Proceedings of the 15th International Workshop on Laser Ranging

Extending the Range

October 15-20, 2006
Canberra, Australia

Book Title

Proceedings of the 15th International Workshop on Laser Ranging, Canberra Australia, October 2006 (editors J. Luck, C. Moore and P. Wilson).

Author and Publisher

EOS Space Systems Pty Limited
111 Canberra Avenue
Griffith ACT 2603
Australia
Telephone: + 61 2 6222 7900
Facsimile: + 61 2 6299 7687

First published

Feb 2008

Printer

QPrint
24 Markus Clarke St, Canberra City, ACT.
Contact: info@qprint.net.au

Sponsors

International Laser Ranging Service

The International Laser Ranging Service (ILRS) provides global satellite and lunar laser ranging data and their related products to support geodetic and geophysical research activities as well as IERS products important to the maintenance of an accurate International Terrestrial Reference Frame (ITRF). The service develops the necessary global standards/specifications and encourages international adherence to its conventions.
Website: http://ilrs.gsfc.nasa.gov/

Geoscience Australia, Australian Government

Within the portfolio of Industry, Tourism and Resources, Geoscience Australia plays a critical role by producing first-class geo-scientific information and knowledge. This can enable the government and the community to make informed decisions about the exploration of resources, the management of the environment, the safety of critical infrastructure and the resultant wellbeing of all Australians.
Website: http://www.ga.gov.au/

Electro Optic Systems Pty Ltd

EOS is a public company, specialising in the design, development and production of sophisticated laser technologies, including supporting software and electronic sub-systems. EOS' advanced technologies are applied to a variety of sighting and surveillance applications in the aerospace and defence markets.
Website: http://www.eos-aus.com

ACT Government

Website: http://www.act.gov.au/

15th INTERNATIONAL WORKSHOP ON LASER RANGING
Canberra, A.C.T., Australia
15 – 21 October 2006

ORGANIZATION

Theme: "Extending the Range"

Venue: Canberra Convention Centre

PROGRAM COMMITTEE

Ben Greene (Chair), Ramesh Govind, Hiroo Kunimori, Ron Noomen, Mike Pearlman, Peter Shelus, Mark Torrence, Georg Kirchner, Ulrich Schreiber

LOCAL ORGANIZING COMMITTEE

Ron Thompson (Chair), Jennifer Mullaney (Coordinator), Craig Smith, John Luck, Chris Moore, Ramesh Govind

SESSION CHAIRS

Opening Ceremony	Ben Greene
Science Products	Steve Klosko, Gerhard Beutler
Network Performance and Results	Cinzia Luceri, Mark Torrence
Lasers and Detectors	John Degnan, Ivan Prochazka
Altimetry	Frank Lemoine
Kilohertz Systems	Georg Kirchner, Graham Appleby
Timing Systems	Yang Fumin
Multiple Wavelength and Refraction	Erricos Pavlis
Telescopes, Stations and Upgrades	Craig Smith
Advanced Concepts and Time Transfer	Hiroo Kunimori
Transponders	Ulrich Schreiber
Uncooperative Targets	Craig Smith
Software and Automation	Jan McGarry, Werner Gurtner
LLR Systems	Tom Murphy
Targets and Return Signal Strength	Tom Murphy
Overflow	Mike Pearlman
Closing Session	Mike Pearlman

EDITORIAL COMMITTEE

John Luck, Chris Moore, Peter Wilson, and Session Chairs

PROGRAM

SCIENTIFIC PROGRAM

Monday 16	09:30	Opening Ceremony
	11:05	Science Products
Tuesday 17	09:00	Network Performance and Results
	14:00	Lasers and Detectors
	14:45	Altimetry
	16:00	Kilohertz Systems
Wednesday 18	09:00	Timing Systems
	11:15	Multiple Wavelength and Refraction
	12:00	Telescopes, Stations and Upgrades
	16:00	Advanced Concepts and Time Transfer
Thursday 17	11:00	Transponders
	12:00	Uncooperative Targets
	14:00	Software and Automation
Friday 18	09:00	LLR Systems
	09:15	Targets and Return Signal Strength
	11:00	Overflow
	14:00	ILRS General Assembly
	15:15	Closing Session

SPLINTER MEETINGS

Sunday 15	15:00	Workshop Program Meeting
Monday 16	13:00	WPLTN Executive; Eurolas General Meeting
	17:30	Data Formats and Procedures Working Group with Consolidated Predictions Format Study Group
Tuesday 17	13:00	Missions Working Group
	17:30	Refraction Study Group
	19:30	Signal Processing Study Group
Wednesday 18	13:00	Networks and Engineering Working Group with Transponders Study Group
Thursday 19	08:30	ILRS Governing Board
	13:00	WPLTN General Assembly; T2L2 Planning Meeting
Friday 20	13:00	IERS Working Group 2; LLR Prediction Algorithm
Saturday 21	09:00	Analysis Working Group

SOCIAL PROGRAM

Sunday 15	17:30	Informal Welcome, Crowne Plaza Hotel
Monday 16	19:30	Official Reception, National Gallery of Australia
Wednesday 18	17:30	Observatory Visit and Barbecue, Mount Stromlo SLR
Thursday 19	19:30	Banquet, Old Parliament House

TABLE OF CONTENTS

Science Products Session

Network Performance and Results Session

Lasers and Detectors Session

Altimetry Session

Kilohertz Session

Timing Systems Session

Multiple Wavelength and Refraction Session

Telescopes, Stations and Upgrades Session

Advanced Concepts and Time Transfer Session

Transponder Session

Un-cooperative Targets Session

Software and Automation Session

Lunar Laser Ranging Session

Targets and Return Signal Strength Session

Overflow Session

PARTICIPANTS

Obituary

KAREL HAMAL, 1932 - 2007

Professor, Czech Technical University in Prague

Passed away suddenly, 8 February 2007

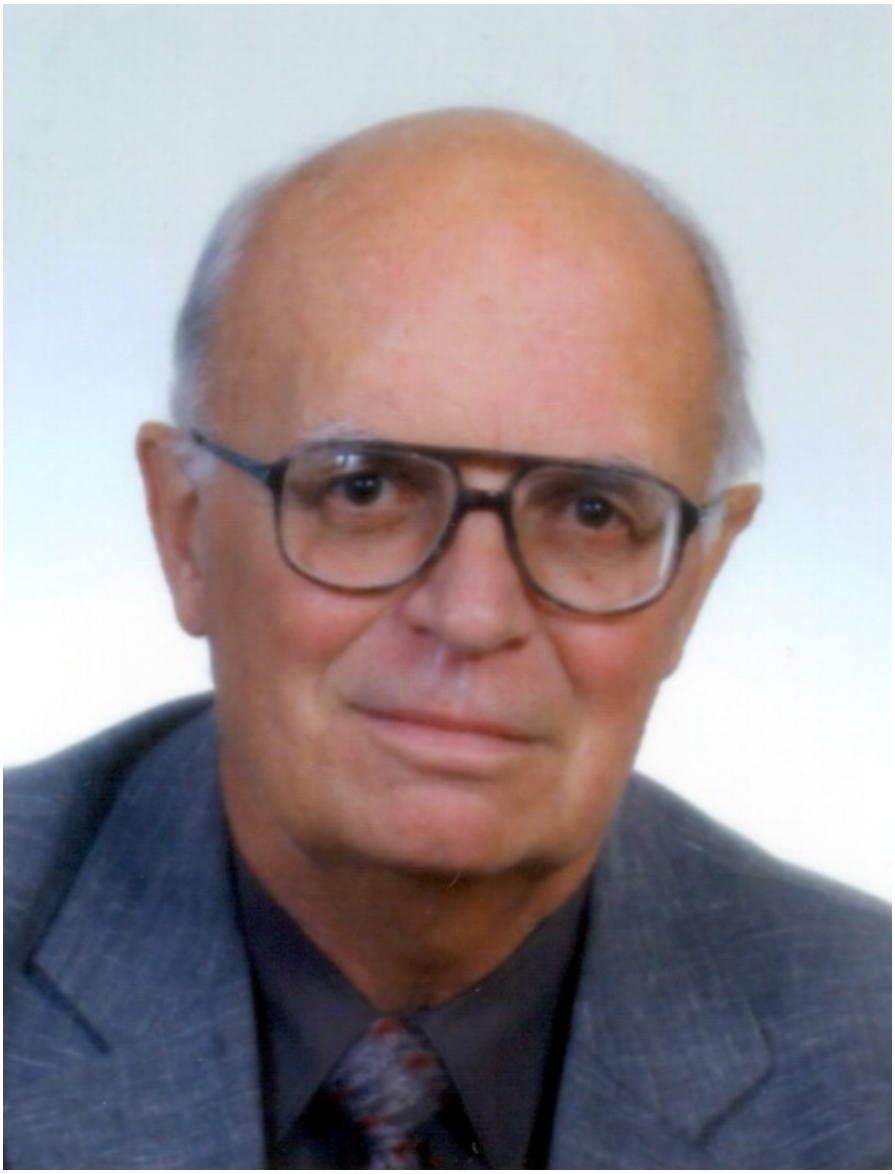

Karel Hamal joined the Czech Technical University in Prague in 1962 after spending some time working for the Tesla radio communication company. His primary interests at that time were in microwaves and radar. At the university he founded the study of a newly emerging technology – solid state lasers. He established a world class laboratory and formed a team of international collaborators. This lab became world famous both for its scientific and educational results.

In the nineteen seventies and eighties he formed international ties between the Czech Technical University and scientists and labs in other countries and he headed the international network of satellite laser ranging stations under the roof of INTERKOSMOS. Satellite laser ranging was his main interest for more than three decades. He was one of the initiators of the international workshops on laser ranging and was involved in the organization of all the workshops for 35 years. The International Laser Ranging Service represented by its Central Bureau awarded Karel Hamal with the "SLR Pioneer Award" in 2002, for his longstanding contributions the subject, in particular, for his early technical leadership in developing and deploying the INTERKOSMOS systems, which helped to create a truly global satellite laser ranging network. Recently Karel Hamal was involved in research and development of solid state photon counters and their applications in laser ranging and space science, in millimeter precision laser ranging and new trends in information technology. Two deep space probes carried his laser ranging and photon counting devices toward the planet Mars late nineties, another two space mission are under completion in Europe and in China to be launched on Earth orbit soon.

Along with the science, Karel Hamal taught several generations of students Physics, ranging from MSc students, PhDs up to research scientists. In the early nineties, he was the driving force behind the reorganization of education at the university.

The passing of Karel Hamal is a significant loss for the University and to the world scientific community. Education and science are losing an expert and unparalleled organizer, the students are losing an excellent teacher and his colleagues are losing a man, who always erupted with new ideas and human energy.

We all will miss him.

Ivan Prochazka

PREFACE

These Proceedings are dedicated to the memory of Karel Hamal, a veritable stalwart of the laser ranging community and one of its prime movers over many years. He attended every International Workshop on Laser Ranging (Instrumentation) since the first at Lagonissi, Greece in 1973. Only Mike Pearlman remains who can match that record. Karel was a great believer in these Workshops and was dynamic on many of their Program Committees. As well as being a brilliant and innovative scientist, he was also a thorough gentleman and a friend to many. Vale Karel.

This volume is being published in three forms:

1. A CD;
2. A book (paper) containing all received papers and some details of the Workshop;
3. On the Internet, most likely on:

   http://ilrs.gsfc.nasa.gov/reports/workshop/

All papers received are included. Where authors have withdrawn their full papers, or not responded, their abstracts have been included when available.

Nearly all the PowerPoint presentations at the Workshop are available at:

http://ilrscanberraworkshop2006.com.au

and are useful adjuncts to the full manuscripts.

Originally, the deadline for submission of papers was set at mid-December 2006, i.e. about six weeks after the Workshop. This was hopelessly idealistic! About 60% of papers were in by the end of February, although not many from the Science Products session. It was felt that this was insufficient to proceed at that time. By 24th August, 113 papers had been received including session summaries, 6 were withdrawn by the authors and 6 were not received at all. I would like to thank the authors, especially those who submitted by the end of February, and the Session Chairs who harassed authors to submit. I also heartily thank Chris Moore, Peter Wilson, Nathan White, Ron Thompson and Jen Mullaney (and her successor, Sarah-Louise McHugh), all of EOS, for their great assistance in the production process.

A “Golden Gong” award was instituted for the last paper to be received and accepted. Several candidates were notified of their eligibility, and competition was fierce. The winner will be formally announced on a suitably sauspicious occasion. Finally, I profusely apologize to all previous editors for my own tardiness in submitting manuscripts. I can now feel that I have been adequately punished!

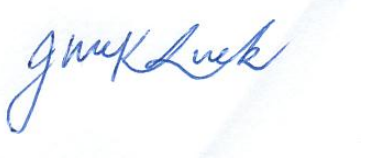

John Luck
Editor

Foreword

It is my pleasure to be involved in the 15th International Laser Ranging Service (ILRS) Workshop in Canberra from 15 to 20 October 2006.

This will be the second time in 30 years that Australia has hosted this prestigious meeting of space scientists. This is an honour for Canberra and for Australia, due to the leading role that Australian scientists and technologists play in this field.
I would like to thank all of you who have travelled to our shores to participate in this event, and also those who have made contributions but were not able to be here.

I would particularly like to acknowledge our sponsors whose generosity has made this Workshop possible:

ACT Government
Geoscience Australia
Electro Optic Systems Pty Limited

Welcome to our beautiful city. We hope you enjoy your stay and find great benefit in the Workshop discussions.

Ron Thompson
Chair, Local Organising Committee

15th International Laser Ranging Workshop
16-20 October 2006-10-13

Welcome Note

Werner Gurtner
Chairman of the ILRS Governing Board

Dear Dr Ben Greene, dear Dr. Williams,
ladies and gentlemen, dear colleagues,

this is the second time that I have the honor to welcome you to an international laser ranging workshop, and it is also the second time that I attend a laser workshop here in Canberra.

For me it is a special honor to attend this meeting in the country and continent with the top two laser tracking stations of our service: Yarragadee has been leading the chart for years, without danger of ever being relegated to a lower position by any other station. The most recent chart, prepared a few days ago by our Central Bureau, awards Mount Stromlo the silver medal for the number of passes collected during the previous 12 months. All our analysts are extremely pleased with this performance of the Australian stations, because it significantly attenuates the well-known weakness of our tracking network in the southern hemisphere.

We have seen several remarkable achievements since the last workshop in San Fernando, four of which I would like to address:

- With Icesat and Alos we have demonstrated that we can successfully track satellites with vulnerable sensors
- Within a year we have introduced a new orbit prediction system with significant improvements in the satellite acquisition
- We are tracking the first Galileo test satellite, Giove-A, although I think that we have to study how to improve our performance for such weak targets
- I was especially pleased to see the very efficient and fast installation and consolidation of the new Chinese station in San Juan in South America. It will further and significantly improve our coverage of the southern hemisphere.

The two space-geodetic techniques VLBI and SLR still form the basis and nucleus of any research in need of high-precision global positions, especially with regard to the referencing to the center of the earth and the height components or the scale of the earth. It is very disturbing that due to budgetary reasons major contributors to the infrastructure needed to maintain these fundamental activities decide to withdraw their support, as we have learned a few days ago from our Canadian VLBI network, and we also had such experiences in our own ranks.

It is extremely important that we can demonstrate the high quality of our products to our parent organizations to convince them of the necessity of space geodesy for modern research in earth sciences. And we have to carefully avoid any activities or statements that could send wrong signals to the external community. There has to be a

healthy competition among the different space-geodetic techniques, internally, in our groups. However, to publicly play one technique off against the another would be disastrous. We will support our sister service, the International VLBI Service, in its activities to convince the Canadian government to re-evaluate these unfavorable decisions.

I would like to thank the local organizing committee for the excellent preparations for this workshop and the sponsors without which it would not be possible to organize and hold such an event.

I wish you all a fruitful and successful workshop. Please enjoy the various activities prepared for the evenings by our hosts. Some of you may even take the opportunity to append a few days to the workshop to see more of this fascinating country.

15th International Workshop on Laser Ranging; Canberra, Australia

Workshop Summary

Michael Pearlman

Electro Optic Systems Pty. Ltd, Geoscience Australia, the Australian Capital Territory Government, and the ILRS sponsored the 15th International Workshop on Laser Ranging in Canberra, Australia during the week of October 16 – 20, 2006. About 111 people from 19 countries participated in the workshop, which included oral and poster presentations on scientific achievements, applications and future requirements, system hardware and software, operations, advanced systems, and analysis.

After the Opening Ceremony, which featured an Aboriginal father-and-son duo welcoming delegates and distinguished guests on didgeridoos, sessions were organized around the following topics:

- Science Achievements, Applications, and Products
- Network Performance and Results
- Lasers and Detectors Session Summary
- Laser Altimetry
- Kilohertz Systems
- Timing Systems
- Multiple Wavelength and Refraction
- Telescopes, Stations, and Upgrades
- Advanced Concepts
- Eye safe Systems
- Laser Transponders
- Uncooperative Targets
- Software and Automation
- Lunar Laser Ranging
- Targets and Return Signal Strength

Some of the key items of interest were:

- Geophysical results through long-term monitoring of SLR data supporting work in gravity field, reference frame, Earth rotation, non-conservative forces on satellites, calibration of GNSS, ocean and ice surface altimetry, lunar science, relativity, and planetary science;
- New event timing systems including the new PICO event timer and control system from TU in Prague;
- Impressive performance (including spin and atmospheric measurements) of the 2 KHz laser at Graz;
- The operation of the new San Juan SLR;
- The SLR progress at Arequipa and Maui;
- Transponder developments for interplanetary ranging;
- Laser altimetry technology and its future application in satellites;

- Automated operations at Stromlo and Zimmerwald;
- Web Application for data engineering files;
- The new climatic facility at INFN for retroreflector array testing;
- Very impressive Lunar Ranging results from the Apollo Station; and
- Systematic time biases in the SR620 counters

Abstracts, most PowerPoint presentations and other information on the workshop can be found at: http://www.ilrscanberraworkshop2006.com.au/. Proceedings from the workshop will be available in mid-2007 on CD with selections in hardcopy, and on the web at that address and at http://ilrs.gsfc.nasa.gov/.

Workshop participants also had the opportunity to visit the SLR station at Mt. Stromlo which has had an extremely impressive recovery after the devastating forest fire in 2003.

The 16th International Workshop on Laser Ranging will be held in Poznan, Poland in the fall of 2008. A specialized SLR workshop similar to those held in Eastbourne and Koetzting will be held in Grasse, France on 24-28 September 2007.

SCIENCE PRODUCTS SESSION SUMMARY

Chairs: Steven Klosko and Gerhard Beutler

The 15th International Laser Ranging Workshop held in Canberra, Australia in October 2006 provided an overview of the state of SLR technologies, campaign activities, and science products. The Science Products Sessions began the meeting and consisted of 16 papers. These presentations demonstrated that satellite laser ranging continues to provide an important resource for satellite orbit determination, verification and validation of active remote sensing systems, and for producing science products that are needed to support a wide range of space geodesy and geodynamic investigations.

A theme of the meeting was the continued contribution of SLR to the progress being made in studying the Earth's system in four dimensions. At the same time, the SLR techniques are being used to both directly provide precision orbits and calibrate precise orbit positioning provided by other tracking systems. And by being a dynamic as opposed to reduced dynamic technique, SLR investigators have contributed significant insight into the intricate force modeling needed to produce cm-level orbit accuracy. All of these topics were discussed during the Science Products Session of the Workshop.

The first set of presentations of the session focused on the orbit determination capabilities of SLR. While GPS analyses benefit from continuous 3-D tracking, which allows "reduced" dynamic orbital techniques, SLR satellites are only observed and directly tracked for a small percentage of the time. Thereby precision orbit determination for SLR requires a high level of sophisticated conservative and non-conservative force modeling.

R. Noomen (1) gave a presentation demonstrating the state of the art in modeling the thermal imbalance and radiative forces acting on the LAGEOS 1 and 2 satellites. These satellites, given their specific design and highly stable orbits, provide an excellent laboratory to study very subtle thermal and drag-like effects acting on these orbits. The thermal perturbations acting on these satellites evolve over time as the satellite spin rate slows and the satellite experiences larger levels of thermal imbalance. R. Noomen presented results obtained at the Delft Technical University of the detailed modeling they have undertaken for the pair of LAGEOS satellites to determine the spin orientation and spin rates for the LAGEOS satellites. In the analysis they account for the complete regime of the spin behavior of the LAGEOS satellites as well as a complete description of the satellites' material composition. This has allowed them to greatly improve the orbit accuracy and fit to the SLR data while reducing the need for empirical correction parameters. SLR provides important and in many cases key independent validation capabilities for a variety of orbit applications. Herein, SLR is complementing GPS and measurements being acquired by these missions to validate orbit accuracy, detect manoeuvres, and provide a back up, fail safe orbit determination capability. Papers given by Urschl (2,5), Govind (4), and Deleflie (3) focused on SLR orbit determination applications that are being applied to study the orbits of GPS-35 and GIOVE-A.

Dedicated SLR satellite missions continue to provide unique long wavelength gravity and decadal time histories of site motions to help establish the geophysical context for many phenomena, a robust reference frame to report these changes within, and place constraints on the geophysical models themselves. Kurt Lambeck (6) gave a paper on the status and future plans for the geodetic network and geospatial modeling framework

within Australia. Australia is moving towards a highly integrated GPS, VLBI, and SLR geodetic reference and geophysical monitoring system. Currently there are two widely e-w separated SLR stations (Yarragadee and Mt Stromlo). Kurt discussed the possibility of deploying a third station in the north central part of the country co-located with VLBI near Katherine.

Contributions are coming from SLR to monitor and better understand long wavelength changes in the Earth's gravity field. Mass flux within the Earth's system over large spatial scales can be observed through the orbit changes they induce on well tracked SLR satellites. The return of the Earth to isostatic equilibrium since the time of the most recent Ice Age is a major source of nearly secular long wavelength gravity field changes. To understand the glacial mass flux apart from the total mass flux dominant over high latitude regions, detailed understanding of the Glacial Isostatic Adjustment (GIA) processes are needed. Dick Peltier of the University of Toronto gave a paper on recent refinements he has instituted to improve GIA modeling (7). Frank Lemoine (8) gave a talk on the long time history of gravity changes obtained from SLR for the longest wavelengths in the field and how they relate to GRACE. To understand contemporary ice sheet mass balance and its contribution to sea level rise, both the high latitude gravity changes and their decoupling from GIA processes are needed.

As knowledge of the long wavelength gravity field has improved, especially with advances coming from the GRACE Mission, further improvements have been made in deriving a constraint on the Lens Thirring effect. Erricos Pavlis (9) of the University of Maryland gave a paper on an improved estimate of the Lens Thirring term. This team has measured the value of this term to approximately 1% of its expected value as predicted by General Relativity. The experiment reported by Ciufolini and Pavlis was based on the long term behavior of the argument of the ascending node of the LAGEOS 1 and 2 satellites. The Lens Thirring predicted "frame-dragging" is seen as an unmodeled node signal for the LAGEOS pair. By evaluating more than eleven years of these data, these authors were able to isolate Lens Thirring from zonal gravity field error sources.

There were a set of papers focused on the reference frame, SLR contributions to the International Terrestrial Reference Frame (ITRF) and www-based tools for comparing time series from different experiments and technologies. D. Delefilie (10) of GRGS gave a presentation on a www-based tool for comparing geodetic times series. D. Coulot (11) of IGN presented a paper on different approaches to accommodate the "least squares mean effect", that is, the effect in a least squares environment of the variation of solved for parameters when a model is imposed on their behavior. H. Mueller of GFZ gave two papers (12 and 16). In the first, he discussed various experiments ongoing to compare SLR solutions using different processes and these results to VLBI and GPS. In the 2nd paper, the authors evaluated the contribution of SLR to the ITRF and presented a comparison of SLR solutions being produced at GFZ with those of IGN. Of high interest in this paper, in contrast to results described below, the GFZ Group is not seeing a scale difference from 2001 onward with their SLR solution and VLBI.

A contrasting paper was given by Z. Altamimi (15) of IGN on the construction and results he derived in computing the ITRF 2005 solution. Therein, this author found a greater than 1 ppb scale difference between SLR and VLBI, and this scale difference seemingly got progressively larger from 2001 onward. Zuheir went into considerable

detail about the use of local survey ties to bring SLR, GPS, and VLBI into a common frame.

The contrast between the IGN and GFZ results with regard to SLR scale, and the decision to use the scale provided by VLBI in the final ITRF 2005 realization caused a great deal of discussion, splinter groups, and involvement of the Analysis Centers in an attempt to better understand, resolve, and develop a strategy for utilizing the ITRF in future SLR analyses.

Also given during this portion of the session were papers by R. Govind (13) who discussed geocenter solutions he has obtained from SLR. This was followed by a paper by D. Gambis (14) of GRGS who presented results for the determination of EOP and Earth rotation using both SLR and LLR and the changing balance of contributions from all technologies over time in the combination solutions produced by IERS.

References:

[1] Andres, J. and R. Noomen, Enhanced modeling of the non-gravitational forces acting on LAGEOS.

[2] Urschl, C., G. Beutler, W. Gurtner, U. Hugentobler, S. Schaer, Calibrating GNSS orbits with SLR tracking.

[3] Deleflie, F., S. Melachroinos, F. Perosanz, O. Laurain, P. Exertier, GIOVE-A and GPS-35 satellite orbits: analysis of dynamical propoerties based on SLR-only tracking.

[4] Govind, R., GIOVE-A using Satellite Laser Ranging Data.

[5] Urschl, C., G. Beutler, W. Gurtner, U. Hugentobler, M. Ploner, Orbit determination for GIOVE-A using SLR tracking.

[6] Lambeck, K., Satellite Laser Ranging in the National Collaborative Research Infrastructure Proposal for Geospatial R&D in Australia.

[7] Lemoine, F., S. Klosko, C. Cox, T. Johnson, Time-variable gravity from SLR and DORIS tracking

[8] Peltier, W., Global glacial isostatic adjustment: target field for Space Geodesy.

[9] Pavlis, E., I. Ciufolini, R. Konig, Recent results from SLR experiments in fundamental physics.

[10] Deleflie, F., A “web-service” to compare geodetic time series.

[11] Coulot, D. Ph. Berio, A. Pollet, Least-squares mean effect: application to the analysis of SLR time series.

[12] Mueller, H., D. Angermann, M. Kruegel, Some aspects concerning the SLR part of ITRF2005.

[13] Govind, R., Determination of the temporal variations of the Earth’s centre of mass from a multi-year SLR data.

[14] Gambis, D., R. Biancale, Contribution of Satellite and Lunar Laser Ranging to Earth orientation monitoring.

[15] Altamimi, Z., Station positioning and the ITRF.

[16] Koenig, R. H. Mueller, Station coordinates, earth rotation parameters, and low degree harmonics from SLR with GGOS-D.

Enhanced modelling of the non-gravitational forces acting on LAGEOS

J.I. Andrés[1], R. Noomen[1]

1. Delft University of Technology, Kluyverweg 1, 2629 HS Delft, The Netherlands.

Contact: j.i.andres@tudelft.nl, r.noomen@tudelft.nl

Abstract

LAGEOS-I and LAGEOS-II orbit Earth since 1976 and 1992 respectively. With 426 Corner Cube Reflectors (CCRs) embedded in a spherical surface and a very low area-to-mass ratio, the LAGEOS satellites are among the best tools for global space geodetic research. By means of SLR observations, geophysical phenomena such as variations of the Terrestrial Reference Frame (TRF) origin w.r.t. the geocenter, global scale, low-degree gravity field terms, Earth Orientation Parameters (EOPs) and plate tectonic motions can be accurately measured, their accuracy directly dependent on that of the ground laser instrumentation and the accuracy of the orbit determination.

Intensive orbital analyses yielded a decrease in the semi-major axis of the orbit of LAGEOS-I, at a rate of 1.3 mm/d, shortly after launch; a similar decay has been observed for LAGEOS-II. Various physical processes (or a combination of them) have been proposed as possible causes for this acceleration: radiation pressure from celestial bodies (Earth and Sun) mismodeling, thermal thrust (re-radiation from the satellite itself), together with eclipse dependencies of the (re-)radiation, and ionospheric drag (neutral and charged particles). This decay can be modeled by an empirical along-track acceleration with a mean value of about -3.4 pm/s^2. The modeling efforts done so far have given a partially successful explanation of the non-gravitational perturbations acting on LAGEOS. However, a clear signal is still present in the calculations, due to a lack of precise modeling of the (unique) physical truth.

This study has concentrated on an accurate modeling of the major factors which could be responsible of the unexplained signal: the geometrical and optical properties, the rotational dynamics of the spacecraft, and poorly modeled forces. Accurate results have been obtained for the rotational dynamics thus eliminating one of the largest uncertainties still present. In parallel, finite element modeling has permitted a detailed characterization of the various elements of the spacecraft, together with an accurate description of their (time-dependent) geometry w.r.t. radiation sources. This has yielded a numerical answer for the thermal accelerations for all possible spinning regimes. Uncertainties in some physical parameters have been dealt within a sensitivity analysis.

Introduction

Although the technique of Satellite Laser Ranging (SLR) dates back more than 40 years [Marshall *et al.*, 1995], it is still one of the main techniques to be used for studying certain elements of System Earth. In particular, global aspects of the terrestrial reference frame, such as origin and scale, are uniquely determined by this technique by virtue of its direct and unambiguous method of observation: the travel time measurements of a pulse of light from a ground station to a satellite and back are typically measurable with high precision, and the various elements that play a role in

converting these 2-way travel times into a 1-way range observation (*e.g.* satellite signature, atmospheric refraction, station delay, etcetera) can be modeled with an accuracy of various mm typically [Otsubo and Appleby, 2005]. To arrive at the best possible solutions for such global parameters, it is mandatory to model the orbit of the satellites as accurately as possible. Typically, the cannonball satellites LAGEOS-1 and LAGEOS-2 (launched in May 1976 and October 1992, respectively) are used for this purpose by virtue of their attractive area-to-mass ratio, making them relatively insensitive to (intrinsically complex to model) surface forces.

In spite of the attractive design of these spacecraft, high-precision orbit determination currently necessitates the estimation of so-called empirical accelerations (typically, in various directions w.r.t. an orbit-referenced frame and with different character – constant or sinusoidal with orbital period). This is a clear indication of the limitations of current analysis models to represent "physical truth" correctly. An illustration of this is given in Figure 1, which shows the residuals of the constant along-track acceleration as observed/estimated for the satellite LAGEOS-1, *i.e.* bi-weekly solutions of such a parameter after subtraction of best known physical mechanisms to explain the acceleration (in reality, the accelerations show a mean value of -3.4 pm/s^2, which can be addressed to a variety of surface forces). The plot clearly illustrates that there is a signal in the residuals at the level of several pm/s^2, which needs a physical explanation in order to advance the contributions of LAGEOS–type missions to geophysical studies further. Candidates for the residuals shown here are (1) thermal radiation exerted by the satellite itself, (2) direct radiation forces, (3) charged and neutral particle drag, and others; of course shortcomings in the modeling of any of these individually, and/or a combination of effects can play a role here. This paper will focus on the so-called thermal forces: minute forces that are introduced by the emission of thermal energy by surface elements of a satellite.

First, a model for the rotational behavior of the satellites will be presented. Previous investigations by other authors show that a proper understanding and description of this aspect is crucial for a good modeling of the thermal behavior. The thermal behavior of the satellites will be the next topic of discussion, and a multi-node model of each satellite will be developed and used to simulate actual temperatures. Then, the temperature distribution will be used to compute contributions to thermal forces as exerted by individual surface elements, resulting in a total acceleration. This acceleration will be used in a first-order assessment of its orbital effect. The paper will end with conclusions and recommendations.

Rotational dynamics

Compared to the orbital motion of the spacecraft, the rotational dynamics of LAGEOS-1 and -2 can be considered as a neglected element of the mission: observations of the attitude and spin rate are few, and models of the rotational behavior are hardly available. One of the reasons for this is the absence of any need for such information: the rotation dynamics plays a subtle role in the orbital behavior of the vehicles, which only come into play when the requirements on orbital accuracies arrive at the level of a single cm and below. A recently developed description of the spin behavior of the LAGEOS pair is given in [Andrés *et al.*, 2004].

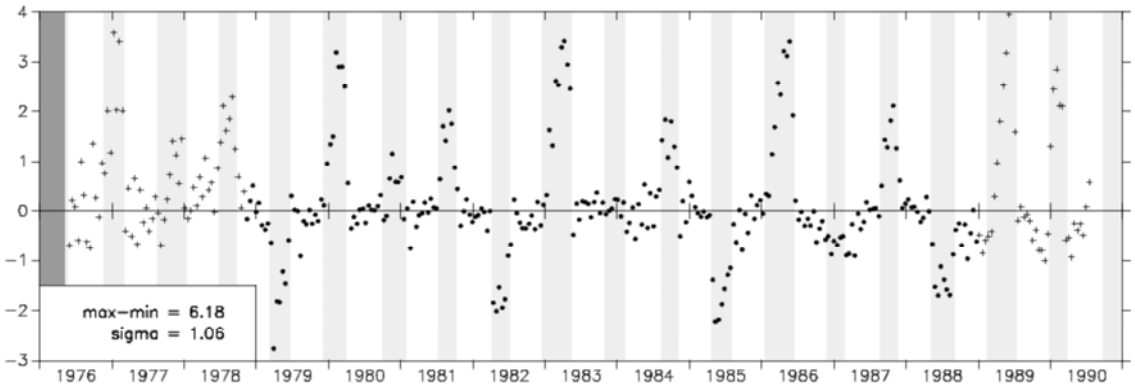

Figure 1. *Residuals of the along-track accelerations as observed for LAGEOS-1, for the time period 1976-1990. Grey areas indicate the periods when the satellite experienced an umbra while orbiting the Earth [Scharroo et al., 1991].*

The LAGEOS Spin Axis Model (LOSSAM) that is developed in this reference is based on a straightforward integration of Euler's equation:

$$\frac{d\vec{L}}{dt} = \vec{M}_{magn} + \vec{M}_{grav} + \vec{M}_{offset} + \vec{M}_{reflec}$$

Here, the external torques represent the influence of the Earth's magnetic field, gravity, a possible difference between the center-of-pressure w.r.t. the center-of-mass, and a possible difference in effective reflectivity between the northern and southern hemisphere of the satellites, respectively. LOSSAM has been obtained after confrontation of the theoretical model as described by the previous equation with independent observations on spin-axis orientation and spin rate taken by a variety of stations and institutes: (*i*) University of Maryland, USA, (*ii*) the laser station in Herstmonceux, UK (owned by the Natural Environment Research Council, NERC), (*iii*) the laser station in Matera, Italy (owned by the Agenzia Spaziale de Italia, ASI) and (*iv*) Lincoln Laboratory [Sullivan, 1980]. Figures 2 and 3 show the behavior of the spin axis orientation of LAGEOS-1 and -2 according to LOSSAM, respectively (spin rate results are withheld here). The plots also show the independent observations that were used in the derivation of the model, and the level of fit. Clearly visible is that LAGEOS-1 is in a different rotational regime currently than LAGEOS-2: the spin-axis orientation of the former satellite follows a more irregular pattern, which is due to a slowing down from a rotational period of 10.5 s at launch (1976) to about 6000 s now (Figure 2). LAGEOS-2 is still spinning with a period of about 360 s currently. Also visible is the fact that the set of observations on the spin axis that is available for LAGEOS-1 is quite restricted: the last ones were taken at the end of 1996, and effectively one cannot do but make predictions of the current behavior of the satellite; the absence of recent observations is directly related to the fact that the rotation of LAGEOS-1 has almost come to a standstill, which makes it extremely difficult to actually apply currently practiced observation techniques on spin axis orientation and rotation rate. For LAGEOS-2, the situation is much better (cf. Figure 3). The reader is referred to [Andrés *et al.*, 2004] for more details.

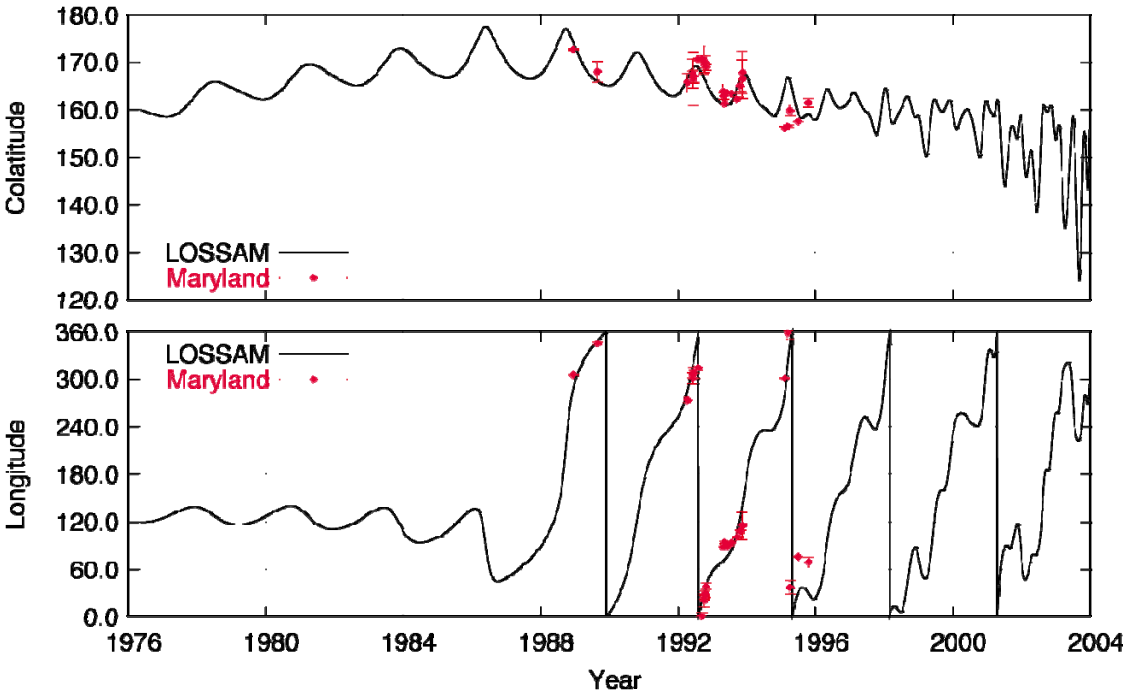

Figure 2. *The LOSSAM spin orientation behavior of LAGEOS-1 as a function of time, as described by the longitude and co-latitude w.r.t. the J2000 reference frame. The red symbols represent the independent observations that were used to derive this model [Andrés et al., 2004].*

Thermal model

Thermal forces, *i.e.* forces that are generated somehow by either direct or reflected radiation, are known to play an important role in the explanation of the observed decay of the semi-major axis of the LAGEOS pair and, directly related to this, of the solutions for the empirical accelerations; many studies have been done into the effects of direct solar radiation (Yarkovsky effect), albedo radiation, earth infrared radiation, the effect of eclipses (Yarkovsky-Schach effect), etcetera (*e.g.* [Rubincam, 1982], [Anselmo *et al.*, 1983], [Barlier *et al.*, 1986], [Rubincam, 1987a], [Rubincam, 1987b], [Afonso *et al.*, 1989], [Rubincam, 1990], [Martin and Rubincam, 1996], [Slabinski, 1997] and [Vokrouhlický and Métris, 2004]). However, none of these investigations has led to a full description and complete understanding of the actual phenomena that influence the orbital behavior of the LAGEOS satellites; if only because simplifications had to be made in order to arrive at first-order estimates of the effects. Clearly, in view of the slow rotation of LAGEOS-1 and a similar trend for LAGEOS-2, the necessity for a more detailed modeling of the satellite and its interaction with various elements in its environment has arisen. As mentioned in the introduction, this paper addresses one of those elements: the thermal interaction with the various radiation sources, and the resulting accelerations. A detailed discussion of procedures, models and results is given in [Andrés *et al.*, 2006].

To model the interaction in detail, making allowance for potential differences in its reaction to various sources of energy, the satellite model needs to be split up into a number of different components. In recognition of the various mechanisms that are effectively responsible for heat transfer (*i.e.* radiation and conduction; any other can be shown to be insignificant [Andrés *et al.*, 2006]) and the differences in thermal and mechanical properties of the various construction elements, a finite-element model of each LAGEOS satellite has been created, with 2133 elements in total: the inner core

(core and stud), two hemispheres, and 426 retroreflector assemblies each consisting of 5 elements: a retainer ring, an upper ring, a corner-cube reflector, a set of ring posts, and a lower ring.

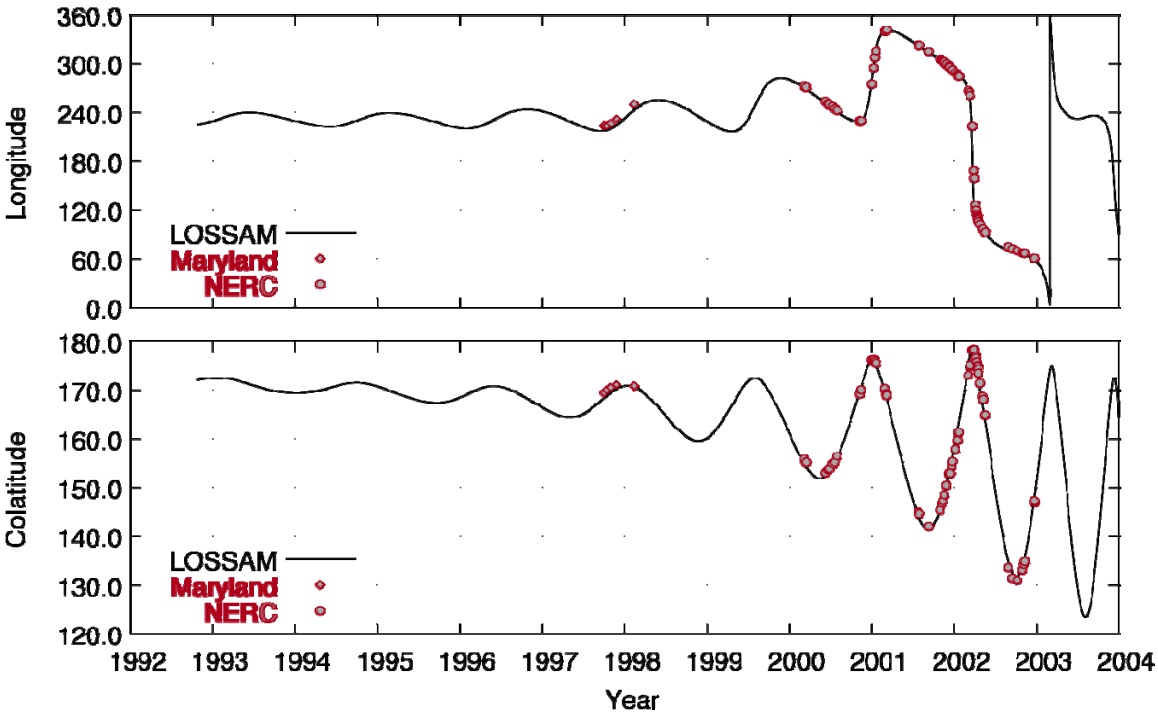

Figure 3. *The LOSSAM spin orientation behavior of LAGEOS-2 as a function of time, as described by the longitude and co-latitude w.r.t. the J2000 reference frame. The red symbols represent the independent observations that were used to derive this model [Andrés et al., 2004].*

For each LAGEOS element *i*, the following (abstract) heat equation can be written:

$$H_i \frac{\partial T_i}{\partial t} = Q_{in} - Q_{out}$$

For more details, see [Andrés *et al.*, 2006]. In combination with cm-level accurate solutions for the orbital motion of the satellites (obtained with GEODYN [Pavlis *et al.*, 1998], the positions of sources of radiative energy (Sun, Earth), models for these radiative flows, models for the thermal and mechanical properties of the spacecraft components, and the LOSSAM model for the rotational behavior of the spacecraft [Andrés *et al.*, 2004] this equation can be integrated over time for each element to yield the thermal behavior of each individual element. This has been done for both satellites from the date of launch onwards, with a step-size of 60 s, and taking care that allowance is made for aspects like shadowing, aliasing (when the rotational period and the integration step size are integer multiples) and rotationally averaged radiation input. An illustration of the result is given in Figure 4, which shows the temperature distribution of the various elements of LAGEOS-1 and -2 for the (arbitrary) epoch January 1, 2002, respectively. The plots clearly show the different temperatures of the Germanium reflectors (3 out of 4 are visible in each plot; the thermal absorption and emission coefficients are very different from the quantities for the 422 Silicium reflectors), and, in a similar fashion, the different temperatures for

the retainer rings. In the case of LAGEOS-1 (Figure 4, left), the Sun is more-or-less located over the satellites equator, resulting in a similar temperature for the northern and the southern hemispheres. In the case of LAGEOS-2 (Figure 4, right), the Sun is at an apparent latitude of about 45°, with a higher temperature for the northern hemisphere as a consequence.

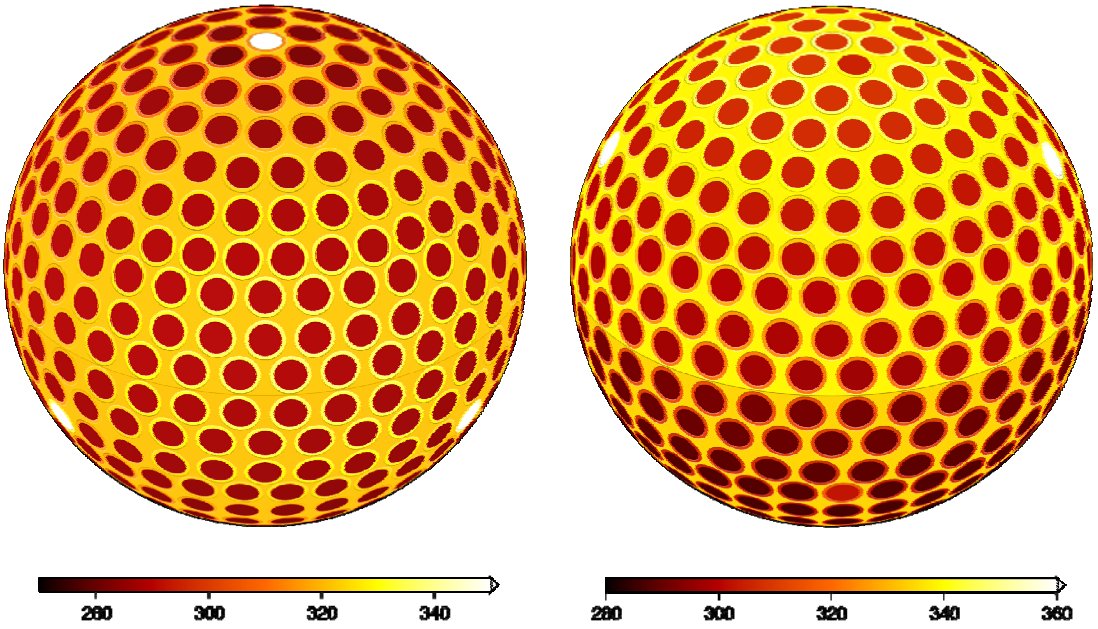

Figure 4. *Temperature distribution on January 1, 2002, for LAGEOS-1 and -2, respectively. All values are in Kelvin [Andrés et al., 2006].*

As an illustration, Figure 5 shows the long-term temperature behavior for a number of elements of LAGEOS-1; a similar behavior has been derived for LAGEOS-2 (not included here; cf. [Andrés *et al.*, 2006]). Figure 5(a) shows the temperatures for representative retainer rings and a Silicium CCR in the northern hemisphere. By virtue of its thermal properties, the CCR has an average temperature which is some 20 K lower than that of the retainer rings. All elements show a variation with time, which is correlated with the occurrence of solar eclipses (indicated by grey bands) and the position of the Sun (the main source of energy) w.r.t. the satellite spin axis; in the case of reflector assembly 89, which is located at a (satellite-fixed) co-latitude of about 58°, temperature variations are relatively humble, but after about 10 years in orbit the attitude of the spacecraft starts to develop into an erratic behavior w.r.t. λ and the spin rate drops off, resulting in extreme temperature variations for the retainer ring located at the satellite's north pole. A similar observation can be made for the retainer rings and the reflectors located in the southern hemisphere of the satellite (Figure 5(b)): the CCRs are typically cooler, show less variation, and big excursions of up to 60 K are visible for the retainer rings closer to the pole (in this case the south pole of the satellite). Figure 5(c), finally, very clearly illustrates the sensitivity of the Germanium CCRs to the actual lighting conditions: the 3 Ge CCRs that are located at co-latitude 121°, show a temperature variation of about 50 K (already large when compared to the behavior of the Si CCRs, cf. Figure 5(a)), but the situation appears to change dramatically for the CCR located at the very north pole of LAGEOS-1: temperature variations of up to 300 K are observed here.

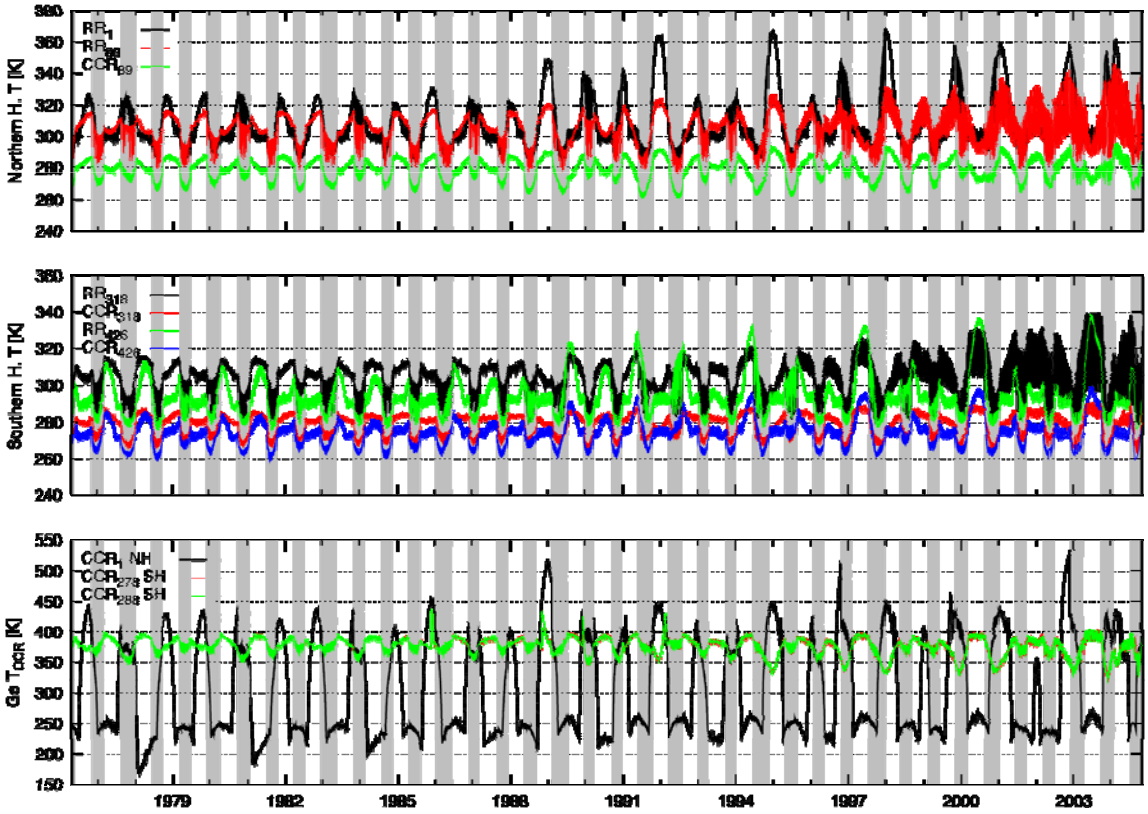

Figure 5. *Temperature behavior of several retainer rings and CCRs for LAGEOS-1 since launch [Andrés et al., 2006].*

Accelerations

Having arrived at a time-series of temperatures for the 2133 elements of each LAGEOS finite-element model, it is possible to derive values for the force that each element exerts (cf. [Slabinski, 1997]):

$$d\vec{F}_i = -\frac{2}{3}\frac{\varepsilon_i\ \sigma\ T_i^4}{c}\ dA_i\ \vec{n}_i$$

Integration of all contributions from all surface elements (clearly, internal elements do not contribute) yields the net thermal acceleration that each satellite experiences. An illustration of that is given in Figure 6: accelerations in the radial, along-track and cross-track directions for one day for LAGEOS-1 and LAGEOS-2, respectively; the right-hand side of the plots zooms in for a particular orbit during that day. It is clearly visible that for both satellites, radial and along-track accelerations of up to 50 pm/s^2 can be obtained (the two follow one another by virtue of the rotation of the orbital, satellite-related reference frame); much larger than the average value of about -3.4 pm/s^2 that is seen in the empirical (constant) accelerations. Since the cross-track orientation of the orbit remains more-or-less constant during one day, this component shows much less of a variation (but can have a very significant value). The plots indicate that an irregular behavior occurs in particular during times of eclipse; in such a situation, the cause for an uneven heating of the satellite disappears (ignoring any

influence form the Earth, that is) and the net acceleration tends to develop towards zero.

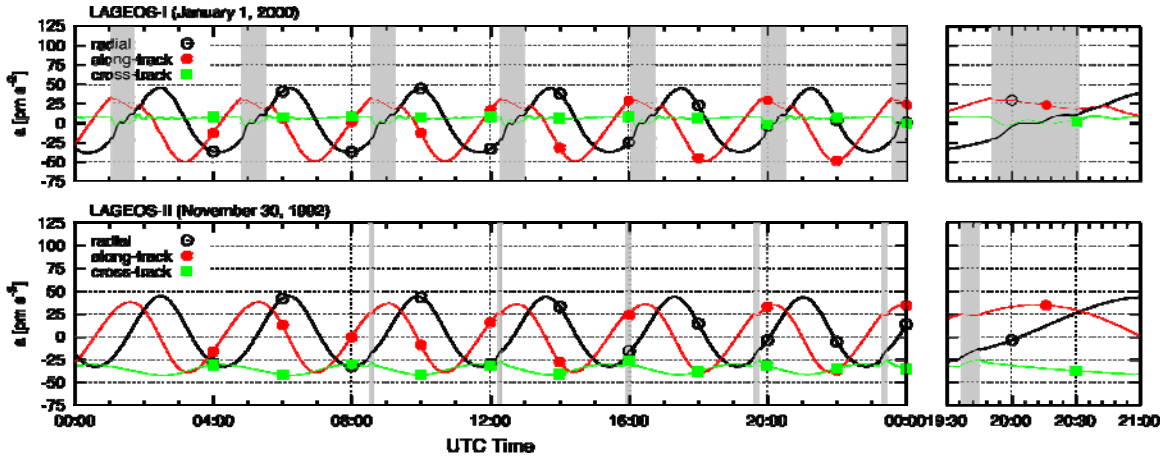

Figure 6. *Net thermal accelerations for (top) LAGEOS-1 on January 1, 2000, and (bottom) LAGEOS-2 on November 30, 1992. The grey bands indicate the exact periods when the satellites are in eclipse [Andrés et al., 2006].*

Extending the presentation to the full lifetime of the satellites (so far), Figure 7 shows the development of the net accelerations as well as the orientation of the Sun in a satellite frame, for each LAGEOS version. Again, the grey bands indicate when eclipses occur (somewhere in the orbit). Starting the discussion with LAGEOS-2 (Figure 7(b)), the long-term behavior is in line with what was shown in Figure 6 already: radial and along-track components interchange by virtue of the definition of the orbital frame, and the variation of the cross-track component is slower. All LAGEOS-2 components have values that go up to about 50 pm/s^2. In the situation that the Sun is located in the equatorial; plane of the satellite (i.e. $\beta_{\text{Sun-SA}}$ is equal to 90°), all 3 components of the net acceleration are effectively zero (by virtue of the rapid rotation of LAGEOS-2). As for LAGEOS-1, a similar story holds (Figure 7(a)), albeit that the relations are a bit more difficult to observe because of the longer time-span covered since launch. Also visible are the larger values for the net accelerations after about 1990, which is due to the specific rotational behavior of the spacecraft (with consequences for the temperature of particular elements of the satellite; cf. Figure 5). Although not included here explicitly, it can be shown that the model for the rotational behavior of the satellites plays a crucial role: net accelerations computed with the LOSSAM model (which is regarded as the state-of-the-art representation of the actual rotational behavior) differ by an amount of about 25 pm/s^2 with the results that would have been obtained with a more traditional (*i.e.* constant) model for the spin axis [Andrés *et al.*, 2006].

Orbit computations

As a very first test of the actual usefulness of the results, two types of orbital computations have been done for LAGEOS-2 only (the choice of this satellite is arbitrary). First, weekly orbital fits have been computed using a model that does not include any external acceleration, and in which the solar radiation pressure force scaling parameter C_R is estimated only (in addition to the state-vector at epoch). Second, similar computations have been done but now with inclusion of the thermal

accelerations as derived by the procedures sketched above (and keeping them fixed at their nominal values). Computations were done for the period October 1993 until

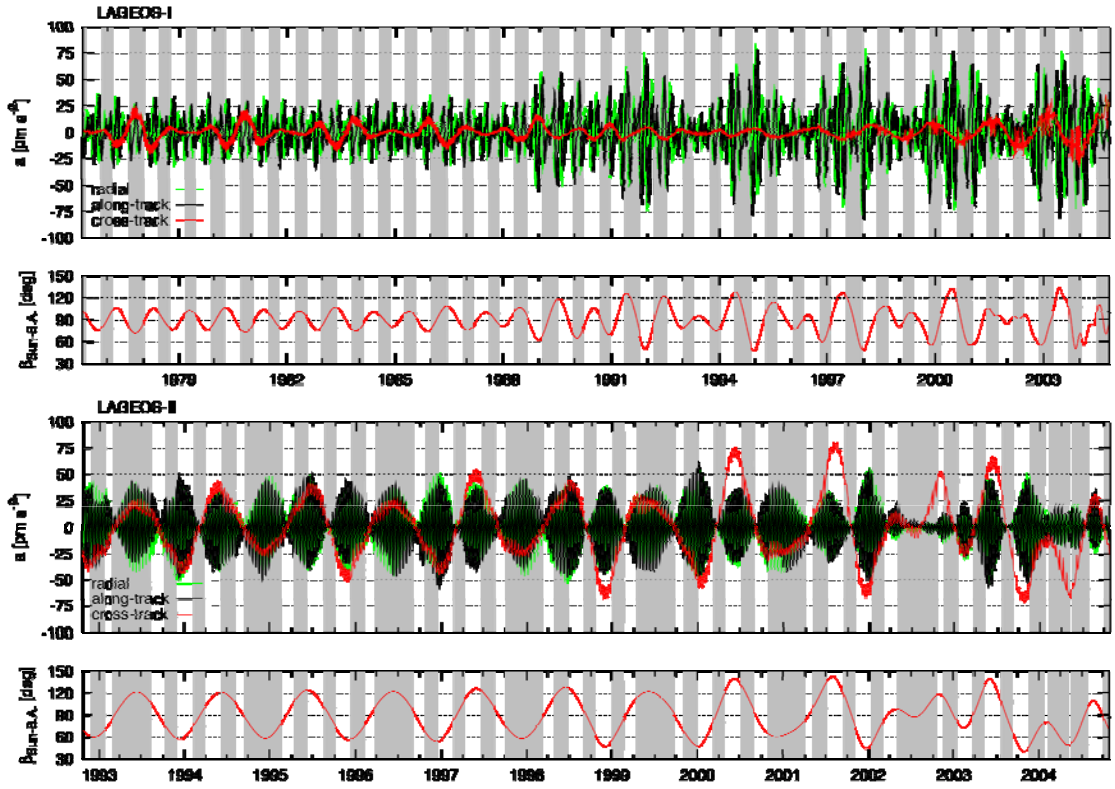

Figure 7. *Net thermal accelerations and solar co-latitude (i.e. position w.r.t. the satellite north pole) for (top) LAGEOS-1, and (bottom) LAGEOS-2. The grey bands indicate the exact periods when the satellites are in eclipse [Andrés et al., 2006].*

December 1994. It should be emphasized here that no effort was done to fine-tune these results, nor to include other (necessary) elements to represent the orbital dynamics of the spacecraft. This explains the relatively high values for the rms-of-fit, which is shown in Figure 8 (typically, one would obtain fits in the order of better than 30 mm (for this period, that is), at the expense of solving for a collection of empirical accelerations; this was explicitly not the purpose of the current test). Figure 8 shows that the use of the thermal accelerations does lead to significant reductions in the quality of the orbit: the fit reduces from a range of 2.5-7.5 cm to a range of 2-4 cm, whereas the stability of the radiation scaling parameter C_R (a physical parameter, which should be constant rather than time-dependent – ignoring adjustments to the space environment during the first months in orbit [Ries *et al.*, 1997] indeed improves as well. The results shown here are very first results; further fine-tune of the computational model will hopefully result in the situation where the (estimation of) empirical accelerations can be discontinued altogether, without any loss of quality of the orbital solution nor of the derived parameters (origin, scale, station coordinates and such); preferably even an improvement of the latter products can be obtained.

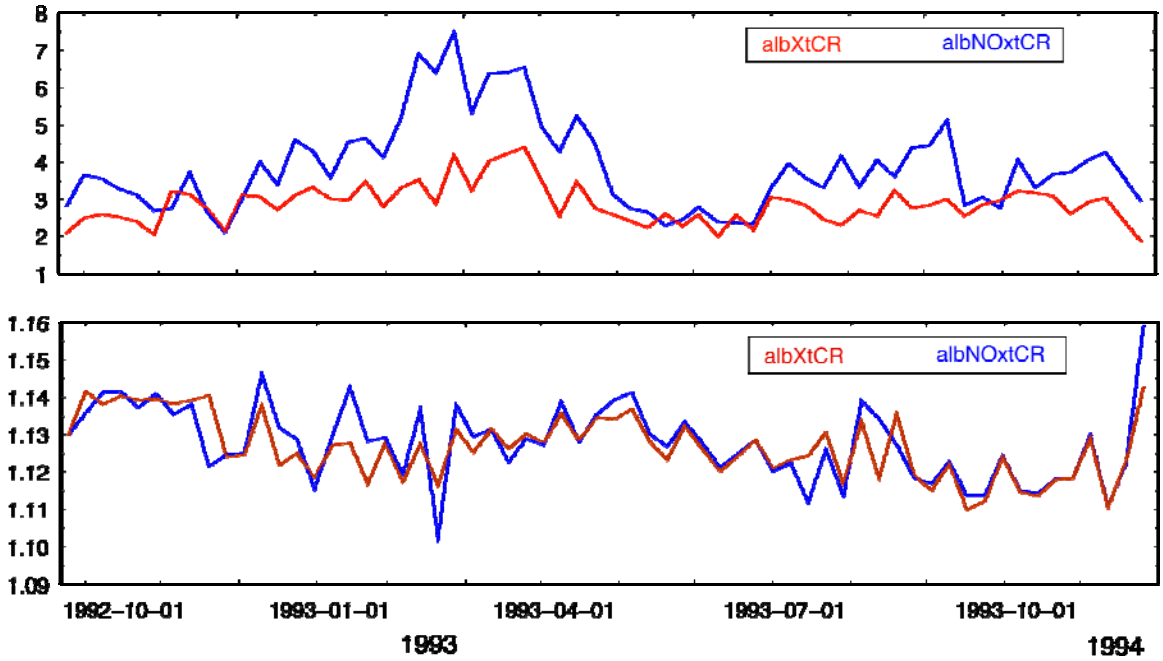

Figure 8. *Rms-of-fit (in cm) and solutions for the solar radiation scaling parameter C_R as a function of time for LAGEOS-2, with and without inclusion of the nominal thermal accelerations as shown in Figure 7.*

Conclusions and recommendations

Based on a detailed finite-element representation of the pair of LAGEOS satellites, and in combination with LOSSAM, the state-of-the-art model for the rotational behavior of each satellite, it has been possible to derive a highly accurate and unprecedented model for the thermal behavior of 2133 different components of each satellite: LOSTHERM. The temperatures appear to show a strong correlation with geometry w.r.t. the Sun as the main source of influx of energy. Also, temperature variations of up to several hundreds of Kelvin are observed by virtue of the sensitivity of particular spacecraft components to irradiation (absorption and emission coefficients). The instantaneous temperature distribution of the outer components in particular can be integrated to yield the net thermal acceleration. These accelerations have magnitudes of up to 75 pm/s^2, much larger than the average value that is typically obtained from orbital computations. The results clearly shows that the rotational behavior of the satellites plays a decisive role in the actual values of these accelerations, and underlines the neccessity of including such formulations in the most demanding orbital computations. It also underpins the need for continuation of independent observations of the rotational behavior of LAGEOS-2, and an answer to the challenge of doing similar things for LAGEOS-1.

References

[1] Afonso, G., F. Barlier, M. Carpino, P. Farinella, F. Mignard, A. Milani and A.M. Nobili, Orbital effects of LAGEOS seasons and eclipses, Ann. Geophys., 7(5), 501-514, 1989.

[2] Andrés, J.I., G. Bianco, D. Currie, R. Noomen and T. Otsubo, The spin axis behavior of the LAGEOS satellites. J. Geophys. Res., 109, B06403, doi:10.1029/2003JB002692, 2004.

[3] Andrés, J.I., R. Noomen and S. Vecellio None, Numerical simulation of the LAGEOS thermal behavior and thermal accelerations, J. Geophys. Res., 111, B09406, doi:10.1029/2005JB003928, 2006.

[4] Anselmo, L., P. Farinella, F. Mignard, A. Milani and A.M. Nobili, Effects of the Earth reflected sunlight on the orbit of the LAGEOS satellite, Astron. Astrophys., 117, 3-8, 1983.

[5] Barlier, F., M. Carpino, P. Farinella, F. Mignard, A. Milani and A. Nobili, Non-gravitational perturbations on the semimajor axis of LAGEOS, Ann. Geophys., Ser. A, 4, 193-210, 1986.

[6] Farinella, P., D. Vokrouhlický and F. Barlier, The rotation of LAGEOS and its long-term semimajor axis decay, J. Geophys. Res., 101(B8), 17,861-17,892, 1996.

[7] Marshall, J.A., S.M. Klosko and J.C. Ries, Dynamics of SLR tracked satellites, Reviews of Geophysics, 33(S1), 353-360, 1995.

[8] Martin, C.F., and D.P. Rubincam, Effects of Earth albedo on the LAGEOS-1 satellite, J. Geophys. Res., 101(B2), 3215-3226, 1996.

[9] Otsubo, T., and G. Appleby, Centre-of-Mass Correction Issues: Towards mm-Ranging Accuracy, in: Garate, J., J.M. Davila, C. Noll and M. Pearlman (eds.), Proceedings 14th International Laser Ranging Workshop, San Fernando, Spain, June 2004, Boletin ROA No. 5, Ministerio de Defensa, Real Instituto y Observatorio de la Armada en San Fernando, Spain, 467-472, 2005.

[10] Pavlis, D.E. et al., GEODYN-II systems description, NASA Goddard Space Flight Center, Greenbelt, Maryland, USA, 1998.

[11] Ries, J.C., R.J. Eanes, G. Métris and D. Vokrouhlicky, Anomalous variations in the LAGEOS and LAGEOS-2 eccentricity, presented at the AGU Fall Meeting, San Diego, California, USA, 1997.

[12] Rubincam, D.P., On the secular decrease in the semimajor axis of LAGEOS' orbit, Celestial Mech., 26, 361-382, 1982.

[13] Rubincam, D.P., LAGEOS orbit decay due to infrared radiation from Earth, J. Geophys. Res., 92(B2), 1287-1294, 1987a.

[14] Rubincam, D.P., Earth anisotropic reflection and the orbit of LAGEOS, J. Geophys. Res., 92(B11), 11,662-11,668, 1987b.

[15] Rubincam, D.P., Drag on the LAGEOS satellite, J. Geophys. Res., 95(B4), 4881-4886, 1990.

[16] Scharroo, R., K.F. Wakker, B.A.C. Ambrosius and R. Noomen, On the along-track acceleration of the LAGEOS satellite, J. Geophys. Res., 96(B1), 729-740, 1991.

[17] Sullivan, L.J., Infrared coherent radar, Proc. Soc. Photo Opt. Instrum. Eng., 227(148), 1980.

[18] Vokrouhlický, D., and G. Métris, LAGEOS asymmetric reflectivity and corner cube reflectors, J. Geophys. Res., 109, B10401, doi:10.1029/2003JB002921, 2004

Calibrating GNSS orbits with SLR tracking data

C. Urschl[1], G. Beutler[1], W. Gurtner[1], U. Hugentobler[2], S. Schaer[3]

1. Astronomical Institute, University of Bern, Switzerland
2. Institute of Astronomical and Physical Geodesy, Technical University of Munich, Germany
3. Federal Office of Topography, swisstopo, Wabern, Switzerland

Contact: claudia.urschl@aiub.unibe.ch

Abstract

SLR tracking data allow for a completely independent validation of GNSS orbits that are derived from microwave data. SLR validation results show mean range residuals of several centimeters for both, GPS and GLONASS satellites, as well as significant seasonal variations for the two GPS satellites that are equipped with retroreflector arrays. It was, however, not clear whether these systematic effects could be assigned to orbit modeling deficiencies or to SLR tracking biases. We present new SLR validation results, which point to serious GPS orbit modeling problems. Moreover, we address the question, whether it would make sense to perform a combined analysis of microwave and SLR data for GNSS orbit determination. With the available low number of SLR observations no significant improvement of the orbit accuracy is found. An a priori variance-covariance analysis shows an improvement of the situation, if continuous SLR tracking data of already a very small number of globally distributed SLR sites were available.

1. Introduction

The International Laser Ranging Service (ILRS) provides Satellite Laser Ranging (SLR) tracking data of Global Navigation Satellite Systems (GNSS, at present consisting of GPS and GLONASS). Two GPS satellites that are equipped with laser retrorereflector arrays (LRAs), and a subset of three GLONASS satellites (all GLONASS satellites carry LRAs) are tracked by SLR.

SLR data allow for an independent validation of GNSS orbits that are derived from microwave data. In Section 2 we present recent SLR validation results, covering about four years of SLR data.

SLR observations may contribute to the GNSS orbit determination in a combined analysis of microwave and SLR observations. The possible improvement of the orbit accuracy is demonstrated on the basis of an a priori variance-covariance analysis in Section 3.

The main results of this work were already presented at the COSPAR 36th Scientific Assembly in Beijing. As this analysis is of a particular interest for the ILRS community, we will briefly introduce and sum up the most important results. We refer to (Urschl et al., 2007) for a detailed discussion.

2. GNSS orbit validation using SLR

For orbit validation we compare the SLR range measurements with the ranges derived from GNSS orbits. We used SLR normal points provided by the ILRS (Pearlman et al., 2002), and final orbits of CODE (Center for Orbit Determination in Europe). CODE is one of the analysis centers of the International GNSS Service (IGS) generating daily orbit solutions for all active GNSS satellites. The orbit determination is based on GNSS microwave observation provided by the IGS (Dow et al., 2005).

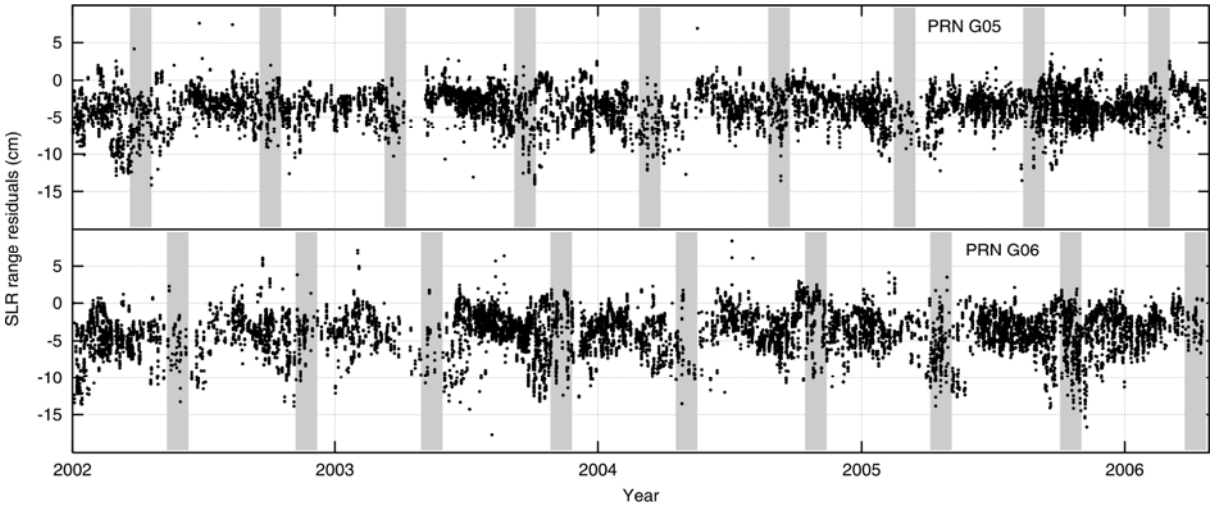

Figure 1. *SLR range residuals in cm for GPS satellites PRN G05 and G06, derived from CODE final orbits. The shaded areas indicate eclipse seasons*

The resulting range residuals indicate the GNSS orbit accuracy, but mainly in radial direction due to the observation geometry. SLR data of about four years starting 2002 were used for the range residual analysis.

Figure 1 shows the range residuals for the two GPS satellites. A standard deviation of the range residuals of 2 cm and 5 cm was estimated for the GPS and GLONASS satellites, respectively. The GPS orbits have a better accuracy compared to the GLONASS orbits due to the much denser GPS microwave tracking network. The GPS range residuals show a mean bias of about –3 to –4 cm. This bias is already known from previous studies, but its origin still remains unexplained. A wrong value for the retroreflector offset, giving the distance from the LRA's center to the satellite's center of mass, could be a possible explanation. It is interesting to note that there is no significant mean bias for the GLONASS satellites.

As part of the analysis, systematic variations were found in the SLR residuals of the GPS satellites, correlated to eclipsing seasons and with amplitudes of up to 10 cm. The largest residuals occur when the satellite is observed within the Earth's shadow during eclipsing seasons (indicated with shaded areas in Figure 1).

We could attribute the periodic signature to orbit modeling problems by displaying the range residuals in the (β,u)-coordinate system. β is the Elevation of the Sun above the orbital plane, and u is the argument of latitude of the satellite with respect to the argument of latitude of the Sun.

Figure 2 shows the range residuals in the (β,u)-system. The residuals are color-coded according to their values. The dependency of the range residuals on the satellite's position within the orbital plane is visible, and rules out SLR tracking biases. The pattern is rather caused by the microwave analysis, indicating attitude or orbit modelling problems.

3. Combined analysis of microwave and SLR data for GNSS orbit determination

Beside the validation purpose, SLR data can be used for GNSS orbit determination in a combined analysis together with microwave observations. But does this make sense in terms of orbit improvement? To answer this question an a priori variance-covariance analysis is performed.

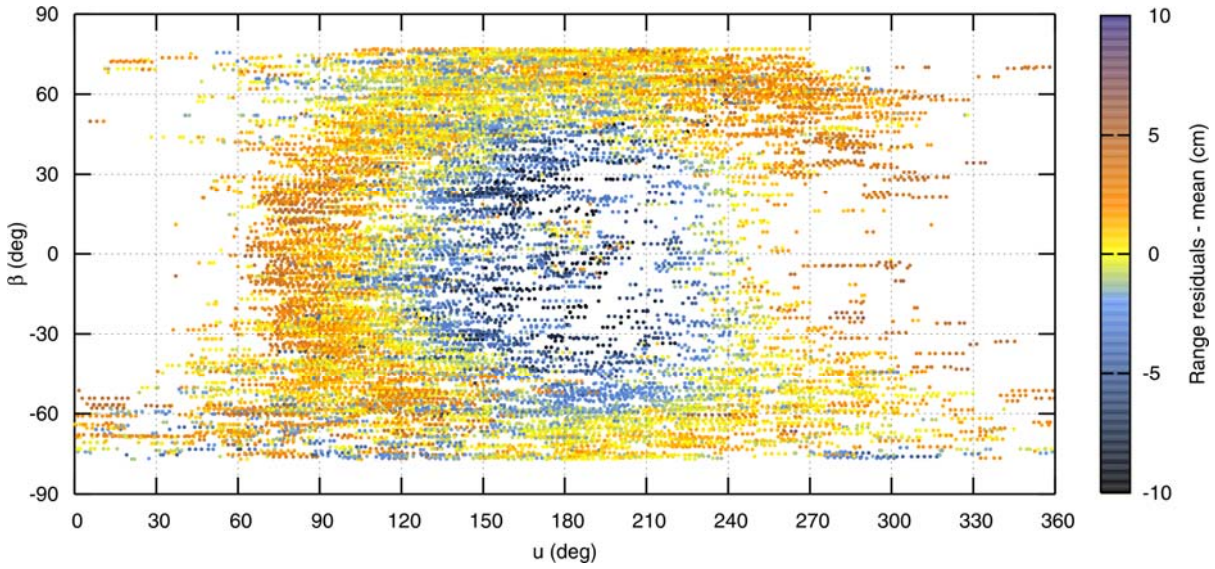

Figure 2. *Color-coded SLR range residuals in cm minus mean value for the GPS satellites PRN05 and PRN06, derived from CODE final orbits*

We used microwave phase observations of about 150 IGS sites and SLR data of 13 ILRS sites. For the variance-covariance analyses only the number, the temporal distribution, and an error model of the observations are needed. The a priori formal errors of the orbit components can be derived from the covariance matrices.

Several experiments were performed using different SLR observation weights. In the first experiment the SLR observation weight is set to zero by setting the a priori sigma of the SLR observations σ_{SLR} to infinity. Thus, the first experiment corresponds to a pure microwave solution. In the second experiment σ_{SLR} is set to 1 cm, similar to that of the microwave observations. In the third experiment the weight of SLR is increased by setting σ_{SLR} to 1 mm.

We compare the a priori formal errors of the orbital parameters of the different experiments. The a priori formal errors only decrease with very strong SLR observation weights (σ_{SLR} = 1 mm) and only around epochs, where SLR observations are available. When using real SLR observations, no significant improvement of the orbit accuracy was found, as SLR tracking data of GNSS satellites are very sparse and not well distributed.

But the situation changes, if SLR data would cover the entire satellite arc. Evenly distributed SLR observations have been simulated with an accuracy of 5 mm, equally spaced at 15 min interval, for altogether four globally distributed SLR tracking sites. SLR data of four sites can cover as much as 90% of a GNSS satellite arc. The a priori formal errors of the orbit parameters decrease significantly for SLR observations with 1 cm accuracy, and even more for SLR observations with increased weighting.

Two additional experiments have been performed using SLR data of only two or three SLR sites. With the data of two sites about 50% of a GNSS satellite arc can be covered, with three sites about 75%. The a priori formal errors in radial orbit component decrease by about 20% including additional SLR data of two sites into orbit determination. The formal error decreases even more if data of three sites are used. Data of the fourth site leads to no further improvement.

For the GLONASS satellites the a priori formal errors of the radial orbit component decrease by about 50%. The impact of additional SLR data on GLONASS orbit determination is larger than for GPS satellites as the number of GLONASS microwave observations is much smaller.

4. Conclusion

The quality of GNSS orbits can be validated using SLR observations of GNSS satellites. An orbit accuracy of about 2 cm and 5 cm was estimated for the GPS and GLONASS orbits, respectively, from a 4-year time series of range residuals covering 2002-2006. A mean bias of –3 to –4 cm for the GPS satellite orbits remains still unexplained. Periodic variations of the GPS range residuals were found, which are highly correlated with eclipsing seasons. We could demonstrate that these variations are not caused by SLR tracking data, but due to deficiencies in the GNSS orbit modeling. An improved solar radiation pressure model might solve the problem. Radiation pressure caused by Earth albedo was not considered in the GNSS orbit determination, but it may have a non-negligible effect on the orbit. Attitude modeling problems might also cause similar periodic variations in the range residuals. Further studies will follow to understand the source of the systematic residual pattern.

The combined analysis of microwave and SLR observations could improve GNSS orbit determination, assuming that the SLR observations are evenly distributed over the entire arc. Already a small network of three globally distributed SLR sites tracking the GNSS satellites continuously may contribute significantly to GNSS orbit improvement.References

References

[1] Dow, J.M., R.E. Neilan, G. Gendt, et al.: “The International GPS Service (IGS): Celebrating the 10th anniversary and looking to the next decade”, Adv. Space Res., 36(6),pp. 320-326, 2005.

[2] Pearlman, M.R., J.J. Degnan, J.M. Bosworth: “The International Laser Ranging Service”, Adv. Space Res., 30(2), pp. 135-143, 2002.

[3] Urschl, C. , G. Beutler, W. Gurtner, U. Hugentobler, S. Schaer: “Contribution of SLR tracking data to GNSS orbit determination”, Adv. Space Res., in press.

GIOVE-A and GPS-35/36 orbit determination and analysis of dynamical properties based on SLR-only tracking data

Stavros A. Melachroinos[1], Felix Perosanz[1,3], Florent Deleflie[2], Richard Biancale1[1,3], Olivier Laurain[2], Pierre Exertier[2]

1. Groupe de Recherche en Géodésie Spatiale/LDTP-UMR5562
2. Groupe de Recherche en Géodésie Spatiale-OCA/GEMINI, Grasse, France
3. Centre National d'Etudes Spatiales, 18 avenue Edouard Belin, 31400 Toulouse, France

Contact: stavros@calc-gen3-ci.cst.cnes.fr

Abstract

SLR tracking data provided by the ILRS (International Laser Ranging Service) network are used to compute orbits of radio-navigation satellites equipped with laser retroreflectors : GPS-35 and GPS-36 for the American GPS constellation, and the first European GIOVE-A (Galileo In-Orbit Validation Element) satellite, launched in December 2005. The equations of motion are computed through an exhaustive dynamical model and is propagated with the two orbit determination softwares of the French GRGS (Groupe de Recherche de Géodésie Spatiale) group: GINS (for high frequency analyses), and CODIOR (for secular orbital elements analyses).

For each of these satellites, a set of SLR (Satellite Laser Ranging) data is processed and the results of the post-fit residuals analysis are shown. The orbit validation for GIOVE-A is based on overlaps between 2-day, 10-day and 30-day arcs calculated with the GINS software. The resulting 3D rms and radial residuals are the primary criteria for the internal accuracy of SLR orbits and may indicate possible dynamical perturbations such as orbit or attitude control manoeuvres. For GPS-35/36 satellites we compare two 10-day arcs to the precise IGS (International Global Navigation Satellite Systems Service) sp3 microwave final orbits. An offset of 2-3 cm in the radial direction appears between the two solutions and may reflect the effect of the non-homogeneity of the SLR tracking network. "Mean observed elements" are also provided.

***Keywords**: GNSS, GIOVE-A, Satellite Laser Ranging, Solar radiation pressure modeling, mean orbital elements*

1. Introduction

GIOVE-A is the first satellite of the future GALILEO global navigation system. It has been developed by Surrey Satellite Technology Ltd and the ESA (*European Space Agency*) . It was launched from Baikonur Cosmodrome on 28 December 2005 and placed into a MEO (*Medium Earth Orbit*) with a semi major axis of 29600 km, an inclination of 56° and an eccentricity of 0.002**.** GIOVE-A is equipped with a LRR (*Laser Retro Reflector*) array having 76 corner cubes with a diameter of 27 mm each (*ESA-EUING-TN/10206*), which provides 40 % more return energy than GPS-35/36 LRR arrays (ILRS). The final constellation of Galileo will consist of 27 operational spacecrafts equipped with such identical LRR arrays. After the launch of GIOVE-A, ESA has requested ILRS an SLR campaign support during spring and summer 2006

(http://www.esa.int). The purpose of these campaigns is to provide data for the characterization of the satellite's on-board clock

The first of theses campaigns has taken place between 22 May and 24 July 2006, with the participation of 13 globally distributed SLR stations. This paper presents the results of the GIOVE-A orbit determination for this period. The orbit validation is based on overlaps of fitted SLR-only orbits of 2-day, 10-day and 30-day duration arcs.

The ILRS community is also actively tracking the only two GPS (*Global Positioning System*) satellites which have LRR arrays on-board, designated GPS-35 and GPS-36. The GPS satellites are equipped with LRR arrays of 32 corner cubes arranged in a flat panel of 19x29 cm (*Degnan and Pavlis, 1994; ILRS, 2004; Urschl et al., 2005***).** The altitude of GPS 35 and 36 is that of 20,195 km and 20,030 km respectively, with a 0.000 and 0.006 eccentricity and a 54 ° inclination for both.

In this study we are using 10 days of SLR data, for the two GPS satellites, in the period of 6^{th} till 16^{th} of June 2006. In this period most of the SLR stations where pointing to the GIOVE-A satellite and the SLR tracking data for the two GPS satellites have always been sparse. In this investigation the challenge consists in discovering the achievable orbit accuracy with sparse tracking data for the two GPS satellites. The analysis of SLR orbits of both GPS satellites is based on overlaps wrt the precise IGSsp3 orbits and the examination of difference residuals in the radial, normal and along-track direction. Transformation parameters between the fitted SLR arcs and the IGSsp3 orbits are adjusted.

Moreover, a propagation of the mean equations of motion, accounting for only the long periodic effects acting on the GIOVE-A orbit, has been led. This study provides the values of the mean observed elements, giving a mean value of each orbital parameter, and of the angles in particular (ascending node, argument of perigee, mean anomaly) for the 10-day arc.

The paper is organized such as follows. The analysis of the SLR-orbit estimation strategy and the solar radiation pressure modeling is outlined in Section 2. Section 3 describes the data set being used for GIOVE-A and GPS-35 and GPS-36 satellites. Section 4 analyses the results of the GIOVE-A internal orbit overlaps. Section 5 makes the analysis of the differences of the estimated SLR orbits of GPS-35/36 wrt IGSsp3 final microwave orbits for the period in question. Section 6 is dedicated to the analysis of GIOVE-A and GPS-35/36 orbit mean elements. Section 7 derives the necessary conclusions and summarizes the results.

2. SLR orbit estimation strategy

Our motivation to process the GIOVE-A and GPS-35/36 satellite SLR data on the period of June 2006 is two-fold: firstly we want to evaluate the implementation of the new box-and-wing SRP (Solar Radiation Pressure) model of GIOVE-A in our software GINS 6.1, and secondly to test the performances of SLR-only orbit determination for these 3 GNSS (Global Navigation Satellite System) satellites.

Our estimation strategy is based on a weighted least squares scheme. The present analysis is made by the orbit determination and analysis software package GINS 6.1 developed by the CNES (Centre National d'Etudes Spatiales) geodetic team of. In table (1) the ad-hoc models and estimated parameters are summarized.

The attitude model used for all three s/c is illustrated in Fig. 1. and corresponds to the following coordinate frame :

- The **Y-axis** points along the solar panels
- The **D-axis** points towards the sun
- The **X-axis** completes the system

For GIOVE-A and GPS-35/36 we have implemented a box and wing solar radiation pressure model including respectively 8 and 19 surfaces with a-priori reflectivity and specularity coefficients

GINS 6.1 soft. package	***GPS 35/36***	***GIOVE-A***
Datum definition	ITRF 2000, EOPC04	ITRF 2000, EOPC04
Tidal displacements	IERS03	IERS03
Gravity field	EIGEN_GL04S(20x20)	EIGEN_GL04S(20x20)
Atmospheric loading Ocean loading	ECMWF FES2004 (K2 cor.)	ECMWF FES2004 (K2 cor.)
Troposphere	Marini-Murray	Marini-Murray
Solar Radiation Pressure	Box-and-wing	Box-and-wing
Albedo and infra-red	Analytical model (10°x10°)	Analytical model (10°x10°)
Satellite's retro-reflector offsets	x=-0.863, y=0.524, z=-0.658	x=0.828, y=0.655, z=-0.688
Attitude model	X, Y, D	X, Y, D
Numerical integration	Cowell 8th order, step size 180s	Cowell 8th order, step size180s
Parameter adjustment	6 orbital parameters, 1 SRP coeff., 1 Y-bias, 1 X, D per revolution (cos, sin)	6 orbital parameters, 1 SRP coeff., 1 Y-bias, 1 X, D per-revolution (cos, sin)

Table 1*. SLR-only orbit processing parameters for GPS-35/36 and GIOVE-A*

We have processed a set of 2-day, 10-day and 30-day arcs for the GIOVE-A satellite and two 10-day arcs for the GPS-35/36 satellites. Depending on the length of each arc, we include 1 per revolution terms for 2-day arcs (with constraints) and 5 per revolution terms (1 every 2d) for 10-day arcs in X, D directions. An additional acceleration along the s/c's Y-axis, the so-called Y-bias, is also adjusted.

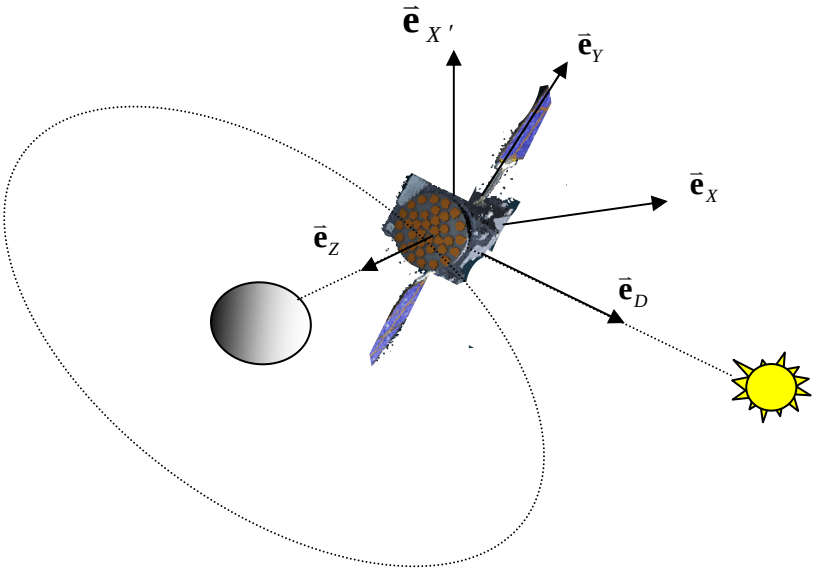

***Fig. 1**. The GIOVE-A and GPS-35/36 attitude model*

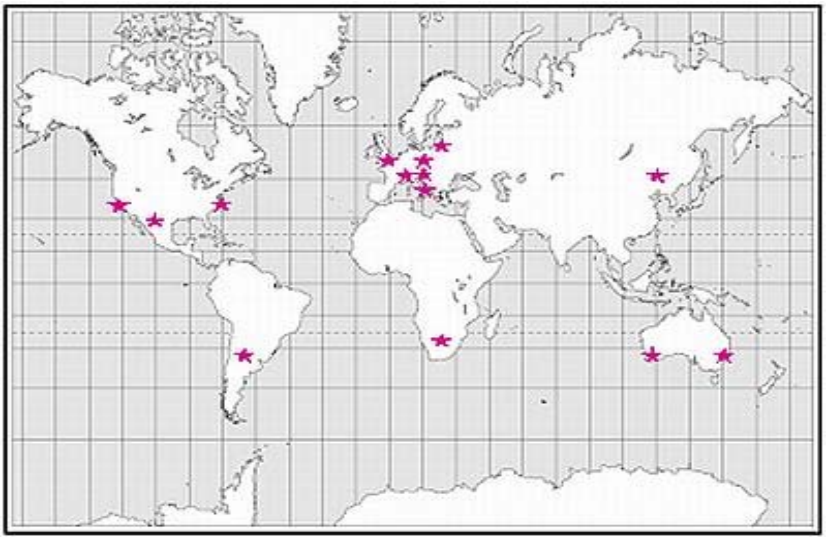

***Fig. 2.** The 13 SLR network stations distributed globally (ESA courtesy)*

3. Data set

Fourteen laser ranging stations (Fig. 2) participated in a campaign to track ESA's GIOVE-A satellite during spring and summer of 2006, providing invaluable data for the characterization of the satellite's on-board clock. The campaign was coordinated by ILRS and the GIOVE Processing Centre at ESA-ESTEC.

See www.esa.int/esaNA/SEM8QOKKKSE_index_2.html .

GIOVE-A satellite data from June to August 2006 used in this study have been processed. Figure 2 illustrates the distribution of the SLR tracking network. The total number of normal SLR points for this period arises up to 2311.

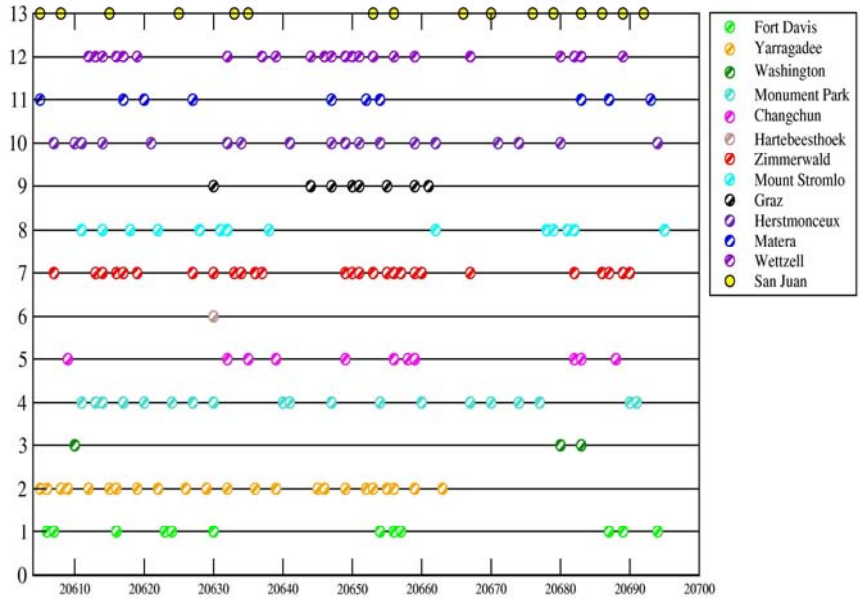

Fig. 3. *3 months (in Julian days 1950) of GIOVE-A SLR data from global tracking stations*

For GPS-35/36 we processed data from the period of June 2006 corresponding to a set of 306 and 402 normal points respectively. For the same period the amount of normal points for GIOVE-A is 900.

4. Orbit analysis of GIOVE-A

In this section we are examining:

- 1-day overlapping SLR-only sessions for GIOVE-A, from JULD50 (Julian day 1950) 20612 (2006/06/05) till JULD50 20623 (2006/06/19),
- a 10-day arc (2006/06/01.5-2006/06/11.5) over a 30-day arc (2006/06/01.5-2006/06/30.5)
- the overlaps with a 90-day arc expanding over the whole period of 3 months.

The illustration of the overlapping strategy is shown in Fig. 4.

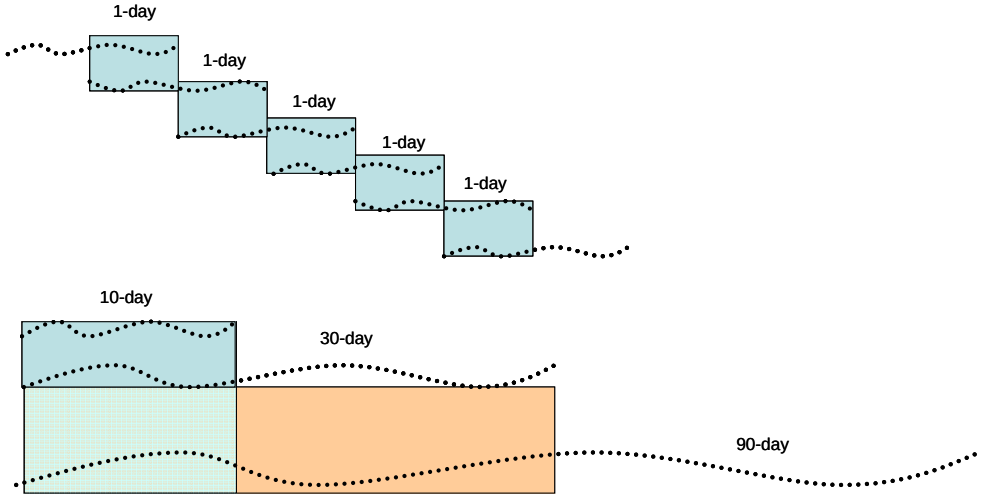

Fig. 4*. The overlapping periods of successive SLR arcs*

The evaluation criteria of the estimated orbit used are the root mean square misfit (RMS) (Eq. 1) and standard deviation (SD) of overlapping periods of successive arcs. An orbit overlap is defined by the comparison of the satellite's position vector between the common time-span of the two successive orbits (e.g. 1-day overlaps over 2 successive 2-day arcs).

$$rms_{misfit} = \sqrt{\frac{\left(\mathbf{x}^{arc1} - \mathbf{x}^{arc2}\right)}{n}}$$
$$rms_{3D} = \sqrt{rms^2_{Radial} + rms^2_{Along} + rms^2_{Cross}} \qquad (1)$$

Figure 5 shows the statistical results of the overlapping period of 2-day successive arcs.

For the arcs between JULD50 20611 (2006/06/08) and JULD50 20613 (2006/06/10), there is a significant change in the estimated accelerations, as well in the overlap mean difference and RMS. This implies that a dynamic perturbation like a manoeuvre occurred. In addition, a degradation of the mean difference of the SLR residuals appears at JJULD50 20620 (2006/06/16). This effect could be related to a reduction in the number of tracking stations for that epoch especially in the southern hemisphere.

The overlapping mean difference for the 2-day arcs is 43 cm in the Radial direction. Without accounting for the possible manoeuvre period it falls down to 14 cm. The same effect can be seen on the residual SD which decreases from 1.41 m to 32 cm for both 2 cases respectively.

Table 2 shows the orbit overlap misfit between a 10-day and a 30-day arc for the

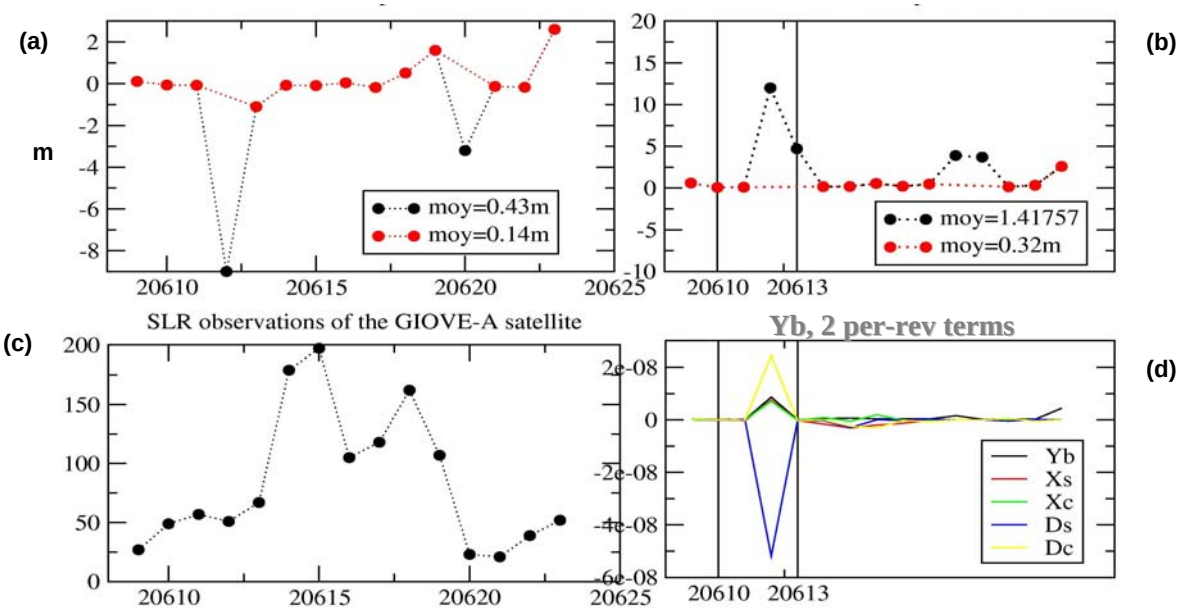

Fig. 5 *statistical results of the overlapping period of 2-day successive arcs: In (a) and (b) are illustrated the mean difference and the RMS misfit in the radial direction respectively. In black are the mean values (in m) including the perturbation days and in red are the mean values without the perturbation days. In (c) is the number of observations for every day and in (d) is the values of the empirical accelerations. Y-b is the Y bias, Xs and Xc are the sin and cos revolution terms in X direction, Dc and Ds are the sin and cos revolution terms in D direction. The perturbation has a stronger influence in the D direction revolution terms.*

period JULD50 20605 (2006/06/01) to 20615 (2006/06/11). The RMS of the satellite positions projected in the radial, normal and tangential directions are respectively 8cm, 45cm and 37cm.

The SLR residuals of a 10-day, 30-day and a 90-day arc are given figure 6 and lead to the same conclusions about the perturbations dates. All arcs agree in the residual level. Outliers up to 8m, verify the existence of dynamical perturbation event and appear in all arcs.

GIOVE-A RMS Misfits (cm)

Earth Along (Tangential)	45.64
Earth Normal	37.46
Earth Radial	8.96

Table 2*. GIOVE-A 10-day orbit overlaps from 2006/06/01.5 to 2006/06/11.5 over a 30-day arc from 2006/06/01.5 – 2006/06/30.5*

5. Orbit analysis of GPS 35/36

One 10-day SLR-only arc has been computed for GPS-35/ 36. The SLR data set spans from JULD50 20610 (2006/06/06) to 20620 (2006/06/16). As already mentioned, this period corresponds to a SLR campaign giving the priority to GIOVE-A tracking. This validation method has been very well known in the last 10 years and many studies, like Pavlis(1995), Appleby and Otsubo (2000), Hujsak et al. (1998) have investigated the undergoing problems of SLR sparse tracking orbit determination.

Tables 3(a) and 3(b) compare the adjusted orbits to the IGSsp3 final precise orbits in terms of position differences in the radial, normal and tangential directions. The RMS is at the level of 3 cm in radial, 47 cm in cross-track and 23 cm in along-track direction for GPS-35.

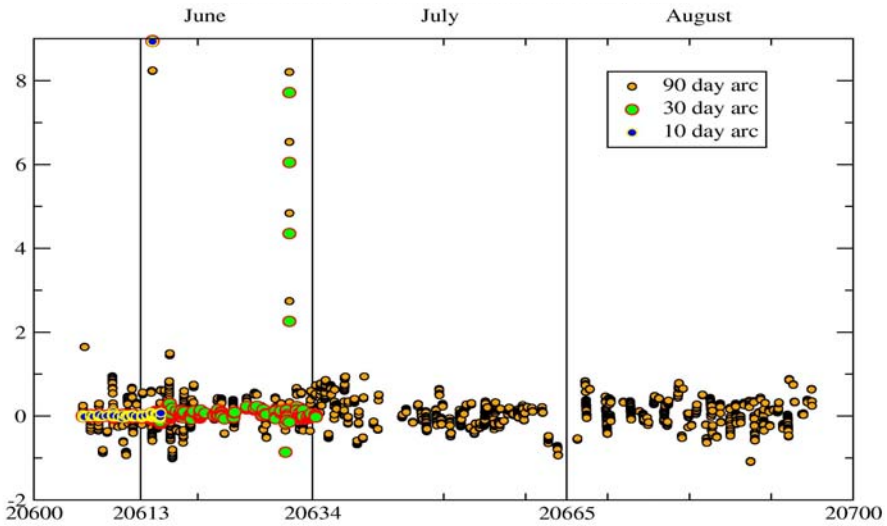

. ***Fig. 6:*** *SLR residuals for the 10-day, 30-day and 90-day arcs from the 1st of June*

GPS-35 RMS Misfits (cm)	
Earth Along (Tangential)	23.81
Earth Normal	47.25
Earth Radial	3.24

Table 3 (a). *GPS-35 10-day SLR arc overlap wrt IGSsp3 final orbits*

GPS-36 RMS Misfits (cm)	
Earth Along (Tangential)	9.55
Earth Normal	25.75
Earth Radial	2.03

Table 3 (b). *GPS-36 10-day SLR arc overlap wrt. IGSsp3 final orbits*

For the case of GPS-36 the level of agreement in comparison with the IGSsp3 radiometric orbits, is respectively in the radial, along-track, cross-track directions: 2-9-25 cm. Obviously, for GPS-35 and GPS-36, this result reflects the poor geographical distribution of SLR tracking stations. When one station in the southern hemisphere tracks GPS-36, for the same period, the factor of disagreement wrt IGSsp3 orbits drops down by a factor of 2.

Tx	-7.8 +/- 9.
Ty	-.4 +/- .9
Tz	**59.8 +/- 9.**
S (ppb)	$.620124 \times 10^{-9}$ +/- $.375 \times 10^{-9}$
S (m)	**16.5 +/- 10**
Rx	-.3 +/- .1
Ry	.01 +/- .1
Rz	**-2.4 +/- .1**

Table 4 (a). *Helmert transformation wrt. the IGS microwave orbits for GPS-35 JJULD 20610-20620 in mm*

In order to further quantify any RF (Reference Frame) systematic differences, we applied a 7-parameter Helmert transformation between SLR-only orbits and IGSsp3 solutions. Table 4 (a) and 4 (b) summarize the statistics from this comparison.

Both translation coefficients in Z for GPS 35/36 are significative with 60 mm (± 10 mm) and 45 mm (± 5 mm) respectively. This offset may reflect systematic problems

in either or both types of orbit as a result of non-homogeneity of SLR tracking stations in the global networks. In addition there is a factor of 8 in scale differences for GPS 35 and GPS 36 wrt the RF defined by IGSsp3 orbit. This statement is probably related to the poor number of southern tracking SLR tracking stations.

Tx	2.2 +/- 5.3
Ty	. 8 +/- 5.3
Tz	**45.3 +/- 5.3**
S (ppb)	$.712820 \times 10^{-10}$ +/- $.2 \times 10^{-9}$
S (m)	**1.9 +/- 5.**
Rx	-.3 +/- .05
Ry	.04 +/- .05
Rz	**-1.4 +/- .05**

Table 4 (b). *Helmert transformation wrt. the IGS microwave orbits for GPS-36 JJULD 20610-20620 in mm*

Furthermore, the overall agreement of SLR-only orbits with sparse data wrt. the radiometric IGSsp3 final orbits, is 2 to 3 cm radially. The consistency of the RF arises up to 6-4 cm in translation along the z-axis.

6. Mean observed elements

A complementary study has been led to give the value of the mean elements of the orbits of GIOVE-A, GPS-35 and GPS-36, namely : the mean semi-major axis, the mean eccentricity and inclination for the metric variables (those providing the computation of secular effects induced on the angles), the mean ascending node, mean perigee and mean “mean anomaly”. Such an approach leads up to an evaluation of the long term validity of gravitational and non gravitational models, and requires a data processing strategy where short periodic effects are removed from the osculating orbit, on each orbital element. This filtering approach has been carried out following the analytic part of the method, developed in (Exertier, 1990).The formulation of (Kaula, 1966) has been used to express the short period acting on the semi major axis, inclination, ascending node, and the one developed in (Deleflie, 2006) for the components of the eccentricity vector, because the investigated orbits are nearly circular.

Figures 7, 8, 9 show the temporal evolution of the mean metric elements of the GIOVE-A, GPS-35 and GPS-36 orbits, respectively. Table 5 gathers up some of these main elements, and Table 6 the main dynamic characteristics of these orbits which can be deduced from this study.

7. Conclusion and perspectives

The capability to estimate SLR-only orbits for GIOVE-A s/c has been implemented and evaluated in the GINS 6.1 CNES/GRGS software. The generated orbits are internally accurate to the level of 5-10 cm radially. This is the case when we are taking into account longer arc periods where orbit dynamics can absorb uniformly in the least square process a possible un-mapped perturbation such as s/c manoeuvres. Unknown manoeuvres are a critical issue for the s/c orbit determination.

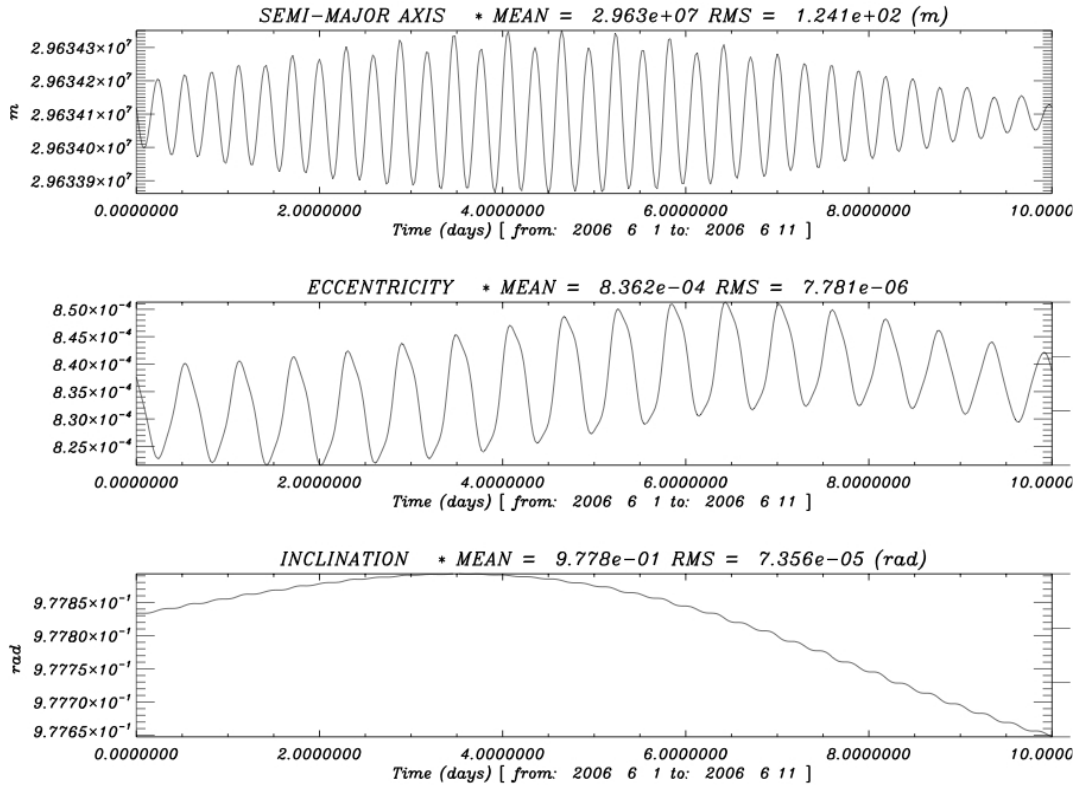

Fig 7. *Temporal evolution of the mean metric elements of the GIOVE-A orbit, from 2006, 1st of June to 2006, 11th of June*

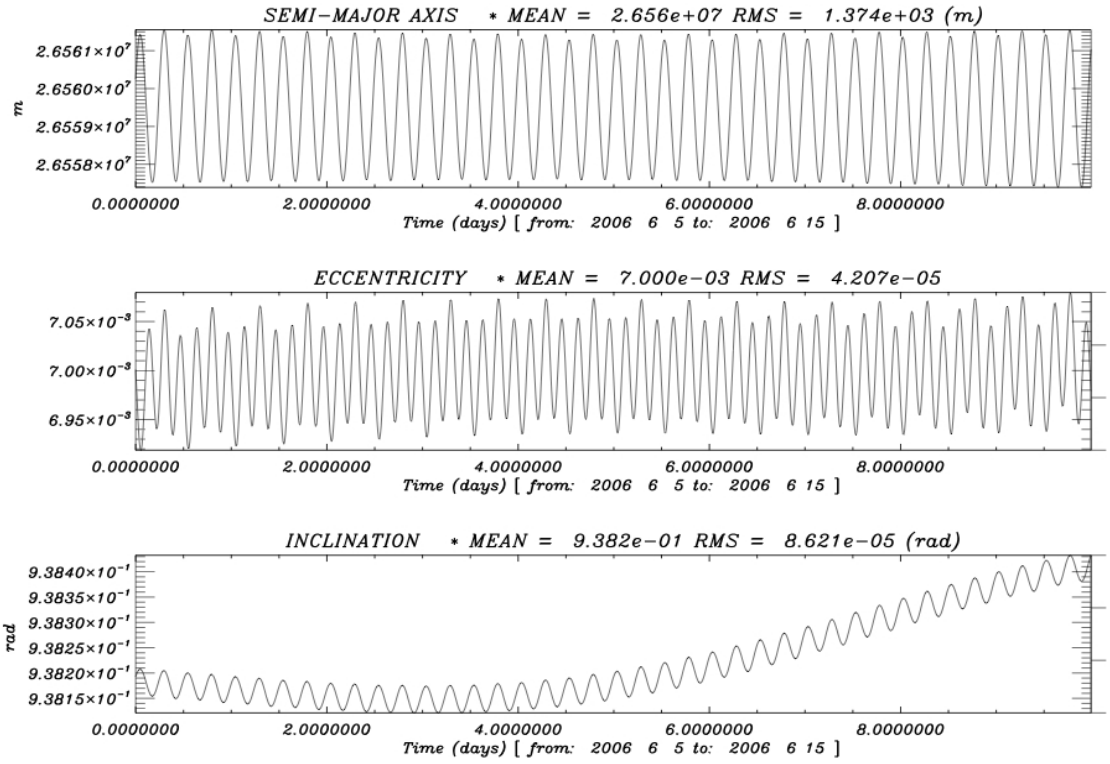

Fig 8. *Temporal evolution of the mean metric elements of the GPS-35 orbit, from 2006, 6th of June to 2006, 15th of June*

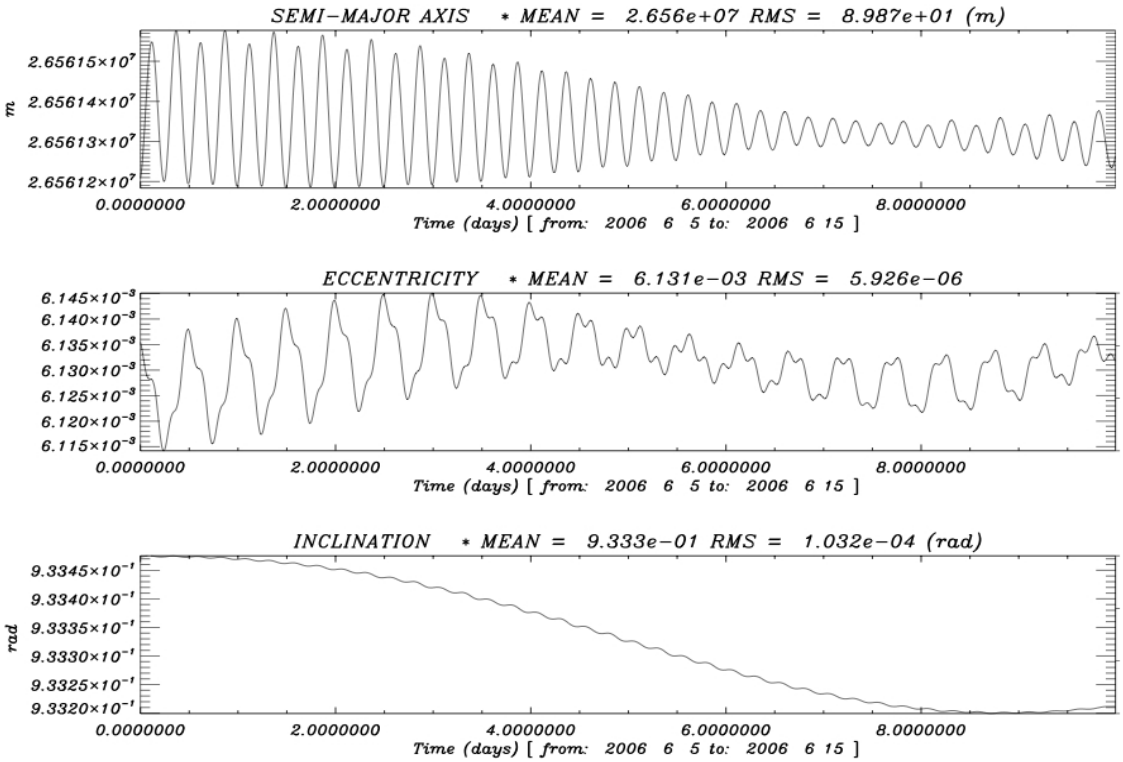

***Fig 9**. Temporal evolution of the mean metric elements of the GPS-36 orbit, from 2006, 6th of June to 2006 15th of June*

By comparing the results for the 90-day, 30-day, 10-day and 2-day orbits we believe that 2-day orbits are the most appropriate for further orbit dynamics investigation. Another critical aspect in the orbit determination of GIOVE-A s/c is the solar radiation pressure model (SRP). We are using an analytical box-and-wing SRP model with approximate specularity and reflectivity coefficients.

	Epoch. (Julian Days 1950)	Semimajor Axis *(m)*	Eccentricity	Inclination °	Ascending node *(rad)*	Argument of perigee *(rad)*	Mean anomaly *(rad)*
GIOVE-A	20605,5	0.29634118E+08	0.83763674E-03	56.025730°	0.32550034E+01	0.57163824E+01	0.11332092E+01
	20615,5	0.29634120E+08	0.83869966E-03	56.015079°	0.32504105E+01	0.57263379E+01	0.12404609E+01
GPS-35	20609,5	0.26560245E+08	0.70009131E-02	53.754485°	0.24052494E+01	0.10521913E+01	0.19530670E+01
	20619,5	0.26561274E+08	0.69619513E-02	53.768426°	0.23981146E+01	0.10572299E+01	0.23138993E+01
GPS-36	20609,5	0.26561208E+08	0.61354695E-02	53.484095°	0.35019663E+01	0.44620688E+01	0.31748379E+01
	20619,5	0.26561276E+08	0.61312841E-02	53.469107°	0.34948338E+01	0.44640863E+01	0.35254203E+01

***Table 5.** Mean observed elements for three orbits, deduced from an analytical filtering of the short periodic terms inside the osculating orbit adjusted on SLR-data.*

	Secular effectsd induced on			riod of revolution of			Altitude of	
	Asc. Node *(rad/s)*	Perigee *(rad/s)*	Mean anomaly *(rad/s)*	Asc. Node *(day)*	Perigee *(day)*	Mean anomaly *(min)*	Perigee *(km)*	Apogee *(km)*
GIOVE-A	-0.520220E-08	0.261182E-08	0.123762E-03	13979	27843	846	23231	23280
GPS-35	-0.807674E-08	0.510770E-08	0.145861E-03	9003	14238	718	19995	20367
GPS-36	-0.812694E-08	0.525981E-08	0.145852E-03	8948	13826	718	20020	20345

Table 6. *Main characteristics of motion.*

A further improvement would be the adjustment of these coefficients in at least one year period time by making use, as well, of the most accurate radiometric observations in L1 and E5. Though an empirical model like those used by CODE orbit analysis center and implemented in the Bernese GPS software, would be further investigated

For GPS 35/36 the presented comparison to the IGSsp3 final orbits for the two 10-day arcs shows a high quality of SLR-only orbits derived with sparse data. RMS residuals are of the order of 2-3 cm radially, 5-10 cm in along and 25-40 cm in cross-track. The systematic patterns of the translation and scale parameters of the RF demonstrate the dependencies in the geographic distribution of the SLR network.

Finally, only two s/c of the GPS constellation are equipped with LRR arrays for orbit validation and the end of their life time could be within the next year. Nevertheless Europe's satellite navigation system Galileo will offer this valuable opportunity of independent orbit validation procedures since all s/c of the constellation will be equipped with LRR arrays.

References

[1] Appleby, G., Otsubo, T. Comparison of SLR measurements and orbits with GLONASS and GPS microwave orbits, in : Proceedings of the 12th International Workshop on Laser Ranging, Matera Italy, 13-17 November 2000

[2] C. Urschl, W. Gurtner, U. Hugentobler, S. Schaer, G. Beutler, Validation of GNSS orbits using SLR observations, Advances in Space Research 36 (2005) 412 – 417

[3] Degnan, J.J., Pavlis, E.C., Laser ranging to GPS satellites with centimeter accuracy. GPS World 62-70, 1994

[4] Deleflie, F., Métris, G., Exertier, P., An analytical solution of the lagrange equations valid also for very low eccentricities. Influence of a central potential, Celest. Mech. 94, 1, 105-134, 2006

[5] European Space Agency, Specifications of Galileo and GSTB-V2 space segment properties relevant for satellite laser ranging, ESA-EUING-TN/10206, Technical note, 2005

[6] Exertier, P., Precise determination of mean orbital elements from osculating elements , by semi-analytical filtering, -V 15, pp 115-123, 1990

[7] Hujsak, R. S., Gilbreath, G. C., Sequential Orbit Determination for GPS-35 and GPS-36 using SLR data from NRL@SOR " SPIE Proceedings, 3380 (32), April 1998

[8] International Laser Ranging Service, GIOVE-A, http://ilrs.gsfc.nasa.gov

[9] Kaula, W. M., Theory of Satellite Geodesy. Blaisdell publ. Co., New York, 1996

[10] Pavlis, E.C, Comparison of GPS S/C orbits determined from GPS and SLR tracking data, Adv. Space Res. Vol. 16, No. 12, pp (12)55-(12)58, 1995

Orbit Determination and Analysis of Giove-A using SLR Tracking Data.

Ramesh Govind[1]

1. Geoscience Australia, Canberra, Australia

Abstract

Using the early available SLR data since its launch, precise orbit determination of the GIOVE-A satellite was undertaken in weekly arcs. A description of the contributing data set, the computation process and the initial results of the orbit quality are presented. From these solutions, the inferred data quality from the individual stations is summarised. Using one estimate of the state vector from these solutions, a spectral analysis of the orbit perturbations due to the Earth's gravity field is shown.

Orbit determination for GIOVE-A using SLR tracking data

C. Urschl[1], G. Beutler[1], W. Gurtner[1], U. Hugentobler[2], M. Ploner[1]

1. Astronomical Institute, University of Bern, Switzerland
2. Institute of Astronomical and Physical Geodesy, Technical University of Munich, Germany

Contact: claudia.urschl@aiub.unibe.ch

Abstract

The first European navigation test bed satellite GIOVE-A was launched on 28 December 2005. SLR observations of GIOVE-A, collected from the ILRS tracking network, are available since 21 May 2006. SLR data are primarily needed for the validation of the microwave-based orbit. As no microwave tracking data are available until now, the orbit determination based on SLR data is of high interest. We present GIOVE-A orbit determination results based on SLR-only data. In addition, the contribution of SLR data to the microwave-based orbit determination is demonstrated.

For the SLR-based orbit determination of GIOVE-A SLR data of the first GIOVE-A SLR tracking campaign were used. Orbits with different arc lengths were determined, as well as orbit predictions. Orbit overlaps were derived to assess the orbit quality. SLR-based orbits of 9-days arc length were determined with an accuracy of about 10 cm in radial orbit component, and about 0.5 m and 1 m in along-track and out-of-plane components.

The microwave-based GIOVE-A orbits as well as the first Galileo orbits in the In Orbit Validation (IOV) phase will rely on microwave tracking data of a very limited number of stations. Therefore, SLR would give an important contribution to the orbit determination through a combined analysis of microwave and SLR data. The possible improvement of the orbit accuracy including SLR observations is demonstrated on the basis of an a priori variance-covariance analysis. For this purpose SLR range measurements and simulated microwave data of GIOVE-A are used.

1. Introduction

Galileo, the European global navigation satellite system (GNSS), is presently being developed. The first of two "Galileo In-Orbit Validation Element" test satellites, GIOVE-A (GSTB/V2A), was successfully launched on 28 December 2005. It carries a retroreflector array and can thus be observed by Satellite Laser Ranging (SLR). For evaluating the characterization of the on-board atomic clocks a first SLR tracking campaign on GIOVE-A was initiated. Between 22 May and 24 July 2006, 14 globally distributed SLR stations participated in the campaign.

As no microwave tracking data are available for scientific use, the orbit determination based on SLR is of high interest. In Section 2, we present first results of the GIOVE-A orbit determination using SLR data of the tracking campaign. Different orbit solutions with varying arc-length were determined. In order to assess the orbit quality, orbit overlaps were computed and compared with each other. In addition, orbit predictions were generated and evaluated by comparing the predicted orbits with the orbits derived from real tracking data.

Orbit determination of GIOVE-A (and the first Galileo satellites as well) based on microwave observations will rely on data of a very limited number of microwave tracking receivers in the beginning. In view of this situation, SLR data would give an

important contribution for precise orbit determination. SLR data may significantly improve the orbit estimates used in addition to the microwave data in a combined analysis. Section 3 shows results of an a priori variance-covariance analysis, demonstrating the possible positive impact of additional SLR data on GIOVE-A orbit determination. For this purpose, simulated microwave data and real SLR data from the tracking campaign were used.

2. GIOVE-A orbit determination using SLR observations

In this Section, we present first GIOVE-A orbit determination results based on SLR data only. SLR data collected during the first GIOVE-A SLR tracking campaign lasting nine weeks (May 22 – July 24, 2006) were used. The SLR data are provided by the International Laser Ranging Service (ILRS) (Pearlman et al., 2002). The triangles in Figure 1 indicate the geographical location of the 11 SLR sites that were included in our analysis. Note that we did not use SLR measurements of San Juan (located in South America), as no official terrestrial reference frame coordinates have been available at the time of analysis.

The temporal distribution of the SLR tracking data is shown in Figure 2. Each line represents 24 hours of a particular day. SLR observation epochs are indicated with a bar. The varying data coverage is clearly visible. Thus, the quality of the orbits derived from these data will vary, depending on the available SLR data.

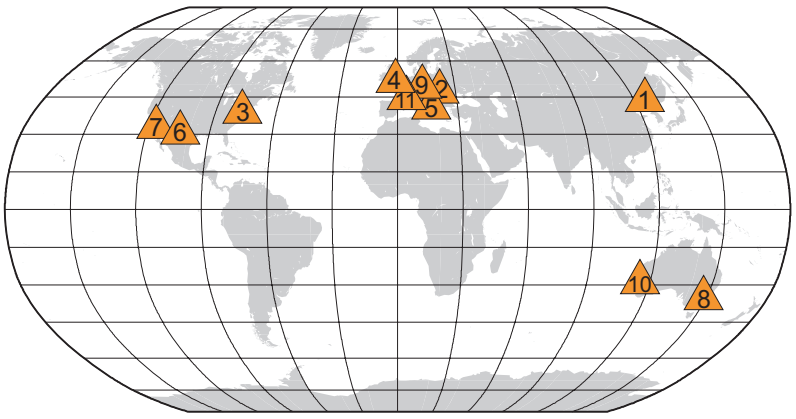

Figure 1. *Geographical location of the 11 SLR sites used for orbit determination*

In each orbit determination process six osculating elements and nine dynamical orbit parameters were estimated. The dynamical parameters represent solar radiation pressure (SRP) parameters defined in the SRP frame (D,Y,X). The SRP frame origin corresponds to the satellite's center of mass. The D-axis points towards the Sun, the Y-axis points along the solar panel axis, and the X-axis completes the right-handed system. The nine estimated SRP parameters are three constant acceleration (in D,Y, and, X direction) as well as six once per orbit revolution sinusoidal accelerations (sine and cosine in D, Y, and X direction).

Different orbits solutions were prepared using arc-lengths of n-days (n = 5, 7, 9, 11, 14) in order to estimate the arc-length that leads to the best possible orbit quality. The Bernese GPS Software Version 5.0 (Hugentobler et al., 2005) was used for the parameter estimation.

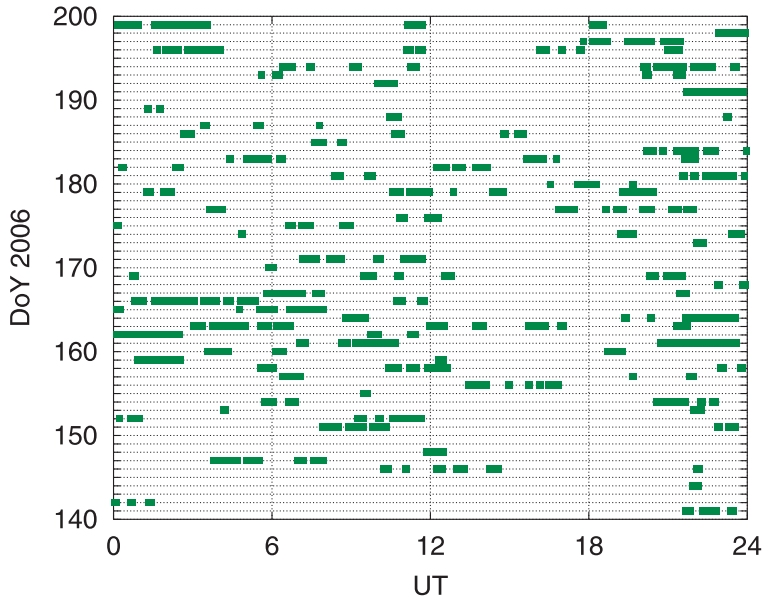

Figure 2. *SLR data coverage of the GIOVE-A SLR tracking campaign*

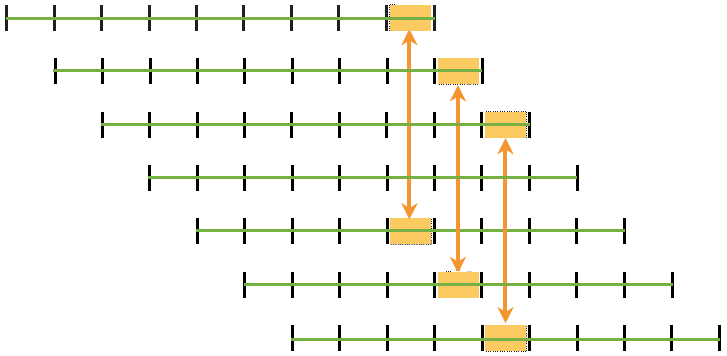

Figure 3. *Sketch illustrating the generation of orbit overlaps for 9-day arcs; orbit overlap is the orbit difference between last and central day*

For each solution we generated between 32 and 50 n-day arcs within the 60 days interval of the SLR tracking campaign of GIOVE-A. Consecutive n-day arcs are shifted by one day each. Thus, overlapping orbits can be generated. The resulting orbit differences (referred to as orbit overlaps in the following) indicate the orbit quality. Small overlaps indicate a good quality, whereas large overlaps indicate a bad quality of the determined orbit. We assume that the central part of an arc is best defined and that the boundary parts of an arc are worst defined. The overlap analysis concept is to compare the last day of an arc with the corresponding central day of another arc of the same arc-length, as illustrated in Figure 3. In the sketch each line represents a 9-day arc, day boundaries are indicated. The arrows show the orbital parts that are compared with each other.

Figure 4 shows the orbit overlaps of the GIOVE-A 9-day arcs. This arc length of 9 days has proved to be the best one, as the overlaps of the other orbit solutions with arc lengths of 5, 7, 11, or 14 days are larger. The orbit overlaps vary significantly, as the orbit quality is highly correlated with the number and temporal distribution of the SLR observations. Arcs with less or badly distributed observations are determined worse. Satellite maneuvers might also cause problems, if they are not considered in the orbit model. The radial orbit overlaps (top chart in Figure 4) show values of up to 10 cm. The radial component is best defined, as the SLR ranges represent observations mainly in radial direction. Orbit overlaps in along-track and out-of-plane components vary up to

1 m and 2 m, respectively. For arcs with a good temporal distribution of SLR data the orbit overlaps are smaller with values up to 0.5 m in along-track and 1 m in out-of-plane component. The formal errors of the satellite positions in the orbit system (radial, along-track, out-of-plane) show corresponding magnitudes similar to the overlap values.

Figure 5 displays the range residuals derived from the 9-day arc solution. The standard deviation of the residuals is about 2 cm, which is within the range of the accuracy of the SLR observations. SLR observations are assumed to be accurate at the 1-2 cm level.

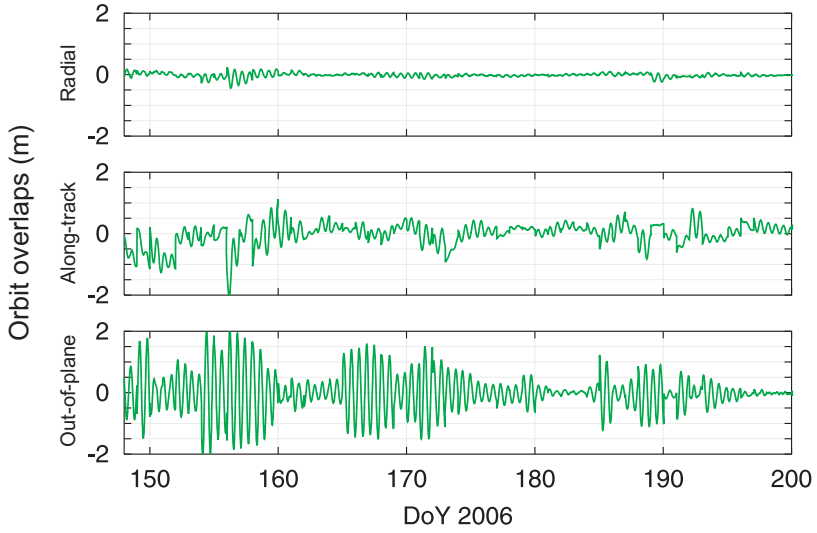

Figure 4. *Orbit overlaps of SLR-based 9-day arcs of GIOVE-A; orbit overlaps are the orbit differences between the central days and the last days of the corresponding 9-day arcs*

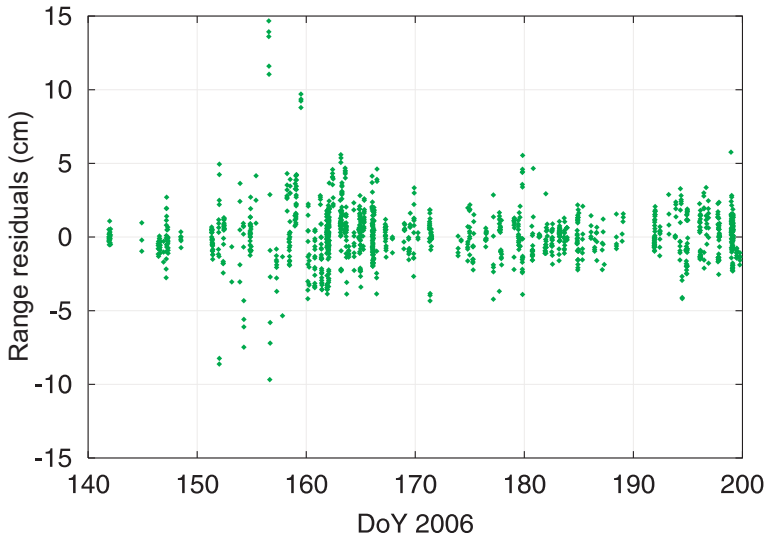

Figure 5. *Range residuals derived from SLR-based 9-day arcs of GIOVE-A*

In addition to the SLR-based 9-day arcs, we computed consecutive 5-day orbit predictions. For the overlap computation, each predicted day is compared with the corresponding central day of the orbit part covered by SLR observations, as illustrated in Figure 6. Thus, for each 9-day arc overlaps of the five prediction days are generated.

Figure 7 shows the orbit overlaps for all prediction days of all orbital arcs. The predictions are getting worse in time due to the accumulated orbit errors. The computed prediction overlaps are dominated by the along-track error of the orbital arc, as this

error increases exponential in time. The overlaps indicate a potential orbit accuracy of about 20-30 m after 5 days of prediction.

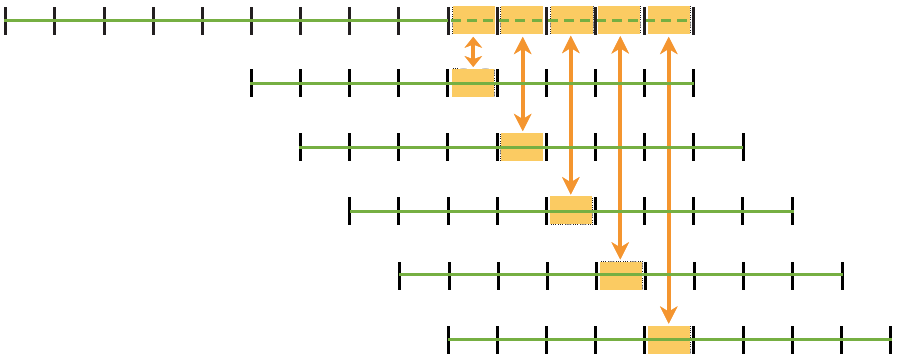

Figure 6. *Sketch illustrating the generation of orbit overlaps for 9-day arcs with 5 day predictions; orbit overlap is the orbit difference between each prediction day and the corresponding central day of the orbit part covered by SLR observations*

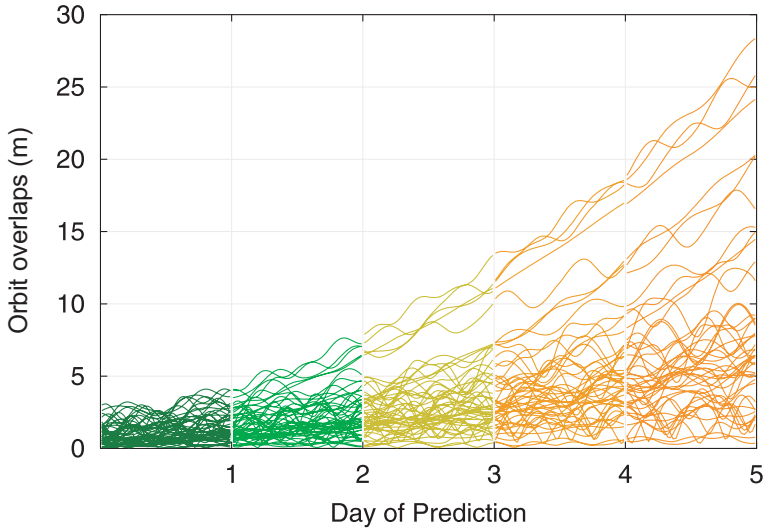

Figure 7. *Orbit overlaps of 5-day predictions based on GIOVE-A 9-day arcs; orbit overlaps are the orbit differences between the prediction days and the central days of the corresponding 9-day arcs*

3. Combined analysis of SLR and microwave observation for GIOVE-A orbit determination

This Section demonstrates the possible contribution of SLR to GIOVE-A orbit determination through a combined analysis of microwave and SLR data. As no microwave tracking data of GIOVE-A were available at the time of our analyses, we performed an a priori variance-covariance analysis. For such an analysis the observations are not needed, rather the number and temporal distribution and the assumed a priori error of the observations. Note that model deficiencies are not considered here.

Microwave phase observations were simulated for 13 GIOVE-A tracking sites, which are chosen similar to the proposed sites of the first Galileo tracking network. Their global distribution is indicated with circles in Figure 8. In addition we used the SLR true observations of the SLR sites represented with triangles.

The microwave phase observations are sampled with 30 s and have an accuracy of 1 mm. Observation equations were set up for microwave phase zero difference observations and SLR normal points. Satellite clocks, ambiguities, and orbit parameters were included in the parameter estimation. Other parameters, as station coordinates,

receiver clocks, tropospheric zenith path delays, and Earth orientation parameters are assumed to be known accurately, as for example from a global analysis of GPS and GLONASS data.

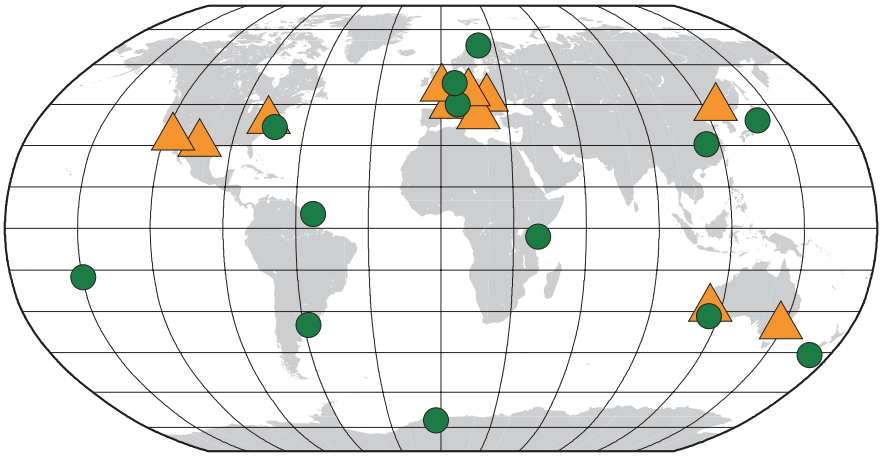

Figure 8. *GIOVE-A tracking sites (circles) and SLR tracking sites (triangles)*

The *a priori* variance-covariance matrix is derived from the obtained normal equation system. The *a priori* formal errors of the orbit parameters are then computed from the variance-covariance matrix. We used the same orbit parameters as in Section 2, i.e. six osculating elements and nine solar radiation pressure parameters in D,Y,X- direction. In summary 57 orbital arcs of 3 days length were determined, shifted by one day each.

To assess the impact of additional SLR observation on GIOVE-A orbit determination, we performed three different analysis with different SLR observation weight scenarios. The first solution corresponds to a pure microwave solution. The SLR observation weight is set to zero by setting the a priori sigma σ_{SLR} to infinity. In the second case, σ_{SLR} is set to 1cm. In the third case, the SLR observation weight is increased (with σ_{SLR} = 1 mm), and corresponds to the microwave observation weight.

We calculate the a priori formal errors of the satellite position in the inertial system from the *a priori* formal orbit errors by applying the law of error propagation. Figure 9 shows the *a priori* formal errors of the satellite position in radial, along-track, and out-of plane component for the three different solutions of a GIOVE-A 3-day arc. The absolute error values must be considered to be much too optimistic, as the error scales with the number of observations. We used 30 s sampled microwave data, but did neglect any temporal correlations between consecutive observations. A sampling rate of 180 s should rather be used for further studies.

The introduced parameters (e.g., station coordinates, troposphere parameters), which are assumed to be known from the GPS/GLONASS analysis, are not error free. Neglecting the formal errors of the introduced parameters, and of temporal correlations between observations causes too optimistic formal errors. However, in this analysis we are not interested in the absolute values of the formal orbit errors, but rather in the relative difference of the formal orbit errors between the three solutions. We may from this assess the impact of additional SLR observations on GIOVE-A (or Galileo) orbit determination in terms of orbit improvement.

The major impact of additional SLR data on the resulting orbit accuracy is given in the radial orbit component. A possible improvement of the radial orbit accuracy of about 60-80% may be feasible, depending on the SLR weight and the number and distribution of SLR observations. The formal orbit error in along-track and out-of-plane components

decreases with strong SLR weights, only. A good temporal distribution of the SLR observations over the entire arc is always necessary. Otherwise, if e.g. SLR observations are only available at the beginning of an orbital arc, the orbital errors as well as the orbit positions will show periodic variations.

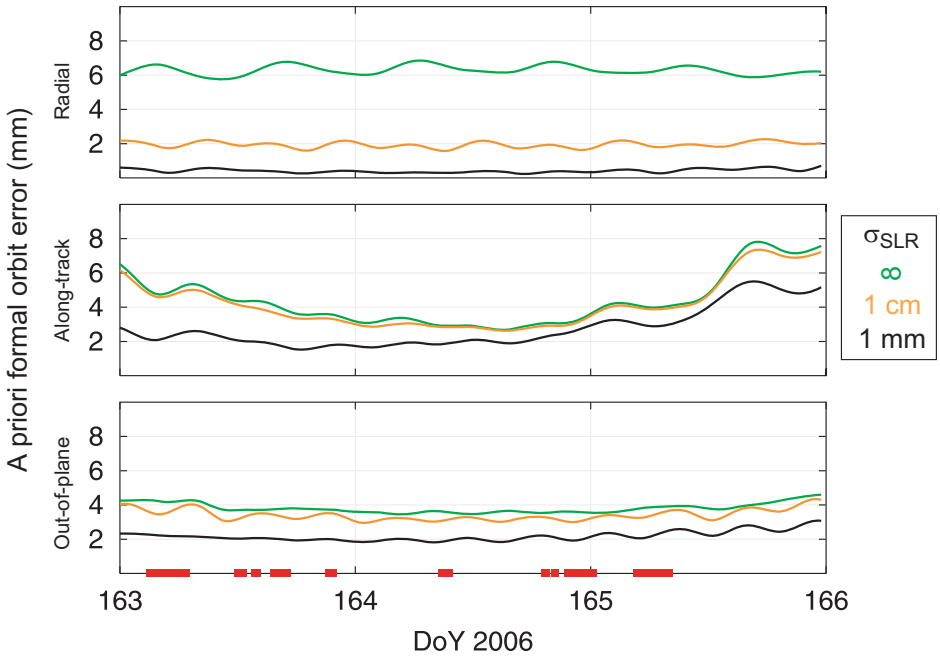

Figure 9. *A priori formal orbit errors in the inertial system; the three lines indicate the different orbit solutions using different a priori sigmas σ_{SLR} for the SLR observations; the bars on the horizontal axis indicate the SLR observation epochs*

4. Summary

We presented GIOVE-A orbit determination results based on SLR observations of the first GIOVE-A SLR tracking campaign. Orbits of several arc-length were determined and compared with each other. Nine-day arcs proofed to provide the best possible orbits with the used orbit model. No a priori solar radiation pressure model was introduced in the orbit determination, but constant accelerations and once-per orbit revolution accelerations were estimated. The orbit accuracy of a 9-day arc is about 10 cm, 0.5 m, and 1 m in radial, along-track, and out-of-plane component, unless the observation coverage of the orbit is poor. If SLR observations are very sparse and not well distributed over the entire arc, the orbit quality decreases. Orbit predictions are at the 20-30 m accuracy level after five days.

The impact of SLR observations used in addition to microwave observations for precise orbit determination of GIOVE-A was demonstrated. An a priori variance-covariance analysis shows a significant orbit improvement mainly in radial direction of about 60%, if additional and well distributed SLR observations are used. This can be addressed to the very low number of microwave tracking sites for the upcoming Galileo system in the very beginning of the system implementation.

References

[1] Pearlman, M.R., J.J. Degnan, J.M. Bosworth: “The International Laser Ranging Service”, Adv. Space Res., 30(2), pp. 135-143, 2002.

[2] Hugentobler, U., P. Fridez, S. Schaer: “Bernese GPS Software Version 5.0”, Druckerei der Universität Bern, Switzerland, 2005.

Satellite Laser Ranging in the National (Australian) Collaborative Research Infrastructure Proposal for Geospatial R&D

Kurt Lambeck[1]

1. The Australian National University, Canberra, Australia

The presentation is at:

http://www.ilrscanberraworkshop2006.com.au/workshop/day2/Monday1400.pdf

Time-variable gravity from SLR and DORIS tracking

Frank G. Lemoine[1], Steven M. Klosko[2], Christopher M. Cox [3], Thomas J. Johnson[4]

1. Planetary Geodynamics Laboratory, NASA Goddard Space Flight Center, Greenbelt, Maryland, USA
2. SGT, Inc., Greenbelt, Maryland, USA
3. Raytheon Integrated Defense Systems, Arlington, Virginia, USA
4. National Geospatial-Intelligence Agency, Reston, Virginia, U.S.A.

Abstract

One of the significant strengths of the tracking of satellites with satellite laser ranging (SLR) is the long time base of data available. This has been exploited to provide us with monthly snapshots of the variations of the low-degree field from approximately 1980 to the present. The analysis of these data by Cox and Chao [2002] revealed an anomaly in the zonal rate for J_2. Cox and Chao [2002] clearly indicated that the contributions to this zonal rate from the cryosphere and surface hydrology, such as glacier melt and ground water storage, are just as important as post-glacial rebound. In this paper, we extend the time series of low degree variations through 2006, describing the satellite data incorporated into the solutions, the method of analysis, and the satellite performance. We compare the SLR/DORIS recovered low-degree variations with those derived from GRACE from 2003 to 2005, through degree four, and investigate the climatological and geophysical connections revealed by the new time series.

Introduction

Although GRACE provides us with a valuable source of high-resolution data for assessment of surface mass transport, the analysis of SLR and DORIS tracking data to low Earth orbiting satellites still provides valuable information. Intercomparison of the GRACE and independent SLR & DORIS results can provide a validation of the GRACE results where the data overlap after launch of GRACE, and an improvement in the quality of the time series through improvements in the dynamic modeling, for example through usage of the GRACE-derived geopotential. In this manner, the joint analysis of GRACE and the SLR and DORIS tracking data can help to leverage these data into the pre-GRACE era. In this manner we can obtain a snapshot of surface mass transport on the Earth over the past 25 years.

Data and Processing

The gravity solutions are based on data to nine satellites: Lageos 1 & 2, Starlette, Stella, Ajisai, Westpac, GFZ-1, TOPEX/Poseidon, and BE-C. The temporal coverage of the tracking data is depicted in Figure 1. For most of the 1980's, only three satellites are available. From the 1990's onward, between six and nine satellites are used, including the SLR & DORIS tracking data to TOPEX/Poseidon.

The modeling applied the ITRF2000 reference frame [*Altamimi et al.*, 2002] with corrections for certain stations, derived principally by the TOPEX/POD team (N. Zelensky, NASA GSFC, personal communications). The GGM01C GRACE-derived gravity model was used [*Tapley et al.*, 2004]. The IERS2003 solid Earth tides were applied including anelasticity [*McCarthy and Petit*, 2004]. The GOT00.2 T/P-derived ocean tide model was applied [*Ray*, 1999]. The atmospheric gravity was forward modeled using atmospheric pressure data from NCEP to 20x20, with an inverse

barometer correction assumed over the oceans. The observed annual gravity terms to 4x4 were forward modeled a priori, based on a previous SLR time series solution. After 1992, the daily arcs are 10 days in length, and constructed to be commensurate with the start and stop times of the near-ten day ground track cycle of TOPEX/Poseidon. Prior to 1992, the arc length was 30 days for Lageos-1, and 15-days for Starlette and Ajisai. For all the arcs, global station biases are adjusted for the SLR data. The gravity solutions consisted of a 30x30 static field, a 6x6 field for the secular rates of the geopotential, annual and semi-annual terms to 4x4, and a 4x4 monthly time series.

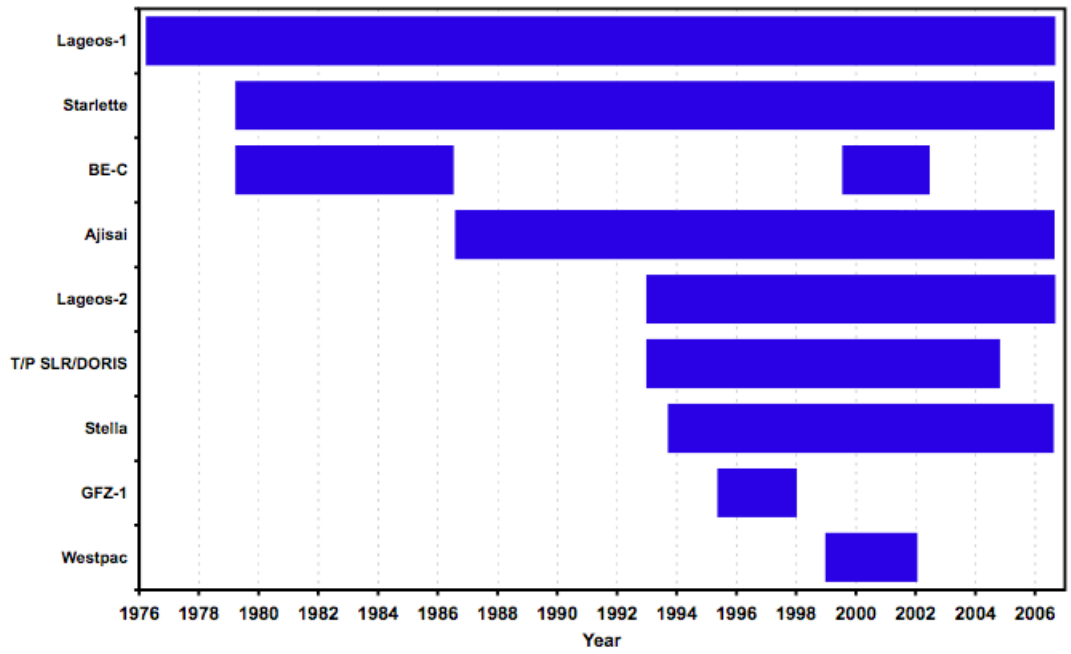

Figure 1. *Temporal coverage of SLR and DORIS tracking data used in the monthly gravity solutions, the solutions for the annual and semi-annual harmonics and the solutions for the secular rates.*

Analysis of the J_2 signal

The full time series is depicted in Figure 2, with respect to the GGM01C. The 1998 J_2 (- C_{20}) anomaly discussed in *Cox and Chao* [2002], appears as an inter-annual variation. The slope in J_2 obtained from 1980 to 1997 of 1.34 x 10^{-11}/year is similar to the post 1997 slope of 1.36 x 10^{-11}/year. It now appears, especially after the application of an annual filter, that a similar interannual variation was observed in 1987-1988. The J_2 time series is visibly much noisier before 1983. The addition of Starlette to the solution, especially after 1983, acts to stabilize the solutions for J_2 and the other low degree harmonics. An additional consideration is that the strength of the network and the quality of the data for 1983 and later is far superior to the pre-1983 SLR data. For reference, we note that a ± 1 x 10^{-10} in J_2 corresponds to a ± 2 mm change for the geoid in a zonal sense from pole to equator.

In Figure 3 we compare the C_{20} time series for GRACE, and from the SLR & DORIS solutions from 2002 to 2006. We show the comparisons for the CSR Release 01 fields (constrained and unconstrained), the NASA GSFC GRACE solutions based solely on GRACE K Band Range-Rate data (KBRR) from *Luthcke et al.* [2006[, and the corresponding SLR & DORIS solution. The unconstrained CSR release 01 (RL01)

C_{20} data have the worst agreement, especially around the period in late 2004 when GRACE entered a deep resonance driven by a close ground track repeat. The solutions lightly constrained by a Kaula constraint are smoother in their performance. The C_{20} from the NASA GSFC spherical harmonic time series is smoother, but still does not have good agreement with the SLR & DORIS solution. We conclude that the GRACE spacecraft are not a good sensor of this very long wavelength harmonic.

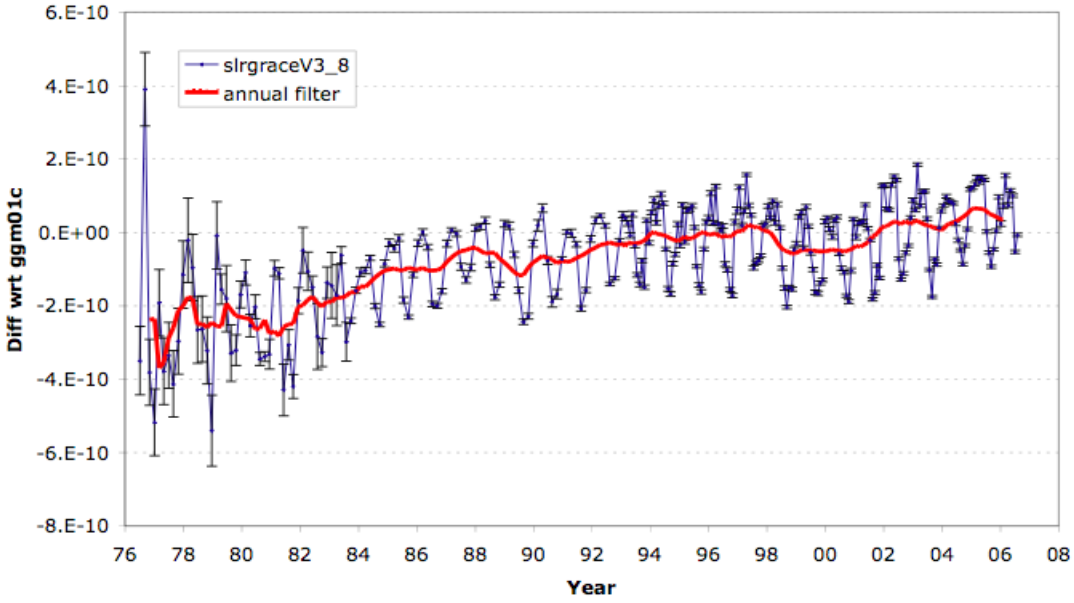

Figure 2. *Monthly J2 solutions from SLR and DORIS tracking from 1976 through 2006. The solutions are shown w.r.t. the GGM01C solution, and with the application of an annual filter (red line).*

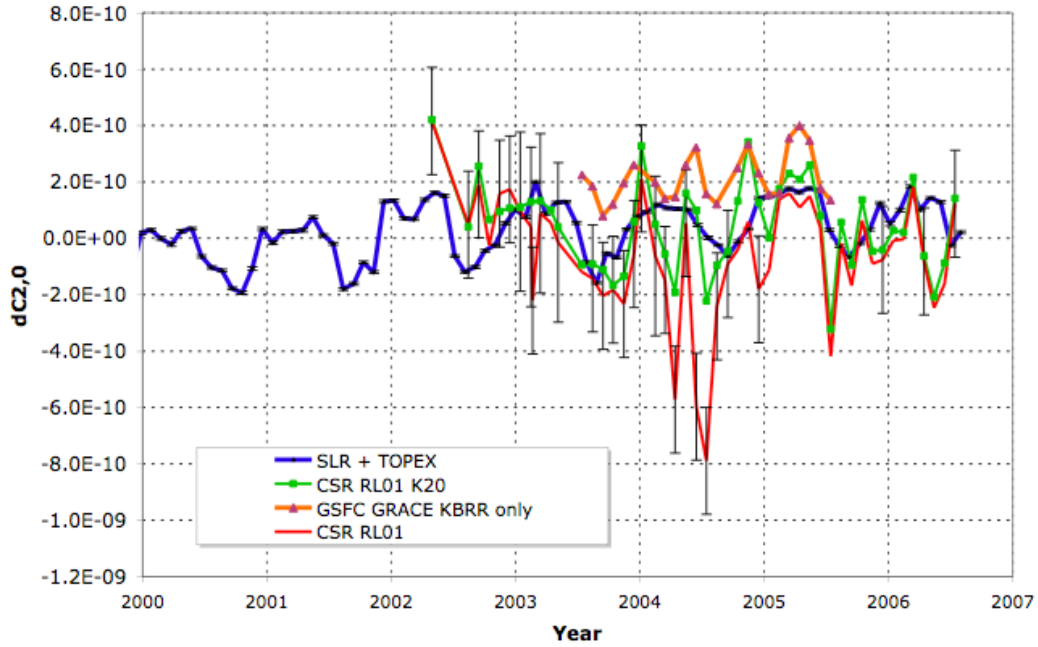

Figure 3. *Comparison of solutions for C_{20} from the SLR and DORIS solutions, and from GRACE.*

Comparison of Other Low Degree Harmonics

The SLR and DORIS monthly time series is compared to the GRACE solutions in Figure 4 for the other low degree harmonics (C_{21}, S_{21}, C_{22}, S_{22}, C_{30} and C_{40}). For C_{21} and S_{22}, the agreement is exceptionally good; For S_{21} and C_{22} there is some agreement on the amplitude of the variation, but the phases really do not match. For C_{30} we obtain the interesting result that the time series for the two GRACE solutions (CSR RL01, and NASA GSFC, KBRR-only) agree perfectly. The SLR and DORIS time series matches more closely the GRACE C_{30} + C_{50} solutions, suggesting that for the C_{30} harmonic, what the SLR and DORIS time series discerns is really a lumped harmonic. In contrast for the C_{40} harmonic, the GRACE solutions completely fail to discern the variations that are visible in the SLR and DORIS time series. We conclude that for C_{40}, just as for C_{20}, the GRACE spacecraft are simply not good sensors of this harmonic.

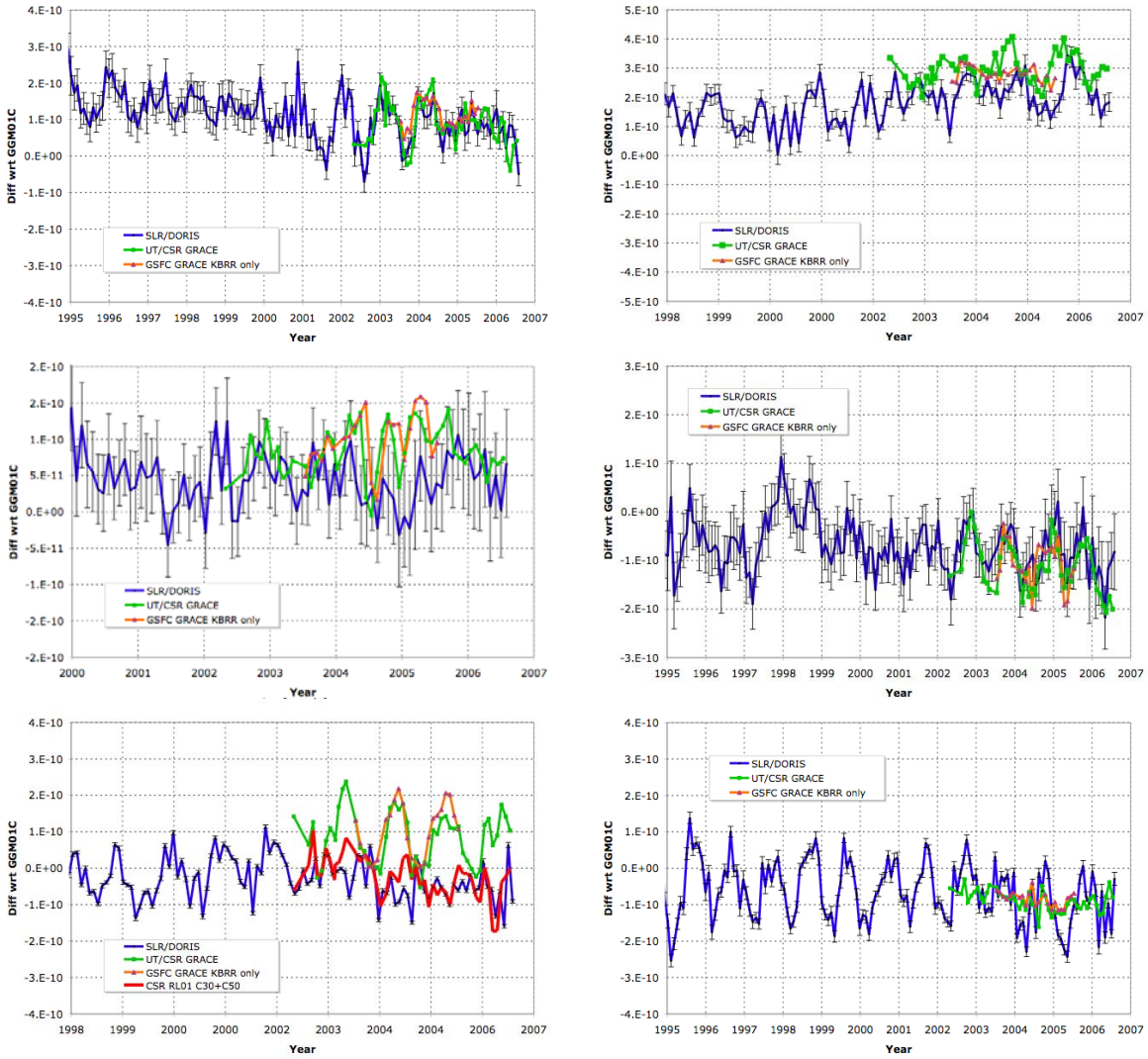

Figure 4. *Comparison time series for the low-degree harmonics between GRACE and the SLR and DORIS solutions (C_{21}, S_{21}; C_{22}, S_{22}; C_{30}, C_{40}). We show the formal errors for the SLR/DORIS solutions. The agreement is exceptionally good for the C21 and S22 harmonics. For the two GRACE solutions tested, the variations in the C40 harmonic cannot be properly resolved.*

Recovery of Annual and Semiannual Harmonics

We are able to use the entire time series of SLR and DORIS data to recover the annual variations in the geopotential through degree six, and the semiannual variations through degree four. In Figure 5, the signal of the annual harmonics recovered from the CSR RL01 GRACE series, is compared to the signal recovered from the SLR & DORIS time series, and the formal uncertainties of the SLR and DORIS recovery. Thus, from this comparison of the degree variances, the SLR and DORIS data can recover signals between degrees five and six.

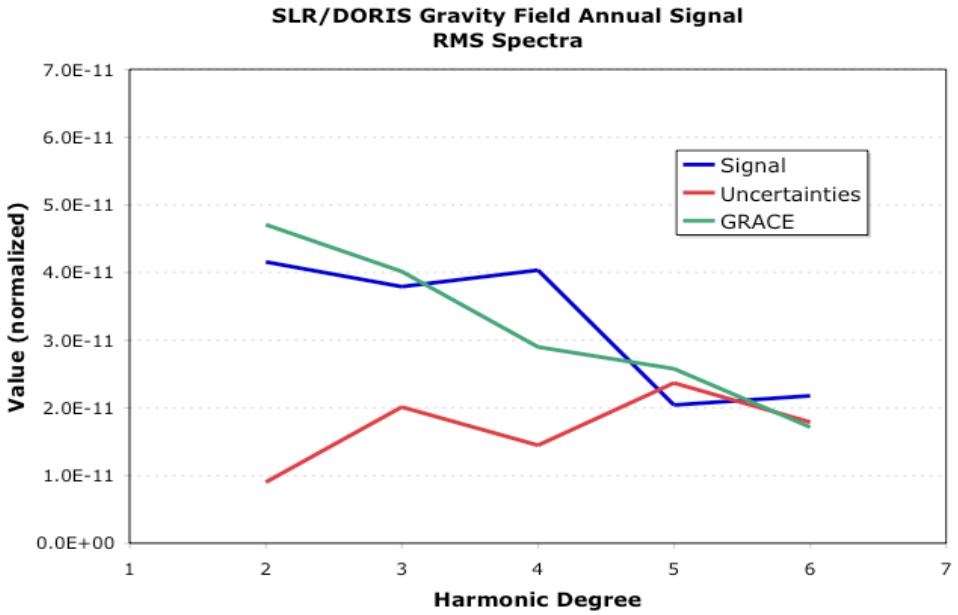

Figure 5. *Degree variances of the annual harmonics recovered from the SLR and DORIS data, and from the GRACE monthly solutions, compared to the formal uncertainties in the SLR/DORIS solutions. The SLR & DORIS time series can resolve the annual variations in the geopotential through degree five over a period of 25 years.*

The SLR/DORIS time series is sufficiently long that we can reliably recover annual and semiannual harmonics over different time scales. For example, if we compare the time-variable gravity variations for two SLR/DORIS solutions (1979-1997, and 1998-2005), we can observe for the most part overall similarities between the solutions. Both show the same patterns of geoid highs and geoid lows in the Amazon region, and Southeast Asia associated with the expected hydrology variations. If we compare the 1998-2005 SLR/DORIS solution to the annual and semiannual harmonics recovered from GRACE (in this case the CSR RL01), both observe the geoid highs in the Amazon in April and May, and the geoid lows in south east Asia and the Bay of Bengal. In addition, both data sets observe the same phase of the Southeast Asia monsoon with a prominent high in August and September over the Bay of Bengal, Bangladesh and the Indian subcontinent. The geoid low observed over the Amazon in November with the GRACE results is more prominent than with the SLR/DORIS observed variations.

Recovery of Secular Geoid Rates

The long time series of SLR and DORIS data allows to solve for secular rates in the geopotential, not just with the zonal harmonics, but for all coefficients through degree

six. The recovered geoid rates are illustrated in Figure 6 for the period from 1979 through 1997. In this figure, the general pattern of post-glacial rebound is observed over Antarctica, Greenland and the Arctic consistent with post-glacial rebound models. Globally the scale of the variations is ± 1 mm/year, with an error of 0.14 mm/year. Secular geoid changes occur in other regions, for example over the Indian subcontinent (+0.5 mm/yr). While we may ascribe the secular changes in the polar regions for the most part to changes in the solid Earth (cf. post-glacial rebound), in other regions, other considerations (long-term hydrology or ocean mass variations) may also play a role. If secular solutions are obtained on shorter time scales (five years) the solutions differ considerably, indicating that on those time scales, annual and inter-annual variations in the geopotential are more prominent than the secular variations.

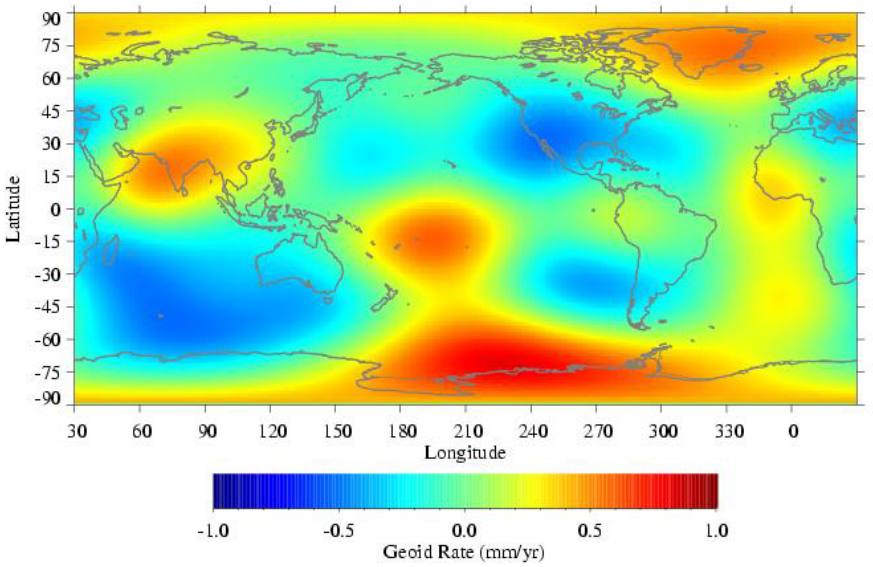

Figure 6*. Geoid rates observed from 1979 through 1997 from SLR and DORIS data. The global error is 0.14 mm/yr.*

Summary

The long time series of SLR and DORIS data allow us to resolve periodic time variations on the time scale of months, and secular variations over the period of many years. These data allow us a window into geophysical mass flux variability over a period prior to the launch of GRACE. We discern that that 1998 C_{20} anomaly was in fact an interannual variation, and that similar variations are observable over the course of the 25-year time series. The GRACE solutions for the low degree even zonals do not agree with those obtained from SLR and DORIS data, although in an overall sense the annual variations observed are similar. The SLR and DORIS data have sufficient strength to resolve secular changes in the geopotential through degree 6 corresponding to a spatial scale of 3300 km.

Acknowledgements

The authors acknowledge the ILRS [*Pearlman et al.*, 2002] and the IDS [*Tavernier et al., 2006*] for making the SLR and DORIS data available for this study as well as for overseeing the networks and the stations responsible for providing the data. Jennifer

Wiser Beal1 (Raytheon Corp, Upper Marlboro, MD) performed most of the GEODYN processing for the SLR and DORIS solutions.

References

[1] Altamimi Z., P. Sillard, and C. Boucher, ITRF2000: A new release of the International Terrestrial Reference Frame for earth science applications, *J. Geophys. Res., 107(B10),* 2214, doi:10.1029/2001JB000561.

[2] Cox, C.M., and B.F. Chao, Detection of a large-scale mass redistribution in the terrestrial system since 1998, *Science, 297,* 831, Aug. 2., 2002.

[3] Luthcke, S.B., D.D. Rowlands, F. G. Lemoine, S.M. Klosko, D. Chinn, and J.J. McCarthy, Monthly spherical harmonic gravity field solutions determined from GRACE inter-satellite range-rate data alone, *Geophys. Res.Lett.,33,* L02402,

[4] doi:10.1029/2005GL024846.

[5] McCarthy, D.D., and G. Petit (Eds.), IERS Conventions, IERS Tech. Note, vol. 32, Verl. Des Bundesamts für Kartogr. Und Geod., Frankfurt am Main, Germany, 2003.

[6] Pearlman, M.R., J. Degnan, and J.M. Bosworth (2002), The International Laser Ranging Service (ILRS), *Adv. Space Research, 30,* 135-143, 2002.

[7] Ray, R.D., A global ocean tide model from TOPEX/Poseidon altimetry: GOT99.2, *NASA Technical Memo. 209478,* NASA Goddard Space Flight Center, 58 pp., 1999.

[8] Tapley, B.D., S. Bettadpur, M. Watkins, and C. Reigber, The gravity recovery and climate experiment: Mission overview and early results, *Geophys. Res. Lett., 31, L09607,* doi:10.1029/2004GL019920, 2004.

[9] Tavernier, G. et al., The International DORIS Service: Genesis and early achievements, *J. Geodesy, 80,* 403-417, doi:10.1007/S00190-006-0082-4, 2006.

Global Glacial Isostatic Adjustment: Target Fields for Space Geodesy

W.R. Peltier[1]

1. Department of Physics, University of Toronto, Toronto, Ontario, Canada M5S-1A7.

Contact: peltier@atmosp.physics.utoronto.ca

Abstract

A very detailed theory of the global process of glacial isostatic adjustment (GIA) is now available that is being employed to address a number of significant problems in both solid Earth geophysics and climate dynamics. A recent focus of the work in this area has been upon the impact of changes in the Earth's rotational state upon postglacial sea level history and the modern field of geoid height time dependence that is being measured by the GRACE dual satellite system that is now in space. Satellite laser ranging continues to play a critical role in the understanding of these processes. This paper summarizes recent progress in modelling the impact of the GIA process upon Earth's rotational state.

Introduction

The origins of highly significant anomalies in the Earth's rotational state, respectively the so-called non-tidal acceleration of the rate of axial rotation and the secular drift (true polar wander) of the pole of rotation relative to the surface geography, have been associated for some time with the influence of the glacial isostatic adjustment (GIA) process. The non-tidal acceleration is equivalent to a value for the time dependence of the degree 2 zonal coefficient in the spherical harmonic expansion of Earth's gravitational field, commonly represented as $\dot{J}_2$ of (-2.67 ± 0.15) x 10^{-11} $year^{-1}$ (e.g. Cheng et al. 1989). The value for the rate of polar wander reported by Vincente and Yumi (1969, 1970) using the data of the International Latitude Service (ILS) was (0.95 ± 0.15) degree/million years, a value that is close to the most recent estimation by Argus and Gross (2004) of 1.06 degree/million years. The latter authors have suggested that the observed direction and speed of polar wander should be corrected for the influence of plate tectonic motions and that this could be a significant effect, depending upon the assumptions on the basis of which the correction is made (see Table 1 of Argus and Gross, 2004).

The development of theoretical explanations for the above discussed anomalies in Earth rotation has been dominated by work over the past two decades that has suggested a close connection of them both to GIA. The earliest discussion of the impact upon polar wander that should be expected due to time dependent surface loading of a visco-elastic model of the Earth was that of Munk and MacDonald (1960) who employed a simple homogeneous model to suggest that wander of the pole could only occur in response to simultaneous variability in the surface mass load. This point was obscured in the later papers by Nakiboglu and Lambeck (1980, 1981) and Sabadini and Peltier (1981) whose analysis was based upon the application of a homogeneous viscoelastic model similar to that employed by Munk and MacDonald (1960). These authors, however, suggested that polar wander would continue on a homogeneous visco-elastic model of the Earth even after all temporal variations of the surface mass load had ceased. This significant error of interpretation was corrected in Peltier (1982) and Wu and Peltier (1984) who showed that, in the case of cyclic loading and unloading, as is appropriate for the computation of the GIA

effect following the series of glacial loading and unloading events that have characterized the Late Quaternary period of Earth history (e.g. Broecker and van Donk, 1970), there would be no polar wander effected once the cycle ended. The homogeneous visco-elastic model of the planet would therefore exhibit no memory of the past history of loading and unloading as correctly pointed out by Munk and McDonald. This was traced to the fact that, specifically for the homogeneous visco-elastic model, there exists an exact annihilation of the polar wander forced by the internal redistribution of mass due to the free relaxation of Earth's shape and that forced by the deformation due to the changing rotation itself (see e.g. Figure 2 of Wu and Peltier 1984).

Based upon the prior analysis of Peltier (1974, 1976), however, it was known that realistic viscoelastic models of the planetary interior were significantly more complex then could be accommodated by the homogeneous visco-elastic model of Munk and MacDonald (1960). Whereas the relaxation under surface forcing of a homogeneous visco-elastic model of the Earth is described by a single relaxation time that is unique for each spherical harmonic degree in the deformation spectrum, realistically layered spherical visco-elastic models have a much more complex relaxation spectrum, a unique spectrum consisting of an (often essentially) finite number of modes for each spherical harmonic degree. In Peltier (1982) and Wu and Peltier (1984) it was demonstrated that this realistic level of complexity endowed the Earth model with a memory of its history of surface loading and unloading such that the pole of rotation would continue to wander even after the surface load had ceased to vary. Deep sea core oxygen isotopic data based upon $\delta^{18}0$ measurements on benthic foraminifera were employed as basis for the construction of a model of cyclic ice-sheet loading and unloading of the continents following the interpretation of such data as proxy for the variation of continental ice volume through time (Shackleton 1967, Shackleton and Opdyke 1973). Analysis based upon the application of rather crude models of the growth and decay of the Laurentide, Fennoscandian and Antarctic ice sheets then demonstrated that both the speed and direction of true polar wander as well as the non-tidal acceleration of rotation could be fit by the model and that the radial visco-elastic structure required to fit both of these observations was essentially the same. This was construed to strongly suggest that both anomalies might to be entirely explained as a consequence of the ongoing global process of glacial isostatic adjustment.

A recent objection to this interpretation was raised in the paper by Mitrovica, Wahr et al. (2005; hereafter MW) who have suggested that the theoretical formulation employed in Peltier (1982) and Wu and Peltier (1984) was mathematically "unstable" insofar as the computation of the polar wander component of the response to the GIA process is concerned. This objection appears to be based upon an error of mathematical comprehension as explicit analyses to be presented in what follows will demonstrate.

Computation of the rotational response of the Earth to the GIA process

The time dependent impact on the Earth's rotational state of the glacial isostatic adjustment process is determined as a solution of the classical Euler equation describing the conservation of angular momentum of a system subjected to no external torques, as:

$$\frac{d}{dt}(J_{ij}\,\omega_i) + \in_{ijk}\,\omega_j\,J_{k\ell}\,\omega_\ell = 0 \tag{1}$$

in which the J_{ij} are the elements of the moment of inertia tensor, the ω_i are as previously and $\in_{ijk}$ is the Levi-Civita (alternating) tensor. Restricting attention to small departures from the modern state of steady rotation with angular velocity Ω_o, we may construct a solution to (1), accurate to first order in perturbation theory, by expanding:

$$\omega_i = \Omega_o\,(\delta_{i3} + m_i)\,;\, m_i = \omega_i / \Omega_o \tag{2a}$$

$$J_{11} = A + I_{11} \tag{2b}$$

$$J_{22} = B + I_{22} \tag{2c}$$

$$J_{33} = C + I_{33} \tag{2d}$$

$$J_{ij} = I_{ij},\, i \neq j \tag{2e}$$

Substitution of these expansions into equation (1), keeping only terms of first order, leads to the standard set of governing equations for polar wander and the length of day, respectively (see Munk and McDonald, 1960), as:

$$\left.\begin{aligned} \frac{dm_1}{dt} + \frac{(C-B)}{A}\Omega_o\,m_2 &= \Psi_1 \\ \frac{dm_2}{dt} + \frac{(C-A)}{B}\Omega_o\,m_1 &= \Psi_2 \end{aligned}\right\} \text{ polar wander} \tag{3a,b}$$

$$\left.\frac{dm_3}{dt} = \Psi_3\right\} \text{ length of day} \tag{3c}$$

in which the "excitation functions" are defined as:

$$\Psi_1 = \left(\frac{\Omega_o}{A}\right) I_{23} - \frac{(dI_{13}/dt)}{A} \tag{4a}$$

$$\Psi_2 = -\left(\frac{\Omega_o}{B}\right) I_{13} - \frac{(dI_{23}/dt)}{B} \tag{4b}$$

$$\Psi_3 = -\left(\frac{I_{33}}{C}\right) \tag{4c}$$

Now it is critical to recognize that there exist perturbations Iij to the inertia tensor due to two distinct causes, namely due to the direct influence of change in the mass distribution of the planet that accompanies the change in planetary shape due to surface loading and unloading and that due to the additional deformation induced by the changing rotation triggered by the surface mass loading and unloading process. The contribution due to the former process may be represented as (e.g. Peltier, 1982):

$$I_{ij}^{GIA} = \left(1 + k_2^L(t)\right) * I_{ij}^R(t) \tag{5}$$

in which $k_2^L(t)$ is the surface mass load Love number of degree 2 and the I_{ij}^R are the perturbations of inertia that would obtain due to the variation in surface mass load if the Earth were rigid. The symbol * in equation (5) represents the convolution operation. The contribution to the perturbations of inertia due to the changing rotation

follows from an application of a linearized version of MacCullagh's formula (e.g. see Munk and MacDonald, 1960) as:

$$I_{13}^{ROT} = \left(\frac{k_2^T * a^5 \, \omega_1 \omega_3}{3G} \right) = \left(\frac{k_2^T}{k_f} \right) * m_1 \, (C - A) \tag{6a}$$

$$I_{23}^{ROT} = \left(\frac{k_2^T * a^5 \, \omega_2 \omega_3}{3G} \right) = \left(\frac{k_2^T}{k_f} \right) * m_2 \, (C - A) \tag{6b}$$

with

$$k_f = \left(\frac{3G}{a^5 \, \Omega_o^2} \right) (C - A) \tag{6c}$$

the value of which is determined entirely by the observed flattening of the Earth's figure. Assuming the validity of the data in Yoder (1995) as listed on the web site: (www.agu.org/references/geophys/4_Yoder.pdf), one obtains the value $k_f \cong 0.9414$, a value that deviates somewhat from the value of 0.9382 employed in MW.

The General Solution for the Rotational Response in the Laplace Transform Domain

Since the solution of equation (3c) for the change in the axial rate of rotation is uncomplicated, it will suffice to focus first in what follows on the solution of (3a) and (3b) for the polar wander component of the response to surface loading. Substitution of (6a) and (6b) into (3a,b), the Laplace-transformed forms of the equations that follow are simply:

$$s \, m_1 + \sigma \left(1 - \frac{k_2^T(s)}{k_f} \right) m_2 = \Psi_1(s) \tag{7a}$$

$$s \, m_2 + \sigma \left(1 - \frac{k_2^T(s)}{k_f} \right) m_1 = \Psi_2(s) \tag{7b}$$

where

$$\sigma = \Omega_o \frac{(C - A)}{A} \tag{7c}$$

is the Chandler Wobble frequency of the rigid Earth, "s" is the Laplace transform variable, and again A=B has been assumed. The Laplace-transformed forms of the excitation functions in (4a) and (4b) are simply:

$$\Psi_1(s) = \left(\frac{\Omega_O}{A} \right) I_{23}(s) - \left(\frac{s}{A} \right) I_{13}(s) \tag{8a}$$

$$\Psi_2(s) = \left(\frac{\Omega_O}{A} \right) I_{13}(s) - \left(\frac{s}{A} \right) I_{23}(s) \tag{8b}$$

with

$$I_{ij}(s) = \left(1 + k_2^L(s) \right) I_{ij}^{Rigid}(s) \tag{8c}$$

Now equations (7a) and (7b) are elementary algebraic equations for $m_1(s)$ and $m_2(s)$ and these may be solved exactly to write:

$$m_1(s) = \left[\frac{1 + k_2^L(s)}{s^2 + \sigma^2 \left(1 + \frac{k_2^T(s)}{k_f} \right)^2} \right] \left[\left(\frac{\Omega_o \sigma}{A} \right) \left(1 - \frac{k_2^T(s)}{k_f} \right) - \frac{s^2}{A} \right] I_{13}^{Rigid}(s) \quad (9a)$$

$$m_2(s) = \left[\frac{1 + k_2^L(s)}{s^2 + \sigma^2 \left(1 + \frac{k_2^T(s)}{k_f} \right)^2} \right] \left[\left(\frac{\Omega_o \sigma}{A} \right) \left(1 - \frac{k_2^T(s)}{k_f} \right) - \frac{s^2}{A} \right] I_{23}^{Rigid}(s) \quad (9b)$$

If we now neglect terms of order s^2/σ^2 in (9a,b), which delivers a highly accurate approximation free of the influence of the Chandler wobble, we obtain:

$$m_1(s) = \left(\frac{\Omega_o}{A\sigma} \right) \left[\frac{1 + k_2^L(s)}{1 - \frac{k_2^T(s)}{k_f}} \right] I_{13}^{Rigid}(s) = H(s)\, I_{13}^{Rigid}(s) \quad (10a)$$

$$m_2(s) = H(s)\, I_{23}^{Rigid}(s) \quad (10b)$$

A convenient short-hand form for the solution vector $(m_1, m_2) = \underline{m}$ is to write:

$$\underline{m}(s) = \frac{\underline{\Psi}^L(s)}{\left[1 - \frac{k_2^T(s)}{k_f} \right]} = H(s) \left(I_{13}^{Rigid}(s), I_{23}^{Rigid}(s) \right) \quad (11a)$$

where $$\underline{\Psi}^L(s) = \left[\left(\frac{\Omega_o}{A\sigma} \right) (1 + k_2^L(s) \left(I_{13}^{Rigid}(s), I_{23}^{Rigid}(s) \right) \right] \quad (11b)$$

An Exact Inversion of the Laplace Transform Domain Solution

From equations (11) it will be clear that the polar wander solution m(s) will depend critically upon the ratio $k_2^T(s)/k_f$. This fact was more fully exposed in the analysis of Peltier (1982) and Wu and Peltier (1984) who re-wrote the Laplace transform domain forms of $k_2^T(s)$ and $k_2^L(s)$ as (e.g. see equation 61 of Wu and Peltier 1984):

$$k_2^T(s) = k_2^T(s=0) - s \sum_{j=1}^{N} \frac{(q'_j / s_j)}{(s + s_j)} \quad (12a)$$

$$k_2^L(s) = (-1 + \ell_s) - s \sum_{j=1}^{N} \frac{(q_j / s_j)}{(s + s_j)} \quad (12b)$$

in which the superscript ℓ=2 on q_j^2, r_j^2, s_j^2 has been suppressed for convenience. Substituting (12a) into (11a) this may be re-written as:

$$\underline{m}(s) = \frac{\underline{\Psi}^L(s)}{\left[1 - \frac{k_2^T(s=0)}{k_f}\right] + \frac{s}{k_f}\sum_{j=1}^{N}\frac{(q'_j / s_j)}{(s+s_j)}} \qquad (13)$$

In their discussion of the formal inversion of (13) into the time domain, Peltier (1982) and Wu and Peltier (1984) made the approximation that the term in square brackets in the denominator of 13 could be safely neglected. In MW it is claimed that this renders the numerical structure employed to compute the time domain response unstable. This appears to be connected to a misunderstanding of the Tauberian Theorem (eg Widmer, 1983) which asserts that the infinite time limit of **m**(t) will be equal to the s->0 limit of the product s**m**(s). Clearly the approximation in which the square bracketed term in the denominator of (13) is neglected, in which case one is assuming that $k_2^T(s=0) = k_f$, the multiplication by "s" on the lhs of (13) cancels the "s" in the denominator of (13), thus rendering the infinite time limit of the approximate form of (13) entirely stable. In this brief paper my purpose is to

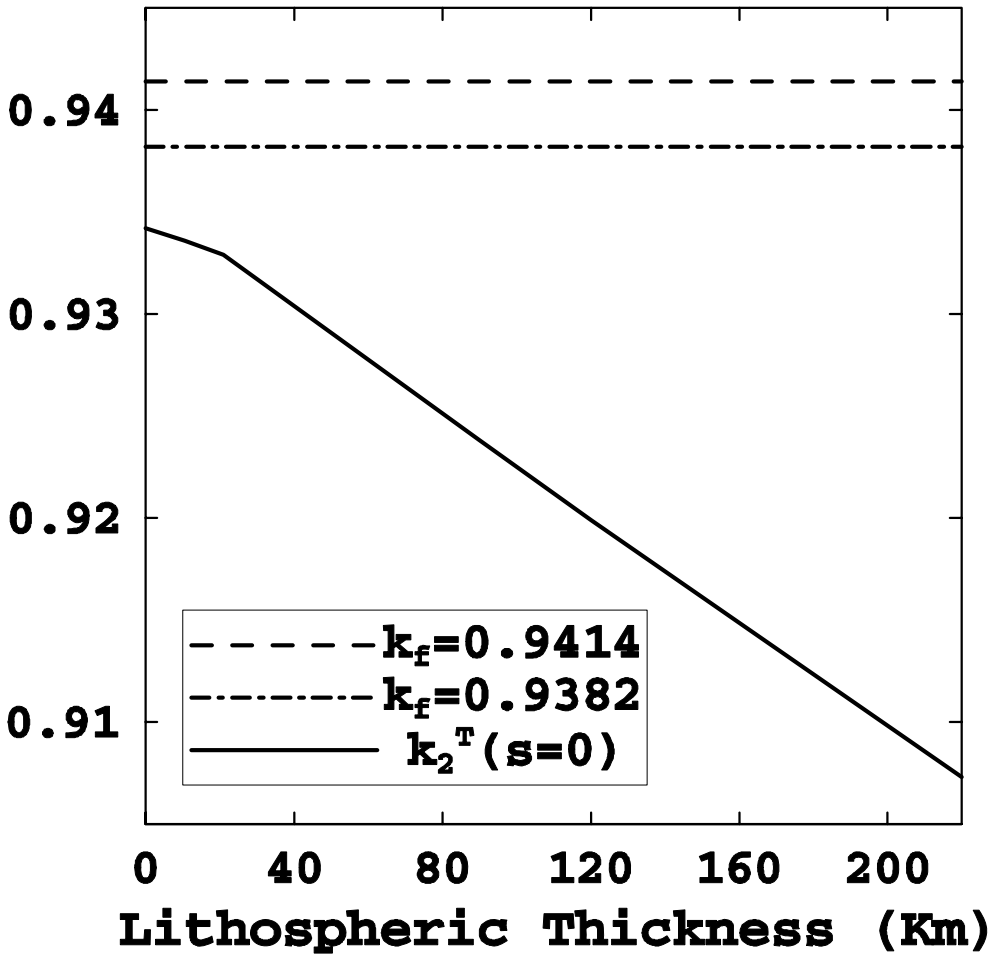

Figure 1. *Compares the value of the degree 2 "tidal Love number" in the limit of zero frequency (s=0) with the two estimates of the "fluid Love number" discussed in the text*

demonstrate this fact by computing exact solutions for the inverse of (13) without making the approximation involved in the neglect of the term in square brackets in the denominator of (13). It is nevertheless useful to start this process by showing explicitly that this term is small. This is demonstrated in Figure 1 where I show $k_2^T(s=0)$ as a function of lithospheric thickness "L". It will be clear by inspection of this Figure, on which the two previously cited values for k_f are also shown, that in the limit of zero lithospheric thickness the approximation made in the analyses of Peltier (1982) and Wu and Peltier (1984) becomes increasingly more valid. That the Earth might be expected to respond to the GIA process such that the flattening of its figure was accurately predictable by the infinite time limit of the first order linear visco-elastic field theory of Peltier (1974) is entirely expected. The fact that it is not "exactly" predictable by this field theory (see Figure 1) is also entirely expected because processes other than the basic rotation of the object, such as mantle convection, may also contribute to this flattening. To demonstrate the impact of the approximation previously made in constructing the solutions for the polar wander speed and direction caused by the GIA process we must invert the Laplace transform domain solution (13) exactly. This was not done in MW and this appears to have clouded their judgement as to what the impact might be.

When the assumption $k_2^T(s=0) = k_f$ is abandoned , the Laplace transform domain impulse response may then be written n the form:

$$H(s) = \left(\frac{\Omega_o}{A\sigma}\right) \frac{1 + k_2^L(s)}{\frac{s}{k_f}\sum_{j=1}^{N}\frac{(q_j/s_j)}{(s+s_j)} + \varepsilon} \tag{14a}$$

where

$$\varepsilon = 1 - \frac{k_2^T(s=0)}{k_f}. \tag{14b}$$

As will become clear, even though ε is a small quantity (especially in the case that the finite thickness of the lithosphere may be neglected in the limit $t \rightarrow \infty$), retaining it in expression (14a) for the impulse response could have a significant impact upon the solution as the rotational stability of the system would be modified. Now the construction of the solution for the time-domain form of the impulse response H(t) proceeds in this case as in the case based upon the Equivalent Earth Model assumption, although the result differs somewhat from a physical perspective. In this case it is useful to make the distinction between the Chandler wobble frequency of a rigid Earth σ and the Chandler wobble frequency of the visco-elastic Earth σo, by employing the definition:

$$\sigma_0 = \frac{\left(k_2^T(s=0) - k_2^{TE}\right)}{k_2^T(s=0)}\sigma. \tag{15}$$

We must then re-write the expression for H(s) as:

$$H(s) = \left(\frac{\Omega}{A\,\sigma_o}\right) \frac{\left(1 + k_2^L(s)\right)}{\left((1-\varepsilon)s\sum_{i=1}^{N}\frac{g_j}{s+s_j}\right) + \varepsilon'} \tag{16a}$$

with

$$\varepsilon' = \varepsilon \frac{\sigma}{\sigma_o}, \tag{16b}$$

and,

$$g_j = \frac{q'_j / s_j}{\sum_j (q'_j / s_j)}. \tag{16c}$$

The inversion of H(s) into the time domain now proceeds by expanding the sum in the denominator of (16a) in the form:

$$\sum_{j=}^{N} \frac{g_j}{(s+s_j)} = \frac{Q_{N-1}(s)}{\prod_{j=1}^{N}(s+s_j)} = \frac{\prod_{j=1}^{N-1}(s+\lambda_j)}{\prod_{j=}^{N}(s+s_j)} \tag{17}$$

since $\sum_j g_j \equiv 1$. Then we have, suppressing for the moment the factor $(\Omega_o / A\sigma_o)$,

$$H(s) = \frac{\prod_{j=1}^{N}(s+s_j)\left[1+k_2^L(s)\right]}{(1-\varepsilon)s\prod_{i=1}^{N-1}(s+\lambda_i) + \varepsilon'\prod_{j=1}^{N}(s+s_j)}. \tag{18}$$

Now substituting for the function $1 + k_2^L(s)$ from (12b) we obtain:

$$H(s) = \frac{\prod_{j=1}^{N}(s+s_j)\,\ell_s}{(1-\varepsilon)s\prod_{i=1}^{N-1}(s+\lambda_i) + \varepsilon'\prod_{i=1}^{N}(s+s_i)} + \sum_{j=1}^{N} \frac{(-q_j/s_j)s\prod_{i\neq j}^{N}(s+s_i)}{(1-\varepsilon)s\prod_{i=1}^{N-1}(s+\lambda_i) + \varepsilon'\prod_{i=1}^{N}(s+s_i)} \tag{19a}$$

$$= \frac{\prod_{j=1}^{N}(s+s_j)\,\ell_s}{(1-\varepsilon+\varepsilon')\prod_{i=1}^{N}(s+\kappa_i)} + \sum_{j=1}^{N} \frac{(-q_j/s_j)s\prod_{i\neq j}^{N}(s+s_j)}{(1-\varepsilon+\varepsilon')\prod_{i=1}^{N}(s+\kappa_i)}. \tag{19b}$$

Where now the κ_i are the N roots of the polynomial in the denominator of the 2 terms in (19a). This expression for the impulse response may be further reduced by re-writing the ratios of products as follows:

$$\frac{\prod_{j=1}^{N}(s+s_j)}{\prod_{j=1}^{N}(s+\kappa_i)} = 1 - \frac{q'(s)}{\prod_{i=1}^{N}(s+\kappa_i)} \tag{20a}$$

where now

$$q'(s) = \prod_{j=1}^{N}(s+\kappa_i) - \prod_{j=1}^{N}(s+s_j) \tag{20b}$$

and
$$\frac{s\prod_{i\neq j}^{N}(s+s_i)}{\prod_{j=1}^{N}(s+\kappa_i)} = 1 - \frac{R'_j(s)}{\prod_{i=1}^{N}(s+\kappa_i)} \tag{21a}$$

with
$$R'_j(s) = \prod_{i=1}^{N}(s+\kappa_i) - s\prod_{i\neq j}^{N}(s+s_i) \tag{21b}$$

We then have, for the Laplace transform of the impulse response, the expression:

$$H(s) = \frac{\ell_s}{(1-\varepsilon+\varepsilon')}\left\{1 - \frac{q'(s)}{\prod_{i=1}^{N}(s+\kappa_i)}\right\} + \frac{1}{(1-\varepsilon+\varepsilon')}\sum_{j=1}^{N}\left(-\frac{r_j}{s_j}\right)\left\{1 - \frac{R'_j(s)}{\prod_{i=1}^{N}(s+\kappa_i)}\right\} \tag{22a}$$

or

$$H(s) = \frac{\ell_s - \sum_{j=1}^{N} r_j/s_j}{(1-\varepsilon+\varepsilon')} - \frac{\ell_s\, q'(s)}{(1-\varepsilon+\varepsilon')\prod_{i=1}^{N}(s+\kappa_i)} + \frac{1}{(1-\varepsilon+\varepsilon')}\sum_{j=1}^{N}\frac{(q_j/s_j)\,R'_j(s)}{\prod_{i=1}^{N}(s+\kappa_i)} \tag{22b}$$

Denoting $\ell_s - \sum_{j=1}^{N} r_j/s_j = 1 + k_2^{LE} = D_1$, say, then we may further reduce the expression for the impulse response to:

$$H(s) = \frac{D_1}{(1-\varepsilon+\varepsilon')} - \frac{1}{(1-\varepsilon+\varepsilon')}\left\{\frac{\ell_s\, q'(s) - \sum_{j=1}^{N}(q_j/s_j)R'_j(s)}{\prod_{i=1}^{N}(s+\kappa_i)}\right\} \tag{23}$$

The inverse Laplace transform of this expression is such that the solution in the present case, in which $k_2^T(s=0) \neq k_f$, is just:

$$m_1(t) = \frac{1}{(1-\varepsilon+\varepsilon')}\left(\frac{\Omega_o}{A\sigma_o}\right)\left\{\left[\ell_s - \sum_{j=1}^{N}\frac{r_j}{s_j}\right] I_{13}^{Rigid}(t) + \sum_{i=1}^{N} E'_i\, e^{-\kappa_i t} * I_{13}^{Rigid}(t)\right\} \tag{24a}$$

$$m_2(t) = \frac{1}{(1-\varepsilon+\varepsilon')}\left(\frac{\Omega_o}{A\sigma_o}\right)\left\{\left[\ell_s - \sum_{j=1}^{N}\frac{r_j}{s_j}\right] I_{23}^{Rigid}(t) + \sum_{i=1}^{N} E'_i\, e^{-\kappa_i t} * I_{23}^{Rigid}(t)\right\} \tag{24b}$$

where

$$E'_i = \left\{-\ell_s\, q'(-\kappa_i) + \sum_{j=1}^{N}\frac{r_j}{s_j}R'_j(-\kappa_i)\right\} / \prod_{i=j}^{N}(\kappa_j - \kappa_i). \tag{24c}$$

The polar wander velocity vector components are obtained simply by time differentiation of equations (24a) and (24b). It is useful to compare the result in (24) to the solutions that obtain under the approximation previously employed. In the limit $\varepsilon \rightarrow o$ we have κN = 0 and κi = λi the N-1 relaxation times that govern the system in this limit. In this case, the parameter E'N in the above becomes:

$$E'_N = -\frac{\ell_1 \, q\,(o)}{\prod_{j=1}^{N-1} (\kappa_j - \kappa_N)} = -\frac{\ell_s \, q(o)}{\prod_{j=1}^{N-1} \lambda_i} \qquad (25)$$

And the previous approximate result is fully recovered.

In order to compare the temporal histories of the rotational anomalies in the two cases, it will be important to proceed by keeping as many features of the Earth model fixed as possible. To this end and for the remainder of this paper, I will focus entirely upon the nature of the solutions that obtain when the recently published ICE-5G model of the glaciation and deglaciation process of Peltier (2004) is employed to determine the rotational excitation functions required for the evaluation of the solution (24). In the next section results will be discussed for a sequence of simple two layered viscosity structures as a function of the parameter ε in order to explicitly demonstrate the highly stable nature of the solution in the limit that this parameter vanishes.

Results

Of particular importance for the purpose of this paper is the sensitivity of the predictions of polar wander speed to the assumption that $k_2^T(s=o)$ may be assumed to be equal to k_f. When this assumption is not made, then the solution is given by equation (24). In the latter, there appears the quantity (1- $\varepsilon+\varepsilon'$), the values in which for the Earth model (VM2) in question are respectively 0.034, 0.05, and 1.017 (for ε, ε' and $1-\varepsilon+\varepsilon'$) when the thickness of the lithosphere is taken to be 90 km. In Figure 2 (bottom) are plotted the predictions of polar wander speed based upon equations (24) as a function of the viscosity of the lower mantle with the upper mantle viscosity held fixed to the value in the VM2 model of Peltier (1996). Results are also shown for several different values of a parameter $\Delta = \varepsilon$ / 0.034 including the value ε = 0.034 (Δ = 1) which is appropriate for the VM2 model with a lithospheric thickness of 90 km, in which case $k_2^T(s=0)$= 0.9263, but also for significantly smaller values of ε including the value ε = 0 (Δ = 0) so as to investigate the "smoothness" of the transition from the value ε = 0 which obtains when k_2^T (s = 0) is assumed to be equal to k_f. The two intermediate values of Δ for which results are shown on Figure 2 correspond to the two values of k_f shown on Figure 1 when the lithospheric thickness L is assumed to be equal to zero. Also shown on Figure 2 (top) is the dependence of the predicted value of the non-tidal acceleration as a function of lower mantle viscosity.

Inspection of Figure 2 clearly demonstrates the fact that the solutions for polar wander speed that obtain in the limit $\Delta = 0$ are almost identical to those that obtain for either of the two non-zero values that correspond to zero lithospheric thickness. This demonstrates that the formulation of Peltier (1982) and Wu and Peltier (1984) based upon the approximation $k_2^T(s=0) = k_f$ was not mathematically unstable as claimed in WM. In fact, careful inspection of Figure 2 will show that the preferred solution for BOTH the non-tidal acceleration and polar wander speed is the model

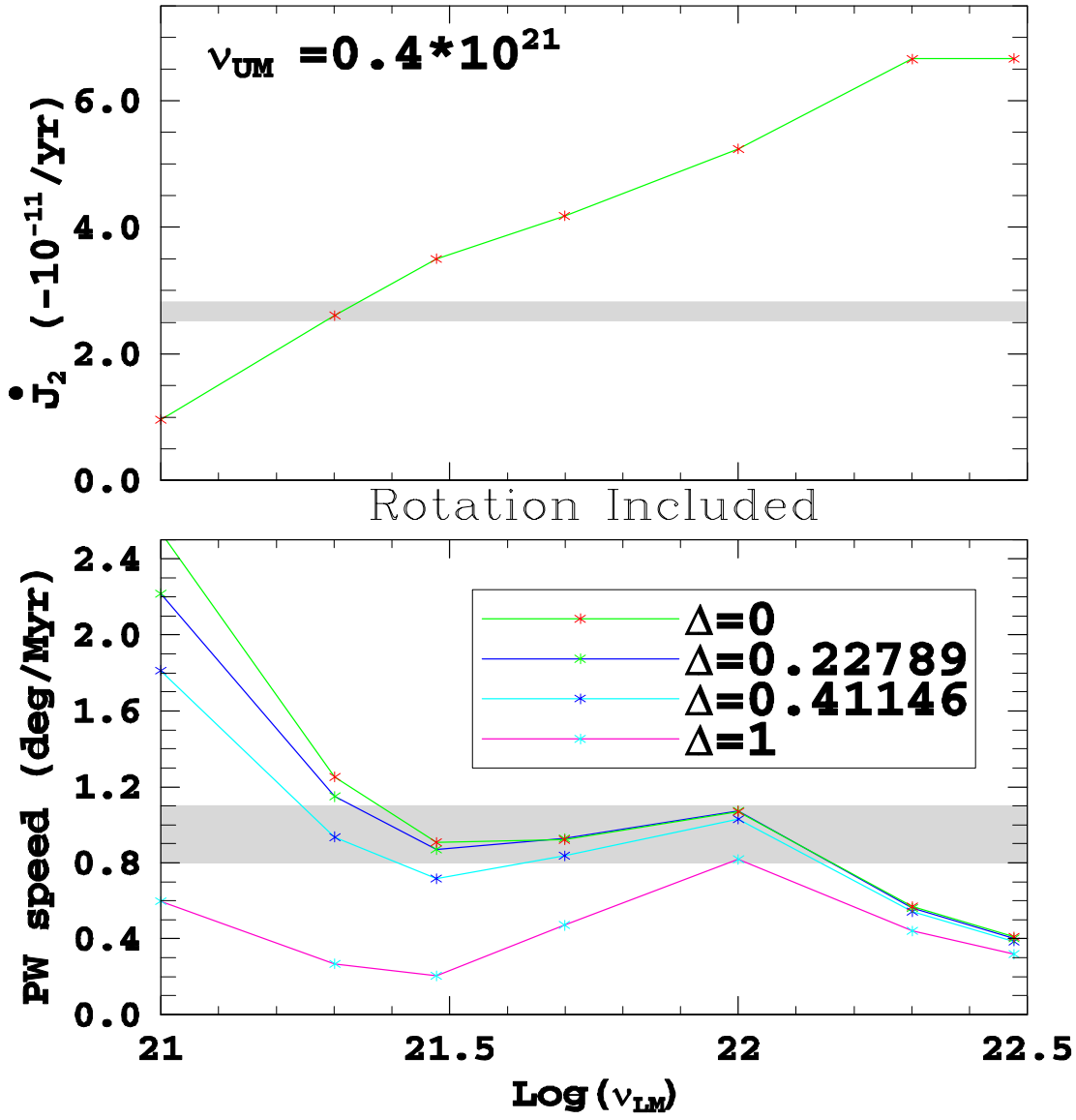

Figure 2. *This Figure compares model predictions of the non-tidal acceleration of rotation (top) and of the speed of polar wander (bottom) as a function of the viscosity of the lower mantle when the upper mantle viscosity is held fixed to the value in the VM2 viscosity model of Peltier (1996). The polar wander speed predictions are shown for several values of the parameter* Δ *which measures the importance of the difference between the fluid Love number* k_f *and* $k_2^T(s=0)$*. The two values of* Δ *that are less than unity, 0.22789 and 0.41146, correspond respectively to the* k_f *values of 0.9382 and 0.9414 and are those that obtain in the limit of vanishing lithospheric thickness. The value* $\Delta = 1$ *is the value appropriate for a finite lithospheric thickness of 90 km.*

with $\Delta = 0.41146$ AND L=0.0. This solution amounts to a very modest adjustment of the earlier result obtained with $\Delta = 0.0$ and L=0.0. The results for finite non-zero lithospheric thickness cannot fit the observed polar wander speed except, marginally, for a model with an upper mantle-lower mantle viscosity contrast that is incompatible with the observed non-tidal acceleration. Such high contrast viscosity models are also firmly rejected by relative sea level data from the previously ice covered area of North America.

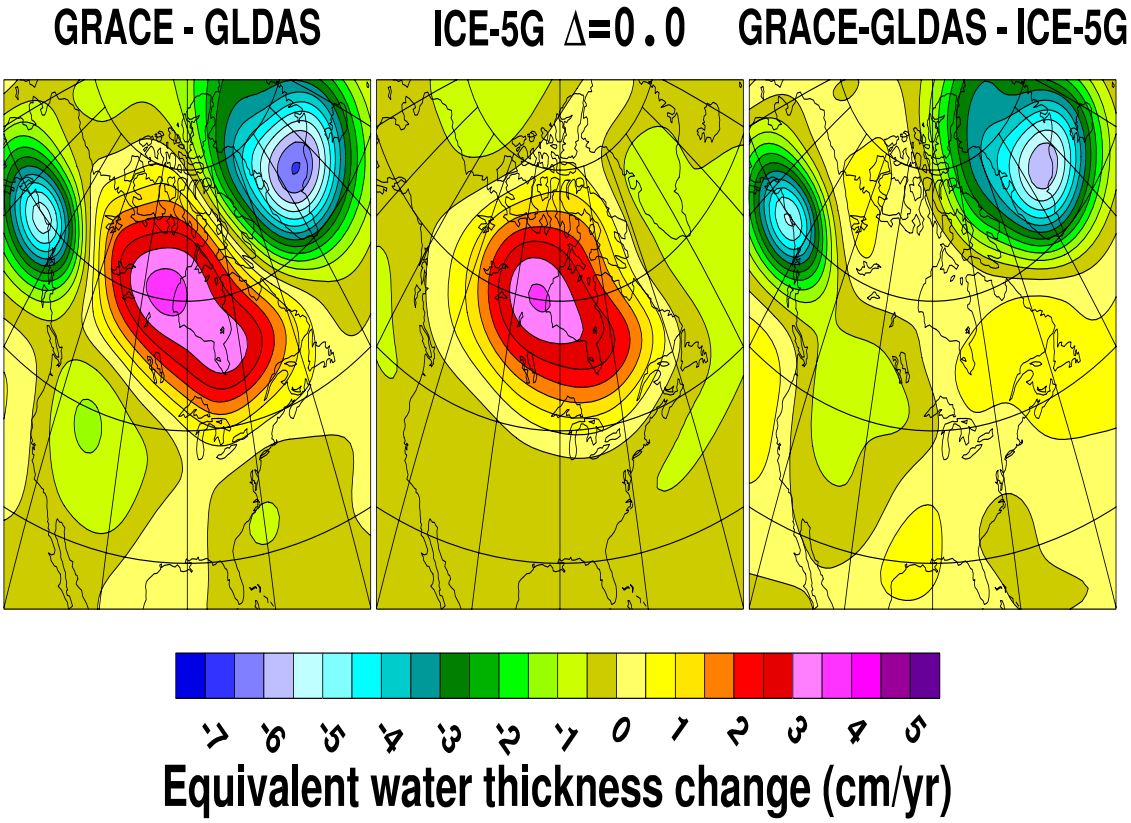

Figure 3. *Demonstrates the ability of the GIA model of Peltier(2004) to accurately explain the observed time dependence of the gravity field over the North American continent. This field is represented by the time rate of change of the thickness of an equivalent layer of water at the earth's surface. This analysis is based upon the level 2 release of the GRACE Stokes coefficients. In this comparison, the degree 2 terms have been excluded, a consequence of the fact that GRACE does not provide accurate measures of these coefficients.*

The quality of this low contrast model is also strongly re-enforced by the recently obtained time dependent gravity field data from the GRACE satellite system. Figure 3 compares the GRACE observed and hydrology corrected GRACE time dependent gravity field observations with the ICE-5G(VM2) GIA model prediction of the same field. In the third frame of Figure 3 the difference between these two data sets is also shown, thus demonstrating the extremely high quality of the ICE-5G(VM2) model. The neglect of the degree 2 coefficients, which are very large for the ICE-5G(VM2) model, as demonstrated in Peltier (2004), is required by virtue of the inability of GRACE to accurately observe these coefficients..

Conclusion

The analyses described in the previous sections of this paper have considerably extended the previously published theory that is employed to compute the response of

the earth's rotational state to the global process of glacial isostatic adjustment. These analyses suffice to refute the claim in MW that the formalism described in Peltier (1982) and Wu and Peltier (1984) was fundamentally unstable mathematically. This error of interpretation appears to have been due to a lack of understanding of the Tauberian Theorem that may be employed to predict the infinite time limit of a solution from the Laplace transform of this solution. The extended version of the theory described herein has allowed a direct investigation of the question of the extent to which the finite thickness of a globally continuous and unbroken lithosphere may contribute to the rotational response to surface mass load forcing. These analyses demonstrate that, in this long timescale limit, the most accurate representation of the rotational response of the Earth is that based upon the assumption of vanishing lithospheric thickness. This is understandable on the basis of the fact that the lithosphere of the planet is "broken" into a series of weakly coupled plates. For planets whose lithospheres are not unbroken in this way, the same assumption would clearly not be appropriate.

References

[1] Argus, D.F. & Gross, R.S. An estimate of motion between the spin axis and the hotspots over the past century. *Geophys. Res. Lett.* **31**, L06614, doi:10.1029/2004GL019657,2004

[2] Broecker, W.S. & Van Donk, J. Insolation changes, ice volumes, and the $\delta^{18}0$ record in deep sea cores. *Geophys. Space Phys.* **8**, 169-198, 1970.

[3] Cheng, Mik, Eanes, R.J., Shum, C.K., Schutz, B.E. & Tapley, B.D. Temporal variations in low degree zonal harmonics from Starlette orbit analysis. *Geophys. Res. Lett.* **16**, 393-396, 1989.

[4] Clark, J.A., Farrell, W.E. & Peltier, W.R. Global changes in postglacial sea levels: A numerical calculation. *Quat. Res.* **9**, 265-287, 1978.

[5] Dahlen, F.A. The passive influence of the oceans upon the rotation of the Earth. *Geophys. J.R. Astron. Soc.* **46**, 663-406, 1976.

[6] Domack, E., Duran, D., Leventer, A., Ishman, S., Doane, S., McCullum, S., Amblas, D. Ring, J. Gilbert, R. & Prentice, M. Stability of the Larsen B ice shelf on the Antarctic Peninsula during the Holocene epoch. *Nature* **436**, 681-685, 2005.

[7] Dziewonski, A.M. & Anderson, D.L. Preliminary reference Earth model. *Phys. Earth Planet. Int.* **25**, 297-356, 1981.

[8] Farrell, W.E. Deformation of the Earth by surface loads. *Rev. Geophys.* **10**, 761-797, 1972.

[9] Farrell, W.E. & Clark, J.A. On postglacial sea level. *Geophys. J.R. Astron. Soc.* **46**, 647-667, 1976.

[10] Imbrie, J., Hays, J.D., Martinsen, D.G., McIntyre, A., Mix, A.C., Morley, J.J., Pisias, N.G., Prell, W.L. & Shackleton, N.J. The orbit theory of Pleistocene climate: Support from a revised chronology of the marine $\delta^{18}0$ record in Milankovitch and Climate, edited by A. Berger et al., pp. 269-306. D. Reidel, Norwell, Mass., 1984.

[11] Lambeck, K. & Chappell, J. Sea level change through the last glacial cycle. *Science* **292**(5517), 679-686, 2001.

[12] Mitrovica, J.X., Wahr, J., Matsuyama, I. & Paulson, A. The rotational stability of an ice-age Earth. *Geophys. J. Int.* **161**, 491-506, 2005.

[13] Nakiboglu, S.M. & Lambeck, K. Deglaciation effects on the rotation of the Earth. *Geophys. J.R. Astron. Sco.* **62**, 49-58, 1980.

[14] Nakiboglu, S.M. & Lambeck, K. Deglaciation related features of the Earth's gravity field. *Tectonophysics* **72**, 289-303, 1981.

[15] Peltier, W.R. The impulse response of a Maxwell Earth. *Rev. Geophys. Space Physics.* **12**, 649-669, 1974.

[16] Peltier, W.R. Glacial isostatic adjustment, II: The inverse problem. *Geophys. J. Roy. Astron. Soc.* **46**, 669-706, 1976.

[17] Peltier, W.R. Dynamics of the ice-age Earth. *Advances in Geophysics*, **24**, 1-146, 1982.

[18] Peltier, W.R. The LAGEOS constraint on deep mantle viscosity: Results from a new normal mode method for the inversion of visco-elastic relaxation spectra. *J. Geophys. Res.* **90**, 9411-9421, 1985.

[19] Peltier, W.R. Ice-age paleotopography. *Science* **265**, 195-201, 1994.

[20] Peltier, W.R. Mantle viscosity and ice-age ice-sheet topography. *Science* **273**, 1359-1364, 1976.

[21] Peltier, W.R. Postglacial variations in the level of the sea: implications for climate dynamics and solid-Earth geophysics. *Rev. Geophys.* **36**, 603-689, 1998.

[22] Peltier, W.R. Comments on the paper of Yokoyama et al. (2000) entitled "Timing of the last glacial maximum from observed sea level minima" *Quat. Sci. Rev.* **21**, 409-414, 2002a.

[23] Peltier, W.R. One eustatic sea level history, Last Glacial Maximum to Holocene. *Quat. Sci. Rev.* **21**, 377-396, 2002b.

[24] Peltier, W.R. Global glacial isostatic adjustment: paleo-geodetic and space-geodetic tests of the ICE-4G (VM2) model. *J. Quat. Sci.* **17**, 491-510, 2002c.

[25] Peltier, W.R. On the hemispheric origins of meltwater pulse 1a. *Quat. Sci. Rev.* **24**, 1655-1671, 2005.

[26] Peltier, W.R., Farrell, W.E., & Clark, J.A. Glacial isostatsy and relative sea-level: a global finite element model. *Tectonophysics*, **50**, 81-110, 1978.

[27] Peltier, W.R. & Jiang, X. Glacial isostatic adjustment and Earth rotation: Refined constraints on the viscosity of the deepest mantle. *J. Geophys. Res.* **101**, 3269-3290, 1996 (Correction, *J. Geophys. Res.* **102**, 10,101-10,103, 1997).

[28] Peltier, W.R., Shennan, I., Drummond, R. & Horton, B. On the postglacial isostatic adjustment of the British Isles and the shallow visco-elastic structure of the Earth. *Geophys. J. Int.*, **148**, 443-475, 2002.

[29] Peltier, W.R. & Fairbanks, R.G. Global glacial ice-volume and Last Glacial Maximum duration from an extended Barbados Sea Level record. *Quat. Sci. Rev.*, 2006.

[30] Sabadini, R. & Peltier, W.R. Pleistocene deglaciation and the Earth's rotation: implications for mantle viscosity. *Geophys. J. Roy. Astron. Soc.* **66**, 553-578, 1981.

[31] Stephenson, E.R. & Morrison, L.V. Long term fluctuations in the Earth's rotation: 700 B.C. to A.D. 1990. *Philos. Trans. R. Soc. London, Serc. A*, **351**, 165-202, 1995.

[32] Shackleton, N.J. Oxygen isotope analysis and Pleistocene temperatures re-addressed. *Nature* **215**, 15-17, 1967.

[33] Shackleton, N.J. & Opdyke, N.D. Oxygen isotope and paleomagnetic stratigraphy of equatorial Pacific core V28-238: Oxygen isotope temperatures and ice volumes on a 10^5-year time scale. *Quaternary Res.* **3**, 39-55, 1973.

[34] Vincente, R.O. & Yumi, S. Co-ordinates of the pole (1899-1968) returned to the conventional international origin. *Publ. Int. Latit. Obs. Mizusawa* **7**, 41-50, 1969.

[35] Vincente, R.O. & Yumi, S. Revised values (1941-1961) of the co-ordinates of the pole referred to the CIO. *Publ. Int. Latit. Obs. Mizusawa* **7**, 109-112, 1970.

[36] Waelbroecke, C., Labyrie, L., Michel, E., Duplessy, J.-C. McManus, J.F., Lambeck, K., Balbon, E. & Labracherie, M. Sea-level and deep water temperature changes derived from benthic foraminifera isotopic records. *Quat. Sci. Rev.* **21**, (1-3), 295-305, 2002.

[37] Wu, P. & Peltier, W.R. Pleistocene deglaciation and the Earth's rotation: A new analysis. *Geophys. J.R. astr. Soc.* **76**, 202-242, 1984.

[38] Yoder, C.F., Williams, J.G., Dickey, J.O., Schutz, B.E., Eanes, R.J. & Tapley, B.D. Secular variation of the Earth's gravitational harmonic J_2 coefficient from LAGEOS and non-tidal acceleration of Earth rotation. *Nature* **303**, 757-762, 1983.

[39] Yoder, C.F., 1995. www.agu.org/references/geophys/4_Yoder.pdf

[40] Yokoyama, Y., Lambeck, K., DeDekkar, P., Johnston, P. & Fifield, L.K Timing of the Last Glacial Maximum from observed sea level minima. *Nature* **406**, 713-716, 2000. (Correction, 2001, *Nature* **412**, 99).

Recent Results from SLR Experiments in Fundamental Physics: Frame Dragging observed with Satellite Laser Ranging.

E. C. Pavlis[1], I. Ciufolini[2], R. König[3]

1. Joint Center for Earth Systems Technology (JCET), UMBC, Baltimore, MD, USA.
2. Università degli Studi di Lecce, Lecce, Italy
3. GeoForschungsZentrum (GFZ), Potsdam, Germany.

Contact: epavlis@JCET.umbc.edu / Fax: +1 410 455 5868

Abstract

Satellite laser ranging provided for decades the most precise measurement of positions and velocities of earthbound tracking stations, as well as the most precise orbits of earth-orbiting artificial satellites. While the latter applies to any satellite carrying the appropriate reflectors, the use of these orbits for precise geodetic products requires the use of specially designed target satellites in high altitude orbits, such as the two LAGEOS satellites. To achieve such high quality, the motion of these satellites must be described with equally accurate models, such as those made available recently, thanks to missions like CHAMP and GRACE. This led to the synergistic application of such precise products to devise tests of fundamental physics theories. Nearly twenty years after conceiving and proposing an initial concept for a General Relativity (GR) prediction test, our recent experiment resulted in a positive and convincing measurement of the Lense-Thirring effect, also known as the gravitomagnetic effect of the rotating Earth. Using state-of-the-art Earth gravitational field models based on data from the CHAMP and GRACE missions, we obtained an accurate measurement of the Lense–Thirring effect predicted by GR, analyzing eleven years of LAGEOS and LAGEOS 2 Satellite Laser Ranging (SLR) data. The new result, in agreement with the earlier one based on Earth models JGM-3 and EGM96, is far more accurate and more robust. The present analysis uses only the nodal rates of the two satellites, making NO use of the perigee rate, thus eliminating the dependence on this unreliable element. Using the EIGEN-GRACE02S model, we obtained our optimal result: $\mu = 0.99$ (vs. 1.0 in GR), with a total error between ± 0.05 and ± 0.1, i.e., between 5% and 10 % of the GR prediction. Results based on processing with NASA and GFZ s/w will be presented, along with preliminary tests with very recent improved GRACE models. Further improvement of the gravitational models in the near future will lead to even more accurate tests. We discuss the LAGEOS results and some of the crucial areas to be considered in designing the future LARES mission dedicated to this test.

Introduction

One of the most fascinating theoretical predictions of general relativity is “frame–dragging” (Misner et al. 1973, Ciufolini and Wheeler 1995), also known as the Lense-Thirring effect, after the two Austrian physicists who predicted the effect based on Einstein’s General Relitivity (GR) theory (Lense and Thirring, 1918). The equivalence principle, at the basis of Einstein’s gravitational theory, states that “locally”, in a sufficiently small spacetime neighbourhood, in a freely falling frame, the observed laws of physics are the laws of special relativity. However, the axes of these inertial frames where “locally” the gravitational field is “unobservable”, rotate with respect to “distant stars” due to the rotation of a mass or in general due to a

current of mass–energy. In general relativity the axes of a local inertial frame can be realized by small gyroscopes, as shown in Figure 1.

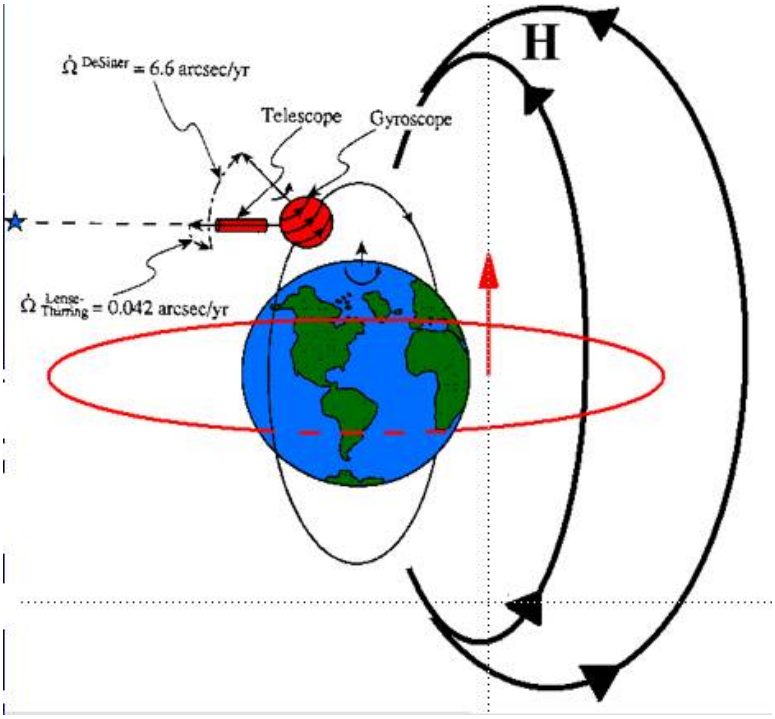

Figure 1. *The gravitomagnetic field and the mass-energy currents that produce the frame-dragging effect on the node of the orbiting gyroscope.*

Methodology

The gravitomagnetic force is by far smaller than the gravitational monopole, so we can use the tools of celestial mechanics and consider this force as a perturbation on an orbiting satellite. From the integrated (to first order) perturbation equations we obtain the most significant effects on the orbital elements, the secular rates of the node and perigee:

$$\begin{cases} \dot{\Omega}^{L-T} = \dfrac{2GJ}{c^2 a^3 (1-e^2)^{3/2}} \\ \dot{\omega}^{L-T} = \dfrac{-6GJ}{c^2 a^3 (1-e^2)^{3/2}} \cos I \end{cases}$$

In the past we used both quantities in our methodology (Ciufolini *et al.*, 1998) due to the lack of accurate enough gravitational models. Since the release of improved models from the CHAMP and GRACE missions though, we only use the node rate in our experiments. Our methodology uses as “source” of the field Earth with its angular momentum, as a test particle the geodetic satellites LAGEOS and LAGEOS 2 at present (and in the future LARES, see more on this later), and our basic observations are the two-way precise ranging with laser pulses from the ground network of the International Laser Ranging Service (ILRS), (Pearlman *et al.*, 2002).

Perturbations due to J_2 are much larger than the Lense-Thirring (LT) effect, so we need to be able to eliminate such uncertainties in order to extract the sought-for LT signal from our data. Thanks to Ciufolini's 1986 idea however, (using a "butterfly" configuration of counter-orbiting satellites in supplementary inclination orbits, Figure 2), the effect of J_2 uncertainties is cancelled.

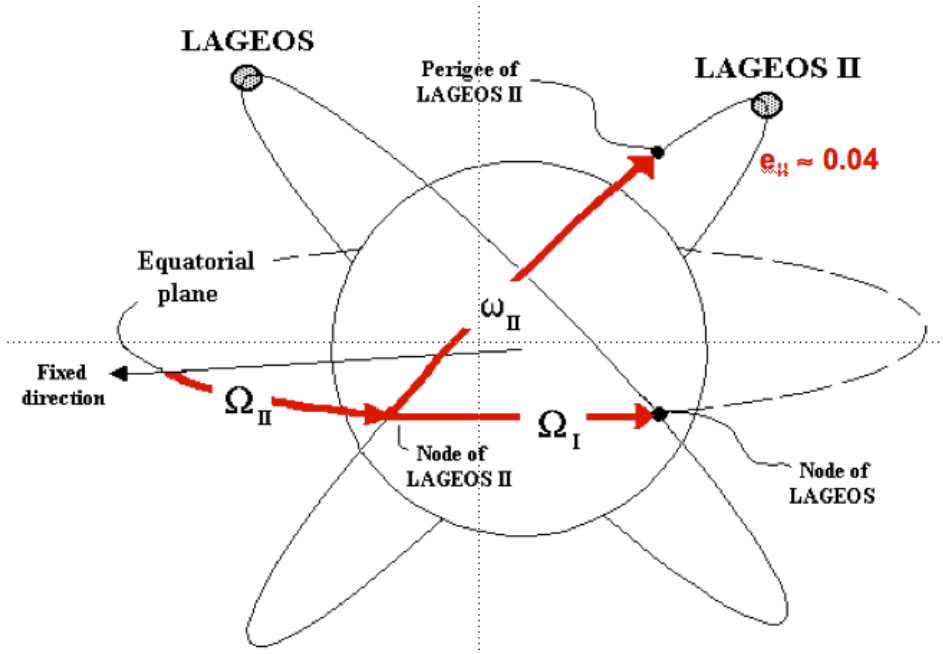

Figure 2*. The nearly-"butterfly" configuration of the retrograde LAGEOS (i = 109.8°) and the prograde LAGEOS 2 (i = 52.6°) orbits.*

When the two orbits are supplementary, one-half the sum of their nodal rate variations would provide a direct observation of the LT effect. However, Ciufolini (1989) generalized his original idea of the butterfly configuration to configurations of *N* nodes of various orbits, to cancel out the effects of the first *N-1* even zonals on the nodal rates of these orbits. Using this modified constraint for the case of two orbits in near- (but not exact) butterfly configuration, such as the LAGEOS and LAGEOS 2 orbits, we obtain:

$$\delta\dot{\Omega}_I + k\,\delta\dot{\Omega}_{II} = 48.2\mu + other\,errors \quad [mas/y]$$

where k (≈ 1/2) is a function of the elements of the two orbits, and μ is our LT parameter to be determined. If μ = 1, GR is correct, if μ = 0 the Newtonian physics are correct. Under "*other errors*" we lump a number of higher order errors and the uncertainty in the background models mapped on the estimated quantity μ. Extensive error analysis of the experiment provides bounds on these errors and allows for a realistic error budget for the result (Ciufolini, Pavlis and Peron, 2006). We separate the error sources in two groups, the gravitational and the non-gravitational. A summary of the results published in detail in (*ibid.*) are given in Figures 3 and 4.

This study supports the errors quoted for our most recent published results for μ, (Ciufolini and Pavlis, 2004), between 5 and 10% of the expected value of 1 for GR. This improved (in accuracy) result compared to our 1998 result, is a direct consequence of the highly improved gravitational model accuracy, thanks to the use

of gravity mapping data from the CHAMP and GRACE missions (Reigber *et al.*, 2002, 2003, 2005 and Tapley *et al.*, 2002 and 2003). These products are the enabling factors for the success of these experiments. Pavlis (2002) and Ries *et al.* (2003) had already forewarned of this leap in accuracy for these models and proposed the continuation of the LAGEOS experiments in anticipation of their release.

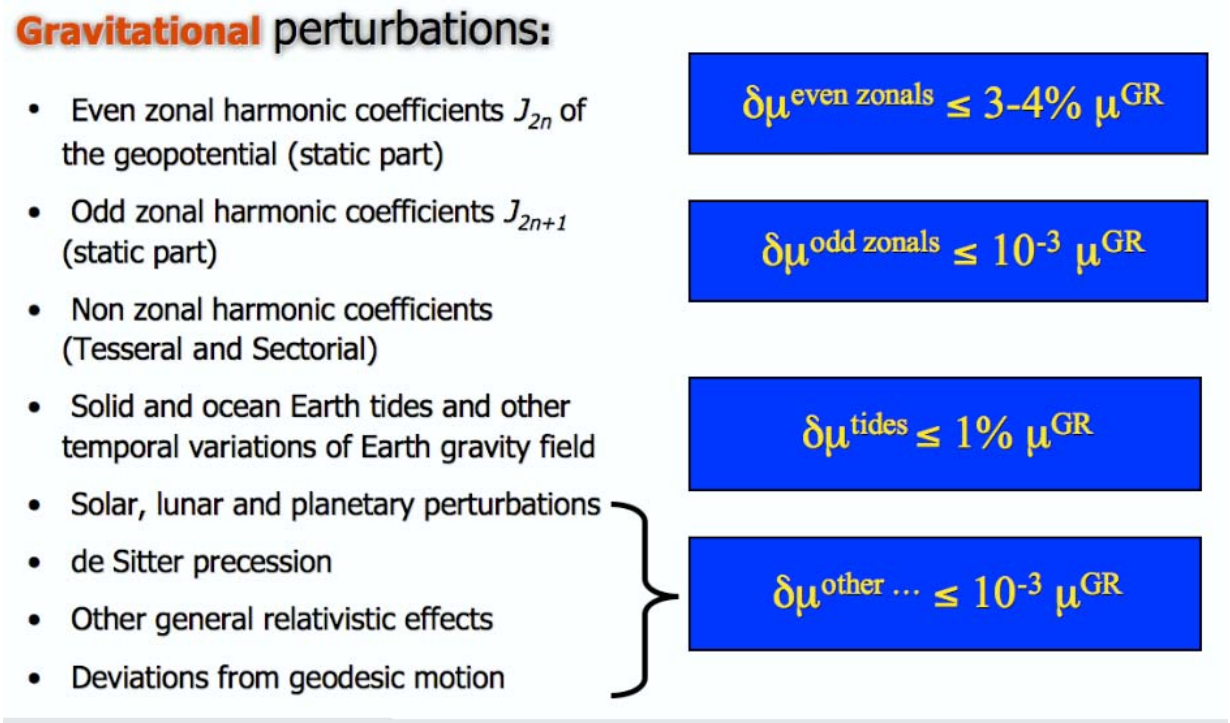

***Figure 3**. The calibrated errors on μ, due to realistic uncertainties of the gravitational parameters.*

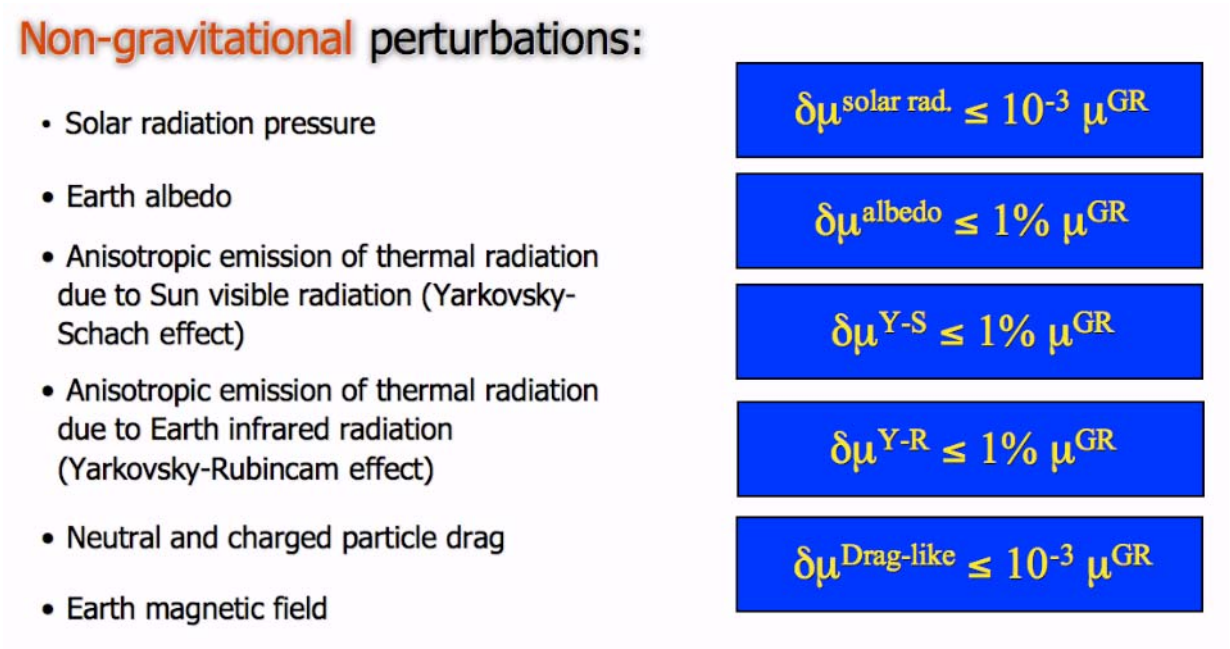

***Figure 4**. The calibrated errors on μ, due to realistic uncertainties of the non-gravitational parameters.*

The 2004 experiment results

The most accurate results on the measurement of the LT effect were published in (Ciufolini and Pavlis, 2004). The methodology and error analysis were subsequently detailed in (Ciufolini, Pavlis and Peron, 2006). These two references describe in detail the technique and the data that were used for the 2004 experiment. The basic points to be noted here are that the analysis covered the period from 1993 (just after the launch of LAGEOS 2) up to 2004, including all SLR data from the two LAGEOS satellites. The data were reduced using 15-day orbital arcs with a one-day overlap. The models used were the most accurate and consistent with the IERS Conventions 2003. All known perturbations were modeled **except** for the LT effect (set to zero). Once all arcs were converged, for each LAGEOS we formed a time series of consecutive arcs' nodal longitude differences, i.e. the nodal longitude at $t_d^{ARC=n+1}$ and the same quantity obtained for the same time from the previous arc at $t_d^{ARC=n}$. These were then integrated and combined using our constraint equation to generate a single time series. The secular trend of these series is the sought-for estimate of the μ LT parameter. Figure 5 shows the final result for the 2004 experiment.

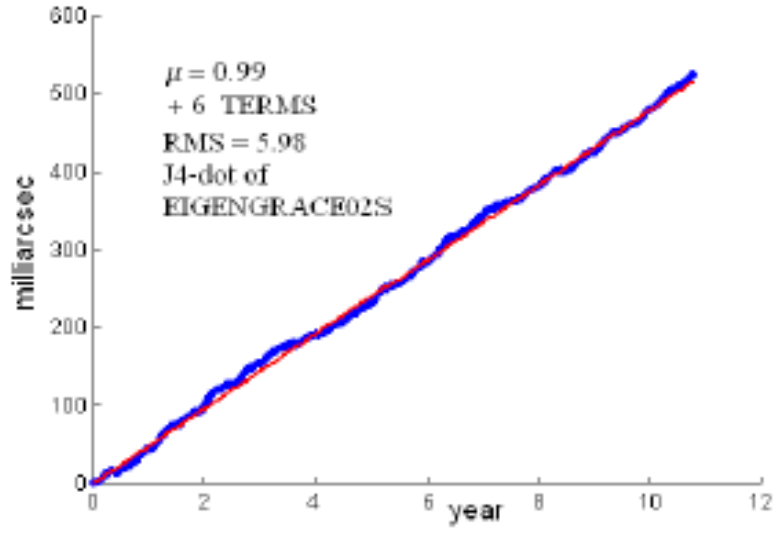

Figure 5*. The linear trend of the LAGEOS and LAGEOS 2 integrated nodal longitude differences time series for the EIGEN-GRACE02S gravitational model. Six periodic signals associated with well-known periods were filtered at the same time.*

We have already discussed the accuracy estimates associated with the 2004 result and the extensive work done to validate these error estimates as much as possible. It is worth noting that the gravitational model improvements from additional years of GRACE data result in an ever-improving estimate of these errors. The converging progression of these accuracy estimates provides a means to validate our quoted accuracy estimates for previous experiments. It is this point that makes the forthcoming new and much improved GRACE model GGM03S so anxiously awaited by all.

Beyond the 2004 experiment

The LAGEOS experiments are a zero-budget verification experiment for the much more accurate (~0.1%) and expensive (>$700M) result expected from NASA's Gravity Probe B mission (Buchman et al., 2000). In particular, with the recent

discovery of unanticipated errors in the gyro design of GP-B (Tomlin, 2007), it is doubtful that the GP-B results will ever break the 10% accuracy level (Kahn, 2007), so the LAGEOS experiments may eventually take a totally unforeseen center role in the area of fundamental physics tests.

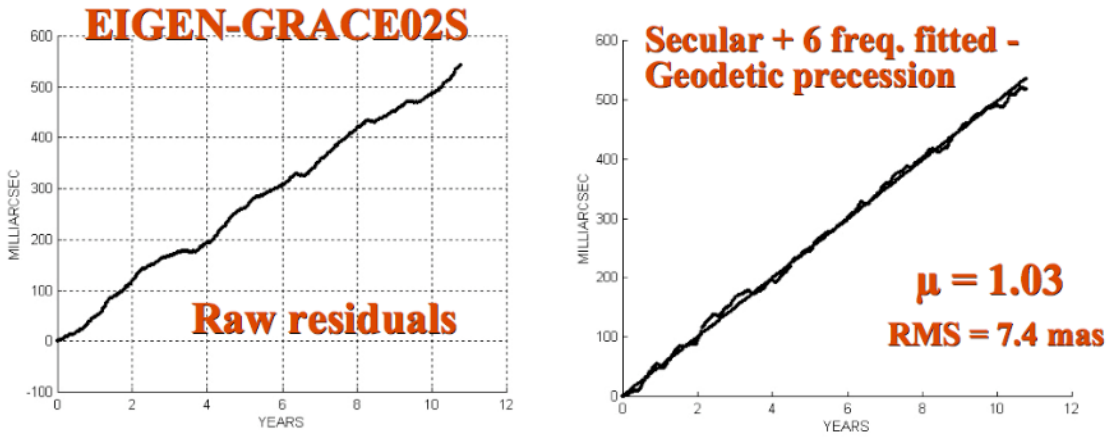

Figure 6. *Results from the GFZ software package EPOS, replicating the 2004 experiment (preliminary, pending small s/w improvements in the force model).*

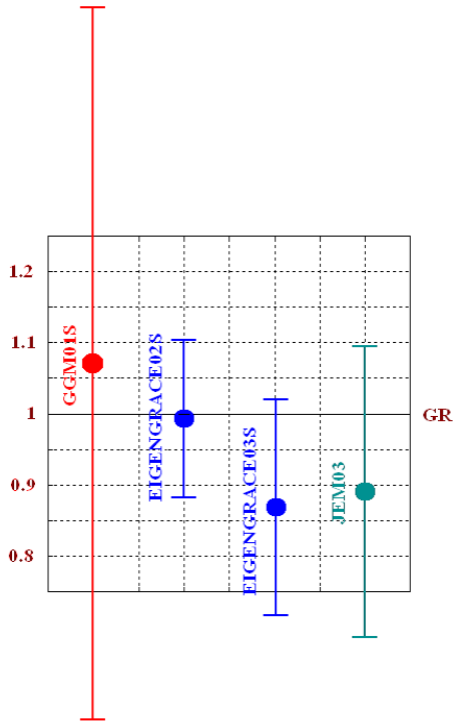

Figure 7. *Results from the joint analysis for four different gravitational models from GRACE (plotted is the value of the recovered μ, with unity signifying GR is correct).*

To improve the validation of our results our original group was extended to encompass analysts from other institutions and allow an independent check of the results with multiple software packages and alternate reduction philosophy. So far, the GFZ group has become an integral and active participant with their software package EPOS. First results from their initial attempts to replicate our 2004 experiment are shown in Fig. 6. The small discrepancy with respect to our 2004 result is due to the

fact that their software needs some small improvements to match the modeling that was used in Geodyn. In addition to the test results for 2004, new models developed by various GRACE science team groups were also used to derive new estimates of μ. Using different gravitational models we also get a good sense of the variability of the μ-estimates due to the change in the model, the development group's strategy and their ability to properly calibrate the errors of their model. The results are shown in a summary plot in Figure 7.

LAGEOS results and LLR claims

It is sometimes claimed that gravitomagnetism, measured already by SLR with the LAGEOS satellites, (might also be detected after refining the GP-B data analysis, see Tomlin, 2007), has already been observed by Lunar Laser Ranging (LLR), (Murphy in these proceedings and Murphy *et al.,* 2007); however the gravitomagnetic effects measured by LLR and the LAGEOS satellites are intrinsically different.

The gravitomagnetic effect measured by LLR depends on the motion of a gyroscope (the Earth-Moon system in the case of the LLR analysis) with respect to a central mass (the mass of the Sun in the LLR analysis) and, by changing the frame of reference used in the analysis, is equivalent to the geodetic precession, already well measured by LLR. The second gravitomagnetic effect measured by the LAGEOS satellites is an intrinsic gravitomagnetic effect (Ciufolini, 1994 and Ciufolini and Wheeler, 1995, Ciufolini 2007) that cannot be eliminated by means of any coordinate transformation.

In general relativity, in the frame in which a mass is at rest the so-called "magnetic" components g_{0i} of the metric are zero (in standard PPN coordinates). However, if an observer is moving with velocity **v** relative to the mass, the "magnetic" components g_{0i} are no longer nonzero in his local frame. These "magnetic" components g_{0i} can be simply eliminated by a Lorentz transformation back to the original frame. This is precisely what has been observed by LLR since the first measurements of the geodetic precession of the lunar orbit. In contrast, a mass object (such as Earth) with angular momentum J generates a gravitomagnetic field intrinsic to the structure of spacetime that therefore cannot be eliminated by a simple coordinate transformation or choice of reference frame. This is the field producing the LT effect on Earth orbiting satellites such as LAGEOS, measured by SLR.

In general relativity, given explicitly a general metric $\boldsymbol{g}$, with or without magnetic components g_{0i}, in order to test for intrinsic gravitomagnetism (i.e. which cannot be eliminated with a coordinate transformation), one should use the Riemann curvature tensor **R** and the spacetime invariants built using it (Ciufolini, 1994 and Ciufolini and Wheeler, 1995). Ciufolini and Wheeler (1995) give the explicit expression of the Riemann curvature invariant ***R•R**, where ***R** is the dual of **R**. Irrespective of the frame of choice, this invariant is non-zero in the case of the Kerr metric generated by the angular momentum and the mass of a rotating body. When however we evaluate it for the Schwarzschild metric generated by the mass of a non-rotating body, it is equal to zero for any frame and coordinate system of choice. In (*ibid.*) it is shown that the gravitomagnetic effect measured by LAGEOS and LAGEOS 2, due to Earth's angular momentum, is intrinsic to the spacetime's curvature and cannot be eliminated by a simple change of frame of reference since the spacetime curvature invariant ***R•R** is different from zero. However, the effect measured by LLR is just a gravitomagnetic effect that depends on the velocity of the Earth-Moon system and whose interpretation depends on the frame used in the analysis.

Murphy *et al.* (2007) show that on the lunar orbit there is a gravitomagnetic acceleration that changes the Earth-Moon distance by about 5 meters with monthly and semi-monthly periods. In a frame of reference co-moving with the Sun, the lunar gravitomagnetic acceleration in the Moon's equation of motion, is $\sim \mathbf{v}_M \times (\mathbf{v}_E \times \mathbf{g}_{ME})$; where $\mathbf{v}_M$ and $\mathbf{v}_E$ are the velocities of Moon and Earth in the frame of reference co-moving with the Sun and $\mathbf{g}_{ME}$ is the standard Newtonian acceleration vector on the Moon due to the Earth mass; this is the term discussed in (Murphy *et al.*, 2007). However, in a geocentric frame of reference co-moving with Earth, the lunar gravitomagnetic acceleration can be written: $\sim \mathbf{v}_M \times (\mathbf{v}_S \times \mathbf{g}_{MS})$: where $\mathbf{v}_M$ and $\mathbf{v}_S$ are the velocities of Moon and Sun in the frame of reference co-moving with Earth and $\mathbf{g}_{MS}$ is the standard Newtonian acceleration vector on the Moon due to the Sun mass. This acceleration can be simply rewritten as a part equivalent to the geodetic precession (Ciufolini 2007) and another one too small to be measured at the present time.

This argument can be made rigorous by using the curvature invariant ***R•R**. This invariant is formally similar to the invariant ***F•F** equal to **E•B** in electromagnetism. In the case of a point-mass metric generated by Earth and Sun, this invariant is: $\sim$ **G•H**, where **G** is the standard Newtonian electric-like field of the Sun and Earth and **H** the magnetic-like field of the Sun and Earth; this magnetic-like field is $\sim \mathbf{v} \times \mathbf{G}$ and then clearly, on the ecliptic plane, the invariant ***R•R** is null. Indeed, this invariant has been calculated (Ciufolini 2007) to be zero on the ecliptic plane, even after considering that the lunar orbit is slightly inclined on the ecliptic plane, this component would only give a contribution to the change of the radial distance too small to be measured at the present time.

***Figure 8**. A 1:2 model of the proposed LARES (Bosco et al., 2006) geodetic satellite for SLR applications in relativistic tests and geodetic TRF development.*

Summary and future plans

The analysis of nearly twelve years of SLR data from LAGEOS and LAGEOS 2 has demonstrated the measurement of the LT effect at the 5-10% level for the first time. This result was possible because of the extremely precise gravitational models developed from the gravity-mapping missions CHAMP and GRACE. The results have been validated with independently developed s/w and our future plans include further additional validation with even more groups.

Interim results are also exchanged and compared with John Ries of Univ. of Texas, who is now using the UTEX software UTOPIA, in a similar reduction approach and obtains similar results. We hope to have UTOPIA results regularly in the near future, as the UTEX group makes time for participation in these experiments. It is our intention to have a new experiment using the new and soon to be released 3rd-generation UTEX model GGM03S, using all s/w packages (GEODYN, EPOS and UTOPIA) and groups, extending our LAGEOS data span by several years (3+) to the present, and incorporating many small but significant model improvements, especially in the temporally varying gravitational signals area due to climate change and global mass redistribution.

In a parallel process we are actively pursuing the optimal design and likely contribution of a new dedicated mission, LARES (Bosco *et al.*, 2006), which is currently in pre-phase B and expected to be in orbit in the next two years. Although not identical to LAGEOS, the improved design of LARES will result in a better LT measurement and expand the list of high-accuracy geodetic targets for TRF and low-degree temporal gravity observations. As explained in (*ibid.*), LARES is being designed with the utmost care for the definition of its "signature", i.e. the precise offset between the effective reflection plane and its CoM, to minimize errors that affect the origin and scale of the TRF. A half-scale model of LARES is shown in

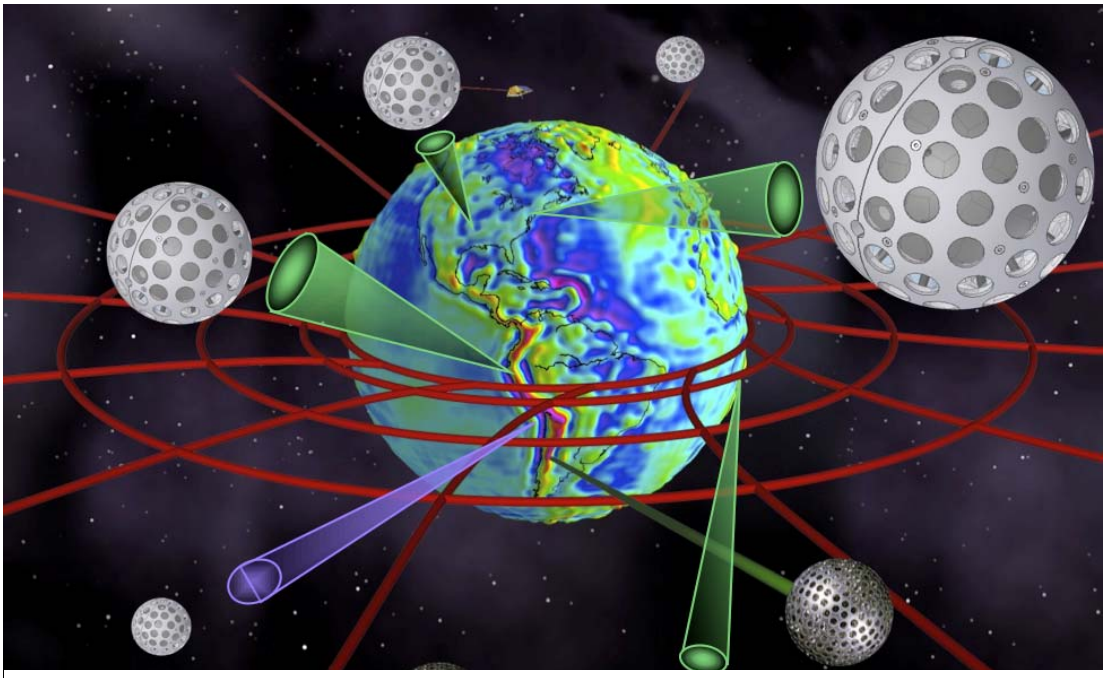

Figure 9*. A visualization of the LT effect on frame coordinate lines and a constellation of geodetic satellite targets which with a small effort could be a reality by the end of this decade.*

Figure 8 along with a mechanical drawing of the current design.

The future launch of LARES and other similar geodetic targets will go a long ways towards the development of a "SLR" constellation (Figure 9). The near-continuous availability of targets at all SLR stations and the improved geometry from the mix of inclinations and nodal longitudes, etc., will lead to a more robust set of SLR products for TRF and POD. Improvement of the gravitational static and temporal models and the availability of other data sets from Earth observing missions will soon allow us to use most of the currently available and future geodetic satellites with laser arrays for highly precise geophysical products.

References

[1] Bosco, A. *et al.*, 2006. "Probing Gravity in NEO with High-Accuracy Laser-Ranged Test Masses," proceedings of "*Quantum to Cosmos"* NASA Int. Workshop, Warrenton, VA, USA, May 2006, *Int. J. Mod. Phys. D*, 8.

[2] Buchman, S. *et al*, 2000. "The Gravity Probe B Relativity Mission," *Adv. in Space Res.* 25(6), p. 1177.

[3] Ciufolini, I., 1989. *Int. J. Mod. Phys.* A 4, 3083.

[4] Ciufolini, I., 1994. *Class. Quantum Grav.* 11, 958.

[5] Ciufolini, I. and J.A. Wheeler, 1995. *Gravitation and Inertia*, Princeton University Press, Princeton, New Jersey.

[6] Ciufolini, I. et al., 1998. Science 279, 2100.

[7] Ciufolini, I. and E. C. Pavlis "A confirmation of the general relativistic prediction of the Lense-Thirring effect", *Nature*, 431, 958-960, 2004.

[8] Ciufolini, I., E. C. Pavlis and R. Peron, 2006. Determination of frame-dragging using Earth gravity models from CHAMP and GRACE, *New Astronomy*, 11, 527-550, 10.1016/j.newast.2006.02.001, Elsevier Science B.V., Amsterdam.

[9] Ciufolini, I., 2007, to be published (arXiv:0704.3338v2).

[10] Everitt, C.W.F., *et al.*, 1980. Report on a program to develop a gyro test of General Relativity in a satellite and associated technology, Stanford University.

[11] Kahn, B., 2007. *StanfordNews*, Press release of April 14, 2007, http://www.stanford.edu/dept/news/pr/.

[12] Lense, J., Thirring, H., 1918. *Phys. Z.* 19, 156. See also English translation by Mashhoon, B., Hehl, F.W., Theiss, D.S., 1984. Gen. Relativ. Gravit. 16, 711.

[13] Murphy, T.W., K. Nordtvedt and S.G. Turyshev, 2007. *Phys. Rev. Lett.* 98, 071102.

[14] Pavlis, E. C., 2002. Geodetic Contributions to Gravitational Experiments in Space, in *Recent Developments in General Relativity, Genoa 2000*, R. Cianci, R. Collina, M. Francaviglia, P. Fré eds., 217-233, Springer-Verlag.

[15] Pearlman, M.R., Degnan, J.J., and Bosworth, J.M., 2002. "The International Laser Ranging Service", *Adv. in Space Res.*, Vol. 30, No. 2, pp. 135-143, 10.1016/S0273-1177(02)00277-6.

[16] Reigber, Ch., *et al*., 2002. GRACE Orbit and Gravity Field Recovery at GFZ Potsdam - First Experiences and Perspectives, Eos. *Trans. AGU*, 83(47), Fall Meet. Suppl., Abstract G12B-03.

[17] Reigber, Ch., *et al.*, 2003. The CHAMP-only Earth Gravity Field Model EIGEN-2, *Adv. in Space Res.* 31(8), 1883-1888 (doi: 10.1016/S0273–1177(03)00162-5).

[18] Reigber, C., Schmidt, R., Flechtner, F., König, R., Meyer, U., Neumayer, K. H., Schwintzer, P., and Zhu, S. Y., 2005. An Earth gravity field model complete to degree and order 150 from GRACE: EIGEN-GRACE02S, *J. Geodyn.* 39, 1.

[19] Ries, J.C., Eanes, R.J., Tapley, B.D., 2003. In: *Non-Linear Gravitodynamics*, The Lense–Thirring Effect. World Scientific, Singapore.

[20] Tapley, B. D., 2002. The GRACE Mission: Status and Performance Assessment, Eos. *Trans. AGU*, 83(47), Fall Meet. Suppl., Abstract G12B-01.

[21] Tapley, B.D., Chambers, D.P., Bettadpur, S., Ries, J.C., 2003. *Geophys. Res. Lett.* 30 (22), 2163.

[22] Tomlin, S., 2007. Interim view from NASA relativity probe, *Nature*, 446, 19 April 2007.

A "Web Service" to Compare Geodetic Time Series

Florent Deleflie[1]

1. Geodesie and Mecanique Celeste Team, Grasse, France

Abstract

We have developed a geodetic database built on the concept of "Virtual Observatory" (http://www.ivoa.net). These time series come from our solutions of Earth Orientation Parameters, stations coordinates and velocities, polar motion, and start at the beginning of the 1990's. Solutions deduced from various techniques are available (SLR data, combined or not...)

This tool enables one to directly compare, in an easy, homogeneous and coherent way, results coming, for example, from various groups. One of the scientific goals consists in making different results be comparable one from another, and to check, for example, if there is or not systematic differences, or if the used reference frames are fully compatible or not.

I will show how this database works (directly through the Web, if it is possible), and I will mention some interesting scientific applications for the future.

Least-square mean effect: Application to the Analysis of SLR Time Series

D. Coulot[1], P. Berio[2], A. Pollet[1]

1. IGN/LAREG - Marne-la-Vallée – France
2. CNRS/OCA/GEMINI - Grasse - France

Contact: David.Coulot@ensg.ign.fr Fax: +33-1-64-15-32-53

Abstract

In this paper, we evidence an artifact due to the least square estimation method and, in particular, to the current modeling used to derive station position time series from space-geodetic measurements. Indeed, to compute such series, we in fact estimate constant (typically over one week) updates of station positions with respect to a priori models (ITRF2000, solid Earth tides, polar tide and oceanic loading effects). Thus, these estimations must underline the physical models which were not taken into account in the a priori modeling (atmospheric and hydrologic loading effects and even unknown signals, in our case).

As shown through the example of the Satellite Laser Ranging measurement processing, it is not the case: the weekly position time series exhibit weekly means of these physical signals but with a supplementary signal at the level of a few millimeters. This is the so-called "least square mean effect".

To avoid this effect, alternative modeling such as periodic series can be used. A method to compute such periodic series for the station positions together with the geocenter motion is also presented in this paper.

Introduction

This paper comprises four parts. First of all, we present the least square mean effect from two points of view, theoretical and numerical. Secondly, we propose alternative models to reduce this effect. Then, we study a new method to process Satellite Laser Ranging (SLR) data. This method should help to use alternative modeling for a global network. Finally, we provide some conclusions and prospects.

1. Least square mean effect

The quality presently reached by space-geodetic measurements allows us to study geodetic parameters (Earth Orientation Parameters (EOPs), station positions, Earth's gravity field, etc.) under the form of time series. The modeling currently used to derive such time series is the following. The physical effects which are well understood are modeled (take as examples solid Earth tides or oceanic loading effects for station positions). These models are used to compute a priori values for the parameters worthy of interest and we compute the parameters with respect to these a priori values. These estimations are supposed to be constant over a given time (typically one day for EOPs and one week for station positions). And these estimations should help us to study the underlying physical effects (atmospheric loading effects, for instance). But, to do so, we need exact and judicious representations. We show that it is not really the case for the current modeling in this section.

1.1. Theoretical considerations

We consider a vector of physical parameters $\vec{X}$ which vary with time. According to the modeling used, we split this vector in two parts: the modeled effects $\vec{X}_0$ and the effects we

want to study through time series $\delta\vec{X}$, $\vec{X}(t) = \vec{X}_0(t) + \delta\vec{X}(t)$ .We know that the vector $\delta\vec{X}$ varies with time but, in order to get a robust estimation, we suppose it constant over a given interval $[t_1, t_m]$. And, doing so, we hope that the constant estimations $\delta\hat{\vec{X}}$ will correspond to the averages of the underlying physical signals over this interval. The measurements used are modeled with a function f ($m(t) \cong f(t, \vec{X})$) which is linearized

$$m(t) \cong f(t, \vec{X}_0(t)) + \frac{\partial f}{\partial \vec{X}}(t, \vec{X}_0(t)).\delta\vec{X} \qquad \text{with} \frac{\partial f}{\partial \vec{X}}(t, \vec{X}_0(t)),$$

the partial derivative matrix of f at the point $(t, \vec{X}_0(t))$) to get the least square model. Furthermore, we can also linearize the measurements but with respect to the true signal to be studied ($m(t) \cong f(t, \vec{X}_0(t)) + \frac{\partial f}{\partial \vec{X}}(t, \vec{X}_0(t)).\delta\vec{X}(t)$).

As a consequence, on one hand, we have a relation between the measurements and the constant updates to be estimated and, on the other hand, a relation between these measurements and the true physical signal to be studied. From these two relations, we get the following observation equation:

$$f(t, \vec{X}_0(t)) + \frac{\partial f}{\partial \vec{X}}(t, \vec{X}_0(t)).\delta\vec{X} \cong f(t, \vec{X}_0(t)) + \frac{\partial f}{\partial \vec{X}}(t, \vec{X}_0(t)).\delta\vec{X}(t)$$

This observation equation allows us to build the following system:

$$A.\delta\vec{X} \cong \widetilde{A}.\delta\vec{\widetilde{X}}$$

with $A = \begin{bmatrix} \frac{\partial f}{\partial \vec{X}}(t_1, \vec{X}_0(t_1)) \\ \frac{\partial f}{\partial \vec{X}}(t_2, \vec{X}_0(t_2)) \\ \vdots \\ \frac{\partial f}{\partial \vec{X}}(t_m, \vec{X}_0(t_m)) \end{bmatrix}$,

$$\widetilde{A} = \begin{bmatrix} \frac{\partial f}{\partial \vec{X}}(t_1, \vec{X}_0(t_1)) & 0 & \cdots & 0 \\ 0 & \frac{\partial f}{\partial \vec{X}}(t_2, \vec{X}_0(t_2)) & \cdots & 0 \\ \vdots & \vdots & \ddots & \vdots \\ 0 & 0 & \cdots & \frac{\partial f}{\partial \vec{X}}(t_m, \vec{X}_0(t_m)) \end{bmatrix},$$

and $\delta\vec{\widetilde{X}} = \begin{pmatrix} \delta\vec{X}(t_1) \\ \delta\vec{X}(t_2) \\ \vdots \\ \delta\vec{X}(t_m) \end{pmatrix}$.

This system is then used to compute the least square solution with a weight matrix *P*:

$$\delta\hat{\vec{X}} \cong \delta\vec{X}_{average} + \left(A^T PA\right)^{-1} A^T P\tilde{A}.(\delta\tilde{\vec{X}} - \delta\tilde{\vec{X}}_{average})$$

$$\text{with } \delta\tilde{\vec{X}}_{average} = \begin{pmatrix} \delta\vec{X}_{average} \\ \delta\vec{X}_{average} \\ \vdots \\ \delta\vec{X}_{average} \end{pmatrix} \text{ and } \delta\vec{X}_{average} = \frac{1}{t_m - t_1}\int_{t_1}^{t_m} \delta\vec{X}(u)du \,.$$

In this solution, we can see that the estimations effectively contain the averages of the involved signals over the time interval but with a complementary term. We have called this term the "least square mean effect".

1.2. Numerical examples

In this section, we provide some numerical examples based on simulations. Here is the method used to carry out these simulations (cf. Fig.1). The first step is the two LAGEOS satellite orbit computation with GINS software. These orbits are used, in a second step, with ITRF2000 [Altamimi et al., 2002a] and a model for atmospheric loading effects to compute simulated range measurements and partial derivatives of these latter with respect to station positions. Then, we estimate station positions without any atmospheric loading effect in the a priori model. Thus, the estimated positions must reflect these non modeled effects. These estimations are finally compared with the temporal averages of the atmospheric loading effect models. We use real orbits and real SLR measurement epochs in order to get the most realistic simulations. European Center for Medium-range Weather Forecasts (ECMWF, http://www.ecmwf.int/) pressure fields were used to derive the atmospheric loading effect models.

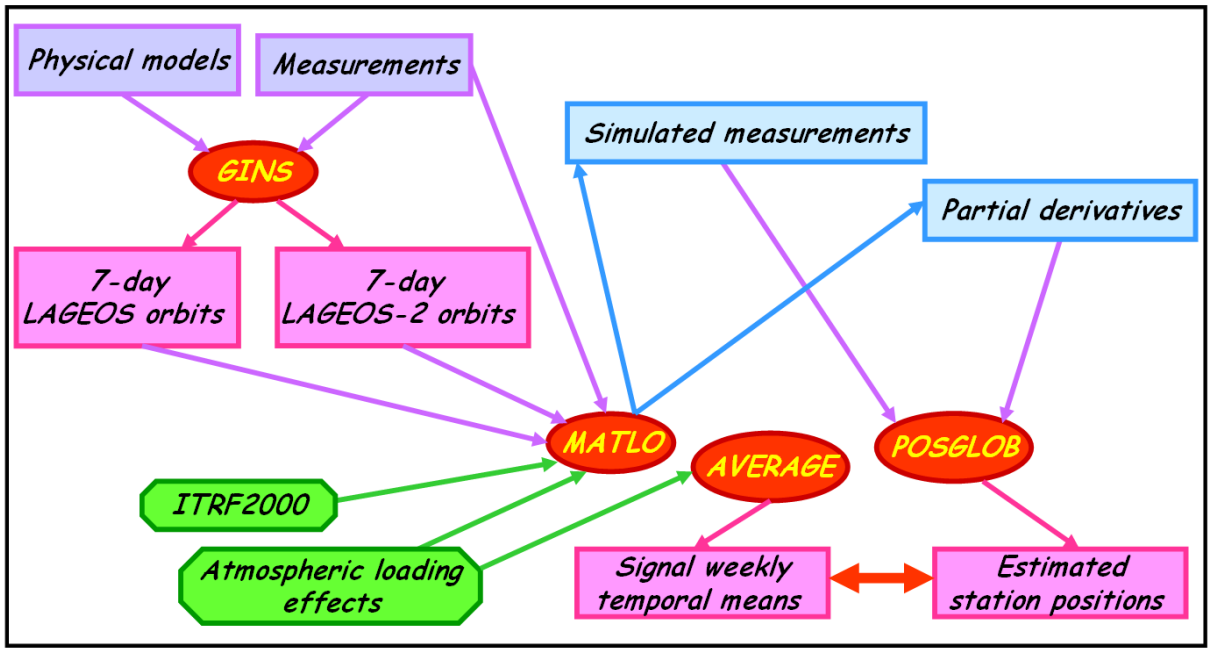

Figure1. *Simulation method.*

Fig. 2 shows the results produced for the station Yarragadee (7090) regarding the three components East, North and Up, in mm. In the graphs above, black curves correspond to the weekly temporal averages of the atmospheric loading effects and red curves to the estimated

weekly time series. The graph below shows the absolute differences between black and red curves, so the least square mean effects.

Table 1 provides maximum values of differences of a few millimeters (2 mm for the Up component). And, on average, the least square mean effect is approximately 10 % of the amplitude of the loading effects.

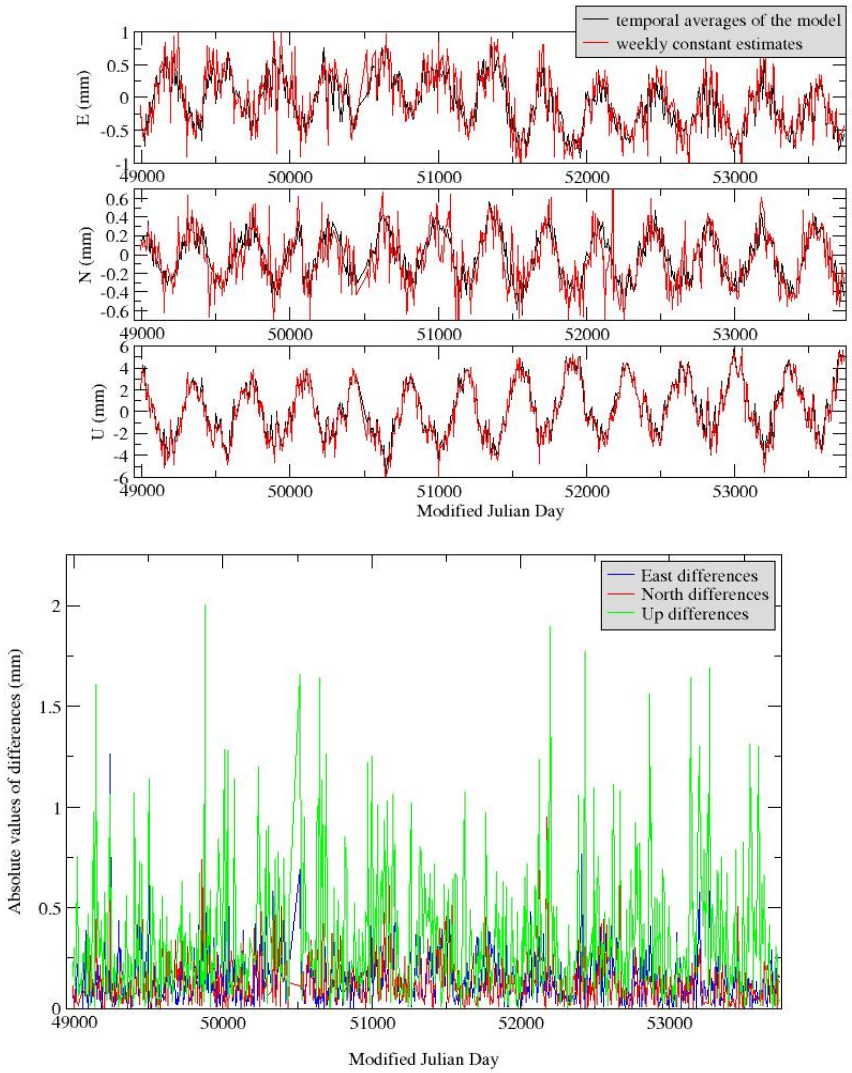

Figure 2. *Simulation results for the station Yarragadee (7090).*
Graphs above: black (resp. red) curves correspond to the weekly temporal averages of the atmospheric loading effects (resp. to the estimated weekly time series) in mm.
Graph below: absolute values of least square mean effects per component in mm.

Table 1. *Statistics of the results shown on Fig. 2.*

Values (mm)	Minimum	Maximum	Average	RMS
East	2.37 10-4	1.26	0.15	0.13
North	1.86 10-5	0.95	0.13	0.12
Up	2.29 10-5	2.00	0.34	0.32

Fig. 3 shows the equivalent results for the Monument Peak station (7110).

Table 2. *Statistics of the results shown on Fig. 3.*

Values (mm)	Minimum	Maximum	Average	RMS
East	1.57 10-4	2.28	0.19	0.21
North	3.87 10-4	1.96	0.19	0.22
Up	3.14 10-5	4.49	0.42	0.51

As shown in Table 2, the effects are even stronger than those obtained for Yarragadee (see Fig.2 and Tab. 1). Indeed, the maximum effect is 4.5 mm for the Up component.

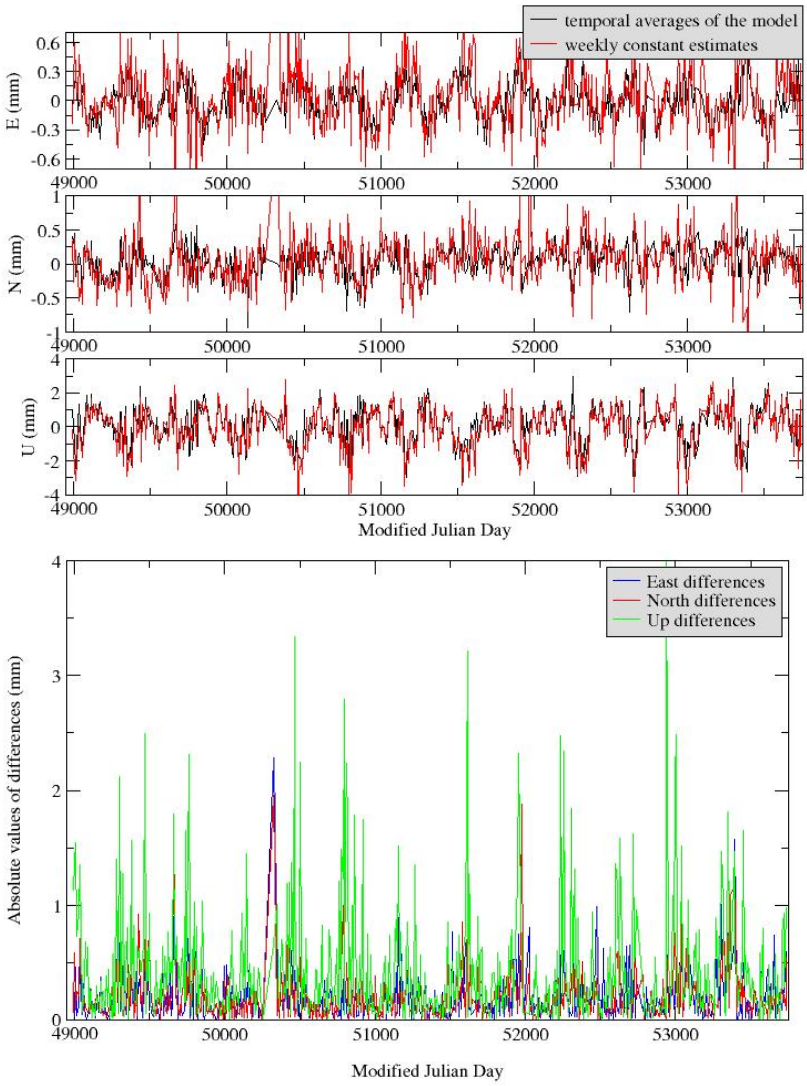

Figure 3. *Simulation results for the station Monument Peak (7110).*
Graphs above: black (resp. red) curves correspond to the weekly temporal averages of the atmospheric loading effects (resp. to the estimated weekly time series) in mm.
Graph below: absolute values of least square mean effects per component in mm.

Thus, this effect is clearly not negligible and we have to take it into account in a geodynamical framework. Indeed, due to this effect, weekly station position time series can not be directly compared to geodynamical models, [Coulot and Berio, 2004] and [Coulot,

2005]. Furthermore, the results provided in [Penna and Stewart, 2003], [Stewart et al., 2005], and [Penna et al., 2007] show that this effect could create spurious periodic signals in the estimated time series. To reduce this effect, we have studied some alternative models.

2. Alternative models

We have studied two alternative modeling. The first one uses periodic terms and the second one is based on wavelets.

2.1. Periodic series

The first model is a periodic one. Each of the three positioning components φ is modeled as periodic series: $\varphi(t) \cong \sum_{i=1}^{n} a_i \cos(\frac{2\pi}{T_i}t) + b_i \sin(\frac{2\pi}{T_i}t)$ where the periods $(T_i)_{i=1,n}$ are the characteristic periods of the involved signals. Instead of estimating weekly φ time series, all available measurements are stacked to compute the coefficients $(a_i)_{i=1,n}$ and $(b_i)_{i=1,n}$.

Fig. 4 shows the results (in mm) provided by simulations for the station Yarragadee (7090). The computational scheme is the same than the one shown on Fig. 1 but the simulated measurements are now used to compute the periodic series. On Fig. 4, blue curves correspond to the model of atmospheric loading effects used to compute the simulated measurements and red curves to the estimated periodic series. We can see a good coherence for the Up component and artifacts near the limits of the considered interval for all components. The less satisfying agreement for the horizontal components is certainly due to the low amplitude of the involved signals and to the poorest sensitivity of SLR measurements with respect to horizontal motions.

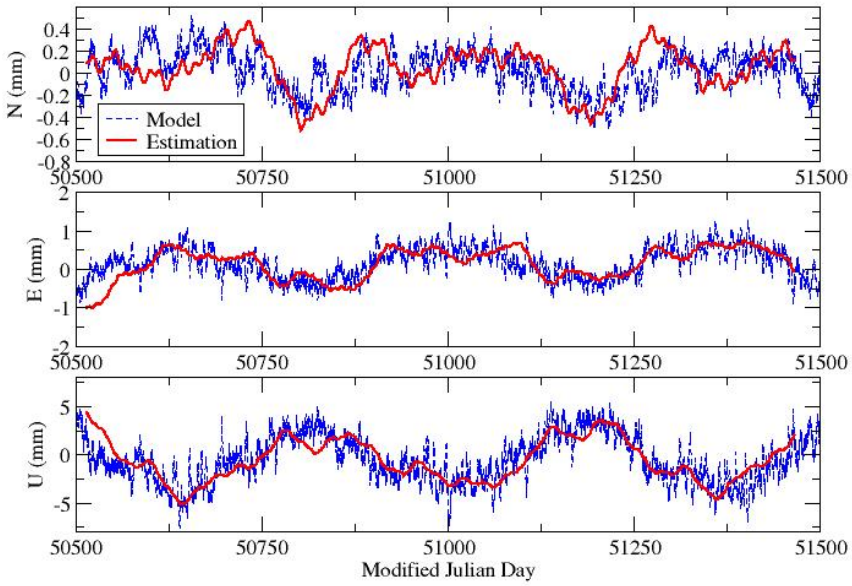

Figure 4. *Periodic series estimated with simulated measurements for Yarragadee station (7090), in mm. Blue (resp. red) curves correspond to the atmospheric loading effect models used to simulate the range measurements (resp. to the estimated periodic series).*

The main advantage of this approach is that no sampling is a priori imposed for estimations but

- the minimal period to be estimated may be imposed by the measurement sampling;

- regarding unknown signals, it will probably be difficult to find the involved periods;
- this model can difficultly take into account discontinuities such as earthquakes.

2.2. Wavelets

To go further, we have also studied a model based on wavelets. We have used, as a first test, the simplest wavelet, Haar's wavelet, for which the core function ψ is defined as follows:

$$\psi(t) = \begin{cases} 1 \text{ if } 0 \le t < \frac{1}{2} \\ -1 \text{ if } \frac{1}{2} \le t < 1 \\ 0 \text{ if not} \end{cases} .$$

Each of the three positioning components φ is modeled by the decomposition of the involved physical signal on the wavelet basis: $\varphi(t) = \sum_{j=-j_1}^{j_2} \sum_{n=0}^{n_{\max}} a_{j,n} \psi_{j,n}(t)$ with

$$n_{\max} = \begin{cases} 2^j - 1 \text{ if } j < 0 \\ 0 \text{ if not} \end{cases} \text{ and } \psi_{j,n}(t) = \frac{1}{\sqrt{2^j}} \psi\left(\frac{t - 2^j n}{2^j} \right).$$

All available measurements are stacked to compute the coefficients $a_{j,n}$. The discontinuities can now be taken into account with the help of this time-frequency representation.

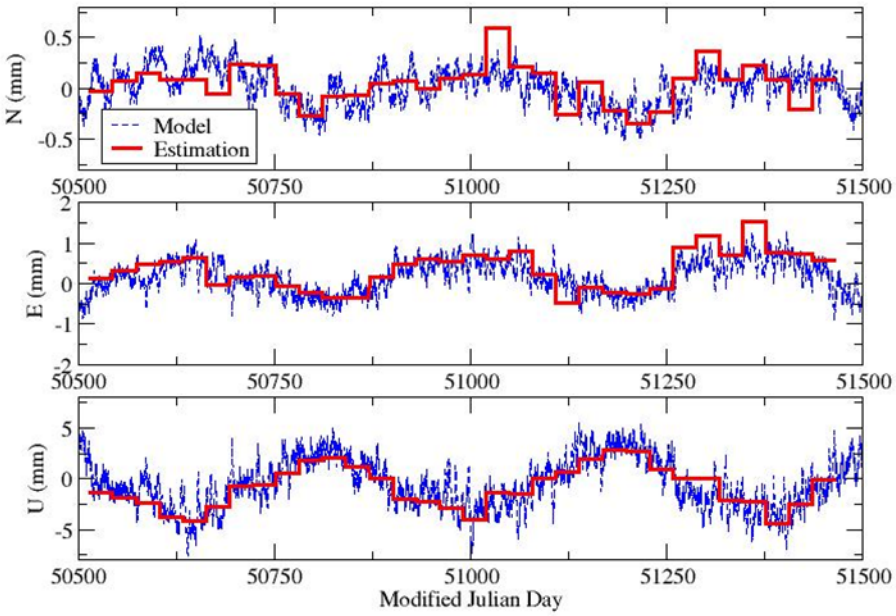

Figure 5. *Wavelet decompositions estimated with simulated measurements for Yarragadee station (7090), in mm. Blue (resp. red) curves correspond to the atmospheric loading effect models used to simulate the range measurements (resp. to the estimated wavelet decompositions).*

Fig. 5 shows the results provided by simulations for Yarragadee station (7090). We can notice the good agreement for the Up component and also the great importance of the smallest scale used for wavelets.

These preliminary results are encouraging but, whatever the model used, we need to guarantee the homogeneity of the involved Terrestrial Reference Frames (TRFs) to carry out such

computations for a station network. Furthermore, we can take the opportunity of such global computation to derive geodynamical signals contained in global parameters such as translations. To reach this goal, we have developed a new approach to process SLR data [Pollet, 2006].

3. New model for SLR data processing

3.1. General considerations

In the "classical approach", the starting point is the observation system Y=A.δX composed by the pseudo measurements Y, the design matrix A and the parameters to be computed δX. By applying weak or minimum constraints, we are able to derive weekly solutions [Altamimi et al., 2002b] (usually, daily EOPs together with weekly station positions for the considered network). On the basis of these weekly solutions, with the help of Helmert's transformation - here are the well-known formulae for station positions and for EOPs [Altamimi et al., 2002a]:

Station positions

$$\delta X = T + DX_0 + RX_0$$

with $T=(T_X, T_Y, T_Z)^T$

and $R=\begin{bmatrix} 0 & -R_Z & R_Y \\ R_Z & 0 & -R_X \\ -R_Y & R_X & 0 \end{bmatrix}$

Earth Orientation Parameters

$$\begin{cases} \delta x_P = R_Y \\ \delta y_P = R_X \\ \delta UT_1 = -\frac{1}{f} R_Z \end{cases}$$

with f=1.002737909350795

we can compute station positions in the a priori reference frame (ITRF2000, for instance) together with coherent EOPs and also 7-parameter transformation between involved TRFs.

The new model we have developed allows us to compute all these parameters in the same process, directly at the observational level. To derive this new approach, we have directly translated Helmert's transformations at the level of the previous observation system: Y=A.δX with δX=δXC+T+DX0+RX0 and δEOP=δEOPC+εR{X,Y,Z}. Doing so, we have replaced the parameters δX and δEOP by new ones: δXC, T, D, R{X,Y,Z} and δEOPC.

Theoretical considerations and numerical tests with SLR data have shown that the rotations R{X,Y,Z} were not needed at all in this model. We did not keep them.

The normal matrices provided by this new approach present a rank deficiency of 7, coming from:

- the fact that SLR data do not carry any orientation information (deficiency of 3);
- the estimation of three translations and a scale factor (deficiency of 4).

This rank deficiency in fact corresponds to the definition of the totally unknown TRF underlying the estimated δXC for which the seven degrees of freedom need to de defined. To do so, minimum constraints [Sillard and Boucher, 2001] are applied with respect to the ITRF2000 and with the help of a minimum network.

3.2. First results

In this section, we provide the preliminary results produced with this new model for SLR data processing over 13 years.

Fig. 6 shows the minimum network used to apply the minimum constraints to define the homogenous weekly TRFs.

Figure 6. *Minimum network used to apply the minimum constraints to define the homogeneous weekly TRFs.*

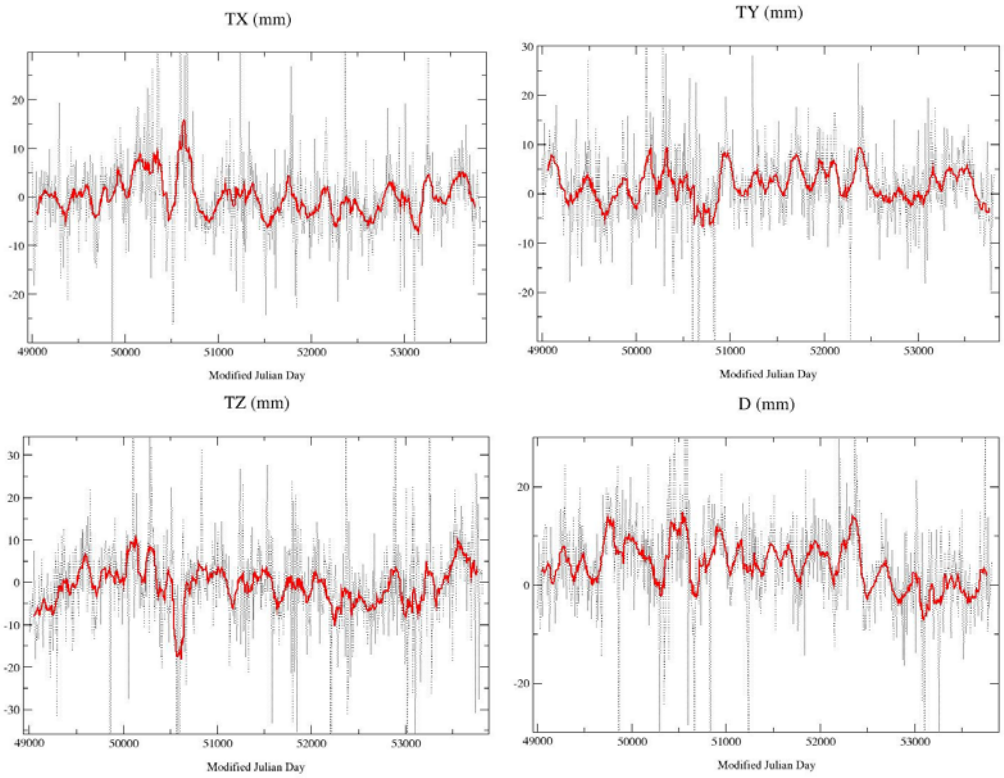

Figure 7. *Weekly time series of the three translations and the scale factor, in mm. Red curves correspond to running averages.*

Fig. 7 shows the four estimated transformation parameters between the weekly TRFs underlying the SLR measurements and directly linked to the two LAGEOS orbit references and the weekly TRFs constrained to be realized in ITRF2000. The three translations exhibit periodic signals (mainly annual) certainly linked to the geocenter motion.

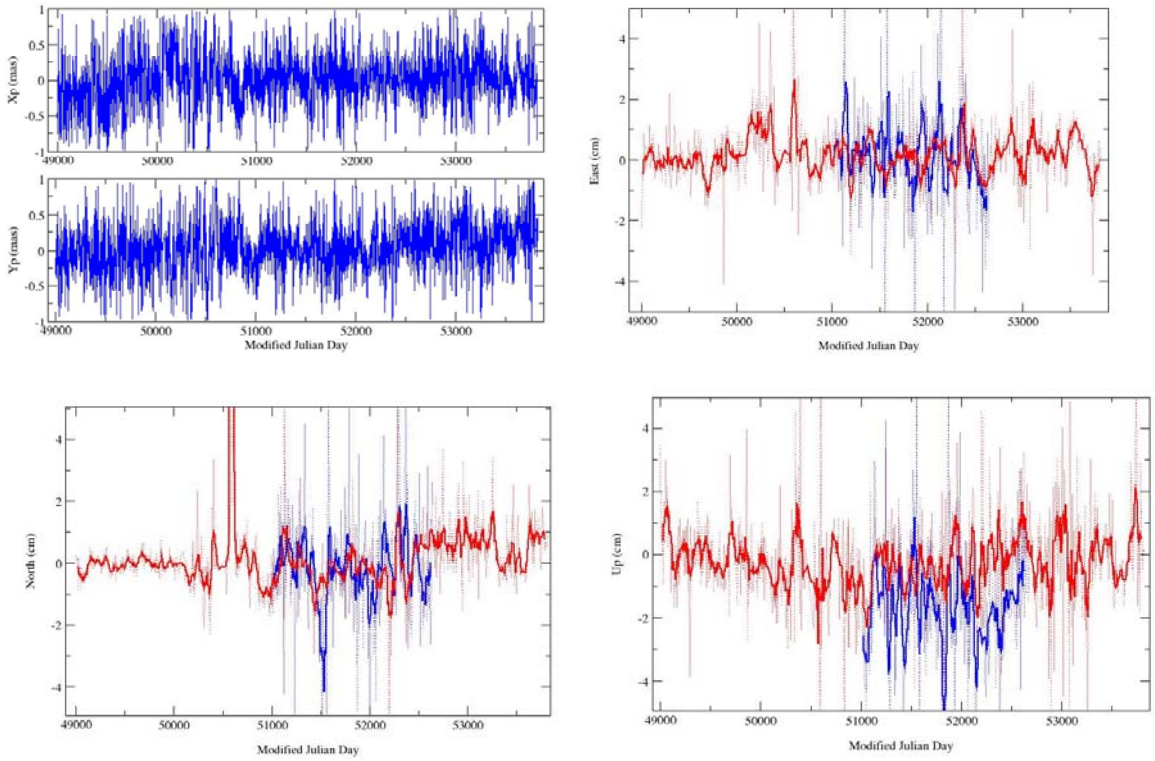

Figure 8. *Results produced with the new method for EOPs and station positions. Graph up left: EOP residuals (mas) with respect to EOPC04 time series [Gambis, 2004] consistent with the estimated station positions. Three other graphs: Mount Stromlo - 7849, in blue- and Yarragadee - 7090, in red- station three positioning component estimated time series (cm).*

Fig. 8 shows the results provided by the new method for EOPs and two Australian SLR stations, Mount Stromlo (blue curves) and Yarragadee (red curves). Regarding EOPs, the weighted biases (resp. the WRMS) are respectively 5µas for Xp and 23µas for Yp (resp. 280µas for Xp and Yp). Regarding the station position time series, we can notice the similarities between these series. The constant difference between the two Up time series is certainly due to range biases which were not taken into account for these computations.

3.3. Toward global estimations over long period

How this new model can help us to reduce the least square mean effect? We can replace the new parameters of the model by previous alternative models such as periodic series in the following example (new parameters to be estimated are underlined in green):

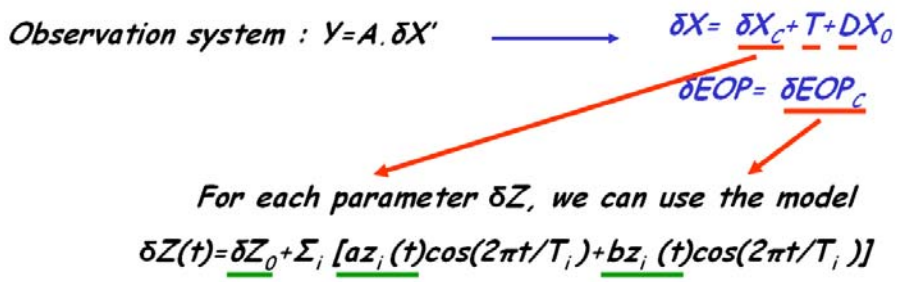

But, each harmonic estimated on station positions generates new rank deficiencies. Consequently, we have to generalize the minimum constraints for harmonic vectors. Furthermore, the number of involved parameters is very large (close to 50 000 in the next example).Thus, we have to use tools allowing the handling of large normal systems.

As a very preliminary computation, we have used this approach to compute amplitudes of annual signals contained in the four global parameters involved. The computation was carried out over 3 years of data. Amplitudes obtained are relatively satisfying (*TX*: 2.1 mm, *TY*: 3.6 mm, *TZ*: 1.1 mm and *D*: 0.9 mm). Moreover, the periodic series really absorb the annual signals as the annual harmonic totally disappears in the residual weekly parameters (the previous parameters called δZ_0) computed with respect to this annual term.

4. Conclusions and Prospects

All these results are satisfying but we of course need to go further by:

- using this periodic approach not only for global parameters but also for station positions;
- computing periodic series directly linked to oceanic loading effects together with series corresponding to atmospheric and hydrologic loading effects;
- deriving diurnal and semi-diurnal signals affecting EOPs with this approach;
- studying the spurious effects provided by this least square mean effect in the International Laser Ranging Service (ILRS) operational products.

We could also couple periodic series with more complex wavelet bases to get a more robust model and, eventually, with stochastic modeling in a filtering framework.

References

[1] Altamimi, Z., P. Sillard, and C. Boucher: “ITRF2000: a new release of the International Terrestrial Reference Frame for Earth science applications”, J. Geophys. Res., 107(B10), 2214, doi: 10.1029/2001JB000561, 2002a.

[2] Altamimi, Z., C. Boucher, and P. Sillard: “New trends for the realization of the International Terrestrial Reference System”, Adv. Space Res., 30(2), p. 175-184, 2002b.

[3] Coulot, D. and P. Berio: “Effet de moyenne par moindres carrés, application à l’analyse des séries temporelles laser”, Bulletin d’Information Scientifique & Technique de l’IGN, 75, p. 129-142, IGN (Eds), IGN-SR-03-083-G-ART-DC, 2004.

[4] Coulot, D.: “Télémétrie laser sur satellites et combinaison de techniques géodésiques. Contributions aux Systèmes de Référence Terrestres et Applications”, Ph. D. thesis, Observatoire de Paris, 2005.

[5] Gambis, D: “Monitoring Earth orientation using space-geodetic techniques: state-of-the-art and prospective”, J. Geod., 78, p. 295-305, 2004.

[6] Penna, N.T. and M.P. Stewart: “Aliased tidal signatures in continuous GPS height time series”, Geophys. Res. Lett., 30(23), p. 2184-2187, doi: 10.1029/2003GL018828, 2003.

[7] Penna, N.T., M.A. King, and M.P. Stewart: “GPS height time series: Short-period origins of spurious long-period signals”, J. Geophys. Res., 112, B02402, doi: 10.1029/2005JB004047, 2007.

[8] Pollet, A.: “Combinaison de mesures de télémétrie laser sur satellites. Contributions aux systèmes de référence terrestres et à la rotation de la Terre.”, Master research course report, Observatoire de Paris, 2006.

[9] Sillard, P. and C. Boucher: “Review of algebraic constraints in terrestrial reference frame datum definition”, J. Geod., 75, p. 63-73, 2001.

[10] Stewart, M.P., N.T. Penna, and D.D. Lichti: “Investigating the propagation mechanism of unmodelled systematic errors on coordinate time series estimated using least squares”, J. Geod., 79(8), p. 479-489, doi: 10.1007/s00190-005-0478-6, 2005.

Some Aspects Concerning the SLR Part of ITRF2005

H. Mueller[1], D. Angermann[1]

1. Deutsches Geodaetisches Forschungsinstitut (DGFI) Alfons-Goppel-Str. 11 80539 Muenchen.

Contact: mueller@dgfi.badw.de Fax: +49 89 23031 1240

Abstract

Two combined solutions for the ITRF2005 were generated independently by two ITRS Combination Centres, IGN, Paris and DGFI, Munich. A comparison of the two ITRF2005P solutions shows in general a good agreement, but the scale and scale rate of the SLR network differs significantly. To investigate this difference a number of tests were performed. It was found that the actual SLR results are consistent with the ITRF2005 solution of DGFI, whereas there is a bias of about 2 ppb compared to the IGN solution. The translation parameters between both ITRF2005 solutions are in good agreement. We also compared the VLBI and SLR scale through co-locations with GPS. This comparison showed the importance of a proper choice and weighting of local ties at co-location sites for the connection of the technique-dependent reference frames. Especially the sites at the southern hemisphere influence the resulting scale of the combined product.

Introduction

Within the re-organized IERS structure, there are three Combination Centres for the International Terrestrial Reference System (ITRS) at Deutsches Geodätisches Forschungsinstitut (DGFI), Munich, Institute Géographique National (IGN), Paris, and National Resources Canada (NRCan), Ottawa. The ITRS Product Center at IGN is coordinating the processing. DGFI and IGN provided each one solution for ITRF2005. Both used their own software and applied their preferred strategy. This guarantees independent results and allows a decisive validation and quality control of the results.

The combination strategy of IGN is based on the solution level by simultaneously estimating similarity transformation parameters w.r.t. the combined frame along with the adjustment of station positions and velocities. The ITRF2005 computations done at DGFI use unconstrained normal equations from the solutions of the different techniques.

This paper briefly summarizes the combination methodology of the ITRS Combination Center at DGFI. Main subject is a comparison of the ITRF2005 solutions of IGN and DGFI. The focus thereby is on the SLR part of ITRF2005.

Combination methodology of DGFI

The general concept of the ITRS Combination Center at DGFI is based on the combination of normal equations and the common adjustment of station positions, velocities and EOP. The computations are performed with the DGFI Orbit and Geodetic Parameter Estimation Software (DOGS). Details on the combination procedure and the mathematical background are given in various publications (e.g., Angermann et al., 2004; Angermann et al., 2006; Drewes et al., 2006; Krügel and Angermann, 2006; Meisel et al., 2005). Figure 1 shows the data flow and the combination methodology for the ITRF2005 computation.

The combination methodology of DGFI comprises the following major steps:

- Analysis of ITRF2005 input data and generation of normal equations
- Analysis of time series and accumulation per-technique (intra-technique combination)
- Comparison and combination of different techniques (inter-technique combination)
- Generation of the ITRF2005 solution by applying minimum datum conditions

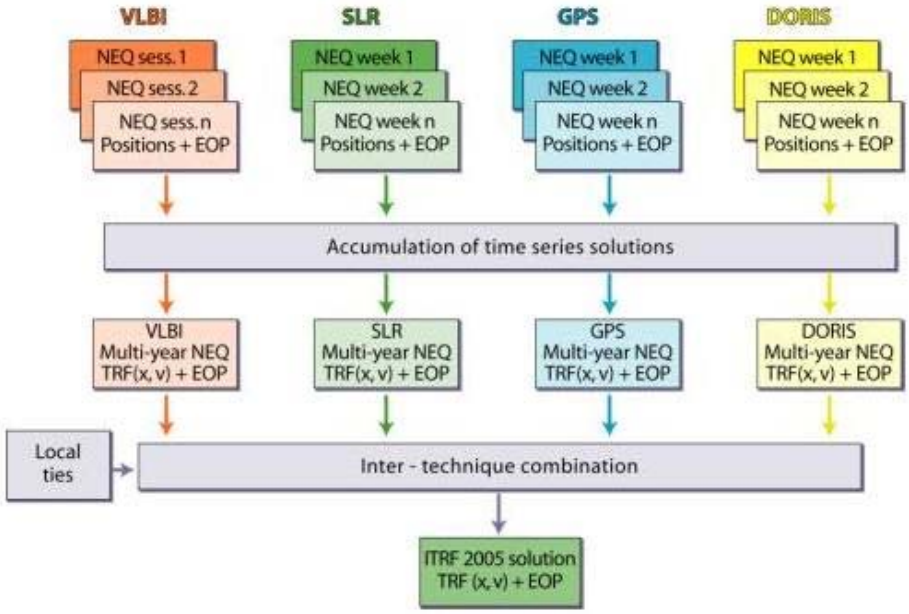

***Figure 1**. Data flow and computation procedure for the ITRF2005 solution of DGFI*

The final ITRF2005 solution comprises station positions, velocities and daily EOP estimates as primary results. In addition epoch position residuals and geocenter coordinates are obtained from the time series combination. The reference epoch for station positions is 2000.0. The rather inhomogeneous data quality and quantity of the space geodetic observation stations is reflected in the accuracy and reliability of the ITRF2005 station position and velocity estimations. This holds in particular for a number of SLR and VLBI stations, but also for some GPS and DORIS stations with few observations. Another aspect is that the new type of ITRF2005 solution contains many stations with several solution ID's. As a consequence the station positions and velocities are valid only for a certain period of time, which has to be known and considered by the users. Furthermore co-location sites may have different station velocities for co-located instruments, if their estimated velocities differ significantly.

Comparison of the ITRF2005 solutions of DGFI and IGN

For comparisons we performed similarity transformations between both solutions. These transformations were done separately for each technique by using good reference stations. The RMS differences for station positions and velocities show a very good agreement (after similarity transformations). This holds in particular for "good" stations with several years of continuous observations without discontinuities (Table 1). For weakly estimated stations (e.g., observation time < 2.5 years, different solutions caused by discontinuities) larger discrepancies do exist, which are in most cases within their standard deviations.

Most of the transformation parameters agree within their estimated standard deviations, except for the scale and its time variation of the SLR network. A significant difference of about 1 ppb (offset) and 0.13 ppb/yr (rate) between the ITRF2005P solutions of DGFI and IGN has been found, which accumulates to nearly 2 ppb in 2006 (see Table 2). The scale difference is not visible in the pure SLR intra-technique solutions of IGN and DGFI. This indicates that the difference between both ITRF2005P solutions is caused within the inter-technique combination.

From these comparisons it is obvious that the major problem of the ITRF2005 is the significant difference in the SLR scale. The analysis of weekly SLR solutions in 2006 has shown that the scale is in good agreement with the ITRF2005P solution of DGFI, whereas

there is a significant scale bias of about 2 ppb w.r.t. the IGN solution (see Figure 2), which is equivalent to a difference of 1.3 cm in SLR station heights. It was argued by IGN that this "scale problem" is a consequence of a scale bias between VLBI and SLR. Because of the apparent discrepancies the scale of the IGN solution was defined by VLBI only, whereas the scale of the DGFI solution is defined by the SLR and VLBI data.

Table 1. *RMS differences for station positions and velocities between IGN and DGFI solutions for ITRF2005 for "good" Reference stations (25 VLBI, 22 SLR, 57 GPS, 40 DORIS stations).*

ITRF2005P DGFI - IGN	Positions [mm]	Velocities [mm/yr]
GPS	0.31	0.14
VLBI	0.79	0.34
SLR	1.82	0.66
DORIS	3.32	1.11

Table 2. *Scale differences between the pure intra-technique and the ITRF2005P solutions of DGFI and IGN.*

	SLR		VLBI	
	offset [ppb]	drift [ppb/yr]	offset [ppb]	drift [ppb/yr]
Pure intra-technique solutions (IGN – DGFI)	-0.17 ± 0.06	0.01 ± 0.02	0.16 ± 0.05	0.01 ± 0.02
ITRF2005 P solutions (IGN – DGFI)	**0.86 ± 0.12**	**0.13 ± 0.03**	-0.12 ± 0.06	0.03 ± 0.03

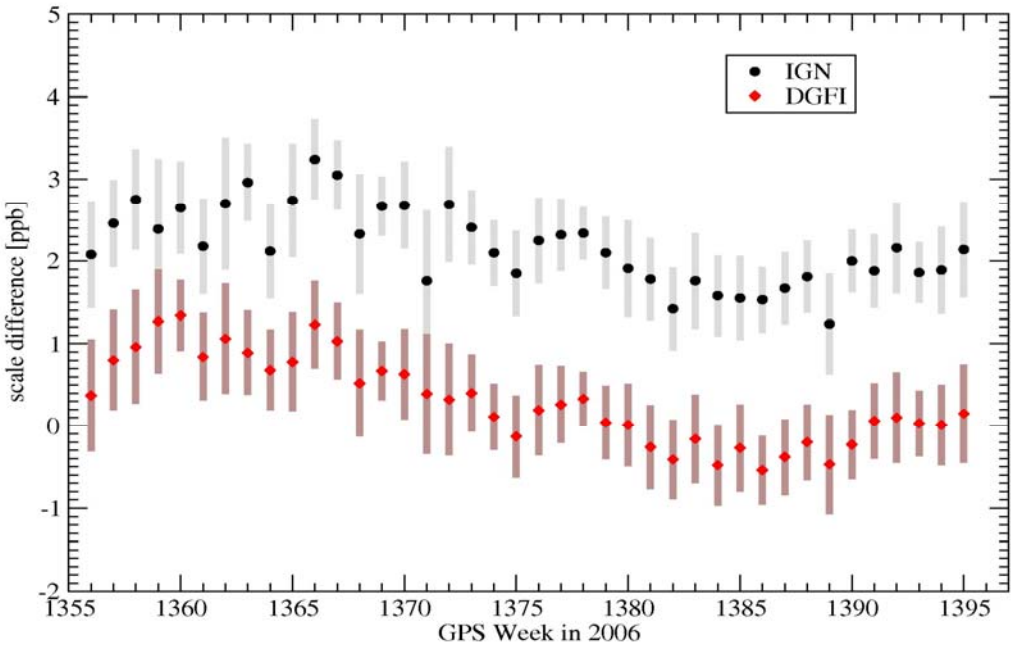

Figure 2. *Scale of ITRF2005P solutions of IGN and DGFI w.r.t. to the combined SLR solution (ILRSA)*

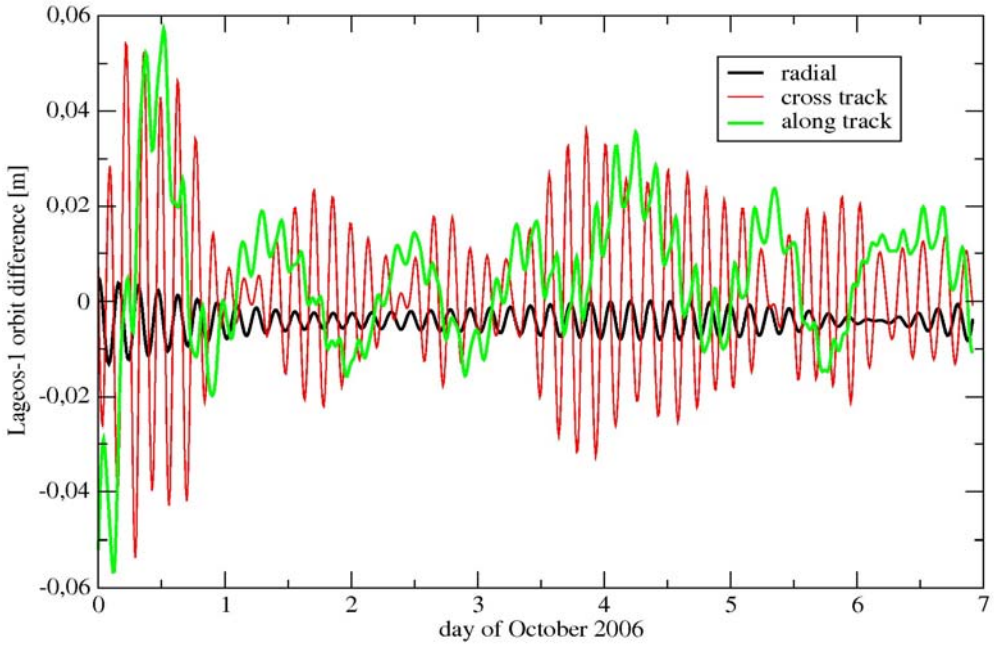

***Figure 3**. Difference between IGN and DGFI solution for a weekly Lageos-1 orbit.*

This scale difference is also reflected in the resulting satellite orbits. For a comparison we solved a weekly Lageos-1 orbit with fixed station coordinates, one with the DGFI solution, the other with the IGN solution, solving for all internal arc parameters and polar motion (X-, Y- pole and dUT1). The resulting orbits were compared in radial, cross- and along track to investigate the influence of the scale difference. In figure 3 the radial offset of about 5 mm is clearly visible. The cross and along track components only show a revolution dependent signal which results from the radial orbit bias, but there is no systematic error. This comparison indicates that the scale of the IGN solution will produce biased satellite orbits.

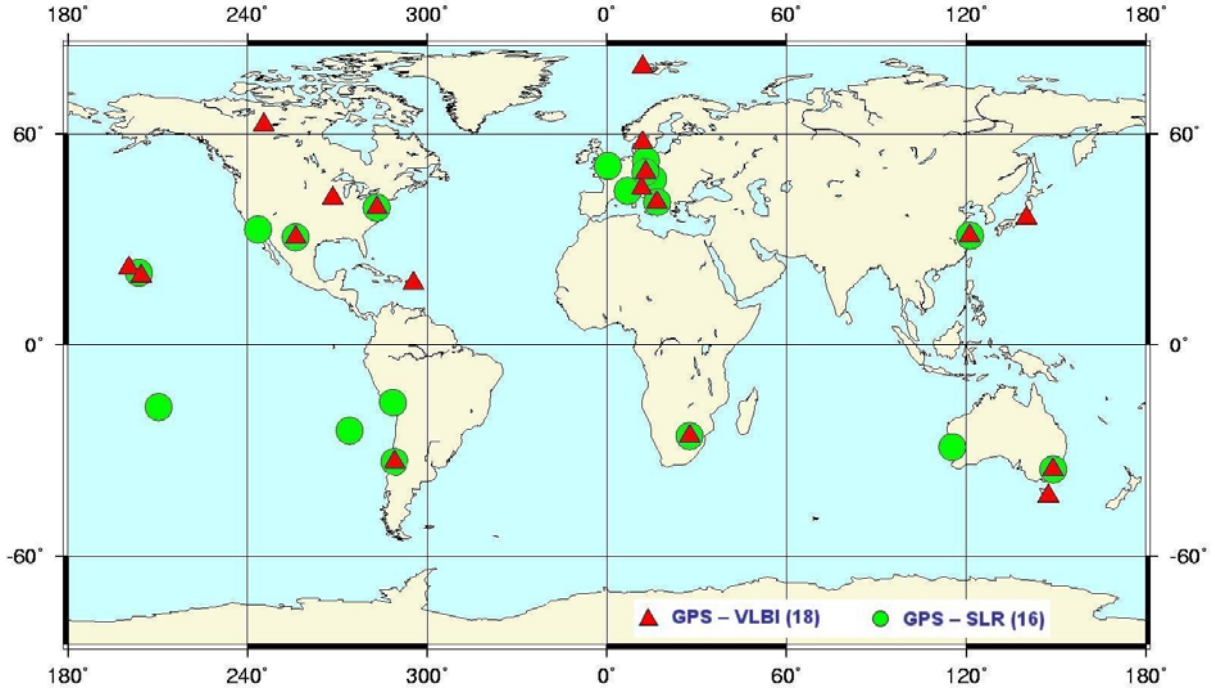

***Figure 4**. Available co-location sites between GPS, SLR and VLBI*

***Figure 5**. Observation period of southern hemisphere collocation sites*

Investigation of the scale differences

We used the intra-technique solutions of the DGFI combination for ITRF2005 to investigate the scale of VLBI and SLR. Since the number and spatial distribution of good co-location sites between VLBI and SLR is not sufficient to get reliable results for a direct comparison of the scale, we used an "indirect" approach via the GPS network and consider the GPS intra-technique solution as reference for this specific study. We used "good" co-location sites and local ties to refer the VLBI and SLR solutions to an "arbitrary" GPS frame (see Fig. 4).

The geographical distribution and quality of SLR tracking stations is in particular problematic in the Southern hemisphere. Therefore we focus on these stations and on the co-locations with GPS. Fig. 5 shows the GPS and SLR observation periods and the estimated ITRF 2005 precision for 8 SLR-GPS co-location sites on the southern hemisphere. DGFI used for the connection of the reference frames all stations except Easter Island and Conception because of poor SLR data. In the IGN solution the Australian sites Yarragadee, Mt. Stromlo, Orroral and Tahiti are down-weighted. Thus the reference frame connection in the IGN solution was realized mainly via the remaining 4 co-location sites on the Southern hemisphere, from which Easter Island and Conception are poorly observed by SLR. This indicates that the integration of GPS and SLR networks in the Southern hemisphere is rather poor in the IGN solution.

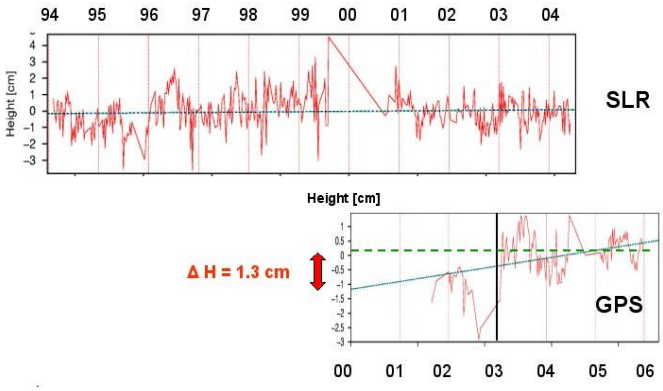

***Figure 6**. Jump in the Haleakala time series*

***Table 3**: Scale difference between SLR and VLBI obtained from DGFI ITRF2005P solution.*

	Δ Scale offset [ppb]	Δ Scale drift [ppb/yr]
SLR - VLBI	0.40 ± 0.42	0.04 ± 0.10
SLR – VLBI *	**0.26 ± 0.41**	**0.03 ± 0.09**

*** : Discontinuity for GPS station Maui introduced**

We also investigated the position time series of co-location sites. As an example Fig. 6 shows the GPS and SLR position time series for the co-location site Maui on Hawaii. A clear jump is visible in the GPS time series at the end of 2002, which affects the height estimation by about 1.3 cm. We have introduced a discontinuity for the GPS station Maui and we solved for two solutions. To test the influence of the jump we performed a 14 parameter similarity transformation between the GPS and SLR solutions and compared the resulting residuals. As shown in Fig. 7 the relatively large height residual for Maui disappeared completely.

The scale parameters obtained from the singularity transformations of the SLR and VLBI solutions w.r.t. GPS are arbitrary numbers, but the difference of the scale parameters is independent from the "arbitrary" GPS scale. The estimated scale difference between VLBI and SLR are shown in Table 3. If the discontinuity for GPS station Maui is introduced the scale differences are 0.26 ± 0.41 ppb for the offset and 0.03 ± 0.09 ppb/yr for the drift. Thus the results of the DGFI ITRF2005P solution do not indicate any evidence for a scale bias between VLBI and SLR.

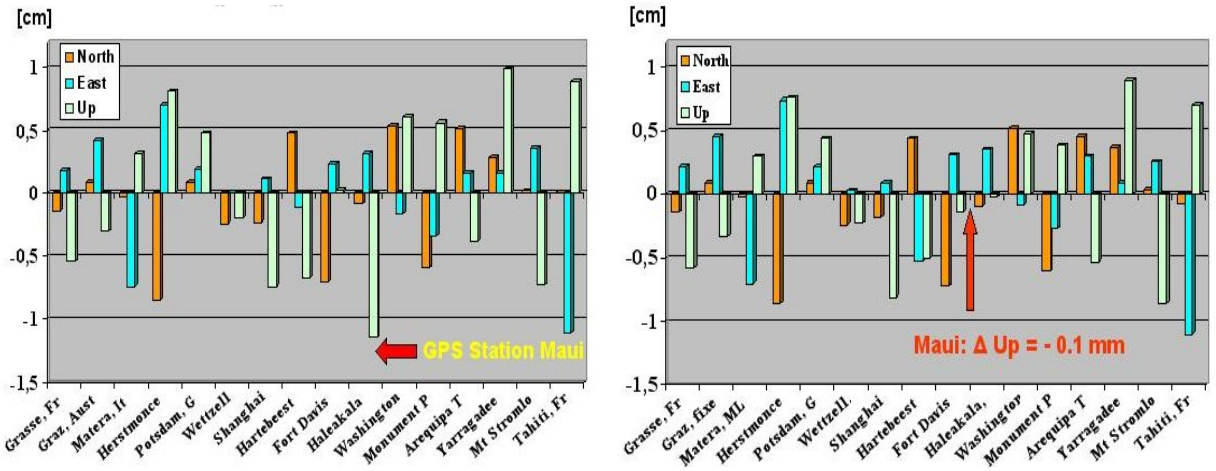

***Figure 7**. Station position residuals for 16 SLR-GPS colocation sites. The left figure shows a height residual for Maui of 1.2 cm, which is reduced to almost zero, if the jump for GPS station is introduced (see right figure).*

Conclusion

The DGFI and IGN for the ITRF2005 are in good agreement for the station positions and velocities (after similarity transformations), but a significant difference has been observed for the scale of the SLR network. As the discrepancies are not visible in the pure SLR intra-technique solutions of IGN and DGFI, they are most likely caused by a different combination procedure and in particular by the implementation of local tie information. Furthermore the IGN solution reveals an apparent difference in SLR and VLBI scales, which led to the exclusion of SLR data for the scale definition of the ITRF2005. The ITRF2005 solution of DGFI does not show this apparent scale difference between SLR and VLBI and it relies on the data of both techniques to define the scale. The analysis of the actual SLR tracking data show a good agreement with the scale of the ITRF2005 solution of DGFI, whereas there is a misfit of about 2 ppb w.r.t. the IGN solution.

Acknowledgement

The authors thank the ILRS (Pearlman et al,2002) for providing the SLR data and the combined weekly SLR intra-technique solutions. For the investigations on the SLR scale we used also the time series of GPS and VLBI intra-technique solutions kindly provided by the IGS and the IVS, respectively.

References

[1] Angermann D, Drewes H, Krügel M, Meisel B, Gerstl M, Kelm R, Müller H, Seemüller W, Tesmer V (2004) ITRS Combination Center at DGFI: A terrestrial reference frame realization 2003, Deutsche Geodätische Kommission, Reihe B, Heft Nr. 313.

[2] Angermann D, Drewes H, Krügel M, Meisel B (2006) Advances in terrestrial reference computations, IAG Symposia Cairns, Springer.

[3] Drewes H, Angermann D, Gerstl M, Krügel M, Meisel B, Seemüller W (2006) Analysis and Refined Computations of the International Terrestrial Reference Frame, Observation of the Earth System from Space, Flury, Rummel, Reigber, Rothacher, Boedecker, Schreiber (Eds), 343-356, Springer.

[4] Krügel M and Angermann D (2006) Frontiers in the combination of space geodetic techniques Proceedings of IAG Symposia Cairns, Springer.

[5] Meisel B, Angermann D, Krügel M, Drewes H, Gerstl M, Kelm R, Müller H, Seemüller W, Tesmer V (2005) Refined approaches for terrestrial reference frame computations, Adv Space Res 36, 350-357, Elsevier.

[6] Pearlman, M.R., Degnan, J.J., and Bosworth, J.M., "The International Laser Ranging Service", Advances in Space Research, Vol. 30, No. 2, pp. 135-143, July 2002.

Determination of the Temporal Variations of the Earth's Centre of Mass from Multi-Year Satellite Laser Ranging Data

Ramesh Govind[1]

1. Geoscience Australia, Canberra, Australia

Abstract

Temporal variation of geodetic parameters (station positions, Earth's gravity field) that are used to monitor global change are referred to a time-varying terrestrial reference system (geocentre, orientation). The time evolution of the geocentre referred to the origin of the terrestrial reference system can be determined from estimates of degree one spherical harmonic representation of the Earth's gravity field. Weekly estimates of the degree one coefficients were undertaken for the period spanning 1993.0 to 2006.8 using SLR data from the global network for four satellites (Lageos-1, Lageos-2, Stella, Starlette). The data set, computation process and results of the geocentre estimates are presented. A comparison of the geocentre estimates from the satellite pairs at two different altitudes is shown. A system to "visualise" the motion of the geocentre as an indicator of mass transport is proposed.

Contribution of Satellite and Lunar Laser Ranging to Earth Orientation Monitoring

D.Gambis[1], R. Biancale[2]

1. Paris Observatory, France
2. CNES Toulouse, France

Abstract

Lunar and Satellite Laser Ranging have been contributing for several decades to Earth orientation variations monitoring. UT0 derived from LLR was used for the period 1976 to 1982 and made the transition between Astrometry and VLBI techniques. Polar motion derived from Lageos observations has a significant contribution in the IERS combinations, mainly thanks to its long term stability. So far Earth orientation parameters and ITRF are derived separately leading to inconsistencies. Rigorous approaches to simultaneously determine a terrestrial reference frame (TRF) and Earth Orientation Parameters (EOP) are now being developed either using SINEX files derived from the different techniques or at the observation level. We present here the results from a coordinated project within the Groupe de Recherches de Geodesie Spatiale (GRGS). Observations of the different techniques VLBI, SLR, LLR, DORIS and GPS) are separately processed by different Analysis centres using the software package GINS DYNAMO. The strength of the method is the use of a set of identical up-to-date models and standards in unique software. The normal equation matrices obtained by the different groups are then stacked to derive weekly solutions of station coordinates and Earth Orientation Parameters (EOP). Results are made available at the IERS site (ftp iers1.bkg.bund.de) in the form of SINEX files.

The analyses we have performed show that for the accuracy and stability of the EOP solution is very sensitive to a number of critical parameters mostly linked to the terrestrial reference frame realization, i.e. minimum constraints application and localities. We present the recent analyses and the latest results obtained.

Station Positioning and the ITRF

Zuheir Altamimi[1]

1. Institut Geographique National, ENSG/LAREG, 6-8 Avenue Blaise Pascal, 77455 Champs-sur-Marne, FRANCE

Abstract

The International Terrestrial Reference Frame (ITRF) as a realization of the International Terrestrial Reference System is one of the scientific products of the International Earth Rotation and Reference Systems Service (IERS). The ITRF is the standard frame recommended for a variety of applications, from surveying to the very fine studies in Earth Sciences. In order to satisfy science requirements, the ITRF should be accurate, reliable and internally consistent over time with unambiguously specified datum definition (origin, scale, orientation and their respective time evolution). Starting with the ITRF2005, the input data requested for the ITRF construction are under the form of time series of station positions and Earth Orientation Parameters (EOPs). Such data do not only allow an appropriate evaluation of the frame accuracy and internal consistency, but also are adequately suited to measure the positioning performance of space geodesy techniques. This paper attempts to review the positioning performance of space techniques via the analysis of the submitted time series to ITRF2005. A special focus will also be given to address the current accuracy level of the ITRF datum definition.

Introduction

The concept of reference systems and frames is one of the fundamental mathematical foundations of modern geodesy with the advent of space techniques since the early eighties. We refer to the pioneering work by a certain number of geodesists and astronomers in (Kovalevsky et al., 1989) who established the foundation of the concept of reference systems and frames followed and used as a basis for the ITRF derivation. Indeed, it is fundamental to adopt that clearly defined concept which distinguish between the system as a theoretical inaccessible mathematical model and the frame as the numerical realization of the system. Moreover, the frame is not only accessible to the users but it is also by essence perfectible, being based on and derived from space geodesy observations.

Using the commonly accepted model of 7(14)-parameter euclidian similarity (also known as Helmert or Bursa-Wolf parameters), it becomes then straightforward to estimate discrepancies between solutions over the frame physical parameters. This is the case for instance where large translation components are often found between SLR on one hand and GPS or DORIS solutions on the other hand. Less scattered temporal behavior of the SLR translation components (as seen from time series analysis), compared to GPS or DORIS, leads to privilege SLR for the ITRF origin definition. Regarding the scale, it is of course admitted that from the theoretical and technology point of view, VLBI and SLR techniques should agree on the TRF scale. However, because we have the possibility to check for their scale consistency (or inconsistency), then when comparing their respective solutions, the possible inconsistency is obviously due to some systematic errors that should be investigated.

The ITRF Product Center hosted by the Institut Géographique National, France, together with the contribution of the ITRF combination centers (DGFI and NRCan) released the ITRF2005 solution in October 2006. Contrary to previous ITRF versions,

the ITRF2005 integrates time series of station positions and daily Earth Orientation Parameters (EOP's). The ITRF2005 input time-series solutions are provided in a weekly sampling by the IAG International Services of satellite techniques: the International GNSS Service-IGS (Dow et al. 2005), the International Laser Ranging Service-ILRS (Pearlman et al., 2002) and the International DORIS Service-IDS, (Tavernier et al., 2006), and in a daily (VLBI session-wise) basis by the International VLBI Service-IVS (Schlueter et al., 2002). Each per-technique time-series is already a combination, at a weekly basis, of the individual Analysis Center (AC) solutions of that technique, except for DORIS where two solutions are submitted by two ACs, namely the Institut Géographique National (IGN) in cooperation with Jet Propulsion Laboratory (JPL) and the Laboratoire d'Etudes en Geophysique et Oceanographie Spatiale (LEGOS) in cooperation with Collecte Localisation par Satellite (CLS), designated by (LCA).

Reasons for which it was decided to use time series of station positions and EOPs as input to ITRF2005 include:

- monitoring of non-linear station motions and all kinds of discontinuities in the time series: Earthquake related ruptures, site instability, seasonal loading effects, etc;
- rigorously and consistently including EOPs in the combination and ensuring their alignment to the combined frame;
- examining the temporal behavior of the frame physical parameters, namely the origin and the scale;
- assessing space geodesy positioning performance, through the estimation of the weekly (daily) Weighted Root Mean Scatter (WRMS) with respect to the long-term solution resulting from the stacking of the time series.

In the following sections we will primarily focus on two main issues: the positioning performance of space geodesy techniques and the temporal behavior of the SLR origin and the scale and the VLBI scale of the contributed solutions to the ITRF2005.

Combination Methodology

The approach that is currently adopted for the combination of various TRF solutions provided by a single or several space geodesy techniques is built on the construction of a unique (combined) TRF, making use of the mathematical (7)14-parameter euclidian similarity. It considers defining the combined TRF at a given (arbitrary) reference epoch and adopting a TRF time evolution law that is supposed to be linear (secular). Consequently, 14 degrees of freedom are always necessary to completely ensure the TRF datum definition: 6 for the TRF origin and its rate (time derivative), 2 for the scale and its rate and 6 for the orientation and its rate. The inclusion of EOPs into the combination requires additional equations where the link between the TRF and EOPs is ensured via the 6 orientation parameters. The combination model considered by the ITRF Product Center allows the estimation of station positions and velocities, transformation parameters of each individual TRF solution with respect to the combined TRF and, if included, consistent series of EOPs. The input solutions usually used in this kind of combination are either (1) time series of station positions and EOPs or (2) long-term solutions composed by station positions and velocities and EOPs. In the first case where the combination amounts to rigorously stacking the time series, the un-modeled non-linear part of geodetic parameters are implicitly embedded in the combination output: possible seasonal (e.g. annual or semi-annual) station or/and geocenter motions are respectively left in the output time series of

station residuals and the transformation parameters. For more details, regarding the combination methodology the reader may refer to (Altamimi et al. 2007a, 2007b).

Positioning Performance

When stacking station positions time series (weekly for satellite techniques and daily for VLBI), global WRMS per week (day) is computed, that is to characterize the internal precision and repeatability over time of each individual position time series. Figure 1 illustrates the WRMS per week (day) for each one of the 4 technique time series over the horizontal and vertical components and Table 1 summarizes the WRMS range. It is to be noted that the WRMS values do not qualify the techniques, but rather the solutions of the techniques which were submitted to the ITRF2005, and they are highly dependent on the quality of each station/instrument. Other factors are also important such as the number of the satellites available, e.g. in case of DORIS it was shown (Altamimi et al. 2006) that the quality (WRMS) improves when the number of satellites increases. However, from Figure 1 and Table 1, we can postulate that the current positioning performance for the best cases is around 2 mm for the horizontal component and around 5 mm for the vertical component.

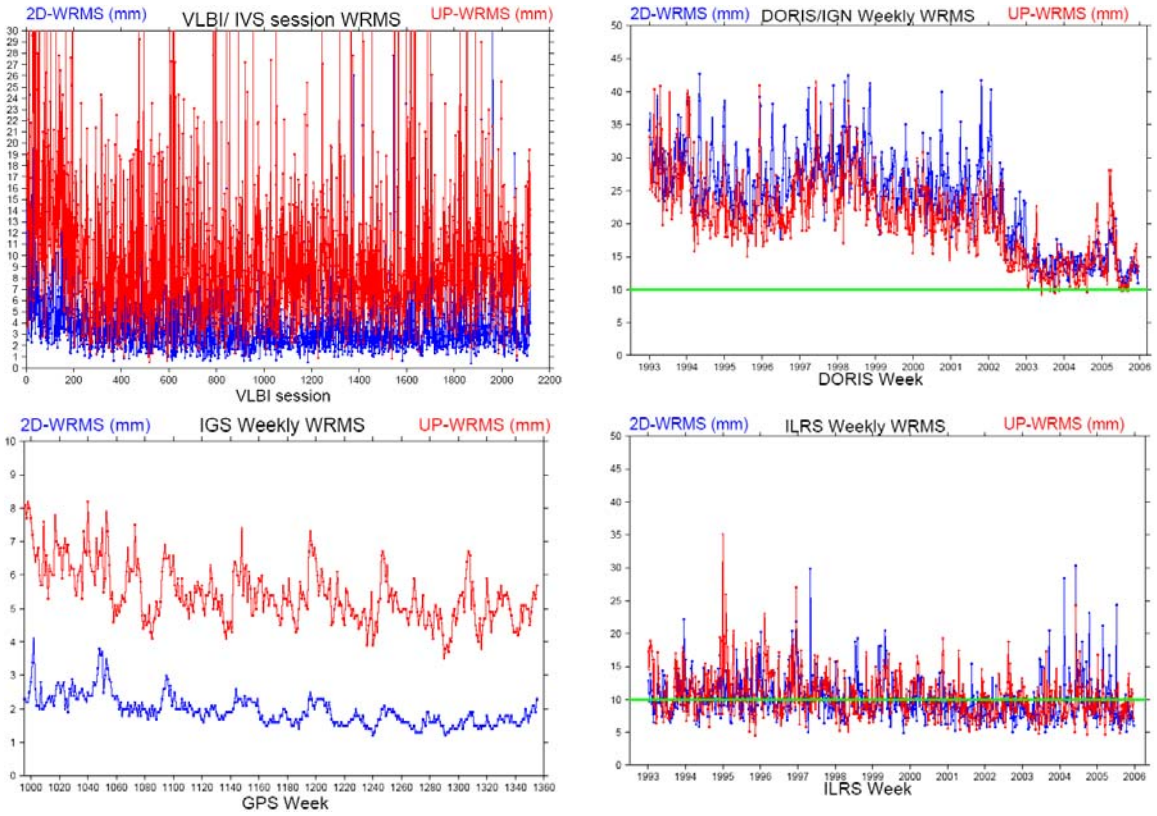

***Figure 1**. Weekly (daily) WRMS as results from the time series stacking.*

Accuracy of the ITRF Origin and Scale

The Origin

Although it is hard to assess the origin accuracy of the single ILRS solution that is submitted to ITRF2005, we attempt however to evaluate its consistency with respect to ITRF2000. Figure 2 shows the 3 translation time variations with respect to ITRF2000, using a reference set of 12 stations. Given their observation history and good performance, these are the only stations that are usable to link the combined

Table 1. *WRMS range per technique*

Solution	2-D WRMS mm	Up WRMS mm
VLBI	2-3	5-7
SLR	5-10	5-10
GPS	2-3	5-6
DORIS	12-25	10-25

SLR TRF resulting from the stacking of the time series to the ITRF2000 frame. Because the estimated transformation parameters are heavily sensitive to the network geometry, the distribution of the reference set of 12 stations is far from being optimal; only two of them are in the southern hemisphere (Yaragadee, Australia, and Arequipa, Peru). Apart from the seasonal variations that could be estimated over the translation parameters, the linear trends are of great importance to the ITRF origin stability over time. From Figure 2 we can easily see that the most significant trend is that of the Z-translation component, being of the order of 1.8 mm/yr. This bias will therefore exist between ITRF2000 and ITRF2005, and could be regarded as the current level of the origin accuracy as achieved by SLR. From that figure we can also distinguish a "piece-wise" behavior of the Z-translation: between respectively 1993-1996; 1996-2000 and 2000-2006. In our opinion, this is completely related to and correlated with the change of the ILRS network geometry over time. In order to illustrate that effect, we plotted on Figure 3 the number of SLR stations available in each weekly solution. From this plot, one can easily see the decreasing tendency of the number of stations, starting around 2000, which should be correlated with the Tz component that starts to significantly drifting at this same epoch (see Figure 2). In addition, among the approximately 80 SLR stations available in the ITRF2005, approximately 20 of them have sufficient time-span of observations to be considered as core stations for useful and comprehensive analysis.

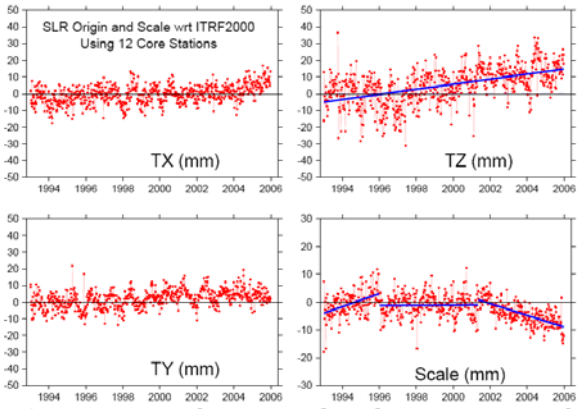

Figure 2*. Translations and scale variations with respect to ITRF2000 of the ILRS SLR time series submitted to ITRF2005.*

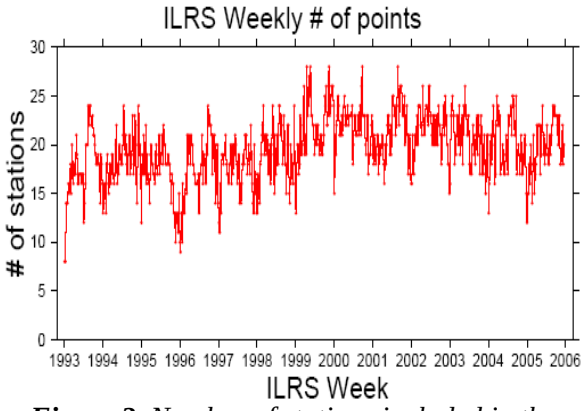

Figure 3*. Number of stations included in the weekly ILRS SLR time series submitted to the ITRF2005.*

The Scale

The ITRF2005 combination (making use of local ties in co-location sites) revealed a scale bias of 1 ppb between VLBI and SLR solutions at epoch 2000.0 and a scale drift of 0.08 ppb/yr. VLBI scale selected to define that of ITRF2005 is justified by (1) the availability of the full VLBI history of observations (26 years versus 13 for SLR)

embedded in the submitted time series and (2) the the non-linear behavior (discontinuities) observed in the ILRS scale (see Figures 3). In order to illustrate more the inconsistency between the two scales, Figure 4 displays both scales with respect to ITRF2005, showing a clear bias both in the offset and the linear trend.

The accuracy assessment of the ITRF scale is not easy to evaluate, being dependent on several factors, as for instance, the quality and distribution of the local ties, the SLR range bias effect, the tropospheric modeling in case of VLBI and other possible systematic errors of the two techniques. However, given the level of consistency mentioned above between VLBI and SLR scales and despite the optimistic accuracy estimate of the ITRF2000 datum definition as stated in (Altamimi et al., 2002), and to be more conservative, we can postulate that the current level of accuracy of ITRF scale is around 1 ppb and 0.1 ppb/yr.

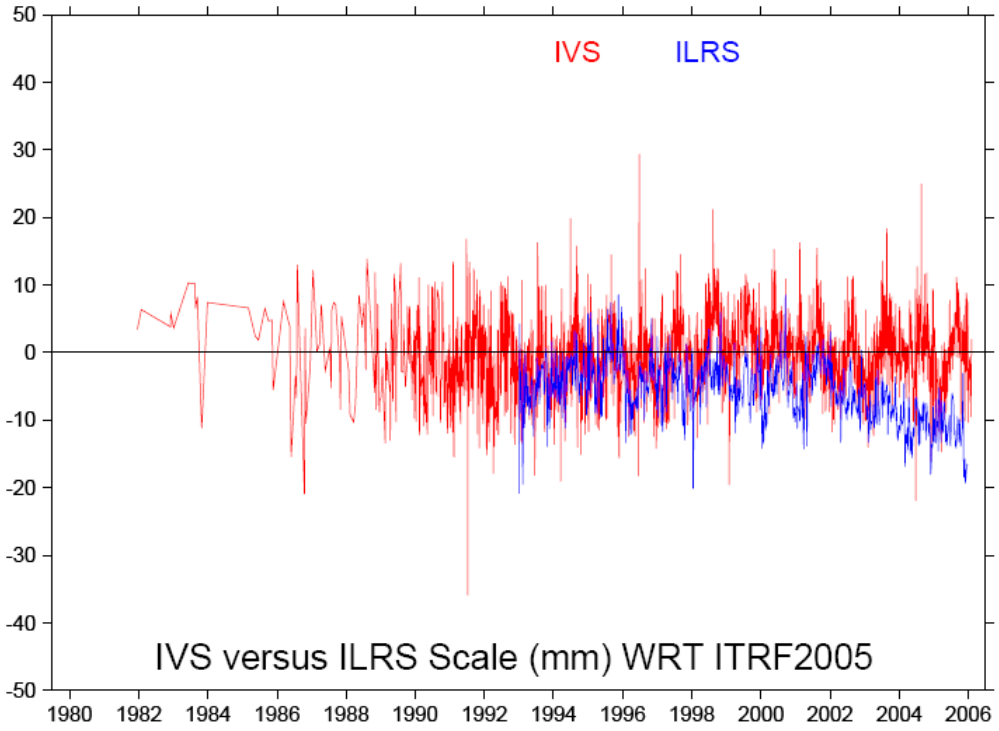

***Figure 4**. VLBI and SLR Scale factor variations with respect to ITRF2005.*

Conclusion

The ITRF2005 experience, using time series as input data, showed how sensitive the frame parameters are to the network geometry and in particular in case of SLR and VLBI and their co-locations. The scale bias between VLBI and SLR solutions revealed by the ITRF2005 combination is most probably due to multiple reasons that include poor VLBI and SLR co-locations, local tie uncertainties, systematic errors and possible differences in correction models (e.g. troposphere, SLR range bias, relativity) employed in the data analysis of both techniques. As results from the ITRF2005 analysis, the positioning performance at the weekly/daily basis, range between 2 to 25 mm, depending on the measurement technique, the instrument quality or station performance.

References

[1] Altamimi, Z., P. Sillard and C. Boucher (2002), ITRF2000: A New Release of the International Terrestrial Reference Frame for Earth Science Applications, Journal of Geophys. Res., 107(B10), 2214, doi:10.1029/2001JB000561.

[2] Altamimi, Z., X. Collilieux and C. Boucher, (2007a), Accuracy assessment of the ITRF datum definition, VI Hotine-Marussi Symposium of Theoretical and Computational Geodesy: Challenge and Role of Modern Geodesy, International Association of Geodesy, in press.

[3] Altamimi, Z., X. Collilieux J. Legrand, B. Garayt and C. Boucher, (2007b), ITRF2005: A new release of the International Terrestrial Reference Frame based on time series of station positions and Earth Orientation Parameters, Journal of Geophys. Res., in Press.

[4] Altamimi, Z., X. Collilieux, C. Boucher, 2006, DORIS Contribution to ITRF2005, Journal of Geodesy, doi: 10.1007/s00190-006-0065-5.

[5] Dow J.M, R.E. Neilan and G. Gendt, 2005, The International GPS Service (IGS): Celebrating the 10th Anniversary and Looking to the Next Decade, Adv. Space Res. 36 vol. 36, no. 3, pp. 320-326, doi:10.1016/j.asr.2005.05.125.

[6] Kovalevsky, J., Mueller, I. I., and B. Kolaczek (Eds.), 1989, {\it Reference Frames in Astronomy and Geophysics,} 474 pp., Kluwer Academic Publisher, Dordrecht.

[7] Pearlman, M.R., J.J. Degnan and J.M. Bosworth, 2002, The International Laser Ranging Service, Adv. Space Res., Vol. 30, No. 2, pp. 135-143.

[8] Schlueter W., E. Himwich, A. Nothnagel, N. Vandenberg, and A. Whitney, 2002, IVS and Its Important Role in the Maintenance of the Global Reference Systems, Adv. Space Res., Vol. 30, No. 2, pp. 145-150.

[9] Tavernier, G., H. Fagard M. Feissel-Vernier, K. Le Bail, F. Lemoine, C. Noll, R. Noomen, J.C. Ries, L. Soudarin, J.J Valette, and P. Willis, 2006, The International DORIS Service: genesis and early achievements, in DORIS Special Issue, P. Willis (Ed.), Journal of Geodesy, 80(8-11):403-417, doi: 10.1007/s00190-006-0082-4.

Station Coordinates, Earth Rotation Parameters, and Low Degree Harmonics from SLR within GGOS-D

R. Koenig[1], H. Mueller[2]

1. GeoForschungsZentrum Potsdam (GFZ)
2. Deutsches Geodaetisches Forschungsinstitut (DGFI), Alfons-Goppel-Str. 11, 80539 Muenchen.

Contact: koenigr@gfz-potsdam.de

Abstract

Time series of station coordinates, Earth rotation parameters, and low degree harmonics of the gravity field are generated in weekly batches from Satellite Laser Ranging (SLR) measurements by two independent German institutes, the Deutsches Geodaetisches Forschungsinstitut (DGFI) and the GeoForschungsZentrum Potsdam (GFZ) and their two software packages for parameter and orbit determination, DOGS (DGFI Orbit and Geodetic Parameter estimation Software) and EPOS (Earth Parameter and Orbit System) respectively.

The products are based on common standards laid down by a consortium of some more German institutes joined in the GGOS-D (Global Geodetic Observing System - Deutschland (Germany)) project. GGOS-D strives for a rigorous and proper combination of the various space-geodetic techniques. The details of the processing and model standards and the differences with the International Laser Ranging Service (ILRS) "pos&eop" products are presented. A first series covering the years 1993 to 2006 has recently been provided by DGFI and GFZ to the project, initial results are shown and compared.

Introduction

The overall objective of the GGOS-D project is the investigation of the technological, methodological and information-technological realization of a global geodetic-geophysical observing system. The main fields of research are the development and implementation of data collection and data management systems as well as the generation of consistent and integrated geodetic time series for the description and modelling of the geophysical processes in the Earth system. The time series have to be referred to a unique, extremely accurate reference frame, stable over decades, and should be generated in such a way that they can be made available in near real-time to all users in science and society. Methods for a careful internal and external validation shall guarantee a very high reliability.

The space-geodetic techniques, i.e. Global Positioning System (GPS), SLR, and Very Long Baseline Interferometry (VLBI) with the exception of Doppler Orbitography and Radiopositioning Integrated by Satellite (DORIS), contribute to the processing with the models and as far as possible with the same set of parameters being applied by all the participating institutions, the Forschungsgruppe Satelliten Geodaesie (FSG), the Geodetic Institute of the University of Bonn (GIUB), the GFZ, the Bundesamt fuer Kartografie und Geodaesie (BKG), and the DGFI. The SLR part is covered by two independent contributions from DGFI with its DOGS and from GFZ with its EPOS software packages. The analysis should span the period 1983 until present date. A first solution beginning in 1993 up to early 2007 has recently been provided.

Processing

Geometric and dynamic models mainly coincide with those recommended for the routine processing of the so-called “pos&eop” product, weekly station coordinates and Earth Orientation Parameters (EOPs) based on SLR, by the ILRS (see Pearlman et al., 2002) analysis centers (DGFI and GFZ being part there as well). In case of the dynamic models however, the ocean tide model FES2004 (Letellier et al., 2007), and the gravity field model EIGEN-GL04S1 (the satellite-only solution of the EIGEN-GL04C model, see Foerste et al., 2006) have been chosen. Also the ocean tide loading site displacements as provided by Bos and Scherneck (2007) corresponding to the FES2004 are applied.

In a first step we processed weekly arcs for the years 1993 to 2006 solving for weekly stations coordinates, daily EOPs, i.e. X-, Y- pole, and UT1 at 0:00 h UTC, all piecewise linear and continuous (in case of “pos&eop” instead X-, Y- pole, and, notably, LOD at 12:00 UTC, all piecewise constant, are solved for). The GFZ solution additionally incorporates the low degree coefficients of the spherical harmonic representation of the Earth's gravity field (shortly “low degree harmonics”) of degree 0 to 2 (in case of “pos&eop” the low degree harmonics are not solved for). In order to overcome the datum defect, the coordinates, the EOPs, and the low degree harmonics are endowed with an a priori sigma of 1 meter or its equivalent.

First Results

The overall orbital fit and statistics for the whole period are shown in Table 1. The intention was to include as many stations as possible in the solutions. As a minimum however, stations should contribute with more than 10 observations per weekly arc. Besides that, iterative editing has been performed according to some criteria chosen individually by both institutes. This becomes evident in the number of observations used for the processing and the resulting orbital fit, and could end up in some differences of the solved-for parameters. In a next step, DGFI and GFZ are going to compare their editing procedures and to analyse the effect on the solution.

Table 1*. Global orbital fit of the two solutions.*

	EPOS	**DOGS**
No. of Arcs	742	759
Period	25-Oct-1992 - 13-Jan-2007	11-Nov-1992 - 20-May-2007
Global Orbital Fit RMS (cm)	1.04	1.07
No. of Observations	1,749,965	1,997,569
No. of Observations per Arc	2,358	2,632

In Figure 1 the weekly orbital fits of the DGFI solution show that some weeks are determined with worse accuracy, especially prior to 1999 or GPS week 990. This is mainly induced by some poorly performing non-core stations, the orbital fit for the core stations remains stable mostly below 1 cm all over the analysis period. In general, Lageos-1 turns out slightly more accurate than Lageos-2. Once up-to-date corrections for the Stanford-counter range bias problems or for the station dependent centre of mass corrections become available, we expect improved orbits and hence an improved quality of the resulting parameters.

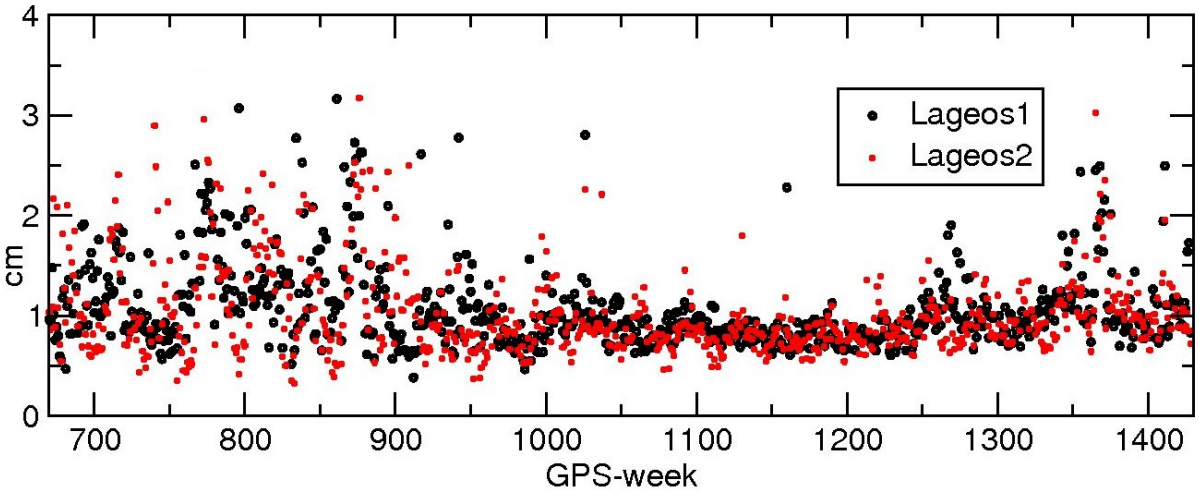

***Figure 1**: Weekly orbital fits of the DOGS solutions.*

Figure 2 shows a comparison of the GFZ C_{20} time series to the recently published series by Cheng and Tapley (2005). Obviously the GFZ series shows a larger scatter, being mainly an effect of the dense resolution of the parameters and of the multitude of solved-for parameters. A generalization of the coordinate and low degree harmonic parameters would presumably stabilize the solution. Underneath the scatter, the general agreement of the curves is visible.

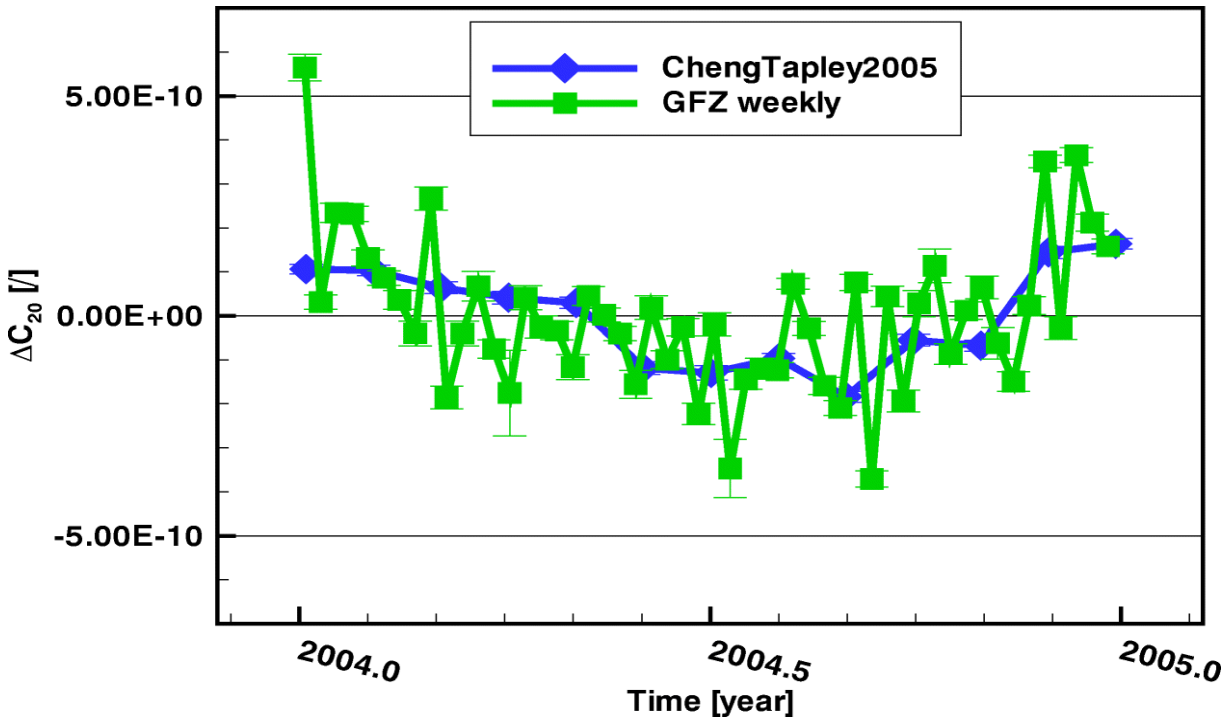

***Figure 2**: Comparison of the EPOS C_{20} time series to the Cheng and Tapley (2005) series.*

The scale differences between the DOGS and the EPOS coordinate solutions are shown in Fig. 3. A small offset of about 1 ppb is visible and may be related to the different editing and to the fact that the GFZ solution has solved in addition for the low degree harmonics including C_{00}, the dynamic scale parameter. The alignment of the editing criteria for DOGS and EPOS, and solving for the low degree harmonics in the DOGS solution as well, should improve the agreement. Also, Fig. 3 reveals a

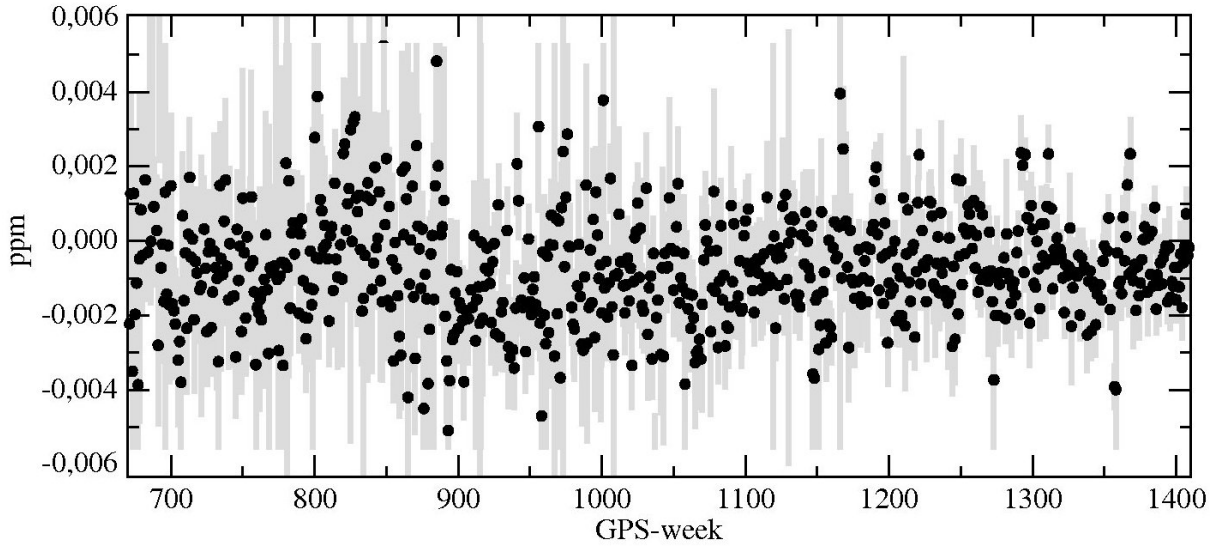

***Figure 3**: Scale differences between the DOGS and EPOS coordinate solutions 1993-2007.*

decrease of the scatter in the course of time, demonstrating the improvement and stabilization of the SLR technique.

Conclusions

Within the GGOS-D project, DGFI and GFZ are processing SLR data with their independent software packages DOGS and EPOS based on common, modern standards. In a first iteration, a 14 year long time series of weekly solutions for coordinates, EOPs, and, in case of GFZ, for low degree harmonics, has been generated. The standards adopted here are different with respect to those of the routine ILRS analysis centre processing.

First results show an excellent quality of the two SLR solutions. Some efforts have to be undertaken to harmonize in particular the editing of the weekly arcs and to include the low degree harmonic parameters to the DGFI solution.

The combination of all space-geodetic techniques within GGOS-D is pending, but first preliminary combinations of GPS and VLBI results indicate an excellent agreement, better than that experienced earlier during the ITRF2005 combinations by DGFI (Meisel et al., 2005).

References

[1] Bos, M.S., Scherneck, H.-G.: *The free ocean tide loading provider website*. http://www.oso-.chalmers.se/~loading, modified 02/03/2007.

[2] Cheng, M., Tapley, B.D.: *Correction to „Variations in the Earth's oblateness during the past 28 years“*. Journal of Geophysical Research, 110, B03406, doi:10.1029/2005JB003700, 2005

[3] Förste, C., Flechtner, F., Schmidt, R., König, R., Meyer, U., Stubenvoll, R., Rothacher, M., Barthelmes, F., Neumayer, H., Biancale, R., Bruinsma, S., Lemoine, J.-M., Loyer, S., *A mean global gravity field model from the combination of satellite mission and altimetry/gravimetry surface data – EIGEN-GL04C*. Geophysical Research Abstracts, 8, 03462, 2006

[4] Letellier, T., Lyard, F., Lefebre, F.: *The new global tidal solution: FES 2004.* http://www.joss-.ucar.edu/joss_psg/meetings/Archived/TOPEX2004/abstracts/D/Letellier.htm, modified 06/-27/2007.

[5] Meisel B, Angermann D, Krügel M, Drewes H, Gerstl M, Kelm R, Müller H, Seemüller W, Tesmer V: *Refined approaches for terrestrial reference frame computations.* Advances in Space Research, Vol. 36, 350-357, Elsevier, 2005

[6] Pearlman, M.R., Degnan, J.J., Bosworth, J.M.: *The International Laser Ranging Service.* Advances in Space Research, 30, 135-143, doi:10.1016/S02731177-(02)00277-6, 2002

An original approach to compute Satellite Laser Range biases

D. Coulot[1], Ph. Berio[2], O. Laurain[2], D. Féraudy[2], P. Exertier[2]

1. IGN/LAREG - Marne-la-Vallée – France
2. CNRS/OCA/GEMINI - Grasse – France

Contact: David.Coulot@ensg.ign.fr / Fax: +33-1-64-15-32-53

Abstract

Although they are permanently calibrated, the Satellite Laser Ranging (SLR) stations can present residual systematic errors, the well-known "range biases". These biases must be considered in any SLR data processing. Indeed, they are strongly correlated with the Up component of the station positions. Thus, if they are not computed together with these positions, they can induce jumps in these latter and consequently damage the global scale factor of the underlying Terrestrial Reference Frame with respect to any given reference.

On the other hand, estimating range biases together with station positions is not so easy, due to the previously mentioned correlations. In this paper, we describe a new approach to derive range bias values together with station positions: the so-called "temporal de-correlation" approach. This method consists in computing station range biases per satellite over a "long" period of time (determined by instrumental changes) together with weekly station position time series in order to significantly reduce the correlations.

Introduction

This paper comprises four parts. First, we provide general considerations about the Satellite Laser Ranging (SLR) technique range biases. Second, we demonstrate the strength of our temporal de-correlation approach through numerical illustrations based on simulations. Then, we analyze the first results produced by this method which has already been used for CALVAL (CALibration/VALidation) experiments and for a SLR data analysis carried out over 12 years. Finally, we describe the recent method improvements, provide the results of this new approach, and produce some conclusions and prospects.

1. General considerations

Fig. 1 shows the Grasse SLR station (7835) Up component time series computed in ITRF2000 without considering any range bias. We can clearly detect a jump in these time series and the epoch of this jump (September 1997) corresponds to a modification of the detection system of the station. This detection system modification has certainly modified the station detection and, as a consequence, its associated systematic errors. As shown by this example, a great attention must be paid to the SLR biases.

As shown on Fig. 2, the International Laser Ranging Service (ILRS) monitors these range biases. Indeed, among all the quality criteria used to qualify the tracking stations, two are directly linked to these biases: the short and long-term bias stabilities.

- The short-term stability is computed as the standard deviation about the mean of the pass-by-pass range biases.

- The long-term stability is the standard deviation of the monthly range bias estimates.

Regarding the data analysis, the situation does not seem to be so clear. Indeed, there are various strategies used to take into account these range biases: not to take biases into account, to correct a priori data with estimated bias values, to compute weekly range biases, etc. This paper aims to describe a method close to the instrumental evolutions of the considered stations. This method allows us to derive range biases by taking into account the problems linked to the simultaneous computation of these latter and station positions.

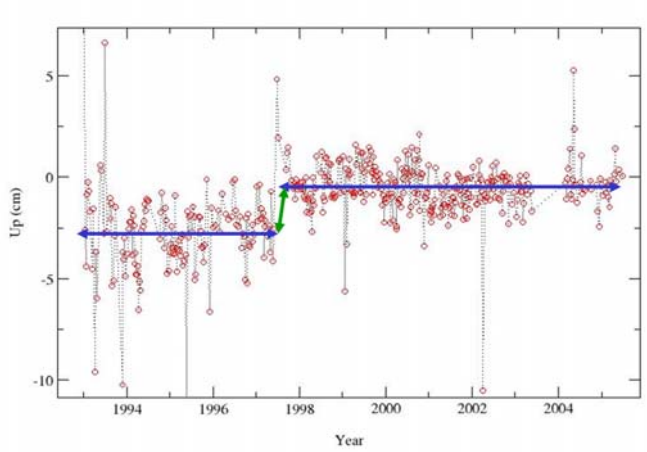

Figure 1. *Up component time series (in cm) of Grasse SLR station (7835) in ITRF2000. No range bias has been estimated nor applied during this computation.*

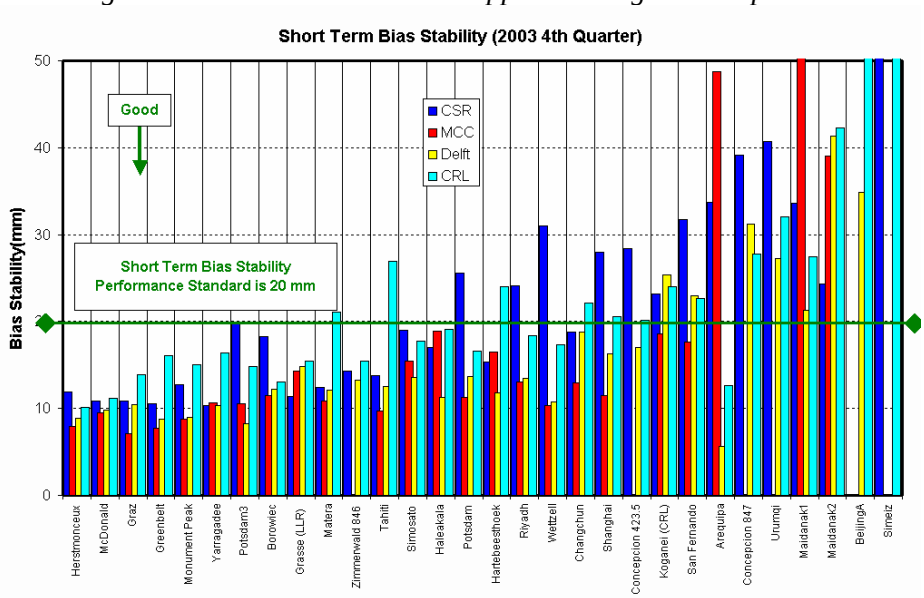

Figure 2. *Example of short-term range bias stabilities provided by ILRS for 2003.*
Source: http://ilrs.gsfc.nasa.gov.

2. Numerical illustrations

The simulations provided here aims to evidence the impact of range biases on any SLR data processing results. Fig. 3 shows the global simulation scheme. The first step consists in estimating the two LAGEOS satellite orbits. Then, these orbits are used with SLR measurements together with ITRF2000 [Altamimi et al., 2002], a model of atmospheric loading effects, and some range bias values to derive, on one hand, simulated range measurements and, on other hand, the partial derivatives of these simulated data with respect to station positions and, eventually, to range biases.

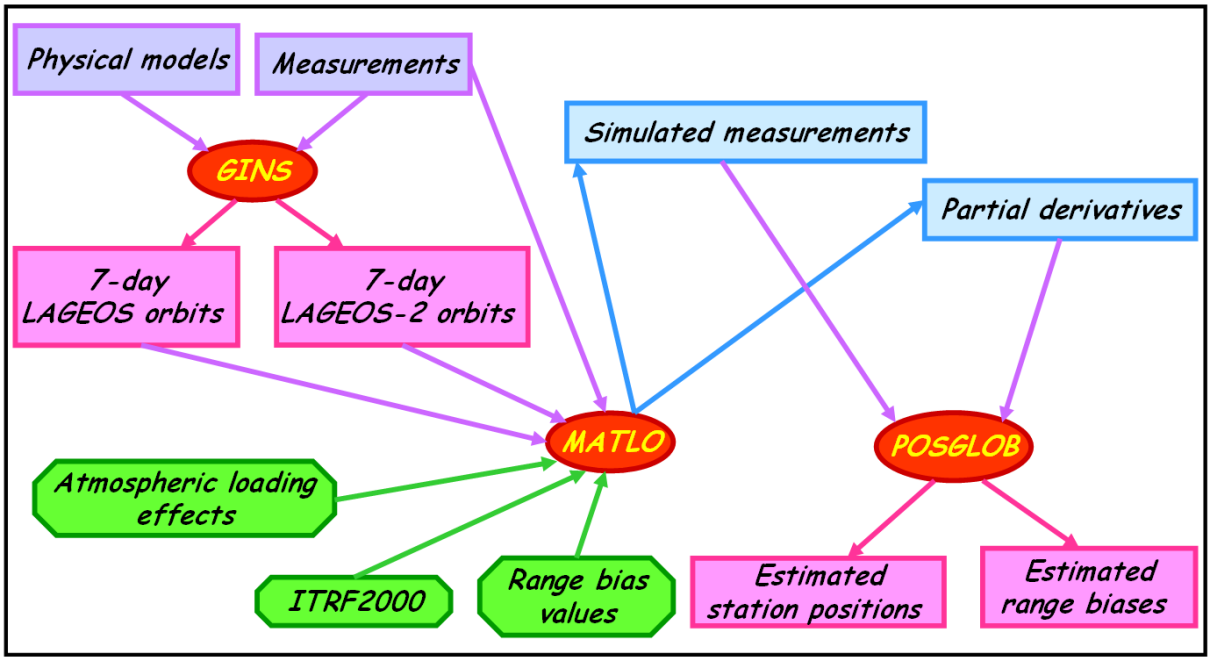

Figure 3. *Simulation method.*

Real orbital arcs and real SLR measurement epochs are used in order to get the most realistic simulations. Atmospheric loading effects are derived from the European Center for Medium-range Weather Forecasts (ECMWF, http://www.ecmwf.int/) pressure grids. As these loading signals are not modeled in the a priori values used, estimated station position time series must evidence them.

For the first simulation (cf. Fig. 4), range biases are applied in simulated measurements but they are not estimated with the Yarragadee SLR station (7090) position time series. The results clearly show that the range biases make a great impact on the Up component time series. Indeed, the time series is completely biased (the mean difference value almost reaches the centimeter level) and is no more stable (the RMS value of the differences is near 5 mm, while the horizontal component RMS values of differences are only at the millimeter level). Thus, range biases must be

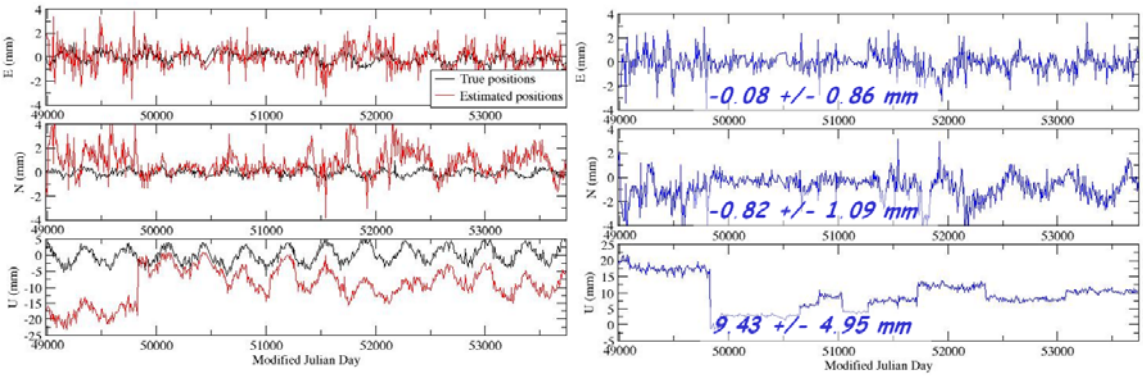

Figure 4. *Results of the first simulation carried out for the Yarragadee SLR station (7090). Values are provided in mm for the three positioning components East, North, and Up. Graphs on the left: black (resp. red) curves correspond to the position time series computed without any bias in simulated measurements (resp. the time series computed with biases applied in simulated measurements). Graphs on the right: differences between red and black curves. Numerical values correspond to the mean and the RMS values.*

estimated together with station positions.

In a second simulation, range biases are applied in simulated measurements and weekly range biases are estimated with the Yarragadee SLR station weekly position time series.

The results shown on Fig. 5 are clearly improved in comparison with those shown on Fig.4. Indeed, the mean value of the Up component differences is divided by 23 and the RMS value by 3.5. Furthermore, the values are also improved for the horizontal components (the difference RMS values are almost divided by 2), proof that range biases can also make an impact (of course lower than the one on the vertical component) on these components. But,

- we can notice large correlations between estimated bias and Up component values (96% on the average);
- spurious signals clearly appear in the weekly estimated biases, even if these latter have made the piece-wise behavior of the Up component time series disappearing.

Thus, range biases must be estimated over a longer period. For the third and last simulation (see the results on Fig. 6), range biases are still applied in simulated

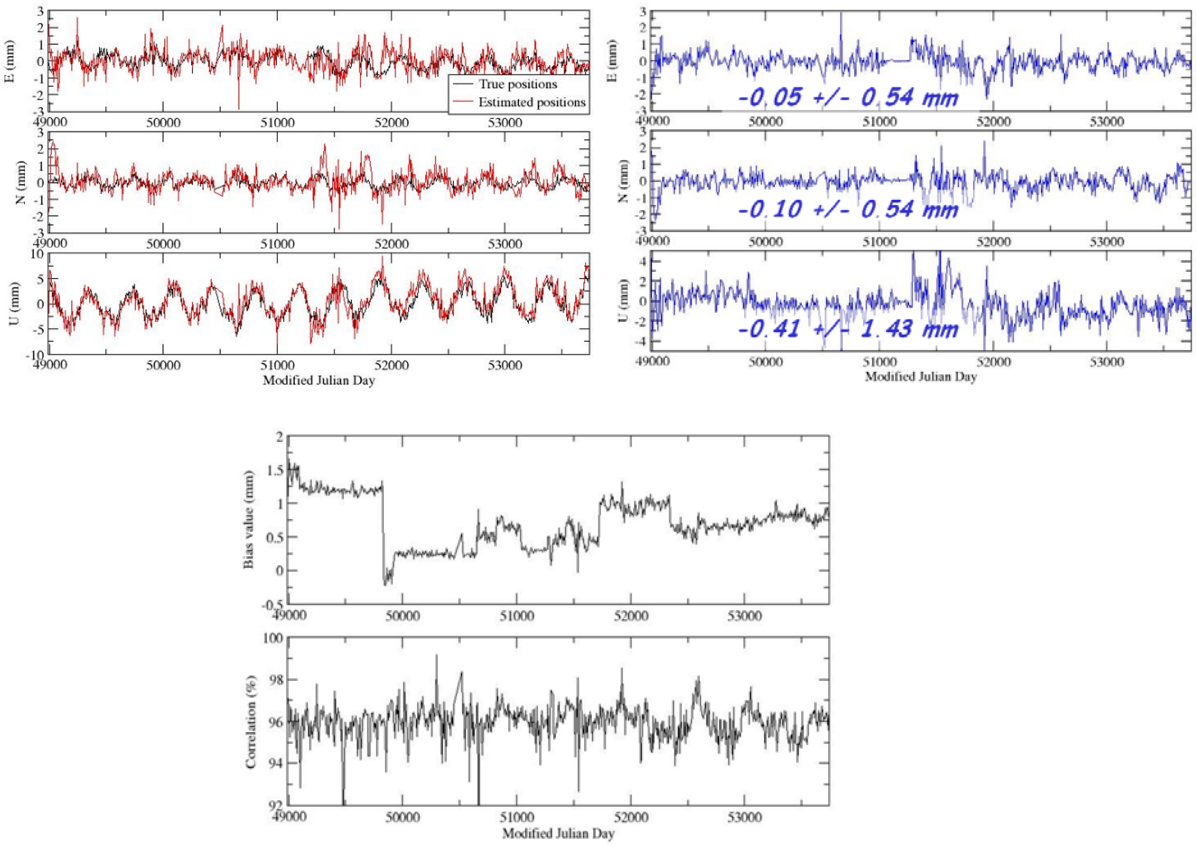

Figure 5. *Results of the second simulation carried out for the Yarragadee SLR station (7090). Values are provided in mm for the three positioning components East, North, and Up. Graphs on the top left: black (resp. red) curves correspond to the position time series computed without any bias in simulated measurements (resp. the time series computed together with weekly range biases with biases applied in simulated measurements). Graphs on the top right: differences between red and black curves. Numerical values correspond to the mean and the RMS values. Graphs below: weekly computed range biases and correlations between bias and Up component estimated values.*

measurements but range biases are now estimated over “long” periods together with the weekly Yarragadee SLR station position time series. The produced results are very satisfying. Indeed, the differences are quite negligible (the mean and the RMS values are below 0.5 mm). Moreover, estimating range biases per satellite allows us to take into account the possible constant signature effects. The correlations have decreased but they are still large (86% on the average).

This approach (that we have called the “temporal de-correlation method”) is the most satisfying one. Moreover, it is fully justified from an instrumental point of view. Indeed, the range biases are directly linked to the tracking instrumentation and we can suppose (at least for the most stable stations) that these instrumentations do not change all the time. As a result, the range biases can be supposed constant over given time intervals.

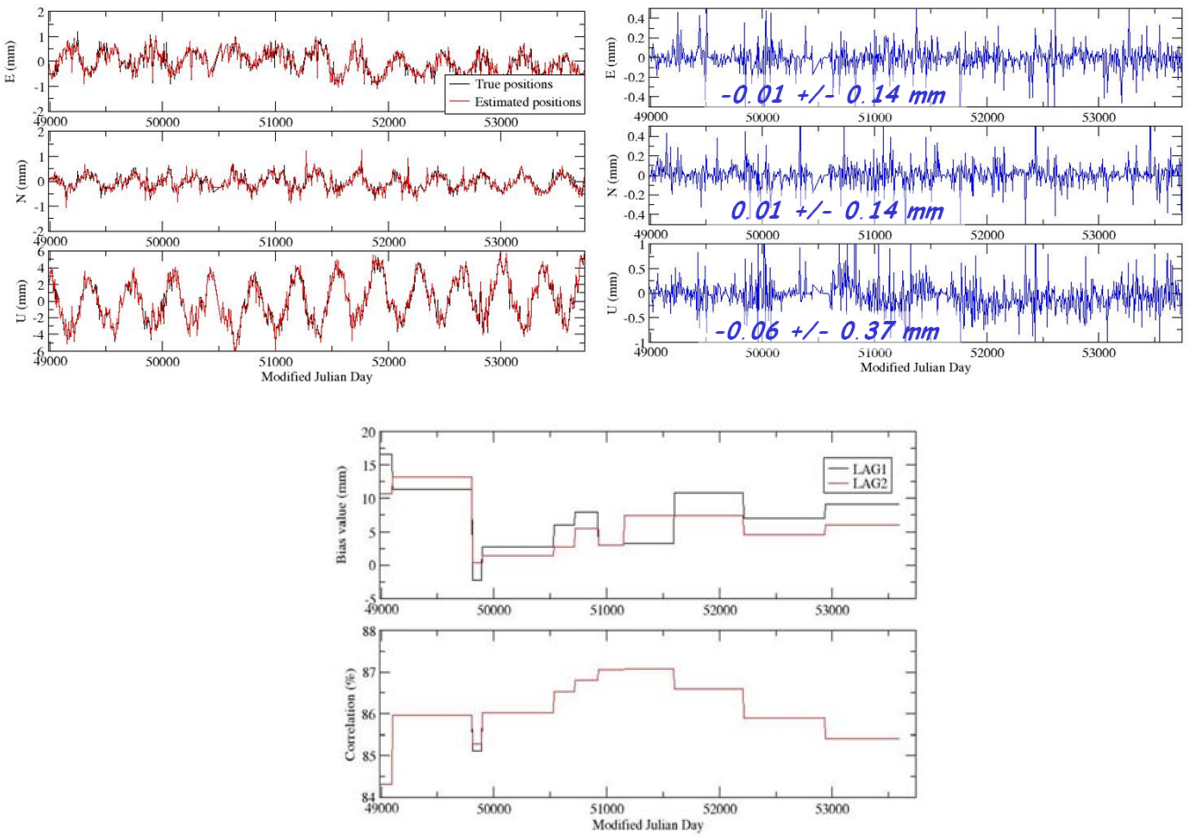

Figure 6. *Results of the third simulation carried out for the Yarragadee SLR station (7090). Values are provided in mm for the three positioning components East, North, and Up. Graphs on the top left: black (resp. red) curves correspond to the position time series computed without any bias in simulated measurements (resp. the time series computed together with the “long-period” range biases with biases applied in simulated measurements). Graphs on the top right: differences between red and black curves. Numerical values correspond to the mean and the RMS values. Graphs below: “long-period” computed range biases per satellite and correlations between bias and Up component estimated values.*

3. First results of the temporal de-correlation method

3.1. CALVAL experiment

These experiments were carried out with the French Transportable Laser Ranging System (FTLRS, see [Nicolas, 2000]) in Corsica in 2002 [Exertier et al., 2004] (and, more recently, in 2005) and in Crete in 2003 [Berio et al., 2004]. As an illustration of the use of our temporal de-correlation method, here is the example of the GAVDOS project, e.g. of the Crete campaign carried out in 2003. During such campaign, the FLTRS aims to calibrate the satellite altimeter (see Fig. 7) with the help of a short-arc technique [Bonnefond et al., 1995]. Thus, we need the most accurate positioning for this transportable station as well as an exhaustive knowledge of its error budget and, in particular, an accurate estimate of its range bias.

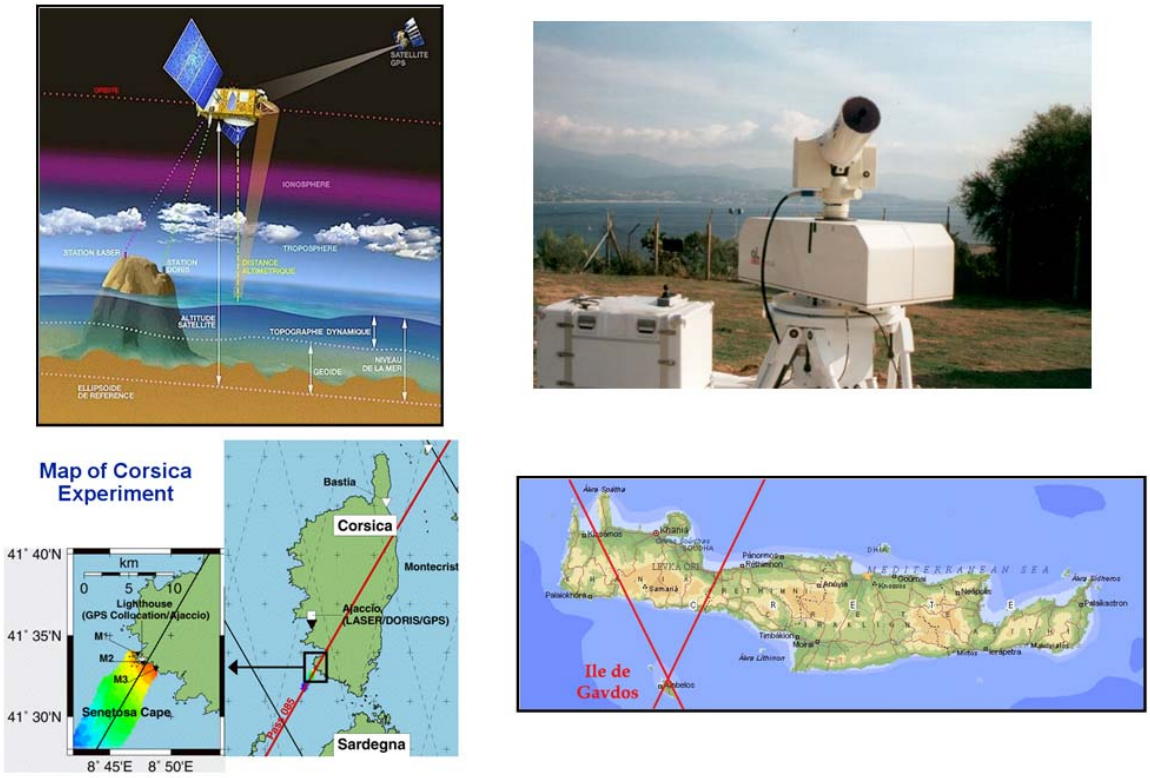

Figure 7. *CALVAL experiments with the FTLRS in Corsica and in Crete.*

Regarding the number of normal points collected on the two LAGEOS satellites by the FTRLS during this campaign (see Tab. 1), it is clear that we need to use the four satellite data to compute the FTLRS positioning. To do so, we have carried out two kinds of computations:

1. the FTLRS position and the range biases per satellite are computed over the whole period of time;
2. we compute weekly FTLRS positions together with range biases per satellite which are computed over the whole period of time (temporal de-correlation approach).

Satellite	Number of normal points
LAGEOS-1	108
LAGEOS-2	315
STARLETTE	2 902
STELLA	1 479

Table 1. *Number of normal points collected by the FTLRS during the Crete campaign carried out in 2003.*

In the both computations, the FTRLS positions are computed with respect to the ITRF2000 position [Altamimi et al., 2002] corrected for the solid Earth tides and the solid Earth pole tide in agreement with [McCarthy, 1996]. With the first method, the mean FTLRS position is directly computed, while, with the second approach, the mean FTLRS position is provided as the weighted mean value of the weekly estimated positions. The results produced by these two methods are summarized in Table 2.

The horizontal component estimated values are left unchanged between both approaches. And, the correlation is strongly decreased with the temporal de-correlation method. We can also notice a transfer between the biases and the Up components (the value is close to 1 cm) between both methods. Only the results of the second method are retained and, as a result, the mean FTLRS range bias value is -13,8 mm. [Nicolas et al. 2002] provides - 5 mm. This difference is explained. Indeed, during the whole campaign, the internal and external FTLRS calibrations exhibited a constant 1-cm difference.

Method	East	North	Up	BLAG1	BLAG2	BSTE	BSTA	Corr.
Method 1	2,5	-5,9	0,3	-19,7	-20,6	-28,3	-22,4	0,93
Method 2	1,6	-5,8	12,5	-9,6	-9,7	-20,2	-15,7	0,57
Absolute differences	0,9	0,1	12,2	10,1	10,9	8,1	6,7	.

Table 2*. Results (in mm) produced by the two methods studied to compute the FTLRS mean position and range bias during the Crete campaign carried out in 2003. The FTLRS mean positions are provided in the ENU local frame. BXXXX corresponds to the FTLRS bias computed for the satellite XXXX and corr. is the maximum value of the correlations between the estimated FTLRS range bias values per satellite and its Up component positioning values.*

Finally, we can see differences between the bias estimated values per satellite (both LAGEOS satellites versus STELLA and STARLETTE satellites). These differences could be explained by a radial constant error of 1 cm found for STELLA [Bonnefond, 2006] and by the fact that the signature effects depend on satellite and on detection system [Nicolas, 2000].

3.2. 12-year SLR data analysis

The temporal de-correlation method has also been applied over 5-month running windows in the framework of a 12-year SLR LAGEOS satellite data analysis (see [Coulot et al., 2005] and [Coulot, 2005] for more details).

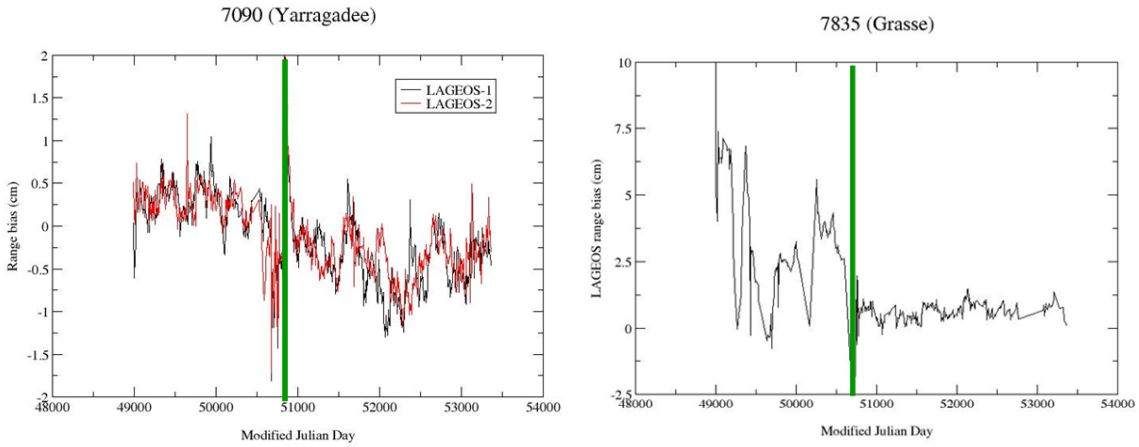

Figure 8. *Bias (in cm) time series with a 5-month sampling computed for the Yarragadee (on the left) and the Grasse (on the right) SLR stations during the 12-year SLR LAGEOS satellite data analysis.*

Fig. 8 provides two examples of bias time series computed during this study. Regarding the Yarragadee (7090) SLR station results, we can first notice that the bias values per satellite are very close: the RMS of the difference is 0.03 mm! A jump is clearly detected in the two time series. And, the epoch of this jump (January 1998) in fact corresponds to a detection system change.

Regarding the Grasse (7835) SLR station results, a jump is also detected in September 1997 and this jump corresponds to the detection system change previously mentioned in section 1 (cf. Fig. 1). We can finally notice the great stabilization of the range biases after this discontinuity. Indeed, the bias RMS value after this latter is 3.0 mm whereas this value is 20.5 mm before the jump!

4. Method improvement

4.1. New approach

Up to now, the limits of the time interval over which biases are supposed to be constant were not rigorously determined. As previously mentioned, range biases are directly linked to SLR instruments. Thus, biases are now supposed to be constant

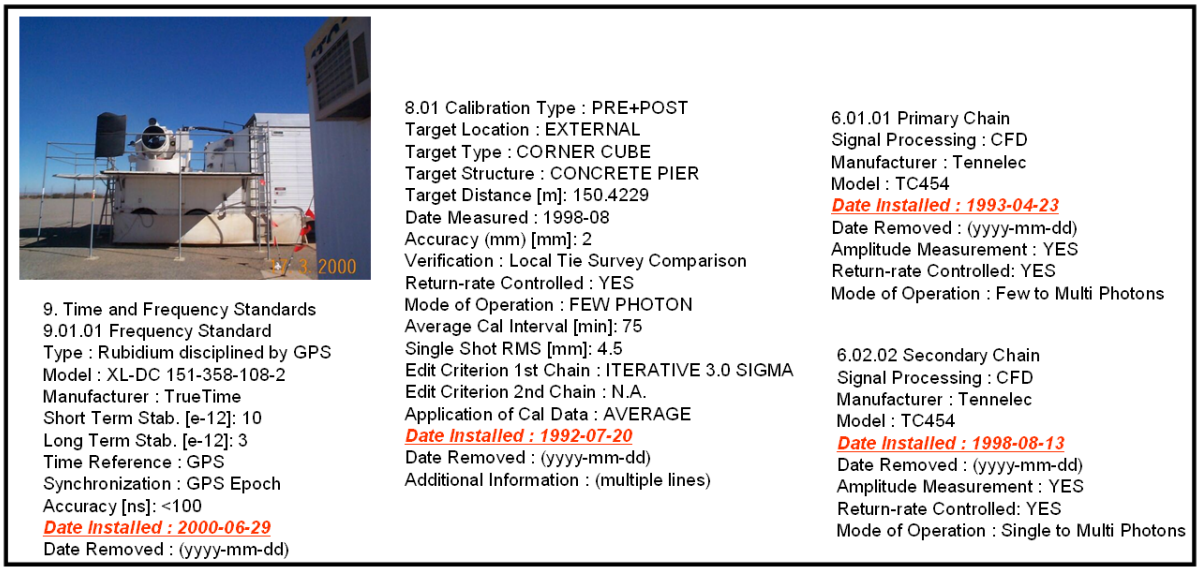

Figure 9. *Examples of instrumental change epochs found in the log file of the Yarragadee SLR station (7090).*

between two instrumental changes. We use station log files to determine these changes. Fig. 9 shows examples of instrumental change epochs used for the Yarragadee station (7090). Examples of so computed biases per satellite are provided in [Coulot et al., 2007].

4.2. Results

Fig. 10 compares the results produced with our improved temporal de-correlation method with those produced without considering any range bias during the data processing. Results are satisfying. Indeed, for instance, the scale factor time series is

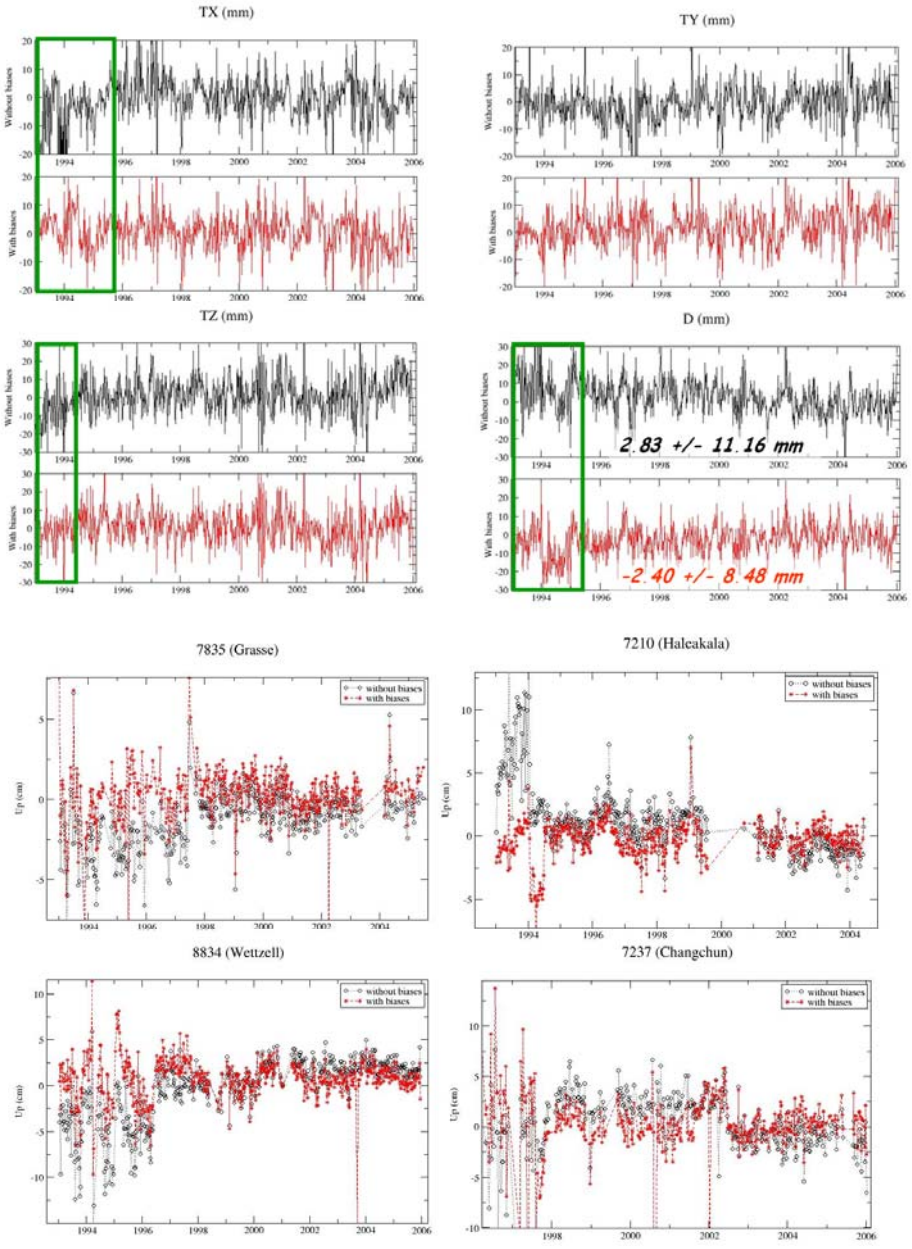

Figure 10. *Translation and scale factor parameters (in mm) computed between the weekly Terrestrial Reference Frames and ITRF2000 and four station Up component time series computed in ITRF2000 (in cm). Black (resp. red) curves correspond to the computation carried out without considering any bias (resp. the computation for which our improved temporal de-correlation method has been applied).*

more stable (RMS value of 8.5 mm to be compared with the 11.2 mm value provided by the computation carried out without bias). Moreover, the drift exhibited by the black scale factor time series disappears when our approach is used. Finally, the station time series are clearly more stable even if some discontinuities are still detected.

5. Conclusions and prospects

The two approaches ("running windows" or "instrumental change epochs") produce very satisfying results. They could be coupled to detect jumps which are not clearly linked to reported instrumental evolutions. Furthermore, it would allow us to rigorously apply the method to "poor quality stations", e.g.. stations for which biases are not stable.

Our method takes into account the correlation between station position Up components and range biases. We should also pay attention to the correlations with the possible radial orbital errors in the framework of a semi-dynamical approach (see [Coulot et al., 2007]). It would thus require a global estimation of all parameters for the whole network involved.

References

[1] Altamimi, Z., P. Sillard, and C. Boucher: "ITRF2000: a new release of the International Terrestrial Reference Frame for Earth science applications", J. Geophys. Res., 107(B10), 2214, doi: 10.1029/2001JB000561, 2002.

[2] Berio, P., P. Exertier, F. Pierron, J. Weick, D. Coulot, and O. Laurain: "FTLRS support to the Gavdos project: tracking and positioning", in Proceedings of the 14th International Laser Ranging Workshop, 2004.

[3] Bonnefond, P., P. Exertier, P. Shaeffer, S. Bruinsma, and F. Barlier: "Satellite Altimetry from a Short-Arc Technique: Application to the Mediterranean", J. Geophys. Res., 100(C12), p. 25 365-25 382, 1995.

[4] Bonnefond, P., personal communication, 2006.

[5] Coulot, D., P. Berio, O. Laurain, D. Féraudy, P. Exertier, and K. Le Bail: "Analysis of 12 years (1993-2004) of SLR data", poster presented at the 2nd European Geosciences Union General Assembly, Vienna, Austria, 2005.

[6] Coulot, D.: "Télémétrie laser sur satellites et combinaison de techniques géodésiques. Contributions aux Systèmes de Référence Terrestres et Applications", Ph. D. thesis, Observatoire de Paris, 2005.

[7] Coulot, D., P. Berio, O. Laurain, D. Féraudy, P. Exertier, and F. Deleflie: "Analysis of 13 years (1993-2005) of Satellite Laser Ranging data on the two LAGEOS satellites for Terrestrial Reference Frames and Earth Orientation Parameters", same issue, 2007.

[8] Exertier, P., J. Nicolas, P. Berio, D. Coulot, P. Bonnefond, and O. Laurain: "The role of Laser Ranging for calibrating Jason-1: the Corsica tracking campaign", Mar. Geod., 27, p. 1-8, 2004.

[9] McCarthy, D.D.: "IERS Conventions", IERS Technical Note 21, Observatoire de Paris, 1996.

[10] Nicolas, J.: "La Station Laser Ultra Mobile. De l'obtention d'une exactitude centimétrique des mesures à des applications en océanographie et géodésie spatiales", Ph. D. thesis, Université de Nice-Sophia-Antipolis, 2000.

[11] Nicolas, J., P. Bonnefond, O. Laurain, F. Pierron, P. Exertier, and F. Barlier: "Triple laser ranging collocation experiment at the Grasse Observatory, France - September - November 2001-", in Proceedings of the 13th International Laser Ranging Workshop, 2002.

Analysis of 13 years (1993-2005) of Satellite Laser Ranging data on the two LAGEOS satellites for Terrestrial Reference Frames and Earth Orientation Parameters

D. Coulot[1], Ph. Berio[2], O. Laurain[2], D. Féraudy[2], P. Exertier[2], F. Deleflie[2]

1. IGN/LAREG - Marne-la-Vallée – France
2. CNRS/OCA/GEMINI - Grasse - France

Contact: David.Coulot@ensg.ign.fr /Fax: +33-1-64-15-32-53

Abstract

The quality presently reached by space-geodetic techniques, regarding precision, accuracy such as spatial and temporal distributions of their measurements, allows us to compute time series of geodetic products.

In this context, we have developed a method to compute time series of Earth Orientation Parameters (EOPs) and terrestrial station positions through the analysis of Satellite Laser Ranging (SLR) data. This technique being an important basis for the computation of the International Terrestrial Reference Frame, it is crucial to derive accurate time series with a rigorous approach. Furthermore, this method will be used by the scientific department GEMINI of the Observatoire de la Côte d'Azur when it will become an official ILRS analysis center.

These times series are obtained with a good accuracy and a reasonable sampling (1 day for EOPs and 1 week for station positions). This good accuracy is ensured by i) a rigorous weighting of SLR measurements per satellite and per station; ii) a kinematic approach to compute orbital residual errors; iii) a rigorous control of range biases which is detailed in [Coulot et al.,2007].

In this paper, we first present the two aspects i) and ii) of our method. In a second part, we analyze 13 years (1993-2005) of SLR data on both LAGEOS satellites in order to study the Terrestrial Reference Frames and the EOPs so computed.

Introduction

This paper comprises four parts. First, we detail the two LAGEOS satellite orbit computation. Second, we provide general considerations about the Satellite Laser Ranging (SLR) data processing, regarding the data weighting, the orbital residual errors, and the range biases. Then, we describe the time series computation method and produce the results and, finally, we provide some conclusions and prospects.

1. Orbit computation

This section aims to briefly describe the two LAGEOS satellite orbit computation. Tables 1, 2, and 3 respectively show the physical models used for the orbit computations and for the Earth Orientation Parameters (EOPs) and the station positions during these computations.

Fig.1 shows the orbit residual WRMS and the numbers of data used and rejected for both satellites. Tab. 4 provides some statistics of these values. We can see that, on average, the residual WRMS are at the centimeter level for both LAGEOS satellites.

The sampling used for these computations is the GPS week but, in order to reduce the impact of the residual orbital errors, we in fact compute 9-day orbital arcs and only keep the 7-day central arcs. As a result, our orbital arcs provide 2-day overlaps. Fig. 2

shows the bias and the RMS values of the orbit differences so computed in RTN frame for both satellites. Table 5 provides the mean values of these difference bias and RMS values.

Table 1. *Physical models used for the orbit computations.*

Type	Description
Earth's gravity field	GRIM5_C1 [Gruber et al., 2000]
Atmospheric density	DTM94 [Berger et al., 1998]
Planetary ephemerides	DE403 [Standish et al., 1995]
Earth's time varying gravity field	
Solid Earth tides	Model in [McCarthy and Petit, 2004]
Solid Earth pole tide	Model in [McCarthy and Petit, 2004]
Oceanic tides	FES2002 [Le Provost, 2002]
Atmospheric pressure	ECMWF, http://www.ecmwf.int/

Table 2. *Physical models used for the EOPs during the orbit computations.*

Type	Description
Reference time series	EOPC04 [Gambis, 2004]
Quasi-diurnal Variations	Model in [McCarthy and Petit, 2004]
Precession	Model [Lieske et al., 1977]
Nutation	Model in [McCarthy, 1996]

Table 3. *Physical models used for the stations positions during the orbit computations.*

Type	Description
Terrestrial Reference Frame	ITRF2000 [Altamimi et al., 2002]
Celestial Reference Frame	ICRF [Arias et al., 1995]
Solid Earth tides	Model in [McCarthy and Petit, 2004]
Solid Earth pole tide	Model in [McCarthy and Petit, 2004]
Oceanic loading (only tidal components)	Computed with FES2002
Atmospheric loading (only non-tidal components)	Computed with ECMWF fields

Table 4. *Statistics of the values shown on Fig. 1.*

Satellite	Mean residual WRMS	Mean number of data used	Mean number of rejected data
LAGEOS	1.11 cm	1433	49
LAGEOS-2	0.95 cm	1320	35

Their interpretation is not easy, and yet these overlaps provide a way of controlling the orbit quality. From Table 5, we can see that the two LAGEOS satellite orbits provide differences with mean RMS values between 1 and 4.5 cm.

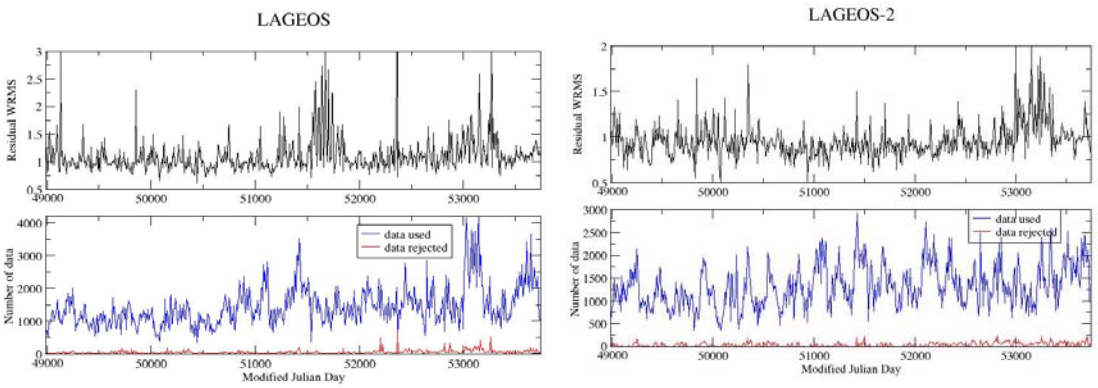

Figure 1.*Orbit residual WRMS (cm) (black curves) and numbers of data used (blue curves) and rejected (red curves) per orbital arc for both LAGEOS satellites (LAGEOS on the left and LAGEOS-2 on the right).*

Table 5. *Statistics of the values shown on Fig. 2.*

Satellite	R (cm)	T (cm)	N (cm)	.
LAGEOS	-0.02 2.57	-0.01 4.37	0.01 2.59	Mean bias Mean RMS
LAGEOS-2	0.01 1.32	-0.05 2.26	0.00 2.66	. .

2. General considerations

The SLR data processing method we have developed is divided in three steps. Fig. 3 shows the global computational scheme. First, GRGS (french Groupe de Recherche en Géodésie Spatiale, Spatial Geodesy Research Group, in English) GINS (Géodésie par Intégration Numérique Simultanée, Geodesy by Simultaneous Numerical Integration, in English) software provides the two LAGEOS satellite orbits with the help of physical models and SLR measurements (see previous section 1). Second, GRGS MATLO (MAThématiques pour la Localisation et l'Orbitographie, MAThematics for Localization and Orbitography, in English) software uses these orbital arcs and the SLR data to compute pseudo measurements as well as partial derivatives of these latter with respect to the parameters worthy of interest. Finally, an estimation software (POSGLOB for POSitionnement GLOBal or GLOBal POSitioning in English) produces parameter estimates from MATLO outputs.

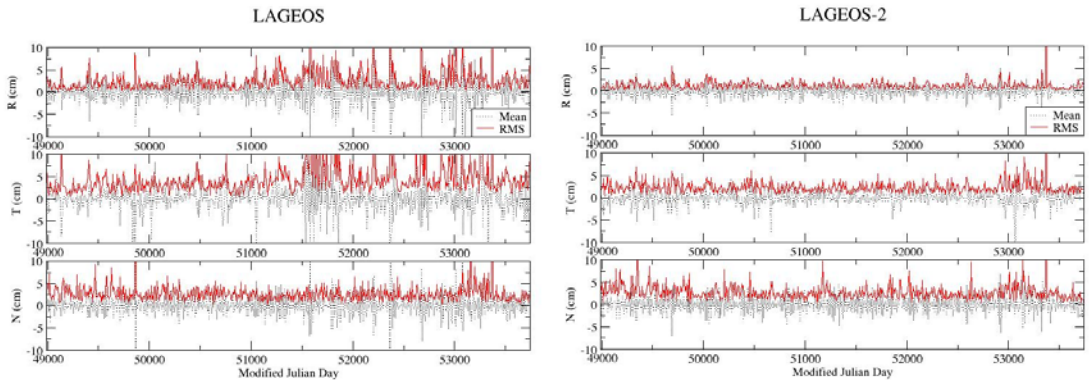

Figure 2. *Orbit differences (biases - in black - and RMS values - in red -, in cm) in the RTN frame computed over the two overlapping days for both LAGEOS satellites (LAGEOS on the left and LAGEOS-2 on the right).*

As shown in green boxes on Fig. 3, there are three critical issues in such computation: the range bias and residual orbital error handling and the data weighting. Thus, we try to build the optimal method to take these issues into account.

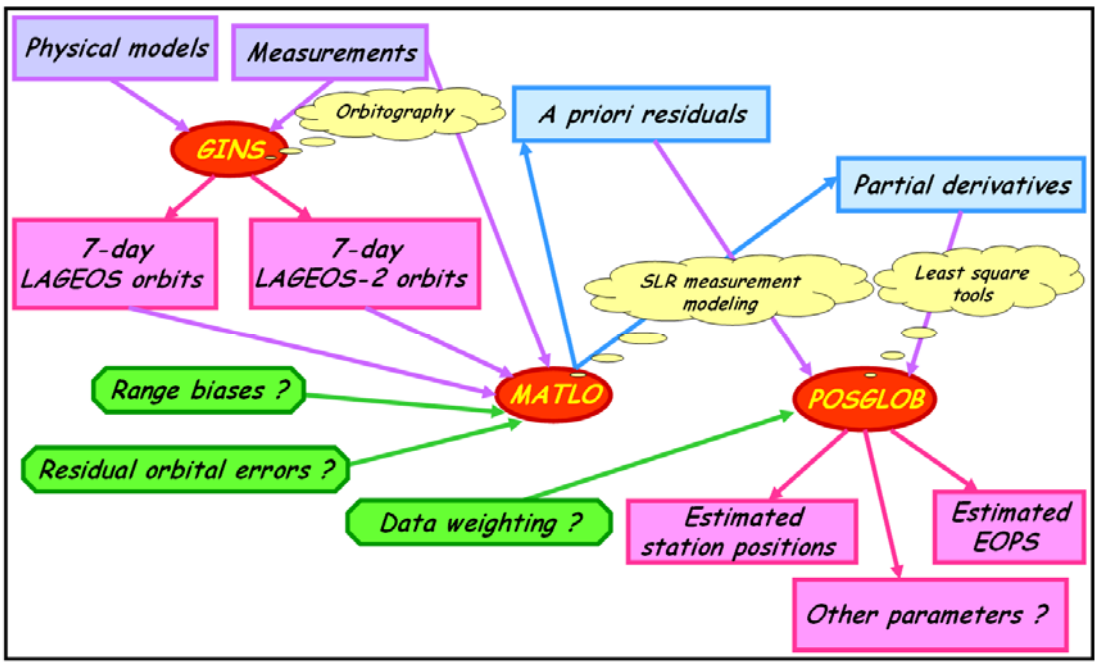

Figure 3. *SLR data processing scheme.*

2.1. Data weighting

SLR stations do not provide measurements of the same quality. As a consequence, we can not use the same weight for all SLR measurements but we have to find weights which really correspond to the quality of these measurements. To do so, we use an optimal variance component analysis method: the degree of freedom method inspired by [Persson, 1982]. The following scheme on Fig. 4 summarizes the method (see [Sillard, 1999] and [Coulot, 2005] for more details).

As shown on Fig.4, this method (as a great part of such variance component analysis method) is based on common parameters for all considered observation groups. In our case, the only real common parameters are EOPs as we consider that observation groups are measurements per station and per satellite. Thus, our variance component analysis approach only relies on these EOPs.

Fig. 5 shows the method used to derive the optimal weighting per station and per satellite. First of all, MATLO software is used to derive pseudo measurements and partial derivatives of these latter with respect to station positions and EOPs from the 7-day LAGEOS satellite orbits and the range biases computed with the temporal de-correlation method (see section 2.3 and [Coulot et al., 2007]. Then, a first computation is carried out with an empirical weighting derived from the mean orbit residual WRMS per station and per satellite.

For this computation, we apply weak constraints on station positions and EOPs. From this data processing results, we get estimated station positions which are used for the second computation. Indeed, for this latter, station positions are held fixed to the previous estimated values and, consequently, the only parameters to be computed are EOPs, the common parameters. From this computation, we then get the weekly

optimal weights per station and per satellite which can now be used for any SLR data processing.

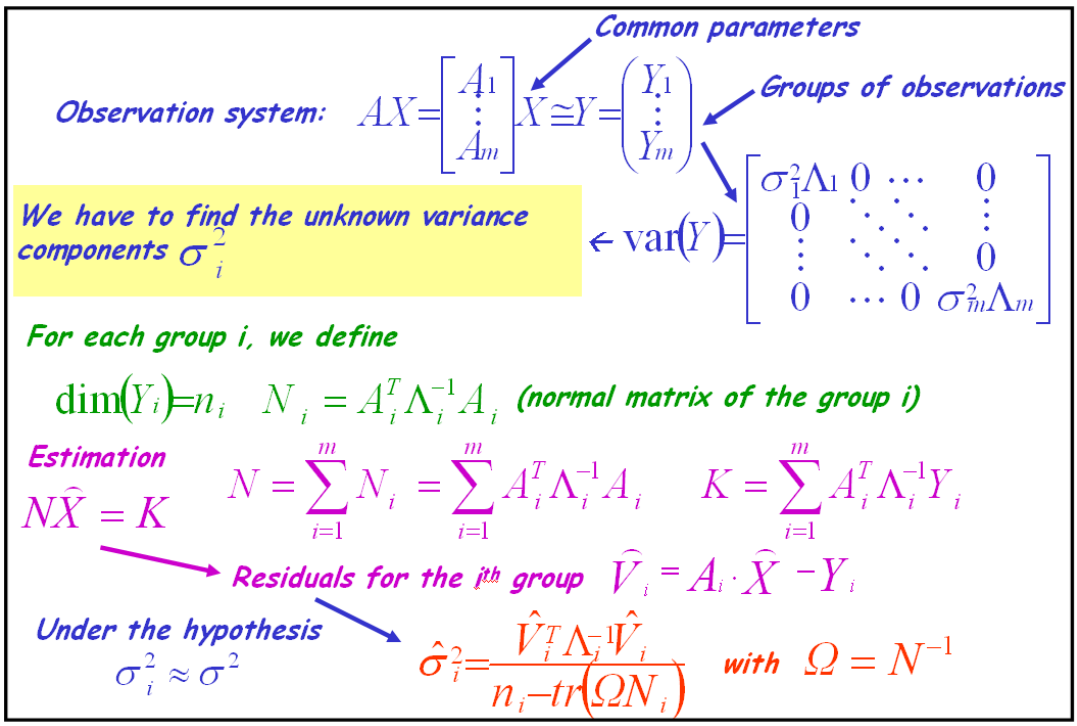

Figure 4. *Scheme of the degree of freedom method.*

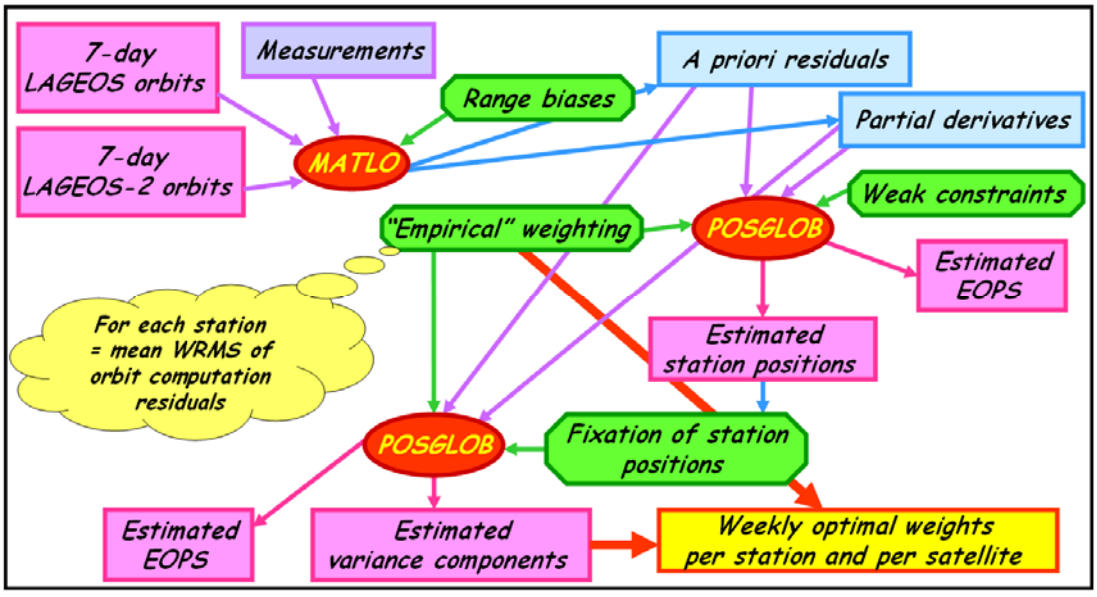

Figure 5. *Scheme of weekly optimal weight per station and per satellite computation.*

Table 6 provides the mean WRMS values of residuals per station and per satellite computed with the optimal weighting. On the whole, the values are consistent with the a priori knowledge one can have on the SLR network station quality but our approach should be more improved by the use of all the involved parameters to compute the optimal weighting. Indeed, orbital residual error parameters (see next section) are common parameters for measurements per station and we should study the impact of the non common parameters (namely, the station positions) on the results produced by variance component analysis methods. Moreover, these values

also evidence the fact that the model used to compute the optimal weighting does not explain the SLR measurements at the millimeter level (the best values are few millimeters). It is certainly mainly due to the fact that the residual orbital errors were not estimated.

Table 6. *Mean WRMS (in cm) values of residuals per station and per satellite computed with the weekly optimal weights derived from the method shown in Fig. 5. For each station, the first (resp. second) column corresponds to the mean WRMS for LAGEOS (resp. LAGEOS-2) satellite. Evidenced stations are present in less than 50 weeks over the 13-year time interval.*

1824	20.5	20.3	7210	1.0	0.9	***7502***	2.3	1.9	7840	0.9	0.9
1831	4.0	3.9	***7231***	5.1	6.2	***7505***	1.6	2.0	7841	1.1	1.1
1863	2.6	2.5	7236	11.4	10.4	7520	1.5	1.3	7843	1.8	1.6
1864	4.0	3.6	7237	2.0	1.9	7548	11.6	6.8	7845	1.0	0.9
1867	30.9	16.2	7249	5.1	4.5	***7597***	2.5	3.1	***7847***	9.9	12.9
1868	9.4	8.1	***7295***	0.9	0.9	***7805***	13.2	15.0	***7848***	2.3	1.9
1873	13.8	14.1	7308	2.0	1.9	***7806***	1.9	1.5	7849	2.3	1.1
1884	2.3	2.1	***7335***	1.0	0.9	7810	1.4	1.4	***7850***	0.7	0.8
1885	8.9	13.0	***7337***	1.0	2.2	7820	2.3	2.4	***7882***	0.5	0.6
1893	3.3	3.3	7339	1.2	0.8	***7821***	2.0	2.9	***7883***	0.5	0.6
1953	9.9	11.5	***7355***	4.3	3.7	7824	2.4	2.3	***7884***	1.2	0.6
7080	1.0	0.8	***7356***	2.8	2.8	7825	1.8	1.9	***7918***	0.9	1.1
7090	1.7	1.4	***7357***	4.9	6.0	***7830***	1.6	1.5	7939	6.9	6.8
7105	0.9	0.8	***7358***	5.0	6.9	***7831***	2.7	2.0	7941	0.9	0.8
7106	7.6	.	7403	1.5	1.1	7832	1.2	1.2	***8833***	2.8	2.7
7109	0.7	0.6	***7404***	4.9	1.8	7835	1.0	0.9	8834	1.4	1.4
7110	0.9	0.8	7405	2.7	2.7	7836	1.0	0.9	7811	1.8	1.6
7122	0.7	0.7	***7410***	0.7	0.6	7837	2.1	2.0			
7124	1.7	1.2	***7411***	0.5	0.6	7838	1.7	1.6			
7130	1.3	1.4	7501	2.2	2.1	7839	0.8	0.8			

2.2. Orbital residual errors

As previously shown in section 1, the LAGEOS satellite orbital arcs may be affected by some residual errors (cf. Fig. 2 and Tab. 5). The integration of Hill's satellite first-order motion differential equations ([Cretaux et al., 1994] and [Coulot, 2005]) provides the empirical form of such orbital residual errors in the RTN frame:

$$\delta R(t) = a_R t\cos(\bar{n}t) + b_R t\sin(\bar{n}t) + c_R\cos(\bar{n}t) + d_R\sin(\bar{n}t) + e_R + f_R t$$
$$\delta T(t) = a_T t\cos(\bar{n}t) + b_T t\sin(\bar{n}t) + c_T\cos(\bar{n}t) + d_T\sin(\bar{n}t) + e_T + f_T t + g_T t^2$$
$$\delta N(t) = a_N t\cos(\bar{n}t) + b_N t\sin(\bar{n}t) + c_N\cos(\bar{n}t) + d_N\sin(\bar{n}t) + e_N$$

The coefficients evidenced in yellow can be estimated. Thus, doing so, we can carry out a kinematic (or semi-dynamic) estimation of the orbital residual errors; see Fig. 6 for examples.

In order to avoid spurious transfers between the terrestrial and the orbital parameters, we should compute all the involved parameters (station positions, EOPs and orbital residual errors) in a same process. But, doing so gives rise to problems. Indeed, it creates supplementary reference system effects [Sillard and Boucher, 2001] on the third translation and on the scale factor of the underlying Terrestrial Reference Frame

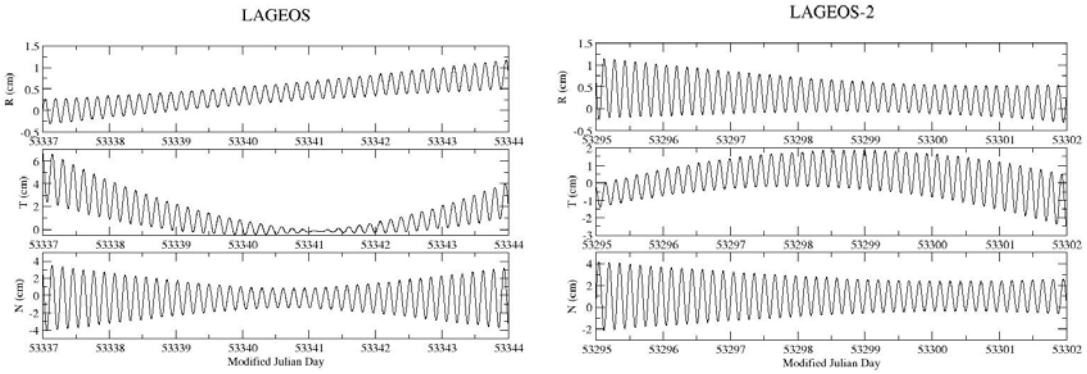

Figure 6. *Examples of orbital residual errors estimated, in cm, for both LAGEOS satellites in the RTN frame.*

(TRF). These parameters are thus damaged and the estimated orbital errors so computed are completely eccentric! Consequently, we have to find a rigorous balance between minimum constraints used to define the weekly TRFs and possible constraints applied on the orbital error coefficients. Furthermore, we have to take into account the physical coupling between the radial and tangential components [Coulot, 2005]. Finally, we have to carry out a sensitivity analysis to determine which coefficients can be optimally computed each week.

2.3. Range biases

Regarding range biases, we have developed a temporal de-correlation method in order to get the most accurate and consistent range bias values (see [Coulot et al., 2007] for more details). Fig. 7 provides an extract of the raw output file provided by this method. We can see that, when they are estimated over long periods, biases per satellite are very coherent. In other cases, the differences are at a few millimeter level.

Station	Validity (CNES J. Dates)		Values obtained for LAGEOS (m) Bias + precision		Values obtained for LAGEOS-2 (m) Bias + precision	
7835	15340	16544	1.395828547040809E-002	1.158416922784649E-003	1.234432517595224E-002	1.203503017002734E-003
7835	16544	16564	3.529396209728985E-002	1.475235139678072E-002	6.300895927387962E-002	1.990854928253546E-002
7835	16564	16679	3.320933374887905E-002	3.232515758791523E-003	2.891112857748582E-002	3.484324601453627E-003
7835	16679	17413	1.664937112299916E-002	1.430681097343033E-003	1.540554934193744E-002	1.520702451478579E-003
7835	17413	18143	-1.971404917293083E-003	3.328628424293636E-004	-6.434411963804878E-004	3.564485287931656E-004
7835	18143	18873	2.129710997299538E-003	3.360069389674007E-004	3.901844189266957E-003	3.633585927952743E-004
7835	18873	19603	9.131760532044128E-003	4.467022182450903E-004	5.700719983120365E-003	4.759540373836256E-004
7835	19603	20300	7.851262565453349E-003	9.554258819448195E-004	2.842151050185370E-003	1.004394426948261E-003
7845	17521	18305	-4.428851680859768E-003	6.223534556697570E-004	-1.201192209408536E-003	6.893149034575394E-004
7845	18305	19305	8.113087278820413E-003	4.018334706229168E-004	7.840983271450021E-003	4.356245988090018E-004
7845	19305	20035	1.285646431835049E-002	5.459565786674019E-004	1.654336641325428E-002	5.438026909611077E-004
7105	15317	16047	-3.746952854385001E-003	4.944474970946950E-004	-6.864306478378965E-003	5.264430332363305E-004
7105	16047	16777	-1.549706818118012E-002	6.921317933826075E-004	-1.064881791710468E-002	7.505764408214999E-004
7105	16777	16940	-1.105482201853714E-002	5.900205316694585E-004	-7.750502221599706E-003	6.391419698574262E-004
7105	16940	17670	-4.330403233925809E-003	3.766190351993729E-004	-2.921756834785135E-003	4.000337192808937E-004
7105	17670	17877	-8.797353166941418E-003	6.028898715788532E-004	-4.826611780213416E-003	6.371640591200326E-004
7105	17877	17959	-8.741490387424361E-003	1.310118230413150E-003	-1.019322123979381E-002	1.342775122007329E-003
7105	17959	18039	-4.648690714335582E-003	8.785822392202415E-004	-2.871015614103231E-003	9.488477693905651E-004
7105	18039	18666	-5.169111580414628E-003	3.867953242580351E-004	-4.312745700605802E-003	4.185257805300395E-004
7105	18666	18877	-3.472024871091189E-003	5.657230028905748E-004	-2.899406111483316E-003	6.018937033126987E-004
7105	18877	19607	-4.193980900330184E-003	3.817904507077791E-004	-5.491238818875488E-003	4.105820099047128E-004
7105	19607	20337	-6.548560807830205E-003	4.924245800410994E-004	-7.645452603994796E-003	5.332010012145024E-004
7105	20337	20500	-7.040431351813800E-003	9.396523059811853E-004	-6.322205532930170E-003	1.035964446496983E-003

Figure 7. *Examples of range bias values (m) per station and per satellite computed with the temporal de-correlation method [Coulot et al., 2007]. CNES JD=MJD-33 282.*

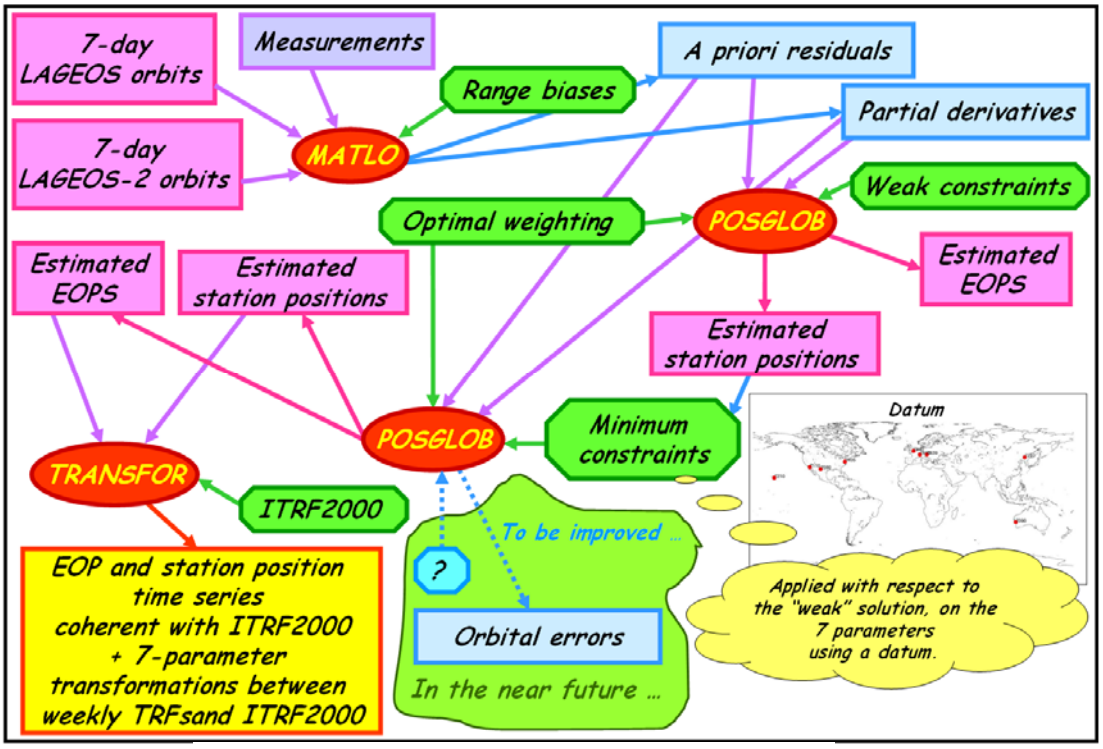

Figure 8. *Time series computation method scheme.*

3. Time series computation

3.1. Method

Fig. 8 shows the global method scheme. For the time series computation, the range bias values computed with our new method as well as our optimal weights are applied. For this first "long period" data processing carried out with MATLO/POSGLOB software, no orbital residual error is estimated nor applied.

3.2 Results

Fig. 9 shows the results produced with TRANSFOR software (cf. Fig. 8) for the three translation parameters. We have carried out frequency analyses of these time series. These analyses have been carried out with FAMOUS (Frequency Analysis Mapping On Unusual Sampling) software developed by F. Mignard (OCA, France) in the framework of the GAIA project [Mignard, 2004]. The TX (resp. TY) time series exhibit a 2.9 mm (resp. 3.2 mm)-amplitude annual signal and the TZ time series exhibit a 2.4 mm-amplitude annual signal as well as a 1.7 mm-amplitude semi-annual signal. Moreover, the scale factor time series are shown in [Coulot et al., 2007], Fig. 10. They exhibit a 2.6 mm-amplitude annual signal. This annual signal may be an artifact due to the SLR network geometry and the fact that the atmospheric loading effects have not been considered in the a priori modeling used for station positions (see next results for these station positions).

Regarding EOPs, the results are shown on Fig. 10. The weighted biases are respectively -119 and 7 µas for Xp and Yp and the WRMS are respectively 299 and 256 µas for Xp and Yp. Moreover, the opposite drifts detected between 2000.0 and 2006.0 certainly come from some network effects.

The station position time series are estimated with respect to the ITRF2000 mean position corrected for plate tectonics (ITRF2000 velocities), Earth solid tides, pole tide and oceanic loading effects in agreement with the IERS conventions [McCarthy

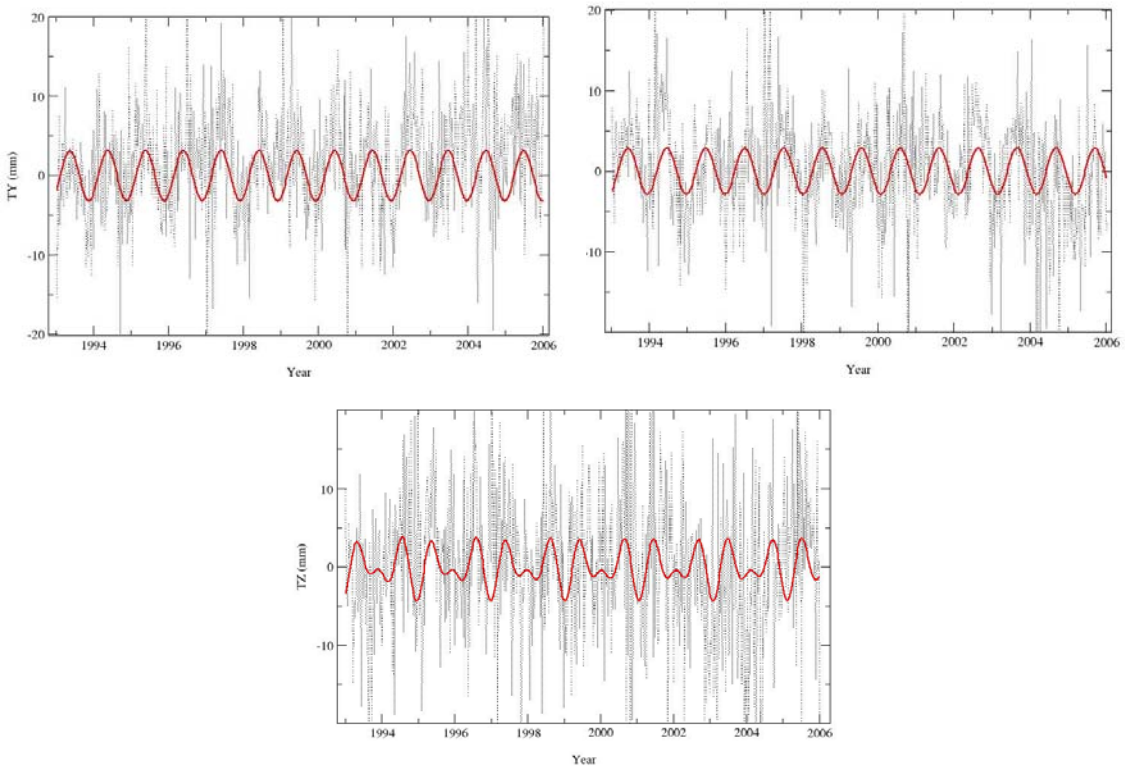

Figure 9. *Weekly translation parameter time series (mm) between weekly SLR TRFs and ITRF2000. Red curves correspond to the periodic signals detected and estimated with FAMOUS software.*

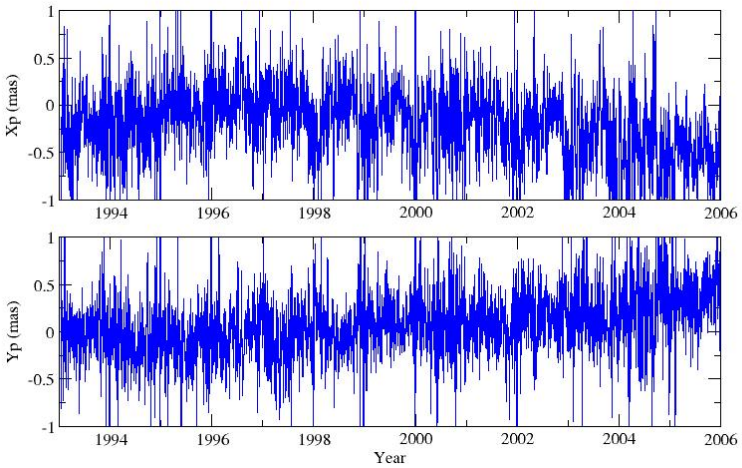

Figure 10. *Daily EOP time series (mas) computed with respect to the EOPC04 time series.*

and Petit, 2004]. These time series must consequently evidence the atmospheric and hydrologic loading effects.

Fig 11 shows 7839 and 7840 SLR station position time series in ITRF2000. Annual and semi-annual signals with amplitudes between 5 mm and 1 cm are detected by FAMOUS software in such Up component time series for some stations. These annual signals may be linked to the previously mentioned loading effects.

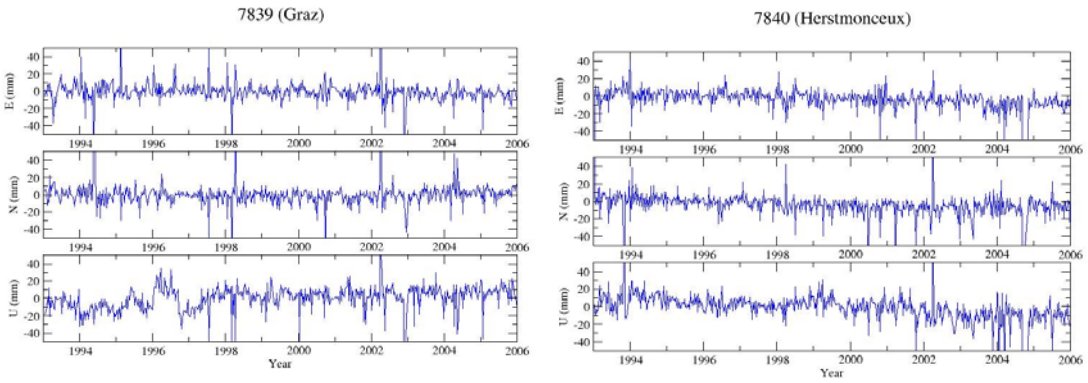

Figure 11. *Examples of station position time series computed (in mm) in the ENU local frame in ITRF2000. On the left: Graz, 7839. On the right: Herstmonceux, 7840.*

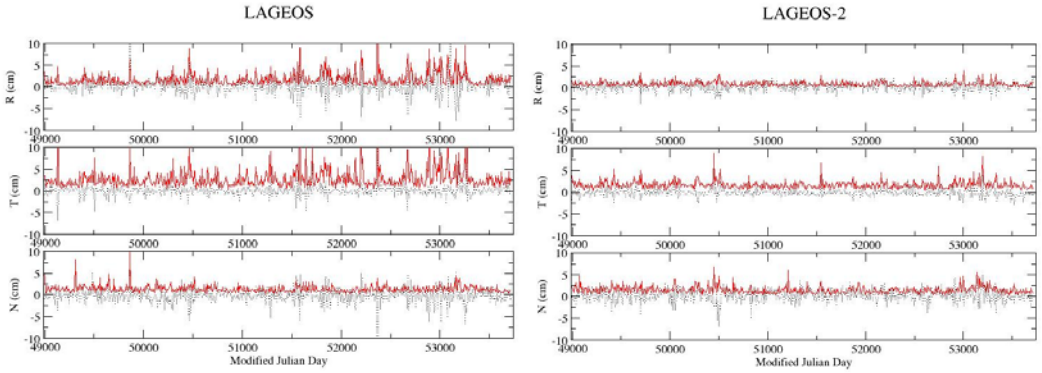

Figure 12. *Empirical orbital errors (biases - in black - and RMS values - in red -, in cm) in the RTN frame computed with our semi-dynamic approach for both LAGEOS satellites (LAGEOS on the left and LAGEOS-2 on the right).*

Table 7. *Statistics of the values shown on Fig. 12.*

Satellite	R (cm)	T (cm)	N (cm)	.
LAGEOS	0.38 1.71	0.06 2.73	-0.13 1.32	Mean of means Mean of RMS
LAGEOS-2	0.31 0.90	-0.11 1.65	0.20 1.46	. .

Finally, although our global method (cf. Fig. 8) does not provide any orbital error estimate, we have tested our semi-dynamic approach by keeping station positions and EOPs fixed. Almost all effects are included in the a priori modeling then used for station positions: plate tectonics, solid Earth tides, pole tide, and oceanic and atmospheric loading effects (European Center for Medium-range Weather Forecasts - ECMWF, http://www.ecmwf.int/- pressure fields were used to derive the atmospheric loading effect models) as well as the range biases provided by the temporal de-correlation method. Fig. 12 shows the bias and the RMS values of the empirical orbital errors so computed in RTN frame for both satellites. Tab. 7 provides the mean values of these error bias and RMS values. These values are coherent with the 2-day LAGEOS overlaps (cf. Fig. 2 and Tab. 5).

4. Conclusions and prospects

Our time series estimation method should be operational soon. To do so, we still have to:

- finalize our method regarding orbital errors;
- use all available common parameters to get optimal weekly weightings;
- go further with our temporal de-correlation approach for range biases [Coulot et al., 2007].

New computations should be carried out with ITRF2005 and the improved EOPC04 time series. And, in the near future, we plan to:

- carry out computations with atmospheric loading effect models in the a priori modeling for station positions to quantify their impact;
- use other satellites and study the impact on the involved TRFs.

References

[1] Altamimi, Z., P. Sillard, and C. Boucher: “ITRF2000: a new release of the International Terrestrial Reference Frame for Earth science applications”, J. Geophys. Res., 107(B10), 2214, doi: 10.1029/2001JB000561, 2002.

[2] Arias, E.F., P. Charlot, M. Feissel, and M.F. Lestrade: “The Extragalactic Reference System of the International Earth Rotation Service, ICRS”, Astron. Astrophys., 303, p. 604-608, 1995.

[3] Berger, C., R. Biancale, M. Ill, and F. Barlier: “Improvement of the empirical thermospheric model DTM: DTM94- a comparative review of various temporal variations and prospects in space geodesy applications”, J. Geod., 72(3), p. 161-178, 1998.

[4] Coulot, D.: “Télémétrie laser sur satellites et combinaison de techniques géodésiques. Contributions aux Systèmes de Référence Terrestres et Applications”, Ph. D. thesis, Observatoire de Paris, 2005.

[5] Coulot, D., P. Berio, O. Laurain, D. Féraudy, and P. Exertier: “An original approach to compute satellite laser range biases”, same issue, 2007.

[6] Cretaux, J.F., F. Nouel, C. Valorge, and P. Janniere: “Introduction of empirical parameters deduced from the Hill's equations for satellite orbit determination”, Manuscr. Geod., 19, p. 135-156, 1994.

[7] Gambis, D: “Monitoring Earth orientation using space-geodetic techniques: state-of-the-art and prospective”, J. Geod., 78, p. 295-305, 2004.

[8] Gruber, T., A. Bode, C. Reigber, P. Schwintzer, R. Biancale, and J.M. Lemoine: “GRIM5-C1: combination solution of the global gravity field to degree and order 120”, Geophys. Res. Lett., 27, p. 4005-4008, 2000.

[9] Le Provost, C.: “FES 2002 - A new version of the FES tidal solution series”, paper presented at Jason-1 Science Working Team Meeting, Biarritz, France, 2002.

[10] Lieske, J.H., T. Lederle, W. Fricke, and B. Morando: “Expressions for the precession quantities based upon the IAU (1976) System of Astronomical Constants”, Astron. Astrophys, 58, p. 1-16, 1977.

[11] McCarthy, D.D.: “IERS Conventions”, IERS Technical Note 21, Observatoire de Paris, 1996.

[12] McCarthy, D.D. and G. Petit: “IERS Conventions”, IERS Technical Note 32, Verlag des Bundesamts für Kartographie und Geodäsie, Frankfurt, 2004.

[13] Mignard, F.: “Overall science goals of the GAIA mission”, in Proceedings of the symposium "The Three-Dimensional Universe with GAIA", 2004.

[14] Persson, C.G.: “Adjustment, weight-testing and detection of outliers in mixed SFF-SFS models, Manuscr. Geod., 7, p. 299-323, 1982.

[15] Standish, E.M., X.X. Newhall, J.G. Williams, and W.M. Folkner: “JPL planetary and lunar ephemerides, DE403/LE403”, JPL IOM 314.10-127, 1995.

[16] Sillard, P. and C. Boucher: “Review of algebraic constraints in terrestrial reference frame datum definition”, J. Geod., 75, p. 63-73, 2001

NETWORK PERFORMANCE AND RESULTS SESSION SUMMARY

C. Luceri and M. Torrence, co-chairs

This workshop session was a forum for the assessment of network data production, quality, and ILRS products.

The regular quality control assessments performed by several ILRS analysis centers was discussed by R. Noomen. He showed range bias estimates for LAGEOS 1 and 2 improved in consistency from 2004 through 2006 from 30 to 20 mm level. Other analysis centers contributions to regular and rapid data quality analyses will help the overall assessment of the results as there are, as of this writing, only two AC contributing to this effort. T. Otsubo showed that characterization of possible intensity-dependence station effects should be considered to achieve mm level data accuracy and calibrations may show possible correlations with seasonal loading effects. M. Torrence showed examples of plots of station's data as a function of local time and range measurement.

J. Luck reported on upgrades to the WPLTN sites and reported the data yield from southern hemisphere tracking sites has increased to 40% of the total data available data with the quality generally comparable with the data from the northern hemisphere. Luck also commented that all stations should pay close attention to their system delay and calibrations. A report on mm level bias due to measurement characteristics of the Stanford counter in the data from Herstmonceux was given by P. Gibbs, with the suggestion that all Stanford counters should be characterized. F. Pierron showed results of the FTLRS occupations at the Ajaccio site, achieving stable position estimation from multi-satellite data analyses using the Eigen-Grace03s gravity model for the two occupations (2002 and 2005).

E. Pavlis discussed the global SLR network and the origin and scale of the TRF in the GGOS era and an SLR-based evaluation and validation studies of candidate ITRF2005 products. An assessment of the ILRS-A standard product was presented by G. Bianco. This routine production process is stable and reliable and those ILRS standard products allow monitoring of site coordinates and EOPs. Additionally, the geocenter motion, geometrically derived from the weekly solutions, could be included among the future ILRS standard products. R. Govind showed results of a simulation to evaluate the contribution of an additional SLR station in northern Australia to the Earth center-of-mass determination.

The session concluded with a light-hearted presentation by P. Shelus on "Evolution of SLR/LLR in Response to Mission Needs." From the summary slide: "As scientific experiments become more complicated, greater pressures are placed upon operational logistics in order to perform necessary operations, and yet retain personnel safety and instrumental integrity. Thorny logistical problems have been solved by a combination of computer power, internet communications, orbital dynamics and precisely defined inter-relationships among several reference frames."

There were several posters presented for this session. C. Noll described the laser ranging archive available at the ILRS data centers and plans for future enhancements. J. Luck showed the result of a minico system delay for the Mt. Stromlo site. C. Moore presented a summary of the observations of GioveA taken from Mt Stromlo SLR Station, the identified patterns that have impacts on tracking productivity and the use of Giove A data for an empirical analysis of link budget requirements for potential gain in tracking GioveA, Galileo and similar satellites. T. Otsubo showed plots of intensity-dependent effects for all stations. M. Torrence displayed plots of data as function of local time and range for all stations.

The SLR network from a QC perspective

R. Noomen[1]

1. Delft University of Technology, Kluyverweg 1, 2629 HS Delft, The Netherlands.

Contact: r.noomen@tudelft.nl / Fax: +31-15-2785322

Abstract

Although it can be considered as a traditional if not classical technique, Satellite Laser Ranging (SLR) (still) plays a crucial role when it comes to assessing and monitoring a number of global aspects of System Earth: scale and origin of the terrestrial reference frame. A proper and timely monitoring of the performance of the network of laser stations is a prerequisite to provide an optimal contribution to the space geodetic community. In order to detect possible data problems at an early stage, a number of analysis centers perform a regular quality control (QC) of the SLR measurements on a variety of satellites. This paper addresses a number of issues relating to that: the development of the global network in terms of stations and their distribution, and the development of the (raw) data quality. The quality and consistency of reported range biases will be studied in this paper as well. Although the analysis done here covers the years 2004-2006 only, the results show an improvement in consistency for most of the QC centers, from about 30 mm in 2004 to about 20 mm in 2006 (total network) or from 25 mm to 15 mm (AWG core network). Two points of concern are the global coverage of the network of SLR stations and the decrease in the number of QC centers.

Introduction

With its highly accurate absolute distance measurements between satellites and ground stations, the International Laser Ranging Service (ILRS) supports a wide range of space geodetic missions: gravity field missions, altimetry missions, missions aimed at the assessment and monitoring of the terrestrial reference frame, and others. To obtain the best possible contribution from such SLR observations, a good global coverage of the network of ground stations, a good production rate and a high quality of such observations are prerequisites.

In this paper, both network geometry and data quality aspects are addressed. In particular, the overall development of the network in terms of geometry, data yield and data precision is described. Also, the various possibilities to monitor the quality of these observations and to alert stations in case of systematic errors (range biases) are examined. The paper compares a number of QC institutes, and derives recommendations for the threshold at which a reported bias can be considered to be real. This is primarily done by comparing independent bias estimates for common passes on LAGEOS-1 and on LAGEOS-2.

SLR network development

Figure 1 shows the number of stations that have tracked the satellites LAGEOS-1 and/or LAGEOS-2, during a particular year. Considering the central role of these two spacecraft, an inventory of the data acquisition on either of these satellites can be considered as a direct measure for the amount of stations that were active in a particular year. It is clearly visible that the number of stations in the global network has increased from about 30 in the mid-1980s to about 40 now; variations and developments in this number are typically related to the operations of transportable SLR stations, and the installation of new stations at various places around the world.

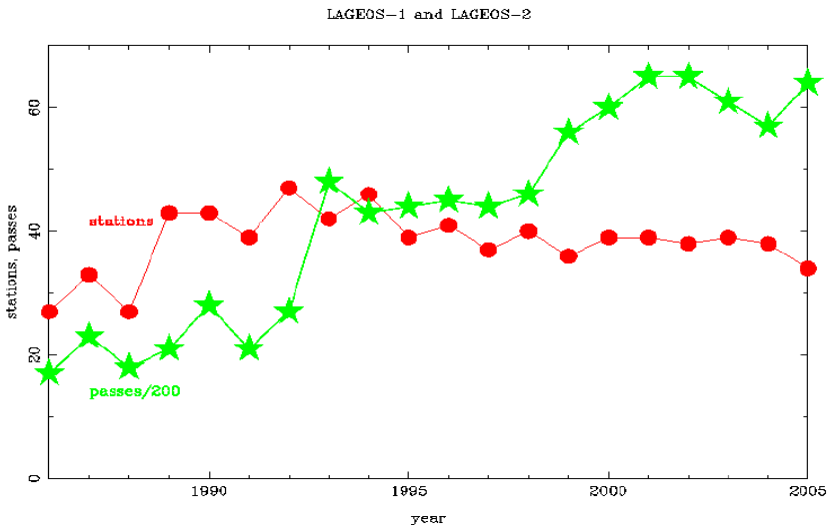

Figure 1. *The yearly number of stations that tracked LAGEOS-1 and/or LAGEOS-2, and their production in terms of number of passes.*

In spite of the reasonable stability of this number over the past decade, the plot shows a remarkable reduction from a recent maximum of 39 in 2003 to 34 in 2005. This will be discussed further shortly.

The figure also shows the total number of passes (on LAGEOS-1 and LAGEOS-2) that have been taken during the same year. In spite of the reduction of the number of stations, the total number of individual passes has been stable if not on the rise: in 2005, about 13,000 passes were obtained, or almost 400 on average per station. Clearly visible is the increase of this number of passes in 1993, the first full year after the launch of LAGEOS-2, on October 25, 1992. Contrary to the decline in number of stations in the past few years, the total data yield of the network appears to be stable (if not increasing). This can be attributed to a higher level of efficiency (automation), improvements in scheduling and increasing number of shifts.

The geometry of the SLR network is illustrated in Figure 2. Here, the tracking network in 2003 is compared to that in 2005; note that no allowance for the number of passes is made. It is clearly visible that the majority of the network has been in operation permanently, whereas a relatively small number of stations (Hawaii, Arequipa/Peru, Chania/Crete and Komsomolsk-na-Amure/Russia; open red circles) did not range in 2005 whereas they did in 2003. New stations in 2005 (or 2004, at least w.r.t. 2003) are Ajaccio/France and Tanegashima/Japan. The plot shows that the distribution of stations has a preference for the Northern Hemisphere, and that the termination of activities in Hawaii and Arequipa has dramatic consequences for the coverage in particular in the Pacific region. In view of the important role of SLR in its unique determination of global parameters of System Earth like geocenter and scale, such flaws in station distribution are an absolute point of concern. Fortunately, the situation has improved again with the installation of new stations in San Juan/Argentina, Hawaii and Arequipa in mid-2006.

To get an idea of the advancement of the technical quality of the network, Figure 3 gives a comparison of single-shot precision values of raw SLR observations. It is clearly visible that these values have improved dramatically in 2002 when compared to 1997. These numbers are to be considered as representative for the current network of stations: on average, the single-shot precision is at the level of a few mm for the major part of the network.

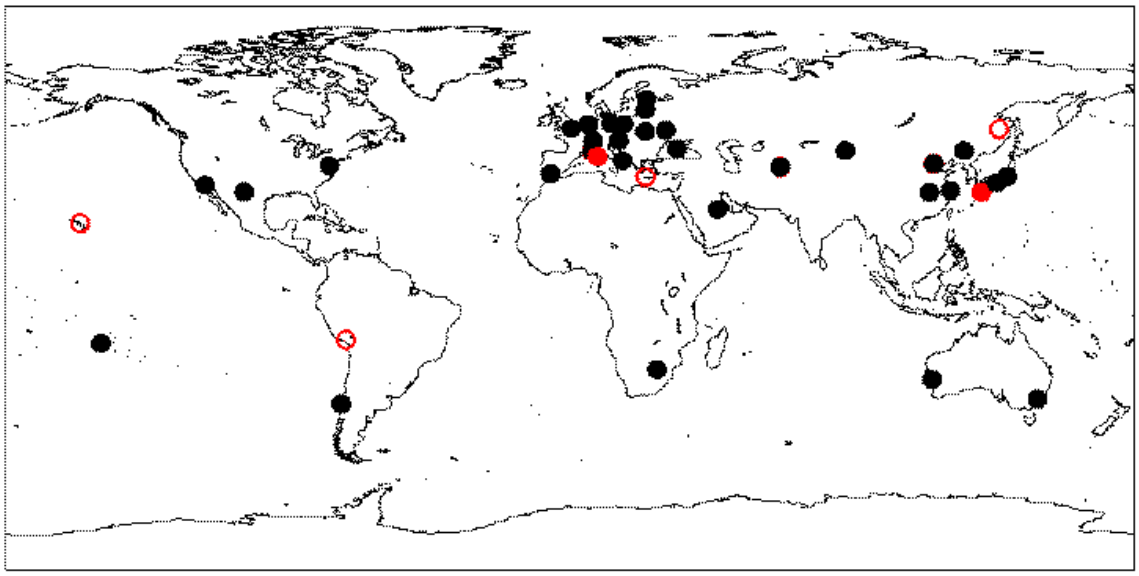

Figure 2. *The global network of SLR stations, Black circles indicate stations that have been active in both 2003 and 2005. Open red circles represent stations that were active in 2003, but not in 2005. Solid red circles represent stations that were active in 2005, but not in 2003.*

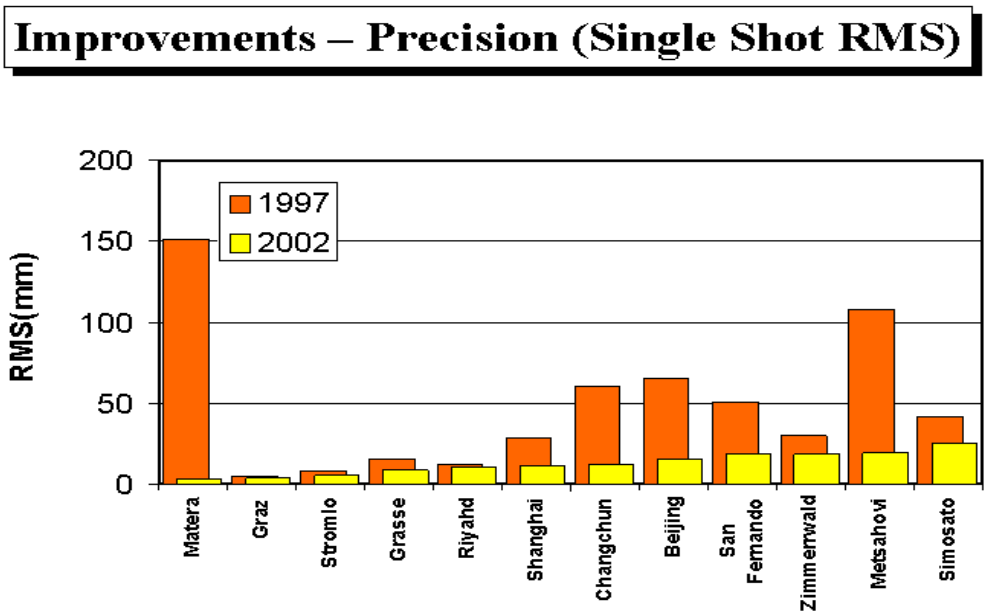

Figure 3. *A comparison of the single-shot precision of a number of representative SLR stations, in 2002 as compared to 1997 (courtesy Van Husson).*

Bias detection capability

SLR observations are reputed for their absolute, unambiguous value, and therefore they play an essential role in the determination of the origin and scale of the International Terrestrial Reference Frame (ITRF) (*e.g.* [Altamimi *et al.*, 2002]). In order to do so properly, it is of utmost importance to monitor the quality of the observations taken by the SLR stations, not only on a precision level (*i.e.* in terms of internal consistency) but especially on absolute accuracy. To this aim, possible systematic errors (range biases) need to be computed and evaluated on a pass-by-pass basis and scrutinized constantly. To do so, a number of options exist. First, one can do so at the tracking station itself; actually the monitoring of such items is already being done, on the basis of orbit predictions and/or short-arc, rapid-return orbit solutions.

Although the capabilities are limited, the stations and analysis centers involved in this are encouraged to continue to do so. The second option is to derive such biases from the official ILRS product; here, a group of 6 analysis centers cooperate in a concerted effort to generate a weekly solution for station coordinates and Earth Orientation Parameters (EOPs) [ILRS, 2006]. A drawback of this technique is that station position and biases become highly correlated below a certain level, and the possibility to monitor range biases at the level of a few mm is therefore not possible. Also, by virtue of the (inherent) scatter in the weekly coordinates solutions for an arbitrary station, the corresponding range biases would also reflect this scatter to say the minimum. The third option is most attractive: a dedicated analysis in which the satellite orbit and related parameters are estimated to come to a most accurate description of the relevant elements of our system, but in which the position of the stations is kept fixed at a highly accurate model value (of course, allowing for temporal effects like crustal deformation, tidal motions, and ocean and atmospheric pressure loading deformation). This paper focuses on results obtained by the latter techniques.

An overview of the analysis centers active in such analyses (not necessarily exhaustive) is given in Table 1. In order to assess the quality of the bias values as reported by these groups on a regular (daily, weekly) basis, only values reported for the satellites LAGEOS-1 and LAGEOS-2 will be treated further here.

Institute	Altimetry, gravity missions	LAGEOS-1, -2	Navigation missions
Astronomisches Institut Universität Bern, Switzerland			X
Center for Space Research, Texas, USA		X	
Deutsches Geodätisches Forschungs Institut, München, Germany		X	
Delft University of Technology, Netherlands		X	
Mission Control Center, Moscow, Russia		X	
National Institute of Information and Communications Technology, Kashima, Japan	X	X	
Shanghai Astronomical Observatory, China		X	

Table 1. *Overview of the dedicated QC efforts done by various SLR analysis groups.*

Although Table 1 shows that quite a number of analysis centers are involved in the operational QC assessments, and might suggest that the results are consistent, a simple illustration (Figure 4) shows that this is not necessarily the case: differences in the "verdict" for individual passes of up to several tens of millimeter can easily be present, sometimes even exceeding decimeter values. This aspect has been known for quite a number of years already [ILRS, 1999]. One of the main reasons for this is the modeling of the ground station positions: differences in this analysis component will immediately show up as consistent bias differences. To remedy this (aspect of the) situation, QC centers have been urged to use a common representation, which has been put into practice during the last years with reasonable success: at this moment, almost all QC centers use the ITRF2000 [Altamimi *et al*., 2002] model, with just a single exception: MCC still uses its own set of station coordinates (status October 2006).

The consistency of the reported bias values is the subject of the remainder of this paper. The results as they are included in the weekly so-called ILRS Combined Range Bias Reports [Gurtner, 2006] are used as input for this evaluation. These reports basically merge the information from a number of individual bias reports, and have been available since 2004. An example of (a few lines from) such a report is given in Table 2, for one (arbitrary) station only.

1864 MAIL Maidanak			CSR		DGFI		DUT		MCC		NICT		SAO	
	sc	wl	rb	pr	rb	pr	rb	pr	rb	pr	rb	pr	rb	pr
1864 2005-11-30 19:49	L2	532	-8	6	-72	12			5	5	-27	12	-2	3
1864 2005-11-30 21:03	L1	532	-18	5	-49	23			-14	10	-28	16	13	20
1864 2005-12-01 17:43	L2	532	29	14	-36	11	-10	15	48	6	13	11	23	1
1864 2005-12-01 19:41	L1	532	4	11	-27	12	-54	11	8	5	-15	12	30	12
1864 2005-12-02 19:40	L2	532	-35	0	-91	11	82	4	*	*	-81	5	171	4
1864 2005-12-05 18:10	L2	532	-31	7	29	8	-62	7			-38	7		
1864 2005-12-05 21:07	L1	532	-50	15	19	14	-16	18			-2	16		
1864 2005-12-05 22:19	L2	532	-40	5	4	9	-64	12			-74	6		
1864 2005-12-06 16:15	L2	532	4	7	50	9	-36	6			-17	7		
1864 2005-12-06 16:29	L1	532	12	4	-52	4	-12	3			-6	3		
1864 2005-12-08 14:03	L1	532	-16	13	-55	12	-64	12			-53	13		
1864 2005-12-08 16:35	L2	532	-5	9	10	15	-70	21			-56	13		
1864 2005-12-08 17:12	L1	532	28	1	-80	6	-32	0			-49	9		
1864 2005-12-08 20:36	L1	532	3	10	-3	9	-5	10			-32	10		
1864 2005-12-08 20:42	L2	532	8	7	26	10	-24	11			-27	11		
1864 2005-12-09 16:02	L1	532	10	5	-61	9	-59	9			-29	9		
1864 2005-12-10 14:29	L1	532	22	13	-13	12	-7	12			12	13		
1864 2005-12-10 16:39	L2	532	-5	11	40	27	-54	28			-27	20		
1864 2005-12-10 17:58	L1	532	-5	16	-29	15	-39	15			-28	16		
1864 Average		532	-4	8	-20	12	-38	11	11	6	-29	11	47	8

Table 2. *An example of en entry in the ILRS Combined Range Bias Report [Gurtner, 2006], for station Maidanak in December 2005. All values are in mm.*

To compare the reported biases in a useful fashion, statistics on a large number of values will be derived. In principle, one can do so in two ways. First, it is possible to do a covariance analysis (cf. Figure 5), where common biases from an arbitrary pair of QC centers are plotted against one another and trend line(s) and correlation coefficients are computed. The advantage of this method is that it allows/eliminates systematic differences between the two series. However, the results can be interpreted with either of the two series as a reference, so this comparison technique will not yield unambiguous results. Instead, a direct comparison is opted for here, where the bias values reported for common passes as reported by an arbitrary QC center pair will be subtracted (cf. Figure 4) and simple, straightforward statistics will be computed. It should be noted that the QC centers may have developed/refined their analysis procedures over the course of time, and therefore allowance will be made for time-depending answers, reflecting differences in quality. An indication of this is shown in Figure 6, which gives the rms-of-fit of orbital solutions on LAGEOS-1, as obtained by Delft University of Technology over the period 1985-2005; improvements in the quality of the orbital fit and therefore also in the bias detection capabilities are clearly visible.

Results

A summary of these computations is given in Table 3: the rms values of the differences. Typically, some 20,000 common LAGEOS-1 and LAGEOS-2 passes went into the computation of a single entry in this table. It should be noted that individual biases of 100 mm and larger (in absolute terms) were ignored here for

various reasons: (*i*) they may be real in some cases, but not representative for a normal situation; (*ii*) they may be very weak because of a small number of observations during such a pass; and (*iii*) they may reflect problems with the model

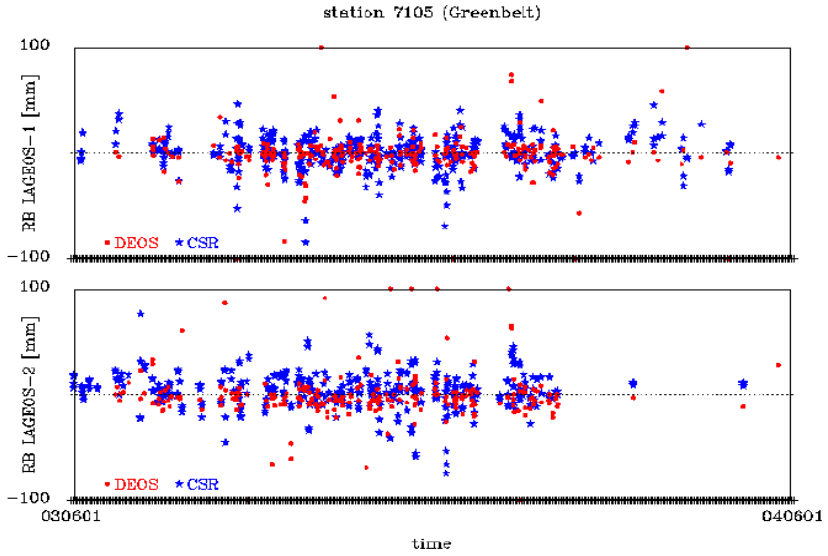

Figure 4. *A comparison of bias values reported for common LAGEOS-1 passes over station Greenbelt by QC centers CSR and Delft, as an illustration of the scatter and uncertainties in these values (direct comparison).*

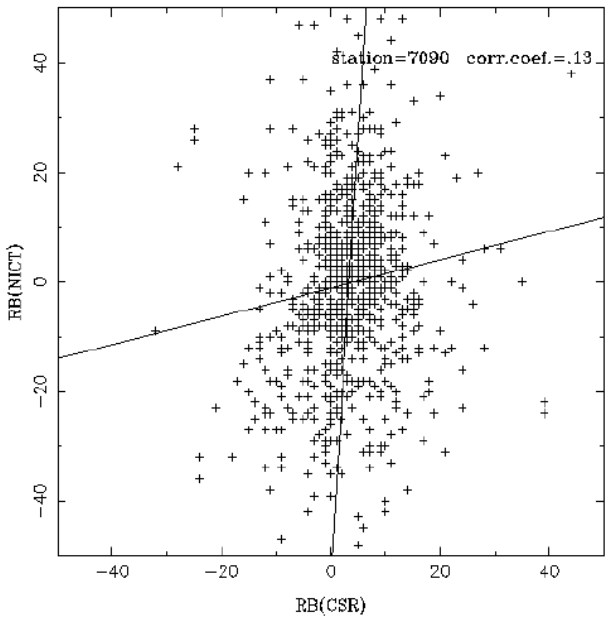

Figure 5. *A comparison of bias values reported for common LAGEOS-1 passes over station Yarragadee by QC centers CSR and NICT, as an illustration of the scatter and uncertainties in these values (covariance-style comparison).*

for station coordinates for the pertinent QC center. However, this represents a very small fraction of the total number of common passes. Another aspect to be noted is that the statistics have been computed in an unweighted fashion. Although passes with a relatively large number of normal points will lead to more stable (consistent) bias values, it is expected that this actually will average out, and straightforward statistics are given here only. After all that is what a station operator or manager is confronted with when reviewing the various bias reports.

As reported, the values have been computed for various periods: the years 2004 (when the Combined Bias Reports were initiated), 2005 and 2006. To better illustrate any trend, the rms differences are also shown in a graphical form: Figure 7.

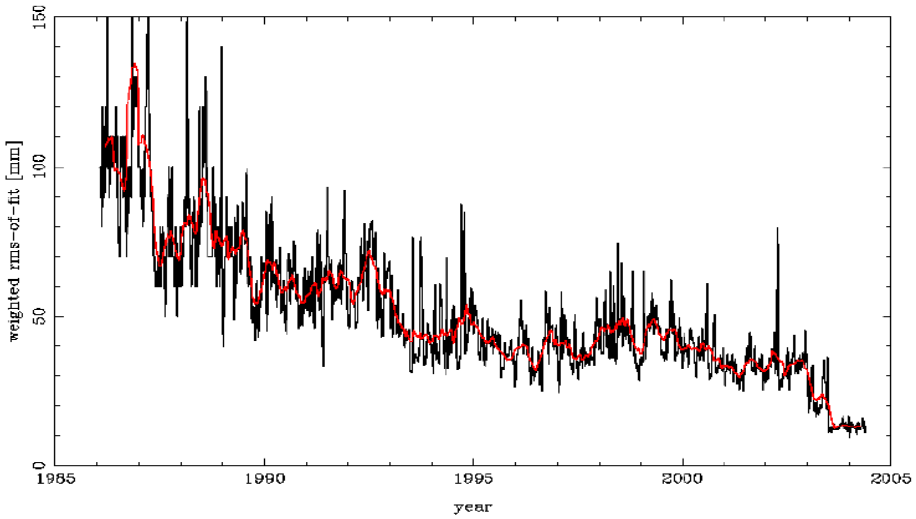

Figure 6. *Overview of the LAGEOS-1 rms-of-fit of the weekly orbital computations as done by Delft University of Technology.*

	DGFI	DUT	MCC	NICT	SAO
CSR	- / 26 / -	25 / 22 / -	28 / 25 / -	29 / 18 / -	34 / 21 / -
DGFI		- / 28 / 34	- / 29 / -	- / 29 / 28	- / 30 / 32
DUT			22 / 22 / -	25 / 22 / 21	24 / 22 / 22
MCC				26 / 25 / -	28 / 25 / -
NICT					32 / 26 / 21

Table 3. *Statistics of the differences between bias values for common LAGEOS-1 and LAGEOS-2 passes observed by the global network of SLR stations, as reported by various pairs of QC centers. Entries are for 2004, 2005 and 2006, respectively. All values are in mm.*

The discussion of the results is postponed until the next section. It is an unfortunate but real fact that the quality of the global SLR network is quite diverse: it is a mixture of top-quality stations and stations that do a little bit less in terms of performance. This might lead to the situation where the numbers reported in Table 3 and Figure 7 are indeed representative for the global network, but do not reflect the bias detection capabilities for the state-of-the-art stations properly. To that aim, the consistency computations have been repeated, but now for a subset of stations which has been given a preferential role in the derivation of the weekly official ILRS product on station coordinates and EOPs only: Graz, Greenbelt, Hartebeesthoek, Herstmonceux, McDonald, Monument Peak, Mount Stromlo, Riyadh, Wettzell, Yarragadee and Zimmerwald. These stations excel in terms of data quantity and quality, and it is expected that the bias values reported for these stations are more consistent than the values reported for the overall network. Results are presented in Table 4 and Figure 8, with similar definitions.

Discussion

The numbers as reported in Tables 3 and 4 and illustrated in Figures 7 and 8 give a very clear message: on average, the reported range bias values are consistent at the level of about 20 mm when considering the total network of SLR stations, and at the

level of about 15 mm when considering the so-called AWG core stations only. If these numbers were to be reduced to an average quality verdict on a bias value reported for an individual pass in an individual analysis report, these numbers can be divided by √2 (first order; one can argue about the level of formal correlation between the pairs of numbers).

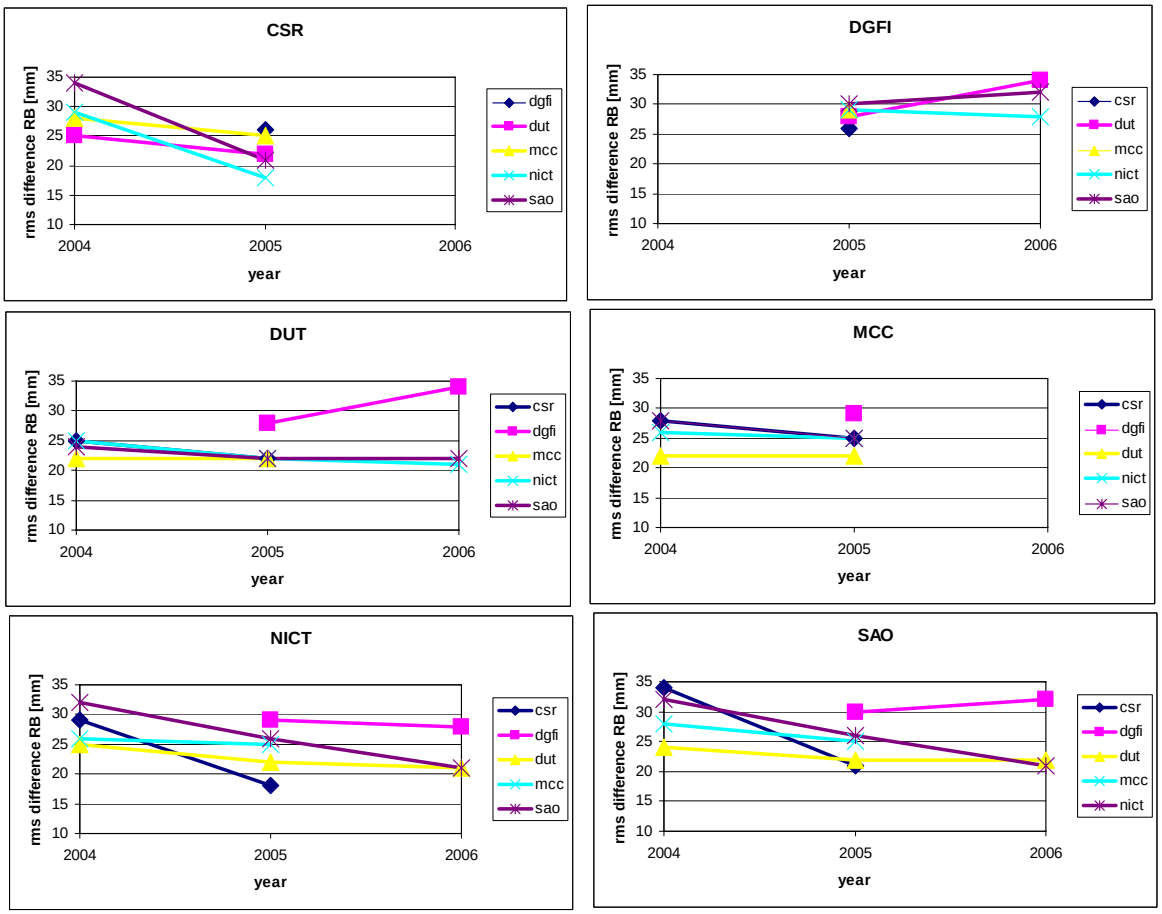

Figure 7. *Statistics of the differences between bias values for common LAGEOS-1 and LAGEOS-2 passes observed by the global network of SLR stations, as reported by various pairs of QC centers. Entries are for 2004, 2005 and 2006, respectively. All values are in mm*

The plots in particular show that the general trend of the agreement between QC center pairs is positive: the consistencies become better with time for most of them. A good illustration of this trend are all statistics involving NICT, where the level of agreement has gone down from about 30 mm (2004) to about 20 mm (2006) (Figure 7, all stations). Similar observations can be done for the AWG core stations only.

	DGFI	**DUT**	**MCC**	**NICT**	**SAO**
CSR	- / 22 / -	20 / 15 / -	20 / 15 / -	25 / 15 / -	29 / 17 / -
DGFI		- / 24 / 32	- / 26 / -	- / 26 / 25	- / 28 / 30
DUT			17 / 15 / -	22 / 18 / 14	22 / 18 / 18
MCC				23 / 19 / -	22 / 18 / -
NICT					29 / 23 / 18

Table 4. *Statistics of the differences between bias values for common LAGEOS-1 and LAGEOS-2 passes observed by the so-called AWG core stations, as reported by various pairs of QC centers. Entries are for 2004, 2005 and 2006, respectively. All values are in mm.*

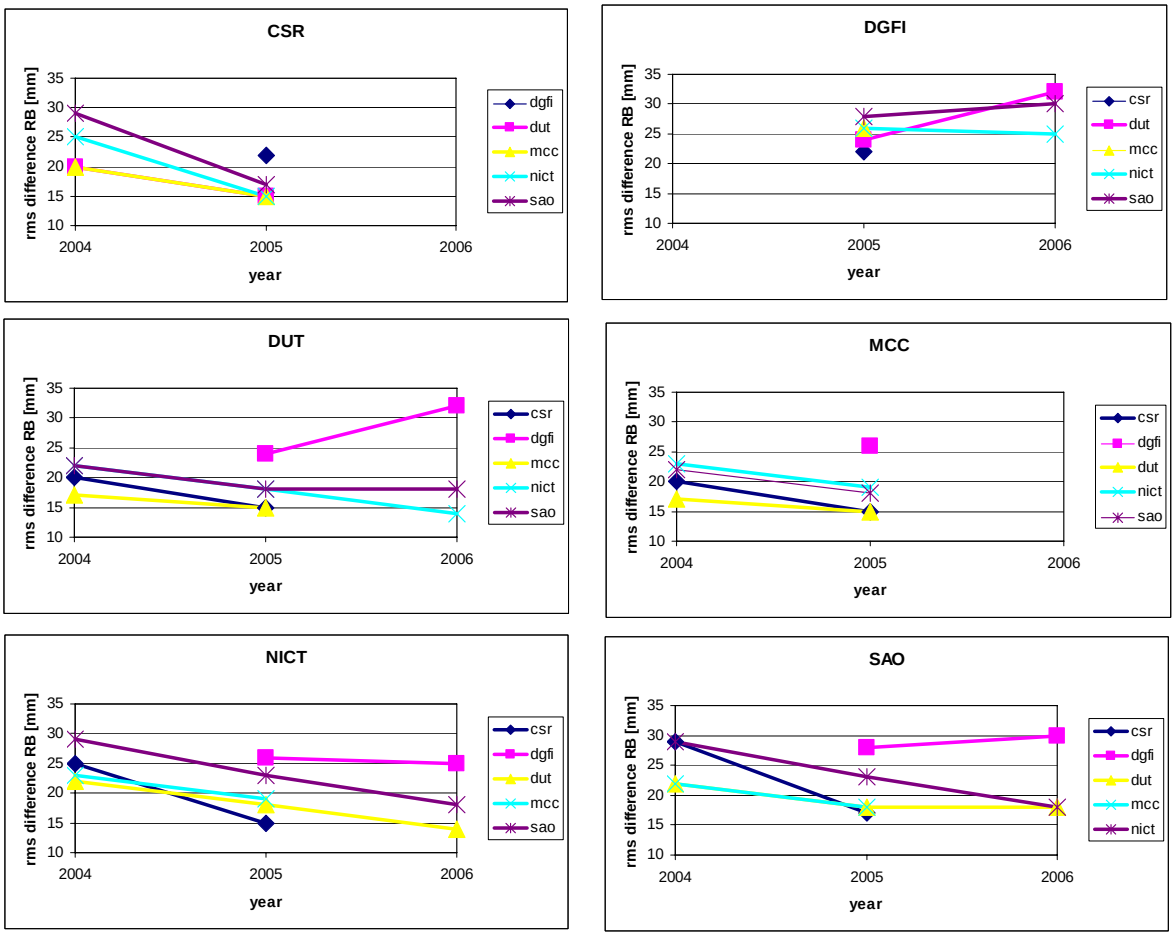

Figure 8. *Statistics of the differences between bias values for common LAGEOS-1 and LAGEOS-2 passes observed by the so-called AWG core stations, as reported by various pairs of QC centers. Entries are for 2004, 2005 and 2006, respectively. All values are in mm.*

Two points of concern remain: first of all, it is clear that the number of analysis centers involved in such analyses fluctuates quite a bit over time. In particular, the situation has become quite worrisome for 2006, with CSR and MCC not contributing anymore (and, although not visible, DUT in a similar situation since mid-2006) for various reasons. Every effort should be undertaken to improve this situation. Secondly, the plots also show that the trends are not so favorable for every QC center involved, and the consistency numbers get worse with time. This holds in particular for DGFI, and an effort should be started to remedy this.

Finally, coming back to the subject of the first part of the paper, the SLR network itself remains a continuous point of attention: only if the laser stations are distributed evenly on a global scale, can the space geodetic (and geophysical) community really take benefit from the unique capabilities of the technique to its fullest.

References

[1] Altamimi, Z., P. Sillard and C. Boucher: A new release of the International Terrestrial Reference Frame for earth science applications, *J. Geophys. Res.*, *107*(B01), 2214, doi:10.1029/2001JB000561, 2002.

[2] Gurtner, W., ILRS Combined Range Bias Report, http://aiuas3.unibe.ch/ftp/slr/summary_report.txt, 2006

[3] ILRS, http://ilrs.gsfc.nasa.gov/working_groups/awg/awg_activities/awg_min_florence1999.html, 1999.

[4] ILRS, ftp://cddis.gsfc.nasa.gov/pub/slr/products/pos+eop/, 2006.

The ILRS Standard Products: A Quality Assessment

G. Bianco[1], V. Luceri[2], C. Sciarretta[3]

1. Agenzia Spaziale Italiana, Centro di Geodesia Spaziale, Matera, Italy
giuseppe.bianco@asi.it / fax: +39-0835-339005
2. e-Geos S.p.A., Centro di Geodesia Spaziale, Matera, Italy
3. Telespazio S.p.A., Roma, Italy

Abstract

In June 2004 the Space Geodesy Center (CGS, Matera, Italy) of the Agenzia Spaziale Italiana (ASI) has been selected by the International Laser Ranging Service (ILRS) as its Primary Official Combination Center for station coordinates and Earth Orientation Parameters.

From the beginning, the CGS has been providing the weekly operational combined ILRS solutions (SSC/EOP), also supporting the IERS B Bulletin production; moreover, CGS has produced the official ILRS contribution to ITRF2005, by combining the weekly solutions, from 1993 to 2005, submitted by the contributing ILRS Analysis Centers.

The CGS combination methodology relies on the direct combination of loosely constrained solutions. This methodology has been implemented and tested to handle site coordinates, site velocities, EOP, LOD coming from the same and/or different techniques.

The whole set of weekly combined solutions, those produced in support of ITRF2005 as well as the operational ones, is analyzed in detail in this contribution, to show the coherence and robustness in terms of global parameters as well as station coordinates.

Introduction

Soon after the establishment of the ILRS a strong need was felt to coordinate the work and combine the results of the various SLR data Analysis Centers (AC's) in order to define and distribute a series of "certified" ILRS products to the users community.

In 1999 the ILRS Analysis Working Group, chaired by Ron Noomen (TU Delft), outlined two Pilot Projects for the estimation of site coordinates and EOP, separately, from different AC solutions; the year after the two Pilot Projects were joined and the first results discussed. In 2003 the ILRS issued a formal Call for Participation for the generation of ILRS products,

In 2004 the ILRS AC structure was finalized and official delivery of standard products started; the CGS was selected as the Primary Official Combination Center, referred to as ILRSA, while DGFI was selected as Backup Official Combination Center or ILRSB.

In 2005 the ILRS contributed to the definition of ITRF2005 with its official time series.

The ILRS Standard Products

Presently, the following six AC's regularly contribute to the production of the ILRS standard products by means of weekly solutions:

ASI, Agenzia Spaziale Italiana, I

BKG, Bundesamt fuer Kartographie und Geodaesie, D
DGFI, Deutsches Geodatisches Forschungsinstitut, D
GFZ, GeoForschungsZentrum Potsdam, D
JCET, Joint Center for Earth System Technology, USA
NSGF, NERC Space Geodesy Facility, UK

Those ACs have been recognized after passing the benchmark tests as requested by the AWG. Other institutes are now under test and on the way to become official ILRS Analysis Centers.

The standard weekly ILRS combined solutions (either the primary and the backup) are made available each Wednesday at CDDIS and EDC, together with the single contributing AC solutions. The complete time series, starting from 1993, is available at CDDIS and EDC. A backwards extension of the time series, back to 1980, in now under construction.

A complete description of standards and methods adopted in the combination is given in [Bianco et al, 2003].

The ILRS coordinate solution in the ITRF 2000 and ITRF 2005

The first quality assessment has been done comparing the ILRS coordinate solution with the ITRF2000 as well as with the newly issued ITRF2005.

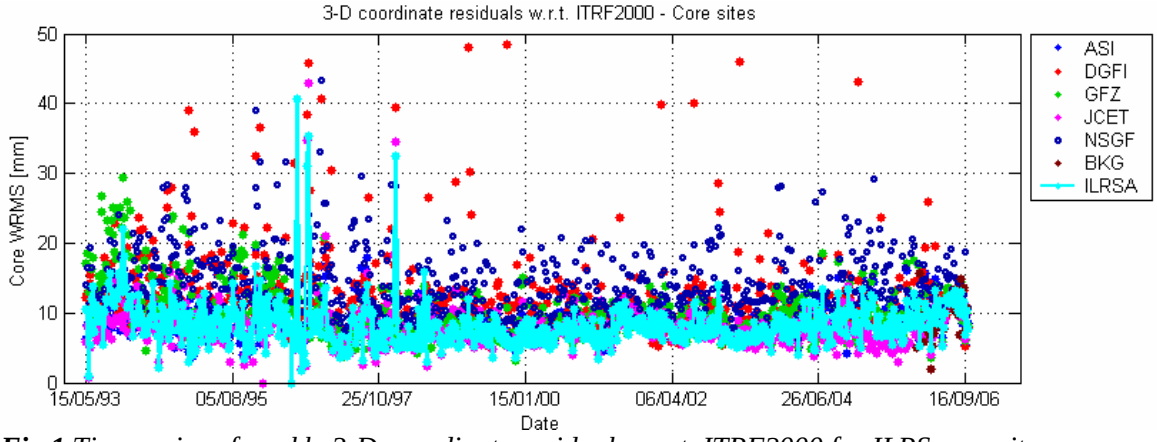

Fig 1 *Time series of weekly 3-D coordinate residuals w.r.t. ITRF2000 for ILRS core sites from individual AC solutions as well as from the combined ILRSA solution.*

Generally speaking, the plot in Fig. 1 shows that the combined solutions represents a real improvement, in terms of consistency and dispersion, with respect to the individual AC solutions. The average 3-D residuals with respect to ITRF2000 are consistently at or below the 1 cm level, as confirmed by the plot in Fig. 2, which shows the 3-D coordinate residuals WRMS as a function of time.

It shows very clearly the fundamental role of the so called “core” sites (i.e., SLR stations with a consolidated tracking history in terms of data quantity and quality). The behavior of the total network worsens after year 2000 due to the introduction of several new observing sites which are not properly modeled in ITRF2000.

As expected, the situation improves with the ITRF2005, as shown if the plots in Figures 3 and 4 below. In particular, the new stations appear properly accounted for; moreover, the 3-D coordinate residuals for the “core” stations behave remarkably well, with an average value constantly below the 1 cm level.

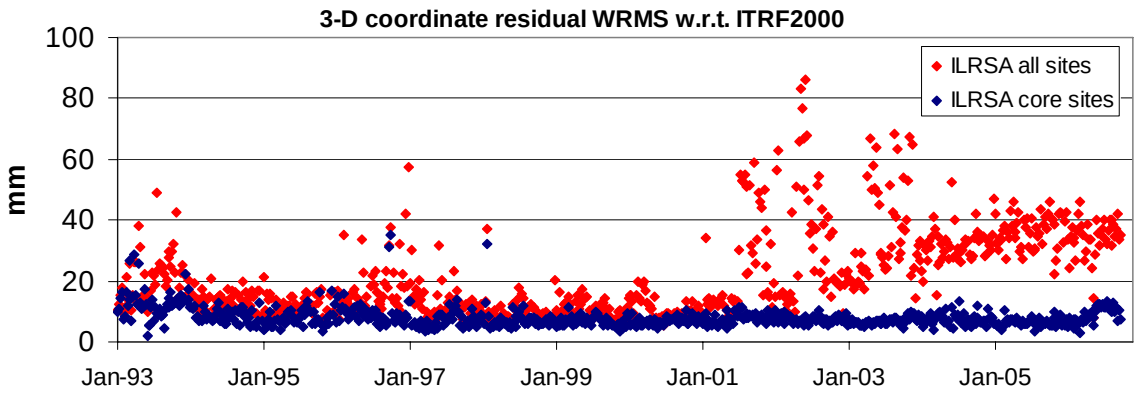

Fig. 2 *Time series of weekly 3-D coordinate residuals WRMS with respect to ITRF2000*

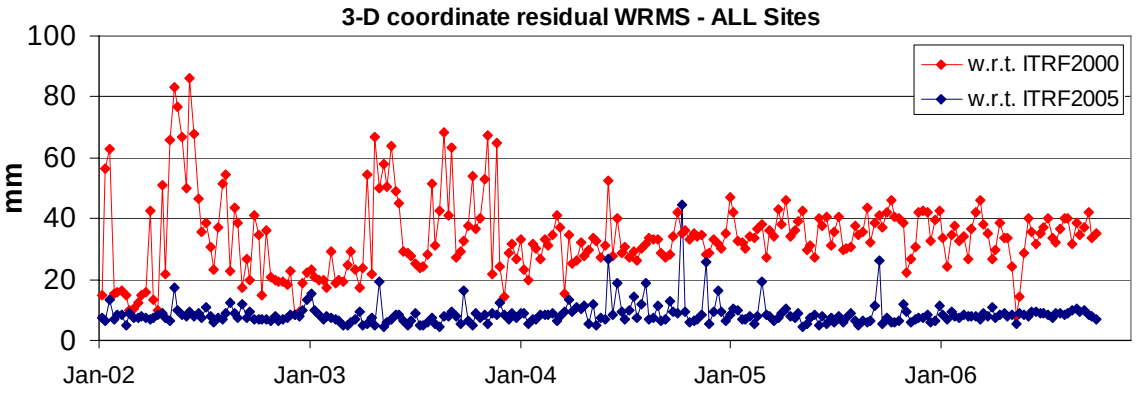

Fig. 3 *Time series of 3-D coordinate residual WRMS for all ILRS sites with respect to ITRF2000 and ITRF2005, as computed in the ILRSA combined solution*

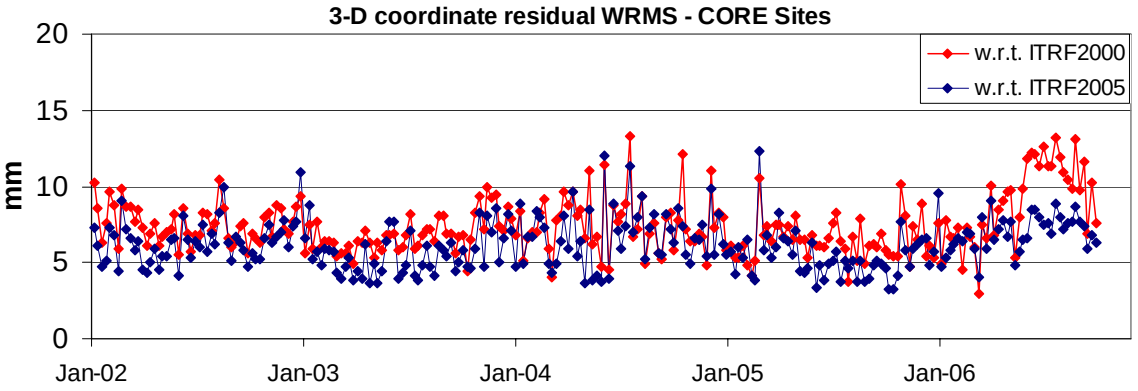

Fig. 4 *Time series of 3-D coordinate residual WRMS for ILRS "core" sites with respect to ITRF2000 and ITRF2005, as computed in the ILRSA combined solution*

ILRS TRF origin with respect ITRF 2000/2005 origins

Another quality assessment has been done by looking at the time series of the 3-D distances of the ILRS Terrestrial Reference Frame origin with respect to another ITRF origin. Each TRF realized by the SLR stations in a loose solution places naturally its origin in the center of mass of the Earth: its Cartesian coordinate offsets from a conventional origin describe the geocenter location. This time series, often referred to as "geocenter motion", is particularly interesting since it can be proposed as a new standard ILRS product.

The plots in Fig. 5 represent respectively the X, Y and Z components of the distance between the ILRS weekly origin with respect to the ITRF2000 and ITRF2005 origins, computed by roto-translations ("geometric" method) in the period 2002-2006. A clear annual signature is visible in all three components. The two series look pretty similar, with a slightly more evident drift in the Z component with respect to the ITRF2005 origin.

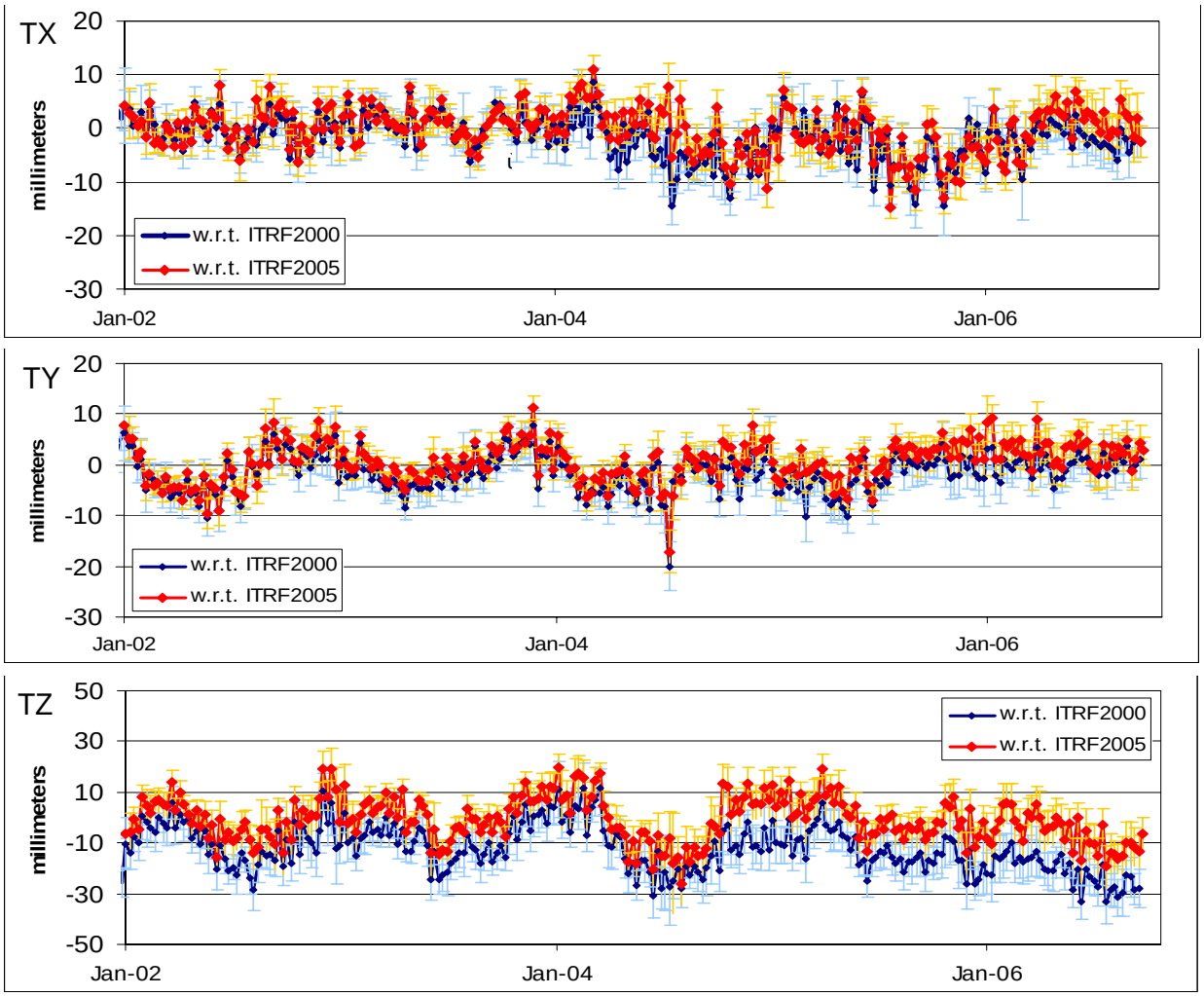

Fig. 5 *Time series of distance between the ILRSA geometric origin and the ITRF2000 and 2005 origins*

The translations of the ILRS TRF origin can also be obtained with a more rigorous data analysis strategy: through the estimates of the C_{10}, C_{11}, S_{11} geopotential coefficients, ("dynamic" method).

The plots in Fig. 6 show a direct comparison between the geometric and the dynamic ILRS TRF origin translations, with the latter obtained via the dynamic solution done by ASI. The behavior of the two time series is remarkably similar; the dynamic origin evolution looks smoother but the main features are present in both series.

This confirms that the geometric offsets, as defined by the standard ILRS combined solution, could be used to properly represent the geocenter motion.

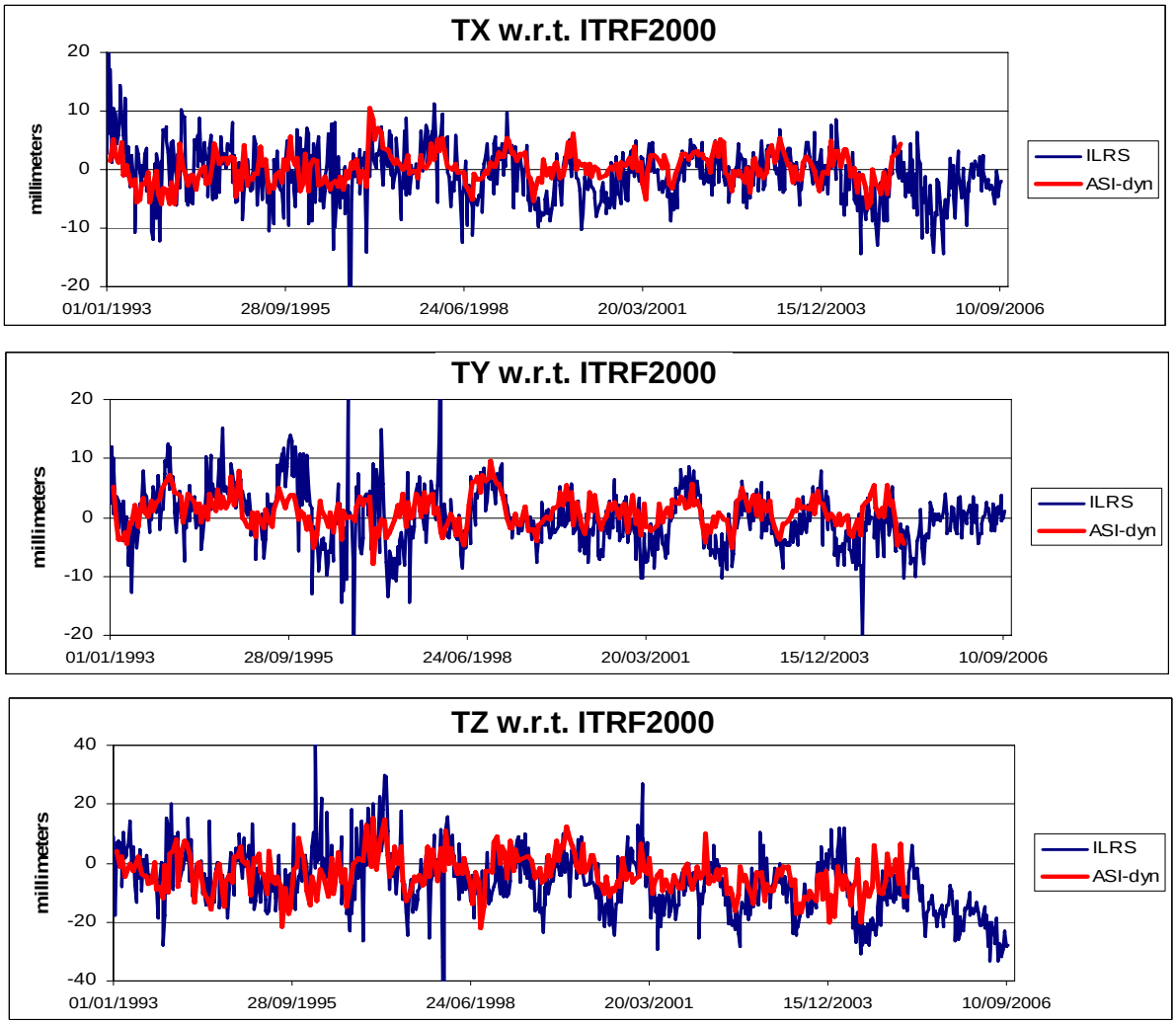

Fig. 6 *ILRSA geometric vs ASI dynamic geocenter motion.*

The scale factor

Much debate has been generated soon after the publication of the ITRF2005, whose scale has been defined without taking into account the ILRS contribution, due to an apparent strange behavior of the ILRS scale itself.

However, based on our work, we do not find evidence of any strange effect in the ILRS scale, as shown in the plots hereafter, covering the period January 2002 to mid 2006.

The ILRS scale with respect to the ITRF2000 is nicely flat, while a clear trend shows up in the scale time series with respect to the ITRF2005.

The selection of the core sites to be used when comparing different reference frames is crucial and can introduce artifacts.

Earth Orientation Parameters

In Fig. 8, ILRS X-pole, Y-pole and Length of Day (LOD) residuals with respect to the USNO “finals.daily” EOP time series, are plotted. The ILRS EOP products look pretty good and stable, with a WRMS of the residuals of the order of 0.25 milliarcseconds.

We've also made an external comparison between ILRS EOP's and those computed by other space geodetic services, namely IVS and IGS (CODE solution). The results for the Y component are shown in Fig. 9 below.

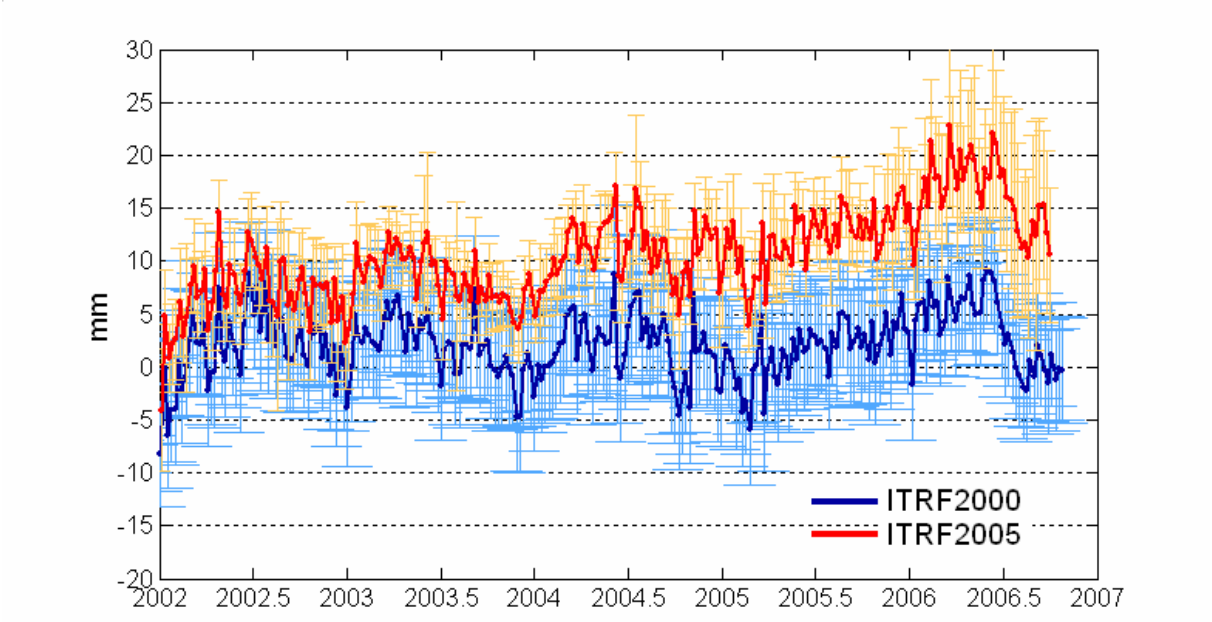

Fig. 7 *ILRSA scale with respect to ITRF2000 and ITRF2005*

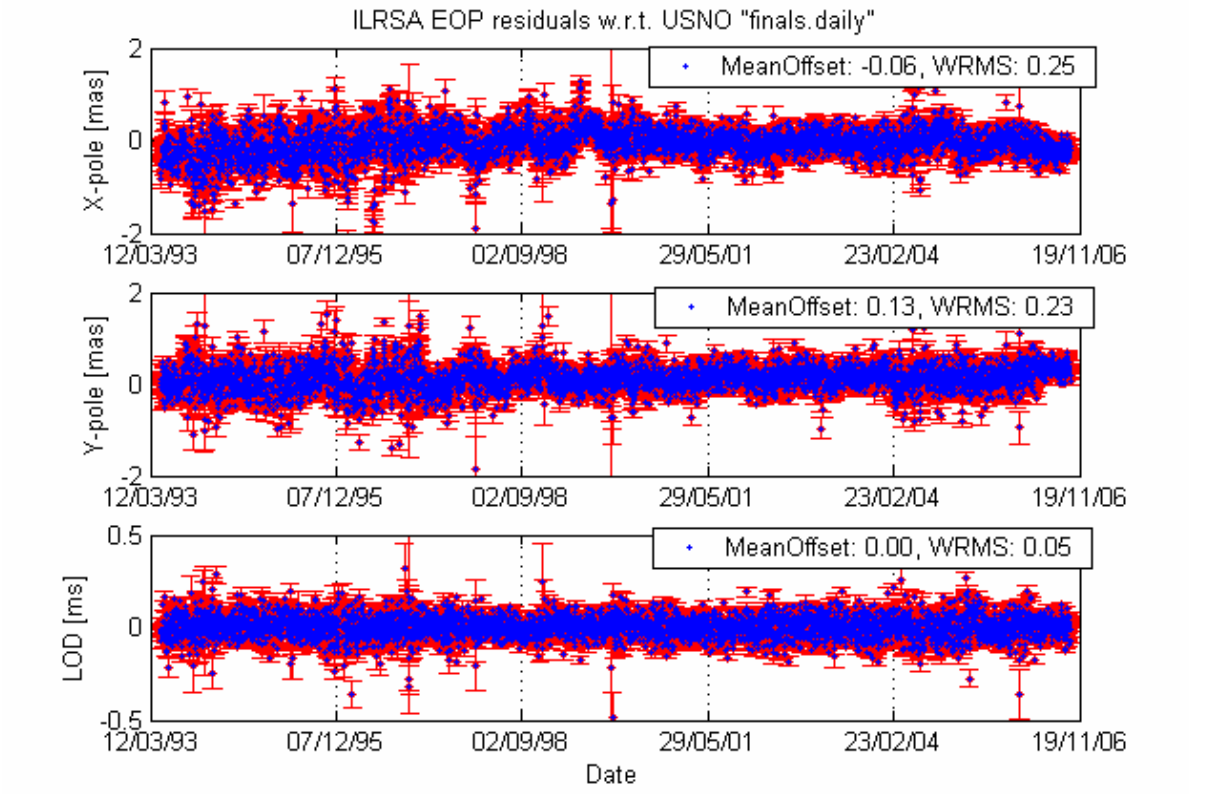

Fig. 8 *ILRSA EOP residuals with respect to USNO "finals.daily" EOP's*

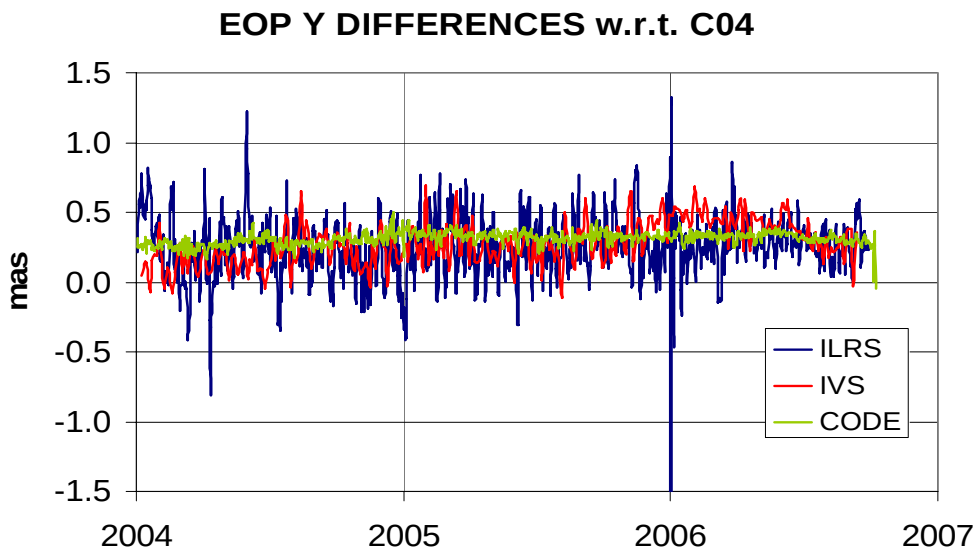

Fig. 9 *ILRSA EOP differences with respect to IERS EOPC04*

Conclusions

After two years of continuous operations, the routine ILRSA combination production process is stable and reliable. The processing chain has been made almost completely automatic and has already demonstrated a high degree of dependability.

Other than for the definition of origin and scale, almost unique to SLR, the ILRS standard products are a very valuable monitoring tool for site coordinates and EOPs, with a very fast response time.

This work has also shown that the geocenter motion, geometrically derived from the weekly solutions, is reliable enough to be included among the future ILRS standard products.

References

[1] Bianco, G., Devoti, R., Luceri, V., 2003, Combination of loosely constrained solutions, Proceedings of the IERS Workshop on Combination Research and Global Geophysical Fluids (Munich, 18-21 Nov 2002), IERS Technical Note 30, 107-109, 2003

Systematic range bias 2005-06

Toshimichi Otsubo[1], Naoko Obara[1]

1. Kashima Space Research Center, National Institute of Information and Communications Technology, 893-1 Hirai, Kashima 314-8501 Japan.

Contact : otsubo@nict.go.jp / Fax: +81-299-84-7160

Introduction

Most of modern laser ranging systems potentially have 1-millimetre-precision measurement ability in a normal-point basis. However, when it comes to 1-millimetre 'accuracy', it has not been fully achieved yet and it is still a challenge for the International Laser Ranging Service (ILRS) network.

At National Institute of Information and Communications Technology (NICT), Kashima, Japan, we check the quality of laser ranging data from the whole ILRS network, in two folds. One is routine automated quality check analysis which gives quick alarms for large and obvious anomalies, and the other is precise residual analysis for sub-centimetre systematic range biases.

Routine quality check analysis

We started the 3-satellite (two LAGEOS and AJISAI) routine bias report in 1997 (Otsubo and Endo, 1998) and enhanced it to the 7-satellite (plus STARLETTE, STELLA and two ETALON) analysis in 1999 (Otsubo, 2000). It was again significantly upgraded in May 2005 as follows.

Firstly, we further added satellites: ERS-2, JASON-1, ENVISAT, GPS-35, GPS-36, GLONASS-87, GLONASS-89 and GLONASS-95. Note that some of these satellites might be omitted from the analysis report in the case of failing a certain criteria in terms of data quality and quantity. Nevertheless, the analysis reports constantly include well more than 10 satellites. The increase of number of satellites and the variety of satellite altitudes will certainly help the ILRS stations easily point the problem and the cause.

We have switched the orbit analysis software from 'concerto v3' to 'concerto v4'. The new version is almost compatible to the physical models recommended in IERS Conventions (2003). The station coordinates basically unchanged to ITRF2000, but those of new or significantly improved stations after the year 2000 were readjusted. Therefore the quality of our analysis reports should be more accurate.

We now publish the report every day, which used to be a week interval before May 2005. The report timing was also improved from 48-hour delay to 24-hour delay. Every morning in Japanese Standard Time (around 0 to 1 hr UT), a report covering up to two days before is being released. Such a quick reporting scheme became possible thanks to the rapid submission (typically within a few hours after the observation) and the rapid archive service (at CDDIS and EDC) of normal point data. The daily reports are available at our website and also via email. See figure 1 for previous website page. New website is: http://www.science.hit-u.ac.jp/otsubo/slr/bias/ [ed].

The reports are distributed through the SLReport mailing list every Wednesday, and they are being sent to registered users even on a daily basis.

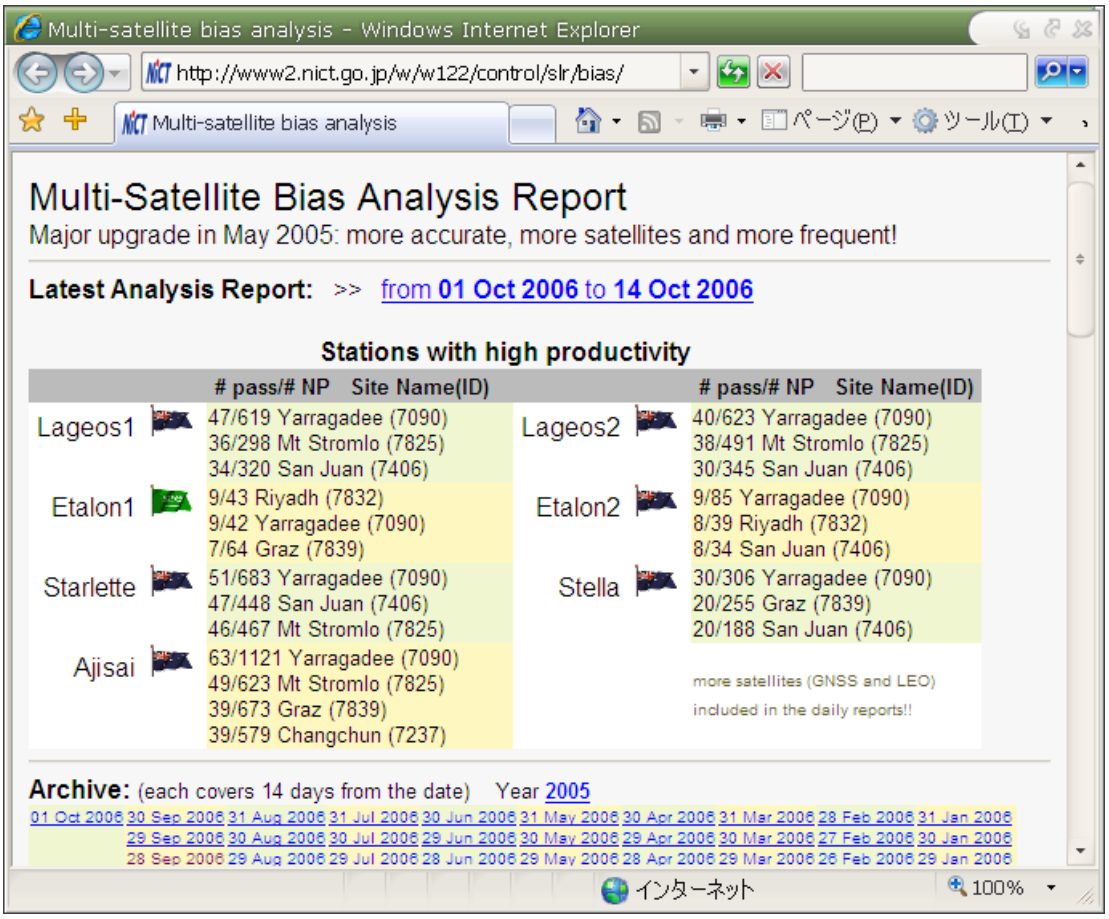

Figure 1. *Multi-satellite bias analysis webpage at NICT.*

Range bias vs intensity

We have proposed a quality assessment method for the intensity-dependent biases (Otsubo, 2000). The post-fit residual data were sorted by the number of single-shot returns per normal point bin which should be strongly related with the signal intensity into a detector. If the detection signal intensity varies, and if the detection timing is dependent on it, there will be intensity dependent bias. Our previous studies also pointed out it is also related to the so-called target signature effect, which is now the major error source of laser ranging technique due to the reflection from multiple retroreflectors on board. The range measurement can differ, at maximum, by 4 to 5 cm for AJISAI and ETALON, and 1 cm for LAGEOS (Otsubo and Appleby, 2003).

We applied the same procedure to the 2005-2006 data set. Three sets of satellite types were chosen: LAGEOS-1 + LAGEOS-2, AJISAI, and STARLETTE + STELLA. For each satellite, the worldwide laser ranging data for 360 days from September 2005 to August 2006 were used for orbit determination. Orbits were solved for every 5 days for LAGEOS satellites and 2 days for others. The station coordinates and range bias were adjusted for all stations. The post-fit residual weighted rms of normal points was 1.0 to 1.2 cm for LAGEOS satellites and 1.5 to 2.5 cm for others.

The intensity dependent tests were carried out for most productive 24 stations during the period. The whole results are available at:

http://www.nict.go.jp/w/w122/control/pod/bias-intensity-0506.pdf

Fig. 2 (a) to (c) shows the three typical samples of them. The first case of Herstmonceux is the station where the return signal energy is almost strictly controlled to single photoelectron. This observation policy successfully results in the flat trend, that is, no intensity dependence seen for this station, in Fig. 2 (a). The Yarragadee station in Fig. 2 (b) represents good MCP stations. There is no intensity dependence larger than a few millimeters either. The typical result of (C-) SPAD stations is shown by Mt Stromlo in Fig. 2 (c). As the target signature studies suggested the strong signal makes the range measurement shorter. The AJISAI case is the largest in most cases, but a number of stations show significant trend (mostly negative) even for LAGEOS and STARLETTE + STELLA.

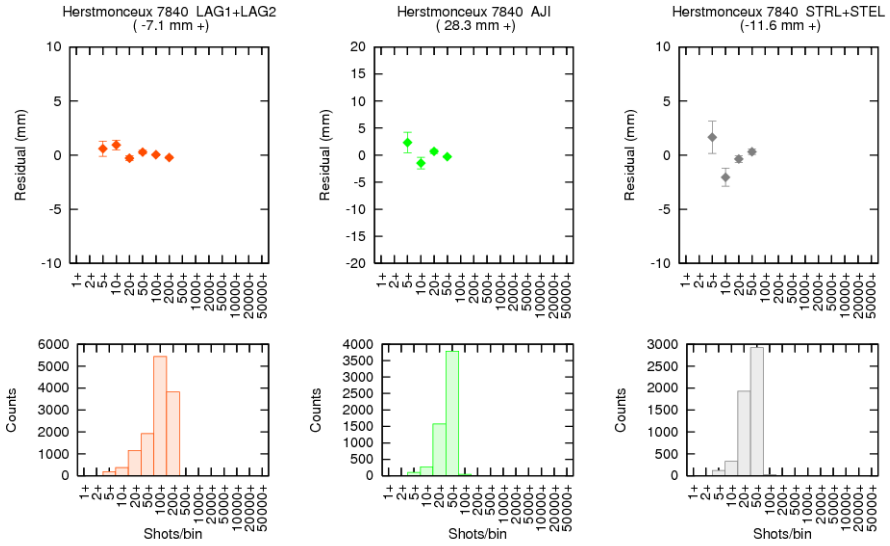

Figure 2 (a). *Intensity dependence test. Single photon Herstmonceux station.*

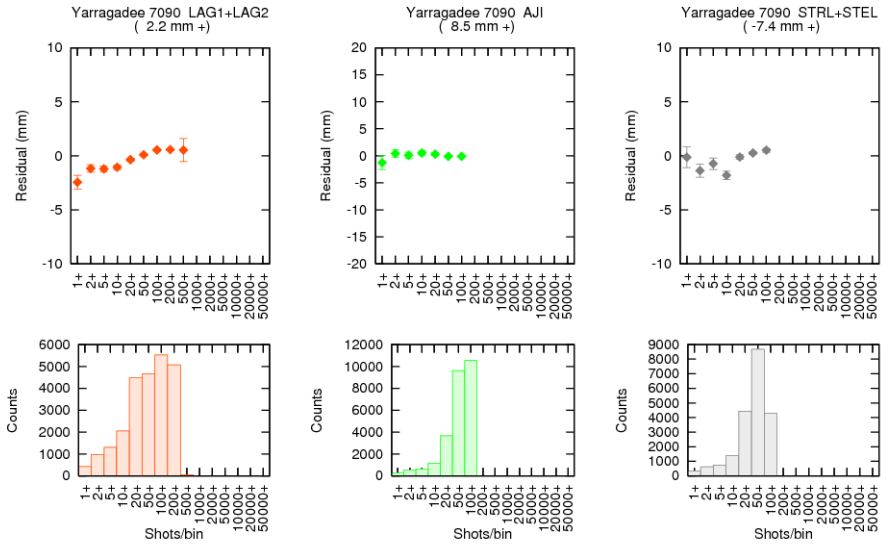

Figure 2 (b). *Intensity dependence test. MCP Yarragadee station.*

It is strongly recommended for every ILRS station to look into the result, and consider how the intensity dependent bias can be removed if it exists. As proven in previous

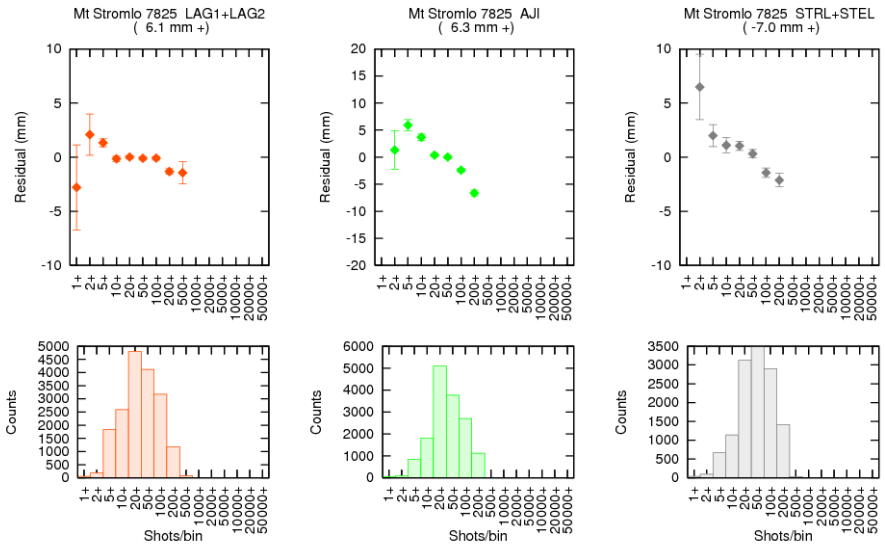

Figure 2 (c). *Intensity dependence test. C-SPAD Mt Stromlo station.*

studies (Otsubo and Appleby, 2004), the signal intensity is closely related to the elevation angle, and as a result the height component of station coordinates can be affected. This study probably underestimates the true intensity dependence. Note that the results from this study are just a guideline - it is the best to check the intensity dependence at each station, for example by inserting and removing the neutral density filter in front of the detector.

Range bias vs applied system delay

The alternative approach is the use of the applied system delay (given in the ILRS normal point format) as a sorting parameter.

The applied system delay is the value to be subtracted from the raw range observations, and it is not constant. Therefore it is to be regularly observed by ranging to terrestrial targets, what we call ‘calibration’. There should not be any correlations between the range residuals and the applied system delay, in the ideal case. If there were, the station would have a systematic error in its ranging procedure to a terrestrial target or in its data processing stage.

We used the same set of the residual data as the previous section. At a number of stations, there have been jumps in the applied system delay itself probably due to some changes in optical or electronic path. Some stations seem to have multiple configurations (dual detectors, etc.) each of which gives different applied system delay. Such discontinuities themselves are not a problem at all as long as the reason is exactly known.

The bin size was set to the two-way range of 66 ps (1 cm in one-way distance). We applied the sorting procedure to the same 24 station as the previous section. The sorting procedure was chopped into a few portions for stations with large jumps. The graphs are also available at our website:

http://www.nict.go.jp/w/w122/control/pod/bias-delay-0506.pdf
(graphs for calibration dependent bias)

http://www.nict.go.jp/w/w122/control/pod/delay-0506.pdf
(auxiliary graphs for variation of applied system delay for the 1-year period)

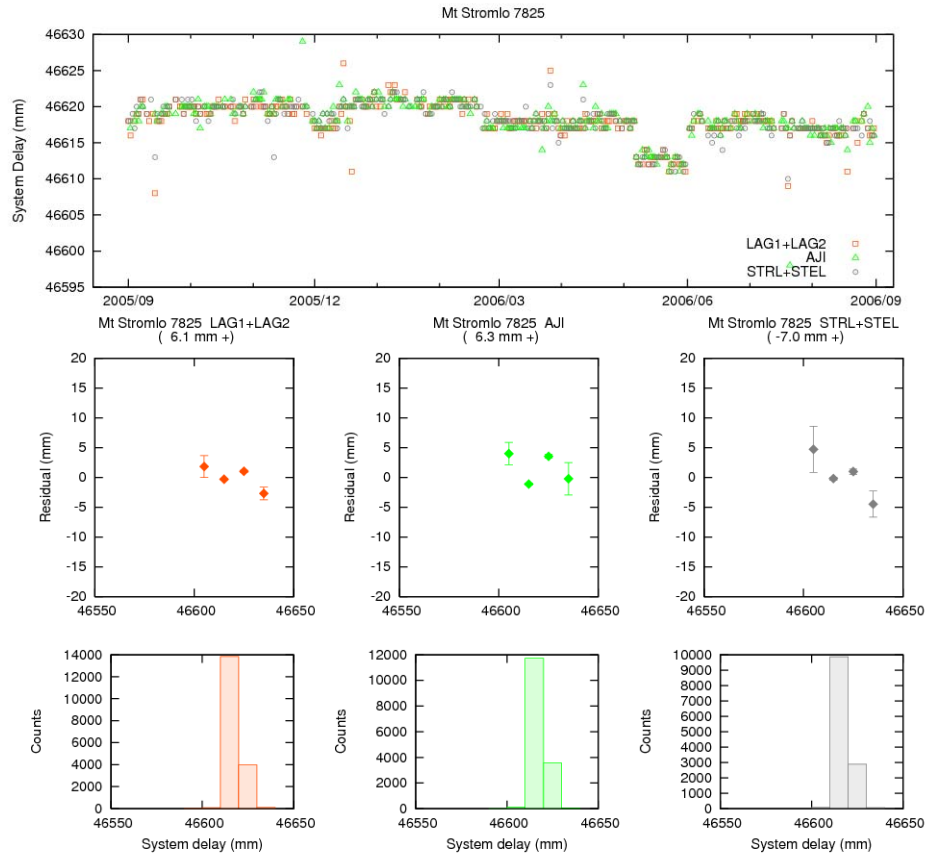

Figure 3 (a). *Calibration dependence test. Mt Stromlo station.*

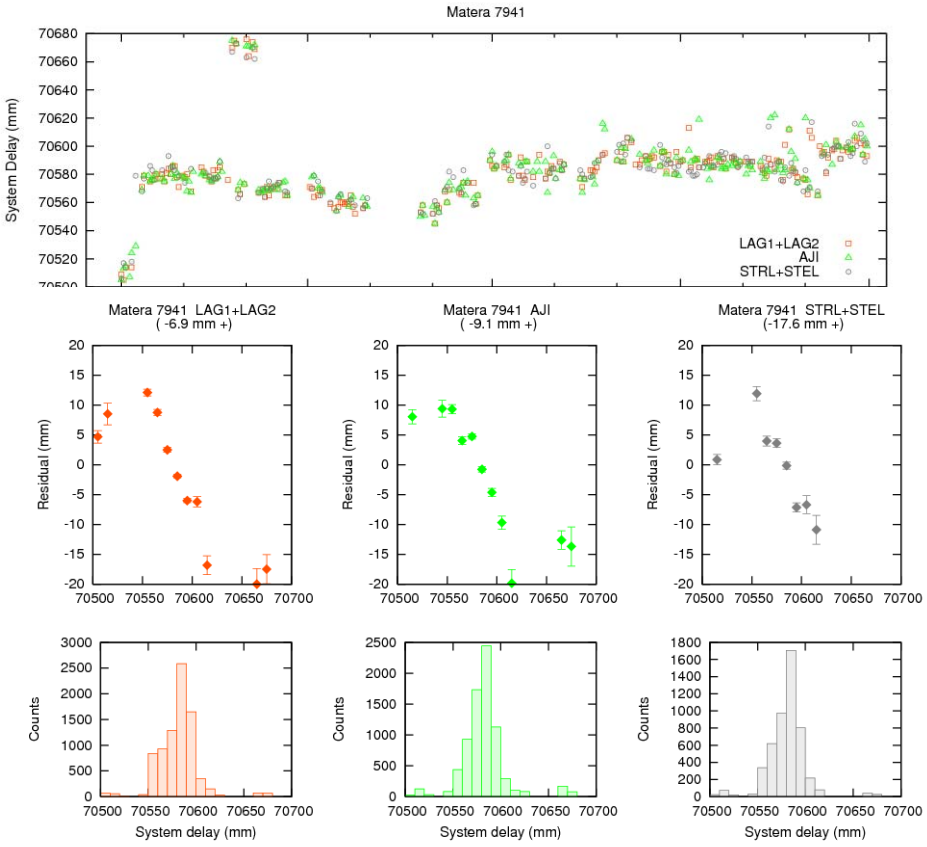

Figure 3 (b). *Calibration dependence test. Matera station.*

Two results are shown in Fig. 3 (a) and (b) among the 24 cases. The first case (Fig. 3 (a)) is probably the best one of all: Mt Stromlo. Its applied system delay has been very stable throughout the year, almost within ± 1 cm (top). There has been no significant calibration dependent bias (bottom). Such long-term stability of calibration ranging helps the long-term stability of satellite ranging. The next graph of Fig. 3 (b) shows those for Matera station. The stability of applied system delay is also good (± 3 cm) for this station. However, there is a steep negative trend for all three types of satellites. A possible reason is that a part of the variation in calibration ranging might not be true and therefore the raw observation would be 'wrongly calibrated' by the calibration procedure.

The long-term variation of terrestrial target ranging is hardly separable from the seasonal or secular variation of station height. Therefore, the result from this approach has a risk of sending a wrong alarm if the station coordinates experience unmodelled effects like loading displacement. It is strongly recommended for each station to understand why the calibration measurement varies and strive to reduce the variation.

Conclusions

In addition to the multi-satellite daily bias reporting system, we demonstrated the more precise ways for quality assessment of laser ranging data. We use the single shot returns per normal point bin, and the applied system delay, as a sorting parameter. Some correlations were found between the range data and these sorting parameters.

It is important to note that most of the information that is potentially useful to assess the quality is lost in the process of normal point generation. It is essential that each station performs extensive tests on site in order to eliminate any systematic bias and to keep the data quality stably high.

References

[1] Otsubo, T., and T. Endo, "Quick bias report for LAGEOS and AJISAI data," Proc. 11th International Workshop on Laser Ranging, Deggendorf , 2, 650-653, 1998.

[2] Otsubo, T., "New approach to quality check: multiple satellite and intensity dependence," Proc. 12th International Workshop on Laser Ranging, Matera, CDROM, 2000.

[3] Otsubo, T., and G. M. Appleby, "System-dependent Centre-of-mass Correction for Spherical Geodetic Satellites," Journal of Geophysical Research, Vol. 108, No. B4, 2201, doi:10.1029/2002JB002209, 2003.

[4] Otsubo, T., and G. M. Appleby, "Centre-of-mass correction issues: toward mm-ranging accuracy," 14th International Laser Ranging Workshop, San Fernando, pp. 467-471, 2004.

A reassessment of laser ranging accuracy at SGF Herstmonceux, UK

Philip Gibbs[1], Graham Appleby[1] and Christopher Potter[1]

1. Space geodesy facility, Herstmonceux, East Sussex, UK.

Introduction

Gibbs et al (2007, these proceedings) reports on a major upgrade and expansion of capability at the Space Geodesy Facility, Herstmonceux, UK. A prerequisite of the laser ranging upgrade to kHz repetition rate is the in-house build of a ps-level precision event timer, based on Thales clock units and dubbed HxET. Extensive use has been made of HxET since it was completed during the summer of 2006 to calibrate the existing cluster of Stanford counters prior to making routine use of HxET. In particular, we are very interested in back-calibrating all the Herstmonceux data for the period 1994-present, during which time the Stanford counters had been exclusively used. In this paper we detail the results of this re-calibration, and also consider the effect the correction to our LAGEOS data will have on the published site coordinates in the ITRF.

Previous calibrations

Extensive tests on the linearity of the Stanford counters at satellite ranges, from a few to approximately 150ms were carried out by Gibbs (Appleby *et al*, 1999, Gibbs *et al*, 2002) using an early version of the Portable Pico Event Timer (P-PET, Hamal *et al*, 2007). The method used is to record start signals and subsequent noise events simultaneously by the P-PET and by the Stanford counter(s) that are under test. A hardware delay is used to move the average interval between start events and detected noise events from a few ms up to 150ms, the range encountered during real satellite ranging. For each event, comparison of the time interval as measured by each Stanford relative to that determined by the highly-linear P-PET, gives an estimate of the error in time interval determined by each Stanford. From this work, a correction table as a function of range was compiled and issued in SLRMail 0891 in 2002 January. The effective dates of application of the results are 1994 October to 2002 January and the magnitude of the corrections reaches 8mm. From 2002 February the corrections are applied at the station as part of pre-processing.

With the availability of HxET, these linearity tests were repeated during 2006 October; the results were found not to be significantly different from those determined in 1999 and 2001, confirming the ongoing validity of the correction table given in SLRMail 0891. The comparison between HxET and the three Stanfords in use at Herstmonceux (coded SRa, SRb and SRd) is shown graphically in Figure 1. The horizontal axis gives the time delay after which each set of measurement comparisons are made of 'flight time' as recorded by the Stanford counters and by HxET. The vertical axis records the mean difference of each Stanford-recorded flight time from that recorded by HxET. It is noted that SRd, the counter currently in use at the station, exhibits close-to linear behaviour over the entire time-range. Excursions from linearity of up to 100ps (15mm in range) are seen for the other two counters.

New Calibrations

The availability of HxET has meant that more detailed measurements of non linearity effects can be made on the Stanford counters. In particular, we are interested in the behaviour at close ranges, within the first few micro-seconds. Time constraints on our previous experiments with the PPET precluded such a detailed study, and errors in

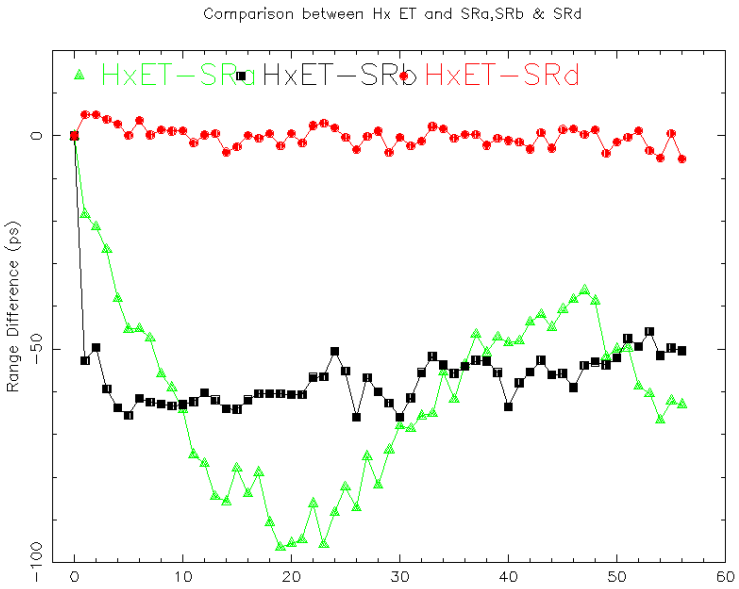

Figure 1 *SGF long-range linearity determination of three Herstmonceux Stanford counters relative to the event timer H*xET.

this time-region will directly affect calibration ranging results and thus all satellite ranges from the station. We expect some significant effects in this region since the Stanford manual shows both high-frequency periodic signatures and more random departures from linearity in the critical range of about 1micro-second, the distance of the prime SGF calibration target. A figure from the Stanford manual is reproduced here as Figure 2, with the time-range locations of the calibration targets marked. We carried out our tests on the behaviour of SRa, SRb and SRd against HxET in this critical range of from zero to 5μs; the results are shown in Figure 3 below and are to be compared with the Stanford manual results reproduced here in the right-hand plot of Figure 2.

In the range of from zero to 2μs the measured behaviour of our three Stanford counters is close to that expected from the specifications, with maximum departure from linearity of from 50 to 100ps, at a range of 1μs. Beyond a range of 2μs, the behaviour of the counters diverges. A probable explanation for the inter-counter scatter evident in these results is the high-frequency periodic structure shown in the

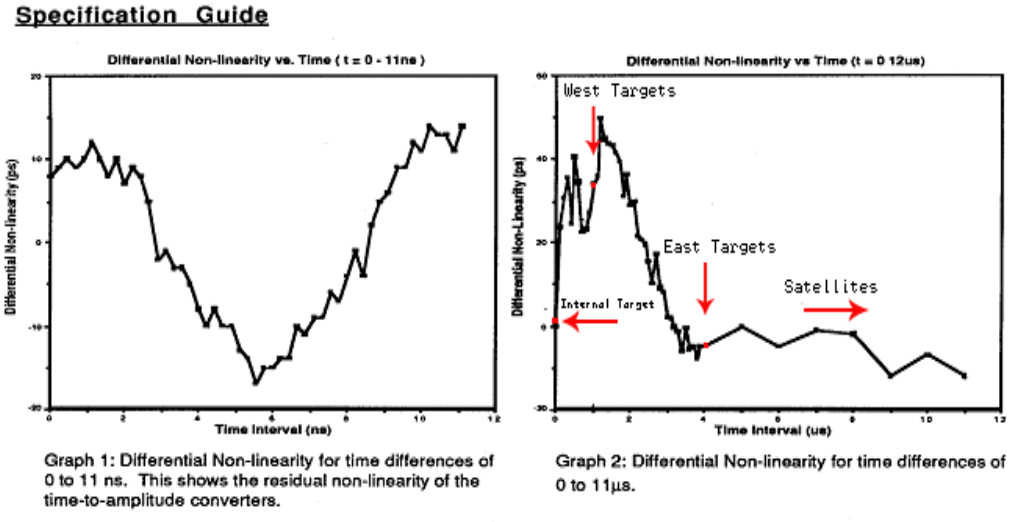

Figure 2 *Short-range non-linearity of Stanford counters as given in specification*

specification (Figure 2, left-hand plot) and in our high-resolution results shown in Figure 4 where we find 22ns periodic effects (cf 11ns expected from specifications) of amplitudes up to 20ps (~3mm). This final result places a limit to the accuracy with which we will be able to determine corrections to range measurements made with the Stanford counters.

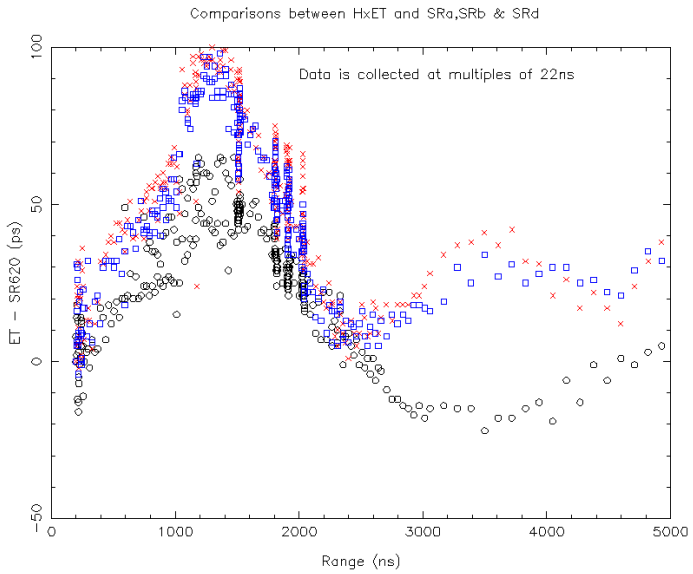

Figure 3 *SGF close-range linearity determinations of three Herstmonceux Stanford counters relative to the event timer HxET.*

In summary, at the effective range of the SGF primary calibration target (890-930ps, dependent on electronic set-up), the non-linearity of the counters imparts an average of ~50ps error into the observed range; this value is dependent on the range itself and the uncertainty of the value is ~20ps due to the observed 22ns periodicity in the non-linearity function.

Effect on LAGEOS data 1994-2006

We have taken from Figure 3 the results for the appropriate counter and also recovered the actual calibration range as given in the ILRS normal point header of

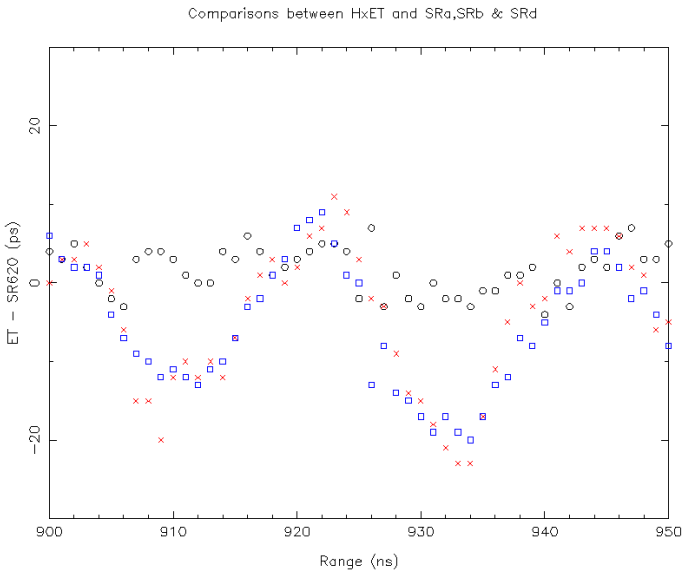

Figure 4 *Observed periodic behaviour in Stanford counters' error functions.*

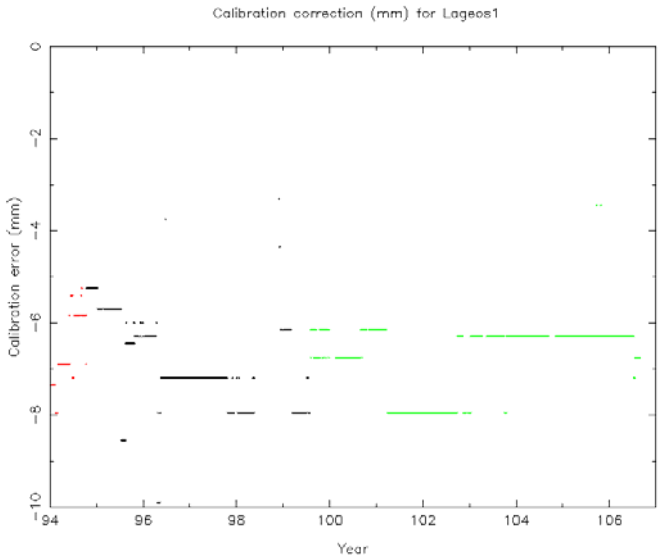

Figure 5 *Correction to calibration values used for LAGEOS during 1994-2006*

SGF LAGEOS data for the period 1994-2006. From these values we have estimated the corrections in mm to be applied to our calibrations taken over that period.The results are displayed in Figure 5, where it is apparent that errors of between 5 and 8mm have been made to the calibration values. However, given our estimate of the uncertainty of these average values, we finally derive an average calibration error of 7±2 mm, and in the sense that the calibration correction is too large by that amount. During this re-assessment we also discovered that no account had been taken for the effect on total delay of a glass neutral density filter that is placed in the optical path during calibration but not during satellite ranging. This correction amounts to 1.5mm, again in the sense that the calibration correction derived from target-board ranging is too long. Therefore our calibration corrections in the period 1994-date are too long by 8.5±2 mm and thus calibrated satellite ranges short by the same amount. This correction, which affects all satellite data equally, is of course in addition to the range-dependent correction discussed under 'previous calibrations' above and announced for the period 1994 October to 2002 January in SLRMail 0891 in 2002 January.

Assuming that the corrections presented in SLRMail 0891 have been made to the Herstmonceux ranges, it is interesting to look at the implications for and evidence in geodetic solutions of this newly-discovered correction of 8.5±2 mm. The centre-of-mass (CoM) correction for LAGEOS for 7840 Herstmonceux single photon data is 245 ± 1mm (Otsubo and Appleby, 2003). However, in computing ITRF2000, the Analysis Centres used the 'standard' 251mm CoM for all stations, thus effectively *increasing* Herstmonceux ranges by 6mm and nearly cancelling the bias of -8.5mm present since 1994. Thus the coordinates (height) of Herstmonceux in ITRF2000 should have only a small bias from the true value, given that a range bias (RB) affects primarily the solution for height. Indeed, the mean of Herstmonceux LAGEOS 1/2 residuals in our daily QC based on fixed ITRF2000 coordinates is currently -11 ± 2mm, close to the expected bias of -8.5mm. Thus it appears that the coordinates have not absorbed the range error and the full range bias remains. Further evidence comes from an analysis of LAGEOS 1/2 data between 1992 and 2006, where J Ries (personal communication, April 2006) finds a range bias of -10 to -12mm and a height change of ~7mm; from an analysis of LAGEOS 1/2 data in the period from 2001-

2005, Otsubo, Appleby, Gotoh and Kubooka (2006) find a range bias of -9mm, and a similar value for Etalon data.

For the ILRS combined product included in ITRF2005, the individual Analysis Centres used the correct value of 245mm for Herstmonceux's LAGEOS CoM, and did not solve for a bias for this station (AWG resolution at ILRS Fall Meeting, Eastbourne 2005). Thus it is likely that in particular station height will be in error in the ITRF2005. To test this, we apply the +8.5 mm range correction to LAGEOS 1/2 data for 2004, and solve simultaneously for correction to station coordinates as given in ITRF2005, and a range bias for 7840 Herstmonceux. On average, we find RB = +1 ± 2 mm and $\Delta H = -5 \pm 1$ mm, implying that station height in ITRF2005 had absorbed half the RB and is in error by +5mm.

Conclusion

All range data from 7840 Herstmonceux will from early 2007 be determined using HxET and will then be free of systematic error greater than 1 or 2mm. An SLRMail will announce the date and confirm that 8.5 mm should be *added* to all Herstmonceux satellite ranges from 1994 to that date, and re-iterate that the range dependent corrections given in SLRMail 0891 should also be applied for the period 1994 October to 2002 January. As a consequence of these counter problems, we estimate that the station height for 7840 Herstmonceux as given in ITRF2005 is approximately 5mm too large. We regret this long-term error that affects all laser data from Herstmonceux and encourage other stations, mostly among the EUROLAS sub-network, that use or have used Stanford counters, to investigate possible similar effects in their data. To this end, we will work with the ILRS Network and Engineering and Signal Processing Working Groups to calibrate the counters of all stations that are interested in collaboration.

References

[1] Appleby, G.M., Gibbs, P., Sherwood, R. and Wood, R., 1999. Achieving and maintaining sub-centimetre accuracy for the Herstmonceux single-photon SLR Facility, *Proceedings of Laser Radar Ranging and Atmospheric LIDAR Techniques II, Proc. SPIE Int. Soc. Opt. Eng.*, 3865, 52-63.

[2] Gibbs, P., Potter, C., Sherwood, R., Wilkinson, M., Benham, D., Smith, V. and Appleby, G.M., 2007. Some Early Results of Kilohertz Laser Ranging at Herstmonceux, these proceedings.

[3] Gibbs, P., 2002. Stanford Counter Comparison Results, Proceedings of EUROLAS Workshop 'Detecting and eliminating errors in the EUROLAS network', Herstmonceux, UK. http://ilrs.gsfc.nasa.gov/reports/special_reports/eurolas_workshop.html

[4] Hamal, K., Prochazka, I. and Fumin, Y., 2007. Portable Pico Event Timer and SLR Control (P-PET-C) System, these proceedings.

[5] Otsubo, T. and Appleby, G.M., 2003. System-dependent center-of-mass correction for spherical geodetic satellites, JGR, 108, no. *B4*, doi:10.1029/2002JB002209.

[6] Otsubo, T., Appleby, G.M., Gotoh, T. and Kubo-oka, T., 2006. Potential TRF Improvements through better understanding of Laser Ranging Target Signature Effects, (abstract and oral presentation), *Geophysical Research Abstracts, Vol 8, EGU*.

The Global SLR Network and the Origin and Scale of the TRF in the GGOS Era

E. C. Pavlis[1]

1. Joint Center for Earth Systems Technology (JCET), UMBC, Baltimore, MD, USA.

Contact: epavlis@umbc.edu / Fax: +1 410 455 5868

Abstract

Satellite Laser Ranging (SLR) data contribute to the realization of the Terrestrial Reference Frame (TRF), defining primarily its origin—geocenter, and in combination with VLBI, its scale. Both entities are fundamental in monitoring vital global change parameters, such as mean sea level, Earth rotation and orientation, etc. The Global Geodetic Observing System (GGOS), places the utmost importance on the development, maintenance and wide distribution of a TRF with very stringent attributes, an origin definition at 1 mm or better at epoch and a temporal stability of 1 mm/y, with similar numbers for the scale and orientation components. The stability, integrity and applicability of the TRF are directly related to the accuracy and fidelity with which mass redistribution can be observed or modeled during its development. Variations in the very low degree and order harmonics, produce geometric effects that are manifested as changes in the origin and orientation relationship between the instantaneous and the mean reference frame.

The unambiguous nature of SLR measurements and absence of significant biases, results in a very precise height determination, and thus the scale of the TRF. SLR has demonstrated millimeter level accuracy for weekly averages. Nevertheless, weather- or failure-induced changes in the network, and the small number and poor spatial distribution of the sites comprising the SLR network, generate additional signals aliased in the results. "Secular trends" seen in the recovered geocenter time series for example cannot be explained by any geophysical phenomena, and are primarily the result of these deficiencies of the present SLR network (poor geometry, lack of redundancy, N-S hemisphere unbalanced distribution, etc.). We investigate here through a number of alternate solutions the robustness of our results, using our SLR analyses spanning the past thirteen years.

Introduction

The Global Geodetic Observing System (GGOS), places the utmost importance on the development, maintenance and wide distribution of an International Terrestrial Reference Frame (ITRF) with very stringent attributes, an origin definition at 1 mm or better at epoch and a temporal stability of 1 mm/y, with similar numbers for the scale and orientation components (Pearlman et al., 2006). The stability, integrity and applicability of the TRF are directly related to the accuracy and fidelity with which mass redistribution can be observed or modelled during its development. Satellite Laser Ranging (SLR) data contribute to the realization of the Terrestrial Reference Frame (TRF), defining primarily its origin—geocenter, and in combination with VLBI, its scale. Both entities are fundamental in monitoring vital global change parameters, such as mean sea level, Earth rotation and orientation, etc., (Altamimi *et al.*, 2002). The motivation behind this contribution was to examine the robustness of the ILRS (Pearlman *et al.,* 2002) contribution to the ITRF in light of the forthcoming developments under GGOS and NASA's effort to upgrade and integrate the space geodetic networks of the future.

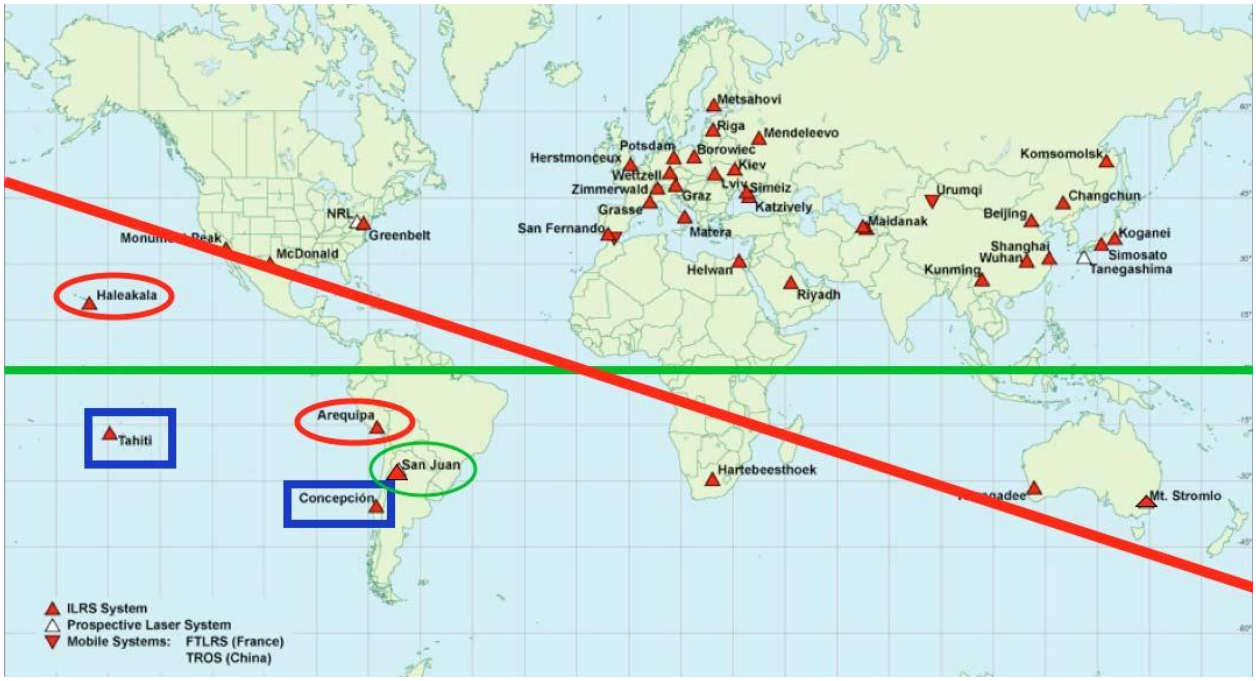

***Figure 1**. The current ILRS network with mark-ups of sites that were recently established (green), poor-yield southern hemisphere sites (blue),and sites that were shut down in 2004 (red).*

SLR contribution to ITRF

The SLR network never achieved an optimal, uniform distribution of stations globally (Figure 1). Furthermore, the closing of two key-sites, Arequipa, Peru and Haleakala, Hawaii in 2004 led to a disastrous lopsided distribution, where one-half the globe is totally void of any SLR observations! This eventually manifested itself in the SLR products as a serious and systematic degradation of the network scale as realized through the SLR observations. Aside from this recent degradation (which is addressed with the re-establishment of the closed down sites and improved performance for the others), this network has produced valuable TRF contributions over the decades. ITRF2000, (Altamimi et al., 2002), was a product that for the first time included a vast number of sites around the world and input from all geodetic techniques with rather strict and rigorous editing in its development. Weekly "geocenter" monitoring with respect to that frame yields a significant and systematic motion in the z-axis, at a rate of ~ 1.7 ± 0.1 mm/yr! Most of this is eliminated in the new realization ITRF2005, but not all. In particular, our SSC (JCET) L 06 analysis resulted in the following rates for the three axes:

$$\Delta x = -6.55 - 0.0848\times(t\text{-}2000) + \textit{periodic terms} \quad [\text{mm}]$$

$$\Delta y = 4.99 - 0.0898\times(t\text{-}2000) + \textit{periodic terms} \quad [\text{mm}]$$

$$\Delta z = 0.91 + 1.6981\times(t\text{-}2000) + \textit{periodic terms} \quad [\text{mm}]$$

The formal accuracy of these estimates is at 0.1 mm/y, however, without an independent estimate to compare, we have no sound way to calibrate this error. Interpreting these signals is even more difficult, since they can be caused by a number of different geophysical phenomena, none of which is easily or fully understood. Table 1 gives some estimates due the main sources that could cause such a systematic signal. It's worth noting that recently, Peltier (private communication), has been able to develop models

for Greenland and Antarctica melting in recent times that support this level of "geocenter" motion, especially in the axial component.

Table 1. *Secular geophysical signals in the axial component of the "geocenter".*

Source	Magnitude	Induced motion	Reference
Sea level	1.2 mm/y	0.064 ± 0.02 mm/y	[2]
Ice sheets (G)	2 mm/y	0.046 ± 0.20 mm/y	[2]
Tectonics	AMO-	0.309 ± 0.05 mm/y	[2]
Postglacial rebound	ICE-3G	0.2 - 0.5 mm/y	[1]

(1) Marianne Greff-Lefftz (2000)
(2) Yu. Barkin (1997)

Methodology

Our conjecture is that the remaining unaccounted-for motion is due to the evolving network, the uneven global distribution of the tracking sites with strong yields, and the poor coverage of some of the major tectonic plates. To test the effect of the "network evolution" we have performed a number of re-analyses of the data, defining TRFs from independent sub-sets of the data in various combinations. As for the effect of the lopsided distribution of the main tracking sites, a large-scale simulation is in progress, within a technique-wide coordinated effort to design the optimal space geodetic networks of the future. The initial results of this investigation will be available by late 2007. A third test involves the so-called effect of the "missing" historical SLR data, i.e. SLR data to LAGEOS prior to 1992. ITRF2000 contained that data, while ITRF2005 does not, due to its tight and firm release schedule. We have generated a TRF that includes the data obtained from LAGEOS since 1976. A comparison of this TRF to a similar one that does not include that data and spans exactly the same period with ITRF2005, should give some idea of whether the missing data contribute to the z-axis secular evolution or the scale difference observed between the SLR and VLBI contributions to ITRF2005.

The effect of the "missing" historical SLR data on the SLR-definition of the scale

To test whether the addition of the "historical" LAGEOS data (1976 to 1992) to the definition of the TRF would eliminate the differences seen between the ITRF2000 and ITRF2005 realizations, we simply reduced that data and added them to the 1993 – 2005 data, generating a new TRF and comparing that through a 14-parameter similarity transformation to the two realizations, ITRF2000 and ITRF2005. The results are tabulated in Table 2.

Our solution is identical to neither ITRF2000 nor ITRF2005, although very close to both. This is expected of course since this is a SLR-only TRF and not a combination product with input from other techniques. Examining the differences in the scale and its rate, we notice that in the case of ITRF2000, our TRF indicates the same level of disagreement as it was originally seen between the SLR-only contributed inputs to this model. Similarly, we see the same for ITRF2005, and the combined difference is exactly what is seen when comparing one ITRF to the other. The fact that a TRF that contains the historical LAGEOS data shows similar differences to the ITRF2005 as does the one without that

data, indicates strongly that the lack of that data cannot be the main reason of the observed differences.

Table 2. *Similarity transformation parameters between SSC (JCET) L 06 and ITRF realizations.*

Parameter	SSC (JCET) L 06.97 vs. ITRF2000	SSC (JCET) L 06.97 vs. ITRF2005
D_x	-8.82 +/- 1.02 [mm]	1.25 +/- 0.91 [mm]
D_y	3.21 +/- 1.01 [mm]	8.37 +/- 0.91 [mm]
D_z	-5.65 +/- 0.95 [mm]	-6.59 +/- 0.86 [mm]
D_s	**0.52 +/- 0.15 [ppb]**	**-0.87 +/- 0.13 [ppb]**
R_x	-0.24 +/- 0.04 [mas]	0.05 +/- 0.04 [mas]
R_y	0.06 +/- 0.04 [mas]	-0.07 +/- 0.04 [mas]
R_z	0.15 +/- 0.03 [mas]	0.32 +/- 0.03 [mas]
$D_{x\text{-dot}}$	0.75 +/- 0.95 [mm/y]	-1.22 +/- 0.85 [mm/y]
$D_{y\text{-dot}}$	0.56 +/- 0.94 [mm/y]	1.37 +/- 0.85 [mm/y]
$D_{z\text{-dot}}$	3.10 +/- 0.73 [mm/y]	1.89 +/- 0.65 [mm/y]
$D_{s\text{-dot}}$	**-0.10 +/- 0.14 [ppb/y]**	**0.05 +/- 0.12 [ppb/y]**
$R_{x\text{-dot}}$	0.12 +/- 0.03 [mas/y]	0.12 +/- 0.03 [mas/y]
$R_{y\text{-dot}}$	-0.02 +/- 0.03 [mas/y]	0.02 +/- 0.03 [mas/y]
$R_{z\text{-dot}}$	0.02 +/- 0.03 [mas/y]	0.01 +/- 0.03 [mas/y]

In addition to the 'geometric' test of the scale implied by different spans of SLR data, we have also examined the dynamic definition of the scale, through the estimation of the GM_E constant from the different data sets. The SLR technique obtains the definition of the scale from the adopted speed of light in vacuum, v_c, however, because it involves satellite orbits, this scale should also be consistent with the size of the orbit as it is constrained by Kepler's third law. With v_c fixed, we can monitor any changes in the intrinsic SLR scale through the estimation of GM_E. The historical data were reduced in three different ways (arc-lengths), in order to verify that this is also not a factor in the development of the TRF: fortnightly (F), monthly (M), and quarterly (Q) arcs. With each expansion of the arc-length, any unaccounted systematic errors in the description of the site-motions is smoothed out by averaging, since more data from other, non-affected sites contribute to the definition of the TRF over that interval of time. Table 3 indicates that a comparison of the GM_E estimates from these solutions to the value that we obtain from the weekly-arc (W) analysis for the 1993- 2005 period, shows no systematic difference, and certainly no scale change larger than the calibrated uncertainty of the estimates.

Table 3. *GM_E estimates from two SLR data spans: 1993 – 2005 and 1976 – 2005.*

Source of displayed GM_E	Value of GM_E
IERS Conventions 2003	398600.441500 x 10^9 [m^3/s^2]
SSC (JCET) L 06 W 1993 - 2005	398600.441659 x 10^9 [m^3/s^2]
SSC (JCET) L 06 F 1976 - 2005	398600.441634 x 10^9 [m^3/s^2]
SSC (JCET) L 06 M 1976 - 2005	398600.441633 x 10^9 [m^3/s^2]
SSC (JCET) L 06 Q 1976 - 2005	398600.441633 x 10^9 [m^3/s^2]

We can reach two main conclusions from the above table: (a) the effect of the historical data in the intrinsic definition of the scale in SLR is at most at the level of 0.1 ppb, and (b) the effect of the arc-length used in the reduction of the data on the scale is even less significant, less than 0.002 ppb. A calibrated estimate of the accuracy of these estimates at the 99% level of confidence is 0.2 ppb or approximately 1.3 mm.

Subset solution results

We investigated the effect of the "evolution of the network" with the development of a number of TRFs from independent sub-sets of the data in various combinations (Figure 2). With only some thirteen years of data to work with, we went as far as ¼ of the data, i.e. the smallest set of data spanned just over three years. This seemed to be marginally acceptable for a quality TRF, with six years being a comfortable minimum for a robust TRF product (specially for velocity estimates). We have two strategies in forming these subsets: (i) using similar amounts of data spanning the same period of time, and (ii) using the same amounts of data sampling totally different time periods. In the first case for example, we used ¼ of the data to generate four different TRFs, each based on the weeks that span the same time-period, every subset formed by choosing every 4th week from the ensemble of all weeks available. In the second case, we also have four TRFs formed on the basis of approximately ¼ the total data, but in this case we broke up the total interval in four equal-length intervals, so each TRFs is fit to data from a different period of time (and a different network with different conditions and performance).

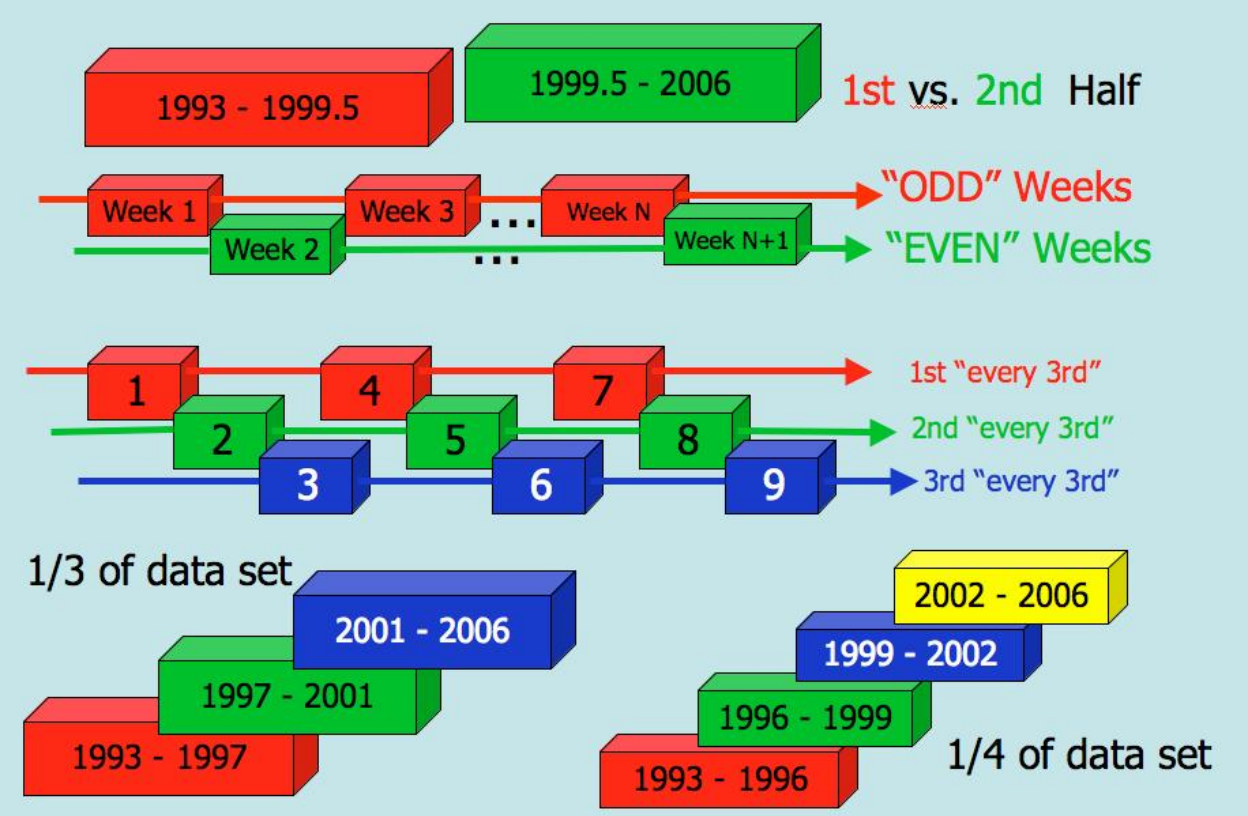

***Figure 2**. The four groups of subset solutions used in this investigation*

Case	ΔX [mm]	$\sigma_{\Delta X}$ [mm]	ΔY [mm]	$\sigma_{\Delta Y}$ [mm]	ΔZ [mm]	$\sigma_{\Delta Z}$ [mm]	3D |Δ| mm	$\sigma_{3D\,\Delta}$ mm
3 **Odd**	-8.37	±10.91	19.25	±10.78	-4.20	±10.32	**21**	± **17**
4 **Even**	-12.62	± 8.93	5.15	± 8.82	-12.50	± 8.44	**18**	± **16**
5 **@ 3rd**	-7.92	± 18.84	-3.87	±18.61	3.56	±17.82	**10**	± **31**
6	-7.61	± 8.66	19.78	± 8.56	-15.33	± 8.19	**26**	± **16**
7	-11.36	± 10.41	9.03	±10.28	-11.58	± 9.84	**19**	± **17**
8 **@ 4th**	-15.62	± 21.76	43.27	±21.49	16.57	±20.57	**49**	± **36**
9	-17.75	± 18.87	16.31	±18.63	-29.03	±17.84	**38**	± **33**
10	-6.61	± 17.18	-5.50	±16.97	-11.56	±16.24	**14**	± **29**
11	-16.72	± 12.01	1.32	±11.86	-9.92	±11.36	**19**	± **21**
1 **1/2**	-41.20	±35.82	6.26	±35.38	-10.10	±33.86	**43**	± **61**
2	1.74	± 6.76	8.06	± 6.68	7.28	± 6.39	**11**	± **11**
12 **1/3**	-49.10	± 22.39	52.74	±22.11	2.73	±21.16	**72**	± **38**
13	-3.07	± 8.21	-13.72	± 8.11	5.90	± 7.76	**15**	± **14**
14	-16.95	± 14.20	5.72	±14.06	4.28	±13.40	**18**	± **24**
15 **1/4**	-60.49	± 23.68	57.43	±23.39	7.48	±22.39	**84**	± **40**
16	18.65	± 31.40	-57.81	±30.88	-6.19	±29.50	**61**	± **53**
17	-0.27	± 18.01	-4.74	±17.79	15.72	±17.03	**16**	± **31**
18	2.07	± 12.29	7.16	±12.18	1.73	±11.60	**8**	± **21**

Figure 3. *The four groups of subset solutions used in this investigation (top cases: same time-span, and bottom cases: disjoint time intervals).*

We will limit the discussion of our conclusions to two items of importance to the ITRF: the definition of its origin and its axial rate. The results are summarized in Fig. 3, in terms of the differences in each component Δx, Δy, and Δz, with respect to the solution obtained from the entire set of data. In order to facilitate their comparison we also formed a figure of merit, defined as the 3D positional difference, and formed as:

$$\Delta = \sqrt{\Delta x^2 + \Delta y^2 + \Delta z^2}.$$

We can draw several conclusions from this table:

- On average, each component is not determined to better than 6-8 mm (depends on time period)
- The 1993 to present data set is significantly non-uniform due to various factors
- There is a steady improvement over the years, however, we can see even 10-fold differences between different time-periods
- With the caveat that our calibrated error estimates are sufficiently realistic, and assuming that the second half of the 1993-2005 period is more representative of current network performance, we conclude that for a reliable definition of the origin of the TRF we need a data spanning more than ~6-7 years.

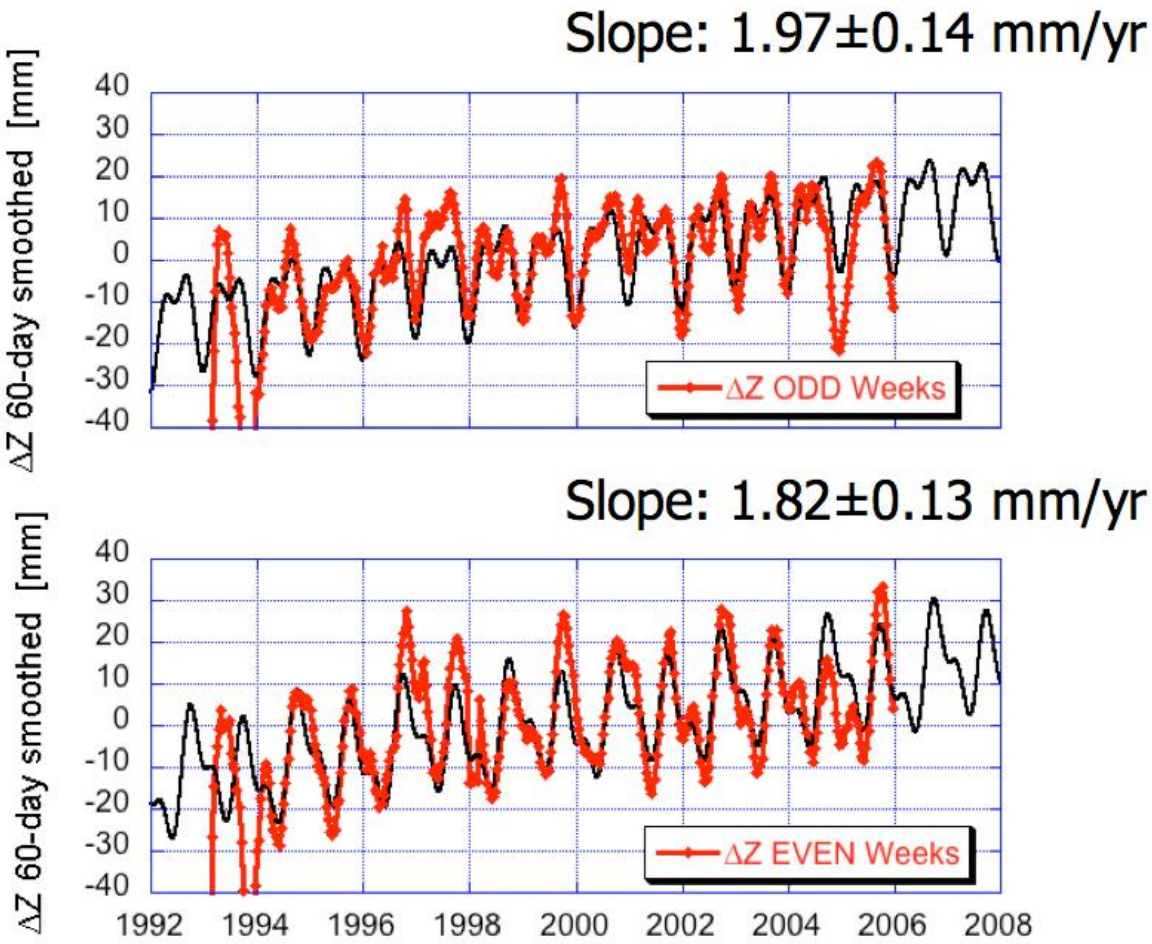

Figure 4. *The time series of Δz (axial component of geocenter) from two independent subset solutions, each spanning the period 1993-2005.*

With each subset solution we also obtained a time series of the weekly variations of the origin with respect to the geocenter. These were analyzed in a similar manner to the origin components themselves, i.e., in comparison to the series we obtain from our ensemble solution that spans the entire time period. The axial component is the only one that shows a significant secular trend, so we will use that in our example. Figure 4 gives an example of the recovered series and their fit to a model that includes a linear trend and three periodic terms, for the two subsets formed from the selection of the "even" and "odd" weeks (i.e. every other week used). The two subsets span the same time period with just one week "offset", but each set has about half the data of the entire data set. It is apparent from these two cases that the secular trend recovered here is statistically insignificantly different from what we obtained from the entire data set (cf. ~1.7 ± 0.1 mm/y). There are differences though in the periodic components' (not magnitude) and when we compare the results from subsets that span even smaller spans of data (less than half), then even the secular trend is not recovered correctly (sometimes we even get sign-reversals!). These observations lead us to the following conclusions:

- Secular trends from same size data span agree to 7-10%
- Secular trends from spans smaller than ~7 years and different periods of time can differ up to 100%, indicating a highly non-stable network (shape, performance or a combination of both)
- The magnitude of the seasonal variations is stable when recovered from various subsets of the entire data set, but the phases seem to be sensitive to

that choice

- For the robust definition of secular trends and seasonal variations simultaneously, it is recommended that more than a decade of data (preferably from a stable network) be used.

Summary and future plans

This study investigated the robustness of the definition of the origin and scale of the TRF from SLR data (only) and with the LAGEOS and LAGEOS 2 data available over the period 1993 to 2005. The conclusions we reached are that these data define the origin at epoch to no better than 10 mm. The monitoring of the secular motion of the origin depends strongly on the network evolution and its performance. For a robust estimate of temporal variations of the geocenter we need data sets that span a decade or more, with a stable network. In such cases, the secular trends can be estimated with an accuracy of about 10%.

For a complete rationalization of the observed error signatures and the performance of future networks, we need a set of very carefully controlled simulations (underway). Extension of this simulation to include the other techniques will give us the advantage to "negotiate" trade-offs between the techniques, since they all act in a complementary manner in the definition of the ITRF. This will allow better use of the available resources and full exploitation of the benefits from each technique.

References

[1] Altamimi, Z., P. Sillard, and Claude Boucher (2002), ITRF2000: A new release of the International Terrestrial Frame for earth science applications, *J. Geophys. Res.*, *107*, NO. B10, 2214, doi:10.1029/2001JB000561

[2] Pearlman, M.R., Degnan, J.J., and Bosworth, J.M., 2002. "The International Laser Ranging Service", *Adv. in Space Res.*, Vol. 30, No. 2, pp. 135-143, 10.1016/S0273-1177(02)00277-6.

[3] Pearlman M., and co-authors (2005), Global geodetic observing system - Considerations for the Geodetic network infrastructure, 2005 IAG/IAPSO/IABO Joint Assembly, Cairns, Australia, August 22-26

[4] Peltier, W. R., 2006, *private communication.*

FTLRS Ajaccio campaigns : operations and positioning analysis over 2002/2005

F. Pierron[1], B.Gourine[2], P.Exertier[1], P.Berio[1], P.Exertier[1], P. Bonnefond[1], D.Coulot[3] and the Grasse/Ftlrs laser staff

1. Observatoire de la Côte d'Azur, GEMINI/UMR 6203-CNRS, Av N. Copernic, 06130 Grasse, France.
2. Centre National des Techniques Spatiales à Arzew (CNTS), Algeria
3. IGN, ENSG/LAREG, 6 et 8 Avenue Blaise Pascal, Cité Descartes, Champs-sur-Marne, 77455, France

Abstract

In the framework of JASON-1 project especially for Cal/Val aspects, Ftlrs has been deployed in Ajaccio for a six months campaign in 2005.

In the continuation of previous operations on the same site in 2002 the observations programs were carefully tuned to be pertinent on both aspects of scientific goals with new tools to optimize sky coverage for the data and technological issues like maintenance and operational costs.

In this paper, we'll present reports and results concerning station positioning with a very interesting combination of LAGEOS -1, -2, STELLA, and STARLETTE observations and comparison over 2002 and 2005 campaigns. An estimation of final accuracy will be discussed in such experiments of multi occupation site and operational issues will be commented.

1. Introduction and Operational issues for Corsica campaigns

The Ajaccio site is the main calibration site of the satellite altimeters in the Mediterranean area

Typical setup of the station (Corsica 2002 and 2005)

The SLR technique is the major contributor to the altimeter calibration: SLR data of the whole network are used to derive ultra precise orbit of altimeter satellites (in combination with DORIS and GPS data) and FTLRS conducts comparative laser distance measurements between the facility and satellite radar altimeters.

The objectives are the following :

- Absolute Sea level monitoring, altimeter calibration and orbit validation (CAL/VAL) of the Topex/Poseidon, Jason-1 and Envisat satellites from the Ajaccio site (Corsica-France)
- Estimation of the satellite altimeters biases and drifts

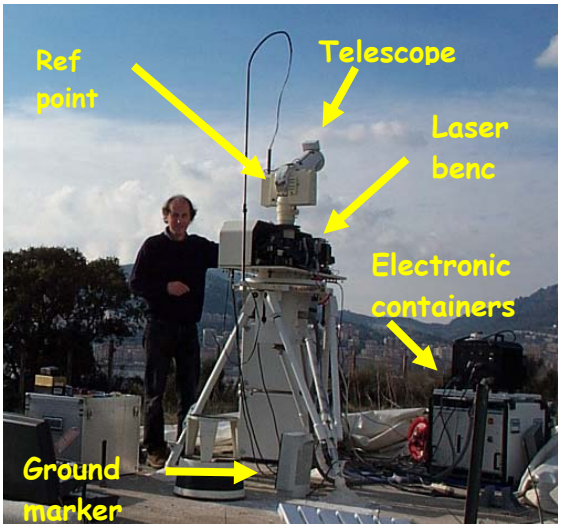

- Need for carrying out accurate SLR positioning from geodetic satellites observations

The FTLRS is a highly mobile Satellite Laser Ranging (SLR) system dedicated to the tracking of geodetic satellites equipped with retroreflectors. This instrument was developed by the Observatoire de la Côte d'Azur (OCA) and the Centre National d'Etudes Spatiales (CNES) in collaboration with the Institut National des Sciences de l'Univers (INSU) and the Institut Géographique National (IGN)

For these campaigns, Ftlrs system is deployed inside a French naval base near Ajaccio on a hill, close the sea and at some thirty kilometer from Senetosa Cape where are installed tide gauges and performed GPS buoys experiments near exact calibration point.

Two major campaigns have been organized at this site: January-September 2002 for 10 months and May-October 2005 for 5 months.

2. Jason1 absolute calibration/validation configuration :

•A geodetic site at Ajaccio with FTLRS settled for some months.
•An in-situ site at Senetosa cape under the track N°85.

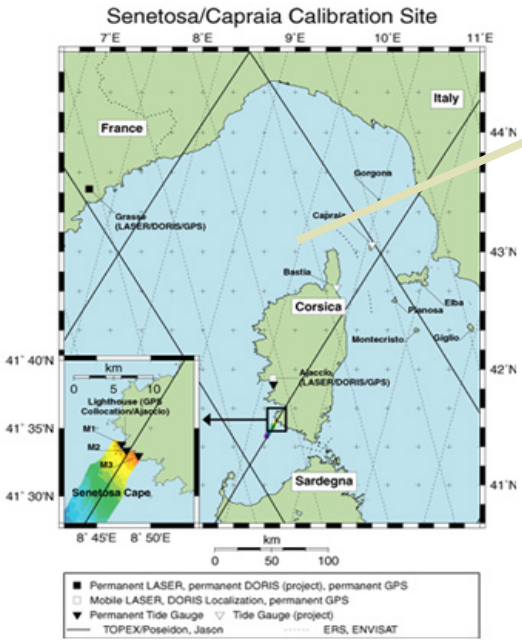

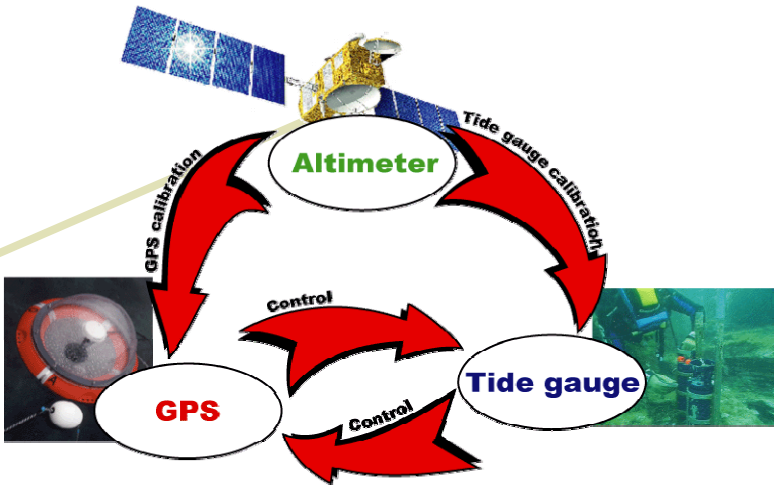

Products used for the study:

- **T/P: M-GDR + TMR drift**
- **Jason-1: GDR**

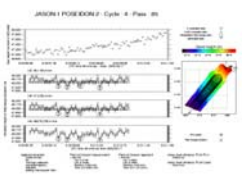

Definition of altimeter bias calibration:

sea height bias = altimeter sea height - in situ sea height

Sea height bias < 0 meaning the altimetric sea height being too low (or the altimeter measuring too long)
Sea height bias > 0 meaning the altimetric sea height being too high (or the altimeter measuring too short)

The Senetosa site allows performance of altimeter calibration from tide gauges as well as from a GPS buoy.

At Senetosa POSEIDON-2 altimeter bias is +100 ±4 mm, based on the whole set of GDR-A products (135 cycles).

The large negative trend is due to JMR (Wet Troposphere) in GDR-A and has been solved in recent analysis works

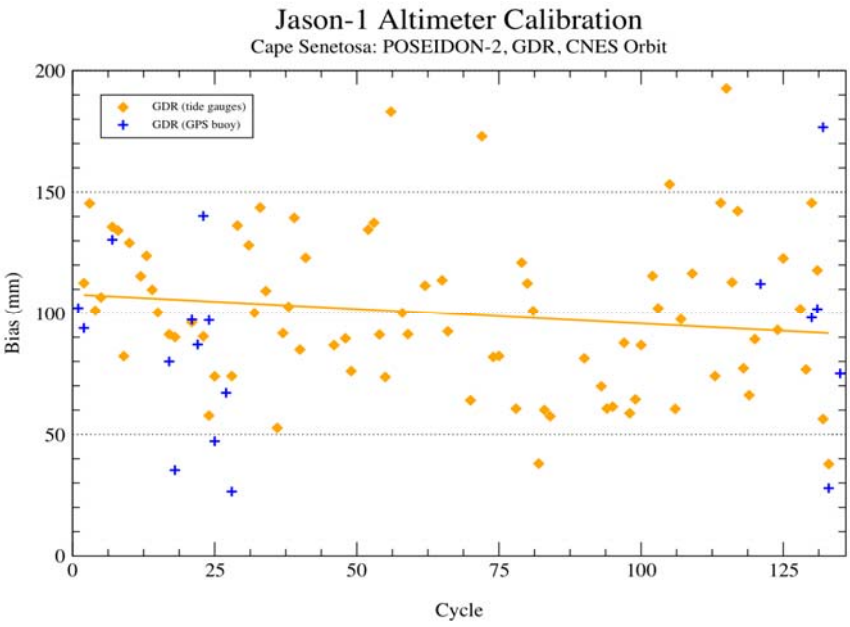

3. Scientific investigation for Positioning

➢ **Positioning with 4 geodetic satellites**

Lageos-1
Lageos-2

Starlette
Stella

➢ **Goals of this positioning :**

-To maintain geodetic accuracy of the FTLRS position in Ajaccio site (Corsica) between the two campaigns

-To provide high accuracy local orbits for the Jason-1 altimeter calibration

➢ **Main steps of the work methodology**

-Orbit computation
-Positioning of the FTLRS Station with Multi satellite combination.

Npts data on the sky for 2005 campaign :

- High Elevation Orbiting Satellites:

Few measurements on Lageos satellites, particularly at low elevation (40°), and irregular distribution of these data over the Ajaccio site

- Low Elevation Orbiting Satellites:

Ten times more range data on Starlette/stella relative to Lageos, and homogeneous distribution of the range data over the Ajaccio site

The quality of FTLRS positioning is very dependent on the accuracy of orbits, and Starlette and Stella are more sensitive to remaining uncertainties in the dynamic models (gravitational and non gravitational effects).

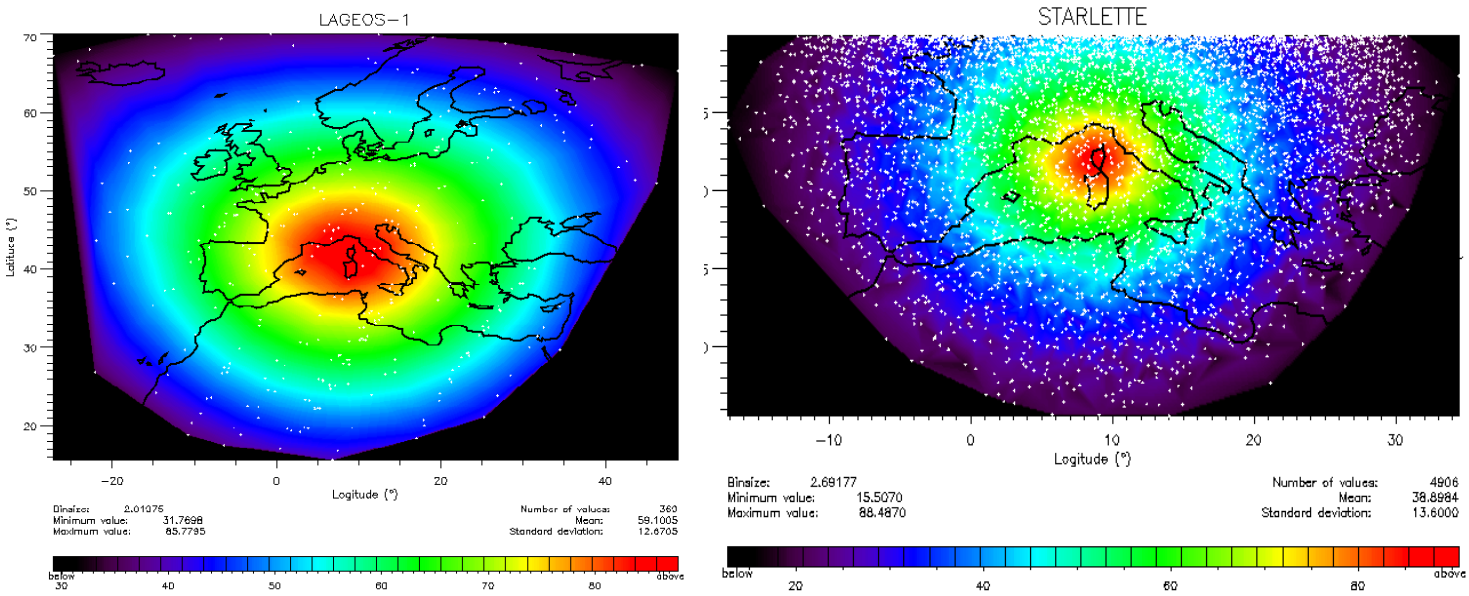

Maps of the range data distribution during the 2005 campaign (05 months) above Ajaccio site

Since few years, thanks to new space mission like Grace, the community got an improvement of the gravity field models. The method in our analysis is to use an accurate field gravity model for the LEO computation and a multi-satellite combination.

A. Parameters for orbit computation :

-Gins software (developed by CNES)

-Dynamical models used :

Model	Designation
Gravity field	*Grim5-c1* or *Eigen-Grace03s*
Atmospheric pressure	*ECMWF*
Solar flow	*Acsol2*
Atmospheric Density	*Dtm-94bis*
Ocean tides	*Fes-2002*
Planets	*De403bdlf.ad.ibm*
Earth Orientation Parameters	*Eop-c04*

-Terrestrial reference frame : ITRF 2000

-Computation by successive arcs (9 days for Lageos 1/Lageos 2 and 6,5 days for Starlette/Stella) with overlapping periods (1 day for Lageos 1/2 and 0,75 days for Starlette/Stella) allowing to control the orbits quality of successive arcs and to limit the "butterfly effect" on the arc computation.

Mean Radial orbit differences (m) geographically correlated of Starlette orbits

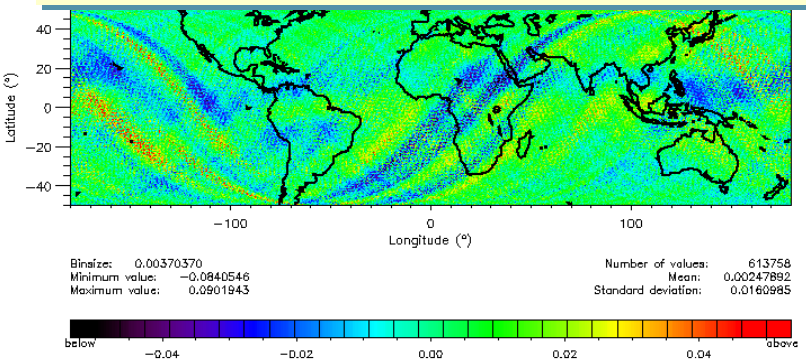

-Effect of gravity field model :

On 32 arcs of Starlette/Stella in 2005, it appears that the Mediterranean area is less affected by a permanent effect.

The lageos orbits are more precise and less affected by the change of gravity field model, but for Stella/Starlette, we have an improvement of orbit precision of +/- 5mm with Eigen-Grace03s model.

	2002 campaign		2005 campaign	
Satellite	GRim5-c1	Eigen-Grace03s	Grim5-c1	Eigen-Grace03s
LAGEOS-1	13	-	11	11
LAGEOS-2	10	-	10	09
Starlette	23	18	23	18
Stella	23	19	21	16

B. Positioning of Ftlrs station :

-Matlo Software (developed by OCA) (Coulot 2005)

This software dedicated to laser positioning (coordinates updates+ range bias/satellite) in a multi-satellite combination compute a global solution and Time series solution.

Range bias	B_{LAG-1} (mm)	B_{LAG-2} (mm)	B_{STAR} (mm)	B_{STEL} (mm)
Glob. Sol. (1)	+12.0	+12.2	-3.9	-6.4
Glob. Sol. (2)	+4.8	+4.6	-4.9	-4.9
7d. Sol. (1)	+11.7	+13.8	-4.6	-5.4
7d. Sol. (2)	+4.9	+3.3	-5.6	-4.3

Coordinate updates	$d\varphi$ (mm)	$d\lambda$ (mm)	dh (mm)	$\rho_{dh\text{-}Bias}$ (%)
Glob. Sol. (1)	+4.3 ± 0.6	-10.1 ± 0.6	+11.7 ± 1.8	94.4
Glob. Sol. (2)	+4.3 ± 0.5	-3.6 ± 0.4	+3.0 ± 1.4	94.4
7d. Sol. (1)	+4.4 ± 0.6	-8.6 ± 0.5	+13.8 ± 0.6	55.4
7d. Sol. (2)	+4.1 ± 0.4	-2.9 ± 0.4	+4.0 ± 0.4	55.4

The Main objective has been to reduce the correlation between the range bias and the vertical component. To do that, we compared a global solution (with coordinates and range biases estimated with the whole data) and 7 days solution (with bias/sat supposed constant remain estimated with the whole data). In the Global solution, the correlation remains to high between biases and dh, some parts of the bias may move to dh and vice versa.

In the 7 days solution, the correlation decreases significantly (55%), this solution is finally held

C. Results and Analysis: adjusted Ftlrs parameters over 2002 & 2005 campaigns:

with :

-Time series solution

-Eigen-Grace03s model

Coordinate updates	$d\varphi$ (mm)	$d\lambda$ (mm)	dh (mm)	$\rho_{dh\text{-}Bias}$ (%)
2002	-0.8 ± 0.7	+1.6 ± 0.7	+0.2 ± 0.8	55.8
2005	+4.1 ± 0.4	-2.9 ± 0.4	+4.0 ± 0.4	55.4

	Lageos-1 *(mm)*	Lageos-2 *(mm)*	Mean Lageos-1&2 *(mm)*	Starlette *(mm)*	Stella *(mm)*	Mean Starlette/Stella *(mm)*	Global mean *(mm)*
2002	-5	-7	-6	-13	-13	-13	-10
2005	+5	+3	+4	-5	-5	-5	0

- **The difference between Lageos and Starlette/stella biases** are probably coming from satellite signature and Ftlrs detection process.
- **adjusted values of Ftlrs range bias in 2002 campaign of -10 mm explained a posteriori:**
  - Non linearity of Stanford chronometer not modelised at this epoch : -4.2 mm
  - Geometrical path for external calibration not adjusted : - 3mm
  - **Total : 7.2mm**
- **The adjusted values of Ftlrs mean range bias for last campaign 2005 is very small and confirm agreement between analysis and technological corrections applied (Stanford non linearity, ground target measurements,..)**

D. Solved coordinates

Geographical coordinates differences from (Exertier et al., 2004) solution:

Coordinates differences	$\Delta\varphi$ (mm)	$\Delta\lambda$ (mm)	Δh (mm)
2002	+0.5 ± 0.7	+2.7 ± 0.7	-1.2 ± 0.8
2005	+4.1 ± 0.4	-2.9 ± 0.4	+4.0 ± 0.4

Stability :

Campaign	Number of solution	σφ (mm)	σλ (mm)	σh (mm)	σ (mm)
2002	28	14.6	13.1	10.5	**12.**
2005	20	7.5	12.3	10.5	**10.**

-Global mean of bias (-5mm): very close to the published one (-7mm)

-Coordinate updates values for 2002 and 2005 are at 3mm level in average relatively to previous solution.

-Coordinates differences are very small at level of residuals errors in the ITRF2000 velocities

-No significant differences between 2002 and 2005 coordinates (at level of the tectonic movement): FTLRS point is locally stable.

4. Conclusion and Prospects:

➢ **Multi-satellite combination** has allowed to palliate lack of measurements on high satellites

➢ The improvement of the dynamical models, notably of the terrestrial gravity field (thanks to the GRACE satellite data **(*Eigen-Grace03s*)** has permitted a precise computation of the orbits, in particular for the low satellites, and so a more precise geographical positioning,

➢ **Interesting decorrelation (~ *40%*)** is obtained between the range bias and the station vertical component, using the time series solution (MATLO),

➢ **The station position is stable** between the two observation campaigns,

➢ In conclusion, the FTLRS has allowed a **precise terrestrial positioning**. That confirms its importance for the absolute calibration process of oceanographic satellites.

SLR-Based Evaluation and Validation Studies of Candidate ITRF2005 Products

Erricos C. Pavlis[1,2], M. Kuzmicz-Cieslak[1] and D. E. Pavlis[3,2]

1. Joint Center for Earth Systems Technology (JCET), Univ. of Maryland Baltimore County, Baltimore, MD, USA
2. NASA Goddard Space Flight Center
3. SGT, Inc.

Contact: epavlis@umbc.edu / Fax: +1 410 455 5868

Abstract

The recent release of candidate solutions for adoption of the new ITRF2005 International Terrestrial Reference Frame (ITRF) initiated numerous tests and comparisons over the past months. This presentation focuses on the evaluation tests we performed with the ITRF2005P and ITRF2005D products, primarily with Satellite Laser Ranging (SLR) tracking data. Since over two decades now, SLR tracking data contribute to the definition of the TRF, primarily in defining its origin and scale. LAGEOS 1 and 2 are the main targets contributing to this, and we use their data, as well as a limited number of independent data to gauge the improvement gained by going from ITRF2000 to either of the two new candidate solutions. An easy and immediate observation is that either of them is only slightly different from ITRF2000, in contrast to what was observed during the release of ITRF2000. This seems natural though, since ITRF2000 dealt with many problems observed with its predecessor and used a uniformly high quality input from nearly all techniques. We concentrate here on the differences between the two and the impact of such factors as the improvements in the analysis methodology, the underlying models, the use of IERS Conventions 2003, and the latest improvements in modelling SLR observations.

Introduction

Since over two decades now, SLR tracking data contribute to the development of the ITRF, primarily in defining its origin and scale. The release of ITRF2000 in 2001 ushered a new era of TRF quality and performance (Altamimi *et al.*, 2002). The recent (mid-2006) release of candidate solutions for adoption of the new ITRF2005 initiated numerous tests and comparisons over the past months. This presentation focuses on the evaluation tests we performed with the ITRF2005P (from IGN) and ITRF2005D (from DGFI) products, primarily with SLR tracking data. In contrast to what was experienced during the release of ITRF2000, the release of the new models did not bring about order-of-magnitude changes, but rather small adjustments and corrections, either for sites that appeared 'after' the release of ITRF2000 or whose ITRF2000 estimates were based on too limited a set of data for meaningful results.

Initial tests for Precision Orbit Determination (POD)

As a first test of the two candidate models we looked at their performance on the LAGEOS and LAGEOS 2 data that were used in their development. From the initial tests on ITRF2005P, which was released first in early summer of 2006, it became obvious that the VLBI-consistent scale imposed on this model because of the observed scale discrepancy between SLR and VLBI, led to a TRF with inferior performance even on the SLR data that were used in its development.

When however we applied a scale adjustment to make it consistent with the intrinsic SLR scale or allowed for a scale adjustment in our tests, the two models performed very similarly, and only marginally better than ITRF2000, except for the few sites that either did not appear in ITRF2000 or had poor ITRF2000 estimates (Table 1).

***Table 1**. Weekly RMS values from the weekly operational ILRS products in comparison to the old (ITRF2000) and new (ITRF2005P), ITRFs (results courtesy Cecilia Sciarretta/Telespazio, S.p.A.).*

Group RMS [mm]	ITRF2000	ITRF2005	ITRF2000	ITRF2005	ITRF2000	ITRF2005
	June 3, 2006		*June 10, 2006*		*June 17, 2006*	
All sites (**24**)	40	**8**	36	**9**	32	**9.6**
Core sites (**16**)	13	**7**	13	**8**	12	**8**

Several SLR analysts did similar POD tests and the main conclusion from all of these tests is that the new models perform very similarly, and not much different from ITRF2000, for the well-determined sites common to both TRFs. The POD tests we performed were limited to data from the period 2003 to 2006.5, and only for the sixteen (16) "Core SLR" sites as identified by the ILRS ACs' operational procedures. A summary of the RMS of fit per site for either of the two new models and ITRF2000 are shown in Tables 2 (for LAGEOS) and 3 (for LAGEOS 2).

A quick observation from Tables 2 and 3 is that overall, ITRF2005D performs slightly better than ITRF2005P does, especially in the case of LAGEOS 2. Note that unlike ITRF2005P, ITRF2005D ***does not*** require any adjustment to its scale or scale rate in order to achieve this performance. Despite this fact, absent any substantiated errors in the development of ITRF2005D, and ignoring all official objections by the International Laser Ranging Service (ILRS), (Pearlman *et al.*, 2002), the final officially adopted model for ITRF2005 was a slightly modified version of ITRF2005P (without any changes with respect to the SLR-VLBI scale issue).

The scale difference between ITRF2005P and SLR

The scale difference between the new and old ITRF (about 1.4 ppb at 2000.0 or ~10 mm, and -0.15 ppb/y or -1 mm/y), intrigued all SLR analysts involved in the evaluation and validation of the new model. Several theories were formed and tested, all of them quickly eliminated following extensive and copious tests, in most cases cross-checked through repetition by more than one group. We list some of the more plausible ones here.

A possible error in the adopted value of GM_E was quickly discarded, since it would require an unreasonably large $\Delta GM_E \approx 0.0025 \times 10^9$ or an equally unreasonable change in the CoM value for the two LAGEOS (~20 mm). Next, the differences in the submitted SLR contributions to ITRF2000 and ITRF2005 were examined closely. The

Table 2. *LAGEOS POD: Core sites' RMS of fit using ITRF2000, ITRF2005P and ITRF2005D, and differences. RMS in red (negative) indicates ITRF2005P performs better than ITRF2005D.*

SITE NAME	SITE ID	ITRF2000 (IGN) RMS [mm]	ΔRMS [mm] 2000-2005P	ITRF2005P (IGN) RMS [mm]	RMS [mm] 2005P-2005D	ITRF2005D (DGFI) RMS [mm]	ΔRMS [mm] 2000-2005D
BEIJING, PRC	7249	22.41	4.90	17.51	1.10	16.41	6.00
GRASSE, FRANCE	7835	10.45	2.54	7.91	-0.12	8.03	2.42
GFZ POTSDAM, DE	7836	13.11	2.60	10.51	-0.84	11.35	1.76
GRAZ, AUSTRIA	7839	9.46	1.48	7.98	-0.19	8.17	1.29
HALEAKALA, HI	7210	17.87	3.29	14.58	2.50	12.08	5.79
MLRO, MATERA, IT	7941	10.87	2.51	8.36	0.67	7.69	3.18
MLRS, TEXAS, USA	7080	13.54	2.00	11.54	1.11	10.43	3.11
YARRAGADEE, AUSTRALIA	7090	11.33	0.48	10.85	1.02	9.83	1.50
GGAO, WASHINGTON, DC	7105	12.35	1.14	11.21	-1.03	12.24	0.11
MON. PEAK, CA	7110	14.41	1.40	13.01	0.92	12.09	2.32
HARTESBESTHOEK, SA	7501	14.45	4.24	10.21	0.43	9.78	4.67
RGO, ENGLAND	7840	9.77	0.78	8.99	0.60	8.39	1.38
SALRO, SAUDI ARABIA	7832	12.59	2.53	10.06	-0.22	10.28	2.31
SIMOSATO, JAPAN	7837	17.13	2.58	14.55	-0.20	14.75	2.38
ZIMMERWALD, CH	7810	8.97	-0.86	9.83	0.51	9.32	-0.35
WETTZELL, DE	8834	11.36	1.75	9.61	0.34	9.27	2.09

Table 3. *LAGEOS 2 POD: Core sites' RMS of fit using ITRF2000, ITRF2005P and ITRF2005D, and differences. RMS in red (negative) indicates ITRF2005P performs better than ITRF2005D*

SITE NAME	SITE ID	ITRF2000 (IGN) RMS [mm]	ΔRMS [mm] 2000-2005P	ITRF2005P (IGN) RMS [mm]	ΔRMS [mm] 2005P-2005D	ITRF2005D (DGFI) RMS [mm]	ΔRMS [mm] 2000-2005D
BEIJING, PRC	7249	19.11	3.60	15.51	0.89	14.62	4.49
GRASSE, FRANCE	7835	10.58	3.47	7.11	0.34	6.77	3.81
GFZ POTSDAM, DE	7836	11.96	1.23	10.73	0.91	9.82	2.14
GRAZ, AUSTRIA	7839	8.63	1.34	7.29	0.30	6.99	1.64
HALEAKALA, HI	7210	16.33	3.61	12.72	1.68	11.04	5.29
MLRO, MATERA, IT	7941	10.60	2.37	8.23	0.62	7.61	2.99
MLRS, TEXAS, USA	7080	13.21	1.93	11.28	1.32	9.96	3.25
YARRAGADEE, AUSTRALIA	7090	10.87	0.09	10.78	2.22	8.56	2.31
GGAO, WASHINGTON, DC	7105	11.80	1.24	10.56	0.10	10.46	1.34
MON. PEAK, CA	7110	12.73	0.53	12.2	1.33	10.87	1.86
HARTESBESTHOEK, SA	7501	16.53	5.19	11.34	1.33	10.01	6.52
RGO, ENGLAND	7840	8.74	-0.08	8.82	1.15	7.67	1.07
SALRO, SAUDI ARABIA	7832	11.22	1.95	9.27	0.25	9.02	2.20
SIMOSATO, JAPAN	7837	17.35	3.10	14.25	-0.60	14.85	2.50
ZIMMERWALD, CH	7810	9.23	-0.09	9.32	0.90	8.42	0.81
WETTZELL, DE	8834	10.92	1.20	9.72	0.83	8.89	2.03

SLR contribution to ITRF2005 had some basic differences from what was submitted to ITRF2000:

- The new submission used the Mendes-Pavlis (2004) refraction model.
- Only the data spanning 1993 to end of 2005 were used instead of the 1976 -2000 that was used in ITRF2000.

The first difference was quickly discarded since the same SLR contributions were used in both ITRF2005 versions, P and D. Additionally, tests that were done to quantify the effect of the new refraction model (~0.4 ppb at most), gave no indication of any such large systematic scale differences between the two solutions with the character of the observed scale differences between the two TRFs. Considering the magnitude of the change in the VLBI-SLR scale difference between the two TRFs, a possibly missing relativistic correction in the formulation of the SLR-modeled time-delay advocated by Ashby (2003), was also investigated. Despite the close agreement in magnitude, this correction was also rejected as the cause of the scale differences, a

conclusion that was also supported by Ashby himself (2006, personal communication). The POD tests were extended to include other SLR targets with orbits markedly different from LAGEOS, such as JASON-1 and Starlette. A corollary benefit from these POD tests was that while LAGEOS data were satisfactorily reduced with the scaled version of ITRF2005P, Starlette data for example showed a slight degradation. This implies either a certain distortion in the ITRF2005P solution, or a significant error in the CoM value used for Starlette. The latter is highly unlikely, but cannot be outright discarded.

A final plausible cause investigated as a possible explanation was the fact that the SLR contribution to ITRF2005 did not contain the historical LAGEOS data from the period 1976-1992. To test this last theory, we reduced all of that data and generated solutions that included that data, which we later compared to the two ITRF2005 solutions. Figure 1 shows the LAGEOS data distribution (weekly resolution) for the ILRS network from 1976 to early 2006. It can be seen that there is no dramatic difference between the two networks that supported the two ITRFs.

The SLR data for the period 1976-1992 is certainly not of the same quality as for the recent years, and the network had undergone several upgrade stages during that period. The initial predominantly NASA-supported network from 1976 to 1980 was more of a research and test-bed outfit than an operational one. The two international MERIT campaigns in the early 80s forced the upgrade of the network, its expansion and strengthening with the addition of several stations outside North America and

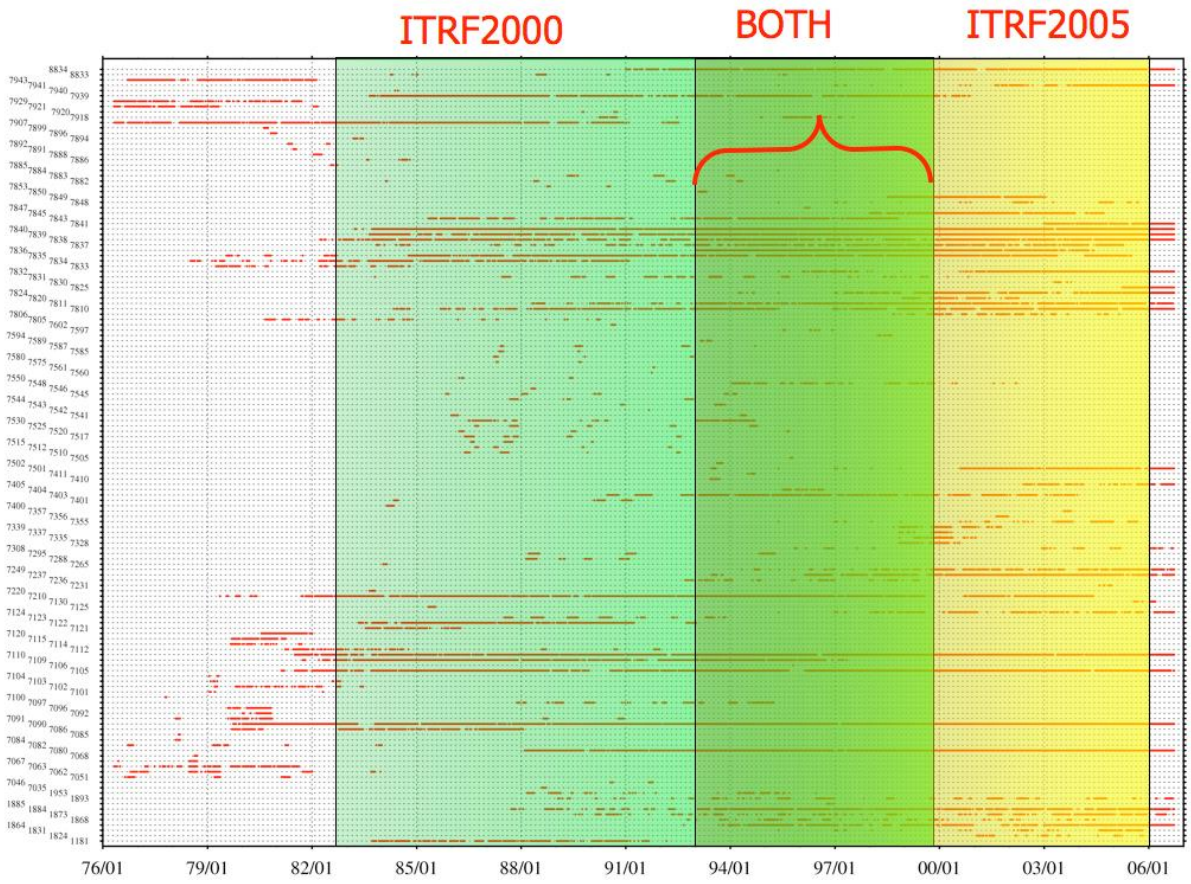

Figure 1. *The LAGEOS and LAGEOS 2 data distribution for 1976 – 2006, and the portions used in the SLR submissions for the development of ITRF2000 (green) and ITRF2005 (yellow).*

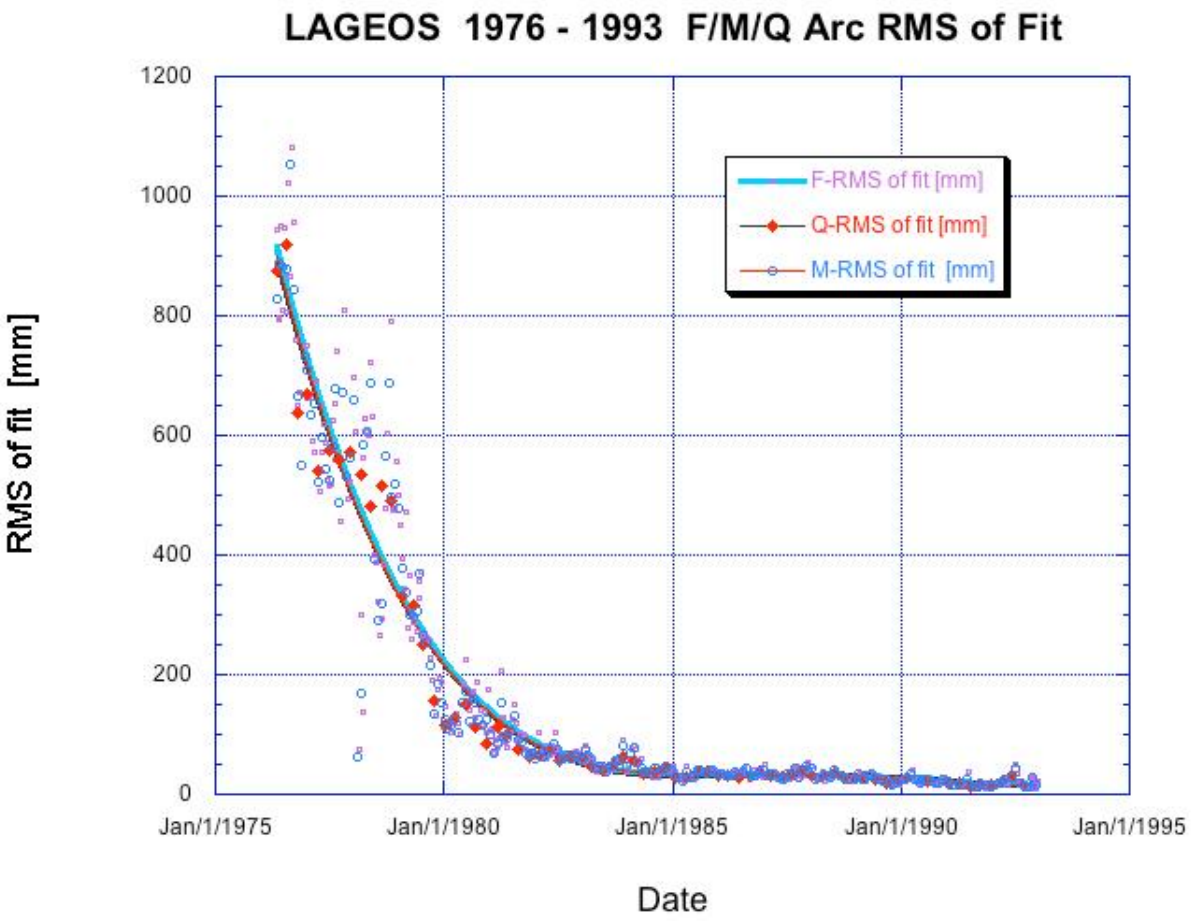

Figure 2. *Orbital arc RMS of fit to LAGEOS data, 1976 – 1992. Results from reductions with three different arc-lengths are shown here, fortnightly (F), monthly (M) and quarterly (Q).*

Europe, and ushered an era of operational mentality across continents, countries and agencies supporting these stations. As a result, the quality of the data improved by an order of magnitude, the quantity increased too, and internationally coordinated scheduling of operations was initiated for improved data yield. The result of these changes is reflected directly in the improved RMS of fit to the collected data, using the same models across all periods of time, as this is illustrated by the graph in Figure 2.

The development of TRFs that included the SLR data from the 1976-1992 period made little difference in their intrinsic scale and scale rate (~10% at most). On the other hand, it does improve the error statistics for sites that span both periods of time and it resulted in capturing in a single consistent frame all SLR sites that ever tracked either or both LAGEOS satellites. This result left the question about the SLR-VLBI scale difference in ITRF2005 open and unanswered, despite the fact that it eliminated a large number of serious candidate explanations.

Recent (spring 2007) developments

During the 2007 General Assembly of the European Geosciences Union (EGU) in Vienna, Austria, MacMillan (2007) brought to the attention of the ITRF community the finding that the official International VLBI Service (IVS) submission to ITRF2005 had an error in the application of the pole tide, which generated a scale bias with respect to the true scale of ITRF.

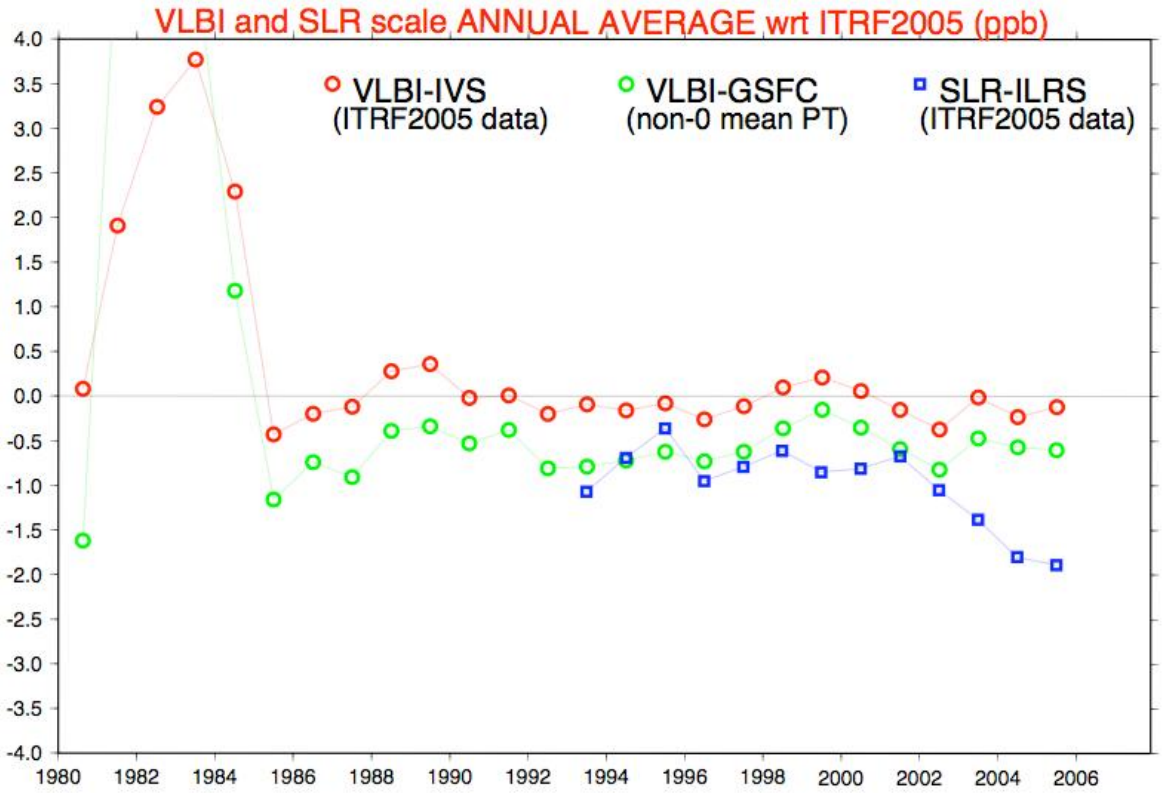

***Figure 3**. Time series of annual scale differences between various VLBI solutions and the SLR submission to ITRF2005, with respect to the ITRF2005 frame, (Altamimi, 2007).*

After an exchange of corrected submission files, Z. Altamimi generated new test solutions that indicate that indeed, this error causes about 0.5 ppb scale bias between the SLR and VLBI frames of reference. This can be seen in the graph that Altamimi (2007) circulated via email on June 18, 2007, under the subject matter: "Pole tide effect on VLBI scale". As you can verify from Figure 3, except for the period after 2004 when the SLR network covers only the one hemisphere of the globe, the scale difference between the two techniques is at the same level of discrepancy as it was during the development of ITRF2000. This means that there is really no reason for the exclusion of SLR from the definition of the scale of ITRF2005. The "significant"scale rate is also a result of the poor network configuration in the latter years and the consideration of some questionable site tie vectors (as pointed out by the DGFI combination center), and could have been dampened by appropriate weighting of the weekly contributions for that period of time, or editing of the ties (as DGFI did for ITRF2005D).

Summary

The release of ITRF2005 in mid-2006 created a great commotion within the geodetic community with its departure from prior tradition, to adopt the scale implied by VLBI only, excluding SLR from the usual 50-50 sharing of this privilege. Additionally, the indication that SLR scale was not only off by more than 1 ppb from the true scale but also suffered from a significant rate change of -0.15 ppb/y, sent SLR analysts scrambling for answers. As we have seen here, none of the most plausible causes

could be found responsible for the observed discrepancy. The matter was never closed, and it was always suspected that in addition to the acknowledged effect of the deteriorating SLR network, either an error in another technique's submission were the cause, or the new way of constructing the ITRF, or a combination of all. The April 2007 findings of MacMillan's investigation in the VLBI scale definition explained for the most part the constant scale offset. The remaining scale rate effect seems to be the result of the new way the ITRF is constructed and the deterioration of the SLR network during 2004- 2006. The recent re-establishment of the SLR sites at Haleakala, Hawaii and Arequipa, Peru, and the new and improved re-analysis of the SLR data this year are expected to resolve many of these remaining issues and restore the faith of the ITRF community in SLR's unique ability to define the ITRF scale in the absolute sense.

References

[1] Altamimi, Z., P. Sillard, and Claude Boucher (2002), ITRF2000: A new release of the International Terrestrial Frame for earth science applications, *J. Geophys. Res.*, *107*, NO. B10, 2214, doi:10.1029/2001JB000561

[2] Altamimi, Z., (2007), email with subject matter "Pole tide effect on VLBI scale", June 18.

[3] Ashby, N. (2003), Relativity in the Global Positioning System, *Living Rev. Relativity*, 6, , 1, available elect. at: http://www.livingreviews.org/lrr-2003-1, (revised 2007).

[4] Ashby, N. (2006), private communication.

[5] MacMillan, D. S. (2007), Determination of the reference frame scale with VLBI, Geophysical Research Abstracts, Vol. 9, 04545, 2007, 1607-7962/gra/EGU2007-A-04545.

[6] Mendes, V.B., G. Prates, E.C. Pavlis, D.E. Pavlis, and R.B. Langley (2002), Improved Mapping Functions for Atmospheric Refraction Correction in SLR, *Geophys. Res. Lett.*, *29*(10), 1414, doi:10.1029/2001GL014394.

[7] Mendes, V.B., and E. C. Pavlis (2004), High-Accuracy Zenith Delay Prediction at Optical Wavelengths, *Geophys. Res. Lett.*, *31*, L14602, doi:10.1029/2004GL020308.

[8] Pearlman, M.R., Degnan, J.J., and Bosworth, J.M., 2002. "The International Laser Ranging Service", *Adv. in Space Res.*, Vol. 30, No. 2, pp. 135-143, 10.1016/S0273-1177(02)00277-6.

An Optimised Global SLR Network For Terrestrial Reference Frame Definition

Ramesh Govind[1]

1. Geoscience Australia, Canberra, Australia

Abstract

It is a continuing debate on the current station distribution and geometry of the global SLR network. In order to design the optimum network for high quality geodetic products, a simulation study was undertaken. Data for previously closed or additional new stations was simulated and augmented into the existing available data set and the relevant geodetic parameters estimated. Weekly estimates of the degree one coefficients of the Earth's gravity field (centre of mass) is used as a measure of the influence of the simulated data with respect to the original solutions -- as determined from the observed data set. The simulated data, observed data, and the computation standards are described. On the basis of these results, an optimised global network of SLR stations is presented.

Performance of Southern Hemisphere Stations

John McK. Luck[1]

1. EOS Space Systems Pty.Ltd., Canberra, Australia

Abstract

The opening of the San Juan station in Argentina, and upgrades to other stations, has lifted the productivity of Southern Hemisphere stations to perhaps 40% of the global total, with a nice distribution in longitude. Various operational statistics will illustrate the improvements achieved up to the start of October 2006.

Introduction

The new San Juan station came on-line in March 2006, in collaboration with NAOC, Beijing. Its performance is highly impressive, and is significantly helping to satisfy the eternal cry for more SLR observations from the Southern Hemisphere.

At the same time, the BKG station TIGO at Concepcion, Chile has been upgraded to hectoHertz ranging with reliability enhancements, and has improved its output considerably in recent months. MOBLAS 8 at Papeete, Tahiti and MOBLAS 6 at Hartebeesthoek, South Africa are also making significant contributions. Of the Australian stations, MOBLAS 5 at Yarragadee continues to be the benchmark and workhorse station for the entire global SLR network, while the re-built EOS/GA station on Mount Stromlo is again one of the top performers.

Statistics for three 28-week time periods in Fig.1 and Table 1 show that data quantities from Southern Hemisphere stations have sustainably improved this year (2006). Other performance metrics are also displayed in this paper.

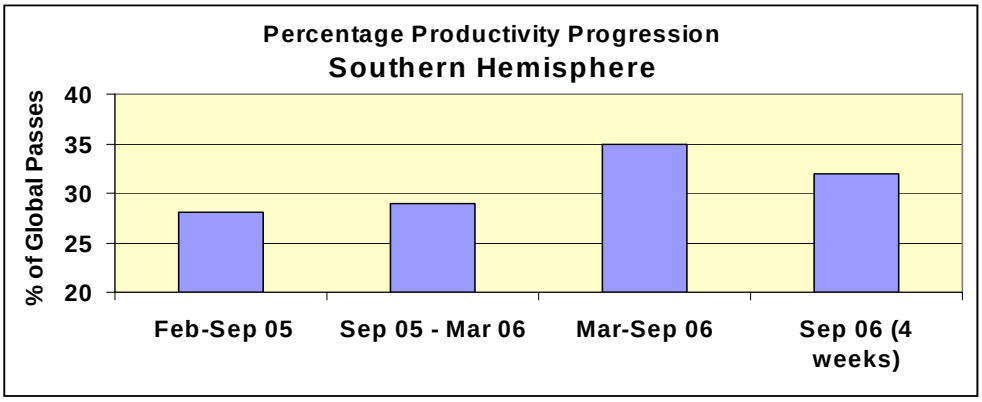

***Figure 1**: Percentages of passes from Southern Hemisphere stations. Data extracted from CDDIS weekly SLRQL reports*

***Table 1**: Pass percentages from S. Hemisphere stations, and also by ILRS Network*

Period	**Southern Hemisphere**	**By Network** (see (Luck, 2006)		
		WPLTN	**NASA**	**EUROLAS**
2005 Feb-Sept	28	38	15	46
2005 Sept – 2006 Mar	29	44	15	41
2006 Mar-Sept	35	42	16	41
2006 Sept 03-30	32	45	12	43

Numbers of passes by station

In Fig.2, station totals are grouped by hemisphere. Some of the least productive Northern Hemisphere stations are not shown. Each point is a 28-week total.

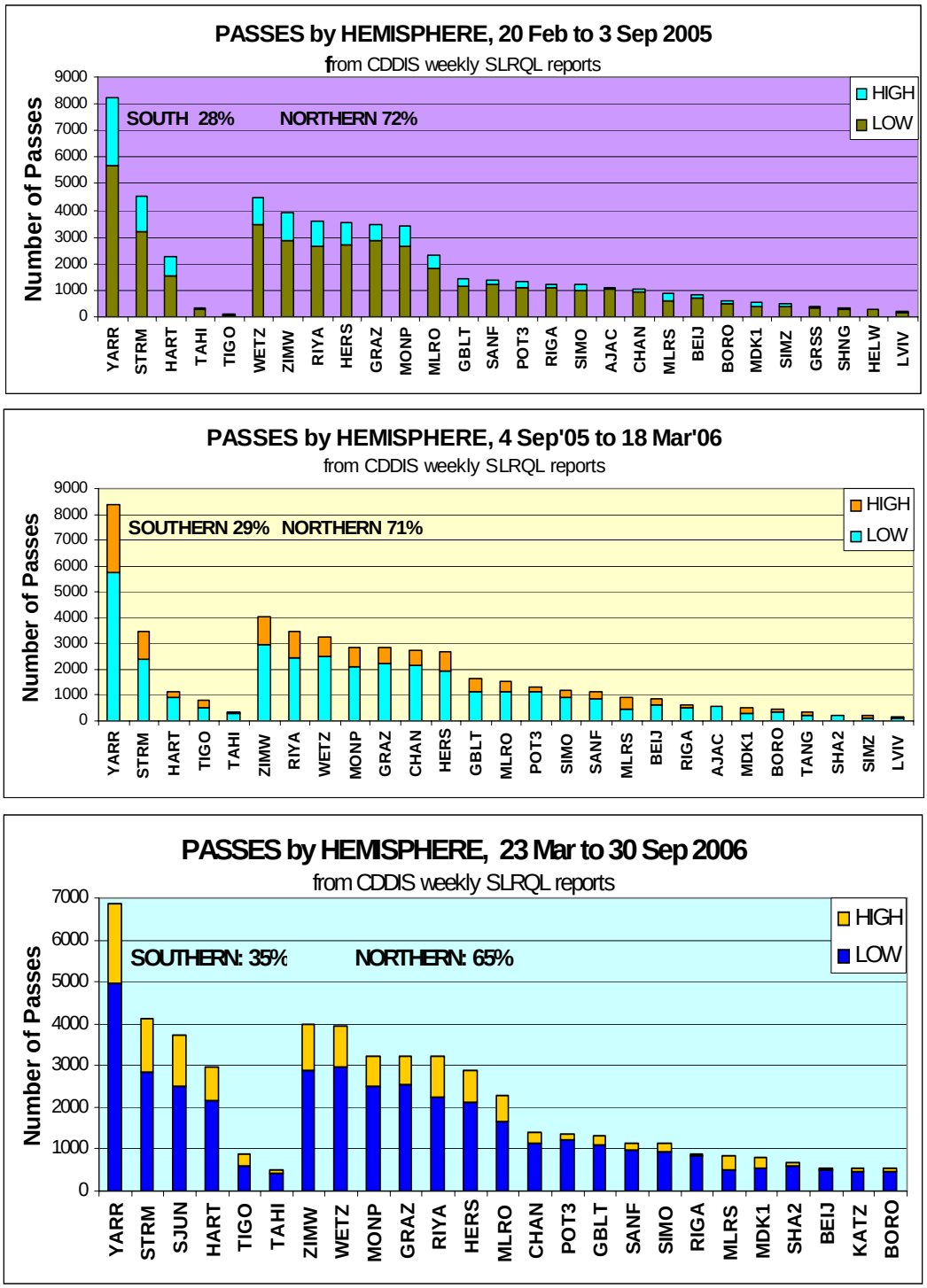

***Figure 2**: Station totals for three 28-week periods, grouped by hemisphere.*

Range bias stability

Fig.3 compares Southern and Northern Hemisphere stations for the RMSs since 19 March this year. They are the RMSs of range biases for LAGEOS I and II combined taken from NICT daily analysis reports, after some outlier editing.

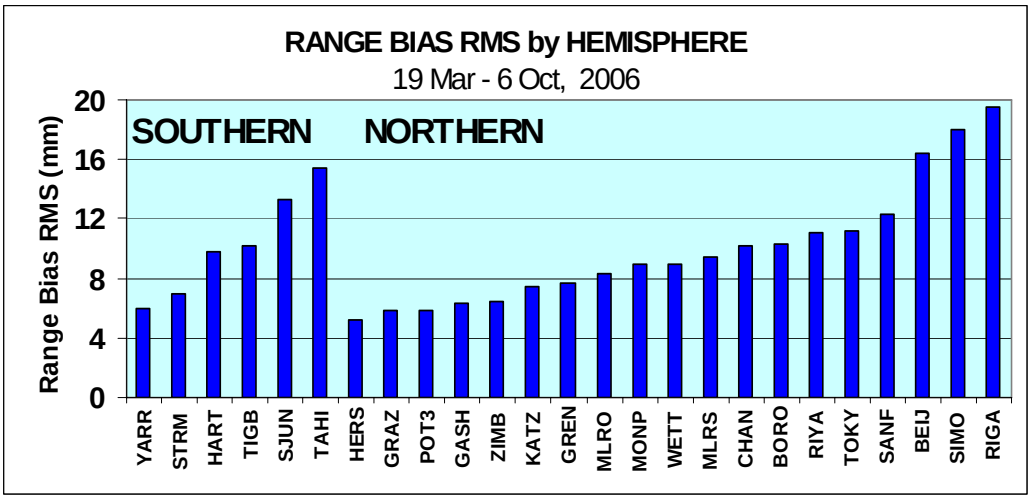

***Figure 3**: RMS of Range Bias per station per hemisphere, L1 & L2*

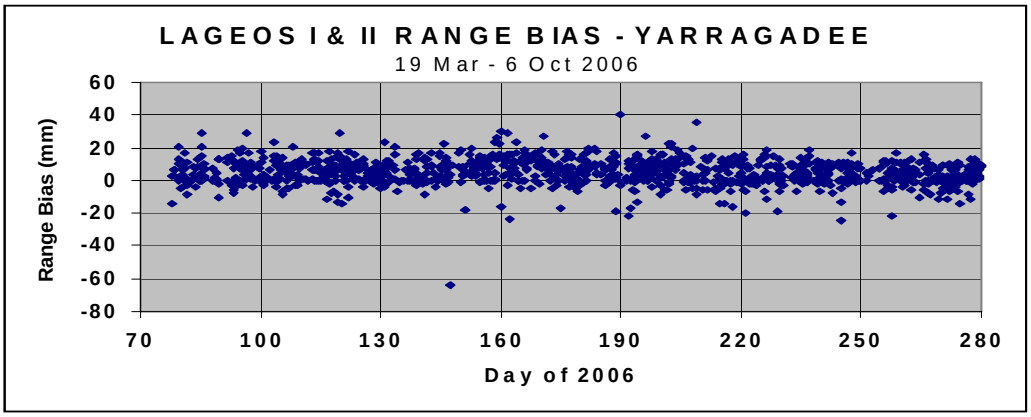

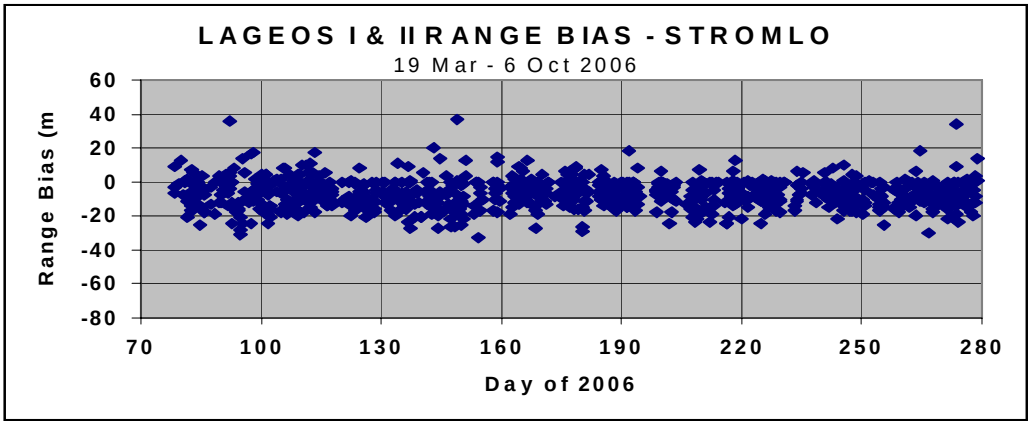

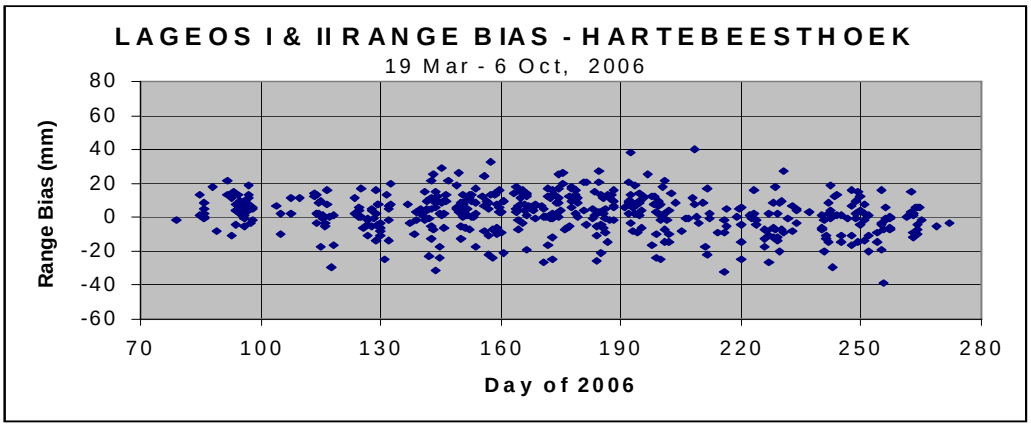

***Figure 4a**: Range Biases for LAGEOS I & II for Yarragadee, Stromlo and Hartebeesthoek .*

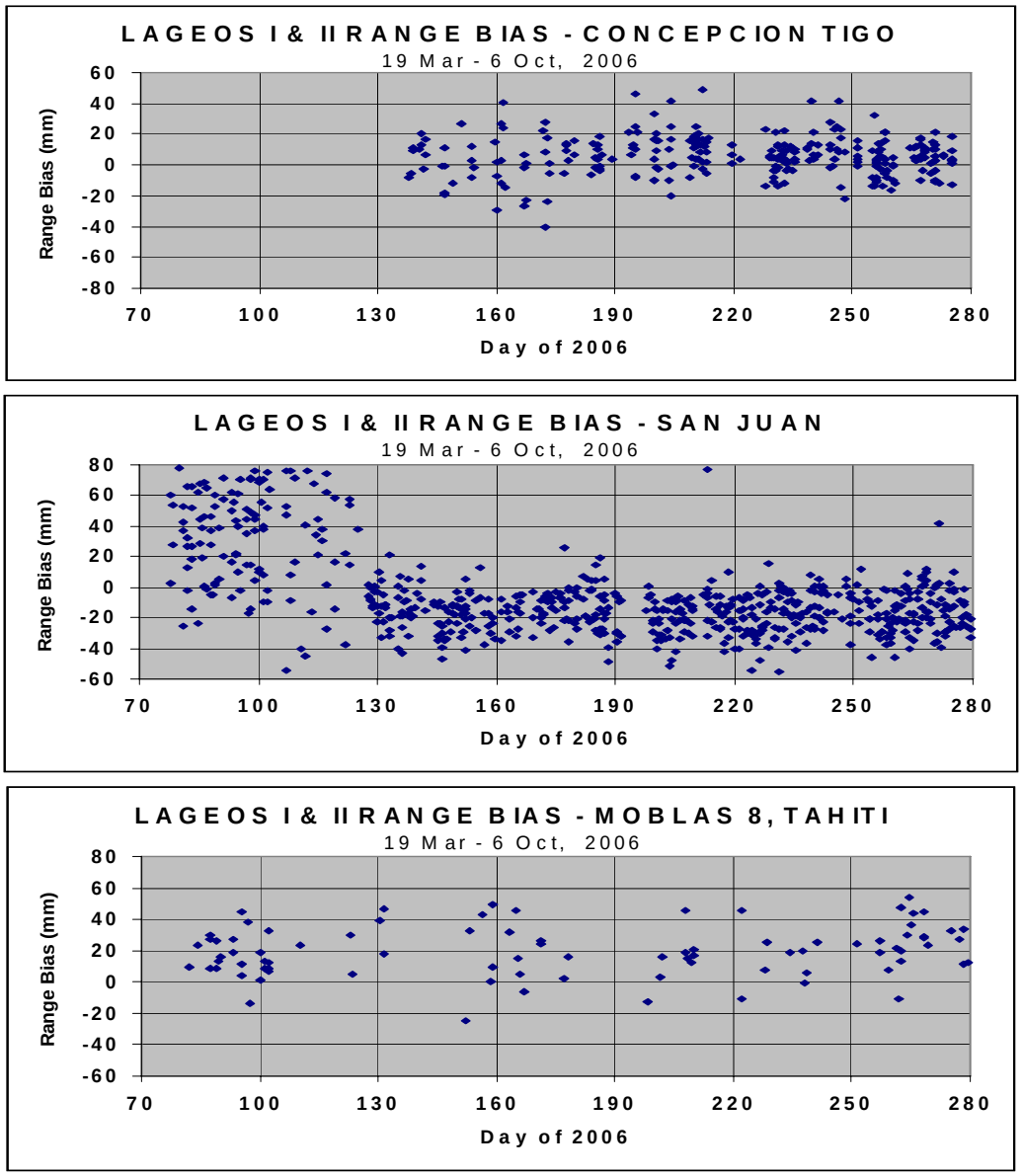

***Figure 4b**: Range Biases for LAGEOS I & II for Conception, San Juan and Tahiti.*

The time series for the 6 stations are shown in Figures 4a and 4b.

Normal points per pass

This category reflects the observing efficiency of the stations, and is affected by skill in acquiring satellites and interleaving passes as well as factors like aperture, laser power, sun avoidance, priorities and bad weather. In general, a low ratio means more uncertainty in determining time bias, unless the few normal points are very well distributed throughout the pass. Fig 5 contrasts northern and southern hemispheres.

Normal point precision

NP precision is calculated as the RMS of normal points about a trend-line fitted through the orbit residuals of the Analysis Centre's global solution. It is thus a measure of a station's internal consistency, and is affected by short-term variations in the station's observations, method of forming normal points, and errors in weather data as well as the Analysis Centre's methods of filtering and fitting. Fig.6 shows the results for the 28-week period Mar-Sep 2006 taken from the NICT daily analysis

reports, but only for passes containing at least four NPs, and Fig.7 shows the time-series for each station over the same period.

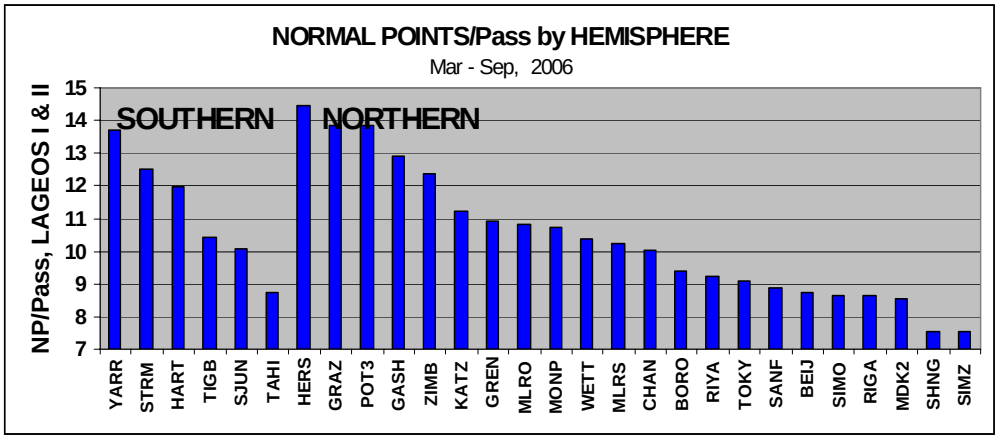

***Figure 5**: Normal points per Pass, LAGEOS I & II combined, extracted from NICT daily Analysis Reports. (Note truncated vertical scale - it looks worse than it is!)*

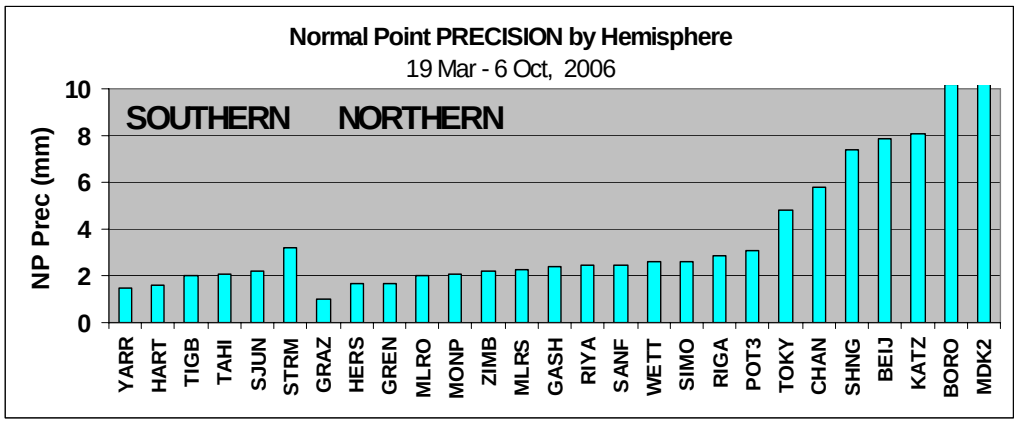

***Figure 6**: Normal Point Precisions Summary*

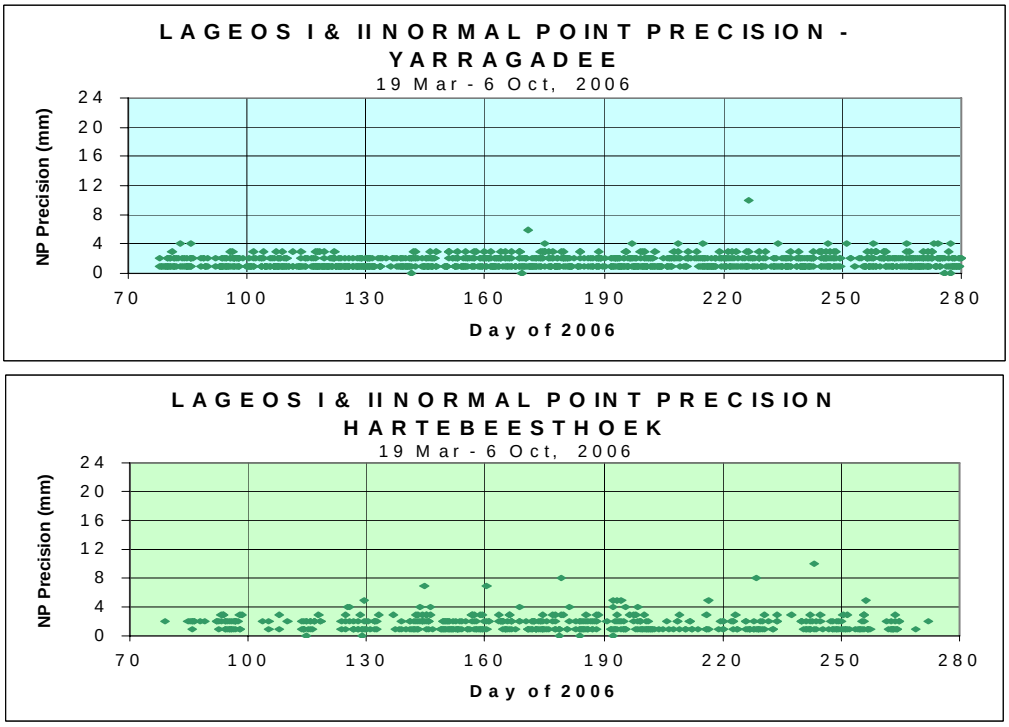

***Figure 7a**: Normal Point Precisions for Southern Hemisphere stations*

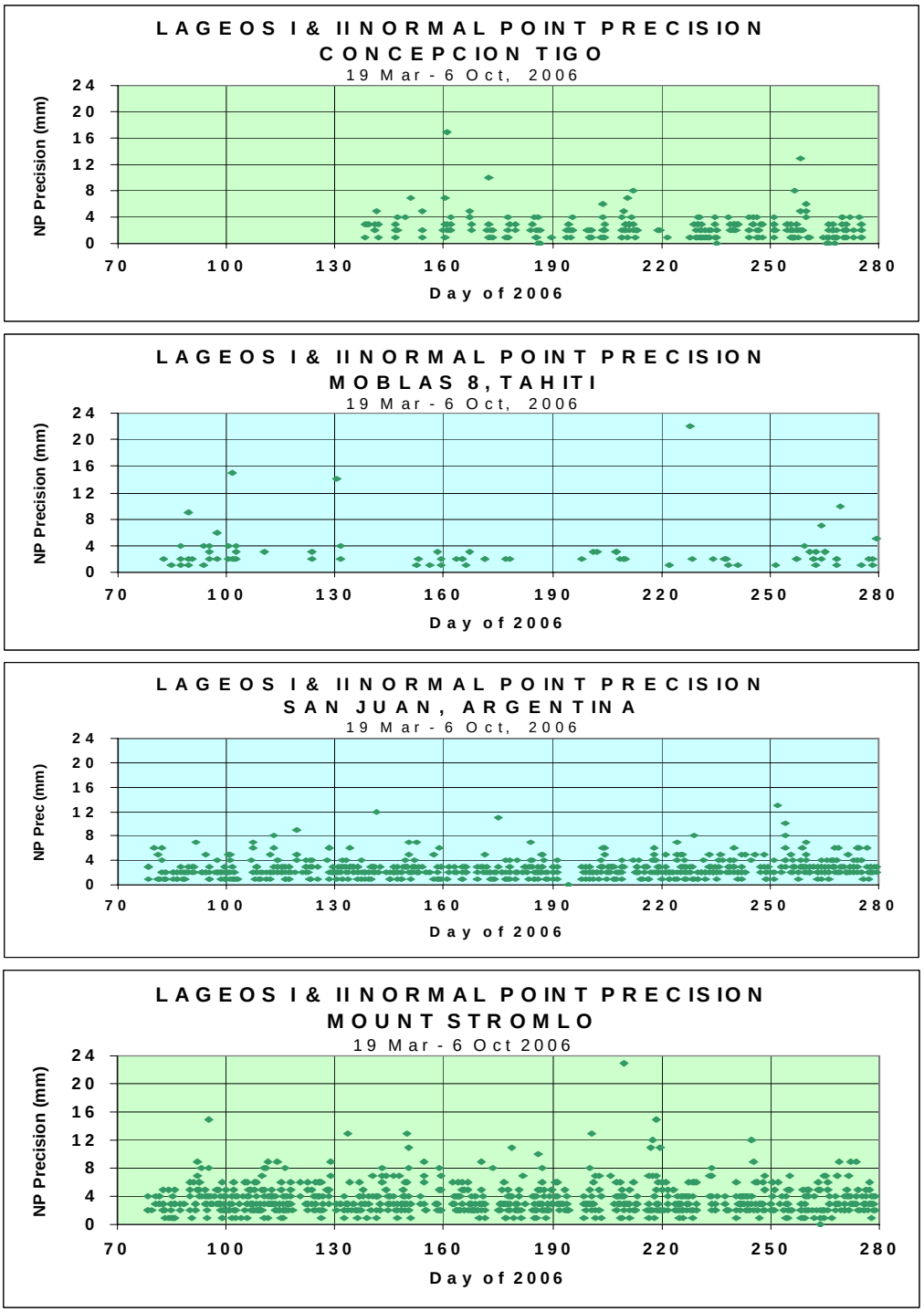

***Figure 7b**: Normal Point Precisions for Southern Hemisphere stations*

System delay

The system delays are the results of system calibration by pre- and/or post-pass ground target ranging, or equivalent. They have arbitrary values and are allowed to jump when, for example, cables are changed in the paths to the timing system, components in the optical path are moved, or other repairs and maintenance are performed. Otherwise, however, they should remain constant. In particular, they should not show drifts such as TIGO has been undergoing since about day 225 in Fig.8. The results in Fig.8 are from Ajisai entries in NICT daily analysis reports, with respect to the average system delay over the 28-week period.

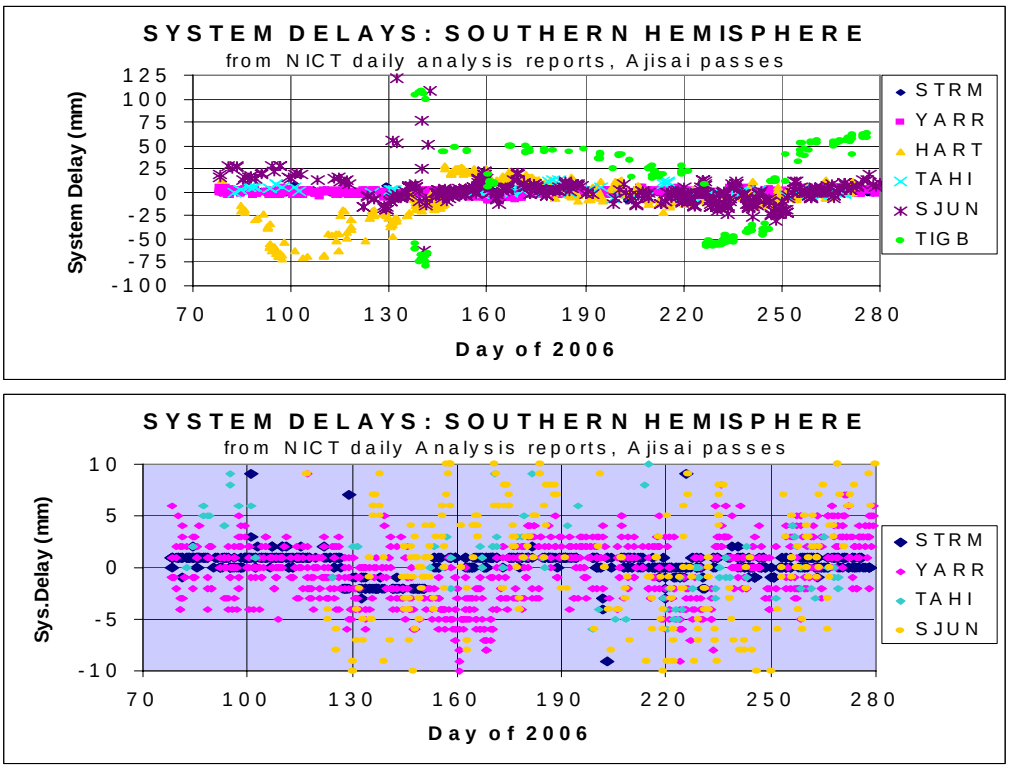

***Figure 8**: System Delays per pass (Ajisai). The lower plot is at expanded vertical scale.*

Conclusions

There has been a boom in Southern Hemisphere ranging in 2006, due mainly to the commissioning of the San Juan station, whose productivity is the more remarkable because it only observes at night-time. Tahiti only has limited day-time tracking.

The quality of ranging is comparable with Northern Hemisphere stations, too, although some stations show worrying trends in their system delay stabilities while Stromlo should be doing far better in its normal point precisions. The imminent resurrection of Arequipa, Peru should further enhance the Southern Hemisphere contribution to global SLR performance.

Acknowledgements

The data used here were extracted from the CDDIS SLR Data Reports, courtesy Carey Noll, and from the NICT daily Multi-Satellite Bias Analysis Reports, courtesy Toshi Otsubo. These reports are produced on behalf of the International Laser Ranging Service (ILRS).

Reference

[1] Luck, J.McK.: "*Performance of WPLTN Stations*", these proceedings (2006)

The Evolution of SLR/LLR in Response to Mission Needs

Peter Shelus[1]

1. University of Texas at Austin/CSR

Abstract

The response of the laser ranging network to the needs of the various missions over the past 40 years or so has been an evolving one. The targets have been varied and the science has been exciting. With the establishment of the International Laser Ranging Service (ILRS) and its Missions Working Group, this planning and coordination has been put on a much more formal basis. This presentation reviews some of the history, provides information on where we find ourselves right now, and tries to look a bit into the future as to where we wish to be.

Assessment of SLR Network Performance

Mark Torrence [1] and Peter Dunn [1]

1. SGT Inc, Greenbelt, Maryland, USA

Abstract

The SLR global performance report card is updated quarterly on the ILRS web-site and presents a broad view of the state of the network. The information summarized in that report can be treated in several different ways to clarify particular features. The usual expression of the station characteristics as a function of calendar time provides a method to monitor the evolution of the health of a station by considering the quantity of normal points collected, as well as the volume of full rate observations and the noise level of these data for each satellite. If the same variables are expressed as a function of local time, the distinction between day-time and night-time performance of a station is high-lighted. Satellite signature effects can be demonstrated by again plotting these same variables but as a function of range value, and this will also vary by station. We demonstrate the use of these alternative representations for all the stations in the network to many satellites and solicit ideas which could enhance the definition of the each observatory's contribution to the Global Network and the analyst's understanding of the data.

Introduction

The motivation for constructing graphs of station performance arose from an assessment of potential corner cube array design for HEO satellites. Looking at the SLR data as a function of local time and as a function of the satellite range may reveal station performance characteristics in SLR data such as whether patterns vary from year to year, and whether there are indications of satellite dependencies.

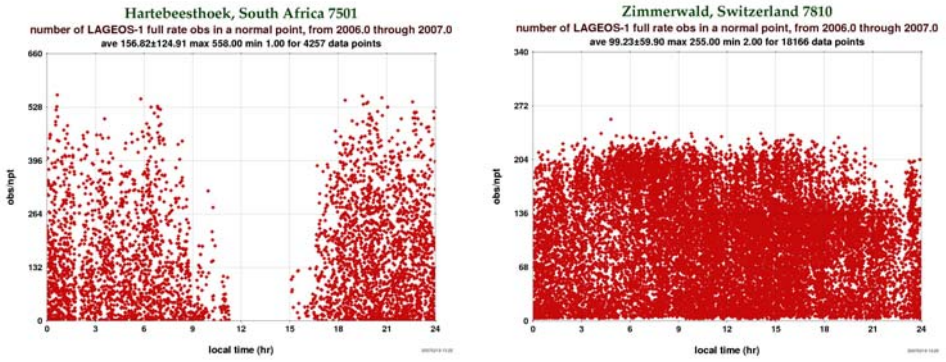

Figure 1 *Number of full rate observations in a normal point for Hartebeesthoek and Zimmerwald.*

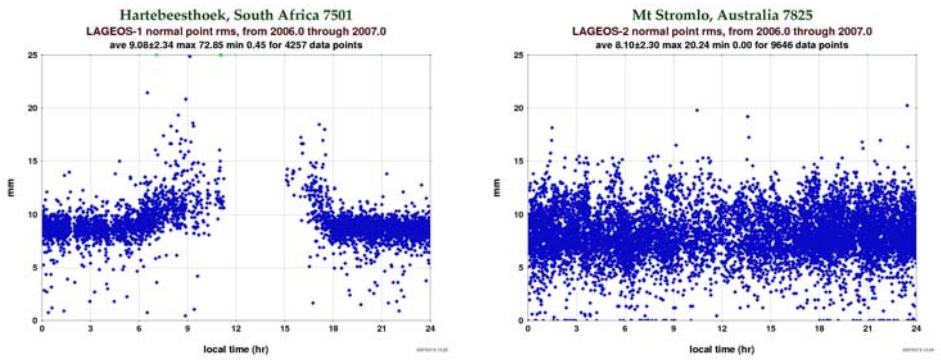

***Figure 2**: Normal point rms as function of local time for Hartebeesthoek and Mt Stromlo.*

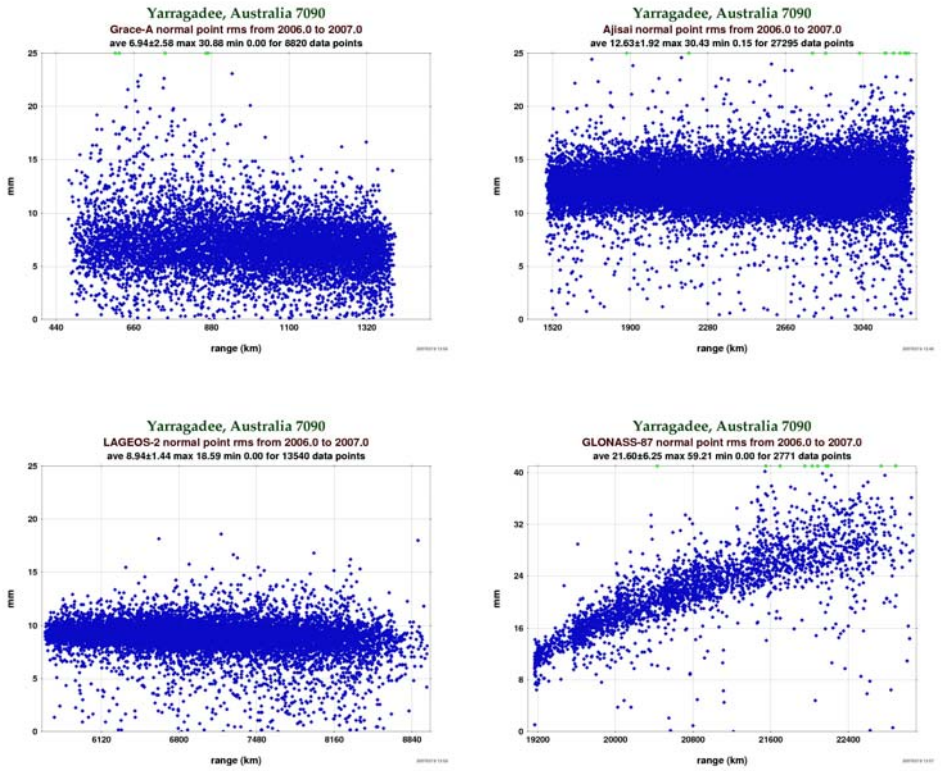

***Figure 3**: Normal point rms as function of range for Yarragadee for Grace-A, Ajisai, LAGEOS-2 and GLONASS-87.*

The pattern seen in the normal point rms as a function of range for Yarragadee tracking GLONASS-87 is most probably due to the large array cross section of GLONASS-87 resulting in center-of-mass offset which is a function of viewing geometry.
See
http://ilrs.gsfc.nasa.gov/cgibin/satellite_missions/select.cgi?sat_code=GL88&sat_name=GLONASS-88&tab_id=com

Plots of this type will be available at the ILRS web site.

Performance of WPLTN Stations

John McK. Luck[1]

1. EOS Space Systems Pty.Ltd., Canberra, Australia

Abstract

There have been significant upgrades to WPLTN stations in the last year. Performance statistics for each station will be presented, which may highlight where further improvements could be achieved.

Introduction

The working and developing stations which constitute the Western Pacific Laser Tracking Network (WPLTN) include Tokyo, Simosato and Tanegashima (Japan), Shanghai, Beijing, Changchun, Yunnan, Wuhan and the CTLRS (China), Yarragadee and Mount Stromlo (Australia), Riyadh (Saudi Arabia), Maidanak (Russia), and most recently the new Chinese-supplied station at San Juan, Argentina. In 2006, as well as the commissioning of San Juan, Shanghai moved to a new site and significant upgrades came to fruition at Simosato and Changchun. San Juan has been accepted as a member of WPLTN, and Yarragadee has dual membership with WPLTN and the NASA network.

These developments have produced a noticeable increase in the productivity and quality of the network as a whole. It is therefore timely to review its performance and to compare it with the NASA and Eurolas networks. (This paper was actually presented at the WPLTN General Assembly.)

For the purposes of this paper, Yarragadee is included in WPLTN, TIGO in Concepcion (Chile) and the Ukraine stations in Eurolas, and Hartebeesthoek and Tahiti in NASA. Data are shown in four periods – three 28-week periods spanning 20 Feb 2005 to 2 Sep 2006, and the 4-week period 3-30 Sep 2006 leading up to the Workshop. In many ways the data displays emulate the ILRS Quarterly Global SLR Performance Reports, arranged differently.

Productivity

The numbers of passes summarized by network are shown in Fig.1 as percentages of the global totals. The increase since 2005 seems to be sustained, at the expense of the NASA network. Data were extracted from the weekly CDDIS SLR Data Reports.

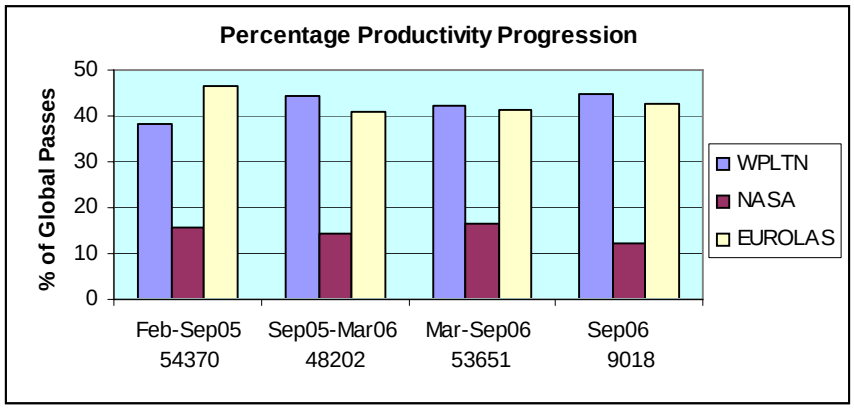

***Figure 1**: Productivity comparison. The global totals of passes are on the bottom line.*

Fig.2 shows the numbers of passes per station per period, grouped by network.

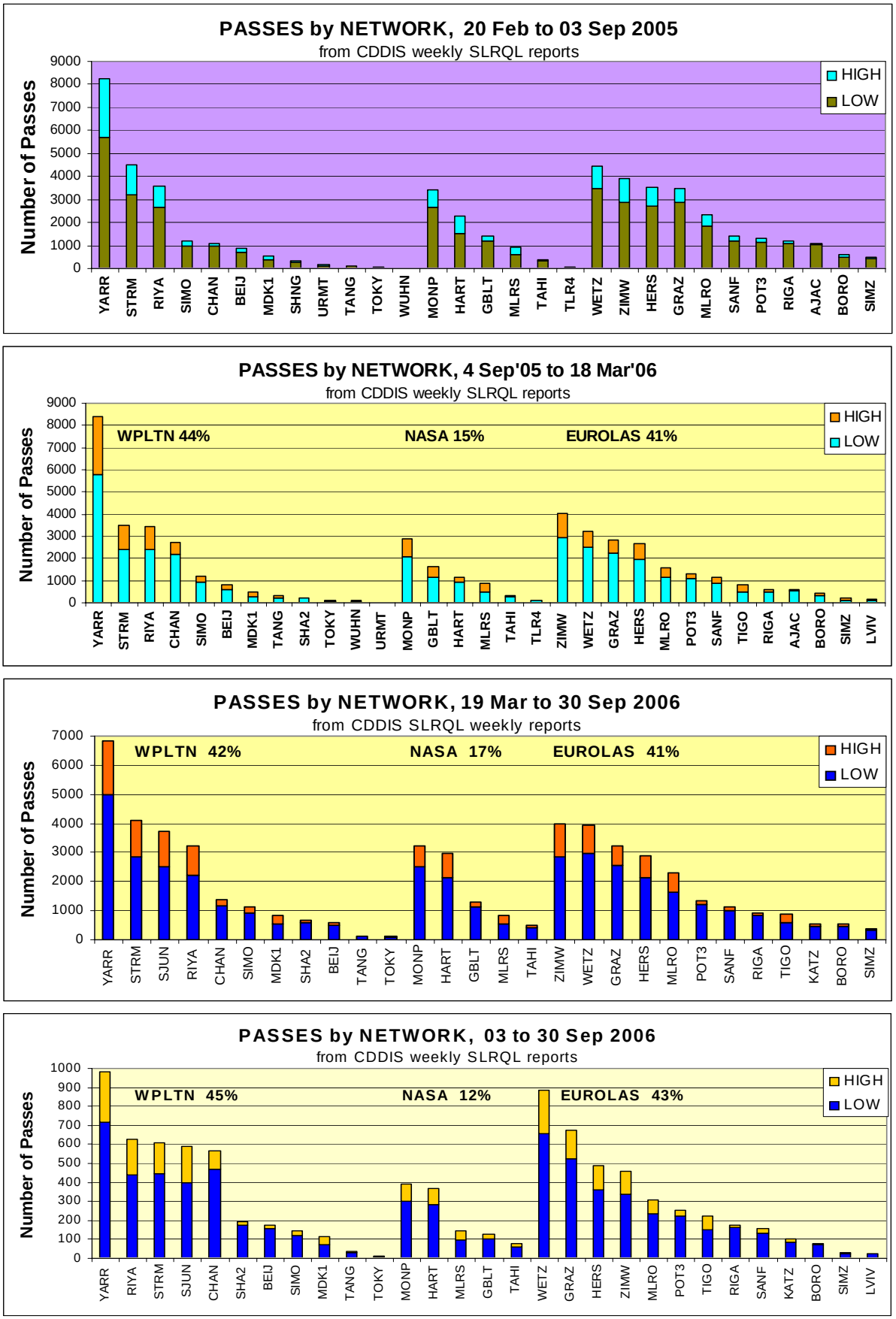

***Figure 2**: Numbers of passes per station in each of the four periods.*

Normal Points per Pass

This category reflects the observing efficiency of the stations, and is affected by skill in acquiring satellites and interleaving passes, as well as factors like aperture, laser power, sun avoidance, priorities, and bad weather. In general, low ratios mean more uncertainty in determining time bias, unless the normal points are very well distributed throughout a pass.

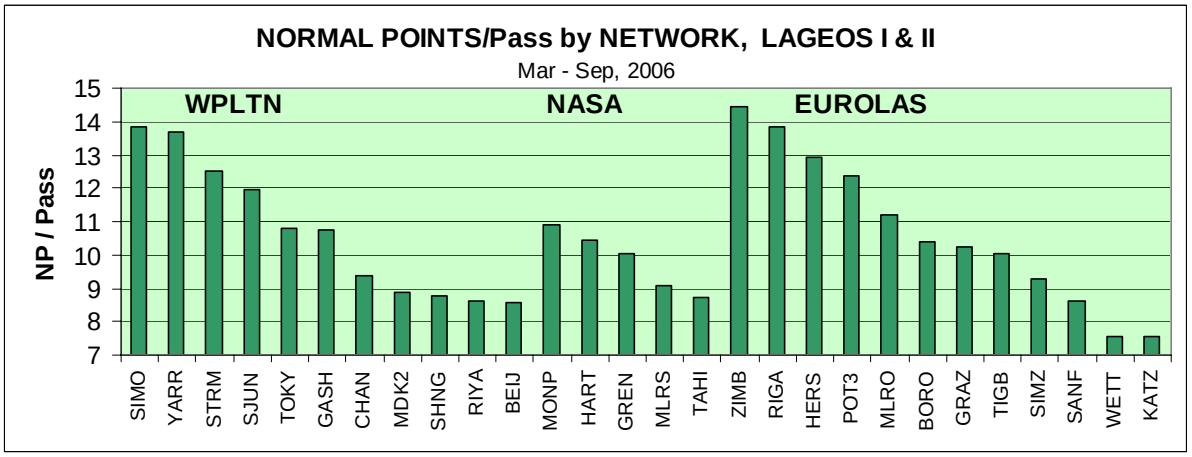

***Figure 3**: Normal points per pass in much of 2006.*
Data from daily NICT Multi-Satellite Bias Analysis Reports.

The best of the WPLTN stations are comparable with Eurolas. Stations with low ratios – in all networks! – should aim to improve coverage during passes.

Normal Point Precision

For Fig.4, the average NP Precision values were calculated after removal of obvious outliers. Stations not shown were off-scale. The best stations achieve 2 mm, and 3 mm should be the aim. Clearly, several WPLTN stations and some from eastern Europe need to improve.

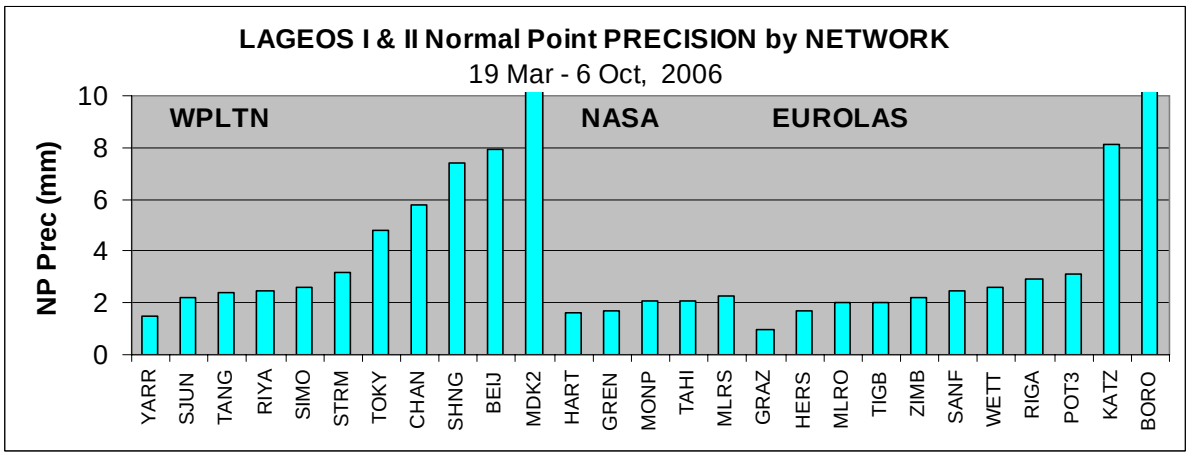

***Figure 4**: Average Normal Point Precisions for much of 2006.*
Data from NICT reports.

Time series graphs for some of the stations are shown in Fig.5. Only passes containing at least 4 Normal Points are plotted. Graphs for Yarragadee, Stromlo and San Juan are given in the companion 'Southern Hemisphere' paper (Luck, 2006).

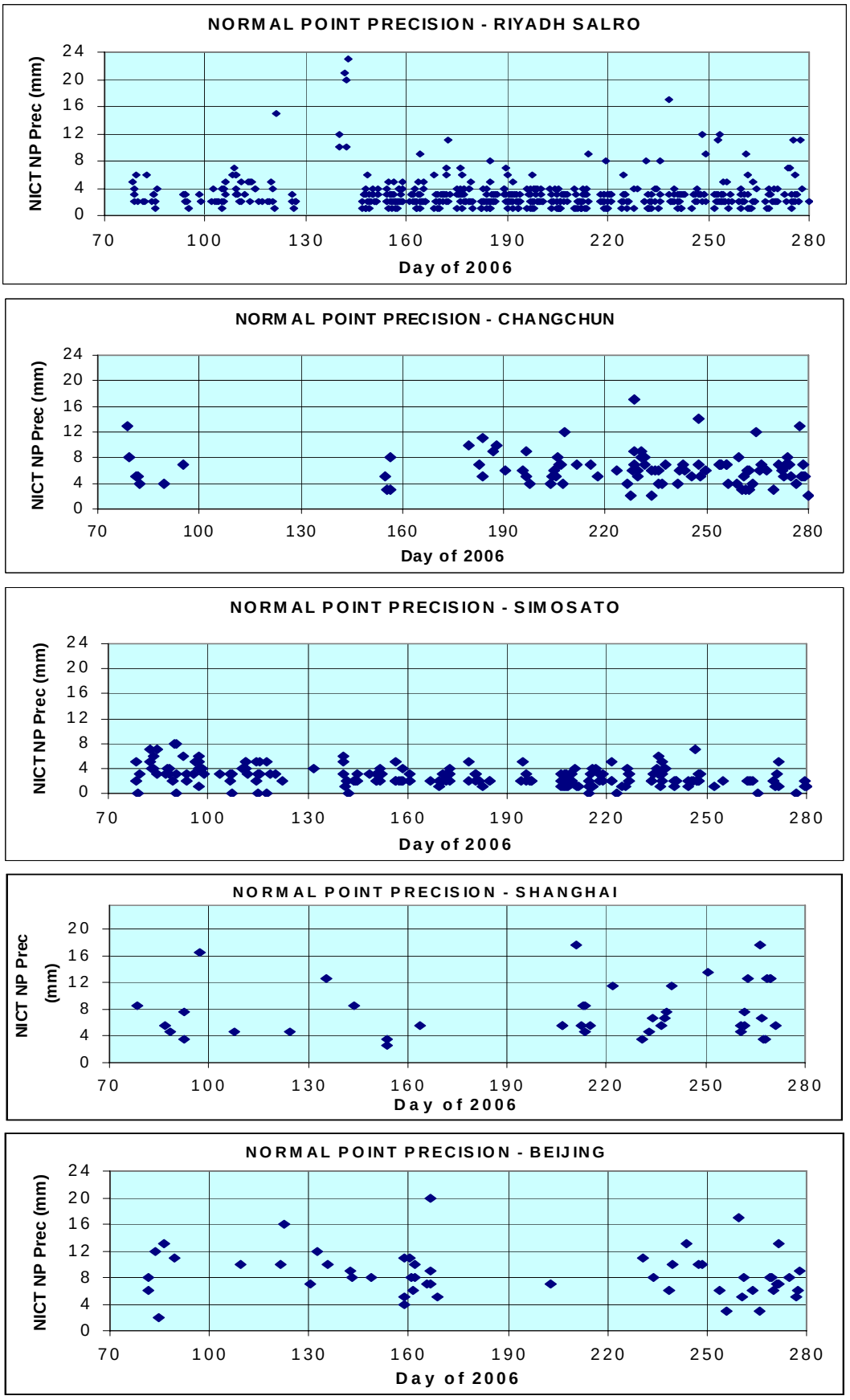

***Figure 5**: Normal Point precisions for selected WPLTN stations. Data from NICT reports. See also (Luck, 2006)*

Accuracy – Range Bias and System Calibration

More important than the precision of the measurements is their accuracy, i.e. how closely the numbers obtained reflect the true distances. There is no perfect way to assess accuracy, so we use range biases, which in a sense give a station's range errors against a sophisticated average over all stations using the satellites' orbits as constraints; and we use ground-target ranging to measure the system delays that are applied to the range measurements. Both these methods have drawbacks. Range biases depend upon the set of station coordinates and the processing philosophy adopted by any particular Analysis Centre. For ground-targets, the distance from invariant point to target must be measured with millimeter accuracy, and preferably be checked frequently by a technique such as MINICO (Luck, 2005).

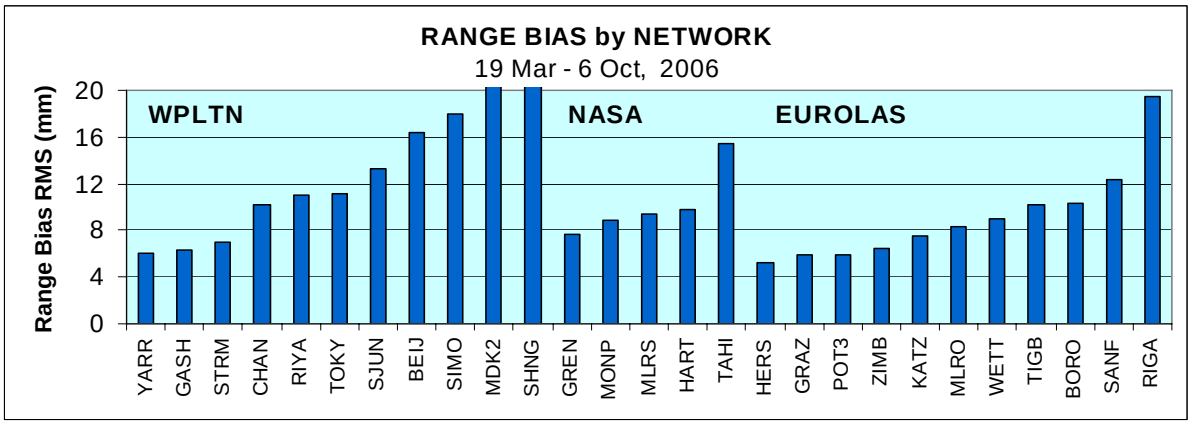

***Figure 6**: Range bias RMS about mean values by station. Data from NICT reports.*

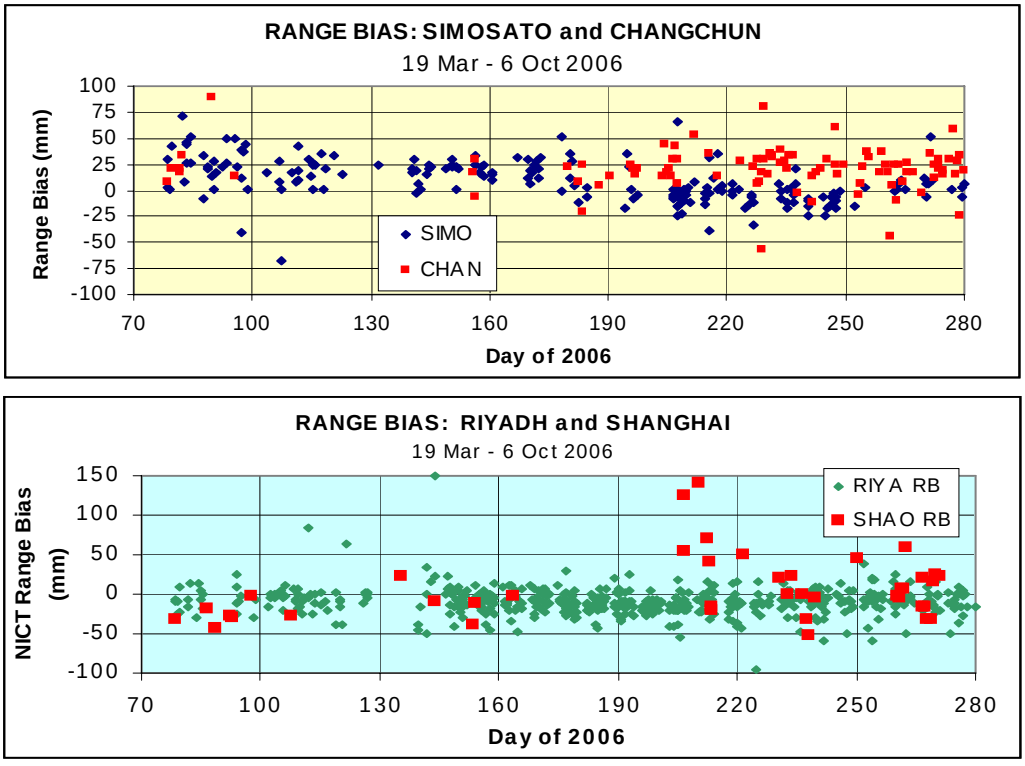

***Figure 7**: Range bias time series for reasonably productive stations. Data from NICT reports.*

RMS variations of LAGEOS I & II range biases about their station means for a period in 2006 are shown in Fig.6, and time series for some of them in Fig.7. Yarragadee,

Stromlo and San Juan are shown in the companion "Southern Hemisphere" paper (Luck, 2006).

System Delays

In Fig.8, the average system delay for each station has been subtracted from its values to clarify the comparisons. Large jumps, which are perfectly valid, occurred during the period at Simosato and Riyadh, so in Fig.9 they are adjusted to their piecewise averages.

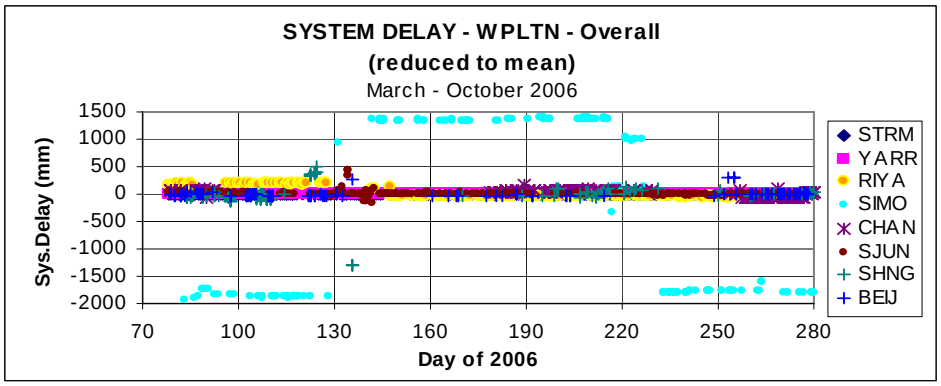

***Figure 8**: Relative system delays for productive stations. Data from NICT reports.*

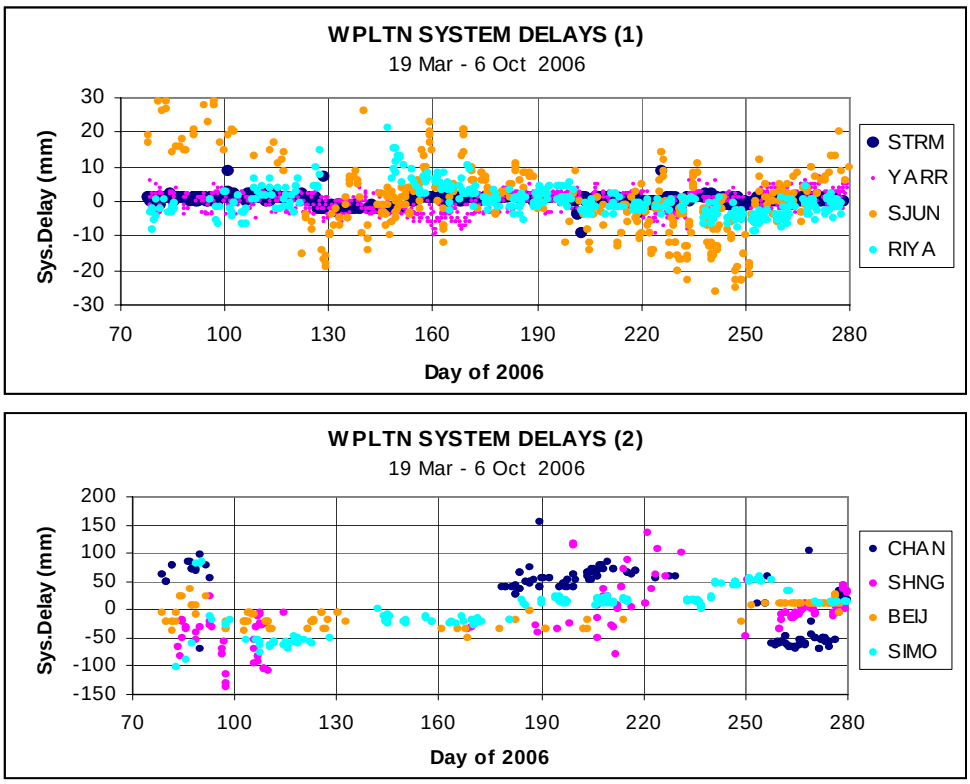

***Figure 9**: Relative system delays at different expanded vertical scales. Data from NICT Reports, AJISAI passes.*

There is substantial scatter for most stations except Yarragadee, Stromlo and Riyadh, and drifts in several, most notably Riyadh and Simosato, which are even more worrying. Stations are strongly urged to investigate the causes of the scatters and drifts, because it is then likely that there are also large scatters and drifts within

passes. Fortunately, there is little evidence of correlations between range bias and system delay (although if there were, it should be easily fixed).

Conclusions

The number of passes acquired by WPLTN stations has improved in the 12 months to October 2006, and now exceeds Eurolas. This is largely due to the commissioning of San Juan and upgrades at some other stations. Most stations now track GPS-35 &-36 successfully, at night. When stations like Changchun and San Juan achieve daylight tracking, the productivity ratios should improve even further.

The analysts prefer passes well tracked from observing horizon to observing horizon, or at worst that include segments near both horizons and at maximum elevation. NPs/Pass is a rough measure of how well this is achieved, but inspection of the NICT reports shows that sparse passes invariably fail to produce a Time Bias of decent quality, which indicates poor NP distribution. Fig.3 indicates that many stations (in all networks) need to improve this aspect of operations.

The quality of WPLTN stations, assessed by Normal Point precision and Range Bias RMS for LAGEOS I & II combined, is an area needing improvement, with only 5 stations showing NP precision better than 3 mm and 3 stations with Range Bias RMS below 8 mm. It is suggested that detailed attention to stabilizing system delays is needed at many stations.

And if you think that this paper is just stating the bleeding obvious, then I have found by long and bitter experience that that is exactly what is sometimes needed!

Acknowledgements

The data used here were extracted from the weekly CDDIS SLR Data Reports, courtesy Carey Noll, and from the NICT daily Multi-Satellite Bias Analysis Reports, courtesy Toshi Otsubo. These reports are produced on behalf of the International Laser Ranging Service (ILRS).

References

[1] Luck, J.McK.: "*Five Target System Calibration*", Proc. 14th International Laser Ranging Workshop, San Fernando, Spain. Boletin ROA No.5/2005, pp.311-321 (2005)

[2] Luck, J.McK.: "*Performance of Southern Hemisphere Stations*", these proceedings (2006)

Archiving and Infrastructure Support at the ILRS Data Centers

C. Noll[1], M. Torrence[2], W. Seemueller[3]

1. NASA Goddard Space Flight Center, Code 690.5, Greenbelt, MD 20771, USA.
2. SGT, Inc., mark.h.torrence.1@gsfc.nasa.gov
3. Deutsches Geodätisches Forschungsinstitut (DGFI), Marstallplatz 8, D-80539 Muenchen, Germany.

Contact: seemueller@dgfi.badw.de /Fax: +49 89 23031-1240,

Carey.Noll@nasa.gov /Fax: 301-614-6015

Abstract

Two global data centers have supported the International Laser Ranging Service (ILRS) since its start in 1998. The Crustal Dynamics Data Information System (CDDIS), located at NASA's Goddard Space Flight Center, and the Eurolas Data Center (EDC), located at DGFI, are active archives of laser ranging data and products derived from these data. The laser data sets consist of on-site normal points and full-rate data. The official ILRS products, currently station positions and EOP, are also made available to the user community through these data centers. Infrastructure support for the ILRS include reports of data holdings and quality, satellite predictions, and station configuration information. This presentation will describe this laser ranging archive available at the ILRS data centers and plans for future enhancements.

Data Center Archive Contents

Currently, the ILRS data and product archive consists of normal point and full-rate data, satellite prediction information, and site positions and velocities. Data since mid-1976 are available at the data centers; ILRS products from January 1993 to the present are also available.

Normal point data is the primary ILRS station data product, gradually replacing on-site sampled data and later full-rate data as the primary data product starting in 1991. Normal points are generated on-site very shortly after the satellite pass and transmitted within a few hours to the ILRS operations centers and, from there, to the ILRS data centers.

Full-rate data were the prime SLR product in the 1970's and early to mid 1980's. In the late 1980's, the normal point generation process was refined and normal points were obtained from the full-rate data during post-processing. In the 1990's, on-site normal point production became the accepted process. In the mid 1990's, the SLR/LLR CSTG subcommission agreed that there was no formal requirement for full-rate due to the transition and acceptance of on-site generated normal points as the prime and only station data product. Many stations, however, continue to provide full-rate data to the ILRS data centers since they are sometimes required for specific needs (e.g., center-of-mass analysis, retroreflector experiments, co-location analysis, etc.). Figure 1 summarizes the data holdings (full-rate or on-site normal point) of the CDDIS archive by year versus satellites tracked and network size.

The ILRS currently provides satellite predictions for the network in two formats: Tuned Inter-Range Vectors (TIRVs) and the newer Consolidated Prediction Format (CPF). The CPF is now considered the operational format for prediction providers and

network stations. However, TIRVs continue to be generated by the prediction providers and made available through email and at the data centers to accommodate stations that are continuing efforts to transition to the CPF.

The CPF information accurately predicts positions and ranges for a much wider variety of laser ranging targets than had been previously possible. Rather than using the tuned IRV's with an integrator, the new predictions provide daily tables of X, Y, and Z positions for each target which can then be interpolated for very accurate predictions. CPF provides an expanded format capability and greatly improves tracking on low satellites because the full modeling potential of the orbit computation at the prediction center will be passed on to the stations. Drag files and special maneuver files are no longer necessary. These predictions are available via email or via anonymous ftp from the data centers.

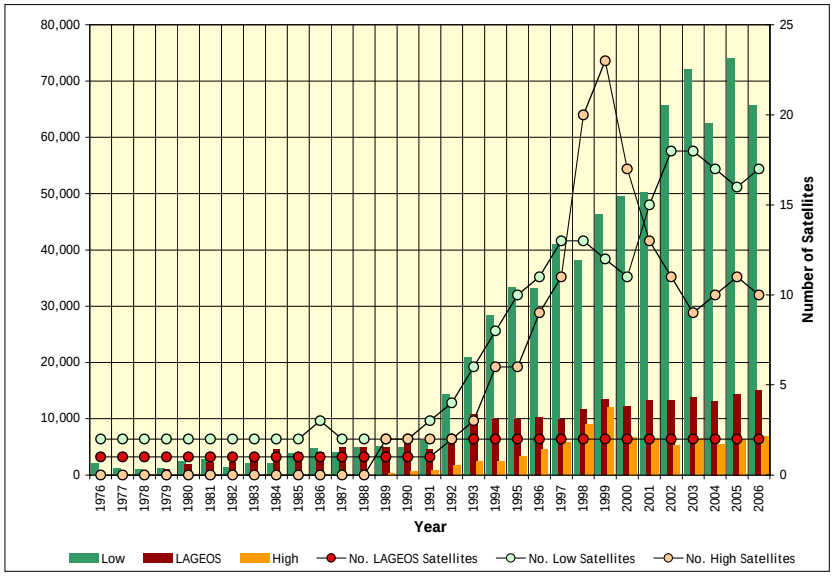

Figure 1. *Laser ranging data volume by year*

Six ILRS analysis centers (AC), ASI/Italy, BKG/Germany, DGFI/Germany, GFZ/Germany, JCET/USA, and NSGF/UK produce weekly solutions on LAGEOS-1 and -2 for global station coordinates and Earth orientation parameters (EOP). Each week, ASI (primary ILRS Combination Center) and DGFI (backup ILRS Combination Center) merge the individual AC solutions into the official ILRS Combination Product. This combination product is available every Wednesday via anonymous ftp from the data centers. The IERS uses this product for the multi-technique Combination Pilot Project and the Bulletin A EOP.

Performance

The ILRS Central Bureau staff has developed various reports and plots to monitor network performance. This information is updated on a frequent basis dependent upon the type of report. Station operators, analysts, and other ILRS groups can view these reports and plots to quickly ascertain how individual stations are performing as well as how the overall network is supporting the various missions. All plots and reports can be accessed through the station pages on the ILRS Web site at URL http://ilrs.gsfc.nasa.gov/stations.

The ILRS performance “report cards” are generated on a quarterly basis and show data volume, data quality, and ILRS operational compliance information. The

statistics are presented in tabular form by station and sorted by total passes in descending order. Plots of data volume (passes, normal points, minutes of data) and RMS (LAGEOS, Starlette, calibration) are created from this information and available on the report card Web site:

http://ilrs.gsfc.nasa.gov/stations/site_info/global_report_cards/index.html

Example plots from the latest report card are shown in Figure 2.

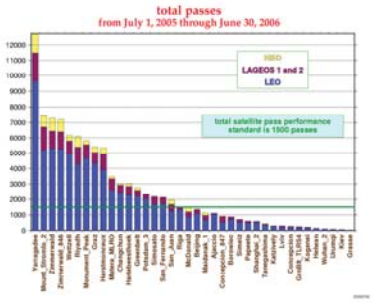

Figure 2a. *Total passes for 2006q3 report card.*

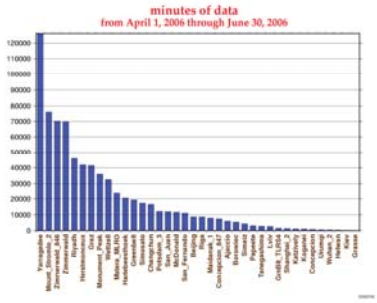

Figure 2b. *Minutes of data for 2006q3 report card.*

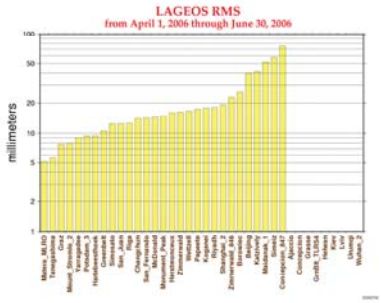

Figure 2c. *LAGEOS RMS for 2006q3 report card.*

A plot of the satellite ground tracks of the last seven days of geodetic satellite data is updated daily and available through the ILRS Web site at:

http://ilrs.gsfc.nasa.gov/stations/recent_groundtrack.html.

The plot, shown in Figure 3 for a week in November 2006, graphs the actual network ground tracks of Etalon, LAGEOS, Ajisai, Starlette, and Stella over the previous seven days based upon the archived normal point data.

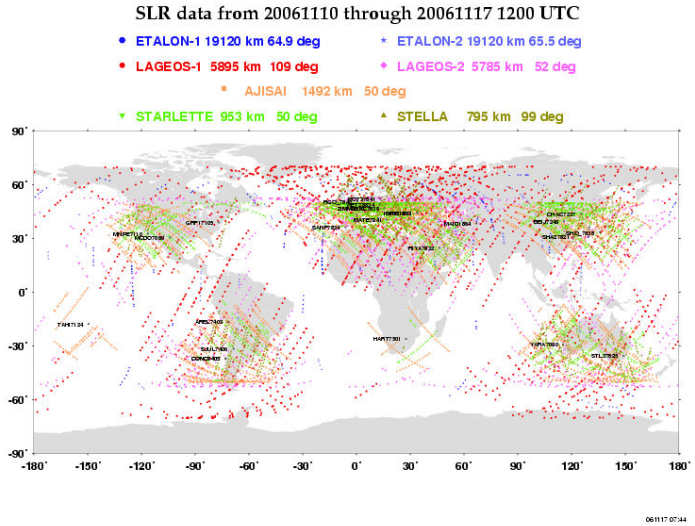

Figure 3. *Plot of the satellite ground tracks of the last seven days of geodetic satellite data.*

Plots of station performance and meteorological data are regularly generated. The plots are sorted by station and come in two forms: for data from the past year and for data since the year 2000. The information presented in these plots for each station in the ILRS network are: total number of normal points, total number of full-rate points, average number of data points per LAGEOS normal point, LAGEOS normal point rms, calibration rms, and system delay, and station temperature, pressure, and

humidity (as recorded in the normal point data). Examples of these plots for the Yarragadee station are shown in Figure 4. The plots are available through the individual station pages on the ILRS Web site (http://ilrs.gsfc.nasa.gov/stations).

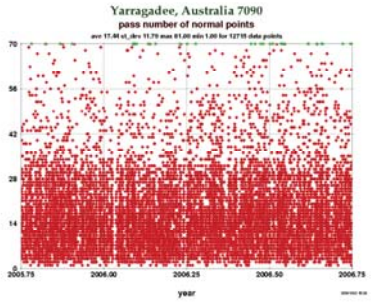

Figure 4a. *Total number of normal points from Yarragadee for the past year.*

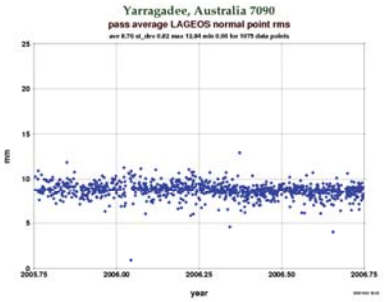

Figure 4b. *Pass average LAGEOS normal point RMS from Yarragadee for the past year.*

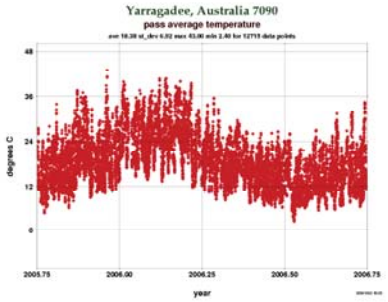

Figure 4c. *Average temperature Yarragadee for the past year.*

Future Plans

Additional plots of station performance are under development for the ILRS Web site. These plots include statistics for all currently tracked satellites and all operational stations as a function of time; full-rate observations per normal point and normal point rms are also computed as a function of range and time. Examples of the new charts for the Yarragadee station are shown in Figure 5 below.

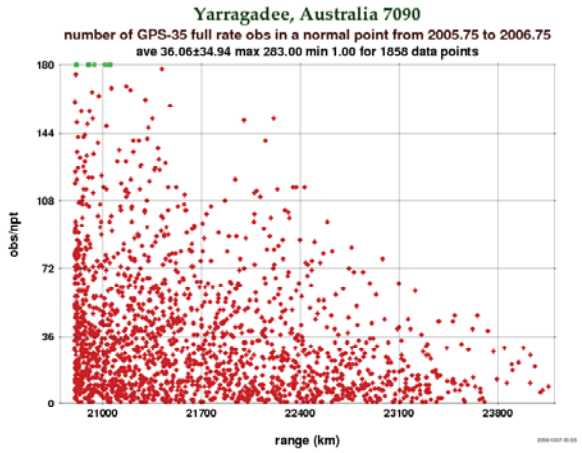

Figure 5a. *Number of GPS-35 full-rate observations per normal point from Yarragadee for the past year.*

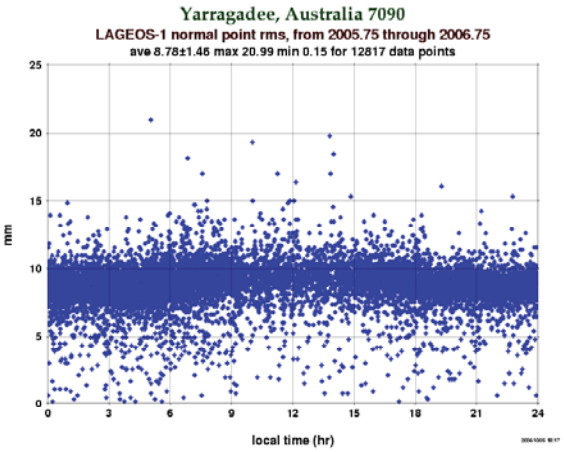

Figure 5b. *LAGEOS-1 normal point rms from Yarragadee for the past year.*

Minico Calibration of System Delay Calibration at Mount Stromlo SLR

John McK. Luck[1]

1. EOS Space Systems Pty.Ltd., Canberra, Australia

Abstract

The MINICO method of ranging to four ground targets in rapid succession has been adopted as a nearly daily routine at Stromlo. In essence, it calibrates the range used for regular pre- and post-pass system delay calibrations. It also provides interesting information on the stability of the calibration pillars and of the telescope pier. There is a clear annual cycle of amplitude 1 mm in the results. The routine biennial precision ground survey was performed in August 2006. Its agreement, or otherwise, with the MINICO determinations of pier ranges will be presented.

A Summary of Observations of GioveA, taken from Mt Stromlo SLR Station

C.J. Moore[1]

1. EOS Space Systems Pty. Limited, 111 Canberra Ave., Griffith, A.C.T. Australia.

Contact: cmoore@eos-aus.com

Abstract

A summary of satellite Giove A SLR data taken at Mt Stromlo over the period from May to August 2006 is presented, and some factors affecting tracking productivity are discussed. Although in a high earth orbit, Giove A has a large optical back scattering cross-section, and this has provided data for an empirical analysis of link budget factors which has allowed potential productivity gains to be assessed.

Introduction

The new Mt Stromlo SLR station has been in operation since December 2004 and data production has been reasonable and overall performance has been very good. Mt Stromlo productivity levels often exceed many other SLR stations. Nevertheless, improvements can be always be made, and this paper describes an analysis of the potential increases to productivity levels that may result from increased laser output energy, particularly as it applies to tracking Giove A and other high earth orbit satellites.

Total number of passes	**77**	**100%**
Number low elevation	**11**	**14%**
Number weather affected	**33**	**43%**
Number available	**33**	**43%**
Number attempted	**21**	**27%**
Number tracked	**12**	**15%**
Tracked/Possible	**12/33**	**36%**

Table 1 *Productivitv Metrics*

SLR productivity (i.e. detection of returns) of high satellites is particularly sensitive to environmental factors such as cloud, air mass water vapour content and photon noise during daylight hours. These high satellites include the Glonass and GPS satellites, Etalon 1 and 2 and the first Galileo test satellite, Giove A. Satellites such as Lageos 1 and 2 are also affected although to a lesser extent. To illustrate the relationships between laser energy and productivity from high satellites, an analysis of Giove A tracking at Mt Stromlo is presented, particularly taking into account actual availability of passes and their distribution with elevation.

Tracking Giove A

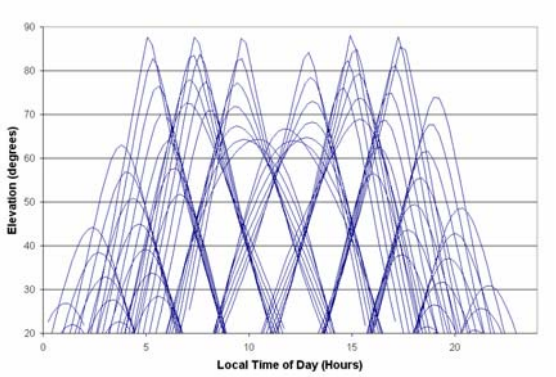

Figure 1:*Giove A passes, June 1 to August 9, 2006*

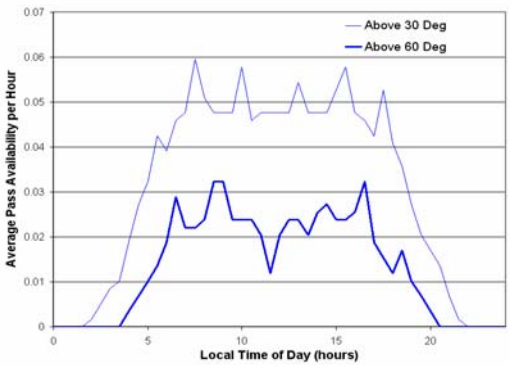

Figure 2: *Giove A Pass Availability*

Although Giove A was launched in December 2005, the ILRS was not requested to commence SLR tracking until late May 2006. The data from Mt Stromlo presented here are from observations taken from June 1st until August 9th (i.e. day 152 to 221). Table 1 summarizes the productivity statistics for this period and Figure 1 shows all of the available passes above the site's 20 degree horizon for this period.

By plotting pass elevations over 24 hour intervals, it was found that Giove A availability during the data period was on average not evenly distributed throughout the day. Figure 2 shows a frequency distribution plot (using time intervals of 0.1 hours) which indicated that there was a gap in passes during the period from approximately 18:00 to 04:00 local time (8:00 to 18:00 UTC) where passes were very sparse. There was also a significant reduction of very high passes in the middle of the day.

Actual Productivity of Giove A at Mt Stromlo

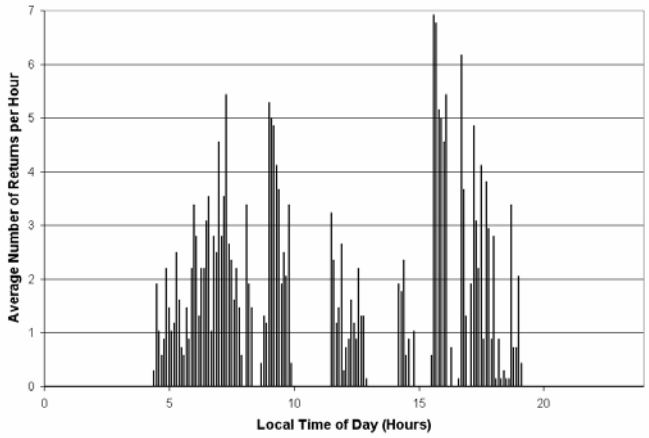

Figure 3: *Giove A Productivity*

While there are many factors affecting successful SLR tracking, it does appear that the distribution of available passes had influenced actual productivity of Giove A. Figure 3 shows the average distribution of number of successful (single-shot) returns over the course of a day, and as expected there were no passes tracked during the middle of the night. The impact of a reduced number of very high passes in the middle of the day is also apparent. However other factors such as sun avoidance and increased daylight noise would have also contributed to reduced productivity.

Figure 2 illustrates that SLR returns were being obtained from a wide range of target elevations (and thus ranges). To assess how productivity was dependent on target elevation a link budget analysis was performed. The following sections describe this analysis and results obtained.

Link Budget Analysis

Estimation of the SLR link budget was made using the standard link budget formulae which determines the average number of detected photons (returns) per laser pulse, N_{pe}, as [1],

$$N_{pe} = \eta_q E_T \frac{\lambda}{hc} \eta_T G_T \sigma_{sat} (4\pi R^2)^{-2} A_T \eta_R \tau_A^2 \tau_C^2 \qquad (1)$$

The transmit gain, G_T is given by $G_T = \frac{8}{\theta_K^2} \exp\left[-2\left(\frac{\theta_P}{\theta_K} \right)^2 \right]$

For Giove-A and Mt Stromlo SLR laser we set the detector quantum efficiency, η_q, to 20%, the transmit and receive path efficiencies, η_R, η_T, to 90%, the laser pulse energy, E_T, to 13.5 mJ, the receive aperture area, A_T, to 0.7 m^2, the beam spread,

θ_P, to 1 arcsec, the pointing accuracy, θ_K, to 2 arcsec and the usual values to wavelength, λ, Planck's constant, h, and speed of light, c. The atmospheric transmittance, τ_A, was determined from an elevation dependent model [2] which gives transmittance at zenith of approximately 81% reducing to 72% at 20 degrees. Clear skies were assumed, so that cloud transmittance, τ_C, was set to 100%.

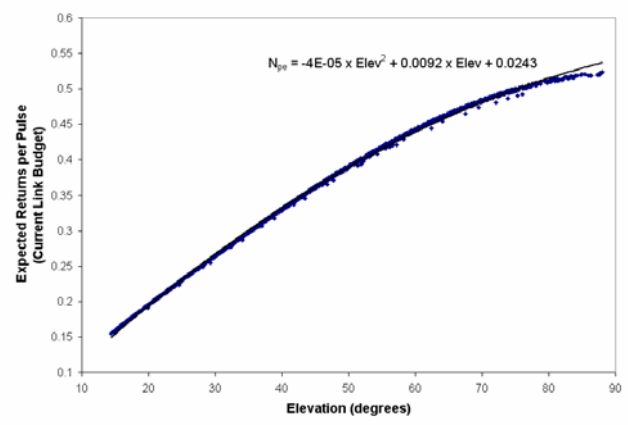

Figure 4: *Link Budget versus Elevation*

The Satellite back scattering cross section, σ_{sat}, for Giove A has been estimated to be in the order of $46\times10^6\ m^2$ (Dave Arnold, private communication). R is the distance from station to satellite (in meters) and is determined from orbit predictions.

The absolute value of estimated link budget is not critical and errors due to these assumptions do not affect this analysis. However, using these values, the average link budget estimates for Giove A against satellite elevation was calculated as shown in Figure 4. The polynomial regression line fitted to the average link budget estimates allows conversion or mapping between elevation, link budget estimates and hence laser energy. This equation is

$$N_{pe} = 0.0243 + 0.0092 \times Elev - 4\times10^{-5} Elev^2 \qquad (2)$$

where the elevation, *Elev*, is valid over the range 15 to 85 degrees.

Elevation Analysis

The mapping between link budget estimates and elevation allowed elevation to be used to provide a relationship between link budget estimates (i.e. laser power) and productivity. This analysis presents statistical analysis based on 5 degree elevation intervals from 20 degrees (the site horizon) to 90 degrees. For each elevation interval, the actual number of returns achieved (productivity) was normalized by the number of available passes in each interval to give the number of returns per pass.

The number of available passes per elevation interval is shown in Figure 5 and the productivity data for each elevation interval is shown in Figure 6. The second plot clearly illustrates that productivity falls with lower elevations (due to a decreasing link budget from an increasing range) and higher elevations (due to a lower number of available passes).

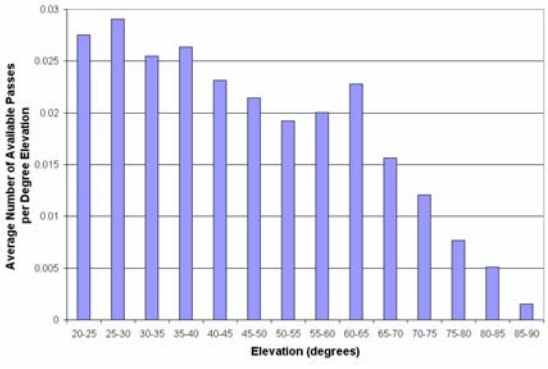

Figure 5: *Available Giove A Passes versus Elevation*

Hence a normalized productivity can be determined by dividing actual productivity data by the data availability. The results for Giove A are shown in Figure 7.

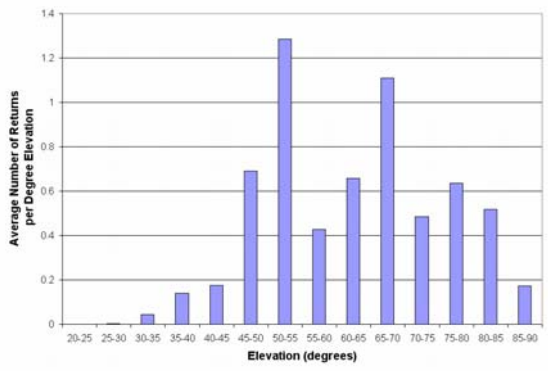

Figure 6: *Giove A Productivity versus Elevation*

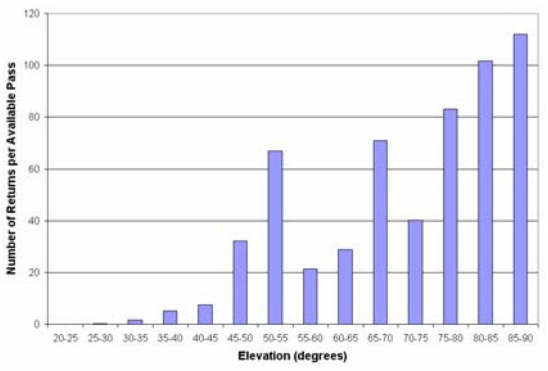

Figure 7: *Giove A Normalized Productivity versus Elevation*

Normalized Productivity

Figure 7 illustrates that, all else being equal, more returns are expected when the satellite is at a higher elevation. Scatter in this data indicates that in practice other factors such as weather are influencing productivity. It also appears that below approximately 40 to 45 degrees elevation, few returns were being detected with the given laser power levels.

When returns were detected at the lower elevations, observation logs indicated that the atmosphere was particularly clear and clean of particles, and that a strong signal had already been detected, and the satellite was being tracked as it descended in elevation.

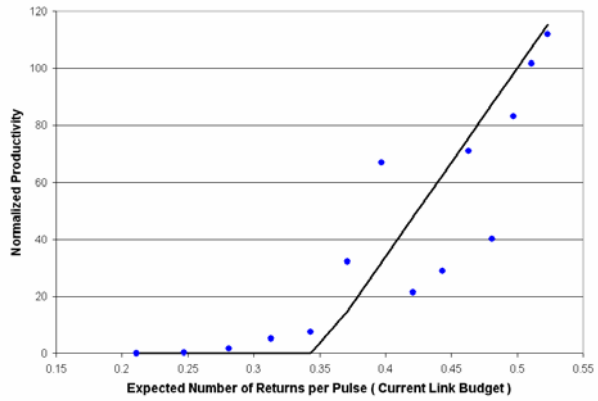

Figure 8: *Normalized Productivity versus Link Budget*

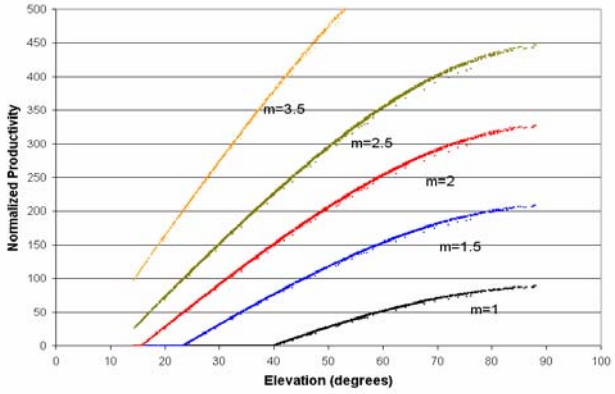

Figure 9: *Normalized Productivity Gains*

Using the conversion equation (2), normalized productivity can be compared to estimated link budget for each elevation interval. The results are shown in the Figure 8.

It appears that for link budget levels below 0.35 there is little or no productivity. For levels above 0.35, normalized productivity (η) appears to increase linearly with estimated link budget. A regression equation gives

$$\begin{aligned} \eta &= 660 \times N_{pe} - 230 \quad N_{pe} > 0.35 \\ \eta &= 0 \qquad\qquad\qquad\quad N_{pe} < 0.35 \end{aligned} \tag{3}$$

Of course ideally, it should be expected that actual return rate is proportional to expected return rate. In practice, it appears that this may be the case once the link budget reaches some “threshold” value.

Potential Productivity Gains

Equation (3) suggests that increasing the link budget (say by increasing laser power) to values less than 0.35 will give little or no improvement to productivity levels. However there should be significant gains by increasing link budget levels that are currently below 0.35 to values in excess of the 0.35.

Consider an increased link budget $N'_{pe} = mN_{pe}$ which is a result of multiplying current levels by a factor of m. From equation (3) the actual normalized productivity rate is expected to be now η', where

$$\begin{aligned} \eta' &= 660 \times mN_{pe} - 230 \quad & mN_{pe} > 0.35 \\ \eta' &= 0 & mN_{pe} < 0.35 \end{aligned} \tag{4}$$

Figure 9 shows plots of increased normalized productivity depending on the link budget multiplier, m.

Using the data gathered on Giove A pass availability, as shown in figure 5, the effect of link budget increases on actual productivity can be determined. Figure 10 shows such productivity plots for various values of m. The heavy line with m =1 is a smoothed curve using current data and is effectively equivalent to the plot shown in Figure 6.

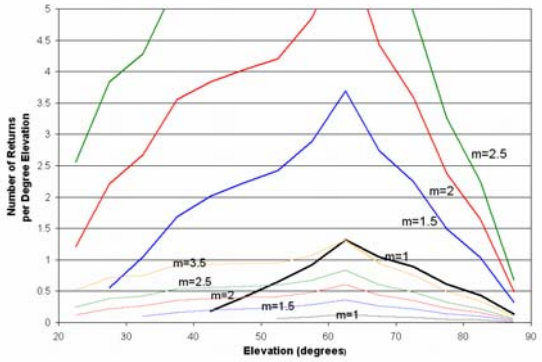

Figure 10: *Productivity Gains*

There are two sets of plots shown in Figure 10. The darker lines represent productivity increases based on current data while the lighter lines represent productivities assuming a factor of 10 (or 1 ND) loss in the number of returned photons. This factor is chosen to represent the loss when the enclosure glass window is installed and to account to some degree the effect of less than ideal sky conditions. The next section describes an analysis on the effect of the enclosure window, and for weak signals, it appears that a factor of 4 in link budget is required to compensate for the glass window.

It is clear that based on current data, increasing the link budget by 50% or 100% should make a substantial improvement to productivity including the possibility of obtaining reasonable number of returns from Giove A at elevations below 30 degrees. However, it is important that improved productivity levels can be maintained when the enclosure window is in place or when sky conditions deteriorate. Assuming a 1 ND loss, the second figure shows that an increase in link budget by a factor of 2 or more will be sufficient to maintain productivity at levels at least as good as current levels, and probably better at elevations below 40 degrees.

Effect of Enclosure Window

The Mt Stromlo SLR station is designed to allow continuous and unmanned operations in all weather conditions. This is in part achieved by having a weather-proof telescope enclosure incorporating a glass window. Such a window has many advantages for operations, but will also attenuate the transmit and receive beams. An assessment of the net impact from operating through the glass window is presented from comparisons made with data obtained when there was no glass window in place, i.e. the glass window is exchanged with an “air window”.

Near Field Target

A comparison of measurements to calibration pier (at a range of approximately 92m) with and without the glass window in place are shown in the Figure 11. The mean difference between the signals is approximately 0.061 ns (in two way time of flight) consistent with having a window with glass thickness of 18.3mm.

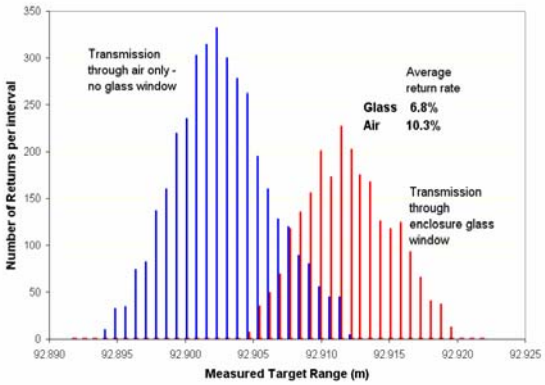

Figure 11: *Near Field Target Histogram*

For a given configuration (i.e. fixed laser power, ND filters etc.) and equal time periods the return rate with a glass window in place is 6.8% while in air the rate is 10.3%. Thus the difference in average return rate gives a loss of approximately 30%.

Far Field Targets

Data from far field targets at ranges of 6,100 to 10,000 km allows a comparison of results for relatively good signals (Lageos 1) and weaker signals (Lageos 2). These satellites are used since comparisons are difficult using much higher satellites when fewer returns are available when the glass window is in place. The second and third plots show average return rates and return rate (suitably normalized by tracking periods) distributions for the two signal levels.

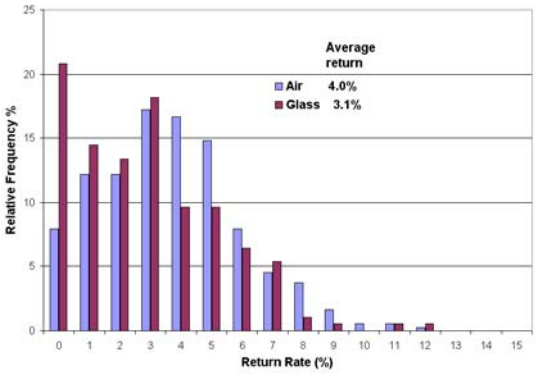

Figure 12: *Lageos 1 Return Rate Distribution*

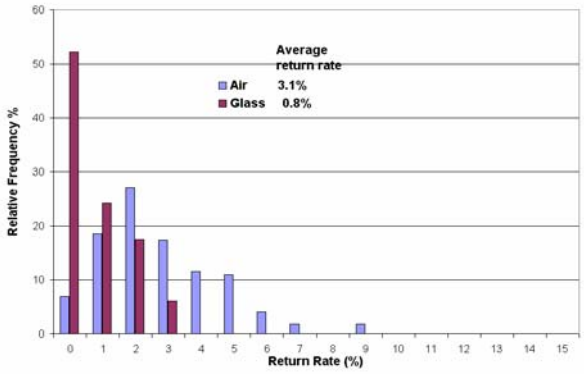

Figure 13: *Lageos 2 Return Rate Distribution*

Good Return Signal

When average return rate is relatively good, above 4% in air, the average return rate decreased to about 3% when the glass window was in place - indicating a 25-30% loss, similar to that for a near field target. The plot clearly demonstrates the relative decline in return rates above 3% when the window is in place and also the greater fraction of time there are no returns.

Weak Return Signal

When the return signal is weaker, in the case around 3% in air, the effect of the glass window is proportionally greater as illustrated in the third plot. In this case, the average return dropped to less than 1% when the glass was in place giving a loss of

over 75%. Return rates with the glass in place do not exceed 4% and there are no returns for at least 50% of the time.

Conclusions

Mt Stromlo SLR station has successfully tracked Giove A for a number of months commencing in June 2006. A link budget analysis of the distribution of productivity data for this satellite with elevation has allowed an assessment of factors that may improve SLR productivity for Giove A (and other high earth orbit satellites).

Threshold effects associated with decreasing link budgets have been identified both during tracking of Giove A (e.g. with decreasing elevation) and also with Lageos 1 and 2 with transmission though air versus a glass enclosure window. Such threshold effects result in a rapid deterioration in detectable signal when return rates fall below approximately 3 or 4% for the current configuration at Mt Stromlo. Because of this threshold effect, it is possible that an increase in the link budget by a factor of two or better may lead to a substantial improvement in productivity. It is hoped that such an improvement can be demonstrated once the planned upgrade of the SLR laser power at Mt Stromlo has been implemented.

References:

[1] Degnan, J., Millimeter Accuracy Satellite Laser Ranging: A Review. Geodynamics Series 25.

[2] Degnan, J., 1993. AGU Geodynamics Monograph Vol.25, p.139-140

LASERS AND DETECTOR SESSION SUMMARY

Chairs: John Degnan and Ivan Prochaska

The Czech Technical University reported the latest results on their space-qualified photon counting module for the Chinese Laser Time Transfer Project [Prochazka et al]. The silicon K14 SPAD has the following properties at 532 nm:

- Active area: 25 micron diameter
- Quantum Efficiency: 10%
- Timing Resolution: 75 psec
- Dark Count Rate: < 8 kHz @ 20^{o}C
- Operating Temperature Range: -30^{o}C to 80^{o}C (no cooling)
- Power Consumption: <400 mW
- Mass: 4 g

In addition, it is highly resistant to solar and ionizing radiation (100 krad) damage and has an expected lifetime of greater than 10 years in space.

Andreev et al reported on a very different laser approach based on Stimulated Raman Scattering (SRS) pulse compression which produced 25 psec, 1 mJ pulses, at a 1 kHz rate and with good spatial mode quality (M^2 = 1.1). Using a Nd:YAG Master Oscillator (MO) and three single pass Nd:YAG amplifiers in conjunction with a Ca_8Fl_{16} SRS cell, they generated 100 mJ, 350 psec pulses at 1319 nm. They used this radiation to pump a $Ba(NO_3)_2$ SRS-MO and two SRS amplifier cells to obtain 50 mJ, 30 psec pulses at an eyesafe wavelength of 1530 nm and a 100 Hz rate. It was observed that the Raman conversion efficiency decreased noticeably at kHz rates for the higher peak pump powers.

Gao et al reported on diode-pumped lasers for tracking satellites and space debris. For SLR, 10 psec pulses are generated from a SESAM (Semiconductor Saturable Absorber Mirror) mode-locked laser oscillator, regenerative amplifier, and power amplifier. For debris tracking, they use two nanosecond pulses from a 230 Watt multistage system consisting of a single frequency oscillator, preamps, power ampfiliers and SBS cells.

Photon Counting Module for Laser Time Transfer Space Mission

Karel Hamal[1] , Ivan Prochazka[1], Lukas Kral[1], Yang Fumin[2]

1. Czech Technical University in Prague, Brehova 7, 115 19 Prague 1, Czech Republic,

2. Shanghai Observatory, Chinese Academy of Science, 80 Nandan Road, Shanghai, China

Contact: prochazk@troja.fjfi.cvut.cz

Abstract

We are presenting the results of research and development of the Single Photon Avalanche Detector (SPAD) for application in a Laser Time Transfer (LTT) space mission.

For the joint project with the Shanghai Observatory, Academy of Sciences of China, we have developed the detector package dedicated for the project of synchronizing the hydrogen maser-based time scales by laser pulses. The technology demonstrator of a dual detector has been built and tested in our labs. The main parameters are: detection efficiency 10% at 532 nm, timing resolution 80 psec, dark count rate 8 kHz, non gated operation. The detector's active area is 25 um in diameter. The total mass, including bias stabilizing circuit, is 2 grams, and the total power consumption is below 0.5 Watt per detecting channel. The detector can be operated in a wide range of temperatures ranging from –30^o C to +60^o C without any additional temperature control.

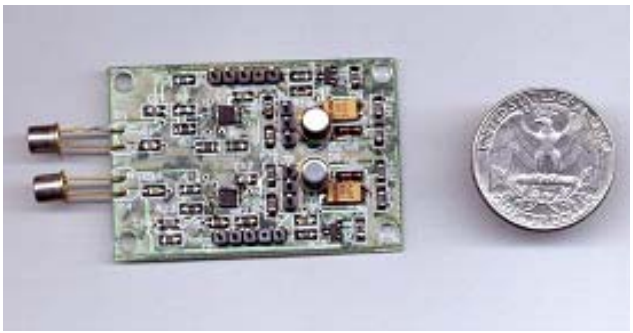

***Figure 1:** The technology demonstrator of the dual photon counting detectors. The detection chips (protective caps installed for handling) are on the left.*

The ruggedness of the detector is superb. Optical power of 2 mW has been focused onto a sensitive area while the detector has been biased for 8 hours. No detectable degradation has been experienced. The overload tolerance negates the need for any mechanical Sun protection shutter in space. The recovery time from optical overload to full functionality is less than 0.1 second. The detector package has been successfully integrated into the LTT timing electronics and the pre-flight test was performed in China during the period July-September 2006.

GOALS

- Fast photon counting detectors for the Laser Time Transfer space mission, China
- BACKGROUND
  the K14 SPAD detectors have been launched onboard MARS 96 (Russia) and NASA Mars Polar Lander (USA) space missions
- REQUIREMENTS
- low mass, power, bias voltage
- high radiation in - sensitivity (> 5 years in space)
- high temperature range
- extreme optical damage threshold (full Solar flux, no shutter)

Prochazka, Hamal, Kral, Yang Fumin, Canberra, October 2006

„LTT Module in Space", China, 2007-2008

- GOALs
- to synchronize the rubidium clocks in space, hydrogen masers in a future.
- Laser Time Transfer (LTT) between space and ground
- employing the existing China Satellite Laser Ranging network consisting of 5 fixed and 2 mobile systems

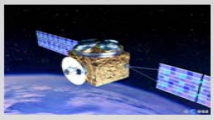

- required ~ 100 ps timing accuracy
- expected accuracy improvement
  >> 10x over RF techniques

Prochazka, Hamal, Kral, Yang Fumin, Canberra, October 2006

Detector Requirements - version LTT China

- single photon timing K14 SPAD chips two channels
- aperture 25 μm each
- timing resolution < 100 psec
- power, mass < 2 W , 100 grams
- operating temperature -30 ... +60°C
- lifetime in space > 5 years
- high opt. damage threshold direct exposure to the Sun (!!)
  in a focal plane of 2 mm aperture collecting optics
  no Sun safety shutter will be installed

- design & construction 3 months (!)

Prochazka, Hamal, Kral, Yang Fumin, Canberra, October 2006

SPAD Bias Temperature Control

- SPAD break down voltage 29 Volts
- bias accuracy required 100 mV
- temperature range requested -30 …+ 60° C
  no temperature control or cooling
- SPAD break voltage temperature drift - 30 mV / K
- => temperature controlled bias circuit

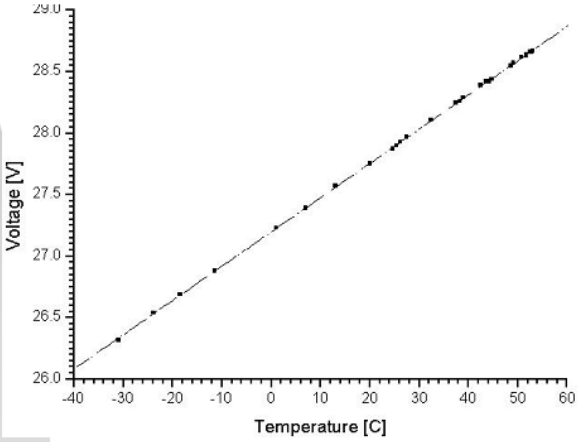

Prochazka,Hamal, Kral, Yang Fumin, Canberra, October 2006

Optical Damage Threshold

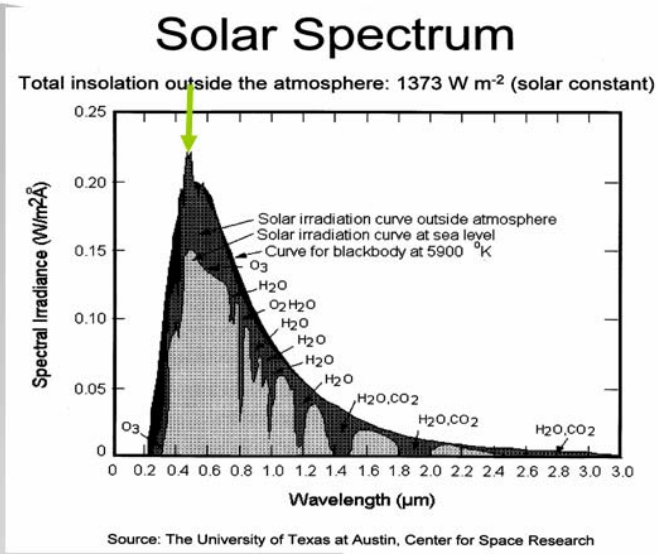

- Irradiance 0.2 W/m²/0.1 nm @ 532nm wavelength
- receiver
  aperture 2 mm
  f / d ~ 1.0
  field of view ~ 0.5°
  entire Solar disc
- bandwidth 100 nm
  blocking glass filter
- => 1 mW max. on SPAD

Surprisingly, the total flux on the detector aperture is not exceeding 1 mW /100 nm for any aperture (!), due to the field of view limitation.

Larger telescope is not capable to focus all the incoming Sun light onto small SPAD aperture.

Prochazka,Hamal, Kral, Yang Fumin, Canberra, October 2006

Optical Damage Tests

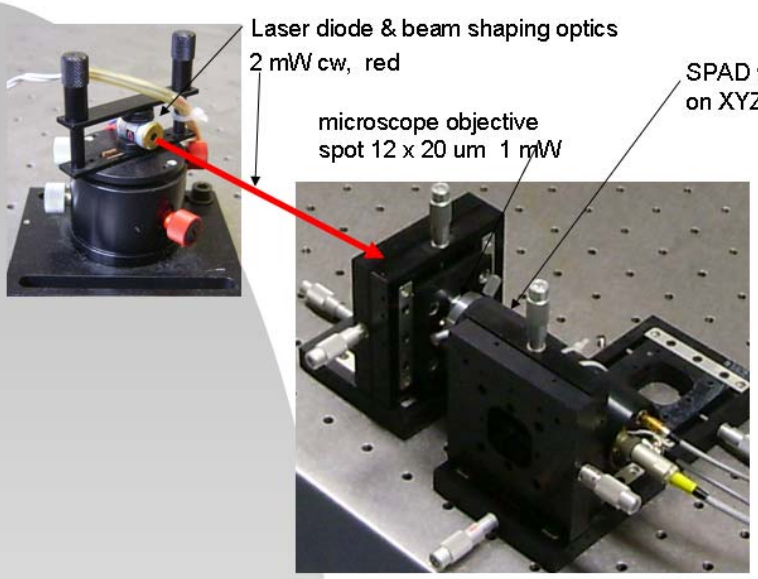

- exposure tests :
- no bias 3 x 8 hr
- biased 3 x 8 hr

- NO detectable detector degradation after all optical irradiation tests
- Any size telescope with SPAD detector may be pointed toward the Sun without the damage (< 100 nm bandwidth)

Prochazka, Hamal, Kral, Yang Fumin, Canberra, October 2006

Optical Saturation Recovery

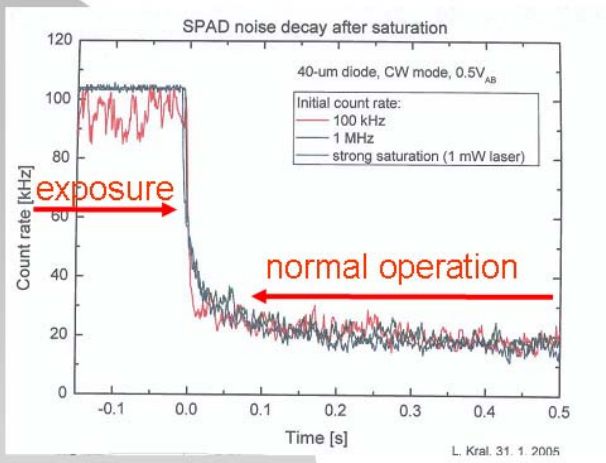

- Detector operation recovery after strong optical signal exp.
- detector illumination
- ambient light 100 kHz
- attenuated laser 1 MHz
  out of range when illuminated
- full laser 1 mW NA
  out of range when illuminated
- instrument time constant ~ 0.02 s

- Detector recovery time after saturation is well below 100 ms
- within this time, the dark count rate drops to 1.1 times the standard value

Prochazka, Hamal, Kral, Yang Fumin, Canberra, October 2006

Photon Counting Module for Space Mission LTT

Technology demonstrator
Prague, March 2005

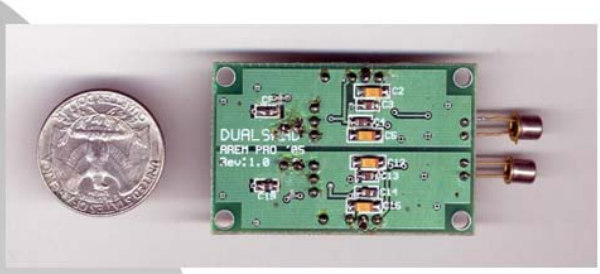

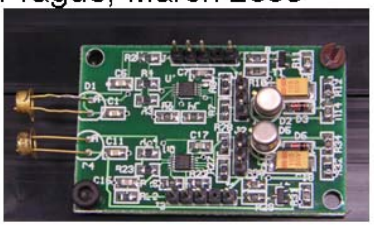

Detector package sample
for pre-flight tests
Shanghai, China, July 2006

Prochazka,Hamal, Kral, Yang Fumin, Canberra, October 2006

SPAD Timing Resolution Tests, Shanghai July 2006

Shanghai SLR, laser 35 ps, HP counter, Detector # 1

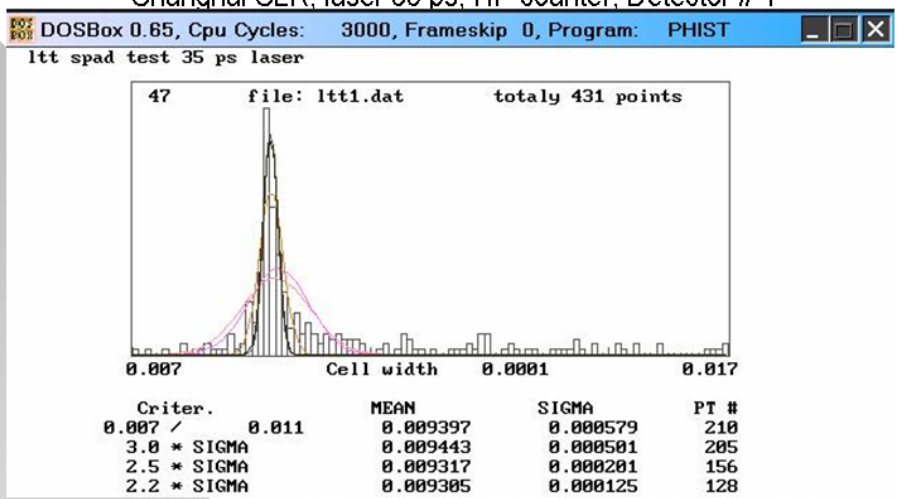

- Jitter detector # 1 125 psec
- detector # 2 120 psec
- Detection delay difference 440 +/- 20 psec

Prochazka,Hamal, Kral, Yang Fumin, Canberra, October 2006

Dual Single Photon Counting Module

Detector Technology Demonstrator - Specifications

configuration	dual photon counting detector based on Silicon K14 SPAD
quenching	active
active area	circular 25 um diameter
quantum efficiency	~ 10 % @ 532 nm
timing resolution	75 psec
dark count rate	< 8 kHz @ +20°C
operating temp.	-30 … +60°C no cooling, no stabilisation
power consumption	< 400 mW
mass	4 grams
optical damage th.	full Solar flux 100 nm BW, > 8 hr
lifetime in space	> 10 years

Prochazka, Hamal, Kral, Yang Fumin, Canberra, October 2006

CONCLUSION

Photon Counting Module for Space Mission LTT

- the Technology Demonstrators have been completed Prague, March 2005

- the Flight Unit detector version has been completed Shanghai, July 2006
- Solar flux resistant using moderate wavelength filtering
- radiation resistant, 100 kRads without parameter change
  => lifetime in space > 10 years
- pre-flight tests, Shanghai, Beijin , fall 2006

Prochazka, Hamal, Kral, Yang Fumin, Canberra, October 2006

Picosecond lasers with Raman frequency and pulsewidth conversion for range finding

N.F. Andreev[1], E.A. Grishin[2], O.V. Kulagin[1], A.M. Sergeev[1], M. Valley[3]

1. Institute of Applied Physics, Nizhny Novgorod, Russia
2. Institute for Precision Instrument Engineering, Moscow, Russia
3. Sandia National Laboratories, Albuquerque, USA

Abstract

We review design issues for short-pulse lasers with Brillouin and Raman pulse compression and frequency conversion. In particular, scheme and material development has enabled us to provide output pulsewidth of 25 ps by SRS at a repetition rate of 1 kHz. Also, advantages of advanced laser ranger based on eye-safe high-power laser are discussed.

Introduction

Solid-state lasers generating high power picosecond pulses are attractive for a wide range of applications. Conventional mode-locked lasers with complex scheme emit ps pulses of widened spectral width at low pulse energies (less than 1μJ) [1-3]. Slightly higher energies are produced by microchip lasers with passive [4] and active [5] Q-switch. Such laser may generate pulses as short as 56 ps [5] with high repetition rate. However, the pulse energy in this case is not higher than a few μJ if $\tau \leq 500$ ps. In both cases such pulses require further amplification in regenerative and multipass amplifiers. But a direct amplification of picosecond pulses is complicated and negatively affects the quality of the beam. The other method to increase the peak power of laser pulses is to use the pulse compression via Stimulated Raman and Brillouin Scattering (SRS and SBS) [6-8].

We present here the results of using SBS and SRS for an efficient temporal compression and frequency conversion of Q-switched laser pulses for range finding systems. High conversion efficiency and simple optical approach make this method rather attractive for the pulses up to several picoseconds. But there non-linear optical pulse compression was applied in pulsed lasers with low repetition rate. Earlier experiments were submitted where for the first time SBS pulse compression technique for diode-pumped solid state lasers (DPSSL) has been demonstrated [9].

It is known that the pulse compression ratio of up to ~17÷20 could be achieved in the optimal pumping geometry of SBS. Besides pulse compression, the phase conjugation (PC) and beam cleanup by SBS have been widely employed in the double-pass laser amplifiers. However, the spatial-temporal distributions and energetic stability of output Stokes pulses dramatically degrades for the pump pulses approaching ~3ns due to unwanted self-focusing or SRS in conventional SBS-active liquids, such as CCl_4, $SnCl_4$, and D_2O. Therefore the short pulses of ~160ps duration and ~0.3mJ energy attained presently in SBS-compressors by neglecting poor energy stability and accompanied by thermal and diffraction distortions introduced by subsequent multi-pass amplifiers.

It is shown here that SBS-cell filled by high purity heavy fluorocarbons C_8F_{18} is capable to maintain order of magnitude higher intensities of pump radiation without

the risk of optical breakdown. This allowed us for the first time to incorporate SBS-compressor into the scheme of double-pass amplifier and employ it as phase conjugate mirror for the beam cleanup. As a result, the exceptionally smooth and diffraction-free Gaussian beam has been achieved at the output of SBS-compressor. Moreover extraordinary high reflectivity (>97%) of novel SBS-mirror allows efficient energy extraction from double-pass amplifier.

This scheme has been incorporated into custom design Nd:YAG lasers (see Fig.1) for plasma and ultrafast flow dynamic research. High-quality spatial and temporal distributions are assured by a two-pass Nd:YAG amplifier with SBS-compressor. The MO is protected by Faraday isolator from unwanted backward high-intensity amplified Stokes radiation.

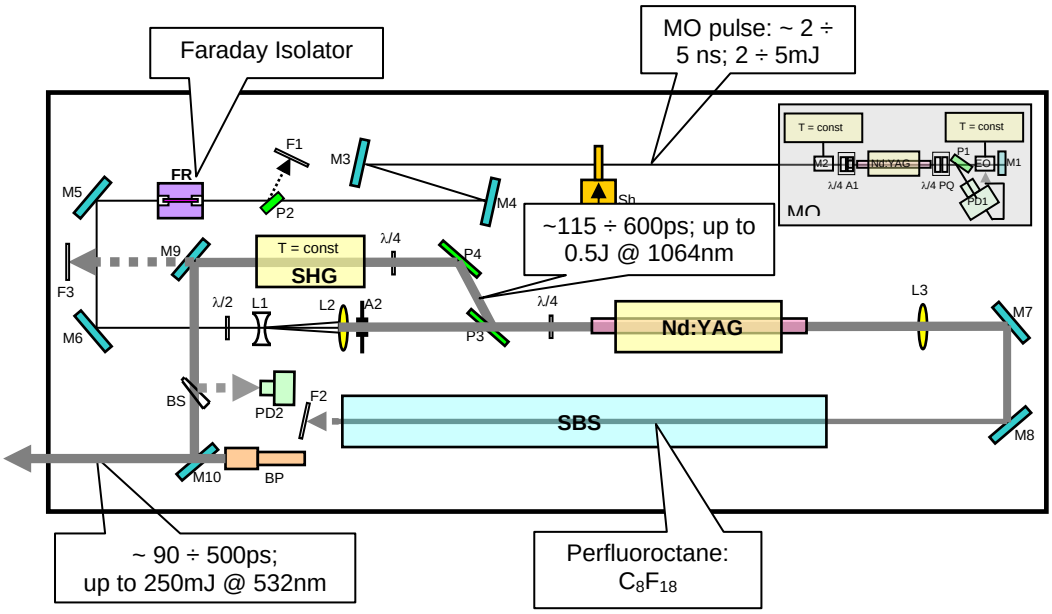

Fig.1. *Schematic of the laser with the SBS compression stage*

In optimised SBS focusing geometry laser provides output pulses of ~100ps at 532nm. RMS energy stability of output laser pulses at 532nm (114ps; 90mJ) was +/- 2.5 ÷ 3%; temporal jitter < 100 ps (RMS deviation) respectively the signal of fast electrical trigger.

The subsequent solid-state SRS-compressor based on $Ba(NO_3)_2$ crystals combined with SBS-compressor allows us to increase compression while ensuring a diffraction-limited output Stokes beam as well as to get output wavelength in a wide range (in particular, in eye-safe range), because of high value of Raman frequency shift. As a result of these investigations, a robust and reliable Nd:YAG laser (see Fig.2, as it is at the operational site for SLR) for satellite ranging has been created. This laser was installed in Altay Optical\Laser Center of Institute for Precision Instrument Engineering.

Here the laser pulses with a pulse width of 3 ns and energy of 1 mJ come from a master oscillator (MO) to the power amplifier (laser heads PA1 and PA2). A Faraday rotator FR was installed between the MO and the power amplifier to protect the MO from residual backward radiation. After positive lens **L2**, we have got a collimated beam with a diameter of about 7 mm, which is a bit smaller than the diameters of Nd:YAG rods (8 and 10 mm) in the laser heads. After the first pass through laser heads **PA1** and **PA2** a laser pulse is reflected in the SBS-cell. Then the laser pulse

passes second time through quarter-wave plate, changes its polarization into orthogonal and leaves the power amplifier with the help of a polarizer. A two-stage SRS pulse compressor was used to provide high efficiency of laser energy into the picosecond region.

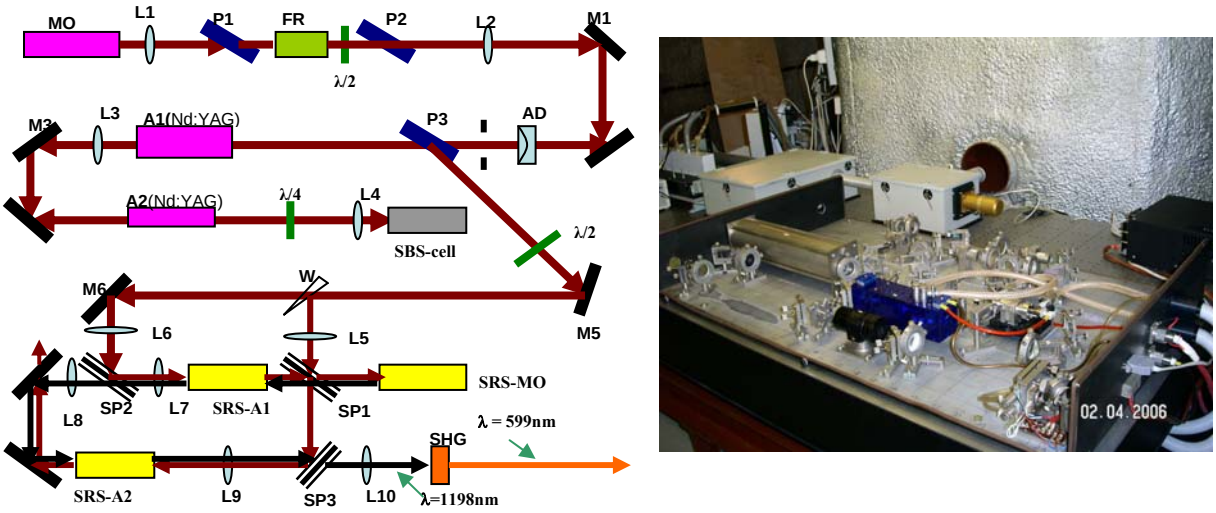

Fig.2. *Scheme and view of the laser with the SBS and SRS compression stages*

On the input to Raman compressor a beam-splitter **W** (a glass wedge) after our Nd:YAG laser reflects about 0.5% of laser output to pump the Raman oscillator. The remaining radiation is sent to pump crystals of the first Raman amplifier by a mirror **M6** and a spectrum-splitter **SP2**. The first Raman amplifier is placed between two spectrum splitters **SP1** and **SP2** - dichroic mirrors which are transparent for the Stokes wavelength of 1198 nm and high-reflected for the 1064 nm pump. For optimal time matching between pump and Raman pulses, the both Raman amplifiers were shifted along optical axes. When pulse compression conditions are met, 100 mJ 30 ps pulses will be generated at appropriate repetition rates, i.e., the Raman pulses' width is more than 10 times narrower compared to that of the pump pulses, as was measured at the previous stage of the project. After the first Raman compression stage, the conversion efficiency of pump radiation to the Raman output is about 10-20%. It is due to a comparatively low output energy from the Raman oscillator (~ 0.01 mJ) and the length (~ 7-8 cm) of the Raman amplifier crystals relative to the pulse width. The conversion degree was increased by up to 50% - 60% by arranging an additional path of counter-running Raman and pump beams through the second Raman amplifier. As a result, the laser produces spectrally limited pulses of 30 ps duration and ~100 mJ energy at 1198 nm with RMS energy stability of 4%. Moreover, the second harmonic generation was used at the laser output to meet requirements of ranger system specification. In this case we have got output laser energy of 50-55 mJ in 25-30 ps pulses at 599 nm.

Also, an eye-safe high-power Raman picosecond laser is developing now for a project of an advanced laser ranger. Next to atmospheric turbulence, range is the dominant source of uncertainty in acquired laser ranger and tracker Time Space Position Information data. State-of-the-art ranging systems have an operating range and accuracy far below the needs for performance testing and model validation. A new, eye-safe, long operating range, accurate (order of cm) ranger will be developed using an ultrashort pulse (e.g., picosecond) laser system in conjunction with time-of-flight

measurement methods. This laser has the similar scheme as in Fig.2, but a four-pass power amplifier with three laser heads is used instead of two-pass one with two laser heads in Fig.2. In this case Nd:YAG MOPA scheme produces pulses (pulse width ~ 0.35 ns) of energy up to 100 mJ at 1319 nm to pump Raman compressor scheme. The Raman compressor produces Stokes output pulses with wavelength of 1530 nm and picosecond pulse width. As a result of the development of the eye-safe picosecond Raman laser, we achieved the following set of parameters: output of 25-30 ps pulsewidth and 50 mJ pulse energy at 1530 nm and repetition rate of 100 Hz.

Further, Raman compression in the field of two counterpropagating pump beams has been studied for the first time both theoretically and experimentally [10]. It was shown that this geometry allows further increasing the compression ratio of incident laser pump pulses up to 150. To check it experimentally, we used a diode pumped electro-optically Q-switched Nd:YAG laser as a pumping source for the solid-state SRS pulse compressor based on $Ba(NO_3)_2$ crystals (see a lower/left corner of Fig.3). This laser (Master Oscillator for Raman compressor stage) produced single longitudinal mode near-diffraction-limited pulses of 3.3 ns duration and 3 mJ energy at a pulse repetition rate of 1 kHz.

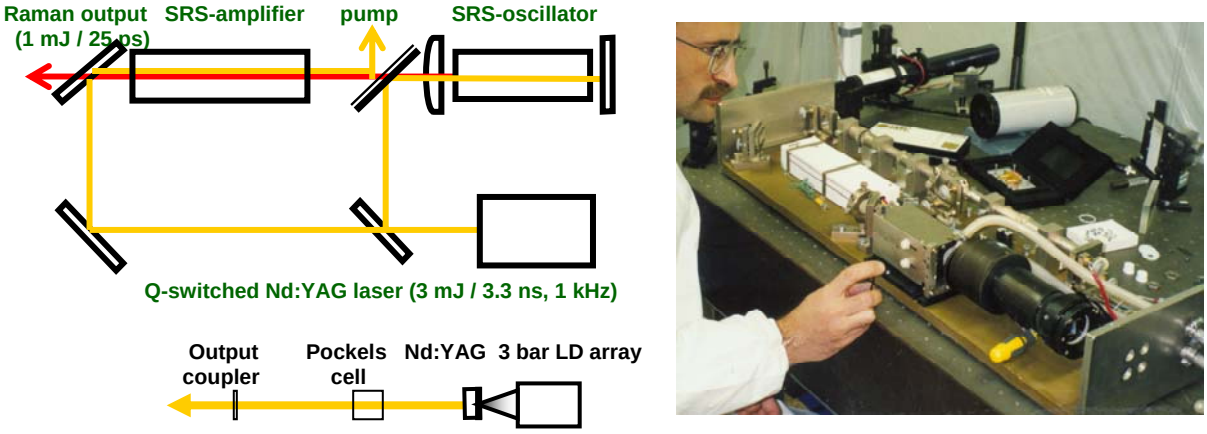

Fig.3. *Scheme and view of 1-kHz diode-pumped Raman laser*

Then the beam-splitter after the Nd:YAG laser reflected 20% of laser output to pump the SRS-oscillator. The rest laser radiation was sent to pump crystals of the SRS-amplifier. It was placed between the couple of dichroic mirrors which were transparent for Stokes wavelength 1198 nm and high-reflected for the 1064-nm pump. The high-reflected mirror for the both wavelengths was placed close to output from the SRS-generator. The alignment of its reflection in back direction provided the SRS threshold decrease by some times. It depended on focusing sharpness and pulse width. For the optimal time matching of pump and Raman pulses the SRS-amplifier was shifted along optical axes. With the carefully adjusted focusing of pump pulses into the crystal we obtained “pump – to Raman” energy conversion efficiency as high as 53% (for 1 kHz). When pulse compression conditions were held, 0.8 mJ - 1 mJ, 25 ps - pulses were generated at 1 kHz repetition rate, Raman pulses’ width being narrower than that of the pump by more than 100 times. Output beam was near-Gaussian shape, i.e. the beam quality was close to the diffraction limit. However, in the “pulse compression mode” the pump to Raman conversion efficiency dropped to 28%. It was caused by the insufficient total length (25 cm) of crystals in the SRS-amplifier

relatively to pulse width. However, the conversion energy efficiency could be increased by the arranging an additional opposite-directed pass of Raman and pump radiation through the SRS-amplifier.

Earlier, to our knowledge, the SBS and SRS pulse compression has not been practically studied for high repetition laser pulses typical for diode-pumped solid state lasers.

As a conclusion, the short pulse lasers with non-linear optical pulse compression are very attractive for laser ranging applications because of appropriate set of output parameters, the scheme simplicity and reliability.

References

[1] J. Aus der Au, G.J. Spuhler, T. Sudeyer, *et al.* "16.2-W average power from a diode-pumped femtosecond Yb:YAG thin disk laser" Opt. Lett. **25**, pp. 859-861 (2000).

[2] T. Beddard, W. Sibbet, D.T. Reid, *et al.* "High-average-power, 1-MW peak-power self-mode-locked Ti:sapphire oscillator" Opt. Lett. **24,** pp. 163-165 (1999).

[3] Z. Liu, S.Izumida, S. Ono, *et al.* Appl. Phys. Lett. **74,** 3622 (1999).

[4] B. Braun, F.X. Kartner, G. Zhang, *et al.* "56-ps passively Q-switched diode-pumped microchip laser", Opt. Lett. **22,** pp. 381-383 (1997).

[5] J. Zayhowski and C. Dill III. Diode-pumped passively Q-switched picosecond microchip lasers", Opt. Lett. **19,** pp. 1427-1429 (1995).

[6] D. Neshev, I. Velchev, W.A. Majevski, *et al,* "SBS-pulse compression to 200 ps in a compact single-cell setup", Appl. Phys. B, **68**, pp. 671-675 (1999).

[7] V. Gidrauskas, A. Dement'yev, E.Kosenko and A.Rodin, "The SRS-amplification of picosecond Stokes pulses", Journal of Applied Spectroscopy, **60**, pp 266-272 (1994).

[8] A.N.Mal'shakov, G.A.Pasmanik and A.K.Potemkin, "SRS-compression of 1ns laser pulses in $SnCl_4$", Quantum Electronics, **27**, pp. 1024-1027 (1997).

[9] A.A. Shilov, G.A. Pasmanik, O.V. Kulagin, K. Deki. "High-peak-power diode-pumped NdYAG laser with a Brillouin phase-conjugation pulse-compression mirror" Opt. Lett. **26,** pp. 1565-1567 (2001).

[10] O.V. Kulagin, A.K. Kotov, G.A. Pasmanik. "Stimulated Raman scattering in counterpropagating pump beams – threshold decrease and pulse compression" CLEO Pacific Rim, Proceedings, v.2, p.475, (2003)

Advanced Solid State Laser Systems for Space Tracking

Yue Gao, Yanjie Wang, Ben Greene, Craig Smith, Amy Chan,
Andrew Grey, Josh Vear, Mark Blundell

1. EOS Space Systems Pty.Ltd., Canberra, Australia

Abstract

A new generation of advanced solid state laser systems has been developed at EOS for space tracking applications.

A completely diode pumped laser system consisting mode-locked laser oscillator, regenerative amplifier, power amplifier and non-linear device with 10 pico-second pulse width has been developed for satellite laser ranging.

A multi-stage and multi-channel completely diode pumped laser system consisting single frequency oscillator, pre-amplifiers, power amplifiers, SBS cells and imaging relays with 2 nano-second pulse width and 230 W output power has been developed for tracking space debris.

Both systems have been in service for more than 2 years with excellent performance and reliability.

ALTIMETRY SESSION SUMMARY

Chair: Frank Lemoine

With the successful return of data on missions such as Mars Global Surveyor, Clementine, Near Earth Asteroid Rendezvous (NEAR), and ICESAT, laser altimeters have been revealed as an essential tool for planetary exploration and Earth monitoring. This session included three papers on aspects of laser altimetry and a fourth paper demonstrating laser communications. Michaelis et al. reviewed the design for BELA, or the Bepi-Colombo Laser Altimeter. This instrument, onboard the Bepi-Colombo spacecraft would globally map Mercury with a 1 m /10 Hz instrument (100 m footprint, 300 m spacing) starting in 2019. Degnan et al. discussed second-generation photon counting imaging lidars. Second generation systems have flown on aircraft (1 km altitude) providing 15-20 cm resolution and contiguous coverage. Future systems could provide high-resolution topographic mapping even from orbital altitudes. Jirousek et al. presented the design of a timing system technology demonstration with sub ns resolution. The range gate delay width was 40 ns; the repetition rate was 24 Hz max, and the unit mass was 2.5 kg. The system was based on tested technology and developed in less than 3 months. Burris et al. presented the results of a demonstration of laser communications at sea. Live video and other data were transmitted on a 125 Mbps fast Ethernet ship-to-ship link over distances of up to 11 nautical miles.

Second-Generation, Scanning, 3D Imaging Lidars Based on Photon-Counting

J. Degnan, D.Wells, R. Machan, E. Leventhal, D. Lawrence, Y. Zheng,
S. Mitchell, C. Field, and W. Hasselbrack

1. Sigma Space Corporation, 4801 Forbes Blvd., Lanham, MD 20706 USA
Contact: John.Degnan@sigmaspace.com /Fax +01-301-577-9466

Abstract

Sigma Space is building a new generation of 3D imaging/polarimetric lidars based on photon-counting for use in small aircraft or mini-UAV's. The most recent system is designed to provide contiguous, high resolution (15 cm horizontal, 3 cm vertical) 3D volumetric images of the underlying terrain on a single overflight from an altitude of 1 km. Based on prior experiments with a first generation NASA prototype system and significant technological improvements, the second generation instruments are expected to have greatly enhanced spatial resolution, areal coverage, and ability to penetrate atmospheric haze, tree canopies, and even water columns for underwater imaging.

Introduction

In 2001, a prototype photon-counting laser altimeter was developed by NASA Goddard Space Flight Center [Degnan et al, 2001]. This first generation NASA system flew at altitudes up to 6.7 km and, using single photon returns in broad daylight, successfully recorded high resolution images of the underlying topography including soil, low-lying vegetation, tree canopies, water surfaces, man-made structures, ocean wave structures, and moving vehicles. The lidar was able to see the underlying terrain through trees and thick atmospheric haze (even when onboard cameras and personnel could not) and performed shallow water bathymetry to depth of a few meters over the Atlantic Ocean and Assawoman Bay off the Virginia coast. An external conical scanner, combined with the aircraft motion, allowed the generation of 3D images as in Figure 1.

Second Generation Lidar

Sigma Space Corporation is presently developing a more compact and higher capability second generation 3D imaging and polarimetric lidar for high resolution

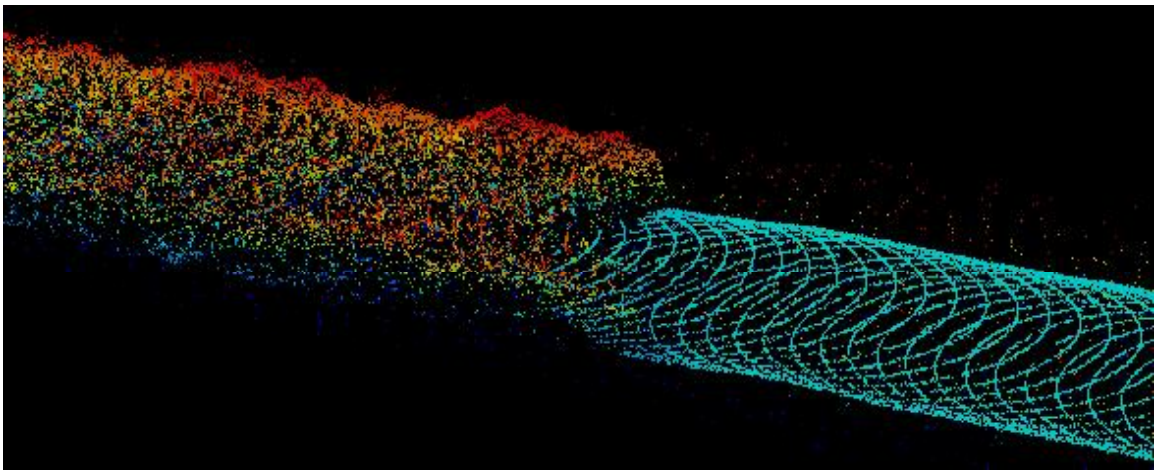

Figure 1: *3D image of a forest edge obtained in daylight by the 1st generation NASA photon-counting microlaser altimeter. (Courtesy Jan McGarry, NASA/GSFC)*

surveying and surveillance from a low altitude, mini-UAV. The shared transmitter is a passively Q-switched Nd:YAG microchip laser oscillator operating at a nominal fire rate of 20 kHz and producing 380 mW of output power at 1064 nm. The photon-counting imager operates at pulse rates up to 22 kHz with approximately 142 mW of frequency-doubled output power at 532 nm; the 238 mW of residual 1064 nm power

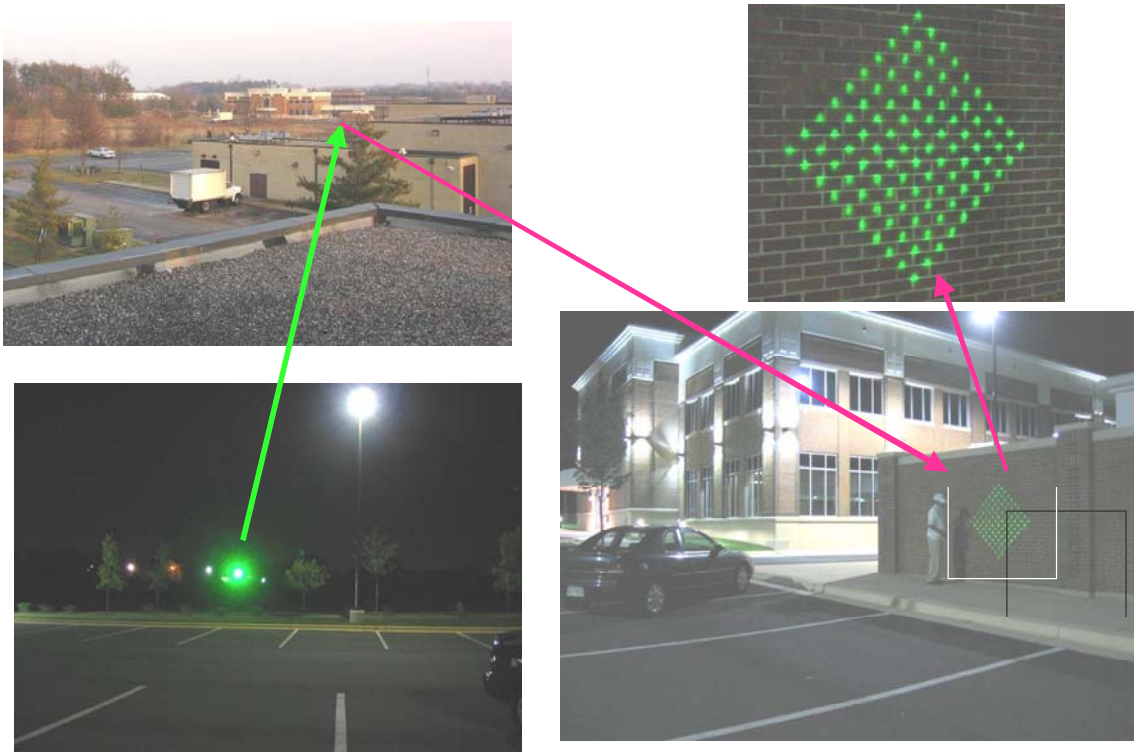

Figure 2: *Counter clockwise from top left: View of target area (most distant building) from the Sigma rooftop; lidar beam as viewed from the target area; projection of holographically altered Gaussian beam on a brick wall at a distance of 250 m; closeup of 10x10 array of beamlets on the brick wall.*

is allocated to polarimetry. Since the green wavelength is near the peak transmission of water, it is suitable for undersea imaging applications. The imager is designed to provide a contiguous, high resolution 3D topographic/volumetric map during a single overflight of the ground scene. From 1 km altitude, the scanner has a swath width of 150 m, a horizontal resolution of 15 cm, and an expected vertical (range) resolution of less than 3 cm. A Holographic Optical Element (HOE) breaks the spatially Gaussian laser beam into a 10x10 array of quasi-uniform eyesafe spots at the target (see Figure 2). The 100 individual far field spots from the HOE are then imaged by the receive optics onto individual anodes of a 10x10 GaAsP segmented anode microchannel plate photomultiplier. The output of each anode is input to one channel of a 100 channel, multistop amplifier/discriminator/timer. Presently, 50 multiple-stop timing channels can be accommodated by one amplifier/discriminator and one Time-of-Flight (TOF) Printed Circuit Board (PCB). The prototype timer has a demonstrated ±100 picosecond timing (± 1.5 cm range) resolution, a multistop capability with a 2 nsec recovery time per channel (corresponding to a capability to resolve objects separated by 30 cm or more in a single pixel for a single laser fire), and an ability to transfer up to 2.2 million ranges per second to onboard memory for long term storage and post-flight processing. Thus, each laser pulse produces a 100 pixel 3D volumetric image of

a 1.5 m x 1.5 m ground area. The individual images are then mosaiced together via the platform velocity and the action of a highly flexible dual wedge optical scanner synchronized to the laser pulse train.

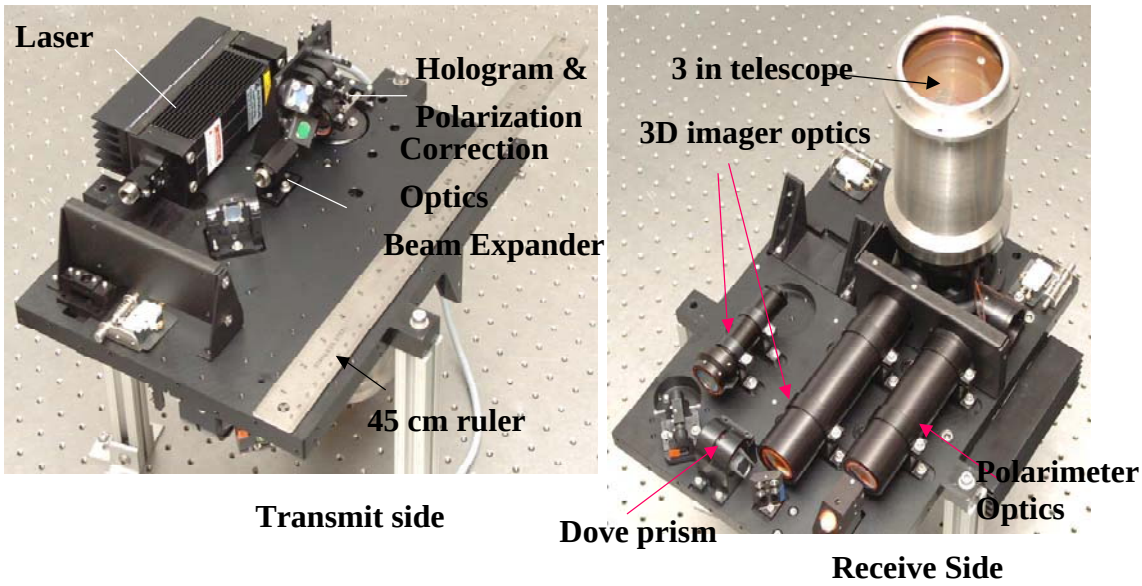

Figure 3: *Optical bench and telescope for second generation 3D imaging and polarimetric lidar. An 18 inch (45cm) ruler is shown for reference*

The transmitter and two receivers (imaging and polarimetry) share a common, 3 inch diameter afocal telescope and optical scanner. This allows the transmitter and receiver to have a common, but narrow, field of view (FOV) to aid in noise rejection and ensures that the imaging and polarimetric data are geographically coregistered. The polarimeter uses the residual laser power (~238 mW) at 1064 nm and two single element detectors to detect two polarization components (although the optomechanical design can accommodate up to 4 NIR detectors for a full determination of the Stokes parameters). Thus, the polarimeter has a nominal horizontal spatial resolution of 1.5 meters. A photo of the lidar optical bench (excluding scanner) is shown in Figure 3. The swath and scan frequency of the dual wedge optical scanner in Figure 4 are tailored to provide contiguous coverage of a ground scene in a single overflight [Degnan and Marzouk, 2003]. The highly flexible servo controller is capable of independently locking the phase and rotation rate of each wedge to the multi-kHz laser pulse train for an infinite variety of precision patterns. These include linear raster scans at various angles to the flight path and conical scans of varying cone angle as well as 2-dimensional rotating line or spiral scans, which might be useful for slow-moving aircraft, helicopters or hovering UAV's. Examples of a 1D linear scan at 45° to the flight path and a 2D rotating line scan are shown in Figures 5a and 5b respectively. The phase locking capability causes the laser beam to be laid down in precisely the same positions with each scan, thereby eliminating the need to record, store, and transfer the scanner wedge positions on each laser fire and greatly reducing data storage and handling. The measured scan repeatability is about 0.07 pixels or about 1 cm at an altitude of 1 km.

The 3D imaging and polarimetric lidar consists of two parts – an optical head and a supporting electronics box. The optical head measures approximately 33 cm x 30 cm x 43 cm and houses the optical bench in Figure 3 (transmitter, imaging and polarimetric optics and detectors, telescope, laser gyros and inclinometer for attitude

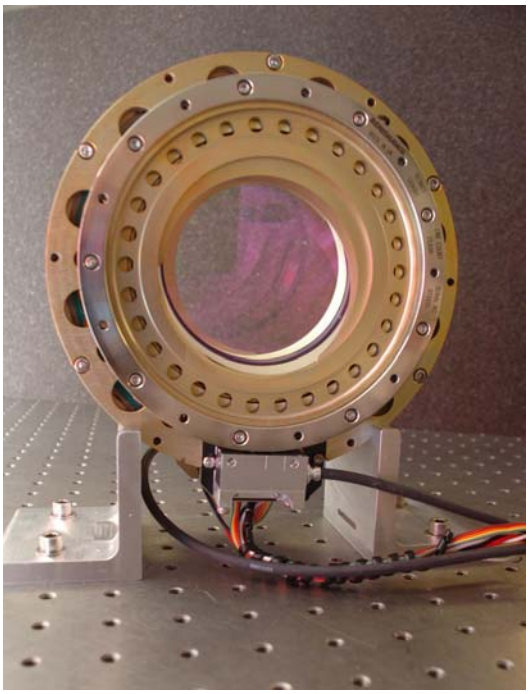

Figure 4: *Photo of the direct drive dual wedge annular ring scanner developed under the NASA JIMO program. The annular ring motors have cryogenic and vacuum compatible counterparts suitable for space use.*

determination, etc) plus the external dual wedge scanner in Figure 4, the MCP/PMT gating PCB, and the Amplifier/Discriminator/Timer PCB boards. The electronics box has a volume of 0.027 m^3 and houses the scanner electronics, GPS receiver, Reference Oscillator and Timing Distribution Circuits, Navigation and Imaging/Polarimeter Data Acquisition Modules, the laser power supply, and various DC/DC converters and voltage regulators. The manner in which the entire lidar system fits within the forward electronics bay of an Aerostar mini-UAV is illustrated in Figure 6.

Summary

Photon-counting altimeters are extremely sensitive and highly efficient, requiring only one photon per range measurement, and, with multistop capability, can be operated day or night with large temporal gate widths for monitoring large elevation changes or simultaneously detecting the tops of tall buildings and city streets or tall treetops and the underlying terrain. Post-detection Poisson filters easily extract the signal from the solar background [Degnan, 2002]. The ability to penetrate obscurants (ground fog, vegetation, water) on a single shot (i.e. without "staring" at a scene while multiple pulses are fired) was demonstrated in the NASA prototype [Degnan et al, 2001]. This penetration capability was the result of the single photon sensitivity and the rapid multiple stop capabilities of the range receiver and will be substantially enhanced in our second generation instruments due to a factor of 12 increase in the effective signal photoelectrons received per ground pixel (~3 pe vs 0.25 pe in the NASA prototype).

Since the laser fires at a rate higher than necessary for contiguous coverage, the 3 pe/pixel is accumulated during multiple interrogations of the pixel during the scan, i.e. typically 3 interrogations at 1 pe which results in a higher probability of detection (~99%) than 3 pe for one interrogation (95%). The integration of a dual wedge scanner in the 2nd generation systems will eliminate the gaps in coverage previously observed with a single wedge conical scanner (see Figure 1) and provide contiguous coverage on a single overflight.

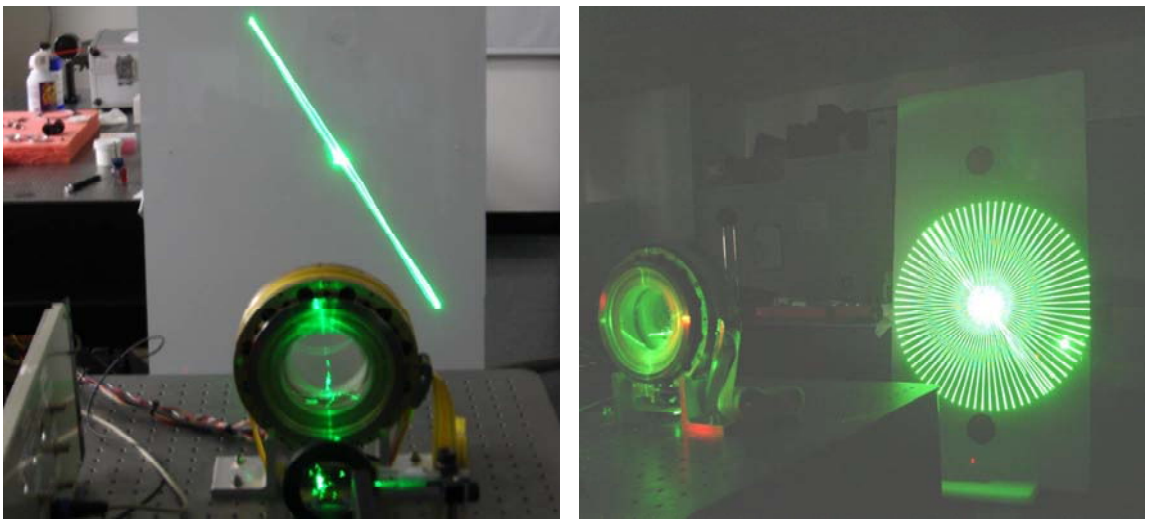

(a) **(b)**

Figure 5: *NASA prototype Direct Drive Internal Scanner generating (a) a linearscan and (b) a rotating line scan on a near field screen. Both scan types were run at 18 Hz and synchronized to a nominal 9 kHz Q-switched microchip laser pulse train. The slight bowing of the linear scan in (a) is due to near field displacement of the beam in the optical wedges but collapses to a true line in the far field. The non-uniformity of the rotating line scan at the 4 o'clock and 10 o'clock positions is due to a slight overlap of two consecutive rotating line scans.*

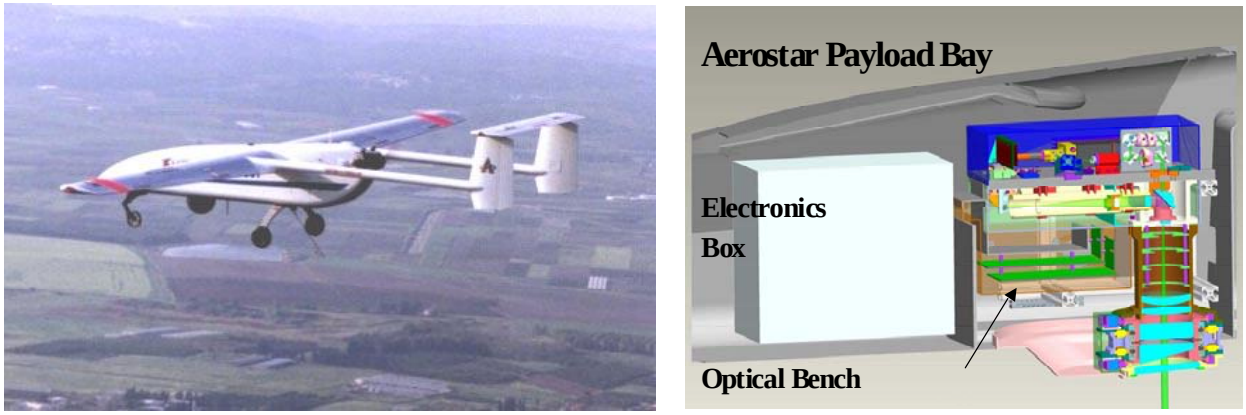

Figure 6: *(a) Aerostar mini-UAV in flight; (b) Packaging of the 3D imaging/polarimetric lidar within the nose electronics bay.*

Acknowledgement

The work presented here was partially supported by USAF Phase II SBIR PO FA8650-05C-1817, Technical Officer: Richard D. Richmond , AFRL, Wright Patterson AFB OH 45433 and by NASA Contract NNH05CC68C, Technical Officer, Dr. Curt Niebur, NASA HQ, Washington DC 20546.

References

[1] Degnan, J., "Photon-Counting Multikilohertz Microlaser Altimeters for Airborne and Spaceborne Topographic Measurements", Journal of Geodynamics (Special Issue on Laser Altimetry), pp.503-549, November, 2002.

[2] Degnan, J. and J. Marzouk, 2003 "An inexpensive 3D imaging lidar for contiguous decimeter resolution topographic mapping from a high altitude aircraft", Proc. AMOS 2003 Technical Conference, Maui, HA, Sept. 8-13, 2003.

[3] Degnan, J., J. McGarry, T. Zagwodzki, P. Dabney, J. Geiger, R. Chabot, C. Steggerda, J. Marzouk, and A. Chu, "Design and performance of an airborne multikilohertz, photon-counting microlaser altimeter", Int. Archives of Photogrammetry and Remote Sensing, Vol. XXXIV-3/W4, pp. 9-16, Annapolis, MD, 22-14 Oct. 2001.

The BELA - The first European Planetary Laser Altimeter: Conceptional Design and Technical Status

Harald Michaelis[1], Tilman Spohn[1], Jürgen Oberst[1], Nicolas Thomas[2], Karsten Seiferlin[2], Ulrich Christensen[3], Martin Hilchenbach[3], Ulrich Schreiber[4]

1. Deutsches Zentrum für Luft- und Raumfahrt, Institut für Planetenforschung, Berlin, Germany.
2. Physikalisches Institut, Universität Bern, Switzerland.
3. Max-Planck Institut für Sonnensystemforschung, Katlenburg-Lindau, Germany.
4. Forschungseinrichtung Satellitengeodäsie der Technischen Universität München, Wettzell, Germany.

Abstract

The BepiColombo Laser Altimeter (BELA) is the first European laser altimeter for planetary exploration which has been selected by ESA for flight aboard ESA's Bepi Colombo mission to planet Mercury. A consortium led by the Physikalisches Institut Bern and Institut für Planetenforschung (DLR-Berlin, Germany) will develop a laser altimeter based on the classical principle of laser pulse time of flight measurement. The instrument is based on a longitudinally pumped Nd:YAG laser with 50mJ pulse energy and pulses of about 3ns duration, operating nominally at 10Hz repetition rate. The BELA requirements, the conceptional design, the technical development activities and their status are presented during the workshop.

Introduction

BepiColombo is the European Space Agencies (ESA) cornerstone mission to the planet Mercury. It consists of two orbiters, the Mercury Planetary Orbiter (MPO) and the Mercury Magnetospheric Orbiter (MMO). Among the instruments that have been confirmed is the Bepi Colombo Laser Altimeter (BELA). BELA's primary goal is:

- develop a full topographic map of the planet with an accuracy (goal) of 1m to support geomorphologic studies,
- explore Mercury's interior structure by joint analysis of topographic, gravity and rotation data,
- determine elastic properties of the planet by measurements of tidal deformation
- measure surface albedo and roughness,
- support spacecraft navigation.

Main Requirements

The instruments key requirements are:

- Global topographic mapping with height accuracy of 10m wrt. COM (goal: 1m),
- Surface spacing 300m (shot to shot),
- High detection probability (>70%) up to 1000km,
- Laser footprint <100m.

The detection probability is defined by the PFD, the probability that a random noise fluctuation in the pulse detection chain is misinterpreted as a laser echo.

These requirements have to be fulfilled under the harsh environmental conditions at Mercury. The main design drivers for the instrument are:

- high thermal- and solar flux,

- to guarantee an alignment stability of a few arc seconds
- cosmic radiation levels,
- low resources (e.g. mass)

The main demands come from the high thermal flux (that is as high as 10kW/m^2) and the high Temperature of Mercury, which can reach surface temperatures of up to 700K. The total instrument mass must not exceed 12kg, which limits the size of the receiver and the laser transmitter.

Technical Approach and Design

The BELA instrument consists of the receiver and the transmitter part which will be developed by institutions from Switzerland, Germany and Spain. The architecture of the instrument is shown in Figure 1.

The receiver telescope with the detector, the laser head and the beam expanding telescope are assembled on the so called Baseplate (BP) unit. The laser head, (OAB), is fibre pumped by the pumped-diode unit (PDU) which is controlled by the laser electronics (LEU). The main electronics of BELA including rangefinder electronics, data processing electronics, transmitter electronics (START-pulse detection and digitization) and the power supply are accommodated in a common electronics box,(ELU).

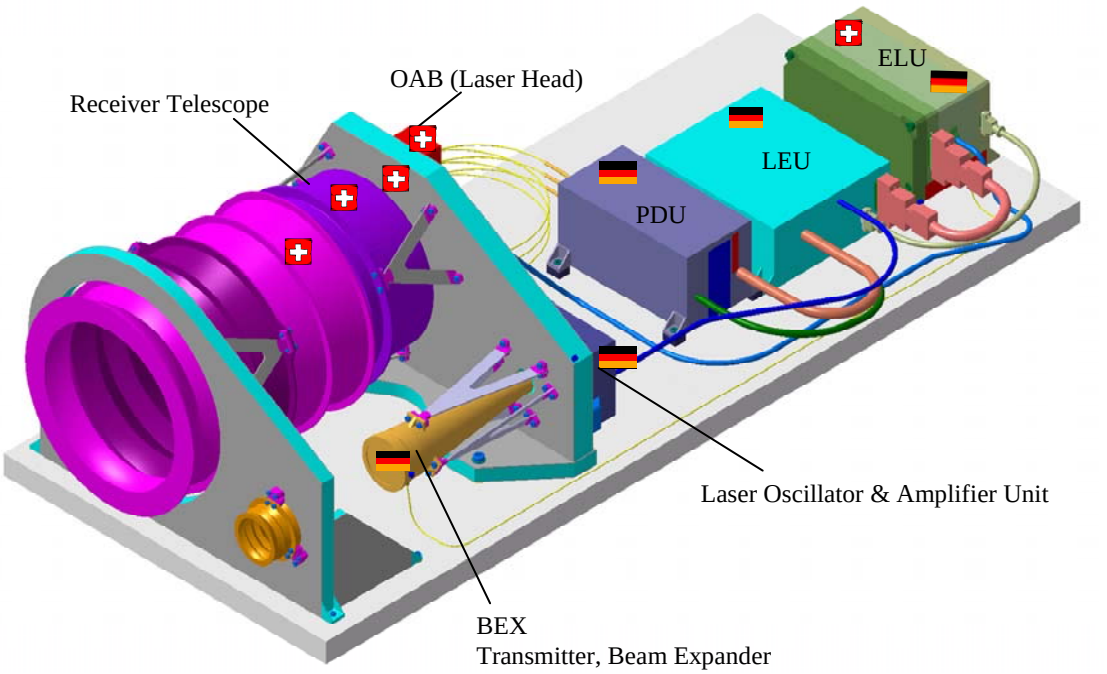

Figure 1: *Main Components of the BELA Laser Altimeter*

The main characteristics of the envisaged instrument are:

- 20-25cm lightweight telescope (1kg) with large baffle for thermal protection,
- backend optics with 1nm filter /FWHM) and >80% transmission,
- high sensitive (low noise) APD detector,
- 50mJ, 3ns diode pumped Nd:YAG laser, 10Hz nominal repetition rate,
- 50mm (20x) beam expander with ~50m footprint @1000km,

- common E box (ELU) with receiver-, START electronics and LEON-3 processor, power converter, thermal controller,
- 12kg, 33W (nominal).

The instrument's characteristics were derived by performance simulations according to the following parameter spreadsheet (see Table 1).

Table 1: *BELA parameter set for performance simulation*

Parameter	Symbol	BELA
S/C		
Destination		Mercury
Altitude	H	400-1500 km
Pointing uncertainty	$\delta\varphi$	25μrad
Laser transmitter		
Pulse energy	E_T	50 mJ[a]
Pulse width	δ_0	3.4 ns[b]
Wavelength	λ_T	1064 nm
1/e² beam divergence	θ_T	25 μrad[c]
Repetition rate	ν_T	10 Hz
Collimator efficiency	ϵ_T	0.80
Receiver optics		
Arperture radius	r_R	125 mm
Focal length	f_R	1250 mm
Field of view	θ_{FOV}	200 μrad[c]
Optical efficiency	ϵ_{RO}	0.70[d]
Filter transmission	ϵ_{RF}	0.80
Filter bandpass	δ_{RF}	0.42 nm[b]
Detector		
Quantum efficiency	ϵ_{QE}	0.38
Gain	M	150
Excess noise index	χ	0.25
Surface dark current	I_{DS}	20 nA[a]
Bulk dark current	I_{DB}	50 pA[a]
Electronics		
TIA Bandwidth	B_0	20 MHz
ADC sample period	T_R	12.5 ns
Noise floor	δI_{NF}	1.0 pA $Hz^{-1/2}$

The most critical parameters are the laser pulse energy, the aperture of the receiver telescope and the performance characteristics of the detector (quantum efficiency, noise). It was estimated that the instrument will be capable of meeting the performance requirements, PFD<0.1 out to a height of 1050km and a height accuracy measurement of down to 1m for a reasonable set of observing conditions.

Key instrument components are presently in development for performance verifications and testing. One key component, the laser units has already been designed and fabricated by MPS and German industry (Laser Zentrum Hannover e.V., DILAS GmbH, Mainz, Von Hoerner & Sulger, Schwetzingen) as a prototype model, which is shortly described below.

The BELA-Laser

The optical design of the BELA laser is based on the concept of Nd:YAG laser crystals for the oscillator and the two amplifier stages, which are longitudinally pumped with GaAs diodes around 804 to 808 nm (@298K). The simplified block diagram of the laser head (OAB) and the pump diode unit (PDU) is shown in Figure 2.

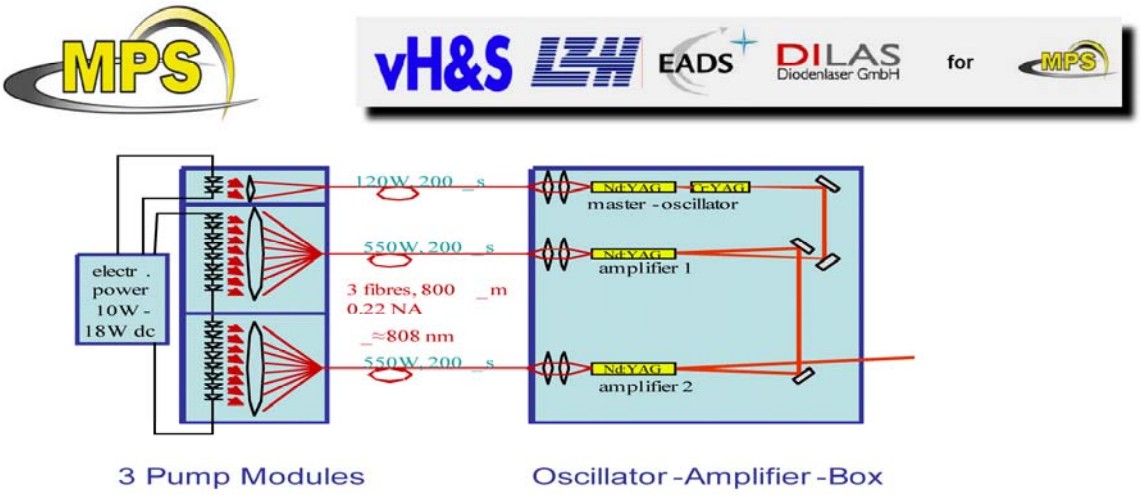

The BELA instrument requirement is to have 3 fibre coupled pump sources (called modules); two of them shall deliver 550W ex fibre each for amplifier pumping while the third has to deliv er 120W ex fibre for oscillator pumping.
The diodes for oscillator pumping shall be available in could redundancy, which means that two bars will be operated and two other bars can be used alternatively (not sketched).

Figure 2: *Block diagram of the laser head (OAB) and the pump diode unit (PDU)*

The OAB is optically pumped via three fibre optics cables between the OAB and the PDU. The output pulse energy of the laser is 50mJ at 3ns pulse duration (measured) and a firing of 10Hz (nominally). The control and the current supply of the laser are provided by the Laser Electronics Unit (LEU). The main parameters of the laser are summarized in Table 2.

Table 2: *Laser Main Characteristics*

Parameter	**Unit**	**Value/Description**
Material		Nd:YAG
Wavelength	nm	1064.x
Pulse Energy	mJ	50 (EOL)
Pulse frequency	Hz	10 (nominal)
Pulse Duration	Ns	3
M2		<1.6 (measured: 1.3)
Q-switch		Passive
Laser Pump		Longitudinal
Efficiency (electro-optical)	%	5.2 (measured)

The first Prototype Model of the laser is shown in Figure 3.

Figure 3: *BELA Laser Prototype Model-1*

Further key components that are presently in development are only shortly listed below:

Beam Expander (BEX)

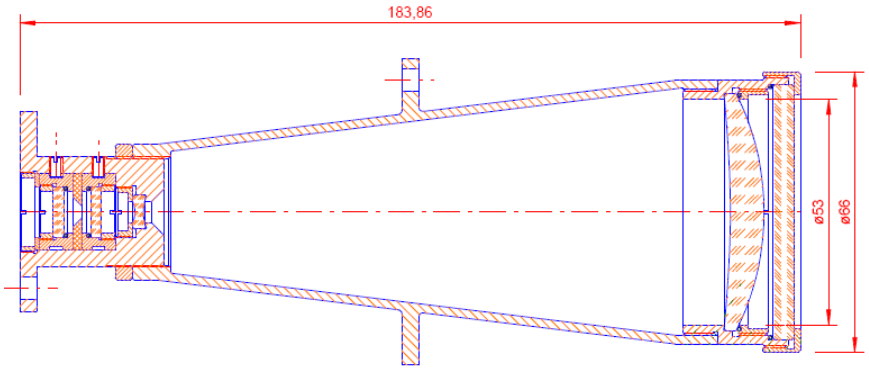

Figure 4: *Opto-mechanical layout of the BELA Beam Expander (BEX)*

The BELA beam expander (Prototype Model) is based on an aspheric lens design for the exit-lens in order to prevent a double-lens and to save mass. The beam direction can be slightly adjusted by wedge prisms at the entrance of the beam expander. The BELA-BEX has a nominal beam expansion ratio of 20. A fibre-optics interface is foreseen for optical detection of the START-pulse.

START Electronics

The START electronics has two functions:

1. detection of the START-pulse, which will be fed to the rangefinder electronics
2. digitization of the START-pulse for energy and shape measurement of the outgoing pulse

The block diagram of the START electronics and the first prototype is shown in Figure 5 and Figure 6 respectively.

The components of the receiver: telescope (incl. base plate), baffle, detector and rangefinder electronics are presently in development in Switzerland, lead by the University of Bern (Nicolas Thomas and Karsten Seiferlin).

Conclusion and Outlook

The BELA team is in process to design the first European laser altimter for planetary exploration which has been selected by ESA for flight aboard of ESA's Bepi Colombo mission to planet Mercury. Numerical models have been developed to assist with design tradeoffs and definition of operational modes. Key components like the laser have been developed as prototype model and further units are in fabrication (beam expander, receiver telescope, detector electronics).

The Forschungseinrichtung Satellitengeodäsie der Technischen Universität München (Wettzell) and DLR are presently in process to design a first performance demonstrator which is based on the BELA prototype models and commercial components with a performance characteristics close to BELA. This performance demonstrator will be used for functional and performance verification of BELA by satellite laser ranging, and it will be used as a transponder demonstrator.

Acknowledgement

The authors would like to thank Reinhard Roll (MPS), Daniele Piazza and Kurt Gunderson (UBE) and the BELA team members of DLR Berlin (Mrs Kerstin Rösner, Wolfgang Bresch, Thomas Behnke, Matthias Tschentscher, Alexander Lichopoj, Kay Lingenauber, Rolf Schrödter) for their contribution to the present design, simulation and test of BELA components.

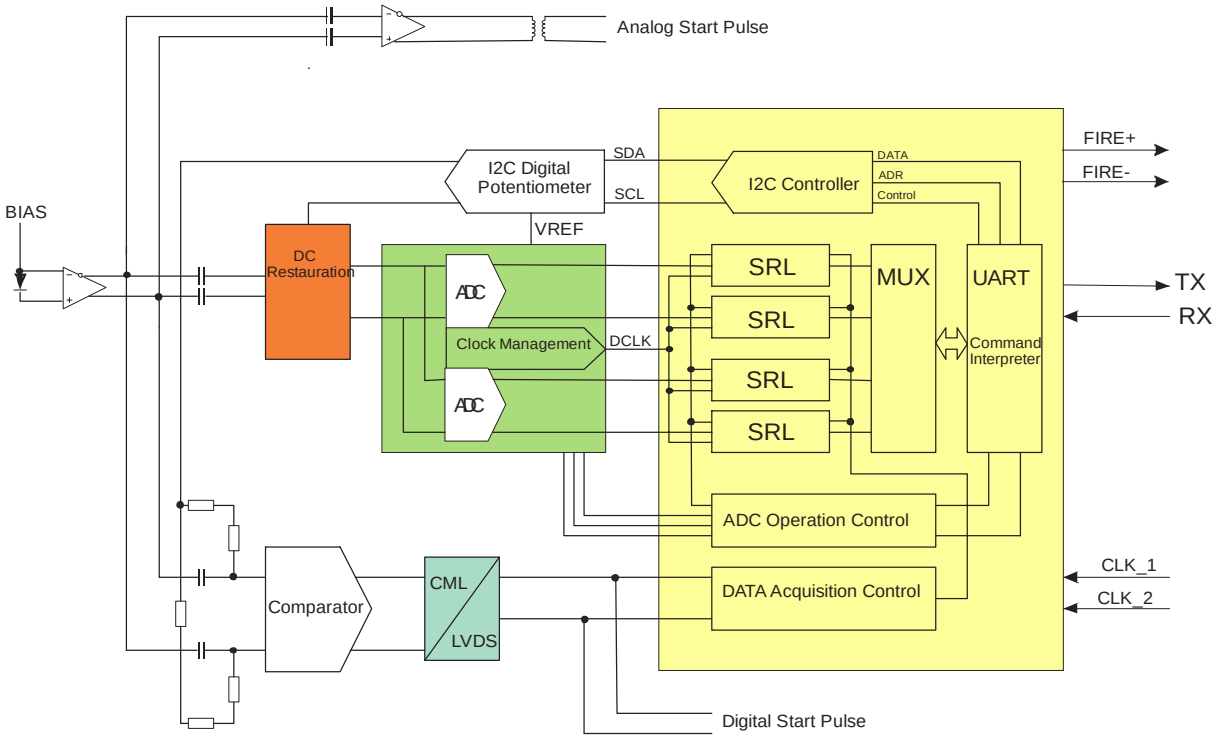

Figure 5: *Block Diagram of the START-Electronics*

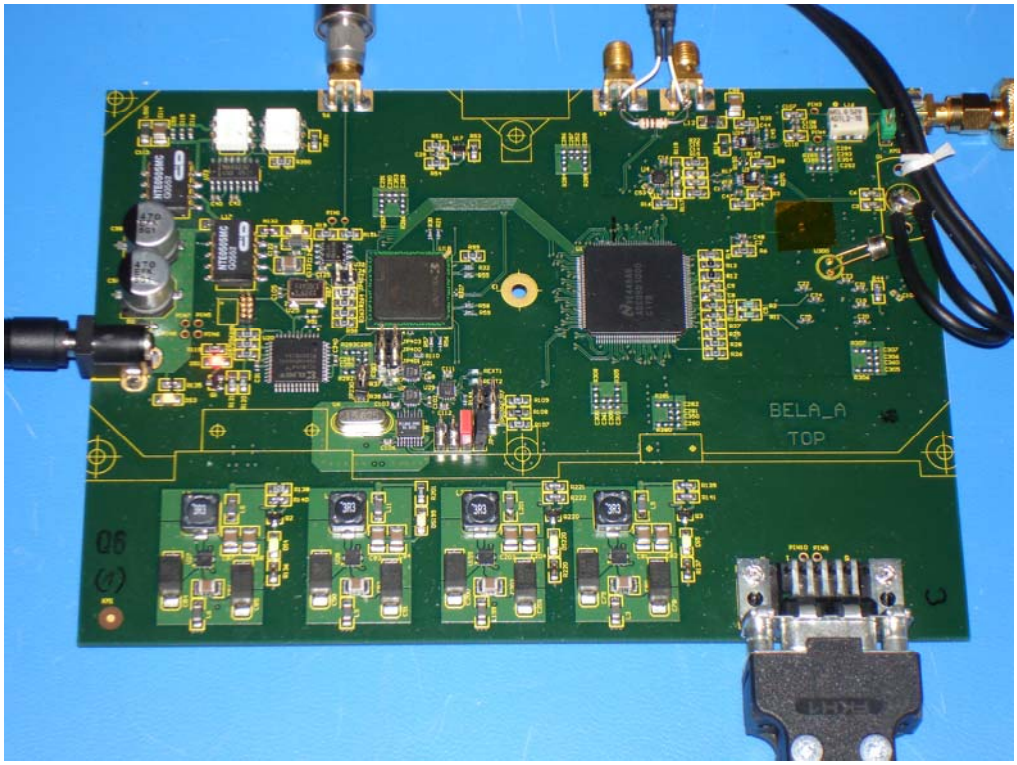

Figure 6: *Prototype of the START Electronics*

Timing System for the Laser Altimeter for Planetary Exploration Technology Demonstrator

P. Jirousek[1], I. Prochazka[1], K. Hamal[1], M. Fedyszynova[1], U. Schreiber[2], H. Michaelis[3], Yang Fumin[4], Huang Peicheng[4]

1. Czech Technical University in Prague, Brehova 7, 115 19 Prague 1, Czech Republic
2. TU Munich, Germany
3. DLR Berlin Adlershof, Germany
4. Shanghai Observatory, Chinese Academy of Science, China

Contact: prochazk@troja.fjfi.cvut.cz

Abstract

We are presenting the design, construction and tests of the timing system for the Bepi Colombo Laser Altimeter (BELA) technology demonstrator. BELA Timing System (BTS) is an universal timing system for laser ranging in ground-ground, air-ground and ground-satellite experiments. It is dedicated to measure precise time interval with subnanosecond resolution. The device for advanced range gating is included. The unit is interfaced to a host personal computer via a serial data link for control, two way data transfer and diagnostics.

The entire BTS has been designed and constructed on the basis of the Portable Calibration Standard (PCS) for satellite laser ranging, which has been developed in our labs within the last ten years. To reduce the complexity, costs, weight and power, considering the modest timing resolution requirements, the sub-nanoseconds instead of picoseconds resolution of the time intervals, the timing part of the original device has been replaced by the Mini counter. The overall design philosophy, the operational control software, the epoch timing, the range gate generation have been preserved along with the concept of the host computer software package for data acquisition, control and data analysis including the communication protocol, data and command formats etc. The use of well tested concept of both the HW and SW enabled to shorten the design, construction and testing phase of the final device down to several weeks.

The BTS consists of the Mini Counter module, the epoch timing and range gate generator module, the control processing unit, the input / output circuits and of the power supplies. The entire control logic hardware including the epoch timing and range gate generator and the input/output board logic is based on the FPGA (ispGAL) programmable logical arrays. There is a significant array capacity still available for future functional extensions and device upgrades, the arrays are field programmable. This fact ensures the maximum device flexibility and upgradability. The main parameters are : resolution 0.25 ns, linearity and stability better than 0.1 ns and 0.1 ns per K and per hour resp. The laser fire epoch resolution is 100 ns, the range gate is programmable in 40 ns steps. The device is small (2 kg), low power, it is capable to operate 3 hours on eight AA batteries.

Goals

- Technology demonstrator of a Compact Laser Rangefinder applicable in future space projects :
  - Mercury planet altimetry
  - Lunar altimetry and surface mapping
  - on-board optical transponder(s) for Earth orbiter(s)
  - airborne range finder
  - ground based Satellite Laser Ranging (SLR)
- Main altimeter parameters:
  - one meter ranging precision
  - multiphoton approach
  - diode pumped laser, ns pulses,
  - modular construction
  - existing / available technology

Jirousek, Prochazka, Hamal, Fedyszynova, Schreiber, Michaelis, Yang, Huang, Canberra 2006

Philosophy

- Technology demonstrator of a Compact Laser Rangefinder
- modular construction
- existing / available technology
- test bench at the Satellite Laser Ranging site Wettzell, WLRS
- applicable in various ground and space projects :
  - Mercury planet altimetry
  - Lunar altimetry and surface mapping
  - on-board transponder for Earth orbiters
  - ground based Satellite Laser Ranging (SLR)
  - airborne range finding

Jirousek, Prochazka, Hamal, Fedyszynova, Schreiber, Michaelis, Yang, Huang, Canberra 2006

Schedule & responsibilities

July 31 st	decision, proposal, quotation	CTU Prague
August 31st	DLR acceptance, contract	DLR
October 30	first version operational	CTU Prague
November	on-site testing	CTU / DLR
November 30	delivery	CTU
December 15	integration at DLR	CTU / DLR

Jirousek, Prochazka, Hamal, Fedyszynova, Schreiber, Michaelis, Yang, Huang, Canberra 2006

Altimeter Timing System Requiremerets

- GENERAL
  universal timing system for laser ranging with sub-ns resolution

- FUNCTIONS
- determining the epoch of laser fire
- measuring the time-of-flight of the laser pulse
- generating the range gate pulse for the echo signal detector
- data acquisition and process control.

- PROPERTIES
- compact, low power (battery operated), low cost
- based on field - proved components HW & SW
- simple to integrate into final device

Jirousek,Prochazka,Hamal,Fedyszynova,Schreiber,Michaelis,Yang,Huang,Canberra 2006

Altimeter Timing System Concept

- Based on P-PET hw and sw concept,
  the Dassault modules are replaced by integrated TDC chips .

- The timing system consists of the range counter module, the epoch timing and range gate generator module, the control processing unit, the input / output circuits and of the power supplies.

- The entire control logic hardware, epoch timing, range gate, and input/output board is based on the FPGA (ispGAL) programmable logical arrays.
  This ensures the maximum device flexibility and upgradability.

Jirousek,Prochazka,Hamal,Fedyszynova,Schreiber,Michaelis,Yang,Huang,Canberra 2006

Timing System Technology Demonstrator Block scheme

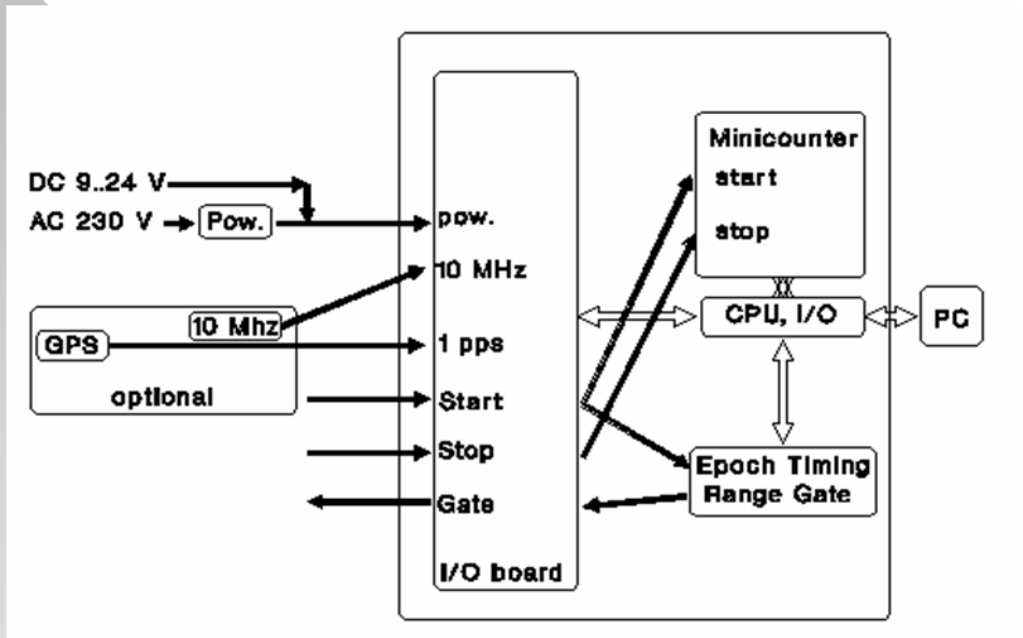

Jirousek,Prochazka,Hamal,Fedyszynova,Schreiber,Michaelis,Yang,Huang,Canberra 2006

Timing System Technology Demonstrator Electronics boards

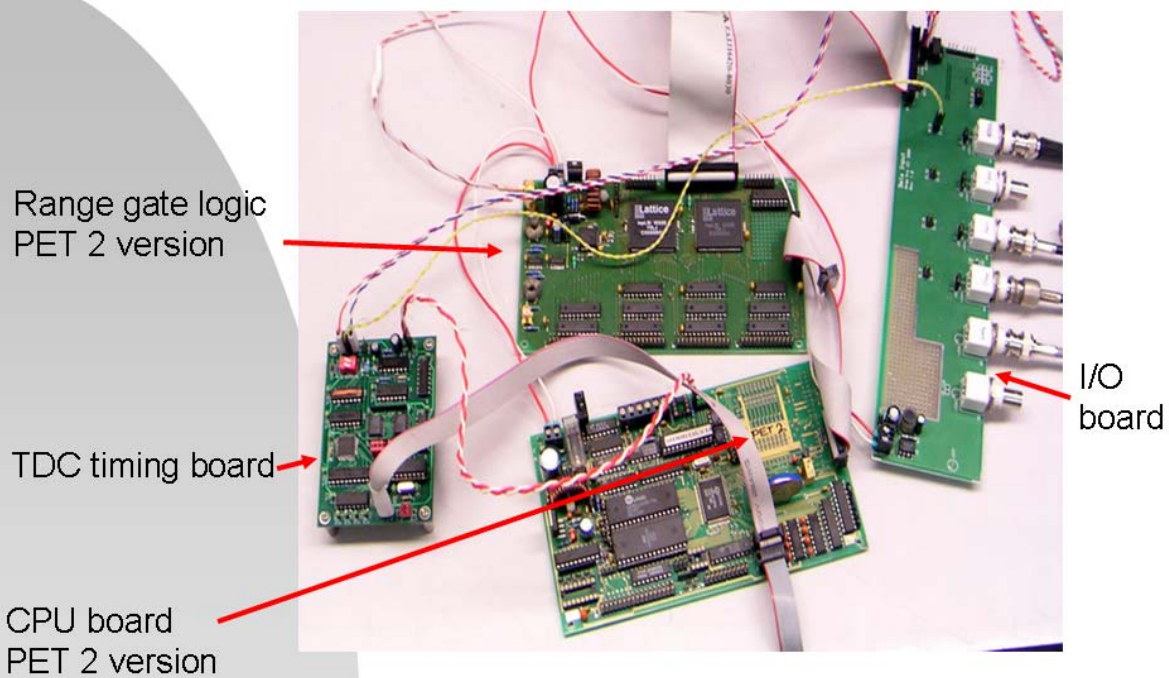

Jirousek,Prochazka,Hamal,Fedyszynova,Schreiber,Michaelis,Yang,Huang,Canberra 2006

Timing System Technology Demonstrator
Temporal resolution

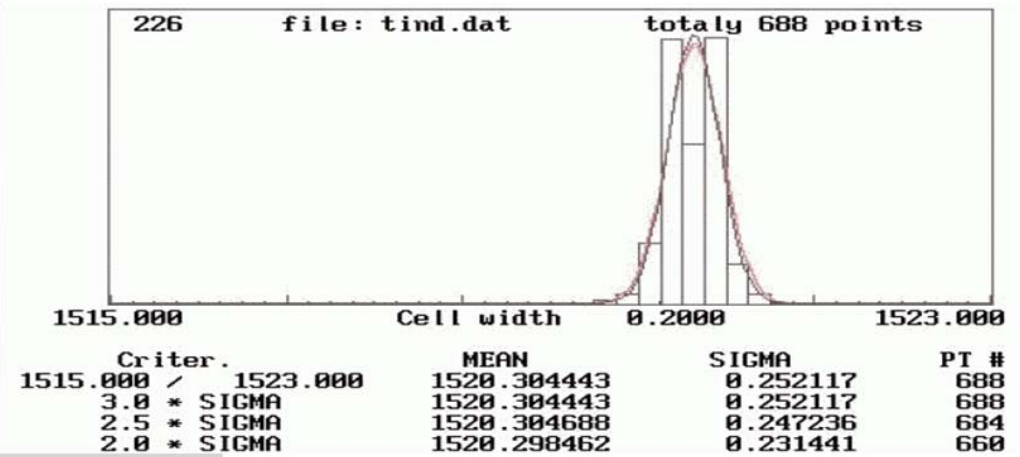

Criter.	MEAN	SIGMA	PT #
1515.000 / 1523.000	1520.304443	0.252117	688
3.0 * SIGMA	1520.304443	0.252117	688
2.5 * SIGMA	1520.304688	0.247236	684
2.0 * SIGMA	1520.298462	0.231441	660

measured time 1.52 μs
the timing resolution of 0.25 ns
normal data distribution

Jirousek,Prochazka,Hamal,Fedyszynova,Schreiber,Michaelis,Yang,Huang,Canberra 2006

Timing System Technology Demonstrator
Long-term temporal stability

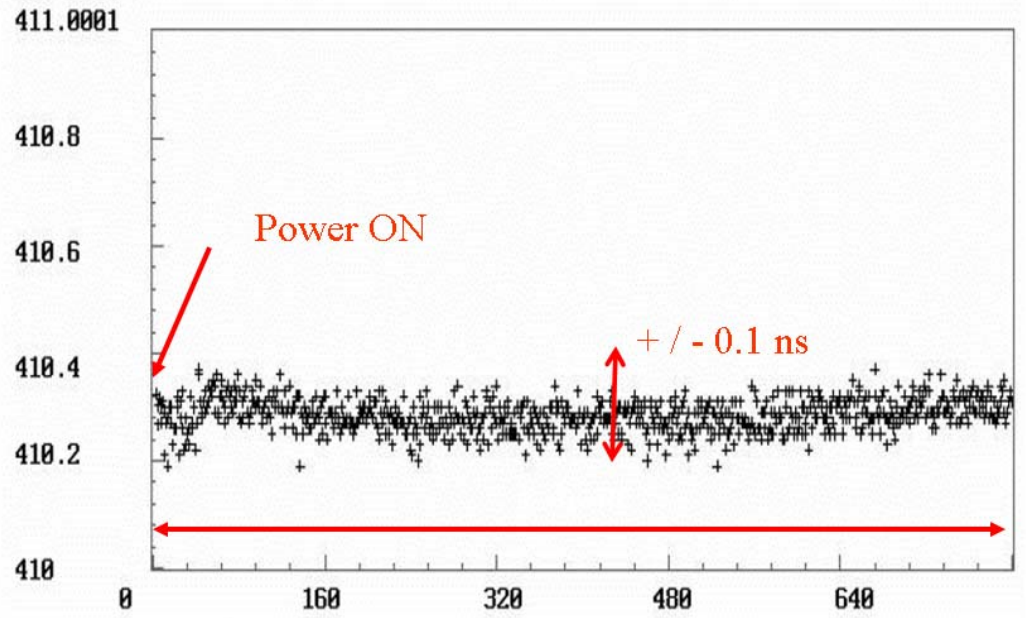

Jirousek,Prochazka,Hamal,Fedyszynova,Schreiber,Michaelis,Yang,Huang,Canberra 2006

Timing System Technology Demonstrator
Parameters

- universal timing system for laser ranging with sub-ns resolution

- resolution, precision — 0.25 ns, 0.25 ns rms
- non-linearity, stability — < 0.1 ns, < 0.1 ns/hour
- range gate delay,width — 40 ns steps
- repetition rate — 24 Hz max.
- mass — 2.5 kg
- power — DC 9-38 V, 7 VA
  > 3 hr operation on AA cells (8x)

Jirousek,Prochazka,Hamal,Fedyszynova,Schreiber,Michaelis,Yang,Huang,Canberra 2006

Altimeter Timing System Technology Demonstrator
Conclusion

- the universal timing system for laser ranging:
  ground-ground, air-ground and ground-satellite
  with sub-ns resolution has been developed and tested
- simple to implement:
  SW package identical to PET devices
- based on tested technology and components
  development period < 3 months :-)
- In perspective the Altimeter Timing System may be applied
  in deep space laser transponder experiments

Jirousek,Prochazka,Hamal,Fedyszynova,Schreiber,Michaelis,Yang,Huang,Canberra 2006

A Compact Low Power Altimetry Laser For Lunar Applications

Thomas Varghese[1], Ralph Burnham[2]

1. Cybioms Corporation, 607 Autumn Wind Way, Rockville, MD 20850
2. Fibertek Inc., 510 Herndon Parkway, Hendon, VA 20170

Abstract

A very compact 10 mJ, 10 Hz, 4ns laser with greater than a billion shots capability is being developed for lunar altimetry applications for a mission projected for 2008. The altimeter will complement other scientific payloads of the mission that includes Terrain Mapping Camera with stereo imaging capability, Hyper-Spectral Imager, and a Low Energy X-ray spectrometer. The laser design exploits the advances in technologies, capabilities, and lessons learned from the NASA Risk Reduction Laser program, Calipso, and others. The Engineering Model and Flight Model are discussed.

KILOHERTZ SESSION SUMMARY

Chairs: Georg Kirchner, Graham Appleby

Talks / presentations given:

- Hamal et al: Portable Pico Event Timer and SLR Control System
- Gibbs et al: Early Results of kHz SLR at Herstmonceux
- Degnan et al: LC Optical Gate for Monostatic kHz SLR System
- McGarry et al: SLR 2000: The Path Towards Completion
- Kirchner et al: Spin Parameters of AJISAI and GP-B from kHz SLR
- Kucharski et al: Lageos-1 Spin Determination from kHz SLR
- Kirchner et al: Measuring Atmospheric Seeing with kHz SLR

In addition: kHz SLR has a lot of unique advantages; just as an example, the graph below shows the significant improvement of the Peak-Minus-Mean value, when going from a standard 10-Hz system (old Graz SLR) to a kHz system; please note that such a statistical improvement is a necessary requirement if we want to think / talk about "mm-SLR" ☺

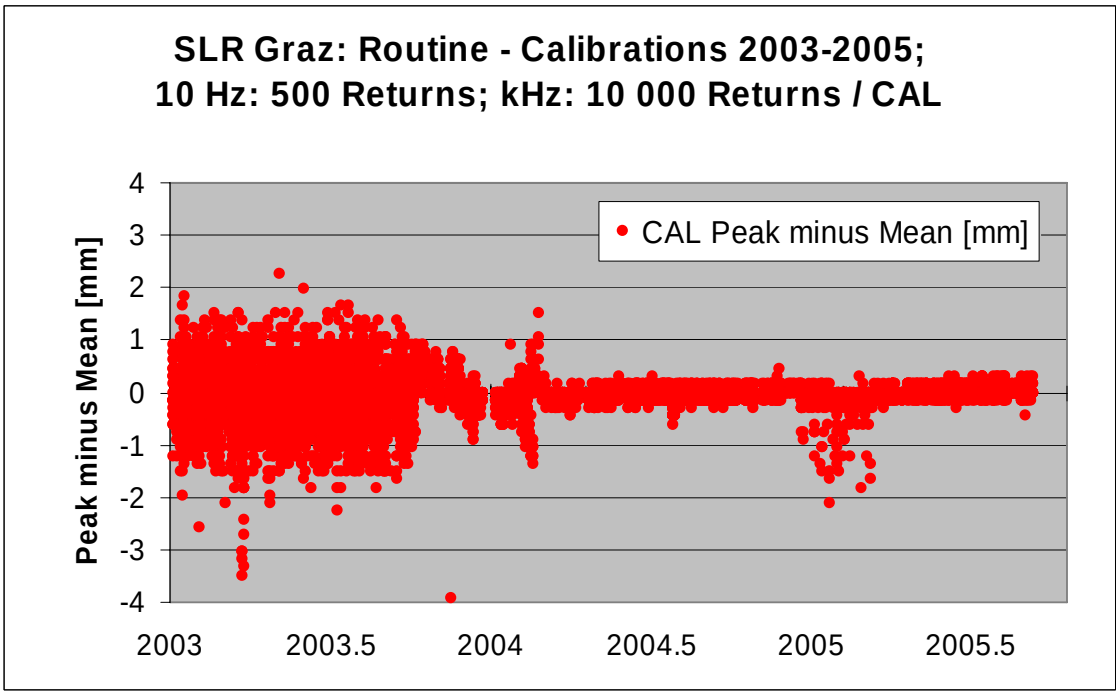

Portable Pico Event Timer and SLR Control (P-PET-C) System

Karel Hamal[1], Ivan Prochazka[1], Yang Fumin[2]

1. Czech Technical University in Prague, Brehova 7, 115 19 Prague 1, Czech Republic

2. Shanghai Observatory, Chinese Academy of Science, 80 Nandan Road, Shanghai, China

Contact: prochazk@troja.fjfi.cvut.cz

Abstract

We are reporting design, construction and parameters of the Portable Pico Event Timer and SLR Control (P-PET-C) System. It has been developed as a self-consistent system dedicated for the millimeter precision satellite laser ranging systems operating at high repetition rates up to 2 kHz. It provides real time control, measurement, data acquisition and data processing of the advanced satellite laser ranging station. It consists of the PET-C hardware and the software package. The system hardware has been developed on the basis of the Pico Event Timer (P-PET), which has been employed in laser ranging stations in Wettzell, Germany, TIGO Chile and in Portable Calibration Standard, a world wide accepted reference for pico-event timing for millimeter laser ranging. These systems have been operated at numerous stations around the world, including China, without any single failure for more than 8 years of continuous operation. The event timing is based on space qualified Dassault units no adjustment or re-calibration is needed. The 200MHz frequency generator was developed in FH Deggendorf. The real time control, measurement, data acquisition and data processing interface is based on the codes developed and operated at the satellite laser station in Graz, Austria, which is world first station operating a high repetition rate millimeter precision laser system. The real time control and data acquisition is provided by the built in PC. The first field operation was performed at the SLR Shanghai, China, 2006.

Portable Pico Event Timer and SLR Control (P-PET-C) System

Goals

- Portable Pico Event Timer and SLRControl 2kHz
- Self-consistent portable unit
- Built in PC
- Dassault Timing Units
- Range Gate Generator
- T/R Pulse Overlap Avoidance
- Dedicated for Portable Calibration Standard 2k

K.Hamal,I. Procházka, Yang Fumin, 15th ILRS Workshop,Canberra,2006

Portable Pico Event Timer and SLR Control (P-PET-C) System

SLR Workshop

Freq module Deggendorf

2 kH SLR PC Card Graz

Pico Event Timer (P-PET)

Portable Pico Event Timer and SLR Control (P-PET-C) System

London 1998

Prague, Shanghai 2006

K.Hamal,I. Procházka, Yang Fumin, 15th ILRS Workshop,Canberra,2006

Portable Pico Event Timer and SLR Control (P-PET-C) System

P-PET-C Block Scheme

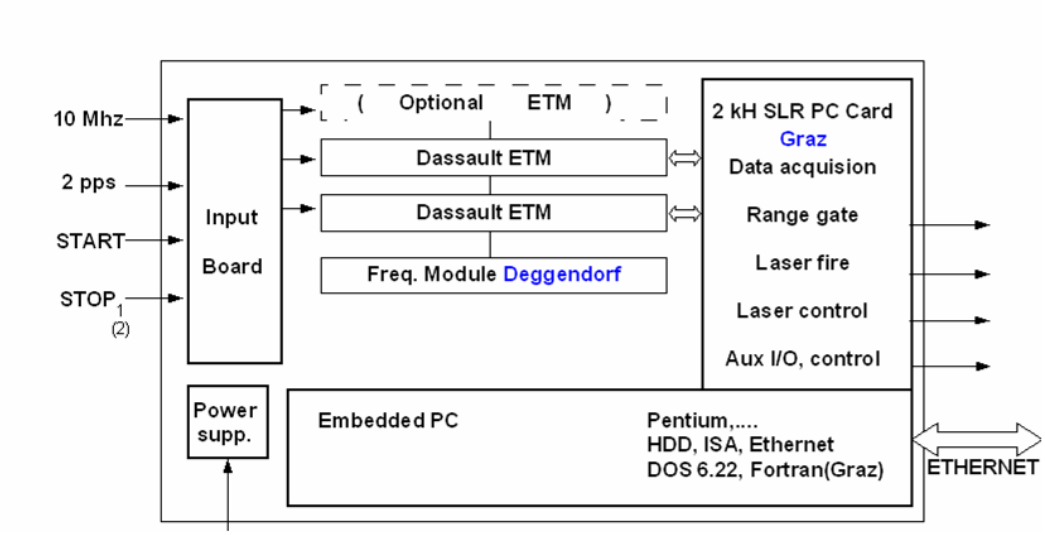

K.Hamal,I. Procházka, Yang Fumin, 15th ILRS Workshop,Canberra,2006

Portable Pico Event Timer and SLR Control (P-PET-C) System

Parametres

timing principle	event timing
timing resolution	1.2 ps
precision	3 ps
timing stability	better than 1 psec / K, / hour
maximum repetition rate	2 kHz
range gate	1 ns steps
	pulses “in space”
	maximum time un-limited
processes under control	epoch and range timing, range gate
	laser fire, laser control
	echo energy monitor interfacing
	T/R pulses collision avoidance
	additional epoch timing devices
	optional I/O
computer	built in, industrial PC
software package	Fortran :-) code, DOS 6.22
	field upgradable
dimension / mass / power	19‘ rack unit, 12‘ high / 30 kg / 200 W

K.Hamal,I. Procházka, Yang Fumin, 15th ILRS Workshop,Canberra,2006

Portable Pico Event Timer and SLR Control (P-PET-C) System

Portable Calibration Standard

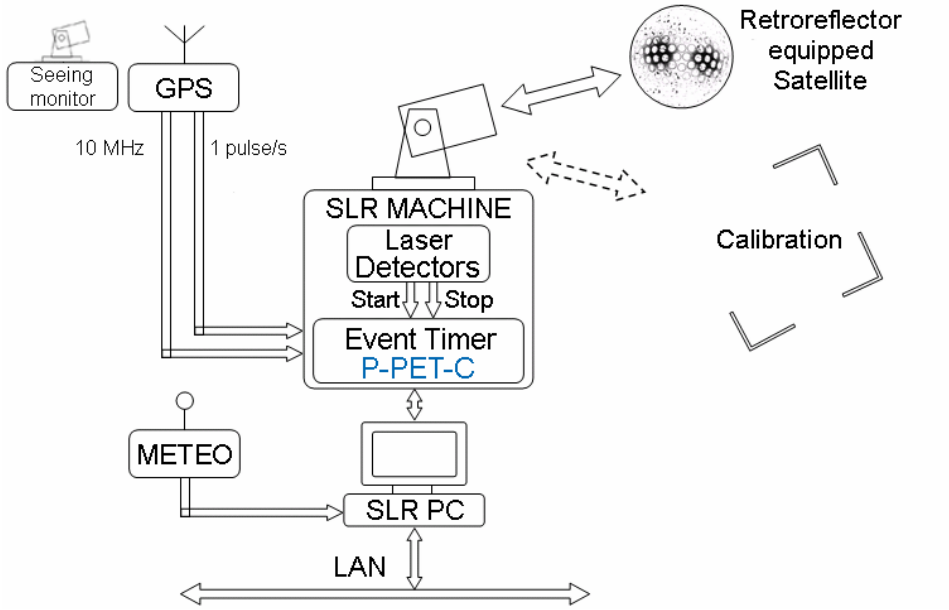

K.Hamal,I. Procházka, Yang Fumin, 15th ILRS Workshop,Canberra,2006

Portable Pico Event Timer and SLR Control (P-PET-C) System

Expected parametres: Equal Graz

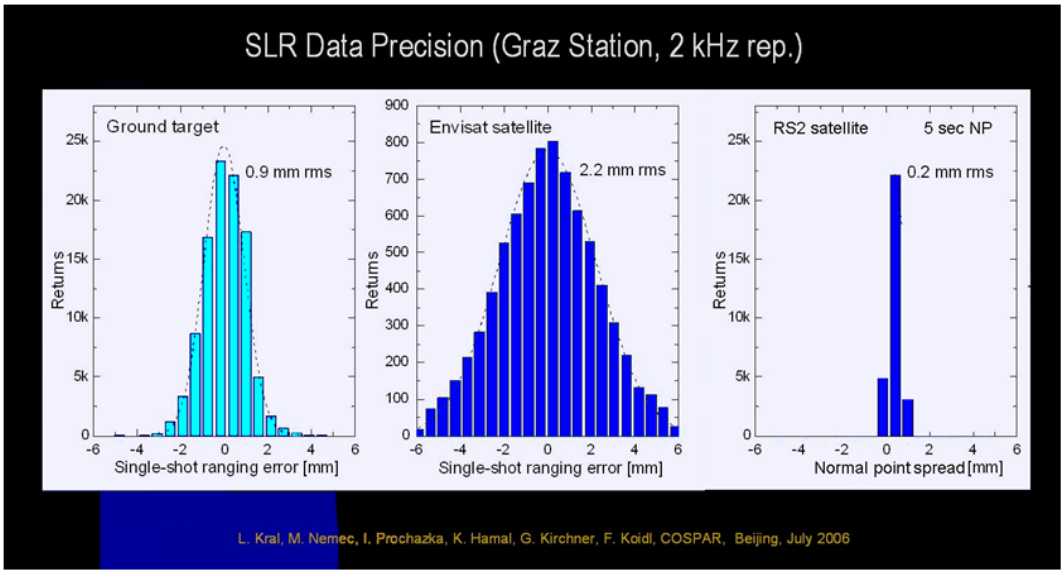

K.Hamal,I. Procházka, Yang Fumin, 15th ILRS Workshop,Canberra,2006

Portable Pico Event Timer and SLR Control (P-PET-C) System

Permanent installations of the PET timing technology

SLR station TIGO operated in Concepcion Chile,

PET4 operational since 1999.

WLRS , Satellite Laser Station Wettzell, Germany

PET4 operational since 1998

8 years no recalibration, no adjustment

K.Hamal,I. Procházka, Yang Fumin, 15th ILRS Workshop,Canberra,2006

Portable Pico Event Timer and SLR Control (P-PET-C) System

Conclusion

- 2kHz
- SLR control system
- Built-in PC
- Portable
- 8 years – no recalibration, no adjustment

- Ground RMS 1 MM Graz
- Satellite ERS2 RMS 2,8 MM Graz
- Normal Point RMS 0,2 MM Graz

- Price

K.Hamal,I. Procházka, Yang Fumin, 15th ILRS Workshop,Canberra,2006

Portable Pico Event Timer and SLR Control (P-PET-C) System

Shanghai indoor test, July 2006

K.Hamal,I. Procházka, Yang Fumin, 15th ILRS Workshop,Canberra,2006

Portable Pico Event Timer and SLR Control (P-PET-C) System

Shanghai outdoor test, July 2006

40W 2J

K.Hamal,I. Procházka, Yang Fumin, 15th ILRS Workshop,Canberra,2006

Some Early Results of Kilohertz Laser Ranging at Herstmonceux

Philip Gibbs, Christopher Potter, Robert Sherwood, Matthew Wilkinson,
David Benham, Victoria Smith and Graham Appleby

1. NERC Space Geodesy Facility, Herstmonceux Castle, Hailsham, UK, BN27 1RN.

Contact: pgib@nerc.ac.uk

Abstract

As part of its support of an upgrade and expansion of capability at the UK Space Geodesy Facility, the UK Natural Environment Research Council has provided funding to enable in-house development of kHz-rate laser ranging at the site. The scientific justification for this upgrade included the expectation of an increase in single shot precision furnished by the much shorter laser pulse-length, an increase in normal point precision from compression of a greater number of raw data points and much more rapid target acquisition via rapid searching.

The upgrade has proceeded in stages. Before we were able to consider kHz ranging we needed an event timing device able to record epochs of multiple events at kHz rates. To this end we built in-house the Herstmonceux Event Timer (HxET), which is based on three modules supplied by Thales. Following completion of HxET in August 2006, the device was thoroughly tested and found to agree with expectations in terms of linearity and precision. With HxET in place we were able to make our first tentative steps by late September into kHz calibration and satellite ranging. This paper presents some of our early problems and successes.

Basic Requirements for Kilohertz ranging

- A kHz laser.
- An event timer to record epochs of laser firing and detector triggering. This must be able to record epochs to an accuracy of a few picoseconds.
- A computer system(s) able to read ET, control the laser, display data and archive the data at kHz rates.
- Software to extract weak return signals from the higher noise levels generated by a C-SPAD running at kHz rates.
- Reduction software that can cope with the new features displayed in kHz data.

kHz Laser

Preparation for a kHz laser system began in 2003 with a visit to the SLR station in Graz, Austria. Graz had at that time recently purchased a kHz laser and was in the process of validating. This visit proved to be exceedingly useful in providing background knowledge necessary for the specification of a laser for the SGF. In 2004 final specifications for the kHz laser system were agreed and suppliers sought. The specification included a final output wavelength of 532nm with a pulse width of 10 – 15 ps at 1 – 2 kHz and a beam quality (M^2) better than 1.5. The ability of the laser to fire at ~10Hz to enable a smooth validation/transition from the old system to the 2 kHz system was also considered important. Other factors needed were the ability of the laser to fire on a shot by shot, variable rate basis under computer control, the ability of all the safety systems (lid locks, door interlocks and radar system) to be able to communicate with and inhibit firing, and the ability of the laser system to recover well after one of the frequent power cuts experienced at the SGF.

Given these specifications, a tender exercise identified two potential systems from High Q Lasers of Austria; one generating a power output of 0.4 mJ at 532nm and the second being capable of 1mJ at 532nm. With these power outputs the link budget calculations, to estimate return rates using a given laser system, were favourable. The following table shows our estimates for the link to the Lageos satellites in daytime, assuming an average amount of cirrus and a horizontal visibility of a poor 8km. The percentage value is the return rate of photons detected by the C-SPAD and the number in brackets is the resultant number of returns per 2-minute normal point:

Elevation	90°	50°	30°	25°
0.4mJ, 2kHz:	20% (12000);	8% (4000);	1% (500);	0.3% (150)
1.0mJ, 1kHz:	50% (15000);	19% (6000);	2% (700);	0.7% (150)

Following these calculations and financial considerations the 0.4mJ system was deemed sufficient but an extra long housing was ordered to enable possible future modification of the laser with an extra amplifier unit.

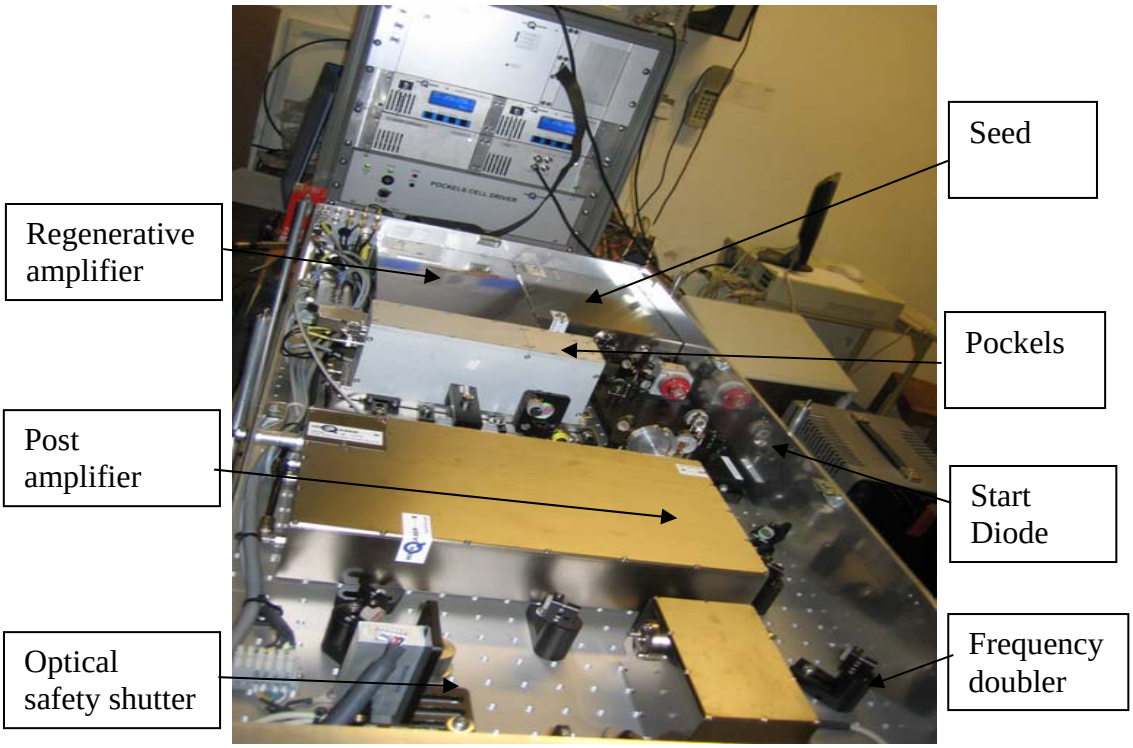

In summary, the specifications for the kHz laser are as follows:

- Nd: Vanadate picoREGEN laser from High-Q Lasers
- Pulse energy 0.5mJ at 532nm at 1kHz
  0.4mJ at 532nm at 2kHz
- Repetition rates of between 10 and 2000 (although large changes may require realignment). To date rates between 100 and 2000 Hz have been used without re-alignment.
- Pulse width is 10ps FWHM at 532nm.
- Upgradeable to >1mJ at 532.
- Firing predictability to 6ns.
- Typical lifetime of pump diode in excess of 10000 hours
- Beam quality – TEM_{00} M^2<1.5

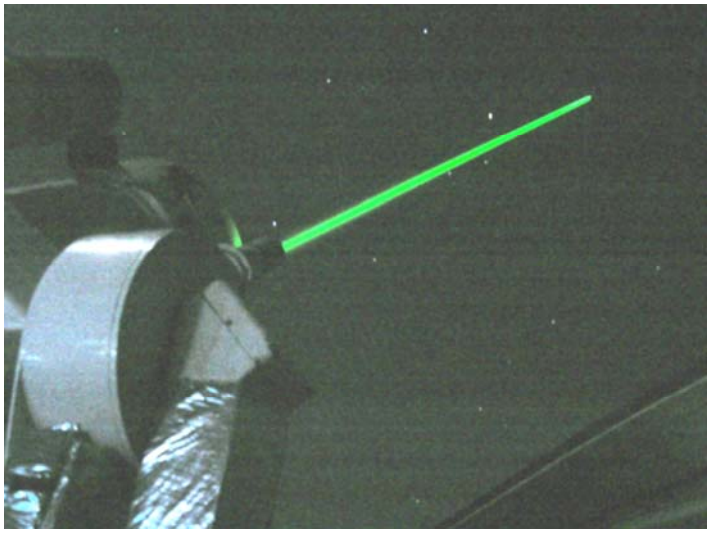

Shown here is a picture of the kHz laser at night

Event timer

A decision was made in 2004 to replace our SR620 timers with a timing system which would be linear across the range of times being measured and also be usable for a Kilohertz system. After investigating various options it was decided to build in-house an event timer with 3 Thales modules (1 clock module and 2 timing modules). The design of HxET included providing power supplies for each module plus some fifteen other power supplies, building an interface between the modules and the ranging computer, the ability to have start and stop signals as either NIM or TTL, and 1pps signal. It also had to include an onboard 1 kHz signal to monitor the difference between the two timing modules. The timer was completed in late July 2006 and ready for use soon after.

Initial tests of HxET using a split signal to the start and stop channels resulted in a total jitter of 7ps. If we assume an equal contribution from both the start and stop channels, this result gives a jitter of 5ps for each, in agreement with the specifications for the modules. Tests were also carried out using HxET to determine the behaviour of our SR620s across the whole timing range from local targets to the GNSS satellites; the results agreed with the results of previous identical tests carried out between PPET and the SR620s (Florence 1998). This we believe shows that there is agreement between PPET and HxET and that HxET is linear across the full range of current timing measurements. This calibration work is the subject of a further paper in these proceedings (Gibbs, Appleby and Potter, 2007).

Computer configuration.

The station computer configuration is as shown below. It comprises a Linux machine that is used to display and archive the data and run the reduction processes. This machine receives in real-time the data from the ranging PC (running under DOS) using TCPIP. The ranging PC communicates with HxET via a Programmable ISA card that was supplied to us by the GRAZ group. The ISA card also controls the Laser and arms the C-SPAD. The ranging PC also controls the telescope tracking, the safety radar, laser beam divergence and an iris in the receive optical path, as well as determining average return rate in real-time and maintaining a single photon return level via a neutral density wheel.

Real Time Display

Recognising that moving to kHz ranging will significantly reduce the signal to noise

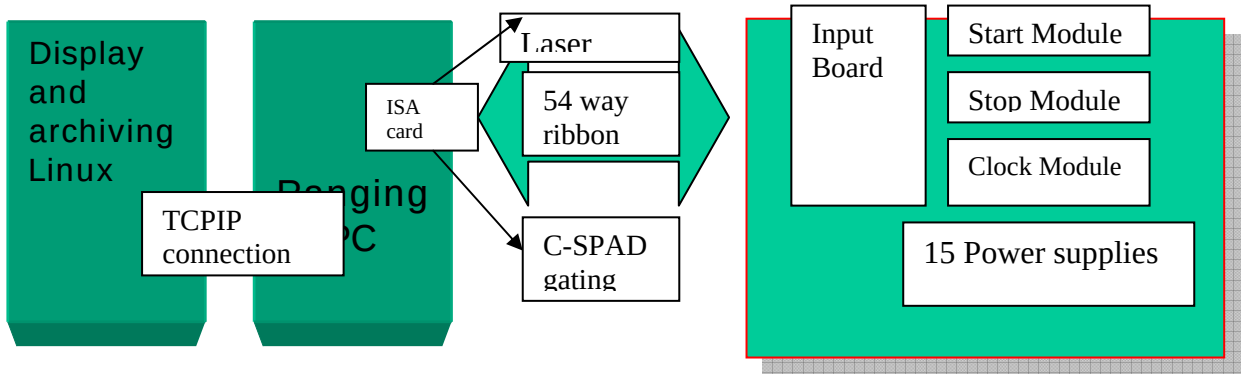

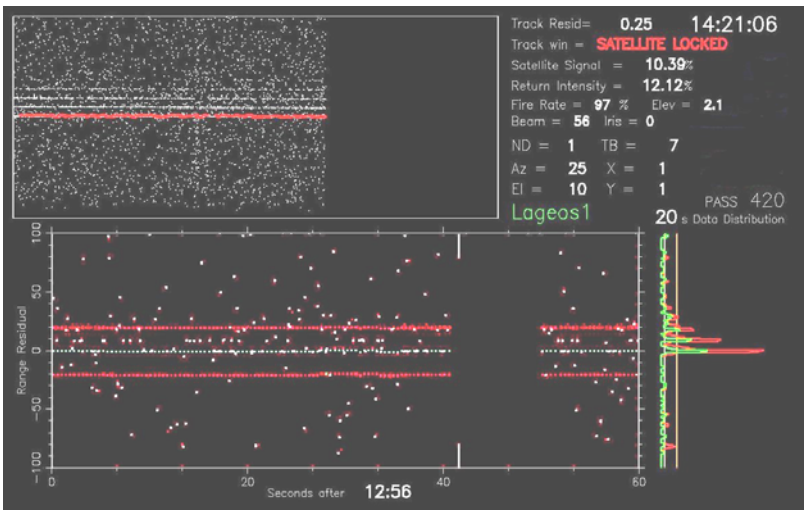

The display process runs on a Linux platform using a TCP-IP connection to the dedicated ranging PC. The display shows long term and short term range gate O-C values as well as a histogram of user defined time span to plot the intensity profile of the data.

ratio of the recorded data, early preparations were made to upgrade the display software. Previously, detection of track in the O-C real-time data within the range gate was aided by the known profile of the semi-train. The high rate data, lack of a semi-train and reduced satellite return signal associated with the low energy laser would make this procedure far more difficult, both for the observer and for the software.

The histogram technique is a very good indicator of the presence and the strength and stability of a satellite return signal and is used for automatic real-time track detection. The technique was developed and implemented for the 13Hz system with the eventual goal of preparing for kHz ranging. The 13Hz laser profile is an initial pulse followed by a significant semi-train, so to avoid tracking the wrong pulse within the semi-train a second histogram was designed in which later pulses are folded in to enhance the initial pulses. This technique exaggerates the first pulse and allows it to be continually tracked. The original (green) and altered (red) histogram profiles can be seen at the bottom right corner of the image above.

A confirmed satellite track is defined by a histogram bin reaching a level of 3-sigma above the background noise in the range gate. Two 3-sigma uncertainties for this track detection are calculated from the instantaneous histogram peaks and from peaks in short blocks of data over the histogram time period. If the satellite signal is strong and stable the software 'locks' onto the track. Once the satellite is locked, the track uncertainties are reduced to 2-sigma and only peaks falling within the newly-defined track window are considered as possible track.

The kHz laser has one dominant pulse and can be tracked with a single histogram. The high firing rate also means that a shorter histogram time span is sufficient, but additionally the histogram can pick out a weak intermittent track if it is given a longer

time span. From experimentation the software can lock on to a 1% satellite return signal with a 3 second time span and lock onto a 2% signal with a 2 second time span.

First Results

Testing of HxET and a full range of comparison tests between HxET and the SR620s were completed in late September 2006. Once completed, we designed the simplest possible software/hardware package that would enable us to obtain some high-rate satellite data as quickly as possible. To this end we simply used a pulse generator to fire the laser at approximately 2kHz. This simple system meant that we had no 'collision' control and as a result periods of high noise can be seen clearly in the data displayed below. We also did not attempt automatic control of return level (although manual control was still available) – in truth we were just happy to see that we were getting data. After just one week we had a software package that could collect data at kHz rates without any losses and then tried observing both in daylight and at night.

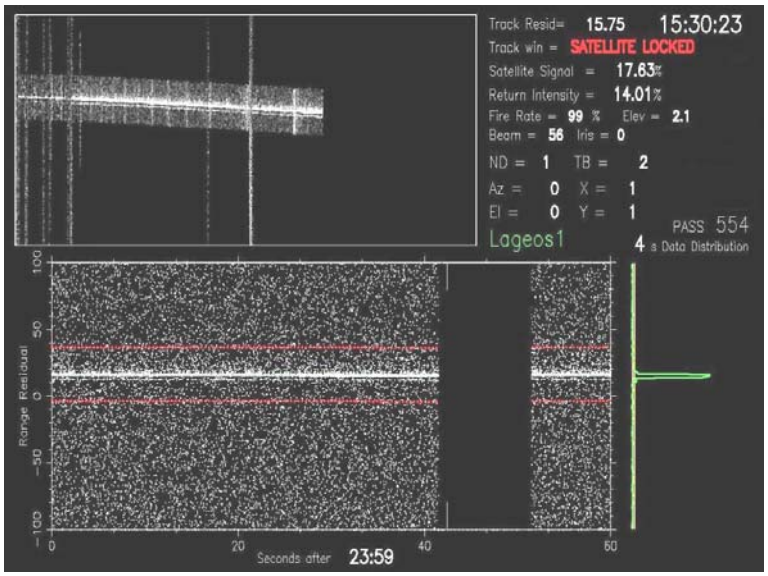

The long-term range gate displays the entire pass, as seen in the image at left. At high repetition rate this window becomes filled with noise points that mask any true track. However, by introducing a grayscale contrast for intensity of points, the track is revealed. This is a very powerful addition to the kHz tracking display, complementing the new histogram-based track determination.

During the daytime we were able to track successfully all satellites from Lageos' heights and lower except for Champ and Grace. At night we were able to range to all the ILRS satellites, again except Champ and Grace. These exceptions were caused by a software problem which has subsequently been solved.

One of the first things that was noticed was that many more noise events were detected than had been expected; initial tests indicated a noise increase of about a

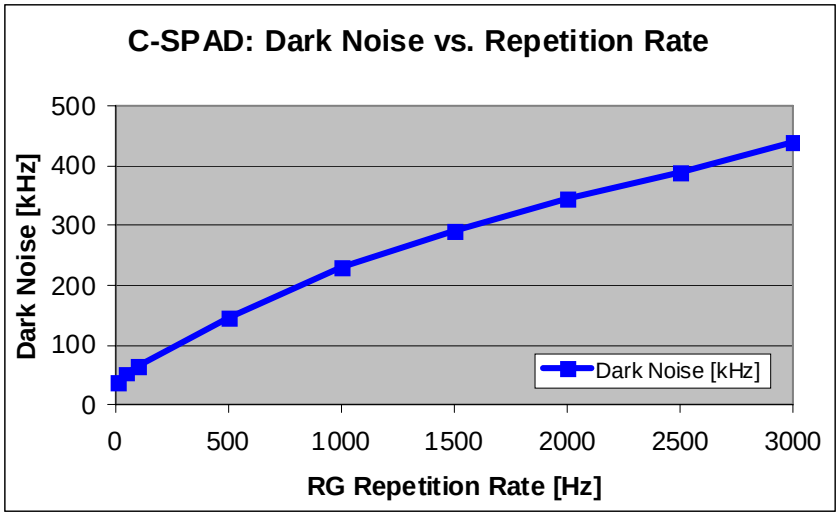

factor of 7 between tracking at 10Hz and at 2kHz. This appears to be due to an increase of dark noise in the C-SPAD as a function of arming rate. This effect had been discovered and quantified by the Graz group, and below is a plot provided by Graz of their results for C-SPAD noise vs. repetition rate.

To estimate the effect this increase of noise would have on our system we examined a histogram of noise collected at 2kHz.

Results from LAGEOS

Shown below is a plot of range O-C for Lageos-2 from October 4th 2006. Present is a number of interesting features. Clearly seen are the 'collision' periods when there are overlaps between incoming return pulses (C-SPAD gated on) and spurious detections of backscatter from outgoing laser light. Also apparent are pre-pulses and spurious other pulses because at the time of the observation the laser pockels cell was not optimally tuned. The uppermost O-C track represents the primary return signal.

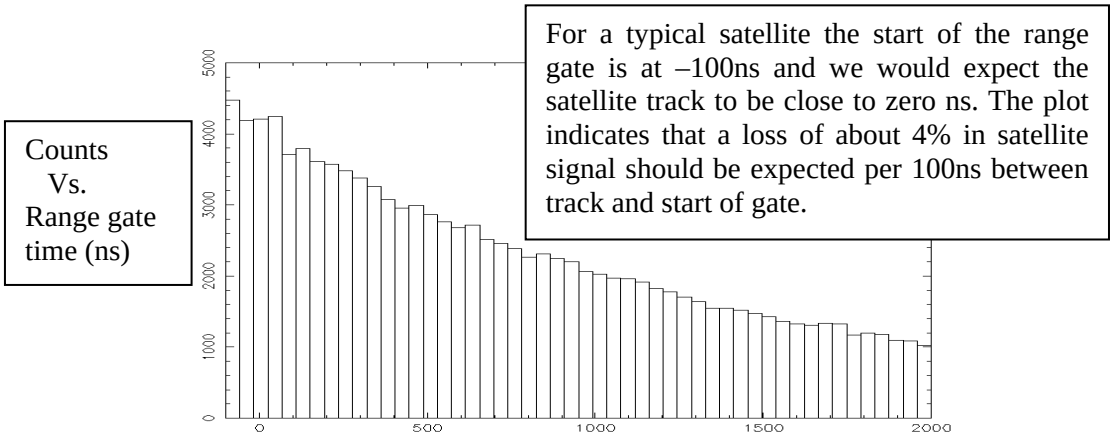

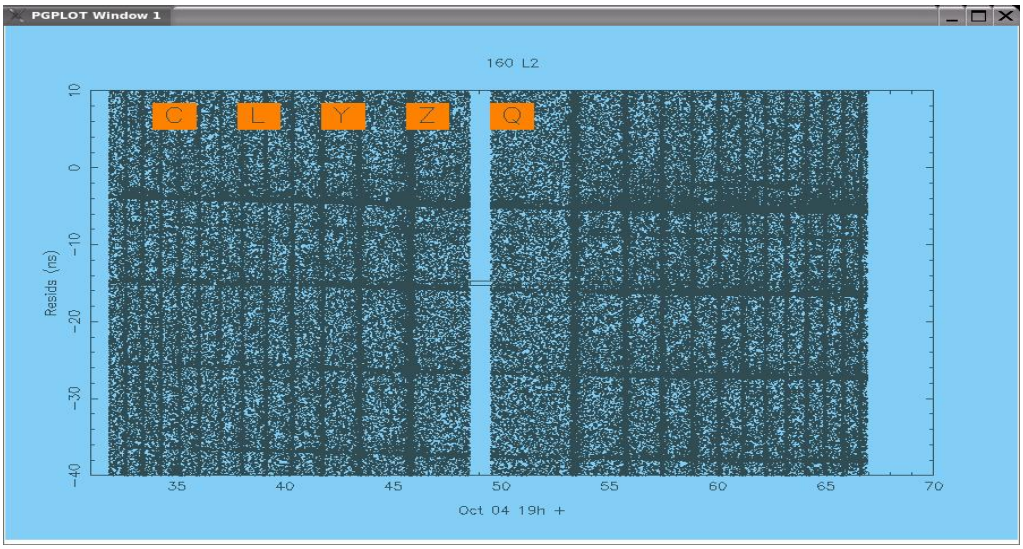

Having collected kHz data the next step was to use our current 10Hz reduction system to check whether there are any significant differences in the data, primarily in systematic effects that may compromise its quality.

The current reduction system comprises the following steps:

1. Extract a data set by a combination of linear and polynomial fitting to the raw O-C data. A minimum limit to the data set of ±0.75ns about the zero mean is imposed by the software to prevent the reduction being biased by the observer.

2. Fit an orbit to the extracted data, iteratively rejecting residuals at a 3-sigma level;
3. Remove this orbit from the entire raw data set and reject at 5-sigma level (yes 5);
4. Fit a smoothing function to this data set, rejecting at 2.5-sigma, using the routine DISTRIB that was produced and made widely available by A. Sinclair (SLRmail 0008).

Extraction of Data.

Below is a plot of the initial data set from which the observer will select the data to be passed to the orbital solution.

Gaussian Fit

Having selected the data as shown in the above plot an orbit is fitted to it. The orbit is then removed from the whole data set and residuals rejected at 5-sigma. We then need to know if this data set is different for the 10Hz and kHz systems

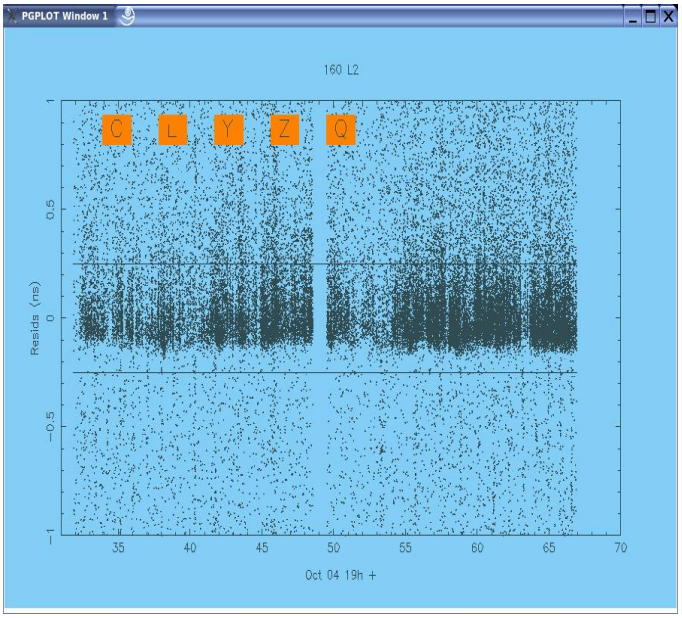

With the increase in background noise apparent at kHz rates it was felt that keeping at least ± 0.75ns of data would introduce too much noise in the preliminary signal extraction. We are currently experimenting with a reduced restriction of ± 0.25ns as shown in the plot, although the observer has the option of overriding these limits. In fact, better predictions, better software and higher-precision data means there is much less scatter in the residuals.

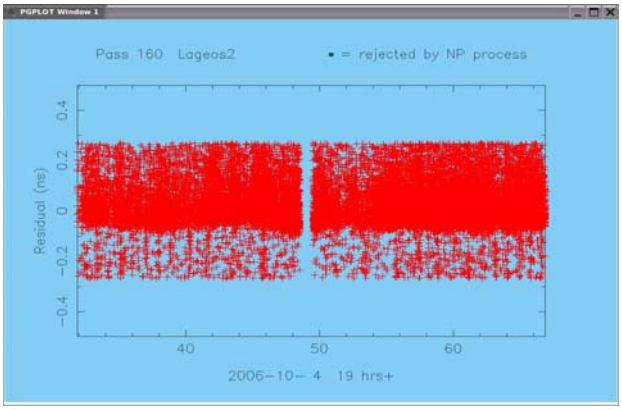

Pictured here is the data set after removing a best-fit orbit and rejecting residuals at a 5-sigma level. Apparent is a “significant” amount of noise below the track and some structure above the track. But is this behaviour significantly different to our current system?

At first glance it would appear that our reduction process is producing the same results for Lageos from both systems, but we have started a more detailed analysis in order both to define a robust reduction process and also to derive an accurate centre of mass correction. Previous work (Otsubo and Appleby, 2003) found that uniquely for the Herstmonceux single-photon system a Lageos centre of mass correction (CoM) of 245mm should be applied (cf 251mm for high-energy ILRS systems). It is important that once our new kHz data becomes available to the analysis community that we have also determined an accurate CoM correction, which may well be a few mm

different from the current 10Hz value. This ongoing work will be reported elsewhere, but the plot below shows the result of an initial investigation of the detailed post-reduction O-C distribution. The rapid rise of the leading edge is as expected and is a result of the short pulse length of the kHz laser, as suggested in the discussions above.

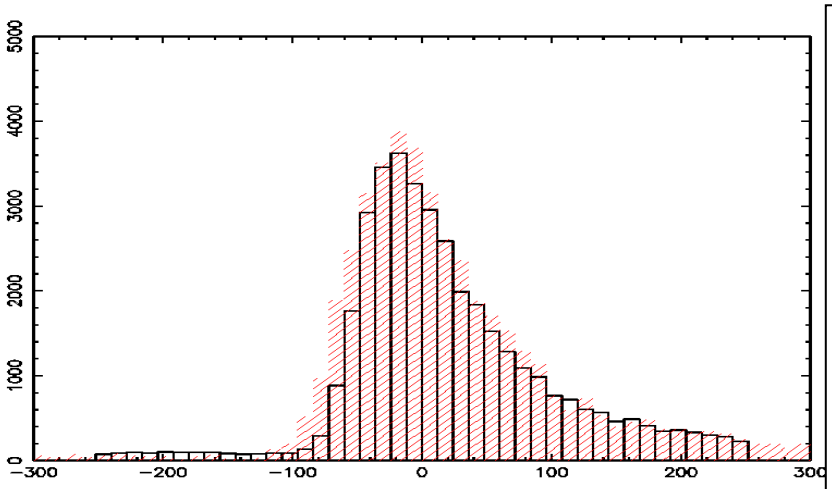

The distribution of the residuals from the two systems is very similar since the Lageos response dominates. As expected, the 10Hz data appears to be slightly broader as the timer and laser contributions are larger:

10Hz: 35ps for SR620
100ps for laser

KHz: 7ps for HxET
10ps for laser

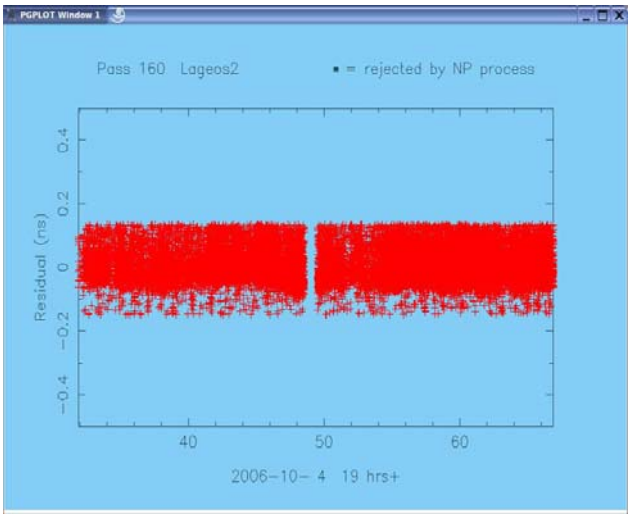

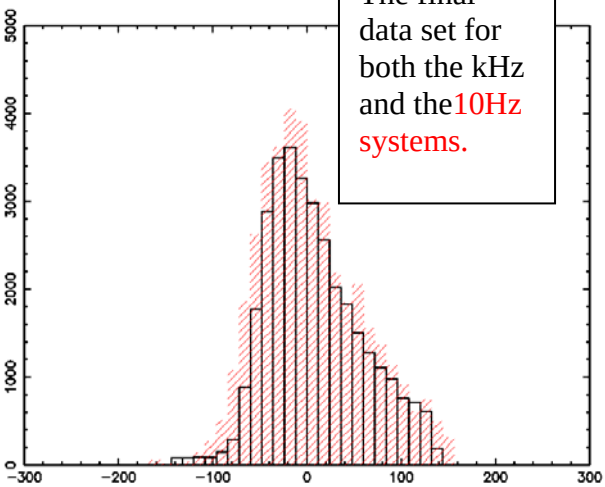

The final data set for both the kHz and the10Hz systems.

Shown above is the final data set for Lageos. There is clearly some noise below the track and the sharp cut off of dense data above may well have removed real observations.

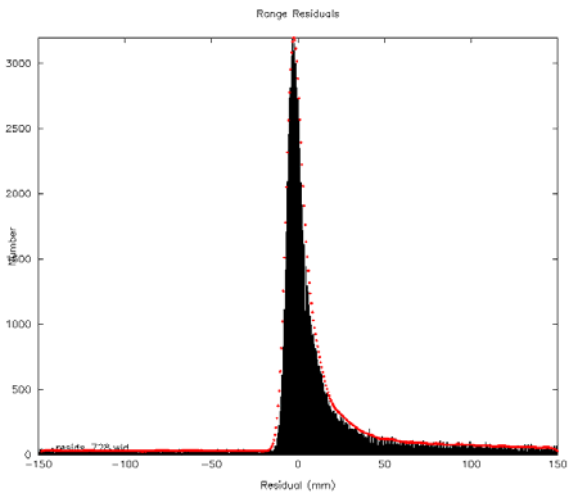

The smoothing function fitted to the distribution is shown in red, and will be used in an asymmetric filtering process to remove primarily leading-edge noise and in a model to determine an accurate CoM value.

Results from a small-array satellite (ENVISAT).

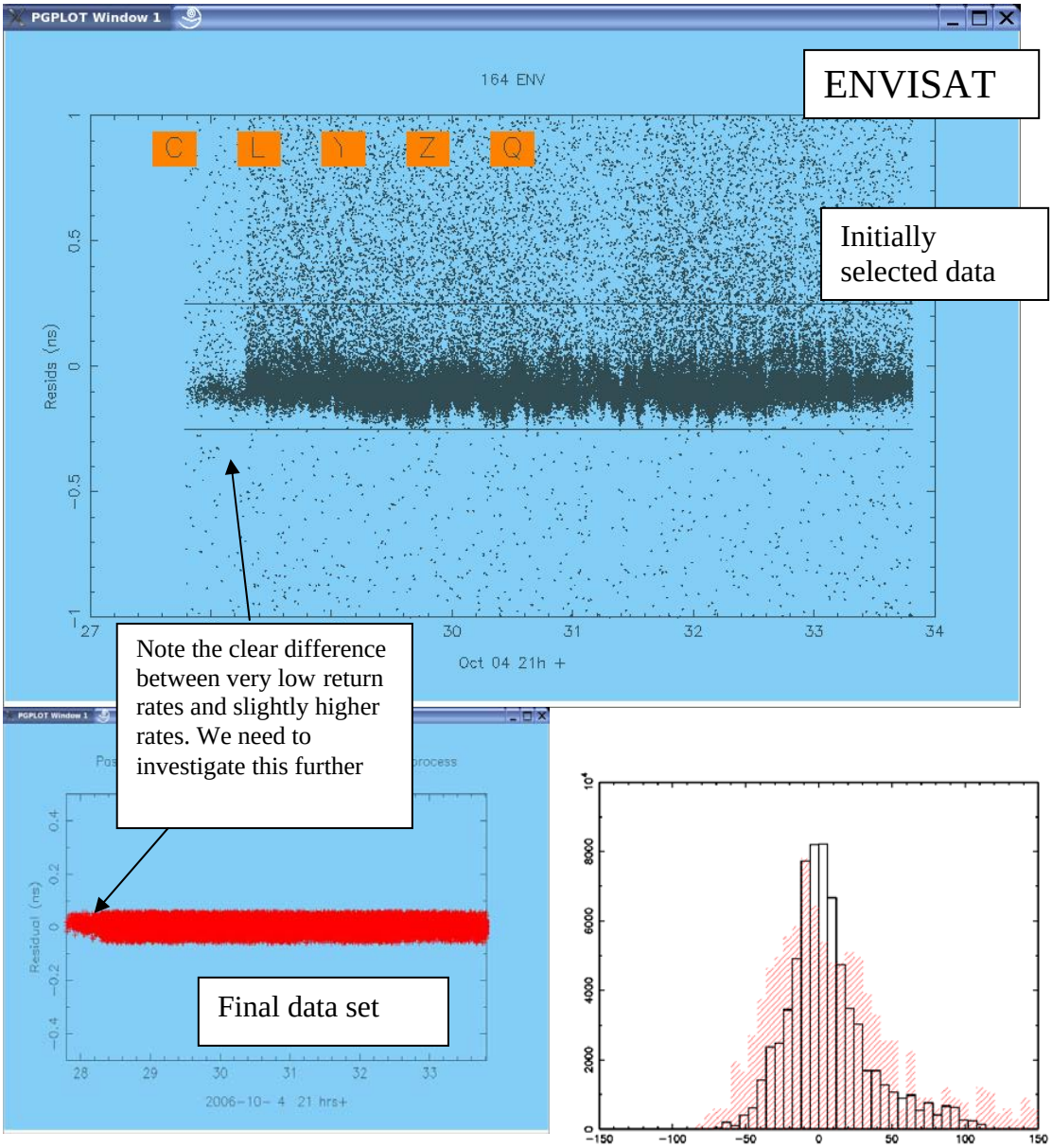

Conclusion

The SLR system at the UK Space Geodesy Facility is at an advanced stage of upgrade to kHz repetition rates, and incorporates a very accurate event timer. Paramount in the upgrade plans is that on-site reduction of the new data should not introduce any discontinuity into the long series of high quality laser data from the site.

Acknowledgement

We would like to thank the staff of the Institut for Space Research, Observatory Lustbuehel at Graz, Austria for their help and encouragement during the development of our kHz system at Herstmonceux.

References

[1] Gibbs, P., Appleby, G.M. and Potter, C.P., 2007. A re-assessment of laser ranging accuracy at SGF, Herstmonceux; *these proceedings*.

[2] Otsubo, T. and Appleby, G.M., 2003. System-dependent centre-of-mass correction for spherical geodetic satellites, JGR, vol. 108, doi:10.1029/2002JB002209.

Performance of a Liquid Crystal Optical Gate for Suppressing Laser Backscatter in Monostatic Kilohertz SLR Systems

John J. Degnan and Daniel Caplan

1. Sigma Space Corporation, 4801 Forbes Blvd., Lanham, MD 20706 USA.

Contact: John.Degnan@sigmaspace.com / Fax:+01-301-577-9466

Abstract

Some of the unique blocking features required by SLR2000 included a large aperture (15 mm), arbitrary polarization returns, a rapid 2 kHz cycle time, long and flexible blocking periods (up to 10% of each 500 microsecond interval between pulses), and adequate switching speeds to minimize data loss. After evaluating numerous potential approaches to optical gating, we determined that the use of a liquid crystal optical gate (LCOG) afforded the best overall protection. We have successfully implemented a 2 kHz LCOG which provides a 50 microsecond "blocked" interval, a 450 microsecond "unblocked" interval, a 10 microsecond rise and fall time on the blocking interval, approximately 90% transmission in "unblocked" mode, and a 659:1 reduction in backscattered radiation in "blocked" mode. Furthermore, the LCOG adapts readily to time shifting of the outgoing pulse.

Introduction

Since SLR2000 operates at a 2 kHz fire rate, multiple pulses are in the air at all times and, at various times within a given satellite pass, reflected signal photons arrive at the SLR2000 telescope at the same time a subsequent transmitted pulse is exiting the system. We refer to these events as "collisions". Since the range gate is open for some period surrounding the expected signal arrival time, the sensitive detector is exposed to backscattered laser radiation from both the instrument and the local atmosphere while in a high gain mode. In principle, backscatter from the atmosphere can be observed for up to 10% of the 500 microsecond laser fire interval. During this time, backscattered photons can cause significant charge transfer from the photocathode to the anode and, since the lifetime of a photocathode is dependent on the number of coulombs transferred, unsuppressed laser backscatter is a potentially life-limiting mechanism. In addition, since SLR2000 is designed to correct telescope pointing by balancing the photon returns in the four ranging detector quadrants, we believe that backscattered photons can interfere with the performance of the pointing correction algorithms by biasing the pointing error in the direction of the transmitter point ahead.

The quadrant segmented anode microchannel plate photomultiplier (MCP/PMT) in SLR2000 has recently been upgraded in order to achieve a factor of 3 to 5 improvement in detection efficiency and sensitivity. The bialkali photocathode tube built by Photek Inc. has been replaced by a significantly more expensive Hamamatsu tube with a less mature but higher efficiency (30% to 40%) GaAsP photocathode. In order to protect the tube from backscattered laser radiation and extend photocathode life, SLR2000 incorporates two design features. The first feature involves periodically changing the laser repetition rate to avoid "collisions" between outgoing pulses and incoming signal photons. This eliminates backscatter during the most critical period when the detector is gated "on", minimizes data loss, and helps to prevent corruption of the quadrant detector pointing correction. We have recently investigated the inclusion of an optical gate which acts as a second layer of defense by

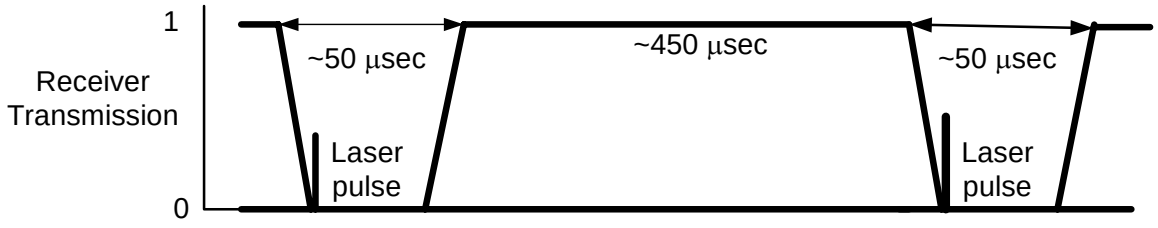

Figure 1. *Performance of the ideal optical gate for suppressing laser backscatter in SLR2000 operating at a 2 kHz rate.*

suppressing backscatter impinging on the photocathode even during less critical times when the detector is gated "off". The ideal performance of the "ideal optical gate" is illustrated in Figure 1. To minimize loss of signal while providing maximum protection, a successful optical gate in SLR2000 must possess the following characteristics:

- Operate at SLR2000 2 kHz laser fire rate,
- Accommodate the 13 mm receiver beam diameter on the optical bench,
- Block atmospheric backscatter for up to 50 microseconds following laser fire,
- Provide high backscatter extinction in blocked mode,
- Provide high signal transmission in unblocked mode,
- Provide a fast transition between blocked and unblocked modes,
- Accommodate variable fire rate used to avoid "pulse collisions",
- Can take advantage of linearly polarized light in two SLR2000 receiver channels if necessary.

We considered various approaches to optical gating including mechanical, electro-optical, acousto-optical, and liquid crystal and rated them with respect to transition speed, aperture, transmission, and ability to provide a long "open" mode. Liquid crystal gates were found to have the best overall performance with electro-optical being deemed less appropriate due to the need to maintain high voltages on the crystals for long periods of time. Our conclusions are summarized in Table 1.

Table 1. *Comparative performance of various optical gating approaches.*

Gating Approach	**Speed**	**Aperture**	**Transmission**	**Gate Duration**
Mechanical	Poor	Poor	Excellent	Poor
Electro-optic	Excellent	Good	Good	Poor (2-3 kV)
Acousto-optic	Good	Poor	Fair	Good
Liquid Crystal	Good	Good	Good	Good ($\pm$30V)

Experiment

The Liquid Crystal Optical Gate (LCOG) takes advantage of the fact that, in SLR2000, the received signal is split based on polarization. This is a consequence of our unique passive Transmit/Receive switch which permits the transmitter and receiver to share the entire telescope aperture simultaneously while experiencing low loss in either path [Degnan, 2004]. In a typical configuration, the LCOG normally acts as a time dependent polarization rotator placed between two crossed polarizers. The first polarizer defines the input polarization. Relatively low voltage (< ±30 VDC) waveforms applied to the crystal align the liquid crystals and rotate the propagating light in a time dependent manner. The action of the second polarizer on the rotated light creates the time varying transmission function of the gate.

As will be described later, the current SLR2000 receiver configuration uses uncrossed polarizers in each receiver leg although crossed polarizers could be employed with a relatively minor design change. For this reason, we conducted our laboratory tests with both crossed and uncrossed polarizer pairs. The signs of the waveform voltages were chosen accordingly to approximate the performance of the ideal gate depicted in Figure 1. Figure 2 provides a block diagram and photo of our test setup.

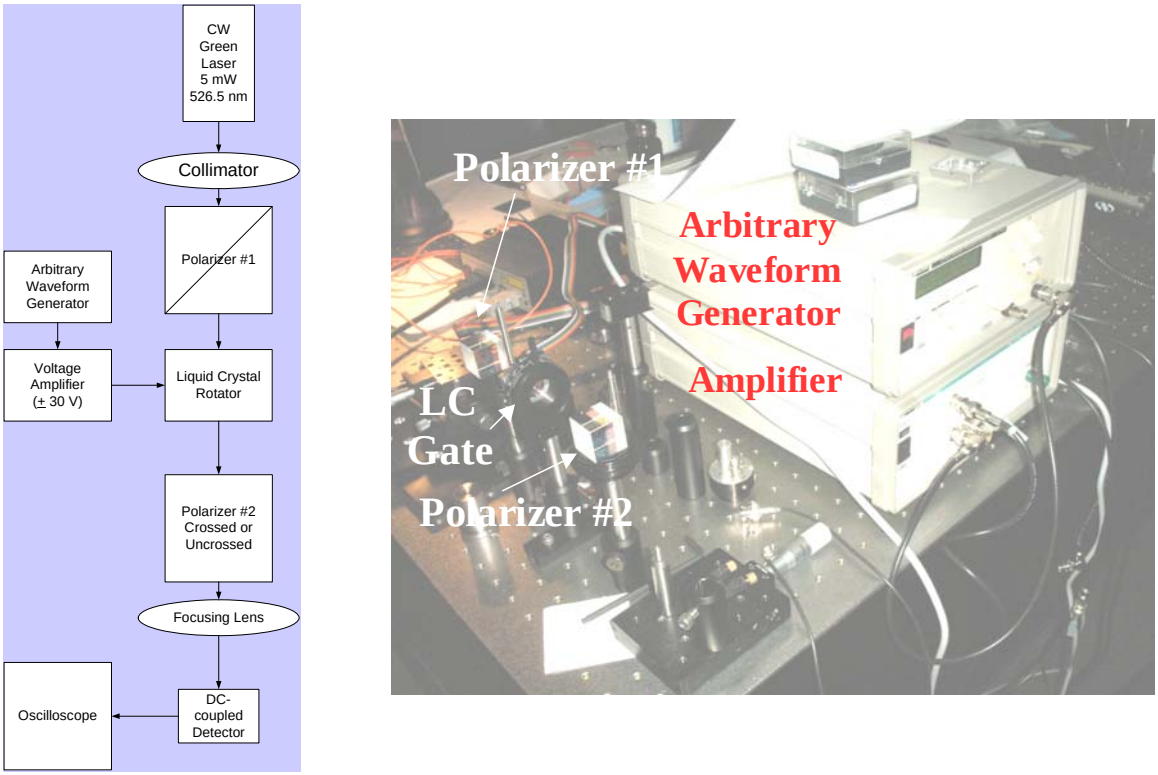

Figure 2: *Block diagram and photo of the laboratory test setup.*

The required waveform was programmed into a high bandwidth Arbitrary Waveform Generator (AWG) and iterated to best approximate the ideal transmission function. The low voltage output of the AWG was amplified to the required ± 30VDC by a separate amplifier module and applied to the flying leads of the Liquid Crystal Rotator manufactured by Boulder Nonlinear Systems, Inc. . Collimated light from a CW green laser was passed through the LCOG and focused onto a DC-coupled detector whose output was displayed on an oscilloscope. Prior to inserting the Liquid Crystal Rotator (LCR), the extinction of the crossed CVI cube polarizers was measured to be 6222:1 in reasonable agreement with the specified value of 10,000:1 and demonstrated the

sensitivity of our measurement approach. A summary of the peak optical gate transmissions and extinctions obtained with different polarizer combinations is given in Table 2. Not surprisingly, the best extinction of 659:1 during "closed" periods was obtained with the normal crossed polarizer configuration whereas the P/P and S/S configurations, corresponding to the current SLR2000 receiver configurations (see Figure 4), provided significantly poorer extinctions of 164:1 and 82:1 respectively. The transmission of the gate during "open" periods was comparable in all cases, varying over a narrow range between 89.3% and 92.1%.

Table 2. *Summary of experimental transmissions and extinctions for various configurations of crossed and uncrossed polarizers.*

Polarizer 1	Liquid Crystal Gate	Polarizer 2	Transmission (gate open)	Extinction (gate closed)
P	No	S	NA	6222:1
P	Yes	S	89.3%	659:1
P	Yes	P	91.3%	164:1
S	Yes	S	92.1%	82:1

Temporal waveforms obtained for the gate with crossed polarizers, as registered in different channels of the oscilloscope, are shown in Figure 3. The "optimized" drive voltage waveform to the LCR, corresponding to the orange curve, is being repeated at the 2 kHz rate of SLR2000. The purple curve, corresponding to the optical detector output, is a good approximation to the "ideal" transmission waveform in Figure 1, where the gate is closed for 50 microseconds and open for 450 microseconds and shows a fast transition between the two states (< 10 microseconds). The upper green curve is the purple curve viewed at high resolution and clearly shows the rapid reversal in the transmission trend as the drive waveform voltage to the LCR changes sign.

It is worthwhile to point out certain required characteristics of the drive waveform. The integral of the waveform over one cycle must equal zero, i.e. the positive area under the waveform must equal the negative area. If the average is not zero, any ions present in the liquid crystal will migrate to the surfaces resulting in a build-up of charge. This will effectively keep the liqud crystal pinned in that state [Bauchert, 2004]. Furthermore, during the "open" mode, one must apply a slight residual positive voltage (~2 to 3V) which holds the molecules in their transmissive state and prevents them from becoming randomly oriented and thereby reducing the transmission when the switch is "open". The width of the blocking gate is determined by the combined widths of the positive and negative going pulses. Because of the zero integral

condition over the full 500 microsecond cycle, the temporal width of the negative drive pulse is necessarily less than that of the positive pulse.

Integration into SLR2000

Figure 4a shows the current SLR2000 receiver configuration where the incoming light is split into s and p polarizations and then recombined on a final polarizer before impinging on the quadrant MCP/PMT. Note that, without the LCR, the polarization of the light is preserved during recombination at the final polarizer. Thus, using the results in Table 2 for uncrossed polarizers, one can project a mean transmission of 91.7% for the open gate and a mean extinction of 123:1 for unpolarized light entering the receiver. Significantly better performance is obtained if a mirror is placed to the left of the combining polarizer as in Figure 4b and the drive voltages to the LCR are reversed. The expected extinction rises significantly to 659:1, and the transmission decreases only slightly to 89.3% for unpolarized input.

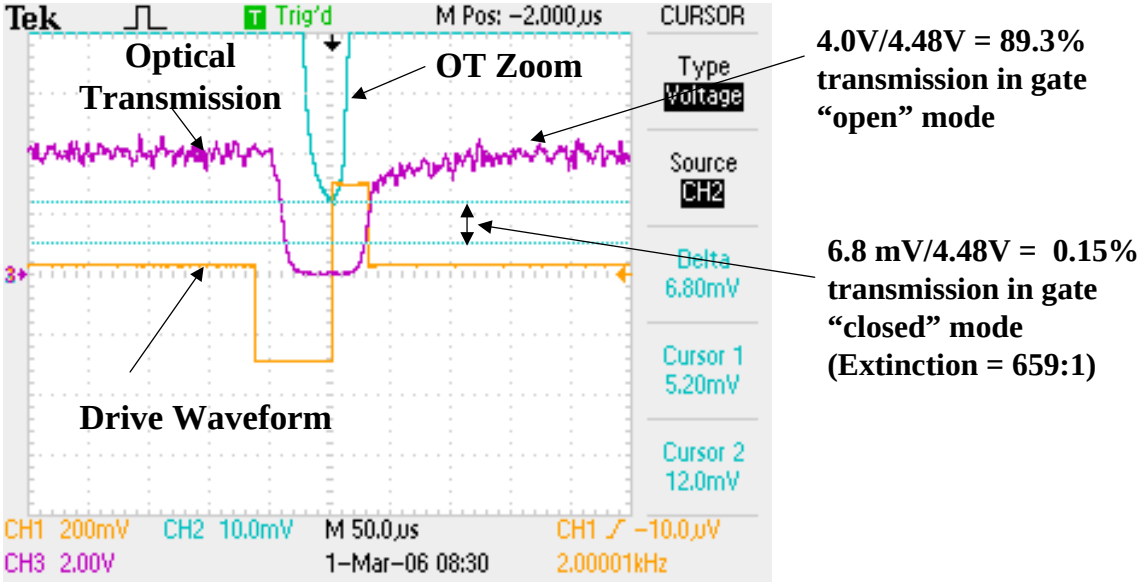

Figure 3: *Oscilloscope traces obtained during transmission/extinction experiments with the normal crossed polarizer configuration. The drive waveform to the LCR is indicated by the orange trace. The purple trace gives the optical transmission from "open" to "closed to "open". The narrow green trace at the top of the figure is a high vertical resolution version of the purple trace and shows the rapid reversal in the optical transmission trend at the point where the sign of the applied LCR voltage is suddenly reversed.*

Summary

We have demonstrated that liquid crystals, when used as a 90^{o} polarization rotator between two cube polarizers, can:

- reduce the amount of laser backscatter by 2 to 3 orders of magnitude in the "closed" state while exhibiting high transmission (~90%) in the "open" state,
- operate at few kHz rates,
- handle large aperture beams (~15 mm),
- switch states in less than 10 microseconds with low voltage (<$\pm$30V),
- produce flexible gate waveforms of arbitrary shape and duration,
- work in tandem with variable laser fire rates to avoid "collisions" between incoming and outgoing pulses.

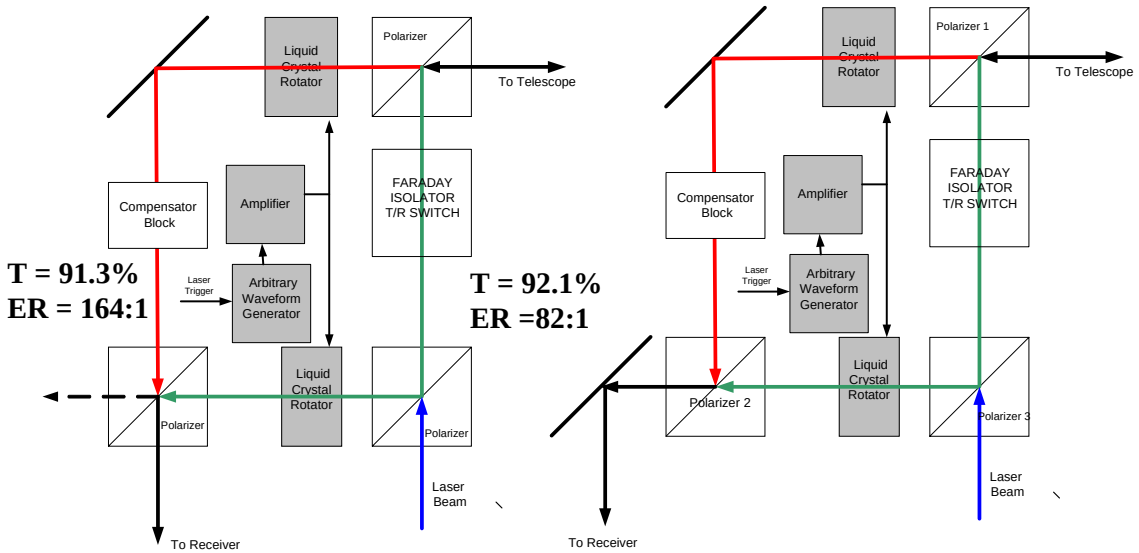

Current SLR2000 Configuration Uncrossed Polarizers (average) T = 91.7% ER = 123:1	Better Configuration Crossed Polarizers T= 89.3% ER = 659:1

Figure 4: *(a) With LCR's installed in both legs of the current SLR2000 receiver and unpolarized signal, the mean transmission and extinction would be 91.7% and 123:1 respectively; (b) a minor modification of the SLR2000 receiver configuration would result in 89.3% transmission and 659:1 extinction.*

We close with certain precautions in the use of these devices. The liquid crystal medium is sandwiched between two optical substrates. Care must be taken when mounting the LCR's to avoid stressing the delicate interface. The voltage to the unit must not exceed the $\pm$ 30VDC maximum or serious damage to the interface may result. Also, as mentioned previously, in designing the drive waveform, the voltage over one repetition cycle must average to zero.

References

[1] Bauchert, K., Boulder Nonlinear Systems, private communication, 2004.

[2] Degnan, J., "Ray Matrix Approach for the Real Time Control of SLR2000 Optical Elements", Proc. 14th International Workshop on Laser Ranging, San Fernando, Spain, June 6-10, 2004.

SLR 2000: The Path toward Completion

J. McGarry, T. Zagwodzki

1. NASA / Goddard Space Flight Center.

Contact: Jan.McGarry@nasa.gov

Abstract

After years of programmatic and technical issues, SLR2000 is finally receiving the manpower and money needed to solve the final technical challenges. This paper describes the progress that has been accomplished over the past year and discusses the final steps that we will take in the coming year to make the system operational.

Introduction

SLR2000 is the prototype for NASA's Next Generation of Satellite Laser Ranging (SLR) Systems. It was originally designed to be completely automated, eye-safe, with a lower cost of operation, a high reliability, and an accuracy comparable to the existing NASA MOBLAS systems [Degnan(1)]. After many years where funding was low, in 2006 SLR2000 development was given a higher priority and more funding.

Much progress has been made in the last year. The system is now tracking low earth orbiting (LEO) and LAGEOS satellites, able to acquire and track most LEOs relatively easily, although the returns are not yet optimized. The system timing, pointing and ranging capability, and accuracy have been tested using MOBLAS-7 return pulses. The software is more robust and the system is more repeatable. We believe that the system is within a year of final collocation with MOBLAS-7.

Recent system developments.

An optical shutter was designed and built by SigmaSpace and installed in the system to reduce the laser backscatter on the detector [Degnan(2)]. In a single telescope common optics transmit-receive system the photomultiplier tube (PMT) is exposed to a significant amount of laser backscatter within its field of view (FOV) as the pulse leaves the system. Even though the PMT is gated off during the laser fire this illumination stresses the photocathode and may shorten its lifetime. Mechanical choppers or shutters were investigated but deemed too problematic for operation at 2 KHz. The solution was an optical shutter in the form of two liquid crystal (LC) polarizing filters, one installed in each leg of the transmit-receive switch which reduce the backscatter by two orders of magnitude (Figure 1).

A new higher quantum efficiency (QE) quadrant PMT was installed in the system. The comparison with the previous detector is shown in the following table.

	Photek(PMT210)	Ham(R4100U- 74-M004C)
MCP stages	2 plates	2 plates
Active diameter	10mm	6mm
Photocathode	S20	GaAsP
Q.E.*	12%	33%
DC current Gain	1×10^6	2.6×10^5
PMT HV bias	-4700V (nom.)	-2250V (nom.)

The relative sensitivity improvement of the Hamamatsu tube over the Photek tube was estimated during an Etalon track to be approximately 5:1. Additional loss in Photek

sensitivity is surmised to be due to aging or degradation of the photocathode over many months of SLR operation.

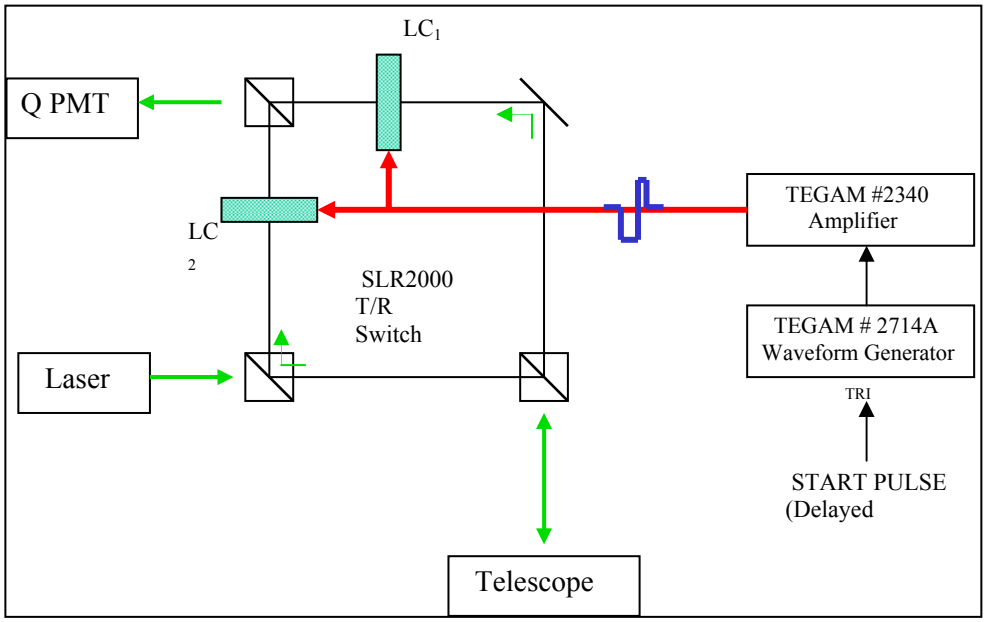

Figure 1: *Optical bench with Liquid Crystal Shutter in both legs of T/R switch*

A laser beam expander was replaced in the system to both control the laser divergence and to give adequate knowledge of the divergence setting. This expander was designed and built by SigmaSpace [Degnan(3)]. Originally the laser transmitter beam divergence could not be adjusted without de-focusing the common beam expander for the receiver. The resultant FOV change in the receiver adversely effected control of background noise and vastly complicated tracking. The solution was to develop a beam expander mechanism which operates solely on the laser transmit beam (independent of the receive path) and which could be focused to accommodate the 10 to 30 arcsecond (full angle) desired beam width.

The Risley prism laser point-ahead optics are now operational in the system [McGarry]. The Risley wedge pair is used to steer the transmit beam ahead of the telescope receive path and put the center of the transmit laser beam directly on the target. The telescope can then be pointed behind to center the receive FOV about the return light. This then allows the FOV to be closed to 10 arcseconds, which reduces the optical noise and allows use of the quadrant detector information to correct the telescope pointing. The Risley optics have successfully undergone testing with an off-line software package. The operational software package interface to the Risleys will be verified in the next few months.

The software now controls the Laser Pulse Repetition Frequency (PRF) to avoid fire/return collisions [Titterton]. This is needed due to the common optics design of the system. Only two different fire intervals are needed for any of the ILRS tracked satellites. The values of the two fire intervals are dependent upon altitude:

- Low Earth Orbiting (LEO): 500 and 510 microseconds
- LAGEOS: 500 and 502 microseconds
- High Earth Orbiting (HEO): 500 and 501 microseconds

The PRF switching is currently being successfully used in all satellite ranging. Figure 2 shows how the laser PRF changes during the course of a LEO (left plot) and LAGEOS (right plot) pass.

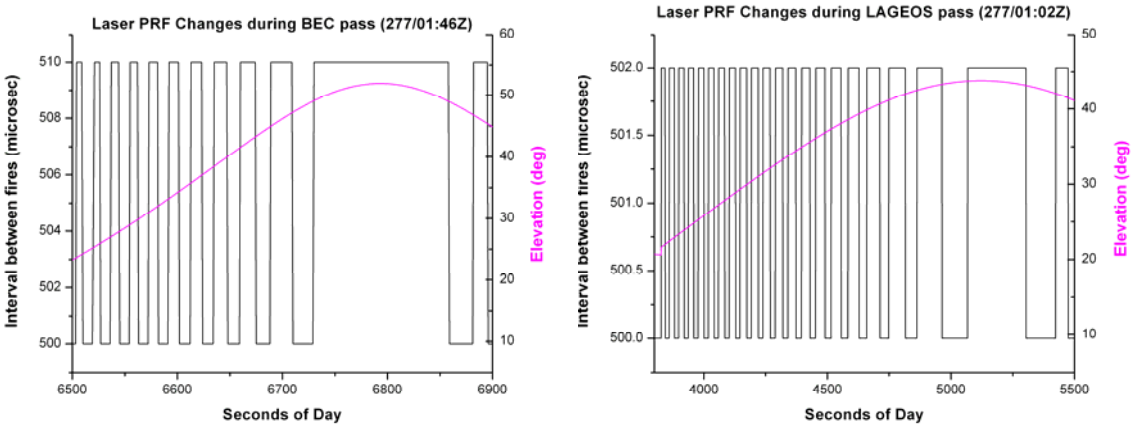

Figure 2: *Examples of laser PRF changes during two passes. The left plot is BEC and the right plot is LAGEOS.*

The new Q-Peak laser was installed into the system. The energy of the previous laser (an earlier Q-Peak version) had degraded to the point where it was transmitting only about 60 microJoules per pulse. The newer laser transmits approximately 120 microJoules per pulse.

Both the star camera (for star calibrations) and the sky camera (for sky condition) failed during 2006 and have been replaced. The star camera had been in use for approximately ten years. The new star camera is the Santa Barbara Instrument Group (SBIG) ST-402ME CCD imaging camera. The CCD chip is 9 microns square with 765 x 510 pixels. It is a low noise, high QE camera with a USB 2.0 interface. It greatly increases the star sensitivity from our old camera, where the dimmest useable star was around magnitude 3.5. The SBIG camera in SLR2000 can resolve better than 8th magnitude stars. The new star camera has been installed and is operational.

The sky camera failed after about five years of more or less continuous operation. The new sky camera is the Jenoptik VarioCam InfraRed (8 – 13 μm) camera. It has an uncooled sensor with a 320 x 240 pixel resolution and a Fire-Wire interface. The new sky camera is installed and working but has not yet been incorporated into the operational software.

Testing with MOBLAS-7

To checkout the system timing, pointing and receive electronics, we took many passes with MOBLAS-7 acting as the transmitter for SLR2000. These tests took two forms: (1) transferring the receive time from the MOBLAS-7 discriminator to the SLR2000 event timer with a cable running between the systems (start/stop via cable), and (2) receiving the actual return light with the SLR2000 quadrant detector. In both cases the MOBLAS-7 fire time was transferred to SLR2000 via cable.

Analysis showed (1) good pointing for SLR2000 (these tracks required no biases to maintain the returns), (2) comparable results between MOBLAS-7 and SLR2000 for data RMS when the cable was used to transfer the MOBLAS-7 fire times, and (3) in general a higher return rates for HEO satellites at SLR2000, due to its singe photon detection capability. Examples of the full rate data RMS for various passes are given in the table below.

Figure 3 shows an example of the LAGEOS return rates for MOBLAS-7 and SLR2000 with MOBLAS-7 providing the fires for both systems and SLR2000 receiving the return light with the quadrant detector.

LAGEOS RMS (mm)
MOBLAS-7 Start/Stop via cable: 10
SLR2000 quadrant detector: 25 – 40
ERS-2/ENVISAT RMS (mm)
SLR2000 quadrant detector: 20 – 25
GLONASS-87 RMS (mm)
MOBLAS-7 Start/Stop via cable: 15
SLR2000 quadrant detector: 35 - 45
ETALON RMS (mm)
SLR2000 quadrant detector: 50 – 60

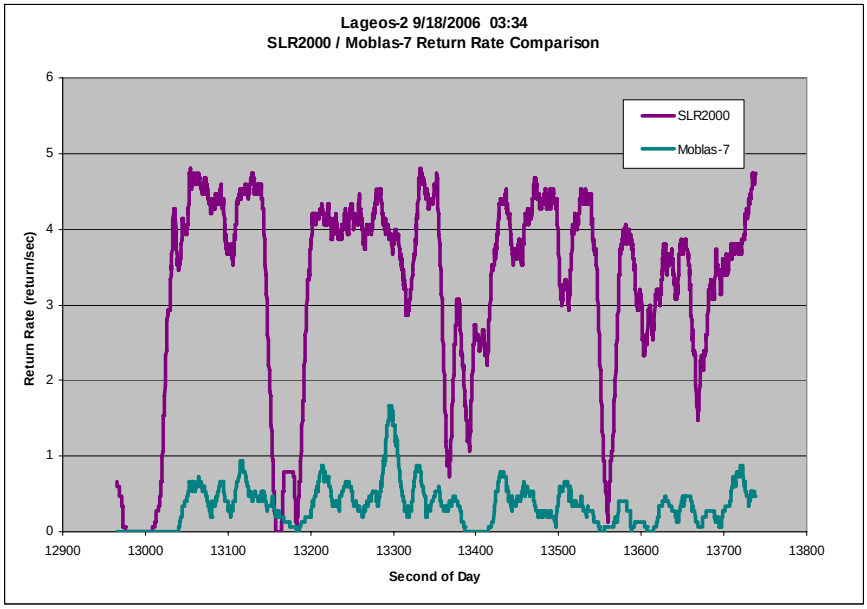

Figure 3: *LAGEOS return rates for SLR2000 (top curve) and MOBLAS-7 (bottom curve) when MOBLAS-7 was used as laser transmitter (5Hz) for both systems.*

Satellite ranging with the 2 kHz eyesafe laser

In the last several months SLR2000 has been ranging to satellites using its own eye-safe 2 kHz laser and pointing the telescope ahead. This configuration removes the need for the Risleys to point the laser ahead, but prevents daylight operation due to the need to keep the receiver field of view open to 25 arcseconds to cover the point-behind angular deviation from the point-ahead.

We have tracked many low earth orbiting satellites as well as a portion of a few LAGEOS passes. The pass RMS values remain relatively high due to our relatively wide pulse width laser (250 picoseconds). An example of the raw data from a STARLETTE pass is shown in Figures 4.

Path to Completion

Our immediate goal for 2007 is to increase our return rate from LAGEOS when ranging with our 2 khz eye-safe laser. We also need to return to our operational configuration where the telescope is pointed behind (toward the receive light) and the Risleys are used to point the laser ahead of the target. In this configuration we will work on finishing the closed-loop tracking. We expect our return signal rate to increase measurably when the system is closed-loop tracking.

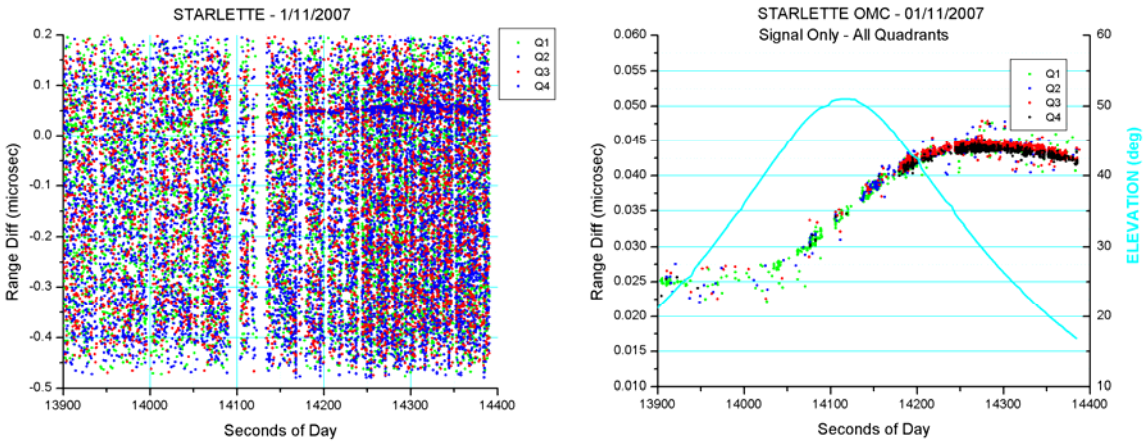

Figure 4: *STARLETTE pass on 1/11/2007. Left plot shows entire range window with signal and noise. Right plot is of signal only (as determined by signal processing).*

Along with this work, a new in-house laser is being built by Barry Coyle and colleagues. This 2 khz laser is expected to have a less than 200 picosecond pulse width with a 100 microJoule to 2 milliJoule variable per pulse output energy. This laser, which will enable us to track the higher satellites (in particular GPS), is expected to be delivered near the end of 2007. Our goal is to complete the SLR2000 prototype system in calendar year 2007 and perform a collocation with MOBLAS-7 in early 2008.

Acknowledgements

The authors would like to thank John Degnan, who developed the concept of SLR2000 and who led the development of this system until recently, for both his original idea and for his continued and unfailing support of this effort. We would also like to thank the SLR Network Manager, David Carter, for his support of our work, and Michael Pearlman who, as chairman of the ILRS Central Bureau, has been a steadfast proponent of SLR2000. We would also like to acknowledge the SLR2000 team, whose efforts were instrumental in SLR2000's progress: Christopher Clarke, John Cheek, Peter Dunn, Howard Donovan, Mike Heinick, Julie Horvath, Anthony Mallama, Anthony Mann, Donald Patterson, Mike Perry, Randall Ricklefs, Mark Torrence, Susan Valett, and Thomas Varghese. This work is being performed with funding from NASA's Science Mission Directorate.

References

[1] Degnan, J., J. McGarry, and T. Zagwodzki, "SLR2000: An Inexpensive, Fully Automated, Eyesafe Satellite Laser Ranging System," Proceedings of 10th International Laser Workshop on Laser Ranging Instrumentation, Chinese Academy of Sciences, Yang Fumin (ed.), 367-377, Shanghai, 1996.

[2] Degnan, J., and D. Caplan, "Performance of Liquid Crystal Optical Gate for Suppressing Laser Backscatter in Monostatic Kilohertz SLR Systems", in this Proceedings.

[3] Degnan, J., G. Jodor, and H. Bourges, "Adaptation of a Commercial Beam Expander for Automated Transmitter Beam Size and Divergence Control in the SLR2000 System", in this Proceedings.

[4] McGarry, J., T. Zagwodzki and J. Degnan, "SLR2000 Closed Loop Tracking with a Photon-Counting Quadrant Detector," Electronic Proceedings of 13th International Workshop on Laser Ranging, Ron Noomen (ed.), Automation and Control Session, Washington, DC, 2002.

[5] Titterton, P., H. Sweeney, and D. Leonard, "System/Usage Impact of Operating the SLR2000 at 2 kHz," Proceedings of the 11th International Workshop on Laser Ranging, 426 – 437, Deggendorf, 1998.

Determination of AJISAI spin parameters using Graz kHz SLR data

Georg Kirchner, Walter Hausleitner, and Elena Cristea

1. Austrian Academy of Sciences, Institute for Space Research, Graz.

Contact: Georg.Kirchner@oeaw.ac.at ; Walter.Hausleitner@oeaw.ac.at ; Elena.Cristea@oeaw.ac.at

Abstract

Using the Graz full rate kHz SLR data, we determined the spin rate and spin direction of the satellite AJISAI as well as its slow down between 2003/10 and 2005/06. The high density of the kHz data results in a precise scanning of the satellite's retro-reflector panel orientation during the spin motion. Applying spectral analysis methods, the resulting frequencies allow identification of the arrangement of the involved laser retroreflector panels at any instant in time during the pass. Using this method, we calculated the spin rate with a high accuracy (RMS of 4.03 x·10^{-4} Hz), and the slow down of the spin rate during the investigated period with a magnitude of 0.0077497 Hz/year. We obtained these results from routine SLR tracking data, i.e. day and night observation, without any additional hardware.

Introduction

The Japanese geodetic satellite AJISAI, launched on August 13, 1986 into a 1500 km circular orbit with a 50° inclination, is a passive sphere with a diameter of 2.15 m [1]. The surface is covered with 318 sunlight reflection mirrors for visual tracking and 120 laser retro reflector (LRR) panels each carrying 12 corner cube reflectors for SLR [2] (see Fig. 1). The satellite's axial rotation causes the mirrors to produce visible flashes of reflected sunlight, which are observable on Earth [4]. This in principle allows a precise determination of the spin rate, but, however, requires dedicated photometric equipment at the ground station. Furthermore, these observations can only be made during night time, and for limited time spans where the satellite is illuminated by the Sun. This method was applied for AJISAI in Japan only in the frame of a few campaigns.

AJISAI was put into orbit with an initial spin rate of 40 rpm, and with the spin axis parallel to the Earth's rotation axis. With the method of photometric timing an axial rotation of 0.67 Hz was measured after launch [5], slowing down to 0.57 Hz by October 1997 [2].

In the present study AJISAI's spin rate has been investigated using the full rate kHz SLR observations of the Graz laser station and was determined to be 0.5064 Hz in July 2005. The main reason for this slowdown is the eddy current resulting from an interaction between the satellite's metallic parts and the Earth's magnetic field [2].

While standard SLR measurements are usually done at a 5 or 10 Hz repetition rate, the SLR station Graz was upgraded and is operating a 2 kHz laser system since October 2003. Due to the capability of detecting return pulses with as few as a single photon, the return rate from AJSAI comes close to 100 %, even with the low energy per shot 400 µJ) of the Graz SLR system. The 2 kHz repetition rate produces up to 1 million measurements per AJISAI pass, which has a duration of typically 16 minutes. This amount of data represents a very dense temporal sampling of the satellite's rotating surface, which allows an accurate determination of the spin parameters.

Fig. 1. *Geodetic satellite AJISAI.*

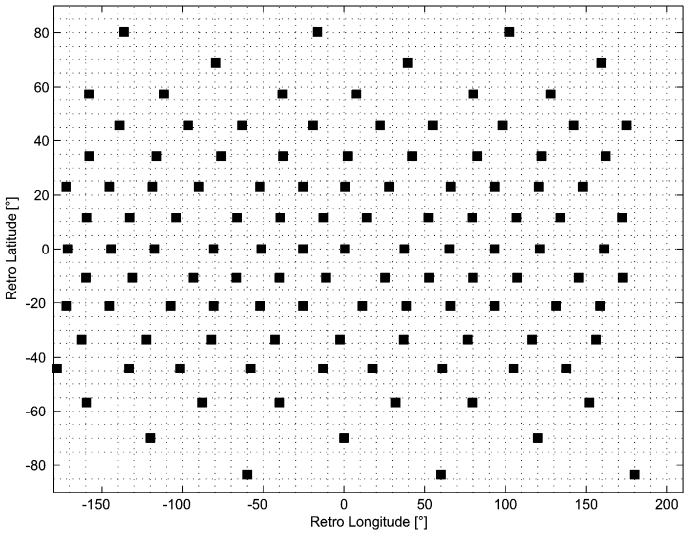

Fig. 2*. Schematic distribution of the LRR panels*

The LRR panels are almost uniformly distributed over the surface, arranged in 15 latitudinal rings [2]. There are 5 rings with 12 LRR's, 4 rings with 9 LRR's, 2 rings with 6 LRR's, and 4 rings with 3 LRR's each. The schematic distribution of these LRR panels in terms of latitude and longitude is shown in Fig. 2.

Ranging Simulations

Due to the axial rotation of AJISAI and the well separated reflector panels, the distance from the observer to each panel varies periodically. The periods are given by the spin rate of the satellite and the number of panels of the involved ring. The amplitudes depend on the dimension of the sphere, the distance between the panels and on the incidence angle of the laser beam. Based on the known location of each reflector panel on AJISAI [6], a ranging simulation was made which clearly shows the expected periodic distance variation.

Fig. 3 shows a full 360° rotation viewing with an incident angle of –18.125° from the satellite's equator, which contains 12 reflector panels, consisting of 3 groups with 4 panels each. The distances between these 3 groups are slightly larger than the distances between the panels within each group (Fig. 2). The resulting pattern shows the corresponding peaks, with 3 larger gaps (at 100°, 220° and 340° longitude) in between.

Spectral analysis of kHz data

In order to verify these simulation results, using the Graz kHz SLR measurements, we calculated a reference orbit from the standard SLR predictions and subtracted the calculated value from the measured distance. A low order polynomial was approximated and subtracted from the residuals in order to remove the remaining low-frequency part (approx. a few minutes in time) of the observations, but keeping the high-frequency variations (less than a few seconds) originating from the rotating reflector panels.

Fig. 4 shows range residuals for a 2 s interval (1 full revolution) of a routinely observed AJISAI pass.. The residual plot clearly shows the bigger gaps (longer ranges) due to the larger distances between the 3 groups as well as small variations in

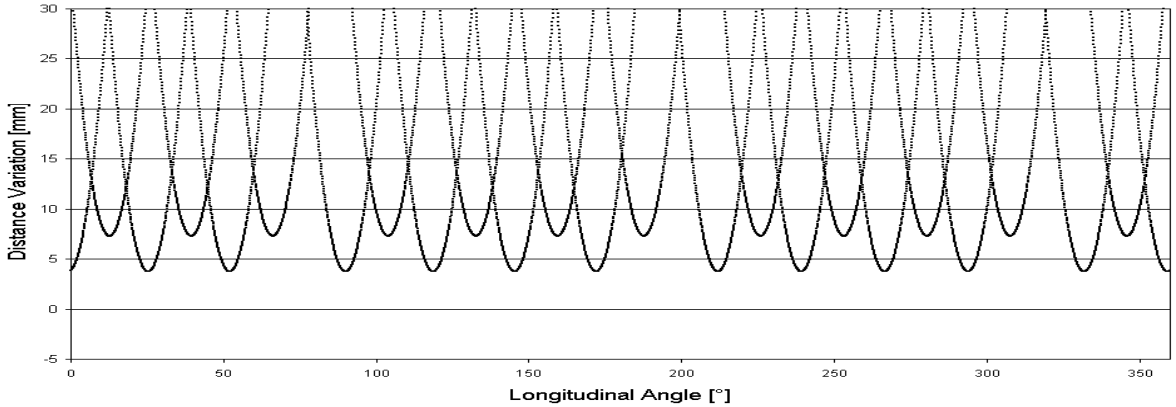

***Fig. 3**. Simulated distance variations of LRR panels at a laser beam incidence angle of -18.125° latitude. The non-symmetric LRR arrangement (Fig. 2) causes the slightly irregular distribution in both the simulation (Fig. 3) and in the ranging residuals (Fig. 4).*

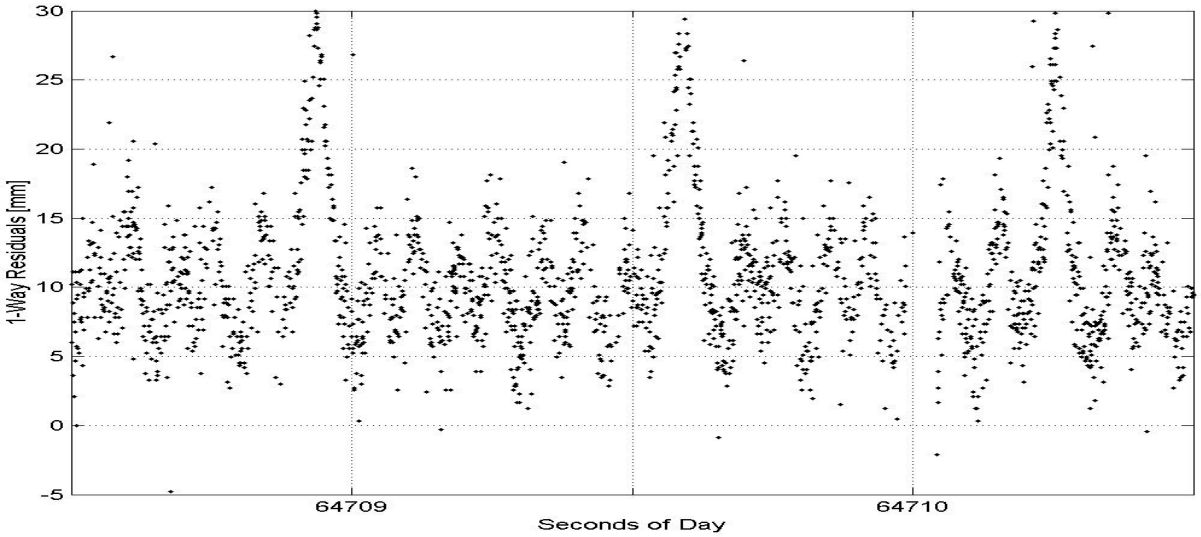

***Fig. 4**. Full rate 1-way range residuals during one full rotation of AJISAI (DOY 122/2005) for comparison with the simulation shown in Fig. 3*

between due to 2 different rings. This residual analysis coincides well with the corresponding simulation shown in Fig. 3.

Frequency Analysis using FFT versus Lomb

Usually, SLR systems do not reach a 100 % return rate, even in good weather conditions. Due to the resulting gaps, the measurements are in general not equidistant in time and therefore the Fast Fourier Transform (FFT) method cannot be directly applied for a frequency analysis. In order to use FFT for the given AJISAI range residuals, the data gaps may be interpolated, but, however, this may induce new frequencies and decrease the accuracy of the results [8]. In [2], the Lomb method for spectral analysis of non-uniformly distributed data was suggested as a useful alternative. This method can handle non-equally spaced data and provides an approximation of the spectrum using the least-squares method.

Connecting Frequencies with AJISAI Geometry

Applying the Lomb method to the residuals of a 10 seconds interval of an AJISAI pass (see Fig. 5), a number of spectral peaks due to the distance variations can be seen clearly. The frequencies of 1.5, 3.1, 4.6 and 6.1 Hz are multiples of AJISAI's basic

spin rate of about 0.5105 Hz in January 2005, and the number of LRR panels (3, 6, 9 or 12) of the involved ring. The higher frequencies of 7.57, 9.09, 10.60 and 12.12 Hz are generated by simultaneous contributions of LRR of two or more adjacent rings. For instance, the clear spectral peak at 12.12 Hz in Fig. 5 cannot be associated with any single ring, but is produced by the combination of two 12-retro rings.

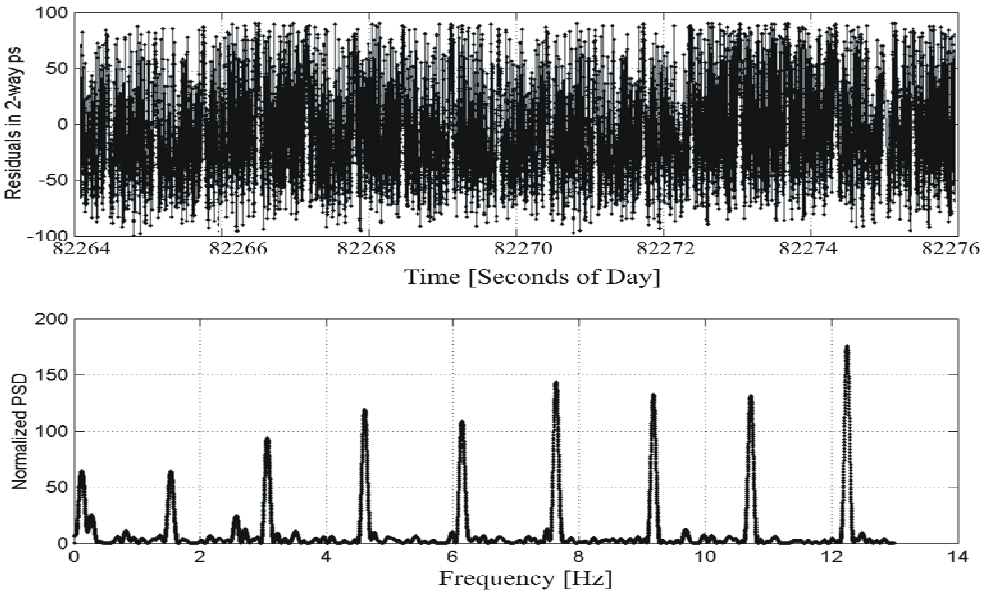

Fig. 5. *Twelve seconds interval of 2-way residuals in time and frequency domain (DOY 019/2005, multiple rings visible).*

Spin rate slow down

It was shown that each calculated frequency corresponds to a specific number of LRR panels. The ratio between frequency and the number of panels of the corresponding ring gives the exact spin rate of AJISAI. The frequency generated by the 3 LRR rings was not used for spin rate calculations, because they generate lower spectral power and lower resolution than the 6, 9 or 12 LRR rings.

For the frequency analysis we selected only passes with high data density (> 300 k returns) observed between 2003/10 and 2005/06. From these passes we used only data of a 1.5 minutes interval centered at the closest approach, containing more than 40 k returns, in order to keep the computation time within reasonable limits (a 3 GHz PC still needed 5 days to analyze the 195 selected passes).

Because the measured spin rate is an apparent spin rate it was corrected for the apparent effect in order to get the sidereal spin rate (see details below). The resulting spin rates for this time span show a well defined slow down rate of 0.0077497 Hz / year (Fig. 6), coinciding well with AJISAI's spin rate slow down calculated for 1997-1999 [2].

Apparent Spin and Spin Direction

The apparent spin rate of a satellite observed at any site on Earth is affected by the axial spin as well as by its orbit around the Earth and by the Earth rotation itself. Therefore the apparently measured spin has to be corrected for these effects, in order to obtain the sidereal spin of AJISAI.

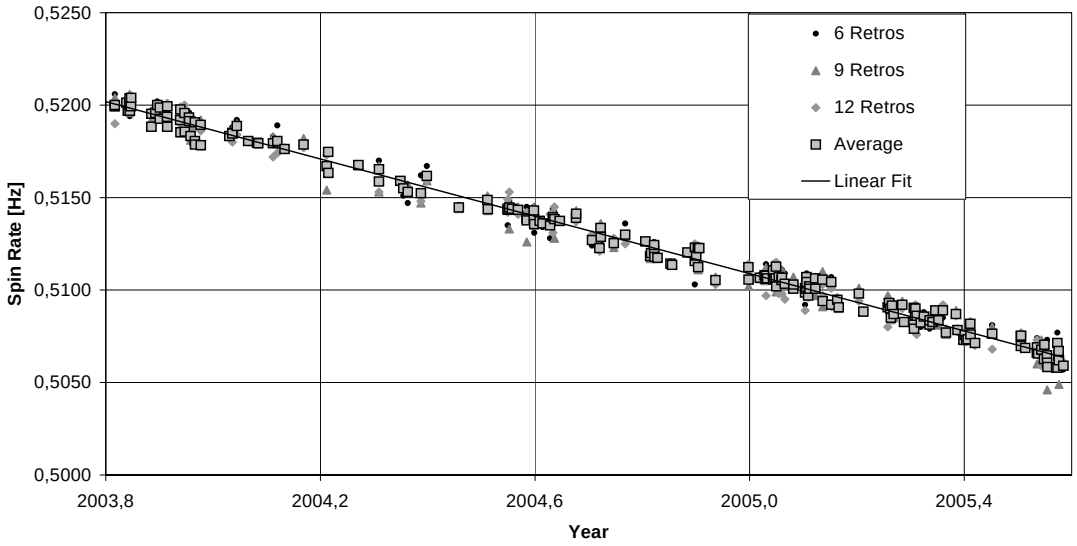

Fig. 6. *AJISAI spin rate decrease determined from the averages of 6, 9 and 12 retro ring spin rates for 195 passes between 2003/10 and 2005/06. The linear fit to these average values yields a slow down rate of 0.0077497 Hz / year, with a standard deviation of 0.000403 Hz.*

As an example, we calculated the spin rate of an AJISAI pass of 2005/01/19 (again for a period of 1.5 minutes around the closest approach). However, in this case, we selected only short slots of 12 seconds (containing at least 5000 residuals), calculated the spin rate with the same approach as above, then shifted the slot time by 6 seconds, and repeated the procedure.

This results in a clearly visible – apparent – increase of the spin rate near the maximum elevation (71.9° for this pass) as shown in Fig. 7, where the values are given together with the corresponding calculated apparent spin rate. The clearly visible outliers at about 82050, 82150 and 82250 seconds can be correlated with according ring transitions, identifiable by detailed analyses of the residuals. The results confirm the high sensitivity of kHz SLR data for the determination of satellite spin rates.

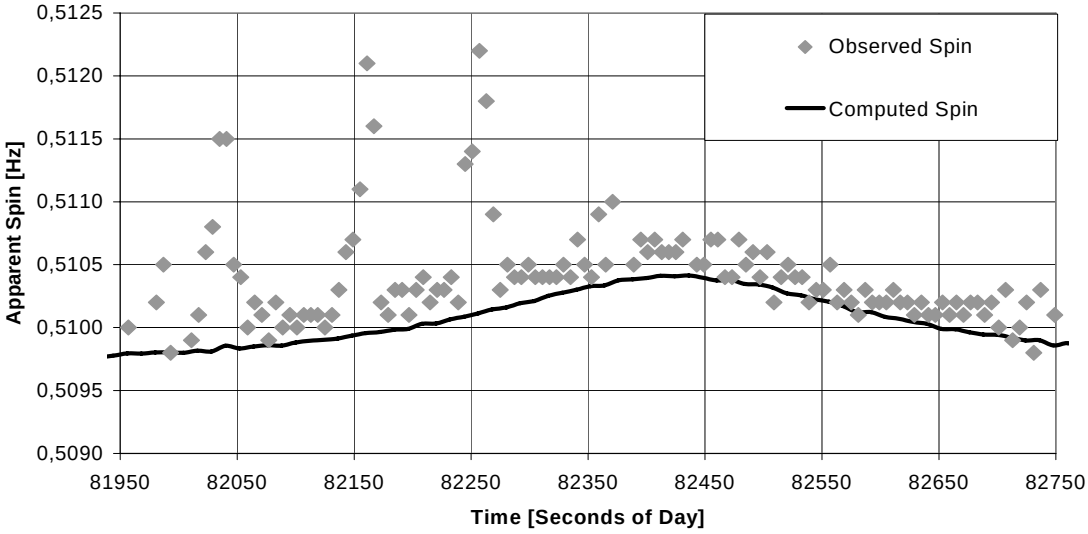

Fig. 7. *Apparent spin motion as observed from the SLR site. Measured rates (diamonds) vs computed values (solid line).*

We assume that the spin direction of AJISAI a priori is not known. From sequences of observed LRR ring transitions in most passes we have evidence that the spin axis is still at least approximately parallel to the Earth axis. Because the closest approach (CA) of the selected pass was at about 160° / 71.9° (as seen from Graz), and the apparent spin shows a slight increase (Fig. 7) at CA, we can conclude that AJISAI is spinning in a clockwise direction.

References

[1] T. Otsubo, J. Amagai, and H. Kunimori, “The center of mass correction of the geodetic satellite AJISAI for single-photon laser ranging”, IEEE Transactions on Geoscience and Remote Sensing, Vol. 37, No. 4, July 1999.

[2] T. Otsubo, J. Amagai, H. Kunimori, and M. Elphick, “Spin motion of the AJISAI satellite derived from spectral analysis of laser ranging data”, IEEE Transactions on Geoscience and Remote Sensing, Vol. 38, No. 3, May 2000.

[3] International Laser Ranging Service (ILRS) Home Page: http://ilrs.gsfc.nasa.gov .

[4] R. Wood, T. Otsubo and R. Sherwood, “Lageos 2 spin rate and orientation”, http://cddisa.gsfc.nasa.gov/lw13/docs/papers/target_wood_1m.pdf

[5] T. Kanazawa, “Determination of the rotation phase angle and the rotation period of AJISAI(II)” in Proc. 70th meeting Geodetic Soc. Of Japan, Kyoto, Japan, 1988, pp. 51-52.

[6] T. Uchimura, Personal communication, July 2005, (uchimura.takashi@jaxa.jp)

[7] M. Sasaki and H. Hashimoto, “Launch and observation program of the experimental geodetic satellite of Japan”, IEEE Transactions on Geoscience and Remote Sensing, Vol. GE-25, No. 5, September 1987.

[8] N. R. Lomb, “Least-squares frequency analysis of unequally spaced data”, Astrophysics and Space Science 39, p. 447-462, 1976.

New Methods to Determe Gravity Probe-B Spin Parameters using Graz kHz SLR Data

Georg Kirchner, Daniel Kucharski, Elena Cristea

1. Austrian Academy of Sciences, Institute for Space Research, Graz.

Contact: Georg.Kirchner@oeaw.ac.at ; Walter.Hausleitner@oeaw.ac.at ;
Elena.Cristea@oeaw.ac.at

Abstract

Using kHz data of the SLR station Graz, spin parameters of the satellite Gravity Probe B (GP-B) are derived; these include spin period and its change over a 1.5 year period, as well as spin direction, and spin axis orientation. The results are compared to the actual data sets - as determined by the GP-B mission itself – thus allowing independent confirmation of the kHz SLR derived results.

Introduction

GP-B was launched on April 20th, 2004, into a polar orbit at 640 km altitude. During its measurement phase, the spacecraft was spinning slowly - with about 77.5 seconds / revolution - around its central axis, defined by a telescope at one end, and the laser retro reflector (LRR) array at the other end. Its orientation was maintained always to point with high accuracy to the star IM-Pegasus; the direction to this star is measured with the on-board telescope with a stability of 0.1 milliarcseconds per year [1] (ed.).

The LRR array (Fig. 1) on GP-B consists of 8 retro reflectors in a ring-like formation, and a central LRR [2]. While such an arrangement only spreads standard SLR measurements, the high resolution of kHz SLR allows to scan the single reflectors, to identify their motion due to the spin of the satellite, and to derive all GP-B spin parameters from kHz SLR data.

Spectral Analysis of kHz Slr Data

The spectral analysis of kHz SLR data is based on residuals obtained by subtracting the calculated, predicted orbit, from the measured distances. Fitting a low order polynomial to these residuals allows elimination of outliers, but keeps the oscillating signal of the eight rotating LRR's (Fig. 2, top).

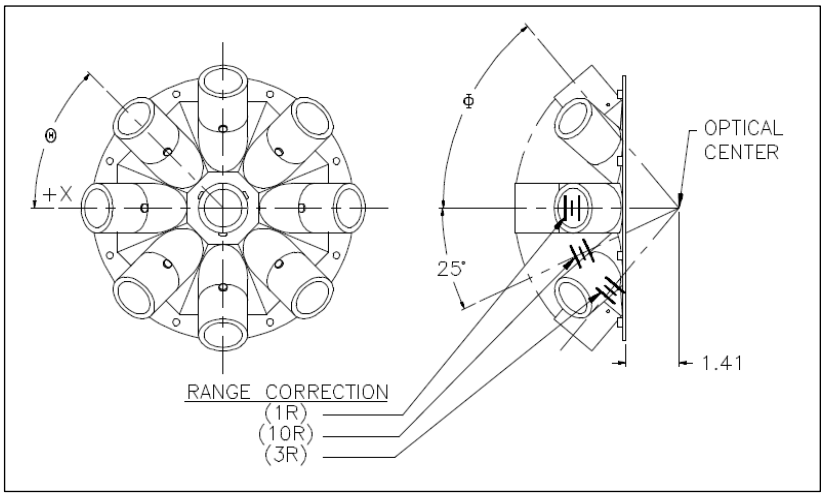

Fig. 1: *GP-B Laser Retro Reflector (LRR) Design*

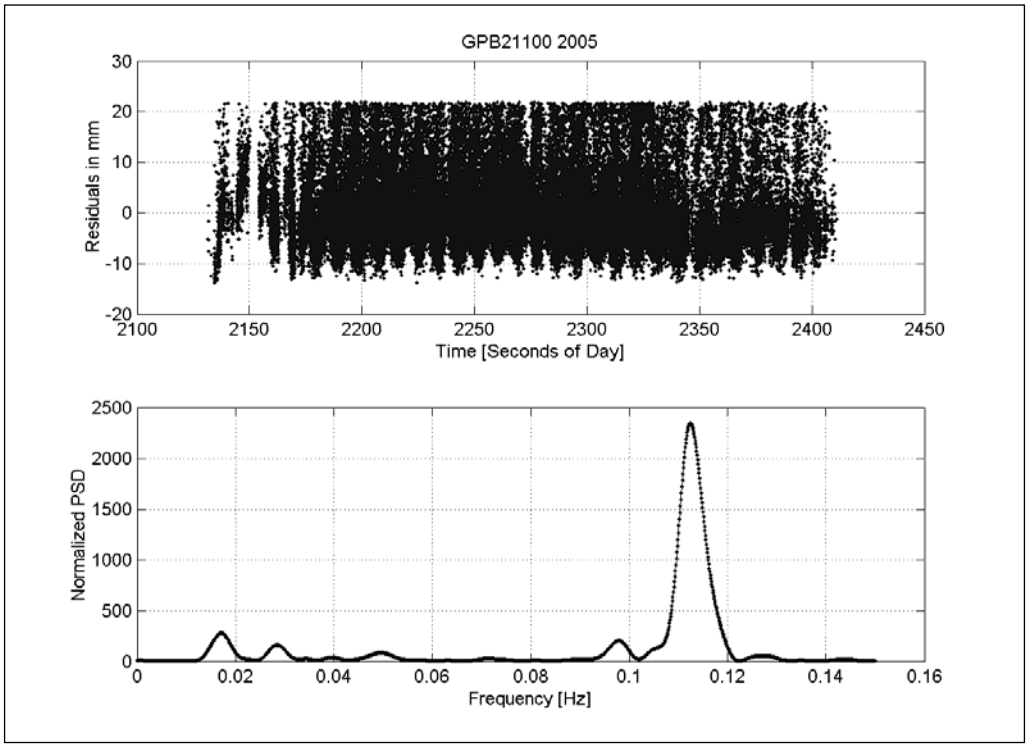

Fig. 2: *Residuals of a 280 seconds segment of a GP-B pass of DOY 211/2005 (top); frequency spectrum generated by these residuals (bottom).*

The Lomb method of spectral analysis was suggested in [3] alternatively to the Fast Fourier Transform (FFT), allowing for non-equally spaced data, as it is the case for such SLR measurements. The FFT could still be used if the data gaps were interpolated, but this would introduce unwanted frequencies. Therefore the Lomb method was preferred.

Taking into account the known inertial spin period of GP-B (77.5 seconds per revolution) during phase A (Fig. 3), and the 8 retro reflectors per revolution, we selected passes with at least 100 seconds to analyze a minimum of 10 oscillations, to get reliable results for the spectral power (Fig. 2, bottom).

This spectral power varies from pass to pass, with the data gaps and the length of the pass being the main corrupting factors. The analysis has been performed also on selected intervals of the longer passes, with high data density, as an additional verification of the frequency obtained for the complete pass.

Spin Period Trend

From all GP-B passes measured by Graz kHz SLR, we selected those with more than 50,000 returns per pass. Applying the Lomb analysis to these passes, we found three different regions of spin periods after the initialization period, as soon as SLR measurements started (Fig. 3, top): phase A: from 10.08.2004 until 6.09.2005, the mean spin period was about 77.5 seconds; phase B: the spin period changed to about 125 seconds; after 11.01.2006 (phase C), the spin period analysis shows an unstable behavior, as expected after termination of the active phase of the GP-B experiments (Fig. 3, top). Comparing the SLR derived spin periods with the GP-B based data set for phase A (Fig. 3, bottom), the RMS of the differences is 4.99 seconds.

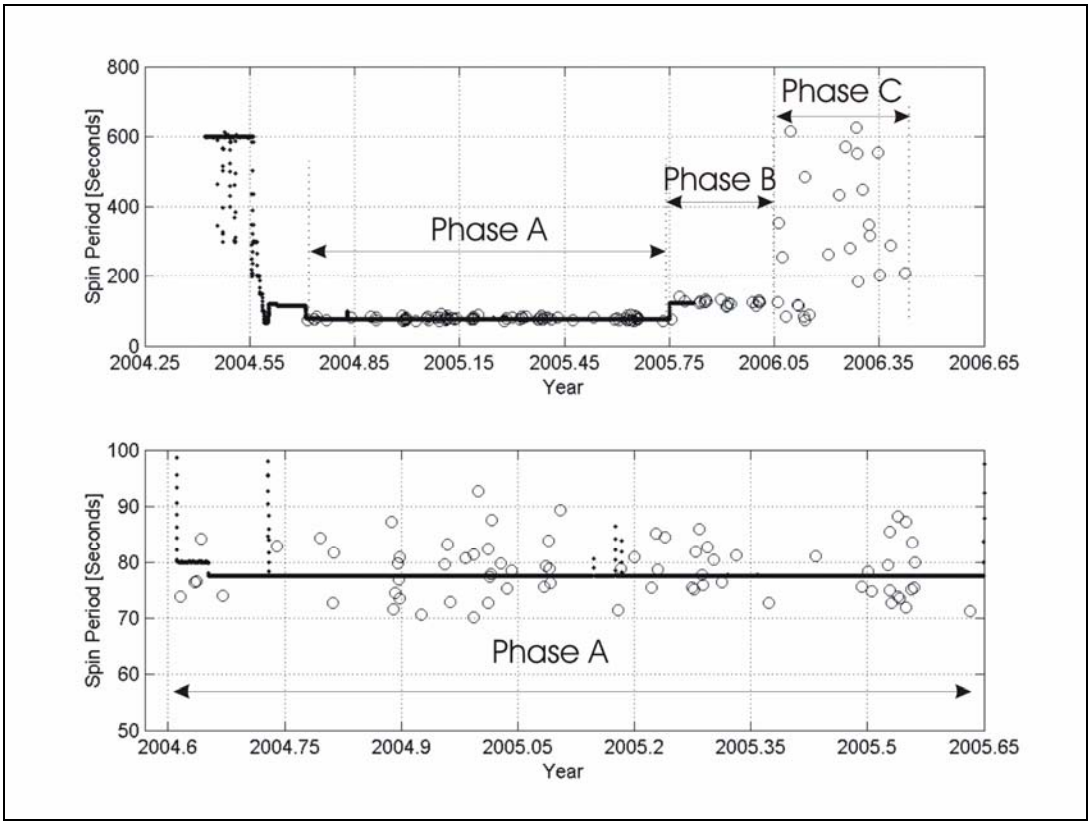

Fig. 3. *GP-B spin period variations. Dots indicate spin periods as measured on-board; circles (o) show results of kHz SLR spectral analysis. Bottom: Expanded view for phase A, showing RMS of 4.99 seconds.*

Apparent Spin

Although the spectral analysis already yields clear results – coinciding with the GP-B on-board measured data sets (Fig. 3) -, the accuracy is not as expected: the frequency peak (Fig. 2, bottom) is well defined, but rather broad; and the RMS of the differences between kHz SLR based periods and the on-board spin measurements (Fig. 3) amounts to rather high 4.99 seconds for phase A.

Simulating the measured GP-B passes, using all known parameters (GP-B orbit, Earth rotation, fixed pointing of GP-B to IM-Pegasus, inertial GP-B spin period as measured by the spacecraft itself, geometry of the retro reflectors, as well as their range corrections, etc.), the influence of the apparent spin - the satellite's spin as observed from Earth – was identified as the main reason (Fig. 4). GP-B's spin period is about 77.5 seconds; because the satellite moves along its orbit considerably during this time, the apparent spin period for even the short part (151 seconds) of the pass in Fig. 4 changes from initial 72.8 seconds (9.1 x 8 retro reflectors) to 70.4 seconds (as determined from peak-to-peak distances; Fig. 5). This change in apparent spin period is the main reason for the mentioned inaccuracies in the spectral analysis. In addition, the change of the incident angle of the laser beam causes a decrease of the "modulation depth", as indicated by the line in Fig. 4.

Spin Period Determination Using Simulation

Due to the low spin rate of GP-B, it is not possible to apply the apparent spin directly to the spectral analysis results, as it has been done in [4]; we therefore checked other

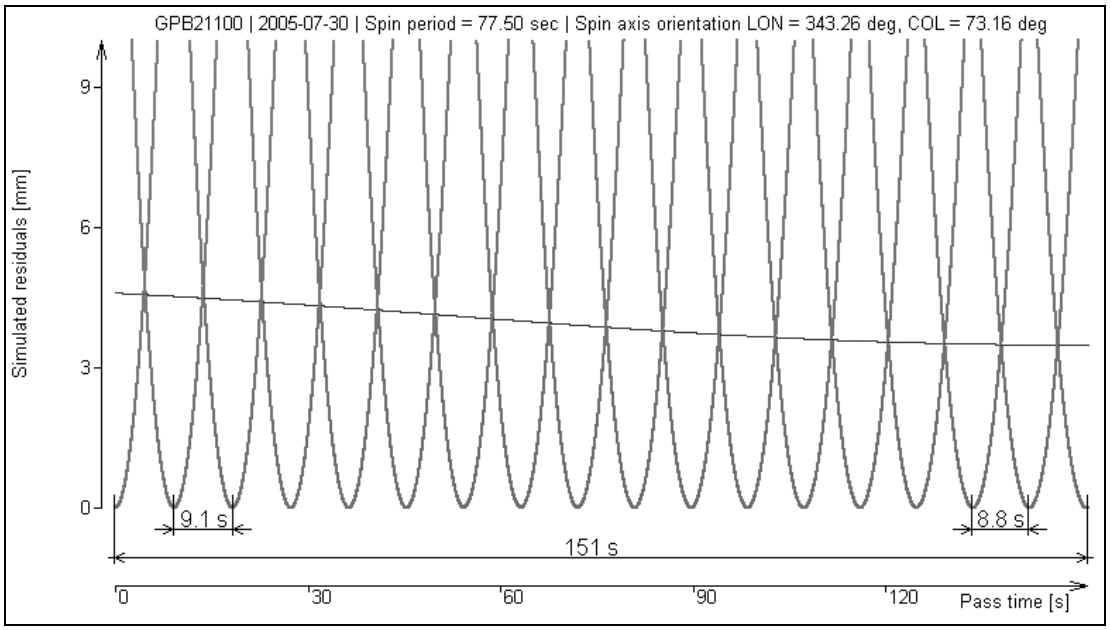

Fig. 4:. *Simulation of GP-B pass DOY 211/2005; spin period slightly changing due to apparent spin. The line shows the decreasing "modulation depth" during the 151 seconds.*

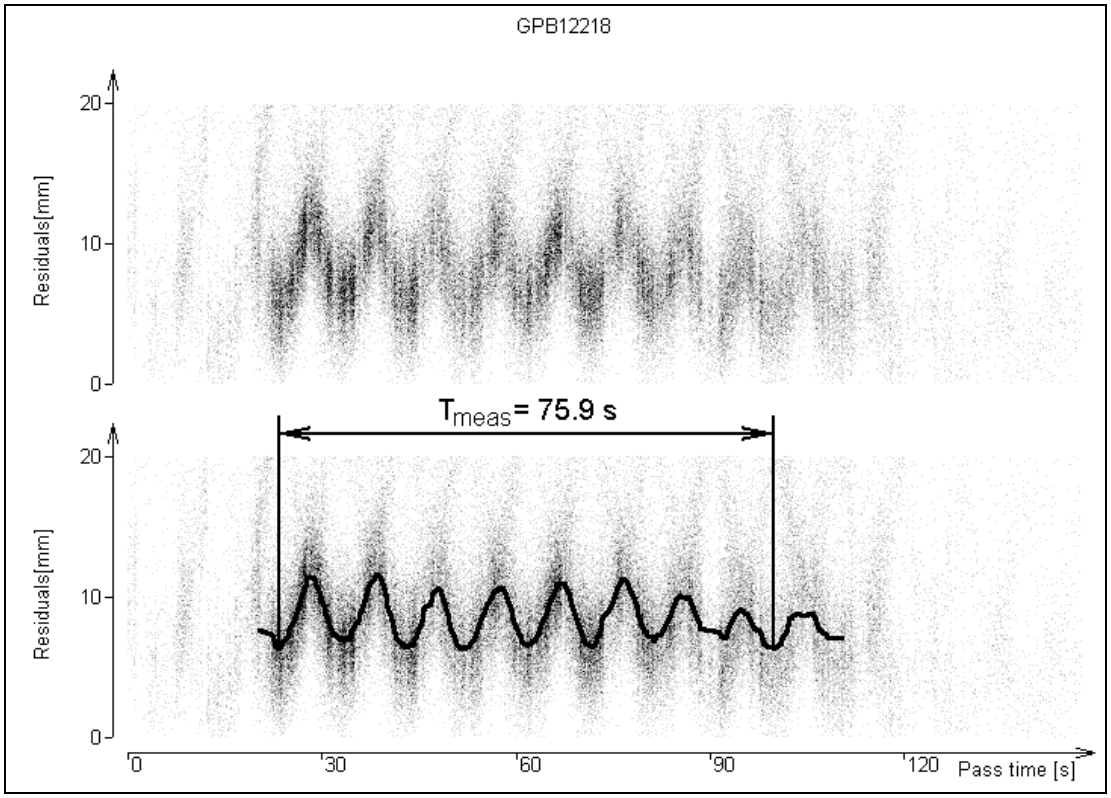

Fig. 5a: *GP-B pass of DOY 122 / 2005, Top: Residuals; about 79200 points in 151 s; bottom: solid line: averaging; 75.9 s from first to last peak (T_{meas}).*

methods to calculate more accurate, inertial spin periods for GP-B using our kHz SLR data.

The simulations, as described above, proved to be a good and powerful tool: for each measured pass, we determined the time period from first to last peak (Fig. 5a, T_{meas}); the same pass was simulated also (Fig. 5b, T_{sim}); however, the inertial spin period of

GP-B was used here as parameter, varying its value from –50 to –100 seconds, and from 50 to 100 seconds, in steps of 0.01 seconds. If the estimated and the true inertial spin periods coincide, the measured and the simulated T values for the same epoch times should be the same. In Fig. 6, the differences T_{meas} - T_{sim} for 100 phase A passes are plotted, allowing for both spin directions. The zero-crossings of these differences determine the inertial GP-B spin periods.

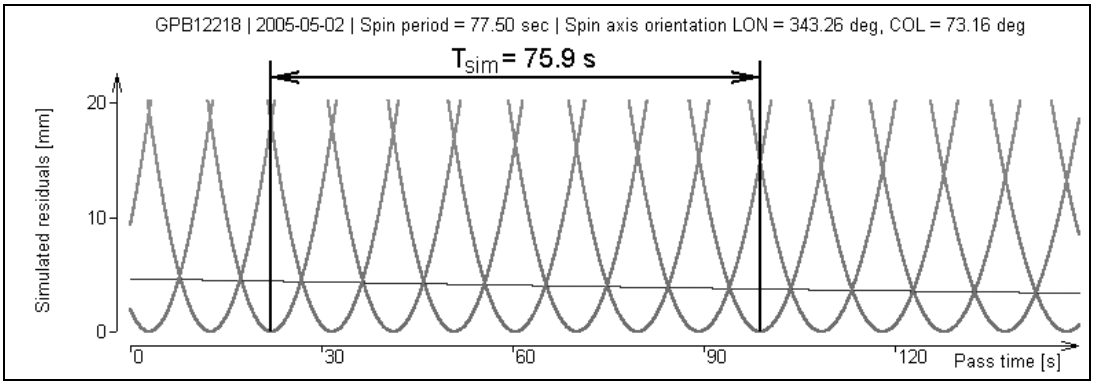

***Fig. 5b**: Simulation of same pass of DOY 122 / 2005: T_{sim} is same as T_{meas} at same epoch time, when simulating with inertial spin period of 77.50 seconds.*

Applying this method to 86 GP-B passes of phase A (selected to contain at least 5 peaks), the resulting spin period values coincide well with spin data as measured by GP-B (Fig. 7a); the accuracy of the resulting inertial spin period is improved now, with an RMS value of 0.98 seconds (Fig 7b).

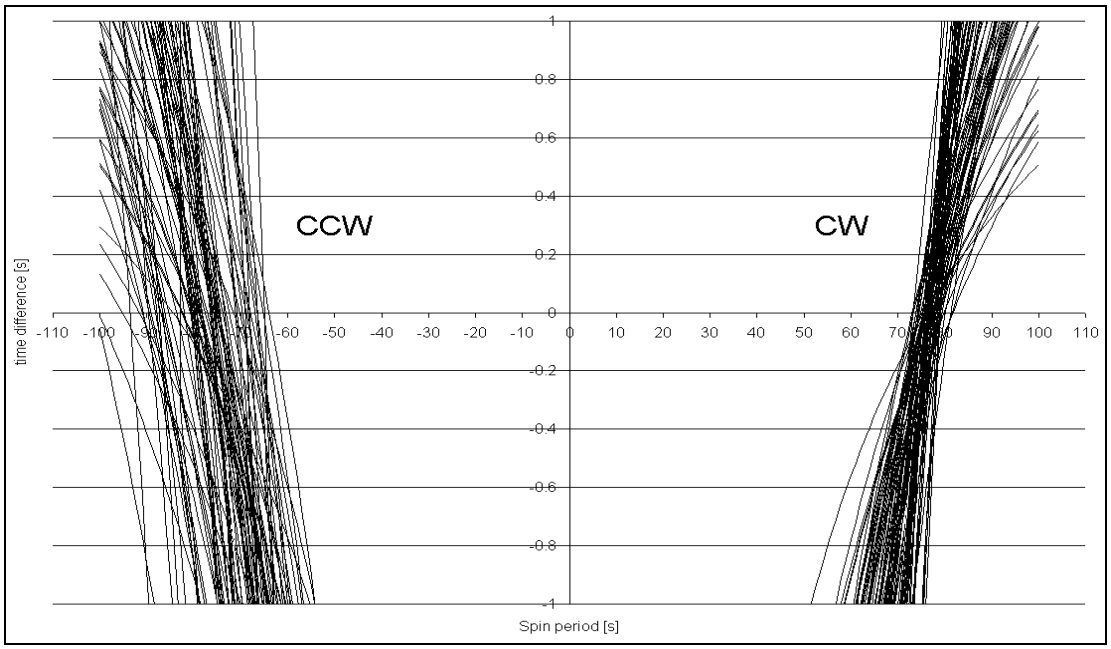

***Fig. 6:** Differences between T_{meas} and T_{sim} for 100 passes of phase A; CCW (left) and CW (right) spin directions have been simulated.*

Determination of Spin Direction

We define clockwise (CW) and counter clockwise (CCW) spin direction here as the spin of the spacecraft when looking on the LRR in pointing direction of GP-B. This spin direction of GP-B is a priori not known to us. To determine it using the kHz SLR

data, both spin directions were simulated (Fig. 6).

The results in Fig. 6 indicate that GP-B spins CW, because the spread of the result here is much less than for the CCW simulation.

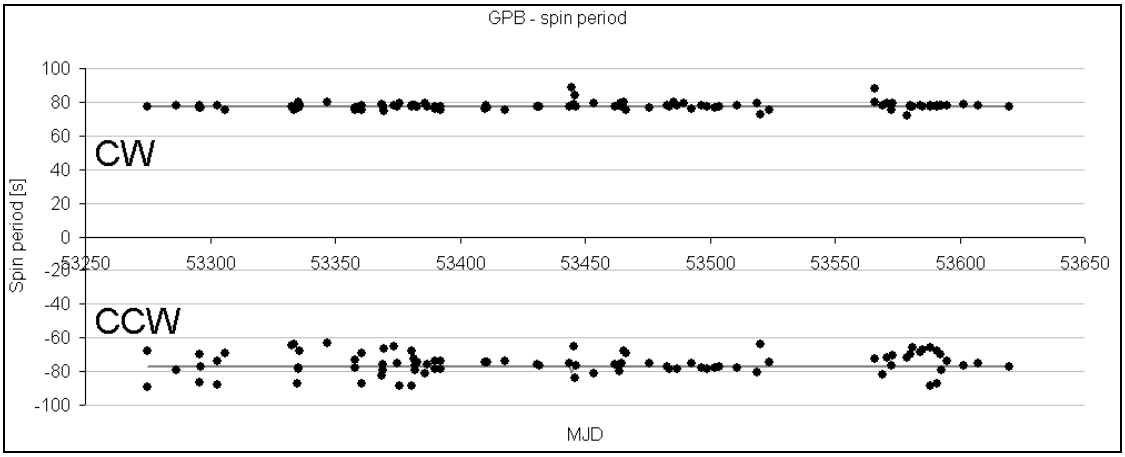

Fig. 7a: *GP-B spin period for 86 passes during phase A; positive values are for CW spin, negative for CCW spin assumed; solid lines at ±77.5 seconds indicate results of on-board spin measurements.*

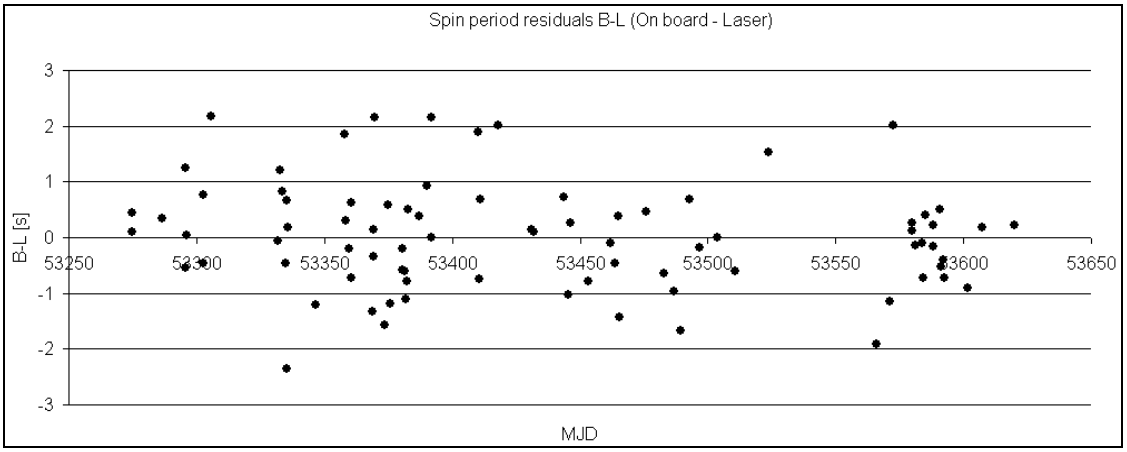

Fig. 7b: *Spin period for 86 passes of phase A with at least 5 peaks: differences to on-board spin period measurements; RMS of differences is 0.98 seconds.*

Determination of Spin Axis

Due to their periodically varying distances as seen by the SLR measurements, the eight laser reflectors generate specific patterns within the return data set, with a "modulation depth" depending on the incident angle between laser beam and GP-B's axis (Fig. 8).

This change of the modulation depth within the pass can be used to evaluate the incident angle (Fig. 8, bottom) and thus at least one orientation angle of the satellite. However, this method proved to be more inaccurate than expected, mainly due to the limited resolution of the modulation depth determination; the instrumental jitter of about 3 mm RMS of the Graz kHz SLR system for GP-B is not really adequate to determine the modulation depth variations of 0 to 6 mm with sufficient accuracy.

Looking for a more suitable method to determine spin axis, the comparison between simulations and measurements once more proved to be appropriate. For this purpose, the returns from the 9th or central retro reflector, which are vaguely visible in a few

passes, were used additionally (Fig. 9). Fitting a parabola to these returns, and determining the minimum value of the oscillations of the other 8 retro reflectors (Fig. 10), allows to fix the minimum distance between the upper and the lower curve (D), and the corresponding epoch time.

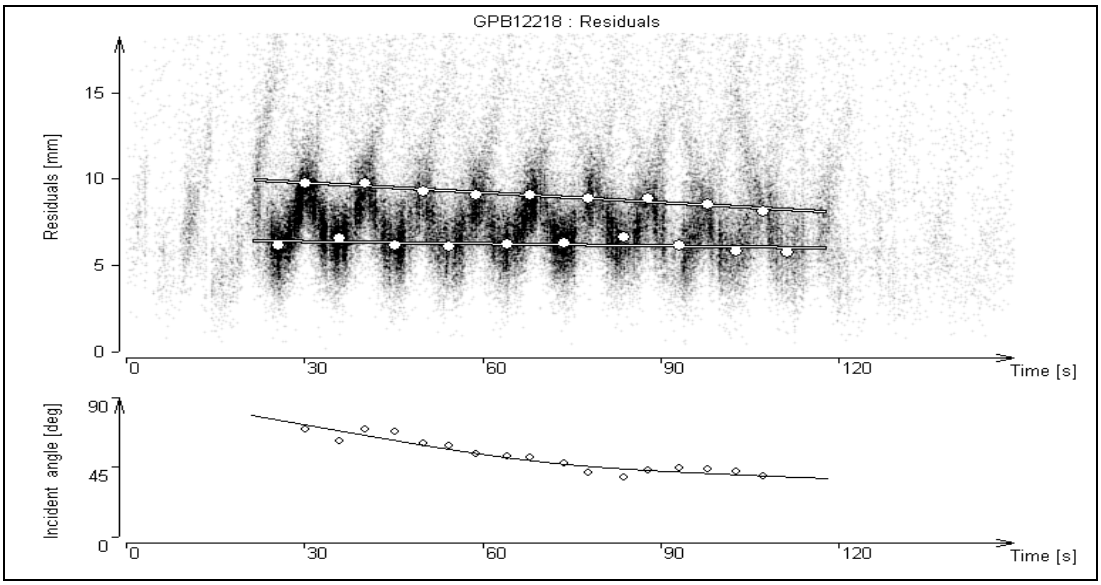

Fig. 8: *GP-B pass of DOY 122 / 2005: "Modulation depth" decreases during the pass (top); applying the known geometry of the retro reflectors, the incident angle of the laser beam can be determined (bottom).*

Running now simulations for this pass, spin axis longitude and colatitude (i.e. spin axis direction) were varied in steps of 1° each; for each spin axis direction, the spin period was calculated with the same method as described above. The goal was to find a combination spin period and spin axis direction, so that epoch time differences (between 9th retro parabola minimums of measurement and simulation) and range differences D (between simulations and measurements) are zero or close to zero.

Fig. 11 plots these differences between simulations and measurements; on the X-axis the differences in epoch time, on the Y-axis the differences in the distances D are shown; each line (set of points) represents solutions for different spin axis longitudes, and each point on these lines represents a solution for different spin axis colatitudes. The lowest line indicates a longitude of 320°, step size is 1°; zero for epoch and range differences means that the correct spin axis angles have been used in the simulation, as well as the correct inertial spin period; using this rough graph, the approximate longitude solution is between 340° and 341°, and the approximate colatitude between 73° and 74° (Fig. 11, left).

Using these values as boundaries for a more detailed simulation run with step sizes of 0.1°, we get about 341.4° for longitude, and 73.3° for colatitude, at an inertial spin rate of 77.42 seconds (Fig.11, right).

Two more GP-B passes were analyzed in this way, and the spin axis parameters determined; all results were coinciding with the on-board values with good accuracy (Table 1): standard deviation of the differences is 1.6° for colatitude, 1.77° for longitude, and 0.6 seconds for spin period.

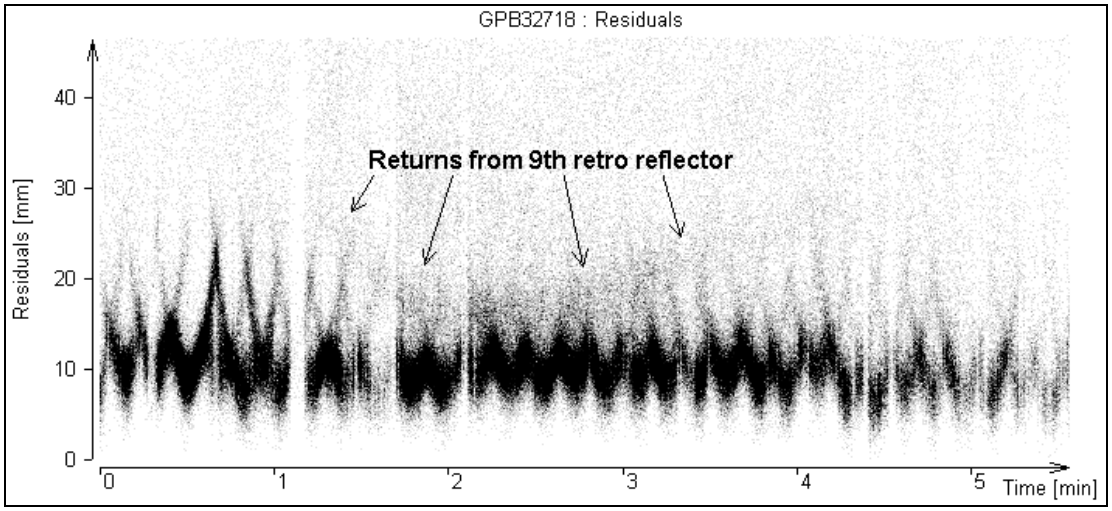

***Fig. 9:**. GP-B pass of DOY 327/2005: Vaguely visible returns from 9th retro.*

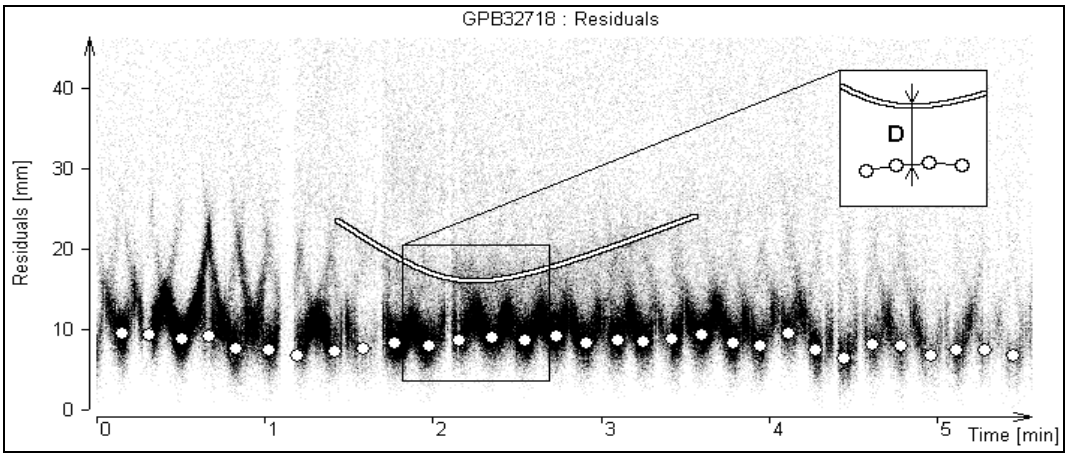

***Fig. 10:**.Parabola fitted to 9th retro returns, gives epoch time and value of "D"*

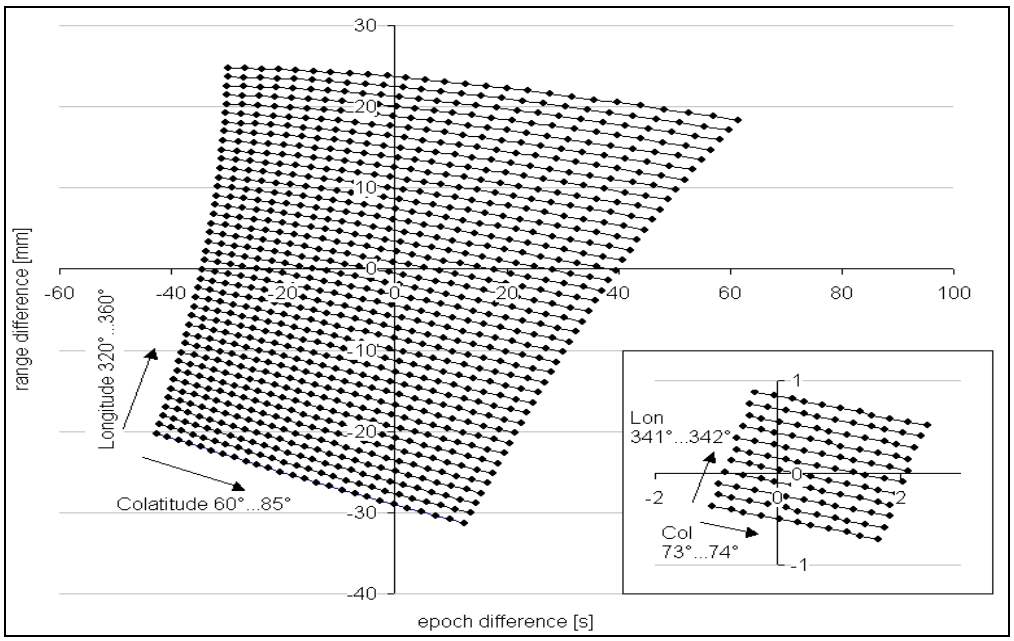

***Fig. 11:**.Simulations for Longitude and Latitude vales of GP-B Spin Axis, varied in 1°-steps (left); same with 0.1° steps around ZERO (right)*

Table 1: *Comparison of complete spin parameters for 3 GP-B passes.*

Pass date	Colatitude [deg]		Longitude [deg]		Spin period [s]	
	Calculated	IM-Pegasus	Calculated	IM-Pegasus	Calculated	On board measurements
2004-11-22 18:06	73.3	73.16	341.4	343.26	77.42	77.48
2005-04-04 9:23	71.7	73.16	339.9	343.26	76.30	77.53
2005-07-29 1:48	74.9	73.16	341.2	343.26	77.05	77.48

Conclusions and Future Aspects

Using only kHz SLR data to derive spin parameters of satellites, opens completely new possibilities and areas for present and especially for future missions; larger separations between the individual elements of the retro reflector arrays automatically would increase the resulting accuracy. Suitable LRR geometries - to allow the identification of returns from single retro reflectors - enables complete spin axis determination from kHz SLR measurements. To get a more uniform distribution of returns from retro reflectors at different locations on the satellite, it would be easy to attenuate all echoes to the single photon level, resulting e.g. in the GP-B case in a much clearer identification of the 9^{th} retro returns (Fig. 9, 10).

As more such kHz SLR stations will be operational in the very near future (Herstmonceux in the UK, SLR 2000 in USA), the availability of kHz SLR data sets will increase, allowing even more accurate spin parameters determination. As the satellite's payload for SLR is only a passive retro array, without any need for power supply or transmission bandwidth – and without major concerns about operational life time - , it might be a good main or backup device to obtain independently spin parameters of satellites, in addition to its main task of precise orbit determination via SLR.

Acknowledgment

The authors would like to thank Paul Shestople of Stanford University for providing the on-board GP-B spin rate data.

References

[1] GP-B Home Page: http://einstein.stanford.edu/

[2] LRR Manufacturer Home Page: http://www.iteinc.net/

[3] T. Otsubo, J. Amagai, H. Kunimori, and M. Elphick, "Spin motion of the AJISAI satellite derived from spectral analysis of laser ranging data", IEEE Transactions on Geoscience and Remote Sensing, Vol. 38, No. 3, May 2000.

[4] G. Kirchner, W. Hausleitner, E. Cristea, "AJISAI Spin Parameters Determination using Graz kHz Satellite Laser Ranging Data", IEEE Transactions on Geoscience and Remote Sensing, Vol. 45, No. 1, January 2007.

LAGEOS-1 spin determination, using comparisons between Graz kHz SLR data and simulations

D. Kucharski[1], G. Kirchner[2]

1. Space Research Centre, Polish Academy of Sciences, Borowiec, ul. Drapalka 4, 62-035 Kornik, Poland.

2. Space Research Institute, Austrian Academy of Sciences, Lustbuehelstrasse 46, A-8042 Graz, Austria.

Contact: kucharski@cbk.poznan.pl / Tel. +48 61 817 01 87;
Georg.Kirchner@oeaw.ac.at / Tel. +43 316 873 4651

Abstract

kHz SLR data contains unique information about the measured targets; this information allows e.g. determination of spin parameters (spin period, spin direction, spin axis orientation) of various satellites, using various methods for different spin periods / satellites: Spectral analysis for spin periods of 2 s (AJISAI (Kirchner et al, 2007)), simulations for spin periods of 77.5 s (GP-B), and comparing simulation results with kHz data for very long spin periods like LAGEOS-1 (about 5000 s).

For the long LAGEOS-1 spin periods, we developed a method to calculate spin axis orientation and spin period from Graz kHz SLR data. This method is based on simulation of returns from each retro reflector, with spin period and spin axis orientation as input parameters. Varying these parameters, the simulation generates retro tracks similar to those seen in the kHz SLR data; comparing simulated and measured tracks, allows determination of spin period, and spin axis orientation. Applying this method to a set of LAGEOS-1 passes - covering a period of 178 days – shows also the slow change of the LAGEOS-1 spin axis direction with time.

***Keywords**: satellite laser ranging, LAGEOS-1, satellite spin*

Introduction

LAGEOS-1 and LAGEOS-2 are identical satellites in circular orbits, about 5,900 km above Earth's surface. Both satellites are spheres with 60 cm diameter, covered with 426 cube corner reflectors (CCRs) arranged in 20 rings symmetrically with respect to the satellite equator (Fitzmaurice et al., 1977) . Because the satellites are totally passive, their orbital motions are affected only by the natural perturbations. In this paper, we analyse only kHz SLR data of LAGEOS-1, due to its very low spin rate.

Perturbations can be of gravitational, non-gravitational (for example: Yarkovsky effect, Yarkovsky-Schach effect) or magnetic nature. SLR distance measurements to the satellites allow precise determination of these orbital perturbations and consequently identification of their origin. The more accurately we can determine the effect of perturbations, the more reliably we can obtain the geodynamical parameters of the Earth, and the relativistic effects in the near space (Ciufolini and Pavlis, 2004). It is expected that a detailed knowledge of LAGEOS-1 spin behaviour should improve the accuracy of such analysis, and will help to identify and confirm the source and magnitude of the (unknown) perturbations, which are introduced presently as empirical accelerations in actual models.

Up to now two methods were used to calculate spin parameters of LAGEOS satellites: frequency analysis of full rate SLR data (Bianco et al, 2001) and analysis of

photometric observations. The frequency analysis works well if the spin rate is not too low (e.g. 23.5 s for LAGEOS-2 in May 2000 gives good results in Bianco et al, (2001), but is not applicable anymore for larger spin periods, like the expected 5000 s for LAGEOS-1 in 2004 (Andres et al., 2004). Photometric measurements of LAGEOS-1 spin parameters were performed until 1997, when they were ceased because of a too low spin rate. In total, 57 photometric observations were carried out for this satellite (Andres et al., 2004), which allowed verification and improvement of the models of its spin motion. The most accurate model describing changes in the parameters of LAGEOS-1 spin is LOSSAM (Andres et al., 2004). According to this model, LAGEOS-1 started the third phase of its life in 1999, where the influences on spin parameters by magnetic, gravitational and non-gravitational torques are of the same order of magnitude. Bertotti and Iess (1991) have predicted that at this phase LAGEOS-1, having reached an extremely low spin rate, will start tumbling more and more, rapidly changing orientation of the spin axis, with chaotic dynamics.

SLR Graz kHz laser measurements

Usually, SLR stations measure distances to satellites with laser repetition rates of 5 or 10 Hz. The Graz SLR station was the first station to measure with a laser repetition rate of 2 kHz (Kirchner and Koidl, 2004). Because of the very short 10 ps laser pulses, and the single photon detection system, the measurements are not only very precise (2–3 mm single shot RMS), but also allow identification of retro – reflector tracks in the data, easily seen due to their slightly different distances.

After a successfully measured satellite pass, the differences between measured and predicted distances are calculated. From these residuals the systematic trends are eliminated, e.g. by using polynomials; plotting these residuals (Fig. 1), different tracks from various retro-reflectors (or groups of them) can be identified easily. Residuals of nearer satellite prisms are on the bottom (satellite front), and residuals originating from more distant prisms are more towards the top in this figure.

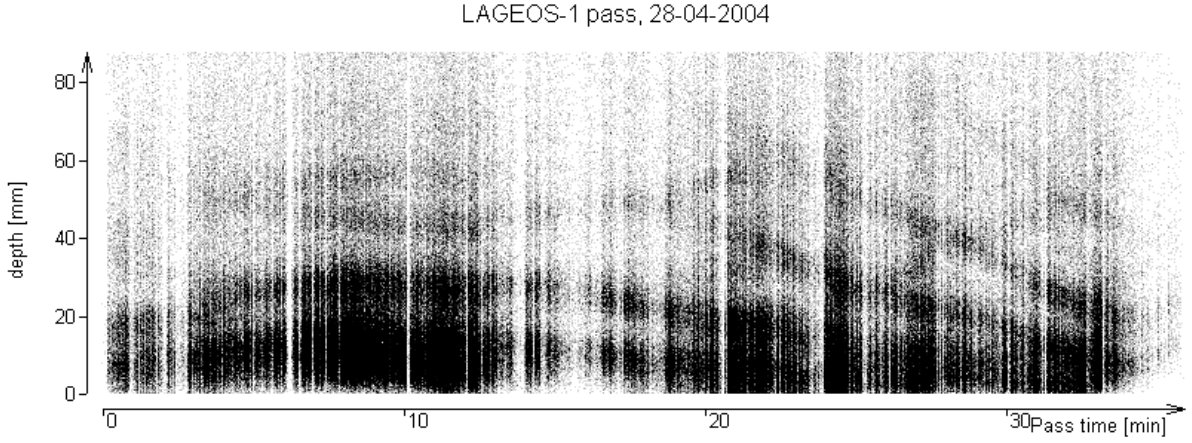

Fig. 1. *Range residuals of a LAGEOS-1 pass, measured by Graz kHz SLR system, 28-04-2004, 2 a.m. (P1)*

The residuals plotted in Fig. 1 refer to a LAGEOS-1 pass of April 28th, 2004 (P1). During the 35 minutes of the pass, more than 500,000 returns were measured. The majority of the returns come from the nearest retro-reflectors; the detection probability for returns from more distant retro – reflectors on the satellite's sphere is decreasing. The reason for this effect is the geometry between the incident laser beam and the CCR. Total internal reflection of LAGEOS-1 optical retro - reflectors depends

on the angle between the incident laser beam and optical axis of the CCR as well as on the azimuth angle giving the direction of the incident beam about the normal to the front face of the CCR (Arnold, 1979; Otsubo and Appleby, 2003).

Identification of the single prism tracks – the method

The tracks in Fig. 1 are due to the passage of retro – reflectors through the field of view of the telescope; thus they contain information on the satellite spin (Arnold et al., 2004). To recognize spin parameters out of the geometry of these spin tracks we developed a new method based on simulations of SLR measurements. The model used in these simulations is divided into two parts. The first part (macro-model) contains the Earth's rotation, the site position in ITRF2000 (Altamimi et al., 2002) and the orbital motion of the satellite. The second part (micro-model) contains the retroreflector-array arrangement and the range correction function (Fitzmaurice et al., 1977). In present study the model does not contain CCR transfer function (Arnold, 1979). The range correction function describes the photon's time of flight delay when the photon is going through the glass of the CCR. This correction depends on refractive index of the glass and the angle of incidence.

The geometry of range residuals distribution depends on spin parameters of the satellite: spin axis orientation and spin period. To calculate spin parameters it is necessary to determine epochs of the spin tracks and their tilt angles. The pass shown on Fig. 1 contains horizontal and tilted CCR tracks.

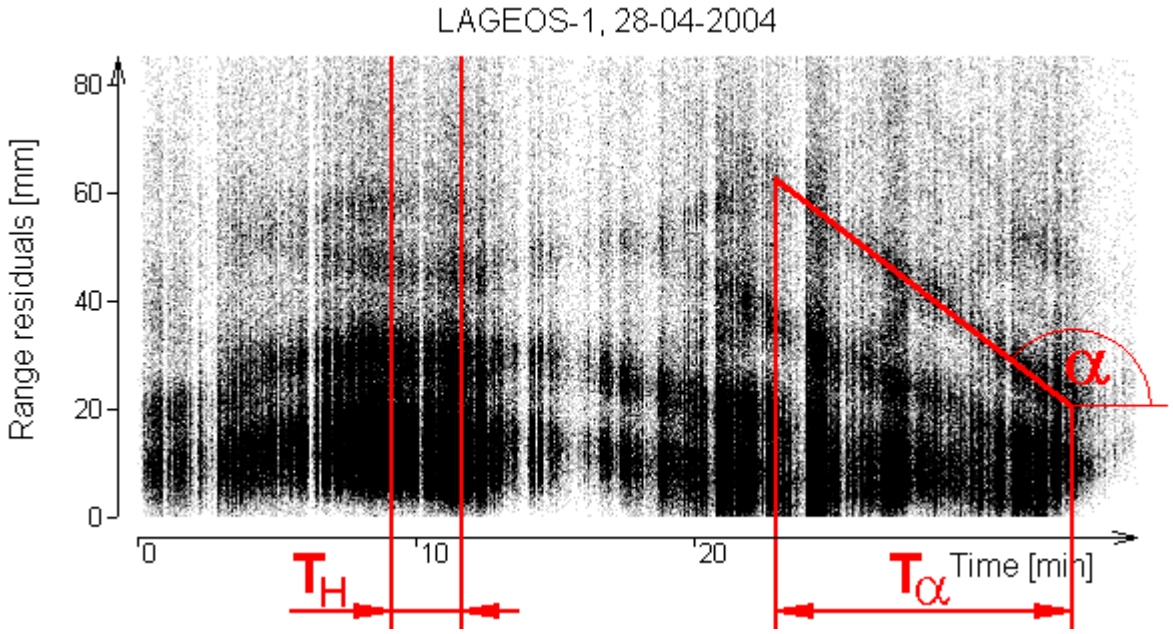

Fig. 2. *Range residuals distribution: T_H - epoch range of horizontal tracks, T_α - epoch range of α-tilted track, pass start 28-04-2004, 2 a.m.*

By using simulations it is possible to generate range residuals for every CCR distributed over the visible satellite's surface. Figure 3 presents examples of simulated CCR's trajectories for different spin parameters of the pass presented on Fig 2. For both charts spin period remains the same, but the second case was generated for different spin axis orientation: both angles (longitude and co-latitude) were increased by 10°. The geometry of the CCRs trajectories is very sensitive for spin parameters.

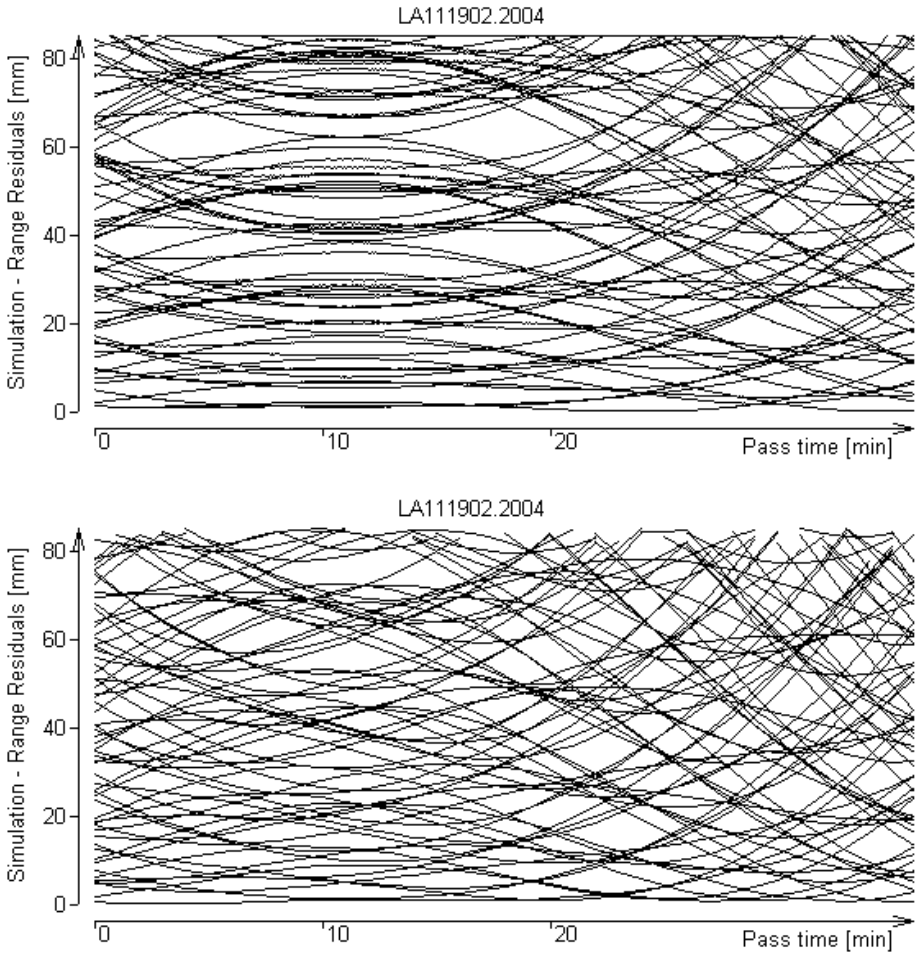

Fig. 3. *Simulations of the CCR's trajectories for the pass presented on fig 1, for both cases spin period stays constant, but spin axis orientation for the bottom situation is shifted by 10° in longitude and colatitude.*

Spin parameters determination

The LAGEOS-1 pass shown in Fig. 2 (P1) shows two significant kinds of range residuals distribution - horizontal and α-tilted - which allows determination of the satellite's spin rate. LOSSAM predicts a spin period of about 5,000 s for LAGEOS-1 for the first half of 2004. Therefore we simulated range residuals for the pass P1 for spin periods T_S from –8,000 s to –3,000 s and from 3,000 s to 8,000 s with 50 s steps, and for all spin axis orientations with 1° steps.

Figure 4 shows results of simulations for all possible spin axis orientations (longitude and colatitude), for a spin periods of T_S=-6,000 s and T_S=6,000 s. The top chart presents amounts (right scale – color bar) of α-tilted spin tracks in T_α epoch range for all spin axis orientations, the middle chart presents amounts of flat spin tracks in T_H (T_α and T_H are given for the pass presented on Fig. 2). During all simulations the algorithm was searching for simulated α-tilted CCR tracks within $\alpha \pm 5$ deg. The bottom charts (Fig 4) show the sum of the top and the middle charts, evaluated pixel by pixel; as can be seen, for some spin axis orientations both kinds of spin tracks can exist. Such common spin axis orientation areas are the biggest for –6,000 s (counter-clockwise rotation) and 6,000 s (clockwise rotation), therefore those spin periods were chosen for further investigation.

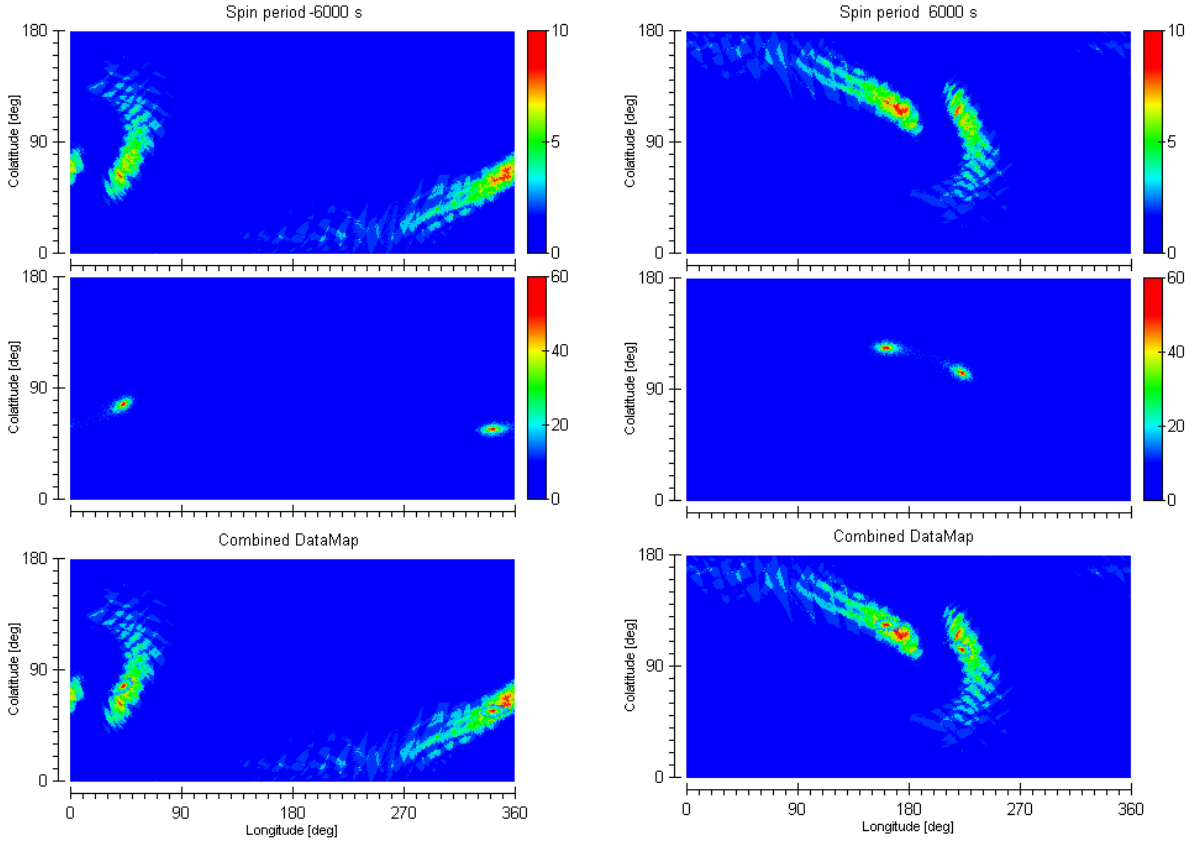

Fig. 4. *Simulation results for spin period of T_S=-6000 s (left) and T_S=6000 s (right); Top: Amounts of a-tilted spin tracks; Middle: Amounts of horizontal spin tracks; Bottom: Sum of Top and Middle, pixel-by-pixel*

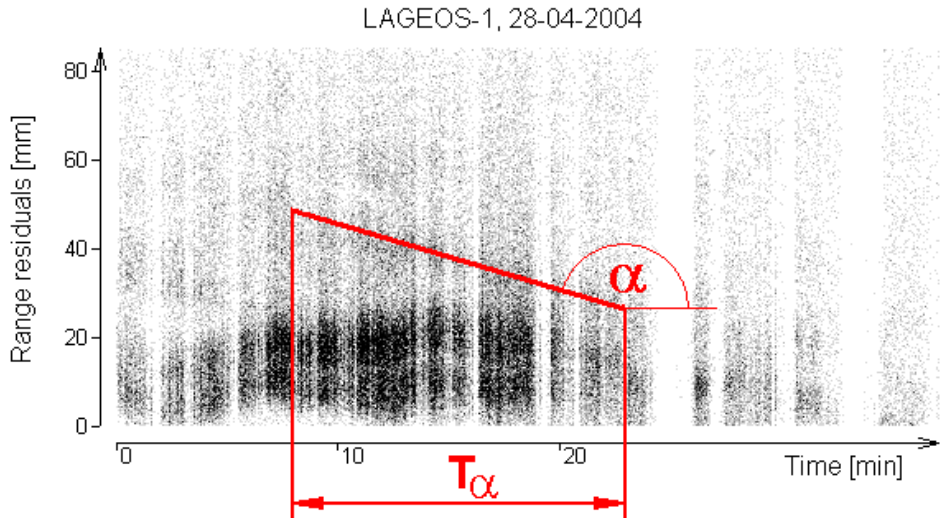

Fig. 5. *Range residuals of LAGEOS-1 pass tracked 12 hours later (P2), pass start 28-04-2004, 2 p.m.*

For both spin periods it is possible to detect two different solution areas (Fig. 4, the bottom charts), due to the symmetrical arrangement of the CCRs over the surface of the satellite. After processing four solutions were obtained, two for CW and two for CCW spinning. To identify which is the real one we used a LAGEOS-1 pass (P2) tracked 12 hours after the main pass (P1) – Fig. 5.

Supposing that spin parameters of the satellite will not change significantly during 12 hours (from pass P1 to pass P2), one of the solutions determined for P1 should be the solution also for pass P2. Figure 6 presents three charts; the top one shows spin axis orientation solution for P1 and the middle chart for P2. The bottom chart shows common area of solutions for these two passes (pixel by pixel comparison); the appropriate spin axis orientation for both P1 and P2 was calculated as a mean value of this area.

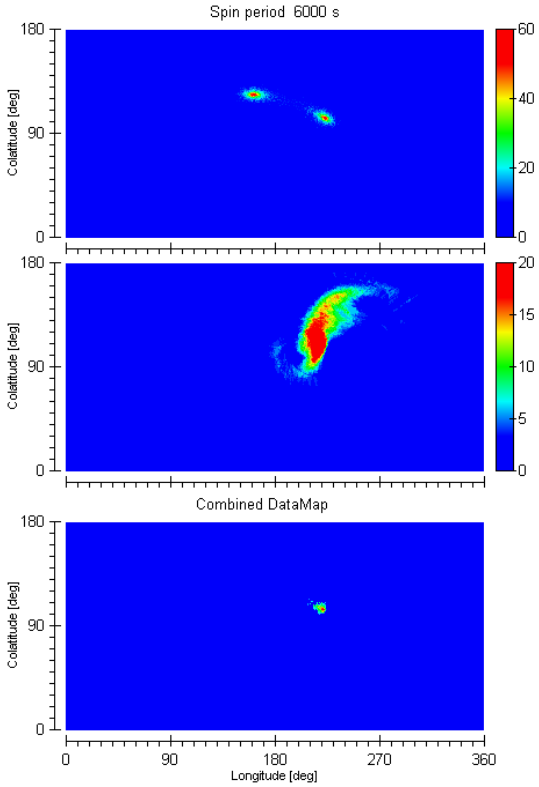

Fig. 6. *Simulation - results; Top and middle: solutions for passes P1 and P2; Bottom: common area of the solutions*

Using this pass-to-pass method reduces the amount of possible solutions from four to one; the spin parameters of LAGEOS-1 calculated from these two passes are: spin period (CW) T_S=6,000 s, spin axis orientation: colatitude=103.8 deg, RMS=3.66 deg, longitude=224.2 deg, RMS=3.76 deg. All parameters are expressed in the J2000 inertial reference frame.

This pass-to-pass method was used to process 33 passes during 178 days of year 2004. Figures 7 and 8 present results for colatitude and longitude of spin axis orientation. The results were obtained for spin period T_S=6,000 s, mean value of RMS for all colatitude results is RMS_{COL_mean}=5.87 deg, and for longitude RMS_{LON_mean}=7.19 deg.

For both angles the scatter around the fitted trend function is visible and has similar magnitude. That may be caused by inaccuracy of the used method or even by chaotic changes of the spin axis precession. The trend function of colatitude values shows sinusoidal decreasing during the investigated time period, while the longitude angle is more stable.

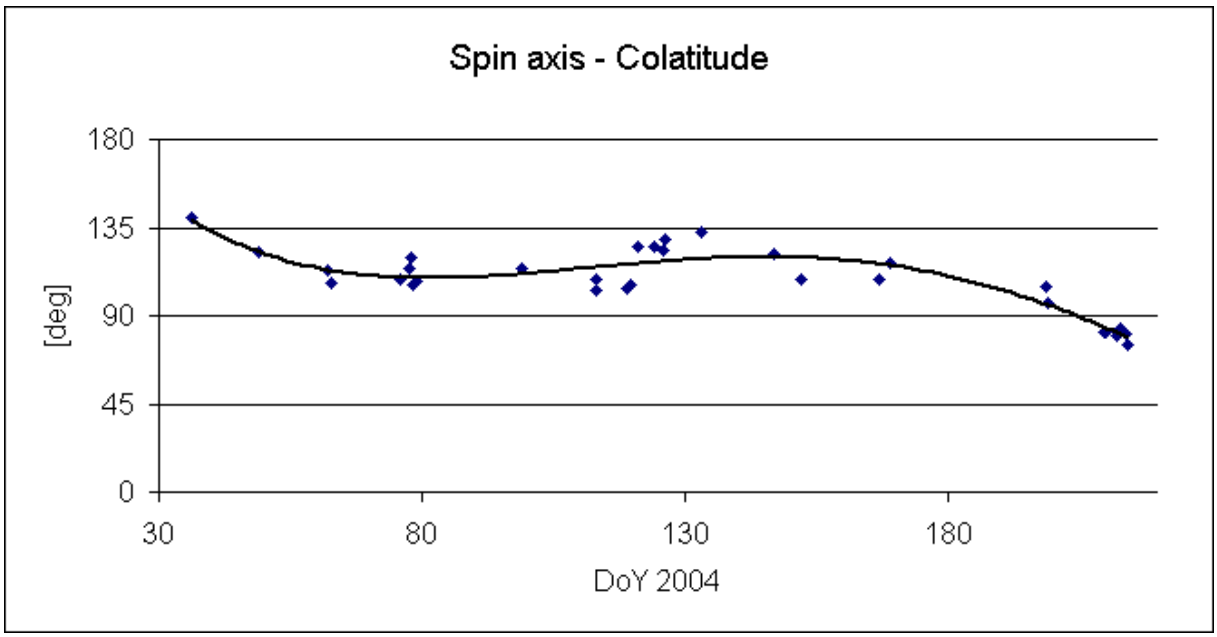

Fig. 7. *Time-series of colatitude angle observations of the spin axis of LAGEOS-1, and trend function*

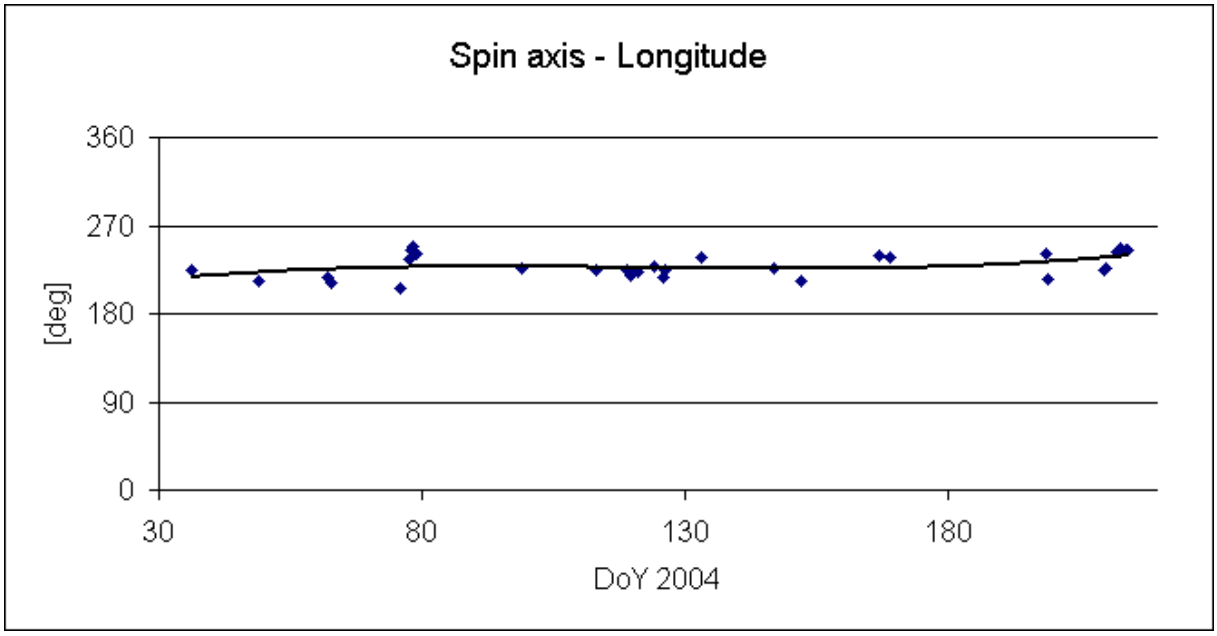

Fig. 8. *Time series of longitude angle observations of the spin axis of LAGEOS-1, and trend function*

Conclusions

The analysis presented in this paper identifies spin tracks in kHz SLR measurements to LAGEOS-1, and uses them to fully determine the spin parameters of this very slowly spinning satellite. This was possible by identifying the geometry of the observed tracks and looking for similar geometries in simulations generated for various spin parameters. This process allows to find several possible solutions, but with the pass-to-pass method it is possible to find a single common solution for two consecutive passes. This method can be applied only when spin parameters do not change significantly between the two analysed passes. Only one out of 33 investigated

passes contains both horizontally and α-tilted CCR tracks, which are both necessary to determine the spin period of the satellite. The simulation model used for presented investigation is missing CCR energy transfer function, thus obtained results contain additional error. The transfer function will be taken into account with next version of the model and then analysis process will be repeated.

The accuracy of our method is a few times worse than that of photometric measurements. However, for long spin periods kHz SLR measurements and this simulation-based method is the only source of information about spin parameters of LAGEOS-1.

kHz SLR measurements, as started for the first time at the Graz SLR station, have opened new possibilities, allowing determination of the satellite spin parameters when all other methods fail. Additionally, the expected increase of the number of kHz SLR stations in the near future will improve the accuracy of spin parameter determination by a few orders of magnitude.

Acknowledgments

This work has been supported by the Ministry of Science and Information of Poland under grant No. 4T12E 062 29.

References

[1] Altamimi, Z., Sillard, P., Boucher, C. ITRF2000, A new release of the International Terrestrial Reference Frame for Earth science applications, J. Geophys. Res. 107(B10), 2214, 2002

[2] Andrés, J. I., Noomen, R., Bianco, G. et al., Spin axis behavior of the LAGEOS satellites, J. Geophys. Res., 109(B6), B06403, doi:10.1029/2003JB002692, 2004

[3] Arnold, D., Method of calculating retroreflector-array transfer functions, Spec. Rep. 382, Smithon. Astrophys. Obs., Cambridge, Mass.,1979

[4] Arnold, D., Kirchner, G., Koidl, F., Identifying single retro tracks with a 2 kHz SLR system – simulations and actual results, 14th ILRS Workshop, 2004

[5] Bertotti, B., and L. Iess, The rotation of LAGEOS, J. Geophys. Res., 96(B2), 2431–2440, 1991

[6] Bianco, G., Chersich, M., Devoti, R. et al., Measurement of LAGEOS-2 rotation by satellite laser ranging observations, Geophys. Res. Lett., 28(10), 2113–2116, 2001

[7] Ciufolini, I., Pavlis, E., A confirmation of the general relativistic prediction of the LenseThirring effect, Nature, 431, 958-960, 2004

[8] Fitzmaurice, M.W., Minott, P.O., Abshire, J.B. et al., Prelaunching testing of the Laser Geodynamic Satellite (LAGEOS), NASA Technical Paper 1062, NASA, 1977

[9] Kirchner G., Hausleitner W., Cristea E., "Ajisai Spin Parameter Determination Using Graz Kilohertz Satellite Laser Ranging Data", IEEE Trans. Geosci. Remote Sens., vol. 45, no. 1, pp. 201-205, Jan. 2007

[10] Kirchner, G., Koidl, F., Graz KHz SLR System: Design, Experiences and Results, 14th ILRS Workshop, 2004

[11] Otsubo, T., Appleby, G., System dependent center-of-mass correction for spherical geodetic satellites, J. Geophys. Res., 108(B4), 2201, doi:10.1029/2002JB00209, 2003

Measuring Atmospheric Seeing with kHz SLR

Georg Kirchner[1], Daniel Kucharski[2], Franz Koidl[1], Jörg Weingrill[1]

1. Austrian Academy of Sciences, Institute for Space Research, Graz
2. Space Research Centre, Polish Academy of Sciences, Borowiec, Poland

Contact: Georg.Kirchner@oeaw.ac.at ; kucharski@cbk.poznan.pl ; Franz.Koidl@oeaw.ac.at ; Joerg.Weingrill@oeaw.ac.at

Abstract

During night-time kHz SLR operation in Graz, we use an ISIT camera to see satellites, stars, and also the backscatter of the transmitted kHz laser beam (Fig. 1). This backscatter image of the laser beam shows a beam pointing jitter in the order of several arcseconds, caused by the actual atmospheric conditions ("Seeing").

Using real time image processing, we determine the area of this beam pointing jitter, and derive the actual astronomical seeing values. These values depend not only – as usual for optical astronomy - on actual atmospheric conditions and on elevation of telescope, but also on the angular speed of telescope motion. In addition, the seeing values are considerably bigger (worse) during winter time, when – due to heating and poor isolation of the Graz observatory - the air above the observatory roof is significantly more turbulent than during the other seasons.

This beam pointing jitter due to atmospheric turbulence can reach a similar magnitude as the laser beam divergence; it spoils our pointing accuracy, affecting our return rate especially from higher satellites. To reduce these effects, we are planning to use a fast steering mirror, which is controlled by the ISIT image derived laser beam pointing offsets.

Introduction

The ISIT camera observes the backscatter of the transmitted laser beam; the image is transferred into the PC via a standard frame grabber. The software (written in C++) now uses the brightness of each pixel, to find out the borders of the laser beam image, and to determine the coordinates of the peak. The offset of the peak from the center (as defined by the illuminated reticle, visible in Fig. 1), is kept as a result for each processed image. This image processing at present is running with 25 Hz, and can handle each ISIT image.

The offsets of the laser beam pointing show variations in the several arcsecond range, and with frequencies between few Hz up to 25 Hz.

Possible reasons for the Laser Beam Pointing Jitter (other than atmosphere)

To verify that this jitter in laser beam pointing is NOT caused by the laser itself, we installed a Laser Beam Monitor at the exit window of the laser box (Fig. 2).

A mirror reflects a small portion of the laser beam (<< 1%) on a CCD chip; the CCD image is monitored by a PC, with up to 30 fps; for each image, the PC calculates the center coordinates (X/Y) of the laser beam, and stores single frame center coordinates and / or averaged values. This data sets (Fig. 3) show that the pointing stability of the laser at the output window of the laser box is in the order of a few microrad (<< 1", more or less within the measurement accuracy); there is no indication of a laser beam induced pointing jitter, as seen in the atmospheric backscatter images. The only visible effect is a very fast (few seconds) warm-up time at start of firing (Fig. 3)

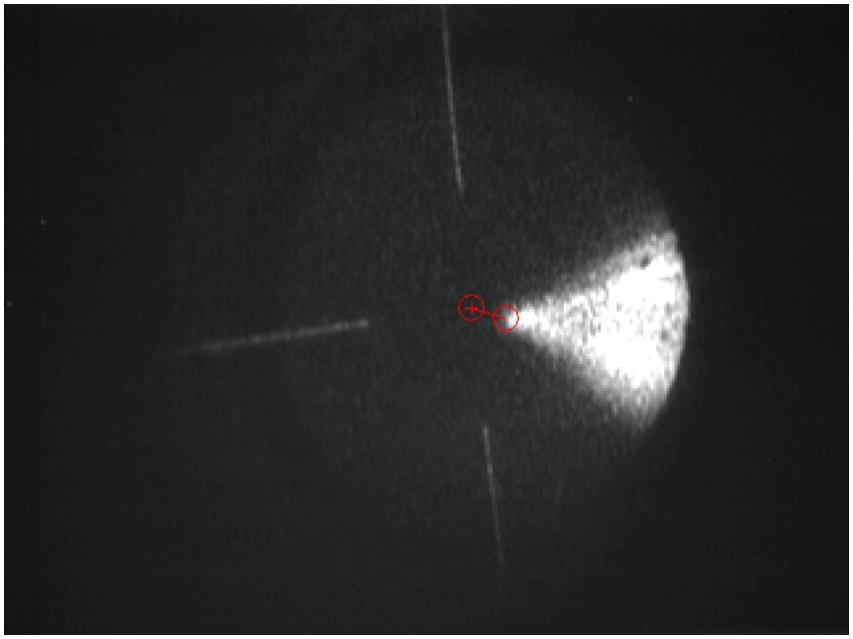

Fig. 1: *ISIT image, with laser beam backscatter, laser beam peak as determined by image processing, and its offset from the center. This offset shows a pointing jitter due to atmospheric turbulence*

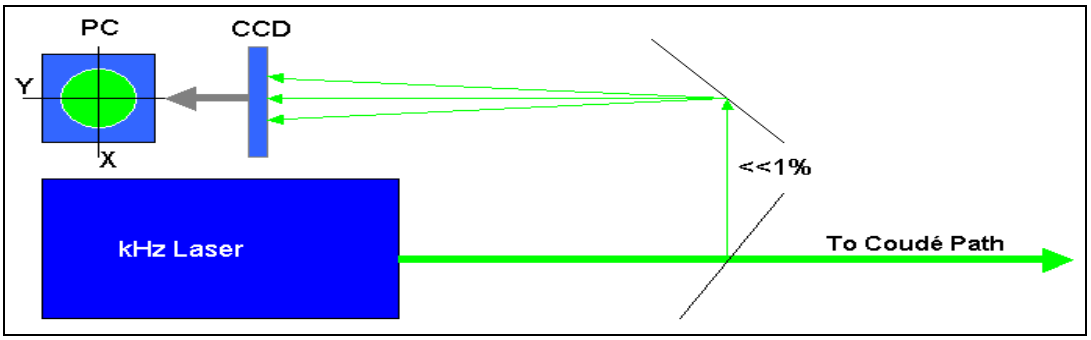

Fig. 2: *Laser Beam Monitor*

Another possibility for the observed laser beam pointing wobble is the mount itself; but tests with fixed mount showed the same wobble of the laser beam pointing.

Laser Beam Pointing Jitter: It is due to atmosphere !

We concluded that the Laser Beam Pointing Jitter is caused by atmospheric micro-turbulences (atmospheric "seeing"); after talking with astronomers working in Graz, we expected seeing values of about 2-4 arcseconds as an average, with expected frequencies from a few Hz up to a few 10 Hz.

However, our measurements usually showed higher seeing values, ranging from about 3" up to more than 8"; there are several reasons for that:

- The fast moving SLR telescope, instead of a more or less constant pointing (or only slow moving) astronomy telescopes; the atmospheric conditions during SLR tracking are therefore changing much faster;
- Heating of the – almost NON-isolated – observatory in cold winter nights; the leakage causes heating of the surrounding air, which heavily degrades seeing; and most astronomy work at the Graz observatory is done usually in autumn, with almost NO heating of the rooms;

- SLR in Graz is usually done down to 10° elevation and lower, where seeing values are increasing.

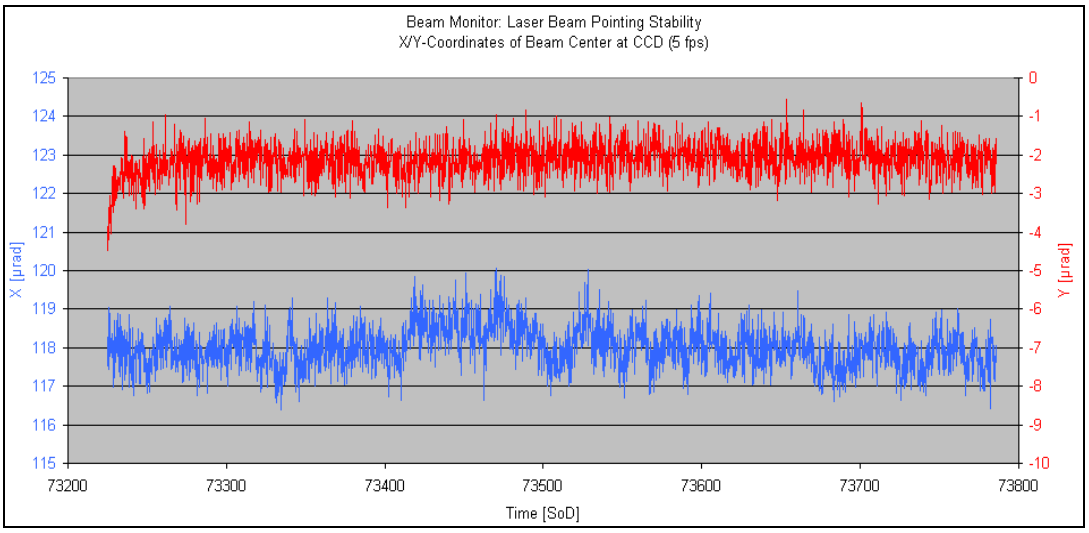

Fig. 3: *X/Y coordinates of Laser Beam Center, 10 minutes of routine SLR operation.*

What are the effects for SLR ?

The minimum laser beam divergence of SLR Graz is about 5”; with a pointing jitter caused by seeing values up to 3” to 8” (and sometimes worse) the “hit rate” or pointing accuracy will decrease (Fig. 4), reducing the return rate.

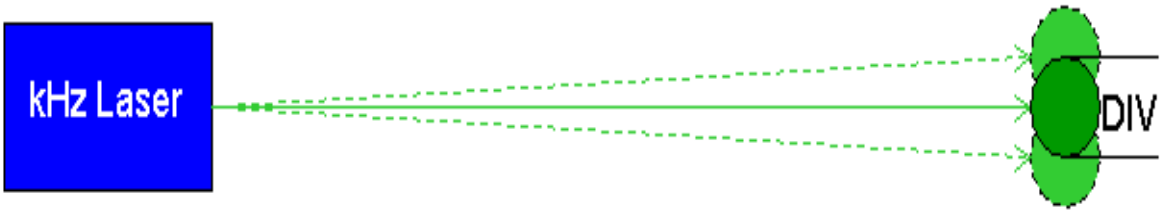

Fig. 4: *Atmospheric turbulences cause laser beam jumping*

Verifying the Seeing Values

To check and verify the seeing values, as measured by the beam pointing jitter, we used the standard DIMM (Differential Image Motion Monitor; Hartmann – Shack) method: With an additional, standard telescope we observed e.g. the polar star; a mask with 2 small holes at a specified distance is placed at the entrance pupil of the telescope (Fig. 5); a CCD (defocused; placed with some offset from the focal plane) monitors the 2 spots created from the star light and the two holes; all images are stored on the PC.

The atmospheric turbulences cause the dual star images to move relatively to each other; this relative motion is measured in the PC, and allows calculation of the atmospheric seeing values.

A typical result of such seeing measurements is shown in Fig. 6; showing an average seeing value of 3” to 4”; it was made in summer time (no heating), at 45° elevation (polar star) and with constant pointing (star).

Seeing Values Derived from kHz Laser

Using the ISIT-Camera and the image processing programs- as described at the beginning - we monitored the atmospheric seeing values automatically during routine

SLR operation for several months; due to the method, we were able to collect seeing values along each tracked pass, and to correlate it with azimuth and elevation of each pass. As an example, an AJISAI pass with about 50° maximum elevation is shown in Fig. 7; tracking started / stopped at about 10° elevation; the correlation between elevation and seeing is obvious for this pass; however, other passes showed sometimes completely different values. Such a different pass is shown in Fig. 8: an ENVISAT pass, with a maximum elevation of <30°, starts with the usual decrease of the seeing value with increasing elevation; however, it then shows a significant INCREASE.

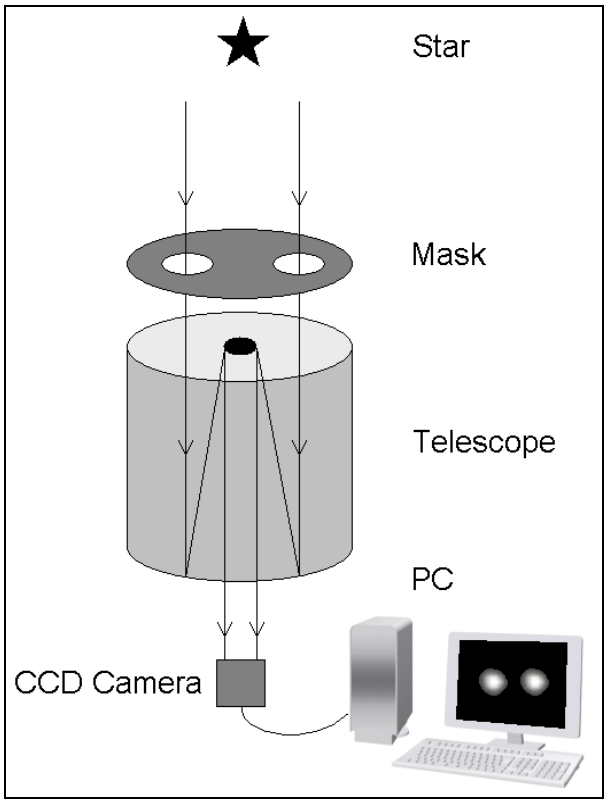

Fig. 5: *Differential Image Motion Monitor (DIMM) / Hartmann – Shack method.*

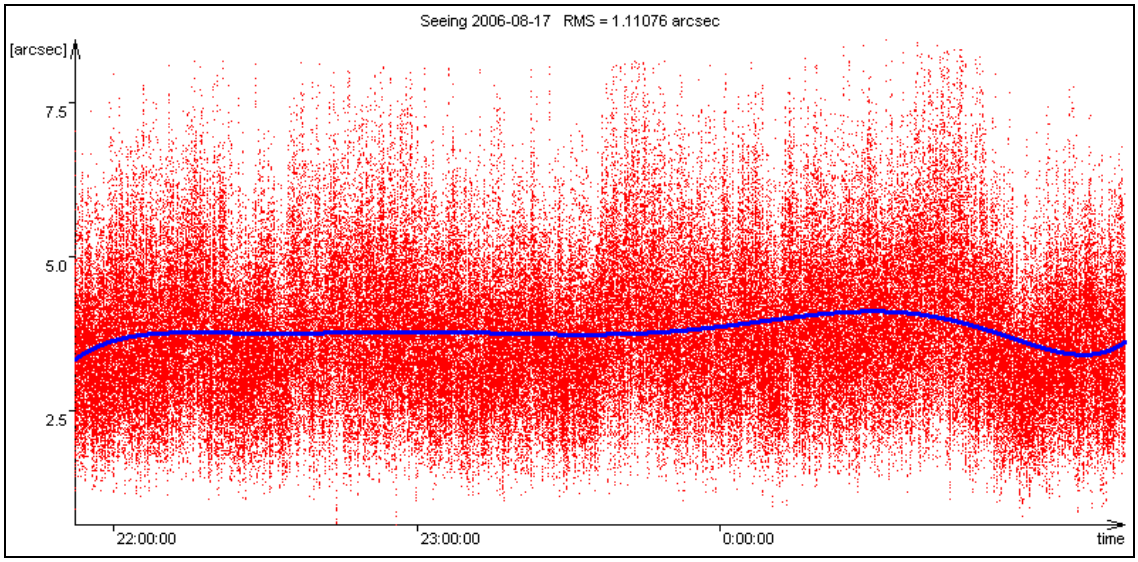

Fig. 6: *Seeing Values measured with DIMM: Summer night, polar star used.*

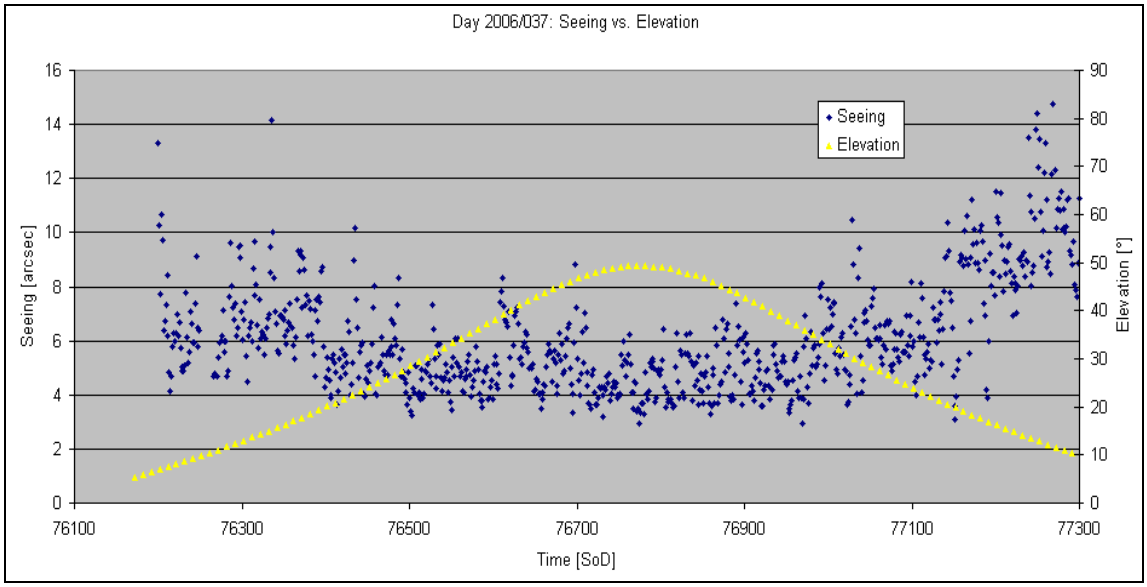

Fig. 7. *Ajisai: day of year 2006 / Day 037: Seeing changes with elevation.*

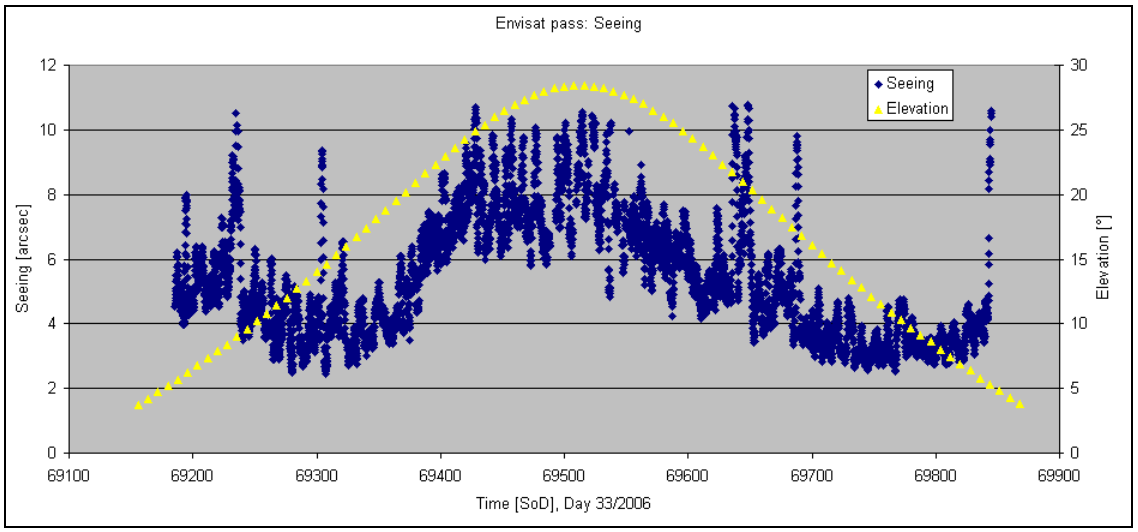

Fig. 8: *Envisat: day of year: 33, < 30° Elevation*

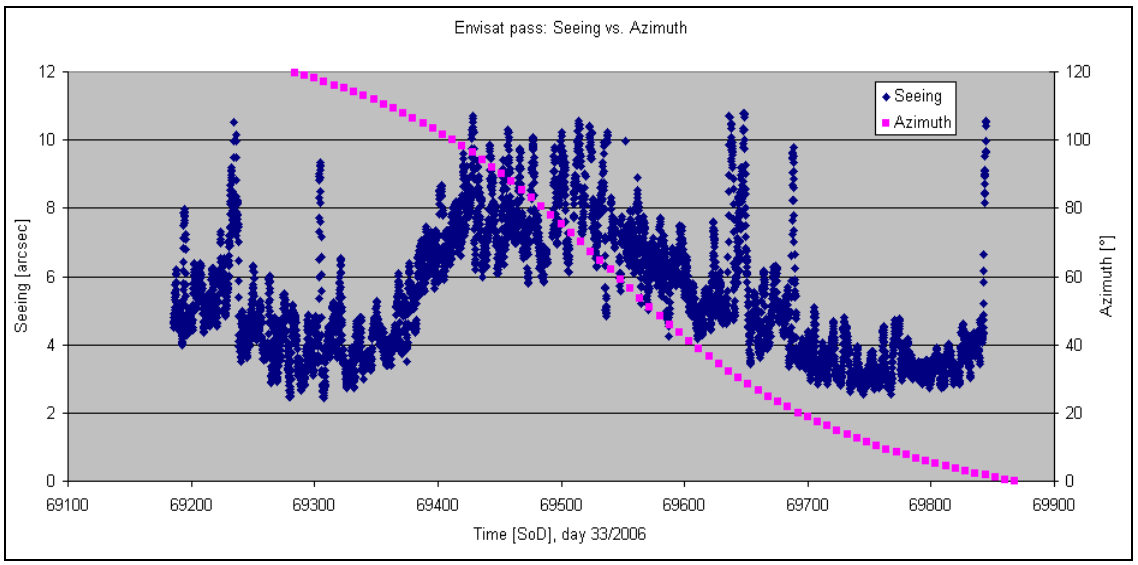

Fig. 9: *At 90° Azimuth: => Obs. Roof, Heating Influence*

The explanation for such a strange behaviour: At this time we started to track (at 90° azimuth) along / above the observatory, where the leakage of the heated building caused increasing turbulence, and hence increasing seeing values (Fig. 9).

Future plans:

We will continue to monitor atmospheric seeing values along the laser beam path during routine SLR operation at night; at least we should get some valuable statistics about the seeing values at the observatory (no such records exist here up to now). In addition, there are plans to install a Fast Steering Mirror (FSM) at the laser bench, to be able to compensate at least partially the beam pointing jitter, using the actual pointing offsets of the laser beam as derived from the ISIT images as control input to the FSM. The goal is to increase return rate from high satellites, like GPS, Giove etc.

TIMING SYSTEMS SESSION SUMMARY

Chair: Yang Fumin

More Event Timers are available, for 2 KHz and even higher repetition rates:

- A032-ET from Latvia, precision 10 ps, 10 KHz
- P-PET-C from Prague, Czech Republic, precision 2.5 ps, 2 KHz
- T2L2 ET from OCA, France, precision 2 ps, ~2 KHz
- ET from HTSI, USA, precision 2 ps, ~50 KHz

With much improved linearity and thermal drift.

Question: Are the prices for these ETs available?

Y. Zhang from Shanghai showed in a poster that only one FPGA chip can work as a timer for future space applications or other compact systems.

A032-ET Experimental Test on Changchun SLR

FAN Cunbo[1], DONG Xue[1,2], ZHAO You[1], HAN Xinwei[1]

1. National Astronomical Observatories/Changchun Observatory, CAS
2. Graduate University of Chinese Academy of Sciences (CAS), Beijing

Abstract

This paper introduces the experimental test of A032 Event Timer on Changchun SLR. First, the pulse delay generator DG535 is used to generate two path signals to simulate the start and stop signal, and the A032-ET to measure the intervals. Then, it also gives out the system hardware connection diagram, analyzes signal time sequence and shows the software flow chart. Finally it shows the results of ranging the ground target and the satellites.

Key Words: Event Timer, A032-ET, Satellite Laser Ranging (SLR), Simulation

Introduction

Satellite Laser Ranging (SLR) is the most accurate satellite tracking technique available with single shot positional accuracy under a centimeter and normal point corrected data able to claim precision of just a few millimeters. The SLR tracking method requires a pulsed laser source and a telescope which is used to collect the reflected laser light on its return. The laser provides a detectable link between a fixed station and a distant satellite moving in the space. The telescope and associated equipment determine a very precise location and velocity for both the satellite and station from the data provided by the laser beam. Time interval from station to the satellite and back can be calculated by counters, which is transferred into the range we want.

The SLR data are used to improve the orbital predictions for the tracked satellites which, in turn, make the satellites easier to track. In other words, the more data we get the better precision of orbit prediction we can calculate. Increasing the firing frequency is a convenient way to increase data, and there are many stations around the world trying to do KHz SLR system. SLR, in essence, is a method of satellite tracking. The key equipment for increasing the firing frequency are the counter and laser source. But now the KHz laser source is available in the world. And here we put the emphasis on the counter. There are two kinds of counters: the Time Interval counter and the Event Timer counter. The interval counter measures the time the laser flight from the station to satellite and back. HP5370 and SR620 are the most popular used interval timers in the global SLR society. The Event Timer records the epochs of signals received by both channel A (start) and B (stop) and puts them into buffer. Then the epochs are matched by range gate prediction. Event Timer calculates intervals with epochs, and in theory, with no rate limits but reading and processing data.

While using Event Timer, sending range gate is the most important technical difficulty, and the match of start and stop signals is also very important. Many stations in the world are adopting Event Timer as counter to advance their systems. PET4 has been used in Wettzell station, which is assembled by Dassualt model; P-PET 2000 begun to work in San Fernando in 2004, and Graz station have already completed KHz system; the KHz system in Herstmonceux is on developing stage, and almost finished. A032-ET developed by Latvia University using EET method also fits for KHz system in theory.

Status In Changchun

There are two interval counters in Changchun station: HP5370B is used routinely and SR620 as a standby. The observation in Changchun is excellent these years and the system is steady. The single shot precision is less than 2cm, and the passes observed every year are more than 4,000. However, the laser fire frequency is not very high: 8Hz for low orbit satellites and 5 Hz or 4Hz for high orbit satellites. We plan to use the Event Timer to increase firing frequency to 10Hz and even higher so as to increase the quantity of data. After analyzing all Event Timers, the A032-ET was chosen for Changchun experiment, and the purpose is to increase the firing frequency for all satellites to 10Hz, and even higher. As an Event Timer, A032-ET is superior to interval counter; some specifications are shown in Table 1.

Table 1: *A032-ET specifications*

Single shot RMS		<10 ps
Dead time		60 ns
Nor-linearity error		< 1 ps
Offset temperature stability		<0.1 ps
FIFO depth		1,200
Measurement rate	Option 1	Up to 10KHz continually
	Option 2	Up to 500Hz cycle repetition rate

Figure 1. *Hardware of A032-ET*

There are two currently available options of the A032-ET, which use the same specialized hardware (Figure 1 shows the hardware of A032-ET) but differ by the software. These options provide alternatively two basic kinds of measurement: The option A032.1 provides continuous (gapless) measurement of events at high (up to 10 KHZ) mean measurement rate. It is well suitable to measure the overlapped time intervals between Start and Stop events that come at the separate inputs (either A or B) of the Event Timer in any order. Specifically this is the case of advanced SLR at KHz repetition rate. The option A032.2 provides cyclical measurement of events that come at the separate inputs of the ET-device in the strict order. Specifically this is the case of conventional SLR where the measured Start-Stop time intervals do not exceed the repetition period of Start events. Considering our purpose, we choose A032.1 option to do the experiment, and the range gate has to be redesigned to fit for the new counter.

Experiment test and real observation on Changchun SLR

Before experiment we redesign the range gate control circuit, and the scheme is represented in Figure 2.

Range gate control circuit is assembled by three circuits, which are designed by the same module. The three circuits generate gate signal circularly and then are imported into an OR gate. Finally, the RG_out is transmitted as the range gate we want.

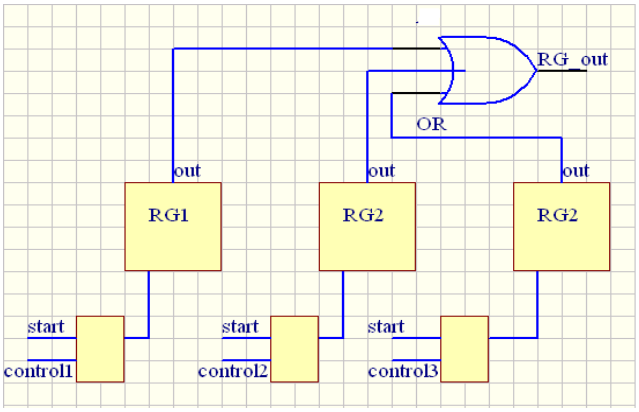

Figure 2. *Range gate control circuit*

Simulation

In this simulation, we use pulse generator DG535 as a signal source. It generates two NIM signals, and the interval was measured by A032-ET. The rate is set to 10Hz for the purpose is increasing the frequency to 10Hz. The interval sent by DG535 is static and the trigger is interior. The hardware connection scheme is shown in Figure 3, and the software flow chart is showed in Figure 4. All through the test, A032-ET worked normally, it measured the interval with the precision of ps under the condition of 10Hz

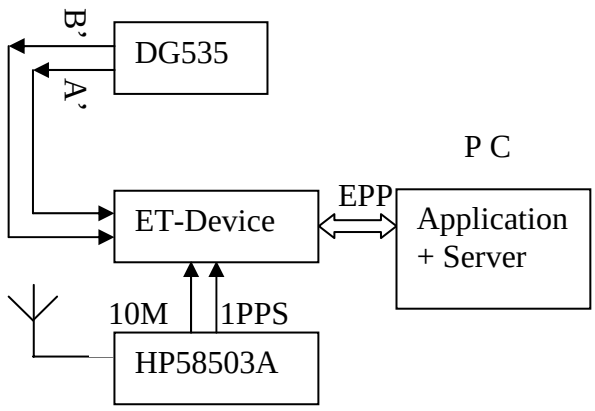

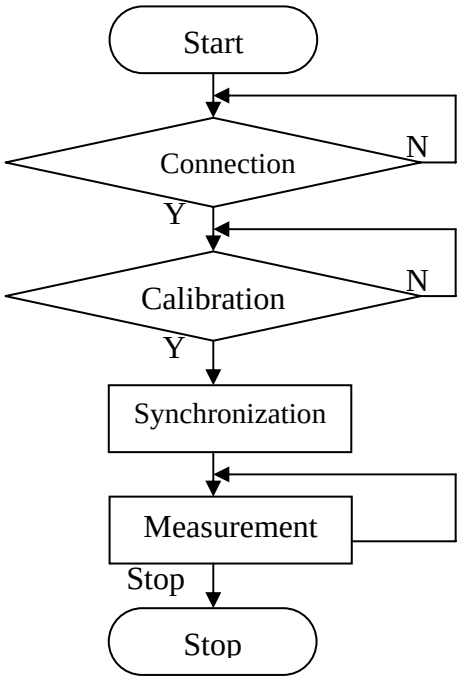

Figure 3. *Simulation scheme*

Figure 4. *Software flow chart*

Range gate measurement

Range gate is measured with A032-ET to find out the matching of start and stop signals. In this experiment, the start pulse is generated by DG535, which is triggered by laser firing, and output of the range gate is used as the stop pulse. Range gate measurement is to simulate observation condition and make some improvement for the software. The main function written in VC++ language is compiled as Dynamic Link Library. The data received by A032-ET is transferred into control software written in VB for

calculating the time interval. The data transferred into VB with the form of an array included time-tags that the events happened in channel A, B. The time-tags are matched well with range gate prediction.

Real Observations

The firing frequency is increased to 10Hz for all satellites and A032-ET is used as a new timer to calculate the time interval instead. The hardware connection scheme is presented in Figure 5. The main pulse is imported into channel A as start signal and the return pulse as stop signal. A032-ET could distinguish only NIM pulses; the 10MHz and 1pps signals are given by GPS HP58503A. Figure 6 shows the time sequence of Changchun SLR system. In the scheme, T1 and T4 is laser fire time, T2 is the epoch time of the main pulse, and T3 is the epoch time of the return pulse.

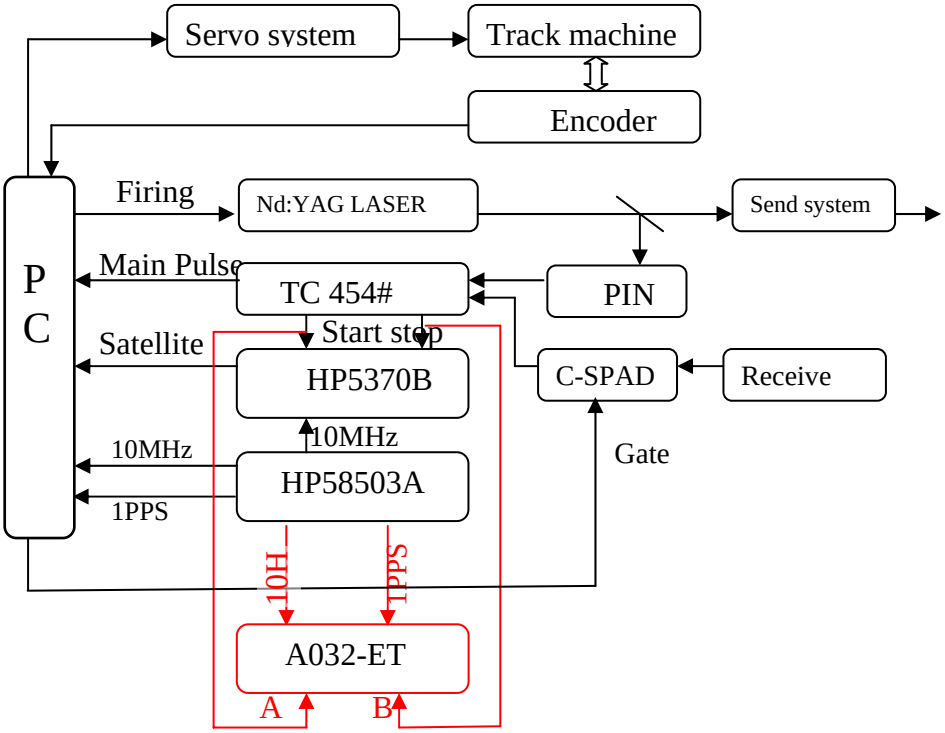

Figure 5. *Hardware connection*

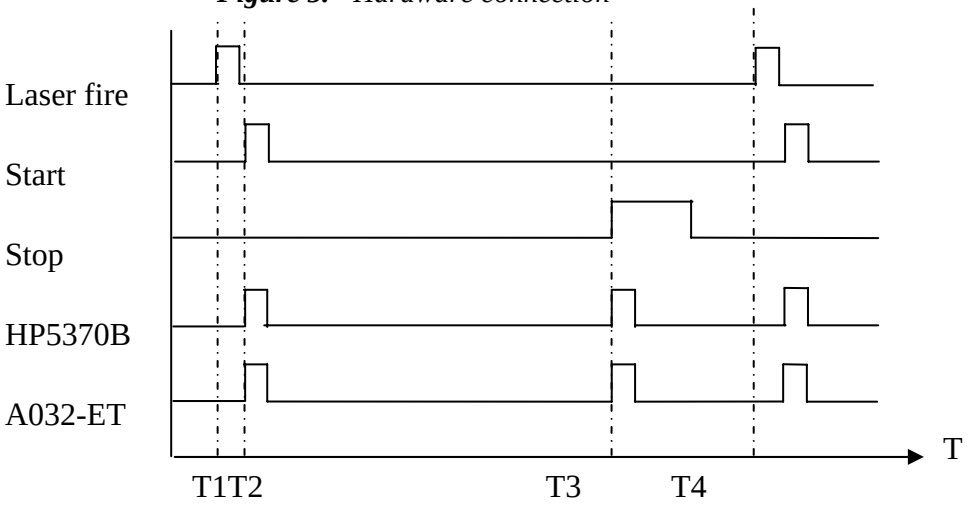

Figure 6. *Time sequence of Changchun SLR system*

Figure 7 shows the Etalon-2 measurement interface. The firing rate is 10Hz. From this picture, the return signal line can be clearly seen. From the satellite observation, we can see that the system works very well with A032-ET under the condition of 10Hz firing frequency. The return signal rate of high orbit satellites is increased.

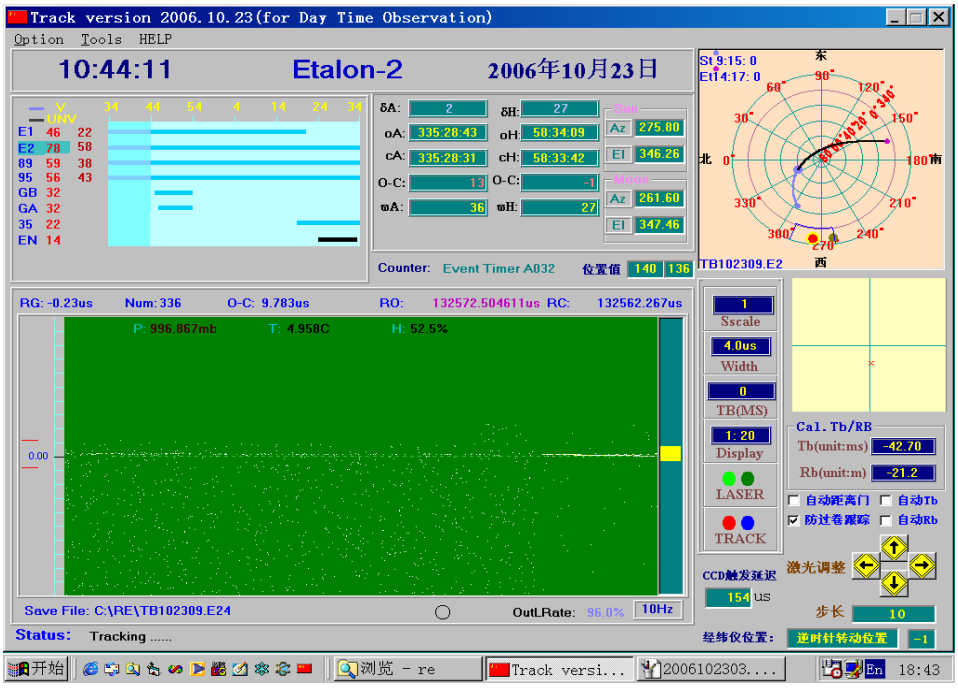

Figure 7. *Etalon-2 measurement interface*

Conclusion

From analysis report such as Toshi's report, we can see A032-ET works well as Event Timer. The precision is 1cm more or less. It could be used in SLR system normally. Because the laser pulse is about 200ps in Changchun station, the precision of the whole system does not increase obviously after the event timer is used. Since Oct.23 of 2006, A032-ET has been used in the satellite laser ranging routinely for the all satellites tracked with the firing frequency of 10Hz in Changchun station. Table 2 shows the data quantity from 2006-10-23 to 2006-12-31. There are too many passes. Now, it works very well and the experiment is very successful. Next, we plan to increase to KHz observation if the laser source is available.

Table 2: *Data of Changchun SLR Station (2006-10-23 to 2006-12-31)*

Site Information		Data Volume			
Column 1	2	3	4	5	6
Location	Station Number	LEO pass Tot	LAGEOS pass Tot	High pass Tot	Total passes
Changchun	7237	1095	153	209	1457

Acknowledgement

The authors would like to thank SHI Jianyong and ZHANG Haitao who partially participate in the work. And also express their appreciation to Prof. Yu. Artyukh and his colleague Eugene Buls of University of Latvia for their technical supports.

The authors gratefully acknowledge the support of K.C.Wong Education Foundation, Hong Kong.

References

[1] Yu. Artyukh: "Selective Time Interval Counter for SLR Applications", Proc. of 11th International Workshop on Laser Ranging, Deggendort, Germany, 1998.

[2] Yang, F.M.: "Current status and future plans for the Chinese Satellite Laser Ranging Network", Surv. Geophys. 22 (6): 465-471 2001.

[3] P. Gibbs: "Comparisons of a single SR620 timer against a variety of timers from the Eurolas network", Proceedings of 13th International Workshop on Laser Ranging, Washington D.C. 2002.

[4] P. Gibbs: "Inter-comparison of Various Timing Devices Against a Single SR Timer", Proceedings of 13th International Laser Ranging Workshop, Washington D.C., USA. 2002.

[5] Yu. Artyukh, V. Bespal: "A New Line of Timing Systems for Satellite Laser Ranging", Proceeding of the 8th Biennial Electronics Conference, Tallinnl, Estonia, 2002, pp. 239-240.

[6] Yu. Artyukh, V. Bespal: "A010 Family of Time Interval Counter Adapted to SLR Application", Proceedings of the 13th International Laser Ranging Workshop, Washington D.C. 2002.

[7] Liu Chengzhi, Zhao You, Fan Cunbo, etc.: "The Performance of Changchun Satellite Laser Ranging Station", Proceeding of 14th International Laser Ranging Workshop, San Fernando, Spain, 2004, pp. 175-177.

[8] Yu. Artyukh, V. Bespal: "A Version of the A032-ET Event Timer for KHz SLR", Proceedings of KHz SLR Meeting, Graz, Austria, 2004.

[9] C. Selke, F. Koidl, G. Kirchner: "Tests of the Stability and Linearity of the A032ET Event Timer at Graz Station", Proceeding of 14th International Laser Ranging Workshop, San Fernando, Spain, 2004, pp. 337-341.

[10] G. Kirchner, 2004, SLR Graz: The RGG (Range Gate Generator), Proceedings of KHz SLR Meeting, Graz, Austria.

[11] G. Appleby, P. Gibbs: "SGF Herstmonseux: Current Status and Future Upgrades", Proceeding of 14th International Laser Ranging Workshop, San Fernando, Spain, 2004, pp. 213-216.

[12] K. Hamal, I. Prochazka: "Portable Pico Event Timer 2 KHz", Proceeding of 14th International Laser Ranging Workshop, San Fernando, Spain, 2004, pp. 333-335.

[13] G. Kirchner, F. Koidl: "Graz KHz SLR System: Design, Experiences and Results", Proceeding of 14th International Laser Ranging Workshop, San Fernando, Spain, 2004, pp. 501-505.

[14] G. Kirchner: "Riga A032-ET in Graz", ILRS 2005 Workshop, Eastbourne, England, 2005.

Event Timing System for Riga SLR Station

Yu. Artyukh[1], V. Bespal'ko[1], K. Lapushka[2], A. Rybakov[1]

1. Institute of Electronics and Computer Science, Riga, Latvia.
2. Astronomical Institute of University of Latvia, Riga, Latvia.

Contact: artyukh@edi.lv, riglas@lanet.lv

Abstract

The new Riga Event Timing System (RTS) is designed and built in 2006 for SLR station Riga-1884 to improve its measurement equipment in precision, functionality and reliability of operation. The RTS is a multimode instrument for satellite ranging at 10 Hz repetition rate with parallel measurement of PMT-pulse amplitudes for the range bias correction. The RTS can support millimetre accuracy of SLR although the overall system accuracy is limited by the other equipment of Riga SLR station. As compared to the previous version of Riga timing system, the RTS offers considerably better performance and functionality and provides a good basis for further improving the Riga SLR station as a whole.

Introduction

The Riga Event Timing System (RTS) is designed and built in 2006 for Riga SLR station to upgrade its measurement equipment. The RTS maintains the basic functional possibilities of the previous Riga timing system but is advanced in many essential respects. Specifically, the RTS is based on employment of the latest Riga Event Timer A032-ET [1]. As compared to the previously used instrument, the A032-ET provides much better single-shot resolution (8 ps RMS instead of the previous 25 ps) and much smaller “dead time” (60 ns instead of the previous 400 ns).

A new hardware design is made to integrate the most of specialized hardware means within a single stand-alone device. There are new functional possibilities of digital signal processing and system control that have to increase the SLR efficiency. Some optional functional capabilities are added for experimental investigations with the aim to improve the performance of Riga station as a whole.

A special feature of the RTS is that it provides pre-processing of STOP pulses coming from either traditional single or special doubled receiver based on Photo Multiplier Tubes (PMT). The doubled receiver generates the pulses overlapping only when the true STOP pulse is being received [2]. It makes possible to reduce the noise influence when the satellite ranging is performed by day. Like the previous Riga timing system, the RTS performs PMT pulse amplitude measurement to correct the range bias [3].

Principles of operation

The RTS supports the following operational modes:

- SLR system calibration in the range from 9 to 375 m with parallel measurement of STOP-pulse amplitudes;
- Satellite ranging to 25,500 km at 10 Hz repetition rate with parallel measurement of STOP-pulse amplitudes;
- Integrated mode when the SLR system calibration and satellite ranging are performed simultaneously (for optional use);
- Measurement of pulse noises.

Structurally the RTS combines the RTS hardware and a PC with the RTS software (Fig.1).

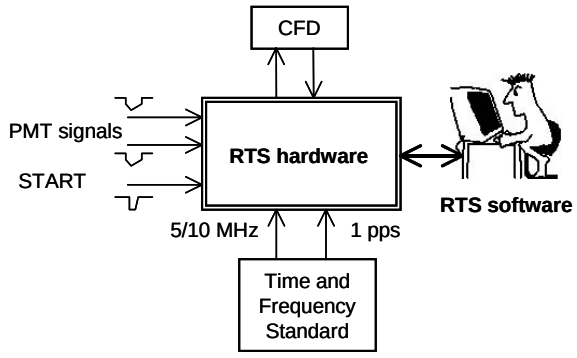

Figure 1. *RTS architecture*

Additionally the RTS includes two commonly used external devices: Time and Frequency Standard and Constant Fraction Discriminator (CFD).

The RTS hardware

The RTS hardware contains three functional units: Signal Processing block, Event Timer Block and Master Clock; each implemented as a separate board. These boards and their power supply are housed in 19'' 2U rack module (Fig.2).

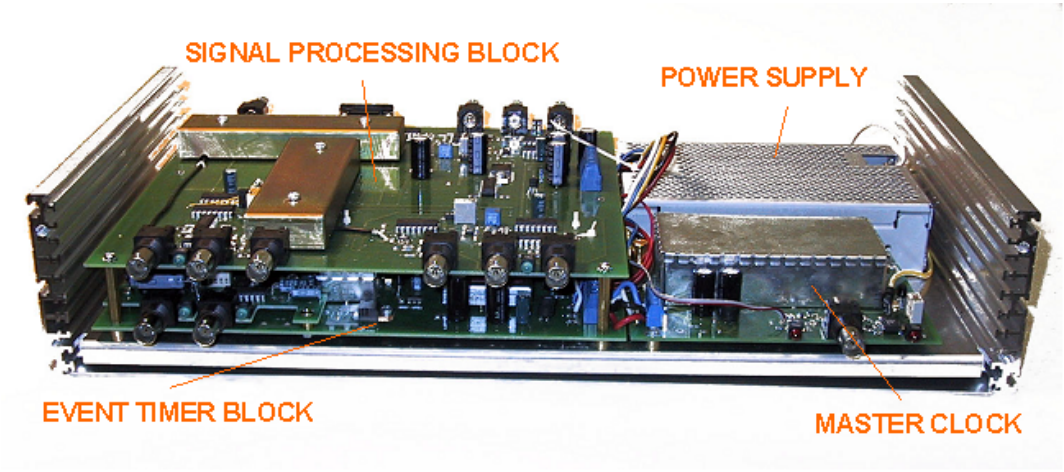

Figure 2. *RTS hardware assembly*

The Signal Processing Block receives the PMT pulses (3 to 7 ns width range; -0.1 to -3.0 V amplitude range) and, in interaction with the CFD, produces normalised NIM pulses for the Event Timer Block. The Event Timer Block measures time instants of these pulses and START pulses coming. Then the measurement results come to PC for further data processing, displaying and memorizing. The Master Clock represents a voltage-controlled crystal oscillator disciplined by an external high-stable 5 or 10 MHz reference frequency using PLL circuit. It generates a low-jittered 100 MHz clock signal required for precise event measurement and synchronization of Signal Processing Block operation as a whole.

Signal Processing Block

The Signal Processing Block performs a few basic operations with PMT pulses before their measurement by the Event Timer Block (Fig.3).

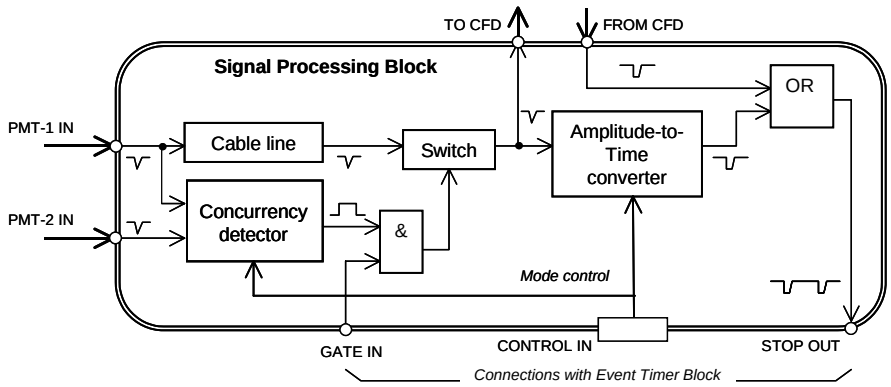

Figure 3. *Functional diagram of the Signal Processing Block*

At first it selects PMT pulses which probably conform only to the returned laser pulses. To do that either single ("PMT-1 IN") input or two ("PMT-1 IN" and "PMT-2 IN") inputs for PMT pulses can be used. In the last case it is supposed that the PMT pulses overlap only when the true return is being received. In the case of concurrency of these pulses one of them ("PMT-1") is selected using the wideband switch. Such selection acts together with the online programmable gating provided by the Event Timer Block.

The selected pulses from the switch output come to the CFD. The CFD generates normalized NIM pulse in response to each input PMT pulse. This NIM pulse comes to the input "FROM CFD" of the Signal Processing Block. However the CFD cannot fully avoid the time-uncertainty of PMT pulse coming. For this reason the amplitude of each PMT pulses is additionally measured as the amplitude values are related to the range bias. To do that, the Amplitude-to-Time converter generates the NIM pulse in response to the same PMT pulse with some delay proportional to the PMT pulse amplitude. In this way every selected PMT pulse is being converted into two NIM pulses where the first one represents directly the returned signal and time interval from the first pulse to the second one reflects its amplitude (Fig.4). Resolution of such amplitude measurement is about 9 bits.

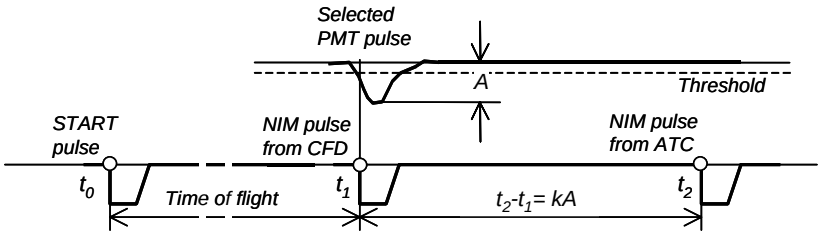

Figure 4. *Time diagram illustrating PMT pulse amplitude conversion*

Then the Event Timer Block measures time instants of these pulses and START pulse coming at each ranging cycle so as to give out complete data for further satellite ranging. As shown in [3], the mentioned technique of PMT signal amplitude measurement makes it possible to effectively correct the range bias caused by the PMT features.

Event Timer Block

The Event Timer Block precisely measures the instants at which input events occur. Every event is associated with certain fixed point on the leading edge of input NIM pulses. Used method of event timing is untraditional in many respects. Specifically, it

supports not only high precision but high speed as well. Using 100 MHz internal clocks this method provides each single measurement with 7-8 ps RMS resolution during 60 ns only.

The event measurement is performed in two stages. At first, the Event Timer Block transforms every input event into single 80-bit timing data block (subsequently referred to as TD-block) and sequentially accumulates them in a FIFO memory. Each TD-block contains the counting data (39 bits; 10 ns resolution) and interpolating data (40 bits), as well as one-bit mark specifying the kind of measured event (either Start or Stop). The interpolating data are presented initially in an intermediate redundant form.

At the next stage the PC takes out TD-blocks from the FIFO memory and processes them to obtain the corresponding epoch time-tags in a unified form. Further these time-tags are additionally processed to display the ranging results in real time. To achieve the best precision, processing of TD-blocks takes into account the actual physical characteristics of time interpolation under actual operating conditions; these characteristics are defined through so called scaling (hardware calibration) before the measurement.

The Event Timer Block is flexibly controllable and allows writing TD-blocks in the FIFO memory and reading them by the PC in different order. Specifically, the RTS provides cyclical measurement of events. In the beginning of each cycle the RTS measures a single Start-event, and only then - a number of Stop-events. According to the modes of RTS operation, the Event Timer Block measures up to 3 events in the System calibration and Satellite ranging modes, up to 5 events in the “Integrated mode” and up to 10000 events when pulse noise is measured. In all cases the Event Timer Block at first accumulates TD-blocks in the FIFO memory during some defined waiting period, starting from Start-event registration. During this time the PC processes TD-blocks that have been read out from the Event Timer Block in the previous cycle. Then the PC stops the event registration, reads the currently accumulated TD-blocks and allows starting the next similar cycle. The waiting period is strictly adapted to the repetition rate (10 Hz) of RTS operation. Optionally the RTS can provide the repetition rate up to 30 Hz.

In addition to the event measurement the Event Timer Block generates NIM pulses, which come to the input “GATE IN” of the Signal Processing Block to provide online programmable PMT pulse gating.

The RTS software

The RTS software performs real-time procedures which depend on the selected operating mode, current user control, etc. There are also various auxiliary procedures to prepare the system to operation (clock synchronization, calibration of measurement hardware, system checking, etc). For example, in the conventional Satellite ranging mode the RTS software performs in real time the following procedures:

- periodically checks the RTS hardware to detect the START pulse coming;
- when the START pulse is detected, triggers the internal time-out and begins processing of the previously taken data;
- when the time-out is finished, stops the measurement, reads the data from the RTS hardware, writes to it a new data concerning the STOP pulse gating and makes next cycle available.

Correspondingly the data processing performed during the time-out includes:

- conversion of TD-blocks to the unified form of epoch time-tags;

- calculation of the gate delay and residual, time interval reflected the STOP pulse amplitude and new data concerning the STOP pulse gating in the next cycle;
- displaying (Fig.5) and memorizing the measurement results.

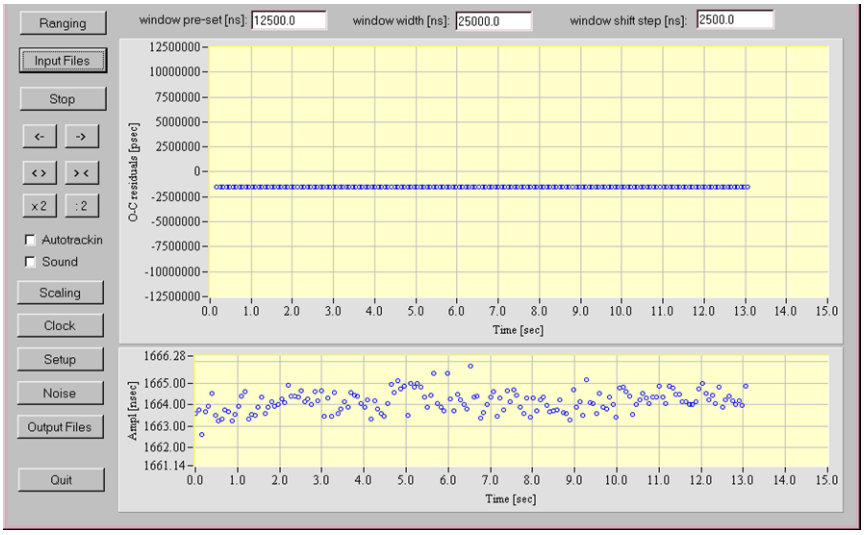

Figure 5. *Example of displaying the measurement results. Upper plot shows residuals; bottom plot indicates amplitudes of PMT pulses*

The RTS software offers optionally an autotracking of satellite in range after its initial acquisition. When the autotracking is on, possible trend of the residuals is actually excluded due to the automatic gate delay correction. Algorithm of the autotracking is based on median selection of current residuals to exclude their possible abnormal values, and continuous generation of a special piecewise-linear function for gate delay correction. Every piece of this function is being determined using regression analysis of the current fraction of residuals. In this case the gate delay correction is performed at 1 Hz rate approx., allowing considerable errors in initial predetermination of the function “RANGE vs. START TIME”.

The RTS software is written in *C* language for LabWindows/CVI ver.6.0 and works under Windows XP.

Conclusion

As compared to the previous version of Riga timing system, the RTS offers considerably better performance in terms of accuracy, functionality, and reliability in operation. This provides a good basis for further advancing the Riga SLR Station as a whole. In 2006 the RTS was involved in trial operation; the first series of successful SLR results has been obtained.

Reference

[1] V. Bespalko, E. Boole, V. Vedin. The Model A032-ET of Riga Event Timers. Proceedings of the 15th International Workshop on Laser Ranging, Canberra Australia, October 16-20, 2006.

[2] ILRS 2003-2004 Annual Report, p. B-38.

[3] Yu. Artyukh, V. Bespalko, K. Lapushka, A. Rybakov. PMT signals caused range-bias correction at the SLR Station Riga-1884. Proceedings of the 12th International Workshop on Laser Ranging. Matera, Italy, November 13-17, 2000.

Instrumentation for Creating KHz SLR Timing Systems

Yu. Artyukh, E. Boole, V. Vedin

1. Institute of Electronics and Computer Science, Riga, LATVIA.

Contact: artyukh@edi.lv

Abstract

The instrumentation provides basic tools for creating SLR timing systems operating at repetition rate up to a few KHz. There is a test setup to simulate the process of ranging to various satellites and to evaluate capabilities of this instrumentation for the KHz system design. The simulation of the CHAMP laser ranging at 2 KHz repetition rate is considered as an example. Test results show that the proposed instrumentation offers sufficient performance to be used in the KHz SLR systems.

Timing system architecture

As known, increasing the SLR repetition rate up to KHz provides a variety of essential benefits. Currently there are a few SLR stations which already use this technique or will have it in the near future. However KHz SLR usually need essential upgrading of SLR equipment, including the timing system for satellite range measurement. In view of that we propose an instrumental basis to create various KHz SLR timing systems adapted to the specific user requirements.

There is the well-known custom timing system for KHz SLR at Graz SLR station [1]. In general terms, architecture of timing systems based on the proposed instrumentation and principles of their operation are similar. But there are distinctions in some essential details. Specifically, in our case the specialized hardware is offered as two compatible stand-alone devices (Event Timer A032-ET and Range Gate Generator). PC interacts with these devices and coordinates their operation via standard parallel ports working in the EPP (Enhanced Parallel Port) mode (Fig.1).

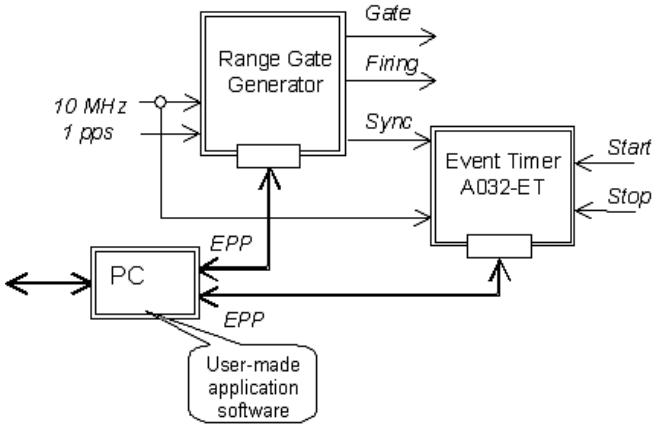

Figure 1. *Timing system architecture*

As for the application software, it should be custom-made according to the specific application requirements with the reference to the sample program (source code written in *C*). This program defines device-specific software functions which can be directly built in the user software to support the interactions with hardware. In this way the instrumentation can be used as a basis for various timing system designs.

System hardware

Event Timer

The basic system hardware component is Riga Event Timer A032-ET. It offers two independent inputs for *Start* and *Stop* measurement with RMS resolution about 7-8 ps. Distinctive feature of this device is exceptionally small "dead time" (60 ns) due to the advanced interpolating technique of event timing. This allows sequential measurement of *Start* and *Stop* using simple single-channel hardware structure (Fig.2). Note that such solution simplifies the timer's implementation and makes it relatively inexpensive.

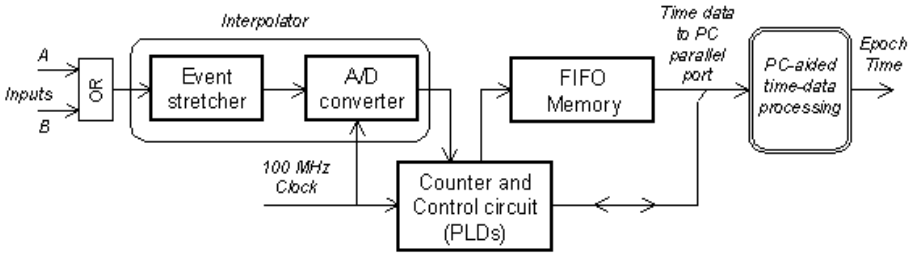

Figure 2. *Schematic block diagram of the Event Timer*

Although small "dead time" allows the burst rate of event timing up to 17 MHz (for up to 12K sequential events), the average rate is limited down to 10-15 KHz by the available speed of data transfer to PC. However it seems that this rate is quite enough for KHz SLR. In more details the A032-ET features are described in [2].

Range Gate Generator

The Range Gate Generator (RGG) is based on the well-known scheme of Digit-to-Event conversion (Fig.3). Continuous counting of 100 MHz clock pulses forms the 25-bit time-scale with 335 ms periodicity. Such periodicity directly conforms to the maximum value of range gate delay.

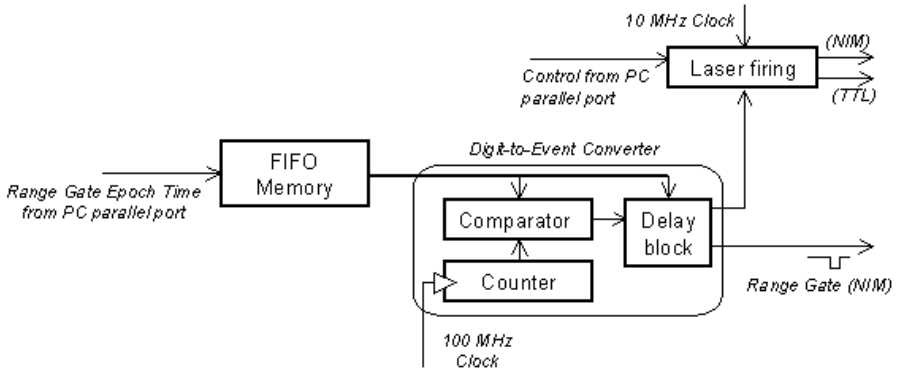

Figure 3. *Schematic block diagram of the Range Gate Generator*

Dual-ported FIFO memory receives the time data (Range Gate Epoch Time) from PC. In this case the data writing to this memory and data reading from it are independent asynchronous processes. Digital comparator compares the data from the FIFO memory with the current state of time-scale, providing the range gate generation with 10 ns resolution. Additional 7-bit controlled delay block (based on MC100EP196 delay chip) increases resolution up to 80 ps. However there is noticeable differential non-linearity for this chip, resulting in a noise-like error of range gate generation (80 ps RMS approx.). Most of the RGG digital functions are implemented on CPLD basis.

An important feature of the RGG is a specific firing generation. As known, the range measurement can be corrupted when a transmitted laser pulse is close to the received one. To avoid such problems each firing is generated so that it never can occur within some protected zone around any gate being generated (Fig.4).

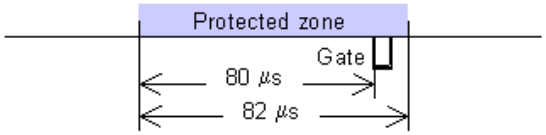

Figure 4. *Zone protected from firing*

To provide such condition, initially specified period of firings may sometimes be automatically (without any pre-calculations) incremented by quarter of its value. The nominal value of firing period can be set in the range from 100 μs to 167 ms with 0.64 μs resolution. In other words, the timing system is able to operate in a wide range of repetition rate, starting from 6 Hz.

Generally the RGG has been designed not only for KHz SLR applications. For this reason it also provides some additional features that are beyond of the direct KHz SLR needs. Specifically, it offers FIFO memory depth up to 16,000 data blocks defining the epoch times, cyclical offline operation, has two selectable outputs for two-channel event generation, etc. These features may be useful for other applications such as tests of timing devices.

General performance limitation

In the process of *Stop* gating each *Start* brings about corresponding control data at the RGG interface with some delay called “response time”. The response time is a system parameter that defines both the SLR maximum repetition rate and allowable minimum of satellite range.

There are three main components of the response time: time of data reading from the Event Timer, time of data processing and time of data writing to RGG. Usually it is desirable to dedicate the maximum time for real-time data processing. Correspondingly the total time of data reading (10 Bytes) and data writing (5 Bytes) via PC parallel ports (see Fig.1) has to be reduced as far as possible. Although formally the EPP should provide the data transfer rate up to 1-2 MB/s, actually it considerably depends on the PC operating system and its configuration. Specifically, our experiments with different MS-Windows operating systems showed that the total time of data reading/writing on average varies from 25 μs (for Windows-98) to 150 μs (for Windows XP). Furthermore, this time is not stable, resulting in significant variation of the response time from cycle to cycle. Unfortunately it was not possible to check other operating systems that could be better suited for real-time operation.

Experimental evaluation of system potentialities

To evaluate the potential of the proposed instrumentation a test setup has been used. This test setup has a structure which is similar to that shown in Fig.1. In this case each firing simulates *Start* and each generated gate simulates *Stop* for the Event Timer. Correspondingly a test program simulates application software. The test program performs the simplest real-time data processing related mainly to the Range Gate Epoch Time calculation and memorizing of the measurement results (no time-consuming operations such as real-time data displaying). Evaluation of the

measurement results is performed offline. The test program works under Windows XP. In this case the average response time was about 250 μs and its maximum value - about 1 ms. Most of the response time was consumed for the data reading/writing. These timing conditions correspond to the possibility of satellite ranging from 1 ms at repetition rate up to 4 KHz.

Other experiments were related to simulations of LEO satellites laser ranging as this represents a worst case for the timing system operation in possible real applications (the higher orbit, the less problems with the response time limitations). Specifically, the simulation of the CHAMP laser ranging at 2 KHz repetition rate was performed (Fig.5). There are 550,000 sequential readings obtained continuously during 275 seconds of the CHAMP pass simulation. The satellite range is from 2.45 ms up to 7.48 ms.

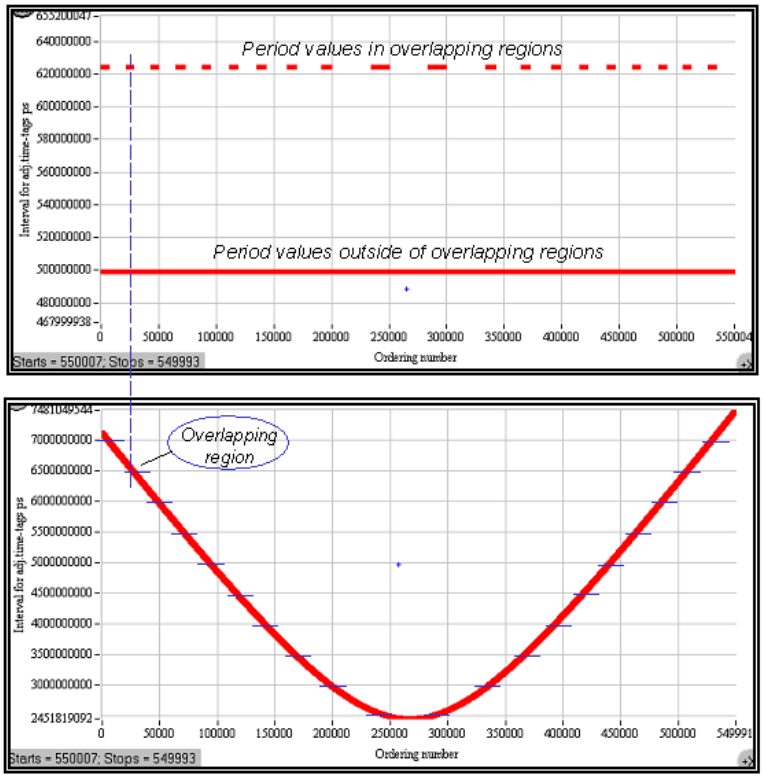

Figure 5. *Period of laser firing (upper graph) and measured range (in bottom) vs. cycle number for CHAMP laser ranging simulation*

As can be seen from the simulation result, there are a number of regions where the transmitting and receiving of laser pulses may overlap. Although the nominal value of repetition period was 499.2 μs, the actual average period was increased up to 502.157 μs (by 0.59%) due to incrementing of some firing periods (~2.4% of total number) by 0.125 ms to avoid these overlaps. Under these conditions any distortions or gaps in the measurement process were not detected. However, it should be taken into account that actually the real-time data processing can be much more complicated than that for the test setup. For this reason it is preferable to use the real-time operating systems to ensure the necessary time for data processing.

Additionally the residuals have been calculated to evaluate the system instrumental errors. When the Range Gate Epoch Times are defined for RGG with the maximum resolution (80 ps), there is a maximum non-linearity in the range gate generation (the

RGG interpolation delay varies in the full 10 ns range). Correspondingly in this case the calculated residuals reflect mainly the non-linearity errors of range gate generation (Fig.6). As can be seen, the peak-to-peak error is about 440 ps.

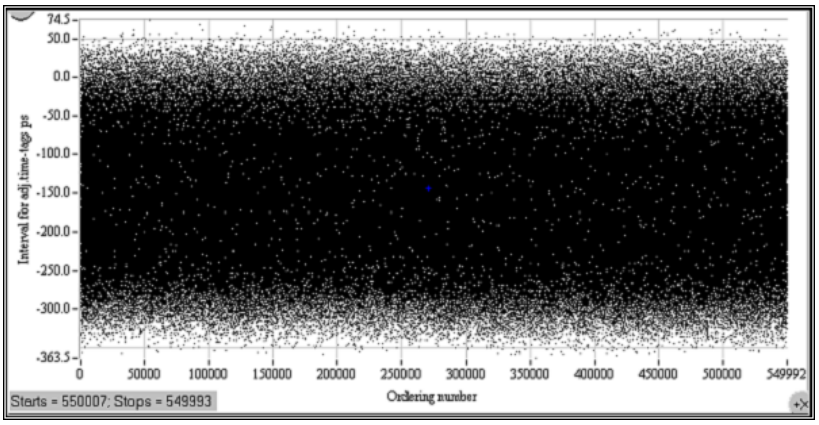

Figure 6. *Residuals vs. cycle number for CHAMP laser ranging simulation*

When the Range Gate Epoch Times are defined with 10 ns resolution, there is no noticeable non-linearity in range gate generation (since the RGG interpolation delay does not vary). Correspondingly in this case the residuals reflect both the errors of event timing and jitter of range gate generation. In our experiment the RMS of residual variation was about 8.9 ps. Since the actual RMS resolution of Event Timer is about 7.5 ps (this is specified by a separate test), it can be concluded that the RMS jitter of range gate generation is about 4.8 ps. Such jitter is negligible as compared to the actual RGG non-linearity.

Conclusion

We presume that KHz SLR is of vital interest for many SLR stations. Taking that into account, the proposed instrumentation offers sufficient performance for such applications and can be useful for creating new timing systems that provide SLR at repetition rate up to a few KHz. In this case the problems of timing system design can be reduced down to the development of user-specific application software.

Special thanks to Dr. Kirchner for his assistance and promotion of our latest designs. His well-known achievements concerning the KHz SLR at Graz station in many respects stimulated our activity in this area.

References

[1] [1] G. Kirchner. Present Status of the Graz kHz SLR System. Proceedings of the kHz SLR Meeting, Graz, Austria, October 27-29, 2004.

[2] [2] V. Bespal'ko, E. Boole, V. Vedin. The Model A032-ET of Riga Event Timers. Proceedings of the 15th International Workshop on Laser Ranging, Canberra, Australia, October 16-20, 2006.

OCA Event Timer

E. Samain[1], Jean Marie Torre[1], D. Albanese[1], Ph. Guillemot[2],
F. Para[1], J. Paris[1], I. Petitbon[2], P. Vrancken[1], J. Weick[1]

1. Observatoire. de la Côte d'Azur, Caussols, France.

2 CNES, Toulouse, France.

Contact: etienne.samain@obs-azur.fr

Abstract

In the framework of T2L2[1,2,3] project, OCA and CNES designed an ultra stable event timer[4]. It includes on a unique card, a vernier, a logic counter, a 100 MHz frequency synthesis and a module for communications and internal calibrations. It has a precision better than 2 ps, linearity below 1 ps and a thermal drift in the range of 0.5 ps per degree. The dead time between two consecutive events is 3 µs.

For the T2L2 ground operations both the start time and the return time of laser pulses are required and not only the differences between the events. In order to run properly the T2L2 project, it will be necessary to upgrade some of the laser stations in that way. A T2L2 questionnaire was sent to the ILRS community to identify precisely the needs of each station.

For these reasons it has been decided to develop from the studies of the space design an event timer dedicated for ground operations. It could have the same characteristics than the flight model even if it seems possible to increase the frequency of the vernier to reach a sub picosecond precision and to decrease the dead time below 1 µs.

Introduction

An event timer is a system able to get the time position of an event in the time scale of a clock. It can be consider as a counter driven by the clock which is the time reference. When an event occurs, the value of the counter is extracted and this value represents the arrival time of the event. The time origin of such an event timer has to be measured with a reference signal like a PPS. A time interval is computed from the difference between two arrival times. The most important characteristics of an event timer are: the precision, the linearity, the time stability and the dead time.

Ideally, the linearity error has to be good enough so that the precision of the timer do not rely on the position of the event in the time scale produced by the clock. A precision of few picoseconds requires then a linearity error in the range of one picosecond. The time stability $\sigma_x(\tau)$ permits to evaluate the performances of the instrument when the events are acquired during τ. In the framework of the laser ranging activities, this is an important characteristic to construct the normal point. In the frame of the time transfer this important to evaluate the noise introduce by the timer as compared to the noise introduce by the clocks. The start time and the arrival time can be measured from the same event timer if the dead time between two consecutive measurements is small enough. A dead time in the range of 3 µs permits to range ground targets at 500 m. This is a minimum requirement to be able to calibrate a laser station with an external ground target.

A first breadboard of the T2L2 space instrumentation was built at OCA in 2002. Since then, T2L2 project was accepted by CNES on the satellite Jason2. We started the development of the space instrumentation in mid 2005. Three models were built: a prototype, an engineering model and the flight model. The flight model is now ready

to be integrated on the satellite.

Description of the T2L2 event timer

The event timer is made with 4 distinct modules on a unique card (figure 1):

- A vernier having a time resolution of 0.1 ps
- Frequency synthesis @ 100 MHz controlled from an external 10 MHz clock signal coming from the DORIS system.
- Calibration module to improve the long term time stability
- Digital module for communication through a RS422 serial bus

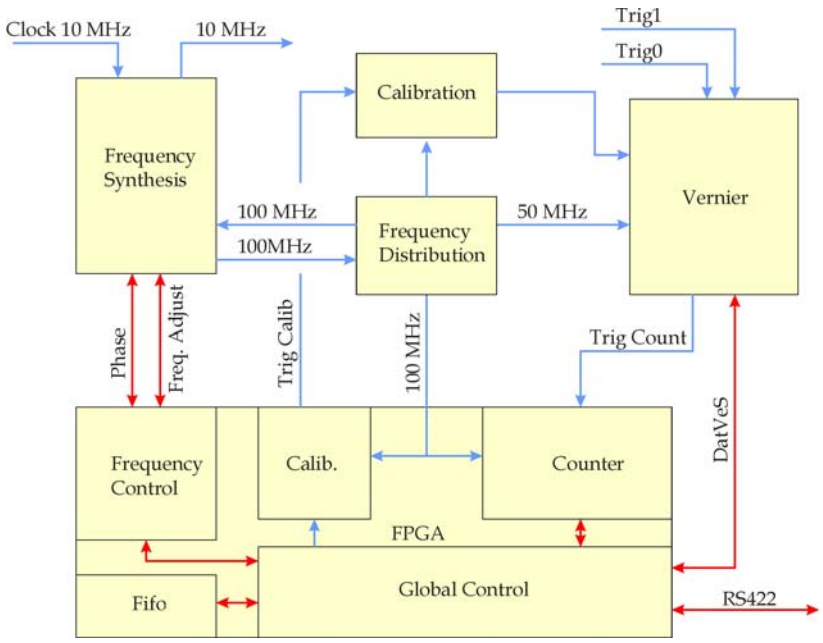

Figure 1 : *Synoptic of the event timer.*

The most important module is the vernier which give the arrival time of the event with a resolution of 0.1 ps. It is driven by the digital frequency synthesis module designed to translate the 10 MHz clock signal to 50 and 100 MHz. The global performances of the timer rely on these two modules. The calibration module permits to improve the long-term stability of the timer. It generates calibrated events that are timed by the event timer. The frequency synthesis is built from an ultra low noise quartz oscillator @ 100 MHz (ArElectronic) controlled with a Phase Lock Loop based on a digital phase measurement. Figure 2 gives the time stability specification of both the DORIS Oscillator and the ArElectronic oscillator. The PLL is tuned to get a frequency cut at 100 Hz with a damping factor of 3. The digital module is divided in 2 parts. The first one is a digital counter driven by the frequency synthesis signal. It gives the arrival time of the event with a time resolution equal to the period of this signal: 10 ns. The second one is the global control of the timer. It controls all the modules and the serial bus.

The complete T2L2 space instrument includes four more cards, two for the detection, one for the computer and memory and one for the power supply. It also includes an optical module made with an avalanche photodiode provided by PESO [5]. All these modules are gathered in a compact aluminium box (figure 3), which is placed inside the satellite payload. The instrument is completed with a detection module located

outside the satellite and very close to the Laser Ranging Array provided by ITE inc.

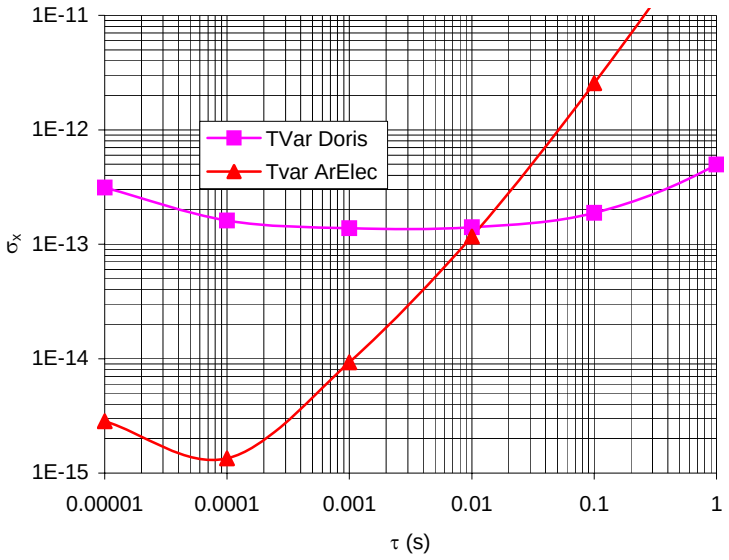

Figure 2 : *Time stability of both the local oscillator and the external oscillator*

The global characteristics of the event timer are:

Input frequency	10 MHz sinus 0 dBm
Event input	2 inputs, ECL level
Local oscillator	100 MHz; noise floor : -165 dBc
Logical frequency	100 MHz
Dynamic	5.7 years
Vernier period	20 ns
Vernier resolution	0.1 ps
Vernier precision	< 2 ps rms
Vernier linearity	< 1 ps rms
Vernier Time Stability	< 30 fs over 1000 s
Vernier Thermal sensitivity	< 1 ps/°C
Vernier Magnetic field sensitivity	< 1ps /100 µT
Calibration Precision	0.9 ps rms
Freq synthesis stability	$\sigma_x = 0.2 \times 10^{-12}\ \tau^{-1/2}$ s @ τ0 = 40 ms
Communication	RS422 @ 1 Mbits
Continuous rate	7000 Hz
Dead time	3 µs
Memory	2 frames
Size	220 x 180 mm²
Power consumption	15 W

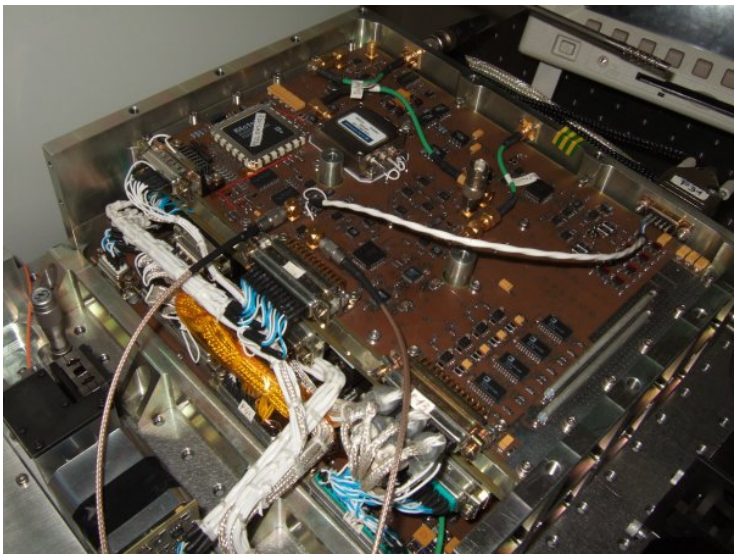

Figure 3 : *T2L2 Electronic instrumentation. The electronic card (in the center of the photography) is the event timer. A part of the Geiger photo detector can be seen on the left side.*

T2L2 ground instrumentation

For the T2L2 ground operations, both the start time and the return time of laser pulses are required and not only the differences between the events. In order for the T2L2 project to run properly, it will be necessary to upgrade laser stations in that way. A T2L2 questionnaire has been sent to the ILRS community to identify precisely the needs of each station. The questionnaire will help us to define the specifications and the design of the event timer: communication, size, number of entry, input frequency, etc.The event timer designed for T2L2 is not dedicated for T2L2: it will also be perfectly well suited for laser ranging. The timer could have the same characteristics than the flight model even if it seems possible to increase the frequency of the vernier to reach a sub picosecond precision and to decrease the dead time below 1 µs.

Conclusions

With an expected improvement of one order of magnitude as compared to existing time transfer techniques, T2L2 will allow the calibration of various existing radiofrequency time and frequency transfer systems like GPS or TWSTFT, and comparisons of cold atomic clocks at a level never reached before. Both the characterizations of the engineering model and the first measurement of the flight model allow us to be confident about the whole performances of the project. The T2L2 space model could also be used in the future in the framework of some interplanetary projects like TIPO [6] (One way laser ranging in the solar system) and Astrod [7] (Astrodynamical Space Test of relativity using optical devices) or LATOR.

Figure 4 : *laser ranging network : Event timer status in September 2006. In yellow laser station requiring an upgrade ; in green, compatible laser station (from the questionnaire)*

For a ground application, the performances of the event timer are at least one order of magnitude better than the performances of the other sensitive elements in the chain: laser – photo-detection. The short dead time between two consecutive measurements (that could be below 1 µs for the ground design) could permit to envision a laser station with only one timer and one photo detection system that will allow a direct accurate laser ranging measurement without any external calibration.

References

[1] P. Fridelance, E. Samain and C. Veillet, "*T2L2 - Time transfer by Laser link: a new optical time transfer generation*", Experimental Astronomy Vol.7 Num.3 Sept.97

[2] Samain, E., J. Weick, P. Vrancken, F. Para, D. Albanese, J. Paris, J.-M. Torre, C. Zhao, Ph. Guillemot and I. Petitbon, "Time Transfer by Laser Link: The T2L2 Experiment on Jason 2 and further Experiments", Int. Journal of Modern Phys. D, World Sci. Publ. Company, (2007), (in press)

[3] Guillemot, Ph., K. Gasc, I. Petitbon, E. Samain, P. Vrancken, J. Weick, D. Albanese, F. Para, J.-M. Torre, "Time Transfer by Laser Link: The T2L2 experiment on Jason 2", Proceedings of the IEEE International Frequency Control Symposium, p. 771-778, (2006)

[4] E. Samain, "*An Ultra Stable Event Timer*", Proceedings of the 13th International Workshop on laser ranging instrumentation, 2002.

[5] I. Procazka , K. Hamal, "*Recent achievements in solid state detector technology for laser ranging*", 2 , 469, Proceedings of the 9th International Workshop on laser ranging instrumentation, 1994

[6] E. Samain, One way laser ranging in the solar system, the TIPO Project (Télémétrie InterPlanétaire Optique), EGS, 2002.

[7] Wei-Tou Ni, Proceedings of the first International ASTROD symposium on laser astrodynamics, space test of relativity and gravitational – Wave astronomy, International journal of modern physics, 2002.

The Model A032-ET of Riga Event Timers

V. Bespal'ko, E. Boole, V. Vedin

1. Institute of Electronics and Computer Science, Riga, LATVIA.

Contact: artyukh@edi.lv

Abstract

The Event Timer A032-ET is an advanced version of the earlier model A031-ET of Riga event timers. As compared to this model, the A032-ET offers better single-shot resolution (<10 ps RMS) and is adapted to KHz SLR, supporting continuous measurement at the mean rate up to 10 KHz. At the same time it satisfies basic demands of conventional (low-rate) SLR. In this paper the principles of operation and basic features of the A032-ET are considered. Typical test results concerning the evaluation of single-shot resolution, linearity and offset drift are presented.

Introduction

Riga Event Timer A032-ET was designed in 2005 as an advanced version of the previous model A031-ET [1] with the main aim to adapt it to KHz SLR and improve its operating characteristics. As a result the following additional features of the A032-ET have been achieved:

- Continuous measurement at mean rate up to 10 KHz;
- Client-Server interaction supporting full remote control from the Client;
- Increased single-shot resolution (better than 10 ps RMS);
- Decreased "dead time" (not more than 60 ns);
- Built-in online programmable Stop pulse gating.

At the same time the A032-ET satisfies basic demands of conventional SLR at repetition rate up to tens of Hz and remains affordable at price. A032-ET is already known for some part of users. In particular, during one year after its designing about 10 instruments were delivered to different SLR stations. In this paper the principles of operation and basic features of the A032-ET are considered in more detail.

A032-ET main features

The A032-ET is a computer-based instrument that precisely measures epoch times when events (input pulse comings) occur. There are two alternative modes of the A032-ET operation that are tailored to the high-rate SLR and conventional low-rate SLR respectively:

- **"True Timer"** provides continuous (gapless) measurement of events at high (up to 10 KHz) mean measurement rate, allowing bursts up to 16 MHz. This mode suits well to measure Start and Stop events that come at the separate inputs (either *A* or *B*) of the A032-ET in any order.
- **"Multi-Stop Counter"** provides cyclical measurement of events that come at the separate inputs of the A032-ET in the strict order: in every cycle at first the A032-ET measures a single Start event coming at the input *A*, and then – a user-defined number of Stop events (up to 12,000) coming at the input *B*. The Stop events can be measured with online programmable gate delay.

Such measurements are performed with 7-9 ps RMS resolution in practically unlimited range. Extreme low measurement non-linearity (<1 ps) is supported.

A032-ET architecture

Like the most of virtual instruments, the A032-ET performs its measurement functions partly by hardware means and partly by software means. The measurement software provides interfacing with a user program via TCP/IP based network according to the well-known "Client/Server" scheme. The application program using TCP/IP service utilities can control the A032-ET and receive measurement data from it for further specific-application processing.

In terms of the Client/Server architecture the A032-ET can be considered as a combination of a specialised timing device (ET-device), and a specialised Server (ET-server) dedicated both to managing the ET-device and primary processing the timing data obtained from it (Fig.1).

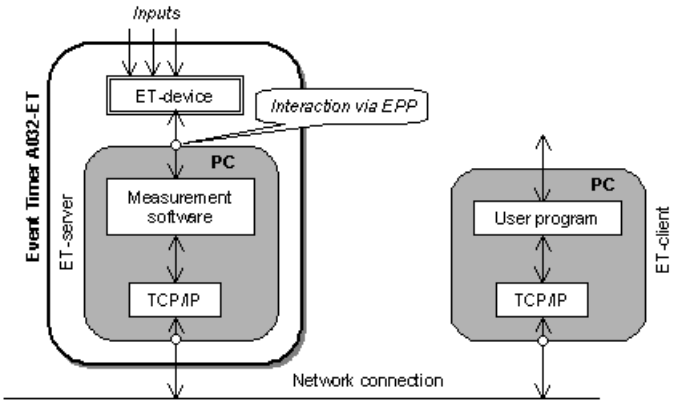

Figure 1. *Network architecture of the Event Timer*

In this case the ET-client is a PC on which user runs his application, using the specific ET-server resources via network. In many cases a single PC under MS-Windows can serve as both the ET-server and the ET-client although a separate PC for the ET-server is preferable to achieve the highest operating speed.

Principles of operation

The A032-ET performs the measurement of input events in two stages. At first, the ET-device transforms every input event into single 80-bit timing data block (TD-block) and sequentially accumulates such blocks in a buffer FIFO memory. Each TD-block contains the clock counter data (39 bits) and interpolating data (40 bits) about the time of event incoming, as well as one-bit mark specifying the input (either *A* or *B*) providing the measured event. The interpolating data are presented initially in an intermediate redundant form and need further an additional processing by the ET-server.

The used unconventional method of event timing supports both high precision and high speed. Specifically, using the 100 MHz internal clocks the method provides each single measurement with <10 ps RMS resolution during 60 ns only. This gives the maximum available rate of event timing about 16 MHz. At this rate the applied FIFO memory is able to accumulate up to 12,000 TD-blocks. An additional attractive feature of this event timing method is that it leads to the relative simplicity of hardware implementation (Fig.2). At the next stage the ET-server reads TD-blocks from the FIFO memory and processes them to obtain the corresponding time-tags in a unified form. Further these time-tags are sent to the ET-client via network.

The ET-device is flexibly controllable and applies two different procedures of TD-

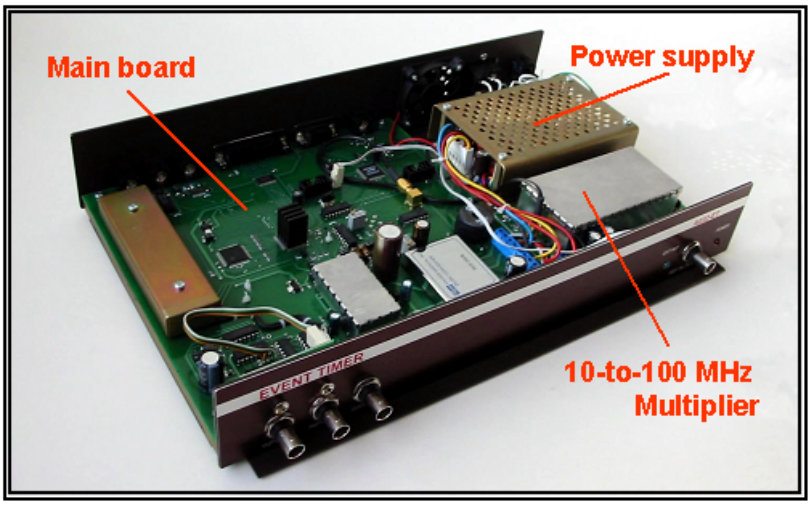

Figure 2. *Hardware design*

block accumulation in the FIFO memory and TD-block reading by the ET-server for two operation modes respectively

In the **"True Timer"** mode the ET-device provides continuous event measurement during practically unlimited time. To do that, the ET-device continuously accumulates TD-blocks in FIFO memory in order of measured event incoming. Concurrently with this process, the ET-server continuously monitors the current state of the FIFO memory with some user-defined period to detect the state when the amount of TD-blocks exceeds the user-selectable value (204, 102, 50, or 25 TD-blocks). The rest of the FIFO memory capacity is used to damp possible bursts of input event intensity. When the specified FIFO state is detected, the ET-server takes out the defined amount of TD-blocks from the ET-device, processes them and sends the corresponding time-tags to the ET-client. Such procedure is being cyclically repeated. In this way continuous event registration goes together with cyclical timing data processing and sending the time-tags to the ET-client via network. The mean rate of such continuous measurement is limited mainly by the available speed of TD-block reading and processing by the PC of the ET-server. Typically (although it may depend on the actual performance of the PC) the total time of single TD-block reading and processing on average is about 0.1 ms, resulting in the maximum mean measurement rate about 10 KHz.

In the **"Multi-Stop Counter"** mode the ET-device provides cyclical measurement of events. In the beginning of each cycle the A032-ET measures a single Start-event coming at the Input *A* of the ET-device, and only then - a number of Stop-events (up to 12,000) coming at the Input *B*. In this case the ET-device accumulates TD-blocks in the FIFO memory during some user-defined waiting period, starting from Start-event registration. During this time the ET-server processes TD-blocks, which are read from the ET-device in previous cycle, and sends the corresponding time-tags to the ET-client. Then the ET-server stops the event registration, reads the accumulated TD-blocks (but not more than the user-defined amount) and starts the next similar cycle. The waiting period can be defined in a wide range with a 1 ms step.

During the waiting period the ET-server can receive a command from the ET-client to restart the measurement with modified gate delay. In this way online cycle-to-cycle controllable gating is possible. However it should be taken into account that the real network may produce some unexpected delays for data exchange, resulting in

episodic loss of synchronism in such interactive operation at a high (more than tens of Hz) repetition rate of measurement cycles.

Precision characteristics

Although, in fact, the A032-ET measures the separate events, its precision is specified for time interval between two measured events. In this case the total measurement error ΔT_j for time interval T_j represented by difference of any two time-tags can be expressed as follows:

$$\Delta T_j = B(t) + E(T_j) + \xi_j,$$

where:

$B(t)$ – time-varying offset in measurement;

$E(T_j)$ – non-linearity error that depends on the value of measured time interval;

ξ_j – unbiased random error.

Specific values of these components of measurement error are evaluated for each instrument. Let's consider some typical examples of such evaluations.

Single shot RMS resolution

The A032-ET provides the best RMS resolution (standard deviation of the error ξ_j) directly after ET-device calibration. Then the resolution may slightly degrade under time-varying temperature conditions (Fig.3).

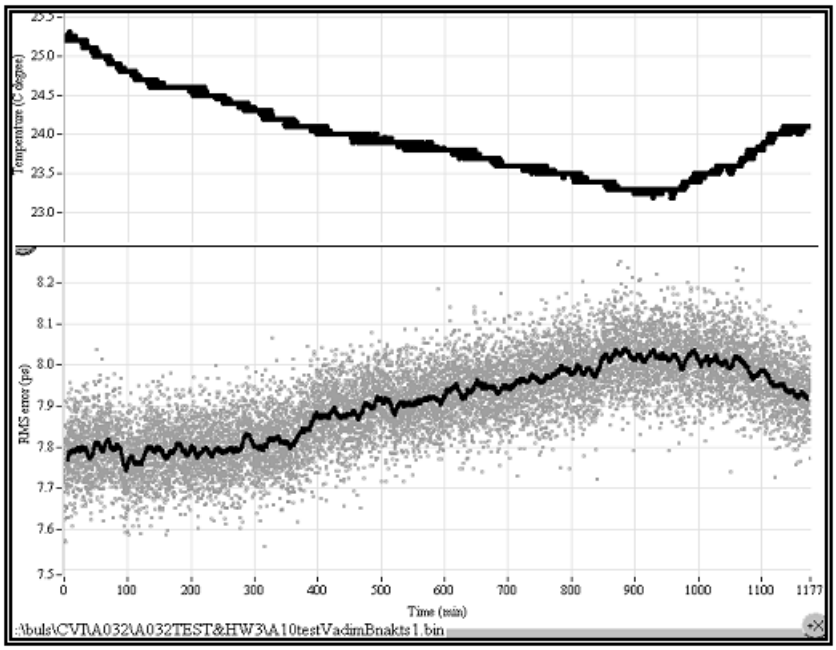

Figure 3. *Ambient-temperature and RMS resolution vs. time*

As can be seen, initially the RMS resolution is about 7.8 ps. During the next 15 hours the ambient-temperature is gradually changed for 2°C, resulting in decreasing of the RMS resolution down to 8 ps (about 0.1 ps/°C).

Linearity

There is some damping transient in electrical circuits responsible for event measurement. If such transient is not completed by the beginning of the following measurement it will be performed with some error. This error depends on the time interval between previous event and event currently measured, causing non-linearity in event measurement.

The A032-ET corrects such non-linearity but cannot exclude it completely, leaving slight, noise-like residual non-linearity in the range up to 2000 ns. This non-linearity appears as errors, which are particular and constant for every 1 ns step of time interval incrementing (Fig.4). In the range exceeding 2000 ns the non-linearity is negligible.

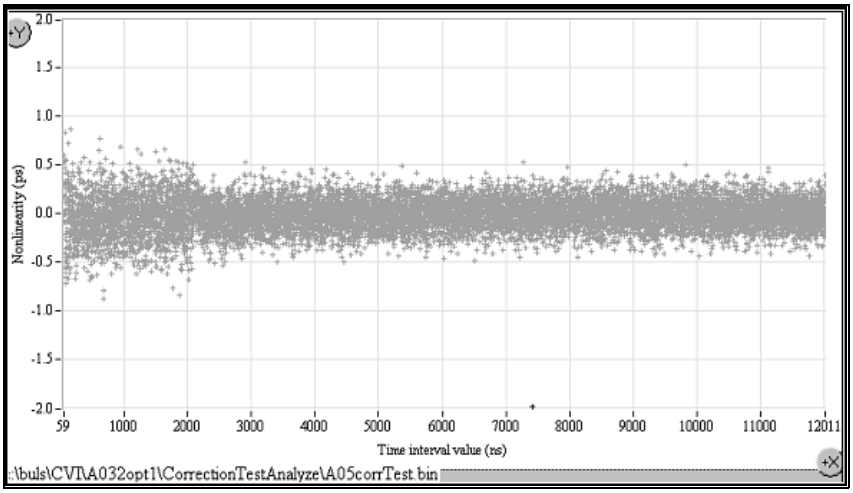

Figure 4. *Typical result of non-linearity error testing*

As can be seen, the maximum non-linearity does not exceed ±1 ps. However such estimate is overstated by reason of the additive evaluation errors (these errors are directly present in the range from 2000 ns). Actually the non-linearity is much smaller.

Offset drift

All events coming at either input of the ET-device are measured sequentially in the same manner and by the same means. Owing to this there is no any noticeable offset in time intervals between measured events when these events come at the same input. However when the events come at the different inputs it results in some offset. The offset is caused by a difference between internal propagation delays of input signals before their coming to the common measurement unit. These delays slightly vary with the ambient-temperature change, thus causing certain offset drift and corresponding long-term instability in time interval measurements.

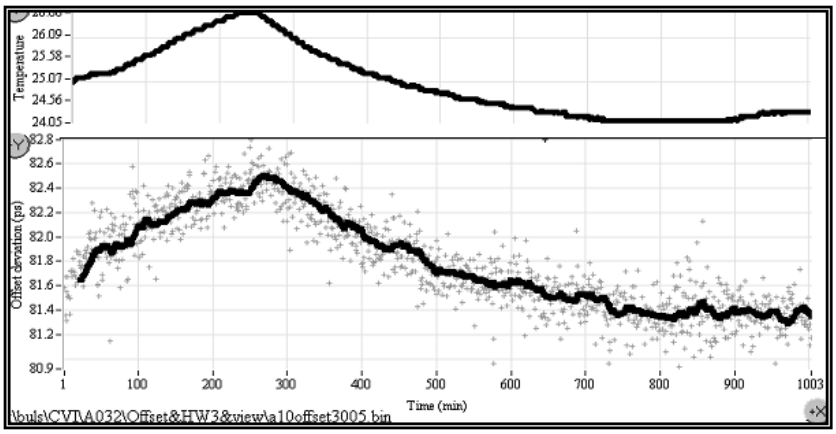

Figure 5. *Ambient-temperature and offset vs. time*

As can be seen from the example shown in Fig.5, the offset variation is directly related to the temperature variation, indicating in this case the offset temperature stability about 0.48 ps/°C. Generally this parameter value depends on the specific operating conditions.

A032-ET summary specification

Generalizing the test results that have been obtained at least for 15 units of the A032-ET, the following summary specification can be stated:

Inputs (BNC): INPUT A	NIM pulse (falling edge; >5 ns width)
INPUT B	NIM pulse (falling edge; >5 ns width)
SYNC IN	TTL pulse (rising edge, 1 pps)
TRIG IN	TTL pulse (rising edge)
REF IN	10 MHz (>0.5 V p-p)
Single-shot RMS resolution	<10 ps
Dead time	60 ns
Non-linearity error	<1 ps (<3-5 ps for time intervals less than 100 ns)
Offset temperature stability	<0.5 ps/^{0}C after warm-up
Warm-up time	2 hours
FIFO depth	12,000 time-tags
Measurement rate (True Timer)	up to 10 KHz continuously
Stop pulse gating (Multi-Stop Counter)	online programmable via network (10 ns LSD, 60 ns to 167 ms range)
Control	fully remote control from a user program via the network
Application interface	over TCP/IP
Hardware interface	via PC parallel port supporting EPP mode
Server software	MS-Windows based
Accessory software	DEMO application software
Hardware dimension, weight	375x60x233 mm (desktop); 3.0 kg
Power supply	100-240 VAC

It should be pointed that the A032-ET is a custom instrument manufactured in a limited quantity and only on request. For this reason such instruments may differ from one to another in some details. Additionally it should be taken into account that the measurement rate may depend on the actual performance of the user's PC and network.

Additional notices

The A032-ET is currently available in the following configuration:

- ET-device;
- Server software A032.1 that provides **"True Timer"** mode;
- Server software A032.2 that provides **"Multi-Stop Counter"** mode;
- DEMO Client software (including source codes in *C*) that illustrates the manner in which the user can create own specific application.

Optionally the Sample program (source code in *C*) is available. This program defines the device-specific software functions to communicate with the A032-ET hardware via PC Parallel Port. These functions can be directly built in the user software when the user desires to create fully integrated timing system.

References

[1] http://ilrs.gsfc.nasa.gov/docs/timing/Event-Timer-A031-ET.pdf

Upgrading of Integration of Time to Digit Converter on a Single FPGA

Young Zhang[1,2], Peicheng Huang[1] and Renjie Zhu[1,2]

1. Shanghai Astronomy Observatory, Chinese Academy of Sciences, 80 Nan Dan Road, Shanghai, China 200030
2. Graduate School of the Chinese Academy of Sciences, 19A Yu Quan Road, Beijing, China 100039

Contact: zhang.young@gmail.com , pchuang@shao.ac.cn and zhurj@shao.ac.cn

Abstract

A Time to Digit Converter (TDC), which can achieve resolution 50-60 picoseconds, is integrated on a single FPGA. Implementing a TDC on an FPGA provides not only higher precision and shorter dead time compared to traditional methods, but also higher scale of integration. As the system can be integrated into single chip, it is especially suitable for portable and satellite-borne system. Besides, the resolution is expected to be improved to less than 30 picoseconds. Principle of operation, architecture of the prototype, the construction of this TDC and the nonlinearity are presented in this paper.

Introduction

Traditional high-precision time interval measurement techniques include time stretching method, time-to-amplitude method and Vernier method, tapped delay line method and differential delay line method [1]. There are two examples of TDC integration on a single FPGA: Jozef Kalisz *et al* adopted differential delay line method on QuickLogic's pASIC2 FPGA, which achieved 100 ps LSB [2]. Zielinski and Chaberski, using tapped delay line method, implemented a module on Xilinx's XCV300 with 100 ps resolution [3]. In this paper, a TDC is implemented on a XC4VSX35 FPGA with 50-60 picoseconds resolution. Table 1 lists main parameters of this module as below.

***Table 1**: Design Summary*

Standard uncertainty	50--60 picoseconds
Resolution/LSB	50--60 picoseconds (expected to reduce to 20-30)
Measurement Range	0-99999 seconds
Input Reference Clock	10MHz Rb Atom Clock
Calibration Mode	Real time Calibration

General Design

Interpolating Principle

Interpolating methods are widely used because of its advantages in both long measurement range and high resolution. With interpolating methods, a time interval T generally consists of three parts. A major part, nT_p, is measured in real time by reference clock. The remaining two short intervals ΔT_1 and ΔT_2 are defined at the beginning and at

the end of time interval *T*, which are measured by insulators. In this design, they are measured by two tapped delay lines. Fig. 1 gives the math relation between them.

Reference clock

The input 10MHz reference clock from Rb atom clock is quite stable but not high enough for interpolating. With built-in DCM on FPGA, it is synthesized into 200MHz. As shown in Fig.1, the time interval nT_p is counted by the reference clock 200MHz. The measurement jitter of 200MHz reference clock is about 60 picoseconds.

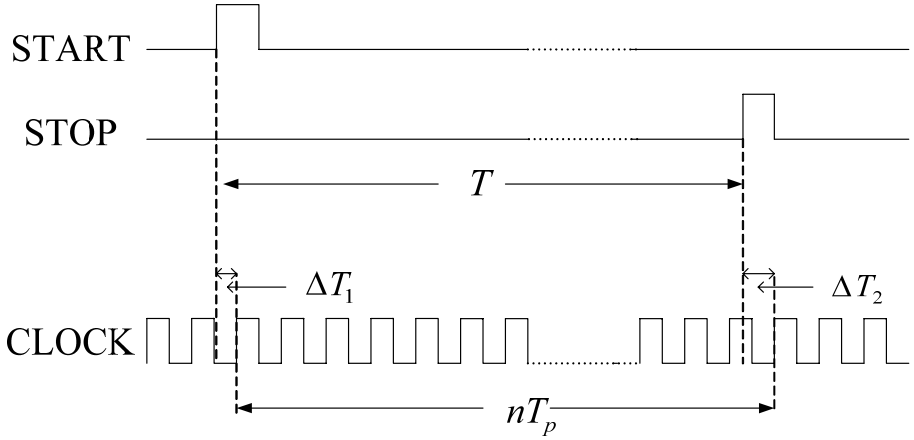

$$T = nT_p + \Delta T_1 - \Delta T_2$$

Figure 1. *Interpolating Principle*

Tapped Delay line

The tapped delay line is made of slices - the basic unit of the Virtex FPGA. As shown in Fig.2, a delay unit and a D flip-flop, is in the dashed line. The dashed part of delay logic can be implemented in a single slice, as shown in Fig. 3. These slices cascade to form a slice chain, i.e., a tapped delay line. Two delay lines of this kind, measure the short time interval ΔT_1 and ΔT_2 respectively.

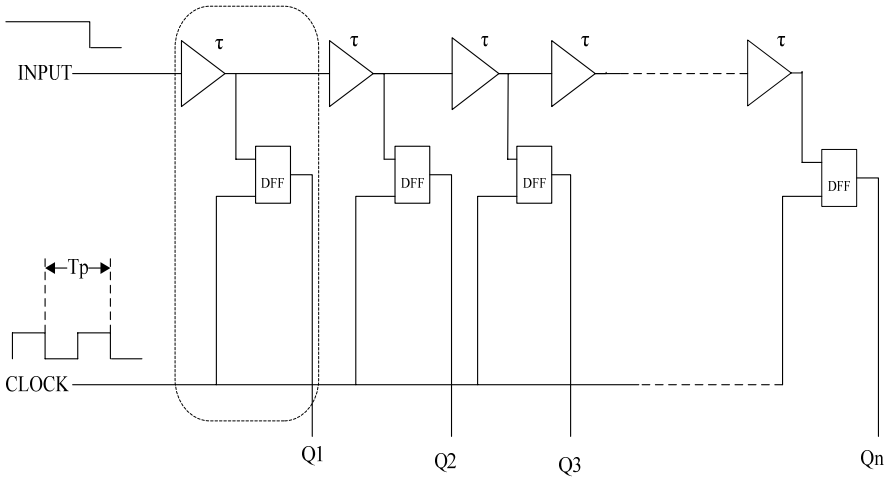

Figure 2. *Tapped delay line made of slices.*

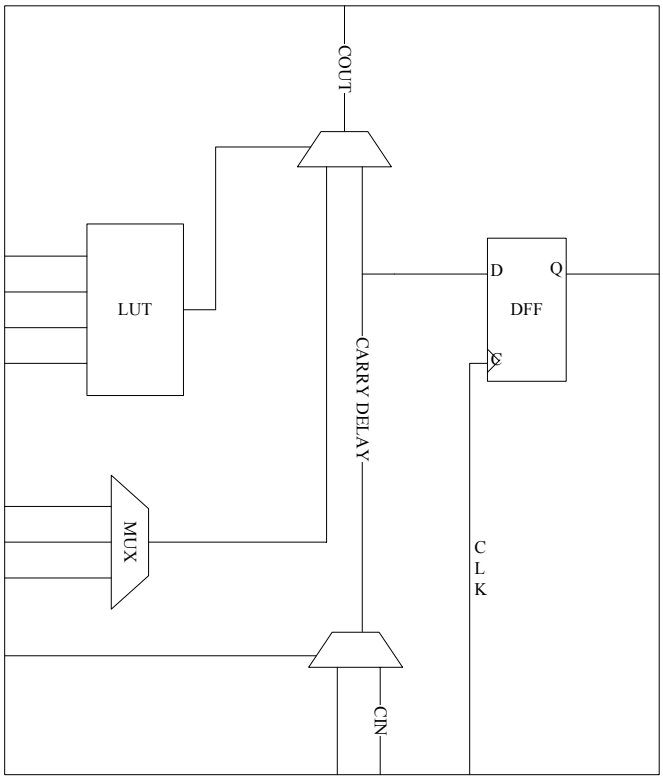

Figure 3. *Simplified slice configuration as delay unit.*

The delay unit of slice utilizes the fastest path, fast carry logic, to obtain the highest resolution. It's assumed that all delay units are of the same delay time τ. The measurement average delay τ, which determines the resolution or least significant bit of this module, is about 50-60 ps. However, this assumption does not fit the facts perfectly. The nonlinearity of the tapped delay line is measured and analyzed in the next part.

Measurement data

In this part, the measurement data of this module is compared with those of SRS's SR620. To demonstrate the resolution of this high-precision TDC, y axis of Fig 4 is marked with TDC measurement, while the x axis is marked with SR620 measurement.

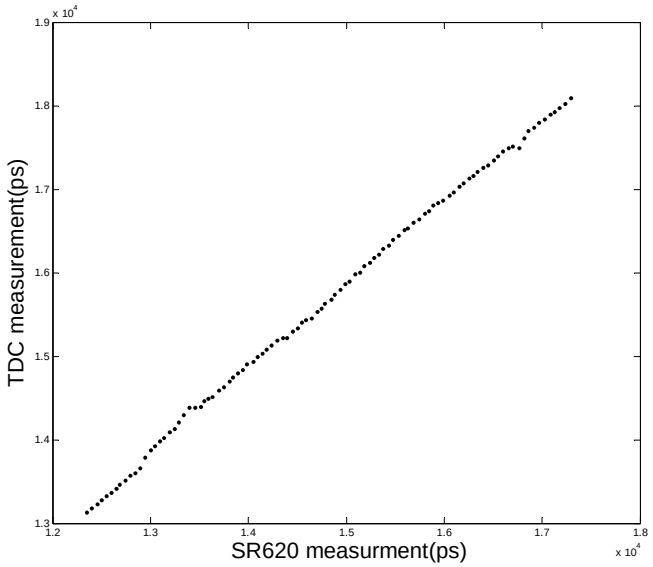

Figure 4*. Comparison of TDC measurement with SR620 measurement*

The difference between two groups of measurement, which is equal to the differential nonlinearity, is given in Fig. 5. In Fig.5, the maximum difference is about 300 picoseconds. The difference measurement can be repeated in other time cycle, which means it can be corrected with prior knowledge of it. This will be part of further research. Besides, with a little internal modification, the resolution is expected to reduce to less than 30 picoseconds, which means 50% improvement in resolution. This will be part of our future work.

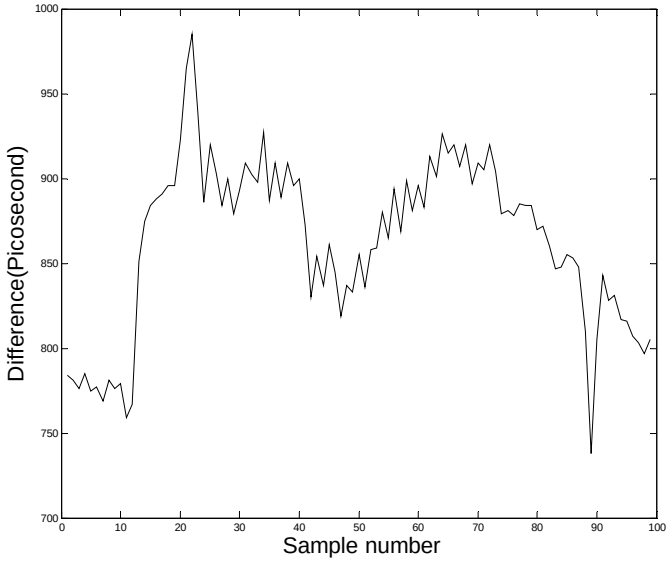

Figure 5. Difference between TDC and SR620

Fig.6 is a snapshot of our measurement experiment.

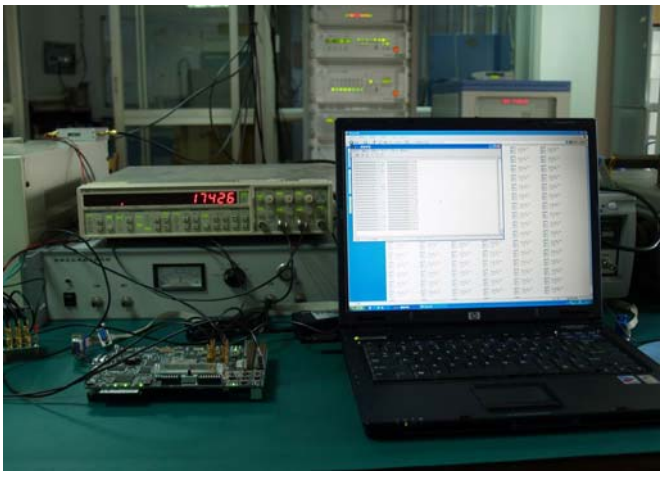

Figure 6. Measurement experiment

References

[1] Józef Kalisz, 2004. Review of methods for time interval measurements with picosecond resolution Institute of Physics Publishing Metrologia, vol 41 pp17-32.

[2] Szplet R, Kalisz J and Szymanowski R., 2000. Interpolating time counter with 100 ps resolution on a single FPGA device IEEE Trans. Instrum. Meas. vol 49, pp.879-883.

[3] Zielinski M, Chaberski D., and Grzelak S., 2003. Time-interval measuring module with short dead-time Metrol. Meas. Syst. 10.

High-Speed Enhancement to HTSI Event Timer System

D. McClure, C. Steggerda, S. Wetzel

1. Honeywell Technology Solutions Inc., 7515 Mission Drive, Lanham, MD USA 20706

Contact: scott.wetzel@honeywell.com

Abstract

HTSI has developed a high-performance Event Timer Controller to pair with the HTSI Event Timer that allows acquisition of UTC tagged event epochs with <2ps jitter and 0.5ps resolution from up to 12 input event channels at continuous asynchronous event acquisition rates of over 50kHz. The increase in sustainable data rate allows easy integration of multiple or arrays of detectors and generation of a single real-time stream of UTC epoch'd event data with associated channel ID flags.

This paper describes the upgrades to the HTSI event timer system that enable the high-speed capability. The content will include a data comparison of ILRS stations utilizing the HTSI event timer as well as a discussion of current usage applications and potentials for future use.

High-Speed Enhancement to HTSI Event Timer System

The HTSI Event Timer was designed and built in the 1990s by Charles Steggerda based on his years of experience designing timing devices. Initial laboratory and MOBLAS-7 test results were reported in July 1998 at the 19th International Laser and Radar Conference in Annapolis, MD in a paper titled *Instrumentation Development and Calibration for the Matera Laser Ranging Observatory*. Today's paper follows up after 8 years of use and describes an important new capability that can be utilized by the current and next generation of high rate laser ranging stations. Figure 1 shows the HTSI Event Timer.

Figure 1: *HTSI Event Timer*

HTSI Event Timer Description

The HTSI Event Timer (ET) generates precise epoch time-tags ideal for Satellite Laser Ranging, Lunar Laser Ranging, and other precision timing applications. The ET facilitates measurement of delays between one or more pulses without a range/delay

dependant effect on timing error and supports applications with multiple shots in the air required by high laser fire rates or extended time of flight to targets (i.e. geosynchronous, lunar, or beyond). The basic design and capability hasn't changed since that reported in July 1998 at the 19th International Laser and Radar Conference. The ET couples a precise synchronous counter with from 1 to 4 analog verniers and a computer synchronized to UTC. In the single vernier configuration, the ET provides better than 2 ps of resolution and less than 4 ps of Root-Mean-Square (RMS) jitter. In the four vernier configuration, the ET provides measurement redundancy and increases the effective resolution to <500 fs with an RMS jitter of < 2 ps.

Clock Speed (Internal)	500 MHz, Locks to external 10MHz
Input Channels	12 SMA inputs; NIM type; 50 Ohm termination; negative pulses (unused channels do not require termination)
Resolution	Better than 2ps (1 vernier), 500 femtoseconds (4 vernier)
Dead-Time	100 Nanoseconds
RMS Jitter	<5ps for 1 vernier; <2ps for 4 vernier
FIFO Depth	512
Interface	32 bit DIO, Optional computer allows additional interfaces
Software	UNIX (HP-UX, Linux), MS Windows, etc.
Power	Auto ranging (100-240V; 50-60Hz)

Figure 2: *Summary of Specifications*

Twelve external inputs are provided and events sampled on each channel are tagged with an identification flag in hardware. When coupled with a computer that receives coarse time via time code or GPS, a full event epoch can be generated. Events can be sampled by the hardware at a rate of 10MHz, but are input into a high-speed FIFO buffer that can only store 512 events. Thus the specification of maximum sustainable event sample rate is dependant on the DIO and processing speed of the specific event timer controller.

HTSI Event Timer Past Performance

The initial HTSI event timer development was started in 1995 to support the Matera Laser Ranging Observatory (MLRO). Initial testing of the ET prototype was performed at NASA Goddard Space Flight Center's MOBLAS-7 reference station. Comparison results between the prototype ET and MOBLAS-7 indicated addition of the Event Timer produced an immediate 30-40% improvement in MOBLAS 7 data quality over the existing HP-5370 counter data decreasing LAGEOS range data RMS from 9mm to 5mm.

Later in 1998, the final 4-vernier MLRO and 1 vernier SLR2000 event timers were built. In 2002, a dual vernier model was built for the Global High Accuracy Trajectory Station (GUTS) to be located in Tanegashima, Japan. The MLRO and GUTS event timers supported both stations in achieving best case performance of 2mm ground calibration and 5mm LAGEOS RMS. Both stations utilized the multiple inputs to support fire, dual color PMTs (MLRO), amplified channels for Lunar (MLRO) and Geosynchronous ranging (GUTS), system calibration inputs, on-time pulses, etc. And in 2006, an Event Timer is being built for the US Naval Research Laboratories (NRL)

- **MOBLAS 7** – (Prototype Event Timer; 1998; 3ps RMS)
  - 5 Hz fire, 2 events per frame
  - Use of the HTSI Event Timer produced an immediate 30-40% improvement in MOBLAS 7 data quality over the HP-5370 TIU (Lageos-1 data improved from 9 mm RMS to 5 mm RMS).
- **SLR2000 Prototype** – (Delivered in 1998; 4ps RMS)
  - 2 kHz fire, multiple events per frame, quad PMT
- **MLRO** – (Used in Greenbelt, MD in 1998 and Matera, Italy since 2000; 2ps RMS)
  - 10 Hz fire, 8 events per frame
  - Multiple laser & PMT detection path signals sampled by one event timer.
  - Supported station in achieving 2 mm calibration and 5 mm LAGEOS RMS.
  - Supported station in acquiring two-color and lunar data.
- **GUTS** – (Used in MD in 2002 and Tanegashima, Japan since 2004; 4ps RMS)
  - 10 Hz fire, 4 events per frame
  - Supported station in achieving 2 mm calibration and 5 mm LAGEOS RMS.
  - Supported station in acquiring data from geosynchronous targets.
- **NRL** – Being developed as a stand alone ET for delivery in 2006/2007
- **GUTS Spare** – Being developed for delivery in 2007

Figure 3: *HTSI Event Timer Past Performance*

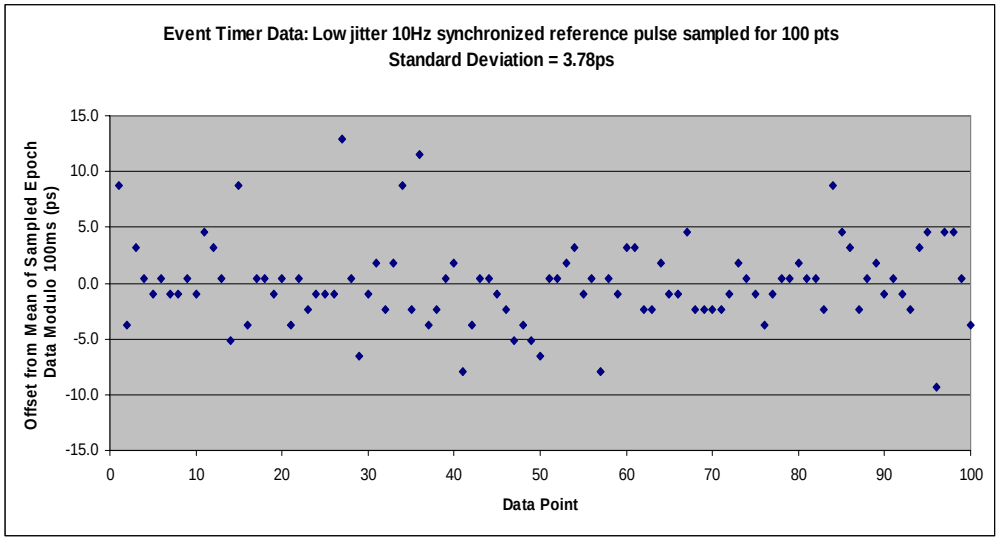

Figure 4: *Event Timer Accuracy*

HTSI Event Timer Data

Figure 4 demonstrates typical Event Timer Accuracy / RMS when configured with a single vernier. To generate this graph, a precise 10Hz electrical reference pulse was sampled 100 times by the event timer. The epoch data was then normalized to the mean repetition frequency. The graph shows raw, unfiltered offset data that demonstrates a 3.78ps RMS jitter. If you look closely, you can see data banding demonstrating that the single vernier bit resolution is <2ps.

Figure 5 demonstrates the potential single shot RMS of stations that utilize the HTSI event timer showing the MLRO and GUTS stations as having the lowest reported LAGEOS single shot RMS in the ILRS network. Note that the event timer, while crucial, is coupled with excellent optics and low-noise optical detection to produce these results.

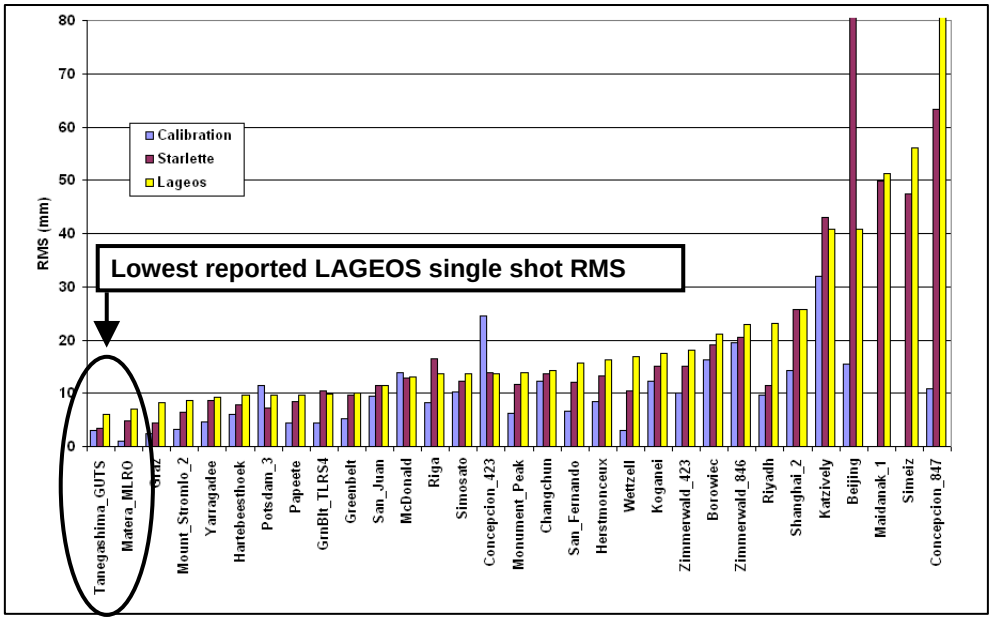

Figure 5: *ILRS Station Single Shot RMS Data for 2Q 2006*

HTSI Event Timer Controller High Speed Enhancement

The HTSI ET has always supported Mega-event per second sample rates, but has been limited by the speed of its control computer in emptying the 512 event deep hardware FIFO. The GUTS and MLRO ET controllers used non-DMA DIO to communicate with the ET at a maximum event rate of approximately 200 events per second (while also performing tracking and controlling other equipment). Counter and verniers were manually addressed by the controller. For SLR2000, HTSI converted the ET to use a high-speed DIO card. In addition, the counter and vernier became auto-addressed allowing for DMA transfer operations. The ultimate data rate was still limited from sharing control computers with other tasks, 10Mbps Ethernet speeds and generation of individual event interrupts.

The advances in computer processing speeds and network bandwidth since 1998 have allowed the design of a high-performance controller to utilize the hardware to its full potential. This high-performance controller enables the HTSI event timer to immediately gain a factor of 10 in sustainable rate (from multi-KHz samples per sec to at least 50ksamples/sec) and promises to allow for further growth in the future as the world transitions to dual core processors and 10GB Ethernet. In addition, the enhanced controller removes the complex issue of DIO interface, driver, and data handling replacing them with a simplistic network accessible design. The enhanced Event Timer controller provides a real-time stream of epoch'd ET data across a dedicated LAN to a station tracking computer. DIO transfer rate is maximized by allowing the ET FIFOs to buffer data. Data is immediately calibrated, combined with UTC coarse time, sent to Ethernet, and received on the tracking computer. A prototype of the enhanced controller has been built in Greenbelt, MD, and is still in the process of software development and testing.

Figure 6 shows the block diagram of the Event Timer Controller that has been built in our integration lab. Notice that all components exist to produce high accuracy time epochs referenced to UTC.

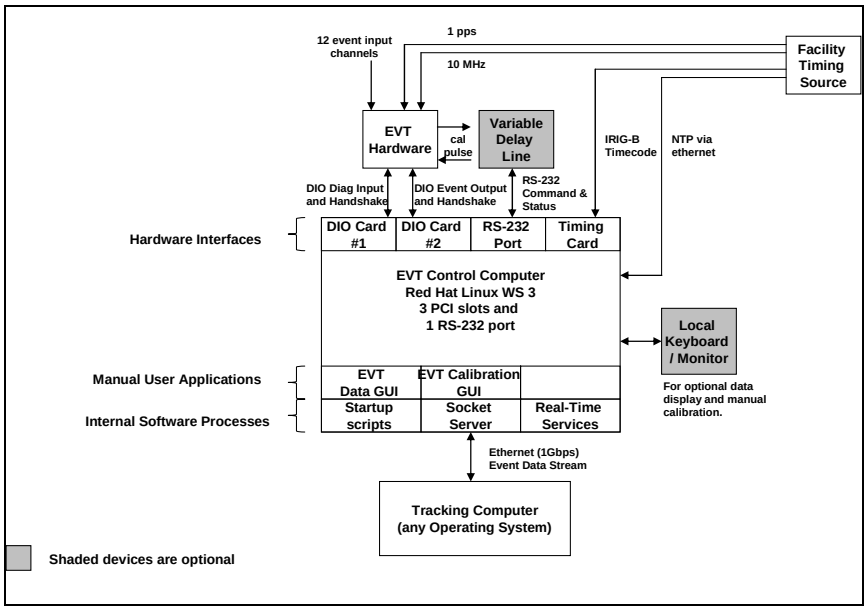

Figure 6: *Enhanced Event Timer Controller: Block Diagram*

Figure 7 shows the internal software architecture and data flows within the Enhanced Event Timer Controller. The Event Timer Software architecture is based on modular C++ UNIX processes inherited from the MLRO and GUTS software heritage. Event Data moves from right to left in this figure. Event Timer and Time Code Generator data is merged to produce a real-time stream of event epoch data. Vernier non-linearity's are then removed via calibration in real-time. The event data is then distributed to client tracking computers via a network socket server.

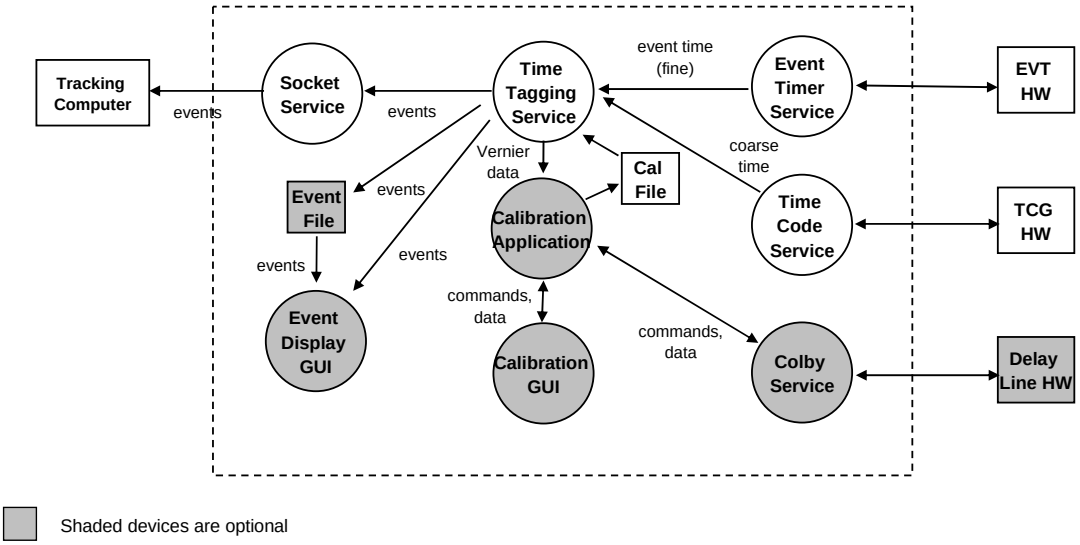

Figure 7: *Enhanced Event Timer Controller Software Architecture*

Optional software modules allow for local calibration of the event timer or independent use of the ET controller by storing event data in a file. Optional modules include a delay line interface, a calibration process and GUI, and an event display GUI.

HTSI Enhanced Event Timer Controller: Initial Results

DIO Performance

Figure 8 shows initial results of high speed testing with the Enhanced Event Timer Controller. Initial DIO laboratory performance tests were able to read reference pulse event times from the ET FIFO buffer at a sustained rate of 5Msamples/sec or **1.25 Million events per second** with a 3 vernier + 1 counter ET. DIO card specifications indicate that the maximum continuous handshaking I/O rate for the DIO-6533 is 17.3 Msamples/sec potentially enabling the reading of. **4.3Million events per second** with a 3 vernier + 1 counter event timer.

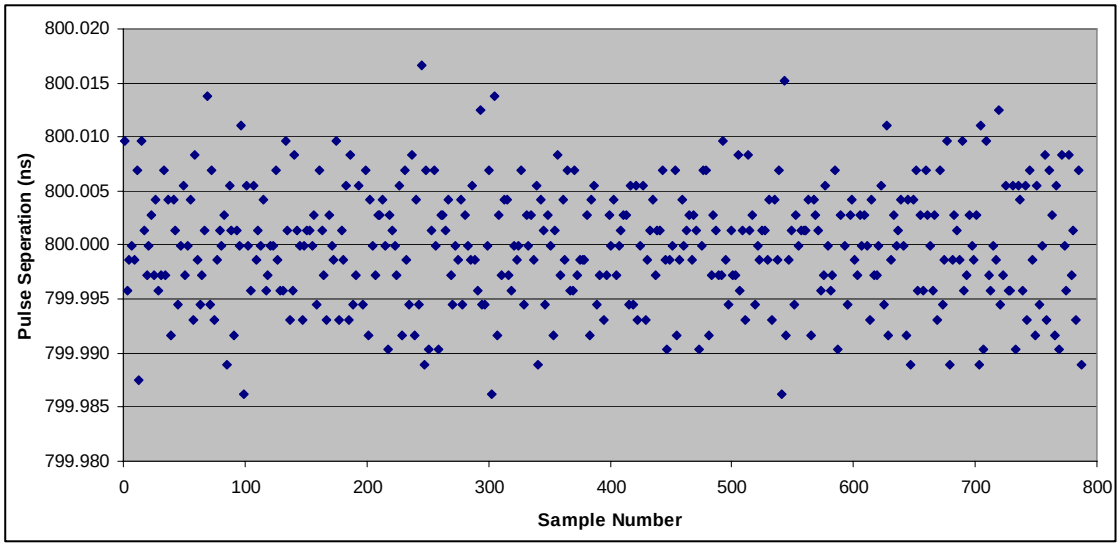

Figure 8: *Initial Enhanced Event Timer Controller High Speed DIO Test Data*

LAN Performance

Preliminary tests demonstrate that it is possible to sustain network transfer rates of **61,035 events per second** on our current 100Mbps testing LAN (no network traffic analysis tool was available to determine actual network bandwidth usage). Further increase in speed is theoretically possible after tuning of packet sizes and enhancing our laboratory with a 1Gbps network switch. These results match initial computations to first order predicting that 50,000 events per second requires a minimum of 25Mbps dedicated network bandwidth on an isolated LAN (assuming 1,024 bit packets holding (8) 112 bit events or 896 bits of user data each and a factor of four compensation for traffic).

HTSI Event Timer: Future Applications

The newly developed HTSI High-Speed Event Timer Controller when combined with the HTSI Event Timer produces a system that can enable many future applications in addition to those currently being supported. Currently the HTSI Event Timer has been used to support:

- 10Hz single and dual laser fire and return with station calibration events (single and multi-wavelength)
- 10Hz geosynchronous and lunar laser ranging (multiple shots in the air)
- 2kHz tracking with 3 high-rate event inputs (6KEvents/sec)

The Enhanced HTSI Event Timer System meets the needs of the SLR data community to acquire data at higher and higher repetition rates with more detectors and enables the design of the next decade of forward reaching experiments. A few of the additional potential applications that can be extrapolated includes:

- 2kHz operations with multiple fire and detection events (i.e. for multiple wavelengths / dual PMTs)
- 2kHz operations with additional station delay diagnostic event inputs
- Use of arrays of detectors at 2kHz (3x3; 3x4; 4x4 would require external event coupling)
- Recording of high rate event epoch data approaching 1 Million events per second
- Laser fire and return pairs several orders of magnitudes faster than 2kHz
- Time transfer experiments (ground and on-orbit)
- Station construction with reduced event timer integration time
- Station construction with reduced real-time tracking controller complexity and cost (ethernet vs. DIO)

References:

[1] *Instrumentation Development and Calibration for the Matera Laser Ranging Observatory*, July 1998, 19th International Laser and Radar Conference in Annapolis, MD, C. Steggerda, M. Selden, C. B. Clarke, R. Stringfellow, J. M. Heinick, D. McClure, Dr. G. Bianco

[2] Time of Flight Devices Manufacturer Specifications Comparison Table, ILRS Web Site, http://ilrs.gsfc.nasa.gov/engineering_technology/timing/tof_devices/manufacture_spec/index.html

[3] SLR Global Performance Report Card 2Q 2006, ILRS Web Site, http://ilrs.gsfc.nasa.gov/stations/site_info/global_report_cards/perf_2006q2_wLLR.html

Low-Noise Frequency Synthesis for High Accuracy Picosecond Satellite Laser Ranging Timing Systems

Josef Kölbl[1], Peter Sperber[1], Georg Kirchner[2], Franz Koidl[2]

1. Deggendorf University of Applied Sciences
2. Austrian Academy of Sciences, Observatory Lustbühel

Abstract

The developed Frequency Multiplier from 10 MHz to 200 MHz is fully compatible to the Thales Multiplier and can be directly interfaced to the Thales Event Timing Modules by "plug and play". The new Multiplier designed at Deggendorf University of Applied Sciences shows high sub-harmonic attenuation in the frequency domain of greater than 110 dB.

Whereas, in the time domain the 200 fs rms cycle-to-cycle jitter specification is observed when measuring the output signal with a high-bandwidth sampling oscilloscope. Measurements in the time domain and frequency domain of the new multipliers show better specifications to existing frequency synthesizers.

The 10 MHz to 80 MHz Frequency Multiplier is in continuous operation at Mount Stromlo SLR Station and in various Keystone SLR Stations in Japan. Modules are available through our partner company MPF Optics Ltd.

Introduction

Tests carried out at SLR station Lustbühel, Graz:
Graz E.T. / Dassault Modules:
Comparison between Dassault Clock and Deggendorf-Clock

- DeggendorfClock is mechanically / electrical connections identical to Dassault Clock;
- Measurements in Graz were made using both clock modules alternatively;
- Measurement description:
    - Standard Laser Firing pulse (TTL), Power Splitter 50 Ohm;
    - 1 Pulse direct into E.T. Start;
    - Splitted pulse delayed with cable, into E.T.Stop;
    - Standard Calibration Program used, Single Time Intervals stored;
    - Results checked with Program DRAW, 2.2 Sigma Iteration;
- For ease of tests: Clock module 200 MHz outputs (both clocks) connected via standard RG58 Cables / SMA connectors into Start / Stop Modules (instead of Dassault Semi-Rigid Cables). All Tests performed in this configuration.
- At each change of Setup: E.T. switched off; new sync / new offsets after each switch on.

Results (in ps) / No Sigma iteration

Cal_1: 9215.94 ± 3.87 [ps]	Dassault Clock	Semi-Rigid Cables (Graz Original Setup)
Cal_2: 9216.04 ± 3.34 [ps]	Dassault Clock	RG 58 cable
Cal_3: 9217.14 ± 3.58 [ps]	Deggendorf clock	RG 58 cable
Cal_4: 9214.83 ± 3.34 [ps]	Dassault Clock	RG 58 cable
Cal_5: 9216.45 ± 3.32 [ps]	Deggendorf clock	RG 58 cable

Results (in ps) / 2.2 Sigma iteration:

Cal_1: 9215.94 ± 2.84 [ps]	Dassault Clock	Semi-Rigid Cables (Graz Original Setup)
Cal_2: 9216.12 ± 2.79 [ps]	Dassault Clock	RG 58 cable
Cal_3: 9217.00 ± 2.82 [ps]	Deggendorf clock	RG 58 cable
Cal_4: 9214.73 ± 3.07 [ps]	Dassault Clock	RG 58 cable
Cal_5: 9216.45 ± 2.57 [ps]	Deggendorf clock	RG 58 cable

Remarks

- Variation in absolute values (1-2 ps): Due to new offsets between start/stop modules after switch ON.
- Several other calibration runs were made, with different cable length etc.; all giving similar results.
- The Deggendorf clock module seems to have at least the same specs than the Dassault; no difference visible.

Editor's Note

The technical data specification for the frequency multiplier unit can be found on the accompanying CD.

MULTIPLE WAVELENGTH AND REFRACTION SESSION SUMMARY

Chair: Erricos Pavlis

Gurtner presented recent changes at Zimmerwald. The system used internal, near realtime calibration until June 2006. The change was necessitated after routine operations with a second wavelength (infrared) revealed differences between the calibrated ranges of the two colors that could not be explained as errors in the applied refraction models. It turned out that the internal calibration values of the infrared chain showed variations that had not much to do with system calibration. The source of these variations could not be identified. In June 2006 the station switched to external calibration and the differential biases were by and large eliminated. One of the concluding remarks was the need of a 100-fold improvement in the dual wavelength data if they are to be used for refraction modeling.

Müller reported that Lageos-1/2 multi-wavelength normal point data from Zimmerwald and Concepcion were reduced with DGFI's s/w, to estimate station coordinates and color dependent biases. The statistics and the history of bias differences for the Marini-Murray and Mendes-Pavlis refraction models were shown. Full-rate tracking data were also analysed to determine if they lead to results different from the use of onsite normal points. The switch from internal to external calibration at Zimmerwald resulted in a significant improvement of the relative biases, mainly for the infrared side. The tests indicated the superior performance of the new refraction model of Mendes-Pavlis.

Pavlis (for Hulley) presented the validation of the new, sub-millimeter accuracy, zenith delay model of Mendes and Pavlis, [2004] and the sub-centimeter accuracy mapping function of Mendes et al., [2002], using global data from the Atmospheric Infrared Sounder (AIRS), the European Center for Medium Weather Forecasting (ECMWF) and the National Center for Environmental Prediction (NCEP). The models however are still far from the required sub-millimeter accuracy goal for future SLR analysis standards and the requirements place on SLR by the Global Geodetic Surveying System (GGOS) [Pearlman et al., 2005]. They thus developed a new technique, using 3D ray tracing that includes the effects of horizontal refractivity gradients. Global statistics for two years indicated delays can reach even 5 cm at an elevation angle of 10° at certain times of the year and at some locations. Application of the method to a two-year set of global SLR data resulted in variance reduction of the residuals by up to 45%, and 3 mm in RMS.

Hamal reported on a joint activity with Chinese groups using multiple wavelength SLR. He described a novel use of a Single Photon Avalanche Detector (SPAD) for sub-centimeter ranging precision in infrared and sub-millimeter precision ranging in the visible region. This optimum configuration was implemented at the Shanghai station. Ranging was done successfully to satellites distances of 30000 km with one-centimeter precision. The results of direct measurements of atmosphere dispersion were compared to existing refraction models.

Sierk gave a lengthy, entertaining and very animated report of the upgrading activities at Wettzell and Conception in an impromptu, unscheduled entry in the session. The brief, 2-slide presentation turned out to be several dozens of slides rolling recollection of every gory detail, of the elaborate steps in upgrading the two systems. At the behest of the anxiously awaiting next presenter, the late Karel Hamal, the chairman had to almost resort to force to put an end to the captivating performance.

Analysis of Multi-Wavelength SLR Tracking Data Using Precise Orbits

H. Mueller

1. Deutsches Geodaetisches Forschungsinstitut, Muenchen.

Contact: mueller@dgfi.badw.de / Fax: +49 89 23031 1240

Abstract

Using precise Lageos-1/2 orbit generated by the DOGS (DGFI Orbit and Geodetic Parameter estimation Software) Package (http://ilrsac.dgfi.badw.de/dogs), multi-wavelength tracking data from Zimmerwald and Concepcion were analysed. We solved for station coordinates and color dependent biases. Some statistics and the history of bias differences for various tropspheric refraction models are shown. Additionally the available full-rate tracking data were analysed to see if there are differences to the biases obtained from the onsite normal points. The results show that the switch from internal to external calibration at Zimmerwald give a significant improvment of the relative biases, mainly from the infrared part. Finally we tried to rate the refraction models from the resulting bias differences.

Introduction

After an email request from Werner Gurtner to investigate if the new calibration scheme for Zimmerwald, Switzerland, since June 21 2006, has improved the quality of the two frequency data, we decided to reprocess all Zimmerwald data for 2005 and 2006 with the new DOGS programme, version 4.07, (Angermann et al. 2004) and strategy.

For the period 2005/06 we solved weekly Lageos-1/2 arcs using the same models as in the weekly position and EOP series. The parameters solved in this weekly arcs are:

- internal arc parameters
- earth orientation parameters
- station coordinates
- weekly biases for selected stations
- for Zimmerwald additionally a colour dependent bias per pass

Analysis

In a first step we looked into the range residual for the two colours, not solving for biases to see if the discrepancy between red and blue range residuals decrease after the calibration change. It is evident, that the range residuals reduced after the change in the Zimmerwald calibration from internal to external. In figure 1 the residuals prior and after the event are plotted. As next test we compared the relative biases between red and blue to see whether we could see an improvement of the data quality, too. In figure 2 the relative biases red-blue are summarized.

Using these results we tried to look for systematic characteristics in the relative biases. Unfortunately we did not see any correlation between bias and elevation resp. atmospheric data. The relative bias between is small after the change in calibration, see figure 3, but the precision is still not good enough to make full use of information contained in the two colors.

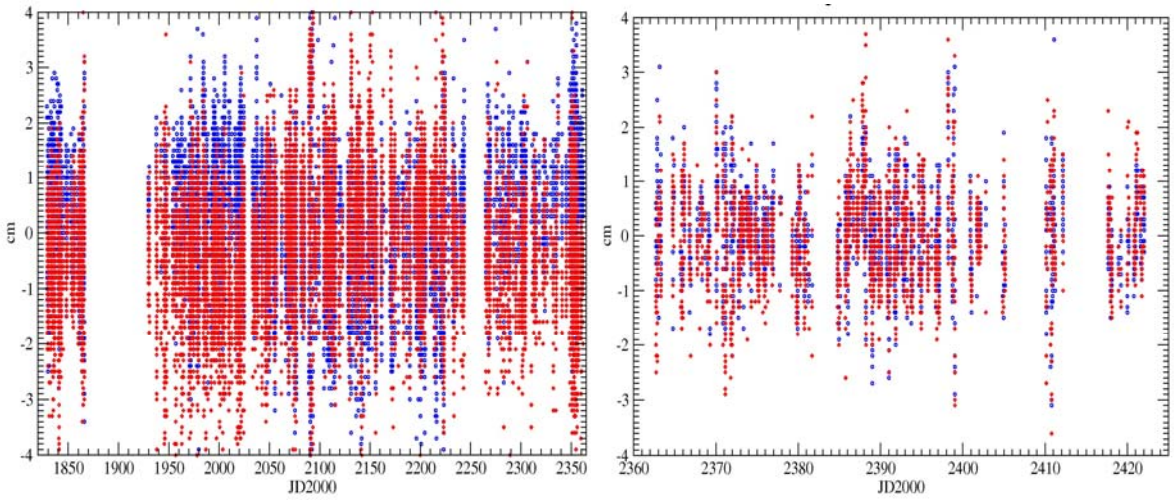

Figure 1. *Lageos-1 range residuals (red and blue Laser) for Zimmerwald*

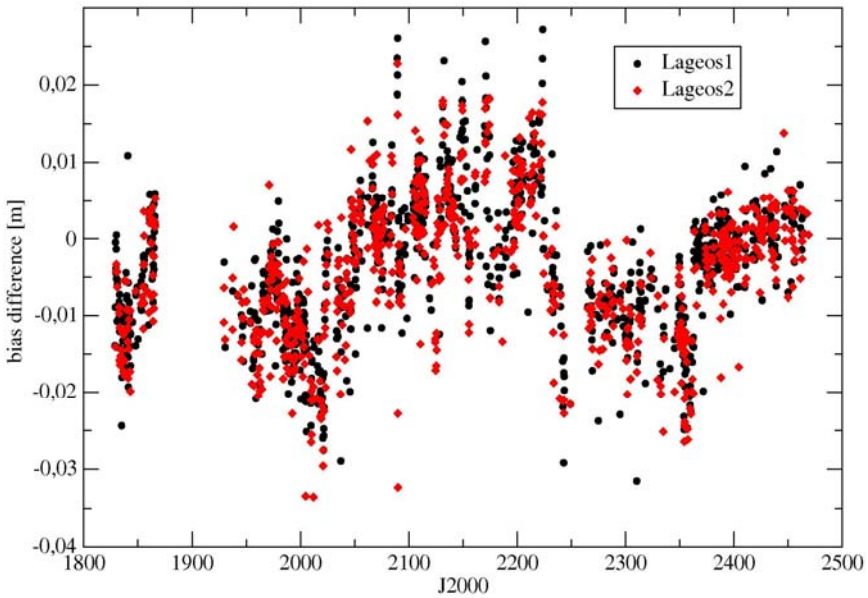

Figure 2. *Relative bias between red and blue Laser (cal. change at 2362.5 JD2000)*

A test to use the full rate tracking data provided for some of the Zimmerwald passes, did also fail because the epochs of the returned pulses are not identical and an interpolation to simultaneous results did not reach the required accuracy.

There is another station, Concepcion in Chile, operated by the TIGO system, which has the capability of two frequency ranging. We also tried to analyse these tracking data, but there is also no evidence of any systematic in the relative residuals. Mainly due to the fact the most of the time TIGO only delivers red wavelength tracking data, see figure 4, for all two-frequency passes available in 2005/06. The only result is that the biases are bigger than the Zimmerwald biases which could indicate that the calibration of the TIGO system is not stable enough because the tropospheric conditions in Chile are not so different to Europe. But there could also be other reasons for that higher noise in the relative biases.

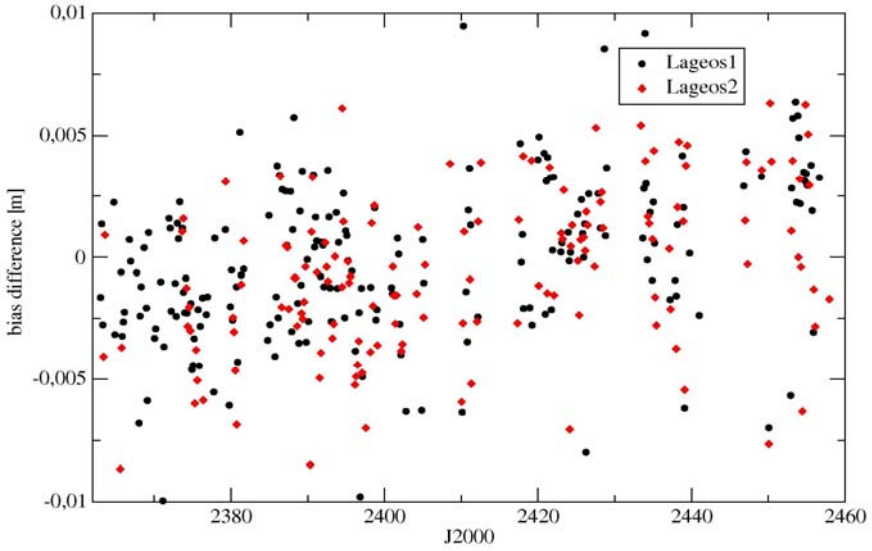

Figure 3. *Relative bias after calibration change for Lageos-1/2*

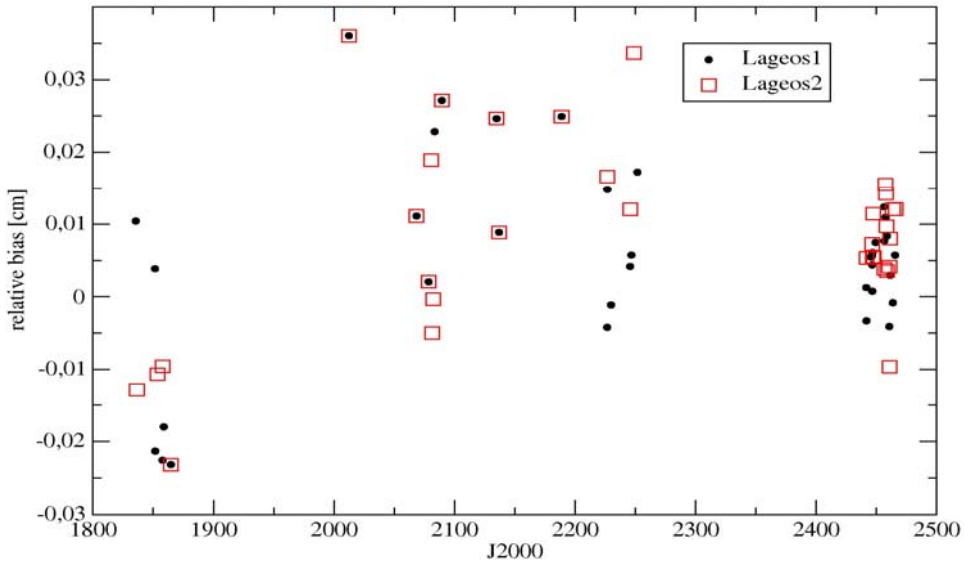

Figure 4. *Relative biases for Concepcion in Chile (TIGO system)*

Analysis of Troposphere Models.

To get at least some results from our computations we tried to see if there is a difference in the relative biases for the presently used Model Marini-Murray and the new Mendes-Pavlis model. There is no direct improvement if we look into the relative biases only, see figure 5. But if we look into the orbital fit, a clear indication that the new Mendes-Pavlis model gives an improvement is the mean weekly r.m.s. fit for the Zimmerwald SLR station which decrease significantly. In figure 6 we see the weekly r.m.s for Lageos-2 for Zimmerwald with solved station coordinates and relative range biases.

Conclusion

The new calibration at Zimmerwald, Switzerland, improved the quality of the two frequency SLR tracking data but there is still not enough precision in the relative biases to make full use of the data. The other two wavelength tracking system TIGO

at Concepcion in Chile has higher relative biases which could be the cause of calibration problems, like the Zimmerwald system.

The new Mendes-Pavlis tropospheric delay model gives, at least for the two frequency systems, an improvement compared to the old Marini-Murray model.

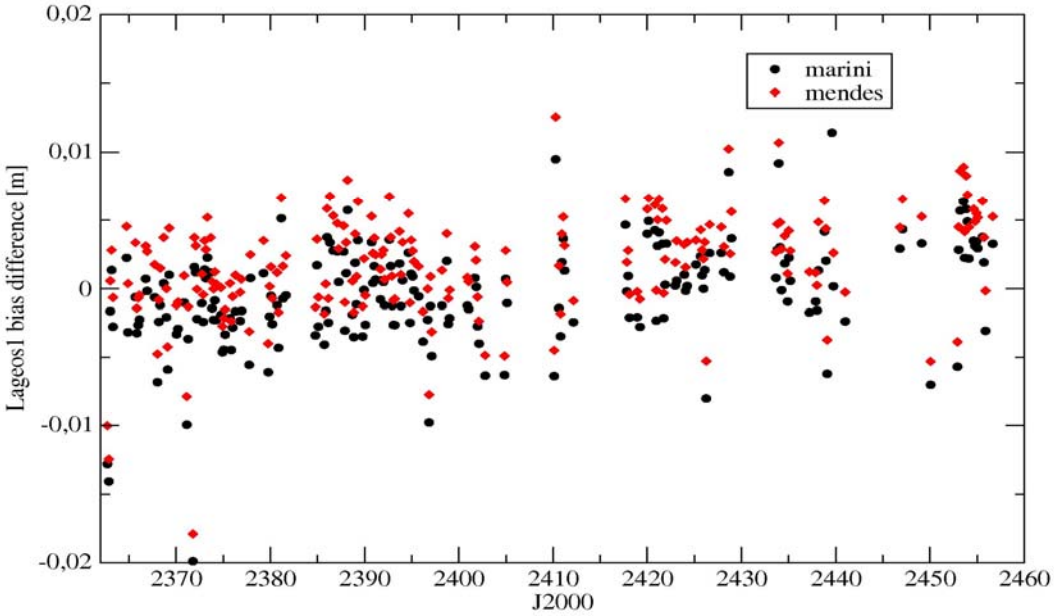

Figure 5. *Relative biases for Lageos-1 using Marini and Mendes refraction model*

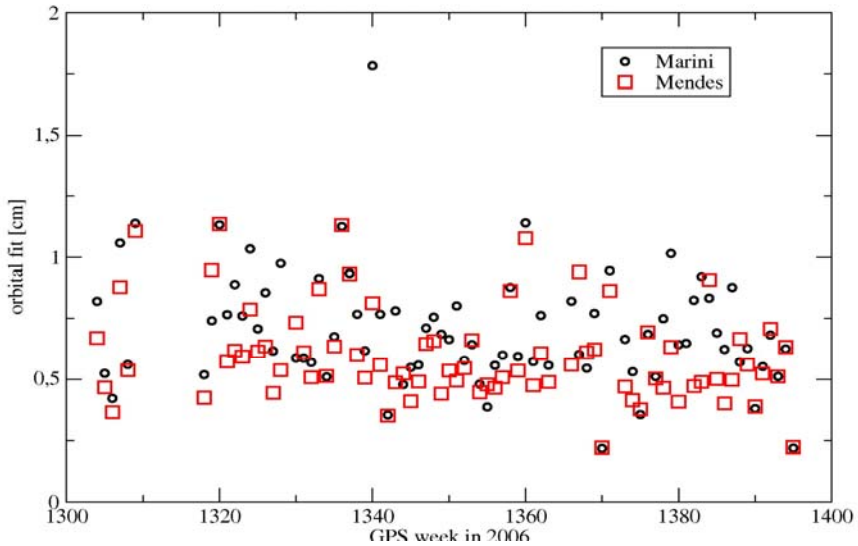

Figure 6. *Mean weekly residuals of Lageos-2 arcs for Zimmerwald*

References

[1] Angermann D, Drewes H, Krügel M, Meisel B, Gerstl M, Kelm R, Müller H, Seemüller W, Tesmer V (2004) ITRS Combination Center at DGFI: A terrestrial reference frame realization 2003, Deutsche Geodätische Kommission, Reihe B, Heft Nr. 313.

[2] Marini, J.W. and C.W. Murray, Corrections of laser range tracking data for atmospheric refraction at elevations above 10 degrees, NASA-TM-X-70555, Goddard Space Flight Center, Greenbelt, MD, 1973.

[3] Mendes, V.B., E.C. Pavlis, High-accuracy zenith delay prediction at optical wavelengths, Geophysical research letters, Vol. 31, 2004.

Improvement of Current Refraction Modeling in Satellite Laser Ranging (SLR) by Ray Tracing through Meteorological Data

G. Hulley and E. C. Pavlis

1. Joint Center for Earth Systems Technology (JCET), UMBC, Baltimore, MD, USA.

Contact: ghulley1@umbc.edu , epavlis@umbc.edu / Fax: +1 410 455 5868

Abstract

The accuracy of current modern space-based geodetic systems such as Satellite Laser Ranging (SLR), Very Long Baseline Interferometry (VLBI), the Global Positioning System (GPS), and satellite altimetry all suffer from limitations in the modeling of atmospheric refraction corrections. The current modeling of atmospheric refraction in the analysis of SLR data comprises the determination of the atmospheric delay in the zenith direction and subsequent projection to a given elevation angle, using a mapping function (MF). Recently a new zenith delay (ZD) model of sub-millimeter accuracy [Mendes and Pavlis, 2004] and a new MF of sub-centimeter accuracy [Mendes et al., 2002] were developed, applicable to the wavelengths used in modern SLR instrumentation.

We have already assessed and validated the new ZD model and MF's using 2-d ray tracing and globally distributed data from the Atmospheric Infrared Sounder (AIRS), the European Center for Medium Weather Forecasting (ECMWF) and the National Center for Environmental Prediction (NCEP). However, the models still remain far from the required sub-millimeter accuracy goal for future SLR analysis standards as set forth by the International Laser Ranging Service (ILRS) based on the requirements place on SLR by the Global Geodetic Surveying System (GGOS) [Pearlman et al., 2005].

To further improve atmospheric delay modeling, we need to look at the application of ray tracing and horizontal refractivity gradients on SLR data collected at the core SLR sites around the globe. We have found horizontal gradient delays of up to 5 cm at an elevation angle of 10° at certain times of year and SLR site locations. The effects of applying ray tracing results, including horizontal gradients to a set of global SLR geodetic data resulted in reduction of the observation residuals by up to 45% in variance, and 3 mm in RMS. This is a highly significant contribution for the SLR technique's effort to reach an accuracy at the 1-mm level this decade.

Introduction

All current models of atmospheric delay for SLR observations assume a spherically symmetric atmosphere, ignoring horizontal gradients in the refractive index of the atmosphere. In order to improve models of atmospheric delay, horizontal gradients in the atmospheric refractive index need to be understood and modeled on a global scale. Currently, ignoring horizontal gradients is the largest source of error in atmospheric delay models for SLR at low elevation angles. We have demonstrated that the contribution of horizontal gradients to the total atmospheric delay is primarily at the few-centimeter level at 10° elevation, and can be as large as 5 cm at certain locations (where SLR stations operate) and times of year. Although centimeter delay corrections seem small, horizontal gradients need to be taken into account because they can lead to significant errors in estimated vertical and to a lesser extent, horizontal station coordinates, which in turn affect the accuracy of the scale and origin of the International Terrestrial Reference Frame (ITRF) [*Altamimi et al.*, 2002].

Presently, we are attempting to develop the infrastructure and enabling science that will allow us to develop future ITRF's with an origin accurate to 1 mm at its epoch of definition and a stability of 0.1 mm/year or better, a tenfold improvement over our current capabilities that are no better than 0.4 parts per billion (~3 mm) in origin stability. Part of this effort requires the improvement of our atmospheric delay corrections to the SLR data with an accuracy of 1 mm or better. In the past, VLBI groups used NCEP fields to calculate refractivity gradients in order to make comparisons with results obtained from their VLBI geodetic data. However, we are entering a new era where global snapshots are available from satellite-borne instruments on a daily basis and at much higher spatial resolution than weather models. We will primarily be using atmospheric profiles from the AIRS instrument on NASA's AQUA Earth Observing System (EOS) platform in order to compute the atmospheric delay by ray tracing and including horizontal refractivity gradient contributions. We also use global data sets from ECMWF and NCEP to supplement, compare, and validate the AIRS results.

Methodology

The optical path length between the tracking station and satellite is defined as the integral of the group refractive index along the path of the ray. We define the atmospheric delay as the difference between the optical path length and the geometric path length:

$$d_{atm} = \int_{ray} n ds - \int_{vac} ds \tag{1}$$

where n is the group refractive index, and $ds = dr/sin\theta$ is a differential element of length along the path of the ray. The subscripts ray and vac in the integral indicate the actual ray path and vacuum path of the signal. If we express the group refractive index in terms of the group refractivity, N

$$n = 1 + 10^{-6} N \tag{2}$$

then the atmospheric delay can be expressed as:

$$d_{atm} = 10^{-6} \int_{ray} N ds + \left[\int_{ray} ds - \int_{vac} ds \right] \tag{3}$$

where the first term represents the excess path delay or velocity error, and the bracketed term is the delay due to the bending of the ray, called the geometric delay (d_{geo}).

By expanding the refractivity, N, in a Taylor's series expansion around the laser site [*Gardner*, 1977], the total atmospheric delay including gradients, can be written as:

$$d_{atm} = 10^{-6} \int_{r_s}^{r_a} \frac{N(r)}{sin\theta} dr + d_{geo} + \left[\int_{r_s}^{r_a} \frac{N_{ns}(r)\rho}{sin\theta} dr \right] cos\alpha + \left[\int_{r_s}^{r_a} \frac{N_{ew}(r)\rho}{sin\theta} dr \right] sin\alpha \tag{4}$$

where θ is the elevation angle at altitude calculated using Snell's law, $\rho = r\phi$ represents horizontal arc distance from the station, r_s is the geocentric radius of the station, and r_a is the geocentric radius at the top of the atmosphere. The third and fourth terms are the contribution to the total delay from horizontal gradients, where N_{ns} and N_{ew} are the North-South (NS) and East-West (EW) components of the horizontal refractivity gradient. The $cos\alpha$ and $sin\alpha$ terms project the NS and EW gradient components onto the azimuth of the observation.

Ray Tracing

The most accurate and comprehensive way of calculating the atmospheric delay is by using a technique known as ray tracing. The computation process is based on geometric optics theory applied over a series of thin spherical shells, concentric with the earth, within which a constant refractivity is assumed. Using Snell's law to calculate elevation changes and horizontal refractivity gradients to calculate azimuth changes along the ray's path, one can trace the ray accurately through the atmosphere in two or three dimensions and calculate the total delay by integrating the incremental delay at each atmospheric layer until the top of the atmosphere using equation (4).

Atmospheric delay modeling has been neglected for decades, with the official model for SLR being that of Marini and Murray [1973], developed in the early 70's. Only in recent years, has an improved ZD model [*Mendes and Pavlis*, 2004] and MF [*Mendes et al.*, 2002] been developed, applicable to the wavelengths used in present day SLR. The new ZD model and MF, called the Mendes-Pavlis (M-P) model, was adopted for the reanalysis of all SLR data from 1976 till present, and in the production of the weekly operational products, beginning January 1, 2007. However, these are still models and the assumption of uniform, spherically symmetric refractive index layers made in their development is unreasonable as it makes the delay only dependent on elevation and not on azimuth. We now have the capability to use atmospheric fields from AIRS that are available at near-real time, twice-daily (day and night), and on a global scale. This enables us to compute the total delay, including gradients, by ray tracing at any elevation and azimuth using real-time atmospheric conditions at any chosen SLR site on the globe. Although ray tracing can be computationally expensive and involves many steps, the results are more physically meaningful than those calculated from delay models, and with the computing facilities available today, the benefits far outweigh the costs. Furthermore, the process can be highly automated at a single, "clearinghouse" type location, with the results disseminated to the users via Internet services and the World Wide Web.

Horizontal Refractivity Gradients

Until now, the contribution from horizontal refractivity gradients to the total atmospheric delay has essentially been ignored in the analysis of SLR data. Previous studies of horizontal gradients (see, for example, *Gardner et al.*, 1978; *MacMillan*, 1995; *Chen and Herring*, 1997) were all based on developing models to account for the gradient delay. We have found these models to be unreasonable in estimating the delay for several reasons: The mapping function used by *Chen and Herring* [1997] ignores higher order terms in the expansion of the continued fraction used in calculating the mapping function, and the development is based on the fact that the gradients have the same direction at all levels in the atmosphere. The model developed by *MacMillan* [1995] includes an extra term, $cot(e)$, that accounts for larger gradient changes at low elevation angles, but the delay becomes infinite at small elevation angles as a result. The *Gardner* [1978] gradient model is dependent on surface gradient values of temperature and pressure, thereby ignoring gradient values at higher altitudes that could introduce significant errors in the magnitude and sign of the gradient delay.

We calculate the gradients in a more direct and accurate way by ray tracing using the third and fourth terms in equation (6) combined with atmospheric profiles from AIRS, ECMWF, and NCEP. Our initial results show that the largest gradient variations occur as a result of seasonal and diurnal changes. Stations situated in mountainous regions,

such as McDonald, TX and Monument Peak, CA had larger horizontal pressure gradients, while stations in close proximity to large bodies of water such as Yarragadee, Australia, had larger horizontal temperature gradients. No significant non-hydrostatic (wet) gradients were found, with maximum wet delays only reaching a few tenths of a millimeter during the summer at Greenbelt, MD. Maximum NS gradient delays of up to 5 cm were found at Yarragadee and Herstmonceux, UK, at an elevation angle of 10°, while standard deviations ranged from 6-12 mm depending on location and time of year. The EW gradients were smaller in magnitude and variability than the NS gradients.

Results

We now look at the impact of using ray tracing with AIRS, ECMWF and NCEP data on the analysis of a set of real SLR data for the geodetic satellite LAGEOS 1 during 2004 and 2005 and for 10 of the globally distributed core SLR stations. We analyze our results by looking at the RMS and variance percent difference between the 'corrected' SLR residuals with the atmospheric delay estimated by ray tracing and including horizontal gradients, and the 'original' residuals, that use the M-P model for calculating the atmospheric delay. The total number of observations used in the statistics for all stations is 47664. Positive values of RMS and variance indicate improvement in the results.

The results when including the gradients in Figure 1 (i.e. delay = model + gradients) show that the residual variances when using AIRS data are reduced by up to 10-15% in variance when only gradient corrections are applied. ECMWF and NCEP results also show improvement with residual reductions ranging from 5-10%. AIRS ray tracing results had a greater improvement in RMS and variance when compared to

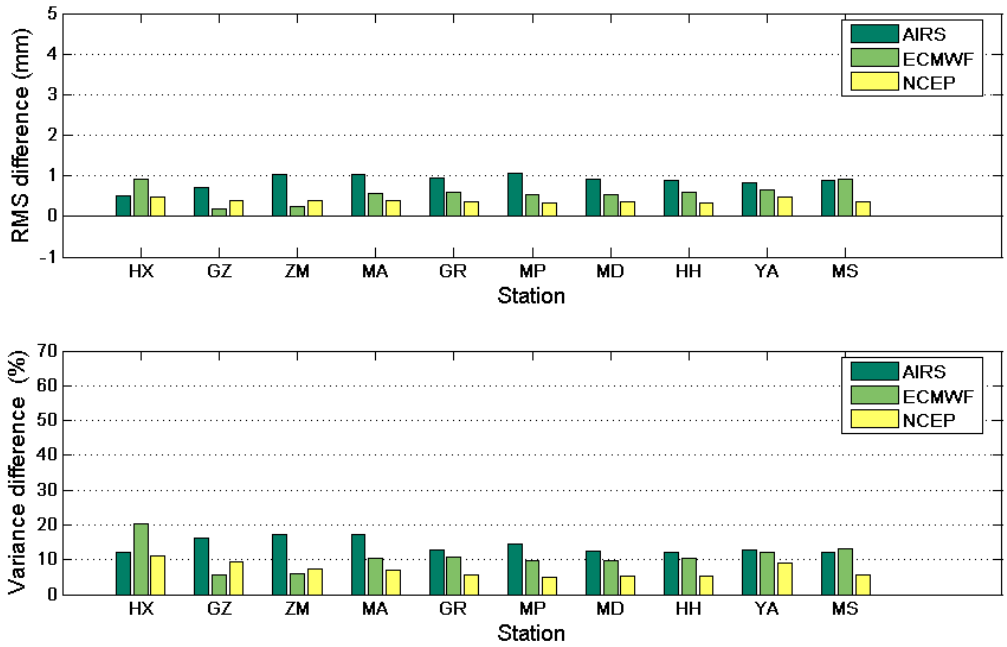

***Figure 1**. RMS (top) and variance (bottom) differences between the original residuals (model) and the gradient-corrected residuals (model + gradients) for stations: HX (Herstmonceux, UK), GZ (Graz, Austria), ZM (Zimmerwald, Switzerland), MA (Matera, Italy), GR (Greenbelt, MD), MP (Monument Peak, CA), MD (McDonald, TX), HH (Hartebeesthoek, South Africa), YA (Yarragadee, Australia), and MS (Mt. Stromlo, Australia).*

NCEP and ECMWF results for all stations. This can probably be attributed to the higher resolution of the AIRS data, providing the ability to calculate the gradients on a much finer scale.

When the total correction is applied (i.e. delay = ray tracing + gradients) with no dependence on the model, the NCEP results actually show larger improvements than AIRS and ECMWF (Figure 2). However, it is interesting to note that there are instances where we see negative RMS differences for NCEP at Herstmonceux, Graz and Greenbelt, even though the corresponding variances show improvement. This is most likely due to either a large positive or negative bias in the mean of the corrected residuals. There is an overall greater improvement in the results when the total correction is applied, and this can be seen as an increase in variance percent difference from Figure 1 to Figure 2. However, at Yarragadee and Mt Stromlo, AIRS total correction actually does slightly worse than the gradient correction. AIRS variances decrease from 12.8% for the gradient correction, to 12.4% for the total correction at Yarragadee and from 12.3% to 9.8% at Mt Stromlo. High AIRS variabilities in boundary layer pressure and temperatures on the interface between land and ocean at these stations could be a factor in this case.

Summary and future plans

Our current and near-term plans are to improve and generalize our 3-d ray tracing process and to include as many sources as presently available. In a second step, we plan to establish an automated daily service for all SLR-tracked targets with high-accuracy requirements (i.e. those used for the ITRF, sea-level monitoring, etc.), and provide the community with value-added data sets including these improved atmospheric delay corrections.

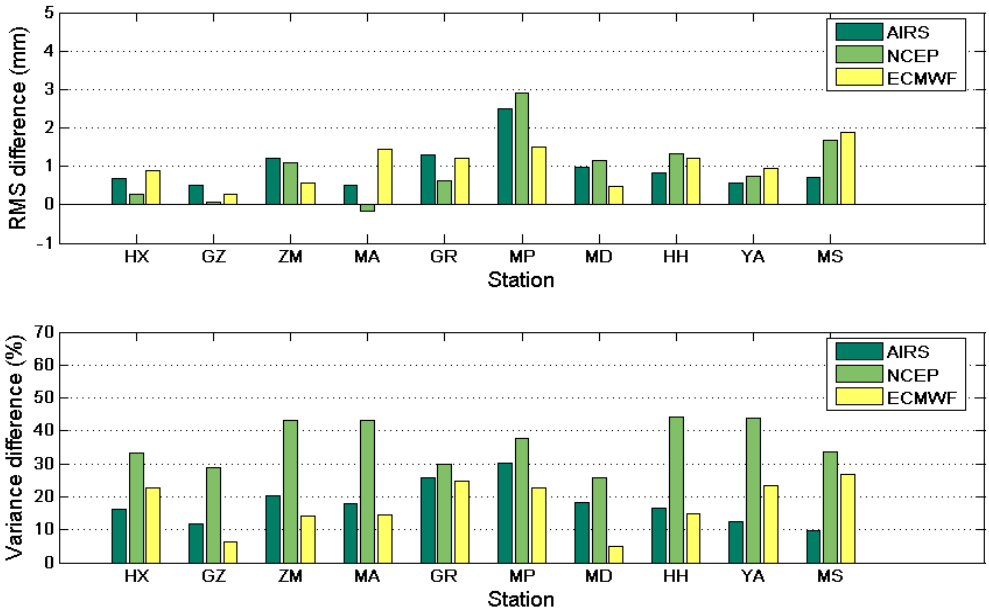

Figure 2. *Differences between the original residuals (model) and the total-corrected residuals (ray-tracing + gradients).*

References

[1] Altamimi, Z., P. Sillard, and Claude Boucher (2002), ITRF2000: A new release of the International Terrestrial Frame for earth science applications, *J. Geophys. Res.*, *107*, NO. B10, 2214, doi:10.1029/2001JB000561

[2] Chen, G.E. and T.A. Herring (1997), Effects of atmospheric azimuthal asymmetry on the analysis of space geodetic data, *J. Geophys. Res.*, *102*, pp. 20,489-20,502.

[3] Gardner, C.S. (1977), Correction of laser tracking data for the effects of horizontal refractivity gradients, *Appl. Opt.*, *16*, *No. 9*, pp. 2427-2432

[4] Gardner, C.S., J.R. Rowlett, and B.E. Hendrickson (1978), Ray tracing evaluation of a technique for correcting the refraction errors in satellite tracking data, *Appl. Opt.*, *17*, *No. 19*, pp. 3143-3145

[5] MacMillan, D.S. (1995), Atmospheric gradients from very long baseline interferometry observations, *Geophys. Res. Lett.*, *22*, pp. 1041-1044.

[6] Marini, J.W., and C.W. Murray (1973), Correction of laser range tracking data for atmospheric refraction at elevations above 10 degrees, *NASA Rep. X-591-73-351*, Goddard Space Flight Cent., Greenbelt, MD

[7] Mendes, V.B., G. Prates, E.C. Pavlis, D.E. Pavlis, and R.B. Langley (2002), Improved Mapping Functions for Atmospheric Refraction Correction in SLR, *Geophys. Res. Lett.*, *29*(10), 1414, doi:10.1029/2001GL014394.

[8] Mendes, V.B., and E. C. Pavlis (2004), High-Accuracy Zenith Delay Prediction at Optical Wavelengths, *Geophys. Res. Lett.*, *31*, L14602, doi:10.1029/2004GL020308.

[9] Pearlman M., and Coauthors (2005), Global geodetic observing system - Considerations for the Geodetic network infrastructure, 2005 IAG/IAPSO/IABO Joint Assembly, Cairns, Australia, August 22-26

Two-Color Calibration of The Zimmerwald SLR System

W. Gurtner, E. Pop, J. Utzinger

1. Astronomical Institute, University of Bern.

Contact: gurtner@aiub.unibe.ch

Abstract

The current and the preceding Zimmerwald SLR systems have used internal, near-realtime calibration with apparently good success. The addition of the second wavelength (infrared) to our system revealed, after some time of routine operation, differences between the calibrated ranges of the two colors that could not be explained with errors in the applied refraction models. It turned out that the internal calibration values of the infrared chain showed variations that had not much to do with system calibration. The source of these variations could not be identified. In June 2006 we switched to external calibration by necessity.

Introduction

The 1-meter Zimmerwald satellite laser ranging system, installed in 1997, has been designed for two-color ranging right from the beginning. In order to have two wavelengths with suitable sensors and reasonable reception signal power at our disposal we chose a Titanium-Sapphire laser with the primary wavelength at 846 nm (near infrared) and the second harmonic at 423 nm (blue).

As receivers we are currently using a compensated SPAD at 423 nm and a Hamamatsu H7422P-50 photomultiplier at 846 nm. The time walk of the latter is compensated using an empirical correction table in function of the measured return pulse energy.

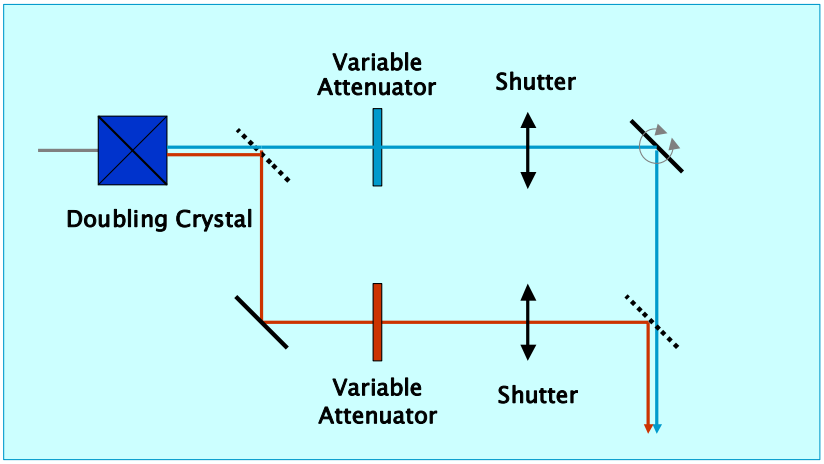

Figure 1: *Transmit path: Individual attenuation*

Single-shot precision is of the order of 60 ps in blue and 150 ps in infrared.
The optical paths to and from the telescope have been optimized for transmission for the two wavelengths. The two beams can be individually attenuated, both in the transmit as well as in the receiving path.

At the International Laser Ranging Workshop 2002 in Washington we reported (Gurtner, 2002) first results of dual-wavelength operation. We concluded;

- *The average difference between infrared and blue residuals per pulse is between 0 and 0.05 ns after a Marini-Murray refraction correction using onsite surface met values.*
- *Apart from the above mentioned tendency we could not yet detect any systematic behavior of the differences so far.*
- *The differential Marini-Murray refraction corrections between 423 and 846 nm seem to be better than < 10 mm.*
- *However, there could still be range biases between the two reception channels of the same order of magnitude.*

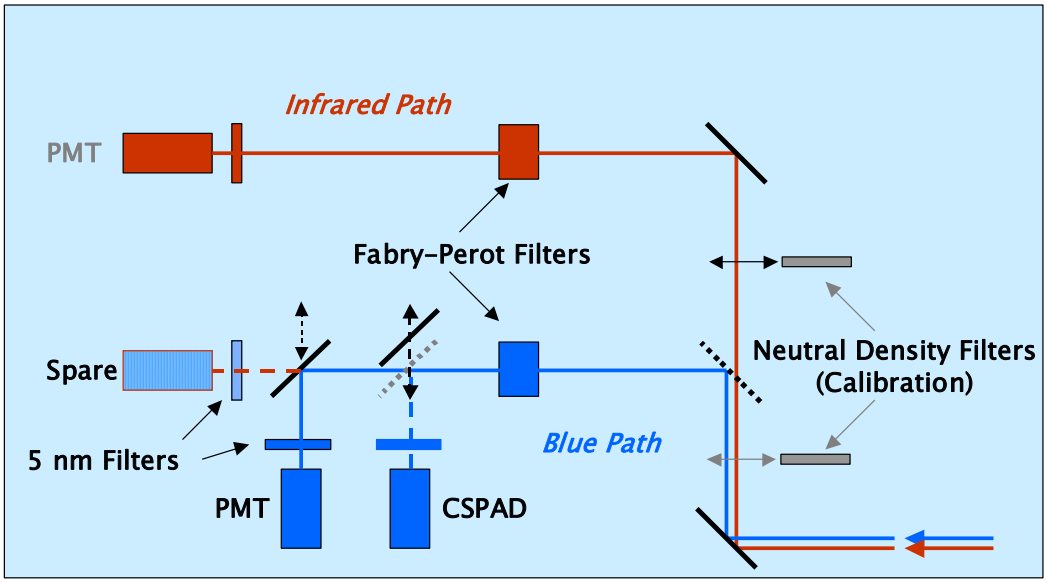

Figure 2: *Receiving path: Separation of the two colors*

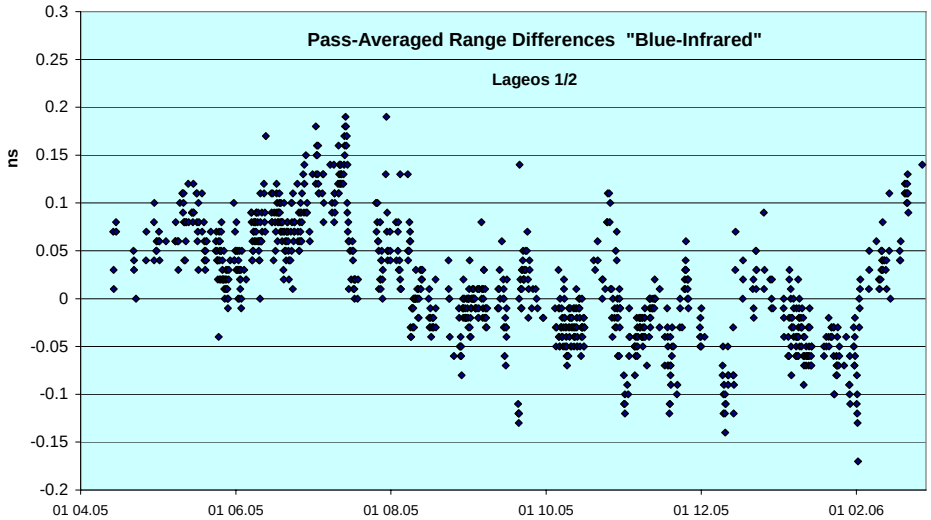

Figure 3: *On-site-determined differences blue-infrared*

Slowly Varying Systematic Differences

In the meantime, however, the refraction-corrected pass-average differences between the two colors showed slowly varying systematic effects that have nothing to do with remaining errors in the applied refraction corrections. These variations could be seen

in on-site generated differences (Figure 3) as well as in the pass-averaged residuals of global analyses performed by ILRS analysis centers (Figure 4). These variations were as large as plus and minus 2 cm!

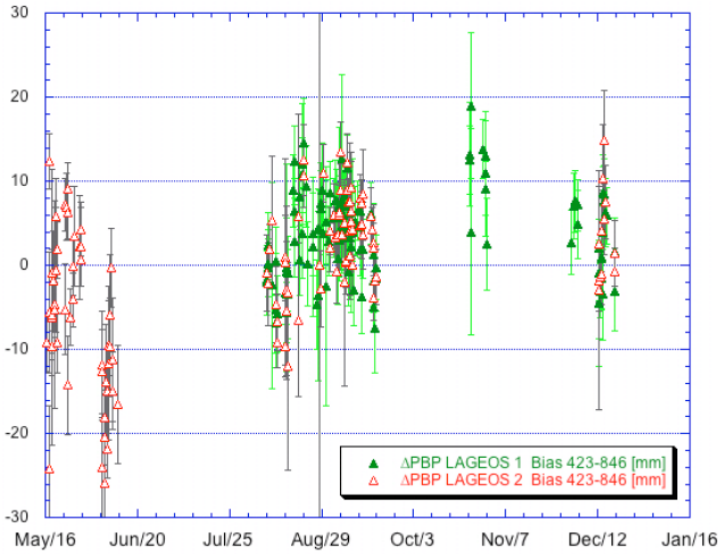

Figure 4: *Pass-averaged biases between blue and infrared (JCET analysis center, 2004)*

A closer investigation showed that these inter-color bias variations highly correlated with the calibration values used to correct the infrared ranges to the satellites (Fig. 5).

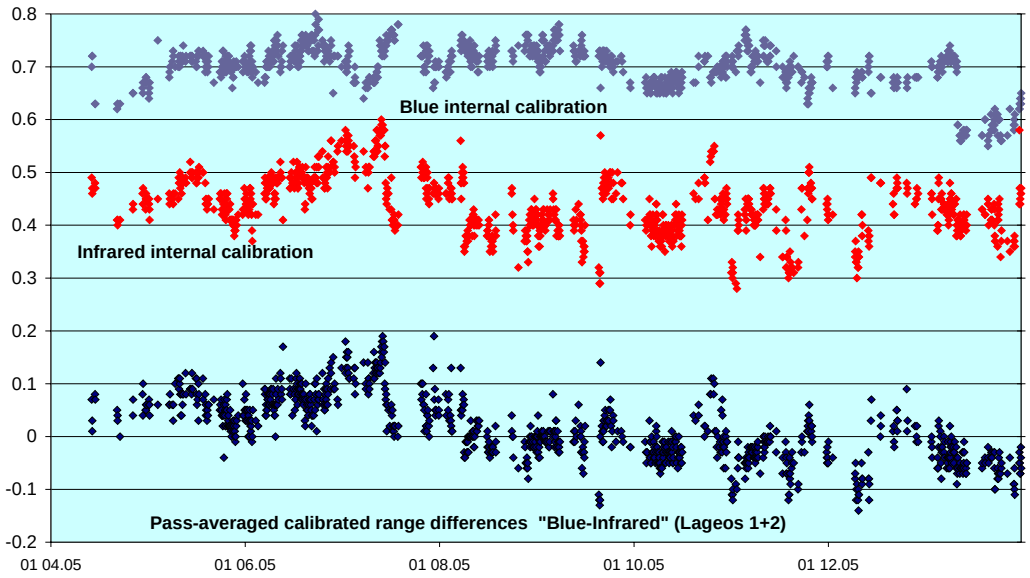

Figure 5 : *Time series of internal calibration values and inter-color biases*

It can be clearly seen that the time series of the infrared calibration values (middle series, covering about 10 months from April 2005 to February 2006) shows the same features as the pass-averaged calibrated range differences between blue and infrared.

The standard calibration procedure used so-called internal calibrations: During the satellite passes, interleaved with the ranging to the satellites, flight time measurements of a weak calibration beam extracted from the main laser pulse and sent through an internal path of known length are performed to keep track of small changes in the

system behavior (e.g. temperature changes) leading to errors in the measured satellite ranges.

The differences between the calibrated ranges (corrected for tropospheric refraction) to the satellites in the two colors should then only contain biases from residual errors in the tropospheric corrections and the applied calibration values, and various random errors from the measurement procedures. The fact that we see slowly varying inter-color biases correlated with the infrared calibration lets us assume that there is a problem with the respective calibration procedure.

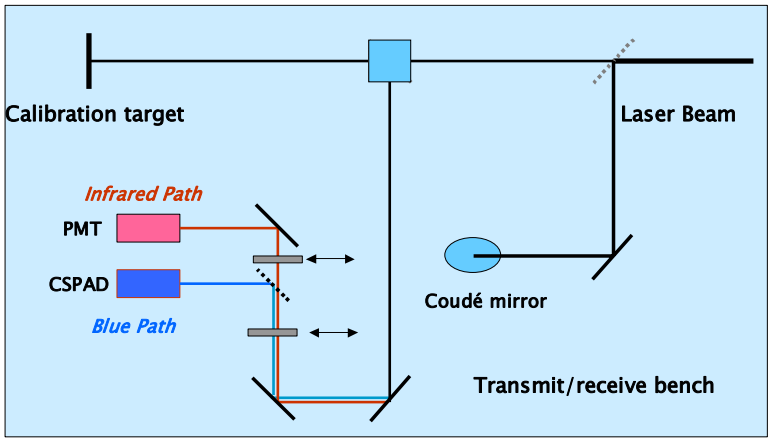

Figure 6: *Internal Calibration*

Occasionally we also perform calibration observations to an external target at about 600 m distance. Figure 7 shows time series of separate internal and external calibration sessions for infrared over the same 10 months and again the pass-averaged differences of calibrated blue-infrared satellite ranges. It is obvious that the external calibrations do not show the same variations.

A possible reason for the problem with the internal calibration (in infrared) could be the behavior of the respective Stanford counter at the very short time of flight (a few tens of nanoseconds). However, a comparison between the two counters used in the two receiver chains (blue and infrared) and the newly purchased A032ET event timers

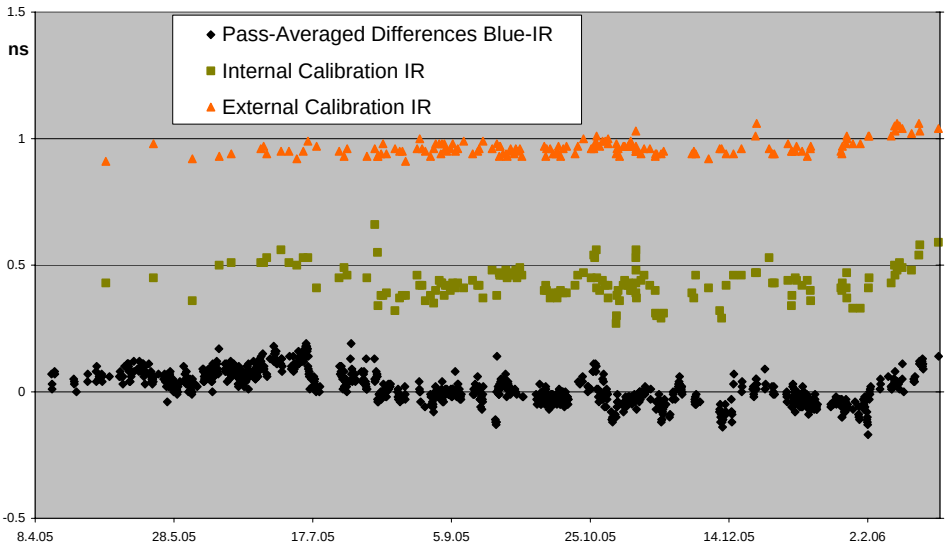

Figure 7: *Internal/external calibration, inter-color biases*

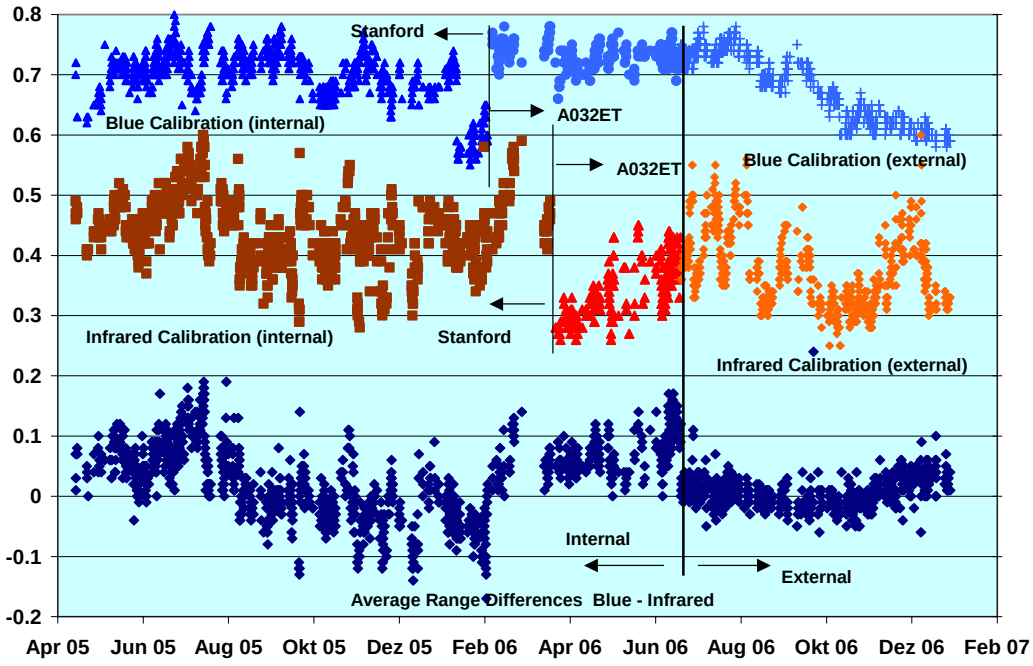

Figure 8: *Calibrations, inter-range biases*

did not reveal anything suspicious. The later replacement of the Stanford counters by the event timers in spring 2006 did not solve the problem either.

Consequently we decided to replace the internal calibration procedure by calibrations to the external target. We modified the observation procedures accordingly: The scheduler inserts now approximately every half hour a short calibration session into the satellite passes.

Figure 8 shows now the behavior of the inter-color biases before and after the modification of the calibration procedures on June 21, 2006. The variations (bottom time series in the Figure) became significantly smaller. There still seems to be a small signature in the time series. We will have to closely monitor these differences and hopefully be able to later correlate these variations with some system parameters.

References

[1] Gurtner, W., E. Pop, J. Utzinger, “Zimmerwald Dual-Wavelength Observations: First Experiences”, 13th International Workshop on Laser Ranging, Washington D.C, October 7-11, 2002

Multi Color Satellite Laser Ranging At Czech Technical University

Karel Hamal[1], Ivan Prochazka[1], Josef Blazej[1],Yang Fumin[2], Hu Jingfu[2], Zhang Zhongping[2], Hiroo Kunimori[3], Ben Greene[4], Georg Kirchner[5], Franz Koidl[5], Stephan Riepfel[6], Werner Gurtner[7]

1. Czech Technical University in Prague, Brehova 7, 115 19 Prague 1, Czech Republic
2. Shanghai Observatory, People Republic of China,
3. CRL, Japan,
4. EOS, Australia,
5. Graz Observatory, Austria
6. Wettzell Observatory, Germany
7. Zimmerwald Observatory, Switzerland

Abstract

We are reporting on our activity on Satellite Laser Ranging (SLR) using multiple wavelengths. The reasons for simultaneous multi-frequency laser ranging of artificial Earth satellites are discussed. Atmospheric dispersion study and the eye-safe wavelength region are both considered. To detect the returned signal, the Single Photon Avalanche Detector (SPAD) is operated in so-called Geiger mode. The silicon, germanium, and gallium arsenide phosphide based SPAD are used depending on wavelength to cover nearly the entire optical region having the single photon response, temporal resolution better than 120ps FWHM, and quantum efficiency of about 15%. The active area size and the compact design of the detector packages permitted their application in satellite laser ranging yielding sub-centimeter ranging precision in infrared and sub-millimeter precision ranging in the visible region. The active area of the detector used is from 100 to 200 µm. Detectors for the visible region are cooled thermo-electrically and detectors for infrared, based on germanium, are cooled cryogenically with a custom design liquid nitrogen Dewar. The design and diagnostics of a hydrogen Raman-shifted picosecond Nd:YAG laser operated at 10 Hz repetition rate are presented. Both the far-field beam structure and temporal picosecond pulse profile are monitored for different laser configurations. The optimum laser configuration has been implemented to the SLR station in Shanghai for two color ranging. To operate the SLR station in Graz in visible range, three color ranging is accomplished by Nd:YAG SHG 532 nm, the first Stokes Raman at 682 nm and the first anti Stokes at 432 nm using Hydrogen. To operate the eye safe SLR in Tokyo at the 1540 nm wavelength, the laser was operating at 1064 nm to pump the first Stokes at 1540 nm using methane. To operate the SLR in Bern and Wettzell (move to Chile) Titanium-Sapphire based laser has been operating at 852 nm and SHG 426 nm. The color set has been established at the Shanghai observatory since 2004. The ranging has been successfully accomplished for retro-reflector equipped satellites up to a distance 30000 km with one centimeter precision. The results of direct measurements of atmosphere dispersion are presented and compared existing atmosphere models.

Introduction

We have the experience in field of SLR since the seventies of last century. To range satellites or Moon one has to consider several “contributors” to the overall accuracy of the SLR measurement chain: the station itself, satellite retroreflector array, and the atmosphere as well. Current SLR technology aims toward millimeter accuracy. From the point of view of the SLR station, rms of the laser pulse duration, Start and Stop detectors rms and the Event Timer jitter are involved. Related to the atmospheric dispersion, the existing models are not yet explaining the contribution at millimeter

accuracy level. The SLR at different wavelengths might help to understand the atmospheric mapping function down to millimeter and consequently sub-millimeter level. In fact, multi-color SLR is a unique method for overall optical path dispersion model direct verification.

Experiment arrangement

Assuming the atmospheric dispersion, to find the right laser for multiple wavelength millimeter SLR, one can consider the Nd:YAG / SHG / THG, Nd:YAG / SHG / Raman First Stokes / First antiStokes in hydrogen, Nd:YAG / SHG / Raman First Stokes in methane and the Titanium Sapphire Fundamental / SHG, all of them at different repetition rates. The basic of Raman conversion is described by eq. 1.

$$\frac{1}{\lambda_{shifted}} = \frac{1}{\lambda_{pump}} + k \cdot \nu_R \text{, where } k \in \left(-\infty, -1\right\rangle \cup \left\langle 1, \infty\right) \quad (1)$$

Where λ is symbol for the wavelength and ν is material constant describing Raman shift for the selected gas. For hydrogen it is 4155 cm^{-1}, for methane 2914 cm^{-1}, and for deuterium 2987 cm^{-1}.

The selection of the laser transmitter concept is influenced by the required reliability in the routine field operation. Considering that the 6 picoseconds round trip time corresponds to one millimeter range, therefore to reach the millimeter goal, the acceptable laser pulse width within the range of 10 to 50 picoseconds is desirable. The experiment energy budget requires the energy in one pulse in order of several tens of millijoules. The selection of the right wavelength pair is determined by the atmospheric dispersion mentioned above, by atmosphere transparency, and by the availability of high effective frequency shifters. In principle it is difficult to use to independent lasers due to the required picosecond synchronization.

The available detectors have to be considered. Our laboratory has long term experience in the field of picosecond temporal resolution solid state detectors[1]. For the visible range we did examine mainly silicon based SPADs, for the eyesafe SLR Germanium based SPADs. The silicon one can be operated at thermoelectrically cooling temperature. The germanium based cooled detector is suitable for eyesafe wavelengths; however it has to be cooled by liquid nitrogen. Using the Quantel YG580 Laser 30 mJ / 1.06 μm, 35 ps, different Raman tubes filled by Hydrogen at different pressure, different focusing lens, we were getting 8 mJ / 0.68 μm, 1 mJ / 0.45 μm. Considering the eyesafe SLR using Raman shift in methane from fundamental we were getting 3 mJ / 1.54 μm.

Conclusion

We are presenting a review of our activities on multiple color SLR and recent results from Shanghai SLR observatory[2]. The selection of the right wavelength pair is discussed and together with our experience with available and effective frequency shifters selection and tuning. The multiple color laser transmitter based on Nd:YAG picosecond laser generating the second harmonic frequency and the Raman Stokes and anti Stokes frequencies is dedicated for the new Shanghai SLR station, the part of Western Pacific Laser Ranging Network.

References

[1] Procházka, I., Hamal, K., Sopko, B.: ”Recent Achievements in Single Photon Detectors and Their Applications”, Journal of Modern Optics. 2004, vol. 51, no. 9-10, pp. 1298-1313. ISSN 0950-0340.

[2] Hu, Jingfu, Yang, Fumin, Zhang, Zhongping, Hamal, K., Prochazka, I., Blazej, J.: ”A Raman laser system for multi-wavelength satellite laser ranging”, Science in China Series G: Physics and Astronomy. 2004, vol. 47, no. 6, pp. 737-743. ISSN 1672-1799

TELESCOPES, STATIONS AND UPGRADES SESSION SUMMARY

Chair: Craig Smith

The session on telescopes, systems and upgrades demonstrated that the field of satellite laser ranging (SLR) is healthy and growing. Speakers during the session described a wide range of new and refurbished SLR instruments all over the globe.

Probably the most ambitious project described came from the Russian Federation where 6 new SLR systems have recently been completed and there are plans to build up to a further 15 stations by 2010, all in support the upgraded Glonass Global Navigation System (GNS).

Not to be outdone, we heard from NASA and US Contractors about a revitalized SLR program that has returned a number of stations to operations (TLRS3 and 4) as well as maintenance and development of the MOBLAS network. SLR 2000 development has also been continued.

Not to be outdone by Russia or the US, China too has entered a new era of significant SLR development as contributions to the Galileo GNS has spurred on rapid SLR activity in this country too. Excellent presentations were provided about a new SLR station built in San Juan, Argentina, as well as significant upgrades to existing stations at Yunnan, Changchun and Shanghai SLR Observatories.

SLR work however, is a global enterprise and from France we heard that after 30 years of operations the old SLR station (7835) at Grasse has been decommissioned. This station has been replaced by new and more capable systems FLTRS and MEO, whilst the old telescope will find new life as an SLR telescope in Matjiesfontein, South Africa. Plans were also presented for new SLR network in South Korea.

We look forward to hearing about the progress of all these ambitious projects and exciting developments at the next ILRS workshop.

Grasse laser stations in evolutions to future and technological developments

F. Pierron[1], E. Samain[1], JM Torre[1], M. Pierron[1], M. Furia[1] and the Grasse laser staff

1. Observatoire de la Côte d'Azur, GEMINI/UMR 6203-CNRS, Av N. Copernic, 06130 Grasse, France.

Abstract

A very important project in term of buildings and technology for telescopes, mount and dome has been started at the Grasse Observatory since September 2005.

A new laboratory has been built in place of historical SLR fixed station (7835) to receive mobile SLR system (FTLRS) for upgrade, development and operations between field missions.

The current LLR station (7845), renamed MeO (for Metrology and Optics), is being completely rebuilt to track and range in the future from "Low Earth orbiting satellites" to the Moon and even further to support new missions in the solar system. The project status will be reported in this presentation with both technological issues and new potentialities for such installations at Grasse.

Introduction and short report 1980-2005 period

The Grasse LLR system with a large and accurate 1.5 meter telescope got first moon returns in 1982.

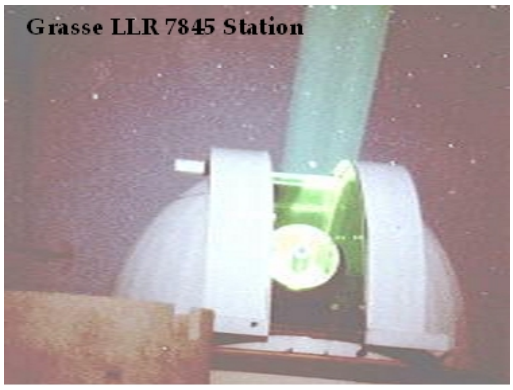

In this configuration (0.2 Hertz ruby laser with 3 nanoseconds pulses), 1166 normal points have been acquired in 5 years with an RMS of about 20 centimeters.

In 1987 a major upgrade was achieved on this system with a new Yag laser (10 hertz-300 ps pulses) and timing system (Dassault event timer).

During this very operational period, about 8500 npts (65% of the global network) were acquired with an rms of 3 cm and a stability at some millimeters level.

The station stopped in summer 2005 for new developments described below in this paper.

This very efficient SLR system installed at Grasse observatory in 1975 at 30 meter from the LLR system tracked in thirty years about 35000 satellites passes.

The quality and quantity of data over the years of this core station is very impressive and scientific community can thanks a lot observers, engineers and scientists involved in this process very consuming in term of manpower.

The station stopped definitively his activity in summer 2005 to involve laser staff in new evolution for SLR/LLR activity.

Historical SLR station definitively stopped, waiting South Africa collaboration

In September 2005, telescope and mount were dismantled and temporarily installed in the old trailer waiting new future abroad.

In fact for some years, South African colleagues are promoting an LLR/SLR development for this country in collaboration with global scientific community.

OCA/CNES/GRGS proposed to participate to this venture in putting this one meter telescope at South African geodesists disposal. Of course the mount and mechanical devices of this system will have to be refurbished (encoders, drive motors, coude mirrors etc.) and a budget is already planned by this partner for renewing this telescope/mount at HartRAO.

In the context of this interesting project in South Hemisphere a new site has been found in a very favorable place for SLR/LLR activity in term of meteorological conditions. We can see here on the next photo, this future site for Space Geodesy Observatory near Matjiesfontein at about 250 km north of Cape Town and 70 km south of GFZ Geodynamics Observatory and South African Astronomical Observatory.

After some administrative agreements in progress, OCA 1 meter telescope/mount should be shipped to South Africa before summer 2007.

Future site for Space Geodesy Observatory in South Africa

1 meter Telescope/mount in trailer at OCA in 2006

New laboratory for FTLRS developments and operations built in place of old telescope :

Just in the place of old one meter telescope, we built a new laboratory perfectly suited to host mobile system between fields campaigns.

The configuration of the setup has very original features.

The group laser /mount /telescope is installed on a platform elevator with two possible positions:

-One down in the laboratory to achieve technological developments tuning and maintenance in good conditions (left picture).

-The other one 1.40m higher (right picture) with the roof open and the telescope able to view the sky and to achieve operations on satellites in normal conditions with operator control facilities inside the building.

The reference point of the station in high position has been designed to be very stable and repetitive at better that one millimeter level. In this observation place, the station is no more supported by but lie on a metallic square embedded in the roof concrete, such a way the platform can be down in this phase**.**

For the campaigns setup the group laser/mount/ telescope is took off from the special support fixed on the elevator in the laboratory and installed in the tripod which can be easily packed for shipping and deployed on site to the concrete pad.

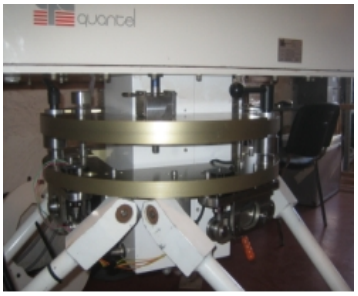

New devices (electric jacks software controlled) to easily adjust leveling in automatic mode have been developed. This new facility is very important to assist local observers with remote control capability during outside campaign.

Ftlrs in campaign configuration – Ajaccio 2005

LLR Station renamed to MEO and completely rebuilt

In summer 2005 we stopped temporarily the old LLR station in order to modernize and to imply it in more goals (science programs and technology).

This important project in term of funding and manpower implied for design and buildings had been prepared for three years with detailed technical studies and looking in the future for emerging new projects on next 20 years.

The main idea is to have flexibility in different configurations :

- **A new generation of Laser Ranging station**
  – From 400 km to the Moon
  – One Way Interplanetary mission
  – Highly Automatic
- **Research & Development facility**
  – New optical links
  – Time transfer experiments
  – One Way Interplanetary missions
  - Detection, Event Timer

A. Telescope/mount

In the future, the mount will be able to have a speed compatible with SLR on lower satellites and this is a very strong constraint on such an heavy system.

We decided to install in this new design powerful and precise direct torque motors on the axes in such a way to have speed multiplied by an important factor .

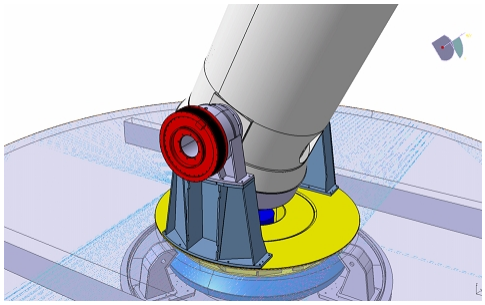

Nevertheless, the pointing accuracy remains an important challenge especially to range moon and future spacecrafts in solar systems.

The quality of the encoders installed on the axes and the mechanical stability of the whole setup are been carefully designed and should lead to an absolute pointing accuracy below 1 arc second.

B. Dome

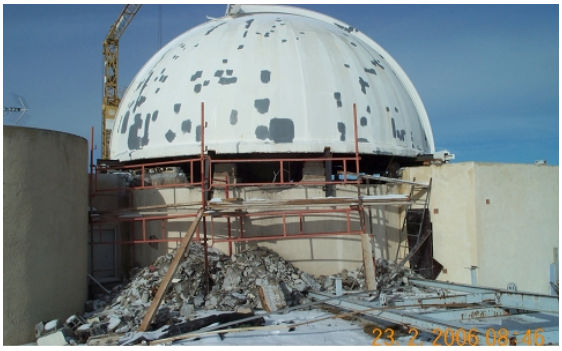

Similar constraints are applied on the dome and in order to remain compatible with mount speediness a lot of modifications are today achieved.

This dome is twenty five years old today and at this occasion the Observatory workshops undertook heavy maintenance works on metallic structures to hope reliable operations in future.

C. Laser and focal laboratories

To track both moon and HEO satellites, two lasers systems in different rooms were operated the past years (Quantel with 300ps and BMI with 20 ps).

A very important work and new design have been achieved to combine both lasers on a single bench with three capabilities

- 800 mJ in 10ns at 10 Hz
- 250 mJ in 300ps at 10 Hz
-250 mJ in 14 x 20ps at 10 Hz

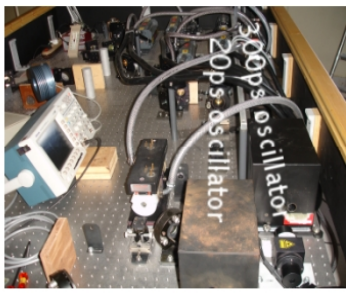

The last configuration with 14 pulses of 20 ps is a very original design to range the moon very accurately comparable with current SLR systems and achieving a return rate similar to previous configuration (single pulse of 300 ps).

In future, at least **3 focal laboratories** will be installed under the telescope to have different R&D experiments and routine operations accessible with a fast and easy mirror switch on the coude.

Conclusion

- **SLR fixed station (7835) stopped in june 2005**
  - 30 years of fruitful operations
  - Telescope and mount moved in the trailer waiting eventual collaboration abroad

- **New laboratory build in this place for FTLRS**
  - Two position capability with elevator system and opening roof
    - Technology developments
    - Operation on satellites to Lageos.

- **Old LLR Station renamed to MEO and completely refurbished.**
  - Earth satellite capability 800 to 36000 km Moon reflectors.
  - R&D studies and new experiments (Time transfer, transponder…).

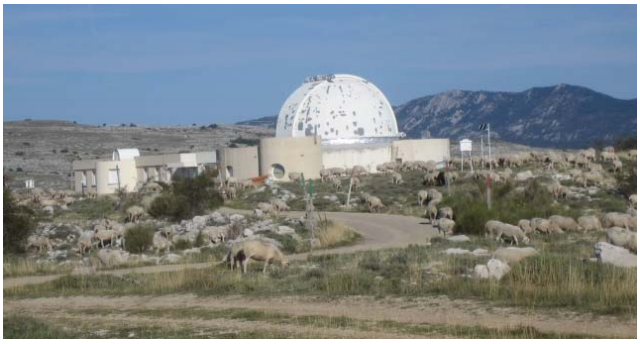

- **New SLR facilities in 12/18 months**
  - Two observing systems (0,13 and 1,50 m telescopes) occasionally collocated.
  - Fields campaign for FTLRS (maximum 6 months/year).

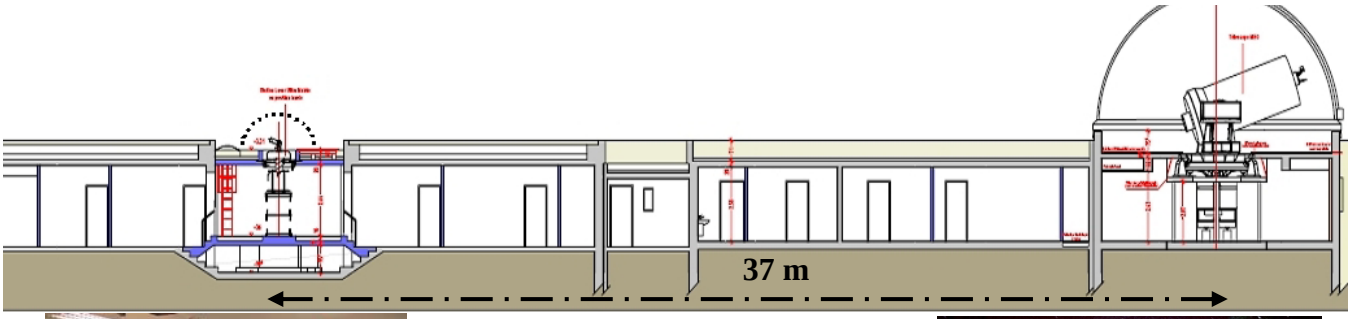

New Russian Systems for SLR, Angular Measurements, and Photometry

V.B. Burmistrov, N.N. Parkhomenko, V.D. Shargorodsky, V.P. Vasiliev

1. Institute for Precision Instrument Engineering, Moscow, Russia.

Contact: www.niipp-moskva.ru

Abstract

A brief description is presented of two novel-type stations providing satellite laser ranging, angular measurements, and photometry (in reflected sunlight), recently developed in the Institute for Precision Instruments Engineering (IPIE). Putting the stations in operation will expand the Russian Laser Tracking Network to six stations.

Compact station

The compact station with two 25-cm diameter optical systems (the first one used for transmission/reception of laser ranging signals, and the second one for angular measurements and photometry) has the following design features:

- The weight of any single unit of the system (in package) does not exceed 50kg, with system total weight less than 300kg. Thus, no special lifting mechanisms are needed for installation.
- An autonomous cover for the optical unit and mount allows installation on a small pier, without erection of a special fixed tower.
- Low power consumption (≤2.5 kW) allows supply from single-phase mains or from a portable power generator.
- Low cost in serial production (about 750K USD) and simple technology provides manufacturing by existing industrial firms.

Compact Laser/Optical Station Parameters

SLR of spacecraft with retroreflectors

- Spacecraft orbit height range: 400 to 40000 km
- Daytime and nighttime measurements for spacecraft with orbit heights 400 to 6000 km
- NP RMS errors 0.5 to 2 cm (averaging interval 60 s)
- Residual (systematic error) 0.5 to 2 cm
- Elevation range 20 to 85 deg.

Angular measurements

- Visual star magnitude: ≤ 12^m
- RMS error for spacecraft angular velocity up to 40 arcsec: ≤ 2’’

Photometry

- Visual star magnitude: ≤ 10^m
- Brightness determination error: ≤ 0.2^m

The option for mounting on a fixed position has a weight of 170 kg (optics + mount). No lifting mechanisms are needed for installation. The station has been tested near the 6-

meter telescope of Russian Academy of Sciences (in Northern Caucasus) during 2005. Currently, serial manufacturing is organized of the compact station for the Russian Laser Tracking Network. It is planned to produce 15 stations more until 2010.

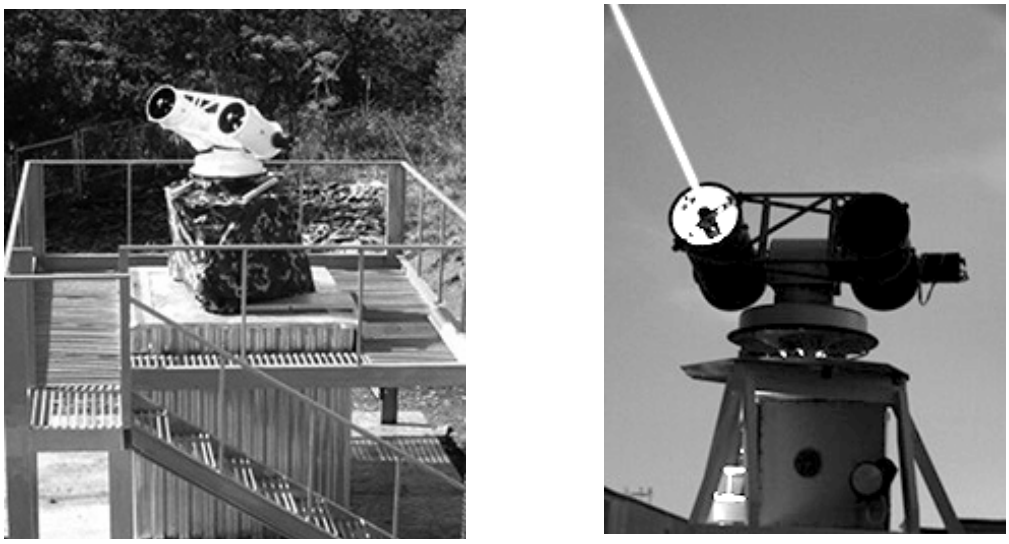

Figure 1: *Compact SLR station in operation*

Mobile Station

The mobile station is placed into 3 containers installed on wheels for transportation. The weight of optics and mount units is 12 tons. Except this unit, the system comprises an equipment container with operator's workplace, as well as a "house" for operator's rest. The mobile station acceptance tests have been completed on the Russian cosmodrome "Baikonur" in Kazachstan.

Pointing/tracking system and mount of the compact station

Mount parameters

- Mount type: Az-El, with two flanges for equipment mounting
- Digitally controlled torque motor drive
- Equipment weight on each mount flange:≤ 20 kg
- The mount is provided with an autonomous cover
- Angular rotation range:
  - Elevation: 5 to 95 deg
  - Azimuth: -278 to +278 deg
- Maximum angular speed 30deg/s;
- maximum angular acceleration 30deg/s^2

Mobile laser/optical station parameters

SLR of spacecraft with retroreflectors

- Spacecraft orbit height range: 400 to 40000 km

- Daytime and nighttime measurements for spacecraft with orbit heights 400 to 6000 km
- NP RMS errors 0.5 to 2 cm (averaging interval 10 s)
- Residual (systematic error) 0.5 to 2 cm
- Elevation range 20 to 85 deg

Angular measurements

- Visual star magnitude:≤ 14^{m}
- RMS error for spacecraft angular velocity up to 40 arcsec:≤2”

Photometry

- Visual star magnitude:≤ 12^{m}
- Brightness determination error: ≤ 0.2^{m}

The mobile station with a 60 cm diameter receive telescope and two separate optical systems for laser beam collimation and TV camera, has the following basic parameters.

Station of both types have similar laser ranging system with the following parameters:

Operation wavelength..... 0.532 μm
Pulse repetition rate..... 300 Hz
Laser pulse duration ..... 250 ps
Laser pulse energy..... 2.5 mJ
Output beam divergence ..... 5 arcsec
Receive telescope diameter
– compact station ..... 25 cm
– mobile station ..... 60 cm
Timing accuracy (measurement position on time scale) ..... 200 ns

Figure 2*: Operation site with installed equipment (containers and telescope)*

***Figure 3**: Mobile station preparation for operation*

***Figure 4:** Mobile station during transportation*

***Figure 5**: Mobile station in operation*

***Figure 6**: Mobile station operator workspace*

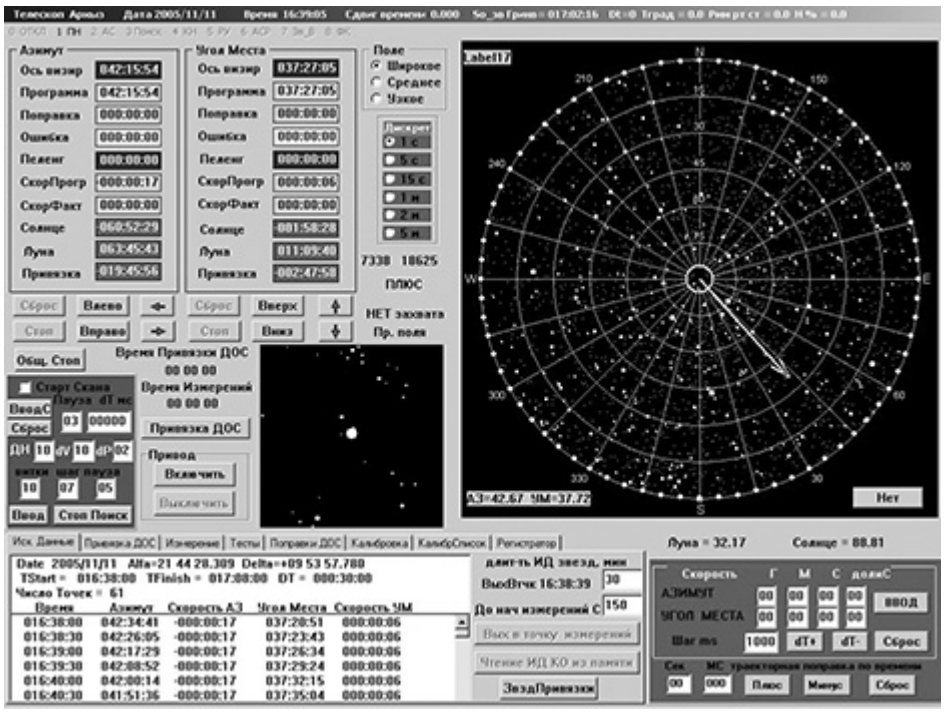

***Figure 7:** Versatile pointing/tracking control virtual panel*

Right: image of star catalog.

Center: image of calculated catalog star positions in the TV camera field of view (around the telescope pointing direction).

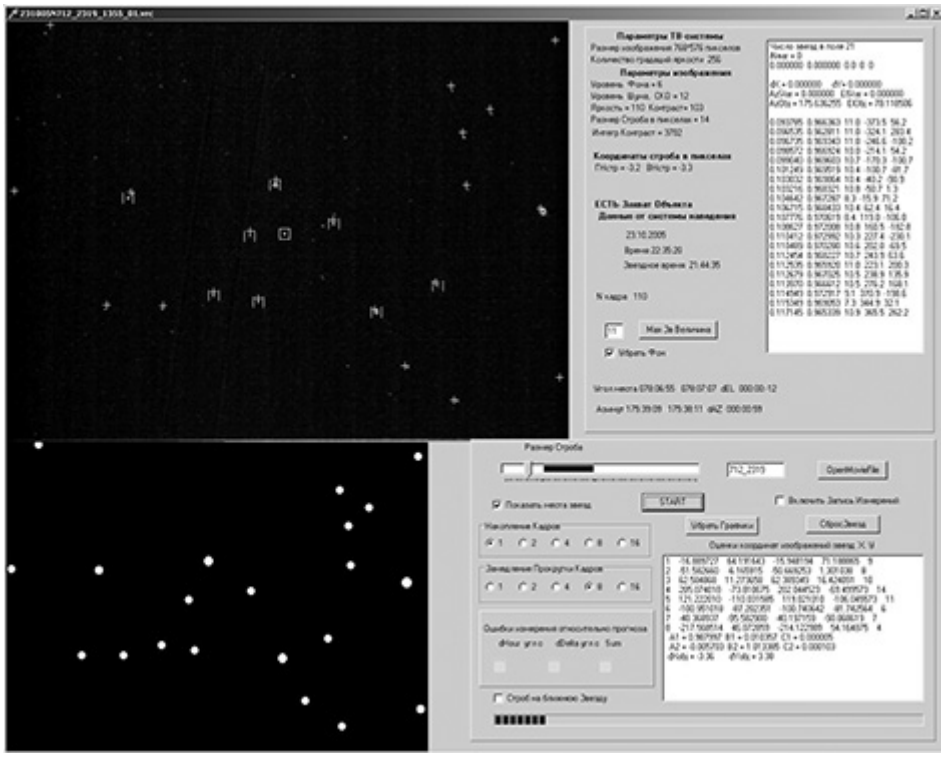

Upper left: TV frame with GLONASS-712 spacecraft in the center.

Lower left: star catalog fragment. + marks: position of catalog stars in the TV frame.

II marks: star tracking gates (stars selected for spacecraft angular position measurements).

Figure 8: *Versatile angular measurement (astrometric) virtual control panel*

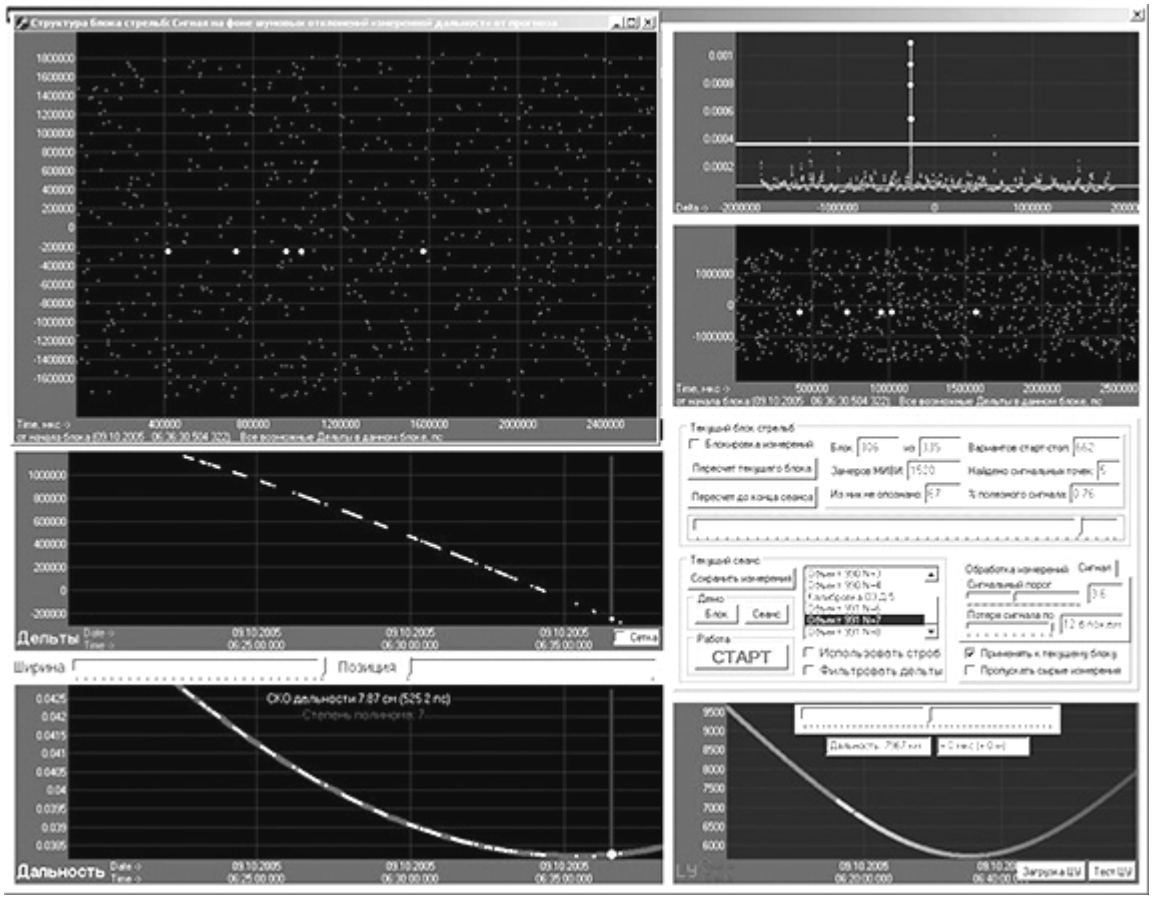

Figure 9: *Laser ranging control virtual panel (daytime observation of LAGEOS)*

TLRS-3 Return To Operations

Howard Donovan[1], Dennis McCollums[1], Don Patterson[1], Julie Horvath[1], Michael Heinick[1], Scott Wetzel[1], David Carter[2]

1. Honeywell Technology Solutions Inc. 7515 Mission Dr., Lanham, MD, USA 20771.

2. NASA Goddard Space Flight Center, Code 453, Greenbelt, MD, USA 20771.

Contact: Howard.Donovan@Honeywell.com

Abstract

The Transportable Laser Ranging Station 3 (TLRS-3) tracked from the Arequipa, Peru site for almost twelve years when the station was decommissioned in January of 2004. Replacing the SAO-2 in 1992 in a partnership between NASA and the Universidad Naciaonal De San Agustin, the TLRS-3 had travelled between Cerro Tololo, Chile and Arequipa, Peru after beginning its first operations in 1988 visiting the Mojave site in Goldstone, California. This paper will discuss the repairs, upgrades, and modifications accomplished at the TLRS-3 as well as the results of the first data collected.

History of TLRS-3 in Arequipa, Peru

The TLRS-3 replaced the SAO-2 system as the primary tracking station in Arequipa, Peru on August 7, 1992 with the tracking of an ERS-1 pass. In an agreement between NASA and the Universidad Naciaonal De San Agustin (UNSA), UNSA provided the operational crew while HTSI provided engineering support. TLRS-3 operated very well for almost twelve years until NASA budget reductions necessitated the closing of TLRS-3. On January 27, 2004 TLRS-3 tracked its last pass, a Starlette. In the fall of 2005, NASA tasked HTSI to return TLRS-3 to operational status. The UNSA crew returned to the station on December 12, 2005 to begin the task of reinitializing the system. HTSI working, with NASA and UNSA, began restoring the TLRS-3 to full operations, returning to the station in January 2006. The task of returning TLRS-3 to operations was done concurrently with the TLRS-4 Return to Operations effort.

TLRS-3 Return to Operations Strategy

With the TLRS-4 Return to Operations effort preceding the TLRS-3 effort by a few months, the TLRS-3 effort was able to take advantage of the multiple enhancements, upgrades and repair strategies used to quickly bring TLRS-4 back to operational status. Unlike the TLRS-4 though, the TLRS-3 had been without power and had not seen any type of maintenance for two years. Scheduled for TLRS-3 would be a full system inspection, implementation of the software and hardware improvements made to TLRS-4, a full system characterization using the System Operational Verification Test (SOVT) process, and a full validation of system performance prior to release of data to the ILRS.

Significant Engineering Issues

The TLRS-3 was off line for over 2 years with no HVAC control, no humidity control, and no air filtration. The system had not been exercised in any way. As a result the integrity of the station computers, system electronics, telescope optics, laser system, and

gimbal were of concern. With the lack of humidity control, corrosion issues were of concern as well, especially with the wire wrap boards, ICs and IC sockets, connectors, switches, etc. and the metal surfaces within the system, especially the laser. Because of the uncontrolled atmosphere within the trailers, temperature cycling presented a connection issue with wire wrap boards, connectors, etc. also. Maintenance of the site and main power system had not been performed either.

Planned and Implemented Upgrades

Upgrades planned for the TLRS-3 had already been implemented and proven to the TLRS-4. The Upper Deck received several enhancements to reduce maintenance and improve lifetime of the optics, improve the accuracy of the star calibration and reduce the time required to accomplish the calibration, and to improve throughput of the daylight filter. The optical system of the entire Upper Deck was enclosed to assist in keeping the optics clean, improve daylight tracking, and provide additional operator safety. A camera system was installed to increase the accuracy of the star calibrations. The optics layout was also redesigned so that optics did not have to be removed to perform the star calibration and so that the laser and star image could be easily co-aligned. The 10 angstrom daylight filter was replaced with a unit that has a 68% throughput and is quite temperature stable. The telescope was returned to NASA SLR Engineering in the USA and was completely disassembled, inspected, cleaned, and realigned. Throughput increased from ~ 50% to 87%. The T/R Switch was upgraded to an improved stepper motor design which was much more temperature stable than the old design. The Photek MCP Upgrade was installed replacing the failing ITT MCP. The upgrade included a newly calibrated CFD as well. The Controller Computer received improved Sattrk and Monitor programs. With these improvements came the Window/Window Upgrade, Mode Change Bias Reset, enhanced “Record All frames” function, 5pps and 4pps Thread Matching and Automated Switching, Sun Avoidance, Horizon Mask, the new Go/No Go software, and the high voltage power supply scaling upgrade. The new TLRS-4 microprocessor based Trackball was installed as well. Maintenance to site power was performed which included refurbishing the site power transformer.

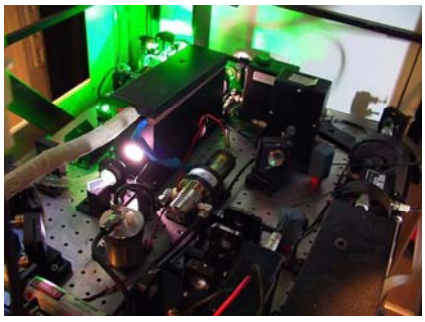

Current Status

The TLRS-3 is producing high quality data. Over 90 pass segments have been acquired with a data quality of <10mm RMS on Lageos and Starlette and <20 mm RMS on Ajisai. CHAMP and Grace B have been tracked. Average ground calibration is excellent at the 5.4 mm level.

Future Plans

Though significant progress has been made in bringing the TLRS-3 back to operational

status, there are still some unfinished tasks. Optimization of gimbal tracking performance, completion of the 4pps upgrade, completion of the Controller and Processor software upgrades and testing, calibration of system test equipment, restocking of system spares, completion of a site safety inspection and the performance of the site survey.

Test Data

Graphical examples of the Lageos satellite data and a listing of all the passes acquired by TLRS-3 during the upgrade are provided below. Included in the pass listing are calibration RMS, satellite RMS, system delay shift, calibration observation count, and satellite observation count.

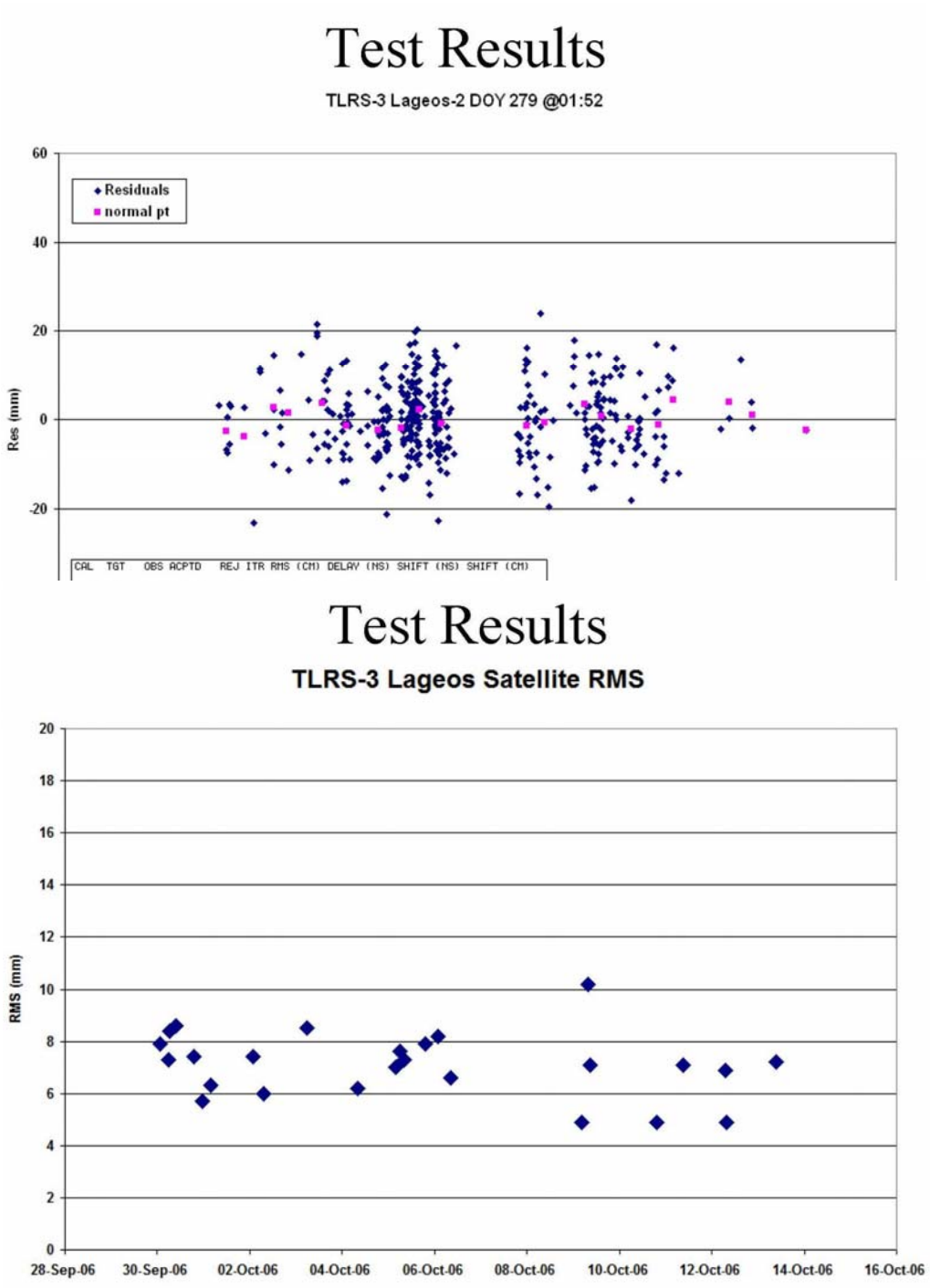

Test Results

PASS DATE	OCC NUM	SATID	TARGET	TARGET DISTANCE	# CAL OBS	# CAL REJ	CAL RMS (mm)	APPLIED DELAY	SHIFT (mm)	# SAT OBS	# SAT REJ	SAT RMS (mm)	MEAN TEMP ©	MEAN PRESS (mbars)	HUMIDITY (%)	NUM NP DATA BINS	NUM NP
29-Sep-06 00:53	03	1500	BC	105981	1948	14	4.5	3637.2	-1.07	93	15	22.2	13.32	761.2	51	30	18
30-Sep-06 01:21	03	5986	BC	105981	2188	9	5.9	3643.9	6.16	92	0	7.9	12.31	760.5	46	4	4
30-Sep-06 01:43	03	4378	BC	105981	2188	9	5.9	3643.9	6.16	19	6	4.2	11.73	760.6	45	28	6
30-Sep-06 02:03	03	1500	BC	105981	2188	9	5.9	3643.9	6.16	341	23	17.3	11.57	760.7	45	20	19
30-Sep-06 05:51	03	5986	BC	105981	2046	5	6.4	3643.5	-1.46	10	0	7.3	10.27	759.7	43	2	2
30-Sep-06 06:11	03	1155	BC	105981	2046	5	6.4	3643.5	-1.46	224	1	8.4	10.29	759.5	42	13	13
30-Sep-06 06:56	03	317	BC	105981	2034	4	6.4	3644.6	0.65	343	23	14.2	9.88	759.5	41	27	19
30-Sep-06 08:05	03	1134	BC	105981	2065	10	5.9	3646.7	1.72	100	7	8.4	8.91	759.6	45	5	5
30-Sep-06 08:52	03	643	BC	105981	2014	1	5.8	3646.2	-0.95	67	3	10	9.51	759.7	42	4	4
30-Sep-06 09:52	03	5986	BC	105981	2043	1	6.4	3646.4	1.37	159	1	8.6	9.15	760	39	14	10
30-Sep-06 18:58	03	1155	BC	105981	2249	10	5	3646.2	-0.35	132	1	7.4	23.14	760.5	15	6	6
30-Sep-06 23:04	03	1134	BC	105981	2022	3	5	3644.5	2.06	372	63	8.9	16.08	761.7	28	19	13
30-Sep-06 23:31	03	5986	BC	105981	2022	3	5	3644.5	2.06	38	1	5.7	14.37	762.1	32	10	8
01-Oct-06 01:11	03	1500	BC	105981	2233	16	4.7	3640	2.66	1063	231	21.7	11.35	762.5	39	17	17
01-Oct-06 02:37	03	6179	BC	105981	2015	32	4.4	3641.1	2.11	43	0	19.9	10.51	762.6	36	5	5
01-Oct-06 03:05	03	6178	BC	105981	2015	32	4.4	3641.1	2.11	127	14	22.4	10.7	762.6	32	6	6
01-Oct-06 03:13	03	5557	BC	105981	2015	32	4.4	3641.1	2.11	109	12	6.1	10.55	762.5	31	7	7
01-Oct-06 03:33	03	5986	BC	105981	2015	32	4.4	3641.1	2.11	109	3	6.3	8.9	762.3	36	13	11
02-Oct-06 00:34	03	4378	BC	105981	2131	39	4.6	3638.1	-0.65	192	3	7.3	12.12	761.9	35	27	23
02-Oct-06 01:13	03	8004	BC	105981	2157	60	4.7	3637.3	-1.4	402	22	14.6	11.46	762.2	35	45	34
02-Oct-06 01:31	03	5986	BC	105981	2157	60	4.7	3637.3	-1.4	405	4	7.4	10.85	762.2	36	21	18
02-Oct-06 02:36	03	6178	BC	105981	2455	66	4.8	3636.3	1.11	59	8	8	10.9	762.2	32	11	10
02-Oct-06 05:14	03	8501	BC	105981	2059	43	5.3	3639.4	-1.09	44	1	6.8	8.48	761.1	37	7	6
02-Oct-06 05:28	03	317	BC	105981	2059	43	5.3	3639.4	-1.09	192	15	14.3	8.69	760.8	35	26	12
02-Oct-06 06:53	03	8501	BC	105981	2083	28	5.3	3638.1	-0.4	8	0	10.1	8.2	760.2	34	2	2
02-Oct-06 06:55	03	1134	BC	105981	2083	28	5.3	3638.1	-0.4	168	10	10.7	8.18	760.2	34	10	10
02-Oct-06 07:05	03	1155	BC	105981	2083	28	5.3	3638.1	-0.4	38	0	6	8.29	760.1	36	3	3
02-Oct-06 07:19	03	317	BC	105981	2083	28	5.3	3638.1	-0.4	371	40	9.3	7.7	760.1	34	34	21
02-Oct-06 07:59	03	643	BC	105981	2025	19	5.4	3638.4	0.16	13	0	5.7	7.41	760.1	36	3	3
02-Oct-06 08:48	03	1134	BC	105981	2035	7	5.5	3640.3	0.91	30	3	7.9	7.8	759.9	34	4	4
02-Oct-06 12:57	03	1500	BA	105981	1018	8	6.3	3645.6	0	460	65	16.3	18.1	761.4	18	12	12
03-Oct-06 01:32	03	1500	BB	105981	1007	32	4.8	3636.8	0	182	5	14.8	10.52	761.4	41	4	4
03-Oct-06 02:48	03	5557	BC	105981	2031	139	5.3	3638.3	-0.94	99	6	7.6	10.69	761.7	40	10	8
03-Oct-06 04:45	03	317	BC	105981	1837	27	5.2	3639.4	-1.4	157	6	9.9	9.58	760.6	40	21	18
03-Oct-06 05:32	03	1155	BC	105981	2034	37	5	3638.3	1.67	243	3	8.5	9.13	760.3	41	12	12
03-Oct-06 06:19	03	8501	BC	105981	2039	41	5	3639.6	-0.1	129	15	16.9	9.6	759.8	36	4	4
03-Oct-06 06:40	03	317	BC	105981	2039	41	5	3639.6	-0.1	119	2	8.5	8.85	759.5	36	11	11
03-Oct-06 07:16	03	1134	BC	105981	2017	34	5.3	3640.5	2.09	17	0	6.9	9.2	759.3	32	1	1
04-Oct-06 05:48	03	8501	BC	105981	2031	6	5.1	3644.3	1.81	165	7	7.2	9.8	759.4	33	9	9
04-Oct-06 07:38	03	1134	BC	105981	2040	8	5.1	3643.3	-0.55	272	8	7.9	8.42	758.6	32	7	7
04-Oct-06 07:49	03	317	BC	105981	2040	8	5.1	3643.3	-0.55	26	0	7.1	8.99	758.5	30	7	7
04-Oct-06 07:53	03	1155	BC	105981	2040	8	5.1	3643.3	-0.55	12	0	6.2	8.61	758.6	34	6	5
05-Oct-06 02:11	03	6179	BC	105981	1237	15	5	3643.2	-1.85	249	55	7.9	10.57	760	41	22	20
05-Oct-06 02:29	03	5557	BC	105981	1237	15	5	3643.2	-1.85	23	1	9.7	10.5	760.1	40	2	2
05-Oct-06 02:40	03	6178	BC	105981	1237	15	5	3643.2	-1.85	346	23	8.9	10.61	760.2	39	20	19
05-Oct-06 02:47	03	8002	BC	105981	1237	15	5	3643.2	-1.85	109	6	10.8	10.47	760.2	39	16	11
05-Oct-06 03:54	03	5986	BC	105981	2277	59	5.5	3642.8	1.2	119	1	7	9.88	759.6	39	17	17
05-Oct-06 05:10	03	317	BC	105981	2046	10	5.5	3643.1	1.29	59	3	10.3	9.7	758.9	34	18	8
05-Oct-06 06:12	03	1155	BC	105981	2146	8	5.5	3647.4	0.67	109	0	7.6	9.37	758.3	22	12	4
05-Oct-06 07:04	03	317	BC	105981	2146	8	5.5	3647.4	0.67	306	20	11.1	8.84	758.1	21	19	19
05-Oct-06 07:54	03	1134	BC	105981	2143	8	5.5	3647.9	1.36	405	51	11.1	9.59	757.8	18	11	11
05-Oct-06 08:20	03	643	BC	105981	2143	8	5.5	3647.9	1.36	130	11	6.7	9.38	757.7	17	6	6
05-Oct-06 08:28	03	5986	BC	105981	2143	8	5.5	3647.9	1.36	54	0	7.3	9.31	757.6	17	8	6
05-Oct-06 18:05	03	8501	BC	105981	2060	10	6.7	3655.7	-7.68	47	2	5.9	23.44	758	16	6	6
05-Oct-06 19:22	03	1155	BC	105981	1687	20	5.5	3654.1	1.19	15	1	7.9	23.11	757.5	17	3	2
05-Oct-06 22:41	03	1500	BC	105981	2064	11	5.6	3654.2	1.87	700	91	21.9	18.21	758.7	22	19	19
06-Oct-06 01:53	03	5986	BC	105981	2590	23	5.3	3646	5.19	417	0	8.2	12.35	760.9	33	24	20
06-Oct-06 03:03	03	5557	BC	105981	2174	5	5.4	3649.3	-1.43	33	3	6.1	10.5	761	35	3	3
06-Oct-06 03:19	03	6179	BC	105981	2174	5	5.4	3649.3	-1.43	127	9	7	11.17	761.1	33	9	9
06-Oct-06 06:16	03	317	BC	105981	2063	5	5.6	3650.2	-0.2	450	19	13.1	10.39	759.9	34	27	25
06-Oct-06 06:28	03	1134	BC	105981	2063	5	5.6	3650.2	-0.2	202	41	9.4	10.33	759.9	33	5	5
06-Oct-06 08:14	03	1155	BC	105981	2021	6	5.6	3652.2	0.49	110	0	6.6	10.14	759.2	30	22	15
08-Oct-06 21:59	03	1500	BC	105981	2026	54	4.7	3655.6	0.51	1417	260	17.7	19.89	760.3	24	25	24
08-Oct-06 23:21	03	4378	BC	105981	2192	106	5.2	3653.8	2.72	116	11	7.5	15.79	761	33	20	14
09-Oct-06 04:10	03	317	BC	105981	1527	175	5.7	3649.4	-1.07	11	0	6.5	11.4	761.6	34	2	2
09-Oct-06 04:30	03	1155	BC	105981	1527	175	5.7	3649.4	-1.07	44	5	4.9	11.34	761.4	32	8	7
09-Oct-06 05:37	03	1134	BC	105981	1540	151	5.5	3647.1	-0.87	134	25	6.9	11.5	760.8	29	5	5
09-Oct-06 07:46	03	1155	BC	105981	2063	181	5.4	3647.1	1.83	39	1	10.2	10.03	760	29	6	4
09-Oct-06 08:15	03	643	BC	105981	2063	181	5.4	3647.1	1.83	33	5	6.5	9.1	759.9	25	2	2
09-Oct-06 08:56	03	5986	BC	105981	2044	259	5.4	3647.1	-2.6	272	23	7.1	9.24	760	23	20	14
10-Oct-06 19:01	03	1134	BC	105981	1234	3	6	3660.7	5.77	241	19	7.1	22.35	761.9	20	20	12
10-Oct-06 19:35	03	1155	BC	105981	1234	3	6	3660.7	5.77	60	1	4.9	22.97	761.8	20	5	5
11-Oct-06 09:10	03	5986	BA	105981	1020	1	5.3	3658.7	0	56	0	7.1	12.22	760.9	17	17	6
12-Oct-06 04:42	03	1134	BC	105981	2048	6	5.1	3660	0.29	156	6	5.9	11.84	762.6	29	14	5
12-Oct-06 06:39	03	8501	BC	105981	2023	5	5	3660.5	-0.34	10	0	8.4	11.4	761.5	31	2	2
12-Oct-06 07:11	03	1155	BC	105981	2124	5	4.8	3661.4	-0.14	108	0	6.9	11.57	761.2	30	6	6
12-Oct-06 07:34	03	1155	BC	105981	2124	5	4.8	3661.4	-0.14	32	0	4.9	11.96	761.2	29	6	6
12-Oct-06 08:31	03	643	BC	105981	2092	9	4.5	3659.8	-0.08	96	12	9.5	11.16	761.1	30	4	4
12-Oct-06 10:03	03	1500	BC	105981	2051	8	5	3658.9	-0.77	1083	111	17	11.35	761.6	30	17	17
12-Oct-06 10:56	03	4378	BC	105981	2019	6	5.6	3662.9	2.36	24	0	6	11.6	762	30	6	6
12-Oct-06 17:52	03	1134	BC	105981	1926	17	5	3666.7	-0.02	133	7	7	24.29	761.1	16	14	10
13-Oct-06 08:09	03	643	BB	105981	1041	47	7.3	3654	0	48	3	16.5	9.6	761.1	36	4	2
13-Oct-06 09:39	03	5986	BC	105981	2085	46	6.3	3656.2	-0.8	377	2	7.2	9.03	761.4	36	14	13

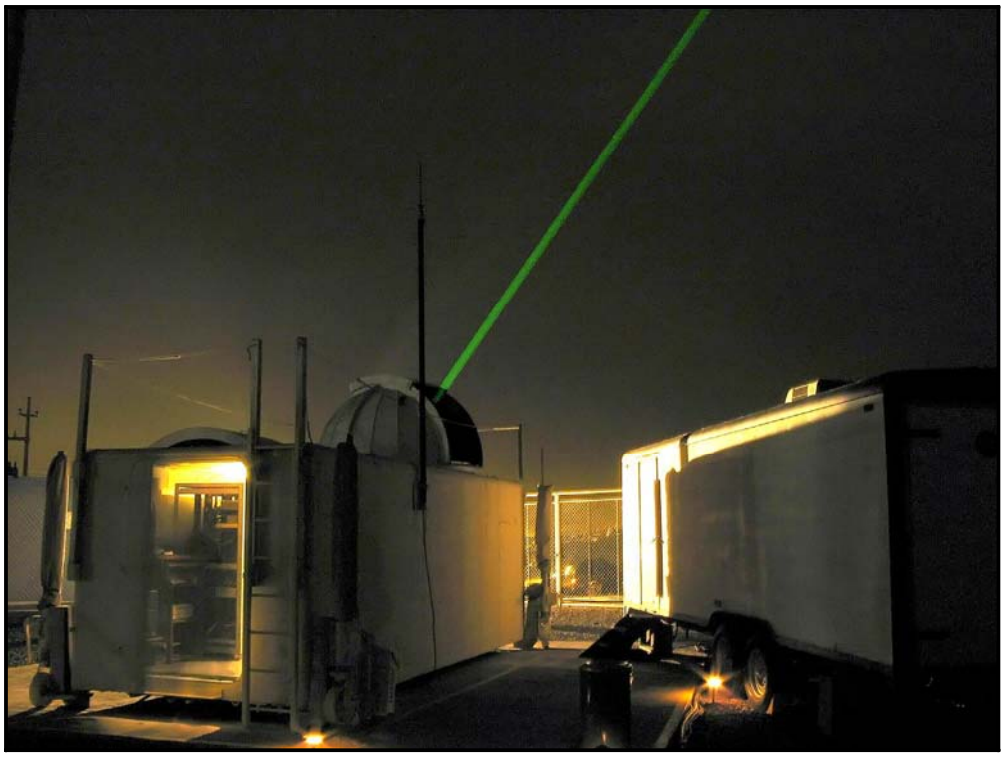

Korean Plan for SLR System Development

Hyung-Chul Lim[1, 2], Jong-Uk Park[1], Sang-Ki Jeong[2], Byung-Su Kim[2]

1. Korea Astronomy and Space Science Institute, Daejeon, Korea
2. Korea Institute of Science and Technology Evaluation and Planning, Seoul, Korea

Contact: hclim@kasi.re.kr

Abstract

There are about 70 GNSS stations in Korea for GNSS applications including space geodesy, and 3 VLBI stations will be constructed by 2007 for astronomical and geodetic research. In addition, two Korean satellites with a laser retro-reflector array, STSAT-2 and KOMPSAT-5, will be launched in 2008 and 2010, respectively. Thus, SLR system is considered to be necessary in Korea for constructed for satellite laser tracking and space geodesy research. KASI has a plan to develop a fixed SLR station and a mobile SLR station in the near future. In this study, future Korean plans of SLR system development will be presented.

Introduction

More than 70 GNSS (Global Navigation Satellite System) stations have been operated by several institutes, including KASI (Korea Astronomy and Space Science Institute), for accomplishing missions of navigation, space geodesy, and so on. From 1995, KASI has been playing an important role in IGS (International GNSS Service) and IERS (International Earth Rotation and Reference Systems Service) as global GNSS station, and operating an IGS global data center from 1996. Except GPS applications, KASI has a wide variety of research areas like optical, radio, theoretical and observational astronomy research, and is expanding its area through astronomical research in space. So, KASI has been constructing 3 VLBI (Very Long Baseline Interferometry) stations with receivers working in the frequencies 2/8, 22 and 43GHz bands which will be completed by 2007 for radio astronomy research including space geodesy. Fundamental stations for geodesy operate three geodetic space techniques at one location: VLBI, GNSS and SLR (Satellite Laser Ranging), which can give a powerful tool for space geodesy such as global reference frame. KASI has a plan of operating a fundamental station in Jeju island in which a GNSS station is already operated and a VLBI station will be completed in 2007. So, KASI wants to develop a SLR system for constructing a fundamental station, and it has tried to raise funds for SLR system development from Korean government.

After KITSAT-1 was launched in 1992, which was the first Korean satellite, Korea launched 6 LEO (Low Earth Orbit) satellites made by Korean technology. They are not all equipped with LRA (Laser Retro-reflector Array) because precise orbit determination is not required in their missions. However, two Korean satellites with LRA will be launched in 2008 and 2010, respectively: Science Technology SATellite-2 (STSAT-2) with a Lyman-alpha imaging solar telescope and Korea Multi-Purpose SATellie-5 (KOMPSAT-5) with a Synthetic Aperture Radar (SAR). STSAT-2 LRA was developed through international collaboration between SaTReC(Satellite Technology Research Center), Korea and Shanghai Astronomical Observatory, China. But KOMPSAT-5 will have the same LRA as Champ, Grace and TerraSAR-X satellites, whose LRA will be made by GFZ (GeoForschungsZentrum Potsdam), Germany.

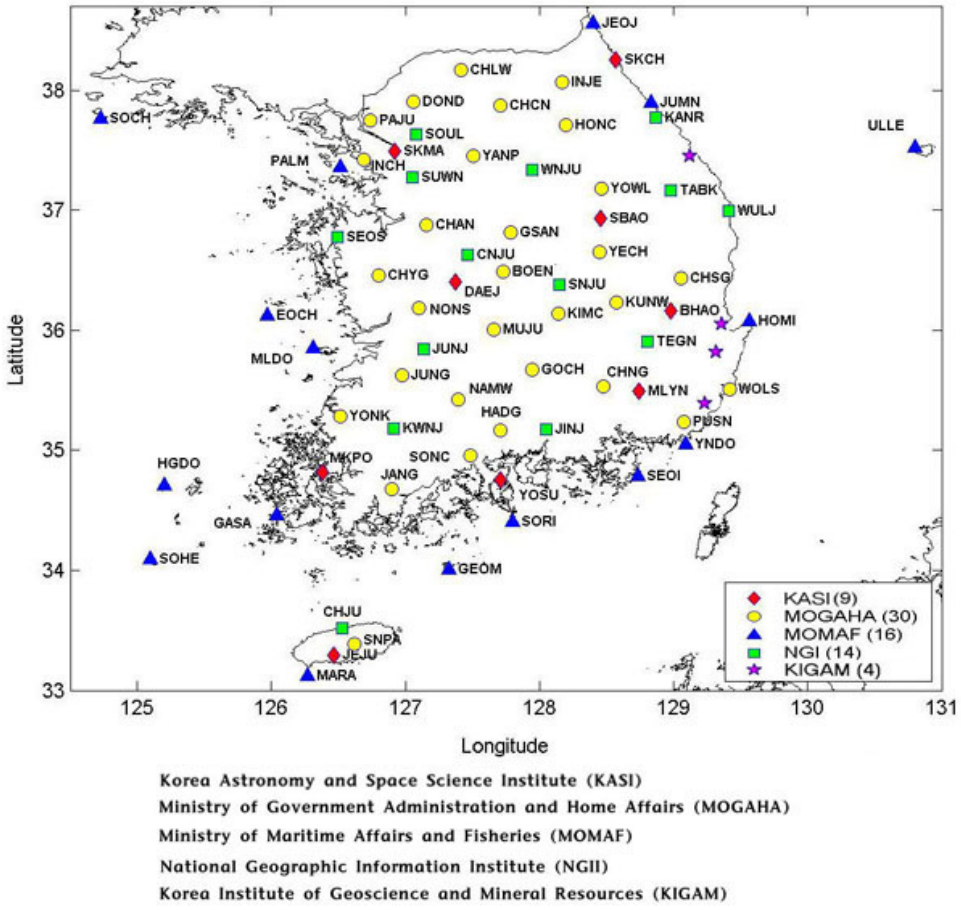

Korea Astronomy and Space Science Institute (KASI)
Ministry of Government Administration and Home Affairs (MOGAHA)
Ministry of Maritime Affairs and Fisheries (MOMAF)
National Geographic Information Institute (NGII)
Korea Institute of Geoscience and Mineral Resources (KIGAM)

***Figure 1**. Korean GNSS Network*

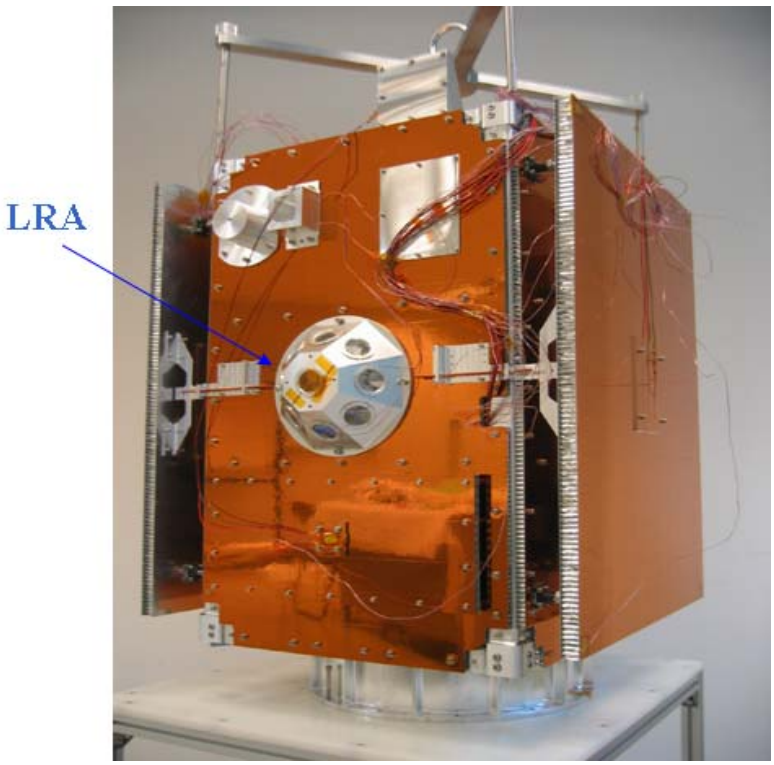

***Figure 2**. STSAT-2(first Korean satellite with LRA)*

Future Plan for SLR system development

KASI conducted the preliminary study for SLR system development from December 2004 to November 2005 with KAERI (Korea Atomic Energy Research Institute), KIMM (Korea Institute of Machinery and Materials) and SaTReC (Satellite Technology Research Center). In the preliminary study, KASI carried out a feasibility study on SLR system development and made the conceptual design of Tx/Rx telescope and Control & Operating System. The conceptual design of the laser generator was done by KAERI, the tracking mount by KIMM, and the Tx/Rx electric system by SaTReC. KASI has tried to obtain the financial support of the Korean government for SLR system development (KSLR project) since this preliminary study, and wants to start the KSLR project in 2008 with KAERI, KIMM and SaTReC. In this project, one fixed system with a 1m Rx telescope and one mobile system with 40cm Rx telescope will be developed for 5 years. The detailed requirements of a fixed system are shown in Table 1. The mobile system will be integrated by introducing the core subsystems from abroad, and the fixed system will be developed through the international and domestic collaboration. So, it will take about 3 years to develop a mobile system but 5 years (subsystem development: 3.5yr, system integration: 0.5yr, test operation: 1yr) to develop a fixed system. After a fixed SLR system is constructed, KASI will join to ILRS (International Laser Ranging Service) for the contribution of the international SLR society.

As mentioned in the previous section, STSAT-2 will be launched in 2008 when Korea will not be capable of tracking it. So a mobile system (TROS, Transportable Ranging Observation System) will be introduced in China this June for laser tracking of STSAT-2 but the detailed schedule is not fixed

Table 1. *Requirements of the future Korean SLR system*

Items	Requirements
Tracking Coverage	• Possible to track satellites in the altitude of 25,000km • STSAT-2, KOMPSAT-5, GPS, Galileo Satellites and so on.
Ranging Accuracy	• Lageos : 10mm(SS), 1-2mm(NP) • GPS and Galileo : 20mm(SS), 3-5mm(NP) • Ground Target : 3mm(SS), 1mm(NP)
Automatic Operation	• Remote control from the remote site via internet or dedicated line. • Aircraft detection using radar and automatic observation according to the schedule.
Etc	• Daylight tracking. • Optical tracking of the space launch vehicle (if possible).

Summary

Two Korean satellites with LRA, STSAT-2 and KOMPSAT-5 will be launched in 2007 and 2009, respectively. Therefore, SLR system is steadily required to be established in Korea not only for satellite tracking, but also for space geodesy research by using GNSS and VLBI. In response to this demand, KASI have prepared for development of SLR system for several years, and expect to launch the project for the development of SLR system from 2008. KASI has a plan to develop one mobile and one fixed SLR systems for 5 years. After a fixed SLR system is constructed, KASI will join ILRS and participate in the international tracking campaign.

References

[1] Lee, J. H., Kim, S. B., Kim, K. H., Lee, S. H., Im, Y. J., Fumin, Y., Wanzhen, C., “Korea’s First Satellite for Satellite Laser Ranging”, Acta Astronautica, 2004.

Study on Servo-Control System of Astronomical Telescopes

Li Zhu-lian, Zheng Xiang-ming, Xiong Yao-heng

1. National Astronomical Observatories/Yunnan Observatory, Chinese Academy of Sciences, Kunming 650011,China

Abstract

Based on recent and modern control theories, this paper describes an analysis of the control system compensation function and its application to astronomical telescope servo control requirements. It discusses corresponding compensation networks for modern astronomical telescopes.

Keywords: *Servo System, Compensation Network, SLR/LLR telescope*

Introduction

Most of modern telescopes servo-control systems are computer closed loop control systems which are based on classical control theories and are composed of one or more feedback control loop. Typical feedback control system is shown in Fig.1. In theory, control system designed according to this block diagram might meet the requirements. However, in a concrete project, control system simply designed like this way is not simultaneously satisfied with all the requirements until it is compensated properly.

C(s) represents controlled output, its value is sent back through feedback controller

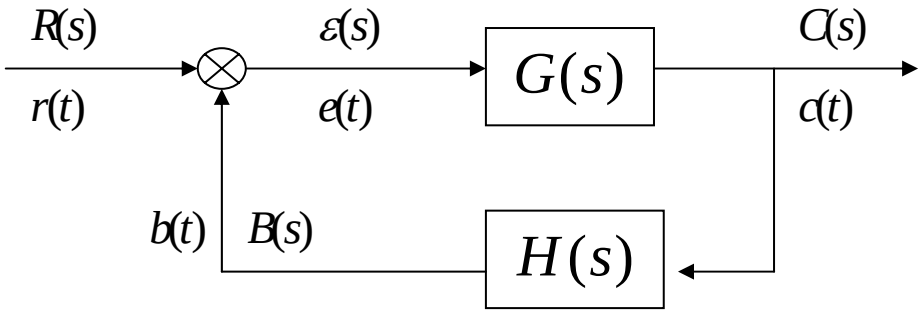

Fig.1 *Typical Feedback Control Loop*

whose transfer function is H(s). Its output B(s) is compared with expected output R(s), i.e. input of whole control system, the error which R(s) substracts B(s) is sent into controller G(s), which adjusts the error to near zero.

Compensation of Control System

In order to carry out expected capability, modifying and adjusting the control system structure is named compensation. In another words, compensation is used to adjust structure for compensating defect of system. PD (Proportion Differential) Compensation Network and PI (Proportion Integral) are often used in modern control system design. Corresponding control loop block diagram is shown as Fig.2. Gc(s) is the transfer function of the compensation network. [1]

PD Compensation Network Function

When compensation network transfer function $G_c(s)$ is:

$$G_c(s) \approx \frac{k}{p} s$$

it is a PD type compensation Network.[2] Fig.3 is its corresponding bode graph, which is magnitude versus phase plot. It could be clearly seen that magnitude gain increases with frequency and phase is greater than zero. This means that PD compensation can offer additional phase for primary system without compensation network.

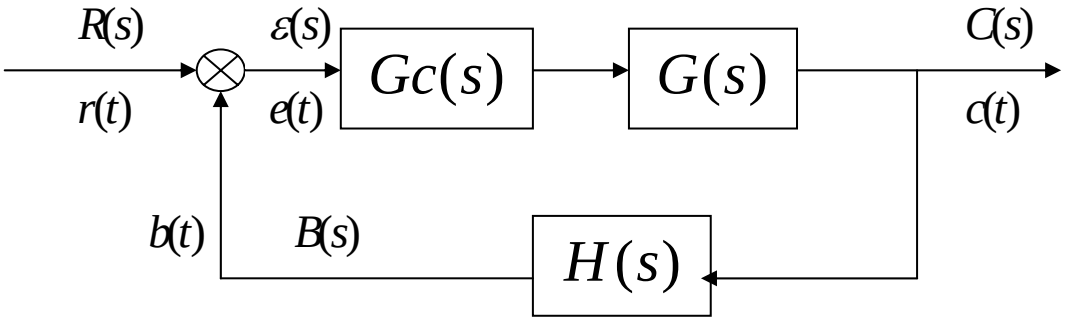

Fig.2 *Feedback Control Loop with Compensation*

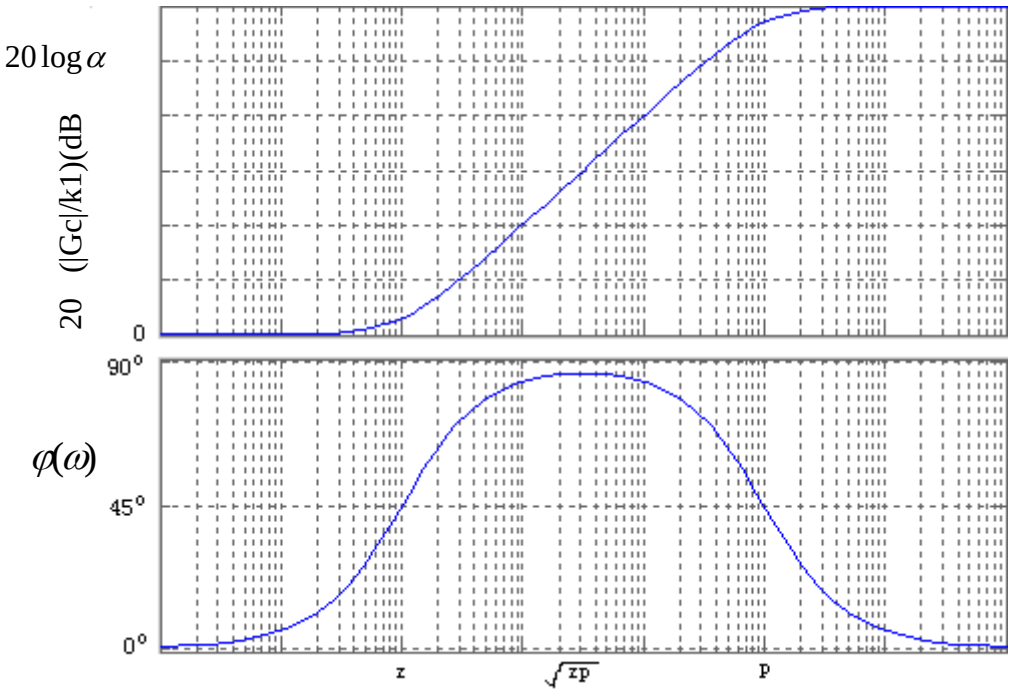

Fig.3 *The Bode Graph of PD Compensation*

Therefore, to make system response more quickly and strengthen system stability is the function of PD compensation.

PI Compensation Network Function

When compensation network transfer function $G_c(s)$ is :

$$G_c(s) \approx \frac{k}{ps}$$

it is a PI type compensation Network.[2] Fig.4 is its corresponding bode graph, which is magnitude versus phase plot. It is obvious that magnitude gain descends with frequency and phase is negative. This shows that PI compensation can offer delay phase for

primary system without compensation network. So, the function of PI compensation is to improve system accuracy of stability. To sum up, PD compensation may be used to improve instantaneous response and PI can be used to meliorate stable response.

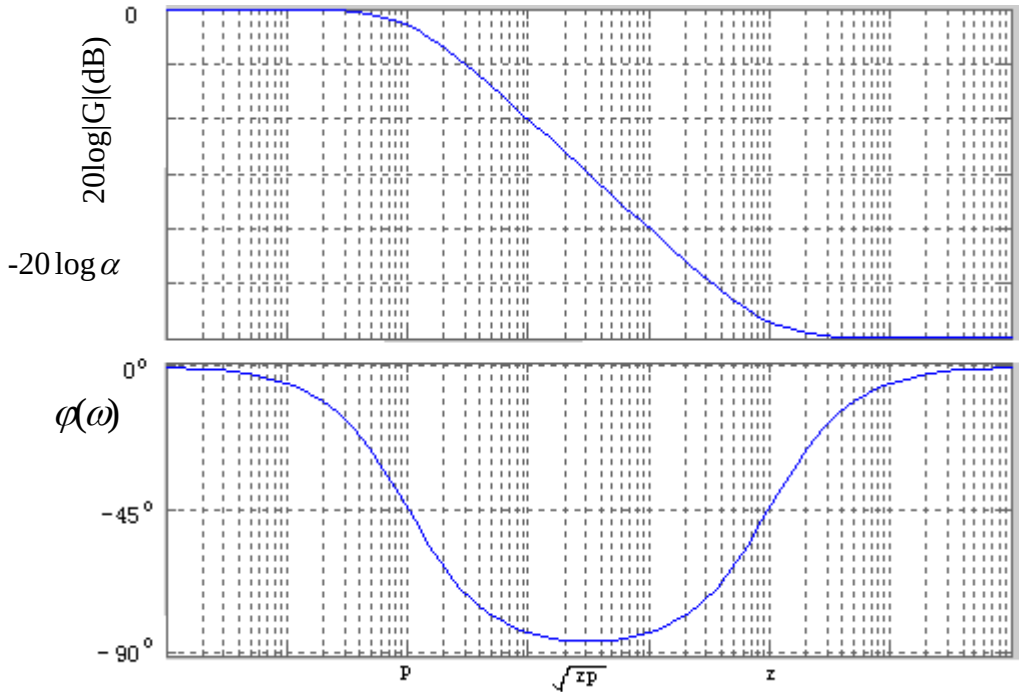

Fig.4 *The Bode Graph of PI Compensation*

Compensation Network Design for Telescope Servo System

According to characters of the compensation network which were analysed above, we could design a proper servo control system for any astronomical telescope.

If a telescope is required to track quick motion celestial bodies, such as satellites near the Earth, we would design the control system compensation network as PD compensation, or PI compensation would be better to observe slow motion celestial bodies for a telescope.

Of course, when a telescope is not require to track quick motion celestial bodies but slow motion bodies, to combine advantages of PI and PD could gain the expected performance or we could directly design the control system compensation network as PID compensation.

Discussion

Though PID compensation network could attain better capability, its disadvantage is that needs more devices and increases design cost. Therefore, if a telescope need track both quick and slow bodies, in order to save resource, we'd better select PD compensation network, then through software methods to compensate the accuracy of stability.

References

[1] Richard C., Dorf, Robert H and Bishop. Modern Control System (eighth edition). Translation by Xie Hong-wei, Zou Feng-xing and Zhang Ming. Beijing Higher Education Press.

[2] Dai Bei-qian, Qian Zhi-yuan. Linear Electronic Circuit. HeFei:University of Science and Technology of China Press.

Russian Laser Tracking Network

V.B. Burmistrov, A.A. Fedotov, N.N. Parkhomenko,
V. Pasinkov, V.D. Shargorodsky, V.P. Vasiliev

1. Institute for Precision Instrument Engineering, Moscow, Russia.

Contact: www.niipp-moskva.ru

Abstract

Basic parameter are presented of six laser tracking stations now installed in Russia. Besides SLR, the stations also provide angular measurement and photometry. Some applications of obtained data are also specified.

Introduction

The Russian SLR stations comprise three optical channels: ranging channel, angular measurement channel, and photometric channel, providing the following accuracy of measurements:

- Ranging: 5 - 10 mm (RMS of NP)
- Angular measurements (in reflected sunlight): 1 arcsec

Photometry (in reflected sunlight): ≈0.2 star magnitude.

Ranging data applications

The high precision of laser ranging allows use of SLR as a single source of calibration data for GLONASS ephemeris determination, providing solution of following problems:

- Estimation of accuracy, and calibration of radio-frequency means for GLONASS orbit measurements.
- Providing SLR stations with geodetic-class RF navigation receivers connected to hydrogen maser frequency standards allows monitoring of on-board clocks and use of the data for operational control of GLONASS time and ephemeris data.
- SLR station coordinates are used as geodetic base for the GLONASS reference frame.
- SLR data are used to provide declared values of ephemeris precision, as well as to provide computation and forwarding of accuracy factor in the navigation frame of GLONASS – M spacecraft.

Angular measurement data applications

Angular measurement data obtained on SLR stations are used for implementation of single-point scheme of flight control for commercial geostationary spacecraft with periodical measurements of orbit inclination to provide retaining of the geostationary spacecraft standpoint within ±0.1 deg. in longitude and ±0.1 deg. in latitude.

Photometric data applications

- The presence of a high-sensitivity TV channel provides registration of flight phases (motors turn-on, booster separation, etc.) during launching of spacecraft on high elliptical and geostationary orbits.

- The photometric channel supports determination of spacecraft motion relative to its center-of-mass, as well as of its attitude stability.

Taking into account the unfavorable astro-climatic conditions on most of the country territory, efforts are made to expand the Russian laser tracking network. Currently, five SLR stations are in operation. In 5 years, the number of stations will increase to 15…20, as declared in the new Global Navigation System Federal program.

Russian laser tracking network

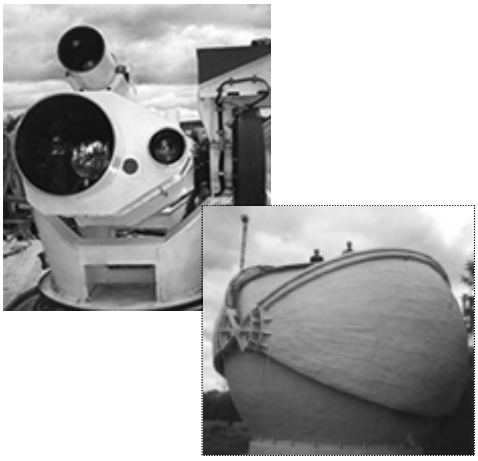

Figure 1: *SLR Station in Shelkovo (near Moscow)*

Figure 2:*Altay Optical and Laser Tracking Center*

Figure 3:*Komsomolsk SLR station*

Figure 4: *Compact SLR station installed in Arkhys (North Cuacasus)*

Figure 5: *Maidanak Optical and Laser stations (Uzbekistan) (currently, an inter-state agreement is under preparation concerning the mutual control and operation of this station).*

Figure 6: *Mobile SLR station installed in Baikonur*

Figure 7: *Russian laser tracking network*

TLRS-4 Deployment to Maui, Hawaii

Scott Wetzel[1], Howard Donovan[1], Maceo Blount[1], Dennis McCollums[1], Craig Foreman[1], Michael Heinick[1,] Daniel O'Gara[2], David Carter[3]

1. Honeywell Technology Solutions Inc., 7515 Mission Drive, Lanham, MD USA 20706
2. University of Hawaii, Institute for Astronomy, Maui, HI, USA 96790
3. NASA Goddard Space Flight Center, Code 453, Greenbelt, MD, USA 20771

Abstract

With the completion of the TLRS-4 Operational Readiness Review in the fall of 2005, Honeywell Technology Solutions Inc (HTSI) working with the University of Hawaii Institute for Astronomy (IfA), deployed the NASA TLRS-4 system to the 10,000 foot summit of the Haleakala volcano on September 7th, 2006. TLRS-4 is returning a critical data point to the ILRS Global solution following the closure of the HOLLAS SLR station in 2004. This paper describes the planning, deployment, current status and future at the Haleakala Observatory.

Background

The NASA Transportable Laser Ranging System (TLRS) number 4, TLRS-4, was returned to operations during spring and summer of 2005, following approximately 10 years of inactivity as an operational station in the NASA SLR Network. A highly successful inter-comparison test with Moblas 7 validated that TLRS-4 was ready for deployment. Following the Operational Readiness Review on September 15, 2005, TLRS-4 was readied for deployment to the 10,000 ft summit of the Haleakala volcano on Maui, Hawaii. The system was to be operated by the University of Hawaii (UH), Institute for Astronomy (IfA) under contract to NASA, returning a critical data point in the Pacific Ocean. As the Hollas system had been decommissioned in 2004 following budget reductions at NASA, the site was converted to the new PanStarrs Observatory. To return SLR to the Haleakala Observatory, the TLRS-4 system was provided and would be moved to a pad within approximately 100 meters of the Hollas station. The figure below shows the location of the former Hollas system and the location of where TLRS-4 system would be deployed.

Haleakala Observatory Site Preparations

As the Hollas site was no longer available for SLR, a suitable location for TLRS-4 was required. One was found near the Mees Solar Observatory, however there was inadequate infrastructure to support SLR operations. Improved infrastructure to be considered included: pad, power, grounding voice and data communications, calibrations piers, site safety and site and system survey. Even though the IfA had no

formal contract in place with NASA, they provided excellent coordination for all efforts of site preparations that would be required to locate TLRS-4 at the observatory.

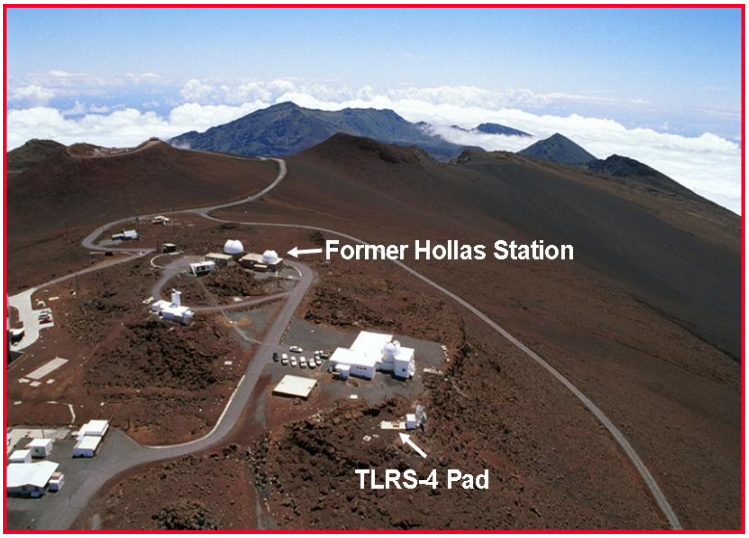

During this period when no contract existed with the IfA, the system remained in a semi-operational mode at the Goddard Geophysical and Astronomical Observatory (GGAO) in Greenbelt, Maryland at NASA SLR Headquarters.

Also, during this time, a dome safety retrofit project occurred in Maryland to provide a remotely operated and weather hardened dome and shutter to meet with the sometimes harsh wind and rain conditions at the summit of the Haleakala volcano. Additionally, an upgrade to provide for 4 Hz tracking for high orbital satellites occurred and the TLRS systems were not originally designed to high satellite tracking.

In April 2006, in anticipation of the IfA, NASA contract being finalized and due to the time required to transport the system from Maryland to Hawaii, it was determined to ship the system to Maui. The system arrived in Maui in late May 2006. As the contract had not been finalized, the shipment consisting of the Ranging Van, the Support Trailer and the radar platform and tracking dome, were placed at the Waiakoa, IfA office property located at 3,000 feet for holding until the system could be sent to the summit. A key milestone to be completed once the contract was in place was a site occupancy permit and permit to perform infrastructure modifications at the observatory.

When the contract was approved in late spring a occupation and building permit was applied for by the IfA. The permit was received in mid-August 2006 and site preparations were begun.

The Haleakala volcano is rich in native Hawaiian history, culture and religion. A cultural observer was required to approve and oversee all work performed on the site

where any disturbance may occur to native soils. Special requirements and permissions for excavation, removal and replacement of ground were followed and it was required that any person working on the project to be provided with a training and a cultural introduction to the religious and historical significance and understanding of working in Hawaii.

Following this training and receipt of the permitting, both HTSI and IfA worked aggressively to ready the site for occupation of the TLRS-4 system. Major components of site infrastructure included the calibration piers and site power. The previous figures show the unoccupied pad and the construction of the calibration piers. Temporary site power was provided from the Mees Observatory.

On September 6, 2006, the TLRS-4 was readied for transport from the IfA offices in Waiakoa to the summit. The newly fabricated dome and radar platform were installed at the Waiakoa office prior to loading the tracking van on the flatbed for the trip to the summit.

The Operations Van and the Support Trailer were delivered and installed on a rainy September 7th and placed on the pad shown above. Since that time, connection to the temporary site power, setup of the two vans and the reenergizing of the system began with the IfA and HTSI team.

An interesting point of working at the Haleakala Observatory is that the crew is required to drive from either sea level or near sea level to the 10,000 foot summit daily. Working conditions with such a daily change in altitude affect how the workers exert effort both mentally and physically. As one never completely adapts to the high altitude, greater concentration in routine physical and mental tasks, are required.

Transition of the TLRS-4 from the HTSI team to the IfA was seamless due to the extensive background in SLR that was retained by the University of Hawaii with key people such as Dan O'Gara and Jake Kamibayashi, the close similarities between the TLRS-4 software architecture and the Hollas system. More significantly, the new TLRS-4 Station Manager, Craig Foreman, spent months in Maryland in the restart effort of the TLRS-4 system and was responsible for many of the modifications of the system to operate in the Haleakala summit environment. Craig's success was ensured by working with the HTSI team especially Maceo Blount who lead the installation team to Maui for the installation and training of the other IfA personal.

Current Status

At the time of this report, the TLRS-4 station setup is completed. During the startup of the system, there was a laser failure that was being troubleshot. Also, during this time, optical alignments were being completed and the other components and subsystems were being verified. Site power to the system was being used on a temporary basis from the Mees Observatory while a permanent source was being developed.

Remaining efforts and future plans for TLRS-4 include completing the System Operational Verification Tests (SOVT), ground calibration testing, satellite tracking and validation of data acquired. Also required actions include completing the site survey analysis and report generation, updating of the Site Log, and completion of the training aspect of TLRS-4 to the IfA crew.

Power switchover to a more permanent solution will require further effort, approval by the cultural observer and contracting with local contractors and the local power company. During this period, the ground field will be enhanced to reduce ground currents on station. Locating an SLR station located at the top of a dormant volcano produce unique grounding opportunities that must be resolved in unique ways.

Conclusion

In conclusion, acknowledgements of the many extra efforts and the dedicated team that worked to reach a successful conclusion to the project that restores an important piece of the global puzzle for the reference frame and for SLR go to NASA with the leadership provided by David Carter. Also to the HTSI Team led by Howard Donovan and his the team of professionals including Don Patterson, Dennis McCollums, Tony Mann, Michael Heinick, Julie Horvath, Bart Clarke, Oscar Brogdon, Maceo Blount, and Craig Foreman. And finally, the team from the University of Hawaii, Institute for Astronomy and the extra efforts provided by Dan O'Gara, Mike Maberry, Jeff Kuhn, Jake Kamibayashi and Les Hieda.

New SLR Station Running in San Juan of Argentina

T. Wang[1], F. Qu[1], Y. Han[2], W. Liu[2], E. L. Actis[3], R. Podesta[3]

1. Chinese Academy of Surveying and Mapping (CASM)
2. National Astronomical Observatories, Chinese Academy of Sciences (NAOC)
3. Observatorio Astronomico Felix Aguilar (FELIX)

Contact: wangtq@casm.ac.cn /Fax:0086-10-68218654

Abstract

The new SLR station in San Juan of Argentina is the result of a kind of cooperation of science and technology between China and Argentina and it was running by the twenty second of February of 2006. The whole SLR system in the station was designed and developed by Chinese Academy of Surveying and Mapping (CASM) and National Astronomical Observatories (NAO) of Chinese Academy of Sciences in the years of 2000 to 2003. The investor for the SLR system is the Ministry of Science and Technology of China. The new station building including the dome in the field of Observatorio Astronomico Felix Aguilar(FELIX), Astronomical Observatories of San Juan National University of Argentina, was designed and constructed by San Juan National University of Argentina. The approximate site position of the station is 31°30´31".050S, 68°37´23".377W and the height is 727.22m. The new SLR facility in San Juan station features a good accurate and prolific SLR system according to the data reports of ILRS data analysis centers. The current status, the future update and some questions for the SLR system in San Juan station are also mentioned in this paper

Background

The new SLR system in San Juan of Argentina is based on the Science and Technology cooperation between National Astronomical Observatories (NAO), Chinese Academy of Sciences and San Juan National University of Argentina. The supporter and investor for the project are the Ministries of Science and Technology of the two countries. In fact, for more than 10 years the Felix Aguilar Astronomical Observatory of San Juan National University of Argentina (OAFA) and National Astronomical Observatories (NAO), Chinese Academy of Sciences have developed friendly cooperation on astronomical research and observation. Under the efforts of the both Observatories the cooperation on cataloguing the Southern Parts of the Earth and astronomy geodynamics using the photoelectric astrolabe MARK II (PA II) has been successful and got lot of interesting results.

At November of 2000, National Astronomical Observatories (NAO), Chinese Academy of Sciences and Felix Aguilar Astronomical Observatory of San Juan National University of Argentina (OAFA) subscribed a cooperation agreement on satellite laser ranging (SLR) to extend the relationship between the two observatories for astronomical observation and research. It is very beneficial to set up a new fixed SLR station in Argentina of South America, which located in the southern parts of the Earth, as the distribution of the SLR stations in the world will be improved better.

According to the agreements of the cooperation the Chinese Academy of Surveying and Mapping (CASM) is responsible for design, developing, installing and debugging of whole SLR system and technical training to the persons from National Astronomical Observatories (NAO) of Chinese Academy of Science and Felix Aguilar Astronomical Observatory of San Juan National University of Argentina (OAFA).The National

Astronomical Observatories (NAO) of Chinese Academy of Science is in charge of packaging of whole SLR system and to ship it to Argentina. And San Juan National University of Argentina with its Felix Aguilar Astronomical Observatory takes charge for whole constructions and decorations of the SLR room including the mobile roof of the building.

The whole SLR system was designed and developed by Chinese Academy of Surveying and Mapping (CASM) and National Astronomical Observatories (NAO) of Chinese Academy of Science in the years of 2000 to 2003 and checked and accepted by China Ministries of Science and Technology at 12th of January, 2004. The main body of the new station building in Felix Aguilar Astronomical Observatory of San Juan National University of Argentina (OAFA) was completed in August of 2005 by San Juan National University of Argentina.

So there are three layers for the scientific and technical cooperation between China and Argentina. The first and top layer, the government layer, is between the two Scientific and Technical Ministries of the two countries and this is on the layer of policy. The second layer is between National Astronomical Observatories (NAO) of Chinese Academy of Sciences and San Juan National University of Argentina and this is on the layer of administration. The third layer is between Chinese Academy of Surveying and Mapping (CASM) and National Astronomical Observatories (NAO) of Chinese Academy of Science and this is on the layer of putting in practice.

Figure 1: *San Juan SLR Station*

Figure 2: *SLR Telescope*

Site Installation

The San Juan SLR station is located in the site of Felix Aguilar Astronomical Observatory in San Juan. San Juan city is 1300km Northwest from Buenos Aires the Capital of Argentina and it is the capital city of San Juan province. San Juan is No.12 of biggest city in Argentina with its population of 20,000 citizens in downtown area. The weather in San Juan region can go up to 50º in summer with very dry character of desert Climate and it is not cold in winter time with the lowest temperature of 5º. There are plenty of fruits and melons in harvest seasons especially the grape. So San Juan is very famous for its good quality and high productivity of the wine.

Felix Aguilar Astronomical Observatory has two observation stations, the Felix Aguilar station and Leonato station. The Felix Aguilar station is about 10 km from the city center of San Juan and the office building of the Observatory is there as well as the

SLR station. The Leonato station near Andes Mountains is 200 km from San Juan city and some astronomical instruments from Germany, America and Spain in use for science and technology cooperation.

So the San Juan SLR station not far from the city San Juan and with 300 good days for SLR observations is a excellent site for astronomical observations. The geographic positions of the site are 31°30´31".050S, 68°37´23".377W and 727.22m. There is an another astronomical device in use for nearly 10 years long the photoelectric astrolabe MARK II (PA II) also cooperated with National Astronomical Observatories of China. The groundwork for the SLR telescope is not good with its screen and sand underground and no base stones within 100 meters in deep.

Installation Time Table

The whole set of the SLR device reached San Juan of Argentina on 6th of Aug., 2005. Then we were waiting for the inspecting from Argentina customs for a month and opened the cargo container on 24th of Sep. From this date to about 20th of Nov., 2005 we were waiting for the decoration of the SLR buildings and for modifying the base pillar of the telescope and the bottom of the laser. On 28th of Nov., 2005 the installing started and the installing ended on 23rd of Feb., 2006 with the first Lageos pass of data returns received last night of the date before. That means we got the first SLR pass of satellites data in San Juan Station on the night of twenty second of Feb., 2006 and sent the data to ILRS and running the station on 23rd of Feb., 2006.

Installation Difficulties

The first difficulty is insufficient for the space of installing. For safety of the transportation from China to Argentina we packaged the whole SLR systems separately to the minimum units. And we needed the base pillar of the telescope and the whole second floor under the dome that must be strong enough and stable enough to the work to do the main mirror and second mirror installing and debugging. But the base pillar still needed to repair and the second floor under the dome was made of thin wood board

***Figure 3**: Installing and debugging*

so the mirrors installing and debugging have to be in a big storage. It was not easy to do such a kind of working in a storage so it takes our nearly a month.

The second thing is the Base pillar of the telescope not fit with the telescope in height and orientation. So we have to change the height of concrete base pillar and some holes in positions and sizes. And that is very hard to do. Base for laser platform is too high and we spend lot of energy to cut the base by electric drilling machine.

Figure 4: *Base of laser platform and Base pillar of the telescope modifying*

Decoration for whole laser building not finished. So we have to do the installing and debugging for the SLR system and the decorating for the SLR building at same time. The mobile roof of the telescope we call it “dome” moves unreasonable. That repeatedly made problems with us and not safe as well.

Installation Personnel

Professor T. Wang from Chinese Academy of Surveying and Mapping (CASM) is responsible for whole installing and debugging and in charge of optics and telescope star calibrations. Professor T. Guo from Institute of Seismology, China Earthquake Administrations is responsible for electronics design and installing. Senior engineer W. Liu from National Astronomical Observatories of China is responsible for electronics and laser installing, debugging and daily maintain. Senior engineer D. Huang also from National Astronomical Observatories of China is responsible for installing and daily observations. Engineer Q. Xiang from Chinese Academy of Surveying and Mapping (CASM) is responsible for installing and daily observations. Senior engineer A. Gonzalez from Felix Aguilar Astronomical Observatory of San Juan National University of Argentina (OAFA) is responsible for electronics installing and The daily observation and maintains. Senior engineer R. Podesta from Felix Aguilar Astronomical Observatory of San Juan National University of Argentina (OAFA) is responsible for daily observations and maintains. Senior engineer E. L. Actis from Felix Aguilar Astronomical Observatory of San Juan National University of Argentina (OAFA) is responsible for daily observations and maintains. Senior engineer E. Alonso from Felix Aguilar Astronomical Observatory of San Juan National University of Argentina (OAFA) is responsible for daily observations and maintains. Senior engineer

Figure 5*: The San Juan SLR Station Team*

A. M. Pacheco from Felix Aguilar Astronomical Observatory of San Juan National University of Argentina (OAFA) is responsible for daily observations and maintains.

Daily Observations and Maintenance

To Argentina side: Monday through Wednesday 4 persons are shift on duty for observations but every day a Chinese people must be present at beginning.
To China side: Thursday to Sunday 3 persons are shift on duty and every day the free person in china side is in charge of cleaning, cooking and shopping for their living. So the work is heavy for every one.

Hope:

We hope getting 6000 passes of satellite data from all SLR satellites a year including 1200 passes from satellites Lageos-1 and Lageos-2 each year. And we hope the all data we get will have good quality.

Figure 6: *Daily Observations and review*

Problems and Questions:

The San Juan SLR station can get 6000 passes of satellite data from all laser satellites per year and they are all night productivities. That means the SLR system in San Juan station has no daytime ability now. This question refers to the laser system itself and we need a stable laser to finish the daytime ability to the SLR system.

In San Juan station the Laser is not only unstable and the spare parts damaged badly. Maybe in the laser system there are some designs unreasonable and we need to adjust the laser system every 3 or 4 days. We have only 3 sets of spare mirrors for the laser and short time after they are all damaged. So recently we have to change the positions of the damaged mirrors maintaining the laser beam output with very unstable some times. This is the second problem in San Juan station.

Some times different persons produce different quality for the data due to laser instability. Not every person can be in control of the laser adjusting so different data quality was produced in the people's shift of on duty from time to time. Dome moves difficulty and not safety are the problems and questions also. At beginning the data have big range bias due to the damaged chip in timing circuit board and now it is ok by change the chip. Running is more difficult compare to in China due to the delay of time for the spare parts transportation from China to Argentina.

Future Plan

The National Astronomical Observatories (NAO) of Chinese Academy of Sciences and Felix Aguilar Astronomical Observatory of San Juan National University of Argentina (OAFA) and Chinese Academy of Surveying and Mapping (CASM) will continue cooperate to the updating of SLR system in San Juan in the near future. The upgrading in first step is to change the SLR system to a new generation system that means we will have KHz and daytime ranging ability of course the semiconductor pumped laser as well.

But it is not soon due to the three layers cooperation and time is needed for finance support from the government and also the performance and the development of the new system need lot of time to do lot of things from China to Argentina.

The Instrumentation

The System Profiles:

The telescope was mostly rebuilt in a storage in San Juan station. It consisted of a Cassegrain receiving telescope of 60 cm aperture and a separated Galilei Telescope which collimated the laser beam with a factor of about 4.

The control computer is a common PC, even a notebook can be also, under windows operating system. All programs like satellite predictions, tracking the targets, ranging the data, data preprocessing and send the data to ILRS etc. are running on the same machine. The control computer is connected to the control interface box by parallel line and the servo system accessed to the control interface box by serial communications.

- Laser system is a Nd:YAG passive mod-locked dye laser with 30ps pulse width and single pulse energy of 30mj in green light.
- The detector is Compensated Single Photon Avalanche Diode (C-SPAD) from Czech Technical University.
- Stanford Counter SR-620

- TV system is Image Intensifier plus CCD and it collect the star and laser beam image by the main receiving telescope.
- Timing and frequency is by HP58503A GPS time and frequency receiver.
- Calibration short distance target, out-install, inside the dome.

The frame diagram of profiles for the whole system is shown as following diagram.

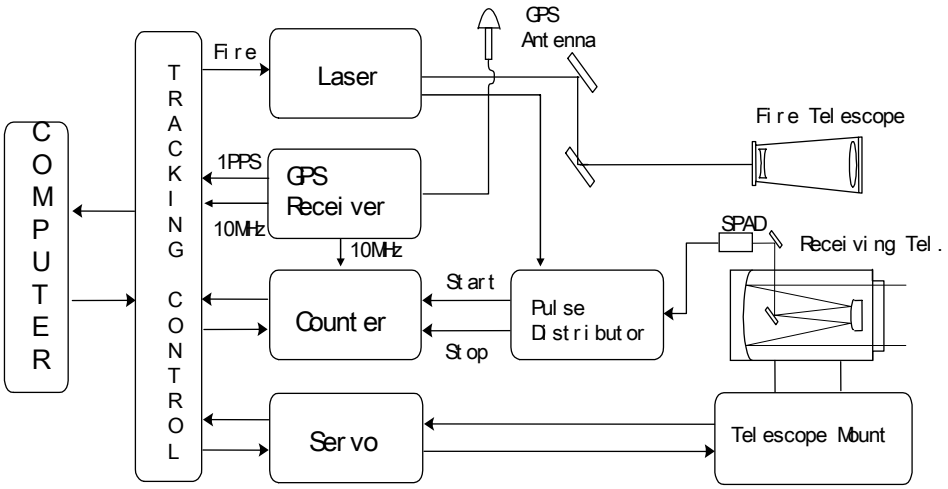

Figure 7: The frame diagram of profiles for the system

***Figure 8**: Control Room for SLR*

***Figure 9:** The Laser System*

***Figure 10**: The short distance Ground Target*

***Figure 11**: Monitoring Screen*

Optical System:

The optical receiving system has a microcrystalline glass main mirror (weight 80kg) with the diameter of 630mm and a microcrystalline glass secondary mirror with the diameter of 200mm. Also there are a spectroscope, an adjustable set of pinhole, an autocollimator and a broadband filter of 10nm in the optical receiving system. The optical receiving system is able to receive both visible light for ICCD and green laser for ranging detector without any additional adjustment due to the spectroscope.

For the transmitting path the laser beam can be guided to the Coude path via 2 reflecting mirrors and a beam expander of 2 times from the laser platform. The Coude path has 6 reflecting mirrors and from the Coude path the laser beam is guided to 16 cm diameter transmitting telescope and to the satellites.

The optical receiving and transmitting path can be shown as following drawing:

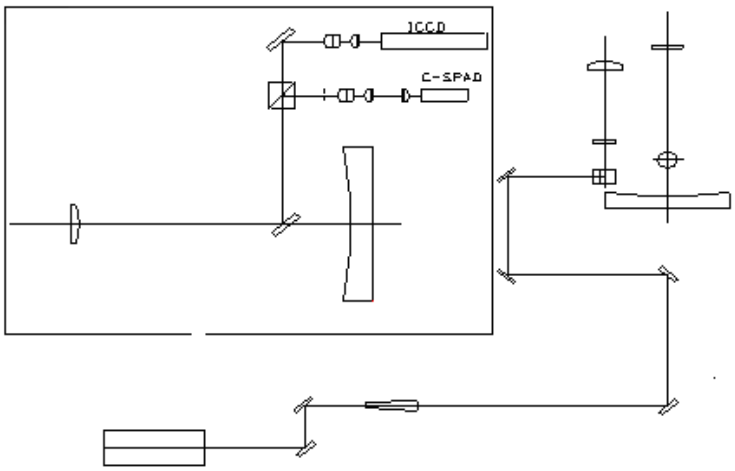

Figure 12: *Optical TR path.*

Laser System:

The computer controlled passive mode-locked laser (Nd: YAG) firing rate up to 10Hz has the pulse width of 30ps and pulse energy of 30mj for wavelength 532nm laser. It is produced by Shanghai Optics and Electronics Institute. The principle diagram of the laser is shown as following diagram:

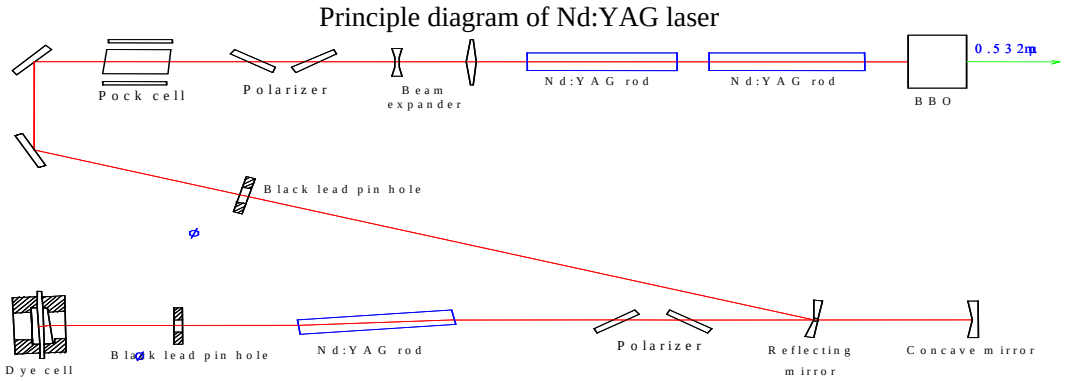

Figure 13: *Laser System.*

Tracking Control and Servo:

A common PC computer is used for telescope control, range gate setting, laser firing and data acquisition etc. All software including satellite predictions and data pretreatment is running in windows operation system and all things can be done just by the computer mouse.

Summaries

The New SLR station in San Juan of Argentina has being running since 23rd of Feb. 2006 and up to 30th of Sep. 2006 nearly 4000 passes of SLR data were sent to the analysis centers of ILRS including 799 Lageos passes and 509 high satellite passes in about 7 months (220 days) from the 2006 3rd quarter report of SLR Global Performance Report Card. That means the San Juan station has the possibility to get 6450 passes for all SLR satellites including 1325 Lageos passes and 844 high satellite passes.

Especially for the Galileo satellite GIOVE-A the San Juan station got 36 passes and it is the number 2 in the quantity line of GIOVE-A satellite by stations only following the station 7090 Yarragadee in Australia which got 45 passes.

The data quality is also very good with the calibration, satellite and Lageos precisions (RMS) of 12.4, 11.0 and 13.3 mm also from from the 2006 3rd quarter report of SLR Global Performance Report Card.

The fact above can prove the cooperation of science and technology between China and Argentina in the field of Satellite Laser Ranging is excellent successful. The SLR system in San Juan station developed by the scientists of China and Argentina has fine capability and stability although the laser is not stable and needs lot of work to maintain. The weather in San Juan station is very good we can say and be reassurance about it.

There are lots of acknowledgments to Professor Guo Tangyong from Institute of Seismology of China Earthquake Administrations and the people from Shanghai SLR station and other stations in China Laser Tracking Network for their efforts in the project.

System Improvement and GIOVE-A Observation of Changchun SLR

ZHAO You[1], FAN Cunbo[1], HAN Xinwei[1], YANG Dingjiang[2], CHEN Nianjiang[2], XUE Feng[2], GENG Lin[2], LIU Chengzhi[1], SHI Jianyong[1], ZHANG Ziang[1], SHAO Baodong[1], ZHANG Haitong[1], DONG Xue[1,3]

1. National Astronomical Observatories/Changchun Observatory, CAS
2. North China Research Institute of Electro-Optics, CGI, Beijing
3. Graduate University of Chinese Academy of Sciences, Beijing

Abstract

This paper introduces the system improvement for tracking GIOVE-A in Changchun station. During the more than two months improvement, the new servo and encoder systems were installed. And primary mirror, second mirror and some other mirrors have been cleaned and recoated. The laser system was adjusted in order to improve the laser efficiency and output. The paper gives out the improvement results, and the GIOVE-A satellite observation results.

Key Words: *system improvement, GIOVE-A observation, SLR*

Introduction of project background

Galileo system consists of 27 satellites distributed in three uniformly separated planes. In 2006, two GSTB-V2 satellites were planned in orbit. The nominal lifetime is 2 years. Four IOV Galileo satellites were planed to be launched towards the end of 2007. Full Deployment Phase and Long Term Operation will be followed the IOV. Galileo In-Orbit Validation Element (GIOVE) satellites: GIOVE-A and GIOVE-B. The objectives of the deployment of these two satellites are to:

- secure use of the frequencies allocated by the International Telecommunication Union (ITU) for the Galileo system
- verify the most critical technologies of the operational Galileo system, such as the on-board atomic clocks and the navigation signal generators
- characterize the novel features of the Galileo signal design, including the verification of user receivers and their resistance to interference and multipath, and
- characterize the radiation environment of the medium-Earth orbit (MEO) planned for the Galileo constellation.

GIOVE-A and -B were built in parallel to provide in-orbit redundancy and to secure the mission objectives. They provide complementary capabilities. GIOVE-A was launched on December 28, 2005, into an MEO with an altitude of 23,260 kilometers. Carrying a payload of rubidium clocks, signal-generation units, and a phase-array antenna of individual L-band elements, GIOVE-A started broadcasting on January 28, 2006, securing the frequencies allocated by the ITU for Galileo. Performance of the on-board atomic clocks, antenna infrastructure, and signal properties is evaluated through precise orbit determination, supported by Satellite Laser Ranging (SLR), an independent high-precision range measurement technique for orbit determination based on a global network of stations that measure the round-trip flight-time of ultra short laser pulses to satellites equipped with laser retro reflector arrays (LRAs). SLR provides instantaneous range measurements of millimeter-level precision which can be compiled to provide accurate orbits and to measure the on-board clock error.

Fig.1. *Changchun SLR telescope*

Due to the urgent need, it is necessary to select an existing SLR station to provide laser ranging service for GSTB-V2 satellites. Given the importance of SLR data for the characterization of the GIOVE clocks, the People's Republic of China contributed to the Galileo program the refurbishing of a Chinese SLR station to provide GIOVE laser-ranging observations. The Changchun station in northeast China was selected among the Chinese stations contributing to the ILRS because it had demonstrated strong MEO satellite tracking; collocation with an existing International GPS Service station; and good weather conditions. There are 5 fixed SLR stations in China nowadays. Among the stations, Changchun station possesses the best performance. Its data quantity is the most in China. It has the ability to range to the distance more than 20,000km with the accuracy less than 2cm. So Changchun SLR Station is selected to service for Galileo in the early stage. Followings are photos of Changchun station and SLR telescope:

Fig.2. *Bird view of Changchun station*

Changchun Observatory (ChO) of National Astronomical Observatory, Chinese Academy of Sciences, is a member of global SLR and GPS networks. It started Satellite Laser Ranging (SLR) since the early of 80th last century. The third generation of SLR in ChO was established during 1985. The system has the ability of tracking satellites with the distance of more than 20000km. Single-shot RMS is less than 2cm. From years ago, ChO SLR has been the best one in Chinese network, and got the No.10 rank in the

global SLR network. It is also an important and high performance station in the International Laser Ranging Service (ILRS). According to the report of ILRS, ChO SLR has the ability of tracking the high orbit satellites, such as Glonass, Etalon and GPS which have orbit height more than 20000km. Based on the Galileo satellite orbit height and the effective area of Laser Retro-Reflectors Array (LRA), the strength of return signal from Galileo satellites will be similar to that from GPS or Glonass satellites. So ChO SLR has the ability of tracking Galileo satellites.

Contents of SLR improvements

Though ChO SLR has the ability of tracking the high orbit satellites such as Glonass, Etalon, GPS and Galileo satellites, it can only get less return signal from above satellites. This is caused by the following causes:

- The coated film of the primary mirror and second mirror are damaged seriously, and now they have low reflectivity.
- The tracking system has lower precision. The mount of the telescope shakes so hard that less data can be obtained from high orbit satellite.
- The energy of output laser pulse is a little low.

Following is the Changchun SLR system structure. The dark color parts are the parts which are to be refurnished for GIOVE-A observation.

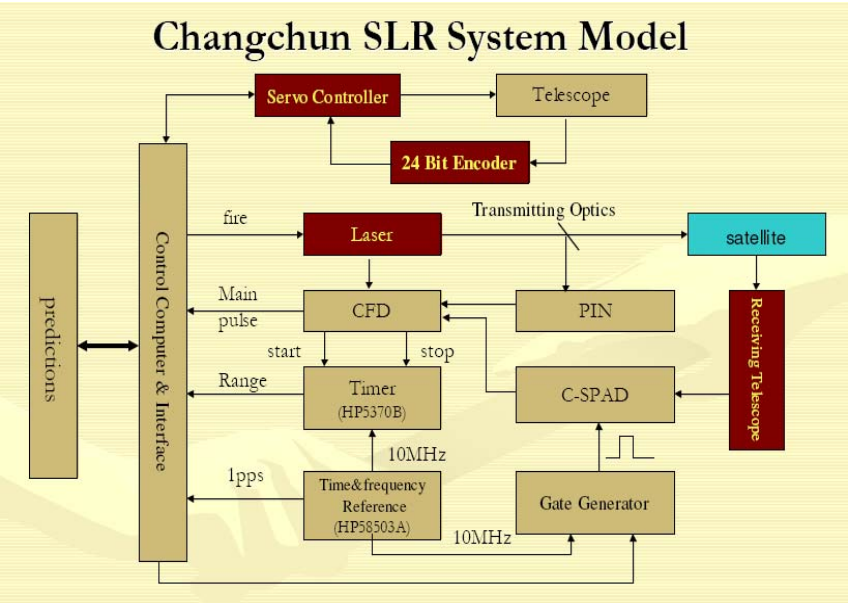

Fig.3. *Changchun SLR System*

If these parts were not improved, it would be very difficult for us to get more data from Galileo satellites and to support a long-term tracking of the satellites routinely. In order to track the Galileo satellites and get more SLR data with high precision, the following things will be done in short-term:

- Telescope. Primary mirror and second mirror of the receiving telescope must be recoated, tested, adjusted and calibrated. This will result in higher transparency of the receiving optics.
- Encoder. A new type photoelectric encoder will be installed in the tracking mount to replace the old one. This will improve the resolution of the angular sensor of the

tracking mount. This can be done in the same period with the telescope modification.

- Servo System. A new type of servo driver will be used to improve the telescope tracking performance. This will heighten the tracking precision.
- Laser System. The old laser components will be replaced in order to heighten the laser output energy up to 70-100mj and improve output stability. This will greatly increase the number of photons reflected back from the satellites.

After the system improvement, the tracking system can have less than 2" tracking precision for high orbit satellites, the output laser energy will be stronger. And these will benefit to improve the return rate and the tracking capability for high orbit satellite of ChO SLR. Finally, the system can execute the Galileo mission and get more data routinely.

Table 1. *System Specifications*

Label	*Unit name*	*Spec. name*	*Spec*	*Listed in Addendum*	*To be Tested*	*Reason*
M1	Mirrors	Reflectivity of Primary Mirror	≧98% (532nm)	Yes (p17)	Yes	
M2	Mirrors	Reflectivity of Secondary Mirror	≧99% (532nm)	Yes (p17)	Yes	
M3	Mirrors	Reflectivity of 45° Mirror	≧99% (532nm)	Yes (p17)	Yes	
E1	Encoder	Temperature Characteristics	Independent	Yes (p18)	No	Determined by principle (digital electro-optic encoder)
E2	Encoder	Current	Tens of mA	Yes (p18)	No	It's a middle spec and can be reflected by accuracy
E3	Encoder	Resolution	0.078″	No	Yes	It's critical spec of a encoder
E4	Encoder	Accuracy	σ≤1"	No	Yes	It's critical spec of a encoder
E5	Encoder	Sampling rate	500Hz	No	Yes	It's critical spec of a encoder
S1	Servo	Elevation Max Speed	8°/s	Yes (p18)	Yes	
S2	Servo	Elevation Max Acceleration	12°/s^2	Yes (p18)	Yes	
S3	Servo	Elevation Min Speed	<5″/s	Yes (p18)	Yes	
S4	Servo	Azimuth Max Speed	10°/s	Yes (p18)	Yes	
S5	Servo	Azimuth Max Acceleration	15°/s^2	Yes (p18)	Yes	
S6	Servo	Azimuth Min Speed	<5"/s	Yes (p18)	Yes	
L1	Laser	Pulse Energy	80mJ	Yes (p18)	Yes	

Performance after improvement

Table 1 lists the specifications to be tested after system refurbishment and the results. All are met the specified value. After recoated, the reflectivity and transparency of the mirrors for 532nm are as follows: primary mirror: 97.29%; second mirror: 99.049%; dichroic mirror: 99.55%; 45°reflector: 99.83%. After system modification, tracking speed and stability of the system greatly improved and output laser energy increased from 30mj to 100mj. Ranging ability increased obviously and points and passes from high satellites increased.

Following are the photos to show the recoated primary mirror, new operation console, laser output on screen, and the encoder system.

The recoated primary mirror

New operation console

Laser output on monitor

New encoder system

Up to Dec.12 of 2006, there are 28 passes of GIOVE-A and 12 passes of GPS-35, -36 to be tracked. Refurbishing work had been finished and acceptance tests were underway. The observations performed by Changchun at the time of the campaign were included in the data set as the data revealed itself to be of high value for the analysis carried out. The geographical location of Changchun (see Figures 4) was of primary importance in providing better laser-ranging coverage of GIOVE-A.

Fig.4. *World map showing geographical distribution of the first GIOVE-A ranging campaign*

Acknowledgement

The authors would like to thank Prof. WANG Jianli, Prof. XU Zhijun (Changchun Institute of Optics, Fine Mechanics and Physics, CAS); Prof. YANG Fuming, Prof. CHEN Wanzhen (Shanghai Astronomical Observatory, CAS); Prof. WANG Tanqiang (Chinese Academy of Surveying and Mapping) who partially participate in the work and their kind help.

The authors gratefully acknowledge the support of K.C.Wong Education Foundation, Hong Kong.

References

[1] Acceptance Test Plan for Phase I of Galileo Project in Changchun Station.

[2] Satellite Laser Ranging For Galileo Project in Changchun Station.

[3] Zhao You: “Upgrade of Changchun SLR System”, Proceedings of 11th International Workshop on Laser Ranging, Sep. 1998 Deggendorf, Germany, pp. 188-196.

[4] Yang Fumin, Xiao Zhikun, Chen Wanzhen, et al, “Design and Observations of the Satellite Laser Ranging System for Daylight Tracking at Shanghai Observatory”, Science in China Series A, Vol 42, No. 2, pp 198-206, 1999.

[5] You ZHAO, Cunbo FAN, Chengzhi LIU, Xinwei HAN, Jianyong SHI, Xinhua ZHANG, Haitao ZHANG: “System Stability Improvement of Changchun SLR”, Proceedings of 13th International Workshop on Laser Ranging, Oct. 2002, USA.

[6] ILRS publications SLR Station Performance Report Card 2005, on the Internet.

[7] You Zhao, Cunbo Fan, Xinwei Han, Chengzhi Liu, Xinhua Zhang, Jianyong Shi: “Progress for daylight tracking in Changchun SLR system”, Proceedings of 14th International Workshop on Laser Ranging, June of 2004, Spain, pp 179-182.

[8] Marco Falcone, Daniel Navarro-Reyes, Jörg Hahn, Michiel Otten, Ricardo Piriz, Mike Pearlman: “Satellite Laser-Ranging Campaigns”, GPS World, Nov 1, 2006.

ADVANCED CONCEPTS AND TIME TRANSFER SESSION SUMMARY

Chair: Hiroo Kunimori

New applications using all or part of SLR instrumentation were the subjects of papers presented in this session. SLR was born and has grown up in the fields of geodesy, geodynamics, and orbital mechanics, and since then has interacted with many other fields to open up new applications and users. In addition to the obvious value of SLR as a contributor to fundamental physics, geodesy and the reference frame, each organization has its own interests to use SLR for different applications. Here we have 5 oral papers and 3 poster papers including Time Transfer, Communications, Radio Astronomy, Lidar and NEO Tracking.

Time Transfer

"Progress on Laser Time Transfer Project" by Y. Fumin et al described the China LTT mission on a satellite, hopefully to be approved in the next three months. It uses dual SPAD, TDC module and Laser Retroreflector Array. The engineering model and testing are in progress. The experiment is now planned only within the China network.

"T2L2 Status Update" by E. Samain, F. Deleflie et al gave news of the Time Transfer by Laser Link project, a LASSO follow-on mission at last approved for the JASON-2 mission for 2008 launch, 30 years after the concept was made. Tests using the space segment engineering model and the ground prototype are ongoing, and an international network is being modelled.

"New Application of KHz Laser Ranging: Time Transfer by Ajisai" by T. Otsubo et al presented a simulation study for AJISAI TT revised 14 years after the concept was introduced in equation form, including a search algorithm and link budget in the KHz SLR era.

Communications

"Satellite Tracking Demonstration on Ground Using 100mm Aperture Optical Antenna for Space Laser Communication" by H. Kunimori et al described how SLR using optical communications equipment were present in a course of development of a next-generation Laser Comm terminal, and present-generation LEO-GND Laser Comm was described.

Also, in another session, a free space Laser Comm experiment over ocean over 10 miles was presented.

Radio Astronomy

"Possibility of Laser Ranging Support for the Next-Generation Space VLBI Mission ASTRO-G" by T. Otsubo et al discussed the role of SLR in POD at altitudes higher than GPS, and the engineering problems.

LIDAR

"LIDAR Experiments at the Space Geodesy Facility, Herstmonceux, UK" by G. Appleby et al.

NEO Tracking and Monitoring

"Electron Multiplying CCD Camera Performance Tests" by D. Lewova et al.

"Possibility of Near Earth Objects Distance Measurement with Laser Ranging Device" by M. Abele and L. Osipova.

Progress on Laser Time Transfer Project

Yang Fumin[1], Huang Peicheng[1], Chen Wanzhen[1], Zhang Zhongping[1], Wang Yuanming[1], Chen Juping[1], Guo Fang[1],Zou Guangnan[2], Liao Ying[2], Ivan Prochazka[3], Karel Hamal[3]

1. Shanghai Observatory, Chinese Academy of Science, Shanghai, China
2. China Academy of Space Technology, Beijing, China
3. Czech Technical University in Prague, Czech Republic

Abstract

The purposes of the Laser Time Transfer (LTT) experiment are to synchronize the atomic clocks in space to ones on the ground, and to verify the relativity theory. The LTT payload in space includes a dual-SPAD detector, a timer based on TDC device, control unit and a LRA. The expected uncertainty of measurement of clock differences for single shot is about 200ps, and the uncertainty of measurement for the relative frequency differences for two rubidium clocks is about 5×10^{-14}/ 1000 seconds. The LTT flight module is ready and is waiting for the flight mission in 2007-2008.

Introduction

Based on the successful time transfer by laser pulses between ground stations in 2003[1], the Laser Time Transfer (LTT) project between satellite and ground stations was initiated in 2004. The goals of the LTT are as follows: 1) Evaluation of performance of space clocks which are rubidium's now, and will be hydrogen clocks in the future. 2) Verification of the relativity

Shanghai Astronomical Observatory, in cooperation with the China Academy of Space Technology in Beijing, has been in charge of the LTT project. The Philosophy of the project is to make a payload as simple as possible on a satellite in a short time to verify the capability of the time transfer by laser pulses between space and ground clocks. So, a simple 40um SPAD detector with 100ps timing resolution[2] and the TDC devices with lower resolution(125ps)[3] have been chosen for the space module. The LTT project has kept going smoothly since 2004. The flight module has been built and has passed the space environmental testings.

Principle of LTT

Fig.1. shows the principle of LTT. ΔT –time difference of second pulses between space and ground clocks. T_G – time interval between the transmitting laser pulse and second pulse of the ground clock. T_S – time interval between the received laser pulse and second pulse of the space clock. τ – flight time of laser pulse between ground station and satellite. So we have:

$$\Delta T = \frac{\tau}{2} - T_G - T_S$$

where the relativity effect, system delays, atmospheric correction and so on are not included.

Fig.2. shows the block diagram of LTT. There are three main parts onboard: detector, timer and retro-reflectors.

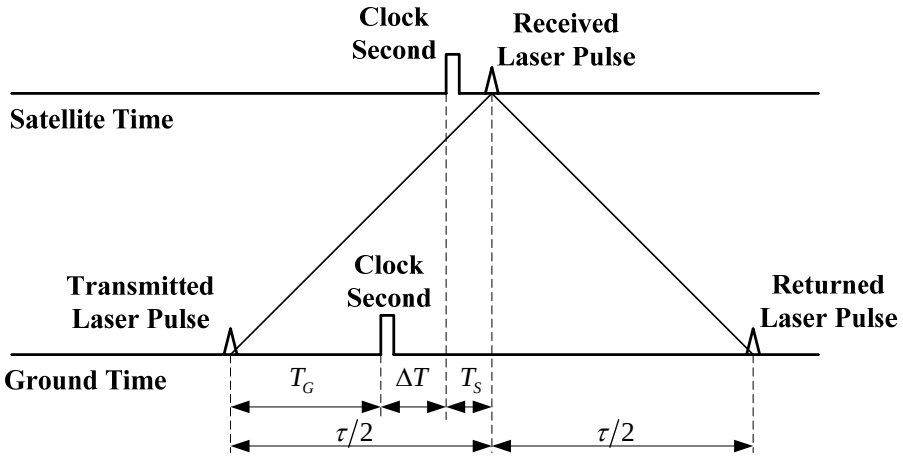

Fig.1. *Principle of Laser Time Transfer*

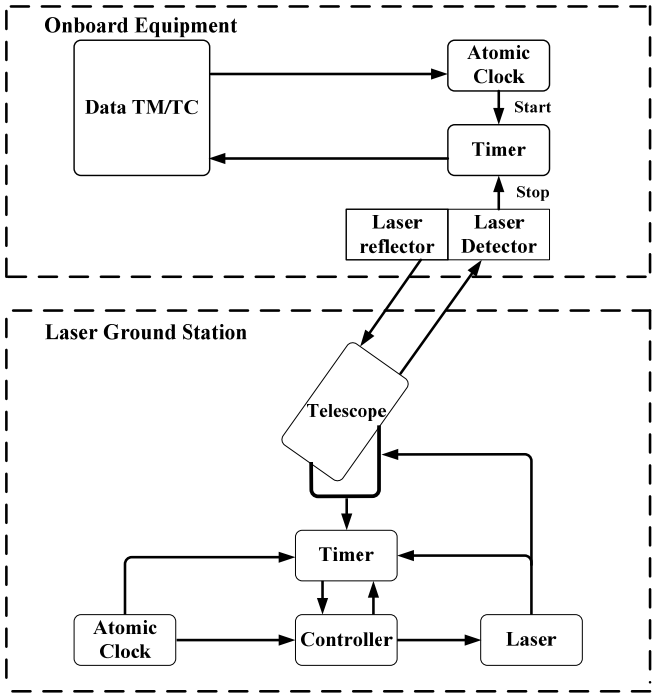

Fig.2. *Diagram of LTT*

Specifications of space module

Laser Reflector Array (LRA)

The LTT module will be installed on the satellite with an orbital altitude of about 20000km. The LRA made by Shanghai Astronomical Observatory has a planar panel with 42 retros. The single retro has an aperture of 33mm without coating on back surfaces. The LRA has the reflective area of 360cm2, and total mass of 2.5kg.

LTT module

Fig.3. is the block diagram of the LTT module. The detector is 40um SPAD made by the Czech Technical University.

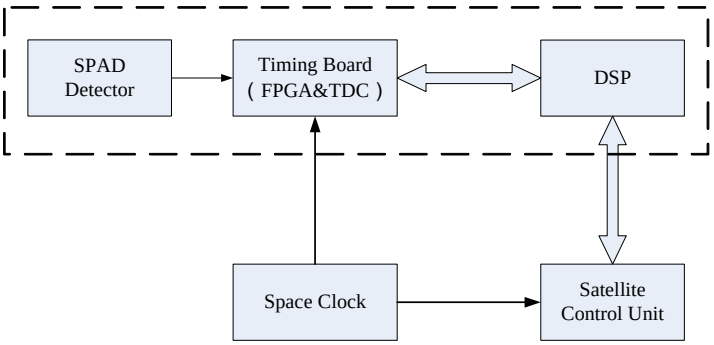

Fig.3. *Block Diagram of LTT Module*

The Specification of the detector is as follows:

- Configuration dual photon counting detector based on Silicon K14 SPAD
- active area circular 25 um diameter
- timing resolution < 100 psec
- operating temp. -30ºC~ +60ºC, no cooling, no stabilisation
- power consumption < 400 mW
- optical damage th. full Solar flux 100 nm BW > 8 hr
- lifetime in space > 5 years

Fig.4. shows the LTT detector. There are two SPAD detectors in the box, one is for spare part and can be switched by telecontrol command from ground. There aren't any lenses in front of the SPAD chips, so the receiving area on board is 40um SPAD chip only. The field of view of the detector is about 30º. There is a 10nm bandwidth filter in front of the SPAD chips.

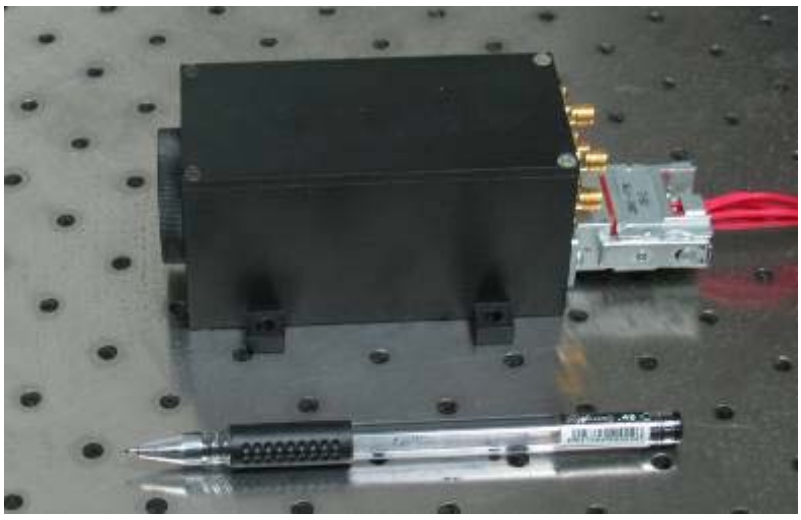

Fig.4. LTT Detector

The received photons onboard NP can be estimated by:

$$N_P = \frac{4 \cdot E \cdot S \cdot A_P \cdot K_t \cdot K_r \cdot T \cdot \alpha}{\pi \cdot R^2 \cdot \theta_t^2}$$

where

E: Laser pulse energy, 50mJ (532nm)

S: Number of photons per joule (532nm), 2.7×10^{18}

A_P: 40μm SPAD without any lenses, diameter of active area, 0.025mm
Kt: Eff. of transmitting optics, 0.60
Kr: Eff. of receiving optics, 0.60
T: Atmospheric transmission (one way), 0.55
R: Range of satellite, for MEO orbit at elevation 30°, 22600Km
θt: Divergency of laser beam from telescope, 10 arcsec
α: Attenuation factor, 0.5

We have, Np=7.0 (Photons)

It can be detected by the 40 μm SPAD detector.

The principle of the LTT timer is shown in Fig.5. The main device is TDC (Time Digit Converter) made by ACAM company in Germany. The TDC-GP1 with resolution of 125ps which had passed the radiation testing in Germany was adopted. Fig.6. shows the LTT timer.

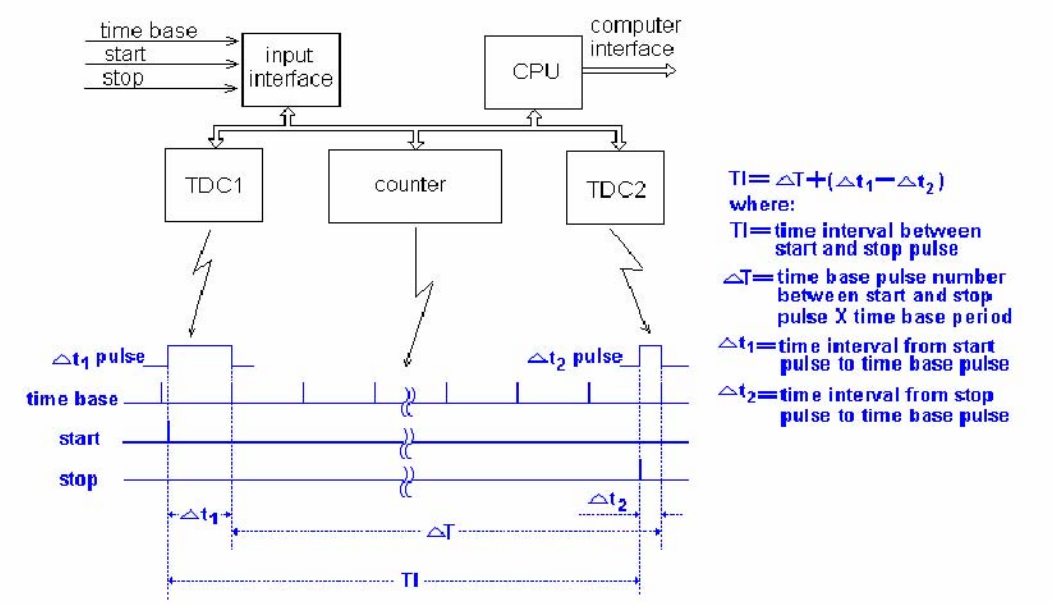

Fig.5. *Principle of the LTT Timer*

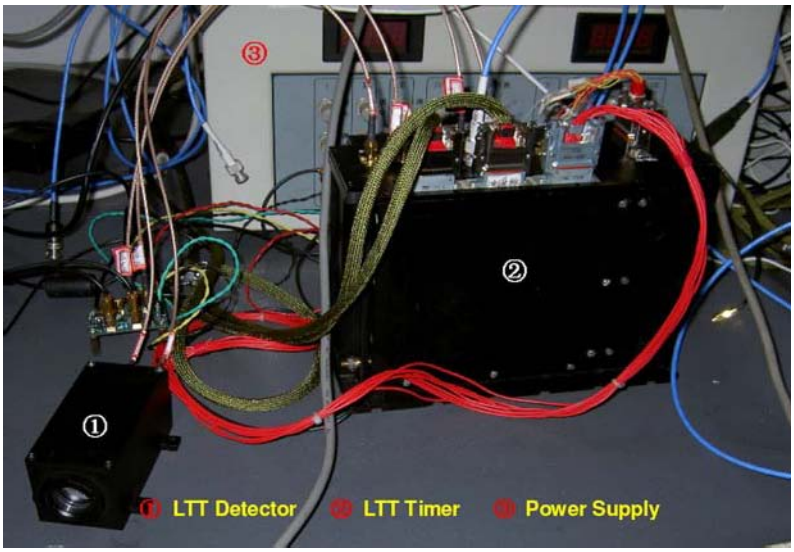

Fig.6. *LTT Timer and Detector*

The specification of the LTT timer is as follows:

- Resolution of timing 10ps
- Precision of timing 100ps
- Mass (dual-timer) 4.3Kg
- Power consumption 17W
- Size 240×100×167mm

Laser firing control for ground stations

For simplification of the module, a 40um SPAD detector without gating circuit and cooling was adopted. In order to keep from the noises produced by the albedo of the ground and the atmosphere, and the detector itself, the ground station will be asked to control strictly the laser firing epoch according to the flight time from ground station to the detector onboard, and let the laser signals arrive at the detector just after the second pulses of the clock onboard, which will start the timer onboard, by 200 ns or so. The laser pulses will stop the timer. So, it is equal to have a gate onboard.

To meet the timing requirement, the laser on the ground station should be actively switched, and the passive switch (or active-passive) can not be used. The accuracy of the prediction of the satellite's range will be about 10m, it equals to 67ns. The uncertainty of laser firing pulses can be controlled within 10ns. The prediction of the difference between the space clock's second and the ground clock's one will be better than 20ns. So we can actually control the received laser pulses with relative to the second pulses of the space clock. Therefore, it means that the time intervals among the laser firings at the station are not constant, and will vary with the distances between the ground station and the satellite.

Ground testing for timing accuracy of LTT module

Fig.7. is the block diagram for the ground testing on the timing accuracy of the LTT module. The specifications of the equipment for the testing are as follows:

- MicroChip Laser
  - Output performance
    - Output power 3μJ
    - Pulse width 650ps
  - Repetition rate 1-100Hz
  - Dimensions (L×W×H) 150×36.4×31mm
  - Weight: 250g
- Rubidium Standard 2 sets, Datum 8000
- Counter (SR620) 2 sets, Stanford Research

Fig.8. and Fig.9. show the instruments for the testing. Table 1 shows the measurement results of the ground testing.

As shown in Table 1, the accuracy of the time difference measurement is 196ps (rms). In Fig.10, line 1 is the result of clock differences by LTT, and line 2 is by the timer SR620 directly. The slope rates of the two lines are: -2.3279×10^{-10} and -2.3285×10^{-10} respectively, and they are coincident very well.

Fig.11. shows several LTT results with 2 sets of Rb clock. The uncertainty for measuring relative frequency difference is about 4×10^{-13} in 200 second and about 5×10^{-14} in 1000 seconds.

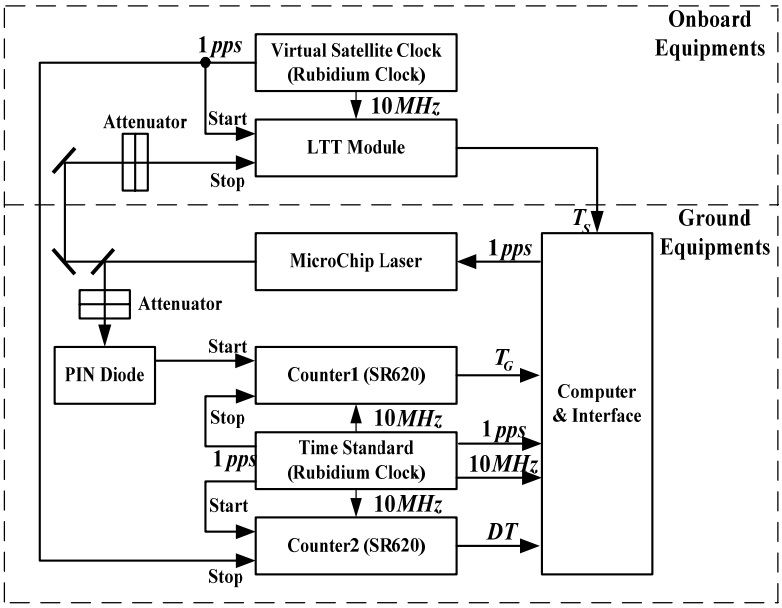

Fig.7. *Diagram of the Testing*

Fig.8. *Ground Testing Instruments*

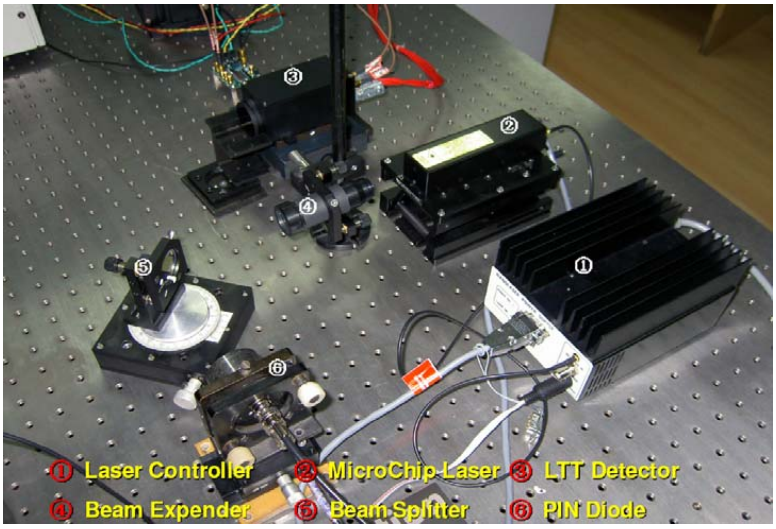

Fig.9. *MicroChip Laser and transmitting Optics*

Table1. *Result of the Ground Testing*

Epoch(s)	(1) Clock Difference by Laser(ns)	(2) Clock Difference by Counter (ns)	(1) (2) (ns)	RMS(ps)	Number of Measurement
3508.7	250300.4	250264.7	35.754	178.4	104
3953.8	250196.3	250160.5	35.783	190.6	139
4246.1	250128.3	250092.6	35.742	165.3	136
4588.9	250048.6	250012.8	35.748	266.7	148
5022.8	249946.8	249911.1	35.751	212.9	84
5498.9	249836.3	249800.5	35.792	73.1	56
5736.5	249781.4	249745.7	35.731	231.2	96
5923.8	249737.7	249702.0	35.687	224.1	103
6187.9	249676.3	249640.7	35.619	199.8	90
6374.8	249633.0	249597.5	35.488	221.6	96
Mean			35.709±0.092	196.4	

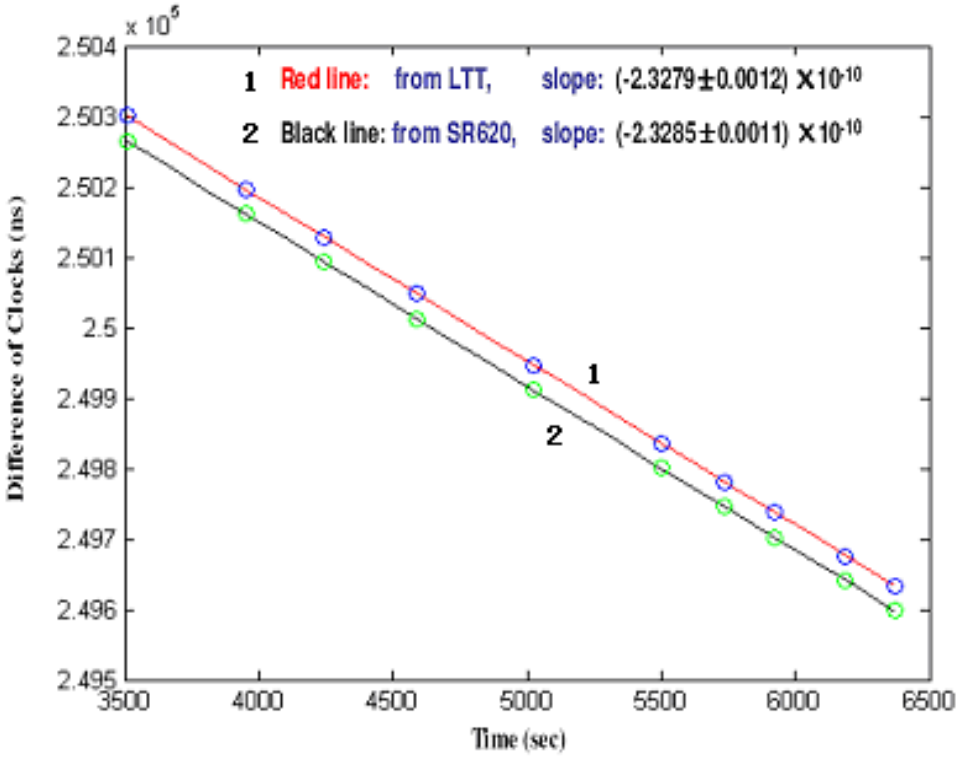

Fig.10. *Results of LTT with two Rb Clocks*

Space Environment Testing

The LTT module has passed the following testing: vibrations, shock, acceleration, thermal circulation, -40--65ºC, thermal vacuum, -40--65ºC, EMC and long term testing in high temperature.

Conclusions

The flight module for Laser Time Transfer experiment has been completed and is waiting for the mission 2007-2008. With the built-in spare parts together, the characteristics of the flight module are as follows:

- Mass 4.6Kg
- Power consumption 17W
- Dimensions:

  - 240×100×167mm (dual-timer, interfaces and power supply)
  - 105×70×50mm (dual-detector)
- Uncertainty of measurement for the relative frequency differences by laser link for two rubidium standards:
  - 4.0×10^{-13} in 200 seconds
  - 5×10^{-14} in 1000 seconds

References

[1] Yang Fumin, Zhang Zhongping, Chen Wanzhen, Li Xin, Chen Juping, Wang Bin, Time Transfer by Laser Pulses between Ground Stations, 14th International Workshop on Laser Ranging, San Fernando, Spain, 7-11 June, 2004

[2] Ivan Prochazka, Karel Hamal, Lukas Kral, Yang Fumin, Photon Counting Module for Laser Time Transfer Space Mission, 15th International Workshop on Laser Ranging, Canberra, Australia, 15-20 October, 2006

[3] TDC-GP1 User Guide, http://www.acam.de/Documents/English/DB_GP1_e.pd

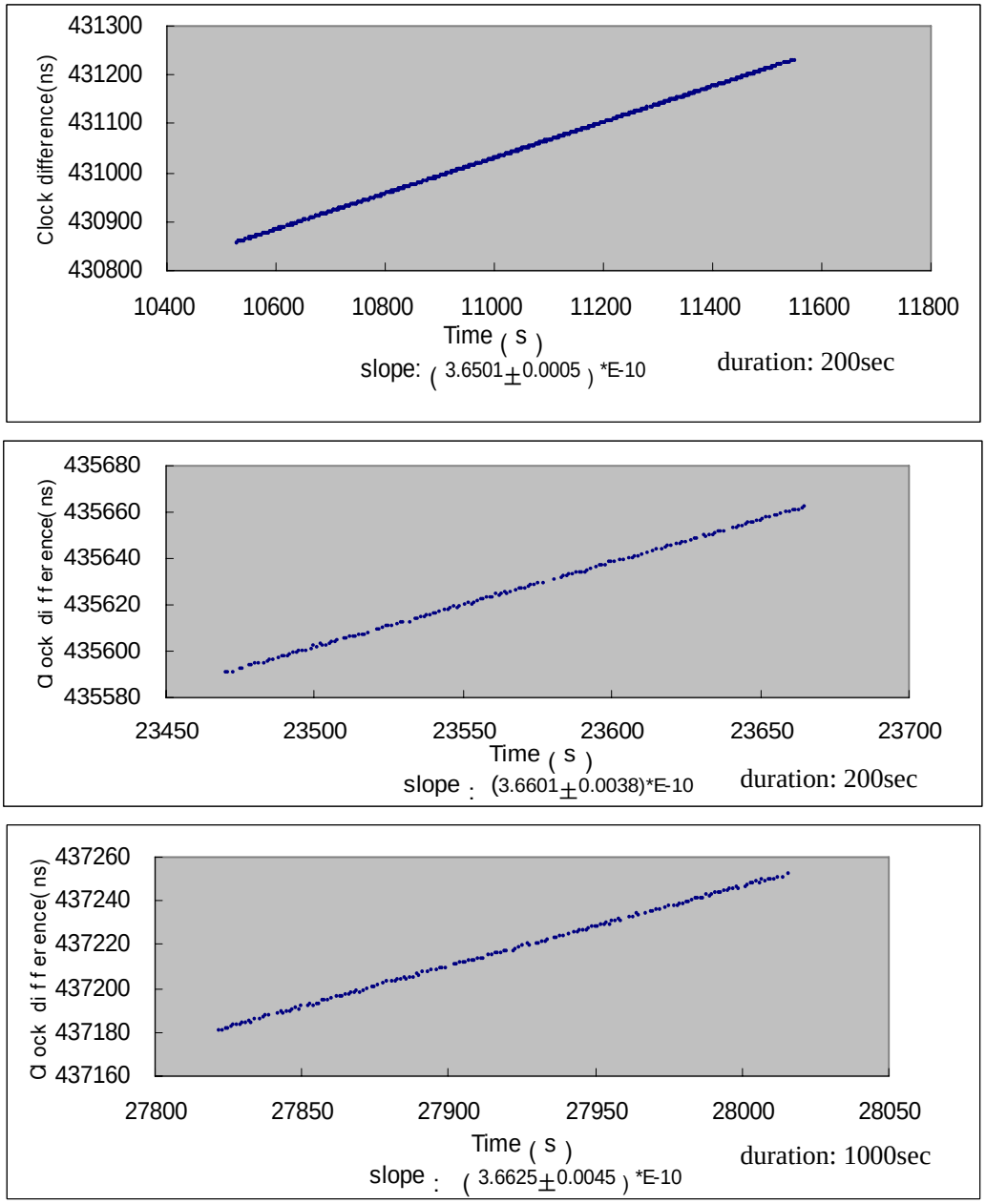

Fig.11. *LTT Results with 2 sets of Rb Clock*

T2L2 – Time Transfer by Laser Link

E. Samain[1], Ph. Guillemot[2], D. Albanese[1], Ph. Berio[1], F. Deleflie[1], P. Exertier[1], F. Para[1], F. Pierron[1], J. Paris[1], I. Petitbon[2], J.-M. Torre[1], P. Vrancken[1], J. Weick[1]

1. OCA - Observatoire de la Côte d'Azur, 06460 Caussols, France.

2. CNES - Centre National d'Etudes Spatiales, 34100 Toulouse, France.

Contact: Etienne.Samain@obs-azur.fr

Abstract

The new generation of optical time transfer T2L2 [1,2] (Time Transfer by Laser Link) has recently been accepted as a passenger of the Jason 2 satellite. The main objective of T2L2 on Jason2 is to compare remote clocks on earth. The project will also permit to follow-up from the ground, the on board clock of the DORIS[1] System. The performances expected are enhanced by one or two order of magnitudes as compared to existing microwave time transfer techniques, like GPS and TWSTFT[2]. After a description of the space instrumentation principle, we will present the metrological performances and give the current status of the project. Jason 2 will be launched in 2008 for a nominal mission duration of 3 years (5 expected) .

Introduction

The Time Transfer by Laser Link experiment (T2L2), initiated by OCA (Observatoire de la Côte d'Azur) and accepted by CNES (Centre National d'Etudes Spatiales), France, will be launched in mid-2008 on the altimetric satellite Jason 2. The experiment principle is issued from the classical laser telemetry techniques, with a specific instrumentation implemented onboard the satellite capable to tag the arrival time of laser pulses.

T2L2 history

T2L2 is the follow-on mission to LASSO (LAser Synchronization from Stationary Orbit) which was proposed in 1972 and launched in 1988 onboard the geostationary orbit satellite Meteosat P2. A first optical time transfer had successfully been achieved in 1992 between OCA, France and MacDonald, Texas [3]. This experiment measured a stability of 10^{-13} over 1000s and validated the feasibility of the concept. In 1996, a T2L2 instrument was proposed in the framework of the French PERSEUS mission to the Russian space station MIR, but the project was finally stopped at the end of the phase A. In the meantime it was accepted by ESA in the ACES (Atomic Clock Ensemble in Space) program scheduled on the International Space Station (ISS). T2L2 was one of the three scientific proposals of ACES, but had to be de-scoped in 2001 for some technical reasons concerning the whole ACES mission. Feasibility studies have been led by CNES and OCA for other flight opportunities (Myriade Micro-satellite, Galileo Test Bed), and finally a new opportunity appeared at the end of 2004, when NASA decided to abandon the WSOA instrument, an American contribution to the Jason-2 mission. A preliminary analysis confirmed the high interest to put a T2L2 instrument onto this altimetry-dedicated space vehicle and CNES decided to select the T2L2 instrument as a passenger on the Jason 2 mission.

[1] DORIS : Radio electric positioning system
[2] TWSTFT: Two-Way Satellite Time and Frequency Transfer

Principle and purpose of the experiment

T2L2 is an optical experiment that is able to establish a temporal link between remote clocks. The principle is based on the propagation of light pulses between laser stations and a satellite equipped with a specific instrumentation. The T2L2 payload is made with a photodetection device, a time-tagging unit, a clock (the DORIS ultra-stable oscillator (USO)) and a Laser Ranging Array (LRA). The ground station emits asynchronous laser pulses towards the satellite. LRA return a fraction of the received photons back to the station, while another fraction is detected and timed in the temporal reference frame of the onboard clock as (t_{board}). Each station records the start (t_{start}) and return (t_{return}) time each light pulse.

For a given light pulse emitted from station A, the synchronization χ_{AS} between the ground clock A and the satellite clock S is then derived from these data:

$$\chi_{AS} = \frac{t_{start} + t_{return}}{2} - t_{board} + \tau_{relativity} + \tau_{atmosphere} + \tau_{geometry} \quad (1)$$

$\tau_{relativity}$ is coming from relativistic effects, $\tau_{atmosphere}$ is the atmospheric delay and $\tau_{geometry}$ takes account of the geometrical offset between the reflection and detection equivalent points, depending on the relative position of the station and the satellite.

The same experiment can be lead from another station B and χ_{BS} can then be measured. The time transfer between A and B is then deduced from the difference between χ_{AS} and χ_{BS}. In a common view configuration, i.e. the two laser ranging stations are firing simultaneously towards the satellite, the noise of the onboard oscillator has to be considered over a very short time (time interval between consecutive pulses), so that it can be considered as negligible in the global error budget.

In a non-common view mode, the satellite local oscillator carries the temporal information over the distance separating laser stations. In the case of Jason 2 (driven by a quartz oscillator), we will have a significant degradation of the performances as soon as the time interval between passes is a few seconds (the maximum distance that allow this common view mode is roughly 7000 km). But in some cases, it will possible to keep a good time transfer performances even if the distance is greater than 7000 km by the use of intermediary laser stations located between station A and B. These stations will permit to build a virtual DORIS time scale from the clocks of each station.

Participation to the T2L2 experiment

The T2L2 ground segment is a laser station equipped with instrumentation to measure accurately both the start and return time of laser pulses. The laser station has to shoot with a 532 nm pulsed Nd:YAG laser having a pulse width between 10 to 200ps FWHM. The station can work between 10 Hz to a few Khz. Concerning the link budget, the conception of the space segment has been studied to detect low energy signals: the detection level onboard is comparable to the level in the ground. As a rule, if the ground station detects the impulse back, the same impulse should have been detected onboard as well.

Among the 40 laser stations in the world, 25 regularly range Jason 1 and will probably track Jason 2. Many laser stations have indicated their interest in participating to the T2L2 experiment (Figure 1).

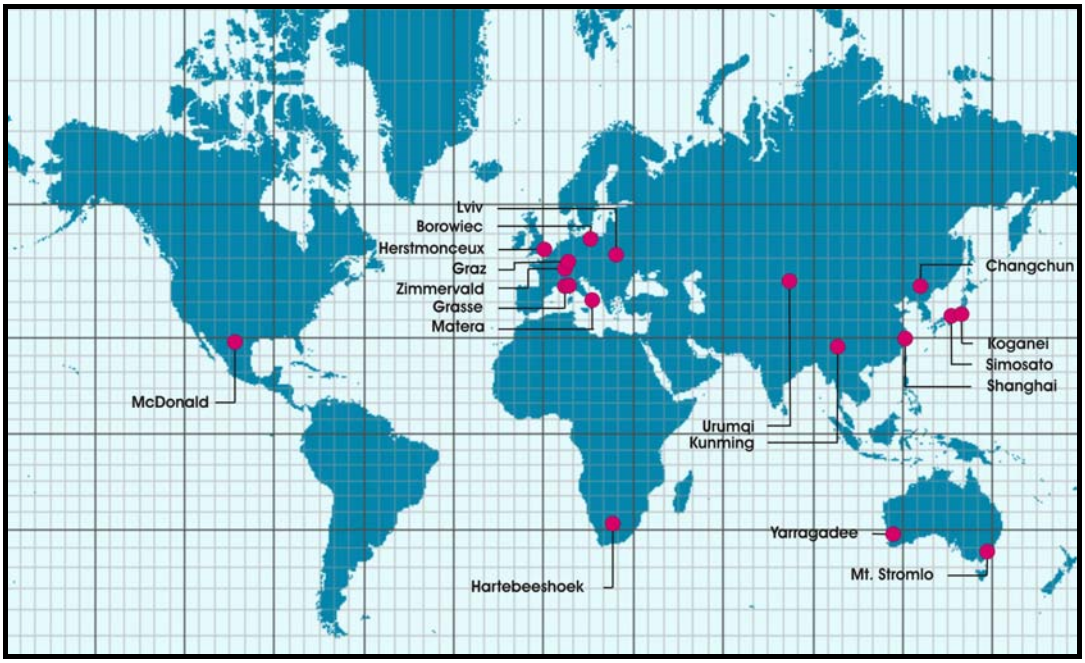

Figure 1: *T2L2 participation (October 2006)*

T2L2 on Jason 2

Jason 2 is a French-American follow-on mission to Jason 1 and Topex/Poseidon. Conducted by CNES and NASA, its goal is to study the internal structure and dynamics of ocean currents mainly by radar altimetry.

Jason 2 is build around a Proteus platform equipped with a dual-frequency radar altimeter Poseidon-3 and a microwave radiometer. For the needs of precise determination of the satellite orbit, three independent positioning systems are embarked: a Doris transponder, a GPS receiver and a LRA (Laser Ranging Array) target. The T2L2 instrument and two radiation studying payloads (Carmen-2, France and LPT, Japan) are supplementing the satellite instrumentation with some complementary objectives.

The satellite will be placed by a Delta launcher on the Jason 1's orbit at an altitude of 1,336 km and an inclination of 66°. This orbit allows common views at continental scale (about 7000 km baseline between stations). The time interval between two passes varies from 2 to 14 hours with an average duration of about 1000 s. The T2L2 specific instrumentation has a mass of 10 kg and a power consumption of 45 W. It includes (Figure 2):

- Two photo detection units located outside the main Jason 2 payload on the LRA boom (figure 3 right). Both are composed of avalanche photo detectors. The first one is working in a Geiger mode for precise chronometry[4,5] The other is in linear gain mode in order to trigger the whole detection chain and to measure the received optical energy and the reflected solar flux (earth albedo). To minimise the false detection rate, the detection threshold may be adjusted either by remote control or automatically as a function of the solar flux measurement.
- The electronic unit, located inside the Jason 2 payload module is composed of two main items (figure 3 right). The detection unit ensures the conversion of the laser pulse into an electronic signal and the event timer [6].

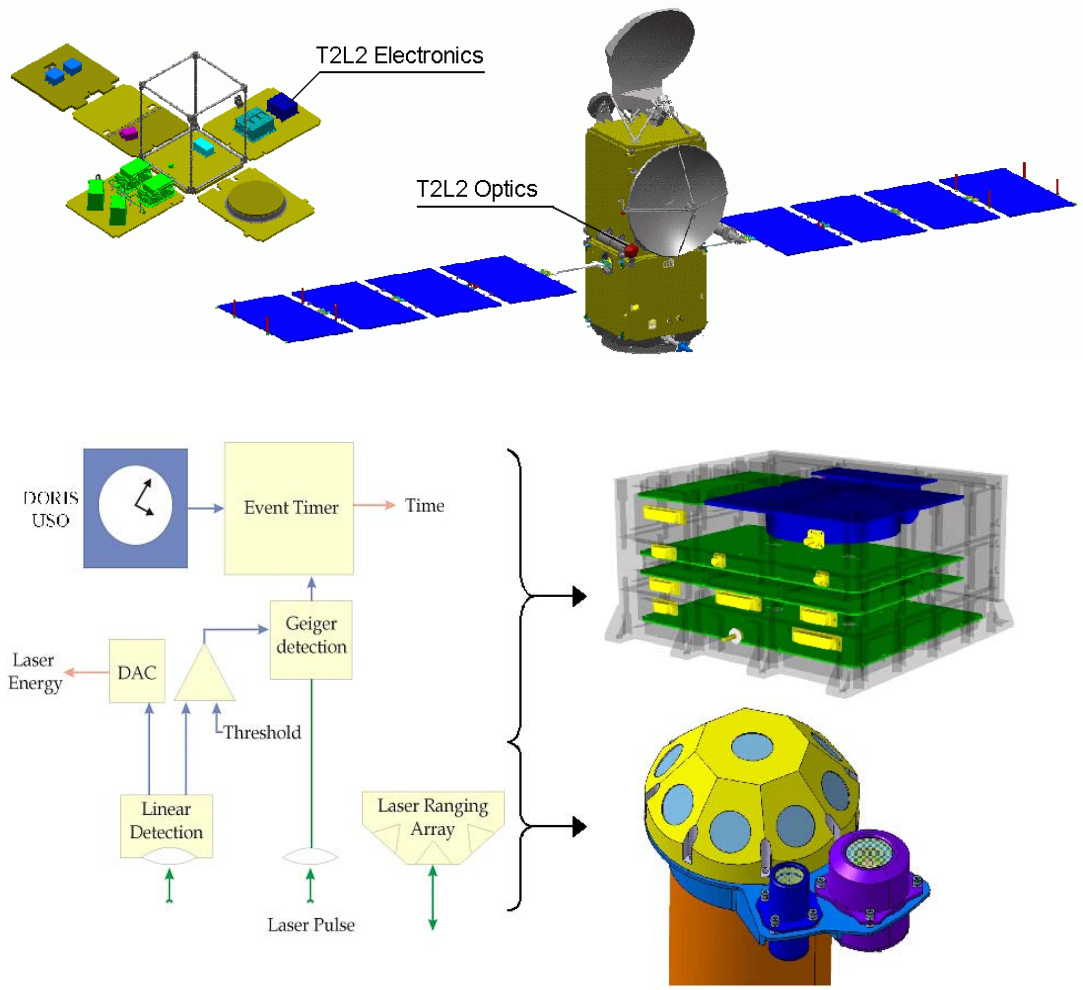

***Figure 2**: The integration of the T2L2 device inside the Jason-2 spacecraft*

Mission's objectives

The objectives of the T2L2 experiment on Jason 2 are threefold:

- Validation of optical time transfer, including the validation of the experiment, its time stability and accuracy. T2L2 will be a first step and a demonstration for future experiment based on one way laser ranging techniques in an interplanetary range: TIPO[3]. It should also allow the de-correlation of the effects coming from the target signature. In that way, it will permit to improve the precision of the telemetry.
- Scientific applications concerning time and frequency metrology allowing the calibration of radiofrequency time transfer (GPS and Two-Way), fundamental physics with the measurement of light speed anisotropy and alpha fine structure constant, Earth observation and very long baseline interferometry (VLBI).
- Characterization of the onboard Doris oscillator's drift, especially above the South Atlantic Anomaly (SAA) where the environment is highly irradiative. The two radiation instruments onboard will give the possibility to find a correlation between the expected and measured drift and propose adequate corrections.

Performance budget

T2L2 has ground-ground time transfer accuracy better than 100 ps. This will allow inter calibration between different time transfer methods by extracting the error

[3] TIPO: *Télémétrie InterPlanétaire Optique* / Optical InterPlanetary Telemetry

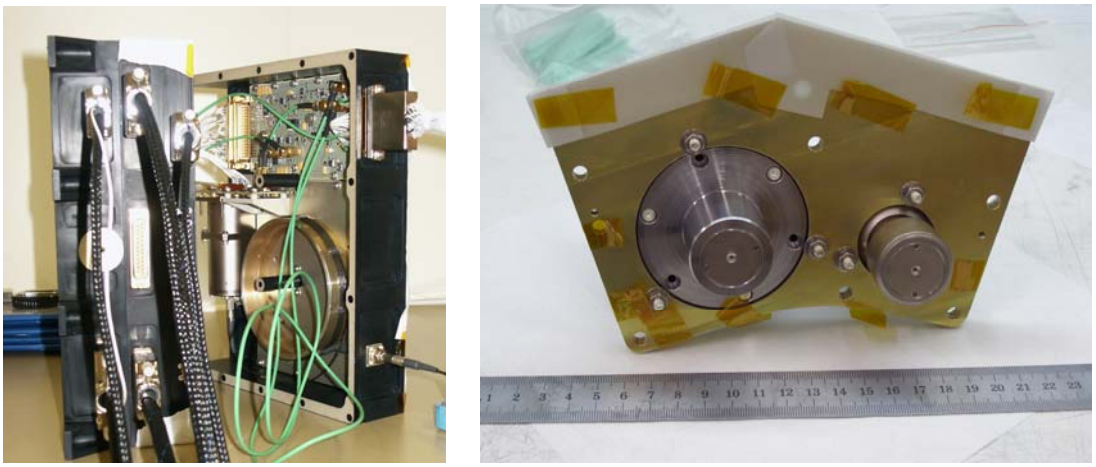

Figure 3: *Left : electronic of the flight model. The cylinder on the right side, support an multi mode optical fiber that generate a delay between the 2 photo detection. Right: the photo detection module (linear photo detector on the left side)*

caused by the transfer techniques themselves. T2L2 is particularly interesting to calibrate the regular time transfer used for the construction of international time scales (TAI) in particular the "Two-Way" (TWSTFT) that is about to become the quality reference for these scales. T2L2 will also permit to validate and to qualify the time transfers of Two-Way phase or GPS phase.

In term of stability, the comparison of T2L2 with the existing microwave links is shown on Figure 4. In a common view configuration (red bottom curve), the stability is better than 1 ps over an integration of 1,000 s. In non-common view, when conditions will not permit to build a virtual DORIS time scale, T2L2 will still offer an interesting alternative for radiofrequency calibration campaigns.

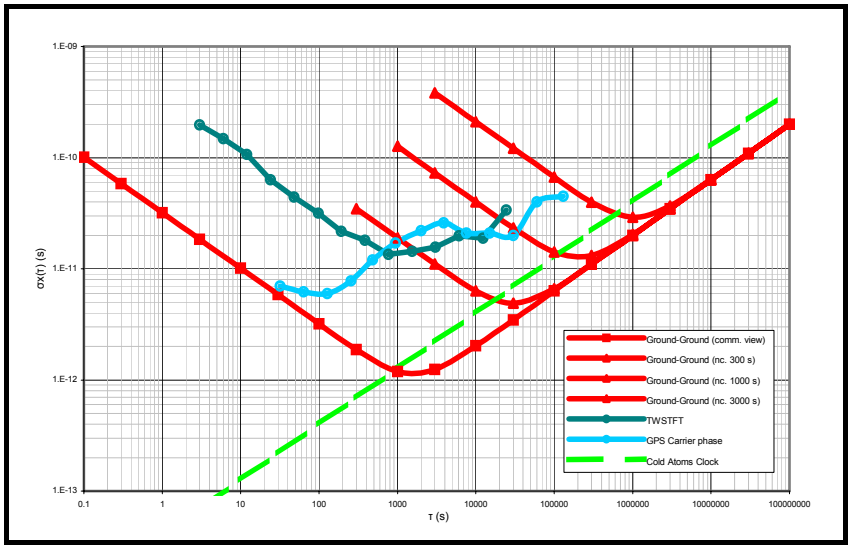

Figure 4: *T2L2 stability in common and non-common view configuration in* $\sqrt{\text{TVAR}}$

Current Status

The decision to put the T2L2 instrument in the Jason-2 satellite was taken on July 2005. The phase B started in September 2005 and entered in phase C/D in January 2006. Only one proto-flight model was built for the optics, while the electronics was developed in three steps: prototype boards, engineering model (EM) and flight model (FM). Metrological tests on EM have been done in July 2006. The flight model is now

fully integrated and the qualification processes is running now. The delivery of the instrument for the integration on the Jason 2 satellite is expected in April 2007.

A test bed has been developed at OCA to evaluate the metrological performances of the T2L2 space instrument and to perform some calibrations of both electronics and optics. This test bed will precisely reproduce the experimental conditions that will meet in orbit. The optical subsystem of the test bed was designed to simulate laser stations by illuminating the optics with faint laser pulses and also background illumination. The T2L2 photo detection module is mounted on 2 axes gimbals able to emulate the attitudes of the satellite in the range of ±60°. A high performance timing system is used as a timing reference. The experimental setup also includes a DORIS space clock engineering model in order to simulate the conditions on the satellite Jason 2, and alternatively a Cesium standard for time accuracy measurements. The tests that were so far conducted on the engineering model show the compliance with the metrology specifications for both the photo detection and the event timer.

Conclusion

With an improvement of one order of magnitude as compared to microwave time transfer techniques, T2L2 will give the possibility to compare cold atoms clocks at a level never reached before. It will allow the calibration of the existing radiofrequency links like GPS and TWSTFT with an improvement of at least one order of magnitude. T2L2 will also allow the precise characterization of the DORIS USO onboard Jason 2. The validation of the time and frequency transfer in space by T2L2 will represent an important step for further missions using this kind of technology, especially in a one-way mode in the solar system [7,8]. Jason 2 will be launched mid-2008 for a nominal duration of 3 years.

References

[1] Fridelance, P., E. Samain and C. Veillet, “Time Tranfer by Laser Link: a new optical time transfer generation”, Experimental Astronomy 7, 191, (1997)

[2] Samain, E., J. Weick, P. Vrancken, F. Para, D. Albanese, J. Paris, J.-M. Torre, C. Zhao, Ph. Guillemot and I. Petitbon, “Time Transfer by Laser Link: The T2L2 Experiment on Jason 2 and further Experiments”, Int. Journal of Modern Phys. D, World Sci. Publ. Company, (2007), (in press)

[3] P. Fridelance, C. Veillet, “*Operation and data analysis in the LASSO experiment*”, Metrologia, 32, 27-33, 1995

[4] I. Procazka , K. Hamal, “*Recent achievements in solid state detector technology for laser ranging*”, 2 , 469, Proceedings of the 9th International Workshop on laser ranging instrumentation, 1994

[5] E. Samain , “*Timing of optical pulses by photodiode in Geiger mode*”, Applied Optics, 37, No 3, pp 502-506, 1998.

[6] Samain, E. et al, OCA Event Timer , this proceedings 2006.

[7] E. Samain, One way laser ranging in the solar system, the TIPO Project (Télémétrie InterPlanétaire Optique), EGS, 2002.

[8] Wei-Tou Ni, Proceedings of the first International ASTROD symposium on laser astrodynamics, space test of relativity and gravitational – Wave astronomy, International journal of modern physics, 2002.

New Application for Khz Laser Ranging: Time Transfer Via Ajisai

Toshimichi Otsubo[1], Hiroo Kunimori[2] and Tadahiro Gotoh[2]

1. Kashima Space Research Center, National Institute of Information and Communications Technology, 893-1 Hirai, Kashima 314-8501 Japan
2. Koganei Headquarters, National Institute of Information and Communications Technology, 4-2-1 Nukui-kita, Koganei 184-8795 Japan

Contact: otsubo@nict.go.jp / FAX : +81-299-84-7160

Introduction

It was 14 years ago when the use of laser ranging technique was proposed for time transfer application for the first time (Kunimori, et al., 1992). The concept is to exchange laser pulses between two laser ranging stations via the curved mirrors carried on the AJISAI satellite (Sasaki and Hashimoto, 1987) shown in Fig. 1. The AJISAI satellite, launched in August 1996, carries 314 mirror panels as well as 1436 retroreflectors. Laser ranging stations usually detect retroreflected signals from the retroreflectors. However, the optical reflection by the mirrors were expected to be useful as if they were a two-way 'zero-delay' optical transponder, although they were originally designed to be used for photographical observations. It should be also emphasised that the optical components on the AJISAI satellite has almost no limit of lifetime, and therefore it can be used for many decades with no risk factors for long-term variation of transponder delay, etc.

This concept has not been realised yet. In this paper, the difficulties we have encountered for the realisation of this concept are briefly reviewed. Then, some new possible approaches, especially the use of the kHz laser ranging technology, are proposed. A possible scenario is lastly given based on the assumption of multiple kHz laser ranging station in Europe region (Kirchner and Koidl, 2004; Gibbs, et al., 2006).

Time Transfer via AJISAI: Concept and Difficulties

As seen in Fig. 1, the surface of the AJISAI satellite is mostly covered by the mirrors whose curvature is 8.5 to 9 metres. The size of each mirror panel is approximately 400 cm2 (~ 20 cm by 20 cm) at maximum. The laser retroreflectors (12 retroreflectors in one holder) are placed in the gap of the mirror panels.

This satellite flashes three or six times per its rotation period when it is illuminated by the sun. This is because three mirror panels located in the same row point toward the same latitudal angle. The placement of mirror panels was arranged so that the flashed mirror panels can be identified by the time intervals between flashes.

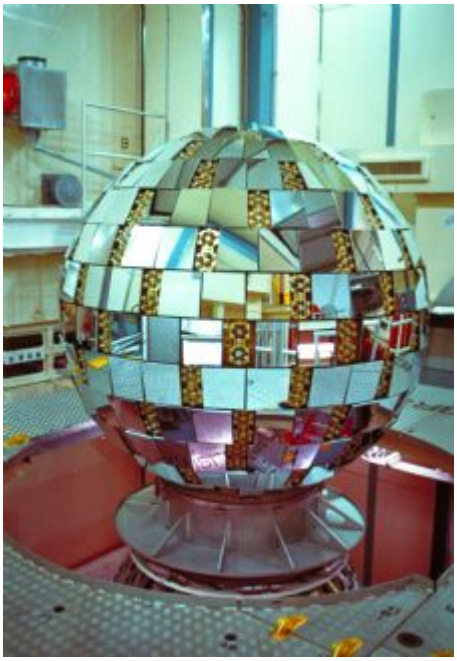

Figure. 1. *Japanese geodetic satellite AJISAI (photo: courtesy of JAXA).*

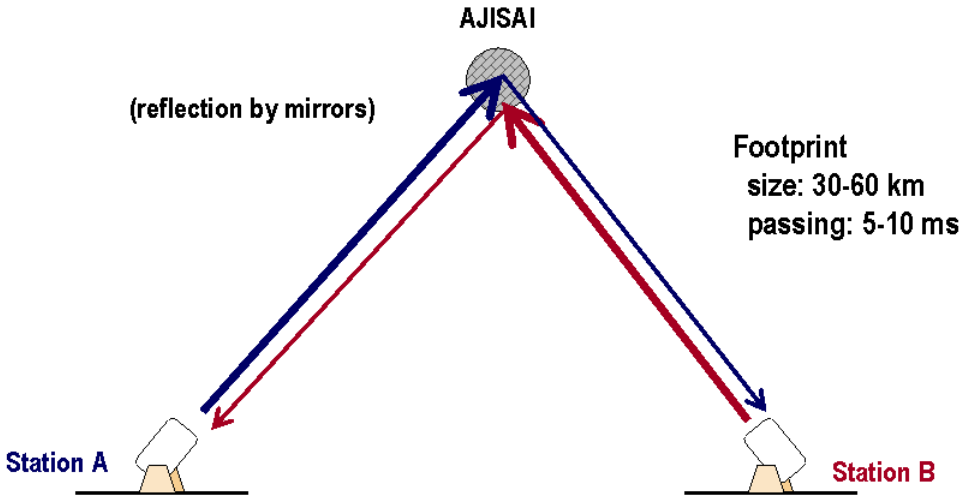

Figure 2. *AJISAI time transfer experiment: basic concept.*

A schematic view of the time transfer experiment via AJISAI proposed by Kunimori et al. (1992) is shown in Fig. 2. Like the radio-based two-way time transfer, the signal transmitted from one station goes to the other and vice versa. The curved mirrors make the reflection beam much wider to about 30 to 60 km size. Such a large footprint passes the receiving station just in 5 or 10 milliseconds.

The time diagram of signal passage between station A and B is illustrated in Fig. 3 where the 'ordinary' ranging of the station A and the signal transfer from the station A to the station B are shown. The signal transfer from the station B to the station A is simply given just by swapping the subscripts A and B. The case [1] is the prediction where the distance (in a time unit) R_{A1}* is the predicted one-way distance from the station A to the satellite and the time duration D_{A1}* is the predicted one-way internal system delay. The laser pulse is intended to hit the satellite at epoch t_0 of an imaginary 'true' clock. Assuming the clock of the station A is fast by ΔT_A compared to the 'true' clock, the station-transmission and the satellite-hit events come earlier by ΔT_A (case [2]). In reality, the laser does not exactly fire at the commanded epoch, and the delay is hereby set to L_A (case [3]). Now the start event $t_T(A)$ is given as:

$$t_T(A) = t_0 - \Delta T_A - R_{A1}^{*} - D_{A1}^{*} + L_A \quad (\text{'true' clock})$$
$$= t_0 - R_{A1}^{*} - D_{A1}^{*} + L_A \quad (\text{station A's clock})$$

Then, neglecting the centre-of-mass correction of the satellite, the reflected signal by retroreflectors comes back to the station A at:

$$t_R(A \to A) = t_0 - \Delta T_A + R_{A2} + (R_{A1} - R_{A1}^{*}) + D_{A2} + (D_{A1} - D_{A1}^{*}) + L_A \quad (\text{'true' clock})$$
$$= t_0 + R_{A2} + (R_{A1} - R_{A1}^{*}) + D_{A2} + (D_{A1} - D_{A1}^{*}) + L_A \quad (\text{station A's clock})$$

where R_{A1} and R_{A2} are the true outgoing and incoming one-way distance and D_{A1} and D_{A2} are the true outgoing and incoming one-way internal system delay.

What we usually use for the laser ranging is the difference (time interval) of the above two:

$$t_R(A \to A) - t_T(A) = R_{A1} + R_{A2} + D_{A1} + D_{A2}$$

from which we subtract the internal system delay D_{A1} +D_{A2} to obtain the two-way distance R_{A1} +R_{A2}. The clock offset ΔT_A and the laser firing delay L_A does not appear here, and therefore they are hardly observable from the ordinary laser ranging measurement.

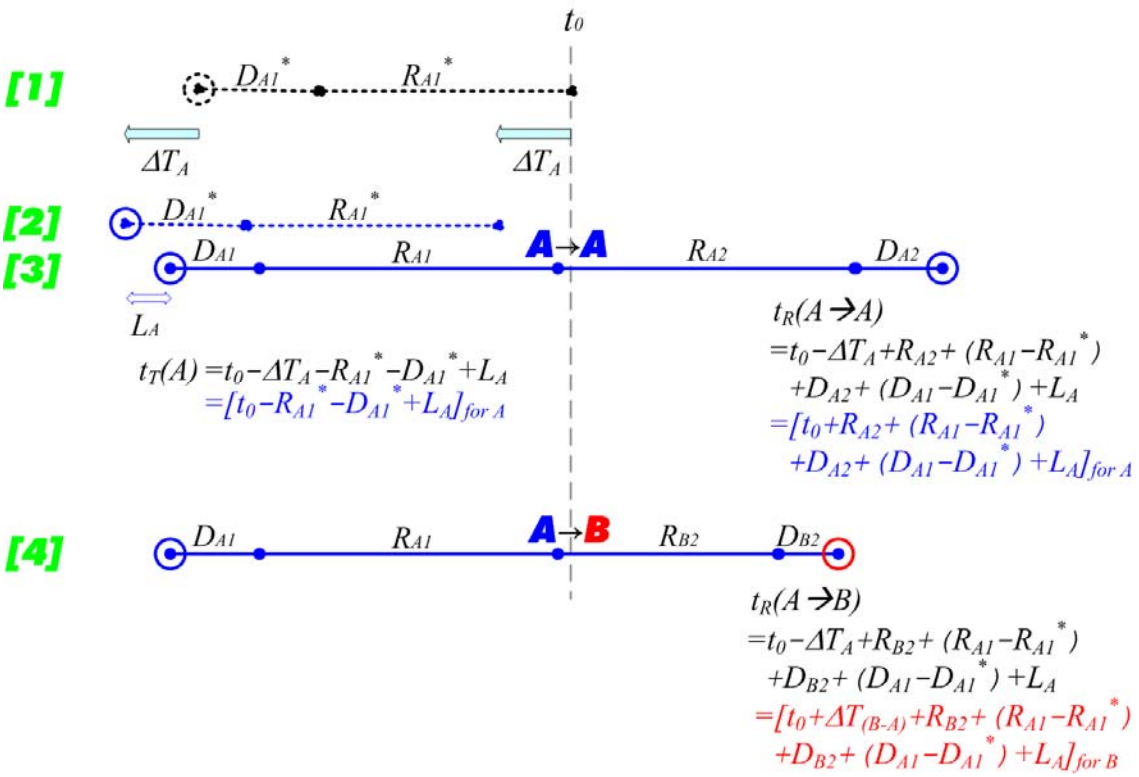

Figure 3. *Time diagram of ordinary laser ranging (A→A) and time transfer (A→B).*

Coming back to Fig. 3, the case [4] shows the signal transfer from the station A to the station B. The stop event at the station B comes at:

$$t_R(A \to B) = t_0 - \Delta T_A + R_{B2} + (R_{A1} - R_{A1}^*) + D_{B2} + (D_{A1} - D_{A1}^*) + L_A \quad \text{('true' clock)}$$
$$= t_0 + \Delta T_{B-A} + R_{B2} + (R_{A1} - R_{A1}^*) + D_{B2} + (D_{A1} - D_{A1}^*) + L_A$$
(station B's clock)

where the subscript B corresponds to variables for the station B. The opposite direction from the station B to the station A is given by an equation of swapping A and B in the above formulae. Using them, the two-way time transfer to obtain the difference of the clock offset, $\Delta T_{B\text{-}A} = \Delta T_B - \Delta T_A$ is given as the difference of two range observations $\rho_{A\text{->}B}$ and $\rho_{B\text{->}A}$, as below:

$$\rho_{A\to B} - \rho_{B\to A}$$
$$= t_R(A \to B) - t_T(A) - t_R(B \to A) + t_T(B)$$
$$\vdots$$
$$= 2\Delta T_{B-A} + [(R_{B2} - R_{B1}) - (R_{A2} - R_{A1})] + D_{B2} - D_{B1} - D_{A2} + D_{A1}$$

Now the double-difference $[(R_{B2} - R_{B1}) - (R_{A2} - R_{A1})]$ can be precisely calculated from the orbital motion of the satellite. On the other hand, the double-difference of the incoming/outgoing one-way internal system delay should be given to obtain the absolute value of $\Delta T_{B\text{-}A}$. That is, either (1) incoming minus outgoing (D_{A1} - D_{A2}) and (D_{B1} – D_{B2}) should be given, or (2) inter-station difference of one-way internal system delay (D_{B1} - D_{A1}) and (D_{B2} – D_{A2}) should be given. These values cannot be easily measured from the ordinary laser ranging systems. Note that, in spite of the difficulties in deriving the absolute accurate $\Delta T_{B\text{-}A}$, the variation of clock offsets would be relatively easily observed, leaving the constant offset of the '*D*' values and assuming them to be constant.

Beside this issue, the experiment itself has seemed unrealistic due to the following problems:

(a) The footprint passage time duration is just 5 to 10 ms. Compared to the laser firing interval of 100 to 200 ms (5 to 10 Hz lasers), it is much shorter. The footprint passage happens usually only three times per the rotation period of AJISAI, currently ~ 2s. Hence, the probability of hitting the laser at the right time was just 2.5 to 10 %. The chance was very limited.

(b) The mirror-reflection signal should reach the other station. If one wants to use a single range gate (common to laser ranging observation), the signals from the station A and the station B should hit the satellite almost at the same time. The multiple stop events should also be recorded, which is not possible by the ordinary time interval counters.

(c) The expected number of photons was just 1 to a few photons for the mirror-reflection signals, assuming a 100mJ/pulse laser. Very high sensitivity (or very strong laser) was required.

Expected breakthrough using kHz laser ranging technology

The problems (a) and (b) in the previous section are likely to be solved by the newly emerging kHz laser ranging networks. Firstly, as for the problem (a), the kHz laser (2 kHz in this case) fires 10 to 20 times per the footprint passage duration. The observation opportunity will not be missed. The kHz laser ranging systems almost automatically requires an event timer, instead of a time interval counter, due to the longer satellite ranges compared to the laser firing interval. The problem (b) will also be solved.

Especially in the European laser ranging network, multiple stations are moving toward the kHz laser ranging, following a very successful achievement at Graz, Austria. This region might be useful to exchange time signals via AJISAI between ~1000 km distant stations.

On the other hand, the link budget issue (the problem (c) in the previous section) gets more serious with kHz lasers. For instance the laser energy transmitted from the Graz system is 400 μJ/pulse, which is only 0.4 % of a traditional 100 mJ/pulse laser. The expected number of photons becomes a few hundredths of photons/pulse, and 1/10 to 1 photons/footprint passage. This would probably be the key issue for the realization of this experiment. We need to increase the laser energy and/or enhance the optical efficiency.

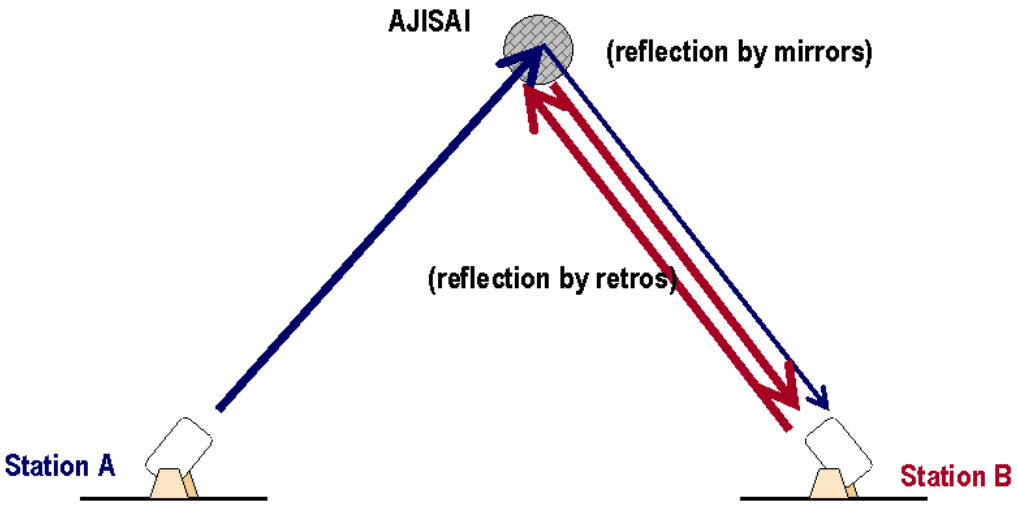

Figure 4. *AJISAI time transfer experiment: new concept.*

New experiment algorithms

As the single (A→B or B→A) signal transfer itself seems an uneasy task due to the weak link, we cannot expect the two-way (A→B and B→A) signal transfer at least at the initial stage. We re-examined the time diagram (Fig. 3) and conceived a novel way to achieve the time comparison experiment, as follows.

Let us assume the situation illustrated in Fig. 4, that is, one gets the single (A→B) signal transfer and the laser ranging (B→B). Subtracting the former range observation $\rho_{A->B}$ by the latter range observation $\rho_{B->B}$:

$$\begin{aligned}
&\rho_{A\to B} - \rho_{B\to B} \\
&= t_R(A \to B) - t_T(A) - t_R(B \to B) + t_T(B) \\
&\quad \vdots \\
&= \Delta T_{B-A} + [R_{A1} - R_{B1}] + [D_{A1} - D_{B1}]
\end{aligned}$$

where the clock offset difference $\Delta T_{B\text{-}A}$ appears. The second term, one-way range difference $[R_{A1} - R_{B1}]$, can be given at a few cm precision from an orbit determination procedure. The centre-of-mass corrections for R_{A1} and R_{B1} are different in this case due to the different reflection point: a mirror and retroreflectors, which should be taken into account for sub-nanosecond time comparison. The third term, difference of one-way outgoing system delay $[D_{A1} - D_{B1}]$, is still a problem to be solved, like the case of the two-way signal transfer. It is, nevertheless, now a difference of outgoing system delay, not the double difference of outgoing and incoming system delay.

Likewise, for example, by subtracting $\rho_{A->B}$ by $\rho_{A->A}$, the outgoing path will be cancelled and the incoming differences should be considered.

In this way, the clock offset information can be obtained by the single signal transfer and the ordinary laser ranging observation. This will ease the difficulties, especially on the weak link budget.

Conclusions

The time transfer via AJISAI is a long-lasting technology potentially with a very high precision/accuracy of 100 ps or even better. This will be one of new fields for a newly emerging kHz laser ranging 'network', especially in Europe. We have also derived a new algorithm which requires only single signal transfer, which will ease the weak link problem.

References

[1] Kunimori, H., F. Takahashi, T. Itabe, A. Yamamoto, "Laser ranging application to time transfer using geodetic satellite and to other Japanese space programs," Proc. 8th International Workshop on Laser Ranging Instrumentation, 1-34—1-42, 1992.

[2] Sasaki, M. and H. Hashimoto, "Launch and observation program of the experimental geodetic satellite of Japan," IEEE Trans. Geoscience and Remote Sensing, GE-25, 5, 526-533, 1987.

[3] Kirchner, G. and F. Koidl, "Graz KHz SLR System: Design, Experiences and Results," Proc. 14th International Workshop on Laser Ranging, 501-505, 2004.

[4] Gibbs, P., C. Potter, R. Sherwood, M. Wilkinson, D. Benham, V. Smith, "Some Early Results of Kilohertz Laser Ranging at Herstmonceux," in these proceedings, 2006.

A Satellite Tracking Demonstration on Ground Using a 100mm Aperture Optical Antenna for Space Laser Communication

H. Kunimori[1], M.Okawa[1], H.Watanabe[1], Y. Yasuda[2]

1. National Institute of Information and Communications Technology
2. Emeritus Waseda University, Japan
Contact: kuni@nict.go.jp , 4-2-1 Nukui-kita, Koganei 184-8795 Japan

Abstract

The Next Generation LEO System (NeLS) optical terminal was designed for 1.5um wavelength and 2Gbps data rate communication between 500 km – 3000 km inter-satellite link. In the course of ground validation test, using Coarse Pointing Mechanism and Optical Antenna, we demonstrated open tracking capability by ranging to a satellite AJISAI.

Introduction

The Next Generation LEO System Research Center (NeLS) in National Institute of Information and Communications Technology (NICT), of Japan, formed in 1997 for the key technology development of space communication network in future [1,2]. Fig. 1 and Fig. 2 show a concept and development schedule for optical communication part, respectively. Since 2002, it has focusing on the development of optical inter-satellite link technology for the future communication demanding a high data transmission for global multimedia service, as well as requirement of earth observation/ science data communication to ground.

Figure 1: *Concept of NeLS: Next Generation LEO System*

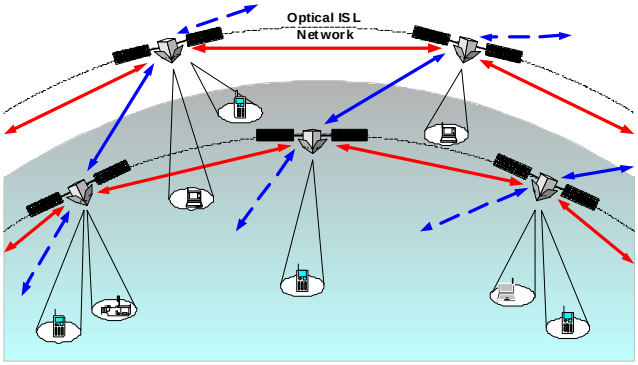

Optical terminal and key components

Fig. 3 shows block diagram of optical terminal. The optical terminal consists of four units, namely 1) Coarse Pointing Mechanism (CPM) located outside the spacecraft on mission panel, 2) Optical Antenna (OANT) as one of fixed part of optics located on mission panel 3) AT&P unit located outside the spacecraft, and 4) Communication Unit which interface both transmit & receive by optical fibers, located inside the spacecraft.

Figure 2: *NeLS Optcal Engineering Model Development Schedule*

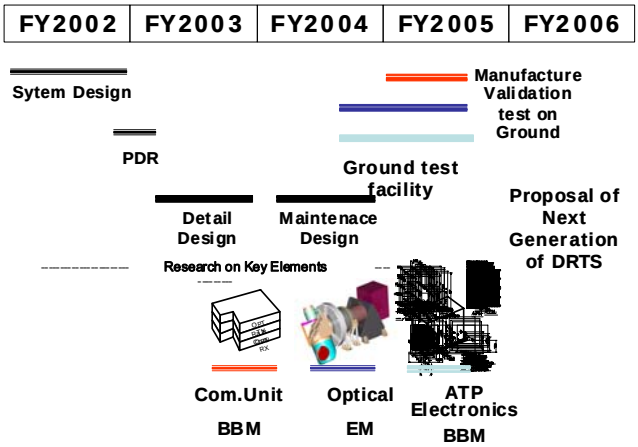

Figure 3: *NeLS Optical Terminal*

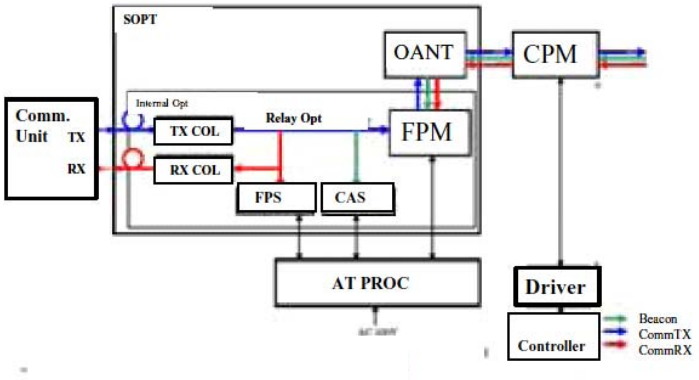

Figure 4: *A 10cm class Coarse Pointing Mechanizm (CPM)*

Item	Specification
Range of drive axis	Az:+/-275deg EL:+/-110deg
Maximum drive speed	3.0deg(slew) 1.0deg(track
Effective aperture size	85mm
Resolution of encorders	2/10000deg
Weight	16kg

CPM utilizes two-flat mirror type 2-axis gimbals (shown in Fig.4 picture and specification) so-called elbow-type has been adopted to cover all direction in space, where optical antenna fixed to satellite body.

In addition to OANT, as a fixed part of optics, a wide range Fine Pointing Mechanism (FPM), a Coarse Acquisition Sensor (CAS), a Fine Pointing Sensor (FPS), a Transmitting Collimator (TX COL), and a Receiving Collimator (RX COL) are integrated onto an optical bench with relay optics. AT&P UNIT includes terminal control processor circuit and power supply.

The Optical Antenna shown in Fig.5 has type of Cassegrain, where secondary mirror is supported by tripod and main reflector diameter of 125mm diameter, made by material of SiC with gold coating. Total effective focal length is 2600mm and magnification is about 20.

Other key components of internal optics include a fine pointing mirror made by voice coil actuators and GAP sensors, and transmitting and receiving fiber couplers has been tested as space qualification devices(Fig.6).

Figure5: *Subsystem - OPTICAL ANTENNA*

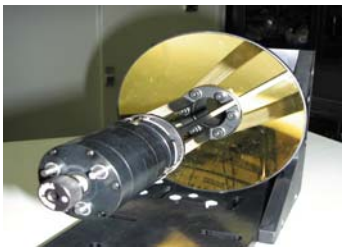

Figure 6: *Key components of internal optics*

Fine Pointing Mirror (FPM)

Transmitting Fiber Coupler (left)
Receiving Fiber Coupler& QD (right)

Utilities for ground test

To perform functional test and validation of optical terminal, we have developed one of utilities an optical tracking simulators utilized in a room spacing several meters between optical terminal and target

Figure 7: *Optical Tracking Simulator for ground experiment*

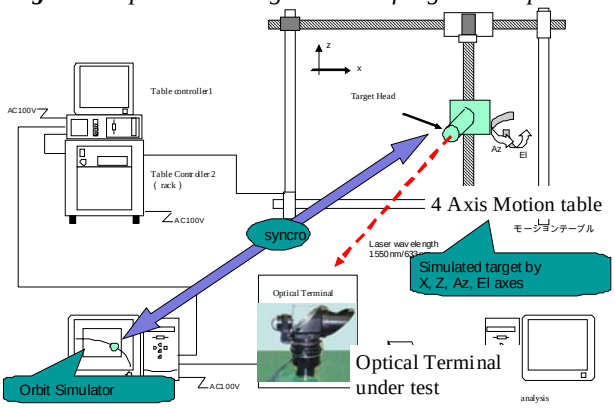

antenna. The target has on 4 axes (X-Z, Tip/Tilt) movement platform and has optical INPUT/OUTPUT capability. Fig.7 shows a schematic configuration of optical tracking simulator. The movement is programmed based on orbit simulation. Although the optical characteristics of terminal is different from that of far field, a basic function of acquisition and tracking during communication has been tested and 2.5Gbps communication BER data acquired and application of HDTV was demonstrated.

Another utility for optical terminal on ground outside, air-conditioned enclosed dome with a 30cm diameter optical window has been developed (Fig.8). The dome has axis of azimuth and rotor on azimuth structure made of stainless steel. The dome is on a box with 2 x 1 x 1 meters dimension, in which there is optical table set as vibration isolated manner, carrying optics and mechanics. Under table there are room and also carrying drivers of dome and electronics and power supply for optical terminal.

Fig.9 shows a schematic view of arrangement in a dome box called MML (Micro Mobile Laser) utility box. It also has optics for satellite laser ranging set that sharing beam through CPM by 45 degrees flat mirror.

Satellite Pointing capability test

Figure 8: *Utility development for Ground outside experiment*

The CPM was set up on optical bench so that mechanical & optical axis is aligned to gravity field (i.e. leveling) and other principal axis of equipments (laser and receivers). Two axis intersection angle offset orthogonality was measured as 80 ± 5 arcseconds. And star calibration of axis resulted in several arcseconds rms after rigorous alignment work done. Fig.10 shows a follow-on error when CPM tracking a Starlette satellite simulation pass which maximum elevation of 85 degrees. Two passes consecutively run shown. Since keyhole effect exists at zenith on Alt/Az axis gimbals, the performance of Az axis about maximum elevation was degraded to 10 arcseconds, however most of errors except key hole was within one arcsecond. Elevation axis has the same characteristics, but mean following error was larger (2 arcseconds rms) than that of Azimuth. Using standard SLR equipment with a nano second pulse width and 20mJ/pulse Nd:YAG lasers set up on table. We have performed laser ranging to a satellite AJISAI. Return proves the tracking system as open loop (means no use of beacon from satellite) working. Fig.11

Figure 9: *Configuration of Optical comm. and SLR equipments*

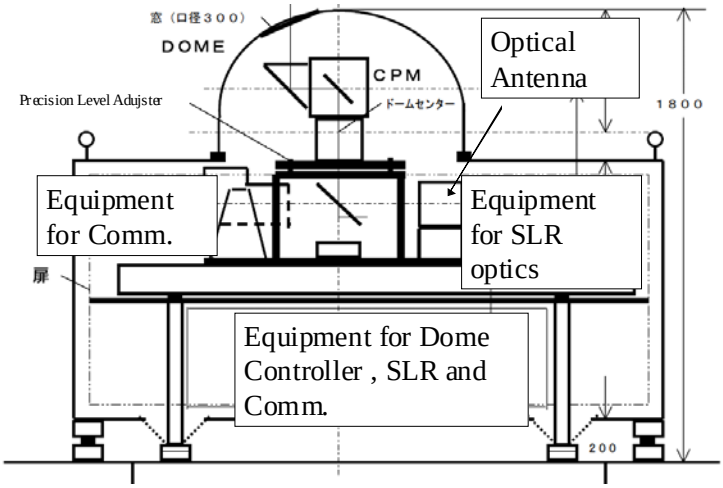

shows range residual vs observation time and there is a series of dots among dark noise and background noises that is from satellite returns. Fig.11 shows range residual vs observation time and there is a series of dots among dark noise and background noises that is from satellite returns.

We have had such four passes acquiring satellite returns during two weeks campaign. During campaign ranging to fix target to a 20meters to 4km distance was used as calibration of range as well as beam divergence and direction. The location of 4km distance is used as fixed distance communication experiment being done almost paralleled.

Figure 10: *LEO Tracking follow-on error evaluation of CPM by Starlette 85 deg elevation pass*

Black dot: Following Error Axis range+- 15arcsec
Red dot error RMS(2sec avarage) Axis range 0-10arcsec

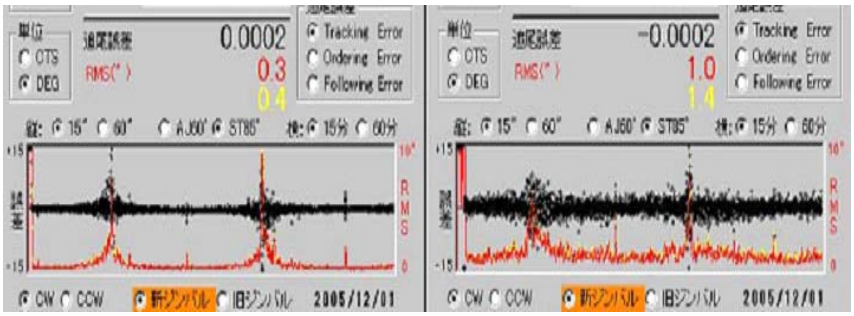

AZ axis:
<1arcsec rms except around zenith about 10arcsec rms

EL axis:
< 2arcsec rms except around zenith about 6 arcsec rms

Summary

The Next Generation Inter-satellite Laser Communication Terminal Optical Part Engineering Model has been developed. By using newly developed utility for ground

test validation, such as 4 axis motion table, mobile dome, optical terminal for 1.5um wavelength and 2.4Gbps data rate was evaluated in near-field (5m-5km) including ATP performance with atmospheric existence. Using Coarse Pointing Mechanism (CPM) and 10 cm class Optical antenna and, and associated 532nm pulse laser connection pass, we have demonstrated open-loop satellite tracking capability by ranging to AJISAI. Next Step is now using evaluation of those, we are proposing the next generation of DRTS (Data Relay Technology Satellite) in early 2010's

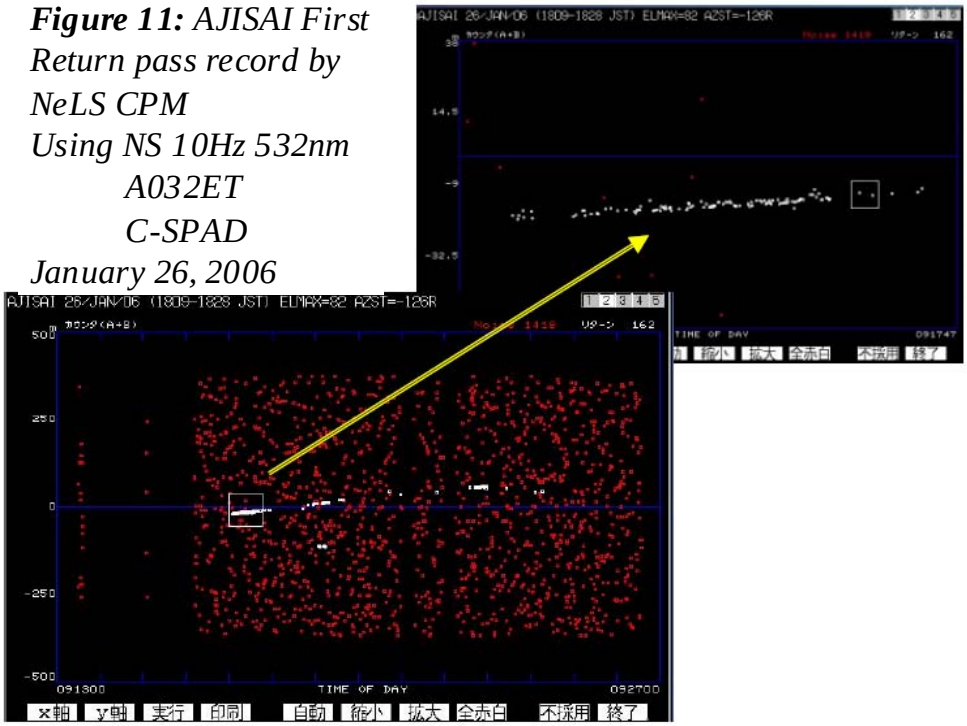

Figure 11: *AJISAI First Return pass record by NeLS CPM Using NS 10Hz 532nm A032ET C-SPAD January 26, 2006*

Acknowledgement

Authors would like to special thanks to who support the NeLS ground-satellite test experiment, namely N.Endo (INDECO), T.Yamaguchi (DENOH), Y.Suzaki (UNIVERSE), A.Hasegawa (SHOTOKU) and J.Guilfoyle (MTP).

References

[1] E. Morikawa, et.al, "R&D of A Next Generation LEO System for Global Multimedia Mobile Satellite Communications", 53th International Astronautical Congress, IAC-02-M.4.02, Huston US, 10-19 Oct. 2002.

[2] Y. Koyama, et.al., " Optical terminal for NeLS in-orbit demonstration", Proc.SPIE .Vo.5338, pp29-36., Jan.2005.

The NASA Satellite Laser Ranging Network: Current Status and Future Plans

David L. Carter[1]

1. NASA Goddard Space Flight Center, Code 453, Greenbelt, Maryland, USA 20771

Abstract

Over the past few years, the NASA Satellite Laser Ranging (SLR) Program has experience a resurgence of energy. In preparation for the completion and deployment of the SLR 2000 Replacement Systems, the NASA heritage SLR network continues to provide quality SLR data products to the International Laser Ranging Service (ILRS). Recently, NASA made the decision to return two critical stations in Maui, Hawaii and Arequipa, Peru back to operational status. NASA has been working hard to bring these two stations back on-line with the replacement of the HOLLAS station with the TLRS-4 system and the re-start of the TLRS-3 system. Other highlights have occurred throughout the NASA SLR network. The current status and the future plans of the NASA SLR Network will be discussed in this paper.

Background

The NASA SLR network consists of eight stations. NASA built five trailer-based Mobile Laser Ranging Stations (MOBLAS) and two highly compact Transportable Laser Ranging Systems (TLRS). The University of Hawaii and the University of Texas have operated two high performing Observatory SLR systems at their respective Universities. The University of Texas system has Lunar Laser Ranging (LLR) capability. NASA also has partnerships with foreign Government agencies and Universities for the operations and maintenance of MOBLAS systems. Under these partnerships, NASA continues to provide the SLR system, training, engineering support, and spare parts to maintain operations. The host country provides the site, local infrastructure, and the operating crew.

In February 2004, a forty percent decrease in the NASA SLR budget caused major reductions to the NASA SLR Network. The reductions included reduced network infrastructure, operational coverage at the stations, sustaining engineering staff, and data operational support. The MOBLAS-7 (Greenbelt, Maryland), McDonald Laser Ranging System (MLRS) (Fort Davis, Texas), and HOLLAS (Maui, Hawaii) stations were reduced to one shift operations. The NASA operator was removed from MOBLAS-8 site in Tahiti. In addition, the TLRS-3 site in Arequipa, Peru closed in February 2004, and the HOLLAS site in Maui, Hawaii closed in June 2004.

Resurgence of NASA SLR Network

In October 2004, the NASA SLR program experienced a resurgence of energy. Additional funding was provided by NASA Headquarters to re-open the TLRS-3 system in Arequipa, Peru. The TLRS-4 system, which was in caretaker status at Goddard Space Flight Center, was returned to operational status and shipped to Maui to replace the HOLLAS station. Another operational shift was added to the MLRS in Fort Davis, Texas. Additional highlights occurred throughout the NASA SLR network which are listed below.

MOBLAS-4 (Monument Peak, California):

NASA continued its collaboration with HTSI for the operations and maintenance of the MOBLAS-4 system. The site installed new Geoscience equipment. A Doppler Orbitography and Radiopositioning Integrated by Satellite (DORIS) instrument and a seismic instrument were installed at the SLR site. The DORIS instrument is from the Institut Geographique National (IGN) in France and the seismic instrument is from SCRIPPS Institution of Oceanography in San Diego, California. The site also installed a newly High Performance forWireless Research and Education Network (HPWREN) high speed internet access. The station is continuing three shift operations, five days per week, twenty-four hours per day.

MOBLAS-5 (Yarragadee, Australia):

NASA continued its collaboration with Geoscience Australia (GA) for operations and maintenance of the MOBLAS-5 system. The MOBLAS-5 crew continues to be one of the top data producing station in the ILRS. The station is continuing three shift operations, seven days per week, twenty-four hours per day.

MOBLAS-6 (Hartebeesthoek, South Africa)

NASA continued its collaboration with the South African National Research Foundation and the Hartebeesthoek Radio Astronomical Observatory (HRAO) for operations and maintenance of the MOBLAS-6 system. The system was originally

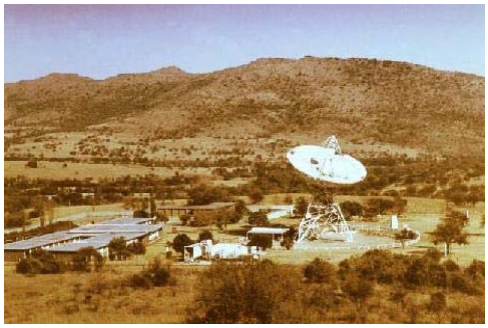

installed in HRAO in June 2000. The MOBLAS-6 operations began in August 2000. The site dedication ceremony occurred in November 2000. The HRAO site is collocated with Very Long Baseline Interferometry (VLBI), Global Positioning System (GPS), and DORIS. The station is continuing three shift operations, five days per week, twenty-four hours per day.

MOBLAS-7 (Greenbelt, Maryland)

NASA continued its collaboration with HTSI for the operations and maintenance of the MOBLAS-7 system. MOBLAS-7 continues to perform outstandingly despite the reduction in operational shifts. The system is used by NASA to test all upgrades and modifications to the NASA network prior to being installed in the field sites. The station is continuing one shift operations, five days per week.

MOBLAS-8 (Tahiti, French Polynesia)

NASA continued its collaboration with Centre National d'Etudes Spatiales (CNES) and the University of French Polynesia (UFP) for the operations and maintenance of the MOBLAS-8 system in Tahiti, French Polynesia. The Tahiti Geodetic Observatory recently named Dr. Jean Pierre Barriot as its new Director. The station was affected by the removal of a NASA operator and trainer due to budget reduction in 2004. The staff has done an excellent job operating and maintaining the station despite poor weather conditions at times. The MOBLAS-8 system was originally shipped to Tahiti in August 1997. The site dedication ceremony occurred in May 1998. The system is collocated with a GPS and DORIS system. The station will be providing two shift operations, five days per week.

TLRS-3 (Arequipa, Peru)

NASA re-newed its collaboration with the Universidad Nacional de San Agustin (UNSA) for the operations and maintenance of the TLRS-3 system in October 2005. The TLRS-3 crew working with Honeywell Technical Solutions Incorporated (HTSI) engineers began restoring the site to full operations. The restoration of the site included repairs to the laser, controller computer, HP5370, gimbal, dome controller, and telescope. The system's first light was September 23, 2006. As of the October 16, 2006, 90 pass segments had been acquired with a data quality of < 10 mm RMS on Lageos. The average ground calibration was at the 5.4 mm level. The station is providing two shift operations, day and night, five days per week.

TLRS-4 (Maui, Hawaii)

NASA renewed its collaboration with the University of Hawaii, Institute for Astronomy (IfA). After the HOLLAS system was decommissioned in June 2004, the site was converted to the new PanStarrs Observatory. NASA decided to bring the TLRS-4 system to operational status and ship it to the Haleakala Observatory in Maui, Hawaii. The TLRS-4 system had a highly successful inter-comparison test with MOBLAS-7. The system passed an Operational Readiness Review in September 2005. After 10 years on non-operations, TLRS-4 was shipped to Maui in April 2006. HTSI working with the University of Hawaii IfA personnel, prepared the site and installed the system on new pad on top of Mount Haleakala. The system's first light was in October 2006. The station will be providing two shift operations, day and night, seven days per week.

MLRS (Fort Davis, Texas)

NASA continued its collaboration with the University of Texas and the Center for Space Research (CSR) for operations and maintenance of the MLRS system in Fort Davis, Texas. MLRS provided SLR and LLR tracking data. CSR continued its data analysis support for the ILRS network. The station will be providing operations seven days per week, twelve hours per day.

Conclusion

The future of the NASA SLR Program is exciting. The resurgence of energy can be seen by the recent accomplishments of the various stations. NASA is increasing its infrastructure as well as plans are in place to increase stations operational shifts. The TLRS-3 system in Arequipa and the TLRS-4 system in Maui will be fully operational in December 2006. Dedication ceremonies for re-opening both sites are being organized for January/February 2007 timeframe. In addition, significant progress continues on the SLR2000 prototype development. We would like acknowledge the extraordinary efforts and dedication of the team supporting the NASA SLR network which includes NASA personnel, contractors, universities, and our foreign partners.

Possibility of Laser Ranging Support For The Next-Generation Space VLBI Mission, Astro-G

Toshimichi Otsubo[1], Toshihiro Kubo-oka[1], Hirobumi Saito[2], Hisashi Hirabayashi[2], Takaji Kato[2], Makoto Yoshikawa[2], Yasuhiro Murata[2], Yoshiharu Asaki[2], and Shinichi Nakamura[3]

1. Kashima Space Research Center, National Institute of Information and Communications Technology, 893-1 Hirai, Kashima 314-8501 Japan
2. Institute of Space and Astronautical Science, Japan Aerospace Exploration Agency, 3-1-1 Yoshinodai, Sagamihara, 229-8510 Japan
3. Consolidated Space Tracking and Data Acquisition Department, Japan Aerospace Exploration Agency, 2-1-1 Sengen, Tsukuba, 305-8505 Japan

Contact: otsubo@nict.go.jp / Fax: +81-299-84-7160

Introduction

Space VLBI (Very Long Baseline Interferometry) missions enable us to extend the baseline length beyond the diameter of the Earth and, as a result, to obtain more precise images of astronomical radio sources. Following the first successful space VLBI mission, HALCA (Hirabayashi, et al., 1998), which launched in 1997 and finished in 2005, JAXA (Japan Aerospace Exploration Agency) approved the next-generation space VLBI satellite called ASTRO-G (Hirabayashi, 2005) in 2006. It is scheduled to be launched in 2012. This new satellite, with a 9.6-metre mesh antenna, will receive high frequency radio signals up to 43 GHz and enhance the resolution of images by approximately 10 times than the former mission. It is expected to provide high-resolution imaging of active galactic nuclei, motion in galactic star forming regions, observations of extragalactic water masers, and so on.

The space VLBI satellite observes stellar objects in collaboration with ground VLBI network. One of the observation modes is called phase compensation observation. That is, the VLBI antenna switches the pointing direction by 2 or 3 degrees every minute to see a target object and a reference object. This makes it possible to compensate the atmospheric delay for ground VLBI stations. In this observation mode, very precise orbits up to a few cm precision are required throughout the trajectory.

Its orbit is highly elliptic. With an eccentricity of 0.62, its altitude varies from 1000 km (perigee) to 25000 km (apogee). The orbital period is about 7.5 hours and the inclination is set to 31 degrees. In contrast to spherical geodetic satellites, the area-mass ratio is large and its shape is very complicated. Therefore, it will experience large and complicated perturbation forces mainly due to solar radiation pressure. Although the cm-order orbit determination for near-circular orbits is nowadays fairly common, that for such an elliptic orbit is a highly challenging problem. We

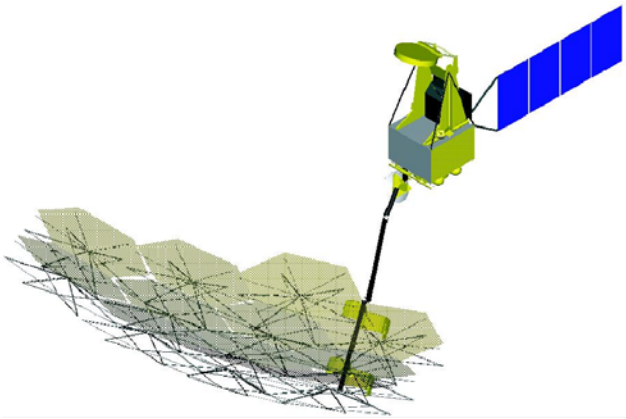

Figure 1. *ASTRO-G satellite.*

are currently investigating possible instruments for high-precision orbit determination. This paper deals a quick-look, first-step simulation of GPS and SLR data.

Possible instruments for precise orbit determination

In the following discussions, we assume these virtual orbital elements of ASTRO-G:

Epoch: 0h UT, 26 Apr 2004
Semimajor axis: 19378 km
Eccentricity: 0.6193
Inclination: 31 deg
Longitude of ascending node: 0 deg
Argument of perigee: 0 deg
True anomaly: 0 deg

After several experiments since 1990's, an onboard GPS receiver is found to be useful for precise orbit determination of low earth orbit (LEO) satellites, and the number of LEO satellites carrying this instrument is rapidly increasing.

We currently consider GPS receiver(s) as the primary instrument for precise orbit measurement. The apogee of ASTRO-G is 25000 km of altitude which is higher than the GPS satellites (20000 km). The beam divergence of GPS microwave signal is almost the size of the earth, so it gets out of the main lobe of the GPS signal (~ 20 degrees for L1 frequency) as its altitude gets high (~ typically a few thousand km).

The number of 'visible' GPS satellites on track was plotted in Fig. 2 using the true GPS constellation on the day. The bottom graph is the geocentric distance of the ASTRO-G satellite. This graph covers 15 hours, almost 2 revolution periods. The 'visibility' is defined so that the ASTRO-G satellite is within the 20-degree beam divergence and it is out of the Earth's shadow. First, assuming a single GPS receiver that always points away from the geocentre, the 'visible' number of GPS satellites is the dotted (blue) line in the top graph. Only when it is close to the perigee, one hour per the 7.5 hours period, it can see more than four satellites. Then, we simulated multiple receivers which provide no limit in terms of direction. The result is plotted as the solid (red) line in the top graph. With the contribution from GPS satellites that locate opposite side of the earth, the 'visible' number increases. Even away from the perigee, a few GPS satellites can be visible, but the number is far less than four in most cases.

In order to overcome this situation, we need to look into the possibility of the use of sidelobe GPS signal. Also, other GNSS satellites like GLONASS and GALILEO are also possible to improve the situation. Nevertheless, we stick to the above condition (solid red line) for the rest of this paper.

In these circumstances, laser ranging seems to play an important role for precise orbits. We have not looked into the specifications, but the reflector array size should be similar to that of GPS or GLONASS satellites. Other possibilities, such as an accelerometer or VLBI delay measurements, are also being considered, but not included in this paper.

Quick-look POD simulations

We simulated the following data set for the 15 hours in Fig. 2:

- GPS: every 30 seconds, pseudorange and carrier phase, L1 and L2 frequency
  (assumed observation error = 10 cm for carrier phase, and 3 m for pseudorange)
- SLR: normal points every 120 seconds
  (assumed observation error = 6 cm)

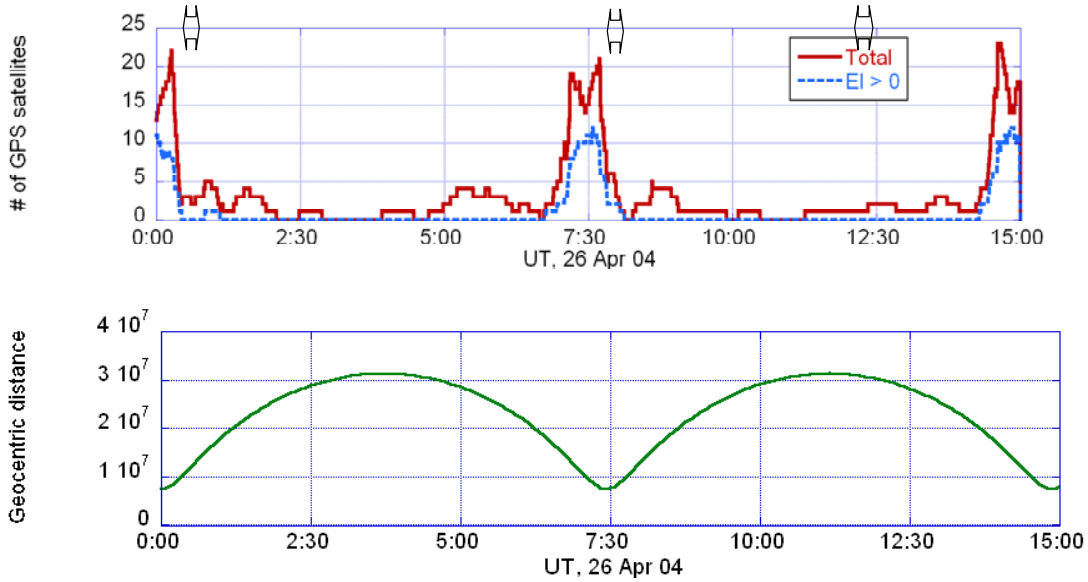

Figure 2. *Number of visible GPS satellites (top) and geocentric distance (bottom) of ASTRO-G simulated orbit. The three two-headed arrows are the duration of assumed SLR observations.*

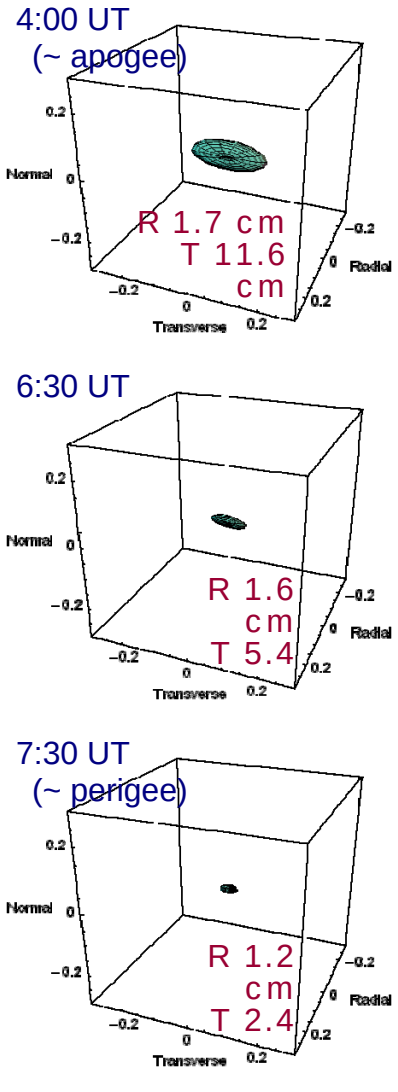

Figure 3. *Error ellipsoids for the GPS-only case.*

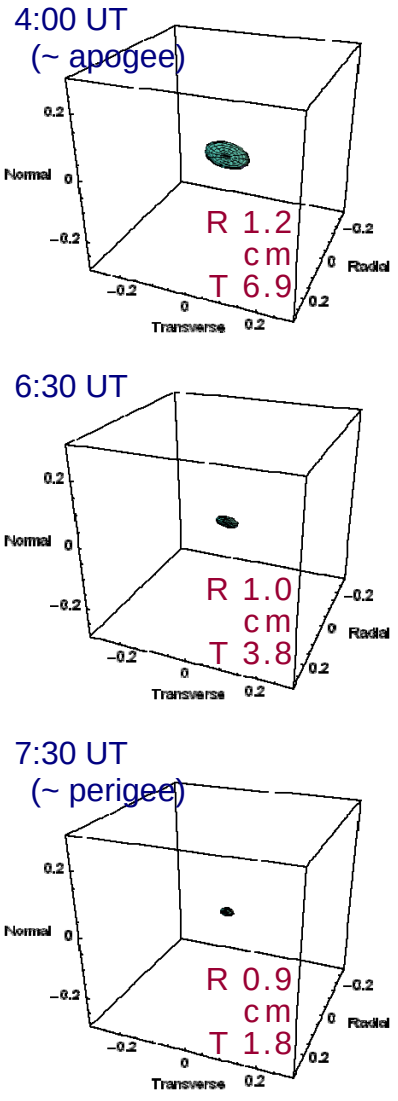

Figure 4. *Error ellipsoids for the GPS+SLR case.*

The orbital parameters, six elements, constant along-track acceleration and once-per-rev along-track acceleration, are estimated at 4:00 (close to the apogee), 6:30 and 7:30 (close to the perigee), instead of the starting time (0:00) of the arc. The clock offsets at each epoch and the ambiguities of ion-free GPS carrier phase are also solved for. We look into the covariance matrix of the orbit positional solution to obtain the estimation error. The covariance matrices given in the XYZ inertial coordinate system are then converted to the RTN satellite-fixed system, that is, in Radial, Transverse and Normal direction.

We firstly simulated the GPS data only. The ellipsoidal bodies in Fig. 3 show the size of three-dimensional errors for the three epochs. The error in the transverse component (= along-track component at the apogee and the perigee) is dominant in all cases. As expected, the ellipsoid gets larger around the apogee where GPS signal is merely detected.

Then we added the SLR data, the three 30-minute passes shown in Fig. 2, to the GPS data. The ellipsoids are shown in Fig. 4. It is obviously seen that the errors in the transverse and radial components are significantly reduced by the addition of the small amount of SLR data. Although we cannot expect dense tracking from the SLR network, this result suggests the SLR data will significantly contribute to the improvement of the orbit of ASTRO-G.

Discussions for future studies

The precise orbit monitoring instrument for the ASTRO-G satellite is being investigated. SLR observations will significantly improve the orbit compared to the GPS-only case. With further analyses we need to consider the details on the instruments such as the number and arrangement of GPS antennas and SLR retroreflectors.

The International Laser Ranging Service (ILRS) had a small experience of highly elliptic orbit satellite in the LRE (Laser Ranging Equipment) test mission launched to a geostationary transfer orbit in 2001 (Otsubo, et al., 2002). If the satellite actually carries retroreflectors for SLR, we would like to ask the ILRS stations to adapt their tracking system to highly elliptic orbits.

Due to the complicated shape of the satellite and the large area-per-mass ratio, this satellite is to experience largely complicated perturbation forces from solar radiation pressure that is about 100 times of LAGEOS. Therefore, along with the orbit measurement instruments discussed in this paper, the establishment of a precise force model is also essential for the precise orbit determination of this satellite.

References

[1] Hirabayashi, H., H. Hirosawa, H. Kobayashi, Y. Murata, P. G. Edwards, E. B. Fomalont, K. Fujisawa, T. Ichikawa, T. Kii, T. Lovell, G. A. Moellenbrock, R. Okayasu, M. Inoue, N. Kawaguchi, S. Kameno, K. M. Shibata, Y. Asaki, T. Bushimata, S. Enome, S. Horiuchi, T. Miyaji, T. Umemoto, V. Migenes, K. Wajima, J. Nakajima, M. Morimoto, J. Ellis, D. L. Meier, D. W. Murphy, R. A. Preston, J. G. Smith, S. J. Tingay, D. L. Traub, R. D. Wietfeldt, J. M. Benson, M. J. Claussen, C. Flatters, J. D. Romney, J. S. Ulvestad, L. R. D'Addario, G. I. Langston, A. H. Minter, B. R. Carlson, P. E. Dewdney, D. L. Jauncey, J. E. Reynolds, A. R. Taylor, P. M. McCulloch, W. H. Cannon, L. I. Gurvits, A. J. Mioduszewski, R. T. Schilizzi, R. S. Booth, “Overview and Initial Results of the Very Long Baseline Interferometry Space Observatory Programme,” Science, 281, 1825, 1998.

[2] Hirabayashi, H., “Next Generation Space VLBI,” EAS Publications Series, 15, 465-478, 2005.

[3] T. Otsubo, H. Kunimori, K. Yoshihara, H. Hashimoto, “Laser Reflector Arrangement on H2A-LRE Satellite for Monitoring the Spin Rate and the Optical Degradation,” Applied Optics, 41, 27, 5672-5677, 2002.

Electron Multiplying CCD Camera Performance Tests

D. Lewová[1], M. Němec[1], I. Procházka[1], K. Hamal[1],G. Kirchner[2], F. Koidl[2], D. Kucharski[3], Yang Fumin[4]

1. Czech Technical University in Prague, Brehova 7, 115 19 Prague 1, Czech Republic,

2. Graz Observatory, Austrian Academy of Sciences, Austria

3. Space Research Centre, Polish Academy of Sciences, Poland

4. Shanghai Observatory, Chinese Academy of Science, China

Contact: lew.dana@gmail.com , nemecm1@troja.fjfi.cvut.cz

Abstract

For satellite laser ranging, TV guiding is widely used to point the laser beam on the satellite. The ISIT (Intensified Silicon-Intensifier Target) camera has been applied in last years for its high sensitivity, which enabled to track all satellites of interest. However, there is a strict limitation to use it for daylight observation. The new type of CCD camera Electron Multiplying CCD (EMCCD) provides high sensitivity for short integration time required for fast real time tracking while maintaining the high ruggedness for daylight tracking. An additional internal gain reaches a factor up to 200 in comparison with regular CCD. During our tests in Graz and Shanghai, we did demonstrate the ability for satellite laser ranging during the daylight and during the night time exploiting the higher sensitivity, as well. The test results and a comparison with ISIT technology will be presented.

EMCCD Camera Performance Tests

- EMCCD provides high sensitivity for short integration time required for fast real time tracking
- In comparison with ISIT, EMCCD offers adjustability of exposure time and EM gain and beside the Analog video output it has very fast native Digital output allowing better image enhancement post-processing
- During our tests in Graz and Shanghai we did demonstrate the ability for SLR during daylight and night operations

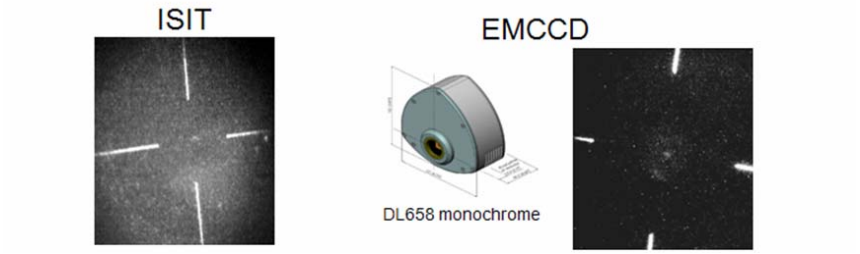

EMCCD Camera Performance Tests

EMCCD Images of GPS, Etalon 2, Glonass and Lageos 2 illuminated by Sun only

Digital output – no enhancement
(Images are captured with the same EMCCD settings and inverted)

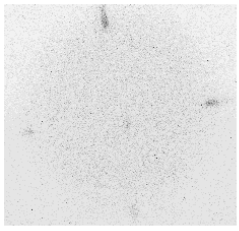

Gps BIIA-24, 0.2s, Gain 250
2006-08-25T20:07:39 UTC
Sun only, Altitude ~ 20,100 km

10x10pixels	Object	Backgr.
Standard Deviation	350,37	243,86
Mean	939,13	818,49
Maximum	2603	2263
Total Counts	375652	327396

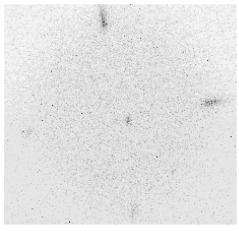

Etalon2, 0.2s, Gain 250
2006-08-25T20:39:42 UTC
Sun only, Altitude ~ 19,100 km

10x10pixels	Object	Backgr.
Standard Deviation	471,25	274,1
Mean	1024,35	820,27
Maximum	4129	2119
Total Counts	375652	328106

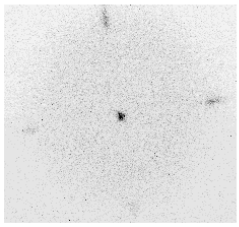

G87- Glonass, 0.2s, Gain 250
2006-08-25T22:53:02 UTC
Sun only, Altitude ~ 19,100 km

10x10pixels	Object	Backgr.
Standard Deviation	1508,39	310,89
Mean	1870,07	869,8
Maximum	10835	2235
Total Counts	748028	347920

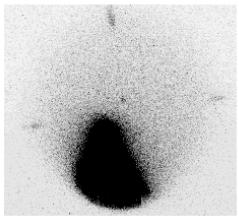

Lageos2, 0.2s, Gain 250
2006-08-25T19:27:57 UTC
Sun only (Laser outside the object)
Altitude ~ 5625 km

10x10pixels	Object	Backgr.
St. Deviation	629,62	503,65
Mean	1713,28	1495,48
Maximum	4375	3389
Total Counts	685310	598194

EMCCD Camera Performance Tests

Analog video output enhancement

On-line video filter - Contrast enhancement
GPS 36

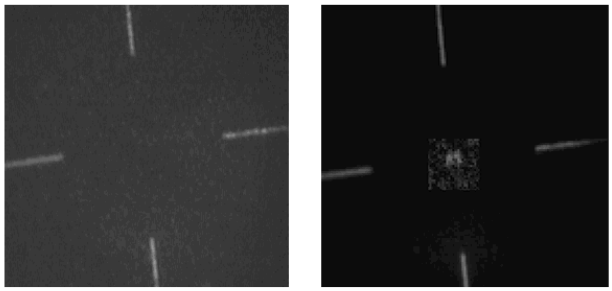

before after

On-line video filter - Pseudocolor mapping

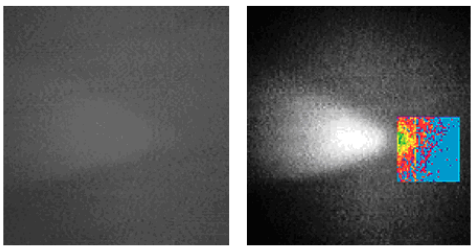

before after

For more details see the following Poster.

Electron Multiplying CCD Camera Performance Tests

D. Lewova, M. Němec, I. Procházka, K. Hamal (1)
G. Kirchner, F.Koidl (2)
Yang Fumin(3), D. Kucharski (4)

(1) Czech Technical University in Prague, Czech Republic, (2) Satellite Laser Station Graz, Austrian Academy of Sciences, Austria
(3) Chinese Academy of Sciences, Shanghai, China, (4) Space Research Centre, Polish Academy of Sciences,Poland

For satellite laser ranging, TV guiding is widely used to point the laser beam on the satellite. The ISIT (Intensified Silicon-Intensifier Target) camera has been applied in last years for its high sensitivity, which enabled to track all satellites of interest. However, there is a strict limitation to use it for daylight observation. The new type of CCD camera Electron Multiplying CCD (EMCCD) provides high sensitivity for short integration time required for fast real time tracking while maintaining the high ruggedness for daylight tracking. An additional internal gain reaches a factor up to 200 in comparison with regular CCD. During our tests in Graz and Shanghai we did demonstrate the ability for satellite laser ranging during the daylight and during the night time while exploiting the higher sensitivity , as well. The test results and a comparison with ISIT technology will be presented.

Andor Luca DL658 (monochrome)

Technology	Electron Multiplying CCD ("gain off" operable)
Active Pixels (horiz x vert)	658 x 496
Pixel Size (horiz x vert; µm)	10 x 10
Image Area (mm)	6.58 x 4.96
Sensor	TIL
Peak Q.E.	52%
Minimum Oper. Temp (°C)	-20
Active Area Pixel Well Depth(e⁻ typical)	25,000
Conventional Register Pixel Well Depth (e⁻ typical)	100,000
Pixel Readout Rate	12.5
Read Noise (e-)	25
Min Operating Temp (°C)	-20
Digitization	14-bit
Max. Frame rate	30 full frames/sec
PC Interface	USB 2.0 only
Price	$8850 / €7500
Software	Solis (Not Recommended) $1500 / €1400

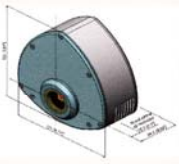

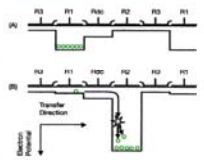

Gain register operation

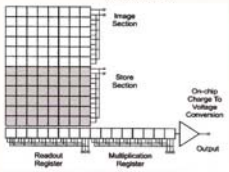

EMCCD structure

EMCCD Camera Tests

Shanghai Observatory

Graz Observatory

Test conditions:

optics	Canon lens TV-16, 1;1.4, f=50 mm, C-mount
optics settings	f/D = 22, additional ND filters 12 x each, 3 pieces
signal source	red LED, 7m distance, dark room
software	ANDOR Solis for imaging, ver. 4.3.0.0
PC notebook	UMAX Vision Book 632LX, Celeron D, 2.5GHz, 512 MB,USB2.0

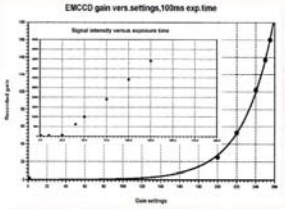

EMCCD and ISIT, Graz, 2006

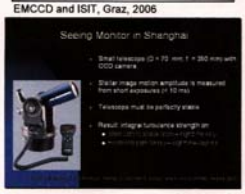

ISIT vs. EMCCD Comparison

Satellite object max/background level : 1,3

ISIT
only night observation
high FPS (30)

Satellite object max/background level : 3

EMCCD
Negs.:
night + day observing
up to 30 FPS
only 5 FPS
(for the same results)
EM ageing / anti-ageing
Pros.:
lower sensitivity
lower noise (EM gain on)
adjustability of exposure time and EM gain

EMCCD Gain experiment :

- green LED
- additional 2 ND filters inserted into optical path
- exposure time set to 100 ms
- the "EMDAC setting" set to values in the range of 1 to 255

Exposure time linearity:

- the gain setting =1 (no EM additional gain)
- one ND filter inserted into optical path
- the image intensity evaluated as a function of image exposure time (linear dependence expected)
- the gain increases with exposure time starting at 1 ms exposures
- the gain increase is linear only for exposure times >= 25 ms !

Gps BIIA-24, 0.2s, Gain 250
2006-08-25T20:07:39 UTC
Sun only, Altitude ~ 20,100 km

10x10pixels	Object	Backgr.
Standard Deviation	350,37	243,86
Mean	939,13	818,49
Maximum	2603	2263
Total Counts	375652	327396

Etalon2 0.2s, Gain 250
2006-08-25T20:39:42 UTC
Sun only, Altitude ~ 19,100 km

10x10pixels	Object	Backgr.
Standard Deviation	471,25	274,1
Mean	1024,35	820,27
Maximum	4129	2119
Total Counts	409740	328106

G87- Glonass, 0.2s, Gain 250
2006-08-25T22:53:02 UTC
Sun only, Altitude ~ 19,100 km

10x10pixels	Object	Backgr.
Standard Deviation	1508,39	310,89
Mean	1870,07	869,8
Maximum	10835	2235
Total Counts	748028	347920

Lageos2, 0.2s, Gain 250
2006-08-25T19:27:57 UTC
Sun only (Laser outside),
Altitude ~ 5625 km

10x10pixels	Object	Backgr.
St. Deviation	629,62	503,65
Mean	1713,28	1495,48
Maximum	4375	3389
Total Counts	685310	598194

Data Mining - HW

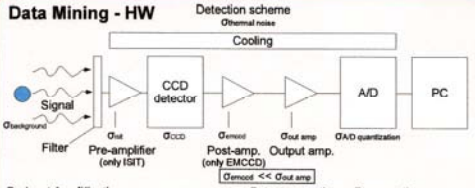

Pre/post Amplification
- decreasing readout noises levels (Low-noise internal amplification of signal before high-noise external output amplification)
- Increasing influence of S/N

Detectors settings - Exposure time
- Internal binning
- Post/pre amplifications

Filtration - interested wave-lengths pass only
- background influence(level) elimination

Cooling - Decreasing thermal noises

GPS BIIA-24 on-line filter
2006-08-25T22:09:39 UTC
Averaging - 25 frames
Selected area – contrast enhanced

Adjusted Contrast and brightness in the selected area

PC – Software methods

Methods for S/N increasing :
SW binning – 3D (integration in time + 2D in space)
SW Exposure - summation of frames
Averaging (mean; time)
Flatfield – Intensity levels calibration
Background Reduction
- Bcg. Frame subtraction(frame without object)
- AVG Filter
- Median Filter

} Artificial Background estimation and subtraction

Original image | Estimated background by median filter | Estimated Background Image subtraction

Visualization

Methods for better visibility of objects in real time :

Levels selection - Image histogram
Adjusting of contrast and brightness
Gama correction
Color inverting
Pseudo-color mapping

Pseudo color mapping

40W, 2J laser Moon shooting

Shanghai observatory

Replacing dichroic mirror

During tests in Graz and Shanghai we did demonstrate the ability for satellite laser ranging during the daylight and during the night time while exploiting the higher sensitivity

15th International Workshop on Laser Ranging, Canberra, Australia,15-20 October, 2006

LIDAR Experiments At The Space Geodesy Facility, Herstmonceux, Uk

Graham Appleby[1], Christopher Potter[1], Philip Gibbs[1] and Roderic Jones[2]

1. NERC Space Geodesy Facility, Herstmonceux, Hailsham, UK

2. Department of Chemistry, University of Cambridge, Lensfield Road, Cambridge, UK

Introduction

We are developing a LIDAR capability, ultimately to run concurrently with satellite laser ranging measurements, at Herstmonceux, UK. Our interest is in monitoring atmospheric pollution, boundary layer heights and cirrus properties over the site. For preliminary testing we have developed a modified version of the laser ranging software and used the existing laser ranging hardware to detect backscatter at a range of heights of from one to 14 km vertically above the site. During experimental runs the C-SPAD detector is gated in few-hundred metre increments from close to the telescope to beyond the tropopause, and time-tagged single-photon backscatter events are detected. Over the experimental period of a few minutes a vertical profile of atmospheric response is mapped and various layers detected. In this paper we discuss some analysis of these preliminary results and state plans for future enhancements.

Backscatter experiments

With the telescope set towards the zenith, we gate the C-SPAD for usually 30-seconds at each height above the site, from 1000 to 14,000m and collect backscatter events. The initial height of 1000m is imposed on this experiment by the separation between the transmit-receive telescopes, whose fields-of-view begin to intersect about 800m from the mount.

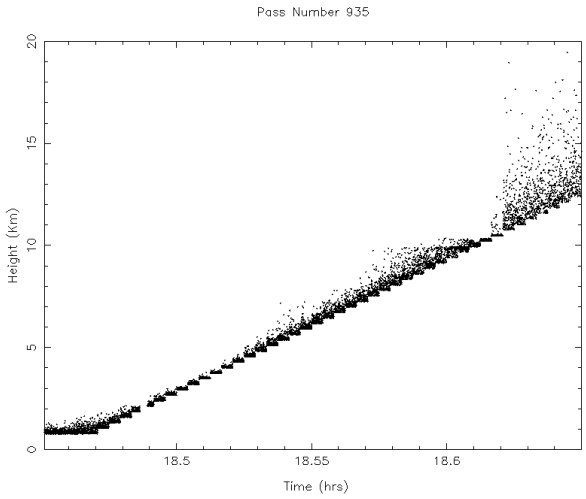

Figure 1. *Raw observations of backscatter events vertically above Herstmonceux*

The plot in Figure 1 shows the 'stepladder' that results when the raw event-height results are plotted against time. During the setup process at the first height, neutral density filters (ND) were entered manually into the receiver optical path to ensure that the range gate was approximately uniformly filled with events. Thereafter, ND values were not changed.

Preliminary analysis

We carry out a preliminary analysis of the backscatter measurements by taking the raw observations and computing for each noise point its distance above the station, on the assumption that for night-time observations all data shown in Figure 1 result from laser backscatter in the atmosphere. On this assumption and, at this stage, ignoring the decrease of laser energy with height, we therefore are able to measure return energy as a function of height and thus probe atmospheric particulate density.

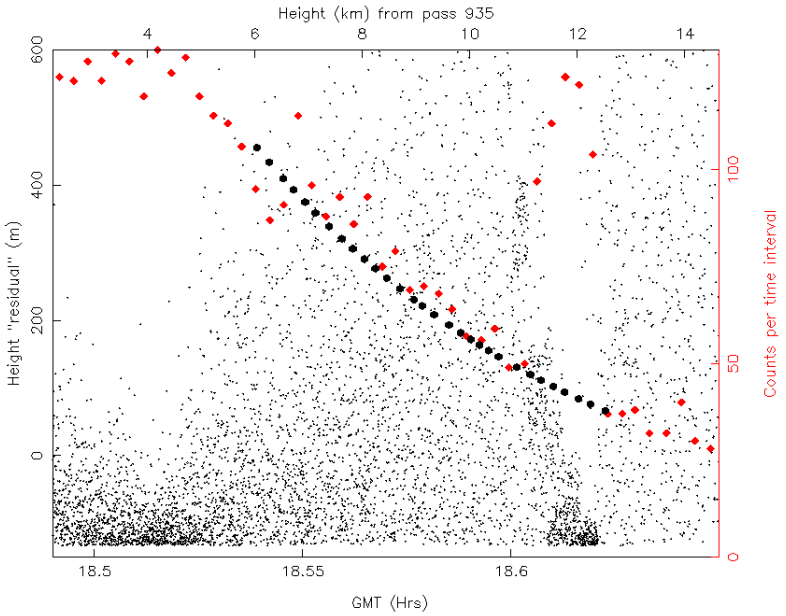

Figure 2. *Backscatter events plotted as a function of time and height in the atmosphere*

Figure 2 shows the results of this simple analysis applied to the observational session of Figure 1. If the degree of backscatter from the atmosphere was independent of height, the plot would show a uniform density of points. However, this is clearly not the case, and from the plot we suggest that a haze layer can be seen at about 4-5Km above the site, followed by a further layer at 12 km, probably identified with the tropopause. The red dots, plotted against the right-hand vertical axis, give the total number of events detected in each 3-minute interval throughout the experiment. We have fitted to those red points, strictly between the two haze layers (6 to 11km), the exponential decay curve shown by the black dots, and determine from it an atmospheric scale height of approximately 6km. Note that this fitted curve is extended in the plot beyond the region of the fit, through the high level layer, where it links with the observational totals for 13km and above. More work will be required to refine this analysis, in particular to estimate the decrease of laser energy with height.

Monitoring cloud and contrail optical density

In a related study, we are interested in the possibility of monitoring contrail and cirrus optical depth during standard laser ranging. The airspace over Herstmonceux is a busy flight path to Gatwick as well as a gateway into the UK for transatlantic routes, and a recent study into contrails over this part of the country (Stuber *et al*, *NATURE*, June 2006) has highlighted the importance of contrails as contributions to warming effects. However, little is known about the characteristics of contrails, and estimates of their optical depth vary greatly.

During laser ranging, the tracking software automatically maintains the average return level at single photons by inserting varying degrees of ND filters in the detector optical path. Compared with a model of the link budget for the ranging process, the degree of ND actually required to achieve single photon returns is a measure of departure of atmospheric transparency from that in the model. In particular, if the pass transits a contrail, the required change (reduction) in ND necessary to maintain single photon returns is a direct measurement of the additional optical depth of the atmosphere due to the trail.

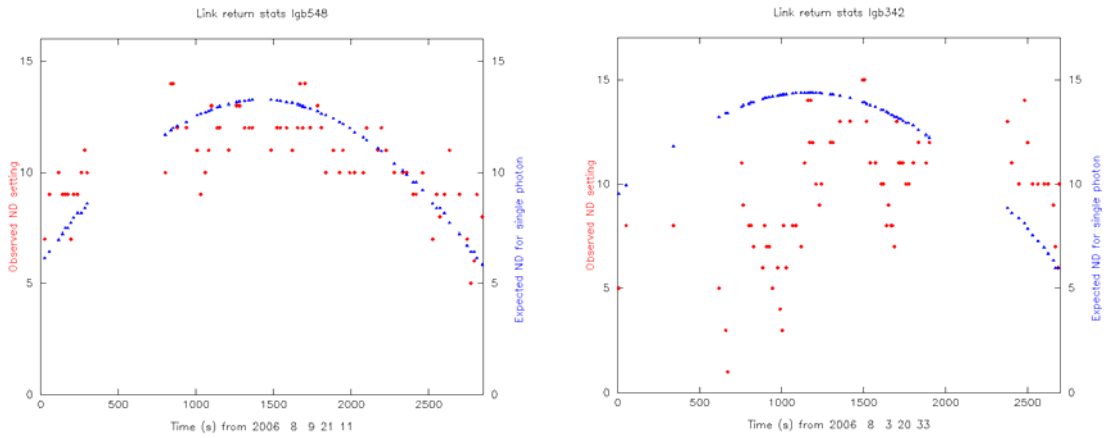

***Figure 3**. Comparison of theoretical (blue) and measured (red) ND required for single-photon laser return from LAGEOS-2.*

The plots in Figure 3 above show two tracking instances of modelled (blue points in smooth curves) and actual ND (red, scattered points) inserted by the operating system; the left plot is in a clear sky and the right plot shows three passages of the satellite behind contrails. The clear sky data follows the predicted ND values fairly well, the small changes being due to pointing variations from optimal. During the contrail passages, ND is systematically removed and replaced, giving a profile of contrail optical density.

Conclusion.

Both the observational experiments reported in this paper are at preliminary stages. Much more work is required to improve and automate the observational methods, quantify systematic effects and analyse the results. We also plan to design and integrate on the telescope a LIDAR system that is independent of, but which will run simultaneously with, standard laser ranging operations.

Possibility of the Near Earth Objects Distance Measurement with Laser Ranging Device

M.Ābele, L.Osipova

Institute of Astronomy, University of Latvia, Raiņa bulv. 19, Rīga LV-1586, Latvia

Abstract

The orbit perihelion of a some of minor planets is nearer from the Sun than the Earth's orbit. Observations are possible only in a small part of the orbit. Orbital elements of them cannot be determined accurately because we have only angular coordinates. The use of a laser ranging device for distance measurements will greatly improve the precision of determining orbital elements.

Keywords: *minor planets, laser ranging*

Introduction

We know a number of minor planets whose orbital perihelion is nearer from the Sun than the Earth's orbit.[1] Accurate forecasting of their motion is not possible, because they can be observed only in the vicinity of aphelion when their lighted sides are turned toward the Earth, and the Sun is located on the opposite side. Observations are possible only for a small part of the orbit because the planets are small in size and it is not possible to observe them from the Earth even with powerful telescopes. In order to determine orbits more accurately, we assess the possibility to measure the distance to these orbits with a laser ranging device. [2, 3, 4]

Possible measurements of minor planets with laser ranging device

A possible scheme of the experiment is shown in Fig. 1. The laser device LAS, which is situated on the Earth, radiates impulses of light in the direction of the minor planet MP. The distance is L and the diameter of the laser beam is d_{la}:

$$d_{la} = 2 \cdot L \cdot \mathrm{tg}\, r_d \tag{1}$$

where r_d is the diffraction, the angle radius $r_d = 1.2197\ \lambda/d_t$ that depends on the radiation optics' diameter d_t and the wavelength λ [5].

As the energy l_i diffraction image is irregular, the energy radiated in the direction of the minor planet E_{ep} can be calculated using formula

$$E_{ep} = E_{las} \cdot c_{at} \cdot c_{op} \frac{\int_0^{d/2} l_i(r) \cdot r \cdot dr}{\int_0^{r_d} l_i(r) \cdot r \cdot dr} \tag{2}$$

where E_{las} – laser emanated energy;

c_{at} – light transmissivity of the atmosphere;

c_{op} – light transmissivity of the optical system;

d – diameter of the minor planet.

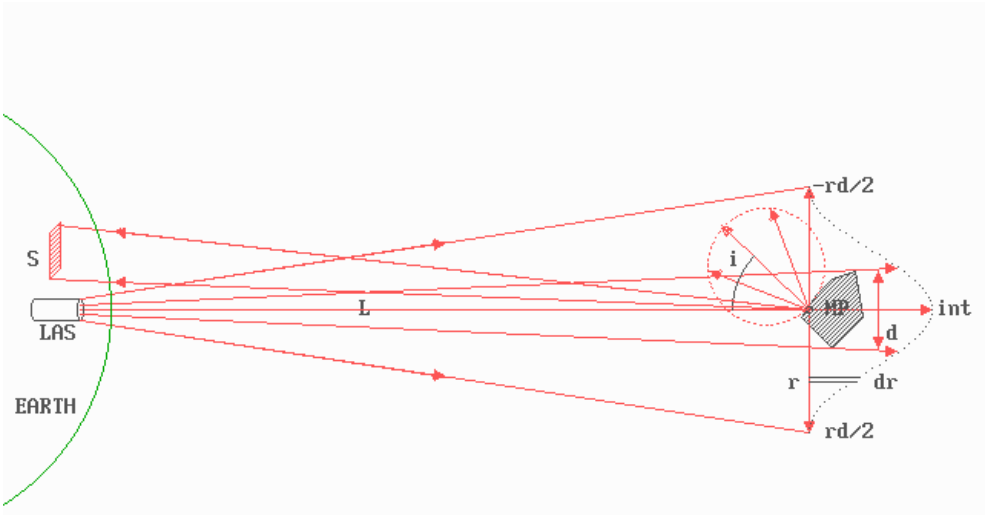

Fig. 1. Measurments of minor planets with laser ranging device

The surface of the minor planet is matted and its each element reflects the light in accordance with the Lambert Law. Area S on the Earth receives radiated energy E_e:

$$E_e = E_p \cdot c_{at} \cdot a \cdot \cos i \cdot \frac{S}{\pi L} \qquad (3)$$

where i – mean surface normal angle turned in the direction of the Earth;

a – reflection coefficient (albedo).

As E_e is very weak, the reflected energy can be described with the number of photons per unit of area $n_f = E_e/E_{fot}$, where E_{fot} – photon energy:

$$E_{fot} = h \cdot \nu \qquad (4)$$

where h – Planck's constant ($h = 6.622 \cdot 10^{-34}$ J·s);

ν – frequency of light wavelength.

The calculation results are showed in Table 1:

Laser energ. = 10 J

Laser wave length = 0.694 mkm

Laser beem diverġence = 0.5819907" (2 r difr)

Atmospher transmitance = 0.8

Telescope transmitance = 0.9

Planets albedo = 10 % (black)

	Planets diameter, m				
	50	100	200	400	800
Range, km	Reflected photons on 1 km^2				
50000	1.953181E+7	6.593346E+7	1.413264E+8	1.583503E+8	1.631335E+8
100000	1275306	4882952	1.648337E+7	3.53316E+7	3.598758E+7
200000	80588	318826	1220738	4120841	8832901
400000	5052	20147	79706	305184	1030210
800000	316	1263	5036	19926	76296
1600000	19	79	315	1259	4981
3200000	1	4	19	78	314
6400000	0	0	1	4	19
1.28E+7	0	0	0	0	1
2.56E+7	0	0	0	0	0

Table 1*. Reflected photons from minor planet.*

The minor planet is irradiated by the Sun. Energy received by the minor planet per second is:

$$E_{sp} = W_s \cdot \pi \cdot \frac{d^2}{4} , \tag{5}$$

where W_s – constant of the Sun (near the Earth W_s = 1360 W/m^2).

Of late, CCD devices with very high sensitivity in red waveband 0.694 μm wavelength laser have been used. In this waveband, the Sun's radiation is less intense than in the visible range. If wavelength is dλ, energy in the zone is

$$\varepsilon_\lambda = \frac{2\pi hc^2 \cdot d\lambda}{\lambda^5 \cdot e^{\frac{hc}{\lambda kT}} - 1} . \tag{6}$$

Energy of the reflected light is

$$E_{st} = E_{sp} \cdot \frac{\varepsilon_\lambda}{\varepsilon} \cdot c_{at} \cdot a \cdot \cos i \cdot \frac{S_{tr}}{\pi L} , \tag{7}$$

where S_{tr} is the area of the reflected light:

$$S_{tr} = \pi \cdot \frac{D_{dt}^2}{4} . \tag{8}$$

And the frequency f_n is

$$f_n = \frac{E_{st} \cdot q}{E_{fot}} , \tag{9}$$

where q – receiver quantum efficiency.

The probability that at least one photon enters the telescope aperture is small. If a telescope with 1.6 m diameter is used, about 50 reflected pulses may be detected in one hour, the noise from the solar background is 249 pulses per second on the average. If a larger receiving telescope is used, a minor planet's trajectory can be spotted better, the measurements can be done at a larger distance and the reflected pulses received with a higher frequency (Fig. 2).

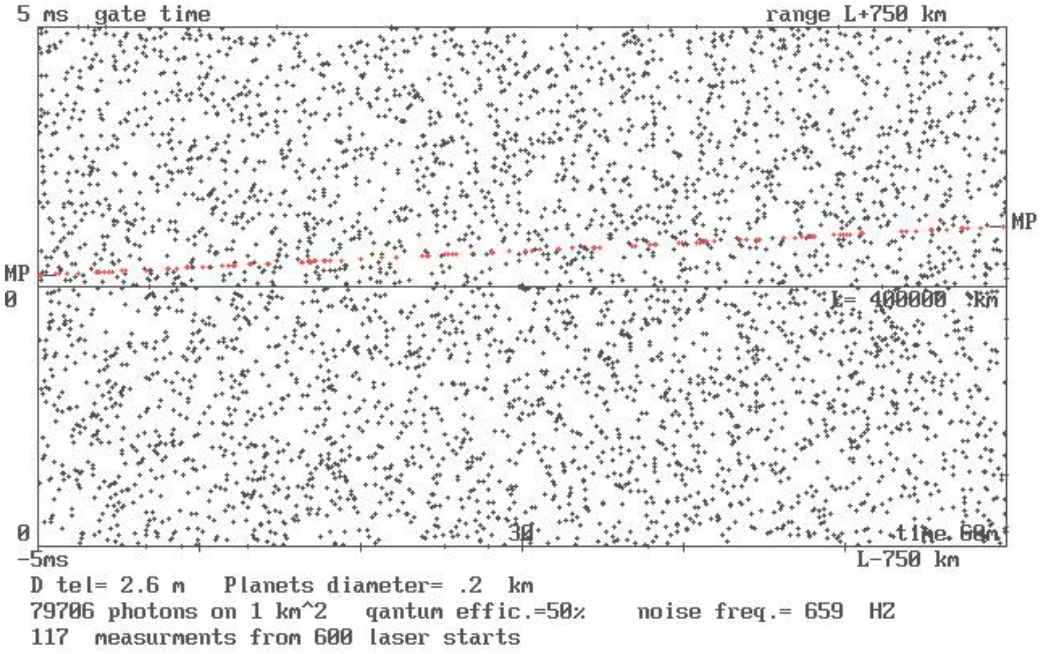

Fig.2. Reflected laser pulses and noise from minor planet

Experiment realization possibility

Described experiment is in planning stage. In order to ensure irradiation of the minor

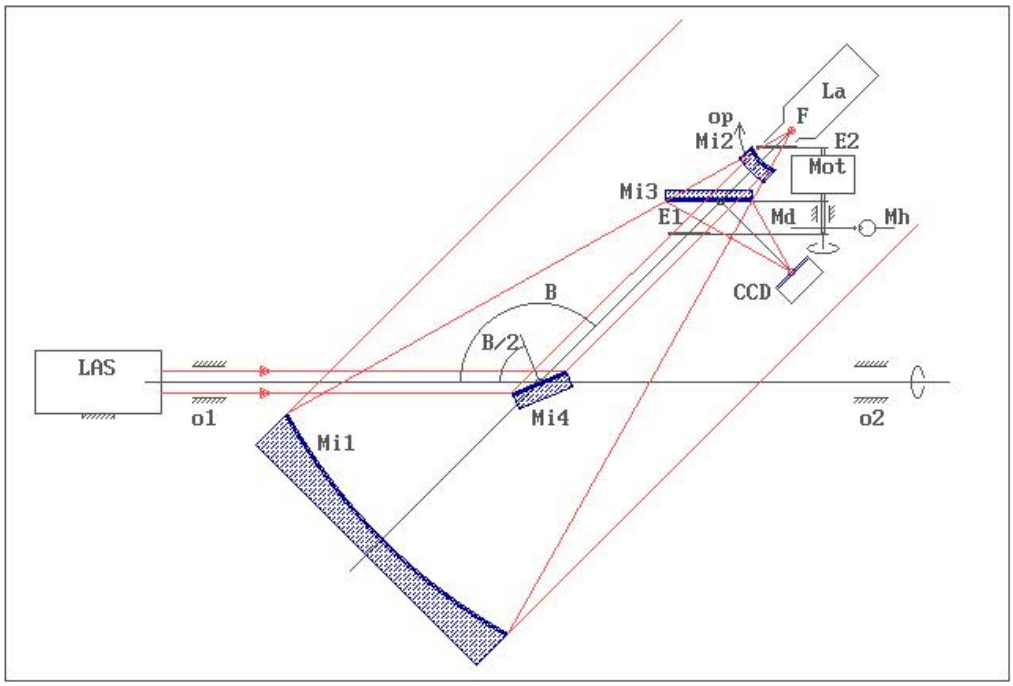

Fig.3. The laser arangement relative to the telescope

planet with a laser beam, a telescope for lighting up cosmic objects from the Earth is being devised at the Institute of Astronomy of the University of Latvia [Fig. 3, 4].

Its main optical element is the paraboloid mirror, 600 mm in diameter, that is put in a special mounting with a horizontal first axis of mounting. It allows for the laser beam to be directed to the irradiation object by a single additional mirror. [6] A laser device with the power level of 10 J can be manufactured in Lithuania by EKSPLA Company.

The receiver telescope of the reflected signal can be placed in a large distance from the transmitting source. Any astrophysical telescope with a mirror of over 1 meter in diameter could be used, and the 1.6 m telescope of the Moletai Observatory (Lithuania) could be a good option. In order to minimize the signals reflected from the Sun, for background impulses the exit of the telescope needs to be equipped with the narrow-band light filter.

Fig.4*. The telescope model.*

Taking into account that the transmitting and receiving devices are situated in a large distance each from the other, it is difficult to harmonize their frequency ranges. The frequencies of transmitted and reflected energy may also differ due to the Doppler Effect. Therefore, it is convenient to make use of a spectrograph with its exit equipped with a charge coupled device (CCD) camera. The scheme of the measurement device is showed in Figure 5.

The spectrum of the minor planet is projected on the outer column of the charge matrix CCD. At the time moment when the re-transmitted impulse from the planet can be expected, a frequency from the silica generator GEN, which moves the accumulated information along j axis, is supplied by the help of an electronic switch whose operation has been synchronized with the GPS time scale. When all matrix cells are filled consistently with the ordinary algorithm with the help of the synchronization scheme SINH through a digital amplitude modifying device, the matrix content is fed to the computer DAT. The available information covers ~ 1000

spectrum zones. One of them can capture the retransmitted impulses from the surface of the minor planet. Any needed zone can afterwards be found from within the absorption zones of the Sun. If a frequency that shifts information from one matrix column to another is 15 MHZ, the distance measurement discreet is 10 m. This allows realization of the showed algorithm of measure.

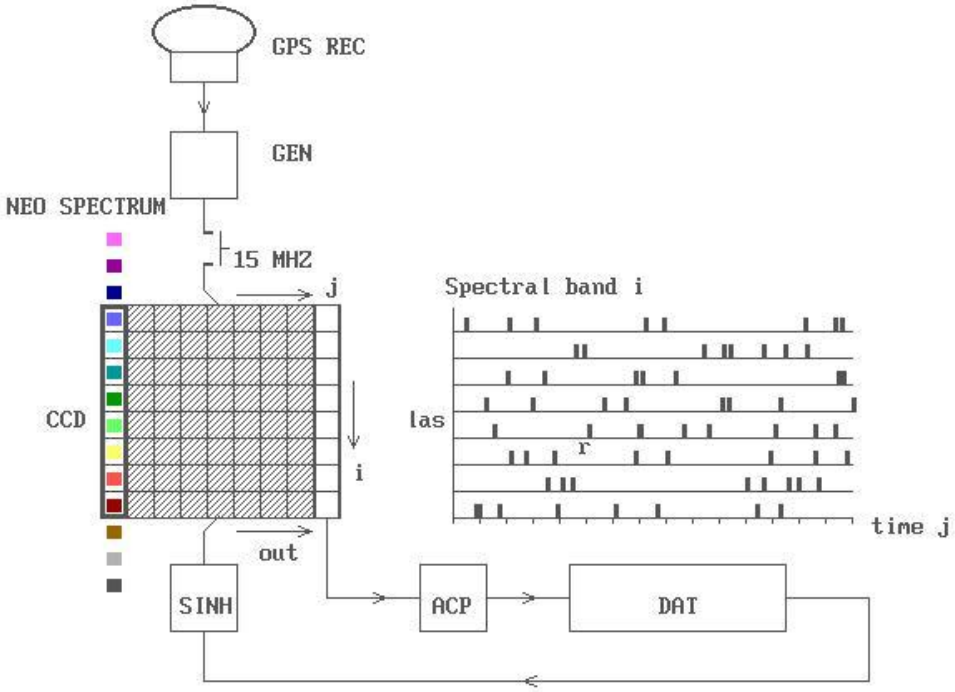

Fig. 5. Spectrograph for reflected pulses measurment

Conclusions

This project can be carried out in co-operation with other astronomers of the Baltic States. Its implementation would enable scientists to improve significantly the orbital elements of the minor planets that present danger to the Earth and to forecast their motion in the future.

References

[1] IAU Minor Planet Center. Unusual Minor Planets. 2002 Sept. 10. http://cfa-www. harvard. edu/iau/lists/Unusual. html

[2] Abele M., Osipova L. Determination of NEO orbits based on laser ranging measurements. Latvian Journal of Physics and Technical Sciences. 2004. 1. p. 31-36.

[3] Abele M., Balklavs-Grinhofs A., Osipova L. Possibility of minor planets distance measurement with laser ranging device. Latvian Journal of Physics and Tehnical Sciences. 2004. 2. p. 54-61,

[4] Degnan John J. Unified Approach to Photon-Couting Microlaser Rangers, Transponders, and Altimeters. Surveys in Geophysics Kluver Academic Publishers. 2002.

[5] Д.Д.Максутов. Астрономическая оптика. 1946. (rus.)

[6] Abele M., Vjaters J., Ubelis A., Osipova L. A telescope to spot space objects from the Earth surface. Latvian Journal of Physics and Tehnical Sciences. 2005. 3. p. 20-28.

TRANSPONDERS SESSION SUMMARY

Chair: Ulli Schreiber

Transponder applications are becoming a real option. Feasibility studies using the optical facility at Goddard and the MOLA on the Mars Explorer and MLA on the Messenger spacecraft have demonstrated successfully one-way and two-way optical ranging at interplanetary distances. These experiments became possible because of the lucky opportunity based on the availability of missions for the test of at least some mission aspects of transponders. A full transponder concept is in preparation for the Lunar Reconnaissance Orbiter (LRO) with the goal of improving the orbit determination for the altimeter application. This will be the first mission where ILRS support is required for a transponder application. Currently there are several simulation and evaluation efforts under way in order to improve the understanding of the potential of transponders, both in simulation and in a collocated ranging experiment.

Laser Ranging at Interplanetary Distances

G. A. Neumann[1], J. F. Cavanaugh[1], D. B. Coyle[1], J. McGarry[1], D. E. Smith[1], X. Sun[1], M. Torrence[1], T. W. Zagwodski[1], and M. T. Zuber[2]

1. NASA Godddard Space Flight Center

2. Massachusetts Institute of Technology

Contact: neumann@tharsis.gsfc.nasa.gov /Tel. 301 614 6026/Fax 301 614 6015.

Abstract

In May 2005, timed observations of short laser pulses of light between the Mercury Laser Altimeter (MLA) instrument aboard the MESSENGER spacecraft, and the Goddard Geophysical Astronomical Observatory (GGAO) measured the two-way range time-of-flight with sub-nanosecond precision. A one-way optical experiment was conducted a few months later from GGAO to the Mars Orbiter Laser Altimeter (MOLA) aboard the Mars Global Surveyor (MGS) spacecraft at a distance of 81 Gm (0.54 AU). These experiments demonstrated the possibility of interplanetary communication and precise ranging using modest power.

Introduction

Laser ranging in space began with ranging to retroreflectors on the Moon placed by the Apollo [Faller et al., 1969] and Luna missions. Pulses fired by a powerful, earth-based laser are reflected back to the transmitting site, where time-of-flight measurements are made using standardized clocks. Such measurements routinely achieve decimeter precision using very short pulses and single-photon detectors. Laser ranges require only small corrections for atmospheric transmission, and provide precise constraints on the dynamics of the Earth-Moon system. With retroreflectors, the number of photons available for timing decreases with the fourth power of the distance, making distances much beyond the Moon's orbit impractical. A transponder, on the other hand, receives pulses and sends pulses back in a coherent fashion so that the photon count decreases only by the square of distance in both directions, making ranging possible at far greater distances. The Mercury Laser Altimeter (MLA) ranging experiment in May, 2005 demonstrated the concept of asynchronous transponders [Degnan, 2002] in which two laser terminals independently fire pulses at each other, with timing recorded for analysis at a common location. The times of the paired observations are then used to solve for two-way range as well as a spacecraft clock offset. Multiple transponder observations can additionally constrain the spacecraft clock drift, the range rate and the range acceleration.

The MLA experiment used the 1.2-m telescope facility of the Goddard Geophysical Astronomical Observatory (GGAO) to fire at and detect pulses from MLA at a distance of 24 Gm, or 0.16 AU. It served to calibrate the instrument transmitter and detector far field characteristics and alignment, as well as confirm the distance inferred from radio tracking. The results of this experiment were communicated in brief [Smith et al., 2006]. In September 2005, one-way laser transmission was achieved to the Mars Orbiter Laser Altimeter (MOLA) instrument at Mars [Abshire et al., 2006] from GGAO using a more powerful laser firing at 49 Hz. MOLA no longer had its laser or timing capability but could record the rate of detector triggers using the spacecraft 8-Hz timing signal. An encoded sequence was transmitted using a 1-Hz shutter. The number of pulses received was strongly correlated with the modulation of the outgoing pulses. This experiment demonstrated the feasibility of laser

communication at 81 Gm, and confirmed the spacecraft clock offset of Mars Global Surveyor to a precision of ~4 ms.

We provide here further details regarding these experiments and prospects for future laser ranging and communication in deep space.

Ground Transmitter and Receiver

The HOMER life-test laser [Coyle and Stysley, 2005] employed in the MLA-Earth experiment produced 16 mJ per shot at 240 Hz. MLA received pulses at 8 Hz, the electronics allowing about 14 ms in each shot interval for returns. Thus it was anticipated that the laser would place three or more pulses inside the timing window. A 10X beam expander collimated the outgoing beam divergence to approximately 50 microradians (90% energy) after transmission through a portion of the 1.2-m telescope of the Goddard Geophysical Astronomical Observatory (GGAO). The energy per shot at the entrance to the 0.0417-m^2 MLA telescope would be 0.6 fJ, neglecting losses in transmission and atmospheric attenuation. The energy at the telescope measured from shots detected at low and high thresholds by the MLA was 0.083 ± 0.04 fJ. After the experiment, it was found that coatings on six folding mirrors in the GGAO optical path had been optimized for 532 nm operation and transmitted only 70% of 1064 nm light, reducing total transmission to about 12%. The effective transmitted energy of the ground system was reduced accordingly, amounting to about 2 mJ per shot. Since the MLA experiment and the Earth-MOLA experiment performed soon thereafter, the mirrors have been recoated and total transmission at 1064 nm is about 70%.

Ground and spacecraft timing

Absolute time and range measurements using a transponder requires tying local event timers to terrestrial time standards. Timing at GGAO was provided by GPS-steered rubidium clocks. A Honeywell precision event time digital counter (TDC) logged the leading-edge times of outgoing and incoming laser pulse triggers with respect to UTC at 10-ps resolution [Kalisz, 2004]. The waveform of each pulse was also digitized by means of a 1-GHz oscilloscope. The centroid time resulting from fitting a Gaussian envelope to the waveforms provided the most precise timing, owing to the extended nature and variable height of the detected pulses (Figure 1). These centroid times were also corrected to UTC seconds of day as recorded by the GPS-steered clock. GPS time errors result in absolute ground clock uncertainty of ~40 ns. Slowly-varying GPS errors do not affect relative times between transmit and receive pulses, which were fit with a root-mean-square residual of 0.39 ns.

Timing was corrected for a 44.2 ns path delay between the transmit laser start detector and the TDC, an optical path delay of 43.8 ns between the transmit detector and the telescope mount reference point, and a 110.2 ns delay from the GPS receiver antenna to the TDC. The latter delay is also applied to the time of the received pulses. The optical path from the telescope mount to the detector assembly and the electronic delay between the detector and the TDC was ~20 ns. Significant forward scattering through clouds likely caused pulse broadening and some delay. Atmospheric refraction delays of tens of ns should also be considered when determining the absolute times of flight, in view of the relatively low 30-35° elevation of the spacecraft above the horizon, but these were not applied. An independent calibration of all timing delays using an earth satellite retroreflector could not obtained during the allotted time owing to cloudy conditions.

The MESSENGER spacecraft [Solomon et al., 2001] employs an ovenized quartz-crystal-based oscillator whose frequency is stable to a few parts in 10^{12} over the course of an hour [Cooper, 2004]. The Mercury Laser Altimeter (MLA) acquires its time base from the spacecraft via a one-pulse-per-second (PPS) tick along with the corresponding mission elapsed time (MET) message over the data bus. The hardware PPS signal provided to MLA was benchmarked at 21 μs uncertainty during ground testing [Cavanaugh et al., 2007]. The PPS offset, and the offset between the MLA event time reference T0 and the PPS tick, are very stable over short intervals of time. The latter is monitored by the instrument at 125-ns resolution. Thus the spacecraft clock can be related to the MLA timing only to tens of microseconds in an absolute sense, but are precisely coupled over intervals of an hour.

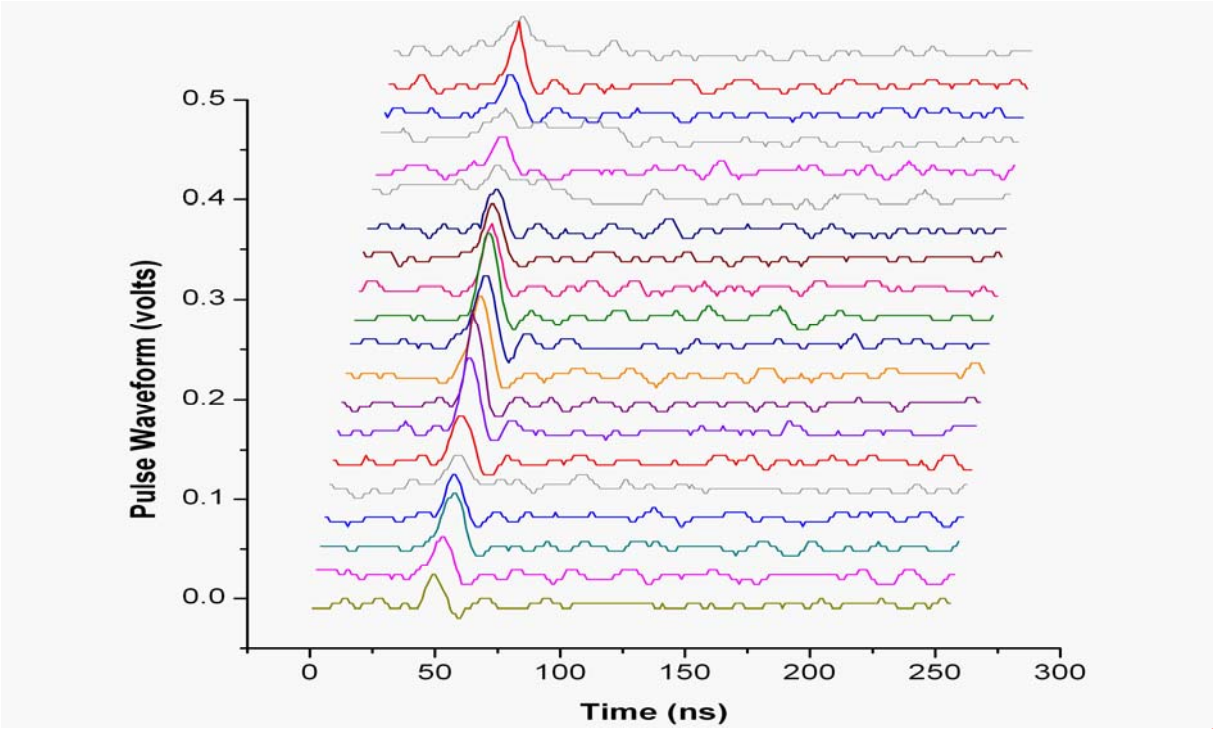

Figure 1. *MLA Pulse waveforms recorded at GGAO on May 27, 2005, along with a few cloud echoes (gray curves) from the ground laser.*

The MLA obtains a 5 MHz clock signal from the spacecraft which drives a coarse event timer. The transmit and receive event timers consist of a set of time-to-digital converters (TDC) based on the tapped delay line technique [Paschalidis et al., 1998]. The tapped lines consist of a series of logic gates that count from an event to the next 5-MHz clock edge. An on-chip delay-lock-loop calibrates the overall delay time against an external reference clock signal, and the delay of each gate is measured on the ground. The combined circuits can time the leading and trailing edges of the transmitted laser pulses and the received echo-pulses to ~400 ps resolution. Coarse and fine clock counts are downlinked via telemetry. A zero-range offset bias of 23.8 ns for high threshold returns and 30.9 ns for low threshold returns is subtracted to account for electronic delays in the receiver relative to the start pulse.

The spacecraft radio telemetry system is used to calibrate MET against time standards at the Deep Space Network (DSN). Spacecraft time must be correlated to a dynamical

time to millisecond accuracy for geodetic purposes, in order to position MESSENGER in space and derive altitude from ranges. The MESSENGER project maintains a clock file giving corresponding MET and Terrestrial Dynamic Times (TDT). An event on the spacecraft at a given MET tick is considered simultaneous with an event at the corresponding terrestrial time, as viewed from the Solar System Barycenter. Owing to special relativity, corresponding times may not appear simultaneous to a terrestrial observer. The Navigation and Ancillary Information Facility (NAIF) toolkit models the travel of light between Earth and MESSENGER in a barycentric inertial frame and was used herein.

MESSENGER Range and Time Transfer Results

During the MLA-Earth experiment, the MESSENGER clock correlation file was updated twice over the course of a week, with coefficients given in Table 1. The clock rate typically varied by <1 part in 10^9 over the period of four days, however, telemetry time coding errors at the DSN on the day before the experiment resulted larger-than-usual variation. Independent verification of the spacecraft timing system integrity was an important goal of the ranging experiment. The downlink time residual was found to be 347 microseconds, while the uplink residual was 351 microseconds. The average residual offset of the spacecraft clock was therefore 349 microseconds. However, post-processing of the spacecraft timing (Stanley B. Cooper, email communication, November 8, 2006) suggests that this clock offset was ~49 microseconds. For reference, the mission requirement is to maintain time correlation to 1 ms.

Table 1*. Spacecraft clock correspondences used during experiment.*

MET	TDT	Rate of MET
25632557	26-MAY-2005T22:11:17.912822	1.00000001564
25963200	30-MAY-2005T18:02:00.917993	1.00000001704
MLA-Earth result, uncorrected for relativistic time delay		
25710307	27-MAY-2005T19:46:03.729662	1.00000001559

Range residuals were calculated via least squares, resulting in a solution from two-way light time of 23,964,675,433.9 m at the 25710307 MET tick, with range decreasing at a rate of 4,154.663 m/s. A spacecraft ephemeris solution using radio tracking data (msgr_20040920_20050823_od032.bsp) predicted a range of 23,964,674,906.35 m. However, the relativistic (Shapiro) delay in the speed of light and bending of light path due to the solar gravitational potential amounted to an equivalent of 486.60 m in each direction, so that the effective range was 23,964,675,392.95 m, or 41 m less than measured by the MLA experiment. There are several sources of error that could account for this discrepancy: the spacecraft ephemeris, errors in the measurement model used for comparison, errors in ground timing and path correction, or combinations of these errors. Such close agreement, to a part per billion in range, is truly remarkable. The formal error in the laser range solution was 0.2 m, or one part in 10^{11}.

MOLA Time Transfer Results

Distances to Mars are well-constrained by years of tracking of spacecraft and landers, and the clock drift on Mars Global Surveyor (MGS) has been very small, so that the

clock correlation file is updated only a few times a year to maintain the specified 10-ms accuracy. The primary purpose of this test was to determine the clock offset between the MOLA data stream and spacecraft time. MGS was commanded to scan twice across a 0.2x0.2° (3.5x3.5 mrad) region of the sky centered on the apparent position of Earth, during each of three nights in September 2005. The 1-3 mrad uncertainty in pointing control of the 9-yr-old spacecraft, as well as the 0.8 mrad detector field of view, made scanning necessary. Passive radiance confirmed that the detector was aimed correctly. MOLA detector threshold was set to produce 1-2 noise counts per second from Earth background light. In each 8-Hz interval, the number of triggers is recorded. A maximum of 6 or 7 shots from the 49-Hz ground laser could have been detected in each interval. In fact, at most 7 triggers above threshold occurred in any single interval, consistent with the expected probability of detection. Roughly 500 such pulses were counted during one successful evening, and from the pattern of counts, it was clear that the pulses were being recorded somewhat later than expected, consistent with a 114-ms skew between the spacecraft time signal and Earth time. Such a bias had earlier been estimated using the altimetry in an eccentric orbit [Rowlands et al., 1999].

Prospects for future experiments

Opportunities to repeat the MLA-Earth experiments occur at several intervals beginning in May 2007, at distances of 100 Gm or more (0.66 to 1 AU). The MESSENGER spacecraft must maintain its sunshade Y-axis within ~12 degrees of the Sun while pointing the instrument Z-axis toward earth, a geometry which also maximizes the elongation of the MLA with respect to the Sun as seen from Earth. The first MLA experiment required several days to complete, even with moderately good visibility. It was severely constrained by the pointing knowledge of the spacecraft, such that no more than 24 shots were received on the ground from MLA during a single observing session. As a result of the experiment, the repeatability of the MLA boresight was determined from passive scans to be within 50 microradians from day to day, and within each scan, the control of each scan line was within its 16-microradian spacing. During several windows through the clouds, the MLA receiver was able to detect ~90 shots from the ground, but never with a probability of detection greater than 1-2%. In 15 events, both a high and a low threshold trigger occurred, with leading and trailing edge times. Such timing allows for estimation of the pulse width and energy, assuming a Gaussian waveform, as detailed in Cavanaugh et al. [2007]. The energy received at the telescope entrance from these events averaged 0.083 fJ, or 0.064 fJ at the detector after transmission losses.

From June 18 to 24, 2007, attempts were made to repeat the MLA experiment at a distance of 104 million km shortly after MESSENGER's second Venus flyby, when the instrument could be safely pointed at Earth. With the improvement in telescope optics, using a single-photon-counting detector, there was sufficient link even with the relatively low ~18 mJ energy of MLA's 1064-nm pulses to range to GGAO at this distance. A 250-mJ laser firing at 48 Hz was employed to improve the probability that a shot would be received within each 14-ms window occurring at 8 Hz, after proper phasing. Communication of a message to the MLA was attempted by modulating the position of each pulse by a variable number of microseconds. However, a myriad of problems with the optical and mechanical ground systems as well as unfavorable weather prevented communication in either direction.

An opportunity for MLA at a similar distance will occur in March 2008, where the elongation of MESSENGER from the Sun will be at a maximum of 44°, with two opportunities in 2009 at elongations of 39° and 36°. It will also be possible to perform the experiment twice per year in Mercury orbit, although solar rejection at the Earth station will require a very narrow field of view. The continued MLA experiments will further demonstrate the ability of lasers to perform precise range measurements, time transfer, and communications throughout the solar system. At these distances the Shapiro delay reaches 10-20 μs. The ability of MLA to see more dramatic effects during solar conjunction is precluded by spacecraft sun avoidance constraints, but the solar avoidance requirements of the MLA optical design itself are minimal. Such experiments could be considered in future interplanetary deployments.

References

[1] Abshire, J.B., X. Sun, G. Neumann, J. McGarry, T. Zagwodzki, P. Jester, H. Riris, M. Zuber, D. E. Smith, "Laser Pulses from Earth Detected at Mars", Conference on Lasers and Electro-Optics (CLEO-06), Long Beach, California, May 2006.

[2] Cavanaugh, J.F., J.C. Smith, X. Sun, A.E. Bartels, L. Ramos-Izquierdo, D. J. Krebs, A. Marie Novo-Gradac, J.F. McGarry, R.Trunzo, J.L. Britt, J. Karsh, R.B. Katz, A. Lukemire, R. Szymkiewicz, D.L. Berry, J.-P. Swinski, G.A. Neumann, M.T. Zuber, D. E. Smith, The Mercury Laser Altimeter Instrument for the MESSENGER Mission, *Space Science Reviews,* in press.

[3] Cooper, S.B., "Design of the MESSENGER Timekeeping System" and "Preliminary Report on MESSENGER Timekeeping Test Results", JHU/APL memos SEA-2003-029, July 11, 2003 and SEA-2004-045, June 7, 2004.

[4] Coyle, D.B., and P.R. Stysley, "The high output maximum efficiency resonator (HOMER) developed for long life, space-based altimetry", IEEE International Aerospace Conference, Big Sky, Montana, 4-11, March 2006.

[5] Degnan, J. J., Asynchronous laser transponders for precise interplanetary ranging and time transfer, *J. Geodynamics* (Special Issue on Laser Altimetry), pp. 551-594, November, 2002.

[6] Faller, J. E., I. Winer, W. Carrion, T. S. Johnson, P. Spadin, L. Robinson, E. J. Wampler, and D. Wieber, Laser beam directed at the lunar retro-reflector array: observations of the first returns, *Science*, 166, 99-102, 1969.

[7] Kalisz, J., Review of methods for time interval measurements with picosecond resolution, *Metrologia*, Vol. 41, pp. 17-32, 2004.

[8] Paschalidis, N., K. Karadomoglou, N. Stamatopoulos, V. Paschalidis, G. Kottaras, E. Sarris, E. Keath, and R. McEntire, "An integrated time to digital converter for space instrumentation", 7th NASA Symposium on VLSI Design, Albuquerque, NM, Oct. 1998.

[9] Rowlands, D.D., D.E. Pavlis, F.G. Lemoine, G.A. Neumann, and S.B. Luthke, The use of laser altimetry in the orbit and attitude determination of Mars Global Surveyor, *Geophys. Res. Lett., 26*, 1191-1194, 1999.

[10] Smith, D.E., M.T. Zuber, X. Sun, G.A. Neumann, J.F. Cavanaugh, J.F. McGarry, and T.W. Zagwodzki, Two-way laser link over interplanetary distance, *Science*, 311, p.53, 2006.

[11] Solomon, S.C., R. L. McNutt Jr, R. E. Gold, M. H. Acu˜na, D. N. Baker, W. V. Boynton, C. R. Chapman, A. F. Cheng, G. Gloeckler, J. W. Head III, S. M. Krimigis, W. E. McClintock, S. L. Murchie, S. J. Peale, R. J. Phillips, M. S. Robinson, J. A. Slavin, D. E. Smith, R. G. Strom, J. I. Trombka, M. T. Zuber, 'The MESSENGER mission to Mercury: Scientific Objectives and Implementation,' *Planetary and Space Science*, Vol. 49, pp. 1445-1465, 2001.

Simulating Interplanetary Transponder and Laser Communications Experiments Via Dual Station Ranging To SLR Satellites

John J. Degnan[1]

1. Sigma Space Corporation, 4801 Forbes, Blvd., Lanham, MD 20706 USA.

Contact: John.Degnan@sigmaspace.com Fax: +01-301-577-9466

Abstract

Laser transponders open up new opportunities for SLR in solar system and planetary science and general relativity, and laser communications offers orders of magnitude more bandwidth in transferring sensor data from our planetary neighbors and their moons. As new missions are proposed by the spacefaring nations to take advantage of these technologies, there will undoubtedly be a need to simulate interplanetary links and test the Earth-based and spaceborne terminals under realistic operational scenarios prior to launch. Dual station ranging to the SLR satellite constellation, in which Station A provides the radiation source received by Station B and vice versa, can provide a realistic testbed for future interplanetary transponder and lasercom systems, simulating not only the high space loss at interplanetary distances (due to the more rapid R^{-4} falloff in signal levels from passive satellites) but also the passage of the transmitted and received beams through the turbulent atmosphere. Satellites which induce minimal pulse spreading are best suited to this application, and the current SLR satellite constellation can simulate interplanetary links as far out as Saturn. The lunar reflectors can simulate distances of 93 AU or more, well beyond the Kuiper belt.

Introduction

In 2005, NASA/GSFC succeeded in performing a two-way asynchronous laser transponder experiment [Degnan 2002] with the Messenger spacecraft at a distance of 24 million km [Smith et al, 2006]. This achievement was followed just three months later by a one way transfer of pulses to the Mars Global Surveyor at a distance of 80 million km. Although these were experiments of opportunity rather than design, they clearly established the feasibility of precise interplanetary laser ranging and wide bandwidth communications. Laser transponders open up new opportunities for SLR in solar system and planetary science and general relativity, whereas laser communications offers orders of magnitude more bandwidth in communicating sensor data from our planetary neighbors and their moons back to Earth. As new missions are proposed by the spacefaring nations to take advantage of these technologies, there will undoubtedly be a need to simulate interplanetary links and test the Earth-based and spaceborne terminals under realistic operational scenarios prior to mission approval and launch. In addition to overcoming large R^{-2} space-losses over interplanetary distances, the laser beams in these future systems must traverse Earth's turbulent atmosphere, which produces effects such as beam spreading, beam wander, and scintillation (fading) [Degnan, 1993]. These effects can become much more pronounced as we attempt to extend the range of transponder or lasercom operations by reducing the uplink beam divergence in order to concentrate more energy on the remote terminal.

End-to-end ground based experiments which can convincingly simulate all aspects of these complex systems are both difficult to envision and expensive to implement. Fortunately, atmospheric transmission and turbulence effects on the uplink and

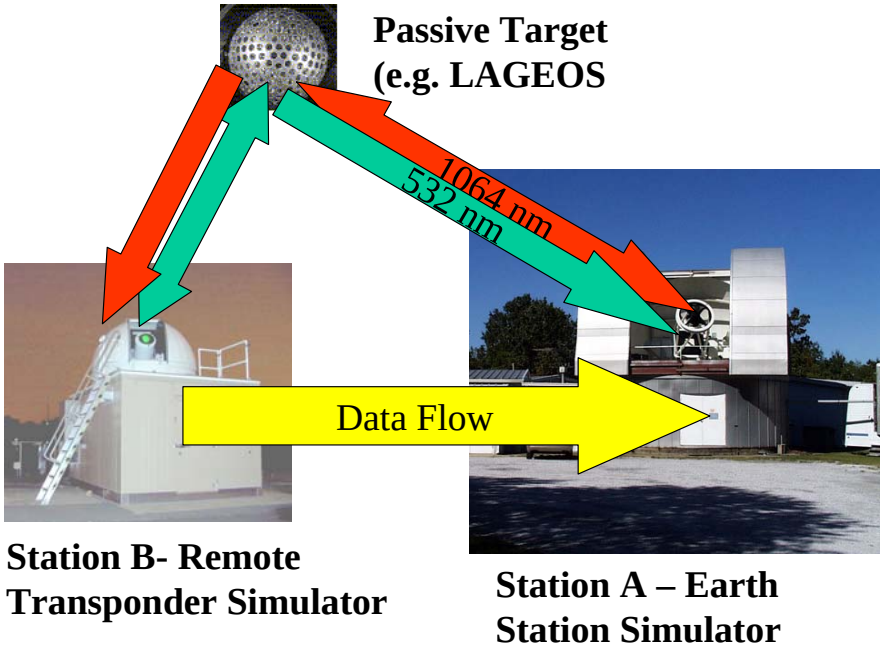

Figure 1: *Dual station laser ranging to LAGEOS with, for example, the GSFC 1.2 meter telescope facility simulating the Earth station and NASA's 40 cm aperture SLR2000 system simulating the remote terminal.*

downlink beams are the same whether the uplink beam is being reflected from a passive high altitude satellite in Earth orbit as in SLR/LLR or transmitted from a distant transponder or lasercom terminal in Deep Space. Dual station ranging to the SLR satellite constellation, in which Station A provides the radiation source received by a nearby Station B and vice versa as in Figure 1, can provide a realistic and inexpensive testbed for future interplanetary transponder and lasercom systems by duplicating not only the high space loss at interplanetary distances (due to the more rapid R^{-4} falloff in signal levels from passive satellites) but also the passage of the transmitted and received beams through the turbulent atmosphere. Each station must be located within the reflected return spot of the other station, and this requirement typically restricts the inter-station separation to within a few hundred meters. The larger terminal, simulating the Earth station, would exchange reflected pulses from the satellite with a smaller station, simulating the remote transponder or lasercom terminal. Figure 1 illustrates GSFC's 1.2 meter telescope facility ranging to LAGEOS in the infrared (1064 nm) while NASA's 40 cm aperture photon-counting SLR2000 system ranges to the same satellite in the green (532 nm). In order to simulate a dual wavelength transponder or lasercom experiment Each station is equipped with a receiver channel at a second wavelength to detect reflected pulses from the sister station. The experiment is self-calibrating since the transponder measures the dogleg defined by Station A – satellite – Station B while the individual ranging systems measure the Station A – satellite and Station B – satellite distances, albeit at slightly different epoch times. Ground surveys typically define the interstation vector, or third leg of the triangle, to better than 2 mm. This provides an accurate way to test the ranging and time transfer algorithms. Similarly, the Bit Error Rate (BER) of an "interplanetary" laser communication system can be obtained by directly comparing the incoming and outgoing bits at the adjacent sites. Such experiments are currently being pursued at NASA [McGarry et al, 2006].

Automated acquisition of the Earth station by the remote terminal can be demonstrated by either turning off or ignoring the closed ranging loop at 532 nm while it searches for the reflected light at 1064 nm. The ability to lock Station A onto the satellite via a closed single ended ranging loop at 1064 nm ensures a steady source of photons from the Earth station for the remote terminal to find and lock onto.

Link Equations

The link equations define the received signal strength at either station. For the infrared link from the Earth station A to the remote terminal B via a passive satellite, the link equation is given by [Degnan, 2001]

$$n_R^{AB} = \frac{4\eta_q^B \eta_t^A \sigma_s \eta_r^B T_A^{2\sec\theta_A}}{h\nu_A \left(\theta_t^A\right)^2 (4\pi)^2} \frac{E_t^A A_r^B}{R_R^4} \tag{1}$$

which depends on the transmitted energy E_t, the receive aperture A_r, detector quantum efficiency η_q, the photon energy $h\nu$, the one-way zenith atmospheric transmission T_a, the satellite zenith angle θ_A, the divergence half-angle of the laser beam θ_t, the target optical cross-section σ_t, measured in square meters, and the optical throughput efficiencies of the transmitter (η_t) and receiver (η_r) optics respectively. The *A* and *B* superscripts and subscripts signify the terminal for which the value applies, and are reversed for the opposite link from terminal *B* to *A*. The quantity R_R.is the slant range to the target satellite. For the nominally circular orbits of typical SLR targets, R_R.can be expressed as a function of the satellite height above sea level *h*, and the satellite zenith angle

$$R_R(h,\theta_A) = -R_E \cos\theta_A + \sqrt{(R_E \cos\theta_A)^2 + h(h + 2R_E)} \tag{2}$$

where R_E = 6378 km is the mean volumetric radius of the Earth and (2) reduces to *h* when $\theta_A = 0$.

For interplanetary transponder or lasercom links, the link equation is given by [Degnan, 2001]

$$n_T^{AB} = \frac{4\eta_q^B \eta_t^A \eta_r^B T_A^{\sec\theta_A} T_B^{\sec\theta_B}}{h\nu_A \left(\theta_t^A\right)^2 (4\pi)} \frac{E_t^A A_r^B}{R_T^2} \tag{3}$$

Setting the mean signal counts equal in (1) and (3), we can derive an expression for the equivalent transponder distance, R_T, in terms of the actual slant range to the satellite, R_R, i.e.

$$R_T(h,\theta_A,\sigma_s) = R_R^2(h,\theta_A)\sqrt{\frac{4\pi}{\sigma_s}\left(\frac{T_B^{\sec\theta_B}}{T_A^{\sec\theta_A}}\right)} \cong R_R^2(h,\theta_A)\sqrt{\frac{4\pi}{\sigma_s}\frac{1}{T_A^{\sec\theta_A}}} \tag{4}$$

where the approximation holds if the remote terminal is in interplanetary cruise phase, in orbit, or sitting on the surface of a planet or moon with little or no atmosphere (T_B ~1).

Since the SLR satellites are normally tracked over the range $0^o \le \theta_A \le 70^o$, Eq. (4) defines a maximum and minimum simulated transponder range for each satellite. These are indicated by the blue curves in Figure 2 for selected satellites where we have assumed a value $T_A = 0.7$ corresponding to the one-way zenith transmission for a

standard clear atmosphere at 532 nm. The red curves are plots of the minimum and maximum interplanetary distances of the Moon and other planets from Earth.

It is worthwhile to note that atmospheric turbulence can influence the effective transmitter beam divergence on the uplink, but this cancels out in our derivation of (4). Furthermore, the fading statistics for the dual station ranging experiment to the passive satellite should be comparable to that of an interplanetary transponder or lasercom experiment, at least to the extent that the satellite adequately mimics a coherent point source of radiation.

Figure 2 demonstrates that a dual station ranging experiment to the lowest of the SLR satellites, Champ, provides a weaker return than a two way lunar transponder. Low elevation angle experiments to Jason are comparable to a Venus or Mars link when they are closest to Earth. Experiments to the LAGEOS and Etalon satellites would simulate ranging to Mercury, Venus, and Mars throughout their synodic cycles while experiments to GPS and LRE (at 25000 km) would simulate links up to and beyond Jupiter and Saturn. Dual station experiments to the Apollo 15 reflector on the lunar surface would simulate transponder links to over 100 AU, well beyond the orbit of Pluto and the Kuiper Belt. These results are summarized in Table 1.

The nine SLR satellites represented in Figure 2 were chosen based on the following criteria:

- The satellite array should not significantly spread nanosecond pulses (important to both transponder and lasercom experiments)
- The satellites should simulate a wide range of equivalent interplanetary distances for experimentation and allow a step-wise demonstration of distance capabilities from the Moon to the inner and outer solar system.
- The satellite suite should permit measurements at a variety of elevation angles to fully explore atmospheric effects which typically worsen at low elevations.

The primary characteristics of these satellites, taken from the ILRS Web Site and used in the computation of equivalent transponder ranges, are also summarized in Table 1.

Another way to interpret Figure 2 is to say that any single SLR station that can track the aforementioned satellites has demonstrated an adequate Energy-Aperture (EA) product for the corresponding transponder link under the same noise background and atmospheric conditions. Since all of the ILRS stations are required to track LAGEOS for membership, they all have adequate EA-product to track out to about 1 AU. About a third of ILRS stations regularly track GPS, which from Figure 2 or Table 1 implies an equivalent transponder range out to 5 AU. The NASA MOBLAS system, with an *EA*-Product of 0.045 Jm^2 and a Power-Aperture (*PA*) Product of 0.23 Wm^2 , falls into this category as does the photon-counting Graz station in Austria with *EA* and *PA* products of only 0.79×10^{-5} Jm^2 and 0.157 Wm^2 respectively. As mentioned previously, three stations have routinely tracked the Apollo reflectors but only at night with low noise background and single photon returns. Nevertheless, the same *EA*-product, which is only about 70% larger than a MOBLAS, should permit transponder links beyond 100 AU under equivalent operating conditions.

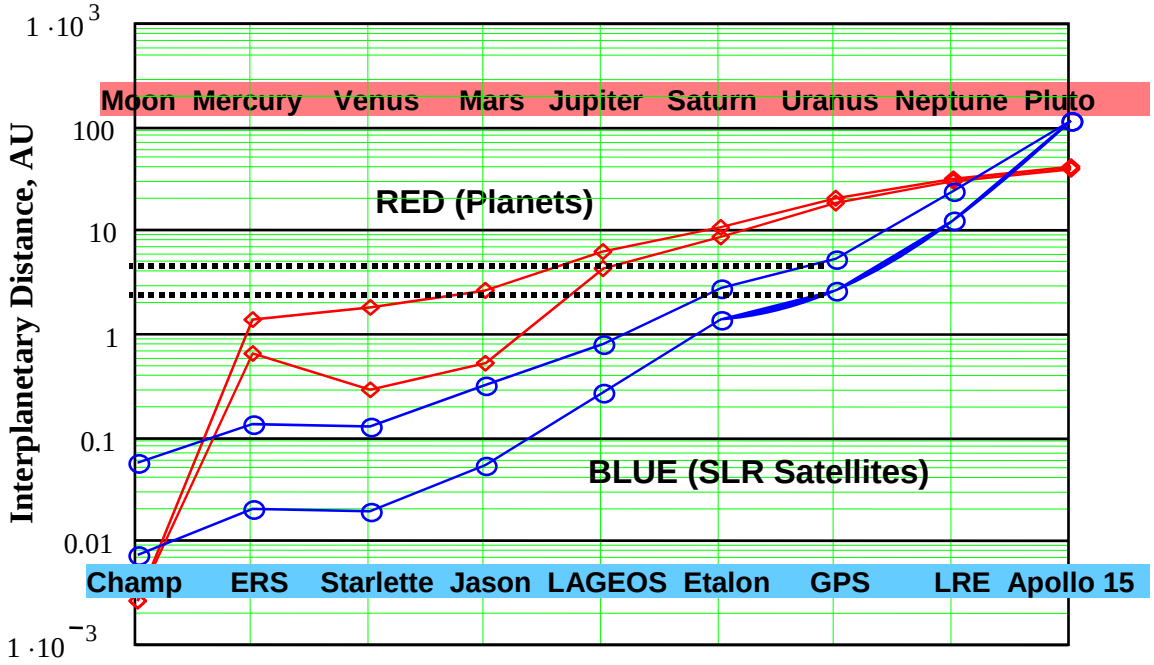

Figure 2: *The minimum and maximum distances from the Earth to the Moon and the 8 planets listed at the top of the graph is illustrated by the two red curves in the figure. The minimum and maximum transponder ranges simulated by the various SLR satellites listed at the bottom of the figure is indicated by the two blue curves.*

Table 1: *Characteristics of selected SLR satellites which can be used to simulate Deep Space transponder or lasercom links (altitudes and cross-sections from ILRS web site).*

Satellite	**Altitude (km)**	**Cross-section (10^6 m^2)**	**Transponder Range (AU)**	**Simulation**
Champ	500	1.0	0.007-0.057	Beyond Lunar (0.0026 AU)
ERS 1 & 2	800	0.85	0.02-0.135	
Starlette/Stella	950	1.8	0.019–0.123	
Jason	1,300	0.8	0.054-0.306	
LAGEOS	6,000	15	0.263-0.771	Mercury, Venus, Mars
ETALON	19,000	55	1.38-2.72	(0.28 to 2.52 AU)
GPS	20,000	19	2.60-5.06	Jupiter near PCA (4.2 AU)
LRE (elliptical)	25, 000 (max)	2	12.52-23.12	Beyond Jupiter, Saturn (4.2 to 10 AU)
Apollo 15	384,000	1,400	111.6	Beyond Outer Planets & Kuiper Belt (40 to 50 AU)

Summary

Based on the recent successful GSFC experiments to the Messenger and MGS spacecraft, the space-qualified technology for decimeter accuracy interplanetary laser transponders is clearly available now. More compact sub-centimeter accuracy photon-counting systems can be made available within 2 to 3 years with very modest technology investments, and interest in fundamental physics experiments using

transponders at NASA is high. Furthermore, detailed exploration of remote planets and moons with modern high data rate sensors previously developed for near-Earth applications will require high bandwidth lasercom systems to transmit the data back to Earth.

The link equations for laser transponders and communications are identical. We have demonstrated that retroreflector arrays on international SLR spacecraft are capable of simulating interplanetary transponder and lasercom links through the turbulent atmosphere. This provides a means for testing potential ground and spacecraft hardware, acquisition procedures, and ranging and time transfer algorithms prior to mission approval. New SLR targets on future HEO/GEO missions could provide an improved testbed with long experiment times and temporally uniform signal strengths. They could also provide better simulations of future missions to the outer planets (e.g. Jupiter and Saturn). In fact, the Jovian moon, Europa, and the Saturnian moons, Titan and Enceladus, have been identified as the top three priorities for exploration by NASA's Outer Planets Advisory Group (OPAG) in their July 2006 report.

The one drawback of using the current SLR target arrays for dual station experiments is that they are composed of large, "spoiled" [Degnan, 1993] retroreflectors. The angularly tight but complex far field patterns produced by these arrays force the stations to lie within a few hundred meters of each other and result in a signal strength which varies with both time and spacecraft-station geometry. Large panels of unspoiled small diameter retroreflectors (~7 mm) placed on future high altitude satellites (GPS/GLONASS altitudes or higher), on the other hand, would relax the proximity requirements for the dual stations to a few km, extend experiment times to several hours or more, and eliminate retroreflector-induced temporal non-uniformities in the return signal strength.

Acknowledgement

This work was initiated following a lively technical discussion on potential ways to demonstrate transponder technologies with Dr. Ulrich Schreiber at the October 2005 ILRS Workshop in Eastbourne, UK.

References

[1] Degnan, J.J., "Millimeter Accuracy Satellite Laser Ranging: A Review", in Contributions of Space Geodesy to Geodynamics: Technology, D. E. Smith and D. L. Turcotte (Eds.), AGU Geodynamics Series, Volume 25, pp. 133-162, 1993

[2] Degnan, J. J., "Asynchronous Laser Transponders for Precise Interplanetary Ranging and Time Transfer", Journal of Geodynamics (Special Issue on Laser Altimetry, pp. 551-594, November, 2002.

[3] Degnan, J. J., "Photon Counting Microlaser Rangers, Transponders, and Altimeters", Surveys in Geophysics, Special Issue on Evolving Geodesy, Vol 22, Nos. 5-6, pp. 431-447, 2001.

[4] McGarry, J., T. Zagwodzki, P. Dabney, P. Dunn, J. Cheek, "Laser Ranging at Planetary Distances from SLR2000", these proceedings, 2006.

[5] Smith, D.E., M. T. Zuber, X. Sun, G. A. Neumann, J. F. Cavanaugh, J. F. McGarry, and T. W. Zagwodzki, *Science*, **311**, p. 53, 2006.

Laser Ranging At Planetary Distances from SLR 2000

J. McGarry[1], T. Zagwodzki[1], P. Dabney[1], P. Dunn[2], J. Cheek[2]

1. NASA / Goddard Space Flight Center
2. Raytheon Information Solutions.

Contact: Jan.McGarry@nasa.gov

Abstract

The SLR2000 prototype system will be participating in two separate planetary transponder laser ranging experiments: (1) as one end of the Goddard in-house asynchronous transponder experiment in 2007, and (2) as the primary ground station for one-way ranging to the Lunar Reconnaissance Orbiter (LRO) in late 2008 and 2009.

The modifications to SLR2000 to participate in these projects are relatively few and are very synergistic with the SLR completion effort. This paper describes the transponder experiments and the changes required at SLR2000.

Introduction

SLR2000 is the prototype for NASA's Next Generation of Satellite Laser Ranging (SLR) Systems. It was originally designed to be a completely automated, eye-safe Satellite Laser Ranging System, with a lower cost of operation, a high reliability, and an accuracy comparable to the existing NASA MOBLAS systems [McGarry]. Because of its arcsecond level pointing capability, its timing accuracy (both absolute and relative) and its ability to independently measure fire and return times, this system is an excellent candidate for transponder work.

The 1.2 metre telescope (aka 48 inch telescope) was developed by Goddard in 1974 as a research and development facility. It has hosted many laser ranging and other experiments over the years including the first successful 2-way asynchronous transponder experiment at 24 million kilometres with the Mercury Laser Altimeter (MLA) on the MESSENGER spacecraft in 2005, and the first successful 1-way laser ranging experiment at ~80 million kilometres with the Mars Obiter Laser Altimeter (MOLA) on the MGS spacecraft orbiting Mars, also in 2005. The 1.2 metre telescope is owned and operated by the Laser Remote Sensing Branch (code 694) at the Goddard Space Flight Center.

Both systems are located at Goddard's Geophysical and Astronomical Observatory (GGAO) which has been the site of most of NASA's ground breaking work in laser ranging, including the some of the first laser ranging returns ever recorded, the development and checkout of the MOBLAS and TLRS systems in the late 1970s and early 1980s, and the MLA and MOLA Earthlink experiments described above. It is also home to MOBLAS-7 which is the NASA SLR Network standard for performance.

Two-way asynchronous transponder demonstration

The goal of this in-house Goddard project is to demonstrate two-way asynchronous acquisition and ranging between two ground systems at Goddard's Geophysical and Astronomical Observatory (GGAO). The 1.2 metre telescope will function as the planetary spacecraft and will transmit at 50Hz in the IR (1064nm) and receive SLR2000's green (532nm) returns. SLR2000 will function as the ground station,

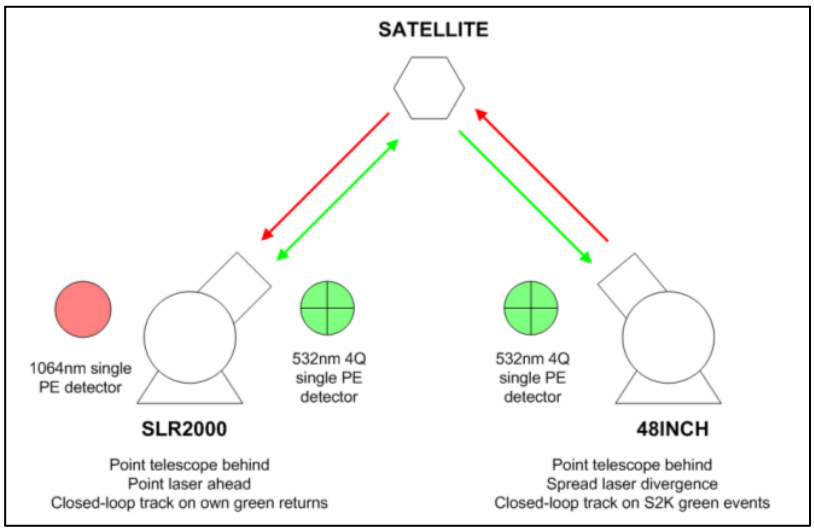

Figure 1: *Two-way asynchronous transponder experiment concept*

firing at 2 khz in the green and receiving the 1.2 metre telescope's IR returns. The laser pulses will be bounced off of retro-reflector equipped satellites to provide the simulation of planetary distances (Figure 1). The stations are sufficiently close that both are within the return footprint from the satellites. SLR2000 will closed-loop track on its own green returns and the 1.2 metre will closed-loop track on the green SLR2000 returns. Fire and return times will be collected by each station. A clock will be used at the 1.2 metre telescope that will simulate the frequency drift of a spacecraft clock. The event information from both stations will be used as input to analysis software that will determine the ranges, clock offset and frequency drift between stations.

Optical breadboard space has been added to SLR2000 to support this experiment along with a dichroic beam splitter (532nm / 1064nm) for the receive channel, beam reduction optics, a narrow band pass filter, and a fiber optic delivery to the 1064nm photodetector (Figure 2). The candidate detector is a Perkin Elmer model SPCM-AQC(4) photodetector with a quantum efficiency of ~2% and better than 500 picosecond jitter. An additional discriminator will be added and one additional event time channel will be used (for the 1064nm returns). There are minimal software changes required to the operational software at SLR2000 to perform this experiment.

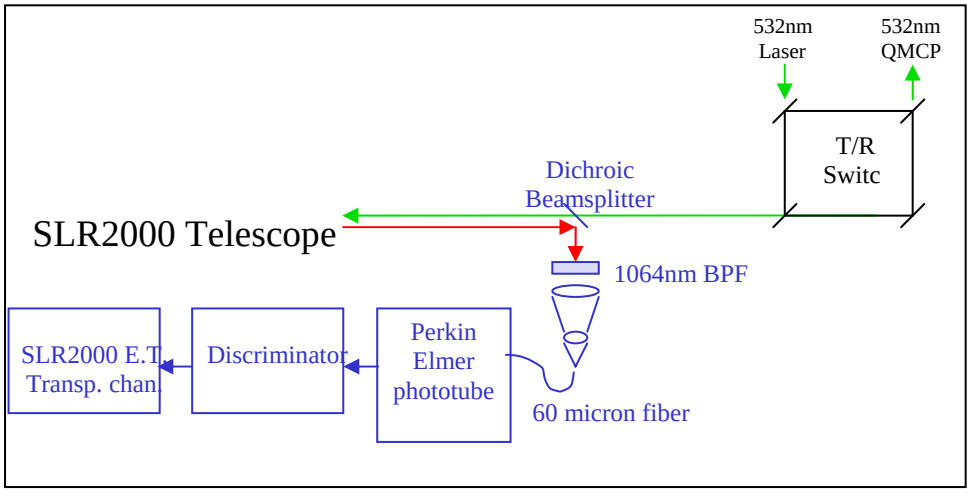

Figure 2: *Additions for 1064nm transponder returns at SLR2000*

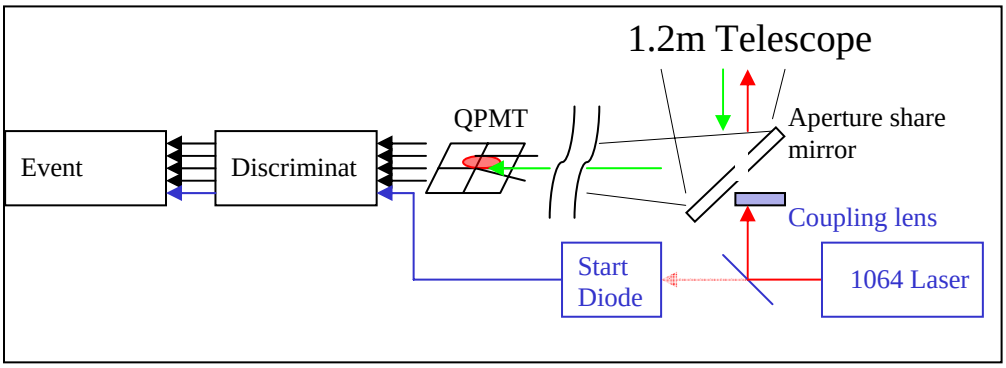

Figure 3: *1.2 meter telescope configuration for transponder experiment*

Modifications to the 1.2 metre telescope configuration include the addition of a 532nm ungated single photon quadrant detector (Hamamatsu metal channel dynode PMT) and four discriminators, along with a band pass filter for the 532nm events from SLR2000 and a 1064nm blocking filter to prevent backscatter from local laser (Figure 3). Much of the configuration used for the MLA-Earthlink and MOLA-Earthlink experiments will be used for this project including the computer, the Time-to-Digital Converter (TDC), the Continuum Inlite II-50 laser (up to 50 Hz at 1064nm with a 6 nanosecond pulse width), and aperture sharing of the transmit-receive. Software modifications include handling of the four quadrant channels for closed-loop tracking.

The transmit and receive times from both SLR2000 and the 1.2m telescope will be processed to remove the noise. The clock bias and drift can be modeled as a linear function of the 1.2 metre telescope's time. The range error can be modeled as a quadratic equation in time. A least squares fit of the fire and receive event data to the resulting equations (shown below in Figure 4) would then provide the ranges as well as the relative clock offset and drift.

Both systems are nearing completion of the required modifications and both have tracked green returns from MOBLAS-7's fires. The 1.2 metre telescope's mirrors are in the process of being recoated in preparation for an upcoming laser communications experiment. When the recoating is complete in the spring of 2007 the two-way asynchronous transponder data collections will begin.

One-way laser ranging to the Lunar Reconnaissance Orbiter

The function of the Earth to LRO laser link is to achieve the mission's precision orbit determination requirement. The requirements on the SLR2000 ground station to accomplish this are:

1. Between 1 and 10 femtoJoules per square centimetre of signal must be delivered to the LRO-LR receiver aperture. For the SLR2000 laser with a 55 microradian laser divergence, this implies 30 milliJoules per pulse.

2. The wavelength must be 532 nm and the 3 Angstrom LRO-LR filter will be tuned to the actual SLR2000 laser in the lab.

3. The laser pulse width must be less than or equal to 8 nanoseconds FWHM.

4. Laser pulses must be delivered into the LOLA earth window at 28Hz.

5. The transmitted pulse time stamp accuracy must be maintained within 100 ns of UTC.

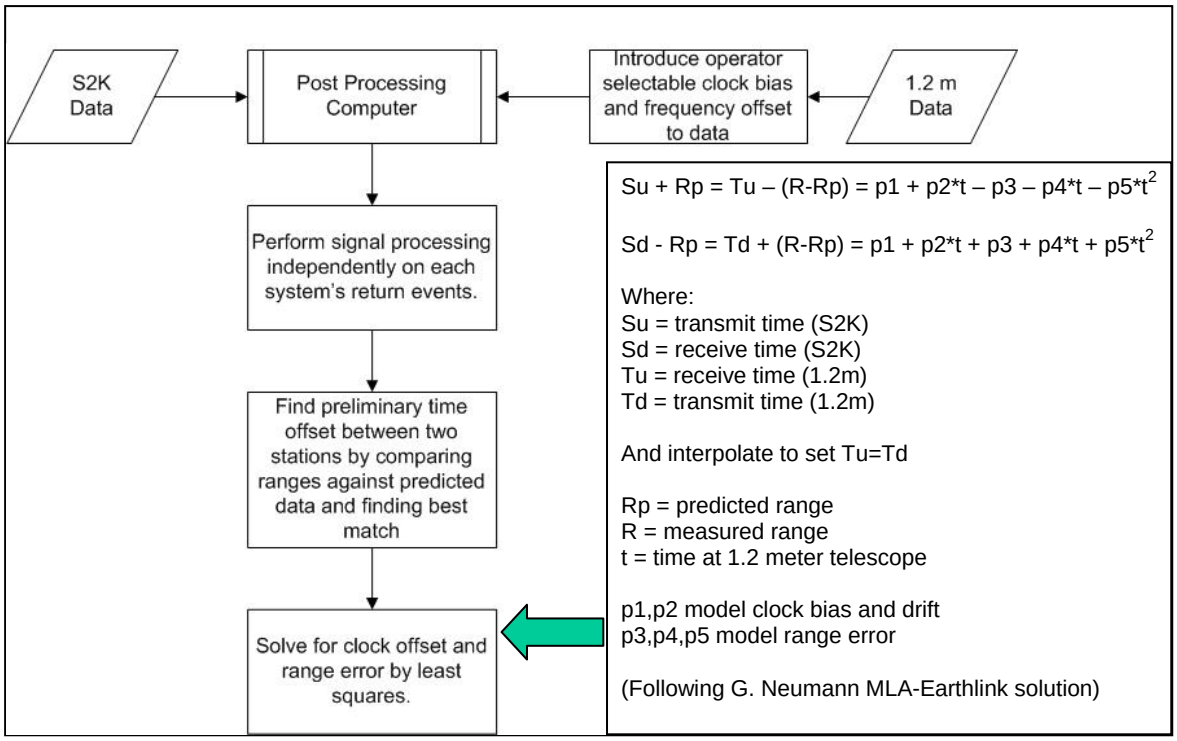

Figure 4: *Post processing of fire and receive event times at two stations*

6. The relative laser time of fire must be measured to better than 200 picoseconds (1 sigma) shot-to-shot over a 10 second period. The laser fire time must be recorded to better than 100 picosecond resolution.

7. The frequency stability of the station's clock must be equal or better than 1.e-12.

8. The system must provide better than 407 hours of ranging data to LRO during year after launch. This number is achievable and takes into account the LRO visibility from the station, the outages due to weather, system failures, as well as aircraft avoidance outages.

To accomplish these requirements SLR2000 is purchasing a 28 Hz diode pumped Nd:YAG master oscillator power amplifier (MOPA) laser that can deliver up to 50 milliJoule per pulse at 532 nm in a 6-8 nanosecond pulse. It is a turn-key system with a projected lifetime of greater than 1 year of continuous use. Additional optical table space has been added for the laser and a removable kinematic mirror mount will be inserted to launch the LRO transmit beam and ensure an easy transition between SLR and LRO lasers. Because this laser is not eye-safe, an aircraft avoidance radar is also being added to the system.

The software for SLR2000 is being modified to handle the new laser parameters, to control the laser fire to hit the earth window on the spacecraft, to take new operator commands for control of the new laser, and to handle predictions for non-earth-orbiting satellites.

LRO-LR will be launched in late 2008. SLR2000 will be staffed to support the mission 10 hours a day, 7 days a week to cover those times when the moon is above 20 degrees elevation. LRO is visible to earth about one hour out of every two.

During the hour that the spacecraft is behind the moon SLR2000 will range to earth orbiting satellites with the eye-safe 2 khz SLR laser.

Summary

Transponder experiments will extend capabilities of SLR2000 and demonstrate the system's ability to do planetary ranging which is the future of laser ranging. Earth orbiting satellite laser ranging and planetary transponder ranging can co-exist in SLR2000 and transitioning between the two will be seamless. The in-house Transponder experiment will complete in late 2007. The LRO mission will run from Fall 2008 through January 2010.

Acknowledgements

The authors would like to thank John Degnan for the original concept of bouncing laser pulses off of earth orbiting satellites to simulate planetary transponder ranging [Degnan].

We would like to thank the LOLA Instrument Principal Investigators David Smith and Maria Zuber for their efforts in getting laser ranging selected for LRO, as well as Xiaoli Sun, Greg Neumann, Ron Zellar, and David Carter for their continued support in the development of the LRO-LR ground system.

We would also like to thank our colleagues who have worked on the transponder experiment and on LRO-LR, including Christopher Clarke, Ray DiSilvestre, Howard Donovan, Julie Horvath, Anthony Mallama, Anthony Mann, Carey Noll, Donald Patterson, Randall Ricklefs, David Rowlands, Mark Torrence, and Susan Valett.

The 2-way asynchronous transponder work is being performed with Goddard in-house IRAD funding. The LRO-LR work is being performed with funding from the Lunar Reconnaissance Orbiter Mission.

References

[1] Degnan, J., "Simulating Interplanetary Transponder and Laser Communications Experiments via Dual Station Ranging to SLR Satellites," in this Proceedings.

[2] McGarry, J., and T. Zagwodzki, "SLR2000: The Path Toward Completion," in this Proceedings.

Laser Ranging to the Lunar Reconnaissance Orbiter (LRO)

David Smith[1], Maria Zuber[2], Mark Torrence[3], Jan McGarry[1], Michael Pearlman[4]

1. NASA / Goddard Space Flight Center, Greenbelt, Maryland, USA,

2. Massachusetts Institute of Technology, Cambridge, Massachusetts, USA

3. SGT Inc, Greenbelt, Maryland, USA

4. Harvard-Smithsonian Center for Astrophysics, Cambridge, Massachusetts, USA

Abstract

LRO will be launched in late 2008 carrying, amongst other payloads, the Lunar Orbiter Laser Altimeter (LOLA) which is a 1064nm laser altimeter for mapping the lunar surface, and the Laser Ranging (LR) receiver which is mounted on the earth-pointed High Gain Antenna (HGA). Laser Ranging with LRO (LRO-LR) is one-way from earth to spacecraft and will be used along with S-band tracking data and the LOLA altimeter data to develop an improved gravity model for both the near and far sides of the moon. SLR2000 will be the primary laser ranging station, but the project would like to extend an invitation to ILRS stations for their participation. The requirements for ranging include satisfying the laser wavelength (to match the onboard filter at 532nm), repetition rate (to hit the range window but minimize impact to the onboard threshold algorithm), transmit energy (to cross the detector threshold), and station timing (to ensure precise transmit time recording). The requirements are very similar to those for earth orbiting satellite laser ranging. We hope that many of you will consider participating in this exciting transponder experiment.

Introduction

LRO is a robotic component of the Moon to Mars vision proposed in January, 2004. LRO will be launched in October 2008 into a polar orbit around the Moon with an average altitude of 50 km. Lunar gravity necessitates orbital maintenance every 30 days (30-70 km altitude range) to maintain the polar orbit for the one-year nominal mapping mission. The LRO spacecraft has a suite of seven instruments: LOLA, a laser altimeter; LROC, a camera; LAMP, a Lyman alpha telescope; LEND, a neutron detector; DIVINER, a thermal radiometer; CRATER, a cosmic ray detector; and the mini-RF, radar technology demonstration. The LOLA altimeter addresses the geodetic measurement objectives of NASA's robotic lunar exploration program, in particular – "Determine the topography of the Moon to geodetic quality from global to landing-site relevant scales." and "Assess metre and smaller-scale features to facilitate safety analysis of potential future lunar landing sites".

The precise determination of the Lunar topography from LOLA data, and positioning of the measurements made by other LRO instrument suite on the lunar surface requires accurate LRO orbits. The LRO orbits will be determined by high quality tracking of LRO and improvement in the knowledge of the Lunar gravity field. To enhance the orbit determination, the LRO mission includes a one-way laser ranging (LR) capability. The LR data will provide a 10 cm precision measurement of the position of LRO. In conjunction with the LOLA data, LRO positional accuracies will be 50 to 100 m along track and 1 metre radially from the Lunar center of mass after improvement of the lunar gravity field. One SLR station (Greenbelt, MD) is presently planned to track LRO; we are hoping for a second US station and help from the international SLR network.

Measurement technique

The LRO-LR measurement is a one way range from earth to spacecraft with the ground station recording the time of the laser fire and the LOLA instrument onboard LRO recording the pulse arrival time. The 2 cm aperture LR receive telescope will be mounted on the spacecraft's High Gain Antenna (HGA). The optical signal will be routed via fiber optic cable to the LOLA instrument (see Figure 1). One of LOLA's five lunar detectors will receive the earth pulses as well as the lunar surface events.

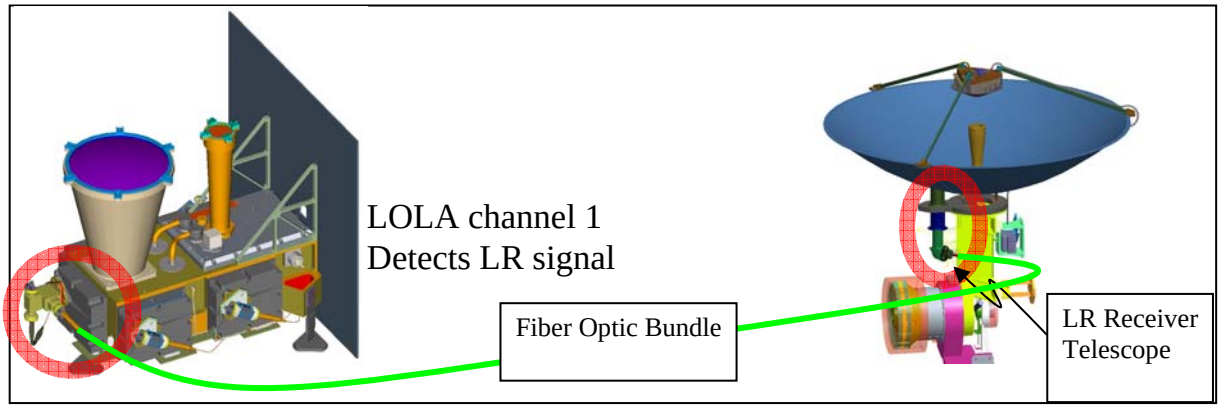

Figure 1: *Optical signal path from HGA to LOLA instrument.*

SLR2000 is the primary ground station for LRO-LR and is required to transmit at 28Hz (the LOLA instrument's fire rate), and to control its laser fire times to ensure that all pulses arrive in the LOLA earth windows as shown in Figure 2 [McGarry]. There is no corresponding requirement for other participating stations to control their laser fire times, however, to ensure a minimum of one pulse per second arrival in the earth window, fire rates of 5 Hz and 10 Hz should be used when the laser fire time is not controlled.

No ground station should fire at LRO faster than 28Hz. Events that occur outside LOLA's range windows (earth or lunar) are interpreted as noise and will affect the threshold level which is controlled by a feedback loop based upon the noise counts outside the windows.

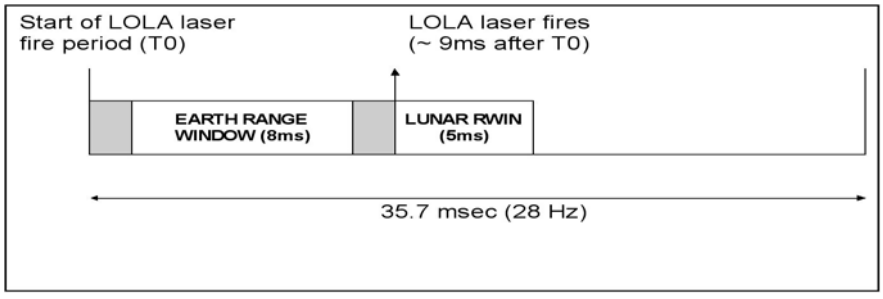

Figure 2: *Timing of LOLA earth window relative to lunar window within the 28Hz laser fire period*

Ground System Requirements

Stations participating in the LRO-LR experiment must satisfy the following requirements:

1. Deliver between 1 and 10 femtoJoules per square centimetre of signal to the receiver aperture. For SLR2000 with its 55 microradian laser divergence this translates into a transmit energy of 30 milliJoules per pulse.
2. The transmitting wavelength must be 532 nm. The exact wavelength will be determined in Spring 2007. The spacecraft filter is 3 Angstroms in width. A filter assembly will be sent to all interested stations later in 2007 to allow each station to determine if its laser meets the requirements.
3. The laser pulsewidth must be less than 8 nanoseconds.
4. The transmitted pulse time stamp accuracy must be maintained within 100 nanoseconds of UTC.
5. The system must measure the relative laser time of fire to better than 200 picoseconds (1 sigma) shot-to-shot over a 10 second period. Laser fire times must be recorded to better than 100 picosecond resolution.
6. The system should deliver at least one laser pulse to the LOLA earth window per second. The laser fire rate cannot exceed 28 Hz.
7. A shot to shot measurement of the output laser energy is desirable.
8. Data should be delivered to CDDIS in new ITDF (simple ASCII format) no slower than daily.

Most ILRS systems should have no problem meeting these requirements.

Other requirements will include coordination with the mission so that coverage can be limited to a single station at a time (at least initially), and reporting so that the mission knows ahead of time which stations will be participating each day.

Operational Considerations

The period of the LRO orbit is approximately 2 hours. The orbit is polar and precesses so that at times the entire 2 hour orbit will be visible from earth. Due to the constraints on the HGA pointing, however, only ~1 hour out of each 2 hour orbit will be available for earth ranging, no matter what the orbital orientation is.

Predictions for LRO will be generated in CPF format. Code for non-earth orbiting satellites will be made available to all ILRS stations by Randy Ricklefs later this year [Ricklefs].

Feedback will be provided from LOLA in its housekeeping telemetry which will be delivered in semi-real-time from the spacecraft, through the LOLA Science Operations Center (SOC), to CDDIS. LOLA will be performing signal processing on the data in the earth window and should be able to recognize earth laser pulses that are fired synchronously to LOLA at 14 or 28Hz. Laser fire rates of 5 and 10 Hz will not be recognized by LOLA, however, the website, http://lrolr.gsfc.nasa.gov ,will contain other information as well (possibly a Go-NoGo flag), so participating stations should check it when ranging to LRO.

The flow of all of the data for LRO-LR is shown in Figure 3.

Stations interested in participating as a ground station for LRO-LR are invited to contact the authors or Michael Pearlman (mpearlman@cfa.harvard.edu).

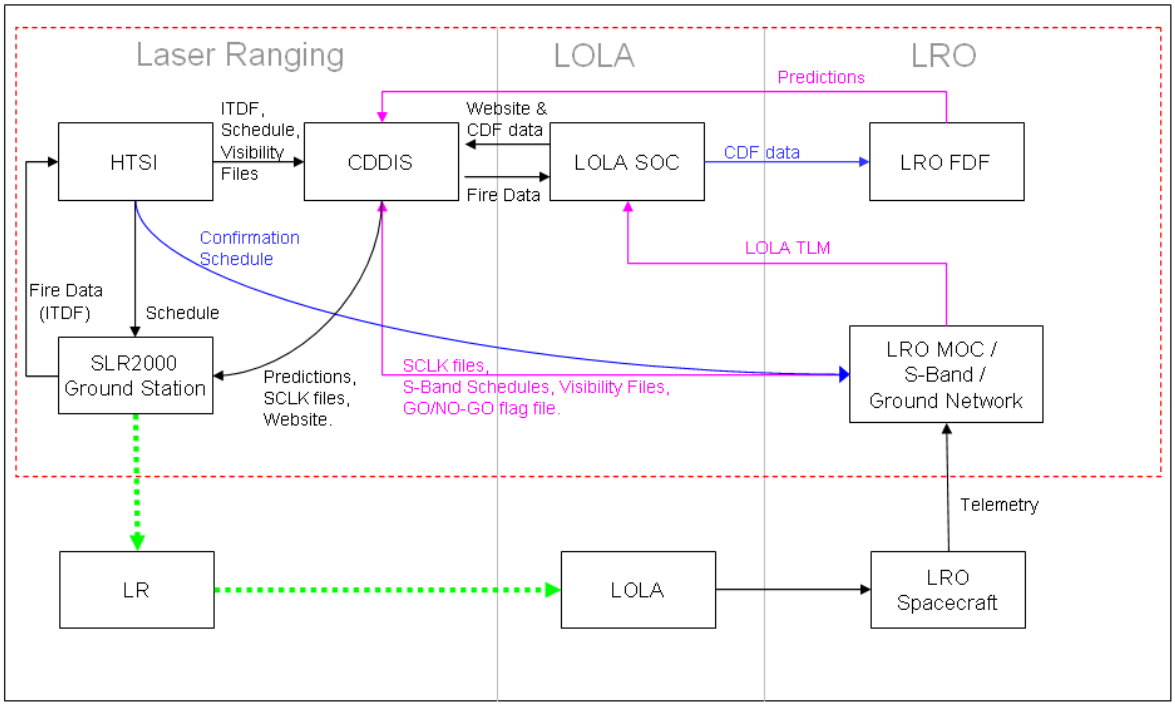

Figure 3: *LRO-LR data flow block diagram.*

References

[1] McGarry, J., and T. Zagwodzki, "SLR2000: The Path Toward Completion," in this Proceedings.

[2] Ricklefs, R., "Consolidated Laser Prediction and Data Formats: Supporting New Technology", in this Proceedings.

UN-COOPERATIVE TARGETS SESSION SUMMARY

Chair: Craig Smith

This short session received fascinating papers from laser ranging groups attempting the most difficult of SLR activities - that is ranging to un-cooperative targets.

From Shanghai Observatory we heard about the numerous upgrades to the system there towards the development of precision tracking for un-cooperative targets (ie targets that do not carry retro-reflectors). We wish Shanghai Observatory well in this endeavor.

From Czechoslovakia and the Graz SLR station in Austria a new technique for provide simultaneous optical and laser tracking of targets was described.

The Experimental Laser Ranging System for Space Debris at Shanghai

Yang Fumin[1], Chen Wanzhen[1], Zhang Zhongping[1], Chen Juping[1], Wang Yuanming[1], K. Hamal[2], I. Prochazka[2)]

1. Shanghai Astronomical Observatory, Chinese Academy of Sciences

2. Czech Technical University in Prague, Czech Republic

Abstract

The paper introduces the performance of the experimental laser ranging system for space debris at the Shanghai Observatory. The output of laser is 2J in 532nm, 10ns, 20Hz, 40W. A new transmitting telescope with the aperture of 210mm is used, and the other parts of the ranging system are the same with the routine SLR system in Shanghai. The ranging system is under testing now.

Introduction

China has launched many spacecrafts into space and had produced many space debris during 30 years. China is one of the members of IADC (Inter-Agency Space Debris Coordination Committee). It is necessary for China to pay great attention to reduce damages from space debris in cooperation with international community. The project of laser ranging to space debris at Shanghai Astronomical Observatory is supported by the Chinese Space Agency. An experimental laser ranging system for space debris at Shanghai is set up in 2006. The goals of the project are as follows: 1) Development of the technology for space debris laser tracking. 2) Experimental observations and orbit determinations for space debris, not routine observations.

2. Performance of the system

The major parts of the space debris ranging system are the same with the SLR system at Shanghai. A China-made 40W Q-switched Nd:YAG laser has been installed and is located at the neighbor room to the mode-locked laser for SLR. There are ten Nd:YAG rods in the laser with the output of 2J in 532nm, 10ns width, 20Hz repetition, 0.6mrad divergence. A new transmitting telescope with 210 mm aperture was installed and replaced the old one with 150mm aperture for better collimating beam. The testing of laser ranging to the satellites with retro-reflectors has been done. The next step will try to ranging to uncooperative space targets soon.

Some photos for the system are shown as follows.

Fig.1. *The Optical Observation Site at Shanghai Observatory, CHINA*

Fig.2. *SLR House in Shanghai*

Fig.3. *SLR Telescope(Aperture 600mm)*

Fig.4. *Electronics Room*

Fig.5. *High Power Laser & Power Supply, Chiller*

Fig.6. *Output of High Power Laser*

Fig.7. *Inside of the 40W Pulsed Nd:YAG Laser*

Fig.8. *Coupling Optics*

Fig.9. *Laser Firing (2J, 20Hz, 40W in 532nm)*

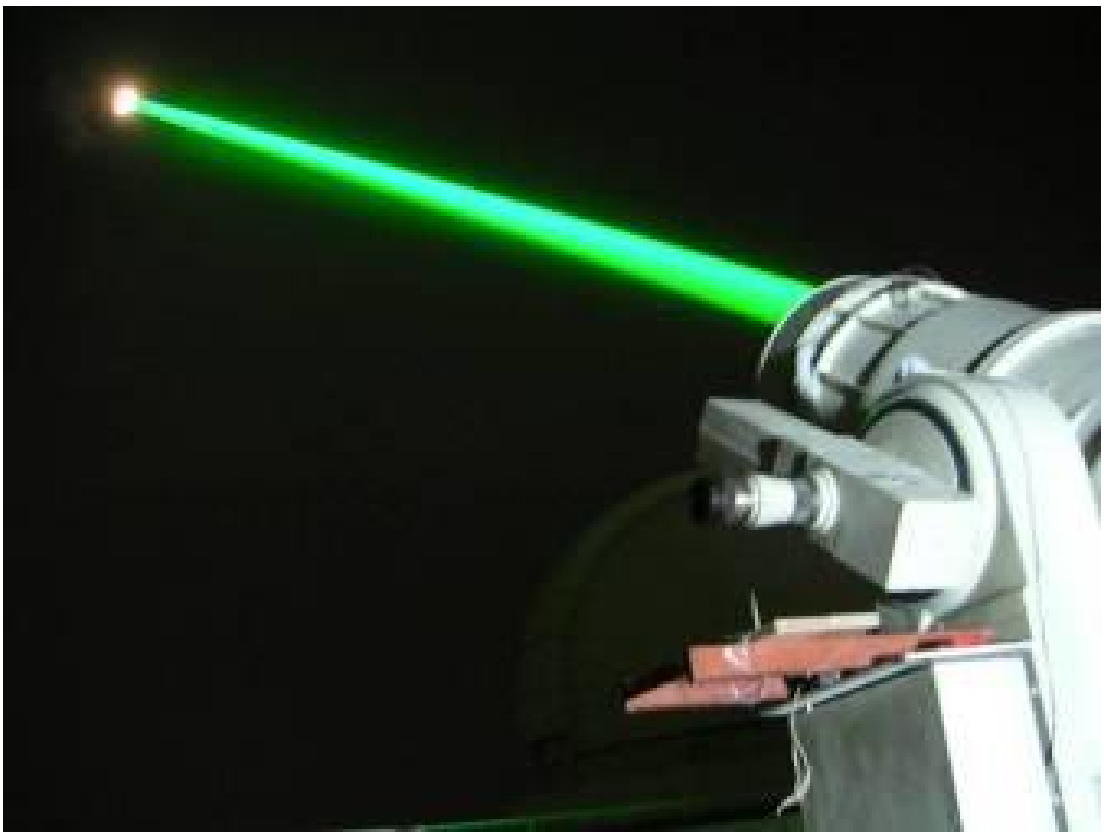

Fig.10. *Laser Firing*

Simultaneous Optical and Laser Space Objects Tracking

M. Němec[1], I. Procházka[1], K. Hamal[1], G. Kirchner[2], F. Koidl[2], W. G. Voller[2]

1. Czech Technical University in Prague, Czech Republic
2. Satellite Laser Station Graz, Austrian Academy of Sciences, Austria

Contact: nemecm1@troja.fjfi.cvut.cz

Abstract

The goal of the presented experiments is the development of new optical tracking techniques for space objects, namely space debris, based on simultaneous CCD and laser measurements: the CCD tracking of a laser illuminated object, the simultaneous CCD tracking and laser ranging and the laser time-tagging of the CCD tracking. The first two experiments can be performed on cooperative - corner retro-reflectors equipped satellites while the third one is applicable to any space object and to space debris in particular. The high accuracy and density of laser ranging data and additional Time-tags in the CCD image, atmospherically back scattered photons, can contribute to the solution stability of computed orbits from data based even on a single tracking location within a single pass.

Simultaneous Optical and Laser Space Objects Tracking

Goals

The goal of the presented experiments is the development of new optical tracking techniques of space objects, namely the space debris, based on simultaneous Optical detection (CCD tracking) and laser measurements:

1) the CCD tracking of laser illuminated object

2) the simultaneous CCD tracking and object laser ranging

3) the nanosecond laser time-tagging of the CCD tracking

The first two techniques can be performed on co-operative retroreflector equipped objects (high power lasers could be further used even for non co-operative [1]).

While the third one is applicable to any space object, the space debris in particular.

Add new applications for Satellite Laser Ranging stations

Martin Němec, FNSPE, CTU in Prague, nemecm1@troja.fjfi.cvut.cz

Simultaneous Optical and Laser Space Objects Tracking

Applications (1/2)
First insight

Classic optical detection

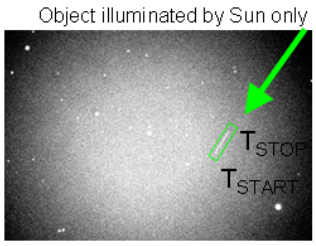

- Technique for determination the orbit of object, based on object's angular positions measurements
- Object illuminated only by Sun
- Telescope synchronized to catalogued stars + object in FOV during exposure -> angular coordinates -> pixels
- 2 Time-tags in the CCD image (Exposure start time and Exposure length) -> times -> pixels
- Problems of the accurate time-tags assigning to subpixels positions in the image (edges detections from signal curve with low SNR)

Laser usage in Optical detection:

- Additional object illumination
  - cooperative objects - Low power laser (usually stronger back reflections (retroreflectros nature) than by Sun only illumination)
  - noncooperative objects - High power laser (object shape reflectivity)
- Additional Time-tags in the CCD images – Low or High power laser
  Time-tags with **nanosecond time precision and subpixel positions** by laser photons backscattered by atmosphere

Martin Němec, FNSPE, CTU in Prague, nemecm1@troja.fjfi.cvut.cz

Simultaneous Optical and Laser Space Objects Tracking

Applications (2/2)
Details

High Precision 3D solution

Object laser ranging + Optical detection with laser time-tagging

- **cooperative objects**
  - Calibration of Optical detection systems
- **noncooperative objects**
  - High power laser strong to get enough returns -> Ranging results -> Orbit estimation
  - Low power laser (only few returns) -> combination of ranging data + high precision angular data (laser time-tagging) -> Orbit estimation

High Precision 2D solution

Optical detection with laser time-tagging

- **cooperative** or **noncooperative objects**
  - several times more of high precision angular data (laser time-tagging) -> Orbit estimation

Martin Němec, FNSPE, CTU in Prague, nemecm1@troja.fjfi.cvut.cz

Simultaneous Optical and Laser Space Objects Tracking

Project scheme

High Precision 3D solution

Optical detection with laser time-tagging

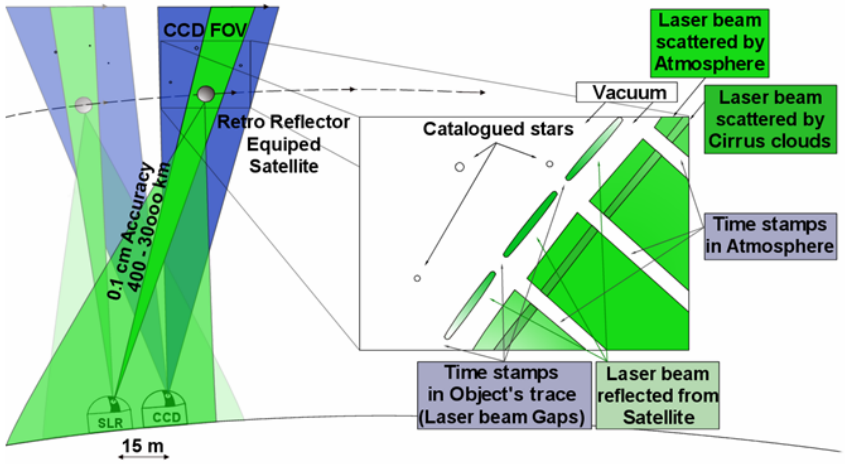

Observatory - Satellite laser ranging station in Graz, Austria

Martin Němec, FNSPE, CTU in Prague, nemecm1@troja.fjfi.cvut.cz

Martin Němec, FNSPE, CTU in Prague, nemecm1@troja.fjfi.cvut.cz

Simultaneous Optical and Laser Space Objects Tracking

Laser Time-Tags without returns

Classic optical detection

- Object illuminated by Sun only
- Only 2 Time-tags (Exposure start time and Exposure length) (more Time-tags using Advanced methods with e.g. rotating shutter)
- Times for Time-tags – milisecond up to microsecond scale (GPS)
- Problems of the accurate time-tags assigning to subpixels positions in the image (edges detections from signal curve with low SNR)
- Accuracy - up to 1 arcsecond
- Nr. of angular measurements during 1 path: usually ~ 10 values/path,

$$\max \sim \frac{\text{path time}}{\text{telescope positioning} + \text{exposure} + \text{image readout times}}$$

Object illuminated by Sun only

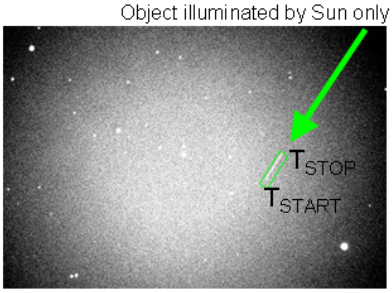

High Precision 2D solution

Optical detection with Laser Time-Tagging

- Object illuminated by Sun and partially by Low-power laser (or by High-power laser only)
- Basic 2 Time-tags (Exposure start time and Exposure length) + **more additional Time-tags** by laser beam modulation or by selection of pulses to be send to the object
- **Higher precision** of the Times for Time-tags – nanosecond scale
- **Higher accuracy** of time-tags assigning to subpixels positions in the image – All image **area** of Atmospherically back-scattered photons could be used - not only edges detections from signal curve
- Accuracy – **better than 1 arcsecond** (first results ~0.2 arcsec/s)
- Nr. of angular measurements during 1 path: **higher productivity**
  Nr. of optical measurements x **Nr. of laser time-tags in image**

Laser beam reflected from satellite

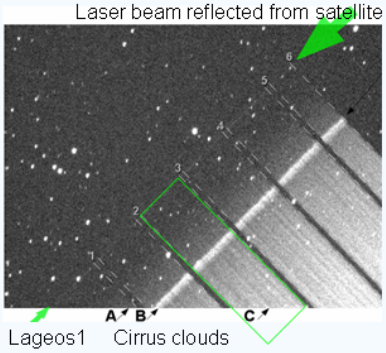

Lageos1 Cirrus clouds

1-5: Laser gaps = 10 Time-tags by laser beam photons backscattered from atmosphere

Simultaneous Optical and Laser Space Objects Tracking

Experiment Setup (1/3)
SLR system

Satellite Laser Ranging System (SLR) station in Graz

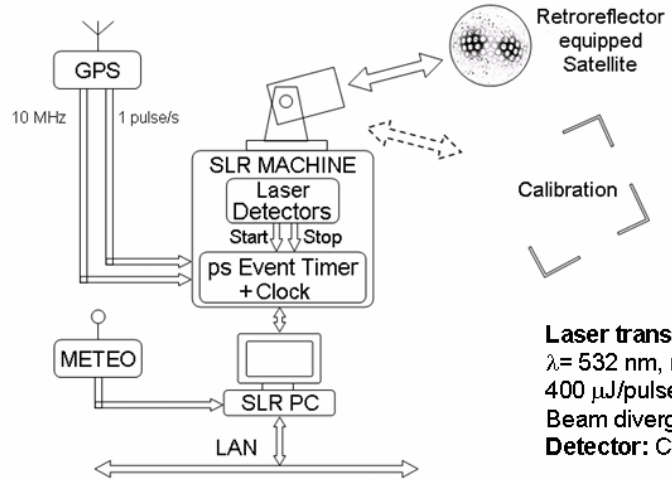

Ranging accuracy ~few mm for Retroreflector equipped satellites in distances of 400-30'000 km

Laser transmitter: HighQLaser, Diode pumped Nd:Van, λ= 532 nm, repetition rate 2 kHz, Pulse length 8 psec, 400 μJ/pulse, Average power up to 1W
Beam divergence θ ~100 μrad
Detector: C-SPAD; Range up to 30 000 km

The SLR station has been modified to provide laser power output modulation (selection of output pulses – gating of Pockel's cells) to serve as a time tagger for the laser illuminated exposures.

The laser is "switched off" for the preset time interval (e.g. 50, 100 or 500 milliseconds, etc.) each one second. The precision of the time-tags is on the nanosecond scale. The time scale accuracy connected to GPS is better than 100 ns.

Martin Němec, FNSPE, CTU in Prague, nemecm1@troja.fjfi.cvut.cz

Simultaneous Optical and Laser Space Objects Tracking

Experiment Setup (2/3)
Telescope and CCD cameras for Optical detection

CCD Telescope:
Meade LX200 16", f/10
Tracking precission 5 arcmin (worse now)

Focal reducers: f/6.3 or f/3.3

Field of View:
CCD1: ~ 23x15 arcmin, 1.8x1.8 arcsec/pixel (bin 3x3)
CCD2: ~ 16.6x12.5 arcmin, 1.2x1.2 arcsec/pixel (bin 2x2)
EMCCD: ~ 9.3x7.0 arcmin, 0.85x0.85 arcsec/pixel

(EMCCD = CCD with internal Electron multiplying register)

CCD cameras:
1: SBIG ST-10ME
Pixel Array:2184x1472
Pixel Size: 6.8x6.8 µmxµm
CCD Size: 14.9x10 mmxmm
Filter:
488-574 nm, green pass

2: SBIG ST-2000XM
Pixel Array:1600x1200
Pixel Size: 7.4x7.4 µmxµm
CCD Size: 11.8x8.9 mmxmm
Filter:
no filter

EMCCD camera:
Andor Luca^{EM}
Pixel Array: 658x496
Pixel Size: 10x10 µmxµm
CCD Size: 6.58x4.96 mmxmm
Filter:
no filter

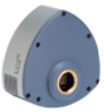

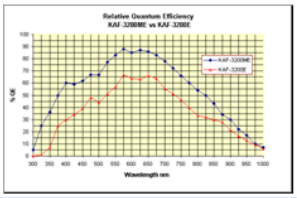

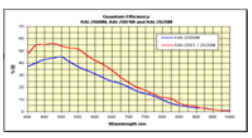

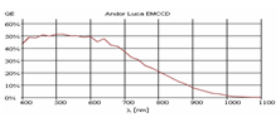

Martin Němec, FNSPE, CTU in Prague, nemecm1@troja.fjfi.cvut.cz

Simultaneous Optical and Laser Space Objects Tracking

Experiment Setup (3/3)
Minimal system configurations

High Precision 3D solution

High Precision 2D solution

* photon detector is not necessary

1. Object path prediction

2. SLR Station:

Telescope - able smooth real-time object tracking (~ 1 arcsecond)

- diameter depending on object shape and reflectivity

Laser – pulse (min. repetition rate > 1 Hz (higher is better)

- depending on Optical detection system FOV, object speed and nr. of laser time-tags)

Pulses gating system + events timing system with high accuracy + photon detector*

Sensitive camera – CCD, EMCCD, ISIT, etc. (optical feedback)

3. Optical detection system:

Telescope

- object tracking precision (~ 5 arcminutes or better, depending on Optical det. system FOV)

- diameter depending on object shape and reflectivity

Sensitive Low-Noise Camera – CCD, EMCCD

- Pixel size, Quantum efficiency depending on object speed, shape and reflectivity (+ telescope properties)

Martin Němec, FNSPE, CTU in Prague, nemecm1@troja.fjfi.cvut.cz

Simultaneous Optical and Laser Space Objects Tracking

Experiment results 1

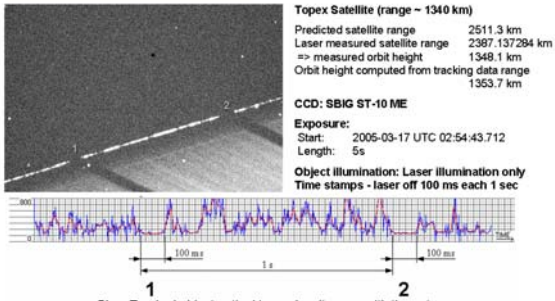

Blue: Tracked object optical trace densitogram with time stamps
Red: Moving AVG (Average) Window graph of optical trace densitogram
(Window: width 5 pixels, height 5 pixels)

Martin Němec, FNSPE, CTU in Prague, nemecm1@troja.fjfi.cvut.cz

Simultaneous Optical and Laser Space Objects Tracking

Experiment results 3

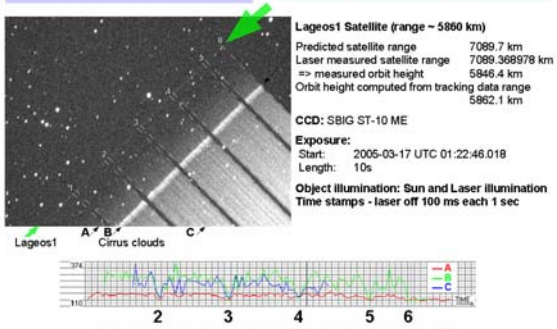

Moving AVG Window graphs of densitograms with time stamps
(Window: width 5 pixels, height 5 pixels)

Martin Němec, FNSPE, CTU in Prague, nemecm1@troja.fjfi.cvut.cz

Simultaneous Optical and Laser Space Objects Tracking

Experiment results 2

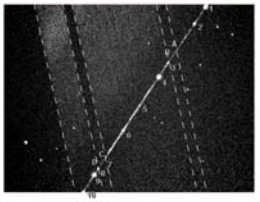

Point	Time [s]	Position [x,y]
A	21.00000002	550.37, 145.97
B	21.10000005	527.67, 180.28
C	22.00000003	323.42, 489.05
D	22.10000001	300.73, 523.36

Base Time: 2005-07-04 UTC 01:47:19.433

Point	Time [s]	Position [x,y]
1	20.5983	641.71, 7.89
2	20.7552	606.01, 61.85
3	21.1217	522.88, 187.52
4	21.2545	492.92, 232.96
5	21.5231	431.77, 325.26

Point	Time [s]	Position [x,y]
6	21.7560	378.69, 405.49
7	22.0012	323.27, 489.28
8	22.1024	300.26, 524.07
9	22.1623	286.64, 544.66
10	22.3192	250.94, 598.62

AJISAI (EGP) is spinning satellite covered with mirrors and retroreflectors.
Adding Time-stamps in atmosphere could increase precision of its spin speed and spin axes orientation measurements

Martin Němec, FNSPE, CTU in Prague, nemecm1@troja.fjfi.cvut.cz

Simultaneous Optical and Laser Space Objects Tracking

Experiment results 4

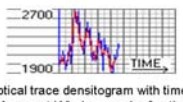

Blue: Optical trace densitogram with time stamps
Red: Moving AVG (Average) Window graph of optical trace densitogram
(Window: width 2 pixels, height 5 pixels)

Martin Němec, FNSPE, CTU in Prague, nemecm1@troja.fjfi.cvut.cz

Simultaneous Optical and Laser Space Objects Tracking

Problems

Atmosphere density – low density => less back-scattered photons

Object tracking Accuracy and Smoothness of the tracking laser movement

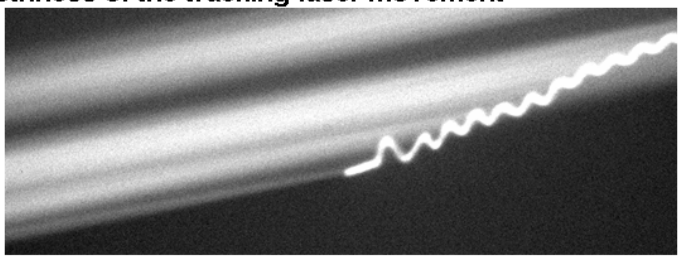

Distance between Laser and CCD telescopes

– too far => low back scattered photons

– too close => low tags resolution - merging

Position of Object, SLR station and CCD telescopes – "Blind Angles"

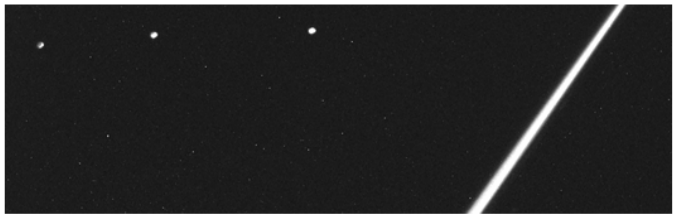

Martin Němec, FNSPE, CTU in Prague, nemecm1@troja.fjfi.cvut.cz

Simultaneous Optical and Laser Space Objects Tracking

Conclusion

Results

The high accuracy and density of laser ranging data **and / or** additional precise laser Time-tags in the CCD image, the atmospherically back scattered photons, can contribute to the high solution stability of computed orbits from data based on a single tracking location within a single pass.

These facts can result in increase the observation productivity and orbit computation stability in comparison to the techniques used recently.

Cooperative targets tracking has been tested by our group in a series of experiments involving combined optical and laser tracking of space cooperative objects at the Observatory of Graz, Austria, March 15-17, 2005 and in September 2006. The laser time-tagging method was also tested on following satellites with retroreflectors: **Champ** (~ 400 km), **ERS2** (~ 800km), **GPS-35** (~ 20ooo km).

Non-cooperative target tracking has been tested by B. Greene [1].

[1] B. Greene et. al., *Advanced Techniques at the EOS Space Research Centre*, 14th International Laser Ranging Workshop, San Fernando, Spain, June 7-11, 2004, published in Boletin ROA No. 4/2004, Real Instituto Observatorion de la Armada, en San Fernando, ISSN 1131-5040, 2004

Future

- Improvement of precision of the image processing methods (now under development)
- Method testing on non-cooperative objects
- Other image time-tagging methods development

Martin Němec, FNSPE, CTU in Prague, nemecm1@troja.fjfi.cvut.cz

SOFTWARE AND AUTOMATION SESSION SUMMARY

Chairs: Werner Gurtner and Jan McGarry

Automation continues to increase throughout the ILRS Network as can be seen in the presentations by Pearson on Mt Stromlo, Pierron on FTLRS, and Xin on TROS. Automation calls for more and more complicated software. Matt Pearson showed that software of the future needs to be modular, loosely coupled, flexible and reusable.

Automation improvements occur in both the hardware and software. Hardware enhancements were presented by Degnan on the SLR2000 beam expander, Wang on new control systems for San Juan, and the use of FPGAs in SLR systems digital design at Beijing by Li and at TROS by Xin.

Chris Moore demonstrated in his presentation that an automated system can perform as well as a manually operated system by giving statistics for Mt Stromlo when it was fully automated and when it was manually controlled.

Werner Gurtner showed that other work can share the telescope system in an automated way with SLR at no performance loss, given the right software to control the system.

New tools and formats are helping SLR stations in their transition to new technologies and in capturing these changes as they happen. This was seen in the presentations by Salminsh on web applications for engineering, and on the Consolidated Prediction and Consolidated Data Formats by Ricklefs.

The presentation by Heiner and Schreiber showed how to improve automated real-time signal processing by reprocessing (looking behind and projecting ahead) which can provide a 10–40% improvement over normal histogram analysis.

Progress in automation, reliability, performance and maintainability continues to be made at stations across the ILRS. Each group has their own approach to improvements. Sharing of these different technical approaches is the most important part of the Workshops.

A Comparison of Performance Statistics for Manual and Automated Operations at Mt Stromlo

C.J. Moore[1]

1. EOS Space Systems Pty. Limited, 111 Canberra Ave., Griffith, A.C.T. Australia.

Contact: cmoore@eos-aus.com

Abstract

The new Mt Stromlo SLR Station was rebuilt in the 12 months following the destruction of the original station by the January 2003 bushfires, and was reopened in April 2004. It became fully operational in December 2004 and since then the station has been operated manually pending completion of the development of a more advanced infra-structure that will support automated operations.

The original station had conducted automated operations for over three years before the bushfires and the performance measures that were in place during this period have continued to be collected for recent operations. This provides a unique opportunity to compare the productivity performance between automated and manual operations undertaken at the same site and with the same management team.

Provided that periods of abnormal events are taken into account, net productivity from these two modes of operation are quite comparable with differences less than about 5% over periods of many months. The fact that automated operations persist for longer periods and in conditions that discourage manual operation appear to compensate for the efficiencies that human interaction can provide.

Introduction

The original Mount Stromlo SLR Station (7849, STRL) was commissioned in Oct 1998, and subsequently performed automated operations from late 1999 until being totally destroyed in the January 2003 Canberra bushfires. A more complete description of the operation of this station has been given by Luck, Moore and Greene (2000). During this period, operations included the automated download of predictions, tracking of satellite and calibration targets, data processing and upload of published data. Automated operations allowed the station to continue operations, collecting and publishing SLR data, while it was unmanned. In fact, such operations were effectively unmanned for 80% of the time.

Productivity metrics were captured for this whole period. As described in Luck et al, these metrics were used for establishing performance criteria required under the contract between EOS and AUSLIG (subsequently incorporated into Geoscience Australia). Processing of productivity data and generation of reports was only partially automated, with a significant component requiring routine, but brief human inspection and assessment of the system and environment.

Subsequent to the 2003 bushfires, the remains of the old station were removed and the new Mount Stromlo SLR Station (7825, STL3) was constructed on the same site. All systems were functional by the official opening in April 2004, less than 14 months later. After undergoing stringent testing of all of the new sub-systems, including a new software system and completing formal acceptance testing, the new station commenced full operations in December 2004. Given the rapid redevelopment of the station, the system (in 2005-2006) was not capable of automation hence the station has been operated manually in a more traditional manner using operators rostered to

cover day and night, seven days a week. The new station was only unmanned when lack of targets or poor weather precluded productive tracking. It should be noted however, that contractual requirements (as well as good practice) required continuing capture of productivity metrics and generation of performance reports. The definition and processing of these data had not changed between the automated and manual operations.

The availability of reasonable long time series in these two data sets, has therefore allowed the relative performance between automated and manual SLR operations to be assessed. It should be remembered that the two stations were both designed by EOS and operated by EOS staff and hence have much in common. It was considered that the physical and technical differences between the two stations did not influence productivity levels to such an extent as data quality and other factors.

Metrics

The metrics used in this assessment include the following;

1. The number of all ILRS satellite passes with a maximum elevation above the 20 degree site horizon.
2. The number of all possible passes – i.e. the number of passes that are trackable, accounting for poor weather, low elevation passes and pass overlaps or priority.
3. The number of attempted passes – i.e. the number of possible passes for which the SLR station fired the laser in an attempt to track the satellite.
4. The number of passes that were successfully tracked – i.e. at least one normal point was generated.

The following figure shows the time series of these metrics for the two periods.

Figure 1: Productivity Metrics

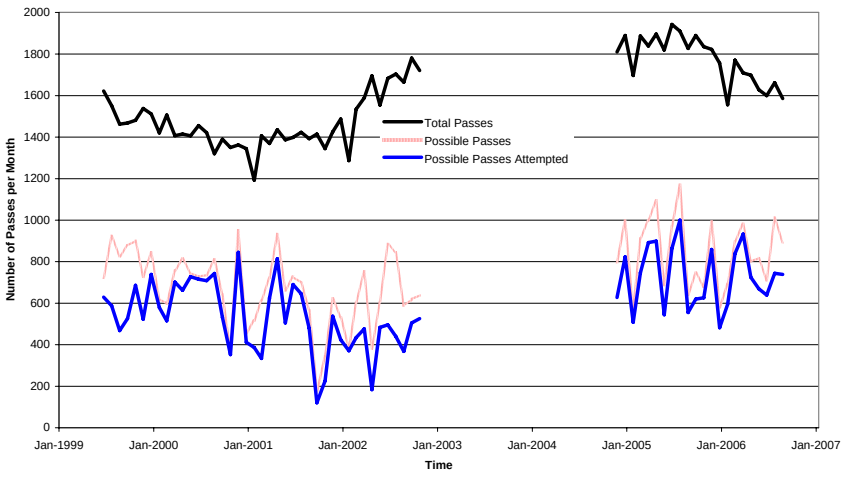

Results

Potential Productivity

Figure 2 provides the number of passes successfully tracked normalized by the number of possible passes. This ratio provides a measure of the system's potential productivity. If the ratio reached 100% then every pass that could realistically be tracked would be tracked. This figure shows that on average the potential productivity of the automated system reached 66% while than manned system was significantly more successful with an average potential productivity of 74%. Note that some exceptional points were excluded from the calculation. The points were associated

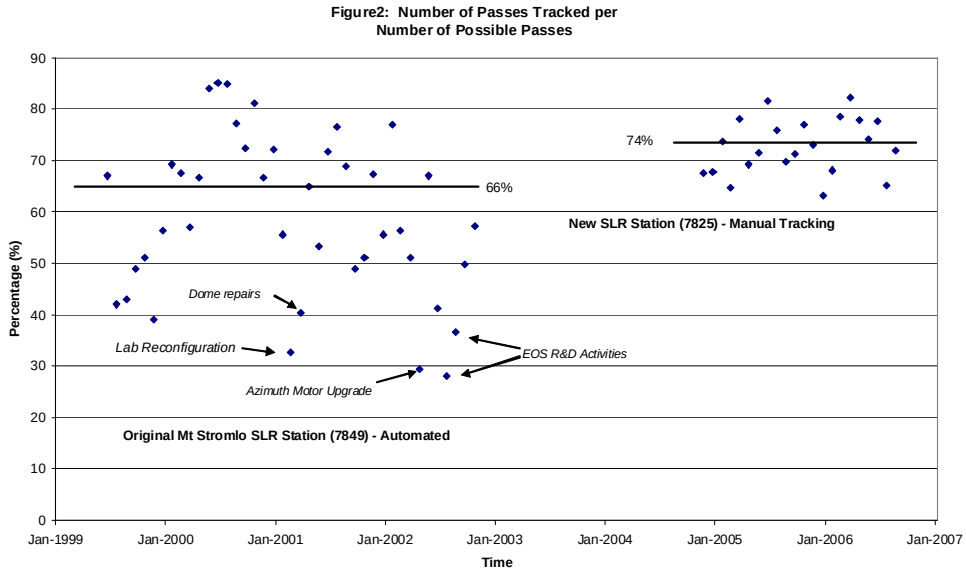

with station activities that significantly affected the ability of the station to perform normal operations. This result suggests that everything else being equal, a human operator should outperform a mechanical system, where for example a human can respond to unusual events such as system failures more quickly.

Tracking Capability

The next figure provides the number of passes successfully tracked normalized by the number of attempted passes. This ratio provides a measure of the system's capability for successfully tracking a target. If the ratio reached 100% then every pass tracked would result in generation of normal points. Figure 3 shows that on average the potential productivity of the automated system was 81% while the manned system was marginally more successful with an average of 87%. Note that a few exceptional points were again excluded from the calculation. For example, at one point the telescope enclosure was slipping due to a mechanical fault such that the system continued to attempt passes, but a misalignment of the telescope and dome meant that no returns were possible.

These results suggest that as long as a pass is attempted, the automated system has on average as nearly as good a chance in successfully acquiring the target as a human operator. Perhaps any skills that an operator may have in acquiring a target is balanced by the persistence of an automated system

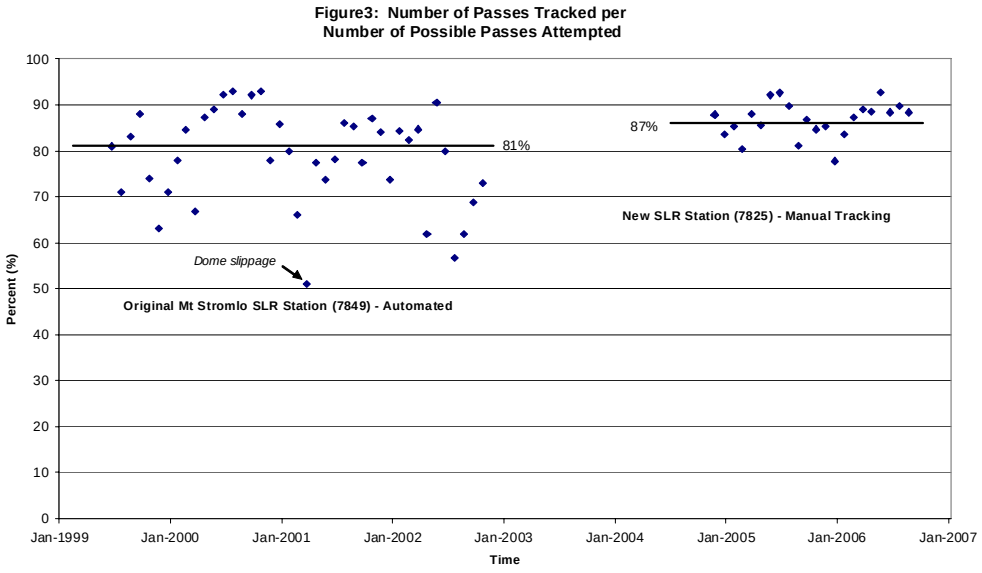

Actual productivity

The final figure provides the number of passes successfully tracked normalized by the total number of passes. This ratio provides a measure of the system's net or actual productivity, or passes tracked irrespective of conditions. In this case if the ratio reached 100% then every pass would have been tracked successfully. Figure 4 shows that on average the actual productivity of the automated system was 32% while that for the manned system was 35%, not a statistically significant difference. Note that some exceptional points were also excluded from the calculation as discussed earlier.

The major contributor to the absolute value of this ratio is of course the weather. It should be noted that during manual operations, the station was often unattended during overcast periods. In contrast, the automated system generally continued operations regardless of weather conditions. It is believed that this difference favoured the automated system, since there would have been opportunities to successful track during breaks in the sky cover or respond quickly to clearing conditions.

Conclusions

Availability of two years or more of productivity data from SLR tracking at one location, using similar techniques and equipment, and the same staff, has allowed an objective assessment of the performance from automation and manual operations.

The results indicate that there was overall very little difference in net productivity between the automated and manual operations. While human operators appear to have an advantage when on-site and undertaking tracking in clement weather, the automated system had an advantage in less ideal condition and could take opportunities that were lost to operators.

Figure 4: Number of Passes Tracked per Number of Total Passes

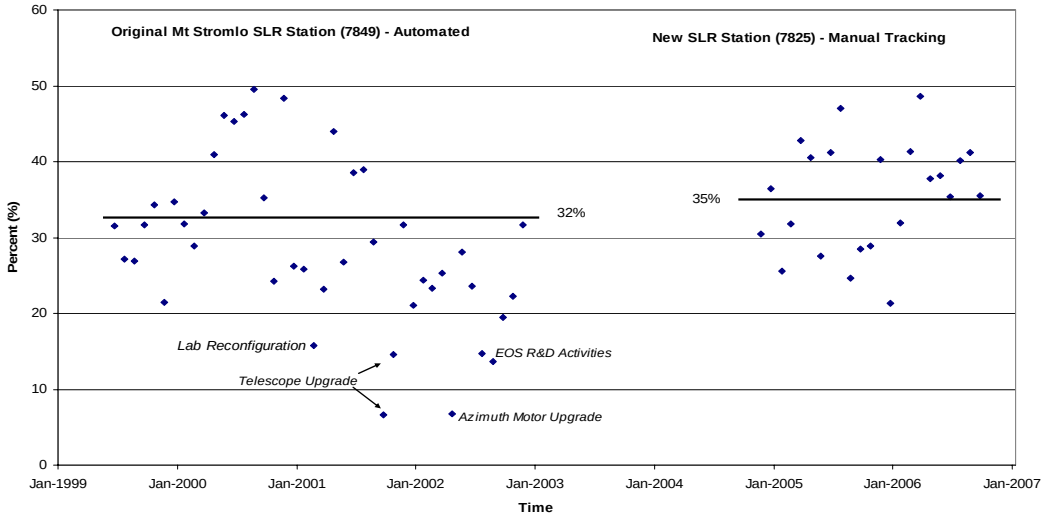

It is therefore clear that sophisticated automation systems can equal, if not better, manual operations. As far as the system at Mount Stromlo is concerned, it is felt that continuing improvements in the software and hardware systems will result in automated operations exceeding manual productivity figures.

References:

[1] Luck, J., C.J. Moore and B. Greene. Autonomous Laser Ranging Results from Mount Stromlo. Twelth International Workshop in Laser Ranging, 2000, Matera.

EOS Software Systems for Satellite Laser Ranging and General Astronomical Observatory Applications

M. Pearson[1]

1. EOS Space Systems Pty. Ltd.

Contact mpearson@eos-aus.com

Abstract

EOS has developed software systems over many years to support Satellite Laser Ranging (SLR) and the delivery of general astronomical observatories to its customers. These software systems are based upon a re-useable software architecture that simplifies systems development. The design objectives of this software architecture are discussed in the context of its evolution and current deployment at the Mt. Stromlo Satellite Laser Ranging facility, located in the Australian Capital Territory.

Introduction

This paper presents a brief overview of the software EOS has developed to support Satellite Laser Ranging at Mount Stromlo, software that has been designed to support not only SLR, but a wide range of astronomical applications.

This software, known as the 'Observatory Control System', supports EOS research and development programmes. It also supports the observatory requirements of several customers, being a flexible and scalable product, which lends itself to re-use across laser ranging and astronomical observatory applications.

Requirements

The basic requirements of the Observatory Control System are:

- it should drive equipment that might be expected at an observatory;
- it should provide some sort of abstraction – an 'Observatory' abstraction – that hides the complexity of the underlying equipment and presents it in terms that end-users and operators are likely to understand;
- it should provide facilities to automate day-to-day operations and routine observatory tasks.

Challenges

With these goals in mind, EOS has developed Observatory Control Systems over many years. But there was a problem; as the complexity of observatories grew, so did the complexity of the supporting software. This led to several challenges which are encountered in all types of software:

- it was becoming monolithic with fewer, larger, more-complex components;
- these components were highly-coupled, so changes to any part of the system could unexpectedly impact seemingly un-related parts;
- these systems were becoming inflexible and difficult to change in order to meet new requirements;
- different observatory solutions were becoming increasingly problem-specific and less re-usable; they were not amenable to solving new problems.

Solution

Under these pressures EOS engaged in a complete re-design of its software, culminating in what is now the 'Observatory Control System'.

The result is that the control system is inherently unaware of its problem domain. It is called an 'Observatory Control System' but it is in fact a generic control system. Its immediate application is to SLR and astronomy, but it could drive any automated industrial facility. It is domain independence that makes the control system highly extensible, flexible and most-importantly for EOS, re-useable.

Basic Architecture

At the highest level the Observatory Control System embodies the system concept:

'a collection of components which work together in order to solve a problem'.

These components include:

- various types of hardware and software;
- usually some sort of network;
- control system and observatory-level software.

The control system software provides facilities including:

- server frameworks;
- client frameworks;
- network interfaces.

The observatory-level software provides facilities including:

- servers;
- clients;
- automation functions.

Refer to Figure 1 for an illustration of these components.

Hardware & Software

Hardware and software include such items as: telescopes, enclosures, lasers, associated software and a variety of other equipment. A common problem with such equipment is that it is often heterogeneous, with different:

- platforms, eg. PC, Mac;
- operating systems, eg. Windows NT, XP, Linux;
- interfaces, eg. serial, CANopen, USB, Bluetooth;
- protocols, eg. sockets, CORBA, COM.

A fundamental feature of the Observatory Control System is that it makes this equipment look, feel and act in a consistent manner. This is achieved by hiding the equipment behind a universal software abstraction – what is called a Device.

Network

Devices are usually accessed through an adapter card and a driver library. But there is a limit to how many devices a given computer can support; at some point a single computer will run out of capacity, or a new device will require a different operating system or computer platform. So most observatories require many computers and the Observatory Control System is network-enabled.

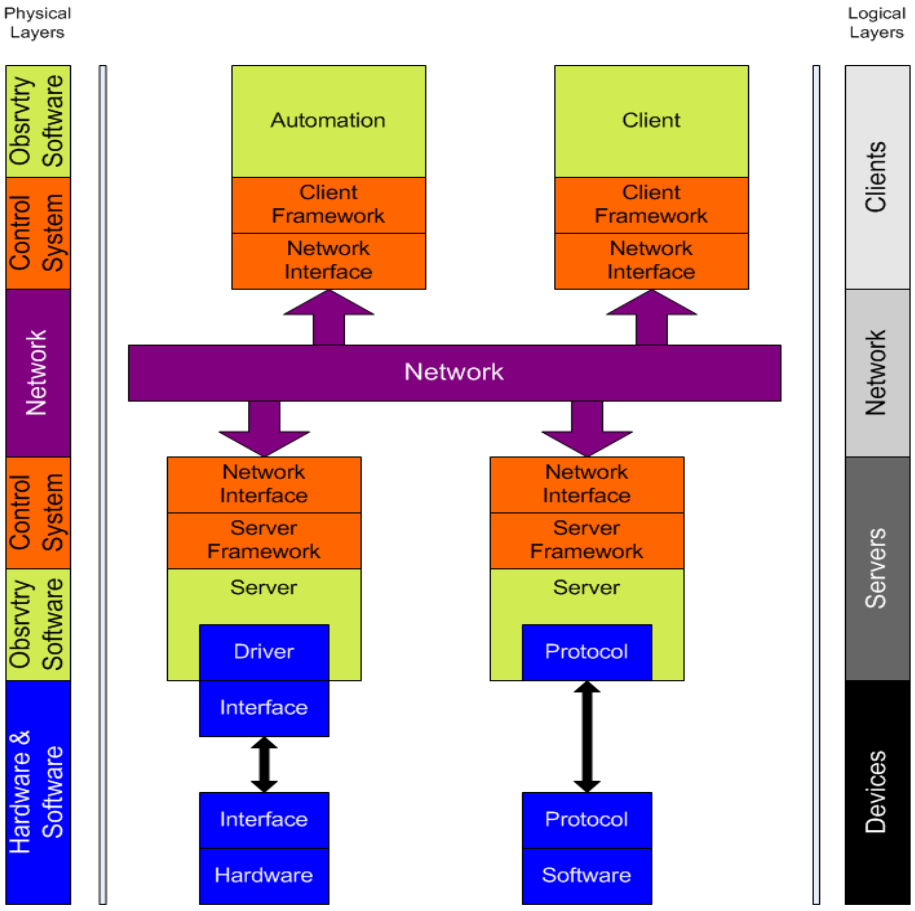

Figure 1. *Basic Software Architecture*

Control System

The Observatory Control System is a Client / Server software architecture. This is a network computing model based on the following concepts; that:

- clients connect to servers;
- clients issue commands to servers;
- servers respond to client commands.

Within the Observatory Control System, device server applications wrap devices and make them available over the network.

Client applications connect to these device servers over the network, or even over the Internet, and drive devices via commands to the relevant device server.

At the heart of the Observatory Control System are several software frameworks; these are code libraries which embody the most-re-useable, but complex and technical aspects of the control system.

These frameworks encourage re-use, and are used by EOS to extend its systems. These frameworks are also available to customers, who can extend their observatories over the longer term, independent of EOS.

Server Framework

Server applications, also known as device servers, are built using a *Server Framework*.

Servers directly manage observatory devices. A device server may manage one or many devices, depending on our requirements.

Servers may be active and/or passive; that is, they may manage devices autonomously and robotically, or in response to user commands.

Servers may participate in a hierarchy, where a parent server may depend on several child servers. Child servers provide services to their parent, which may perform some aggregate function; the parent may itself have a parent, to which it provides services, and so on.

This cooperative, 'building block' approach facilitates a separation of concerns; resulting in simple components from which complex systems can be built.

Client Framework

Client applications are built using a *Client Framework*.

Client applications are the focus of general observatory operators and users. This is where users interface with the observatory. So client applications will usually perform several functions:

- sending commands to / receiving replies from servers;
- displaying server state and responding to server state changes.

The display of server state is by a mechanism called Subscribe / Publish. The subscribing client asks for server state to be delivered at specified intervals, upon which the data is repeatedly published, arriving at the client without the need to keep asking. This asynchronous approach is much more efficient than simply polling for data. It should be noted that efficient network communications are important given the distributed, network-focused nature of the Observatory Control System.

Network Interfaces

In addition to the abstraction which hides the complexities of devices, the network provides its own abstractions – these hide the additional complexity of communicating with devices over the network. The result is that whatever the nature of a device or its location on the network, it can be accessed in a simple manner which is consistent for all devices.

All parts of the Observatory Control System employ the same, universal abstractions to facilitate end-to-end communication between client applications and the device servers which host the observatory devices.

Observatory Software

Observatory software includes client and server applications and automation applications that meet general observatory requirements and specific customer requirements. Domain and problem-specific control system functions are implemented at this level.

Like all parts of the Observatory Control System, this software is built upon a common set of software Frameworks.

It is at this level that the Observatory Control System can be customised, even by customers, with support from EOS if necessary.

Servers

Observatory-level servers will typically drive the hardware and software devices specific to any given observatory.

Clients

Client applications will provide an interface that hides the complexity of the underlying equipment, and present it in terms that end-users and operators are likely to understand.

Automation Functions

Observatory software provides system automation functions at many levels, including:

- device management – automatic management of device behaviour and state by device servers;
- scripted tasks – scripting of automation functions;
- task scheduling – scheduling of robotic tasks to be executed continuously, at scheduled intervals or in response to system events;
- closed loop control – automatic execution of system functions in response to changes in system state.

Case Study – Mount Stromlo

The Mount Stromlo facility contains two ranging systems, for satellite ranging and space debris ranging. These systems have common, but mostly different requirements, and have shared and dedicated components. But both systems were built sharing a single instance of the Observatory Control System.

This integration presented no significant problems or difficulties. Furthermore, no problems are foreseen concerning extensive capability upgrades over the next year. So the Observatory Control System provides technical certainty in terms of EOS' ability to extend and enhance its observatory systems.

Conclusion

The Observatory Control System supports EOS' demanding technical and business requirements. It has evolved over many years and continues to do so. The next evolution may well be a network of stations, where each station is a cooperating instance of the Observatory Control System. This will enable highly coordinated, world-wide observation and ranging programmes.

Currently EOS provides the Observatory Control System with its telescopes and enclosures. There is nothing inherently necessary about EOS' equipment, however; so long as basic requirements are met, the Observatory Control System can operate with any vendor's equipment. So in future EOS may offer the Observatory Control System as a stand-alone product, independent of its telescopes and enclosures.

Finally, the underlying control system is domain-independent. There are no astronomical or observatory-specific concepts embedded in the fundamental control system. So it is plausible that it could be used to drive a range of automated facilities.

Electro-Control System of San Juan SLR Station

Wang Peiyuan[1], Guo Tangyong[1], Li Xin[1], Han Yanben[2], Liu Weidong[2], Wang Tangqiang[3], Qu Feng[3], Tan Yechun[1], Zou Tong[1]

1. Institute of Seismology, China Earthquake Administration
2. National Astronomical Observatories, Chinese Academy of Sciences
3. Chinese Academy of Surveying and Mapping (CASM)
Contact: Yangroot@yahoo.com.cn

Abstract

A new SLR station has been set up in San Juan, Argentina this year, and works well now. Since Feb. 5th, 2006 to the 4th quarter, 2006, a total of 5861 pass (include 1134 Lageos pass) was obtained[1]. Some parts of this station, including servo system, control system, control software, and some observations will be described in this paper.

Telescope Servo System

San Juan SLR station's telescope is a bi-close-loop control system, i.e. position loop and velocity loop. Angle inductosyn and tacho-generator are used for the feedback sensors. When SLR system is tracking, the DAC input is tuned by PC software to drive telescope according to the ephemeris and the telescope position. Then the PID arithmetic theory is used to figure out the PWM voltage, consulting the telescope and theoretical velocity, to drive telescope's moment motor. So using this bi-close-loop control system, the SLR system's tracking can be improved.

The mount is driven by special motion drive IC: LMD18200. Its operating voltage can be up to 55V, and operating current can be up to 3A continuous output.

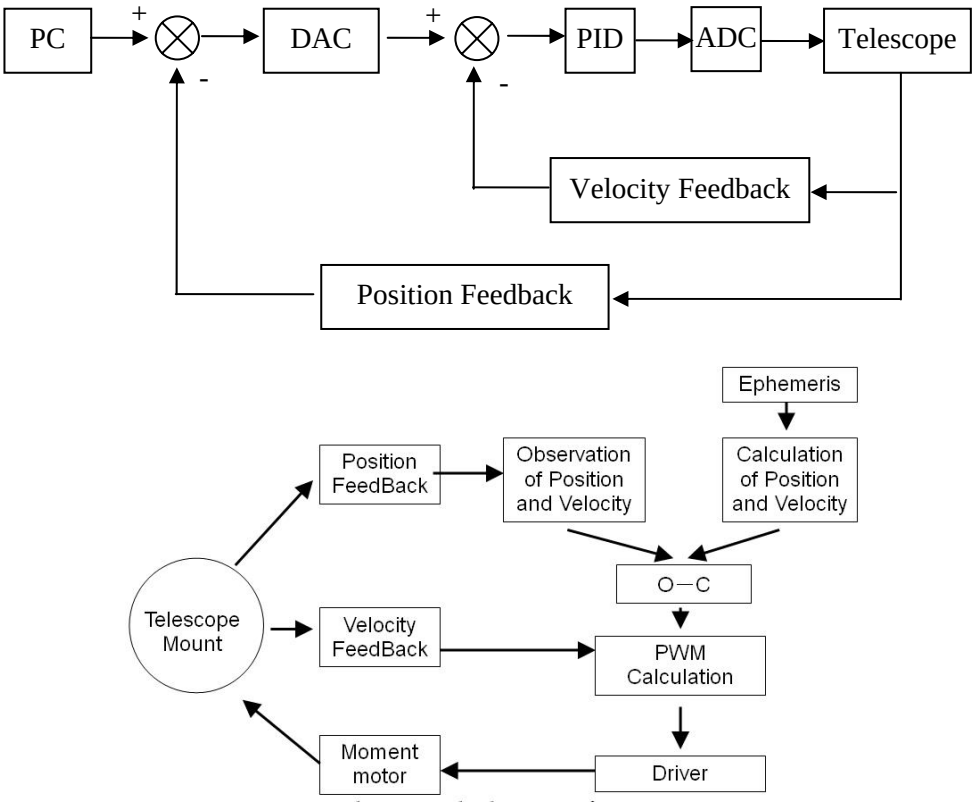

Figure 1: *the principle diagram of servo system*

Control Software

A general computer is needed to run the control software, and Figure 2 is the first picture of San Juan's tracking Lageos. Most control functions are included, such as satellite prediction, data pre-treatment, telescope servo, laser firing, range gate tuning, target measurement, data acquisition, etc.

Figure 2 is the first pass of Lageos in San Juan SLR station on Feb.5th, 2006. In this pass, 1514 samples were achieved between two green lines. The duration is about 15 minutes, and the deviation is very small (white dots).

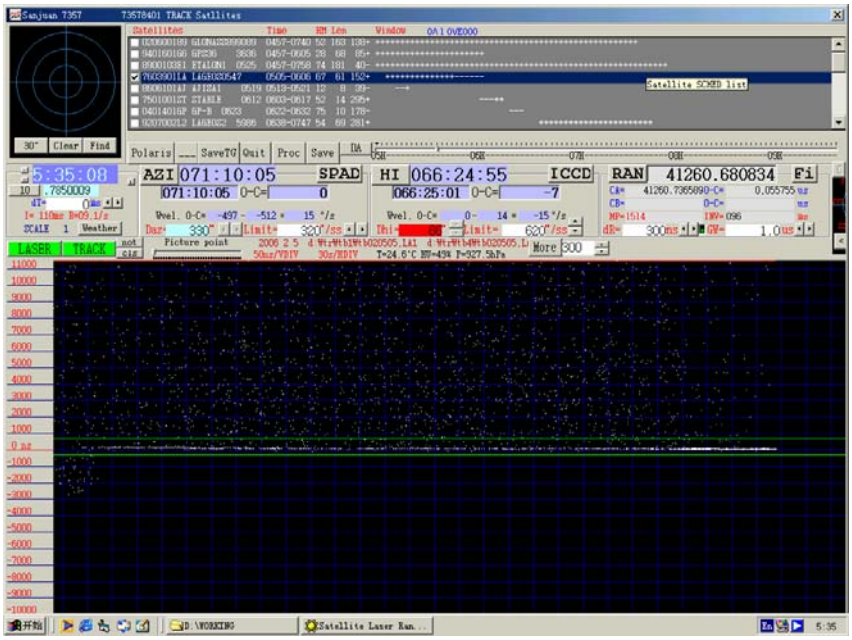

Figure 2: *Interface of control software and the first Lageos pass*

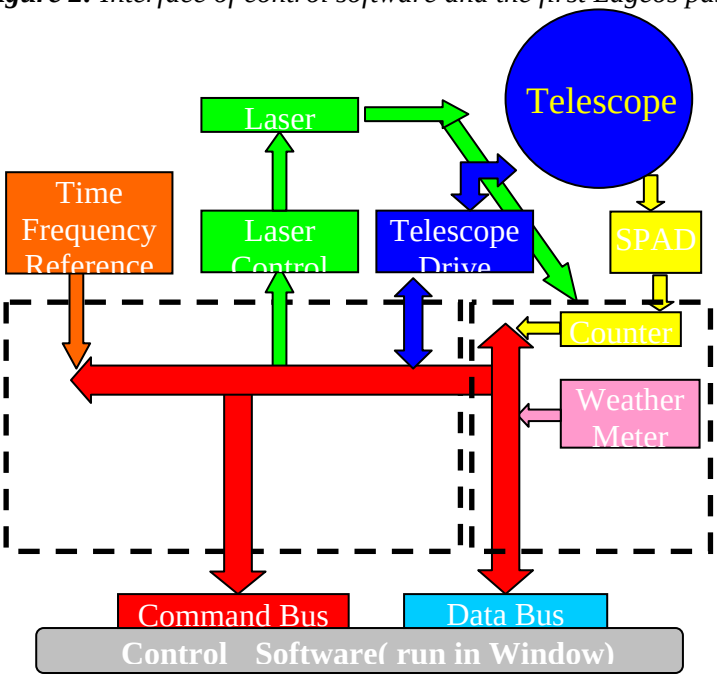

Figure 3: *The diagram of control system*

Results

The South America is lack of SLR station. The running of productive San Juan station will improve performance of the ILRS network.

Site Information		Data Volume									Data Quality		
Column 1	2	3	4	5	6	7	8	9	10	11	12	13	14
Location	Station Number	LEO pass Tot	LAGEOS pass Tot	High pass Tot	Total passes	LEO NP Total	LAGEOS NP Total	High NP Total	Total NP	Minutes of Data	Cal. RMS	Star RMS	LAG RMS
Baseline		1000	400	100	1500								
San_Juan	7406	3846	1134	881	5861	52713	13619	4180	70512	32323	6.5	10.4	12.1

Table 1: *San Juan performance report card[1]*

Reference

[1] SLR Global Performance Report Card July 1, 2005 through June 30, 2006.

[2] Wang Tangqiang, Current Status Of San Juan SLR Station In Argentina, 14th ILRS Workshop Proceedings.

[3] Guo Tangyong, The Performance and Observation of Mobile System TROS-I In China, 14th ILRS Workshop Proceedings.

Integrated Upgrades of Control System for TROS

Li Xin, Guo Tangyong, Zou Tong, Wang Peiyuan, Tan Yechun,
Xia Jiening, Zhou Yunyao, Du Ruilin

1. Institute of Seismology, China Earthquake Administration.

Contact: lxcomcn@yahoo.com.cn /Fax: +86-27-87863471

Abstract

The mobile SLR system TROS has operated for several years. Operations are routine, but the system is not without problems. To solve these problems, we are planning an upgrade to some of the TROS subsystems. These upgrades will enhance the signal return rate, improve the tracking precision and system reliability, provide convenient operational conditions for mobile observation, and relieve the labor intensive nature of the operations and maintenance.

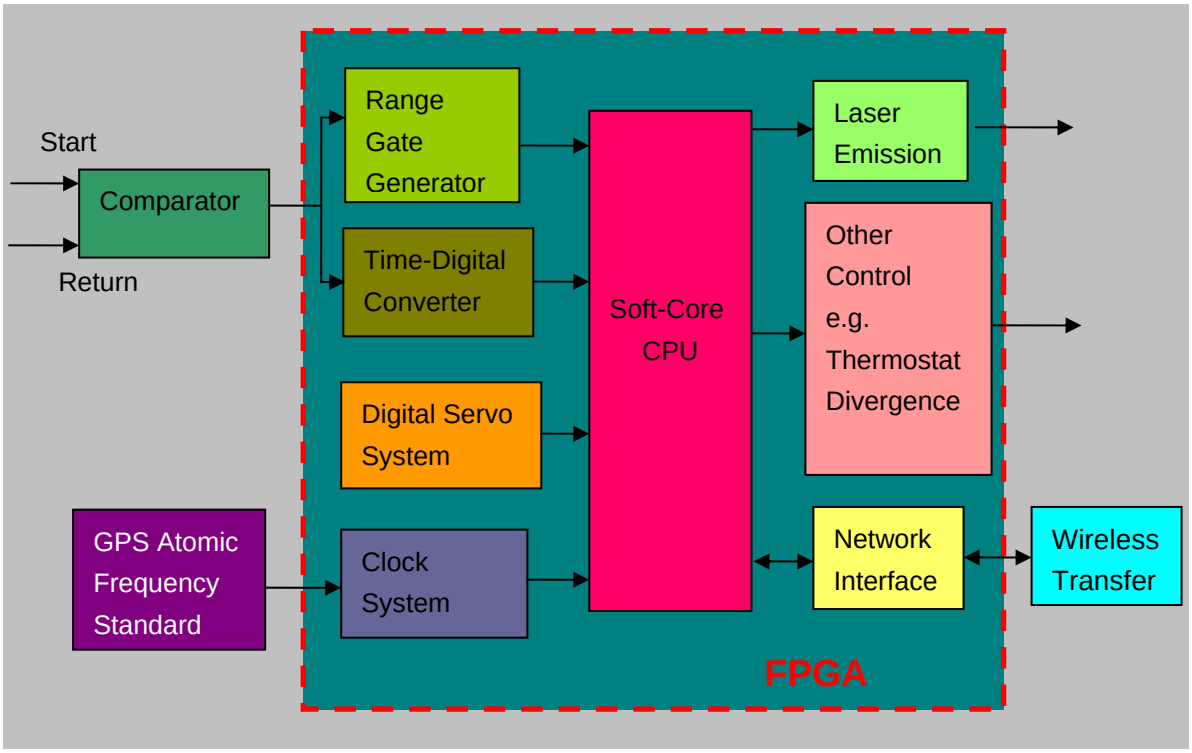

Figure 1. *The principle diagram of the control part*

The new version of TROS will possess the following properties:

1. The electronic components will be integrated into one subsystem, including event counter, GPS locked clock, range gate generator, servo system, and software. This will enhance system reliability.The principle diagram of this part is shown in Figure 1.

2. The control system will provide control for KHz ranging.This will help in target acquisition and tracking and enhance the normal point ranging precision.
3. The integrated event counter will use the time to digital converter to measure the interval in the FPGA.
4. The new electronics will generate the signal of angular position and speed by a photoelectric position encoder for implementing a full digital servo system. This will enhance tracking precision.
5. Operators will be able to run the software to control the system by web browser over wireless link.

CCD and SLR Dual-Use of the Zimmerwald Tracking System

W. Gurtner, M. Ploner

1. Astronomical Institute, University of Bern.

Contact: gurtner@aiub.unibe.ch

Abstract

The Zimmerwald Laser and Astrometric Telescope (ZIMLAT) has been designed for both satellite laser ranging and optical tracking with CCD cameras, the latter mainly for orbit determination of space debris by means of astrometric positions. The paper describes the main characteristics of the control programs, both for CCD and SLR and their interaction during interleaved operation and it summarizes some experiences after several years of dual-use.

Introduction

The Zimmerwald observatory celebrated its 50 years anniversary in 2006. Its original purpose was an astronomical observatory for the University of Bern, Switzerland, mainly designed for sky surveillance (search for supernovae, minor planets and comets). However, it developed more and more into an observatory for space geodesy, starting with optical (photographic) tracking of satellites in the sixties, laser tracking since 1976, permanent GPS (and later GLONASS) tracking since 1991 and finally optical tracking again, mainly of space debris, using CCD cameras and digital image processing. In 1997 we replaced the former SLR tracking system (50 cm telescope, Nd:YAG laser) with a new 1-meter telescope and a two-wavelength Ti:Sapphire laser (846 nm and 423 nm wavelengths). The new ZIMLAT telescope has been designed for dual use, i.e. it serves as transmitting/receiving telescope for satellite laser ranging as well as a telescope for astrometric observations of space objects, mainly space debris.

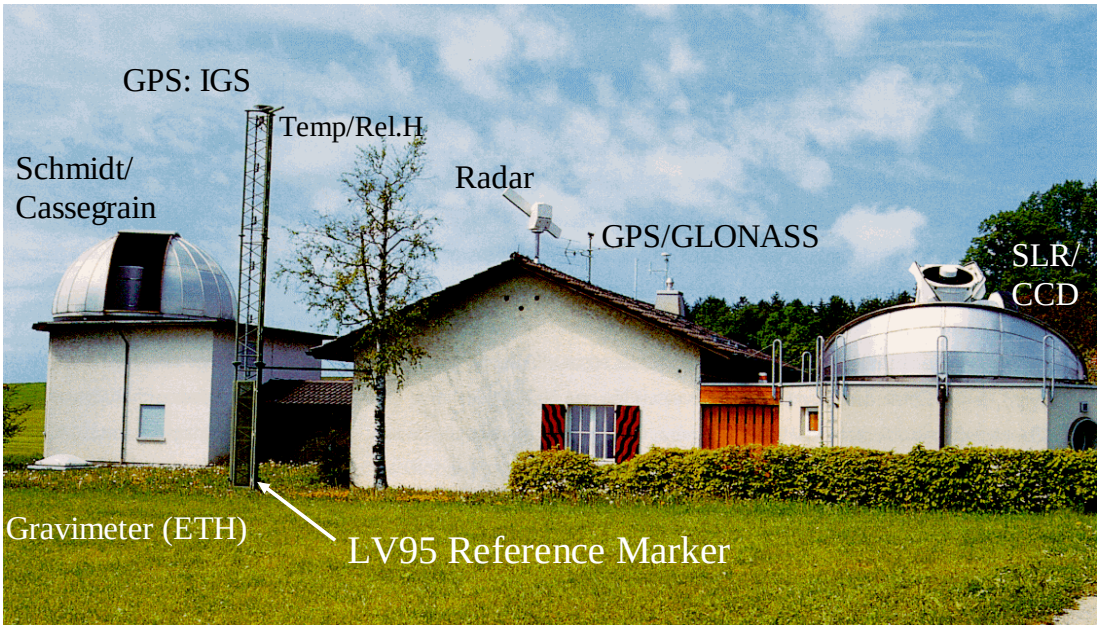

Figure 1: *The Zimmerwald Observatory*

The Zimmerwald Laser and Astrometric Telescope ZIMLAT

The main characteristics of the telescope are as follows:

The diameter of the main mirror is one meter. The telescope is of the Ritchey-Chretien type with main mirror, secondary mirror and a flat 45-degree tertiary mirror reflecting the image sideways into the elevation axis.

A vertical platform on one side of the telescope serves as mounting surface for four optical tables, with reduction optics, filter wheels and CCD cameras (Figure 2). The platform can be rotated around its horizontal axis (independent from the motion of the tube around the elevation axis) to derotate the image on the camera according to various strategies. The camera to be used for observation can be selected by means of a rotating mirror (with four distinct positions) in the center of the platform.

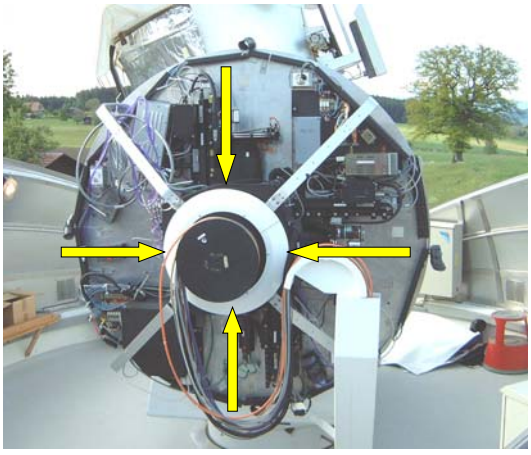

Figure 2: *Instrument platform*

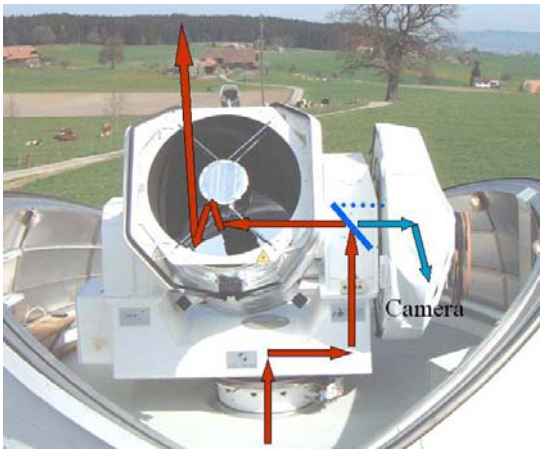

Figure 3: *ZIMLAT telescope*

For Satellite Laser Ranging the laser beam is guided, slightly off-axis, through the Coudé path to the telescope (Figure 3). Its diameter of 1 cm at the exit of the transmit table is increased to 15 cm by the telescope optics. The receiving beam fills the full aperture of the telescope as well as the Coudé path back to the receiving table.

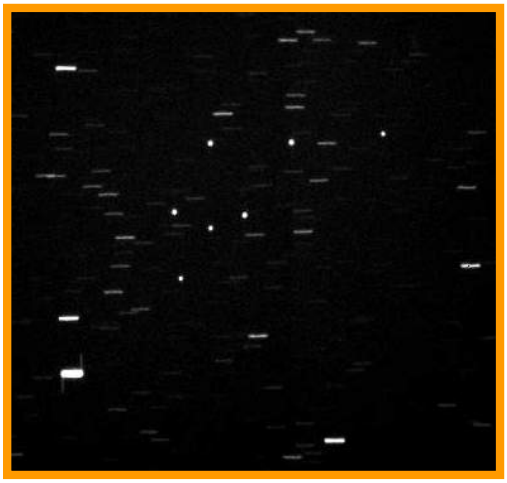

Figure 4: *7 Geostationary Astra satellites (field of view 12x12‘)*

Figure 4 shows a sample image of one of the CCD cameras with 7 geostationary satellites within a field of view of about 12 arc minutes squared. The telescope was

kept fixed during the exposure time, showing the daily rotation of the Earth as short traces of the background stars.

The separation between the CCD and SLR observation modes is done by a fairly large dichroic 45-degree beam splitter mirror in the elevation axis of the telescope. It can be pneumatically removed (tilted) for high-precision CCD imaging. During night-time SLR tracking a video camera on one of the four camera ports can be used for visual verification of the tracking with the dichroic beam splitter inserted.

The Control Systems

The Satellite Laser Ranging part is controlled by the program *ZIMLAS* running on an Alpha workstation (operating system: VMS). It communicates with two specialized PCs for data collection and control of various electronic components and for the control of the telescope. The workstation handles the satellite predictions, generates the observation schedule (example in Figure 6), stores and post-processes the range observations, interacts with the operator in manual mode or controls the whole system in fully automated mode (see also Gurtner et al, 2002).

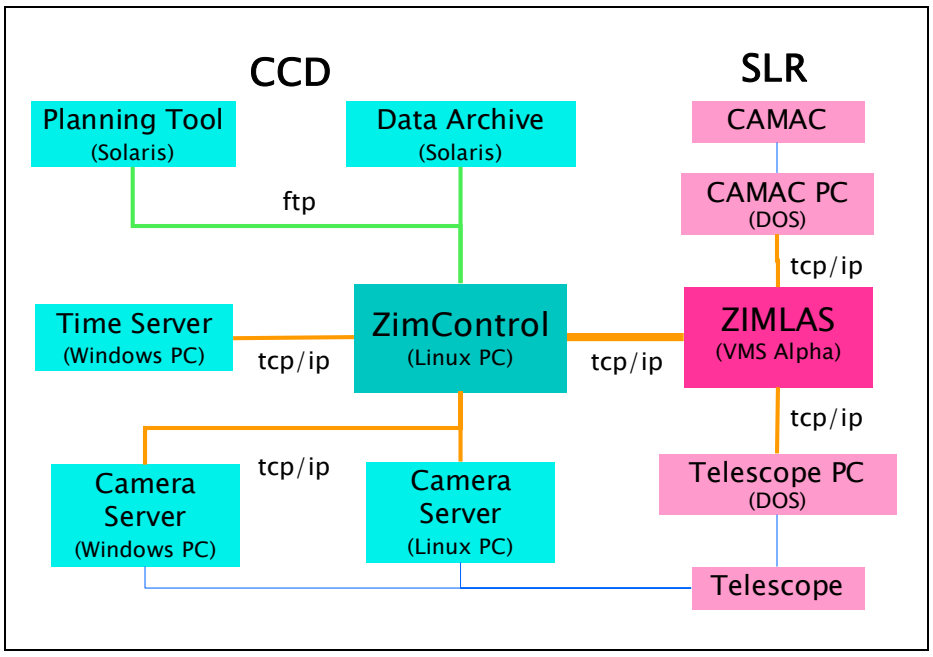

Figure 5: *Control Systems*

The control system for CCD observations (program *ZimControl*) is hosted by a Linux PC. It handles the observation schedule for CCD observations, interacts with the CCD cameras through specialized camera servers, and stores and pre-processes the digital images.

CCD Targets and Observation Plan

The following targets and objects are routinely tracked

- GEO (geostationary objects)
  - Active satellites
  - Space debris
- GTO (geostationary transfer orbit): Upper stages, debris
- Minor planets: Confirmation exposures for Near-Earth Objects

- GPS satellites to check system status (e.g., timing system)
- Photometry: Change of visual magnitude of objects due to their rotation
- Bias and dark current exposures (camera properties)
- Projection parameters, image distortions (telescope and camera properties)
- Focussing exposures (temperature- and elevation-dependent)

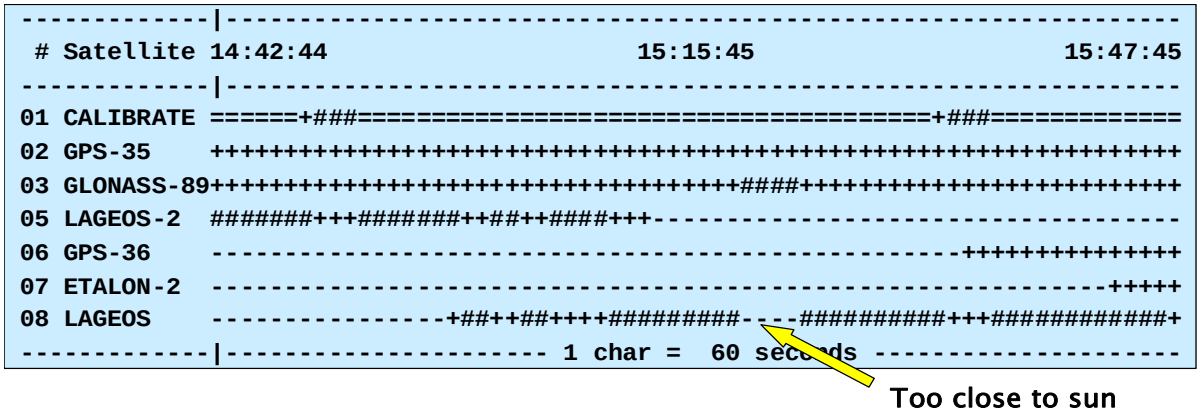

Figure 6: *Automatically generated observation schedule (SLR)*

Figure 7 shows an observation plan with targets and their possible observations periods during one night.

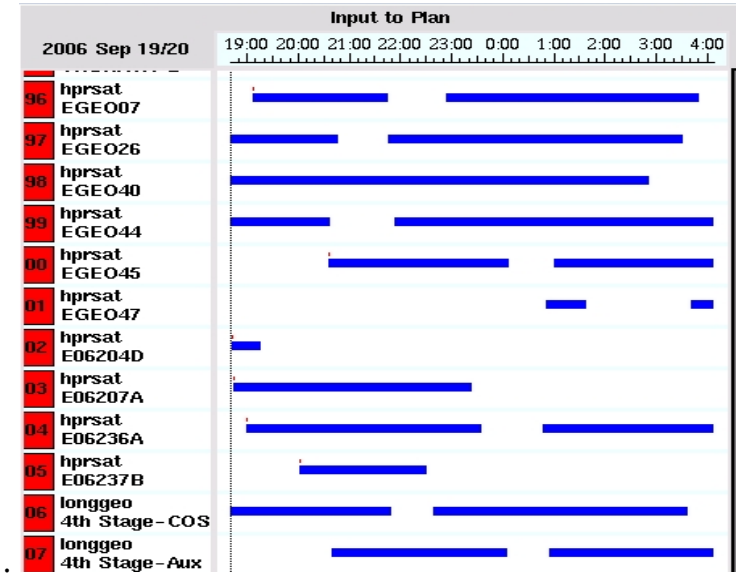

Figure 7: *CCD observation plan*

Insertion of CCD observations into SLR operations

Whenever the sun is more than 9 degrees below the horizon the CCD control system automatically checks if the SLR tracking system is currently operating.

If it is and if there are suitable objects in the observation plan the CCD system starts requesting observation time from the SLR system, starting with a time slot of 10 minutes, gradually reducing its length down to a minimum of 3 minutes if the request is not granted. This process is repeated over and over until a request is granted.

On the other side the SLR system checks each request, compares the requested duration with the current SLR tracking scheme and grants or rejects the request

according to the following conditions:

- Time since last CCD observation “large enough”
- Remaining pass segment of current SLR target “large enough”
- Already a minimum number of successful SLR observations collected
- Currently not in calibration mode
- CCD mode not blocked by operator

“Large enough” depends on the priority of the current SLR target and on the priority assigned to CCD operations.

If the request is granted the SLR system interrupts the current SLR tracking, puts the telescope into CCD mode (removal of the dichroic beam splitter from the elevation axis, pointing of the selection mirror on the platform to the requested CCD camera) and sends the requested object position or trajectory to the telescope control PC for tracking.

The CCD control system commands the camera to take an exposure and stores the digital image for further processing. Depending on the length of the granted observation interval several images of the same object or of different objects may be collected.

At the end of the current CCD observation interval the SLR system puts the telescope back into SLR mode and continues to range to the SLR targets according to the automatically updated tracking scenario.

The CCD control system then starts all over again with new requests for CCD tracking as long as the SLR system is in operation and until dawn.

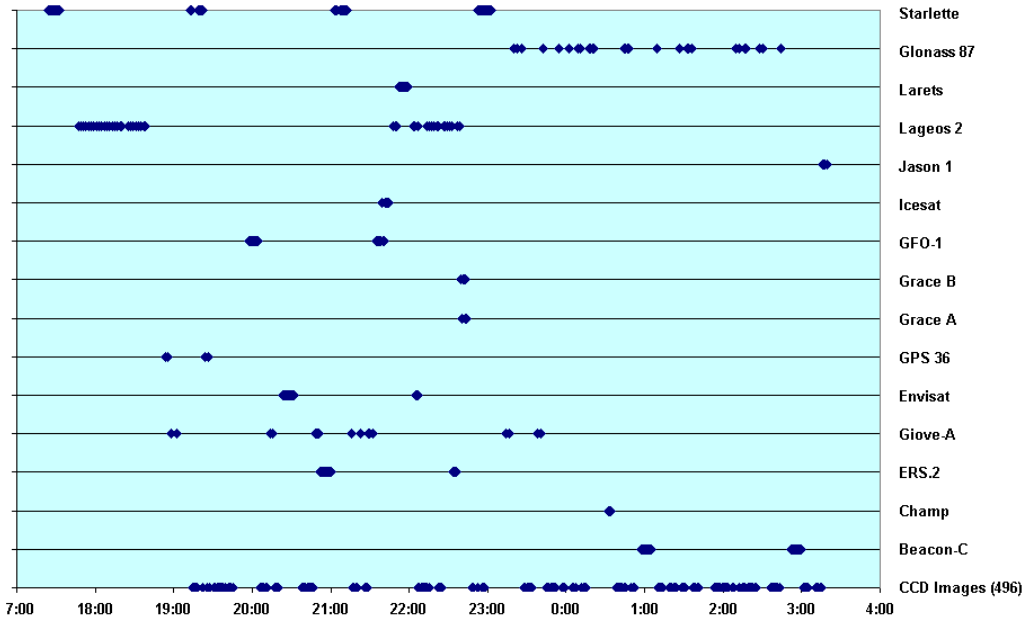

***Figure 8**: SLR/CCD interleaving*

Switching between the two modes SLR and CCD needs all in all less than 30 seconds, repositioning of the telescope included. Figure 8 shows the actual tracking scenario (SLR satellites, CCD observations on the bottom line) of the night of September 1st, 2006. Thanks to the rapid interleaving of CCD into SLR, especially into the long passes of medium-high (Lageos 1,2) and high satellites (navigation satellites and Etalon 1,2) no substantial reduction of the SLR data output could be observed.

Figure 9 shows the monthly number of images collected during the last one and a half years.

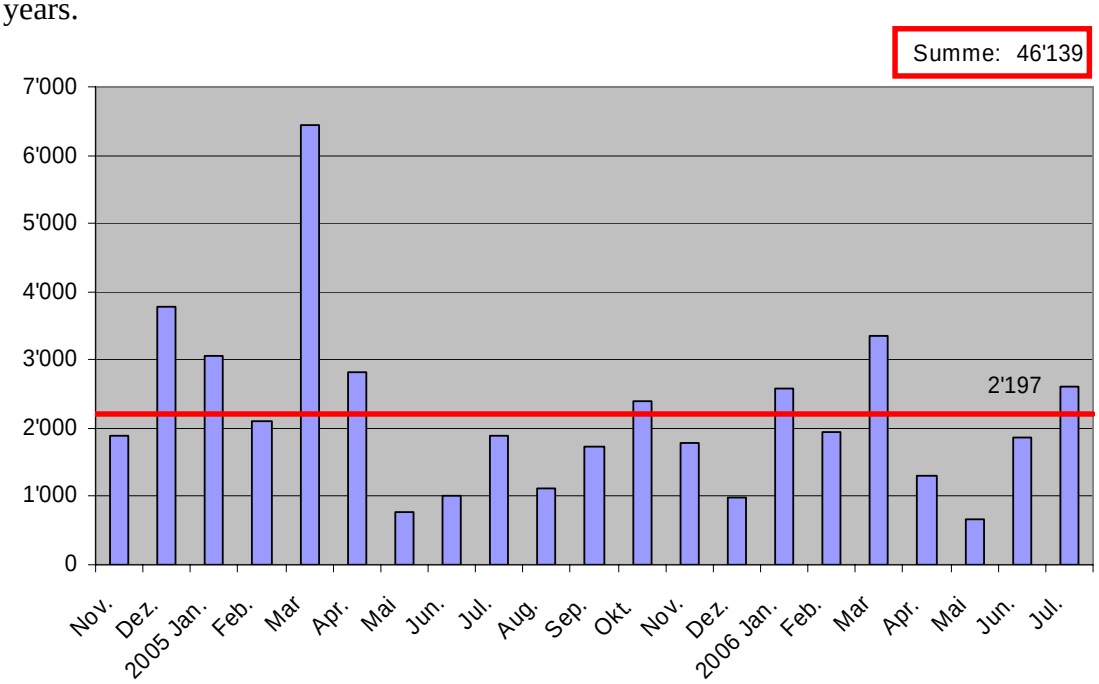

Figure 9: *Monthly number of CCD images Nov 2004 - Jul 2006*

Automation

The two control programs SLR and CCD are independent programs (running on two different computer systems). Either one or both can run completely automatically and unattended or under operator control.

In the extreme case (good and predictable weather conditions provided) several observation sessions of a few hours length each can be set up and submitted in advance by simple commands like

```
AUTO_SLR 20:00 22:00 WG MEDIUM
```

defining start and end time of the session, responsible observer's initials, and the priority assigned to CCD observations. All the rest is taken care of by the two control systems.

Post-processing

SLR data post-processing, i.e.,

- computation and application of an average calibration constant
- data screening
- normal point generation
- exchange format generation and submission of the data to the ILRS data center

can either be done interactively (daylight: mandatory) or fully automatically.

Image processing is automated and runs in the background on a Linux system at the university (the image files are automatically transferred to the university right after acquisition):

- Object recognition
- Reference star selection
- Determine image positions of stars and objects

- Astrometric position of objects
- Image archiving

The automatic processing of the previous night is checked interactively and problematic cases are reprocessed manually.

Conclusions

The dual use of the Zimmerwald Laser and Astrometric Telescope ZIMLAT has proven to be very cost-efficient. Although the telescope's design and operation is more complicated than the one of a single-mode instrument it provides us two different observation techniques for little more than the costs of a simple telescope. Thanks to the high degree of automation the two modes can be used nearly simultaneously without significant reduction of the SLR data output.

References

[1] Gurtner W., E. Pop, J. Utzinger (2002), *Improvements in the Automation of the Zimmerwald SLR Station*, 13th International Workshop on Laser Ranging, October 7-11, 2002, Washington, D.C.

Automated Transmitter Beam Size and Divergence Control in the SLR2000 System

J. Degnan, G. Jodor, and H. Bourges

1. Sigma Space Corporation, 4801 Forbes Blvd., Lanham, MD 20706 USA.

Contact: John.Degnan@sigmaspace.com /Fax: +01-301-577-9466

Abstract

Signal count rates and orbital time bias estimates vary widely over the range of satellite altitudes. In order to obtain an acceptable photon count rate for the higher satellites (e.g. LAGEOS, ETALON, GPS) while still meeting eye safety requirements at the telescope exit aperture, we must tightly control both the SLR2000 transmit beam diameter at the exit aperture and the final beam divergence half angle. For lower satellites, the uncertainty in the satellite angular position and the signal count rates are both relatively high. Thus, the SLR2000 design targets a nominal range of beam divergence half angles between 4 arcsec (larger than the combined effects of mount pointing jitter and atmospherically induced spreading and beam wander) for high satellites and 13 arcsec (adequate to accommodate time bias uncertainties) for LEO satellites. A modified commercial beam expander in the transmitter is used to maintain a constant transmitter beam size at the telescope exit aperture for eye safety while simultaneously varying the beam divergence to accommodate the various satellite altitudes and angular uncertainties.

Introduction

SLR2000 adjusts transmitter beam divergence based on satellite altitude and orbital knowledge, i.e. narrower for high satellites (± 4 arcsec min) and wider for low satellites (± 13 arcsec max). For eye safety reasons, the divergence must be adjusted while keeping the beam diameter at the telescope exit aperture fixed. It has been shown [Klein and Degnan, 1972] that a ratio of telescope diameter to Gaussian beam diameter (between $1/e^2$ intensity points) equal to 1.12 maximizes the amount of energy on the satellite. Thus, for the 40 cm SLR2000 telescope, the optimum beam diameter is 35.7 cm, and final divergence is set by adjusting the phase front curvature of the transmit beam at the telescope exit window. The Special Optics Beam Expander (SOBE) for controlling spot size and divergence is located on the transceiver bench in the transmitter path. This paper outlines our technical approach and additional details can be found elsewhere [Degnan, 2005].

Paraxial ray matrix theory can be applied to Gaussian laser beams if the beam is represented by the complex parameter

$$\frac{1}{q(z)} = \frac{1}{R(z)} - j\frac{\lambda}{\pi\omega^2(z)} \qquad (1)$$

where λ = 532 nm is the laser wavelength in the propagation medium and R(z) and ω(z) are respectively the wavefront curvature and spot radius (measured from the beam center to the $1/e^2$ intensity point) of the Gaussian beam at the location z along the propagation axis. If $q(z_0)$ is the Gaussian beam parameter at the output of the SOBE, then the Gaussian beam parameter at the exit window of the telescope is given by the ABCD Law [Verdeyen, 1989]

$$\frac{1}{q(z)} = \frac{C + D\left(\frac{1}{q(z_0)}\right)}{A + B\left(\frac{1}{q(z_0)}\right)} \tag{2}$$

In (2), A, B, C, and D are the ray matrix coefficients which propagate the rays from the SOBE to the telescope exit aperture. Separating (2) into its real and imaginary parts yields the following expressions for the wavefront curvature and beam spot size at the telescope exit aperture, i.e.

$$R(z) = \frac{\left(A + \frac{B}{R(z_0)}\right)^2 + \left(\frac{B\lambda}{\pi\omega^2(z_0)}\right)^2}{\left(C + \frac{D}{R(z_0)}\right)\left(A + \frac{B}{R(z_0)}\right) + BD\left(\frac{\lambda}{\pi\omega^2(z_0)}\right)^2} \tag{3a}$$

and

$$\omega(z) = \omega(z_0)\sqrt{\left(A + \frac{B}{R(z_0)}\right)^2 + \left(\frac{B\lambda}{\pi\omega^2(z_0)}\right)^2} \tag{3b}$$

We can now compute the ABCD matrix for the transmitter at the satellite target by multiplying the system matrix by the propagation matrix and letting the target range, *r*, approach infinity, i.e.

$$FF = \lim_{r\to\infty}\begin{vmatrix} I & rI \\ 0 & I \end{vmatrix}\begin{vmatrix} A\Gamma' & B\Gamma' \\ C\Gamma' & D\Gamma' \end{vmatrix} = \lim_{r\to\infty}\begin{vmatrix} (A+rC)\Gamma' & (B+rD)\Gamma' \\ C\Gamma' & D\Gamma' \end{vmatrix} \cong \begin{vmatrix} rC\Gamma' & rD\Gamma' \\ C\Gamma' & D\Gamma' \end{vmatrix} \tag{4}$$

Substituting A = rC and B = rD into (3) yields the following expressions for the phase front curvature and spot size at the satellite

$$R(r) = r \tag{5a}$$

and

$$\omega(r) = r\omega(z_0)\sqrt{\left(C + \frac{D}{R(z_0)}\right)^2 + \left(\frac{D\lambda}{\pi\omega^2(z_0)}\right)^2} = r\frac{\omega(z_0)}{m_t}\sqrt{\frac{1}{R^2(z_0)} + \left(\frac{\lambda}{\pi\omega^2(z_0)}\right)^2} \tag{5b}$$

where, for SLR2000, C = 0 and D = $1/m_t$ = 0 where m_t = 30.48 is the total magnification in the transmit path [Degnan, 2005]. As expected, the wavefront curvature in the far field equals the distance from the telescope aperture and the spot size grows linearly with that distance. Equation (5b) can therefore be used to compute the beam divergence half angle (center to $1/e^2$ intensity point) of the transmitter in the far field, i. e.

$$\theta_t \equiv \frac{\omega(r)}{r} = \frac{\omega(z_0)}{m_t}\sqrt{\frac{1}{R^2(z_0)} + \left(\frac{\lambda}{\pi\omega^2(z_0)}\right)^2} = \frac{\lambda}{\pi m_t \omega(z_0)}\sqrt{1 + \left(\frac{\pi\omega^2(z_0)}{\lambda R(z_0)}\right)^2} \tag{6}$$

Note that the far field divergence depends on both the spot size, $\omega(z_0)$, and the phase front curvature, $R(z_0)$, at the output of the SOBE.

Technical Approach

The approach we followed for controlling SLR2000 beam size and divergence was as follows:

1. Measure transmitter gaussian beam radius (.969 mm) at entrance plane to beam expander, raw beam half divergence, and compute gaussian complex q-parameter for the input beam
2. Choose a COTS beam expander with an adequate exit aperture (>40cm/30.48 = 13.1 mm) and magnification range (~13.1 mm/ 2mm = 6.5) and at least two control elements for independently adjusting beam size and phasefront curvature at the output.
3. Develop dynamic ray model for unit including variable lens spacings.
4. Test dynamic ray model against sophisticated ray tracing program such as ZEMAX.
5. Calibrate beam expander servo controllers at various magnifications.
6. For each divergence value, use the gaussian beam propagation law to compute the complex q-parameter of the expander output beam and the lens spacings which produce that parameter.
7. Compute lookup table specific to laser transmitter

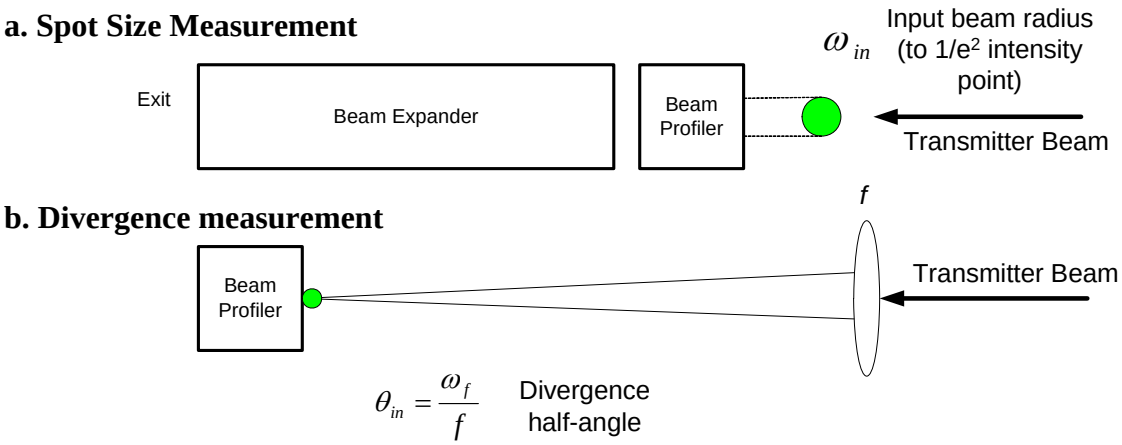

***Figure 1**: Measuring the Gaussian parameters of the raw transmit beam: (a) input radius; and (b) far field beam divergence.*

The beam radius and divergence of the transmitter beam at the input to the SOBE were measured using a standard beam profiler as in Figure 1. The complex Gaussian beam parameter was then computed from the formula

$$\frac{1}{q_{in}} \equiv \frac{1}{R_{in}} - j\frac{\lambda}{\pi\omega_{in}^2} = \frac{\lambda}{\pi\omega_{in}^2}\left(\sqrt{\left(\frac{\pi\omega_{in}\omega_f}{\lambda f}\right)^2 - 1} - j\right) \tag{7}$$

The commercial version of the Special Optics Beam Expander Model 56C-30-2-8X is normally operated under a Labview environment and is designed to provide a wide range of beam magnifications (2X to 8X) at the desired wavelength. Sigma has reconfigured the unit to operate with two National Aperture Motor Controllers under a more flexible software control. The optical unit consists of five lenses: a moving singlet at the input end, a moving doublet in the middle, and a larger aperture stationary doublet at the output end as in Figure 2. The moving singlet and doublet are

driven by two independent stepper motors. Their positions are determined by counting the number of steps from a home position as defined by two limit switches.

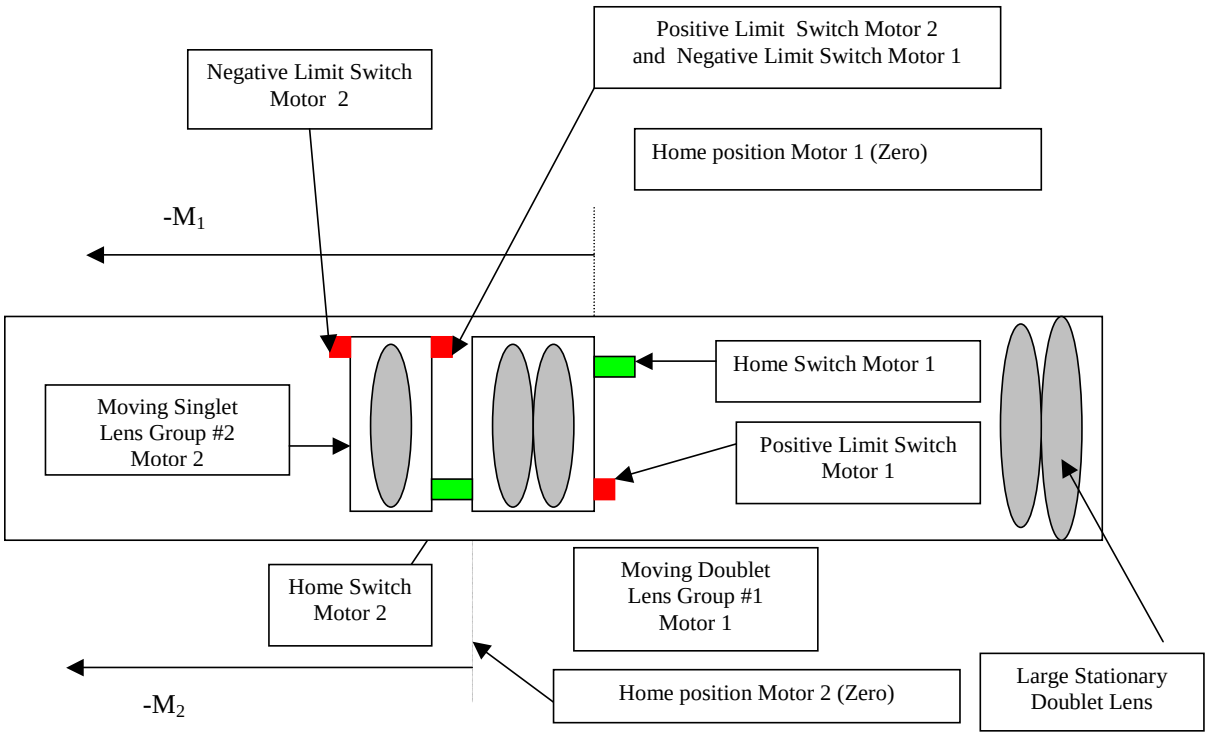

Figure 2: *Optomechanical configuration of Special Optics Beam Expander Model 56C-30-2-8X. The expander has entrance and exit apertures of 10 mm and 30 mm respectively.*

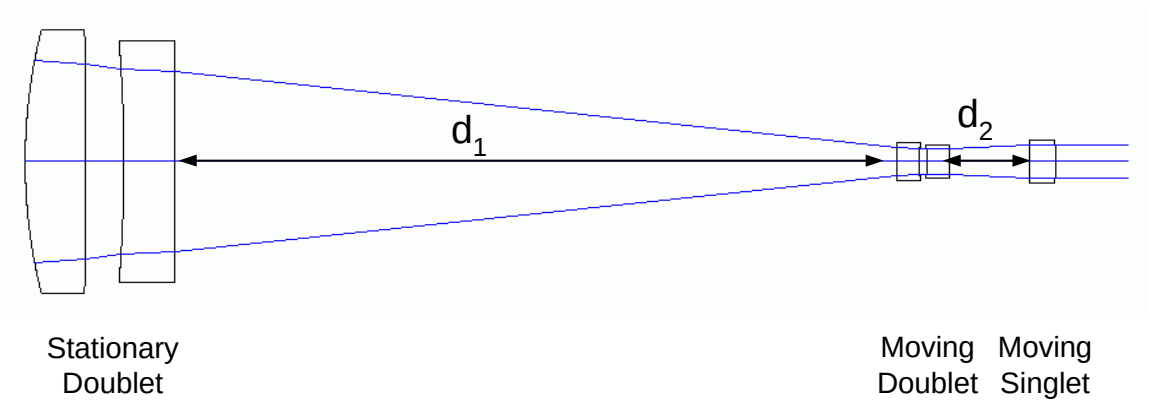

Figure 3: *Optical layout of Special Optics Model 56C-30-2-8X Beam Expander.*

Using an optical prescription provided by Special Optics, we computed a "dynamic ray matrix" for the SOBE depending on the variables d_1 and d_2 defined in Figure 3. The result was

$$M_{SO}(d_1,d_2)=\begin{vmatrix} A_{SO}(d_1,d_2) & B_{SO}(d_1,d_2) \\ C_{SO}(d_1,d_2) & D_{SO}(d_1,d_2) \end{vmatrix} \tag{8}$$

where

$$A_{SO}(d_1, d_2) = A_0 + A_1 d_1 + A_2 d_2 + A_{12} d_1 d_2 \quad (9a)$$

$$B_{SO}(d_1, d_2) = B_0 + B_1 d_1 + B_2 d_2 + B_{12} d_1 d_2 \quad (9b)$$

$$C_{SO}(d_1, d_2) = C_0 + C_1 d_1 + C_2 d_2 + C_{12} d_1 d_2 \quad (9c)$$

$$D_{SO}(d_1, d_2) = D_0 + D_1 d_1 + D_2 d_2 + D_{12} d_1 d_2 \quad (9d)$$

and the computed coefficients appearing in (9) are summarized in Table 1.

Table 1: *Summary of coefficients appearing in the SOBE ray matrix*

Suffix	A	B	C	D
0	1.995665379968	0.028752151456	46.402866180544	1.170293617808
1	63.683551232	1.442710470656	-460.710690944	-10.437108561152
2	-45.765735168	2.505955512	-1230.503704704	67.377646836
12	-1634.569158656	89.502715904	11825.086257152	-647.496210368

Setting C_{SO} =0 and A_{SO} equal to integer magnifications between 2 and 8, the ray matrix predictions of the interlens spacings, d_1 and d_2, computed from (9a) and (9c) were then compared to those of a popular ray tracing program, ZEMAX, and the predictions were found to agree within a few tens of microns for all magnifications. The two motor positions, relative to their respective home limit switches, are related to the interlens spacings via the equations

$$M_1 = a - d_1 \quad \text{and} \quad M_2 = b - d_1 - d_2 \quad (10)$$

Following our inhouse calibration procedure, the constants a = 88.7412 mm and b = 92.9858 mm in (10) were found to differ from the values (a = 88 mm and b = 90 mm) provided by the manufacturer. The next step in the process is to tabulate the values of d_1 and d_2 that produce the desired spot size and divergence at the exit aperture of the telescope. This is accomplished by using the Gaussian propagation law (2) to generate the following approximate expressions for the beam radius and phasefront curvature at the exit aperture of the SOBE

$$\omega_0(\theta_t) \cong \frac{\omega}{m_t} - d_t\theta_t = 0.00585 - 30.84\theta_t(rad)$$

$$\frac{1}{R_0(\theta_t)} \cong \frac{m_t^2\theta_t}{\omega - m_t d_t \theta_t} = \frac{929.0\theta_t\,(rad)}{0.1785 - 940.0\theta_t(rad)} m^{-1}$$

where ω = 0.179 m and θ_t, are the desired beam radius and beam divergence at the telescope exit aperture. For each divergence, we then use the beam expander ray matrix (8) to compute the expander lens positions, $d1$ and $d2$, which yield the above values of ω_0 and R_0. The final step is to compute the corresponding motor positions via (10), convert the latter into encoder counts using a scale factor of 0.304 microns per step, and generate a table lookup of beam divergence versus encoder counts for each motor. Figure 4 gives a graphical representation of the interlens separations in the lookup table as a function of final transmitter beam divergence for SLR2000.

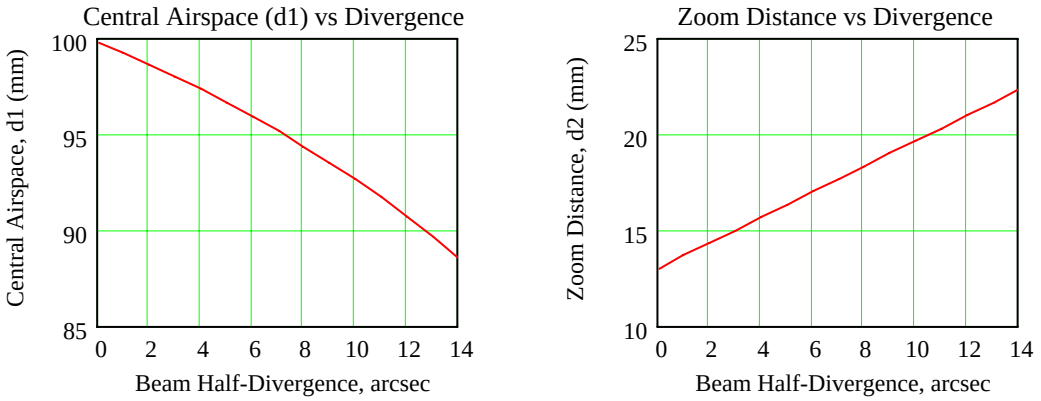

Figure 4: *The computed interlens distances, d_1 and d_2, in the SOBE which produce a given divergence half-angle in the far field while maintaining a constant spot radius of 17.9 cm at the exit aperture of the telescope. A circularized Phase II laser with a mean Gaussian radius of 0.969 mm and a raw half-divergence of 1.265 mrad is assumed as input to the SOBE.*

Summary

Using a computer lookup table, the SLR2000 computer can set two lens spacings in the 5-element transmit beam expander to provide a fixed beam diameter (35.8 cm) at the telescope exit aperture for eye safety while adjusting the phasefront curvature to give the desired final divergence. The lookup table must be updated whenever the transmitter is changed but it is an automated process. The optical half-divergence range of the final SLR2000 transmit beam is theoretically 0.25 arcseconds to 13 arcseconds (1.3 to 65 microradians) but atmospheric turbulence will define the actual lower limit. For verification, GSFC monitors the divergence of the SOBE output via a long focal length lens and CCD camera as outlined in Figure 1 and divides the result by the total magnification in the transmitter path. Presently, an inadvertent defocus in the SLR2000 main telescope is being compensated for by an offsetting defocus in a 3-power telescope on the transceiver bench. As a result, the nominal magnification of 30.48 for perfectly focused telescopes has been reduced to 28.21 for the compensated telescopes [Degnan, 2005].

References

[1] Degnan, J. J., “Ray Matrix Analysis for the Realtime Control of Automated SLR2000 Optical Subsystems”, Chapter 8, Sigma Space Corporation Report, October 2005.

[2] Klein, B. J. and J. J. Degnan “Optical Antenna Gain. I. Transmitting Antennas”, Applied Optics, 13, pp. 2134-2141, 1974.

[3] Verdeyen, Joseph T., Laser Electronics, Chapter 5, Prentice Hall, Englewood Cliffs, New Jersey 1989.

Obtaining the High-resolution Epoch with the FPGA Technology

Q. Li, F. Qu and Z. Wei

1. Chinese Academy of Surveying and Mapping (CASM)

Contact: liqian@casm.ac.cn /Fax:0086-10-68218654

Abstract

In Satellite Laser Ranging it is important to record the transmission epoch of each laser pulse. Currently in the Beijing SLR station many counter-chips are used to accomplish this task. With the popularity of the FPGA technology, engineers find that using FPGA (Field Programmable Gate Array) to design the digital system is a feasible way to reduce the dimension of the circuit board and increase the reliability of the system. We are designing a new epoch measurement system using one Xilinx's Spartan FPGA chip to accomplish what previously had required many counter-chips. The 1pps signals and the time code from the HP58503 are used to get rough epoch information to a one second resolution. The 10 MHz frequency from the HP58503 is used as the system clock. A 24-bit counter module in the FPGA chip, used with the system clock, gives timing information with a resolution of 100 nanoseconds and with a period of one second. To obtain the time code from the HP58503, two UART (Universal Asynchronous Receiver) modules are used, one to communicate with the HP58503, and another to transfer the epoch data to a PC.

Introduction

Fig.1 shows the present module at the Beijing Station that is used to obtain the epoch of the laser pulse. It is the cascade connection of 6 counter-chips. Every chip is only 4 bits, so higher resolution requires more counter-chips. To achieve a higher integrated level, we selected the FPGA chip which would perform the same task in a single module.

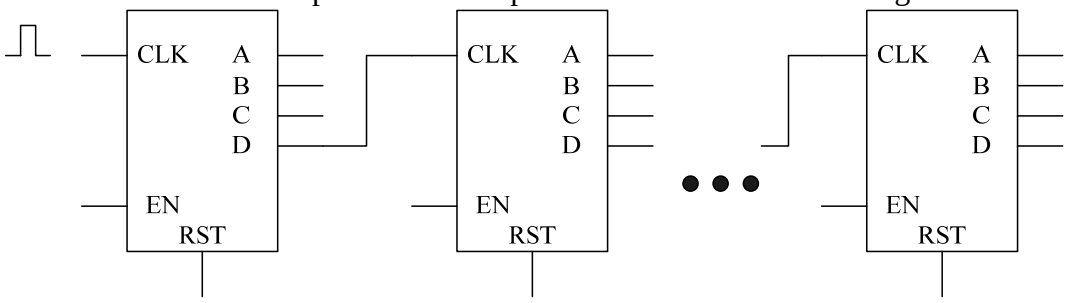

Figure 1: *Present module to obtain the epoch in Beijing Station*

Fig.2 shows the block scheme of the system. The HP58503 supplies the reference frequency, the one-pulse-per-second signal and the time code for the FPGA module to establish a UTC time clock. When a laser pulse arrives, the FPGA module sends the epoch data to the PC through the Serial Interface. MAX3232 is used as the level translator between the RS232 and LVTTL.

Establishment of the UTC time clock

Fig.3 shows the block scheme of the establishment of the UTC time clock. As the input clock frequency is 10MHz, so the time resolution is 100ns. To record one complete second, we must use a counter with at least 24 bits, because,

$$\log_2 \frac{1}{100 \times 10^{-9}} = 23.3$$

It's convenient to design a 24-bit counter in FPGA. Another 16-bit counter is designed to record the number of 1pps events after the reset operation. The 16-bit counter can record the time up to 18 hours, so 18 hours later, another reset operation is needed. Some registers are used to record the time code from the HP58503 to save the datum time.

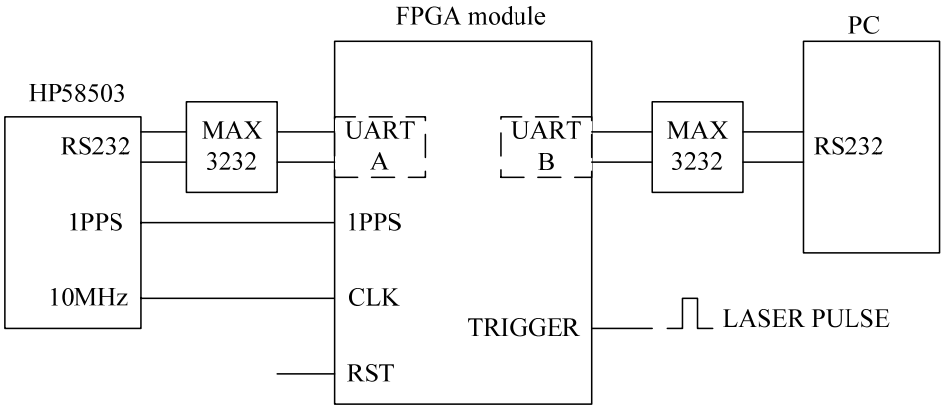

Figure 2: *Block scheme of the system*

Obtaining the epoch of the laser pulse

When a laser pulse arrives, some relative-time-registers are allocated to store the current values of REG1 and REG2. Then the data in the datum-time-registers and relative-time-registers are sent to the PC through UART B. The PC performs the final calculations required to obtain the transmission epoch of the laser pulse.

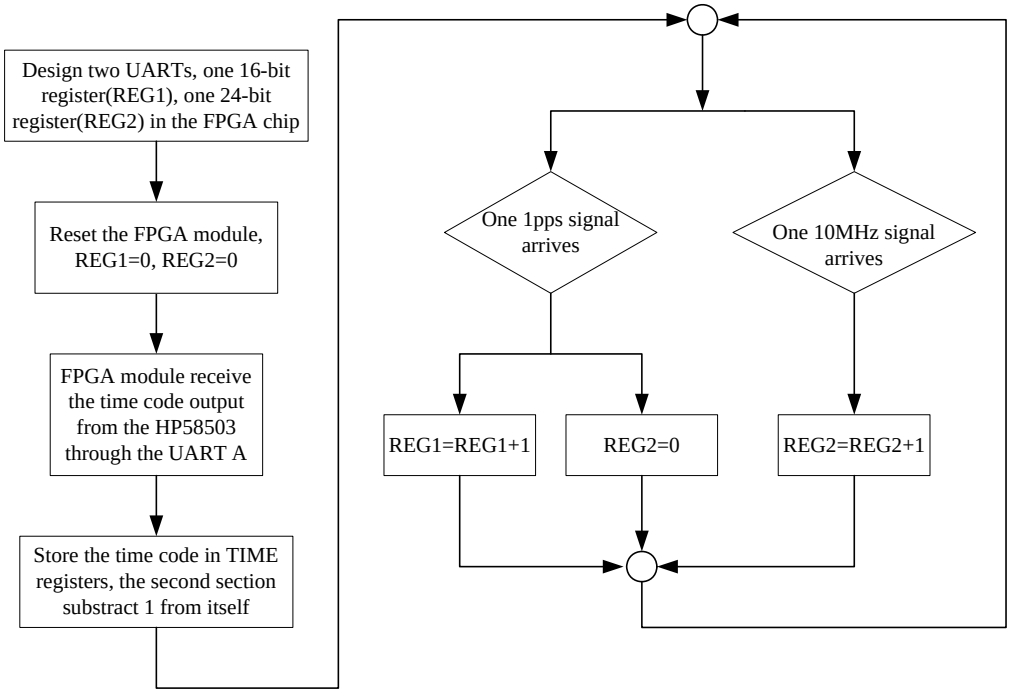

Figure 3*: The Establishment of the UTC time clock*

Comparison experiment and conclusion

A test setup has been designed to make sure that the new module can obtain the time code, 10MHz signal, 1pps signal from HP58503 as well as the laser pulse without disturbing the original system. Comparing the two epoch data shows that the new module has the equivalent function to the original one.

Difficulties in the development process and Future Plans

In the development process, the implementation of the UART is relatively harder than that of the counters. So compared with the microprocessors, the merits and drawbacks of developing a digital system with an FPGA are obvious.

Today, RISC microprocessors with an ARM core are widely used to design digital systems, so the structure “ARM+FPGA” may be a good choice for developing a digital system that can achieve higher resolution, precision, stability, flexibility and integration level as well as shorten the development time.

Platform

- Device:

  - Xilinx’s Spartan FPGA, HP58503, PC

- Software:

  - Xilinx ISE 7.1

  - VC++ 6.0

- Top-level Module type

  - HDL(Verilog HDL)

- Simulator

  - ISE Simulator

- Synthesis

  - XST(VHDL/verilog)

NEW FTLRS software tools for tuning observations schedule and remote control

Monique Pierron and FTLRS staff

1. Observatoire de la Côte d'Azur, Avenue N.Copernic - 06130 Grasse – France.

Contact: Monique.pierron@obs-azur.fr

Abstract

In the goal to facilitate and make more pertinent campaign observations, we have developed:

- *A fully automated mechanism for the CPF predictions: CPF file reception and propagation, prediction generation and orbit display are automatically performed.*
- *An acquired data sky coverage display for any site (per satellite and per date).*
- *A new levelling system for FTLRS, easy to use for observers, efficient and completing the remote controlled capability.*

Introduction

The French Transportable Laser Ranging Station often operates far from our French location in Grasse and it is very important to increase its remote capability, and to facilitate the observer's life.

Fully automated mechanism for the predictions

CPF mail reception

Mail is automatically extracted on the principal computer in Grasse. CPF files are sorted and dispatched in dedicated directories (for example /d/dat/prev/grca if GraceA) and files. File names are based on CPF file headers, for example gracea_060930_7732.gfz is done with target (gracea), date (060930), sequence number (7732) and provider (gfz).

CPF file propagation for FTLRS

For this, we use the rsync command (a free software computer program for Unix) to synchronize CPF files and directories from the Grasse computer to the FTLRS computer. This rsync command is executed every hour via the Crontab unix facility.

Files creation for satellite orbit display

All necessary files to display satellite orbits for the next few hours are created daily on Grasse and FTLRS computers (via cron facility):

- satellite timetable files for one month or more,

- prediction files for satellite passes to come: in this file, the step between positions depends on pass duration, in order to have a continuous curve for orbit display,
- file with next passes list for easy display; each line has the following form: Satellite name, MJD (begin), culmination, azimuth (begin and end), duration, date (hour and minute), prediction file name.

Satellite list and orbit display

At login the following window is displayed and continuously updated.

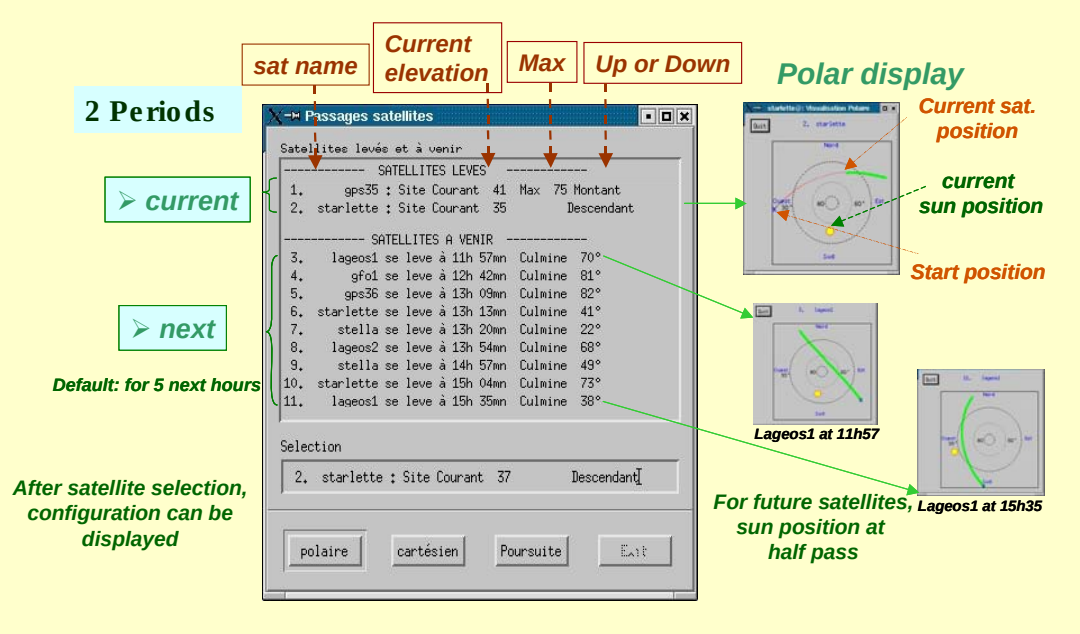

A few minutes before each satellite pass, a window with information appears and a bell rings.

With this mechanism in place, it was then natural and easy to develop the prediction's server on our main computer in Grasse. An executable prediction client (for Windows and Linux) is available. This will be very useful for further operations with MEO station (7845).

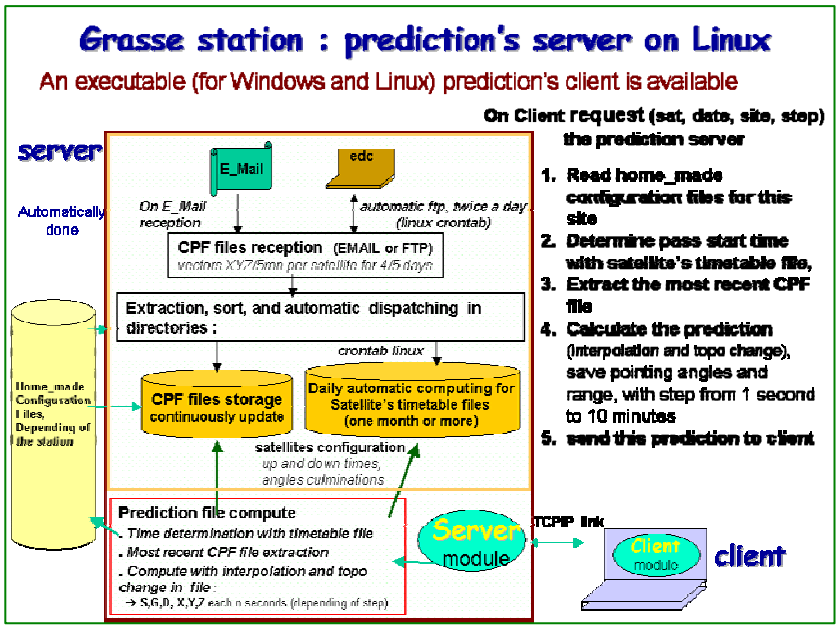

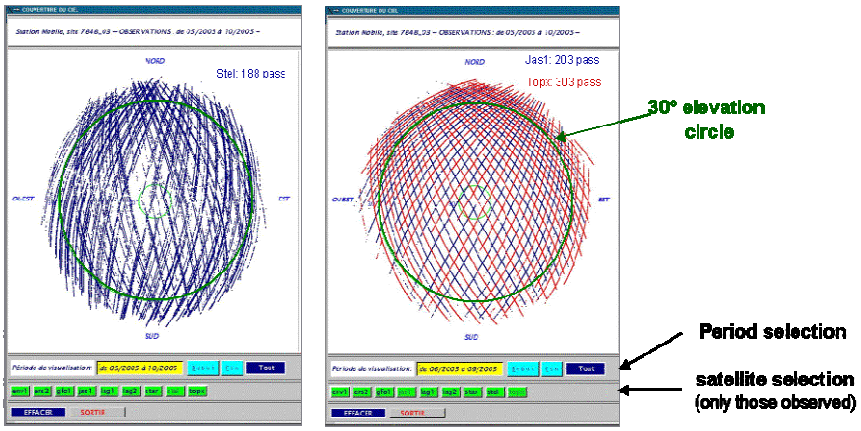

***Figure 1**: Sky coverage for Stella and Jason/Topex - FTLRS - May to October 2005*

Acquired data sky coverage display

This application allows display of data for each Grasse station (FTLRS, MEO and GRSL). Each point on the display is a validated return. The operator has just to choose:

- the satellite(s) in the proposed list, and
- the observation period.

The observation's Grasse station is done with an environment's variable.

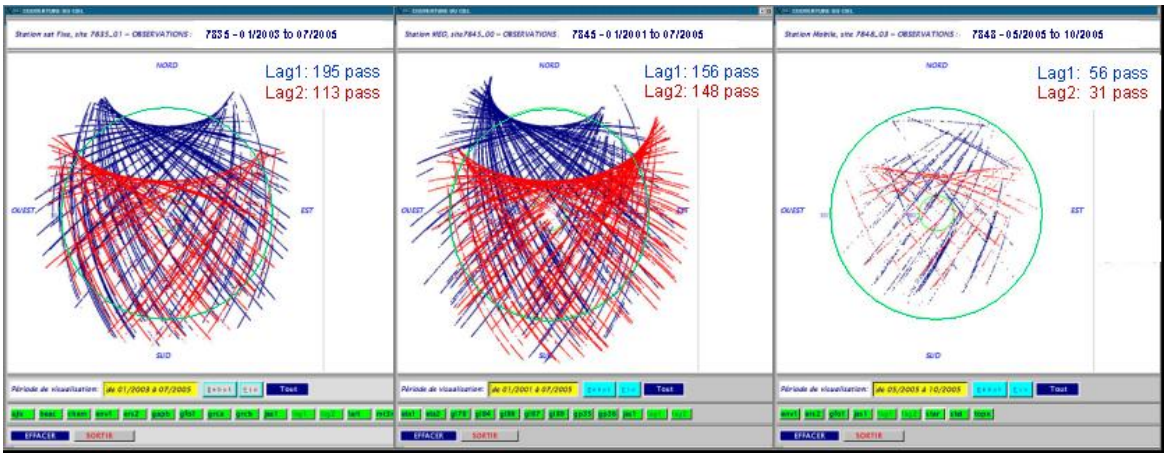

***Figure 2**: Lageos 1/Lageos 2 on Grasse stations: GRSL(7835), LLR(7845) and FTLRS (7848 Ajaccio)*

For FTLRS (7848 station during last Corsica campaign), we observe from the display that:

- the coverage has good repartition on all directions,
- Stella (first part Figure 1) is lost just during culmination,
- for Lageos (third part Figure 2) there were no returns under 30 or 40 degrees.

For GLRS (7835 station) we had a good coverage for all satellites (low satellites to Lageos).

For 7845 station (MEO station used for HEOS) from Lageos:

- the coverage has good repartition on all directions,
- it is easy to have returns when the satellite is low,
- for Lageos, it is very difficult to have returns when higher than 80°; this doesn't exist for higher satellites (Glonass or GPS).

A remote levelling system for FTLRS

We have developed a new system, to process the mount levelling system. The system (laser + telescope) is now on a mechanical device, and this device is levelled with two electrical jacks. These jacks are positioned in perpendicular directions.

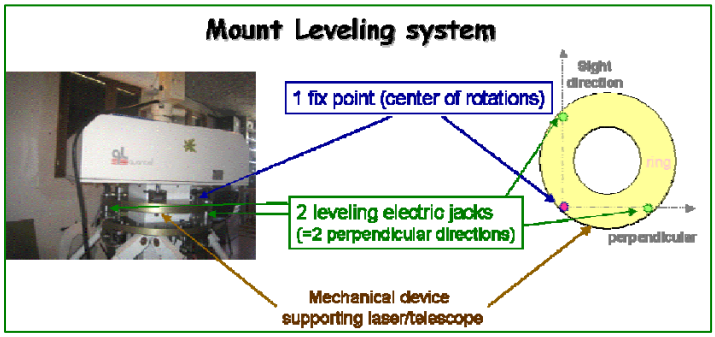

Figure 3: *The new mount Levelling sytem for FTLRS*

These jacks are software controlled via a control panel. Levelling values in two directions are continuously read and displayed, and it is possible to adjust the level:

- manually with the two push buttons on panel, or
- automatically with a servo loop control.

This new remote tool for FTLRS is efficient, easy to use and very important for remote controlled capability.

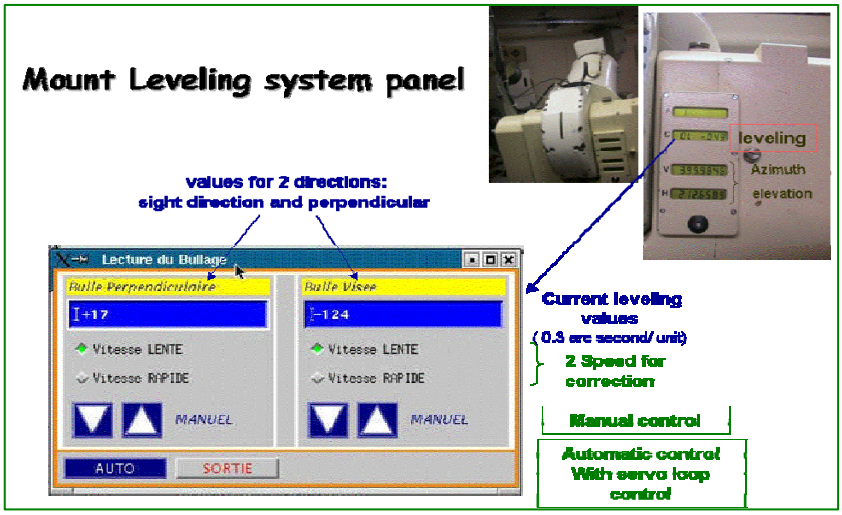

Conclusion

Fully automated mechanisms for the predictions and the new levelling system for FTLRS are major improvements, facilitating the observer's life and completing the remote controlled capability. FTLRS will very soon be operational in our new laboratory in Grasse, and all our staff is very excited to test these new tools and we look forward to our first returns there.

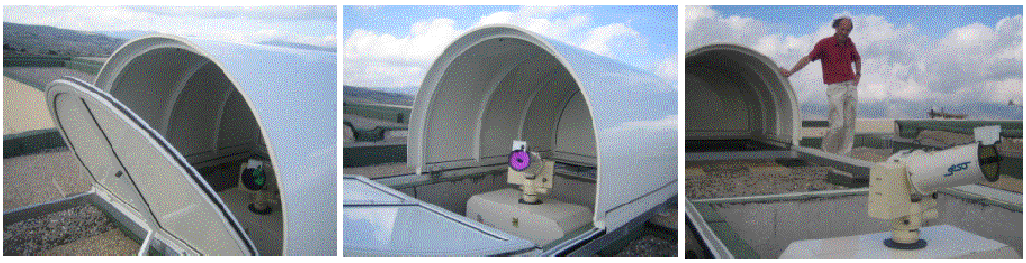

Recursive Filter Algorithm for Noise Reduction in SLR

Michael Hiener[1], Ulrich Schreiber[1], Nikolaus Brandl[2]

1. Forschungseinrichtung Satellitengeodäsie, Technical University of Munich, Fundamentalstation Wettzell, 93444 Bad Kötzting, Germany

2. Bundesamt für Kartographie und Geodäsie, Fundamentalstation Wettzell, 93444 Bad Kötzting, Germany

Contact: schreiber@fs.wettzell.de

Abstract

This report presents the concept and implementation of a recursive filter for the identification of satellite returns in laser ranging in the presence of strong noise. This project was aiming for an increased data yield of automatically filtered satellite laser ranging measurements in order to maximize the number of correctly identified returns. Furthermore the amount of false readings have to be reduced and an automatic timebias-adjustment during ranging was required.

Introduction

Automatic data screening of timer readouts in SLR is widely used by many laser ranging facilities of the ILRS. All of them depend on some type of histogram evaluation of short time slices of measurements throughout the ranging process. The approach uses the fact that return signals from a satellite bunch up at a specific location in the range gate window, while noise readouts caused by background light or intrinsic detector noise are far more spread out throughout the range gate. For satellite passes with reasonable or good signal to noise ratio this method is fully adequate. However, in particular for daylight passes of the GPS and GIOVE satellites, this method is often extracting much fewer returns than actually were recorded by the ranging facility. On top of that a non negligible number of false readings is usually upsetting the normal point generation process, because erratic data points prevent the fitting procedure from converging. Figure 1 shows an example of such a weak satellite pass. One can clearly see time intervals where a reasonable or good signal to noise ratio exists for the measurement. However there are also times where only sparse data is recorded. In order to extract the valid returns out of all the recorded data points in near real-time the control software examines small portions of the pass of a few seconds length. The data is then converted to a histogram and if a suitable bin contains a sufficient number of echoes, these are extracted and stored away as satellite returns. This evaluation process is fast and strictly linear in time. In the presence of very sparse data the threshold criterion is never satisfied and valid data is lost. If on the other side the threshold value is lowered too far, then randomly lumped together background noise events will accidentally be taken as good data and the post-processing can be disrupted.

By using more than one criterion at a time and introducing reprocessing of past data as well as a locally linearized look ahead strategy, one can vastly improve the robustness of the filter procedure. At the same time the data yield improves substantially in particular for passes with a low signal to noise ratio.

Function of the new filter algorithm

The new filter applies two distinctly different methods. A histogram-analysis is used to detect possible satellite returns in a reasonably short time interval. The results then are used to predict the likelihood of valid returns into the future, where it also

successfully recovers valid data-points at a low data rate. Both methods cooperate to not only detect, but also rate identified returns during the ranging activity.

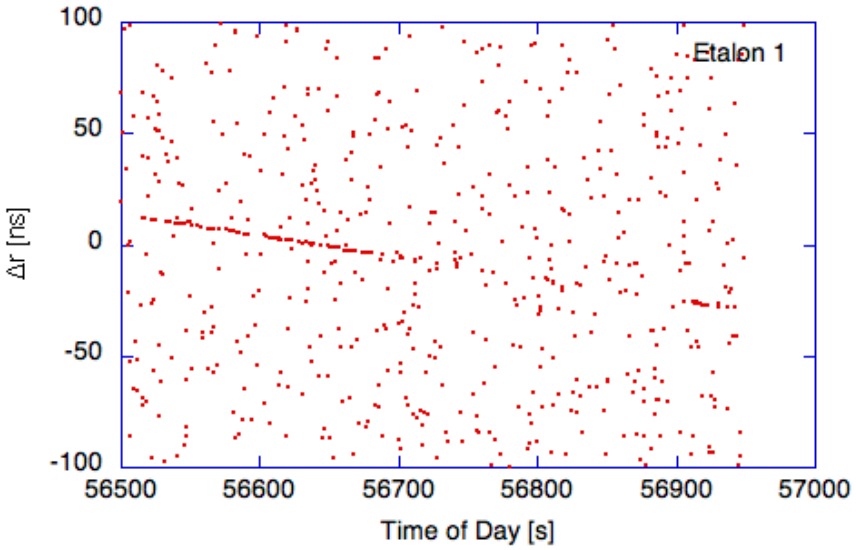

Figure 1: *Example for a measurement window of an ETALON pass with sparse data in daylight.*

From a number of verified satellite returns within a number of time slices, the actually applied time bias value for the momentarily observed satellite pass can be improved. With time bias corrected range residuals the histogram of the analysis process sharpens substantially. As a consequence the width of the rangegate can then be reduced automatically, which in turn enhances the data yield of the ranging operation. The program module works in several layers. The inner loop of the filter procedure is based on time slices of 5 seconds of observations (fig. 2). The length of the time slice is adjusted to the 10 Hz repetition rate and the background noise level typical for the Wettzell Laser Ranging System (WLRS). Other systems will have different settings. If already available a time bias correction is applied to all the data points in that time segment. Then the data is passed on to a histogram analysis routine, which has a bin width of 5 ns. This arbitrarily chosen value too has shown to work well for the WLRS operation parameters.

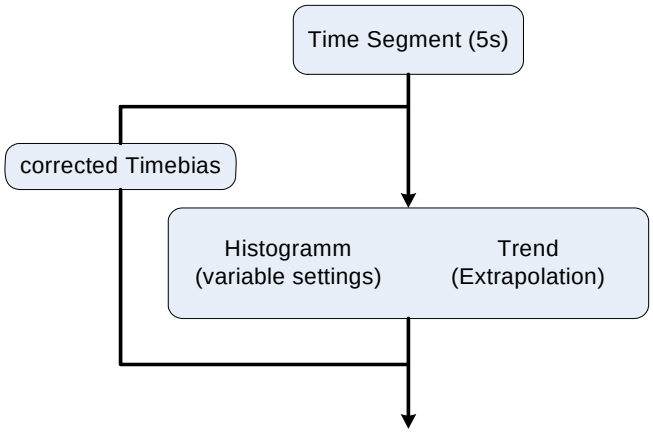

Figure 2: *Flowchart of the inner loop of the data-screening program.*

The threshold value for the histogram evaluation is currently set to 4 events per bin. In order to avoid ambiguities from unfavorable bin boundary settings (see fig. 3) in the histogram analysis, this evaluation is made twice with all the bins shifted to one side by half the bin-width.

When the threshold value of 4 events per bin is exceeded, all data points within that histogram bin are taken as possible returns. If the threshold value is exceeded by a factor of 2 the data within this bin is considered as reliably identified returns. Reliable returns are used twofold for the remainder of the satellite pass. They are used for an updated time bias computation, which feeds back to the next time slice and they are used in order to predict future locations within the range gate for the next few time slices. Figure 5 illustrates the prediction approach. Known trustworthy returns from the most recent past are linked with a straight line. The line is extended into the future and a corridor of ±2.5ns is set around this predicted line. Any single event that happens to fall within this corridor is considered a potential return and subjects it to further verification.

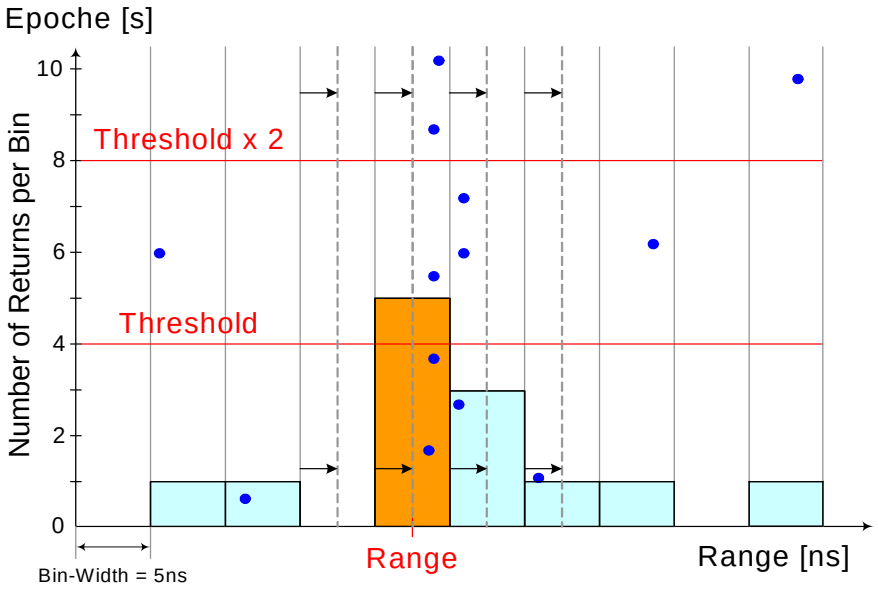

Figure 3: *A histogram of a 5 second long segment of a satellite pass of the WLRS. Unfavorable bin boundary settings are avoided by a re-evaluation with shifted bins.*

Therefore also extremely low return rates well short of the threshold value of 4 can be detected. The predicted linear corridor where future returns are expected expires after about 30 seconds when no further satellite echoes are recorded, because this simplified piecewise linearization of a satellite pass does not represent a valid approximation indefinitely.

Another important aspect of this new approach is a retrospective analysis, which identifies satellite returns that have been overlooked in the near real-time evaluation. A very sparse return rate may cause such lost returns as well as a number of false alarms. The retrospective analysis step revisits the last whole minute of observation. From the time slice analysis a number of returns are found. Some of them will be unambiguously identified as valid returns, while a certain number of returns are only classified as possible candidates. Again a linear regression through all unambiguously identified data points along with a corridor of ±2.5ns selects the part of the range gate where returns are most likely. Three cases may be found:

- All candidates (orange points in fig. 5) within these limits are now recognized as valid returns.
- All candidates outside this corridor are deleted from the list of possible returns.
- All not identified (white) data points inside the corridor are added to the list as possible candidates.

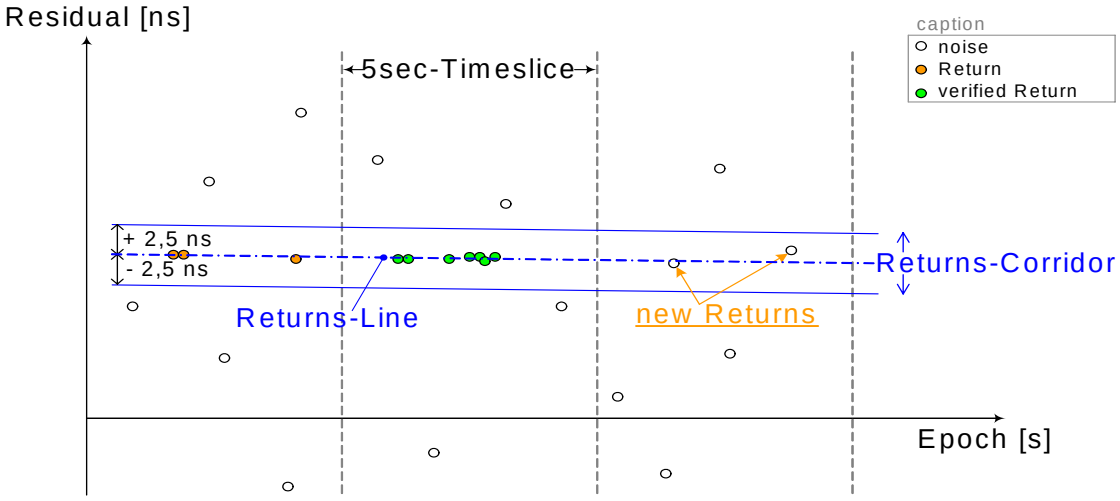

***Figure 4*:** *Reliably identified returns within a time slice of data are extrapolated into the future in order to find otherwise lost data points when the return rate is sparse.*

The linear approach for this screening procedure is justified because only very small segments of a complete pass are analyzed at a time. It has the advantage that this processing is fast and that it does not diverge quickly as polynomials tend to do in the presence of an inhomogeneous data distribution.

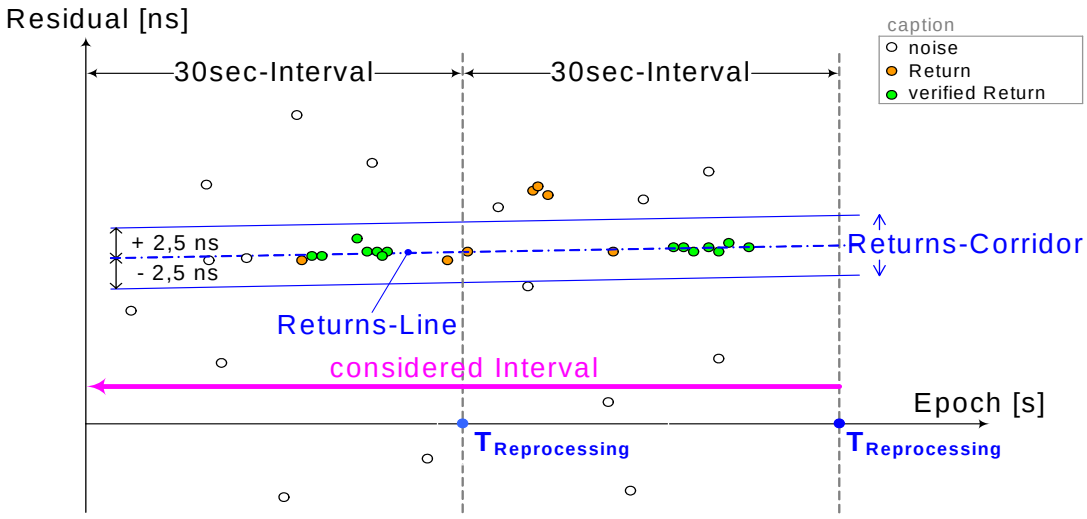

***Figure 5*:** *Reprocessing of the last 60 seconds of data. Reliably identified returns are used to define a return corridor. Potential returns outside this corridor are deleted from the list, while potential returns inside the corridor are turned into verified returns.*

Application Results

When this new data screening approach was integrated into the routine operation software of the WLRS, care was taken that rapid data processing was maintained throughout the ranging operation. We never encountered a situation where the ranging data came in faster than the various processing steps took to evaluate the data. We would expect that this would also apply for higher repetition rate systems, however with an appropriately adapted parameter setting.

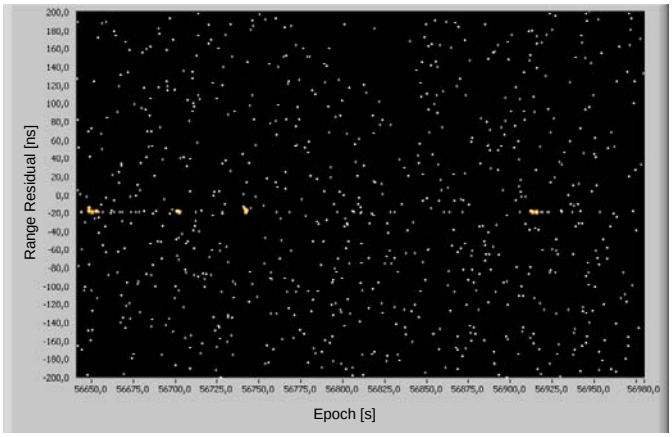

Figure 6*: A Section of an Etalon daylight pass with sparse data with returns identified with the previous screening program. Clearly many valid data points were lost in the past.*

Because of the repeated scanning of recent tracking data some adjustments to the data storage strategy had to be newly introduced. Essentially a larger data buffer is required as a temporal additional storage. As one might expect there is little to no advantage of this recursive screening filter over the simple histogram analysis when there are many satellite returns and almost no noise events. However for a weak signal to noise ratio approaching 1, rather dramatic improvements have been obtained. Figure 6 shows such an Etalon pass. Unfortunate boundary locations of the time slices often cause histograms to remain below the threshold limit. As a consequence a lot of data is lost. In this example only 12 returns were recovered out of the portion of data shown in the diagram.

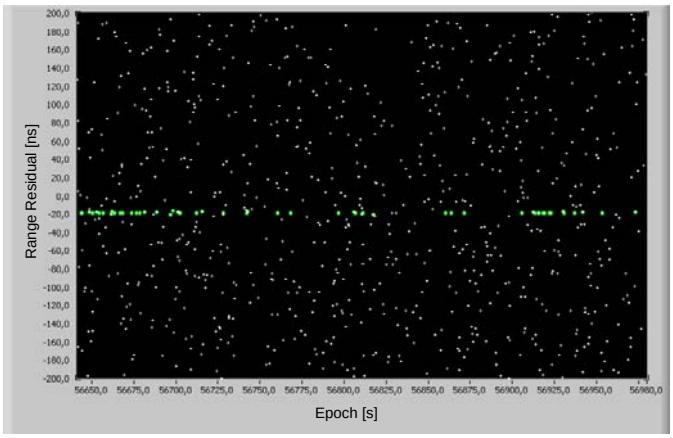

Figure 7: *The same section of the Etalon pass processed with the new screening programme.*

In contrast to fig. 6 the same dataset was re-analyzed with the new screening procedure extracting 50 returns instead of 12. The results are shown in fig. 7. Again this may still not catch all available returns. On the other hand it does not generate false readings either which is also an important aspect for this filter process. The WLRS ranging software was updated to this new filter scheme in December 2006. As far as we can see it improved the efficiency of the WLRS and reduced the number of passes that need manual user intervention for the normal point generation process noticeably.

References

[1] R. Jamal und Herbert Pichlik; LabVIEW Programmiersprache der 4. Generation; Prentice Hall, ISBN 3-8272-589-0, (1999)

[2] M. Chugani, A. Samant, M. Cerna; LabVIEW Signal Processing}; Prentice Hall PTR, ISBN 0-13-972449-4, (www.phptr.com), (1998)

The Impact and Resolution of "Collision Bands" on Tracking Targets at Various Ranges

C.J. Moore[1]

1. EOS Space Systems Pty. Limited, 111 Canberra Ave., Griffith, A.C.T. Australia.

Contact: cmoore@eos-aus.com

Abstract

Symmetric SLR and LLR systems that adopt a spinning disk as an optical switch between transmit and receive laser pulses need to address the problem of losing signal due to transmit and receive pulses being coincident at the disk when targets are at certain "collision band" ranges. These collision bands occur with increasing frequency at larger target ranges and can interrupt tracking of distant targets (> 6,000 km) for significant periods. A general solution to minimize the impact of collision bands based on disk frequency adjustment is presented. Depending on the design of the disk and system requirements, it is possible to eliminate the effect entirely or reduce the impact to a few narrow range bands by applying a relatively simple disk frequency control algorithm.

Introduction

Satellite Laser Ranging (SLR) stations that employ a symmetric (i.e. single telescope) system for their transmit and receive paths must adopt a multiplexing mechanism to allow measurement of the timing of the transmitted and received laser pulses. One popular mechanism involves the use of spinning mirrored disk containing one (or more) small holes that allow passage of the transmit pulse, while the mirrored surface is orientated such that return photons are reflected towards a receive detector. This mechanism has been adopted in recent years by EOS Space Systems for a number of their laser tracking system, including the Mt Stromlo SLR system.

One disadvantage of this mechanism is termed the "collision band" problem where a tracking signal is lost due to coincidence of a transmit hole and returning photons. The collision band thus refers to the band of target ranges that are effectively unmeasurable due to this coincidence. To increase the transmit power it can be advantageous to increase the number of transmit holes, which for a given disk rotation frequency, allows a greater laser fire rate. Unfortunately the greater the number of transmit holes, the greater the number of collision bands that may be experienced with potential loss of signal.

One technique used to minimize of collision bands relies on adjustment of the disk frequency and thus laser fire rate. For example, Titterton (1998) describes this technique to minimize backscatter. This paper describes an analysis of this collision band problem and proposes a technique for the automatic minimization of collision bands and number of disk frequency adjustments for a given range of disk configurations.

Theory

Collision Band Model

Spinning transmit/receive (T/R) disks often have one or two transmit holes, but in general there could be any number subject only to physical restrictions. Figure 1 shows a schematic of such a disk having two transmit holes. In general we can let; **N** = number of holes equally spaced around the disk, **r** = radius of the transmit hole, **R** = radius of 'projected' circle containing the transmit hole centre at fire time, and **f** = disk speed (Hz), giving the laser fire rate as **Nf**. Also let $\boldsymbol{\alpha}$ = angle subtended by each transmit hole such that $\boldsymbol{\alpha} = 2 \sin^{-1} (\mathbf{r}/\mathbf{R})$.

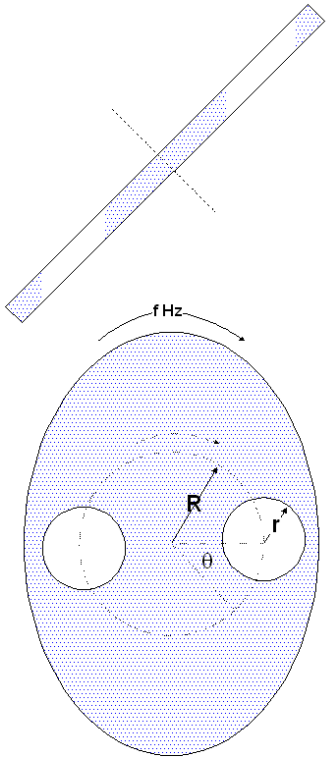

Figure 1: *Schematic of theSpinning T/R Disk*

s = available signal as a ratio, i.e. **s** = 1 when there is no loss and outgoing and incoming signals do not overlap, or **s** = 0 when complete overlap occurs.
d = distance of the target (along the optical path), and **c** = speed of light, such that the two-way time taken for a reflected pulse to leave and return to the disk is $\boldsymbol{\tau = 2d/c}$.
Let $\boldsymbol{\theta}$ = angular displacement on the 'projected' circle. Given the rotation speed of a point on this circle is $\boldsymbol{2\pi f}$, then the disk rotational movement, $\boldsymbol{\Delta\theta}$, in the time it takes for a laser pulse to leave and to return, $\boldsymbol{\Delta\theta = 2\pi f\tau}$, is limited to

$$\frac{2\pi\, i}{N} - s\alpha < \Delta\theta < \frac{2\pi\, i}{N} + s\alpha$$

Here **i** is an integer, equivalent to the number of shots in flight.

Assume that $\boldsymbol{\alpha}$ = 2**r**/**R** to a good approximation and define a geometrical factor, **F** = **sr**/**R**. This equation can be then be rewritten to give the condition for the existence of a collision band, i.e.,

$$\frac{i}{N} - \frac{F}{\pi} < f\tau < \frac{i}{N} + \frac{F}{\pi}$$

which can be expressed simply as,

$$\left| f\tau - \frac{i}{N} \right| < \frac{F}{\pi} \tag{1}$$

The number of pulses in flight, **i**, can be determined from $i = \lceil Nf\tau \rceil$, but it is wise to confirm the inequality using "floor" and "ceiling"values; i.e. $i = \lfloor Nf\tau \rfloor$ and $i = \lceil Nf\tau \rceil$.

Frequency Shifting

Equation (1) indicates that for a given range, **d**, and a given geometrical configuration there is only one parameter that can be adjusted such that the inequality no longer holds and that is the disk frequency, **f**. Hence it may be possible to adopt a scheme where the effect of collision bands can be reduced, or even eliminated, by frequency shifting the spinning disk.

From equation (1) it can be shown that to avoid a collision band at a given range, **d** (or equivalently, $\boldsymbol{\tau}$) then set **f** such that

$$\left| Nf\tau - \lceil Nf\tau \rceil \right| \geq \frac{NF}{\pi} \tag{2}$$

There may be additional system restrictions on the spinning disk frequency, the range of frequency adjustments that can be made and on the rate that adjustments can be made. The restrictions may be such that condition set by equation (2) cannot be met and the collision band cannot be avoided.

The next section describes an analysis of a typical two hole disk used in a laser tracking system and the scheme used to meet, as much as possible, the collision band avoidance condition given by equation (2).

Analysis of a Two Hole T/R Disk

Consider a two-hole disk having a geometrical factor F of 20%. For example, a disk where the transmit holes have a radius (projected at right angles to the laser beam) of 15 mm, at a radius from disk centre of 75 mm, or a disk with transmit holes of radius 12 mm at a distance of 60 mm from the disk centre will have F = 20% assuming no overlap of the return beam footprint on the transmit holes (s = 1.0). For this analysis assume that the maximum laser fire rate is 100Hz and the maximum frequency variation is ±5%. This is just one example of possible design constraints that might apply to systems using this technique. In this case, the value of **f** is limited to a range between 45 and 50 Hz

Table1: *Defined Range Bands*

Range Band	Sample Ranges (km)
Low Earth Orbit (LEO)	500 – 2000 km
Medium Earth Orbit (MEO)	2000 – 12000 km
High Earth Orbit (HEO)	19000 – 29000 km
Lunar	350000 – 400000 km

Table 1 summarises the four range intervals used in this analysis. These represent the typical distribution of earth orbit satellite and lunar targets. Equation (1) was applied to range values in each of these intervals to identify the collision bands occurring over the various ranges. The following sections describe the results from these calculations. In all cases the disk frequency resolution used was 0.05 Hz.

Impact of Tracking LEO Satellites

No collision bands are evident for low earth orbit ranges less than about 1,300 km as shown in figure 2. Unfortunately a collision band occurs for ranges from approximately 1450 km to 1700 km which cannot be avoided using the available disk frequency shift.

An assessment has to be made whether this collision band will cause significant impact on actual target tracking.

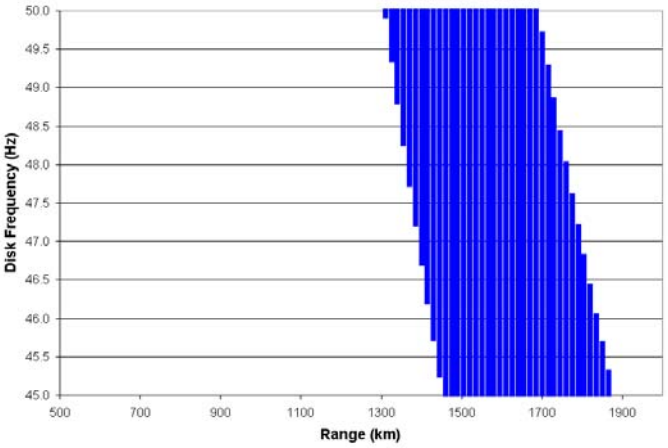

Figure 2*: Collision Bands at LEO Satellite Ranges*

Impact on Tracking MEO Satellites

For ranges between 2,000 and 12,000 km, the collision bands are grouped as shown in figure 3. There are also significant range intervals where there are no collision bands at all. However there is still one range interval where there is an unavoidable collision band, at about 3,000 to 3,200 km. Above this interval there are no ranges that have an unavoidable collision band, as illustrated in figures 3, 4 and 5.

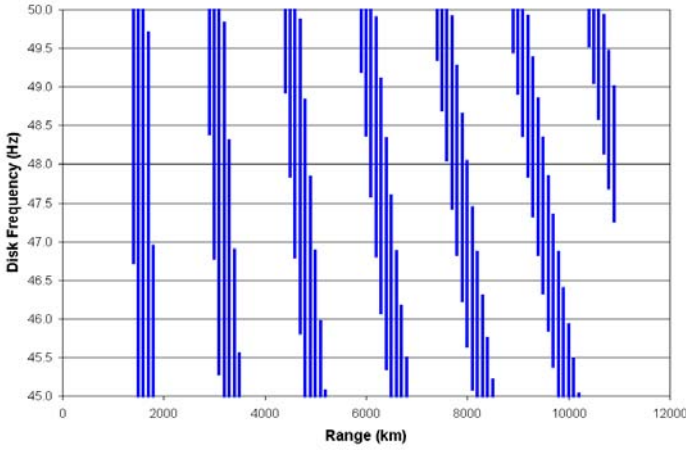

Figure 3*: Collision Bands at MEO Satellite Ranges*

Impact on Tracking HEO Satellites

As ranges increase, the number of collision bands within the disk frequency range increase and become shorter, as illustrated in figures 4 and 5, so the options for avoiding collision bands also increases. However, for any given disk frequency, the probability of a target pass having a number of collision bands also increases.

It is notable that even for one-hole disk systems, the probability that a high satellite pass contains one or more collision bands is quite high, and hence an avoidance scheme is still required.

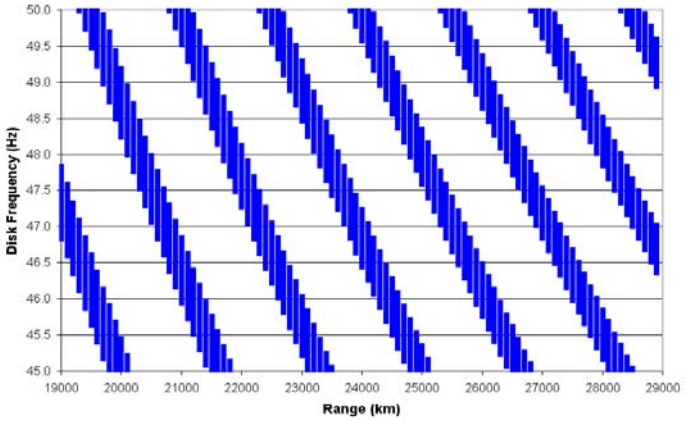

***Figure 4**: Collision Bands at HEO Satellite Ranges*

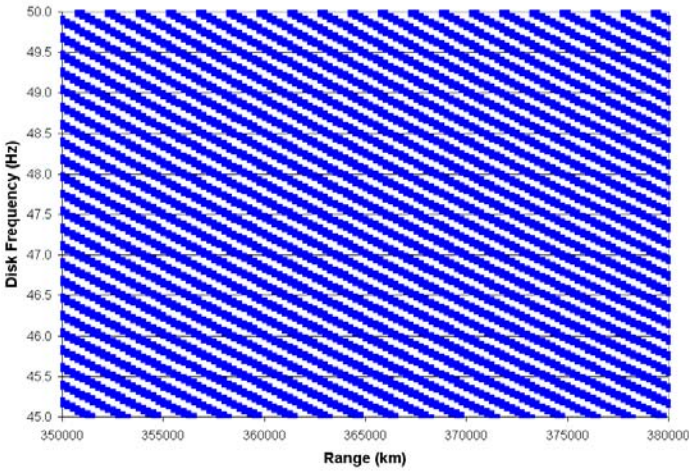

***Figure 5**: Collision Bands at Lunar Ranges*

Impact on Tracking Lunar Targets

At lunar target distances, collision bands are very frequent but very short both in terms of disk frequency and range changes as illustrated in figure 5. With slowly changing ranges, it is possible that a lunar target pass may either be largely free of collision bands or be largely in a collision band. Avoidance at these ranges will require small shifts in disk frequency. Table 2 shows a summary of typical impact of collision bands on tracking a number of ILRS SLR satellites and LLR targets.

***Table 2**: Impact of Collision Bands on ILRS Satellites*

Satellite Groups	Typical Ranges (km)	Impact, no avoidance	Impact with avoidance
GraceA & B, Champ	500 – 1500	None	None
Envisat, ERS2, GFO1, Stella, Starlette	800 – 2000	Lost data around 1500-1700 km (near end of passes)	Lost data around 1500-1700 km (near end of passes).
Ajisai, Jason	1400 – 2900	Lost data near zenith of high passes.	Lost data near zenith of high passes.
Lageos1,2	5900 – 9,000	Lost data in 1 or 2 bands.	None
GPS, Etalon, Giove A, Galileo	19,000 – 27,000	Lost data in 2 or 3 bands.	None
LLR targets	350000 – 420,000	Significant periods of lost data	None

Collision Band Avoidance

Frequency Shifting Algorithm

Using equation (1) it is straightforward to assess, given current range and disk frequency, whether a tracking system is experiencing a collision band. However it is less straightforward to determine what is the best disk frequency to use to avoid such a band. An algorithm was devised such that not only are collision bands avoided (if at all possible) but the number of

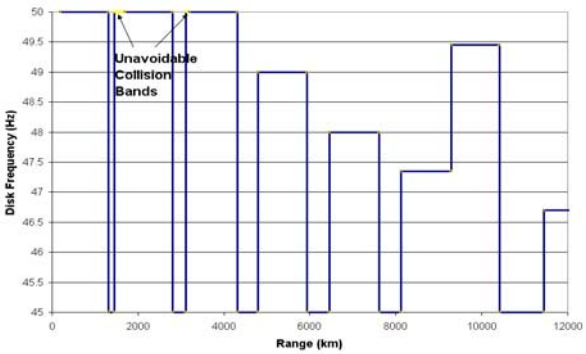

***Figure 6**: Disk Frequency over increasing LEO and MEO Satellite Ranges*

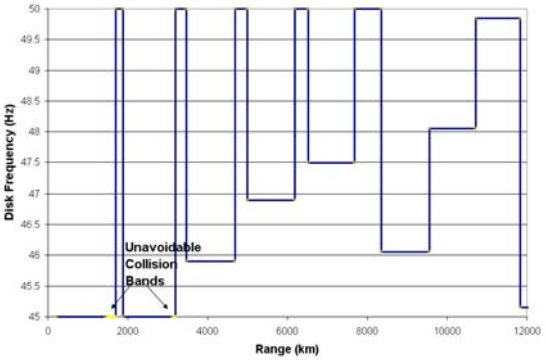

***Figure 7**: Disk Frequency over decreasing LEO and MEO Satellite Ranges*

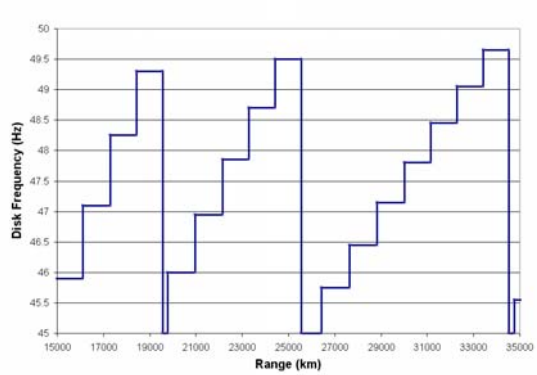

***Figure 8**: Disk Frequency over increasing HEO Satellite Ranges*

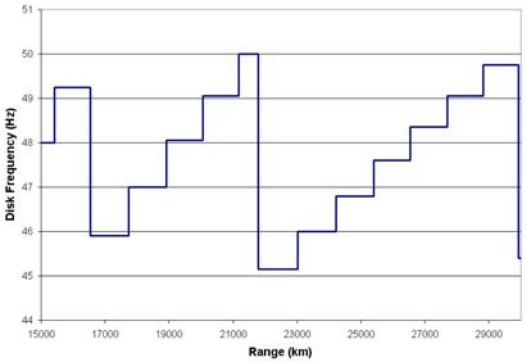

***Figure 9**: Disk Frequency over decreasing HEO Satellite Ranges*

frequency adjustments is minimized. This may be important if the time taken for the laser system to respond to frequency changes is significant.

The algorithm requires determining, for a given range, the disk frequency end points of a given collision band, at the moment that this collision band is first encountered. No action (i.e. frequency adjustment) is necessary when a collision band is not present. If a collision band is encountered when the range is increasing, increase the disk frequency by a small amount and check if the collision band is still present. This is repeated until maximum disk frequency is reached, at which point, the disk frequency is set to the minimum, and then adjusted upwards until no collision band is found or the cycle is completed and avoidance is not possible. A similar procedure is followed when the range is decreasing but in this case the disk frequency is reduced by a small amount.

The following diagrams illustrates the disk frequency changes (for the sample configuration) resulting from the application of this algorithm. Results from increasing and decreasing

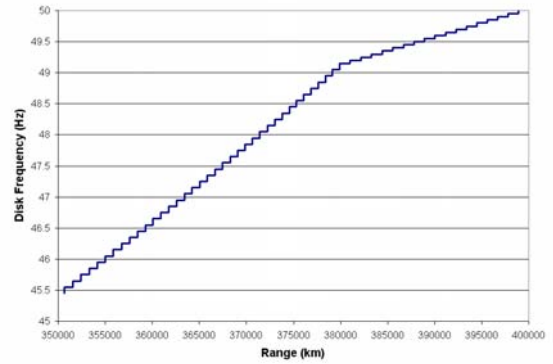

***Figure 10**: Disk Frequency over increasing Lunar Target Ranges*

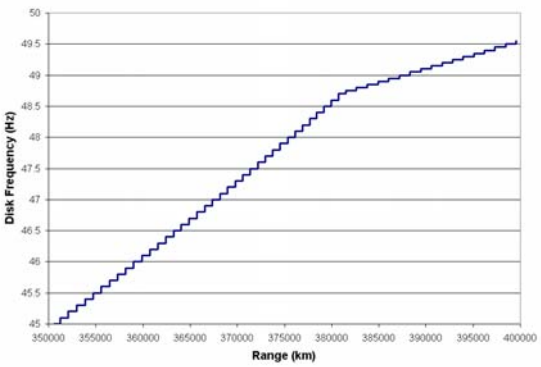

***Figure 11**: Disk Frequency over decreasing Lunar Target Ranges*

ranges are shown.

Low-Medium Earth Orbit Satellite Ranges

The frequency shift patterns for increasing and decreasing distances over the low and medium earth orbit satellite ranges are shown in the figures 6 and 7. Note there are two small ranges where collision bands are unavoidable by frequency shifting for the two hole configuration used.

High Earth Orbit Satellite Ranges

The frequency shift patterns for increasing and decreasing distances over the high earth orbit satellite ranges is shown in the figures 8 and 9. There are no unavoidable collision bands.

Lunar Target Ranges

The frequency shift patterns for increasing and decreasing distances over lunar target ranges is shown in figures 10 and 11. There are no unavoidable collision bands.

Disk Design

Given a geometrical design of the disk, the disk rotation frequency can be used to minimize collision bands as described in the previous section. However can the need for frequency shifting be ameliorated by appropriate disk geometry? The number of transmit holes and the

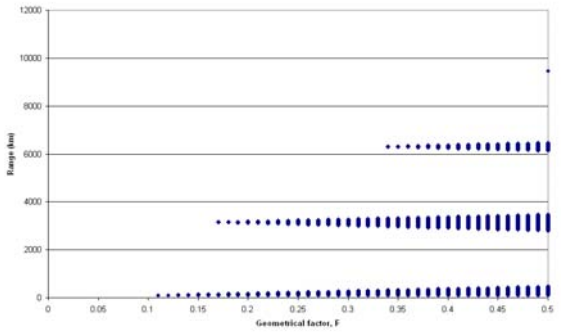

Figure 12: *Unavoidable bands for a 1 hole disk.*

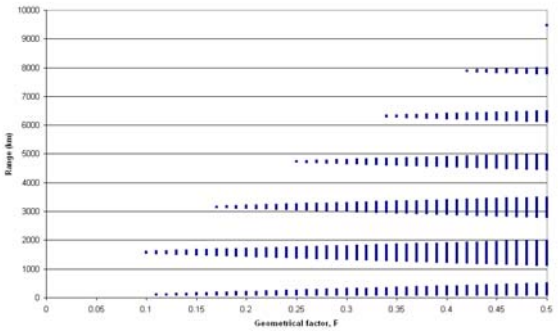

Figure 13: *Unavoidable bands for a 2 hole disk.*

geometrical factor, F, will influence the occurrence of collision bands and this is illustrated in Figure 12 for a 1 hole disk and Figure 13 for a 2 hole disk operating between 45 and 50Hz as in the previous examples. Similar diagrams can be generated for disks having three or more holes. These diagrams show the ***unavoidable*** collision bands at various ranges and various F-factors.

Clearly, more holes will result in a greater number and width of unavoidable bands over ranges up to 8,000 km. However, if the T/R disk and associated transmit hole can be designed such that $F < 0.1$ then the performance of disks with multiple holes (at least up to 3) is greatly improved. If the transmit hole radius had to be greater than, say, 10 mm, to accommodate the laser beam, then to obtain $F = 0.1$, the centre of the transmit hole would have to be greater than 100 mm from the centre of the T/R disk. Whether this is achievable would depend on other design criteria.

References:

[1] Titterton, P., "System/Usage Impact of Operating the SLR2000 at 2 Khz,". Proceedings of the 11th International Workshop on Laser Ranging, 1998, Deggendorf.

Web Application for the Engineering Data Files Processing

K.Salminsh

1. Institute of Astronomy, University of Latvia.

Contact: kalvis@lanet.lv /Fax: +371 7034582

Abstract

One of the problems of introducing new data formats and procedures is a high cost in terms of manpower and time to develop, modify and deploy necessary software across the SLR network. Web applications are a relatively new type of applications located on the server and accessible via the web browsers hence simplifying the software distribution and making any changes and improvements immediately accessible to all users. In this report the web application for the Engineering Data Files (EDF) processing and analysis is considered in more details. Review of the existing functionality and future development is presented.

Introduction

As was shown in [1] the preferable way to handle Engineering Data Files (EDF) processing and analysis is a web application to reduce overall implementation costs accross the ILRS network and to make software and its eventual future changes immediately accessible to the all users. For more detailed information on the EDF's, see [2]. Another advantage of the web applications is their accessibility to everyone with an internet connection and web browser (security restrictions may apply).

EDF Processing Application

Overview of the current implementation of the EDF processing workflow is presented in [2]. Incoming EDF from stations are uploaded via FTP and after preprocessing are moved to the directories for anonymous ftp access and also are inserted in the relational database. Data then can be accessed and processed over the Internet using the dedicated web application. Web application basic functionality, based on the goals stated in [1], can be summarized as following:

- Overview of the used equipment
- Calibration time series and analysis
- Calibration charts
- External interfaces: data export to Excel, web feeds (e.g. RSS)

The use of the application is straightforward. The equipment overview function (Figure 2) allows users to retrieve data about the equipment used in a given period of time for all stations, and to use it as a selection criteria for the calibration time series and to calculate statistics for one or more stations. The selected data can then be compared, plotted or exported to an Excel spreadsheet and downloaded to the user computer. Tabular data view for the Excel export is presented in the Figure 3. Live calibration data can be also published from the database as an RSS feed directly usable in other applications or web sites.

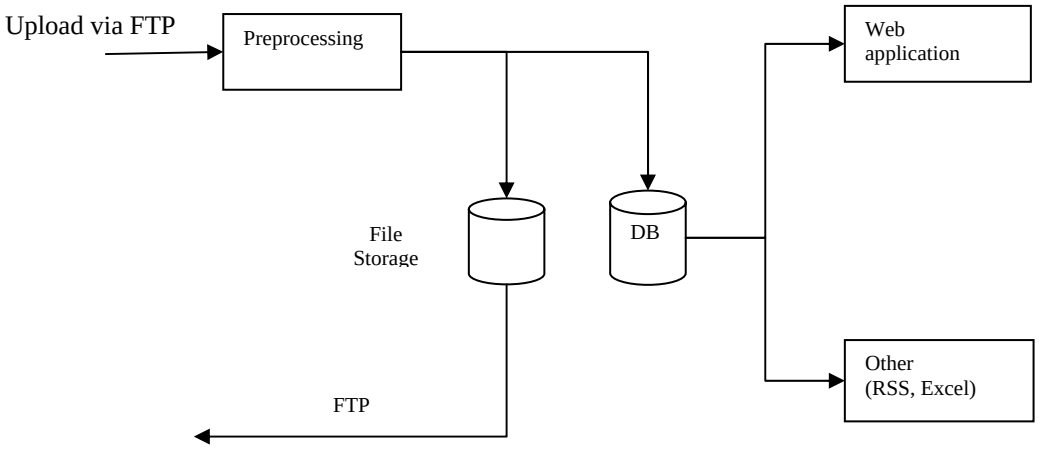

***Figure 1**: EDF processing flow*

Implementation details and future extensions

The EDF processing web application is now deployed on the server at the Institute of Astronomy, Institute of Latvia, and access information will be published on the EDF website [2]. The application is running on a Windows 2003 server and using a Firebird 1.5 relational database for the data storage. The most challenging part of the application is calibration data selection based on the used hardware and data model in the database. This is because it involves optional and station specific data within EDF XML documents and it leads directly to tree data structures which don't map well into the relational database structure. The current solution is to make directly accessible within the database only required parameters from the EDF specification, and to limit the number of parameters available for the data selection. The list of key parameters currently made available for data search and selection are:

- Station
- Calibration epoch
- Detector type
- Timer type
- Laser

Another limitation of the current design and data model is that the station custom data recorded within EDF can be used only as a reference and should be retrieved from the original EDF and stored in the database table as an entity, separately. Hence one of possible future extensions may include migration to the XML database to remove these limitations. Other eventual improvements are related to the user interface and application functionality including improvements in the data model.

Conclusions

One of the main problems in designing the EDF processing application is the absence of a common naming standard for the SLR station basic hardware elements and their parameters which can have an adverse impact on obtaining ranging results. Very likely similar problems will be encountered by others trying to record, process and analyze SLR data.

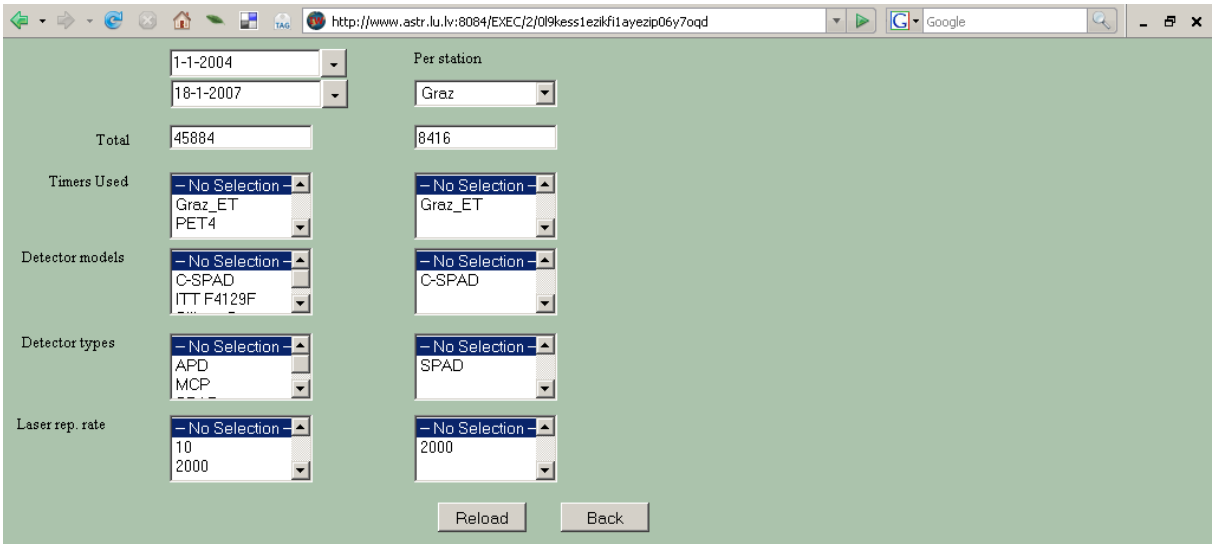

Figure 2: *Hardware overview and selection*

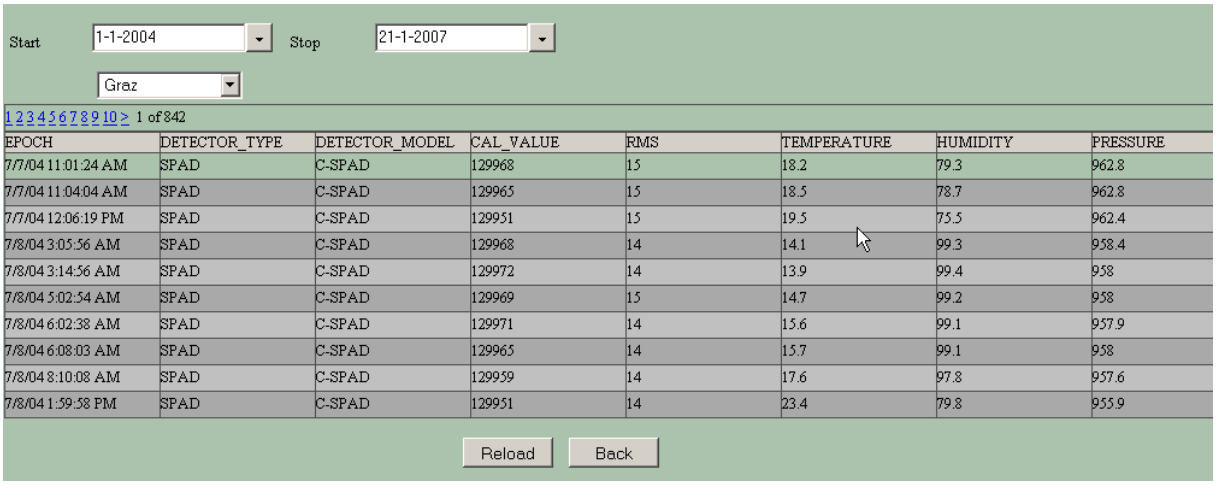

Figure 3*: Calibration time series – table view*

References

[1] Salminsh K. “Engineering Data File Processing and Distribution”, p.377, 14th International Laser Ranging Proceedings, San Fernando 2004.

[2] Website: http://www.astr.lu.lv/EDF

Consolidated Laser Prediction and Data Formats: Supporting New Technology

R. Ricklefs[1]

1. Center for Space Research,The University of Texas at Austin.

Contact: ricklefs@csr.utexas.edu for the ILRS Prediction Format Study Group and the Data Formats and Procedures Working Group

Abstract

The new tabular ILRS Consolidated Prediction Format (CPF) was developed to provide a single format to encompass traditional artificial satellite and lunar ranging targets as well as proposed transponder targets on or around the moon and other planets. As implementation of this format nears completion, the need to effectively handle kilohertz firing rates and transponder data in a new data format has emerged. The proposed Consolidated Laser Ranging Data Format (CRD) carries with it the lessons learned from the CPF: modularity, flexibility, and expandability.

Introduction

At the International Laser Ranging Service (ILRS) Workshop in Matera, Italy in 2000, it was decided that a new prediction format was needed to encompass the existing satellite and lunar ranging targets as well as the often-discussed transponders. In addition, there was a need to improve the predictions for low earth satellites. Thus the consolidated prediction format (CPF) was developed as a single format for all laser ranging targets, present and future. As the process of implementing the CPF is winding down, technological changes, in particular kilohertz repetition rate lasers and the Lunar Reconnaissance Orbiter (LRO) transponder are demanding that the current laser data formats be similarly reformulated. The process of creating the Consolidated Laser Ranging Data Format (CRD) is moving forward to meet LRO mission deadlines.

Consolidated Prediction Format

As described in early documents (Ricklefs, 2004, 2006), the CPF provides a method of ranging to different types of targets using one format. It therefore allows cross-technique ranging attempts, provided that a ranging station has needed hardware capabilities – such as event timers for lunar ranging.

The CPF does not rely on the on-site gravity model, tuning, separate Earth Orientation series, or drag and time bias functions that were required for the older tuned inter-range-vector (TIV) system. Instead, the new format contains untuned state vectors at appropriate intervals, typically in the ITRF system. This so-called format change is actually a change to the entire prediction scheme at the laser station from one of integration to one of interpolation.

Consolidated Prediction Format: Implementation Status

Currently (as of late October, 2006), the CPF is used exclusively in at least 22 out of the 37 ILRS Satellite Laser Ranging (SLR) stations, with one station in late stages of testing and 5 others close behind. Many of the remaining stations are not currently operational. It is expected that all operational stations will be converted by early 2007. In addition, the format is used at the one currently operating Lunar Laser Ranging (LLR) station (McDonald Laser Ranging Station), with other stations experimenting

with the format. The author is also working with the LRO project to generate CPF files. This effort may result in some additional transponder-specific changes to the format.

The results from using the CPF seem to be quite promising. According to one station (Gibbs, 2006), SLR predictions are seen to be much more accurate, with 90% of passes being within +-20nsec and 99% being within +-100nsec of the predicted range.

Consolidated Laser Ranging Data Format: Motivation

The first concern with the existing data formats (ILRS, 1999, 2004) is that transponder data will not fit. Specifically, transponders will often need to deal with one-way ranges. For instance, LRO data will consist of a fire time on the ground and receive time at the satellite. This being the case, there is a need for more accuracy in the fire and receive times, as the difference between the two must accommodate the accuracy expected from a range, usually at the picosecond level. This highlights the third issue, that of clock information. The current time standards, such as GPS are accurate only to about 100ns. Thus, there must be a way of describing the time standard used to record the data – on both the ground station and spacecraft. This is accomplished with a time system flag, a time offset, and a drift rate for both. Calibration is yet another area needing expansion. In the same way that there are laser station system delays, there are similar system delays on the spacecraft that must be accounted for.

In addition to the demand to reshape the data formats for transponders, stations with kilohertz laser firing rates are becoming more common and must be accommodated. Among the advantages, kilohertz laser ranging offers the possibility to study a satellite's signature in more detail than ever before, providing details of the spacecraft rotation rate and corner cube performance (Arnold, et. al., 2004). The existing fullrate data format is cumbersome for use with high-repetition-rate systems, because there is so much redundant information found in each data record. Estimates for the draft version of the format show that fullrate file size should drop by 55-65% at 500 returns/sec and 25-30% at <10 returns/sec.

Consolidated Laser Ranging Data Format: Overview

The intent of the new format is to encompass full rate, sampled engineering, and normal point data in one flexible, ASCII data format. The structure will be similar to that for the Consolidate Prediction Format in that there are several types of header and data records, assembled in a building-block approach, with records capable of specifying data for a particular data type or spacecraft configuration. This makes the format extensible and flexible. An additional section, for system configuration information, is being considered. A configuration section would make the data more self-documenting with more detailed data being available to the analyst. As with the CPF, header records are fixed format, but data (and configuration) records are free format, allowing field sizes to be optimized for each satellite.

Sampled engineering, fullrate, and normal point data could be placed in one file or broken into 3 files. Multiple color data could be included in one file, as could data from one or more satellites or stations. Simple utility programs could facilitate the merging or parsing of files. The hope is to make the format XML-friendly so that the data files could be easily parsed and written into XML files, and an XML representation of the data could easily be written in the CRD format.

In the case of transponders, much of the data required to write the complete CRD file is not available at the ranging stations in real time. The data that is recorded can be transmitted to the mission data center where all the data is collated, quality controlled, and finally submitted to the ILRS data center. Normally, one would expect that the stations would create and submit partially populated CRD files which the mission data center would complete.

Timetable

The LRO mission has become a driver for creation and implementation of the new data format, since its schedule is so tight, with launch in late 2008. At some point a version of the format will need to be frozen for this mission, even if the format is not ready for network-wide implementation. (Fortunately, on-station data for LRO will be written into a compact intermediate format, so 2 versions of the CRD will not be implemented at participating stations.) The version presented here, version 0.09 will probably be used for LRO.

In the near future, the preliminary format will be made available on the ILRS web site. The general community will be invited to submit comments.When the format is finalized, its implementation will take place over a period of a year or so, with stations in most need of the new features implementing it first. These include kilohertz stations, transponders-ranging stations, and lunar stations. The lunar ranging on-station raw format has always contained data not transmitted through the ILRS formats.

There has been some concern on the part of analysts that they would find it disruptive to deal with more than one data format at a time. For this reason, the data centers will translate normal point data received in the new format into the current ILRS format until all stations are using the new format. At some time, historical data, especially normal points, will need to be translated into the new format. This may have to be phased in over a number of years, once the format has been implemented and as resources become available. This topic needs to be discussed in more depth.

Summary

The successful implementation of the new prediction format is drawing to a conclusion at the same time that new technology such as kilohertz ranging and the LRO transponder are demanding that the laser data formats be rewritten. The new data format (CRD) will encompass fullrate, sampled engineering, and normal point data for SLR, LLR, and TLR. As with the CPF, the CRD format will use a building-block approach to permit modularity, expandability and extensibility.

References

[1] Arnold, D., G. Kirchner, and F. Koidl: “Identifying Single Retro Tracks with a 2kHz SLR System – Simulations and Actual Results”, Proceeding of the Fourteenth International Workshop on Laser Ranging, San Fernando, 2004.

[2] Gibbs, P.: Private communications, 2006.

[3] ILRS: “ILRS Fullrate Format Version 3”, http://ilrs.gsfc.nasa.gov/products_formats_procedures/fullrate/fr_format_v3.html, 1999.

[4] ILRS: “ILRS Normal Point Format, Revision 2”, http://ilrs.gsfc.nasa.gov/products_formats_procedures/normal_point/np_format.html, 2004.

[5] Ricklefs, R.: “Consolidated Laser Ranging Prediction Format: Field Tests”, Proceeding of the Fourteenth International Workshop on Laser Ranging, San Fernando, Spain, 2004.

[6] Ricklefs, R.: “Consolidated Laser Ranging Prediction Format”, http://ilrs.gsfc.nasa.gov/products_formats_procedures/predictions/cpf.html. 2006.

Appendix A: New CRD Format Examples

The following data examples are based on the preliminary 0.09 version of the format and are included for demonstration purposes only. Changes being made to the format document will render these examples obsolete.

1. Headers

1.1 Basic header 1

H1 CRD 1 MLRS   2006 9 27 17 0 ENVISAT   test file

Note station and satellite names.

1.2 Basic Header 2

H2   200901 6179   27386 2003 11 11 5 31 24 2003 11 11 5 32 2 52954 7080 24 19 1 0 6 7 2 0

Note the begin and end times and modified julian date of first data record as well as numerical station and satellite IDs.

1.3 Laser color record

H4 1 532.0

One such record is included for each laser color recorded in the file.

1.4 Pass Information

H5 1   -650   0   82   82

This record contains statistical information on the data and calibrations. The final format is likely to include the often-requested skew and kurtosis of the data in addition to the RMS.

1.4 End of Header

H9

Additional headers for transponders and full rate information are not shown here. Headers are fixed format

2. Data records

2.1 Range Record

10 1 2   19880.8466929 1 2   0.010936014472   0

The first long field is the transmit time, and the second long field is either range or receive time at the spacecraft. In the case of a down-link transponder, the first log field would be the transmit time at the satellite, and the second would be the receive time at the ground station. Interpretation of these fields is controlled by flags fields.

2.2 Meteorological record

20   19880.8466929 802.50 288.10   69

This record is written at the beginning of the file and thereafter only when one of the fields change “significantly”. This could be defined as twice the least significant bit of the sensor or an amount based on the field, such as 0.02mB for atmospheric pressure.

2.3 Point angles

30   19880.8466929 1 281.1890 22.4030

Point angles would be written for sampled engineering and fullrate data. After the beginning of the data, additional record are written only when a field changes “significantly.”

2.4 Corrections

40   19880.8466929 1 2   0   0   -650   0

This record includes refraction, center of mass, and system delays. Additional records are written only when a field changes “significantly.”

2.5 Range (with normal point fields)

10 2 2   19884.7472085 1 2   0.010985288919   0   15   37   73   0.0

Note that data records are written in free format.

LUNAR LASER RANGING SESSION SUMMARY

Chair: Tom Murphy

The Lunar Laser Ranging (LLR) session consisted of a single presentation by T. Murphy about the new APOLLO LLR station. Despite this, he McDonald Laser Ranging Station (MLRS) is still actively engaged in LLR. The LLR station at the Grasse is undergoing a major renovation, which was reported by J. Torre in the *Telescopes, Stations, and Upgrades* session. LLR efforts continue at Matera and Mt. Stromlo, Matera having had some success in the past. There is interest in developing a new lunar-capable station in South Africa, though not presented at this conference. A campaign to perform one-way laser ranging to the Lunar Reconnaissance Orbiter (LRO) was discussed by M. Torrence and J. McGarry in the *Transponders* session.

The talk by Murphy, *APOLLO Springs to Life: One-millimeter LLR*, described the progress of the new LLR station at Apache Point in New Mexico. The station began lunar ranging operation in October 2005, attaining science-quality data beginning April 2006. APOLLO routinely achieves a large-enough photon count to achieve one-millimeter statistics. Peak rates approach one photon per pulse at 20 Hz, with ten-minute normal points sometimes consisting of several thousand photons. The 4×4 avalanche photodiode array and 16-channel timing system permits multi-photon returns, the strongest of which to date is 9 photons in a single pulse. Murphy also described the gravitational physics goals of APOLLO, revealing that LLR has already placed 0.1% limits on gravitomagnetism—the phenomenon behind Lense-Thirring precession.

APOLLO SPRINGS TO LIFE: ONE-MILLIMETER LUNAR LASER RANGING

T. W. Murphy, Jr. [1], E. G. Adelberger[2], J. B. Battat[3], C. D. Hoyle[4], E. L. Michelsen[1], C. W. Stubbs[3], and H. E. Swanson[2]

1. UC San Diego, MC-0424, 9500 Gilman Drive, La Jolla, CA 92093-0424, USA;
2. University of Washington, MC-351560, Seattle, WA 98195-1560, USA;
3. Harvard University, Dept. of Physics, 17 Oxford Street, Cambridge, MA 02138, USA;
4. Humboldt State University, Dept. of Physics, Arcata, CA 95521, USA;

Abstract

The Apache Point Observatory Lunar Laser-ranging Operation (APOLLO) obtained its first lunar ranges in October of 2005, achieving over 2000 photons in a 30-minute period. Subsequent operations have seen as many as 2500 photons in less than ten minutes, with a peak photon rate of 0.6 photons per pulse, or 12 per second. The major elements of the system are described, with performance examples and a look at the data precision.

Introduction

Lunar Laser Ranging (LLR) has long provided many of the best tests of gravity, currently claiming the best limits on:

- the weak equivalence principle, to $\Delta a/a < 1.4\times10^{-13}$;
- the strong equivalence principle to $\eta < 4.5\times10^{-4}$;
- time-rate-of-change of the gravitational constant, G, to $< 10^{-12}$ (fractionally) per year;
- gravitomagnetism to < 0.1%;
- geodetic precession to < 0.7%;
- inverse square law to 10^{-10} times the strength of gravity at $\approx 10^{8}$ m scales.

Many of these latest results are presented by Williams et al., (2004) [1]. The gravitomagnetic effect produces six-meter deformations in the lunar orbit at two different frequencies [2], each determined by LLR to sub-centimeter accuracy. Though the phenomenologies of gyroscopic precession (frame dragging) outside a rotating body, orbital (Lense-Thirring) precession of the LAGEOS satellites, and orbital distortions of the lunar orbit may appear to represent distinctly different physics, they all stem from the same term in the equation of motion. This is analogous to the seemingly different rotation of a draining tub and trajectory deflection due to the Coriolis force, though both stem from the same root physical cause.

The APOLLO Apparatus

The APOLLO apparatus is situated at the Apache Point Observatory in southern New Mexico, at 2780 m elevation. The laser is permanently affixed to the 3.5 m telescope, so that a rotation of the telescope tertiary mirror allows efficient sharing with other astronomical programs. The median atmospheric seeing at the site is 1.1 arcseconds (at zenith). The telescope is flexibly scheduled, so that APOLLO is able to get 1.5-hour time slots every few days during the accessible part of the lunar month.

Laser

APOLLO's laser is a Leopard SS-20 model from Continuum Lasers. It is a flashlamp-

pumped Nd:YAG system delivering 120 ps infrared pulses via acoustic mode-locking and cavity dumping, operating at 20 Hz. The infrared is frequency-doubled to 532 nm, delivering about 100 mJ per pulse at a pulse-width < 100 ps.

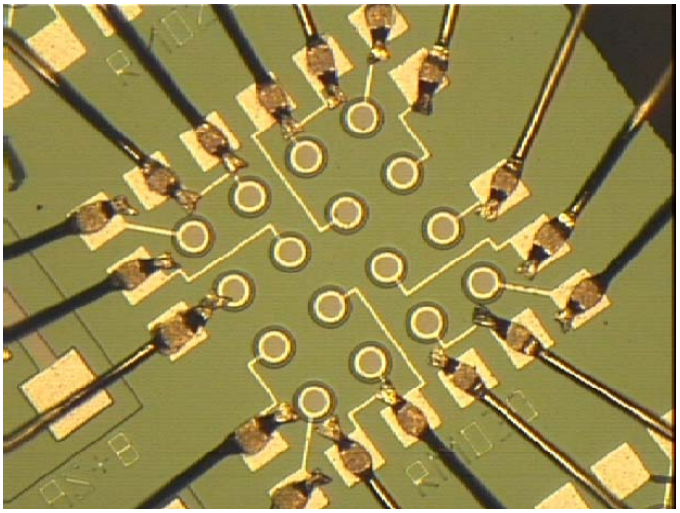

***Figure 1**: 4×4 APD array with 30 μm elements on a 100 μm square grid.*

APD Array Detector

APOLLO uses a 4×4 format avalanche photodiode (APD) array at the re-imaged focal plane (Figure 1). In this way, multiple return photons can be accommodated in a given pulse, each generating a timing signal that is separately time-stamped. A lenslet array placed in front of the detector recovers the fill-factor loss of the bare array. Besides providing multiple "buckets" for the multi-photon return, the resulting 1.4 arcsecond field of view (0.35 arcsec per pixel) yields spatial information about where the telescope is pointing, so that we may maintain tracking lock based on the spatial distribution of the lunar return.

Optical Layout

Figure 2 shows the APOLLO optical layout. Starting at the laser output, the green pulse emerges as a ~7 mm diameter ($1/e^2$) beam with an approximately Gaussian profile, centered 61 mm off of the optical bench. A beam expander (TL1 and TL2) expand the beam to 16 mm diameter prior to the rotating transmit/receive (T/R) optic. Following the T/R optic, the beam encounters a plano-concave lens (L3) that introduces a roughly *f*/10 divergence to the beam so that it may fill the telescope aperture. After L3, the beam experiences two 90° turns on M5 and M4—both of which are multi-layer dielectric coatings for high-efficiency reflection at 532 nm. After this are the telescope's aluminum-coated tertiary, secondary, and primary mirrors (M3, M2, M1). The beam emerges from the primary mirror collimated to well below 0.5 arcsec.

Incoming light from the telescope is brought toward a focus, following the inverse path of the transmit beam, becoming collimated at L3. From here, the path through the T/R optic experiences two 90° turns on M6 and M7, in the process being elevated to ~115 mm off of the optical bench so that it may cross the transmit path. M7 is tip-tilt actuated so that the receiver may be aligned relative to the transmit beam direction. The collimated beam enters the receiver tube via an uncoated glass window, tilted to send the reflected light toward a CCD camera that aids acquisition and alignment. The clear aperture up to this window is maintained to be at least 35 mm so

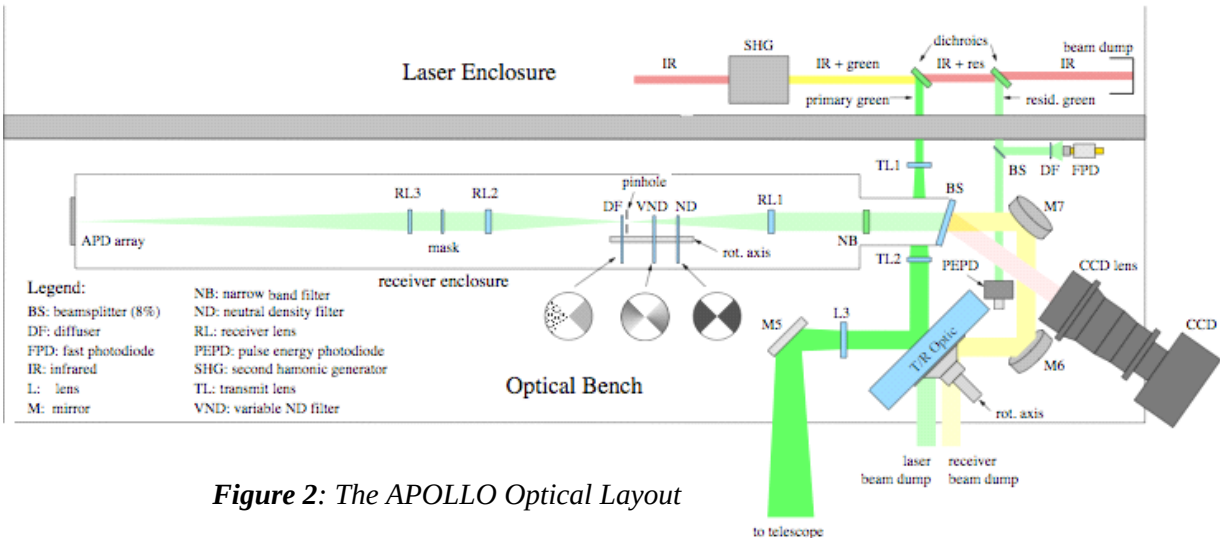

***Figure 2**: The APOLLO Optical Layout*

that a 40 arcsec field of view is preserved for the CCD camera. Past this window, the optics are 25 mm in diameter, which is suitable for the small field of the APD detector array.

A narrow passband filter sits at the front of the receiver tube, with a 1.5 nm FWHM passband centered at 532 nm, and 35% transmission at the center wavelength. Beyond this, a doublet lens (RL1) concentrates the collimated beam to a focus, where a pinhole is placed to act as a spatial filter. The 400 µm hole corresponds to 3 arcsec on the sky. An identical lens (RL2) is placed opposite the pinhole, re-forming the collimated beam. An optional mask in the collimated beam prohibits light originating outside the telescope aperture to proceed. A final lens (RL3) focuses the light onto the detector at the end of the receiver tube. The receiver tube is closely baffled at 50 mm intervals along its entire length so that scattered light from the laser fire is unlikely to survive a trip to the photon-sensitive detector.

Differential Measurement Scheme

APOLLO, like many laser ranging systems, implements a differential timing scheme, referencing its photon arrival times against returns from a local corner cube. This **fiducial** signal (note: often called “calibration” in the SLR community) follows *exactly* the same optical path as the lunar return photons, and is processed by the same timing electronics in the same configuration. The only difference is that optical coatings on the T/R mirror and on the disks near the spatial filter pinhole rotate into

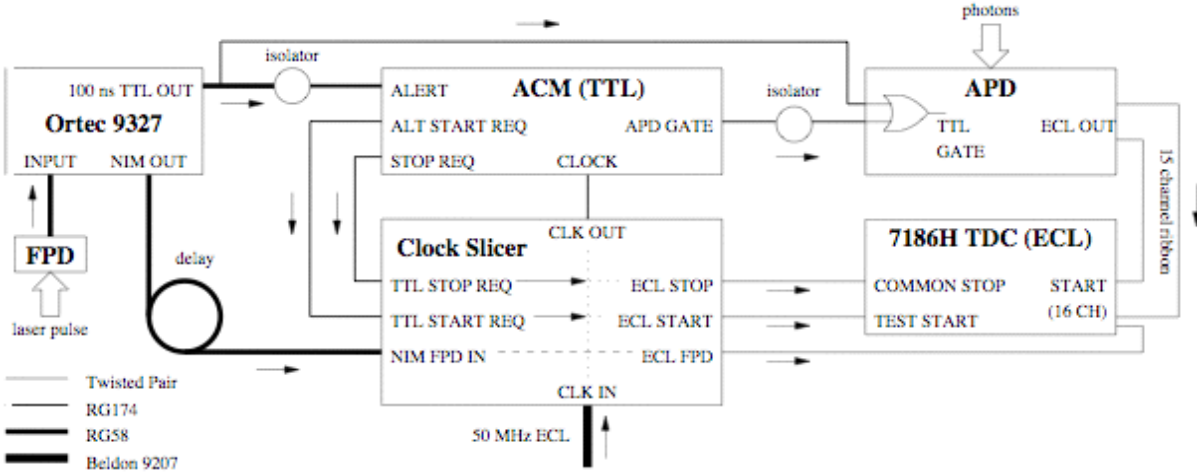

***Figure 3**: The APOLLO Timing System*

the beam to provide an attenuation of ~10^{10}, adjustable over about one order-of-magnitude. The result is a signal level of approximately one photon per pulse (distributed among the APD elements). The disks in the receiver rotate at half the rate of the T/R optic (which itself triggers laser fire events), one side diffusing the fiducial photons to have a roughly uniform distribution within each pupil-imaging APD element. The other side has matching attenuation, but allows the fiducial to be concentrated on each APD element in accordance with the corner cube's spatial location within the telescope entrance aperture. In this way, we can explore the timing bias associated with illumination position within the APD element. See [3] for details on this scheme.

Timing Scheme

The multiplexed timing system for APOLLO is capable of ~20 ps timing on 16 independent channels (common STOP) at rates as high as 4 kHz. The timing system is comprised of:

- a 16-channel time-to-digital converter (TDC): Phillips Scientific model 7186H;
- a Truetime XL-DC GPS-disciplined clock with low phase noise 10 MHz output;
- a 5× clock multiplier producing a 50 MHz ECL clock, preserving low phase noise;
- a custom "clock slicer" module that extracts selected clock pulses out of the train;
- a custom CAMAC module that coordinates gate events and requests clock pulses;
- an Ortec 9327 amplifier/discriminator establishing laser fire time to high precision.

The timing system is depicted in Figure 3. A secondary feature of our setup is the ability to calibrate the TDC by sending pulse pairs based on the 50 MHz clock to the TDC. In this way, we get START/STOP pulse pairs that are integral numbers of 20.00 ns apart. Even so, by arranging the lunar and fiducial photons to use the same 20 ns part of the TDC range (we have control of gate placement up to the clock period), we make the need for this calibration secondary. Running the calibration at 1 kHz at five pulse-pair separations yields 1000 measurements per setting in a five second period.

Example Data Runs

We present here example data from recent APOLLO runs to illustrate the system performance and capabilities.

Figure 4 shows the result of a 10,000 shot (500 second) run on Apollo 15—an array of 300 3.8-cm-diameter corner cubes. The first half of the run was spent optimizing pointing and beam offset. More than three quarters of the return photons fell within the last half of the run, producing an average rate of 0.33 photons per shot.

Figure 5 shows a 10,000-shot run on Apollo 11 (100 3.8 cm corner cubes) that followed the Apollo 15 run shown in Figure 4. Having optimized the signal in the previous run, the signal rate is steady in the Apollo 11 run. The 0.11 photon-per-pulse average return rate is consistent with the 0.33 result from Apollo 15, given the difference in array sizes.

The APOLLO error budget is dominated by the temporal spread arising from the libration-tilted finite-sized corner-cube arrays. Typically contributing about 20–50 mm root-mean-square (RMS) spread (less for the smaller arrays), we need approximately 400–2500 photons to achieve 1 mm random uncertainty. The above examples show that APOLLO is capable of achieving this in few-minute timescales.

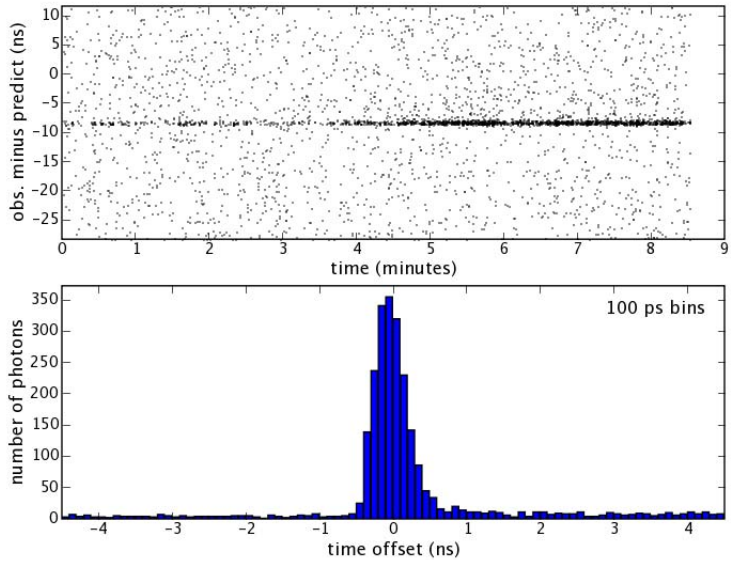

***Figure 4**: Apollo 15 run: 10,000 shots, 2000 lunar returns, 1670 of those in last half (following system optimization). Photon rate average in last half: 0.33 per pulse.*

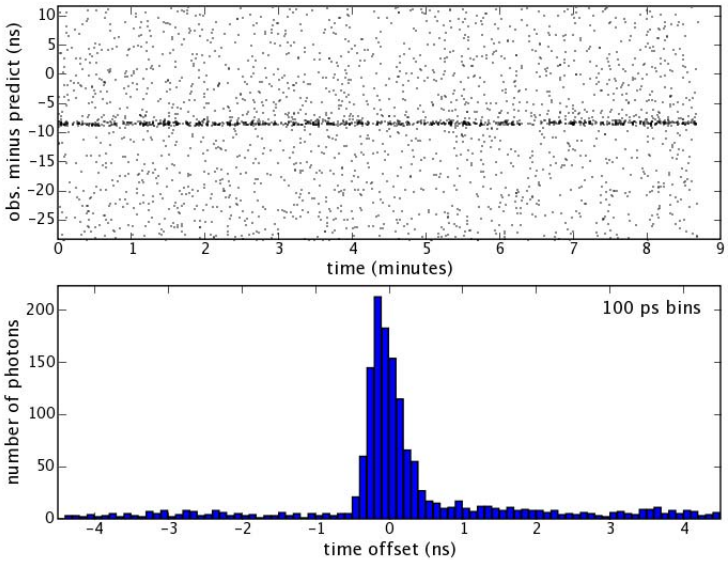

***Figure 5**: Apollo 11 (3 times smaller than Apollo 15) run: 10,000 shots, 1100 lunar returns*

Fiducial Data

An example of APOLLO fiducial data is shown in Figure 6. This particular set coincides with the lunar data presented in Figure 4. Shown here are the time histograms between the arrival of the cable-delayed fast-photodiode signal and the fiducial corner cube APD signal for the various APD channels. The absolute value (about 6 ns on average) is not fundamental, being affected by the cable delay between these signals. The offsets between channels *is* relevant, however, as this information is needed to properly register the lunar return photons among the various APD channels. The consistent shapes indicate that all channels behave similarly in the time domain (channel 8 is an exception). Channels 3 and 5 are inactive. The channel 15 input on the TDC is used to mark the fast photodiode (laser start) reference time. This is expected to fall at a random time relative to our 50 MHz clock, thus producing a uniform histogram 20 ns wide. The time axis is reversed in these histograms

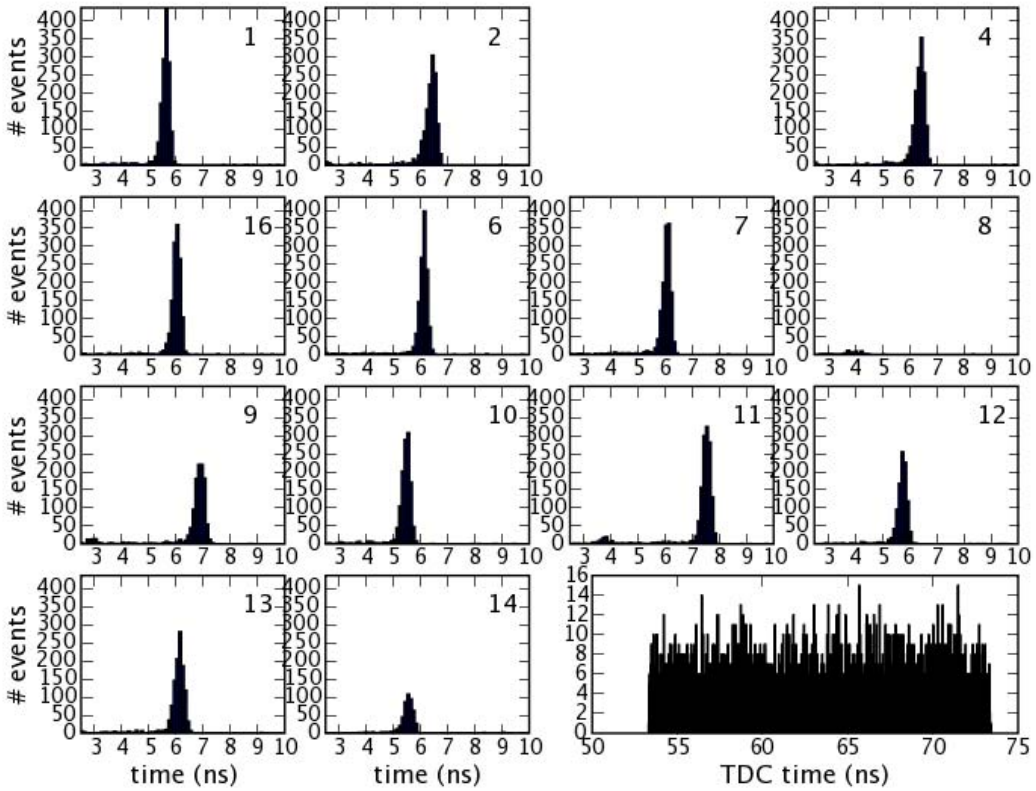

Figure 6*: The fiducial events recorded for the run shown in Figure 4 for each APD channel, at 100 ps per bin. The time axis is reversed from the histogram in Figure 4. Channel 15 is used for the fast photodiode/Ortec signal (pictured in the wide panel), and channels 3, 5, and 8 are effectively inoperative.*

compared to the one shown in Figure 4. The asymmetry is due to the APD response: some photoelectrons take longer to produce an avalanche than the typical, prompt, photoelectron.

APOLLO Performance Summary

APOLLO has achieved routine operational status, and began to gather scientifically useful data beginning in April 2006, with a regular cadence established in October 2006. More than a year of data is needed to see the impact of APOLLO's ranging capability on gravitational physics, so this should come about late in 2007. At this time, some of APOLLO's first year accomplishments are:

- As many as 2500 photons in a 500 second period
- Peak rates of ~0.6 photons per pulse, over 30 second intervals
- Range with ease at full moon (initial October 2005 acquisition at full phase)
- As many as 9 lunar return photons detected in a single pulse
- In strong runs, ~50% of photons arrive in multi-photon groups—even when the average rate is 0.25 photons per pulse

References

[1] Williams, J. G., Turyshev, S. G., and Boggs, D. H., "Progress in Lunar Laser Ranging Tests of Relativistic Gravity," *Physical Review Letters*, **93**, 261101, (2004)

[2] Murphy, T. W., Nordtvedt, K., and Turyshev, S. G., "Gravitomagnetic Influence on Gryoscopes and on the Lunar Orbit," *Physical Review Letters*, **98**, 071102, (2007)

[3] Murphy, T. W. et al., "APOLLO: Meeting the Millimeter Goal," *Proceedings of the 14th International Laser Ranging Workshop*, pp. 165–173, San Fernando, (2004)

TARGETS AND RETURN SIGNAL STRENGTH SESSION SUMMARY

Chair: Tom Murphy

This session consisted of five talks, three of which dealt with target design, testing, and analysis, and two of which dealt with absolute calibration of return signal strengths from laser ranging targets.

D. Arnold presented a summary of analytical results spanning a wide variety of topics, including: range corrections to LAGEOS and LARES; wavelength correction to LAGEOS for 850 and 425 nm light; Apollo lunar array diffraction patterns; hollow cube thermal analysis; retroreflector arrays for high-altitude satellites; diffraction patterns from and thermal analysis of Russian corner cubes; and range corrections associated with multi-photon returns to a single-photon avalanche detector (SPAD).

G. Delle Monache presented an overview of the Space Climatic Facility (SCF) in Frascati—a space/earth/sun simulation facility used to examine the thermal properties of retroreflector arrays in a space environment. The presentation included example thermal images of LAGEOS/LARES corner cubes under simulated space conditions, a description of the SCF's far-field diffraction pattern test capability, preliminary test results of the GPS3 array as part of the ETRUSCO experiment, and plans to test a LAGEOS mock-up in the near future. An invitation was extended to perform thermal tests of other retroreflector systems at the LNF facility.

V. Shargorodsky and V. Vasiliev described a new two-layer nested glass sphere retroreflector target, 17 cm in diameter, 7.5 kg in mass, with a 100,000 m^2 cross-section at 532 nm. The spherical target has been built, and is currently undergoing measurement tests of the return pattern in various conditions. The expected launch date is late 2007. Also presented was a concept possibility for a multi-layer retroreflective sphere that would work at two colors.

T. Murphy presented signal strength results from the APOLLO LLR station, comparing the highest return rates to date with a detailed link budget. Realistic diffraction patterns and de-rating factors were applied to the Apollo arrays. The result was a return signal strength substantially weaker than expected, by a factor of 15. Dust or surface abrasion are likely to blame.

J. Luck and C. Moore presented the results of a study to see if Optus-B or similar targets could be used to calibrate the return strength from other targets. By comparing return strengths from Optus-B and GPS on a variety of nights with similar pointing angles within a given comparison, they found that the measured cross-section ratio agreed with the theoretical ratio to better than 15%—suggesting such inter-comparisons as a viable technique for characterizing the performance of targets in the space environment.

Retroreflector Studies

David A. Arnold

1. 94 Pierce Road, Watertown, MA 02472, USA.

Contact: david-arnold@earthlink.net +1 617-924-3811.

Abstract

This paper discusses studies being done on retroreflectors. Complete reports are available for some, and others are ongoing projects. The studies include a preliminary transfer function for the LARES retroreflector array; computation of the wavelength correction for LAGEOS 850–425 nm; the cross-section of the Apollo lunar retroreflector arrays; parametric thermal analysis of a hollow beryllium retroreflector; retroreflector arrays for high-altitude satellites; measured diffraction patterns of retroreflectors; thermal simulations of coated and uncoated solid cube corners; and modelling of the response of a SPAD detector to various retroreflector arrays.

Introduction

This is an abbreviated version of the paper. The full paper in PDF format is available at http://www.ilrscanberraworkshop2006.com.au/workshop/day6/overview.asp or on the SPWG website in WORD format at http://nercslr.nmt.ac.uk/sig/signature.html.

LARES preliminary transfer function

The variations in range are reduced by the square root of the number of cube corners. Since LAGEOS has 4 times as many cubes as LARES the averaging is better by about a factor of 2. Because the radius of LARES is about half the size of LAGEOS the range correction is smaller. The two effects cancel each other approximately so the variation in the range correction is about the same for both satellites.

Wavelength correction for LAGEOS 850nm-425nm

Table 1 shows the wavelength correction (mm) vs velocity aberration (microradians). The average wavelength correction between 32 and 38 microradians is 2.806 ±.2 mm. The input polarization is circular.

***Table 1**: Range correction as a function of velocity aberration*

30	32	34	36	38	40
2.615000	2.773500	2.891750	2.865250	2.696250	2.465750

Cross section of the APOLLO Lunar retroreflector arrays

The APOLLO Lunar retroreflector arrays use a 1.5 inch diameter uncoated fused silica retroreflector with no intentional dihedral angle offset. The front face is recessed by half the diameter in a cavity with a 1.5 degree flare on the first APOLLO array and a 6 degree flare on the two later arrays. The cutoff angle with no flare would be 27.7 degrees. With the 1.5 degree flare it is 28.3 degrees. With the 6 degrees flare it is 30.3 degrees. Since the APOLLO retroreflectors are uncoated, there is loss of total internal reflection at certain incidence angles. The cross section has been computed vs incidence angle.

Parametric thermal analysis of hollow cubes

Equations have been derived for making order of magnitude estimates of the thermal gradients in a hollow Beryllium retroreflector due to absorption of solar radiation. The performance of the retroreflector can be degraded by thermal warping of the plates or changes in the dihedral angles between the reflecting plates as a result of differential expansion and contraction. The equations consider the case of conduction through the plate and along the plate.

Putting numbers into the equations shows that conduction through the plate is not a problem because the conduction path is wide and the path length short. Conduction along the plate can be a problem because the path length is long and the conduction path is narrow. Thermal distortion of the plates is acceptable as long as the cube corner is not larger than about 2 inches and the plate has a low solar absorptivity such as 7 percent.

Retroreflector arrays for high altitude satellites

Tables 2 and 3 show the area and mass of the cube corners needed to obtain a cross section of 100 million sq meters at the altitude of the GNSS satellites and a cross section of one billion sq meters at geosynchronous altitude.

***Table 2**: GNSS*

Design	# of cubes	Diam. in	Area sq cm	Mass g
uncoated	50	1.3	428	1000
coated	400	0.5	508	460
hollow	400	0.5	508	201
hollow	36	1.4	356	400
GPS	160	1.06	1008	1760

***Table 3**: Geosynchronous*

Design	# of cubes	Diam. In.	Area sq cm	Mass g
Uncoated	165	1.7	2415	7457
Coated	1153	.7	2863	3638
Hollow	1153	.7	2863	1590
Hollow	122	1.8	2003	2863
Single dihedral	22	2.0	446	708

Measurements of Russian cube corners

The data used in this analysis were kindly provided by Vladimir Vasiliev. A measurement of a reference mirror the same size as the cube corner is used for absolute calibration of the cross section of the cube corner. The first cube corner is a very high quality diffraction limited cube and the second is a typical cube corner. The cross section of the typical cube is larger than that of a diffraction limited cube corner past about 20 microradians.

Thermal simulations of Russian cube corner

These simulations were done using a very simple thermal simulation program that has been used only to give order of magnitude effects. The cube corners have no intentional beam spread. The isothermal diffraction does not show sufficient cross section at 26 microradians to account for the nominal cross section of the GPS array. The simulations with solar illumination show that thermal gradients could spread the

beam sufficiently to increase the cross section of the GPS array to 20 million sq meters that is the nominal cross section. The simulations show that the thermal gradients disappear quickly when the solar illumination stops. This could make it difficult to study the effect of thermal gradients in the laboratory. In the absence of a detailed engineering data on the cube corners the only way to know how the Russian cube corners behave is by laboratory testing.

Laboratory tests of cube corners

The space climactic facility at LNF in Frascati, Italy presently has a section of the LAGEOS retroreflector array, a section of LARES cube corners, and the third GPS array that contains Russian cube corners. The plan is to take diffraction patterns similar to those described in section 7 of this report and do thermal vacuum tests to measure the response of the cube corners to solar radiation. These test results can be compared to the simulations given in section 8 of this report. There will probably be significant differences between the simulations and the laboratory tests because of the limitations in the modelling.

Modelling of the response of a SPAD detector to a distributed signal

My analysis programs compute the range correction of a retroreflector array for centroid and constant fraction discriminator detection systems. All single photoelectron systems measure the centroid. For multi-photoelectron signals the range correction for a SPAD detector requires modelling the current vs time as a function of the time of arrival of each photoelectron. The exponential model of a SPAD assumes the number of charge carriers increases exponentially after a photon is detected until the available charge carriers are depleted. Tom Murphy has suggested modelling the number of charger carriers as a quadratic function of time on the assumption that the region of charge carriers is a thin disc whose radius increases linearly with time. The actual behaviour is complex. The rise time of a SPAD detector is a function of the number of photoelectrons. The CSPAD detector compensates for the number of photoelectrons for a point reflector. In the exponential model the rise time is independent of the number of photoelectrons. The exponential model does not explain the observed dependence of the rise time on the number of photoelectrons.

Simulations with the exponential model indicate that the measured range decreases if additional photoelectrons arrive before the current from the first photoelectron has increased to a large value.

***Table 4**: Two-photon bias*

x	0.0	2..6	5.2	10.4	15.6	20.8	26.0	52.0
Δr	3.60	2.66	1.77	0.72	0.28	0.10	0.04	0.00

In Table 4, 'x' is the one-way distance between the reflection points of two photoelectrons. Δr is the decrease in the measured one-way range due to the second photoelectron. For millimeter accuracy ranging the effect is significant for the first centimeter.

The modelling of a SPAD is complex. Unless one has a good model the only way to study the effect of a photoelectron that arrives a short time after the first is to do an experiment. For example, the target calibration vs signal strength could be done with a flat target and with a target where half the area is at position zero and the other half is a few millimeters farther away.

The INFN-LNF Space Climatic Facility for LARES and ETRUSCO

D. Arnold[1], G. Bellettini[2], A. Cantone[3], I. Ciufolini[4], D. G. Currie[5], S. Dell'Agnello[3], G. O. Delle Monache[3], M. Franceschi[3], M. Garattini[3], N. Intaglietta[3], A. Lucantoni[6], T. Napolitano[3], A. Paolozzi[6], E. C. Pavlis[7], R. Tauraso[2] and R. Vittori[8]

1. NASA-GSFC.
2. Univ. of Rome Tor Vergata, Italy.
3. INFN – LNF, Laboratori Nazionali di Frascati, Italy.
4. Univ. of Lecce, Italy.
5. Univ. of Maryland, College Park, USA.
6. Univ. of Rome La Sapienza, Italy.
7. Univ. of Maryland, Baltimore, USA.
8. Italian Air Force.

Abstract

The construction of the LNF Space Climatic Facility (SCF) started in Frascati, Italy, in 2006. The initial purpose was to study the thermal thrusts (TTs) of LAGEOS I/II satellites and to perform the full space-climatic and laser-optical characterization of the new LARES laser-ranged test mass. In late 2004 the construction of LARES was proposed to INFN, which then gave the scientific approval of the LARES experiment in November 2006.

The modular and evolutionary design of the SCF turned out to be well suited to characterize the thermal and optical performance of retro-reflector CCR arrays deployed on GNSS constellations. For this purpose, the groups of INFN-LNF, Rome-Tor Vergata plus R. Vittori in 2006 proposed to INFN a new experiment, ETRUSCO ("Extra Terrestrial Ranging to Unified Satellite COnstellations"). ETRUSCO was approved by INFN in October 2006. This paper describes the SCF and the first preliminary measurements and thermal simulations.

The SCF Apparatus

A schematic view of the SCF is shown in Fig. 1. The steel cryostat is approximately 2 m length by 1 m diameter. Inside this vacuum shell the shield, black painted with the high emissivity paint Aeroglaze® 306, is cooled down to 77 K by forced LNF2 flow. When the SCF is cold, the vacuum is typically 10^{-6} - 10^{-5} mbar.

The thermal input loads are provided by a Solar Simulator (SS) and an infrared (IR) Earth Simulator (ES). The SS is located outside, behind a quartz window (36 cm diameter, 4 cm thickness), which is transparent to the solar radiation up to 3000 nm. The ES located inside, is an Al black-painted disk (diam. 300 mm) held at 254 K by thermo coolers (TECs). A support fixture on the ceiling holds the prototype in front of the simulators. The distance of prototype from the ES is such to provide the CCRs with the same viewing angle in orbit (~60^{o} for LAGEOS). A Germanium window on the right side of the SCF allows for the acquisition of thermograms of the prototypes with an IR digital camera.

The SS (www.ts-space.co.uk) gives a 40 cm diameter beam with close spectral match to the AM0 standard of 1 Sun in space (1366.1 W/m^2), with a uniformity better than ± 5% over an area of 35 cm diameter. The spectrum is formed from the output of two sources, namely an HMI arc lamp (UV-V), together with a tungsten filament lamp (Red-IR). The quartz halogen lamp (with the tungsten filament) has a power of 12 KW, while the metal halide lamp has 6 KW power. These two sources are filtered

such that when the two beams are combined with a beam splitter/filter mirror, the resulting spectrum is a good match to AM0 in the range 400–1800 nm. The spectrum has also been measured also from λ = 1500 nm up to 3000 nm and found to be in reasonable agreement with the AM0 over this extended range. The absolute scale of the SS intensity is established by exposing the beam to a reference device, the *solarimeter*, which is a standard www.epply.com thermopile.

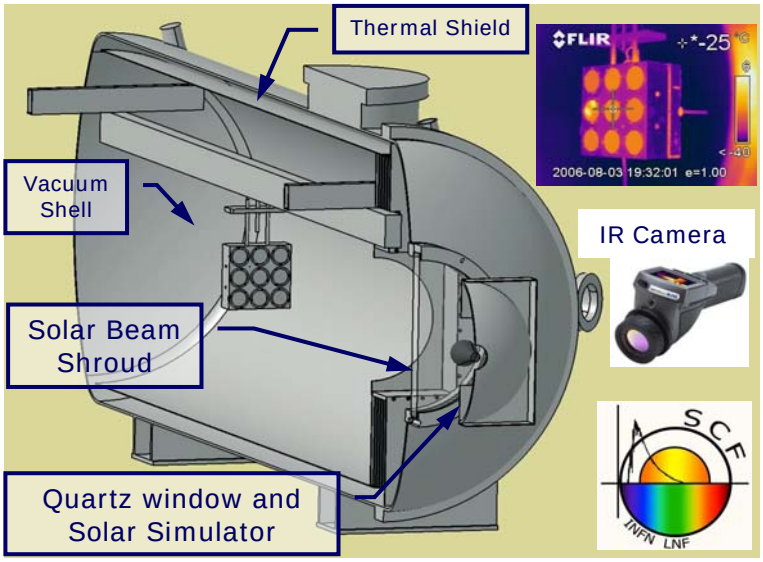

***Figure 1**: The LNF Space Climatic Facility with a retro-reflector array inside.*

The temperature DAQ system consists of an IR camera for non-invasive, high spatial granularity measurements and class-A PT100 RTDs with 4-wire readout. The IR camera is a ThermaCAM® EX320 by http://www.flir.com. The camera focal plane array detector is an un-cooled Vanadium Oxide micro-bolometer with spectral range 7.5 ÷ 13 μm. This camera has a true, built-in 320 x 240 pixel array, field of view/min focus distance 25° x 19° / 0.3 m and thermal sensitivity 80 mK. Since the EX320 factory accuracy is 2 K, the PT100s will be used for cross calibration. The PT100s are certified to have an accuracy of 0.1 – 0.3 K between 273 K and 373 K, which has been checked with a reference thermometer of absolute scale accuracy < 0.1 K, in a range appropriate for LAGEOS. The PT100s are also used below 250 K, outside the working range of the IR camera.

***Figure 2**: The 3×3 LAGEOS matrix built at LNF and the CCR assembly components.*

Thermal Characterization of LAGEOS Retro-reflectors

The thermal relaxation time of LAGEOS and LARES CCRs, τ_{CCR}, has never been measured in realistic climatic conditions. Computations vary by 300%. The goal for LARES and LAGEOS is to measure τ_{CCR} at ≤10% accuracy. This will make the error on the measurement of the Lense-Thirring effect due to thermal perturbations

negligible (permil level; [1] and references therein). A prototype called "3×3 matrix" has been built by LNF to measure directly τ_{CCR} and the time relaxation constant of the retainer Al rings (see fig. 2).

The program of measurements to be done on LAGEOS prototypes is described in [1] and will not be repeated here. The Aluminium base of this prototype has been held at constant temperature by the TECs (for example T(Al) = 298 K), in order to simulate the average temperature of LAGEOS, while the CCR assembly components experience the SS and ES thermal loads in varying climatic configuration. Note that the baseline LARES design uses the same type of LAGEOS CCRs.

The SCF includes thermal software for simulation and parametric design of spacecrafts and/or components. LNF is using the following package from http://www.crtech.com/: Thermal Desktop, the CAD-based geometric thermal modeler, RadCad, the radiation analysis module and orbital simulator, Sinda-Fluint, the solver. With this software, we estimated the overall TTs on LAGEOS during the eclipse due to the Earth shadow (see ref. [1]). With the SCF a preliminary thermal measurement with the ES as the only thermal input has been performed. The measured steady-state temperature of the CCR shows a fair match with the simulated thermal model of the 3×3 matrix (see fig. 3). It should be pointed out, however, that this preliminary test has been carried out with a non-optimized configuration of the screws and retainer rings (in terms of the materials used and of the torque applied to the screws) and that the temperature scale of IR camera was not fully calibrated. Once the thermal model will have been tuned to the final data it can be used for the complete thermal analysis of the LAGEOS satellites (and for the parametric design of LARES).

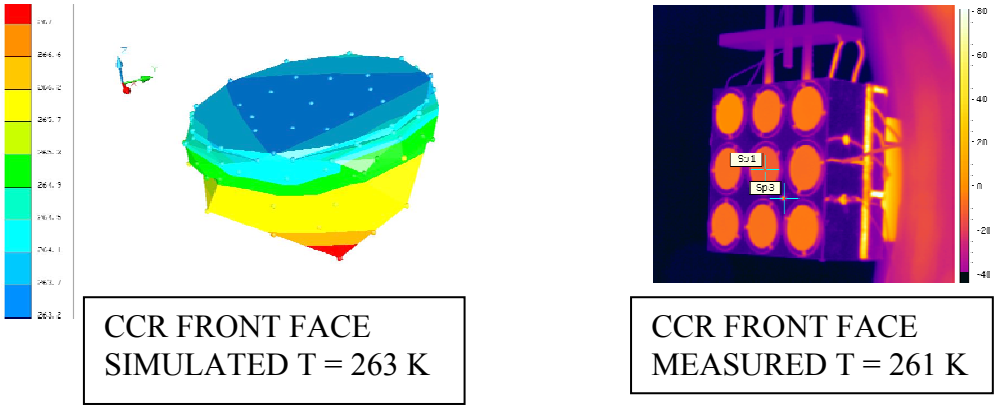

***Figure 3**: Comparison of the steady state CCR temperature measured with the SCF (ES only) and modelled with the thermal software, in a specific test configuration.*

Figure 4 shows the result of another preliminary in-air test at STP conditions, which was performed with the SS as main thermal load (at 75% of the nominal intensity). This was done mainly to exercise the whole system during a maintenance period of the SCF.

The SCF is now being upgraded with one optical-quality fused silica window to measure the far field diffraction patterns (FFDPs) of CCRs inside the SCF in realistic space conditions. Integrated thermal and optical tests will be performed on the CCRs of the LAGEOS "sector" prototype of NASA-GSFC (fig. 5). The finish of its Al surface is believed to be highly emissive (20% - and it will be measured) like for LAGEOS I. The sector contains 37 CCRs of good optical quality (in terms of the

accuracy of the dihedral angle offsets) with an outer diameter of 34 cm, well within the diameter of the SS beam.

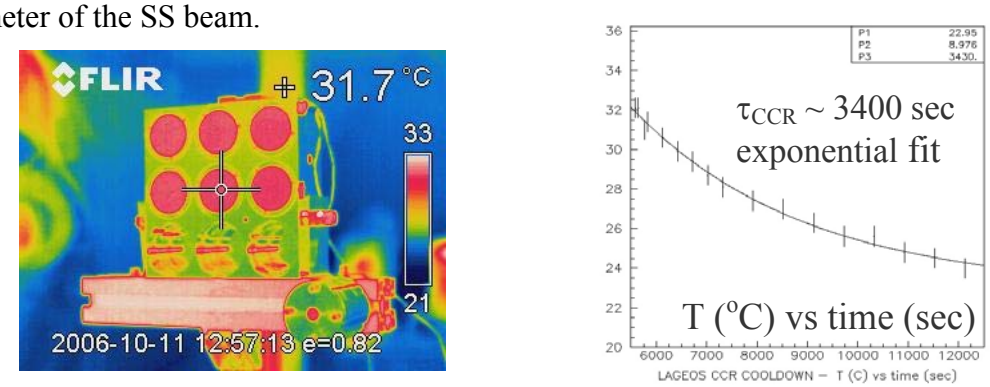

***Figure 4**: Cool-down curve of a LAGEOS CCR in-air and STP conditions.*

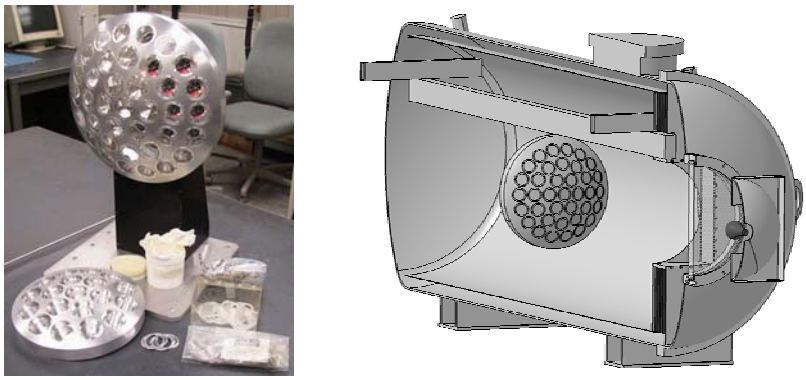

***Figure 5**: Engineering model of LAGEOS (circa 1992) property of NASA-GSFC. This LAGEOS sector is now at LNF for thermal and optical testing at the SCF.*

ETRUSCO (ExtraTerrestrial Ranging to Unified Satellite COnstellations)

The "unification" refers to the addition of laser ranging to the standard microwave ranging of GNSS satellites. Our aim is to perform a complete thermal and laser optical characterization of different CCR arrays used for existing and future GNSS constellations.

A preliminary in-air and STP test of a flight model of the third CCR array to be deployed on a satellite of the GPS block II has been done at LNF. This so-called "GPS3" array is identical to the ones installed on the GPS 35 and 36 satellites in orbit and is property of the University of Maryland (C. O. Alley et al). The three arrays have been manufactured in Russia. Mechanical drawings for its correct modelling have been provided courtesy of V. Vassiliev of the IPIE, Moscow. The GPS3 is currently at LNF, under a special agreement between NASA-GSFC, UMD and INFN-LNF. to be tested at the SCF. A preliminary test was done with the SS as main thermal load (at 75% of the nominal intensity). Two thermograms are shown in Fig. 6.

Figure 7 shows the thermal behaviour of the GPS3 as measured with the IR camera. A space-climatic test will follow in 2007, under the supervision of D. G. Currie of UMD.

Far Field Diffraction Pattern Measurement

The optical circuit for FFPD measurements at STP conditions is shown in fig. 8. The laser beam profiler is a Spiricon CCD camera. Tests are now performed at STP; final one will be performed with the CCR array in SCF.

Figure 9 shows how the SCF is now being upgraded with one optical-quality fused silica window to measure the far field diffraction patterns (FFDPs) of CCRs inside the SCF.

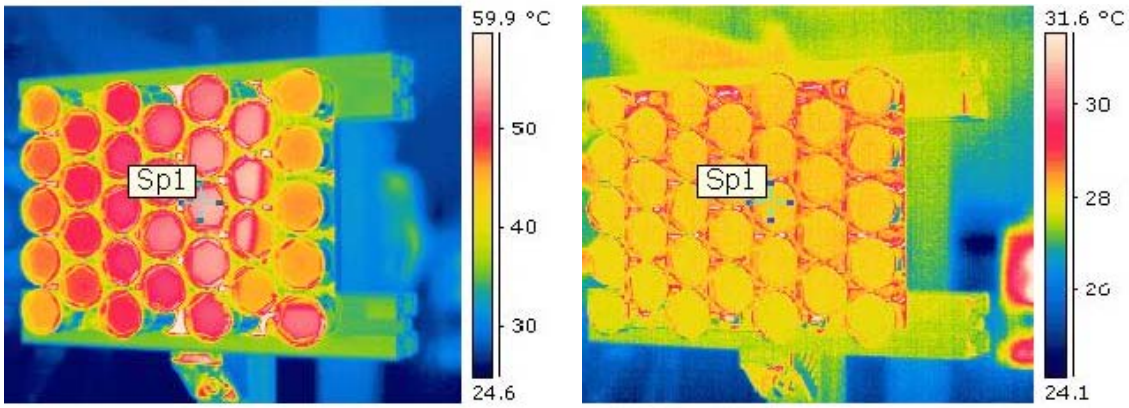

***Figure 6**: Warmest and coolest conditions of the GPS3 retro-reflectors in the LNF STP test.*

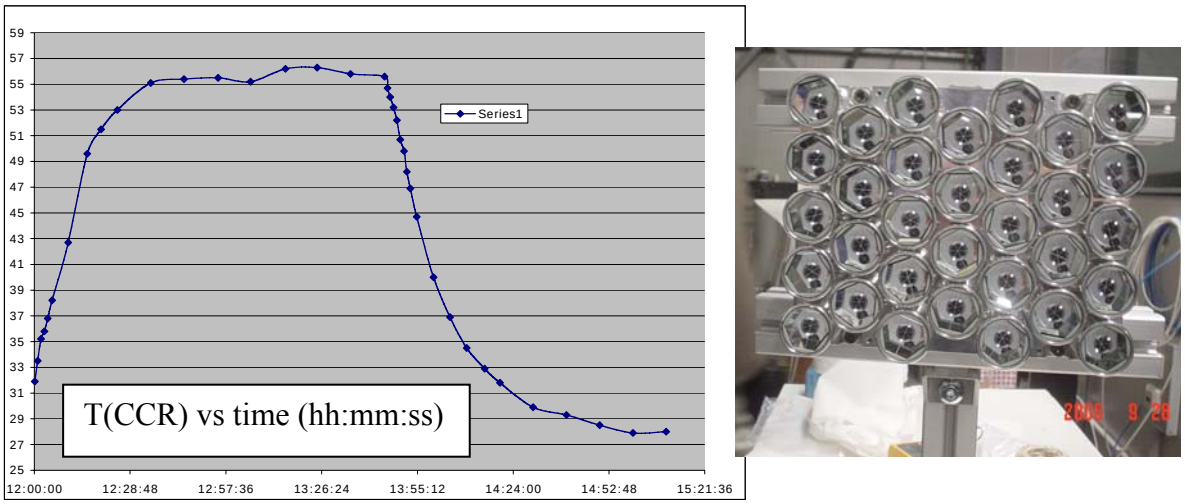

***Figure 7**: Warm-up and cool-down curves of the GPS3, in-ar and at STP at LNF.*

Each CCR will be first exposed to the Sun and the Earth simulators and its thermogram taken by the IR camera from the 45° window. Then, the CCR will be moved in front of the optical window to be exposed to the laser beam and its FFPD recorded (see fig. 10).

Conclusions

At the end of 2006 the SCF has become a permanent, small-size, experimental apparatus of INFN-LNF. The collaboration with ILRS has been very fruitful. Two approved INFN experiments are based for a significant part on the SCF operation: the by-now consolidated LARES mission and the new ETRUSCO experiment. The current upgrade of the SCF, consisting of the integration of the thermal and the laser-optical tests has been funded by INFN, and by LNF, explicitly for ETRUSCO. This funding includes an additional, dedicated optical table to be installed next to the SCF. It does not include the mechanical system(s) for the automated positioning of all the CCRs in the SCF climatic conditions. An endorsement of this work and its scientific motivations by ILRS would be very useful for fund-raising (outside ILRS) and the fulfilment of the ultimate ETRUSCO goals.

References

[1] *Probing Gravity in NEO with High-Accuracy Laser-Ranged Test Masses*, A. Bosco et al, Report INFN-LNF-06-24(P): http://www.lnf.infn.it/sis/preprint/pdf/LNF-06-24(P).pdf. Presented by S. Dell'Agnello at the "Quantum to Cosmos" NASA Int. Workshop, Warrenton (VA), USA, May 2006; to be published in a special issue of Int. Jour. Mod. Phys. D.

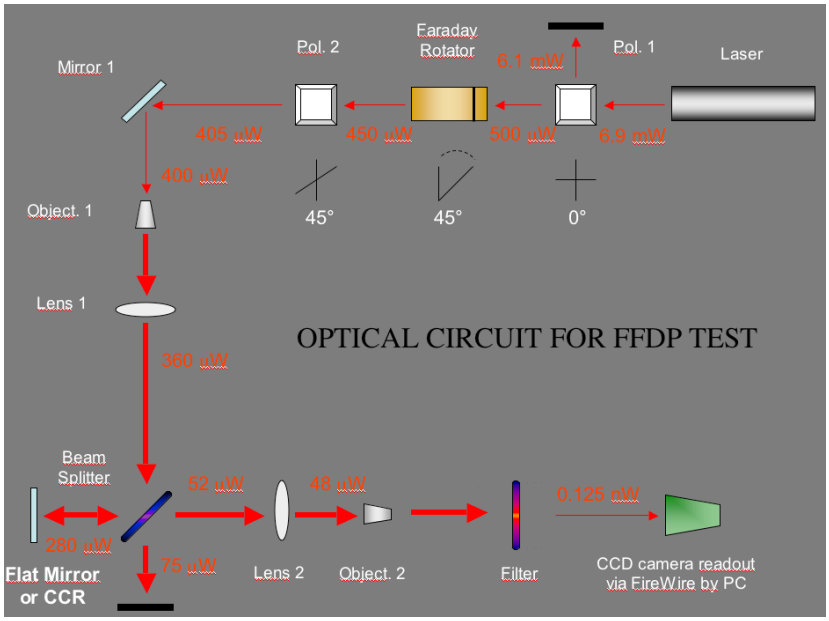

***Figure 8**: Layout of the optical circuit for the FFDP measurement.*

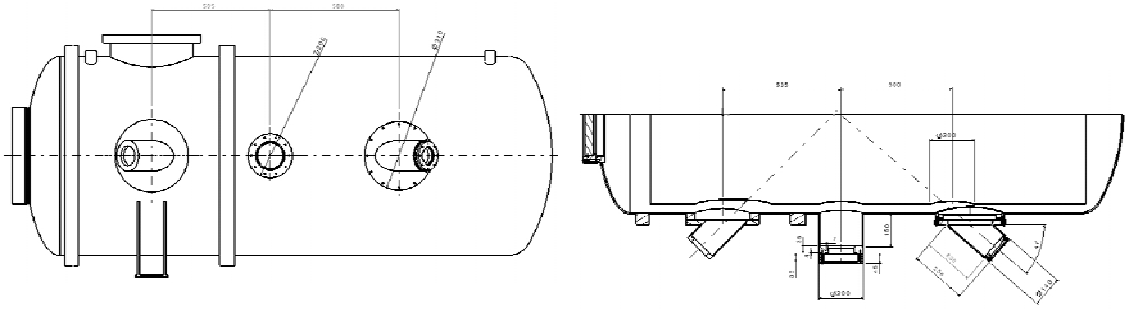

***Figure 9**: Left/central/right windows: IR thermometry, FFDPs and a spare.*

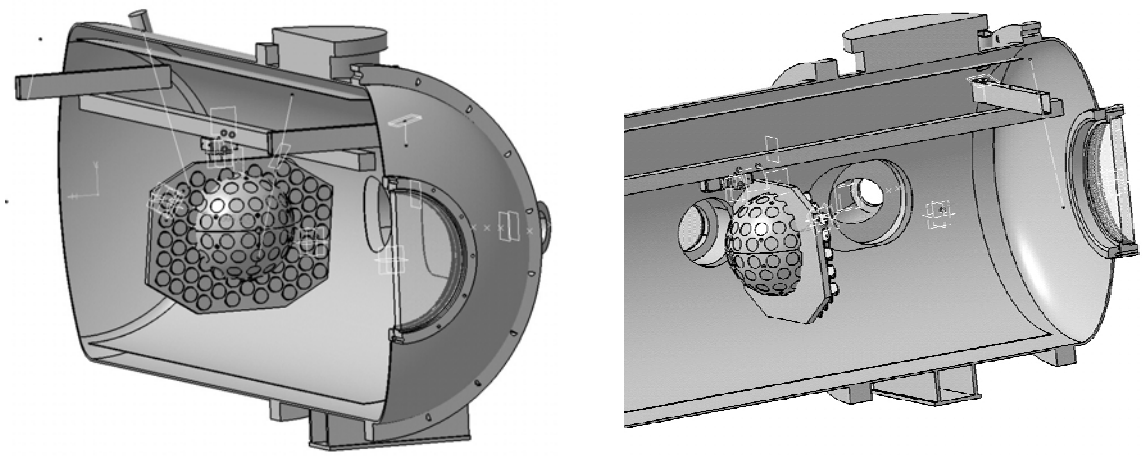

***Figure 10**: The baseline LARES and a GNSS retro-reflector array in the upgraded SCF.*

Absolute Calibration of LLR Signal: Reflector Health Status

T. W. Murphy, Jr. [1], E. G. Adelberger[2], J. B. Battat[3], C. D. Hoyle[4], E. L. Michelsen[1], C. W. Stubbs[3], and H. E. Swanson[2]

1. UC San Diego, MC-0424, 9500 Gilman Drive, La Jolla, CA 92093-0424, USA;
2. University of Washington, MC-351560, Seattle, WA 98195-1560, USA;
3. Harvard University, Dept. of Physics, 17 Oxford Street, Cambridge, MA 02138, USA;
4. Humboldt State University, Dept. of Physics, Arcata, CA 95521, USA;

Abstract

The recently-operational APOLLO lunar ranging station has received lunar return signals as strong as 0.6 photons per pulse over short periods. This signal rate is high enough to allow system optimization and diagnoses that permit careful quantification of system performance. Moreover, observing a spatially flat part of the moon with a well-defined field of view yields a check on the total one-way system efficiency. We are therefore able to compare the lunar signal rate against theoretical expectations as a means of examining the health of the retroreflector arrays after 35 years or more in space. A key part of this analysis is a thorough understanding of the diffraction pattern returned by the corner cube array.

Introduction

Three of the Apollo lunar landing missions placed corner-cube arrays on the lunar surface for the purpose of laser range measurements. The arrays consist of identical 38 mm-diameter uncoated fused-silica corner cubes working via total internal reflection. The Apollo 15 array is three times larger than the first two (Apollo 11 and Apollo 14), making it the preferred target due to its higher return rate. Roughly 85% of laser range measurements to the moon utilize the Apollo 15 array. The present analysis concerns itself only with this array, though results from the others support our conclusions.

The photon count per pulse can be characterized by the link equation,

$$N_{\rm detect} = N_{\rm launch}\eta_{\rm c}^2\eta_{\rm r}\eta_{\rm NB}Qn_{\rm refl}\eta_{\rm refl}\left(\frac{d}{r\phi}\right)^2\left(\frac{D_{\rm eff}}{r\Phi}\right)^2, \qquad (1)$$

where $N_{\rm launch}$ is the number of photons emitted by the laser per pulse, $\eta_{\rm c}$ is the one-way optical efficiency common to both transmit and receive modes, $\eta_{\rm r}$ is the optical efficiency of the receiver, $\eta_{\rm NB}$ is the narrow-band filter peak transmission, and Q is the detector quantum efficiency. The reflector array is composed of $n_{\rm refl}$ corner cubes (300 for Apollo 15), each of diameter, d and efficiency $\eta_{\rm refl}$. The uplink beam has a divergence ϕ, while the downlink divergence is Φ. $D_{\rm ef}$ is the effective diameter of the telescope (such that the collecting area is $\pi D_{\rm eff}^2/4$, and r is the one-way distance between the telescope and the reflector array. The simplified link equation assumes "tophat" diffraction distributions rather than Gaussian or more complicated patterns as a rough estimate of flux in the center of the distribution. We will later abandon this simplification in a refined approach.

The sections below evaluate the terms in the link equation for the recently constructed APOLLO (Apache Point Observatory Lunar Laser-ranging Operation) apparatus [1], comparing the model to observed peak rates. First, the individual terms and their

errors are estimated, followed by a check of the one-way efficiency using the solar-illuminated lunar surface. Then the lunar return is estimated and compared to actual measurements. Ultimately, the calculation is modified to account for a realistic diffraction pattern from the lunar corner cubes. An attempt is made to propagate realistic errors throughout this analysis.

One-Way Throughput

The one-way throughput of the apparatus may be checked by looking at a star or other flux standard using the same detector path employed in detecting lunar laser returns. This checks the quantity $\eta_c \eta_r Q$ in the link equation.

The η_c and η_r terms are composed of a number of optical efficiencies, evaluating to 0.51±0.03 and 0.29–0.58, respectively. Atmospheric transmission, measured to be 0.87 for one airmass at 550 nm at Apache Point, is included in η_c. The large range on η_r stems from the fact that the APOLLO detector only spans 1.4 arcseconds on a side. Therefore, a point source above the atmosphere may overfill the array depending on atmospheric seeing. Despite the large range, given knowledge of the seeing we can estimate this parameter to ~10% precision, leading to a ~12% estimate on η_r. The detector quantum efficiency, *Q*, is roughly 0.30. This number matches theoretical expectations based on device structure, and the flux calibration to a flux standard is in agreement with this figure. The effective diameter of the Apache Point 3.5 meter telescope is 3.26 m.

For the purpose of estimating the one-way throughput when looking at a flux standard, we need to know that the effective bandpass of the narrow-band filter is $\Delta\lambda_{NB}$ = 0.95 nm, and that the integration time is Δt_{APD} = 95 ns per APD gate event. We use the flux calibration standard that a zero-magnitude source at 532 nm wavelength has a flux density of $F_0 = 3.9\times10^{-11}$ W m^{-2} nm^{-1}. The number of photons we see per gate event is then

$$N = \frac{\pi}{4h\nu} F_0 10^{-0.4m} D^2 \Delta\lambda_{NB} \Delta t_{APD} \eta_c \eta_r Q \,, \qquad (2)$$

where *m* is the stellar magnitude, and $h\nu$ is the photon energy. During full moon, we estimate the darker-than-average terrain around the Apollo 15 reflector to have a surface brightness of 3.60 magnitudes per square arcsecond. This translates to 2.87 magnitudes into the 1.4×1.4 arcsecond field of view. Accounting for the fact that only 13 of the 16 APD elements are operational, the expected lunar background rate is: $N_{lunar} = 0.40 \pm 0.08$ photons per gate. Comparing this to the measured full-moon background rate of 0.40 photons per gate, we claim to understand the one-way efficiency of our system. Similar analysis on a focused star yields similar results.

Lunar Return Rate

Simplified Calculation

Populating the terms in Equation (1), we take $\eta_{NB} = 0.35 \pm 0.025$, $N_{launch} = f_{launch} E_{pulse} / h\nu$, with $f_{launch} = 0.6 \pm 0.03$ as the geometrical loss of the Gaussian beam propagating out of the 3.5 meter telescope, and $E_{pulse} = 0.100$ J. Setting $n_{refl} = 300$, d = 0.038 m, $\eta_{refl} = 0.93$, $r = 3.85\times10^8$ m, $\phi = 0.8 \pm 0.12$ arcseconds, and $\Phi = 10 \pm 1.5$ arcseconds, we get an expected lunar return into the APD array (with its particular pattern of dead pixels) of: $N_{detect} = 12.0 \pm 6.1$ photons per pulse. If we use the information we get from the one-way system check, we

reduce the uncertainty by a small amount to ±5.6 photons per pulse.

Observed Lunar Return Rate

The APOLLO lunar return rate is highly dependent on atmospheric seeing and pointing. Not only does the illumination of the reflector scale as the inverse square of the seeing scale, the finite and small APD field of view truncates flux in poor seeing. Seeing of 2.0 arcseconds produces a return rate ten times smaller than at 1.0 arcseconds, if perfectly centered in both cases. For the present analysis, we use the two highest return rates observed in the first six months of APOLLO operation: 9 December 2005, and 17 January 2006. Both nights had exceptional seeing. On each night, we saw return rates of ≈ 0.5 photons per pulse over < 30 second intervals. In each case, telescope pointing and beam offset were optimized for the best signal.

The estimate of expected lunar rate above is 24 times the observed rate. Even though the analysis is a simplified version, the discrepancy is large, and difficult to eliminate through reasonable choices of parameters.

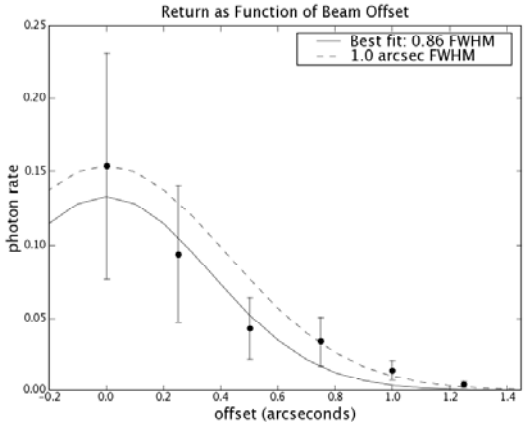

Figure 1*: Beam offset optimization on 9 Dec. 2005. At offset steps of 0.25 arcsec, it is clear that the beam size is less than 1.0 arcsec. Error bars are estimated at 50%.*

The effective beam size on the moon (affected by seeing and optical configuration) is the most obvious place to suspect poor understanding. As for the seeing, the median seeing at the Apache Point Observatory is 1.1 arcsec at zenith. Since the nights used for comparison had especially good seeing, we may assume the seeing to be less than 1.1 arcsec, and likely around 0.8 arcsec. But more convincingly, by rastering the beam pointing on the moon (while keeping the receiver fixed at the same location) we can demonstrate the sensitivity to beam offset, and see directly that the beam illumination footprint on the moon has a full-width at half-maximum (FWHM) less than one arcsecond (Figure 1). Though the best fit in Figure 1 is 0.86 arcsec FWHM, we have chosen 0.8 arcsec in the present analysis because the periods we have chosen for comparison represent the very best 30 second periods within ~10 minute runs. We therefore expect the conditions to have momentarily been better than the average for the run.

It should be noted that the multi-photon capability of APOLLO's detector array renders us insensitive to skewed statistics arising from the structure of the beam's speckle pattern on the moon. In the present analysis, some pulses are seen with as many as 6, 7, or 8 photons. We do not underestimate our return rate by missing these top-heavy events.

Refined Calculation

In the preceding analysis, we made the gross simplifying assumption that the beam patterns were uniform across a circular region—a so-called "tophat" profile. A more realistic calculation should:

- treat the outgoing beam as having a Gaussian profile;
- consider the theoretical diffraction pattern from a perfect corner cube;
- allow for manufacturing tolerance of the corner cubes;
- account for the reduced corner cube throughput as a function of incidence angle;
- de-rate the return strength due to thermal distortions of the corner cube;
- compensate for velocity aberration of the returning beam.

In this section, we treat each of these issues in turn, ultimately producing a more realistic estimate of the return rate, with less uncertainty.

A circularly symmetric Gaussian flux distribution has a peak irradiance that is ln2 ≈ 0.69 times the irradiance of a tophat whose diameter is the same as the Gaussian FWHM and carries the same total flux. Thus we multiply the return rate by this factor.

A corner cube prism employing total internal reflection (TIR) produces a diffraction pattern that is significantly different from that of an equivalent circular aperture. As seen in Figure 2, there is a central core of concentrated flux surrounded by a roughly hexagonal pattern containing significant flux. The core follows the Airy function that would be produced by a perfect circular aperture of the same diameter as the corner cube, but at a peak flux only 27% that of the Airy function, ignoring the two-way reflective surface loss. At normal incidence, the TIR pattern contains 36% of the total energy within the first Airy ring of radius $1.22\lambda/D$, where λ is wavelength and D is the diameter of the aperture [2]. This is compared to 84% for the Airy function.

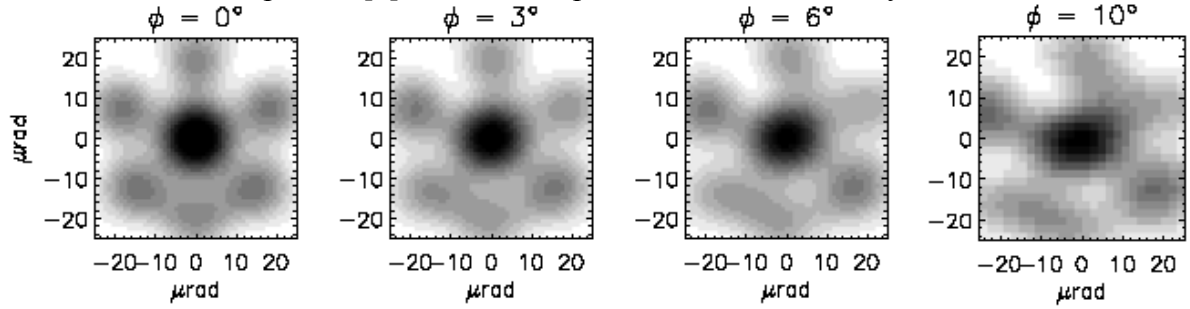

***Figure 2**: Sample diffraction patterns from an Apollo corner cube as a function of incidence angle. Data courtesy David Arnold.*

Compared to a tophat flux distribution with angular diameter λ/D, the normal-incidence TIR diffraction pattern has a central irradiance that is 0.182 times the tophat irradiance if both contain the same total flux. Including the 0.93 two-way front-surface reflection loss from fused silica (η_{refl}), the Apollo corner cubes produce a diffraction pattern with a central irradiance 0.169 times that of the comparison tophat. For the Apollo cubes and $\lambda = 532$ nm, the tophat diameter is 2.89 arcsec.

The manufacturing tolerance for the mutual perpendicular faces of the Apollo corner cubes was specified as ±0.3 arcsec [3]. It was reported that the central intensity of each corner cube selected for flight was at least 90% of the theoretical value. As such, we adopt a factor of 0.93 to provide a representative scaling of manufacturing imperfection.

Corner cubes have an effective cross section that is a function of the incidence angle. For circularly-cut fused silica corner cubes, this function is linear near normal incidence, with 4.3% loss per degree offset. In addition, the Apollo corner cubes are recessed in aluminum mounting structures by half their diameter, or about 1.9 cm. The recesses have conical flares, with half-angles of 1.5° for Apollo 11, and 6° for both Apollo 14 and 15. Together, these factors reduce the throughput by as much as a factor of two for the most extreme libration-induced tilts of 10° (Figure 3).

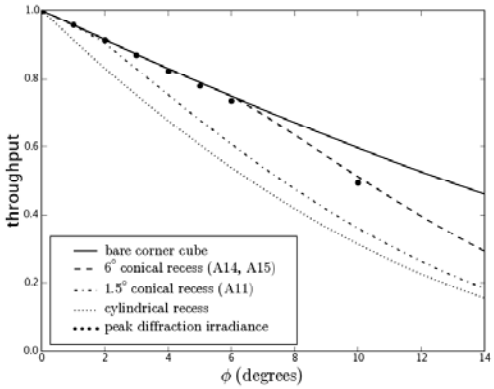

***Figure 3**: Corner cube throughput as a function of incidence angle and recess geometry. The single points come from diffraction patterns (as in Figure 2). Data courtesy Jim Williams.*

The thermal performance of the Apollo reflector arrays in the lunar environment was modeled and tested in great detail prior to flight. The primary performance degradation stems from thermal gradients within the corner cubes, which both deform the optical surfaces and present a refractive index gradient within the material—leading to distortion of the reflected wavefront [4]. For the Apollo 15 array, the central irradiance may be as low as 0.7 times the isothermal value. The original analysis presented plots of degradation as a function of sun angle for the three arrays, from which it is possible to evaluate the thermal degradation factor for any particular lunar phase [5].

Because the lunar reflector is in relative transverse motion with respect to the earth station—due both to the lunar orbit at ≈ 1000 m/s and earth rotation at ≈ 400 m/s—one must account for the angular shift in the diffraction pattern, amounting to $2\Delta v/c$. This amounts to 0.8–1.2 arcsec (4–6 μrad) depending on the vector sum of the relevant velocities. Given the functional form of the central region of the TIR corner cube diffraction pattern, this translates to a signal degradation of 0.64–0.86, or 0.75 on average.

Putting these factors together, we find that the response from the ideal TIR corner cube suffers a factor of 0.20–0.86 degradation. If one then treats the corner cube diffraction pattern as a λ/D tophat function, a pre-factor of 0.034–0.146 must be applied to the link equation. This is equivalent to a tophat function 8–15 arcsec in diameter with no degradation pre-factor.

Analysis of Two Cases

As mentioned before, we use two epochs—both at a return rate of 0.5 photons per pulse—to compare against the return estimate. Table 1 summarizes the various de-rating factors, and estimates resulting from the analysis. The squared atmospheric de-rating as a function of zenith angle has been included (belongs in η_c, technically).

The static factors shown in Table 1 represent the outgoing Gaussian beam profile, the TIR diffraction profile with surface reflection, and the manufacturing tolerance.

***Table 1**: De-rated return rate estimates for the two comparison epochs.*

Parameter	**Epoch 1 value**	**Epoch 1 de-rating**	**Epoch 2 value**	**Epoch 2 de-rating**
Velocity Aber.	1.09 arcsec	0.71	0.86 arcsec	0.81
Angular Offset	3.94°	0.84	4.04°	0.81
Sun Angle	–73°	0.85	35°	0.70
Range	371425 km	1.15	404301 km	0.82
Zenith Angle	50°	0.84	23°	0.97
Static Factors	0.69×0.169×0.93	0.108	0.69×0.169×0.93	0.108
Total de-rating		0.053		0.040
Return Estimate	8.2±3.4 phot./pulse		6.2±2.6 phot./pulse	
Estimate Ratio	16.4		12.4	

Using the de-rating estimates in Table 1 together with Equation (1), and taking the convention that $\Phi = \lambda / D = 2.89$ arcsec, we arrive at the conclusion that we see a return rate approximately 15 times weaker than expected. Given that the estimated net error is about 41%, and considering that this is a multiplicative problem, a one-sigma deviation would correspond to multiplying the estimate by (1 – 0.41) = 0.59. A two-sigma deviation corresponds to multiplying by $0.59^2 \approx 0.35$. To bring the discrepancy down to unity, we must be approximately five standard deviations away—a significant result.

To illustrate the robustness of this result, imagine that our estimate of the beam width—our least certain parameter—is less certain than our ±15% estimate. We could achieve the discrepant ratios by letting the beam profile be as large as 2.8–3.2 arcsec, which is not at all consistent with Figure 1, or APOLLO experience in general.

We conclude that the lunar reflectors have suffered performance degradation (ratios between reflectors are as expected) in their > 35 years on the lunar surface. We cannot tell whether the degradation is due to dust or surface abrasion. Recent work proposing a dynamic fountain of dust on the moon may be relevant [6].

References

[1] Murphy, T. W. et al., "APOLLO Springs to Life: Millimeter Lunar Laser Ranging," *Proceedings of the 15th International Laser Ranging Workshop*, Canberra, (2006)

[2] Chang, R. F., Currie, D. G., Alley, C. O., and Pittman, M. E., "Far-Field Diffraction Pattern for Corner Reflectors with Complex Reflection Coefficients," J. Opt. Soc. America, **61**, 431, (1971)

[3] Kokurin, Y. L., "Laser Ranging to the Moon," *Proceedings of the P. N. Lebedev Physics Institute*, **91**, p. 161

[4] Faller, J. E.., "The Apollo Retroreflector Arrays and a New Multi-lensed Receiver Telescope," *Space Research XII*, Akademie-Verlag, p.235, (1972)

[5] Faller, J. E. et al., "Laser Ranging Retroreflector," Chapter 14 of the NASA post-mission report on the Apollo 15 mission

[6] Stubbs, T. J., Vondrak, R. R., and Farrell, W. M., "A dynamic fountain model for lunar dust," *Advances in Space Research*, **37**, 59, (2005)

Experimental Return Strengths from Optus-B and GPS

John McK. Luck[1] and Chris Moore[1]

1. EOS Space Systems Pty.Ltd., Canberra, Australia

Abstract

The return signal strengths from the retroreflector arrays on the Optus-B satellites in geostationary orbits have been compared with those from GPS targets using the High Energy Laser on the 1.8 metre space debris tracking system adjacent to the Mount Stromlo SLR. In the experiments conducted in mid-2006, we performed alternate ranging to an Optus-B then to a GPS while the two targets were in close proximity to minimize atmospheric differences. Each measurement was the setting of the receive-path Neutral Density filter required to extinguish returns, having first maximized the return rate by fine pointing adjustment.

The ratios of the results, after judicious editing of outliers, were in broad agreement with Dave Arnold's calculations of the respective array cross sections. They suggest that this could be a viable technique for calibrating actual performance of arrays in their space environment.

Satellite Retroreflector Arrays

The constellation OPTUS-B1 and OPTUS-B3 constitutes the space segment of the Australian satellite communications system. They are in geostationary orbits. B1 was launched in 1992 and is at longitude 160°E. B3 (1993) is at 156°E. B2 crashed after launch. Each contains a 20cm x 18cm tray of 14 solid cubes of Herseus fused silica, Amasil grade. Their front faces are tri-roundular with inscribed diameter 38 mm coated with indium tin oxide (ITO) over an anti-reflection dielectric layer. Their rear faces are also coated with ITO and have dihedral angles of 0".8 (James et al, 1990; Luck, 1994). The cross-section of each array is $\sigma_O = 46 \times 10^6$ m^2 (Arnold, 2006).

GPS-35 and GPS-36 each host trays of 32 solid hexagonal cubes 27 mm across with aluminium-coated rear faces. The cross-section of each array is $\sigma_G = 20 \times 10^6$ m^2 (Arnold, 2006). The theoretical ratio of cross-sections is therefore $\kappa = \sigma_G/\sigma_O = 0.43$.

Experimental Method

The method was to range to a pair of satellites, one Optus and 1 GPS, in "bursts" in rapid succession while the selected GPS satellite was "close" to the Optus satellite. During each burst, the Neutral Density (ND) filter was adjusted so that returns were just extinguished. The measurement was the ND value at extinguishment. The UTC, ND setting and GPS elevation angle were recorded at that instant. This method relies on the assumption that the photon detection threshold of the detector is both significant and constant.

"Close" means within a few degrees (<10°) in elevation, to minimize variations in atmospheric attenuation, and also in azimuth to minimize cloud attenuation variation. A "burst" was just long enough to optimize the pointing for maximum return rate, then to adjust the ND until extinguishment, ideally less than 5 minutes. Then a burst was done on the other target.

Observations were made on the 1.8 metre space debris-tracking telescope STRK (7826) adjacent to Stromlo SLR at wavelength 1064 nm, power 2-12 W at 50 Hz.

Data Reduction

Define "brightness" B as the return signal strength (e.g. photons/sec at the detector) when pointing is optimized, and let B_e be the brightness at extinguishment so that it corresponds to the detection threshold. B_e is assumed constant. Let P be the measured average power, effectively equivalent to energy per shot since pulse-width, fire rate etc. are constant. Also let N be the transmission through the ND filter, T be one-way atmospheric transmission, R be the range from station to satellite, and S be the actual array cross-section. Then:

$$B = \alpha P N T^2 . S/R^4$$

where α is a proportionality constant. The observed ratio of cross-sections is then:

$$k = S_G/S_O = (R_G/R_O)^4 . P_O N_O T_O^2 / P_G N_G T_G^2$$

where subscripts G and O refer to GPS and OPTUS respectively. We used $N = 10^{-ND}$ where ND is the Neutral Density wheel setting, and:

$$T = \exp[-0.21072\exp(-h/1.2)/\sin E]$$

where *h* is height above sea level (0.8 Km for Stromlo) and *E* is target elevation angle (Degnan, 1993). The two-way transmission is illustrated in Fig.1.

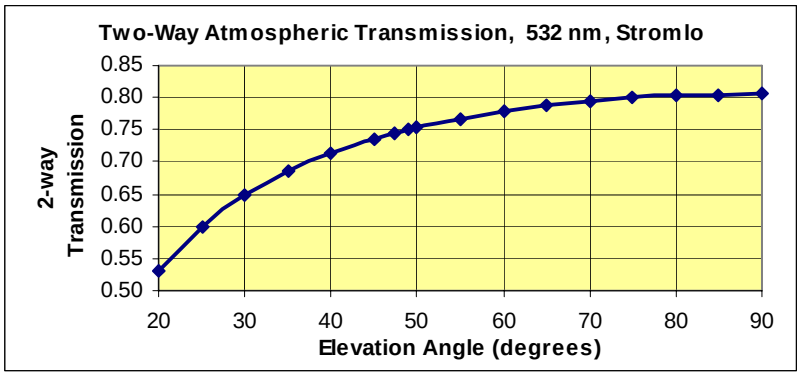

***Figure 1**: Standard atmospheric transmission as a function of elevation angle, Stromlo*

A "standardized brightness" V can be defined for a satellite observed on a given ranging system, as if there was no atmosphere and no ND filter and the transmitted power was 1, normalized to the detection threshold. Thus:

$$V = B_e/PNT^2 \quad \text{and hence} \quad S=R^4V/\alpha.$$

The ratio $\beta = V_G/V_O$ gives the relative standard brightness. Its expected value with R_O = 37180 km (B3, nominal) and RG = 20931 km (GPS36, typical at 49° elevation) is β = 4.28.

Results

Measurements made on 4 clear nights in May 2006 are shown in the Table 1. The column R_G/R_O is the ratio of range (Stromlo to GPS) relative to range (Stromlo to OPTUS). Column S is the cross-sections in square metric (but otherwise arbitrary) units, and column V the standardized brightnesses. There are huge variations, so the greatest and least values of S_G and of S_O were discarded, as were those of V_O and V_G, yielding mean values of:

$S_G = 14.2$ $V_G = 145.8$

$S_O = 34.6.$ $V_O = 34.6$

The ratios of averaged observed cross-sections, and of standardized brightnesses, are:

$S_G/S_O = 0.41$ $V_G/V_O = 4.2.$

The observed cross-section ratio is remarkably close to the predicted $\kappa = 0.43$ given above. The observed brightness ratio similarly is also remarkably close to the predicted $\beta = 4.28$.

Conclusion

It may be that this excellent result is a fluke, but we certainly did not continue observing until we got the right answer! It suggests that this technique might indeed be viable for determining relative cross-sections of retroreflector arrays in actual orbit, provided that a sufficient number of measurements are taken.

***Table 1**: Summary of observations and resulting cross-sections. Optus cross-sections are in green. Rejected outliers are flagged in the right-hand column.*

Date	UTC		Sat	R/R(Opt)	El	P	ND	T	V	S	Rej
May-06	hh	mm			(deg)	(Watts)		(1-way)			
10	9	50	GPS36	0.544	75.9	9	2.75	0.894	78.10	6.84	
	11	2	B1	1	47.4	9	2.15	0.863	21.06	21.06	
	11	9	GPS36	0.598	39.5	9	0.50	0.844	0.49	0.06	*
	11	26	B3	1	48.9	9	4.00	0.866	1480.67	1480.67	*
13	11	0	B3	1	48.9	2	2.00	0.866	66.63	66.63	
	11	10	GPS 36	0.610	40.9	2	3.00	0.848	695.81	96.34	*
	11	20	B3	1	48.9	2	2.00	0.866	66.63	66.63	
15	9	20	B3	1	48.9	12	3.00	0.866	111.05	111.05	
	9	33	GPS36	0.545	85.0	2	1.90	0.897	49.35	4.35	
	9	42	B3	1	48.9	2	0.90	0.866	5.29	5.29	
	9	59	GPS36	0.556	63.6	2	2.30	0.886	127.02	12.14	
	10	3	GPS36	0.560	61.7	2	2.90	0.884	507.80	49.94	
	10	9	B3	1	48.9	2	0.60	0.866	2.65	2.65	
	10	19	GPS36	0.568	55.6	2	2.40	0.877	163.25	16.99	
	10	26	B3	1	48.9	2	0.80	0.866	4.20	4.20	
	10	32	GPS36	0.580	46.2	2	2.10	0.861	84.95	9.61	
	10	42	B3	1	48.9	2	0.80	0.866	4.20	4.20	
	10	44	B3	1	48.9	2	1.00	0.866	6.66	6.66	
	11	0	GPS36	0.603	33.6	2	1.00	0.822	7.39	0.98	
16	9	28	GPS36	0.546	74.8	12	3.50	0.894	329.76	29.31	
	9	44	B3	1	48.9	12	0.60	0.866	0.44	0.44	*
	10	0	GPS36	0.559	62.0	2	1.70	0.885	32.02	3.13	
	10	27	B3	1	48.9	12	2.80	0.866	70.07	70.07	
	10	35	GPS36	0.583	44.4	2	1.20	0.857	10.80	1.25	
	10	42	B3	1	48.9	12	2.30	0.866	22.16	22.16	

Further Suggestions

- Repeat the experiment at 532nm wavelength.
- Extend to GLONASS, GIOVE, ETS-VIII, LARES and others.
- The GPS array is theoretically about 1500 times brighter than Apollo 15, corresponding to ND 3.2, so if GPS is still observable at a station with this setting then LLR should also be acquirable.

- Systems having readouts for return signal strength would be well suited to doing an equivalent of this experiment, more easily. In fact, by using our method as well as their own, our method could be tested.
- Similarly, comparisons of return rates in controlled experiments might assist in validation of the technique.

References

[1] Arnold, D.: Private communications, 2006.

[2] Degnan, J.J.: "*Millimetre Accuracy Satellite Laser Ranging: A Review*", in "Contributions of Space Geodesy to Geodynamics: Technology", David E. Smith & Daniel L. Turcotte (Eds), Geodynamics Series Vol.25, American Geophysical Union, Washington D.C., esp. pp.139-140 (1993)

[3] James, W.E., W.H. Steel & Evans, N.O.J.L: "*Design and Testing of a Cube-Corner Array for Laser Ranging*", SPIE Vol.1400 Optical Fabrication and Testing, p.129 (1990)

[4] Luck, J.McK. & J.R. Woodger: "*Laser Ranging Support for TV Time Transfer Using Geostationary Satellites*", Proc. 8th European Frequency and Time Forum, Technical University Munich, March 9-11, 1994.

Spherical Glass Target Microsatellite

V.D. Shargorodsky, V.P. Vasiliev, M.S. Belov, I.S. Gashkin, N.N. Parkhomenko

1. Institute for Precision Instrument Engineering, Moscow, Russia.

Contact: www.niipp-moskva.ru

Abstract

A new SLR target microsatellite based on the optical Luneberg lens concept is now undergoing ground testing. It will be launched from the carrier spacecraft METEOR-M next year, and will be the first autonomous retroreflector satellite of this type, providing an extremely low target error.

Some parameters are presented of the microsatellite and its orbit, as well as far-field diffraction patterns measured on test bench.

Introduction

Most of the current SLR target satellites are spherical structures carrying a number of corner cube retroreflectors; with the rapid progress in SLR precision during the last decades, some disadvantages of such targets, being insignificant during the first years of SLR development, became increasingly more significant with the passing years.

The disadvantages are:

- It is difficult to obtain target errors less than 1 mm if return signals come from several cube corners having different positions relative to the CoM (Center of Mass) of the satellite.
- Even if the "one direction - one reflector" principle is used (e.g. in the WESTPAC or LARETS satellite design), the active retroreflector position varies relatively to the CoM, and the cube corner internal delay time also varies when the active retroreflector moves away from the line connecting the SLR system with the satellite CoM.
- The return signal strength varies significantly with the satellite rotation.
- The satellite shape is not an ideal sphere, especially for a design using the "one direction - one reflector" principle (WESTPAC, LARETS).
- Interaction with the Earth magnetic field (due to eddy currents induced in the massive metal body): slow-down of spinning, some disturbance of orbital motion.

There is a way to overcome the above difficulties. Instead of a multitude of corner cube prisms mounted on a spherical metal body, the target may be a single spherical retroreflector made of glass.

The initial idea was to use a device similar to the Luneberg lens proposed in 1944 and used in some radio-frequency systems (Figure 1). A planar electromagnetic wave coming from any direction is there focused on opposite surface of the spherical lens and if this surface is a reflective one, the device acts as a retroreflector.

Unfortunately, there are currently no suitable optical materials for correct implementation of such a device operating in the optical waveband.

A possible solution is using of a ball lens made of a glass with an index of refraction exactly equal to 2 (Figure 2). However, it requires a special extra-dense glass of a

high optical quality; this is currently a very hard task. Moreover, calculations show that only a small part of the ball aperture may be effectively used because of the spherical aberration.

The first practical solution was a two-layer glass ball, where the inner part is made of a flint glass having a relatively large index of refraction (1.75), while the outer layer is made of a crown glass with a low index of refraction (1.47). Such a device has been implemented and successfully tested showing acceptable retroreflector parameters [1] (Figure 3).

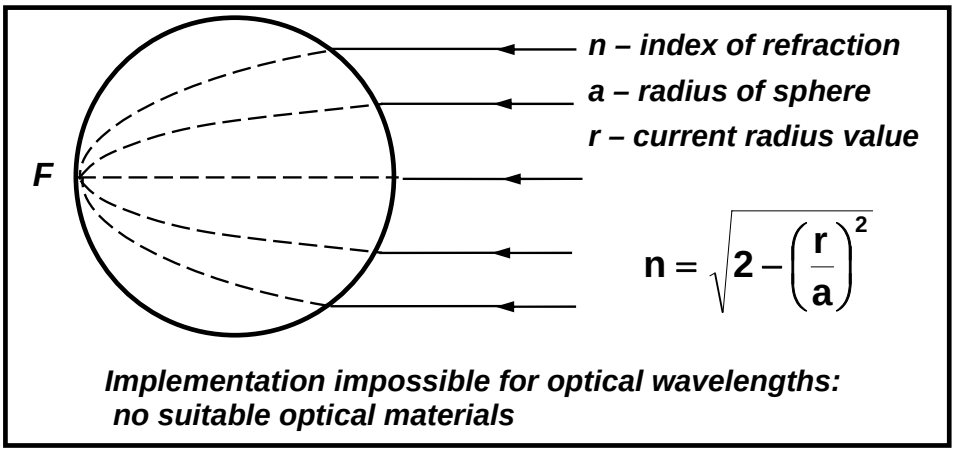

Figure 1. *Luneberg lens principle*

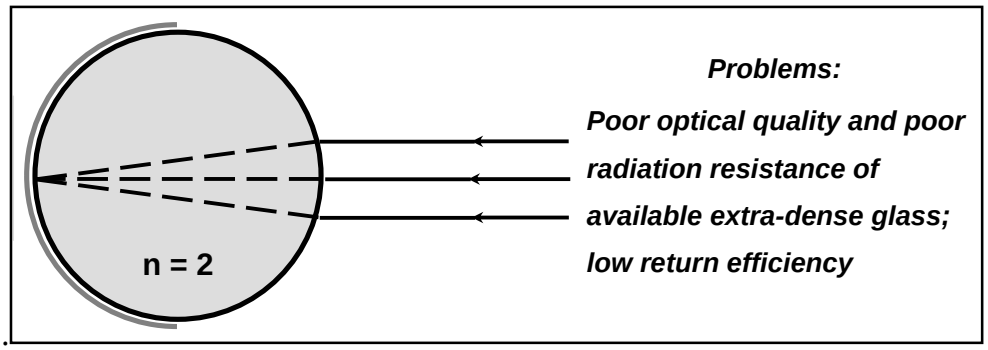

Figure 2. *Ball lens made of glass with index of refraction n = 2*

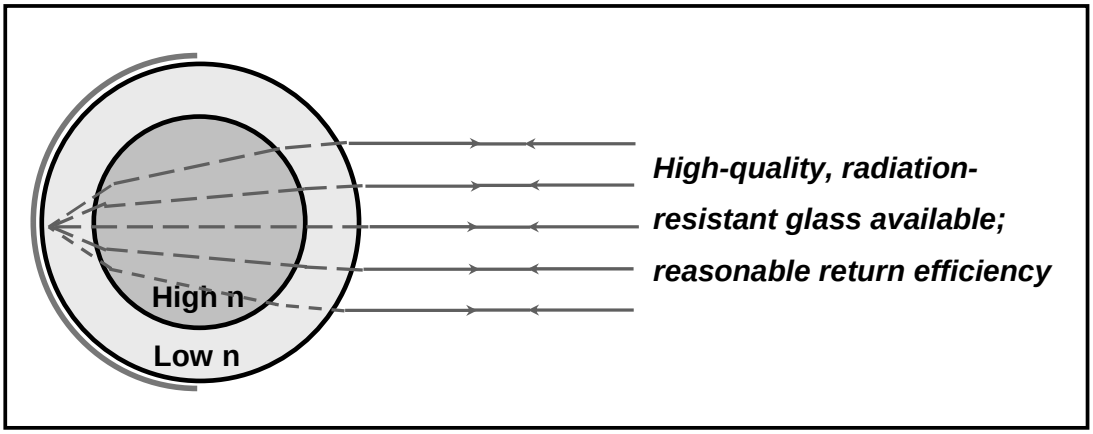

Figure 3*. Spherical retroreflector: a two-layer ball lens*

An experimental 60-mm-diameter spherical retroreflector of this type [2], after being tested in laboratory conditions, has been 10 December 2001 launched into space on board of the METEOR-3M(1) satellite having a 1018.5-km-high circular orbit (Figure 4). During four years of operation, the spherical retroreflector provided precision orbit determination for the SAGE-III experiment.

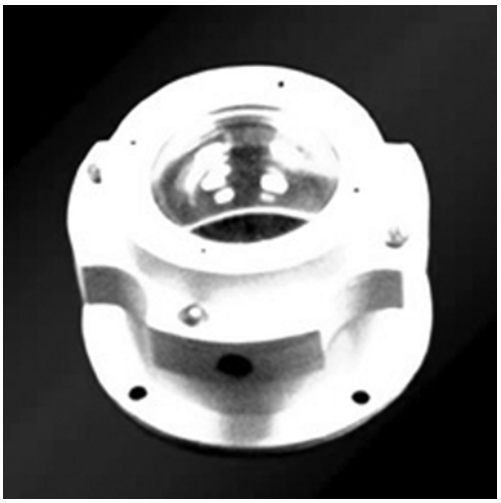

Figure 4*. An experimental 60-mm-diameter spherical retroreflector, launched into space on board of the METEOR-3M(1) 10 December 2001*

The lidar cross-section of this target was low (about 10^4 sq.m at the initial phase of flight), making SLR observations difficult and even impossible for a large part of the ILRS network stations.

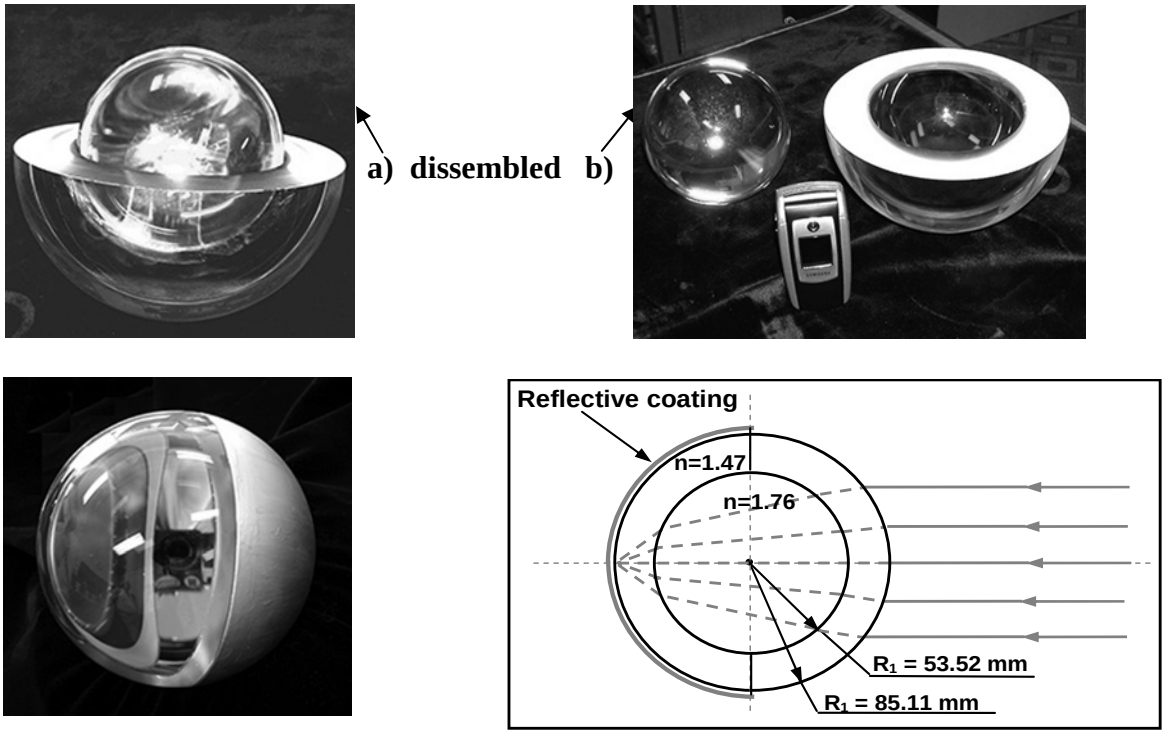

Figure 5. *17-cm-diameter spherical retroreflector*

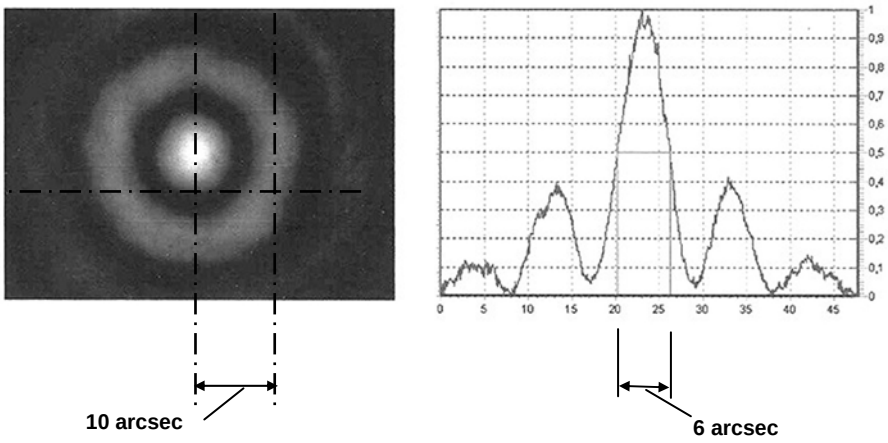

Figure 6. *Far-field diffraction pattern*

We have therefore developed and fabricated a medium-size (17 cm in diameter) spherical retroreflector of this type, which can be used as an autonomous SLR target.

Figure 6 shows the far-field diffraction pattern of this device measured on a test bench. It can be seen from the picture, that most of the return signal energy is in the first-order side lobe (the product of its amplitude and solid angle is more than that of the center lobe).

It is intended to launch this device as an autonomous SLR target, as a piggyback load on the Meteor-M spacecraft. The basic parameters of this micro-satellite are shown in Table 1.

Table 1. *Zero-signature spherical retroreflector micro-satellite*

Microsatellite parameters	
Diameter	17 cm
Mass	7.45 kg
Cross-section	~100,000 sq.m at λ=532 nm
Current status	
Return pattern measurement under varying ambient conditions	
Separation system development	
Mission	
Carrier satellite	METEOR-M
Carrier satellite parameter	Height: 835 km (circular) Inclination: 99.7°
Planned launch date	Late 2007

The separation system (now under development) should provide a spin rate of at least 6 rpm, while the spin axis lies in the plane dividing the ball lens surface into the coated and uncoated parts.

SLR targets of this type may be improved in the following ways:

1. To increase the lidar cross-section, more than two layers of glass may be used. Calculations show that a three-layer ball lens may provide a significantly higher cross-section value than a two-layer one.
2. To provide operation on two widely separated wavelengths (e.g., 532 nm and 1064 nm), a design may be used shown in Figure 7. In the future, such an SLR-target may be attractive for minimization of the atmosphere refraction error using simultaneous two-wavelength ranging.
3. If (or rather when) super-dense optical glass with reflection index values ≥2 with good optical quality becomes available, it may be used for manufacturing of a ball-lens retroreflector microsatellite with a high mass to aperture cross-section ratio.

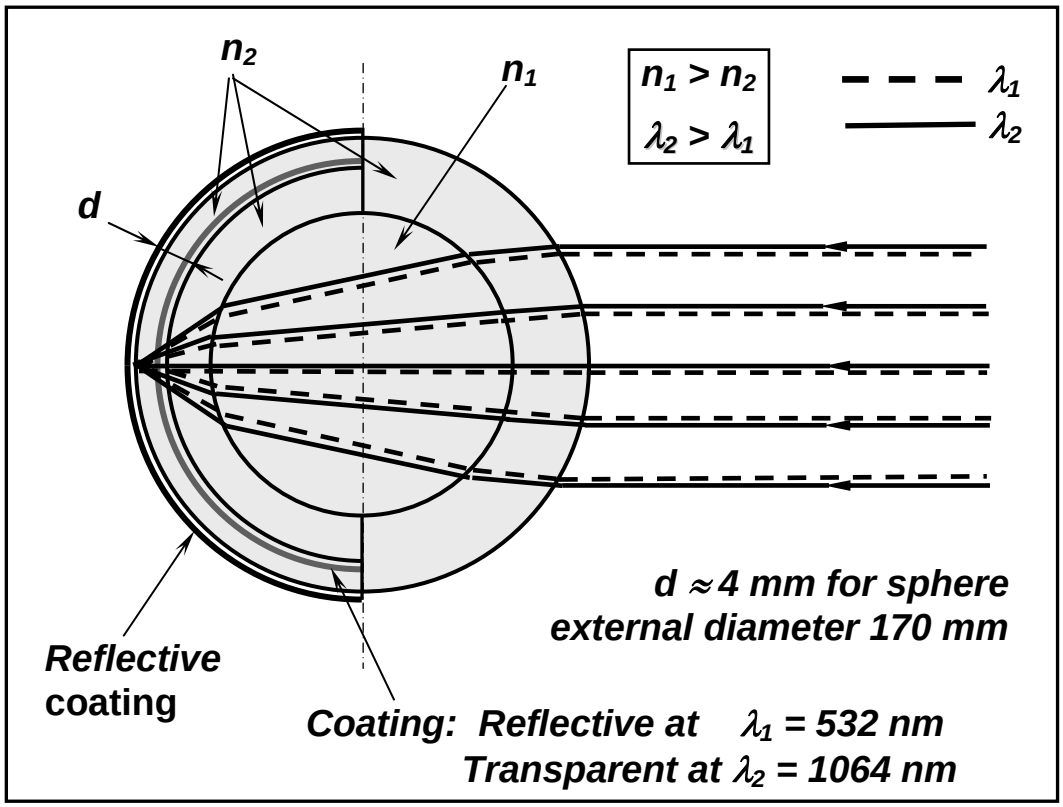

Figure 7. *Spherical retroreflector for operation at two widely separated wavelengths*

References

[1] Vasiliev V. P., Gashkin I. S., Belov M. S., Shargorodsky V. D., A New Approach to a Submillimeter SLR Target Design. Proceedings of 11th International Workshop on Laser Ranging, Deggendorf, Germany, Sep. 1998

[2] Shargorodsky V. D., Vasiliev V. P., Soyuzova N. M., Burmistrov V.B., Gashkin I. S., Belov M. S., Khorosheva T. I., Nikolaev E. A. Experimental Spherical Retroreflector on Board of the Meteor-3M Satellite. Proceedings of 12th International Workshop on Laser Ranging, Matera, Italy, 2000

OVERFLOW SESSION SUMMARY

Chair: Mike Pearlman

Andrew Dmytrotsa gave a paper on the recent upgrading of the Simiez SLR Station. Software and optics upgrades have improved data yield. The laser power supply was replaced with a loaner from the Katzively station after the on-site system failed. Upgrades continue with new servo drivers for the stepper motors.

Julie Horvath reported that the TLRS-4 system has been refurbished, upgraded, and transferred to a new site at Haleakala in Maui. The collocation with Moblas-7 at GSFC achieved closure to 1 - 2 mm and demonstrated full capability on both low satellites and LAGEOS. Operations are anticipated by the end of the year.

Nobuo Kudo gave a paper on "Using SLR, the GPS accuracy verification experiment of ALOS". Twelve selected stations from the ILRS network supported the GPS-SLR validation campaign from August 14 to 31, 2006. The satellite had a payload vulnerable to laser light and this campaign used the new restricted tracking procedures implemented by the ILRS network last year. The campaign showed that the offset between the GPS and the SLR orbits was within a few centimeters RMS, well within the mission requirement.

Hyung Chul Lim presented the "Korean Plan for SLR system development". He described the structure and activities of the Korea Astronomy and Space Science Institute (KASSI). KASSI is building two satellites STSAT-2 and KOMPSAT-5 to be launched in 2007 and 2009 respectively. Both will carry retroreflector arrays for POD. Korea now has about 80 GPS stations and three VLBI stations and plans to build a mobile SLR station and a Fundamental Station that would include a permanent SLR. The development period for these systems will be about 2 years for the mobile system and 5 years for the Fundamental Station. In the meantime, the Chinese will provide a mobile system for use at a site in Korea for some period starting in 2007 to support the STSAT-2 satellites and ILRS requirements.

You Zhao reported on the "Fulfillment of the SLR daylight tracking of Changchun Station". The main thrust of the program is to improve orbit predictions, provide better filtering of sky noise, increase the alignment of the transmitting and receiving beams, and reduce stray light. The plan includes improved spatial, timing, and spectral filtering. The hardware and software improvements are nearly ready for testing. Work had been delayed because the Changchun Station was selected as the main Chinese tracking support for GIOVE-A, and tracking on this satellite took highest priority, but system testing is anticipated by early 2007.

Vladimir Glotov presented "GLONASS status updates; MCC activity in GLONASS Program". The paper reviewed the background and mission of the GLONASS Program which is building toward a 24 satellite complex in the 2009 timeframe. The International GLONASS – Pilot Project (IGLOS-PP) is a pilot service of the IGS to track and analyze data from the satellite constellation. The ILRS provides very important support for GLONASS by tracking three of the constellation satellites as designated by IGLOS. The need will continue and hopefully the tracking will increase. GLONASS provides a "colocation in space", a key tool to strengthening the reference frame. IGLOS-PP demonstrates the ability of IGS to accommodate other microwave satellite systems.

Current Status of ''Simeiz-1873'' Station

A.I. Dmytrotsa[1] , O.A. Minin[1], D.I. Neyachenko[1]

1. SRI Crimean Astrophysical observatory, Crimea, Ukraine.

Contact: dmytrotsa@gmail.com

Abstract

The SLR station "Simeiz-1873" was founded in 1989. After modernization in 2000 we have increased the amount of ranging data by approximately three times. With this modernization we have probably reached a limit of the equipment, due mainly to the shortcomings of the laser transmitter. Independent analysis groups have shown stability problems in of our data.

A permanent GPS receiver was installed at the site in 2000. "Simeiz-1873" became a permanent IGS station (GPS-CRAO) in 2004. Recently in our station began processing GPS data using the GLOBK/GAMIT software. We have obtained and analyzed data for the period 2002-2005.

Introduction

Regular satellite laser ranging started in our observatory in 1976 as an INTERKOSMOS Station with a laser system installed by K. Hamal on a KRIPTON telescope. In 1988 the Crimean Astrophysical Observatory installed a new station (near the old station). Colocations with the IFAG MLTRS system were conducted in 1991.

A modernization program was undertaken in 2000 under a CRDF grant (thanks for M. Pearlman and D. Nugent). New angular encoders and a new time interval counter were installed. After modernization we increased the amount of ranging data by approximately three times (Fig.2).

A permanent GPS receiver has been operating near “Simeiz-1873” since 2000. In 2004 it became an IGS site “GPS-CRAO” (Fig.3, right). The “Simeiz-1873” is a one of four Ukrainian SLR stations. (GLSV-1824, Lviv-1831, KTZL-1893)

Current status

Modernization of station proceeds. It is necessary to carry out the following items:

- Implementation of the new CPF prediction format into the software;
- installation of a new modern control system of engines;
- updating of optical system of a telescope for a new calibration target and replacement of a prism with a mirror;
- ground calibration tests with the new target at 77m east;
- continue processing GPS data with GAMIT/GLOBK.

Ranging and GPS proceeding

In 2006 we suffered appreciable downtime due to two failures of the laser power unit. The Katzively station (1893) has installed a new laser systems and loaned their old power unit to us. The loaned unit also failed and required considerable, time-consuming repair.

As you can see in Fig.2, data has increased with the modernization activities, but we have probably reached the limit with our equipment; the laser transmitter is 18 years

old! The second problem is in tracking. In 2006 we purchased new servo-drivers for the stepper motors and we hope that this will help improve our tracking capability.

Figure 1. *SLR-1873. General view.*

Table 1. *Main elements.*

Element	Description
Mount	Alt-Az. 1m mirror.
Angular encoders	FARRAND CONTROLS, 0.4”
Time interval counter	SR620
PMT	H6533
Time & Freq standard	TC-74, sec. from GPS.
Laser	350 ps, 5Hz. (18 years old)
Software	GUI on a JAVA, server on a C++, low level modules on a C. LINUX.
Ephemeredes	CPF, (on a F77).

Analysis by two independent groups shows that the stability of the station SLR data still needs considerable work. Results from the Ukrainian Center of Determination of the Earth Orientation Parameters (Bolotina, 2006) are shown in fig.3 (left). Similar results were found by S. Schillak by processing our LAGEOS ranging data for period 1999-2003. (See Schillak, 2004).

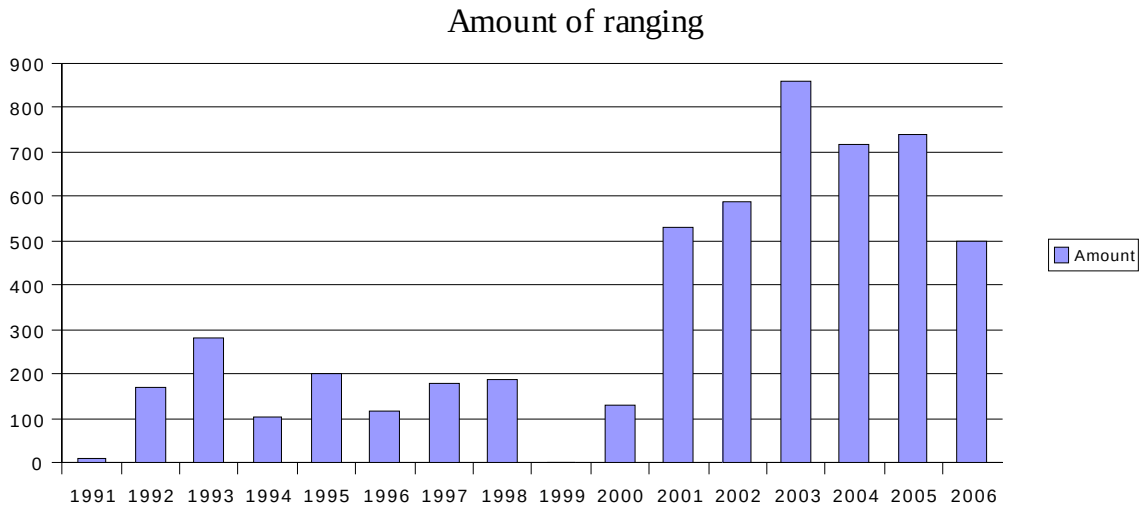

Figure2. *Amount of ranging from 1991 to 2006.*

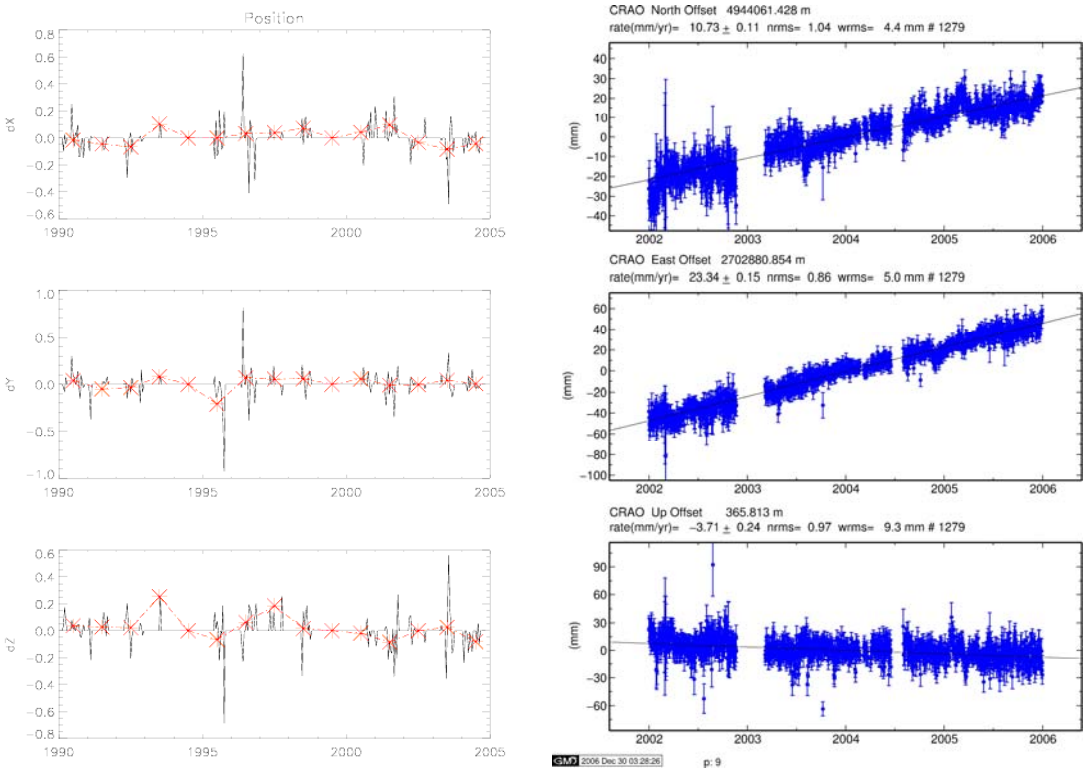

Figure 3. *Geocentric coordinates (delta from mean value) obtained by SLR (left) for 1991-2005 (red is a mean by year), meters; topocentric coordinates (delta from mean value) obtained by GPS (right) for 2002-2006, mm*

We have also processed GPS data with the GAMIT/GLOBK software on our station (fig.3, right). As you see, results from our SLR location are not comparable with results received by GPS. Also on the GPS results a trend is evident. It not detectable in the lower precision SLR data.

Summary

The analysis of results has shown that we still have stability problems with the Simiez ranging systems; likely causes of the problems are the old laser transmitter, inadequacies in the calibration system, and greater breaks in ranging to LAGEOS because of equipment failure and poor weather.

The basic directions of work will be: creation of a new telescope mount model; better operations procedures, and hopefully, replacement of the laser on new.

Acknowledgments

We acknowledge and thank to Stanislaw Schillak and to Olga Bolotina for processing our SLR results. We acknowledge and thank the Local Organize Committee of the 15th Workshop for financial assistance.

References

[1] Bolotina, O., Medvedskij M, Investigation of the stability of the Ukrainian SLR network, preprint, 2006

[2] Schillak, S. Determination of the station coordinates for quality control of the satellite laser ranging data. p387-394, Proc. 14th International Laser Ranging Workshop.

Overview and Performance of the Ukrainian SLR Station "Lviv-1831"

Martynyuk-Lototsky K., Blahodyr Ja., Bilinskiy A., Lohvynenko O.

1. Astronomical Observatory of Ivan Franko National University of Lviv, Ukraine, 79005, Lviv, Kiril and Mephodij St.8.

Contact: langure@mail.ru

Abstract

Satellite laser ranging station "Lviv-1831" was found in 1998. In August 2002, it was registered as an associate SLR station in the ILRS. It is also a member of the Ukrainian network of UCEOP (Ukrainian Center for Earth Orientation Parameters).

The station is based on the following equipment: 1 m telescope TPL-1M on alt-azimuth mounting, an SL-212 laser with 150 ps pulses at 532 nm and a repetition rate 5 Hz, a Latvian A911 timer with internal precision of 40 ps. The current fire-receiving system can only operate at ranges above 900 km [1].

During 2005 the station ranged to 138 passes of LAGEOS with an RMS of 50 mm. The short term stability over 2005 was about 35 mm, and the long term stability was 25 mm.

At present, the station team is testing a new receiver with a Hamamatsu module H6780-20 PMT, a neutral density filters wheel for return signal strength control, and a new electromechanical shutter. Implementation of these improvements in the system should increase the performance and the accuracy of ranging results by a factor of about three. The next step in station modernization is the improvement of fire-receiving system for ranging to very low satellites at altitudes about 500 – 900 km.

References*:*

[1] A.Bilinsky, Ya.Blagodyr, A.Lohvynenko, S.Ternavska Station reports: Lviv, Ukraine // International laser Ranging Service 2003-2004 Annual Report, June 2005, pp.B-26 – B-27.

Results of the TLRS-4 / moblas-7 Intercomparison test

Julie Horvath[1], Maceo Blount[1], Christopher Clarke[1], Howard Donovan[1], Craig Foreman[1], Michael Heinick[1], Anthony Mann[1], Donald Patterson[1], Dennis McCollums[1], Thomas Oldham[1], Scott Wetzel[1], David Carter[2]

1. Honeywell Technology Solutions Inc. 7515 Mission Dr. Lanham, MD USA 20706
2. NASA Goddard Space Flight Center, Code 453, Greenbelt, MD, USA 20771

Contact: julie.horvath@honeywell.com

Abstract

In March 2005, Honeywell Technology Solutions Inc. (HTSI) was tasked to restore the Transportable Laser Ranging System 4 (TLRS-4) to operational capability. This was in preparation for replacement of the Hollas SLR system, located on Mt. Haleakala that had ceased operations in 2004.

Introduction

The TLRS-4 had ended routine operations following a successful tracking campaign in Richmond, Florida on May 22, 1995 and was held at the Goddard Geophysical and Astronomical Observatory (GGAO) at the NASA Goddard Space Flight Center in a semi- operational status until 1999. Less than six months after beginning the restoration of the TLRS-4, the system was providing quality ground and satellite tracking. This culminated in the validation of the TLRS-4 by a direct intercomparison of TLRS-4 with the Network Standard, Moblas-7. The TLRS-4 / Moblas-7 Intercomparison occurred from August 1st – September 6th, 2005. Results of this test were presented at a NASA Operational Readiness Review on September 15th, 2005 to a panel of ILRS members and other NASA management.

This paper provides a description of the work performed to restore the TLRS-4 to operational status, a description of the intercomparison test, the analysis of simultaneous satellite tracking data along with ground target tests and the results of the test.

History

The TLRS-4 system has a history that dates back to the early 1980's when two identical TLRS systems (Transportable Laser Ranging Systems) -3 and -4, were originally designed and built by NASA. These systems were designed as compact and transportable,

and were deployed to many diverse locations for short (2-6 months) SLR tracking campaigns. HTSI, as NASA's mission contractor, was tasked to maintain, operate, and deploy each system for these tracking campaigns. TLRS-4 was assigned to North American locations.

In 1995, after a major decrease in the NASA SLR budget, TLRS-4 returned to GSFC. Since 1995, HTSI maintained the system in caretaker status at the GGAO under NASA SLR Mission contract. HTSI maintained TLRS-4 while supporting all other NASA SLR systems, as well as operating two systems at the GGAO and Monument Peak, CA (Moblas-7 and Moblas-4). TLRS-4 was frequently used as a test-bed to support SLR engineering projects, and was used for spare parts to support operational stations. In March of 2005, NASA tasked SLR to return the TLRS-4 to operational status. The system required a major engineering effort to return the system to regular operations.

Repairs/Upgrades

The TLRS-4 system's pre-upgrade status was that of an inoperable system missing both hardware and software upgrades that had been installed into all other systems in the NASA Network. Major repairs and upgrades were required for every major subsystem of the TLRS-4. The Laser subsystem required new oscillator and amplifier heads, a solid state pulse slicer, a laser interlock system, a laser collimation lens, dye pump power supply, calibration transmit filter, laser bracket, and a laser warning light. The telescope/optics subsystem required a new 10Å Daylight Filter, a complete upper deck upgrade, and a diassembly and cleaning of the telescope. The transmit/receive subsystem required a T/R Switch motor and synch board, installation of the Photek MCP upgrade, and installation of a low-loss receive cable. The computer subsystem required a fully upgraded processing computer, a new administration computer, modifications to software for the controller computer, and upgraded Internet communications. The console subsystem required a new trackball board and microprocessor, a new tracking scope, and a new HP5370B Time Interval counter. The timing subsystem required a modification to the Time Code Generator for 4pps, the modification for 4/5 pps Auto switch, and updated CNS Clock Software. The facility subsystem was upgraded with dome control sensors, dome weather protection, a new remote operated dome shutter, and a complete refurbishment of the Instrumentation van and Support trailer. The safety subsystem was completely overhauled and coordinated through GSFC Code 250 for laser safety compliance.

System Operations Verification Tests (SOVT)

In July 2005, after all system upgrades and repairs were completed, HTSI began SOVT testing of the TLRS-4 system. SOVT Tests are performed subsequent to each relocation and prior to any laser system beginning operational support. SOVT's are comprehensive testing that ensures that the system is ready for operations by addressing every major and minor subsystem. These include tests for verifying station communications; station timing; mount level and dome control; interface of the tracking computer, mount, and data interface system; processing computer; performance of the data measurement

system; operations of the Continuum Laser system; safety interlock system; telescope pointing; star calibration performance; ground tracking; and controller computer operations. All SOVT Testing was successfully completed on July 15th, 2005.

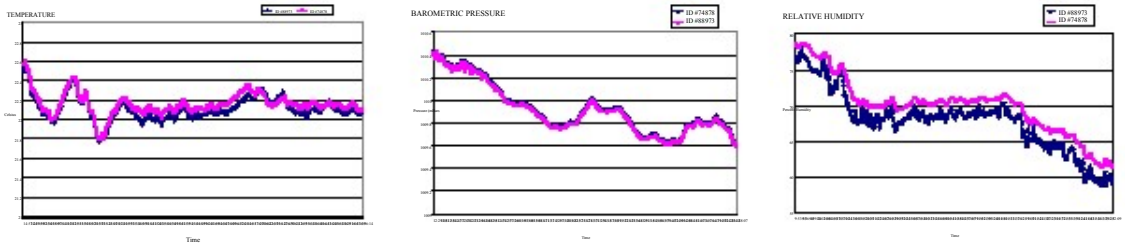

System Validation

The NASA SLR program validates newly built, or newly upgraded SLR systems with an Intercomparison or Collocation Technique developed at NASA and HTSI in the 1980's. Designed to directly compare an upgraded SLR system to an established SLR tracking system (Moblas-7 at GGAO currently operates as the NASA Global Standard SLR system), this technique characterizes and verifies the operational performance and laser ranging capabilities of the upgraded system prior to establishing routine operations. During this project, system performance of the TLRS-4 system was compared, relative to that of Moblas-7 with an Intercomparison between the two systems. Both datasets were also compared against known orbits. The Intercomparison was achieved by using NASA SLR- developed Intercomparison software packaged called Polyquick and orbit comparisons were achieved by using the NASA-developed GEODYN software package. Polyquick was developed to identify laser system ranging anomalies by utilizing intercomparison geometry to isolate station dependent, systematic ranging errors from other external sources of systematic errors such as refraction and orbital errors. Directly comparing these two stations will provide a reliable technique to accurately calibrate the TLRS-4's SLR performance at the centimeter and sub-centimeter accuracy level.

A pre-intercomparison phase was established to ensure that all prerequisites for the Intercomparison were completed. Prerequisites included a first order system survey to establish the DX, DY, DZ components between the two systems, simultaneous ground tests to establish stability and dependency issues, simultananeous satellite tracking to establish performance, comparison of the two systems MET systems, comparison of the two systems station timing, and finally a configuration freeze.

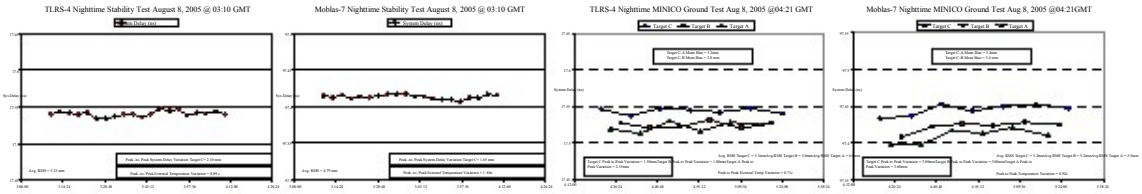

STATION	LATITUDE	LONGITUDE	HEIGHT(m)
7105	39° 01′ 14.17743″ N	76° 49′ 39.69784″ W	19.194
7130	39° 01′ 15.27139″ N	76° 49′ 38.82201″ W	18.632

On August 1st, 2005, the configuration of both the Moblas-7 and TLRS-4 systems were frozen for the formal Intercomparison phase of the TLRS-4 Return to Operations Project. An Intercomparison test consists of simultaneous satellite and ground tracking where an evaluation is done for data quantity and data quality, as well as simultaneous data analysis to establish any biases or dependencies between the two systems. The Moblas-7, the NASA Network standard, was established as the base system because of its known performance, and was to be tested against the unknown TLRS-4 system.

Intercomparison Requirements:

– Data Quantity and Quality:

– Minimum of 15 simultaneous Lageos-1 or Lageos-2 passes must be tracked during the Intercomparison period.

– Minimum of 20 low orbital satellite passes will be tracked during the Intercomparison period.

– Both systems must achieve the specified data quality standards for any pass to be qualified for the test pass total. The quality criteria are as follows:

System Calibration RMS (mm) Calibration Shift (mm)	Lageos RMS (mm)	LEO's RMS (mm)
TLRS-4< 7.0< 10.0	< 15.0	12.0 - 30.0
Moblas-7< 7.0< 10.0	< 15.0	12.0 - 30.0

Data Analysis Requirements:

– All systematic biases between the TLRS-4 and Moblas-7, operating under normal conditions will be less than ±15 millimeters

– Only passes with 30 full-rate observations for Moblas-7 are qualified for Intercomparison data analysis

– Minimum of 10 simultaneous points per Polyquick bin per station.

– Analyses by Polyquick will be performed for each simultaneous pass taken during the Intercomparison test period.

- Range Difference Computation
- Bias Tests
  - – Range-dependent Range Bias Test
  - – Range-rate dependent Bias Test
  - – Elevation Dependent Range Bias Test
  - – Azimuth Dependent Range Bias Test
  - – Energy Dependent Range Bias Test
  - – Test for Long Term Mean Range Bias Stability
  - – Test for Diurnal Effects
  - – System Delay Range Bias Test
  - – Sky Coverage Test
  - – Orbital comparison Test

- Data Analysis:

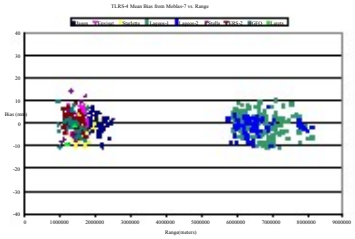
TLRS-4 Mean Bias from Mobllas-7 vs. Range
Range(meters)

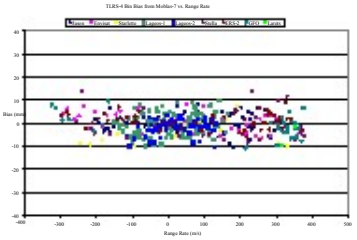
TLRS-4 Bin Bias from Mobllas-7 vs. Range Rate
Range Rate (m/s)

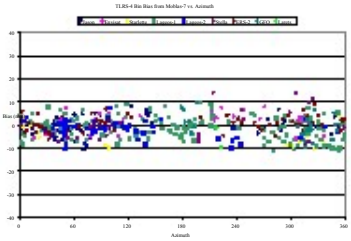
TLRS-4 Bin Bias from Mobllas-7 vs. Azimuth
Azimuth

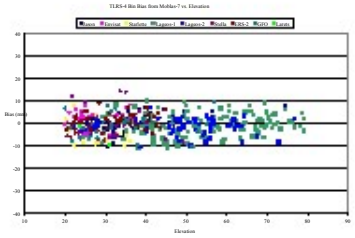
TLRS-4 Bin Bias from Mobllas-7 vs. Elevation
Elevation

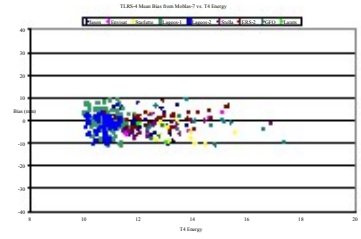
TLRS-4 Mean Bias from Mobllas-7 vs. T4 Energy
T4 Energy

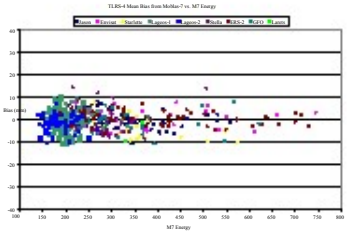
TLRS-4 Mean Bias from Mobllas-7 vs. M7 Energy
M7 Energy

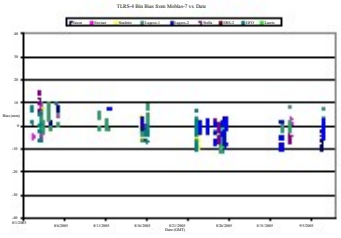
TLRS-4 Bin Bias from Mobllas-7 vs. Date
Date (GMT)

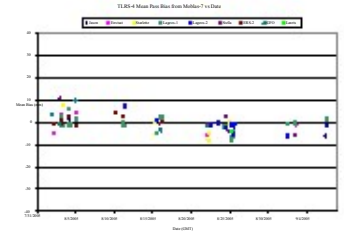
TLRS-4 Mean Pass Bias from Mobllas-7 vs Date
Date (GMT)

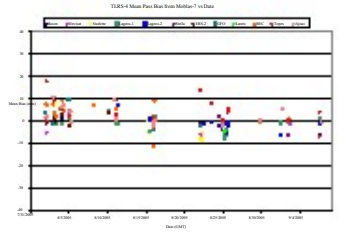
TLRS-4 Mean Pass Bias from Mobllas-7 vs Date
Date (GMT)

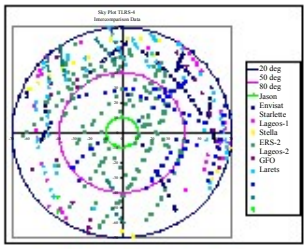
Sky Plot TLRS-4
Intercomparison Data
20 deg
50 deg
80 deg
Jason
Envisat
Starlette
Lageos-1
Stella
ERS-2
Lageos-2
GFO
Larets

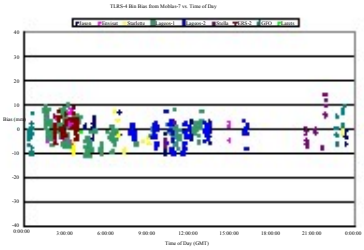
TLRS-4 Bin Bias from Mobllas-7 vs. Time of Day
Time of Day (GMT)

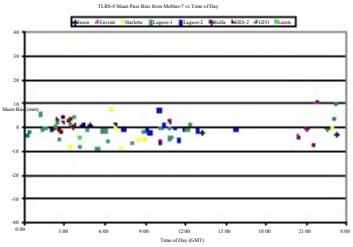
TLRS-4 Mean Pass Bias from Mobllas-7 vs Time of Day
Time of Day (GMT)

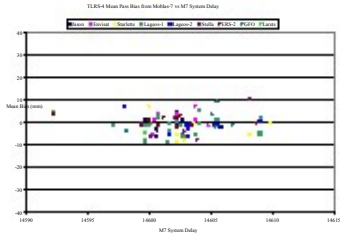
TLRS-4 Mean Pass Bias from Mobllas-7 vs M7 System Delay
M7 System Delay

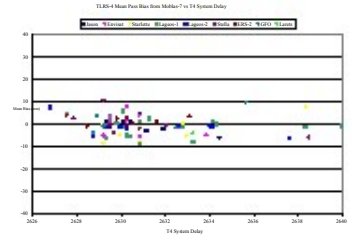
TLRS-4 Mean Pass Bias from Mobllas-7 vs T4 System Delay
T4 System Delay

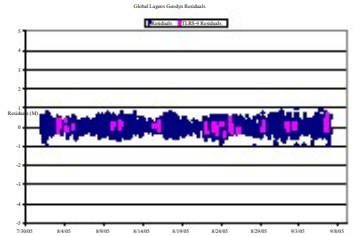
Global Lageos Geodyn Residuals
Residuals
TLRS-4 Residuals

Intercomparison				
TOPIC	TLRS-4	Moblas-7	TLRS-4 Results	Moblas-7 Results
Minimum Simultaneous Passes				
Lageos-1 & Lageos-2	15	15	29	29
LEO's	20	20	123	123
Fullrate Data RMS				
Calibration	≤ 7 mm	≤ 7 mm	5.44 mm	5.49 mm
Calibration Shift	≤ 10 mm	≤ 10 mm	0.31 mm	0.71 mm
Lageos-1 & Lageos-2	≤ 15 mm	≤ 15 mm	11.25 mm	9.17 mm
LEO's	≤ 12 - 30 mm	≤ 12 - 30 mm	16.11 mm	11.21 mm
Ground Test Delay Variations				
Stability Test	≤ 8 mm	≤ 8 mm	2.55 mm	1.73 mm
Extended MINICO	≤ 8 mm	≤ 8 mm	2.95 mm	2.13 mm
Intercomparison Bias				
TLRS-4 Mean Pass Bias from Moblas-7	± 15 mm		1.07 mm	
Lageos-1 & Lageos-2	± 15 mm		0.91 mm	
LEO's	± 15 mm		1.67 mm	

Results

The TLRS-4 / Moblas-7 Intercomparison produced some of the best intercomparison results ever achieved by a NASA system. The TLRS-4 system bias from Moblas-7 was 1.07 mm, far exceeding the ±15 mm requirement. The system exceeded every other intercomparison requirement and was declared an operational system after the NASA Operational Readiness Review on September 15, 2005. TLRS-4 was deployed to Maui, Hawaii on April 19th, 2006. It was then moved to the summit of Haleakala on September 7, 2006, and will return laser ranging to a critical global geographical position in the very near future.

The Accuracy Verification for GPS Receiver of ALOS by SLR

Nobuo Kudo, Shinichi Nakamura, Ryo Nakamura

1. Japan Aerospace Exploration Agency, 2-1-1 Sengen, Tsukuba-city, Ibaraki, 305-8505.

Contact : kudoh.nobuo@jaxa.jp / Fax: +81-29-868-2990

Abstract

The Advanced Land Observing Satellite (ALOS) provides precise geographical data for making global precise map. ALOS has a dual-frequency GPS receiver to determine geographic positions corresponding to points on satellite images. In order to confirm the orbit determination accuracy by GPS, we carried out a restricted laser ranging campaign with the support of the International Laser Ranging Service (ILRS). We found the GPS orbit agreed with the SLR orbit to within the resolution range of the SLR analysis.

Introduction

Recently, the positioning accuracy achieved by dual-frequency GPS receivers is within few dozens of cm. However we needed to verify the ALOS onboard GPS receiver because it was newly developed.

Overview of ALOS

Advanced Land Observing Satellite (ALOS), also called “DAICHI”, was launched from Tanegashima Space Center in Japan on 24 January 2006. ALOS performs earth observations at a high resolution, which is expected to contribute to a wide range of fields such as map compilation, regional observation, notice of disaster situations and resource mapping. Detailed review of the ALOS mission and its advanced technology were reviewed in Iwata et al [1] and Hamazaki [2]. The orbit information of ALOS is described in Table 1.

Table 1: *The value of the orbit*

Orbit Type	Solar synchronous, sub-recurrent, frozen
Height	691.65km (above the equator)
Period	98.7 min
Eccentricity	1/1000
Inclination	98.16deg
Recurrent days	46 days

ALOS is one of the largest Earth observing satellites ever developed. ALOS has a GPS receiver and a laser reflector as tools for orbit determination.

Orbit Determination accuracy of ALOS

In order to make a precise map, it is necessary to observe the earth with high resolution and specify geographical positions corresponding to observed images. Thus, high positioning accuracy and directional precision are required for ALOS [3]. Orbit determination accuracy is required to be within 1m after processing on the ground. There are two tools for precise orbit determination for ALOS, that is, GPS receiver and laser reflector (LR) for Satellite Laser Ranging (SLR). The ALOS GPS receiver was newly developed for this mission. Detailed description of the GPS receiver is given in Toda *et al* [4]. The result of orbit determination using the GPS data is reported in

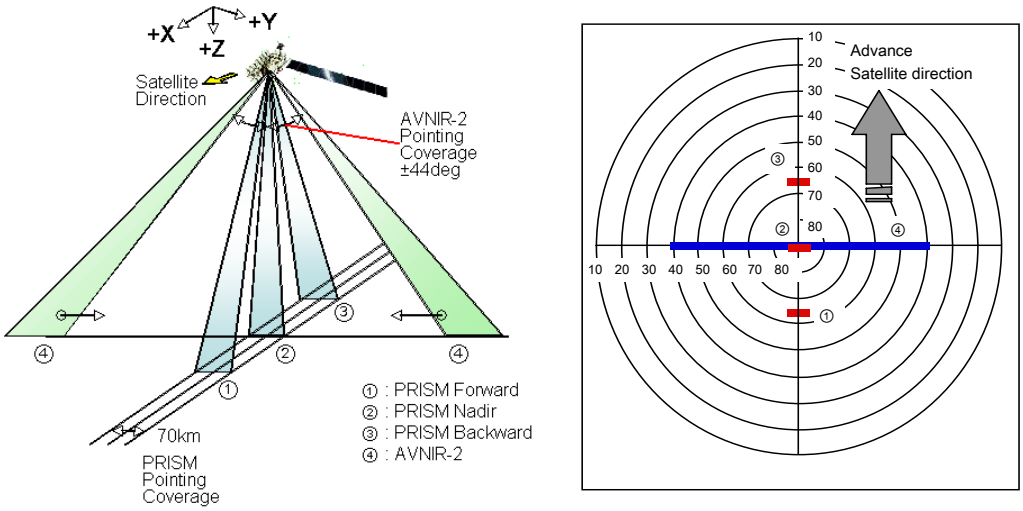

Figure 1. *Image of the ranging restriction.*

Nakamura *et al* [5]. The ALOS LR consists of nine Corner Cube Reflectors (CCR). A more detailed analytical result is described in the ALOS Tracking Standard [6].

Interference between ALOS's earth observation sensors and SLR laser beam

ALOS has two earth observation sensors (PRISM, AVNIR-2) which are vulnerable to the SLR laser radiation wavelength at 532nm. The CCD of each sensor can be destroyed when the incident energy exceeds $5x10^{14}$[W/m^2]. We checked the possibility of damage to these sensors using the specifications of some typical SLR stations. As a result, the laser of SLR could damage the CCDs of sensors if the laser beam impinges on the sensors. The results are similar for almost all stations of the world. Therefore we needed to carry out restricted laser tracking to avoid damaging sensors.

Restricted Laser Tracking

The method of restricted laser tracking is standardized by the ILRS[7]. JAXA carried out restricted laser tracking to ALOS using this method. Figure 1 shows the restricted area. The pass of ALOS is sometimes divided into two, three, or four regions.

Table 2: *List of participating station for ALOS Tracking*

SLR Stations	**ID**	**Nation**
Mt. Stromlo	STL3	Australia
RIGA	RIGL	Latvia
Koganei(KOGC)	KOGC	Japan
Simosato	SISL	Japan
Monument Peak(Moblas-4)	MONL	USA
Hartebeesthoek (Moblas-6)	HARL	South Africa
Yarragadee(Moblas-5)	YARL	Australia
Tanegashima	GMSL	Japan
Zimmerwald	ZIML	Swiss land
Herstmonceux	HERL	United Kingdom
Greenbelt (MOBLAS-7)	GODL	USA

SLR data acquisition and ILRS campaign

We asked ILRS to provide support for ALOS SLR. Thanks to ILRS support, eleven SLR stations (Table 2) participated in the ALOS SLR campaign. We carried out the

ALOS SLR campaign from UT 00:00:00 on 14 August 2006 to UT 16:00:00 on 31 August 2006. We obtained 100 passes and 2979 data points.

The accuracy of orbit determination using GPS data

First, we review the accuracy of orbit determination using GPS data. The details of method of orbit determination using GPS are described in Nakamura *et al*[5].

The accuracy of orbit determination using GPS data

Figure 2 and Table 3 shows the accuracy of orbit determination using GPS data during ALOS SLR campaign. The accuracy of orbit determination is evaluated by overlap comparison and expressed in terms of the RMS value during the orbit determination period. Figure 2 and Table 3 show that the accuracy of orbit determination using GPS data is within a few cm.

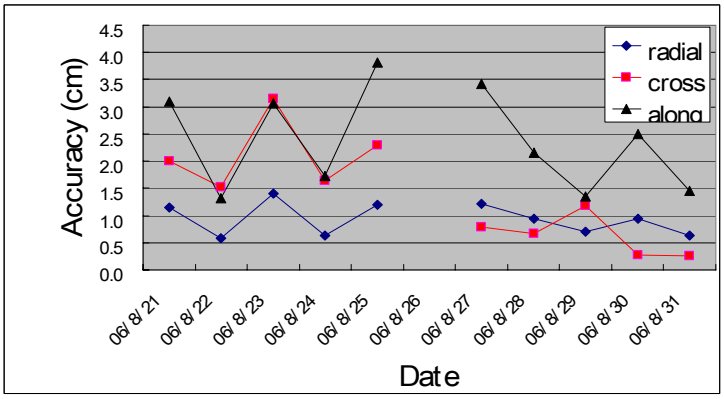

Figure 2. *Accuracy of orbit determination using GPS data (RMS) The horizontal axis is date and the vertical axis is the accuracy of orbit determination.*

Table 3. *Summary of GPS OD Accuracy (cm)*

	Radial(ave)	Radial(sig)	Cross(ave)	Cross(sig)	Along(ave)	Along(sig)
GPS Overlap	-0.04	0.94	0.03	1.38	0.56	2.39

Analysis

Our SLR analyses used both global arc and short arc methods.

Global arc analysis

We compared GPS data with SLR data and evaluated the residual of SLR data. Figure 3 shows a typical result and Table 4 shows the statistic result.

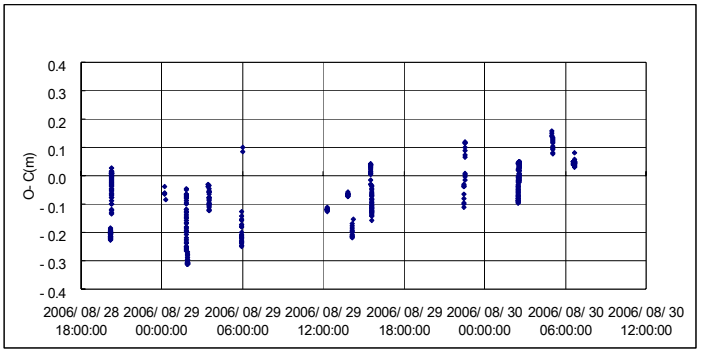

Figure 3. *Difference between GPS orbit and Laser ranging data (as example)*

Our analysis shows that the SLR data is within -4.8 ± 12.0 cm of the GPS orbits. What is noteworthy is that the standard deviation value is larger than the average value. This means that the difference between GPS-determined orbit and SLR data is well within the margin of error; there is no significant difference.

Table 4. *Results of residual (cm)*

	Average	St Dev
SLR O-C Analysis	-4.78	12.03

Short arc analysis

The above analysis cannot separate the radial, cross, and along components of GPS-determined orbit. Next we performed the orbit determination using only SLR data and compared it with the orbit determination using GPS data in each direction. Because SLR is an independent method from GPS, this analysis provides an objective evaluation of the ALOS onboard GPS receiver specifications.

Several passes are needed to perform orbit determination using SLR data. If we used daily data sets, the accuracy of orbit determination would be degraded because of the irregularity in data density. Therefore we performed the orbit determination using SLR data acquired during periods when more than three stations carried out SLR within a few orbital cycles. This means that our analysis is not the short arc analysis in a strict sense.

We calculated only the six orbital elements for the orbit determination using SLR data. We used a polyhedral model to represent the satellite and also considered the attitude model of ALOS. We didn't estimate the range bias for each station data. (We used the calibration data of each station.) And the analysis was performed for the periods where SLR data existed.

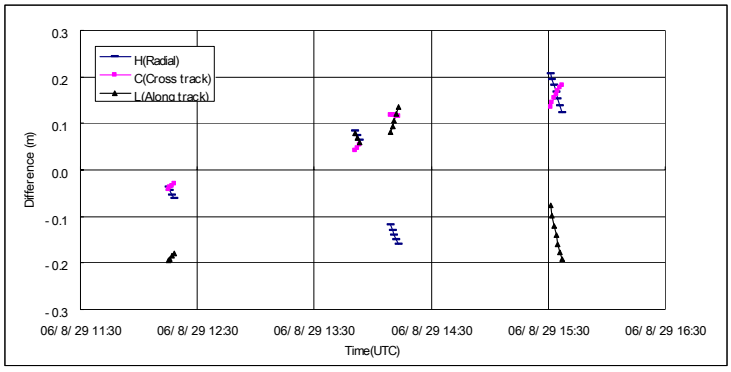

Figure 4. *The difference between the orbit determinations using SLR and* GPS

We compared the two orbit determinations of SLR and GPS approaches, and verified each direction (Cross, Along, Radial) result. The summary of result is shown in Table 5.

Table 5. *Summary of Difference between SLR and GPS (cm)*

	R(ave)	R(sig)	C(ave)	C(sig)	A(ave)	A(sig)
SLR-GPS	-2.98	20.54	-4.69	38.32	-5.44	28.76

These results show that the position estimated by GPS overlap method, and the position estimated by comparison of GPS orbit determination and SLR orbit determination fell within the margin of error (1sigma).

Conclusion

The analysis using the overlap method is a relative evaluation of GPS-based orbit determination and the analysis using SLR data is an absolute evaluation of GPS-based orbit determination. In other words, the overlap method is the evaluation of random error and the analysis using SLR data is the evaluation of bias error.

From this analysis, the error estimated by GPS overlap method was small compared to the error estimated by the analysis using SLR data. This means that the error estimated by GPS overlap method is negligible. The result of global arc analysis shows that there is no significant difference between the SLR and GPS data. Next we checked the difference in each direction between SLR determined-orbit and GPS determined-orbit by short arc-like analysis. As a result, the position estimated by GPS overlap method, and the position estimated by comparison of GPS orbit determination and SLR orbit determination agreed to within the margin of error (1sigma). Because the ALOS onboard GPS receiver was newly developed, we needed to verify the specifications. The result of this analysis showed that ALOS GPS receiver provides correct positioning information, to at least within the accuracy confirmed by our SLR-based analysis. In this analysis, 1 sigma was about 30 cm. This means that the accuracy of the ALOS onboard GPS receiver satisfies the requirement from ALOS mission, which is within 1m (peak to peak).

Acknowledgements

ALOS tracking campaign was performed successfully with the cooperation of ILRS and participating SLR stations, to all of whom we would like to express our deep appreciation. And we also would like to express our deep appreciation to Mr. Iwata, Mr. Toda and Mr. Matsumoto of ALOS project team, who explained the structure of ALOS in detail.

References

[1] Iwata. T et al, “The Advanced Land Observing Satellite (ALOS) – Preliminary Design”, 49th IAF, IAF-98-B.2.01, Melbourne, Australia, 1998.

[2] Hamazaki. T, “Key technology development for the Advanced Land Observing Satellite”, XIXth ISPRS Congress, Amsterdam, The Netherlands, July 2000

[3] Iwata. T, “Precision attitude and position determination for the Advanced Land Observing Satellite (ALOS)”, SPIE 4th International Asia-Pacific Environmental Remote Sensing Symposium: Remote Sensing of the Atmosphere, Ocean, Environment & Space, Honolulu, U.S.A., November 9,2004

[4] Toda. K et al, “GPS Receiver and Precision Position Determination for the advanced Land Observing Satellite (ALOS): Flight Result”(in Japanese), in print

[5] Nakamura. S et al, “Precise Orbit Determination for ALOS” (in press)

[6] Uchimura. T, “ALOS Tracking Standard”, http://god.tksc.jaxa.jp/al/source/source.html

[7] Werner Gurtner, Restricted Laser Tracking of satellites, May 2, 2005, http://ilrs.gsfc.nasa.gov/satellite_missions/restriction.html

Fulfilment of SLR Daylight Tracking In Changchun Station

ZHAO You, HAN Xinwei, FAN Cunbo, DAI Tongyu

1. National Astronomical Observatories/Changchun Observatory, CAS

Abstract

The paper introduces the performance and progress for Satellite Laser Ranging (SLR) system daylight tracking in Changchun station. This paper first introduces the problems and difficulties facing this system for daylight tracking—mount model, the separation of emitting and receiving parts of the telescope, control range gate, installing narrower filter. Third it presents some work which was done in the system for daylight tracking: system stability improvement, laser stability improvement, mount model adoption, control system, etc. From these analysis and work which have been done, the system performance has been greatly improved. A routine operation system in daylight tracking has been set up.

***Keywords*:** SLR, daylight tracking

Introduction

Some main technical problems for daylight tracking

The daylight tracking is necessary and the tendency of SLR in the future. Many stations in the world can take the daylight observations. According to the experience at the most successful station, recent years, Changchun station has been working on the daylight tracking technique. Some things to consider:

- Precise orbit prediction

Predictions of position and range of satellites and pointing of tracking mount with high accuracy. No problem for current CPF predictions.

- Reduce the effect of daylight sky background noise on photoelectric detector

Day background noise level is higher in SLR daylight tracking. Pointing of the telescope; Mount model problem for the telescope; Generating control range gate narrower; the application narrow Spectrum filter; the receiver filed of view want to be small, above all will efficiency reduces amount of background light.

- Parallelism of transmitting and receiving paths

For our station using telescopes with separated transmit and receive, it is sometimes difficult to maintain correct laser beam pointing due to Coude path mirror drifts. It required good collimation.

- Intensive light protective methods

To avoid the damage of the detector by focused Intensive light.

Progress for Daylight Tracking in Changchun SLR System

Even there are so many difficulties, we still have done some work to try to fulfill daylight tracking, such as system stability improvement, laser stability improvement, mount model adoption, control system, etc. In order to improve the system stability, a new control system has been adopted, including an industrial control computer, data collecting board and counter card for timing and range gate. Control and data preprocessing software are also updated so that all work can be done automatically. For

laser stability, the room is air-conditioned. The cooling system is also improved for its liable working, including some system protections. In order to improve the pointing accuracy, mount model correction is also adopted in the satellite prediction. A spherical harmonics pointing model was built by using astronomical observation at our telescope system. It is proved that the pointing model is an effective correction to the system error. This makes the pointing bias become very small in most directions. The design of tracking optical scheme on Changchun SLR system is shown in Figure 1.

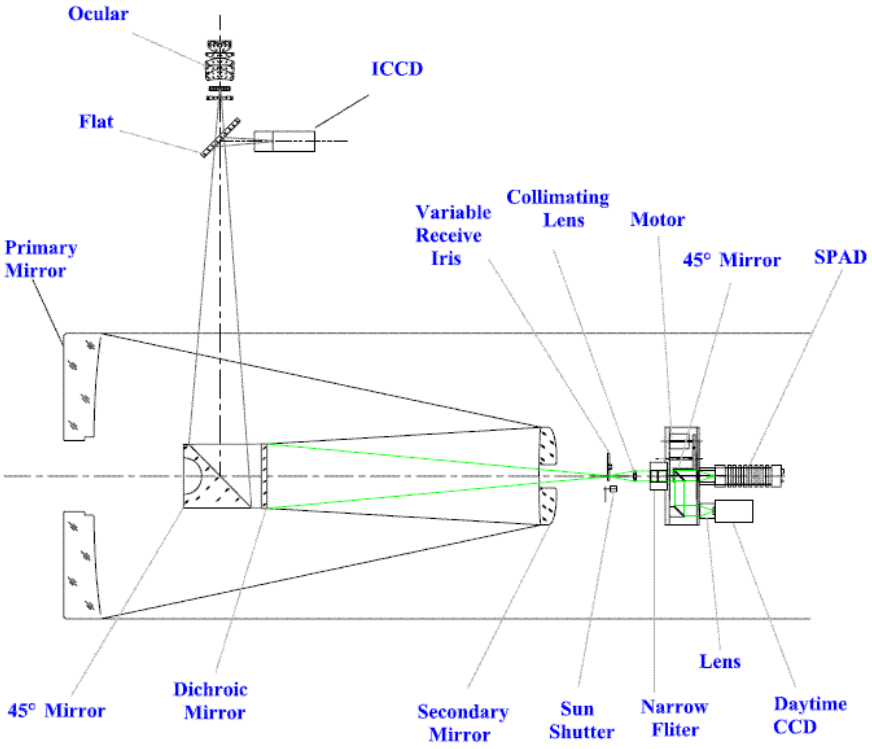

Figure 1. *Optical scheme of Changchun SLR system*

Ways to reduce effect of daylight background noise

Space filter

The electric-powered adjustable iris is used for field of view.
Receiving Field of view: 45"-12'. Figure 2 shows receiving iris diaphragm.

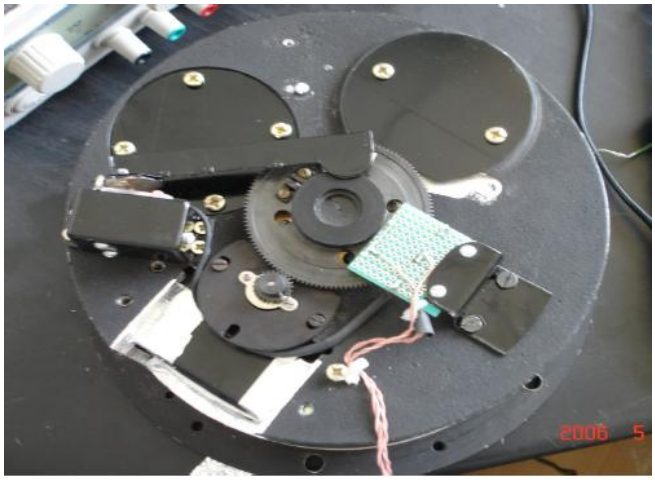

Figure 2. *Variable Receiving Iris diaphragm*

Timing filter

We designed and developed the precise range gate generator.
It can produce 1ns range gate to make the time closer to the arrival echo. We provide two devices to generate range gate:

AD9501: Programmable digital delay generator.10ps precision time delay, delay: 2.5ns—10us (capacitance and resistor);

DS1020: 8 bit programmable delay device, serial parallel mode. Max. Delay time: 48.25ns (fast mode), 520ns (slow mode). Figure 3 is the control precise range gate Generate Circuit Chart.

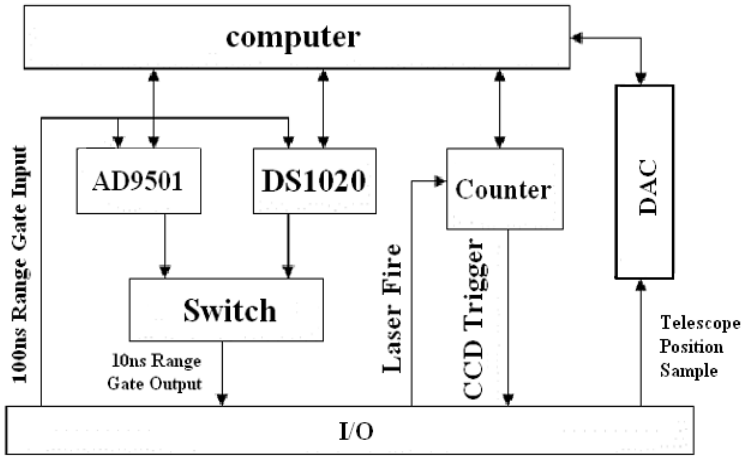

Figure 3. *Control precise range gate Generate Circuit Chart*

Spectrum filter

The application of 0.3nm narrow band pass interference filter form Andover Corp**.** and the constant temperature box to cut more background noise and to make the filter working in a constant temperature environment. The temperature controller provides protection against the influences of ambient temperature fluctuation. The specs of Andover Narrow Band Interference Filter are: Center Wavelength: 531.9 nm; Bandwidth: 0.3±0.1 nm; Peak transmission: 41.30 %; Ambient temperature: 23ºC; Size:Φ25.00 ± 0.25 mm. Figure 4 is the photograph.

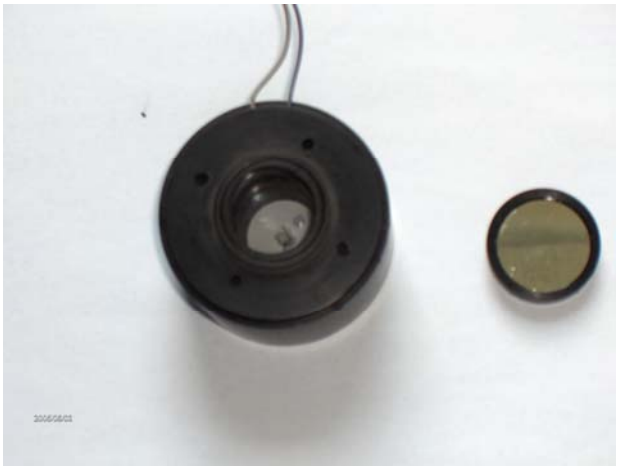

Figure 4. *Spectrum filter and constant temperature box*

Pointing of the telescope

- Mount leveling Collimation measurement

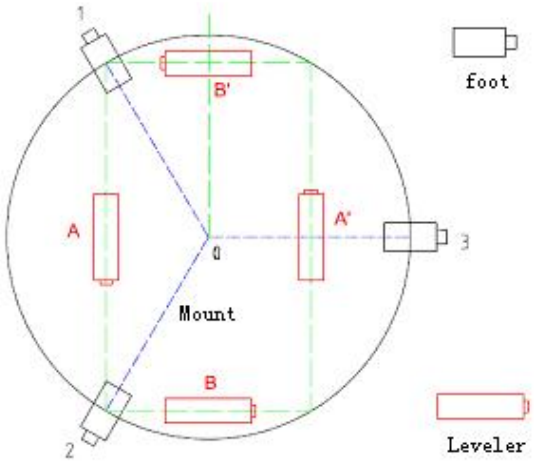

Figure 5. *Mount leveling Collimation measurement*

The first step is mount leveling. The data of mount leveler is recorded each 30 degree.

After leveling

$$i = \sqrt{a_1^{\,2} + b_1^{\,2}}$$

$$A = \arctan\left(\frac{a_1}{b_1}\right)$$

where

$$a_1 = \frac{1}{6}\sum_{j=0}^{11} f(\alpha_j)\cos(30^\circ \cdot j); b_1 = \frac{1}{6}\sum_{j=0}^{11} f(\alpha_j)\sin(30^\circ \cdot j)$$

After calculation: the azimuth angle perpendicular to the slant direction is A=1.2"

- Collimation measurement

$$C = (A_R - A_L \pm 180^o)/2$$

RMS = 3'02"

- Zero error measurement of encoder

Polestar observation the error of encoder zero position:

$$\Delta A_0 = 180.682431^o$$

$$\Delta E_0 = 0.01684^o$$

- Star Calibration

Observe positions of known stars (calculation from FK5) using night camera. Mark reference position on screen of night camera. Our system can to gather data from 48--60 stars in 1 hour. Compare observed (encoder readings) with calibration position (O-C). The Least Squares to fit the mount model parameters (13 parameters each axis). Application of current mount model provides a good fit for elevations from 15 degrees to 80 degrees. System pointing is at the few arc second level.

RMS of fit: Azimuth: 5.5"

Altitude: 4.8"

Parallelism of transmitting and receiving paths

1) Adjustment of sensitive area of detector.
2) Coude path fine adjustment.
3) Monitor laser beam during daylight.

We have installed a CCD camera in the receiver path; a switched mirror can direct this green light into the CCD or into the SPAD. This CCD is triggered by the laser start pulse that is delay 153us; an exposure time of down to 1/20000 s. Using software image / contrast enhancement techniques to display the backscatter of laser beam in real time.
4) Directional adjustment of output laser beam.

To adjust the laser beam direction with remote control of the last Coude mirror to fit the parallelism of transmitting and receiving path. Figure 6 is the image of daylight laser beam.

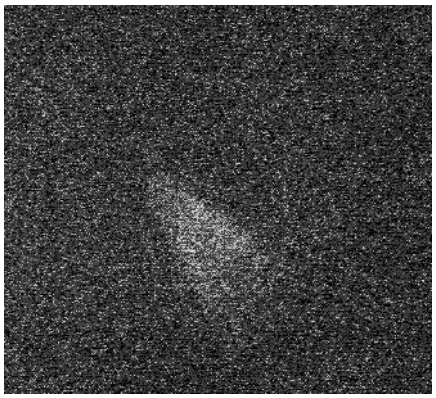

Figure 6. *Image of Daylight Laser Beam*

Intensive light protective methods

In order to avoid the damage of the C-SPAD detector by focusing sunlight, we must prevent the mount from pointing to the Sun. The double methods were used:

Hardware protection

Four strong light detectors were adopted on the top of mount, when the telescope moves to the place with strong light (such as to the sun or moon), the detectors will trigger a circuit to shut off the emergency shutter of the field of view. Figure 7 shows the electronic circuit diagram.

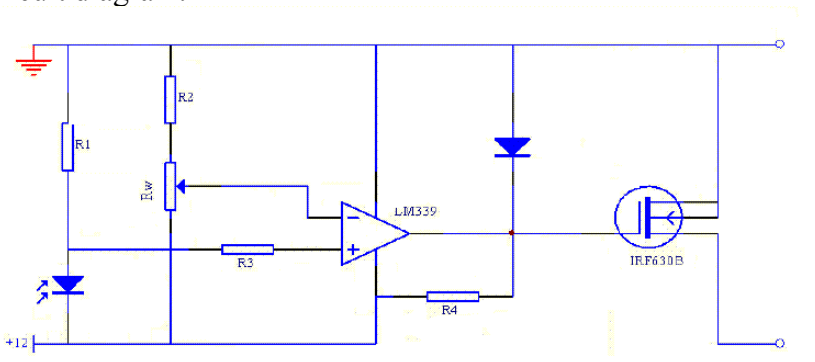

Figure 7. *Electronic diagram of light protective circuit*

Software protection

The software will control the telescope to avoid the sun when the satellite path travels across the sun area (less than 15º distance to sun) and stop the laser. It can choose a tracking path automatically when multi-satellite alternative tracking.

Conclusion

Almost everything, including hardware and software, is ready since the end of last year. Because of the cold weather we decided to do the test at the beginning of this year. In March of 2006, Galileo project was launched. Changchun station was selected to track Galileo satellite by Chinese government and ESA. So we have to change our plan and daylight tracking test has to be delayed. The Galileo project of first phase was finished, but the acceptance is not done. We have to wait for until it is over. But we are sure the condition is suitable for daylight tracking. And we will try the daylight tracking in the near future.

Acknowledgement

The authors would like to thank the financial support of the knowledge innovation project of the Chinese Academy of Sciences. And helpful discussion with Prof. Yang Fumin, Ms. Chen Wanzhen of Shanghai Astronomical Observatory, CAS of China, Dr. George Kirchner of Graz station of Austria.
The authors gratefully acknowledge the support of K.C.Wong Education Foundation, Hong Kong.

References

[1] ZHAO You, ZHANG Jun-rong, CUI Dou-xing: “The improvement of Changchun satellite laser ranging system”, Proceedings of SPIE Vol. 3501, pp.453 -460, 1998 Beijing, China.

[2] Zhao You: “Upgrade of Changchun SLR System”, Proceedings of 11th International Workshop on Laser Ranging, pp. 188 - 196, Sep. 1998 Deggendorf, Germany.

[3] Zhao You, Kunimori H., Hamal K., Prochazka I: “PCS in Changchun Station”, Proceedings of 11th International Workshop on Laser Ranging, pp.174 - 180, Sep. 1998 Deggendorf, Germany.

[4] LIU Chengzhi, ZHAO You, FAN Cunbo, CUI Douxing, HAN Xingwei, YANG Fumin: “Performance and observation summary of Changchun Satellite Laser Ranging Station”, Chinese Science Bulletin, Vol. 47, No. 13, pp.1070 - 1072, July 2002.

[5] You ZHAO, Cunbo FAN, Chengzhi LIU, Xinwei HAN, Jianyong SHI, Xinhua ZHANG, Haitao ZHANG: “System Stability Improvement of Changchun SLR”, Proceedings of 13th International Workshop on Laser Ranging. Oct. 2002, USA.

[6] ILRS publications SLR Station Performance Report Card 2003, on the Internet.

[7] Werner Gurtner, Ulrich Schreiber: “Daylight Tracking”, ILRS Technical Workshop, Kötzting, Germany, October 28 - 31, 2003.

[8] Yang Fumin, Xiao Zhikun, Chen Wanzhen, et al., “Design and Observations of the Satellite Laser Ranging System for Daylight Tracking at Shanghai Observatory”, Science in China, Series A, Vol.42, No.2, pp.198 - 206, 1999.

[9] Zhao You, Cunbo Fan, Xinwei Han, Chengzhi Liu, Xinhua Zhang, Jianyong Shi: “Progress for daylight tracking in Changchun SLR system”, Proceedings of 14th International Workshop on Laser Ranging, June of 2004, Spain, pp179 – 182.

GLONASS status update. MCC activity in GLONASS program.

V.D. Glotov, S.G. Revnivykh, V.V. Mitrikas

1. Russian Mission Control Center

Introduction

The Global Navigation Satellite System (GLONASS) is a government satellite navigation system which is designed for providing a continuous all-weather support of an unlimited number of aeronautical, maritime, terrestrial and space-born users with high-precision position-fixing and timing information at any point of the Earth and in the near-Earth outer-space. The Russian Federation Presidential Directive No. 38-RP of February 18, 1999 designated the GLONASS system as a dual-purpose space facility applied for solving the scientific, industrial, economical, social, defense, security and other relevant problems. It was also specified that the Federal Space Agency (Roscosmos) is a co-customer of the GLONASS system on equal footing with the Russian Ministry of Defence.

GLONASS Status

The first GLONASS satellite was launched into orbit on October 12, 1982. The GLONASS system formally attained the initial operation capability with a reduced-scale orbital configuration on September 24, 1993. The fact was approved with Presidential Directive No. 658 RP. Russian Federation Government Directions No. 237 of March 07, 1995 assigned a mission to implement a full-scale deployment of the GLONASS orbital constellation (24 satellites), to provide for mass-production of user equipment and to introduce the GLONASS system as an integral element of the international satellite navigation system for civil users.

The Russian Federation Government approved a long-term program of the GLONASS system modernization on August 20, 2001. It is designated as the Global Navigation System (GNS) federal objective program. The GNS Program covers improvement of space, ground-based and user equipment segments of the GLONASS system. Government commitments are associated with appropriation of funds to the Program for ten years by the State Budget Act.

There are new main tasks with the Presidential Directives issued at January 18, 2006 and at April 19, 2006:

- To ensure GLONASS minimum operational capability (constellation of 18 NSV) by the end of 2007
- To ensure GLONASS full operational capability (constellation of 24 NSV) by the end of 2009
- To ensure GLONASS performance comparable with that of GPS and GALILEO by 2010
- To ensure the navigation equipment mass production: encourage the industry in the manufacture renovation
- Mass market development

The Federal GLONASS Program update was approved by the Government Resolution at July 14 2006, No423.

Main reasons for SLR data application to GLONASS

There are a lot of the civil and scientific applications where navigation data from GPS are not enough for the complete analysis. The GLONASS navigation data are useful and helpful in these situations. Thus it's very important to use the same geodetic base with GPS by the GLONASS data generation. From this point of view it is necessary to calibrate geodetic base, the navigation signals accuracy for GLONASS system as good as possible. On the other hand the Russian Ground-Based Control Facility (GBCF) provides for management of the GLONASS orbital constellation and consists of the GLONASS Control Center and a network of tracking/control stations deployed in different areas of the Russian Federation only. SLR data from world wide stations net is the source of calibration data for ephemeris determination, international geodetic base providing and accuracy factor improving for GNSS etc.

So SLR data from ILRS network provide:

- Improving of the geodetic base for GLONASS on the way to ITRF
- Studying and improving of the SC motion model etc.
- Calibration and validation of the microwave means
- Testing and validation of the software and analysis results
- Monitoring of the real on-board ephemeris and clock

IAC activity in GLONASS Program

Informational Analytical Center (IAC - the department of the Russian Mission Control Center) since August, 15, 2006 has been formally assigned by the Federal Space Agency as the GLONASS official information portal for users with the next issues:

- Daily brief bulletins for GLONASS and GPS status based on the global data available (IGS network)
- GLONASS Control Center (Space Force) information
- NAGU generation
- Monthly bulletins with deep analysis of GLONASS performance
- GLONASS news
- GLONASS ICD, etc.

So, IAC is now acting as positive feed-back in the GLONASS control segment.

The IAC has been making contributions to the International GPS Service (IGS) by providing precise orbits based on SLR observations for those GLONASS satellites that are observed by the ILRS network. These independent orbits help to validate and evaluate precise orbits computed by Analysis Centers from the IGS tracking network observations. Since 1995, the MCC has permanently supported orbit determination of GLONASS satellites based on SLR data. Orbits for GLONASS satellites (in SP3 format) are regularly sent to the CDDIS for the determination of the final orbits based mainly on the GLONASS "phase" data.

GLONASS SLR data analysis

The global products from the International GLONASS service as part of the IGS should facilitate the use of combined GLONASS and GPS observations and analysis results for the civil scientific and engineering applications in the frame of the prototype Global Navigation Satellite System (GNSS). The ILRS supports this effort by a continuous tracking of three GLONASS satellites as part of their standard tracking protocol and by delivering precise GLONASS orbits through one of its Analyses Centers (MCC). Average number of the SLR data pro month for three GLONASS satellites is 500 – 700 passes from 15-18 stations (see the Table 1 as example of the month SLR tracking.)

Table 1.
Time interval: 30.07.2006 – 26.08.2006

SC	Passes	Stations
GLONASS-07	**133**	**14**
GLONASS-22	**154**	**15**
GLONASS-03	**220**	**16**
Total	**507**	**18**

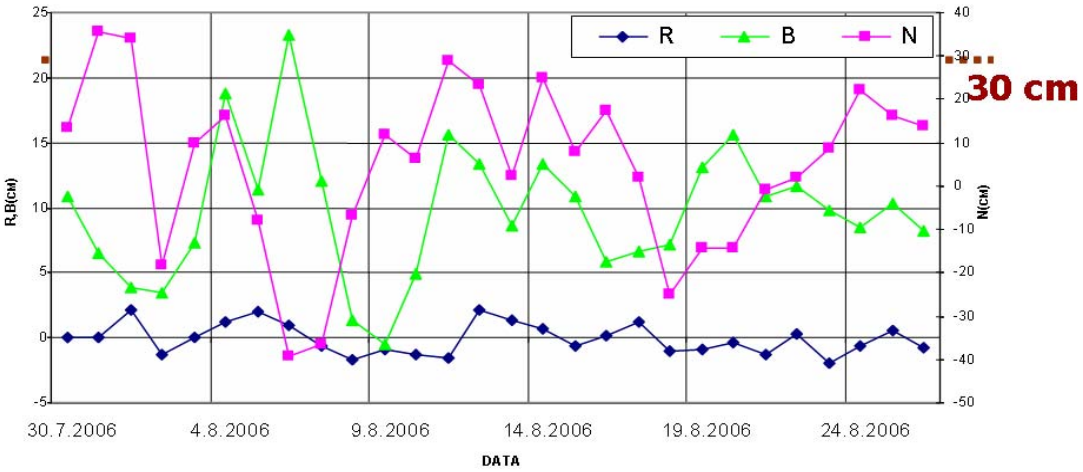

Figure 1. *The average difference between SLR and navigation orbits for GLONASS-89 (August 2006)*

Figure 1 shows the average difference between SLR and "microwave" orbits as potential GLONASS Performance (R-radial, B-across orbit, N- along orbit).

Figure 2 shows the improving of the on-board ephemeris & clock data for GLONASS constellation in the last years (since July 2005).

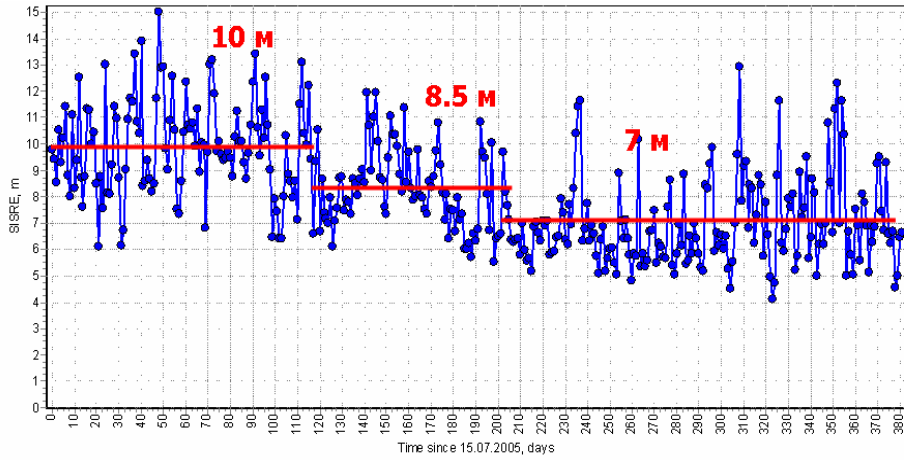

***Figure 2**. Average Signal In Space Range Error (SISRE), м (Since July, 2005)*

Conclusions

- ILRS support is very important for GLONASS modernization by the way to the Global Navigation Satellite System
- Need to continue/increase tracking of GLONASS satellites by ILRS for the realization of the real collocation in space (Microwave / Laser)
- The International GLONASS - Pilot Project demonstrates the extensibility of IGS to accommodate other microwave systems (GLONASS, GALILEO).

REGISTRANTS

Last Name	First Name	Organisation	Email
Altamimi	Zuheir	Institut Geographique National, France	altamimi@ensg.ign.fr
Appleby	Graham	NERC Space Geodesy Facility, UK	gapp@nerc.ac.uk
Arnold	David	Watertown, MA, USA	david-arnold@earthlink.net
Baltuck	Miriam	CSIRO, Canberra Deep Space Complex, Australia	mbaltuck@cdscc.nasa.gov
Beutler	Gerhard	Astronomical Institute of the University of Bern, Switzerland	Gerhard.beutler@aiub.unibe.ch
Bianco	Giusseppe	ASI/CGS, Matera, Italy	Guiseppe.bianco@asi.it
Burmistrov	Vladimir	Institute for Precision Engineering, Russia	Natalia.n@g23.relcom.ru
Burris	Harris	NRL / RSI, USA	
Carman	Randall	MOBLAS 5 Yarragadee, EOS, Australia	moblas@midwest.com.au
Carter	David	NASA Goddard Space Flight Centre, USA	david.l.carter@nasa.gov
Chuanyin	Zhang	Beijing SLR Station of Chinese Academy of Surveying and Mapping, China	bjslr@casm.ac.cn
Clarke	Christopher	NASA SLR / Honeywell TSI, USA	christopher.clarke@honeywell-tsi.com
Coulot	David	IGN/LAREG, France	David.Coulot@ensg.ign.fr
Davis	Mark	Naval Research Lab, Honeywell TSI, USA	mark.davis@nrl.navy.mil
Degnan	John	Sigma Space Corporation, USA	John.Degnan@sigmaspace.com
Deleflie	Florent	OCA/ GEMINI – GRGS, Grasse, France	Florent.deleflie@obs-azur.fr
Delle Monache	Giovanni	INFN LNF, Italy	Giovanni.dellemonche@lnf.infn.it
Dmytrotsa	Andriy	SRI Crimean Astrophysical Observatory, Ukraine	dymtrotsa@gmail.com
Donovan	Howard	NASA Satellite Laser Ranging Program, USA	howard.donovan@honeywell-tsi.com
Dunn	Peter	SGT Inc, USA	Peter.Dunn@raytheon.com
Feng	Qu	Beijing SLR Station of Chinese Academy of Surveying and Mapping, China	bjslr@casm.ac.cn
Forman	Michael	EOS, Canberra, Australia	mforman@eos-aus.com
Fumin	Yang	Shanghai Astronomical Observatory, China	yangfm@shao.ac.cn
Gambis	Daniel	Observatoire de Paris, France	daniel.gambis@obspm.fr
Gao	Yue	EOS, Canberra, Australia	ygao@eos-aus.com
Garate	Jorge	San Fernando Naval Observatory, Spain	jgarate@roa.es
Gibbs	Philip	NERC Space Geodesy Facility, UK	pgib@nerc.ac.uk
Glotov	Vladimir	Russian Mission Control Centre, Moscow, Russia	Vladimir.glotov@mcc.rsu.ru
Govind	Ramesh	Geoscience Australia, Canberra, Australia	Ramesh.Govind@ga.gov.au
Greene	Ben	EOS, Canberra, Australia	bengreene@bengreene.net
Gurtner	Werner	Astronomical Institute, University of Bern, Switzerland	werner.gurtner@aiub.unibe.ch
Hamal	Karel	Czech Technical University, Prague, Czech Republic	prochazk@troja.fjfi.cvut.cz
Horvath	Julie	NASA SLR / Honeywell TSI, USA	julie.horvath@honeywell-tsi.com
Izumi	Tadashi	NICT, Kogenai, Japan	slr-kog@slr.nict.go.jp
Jianli	Wang	Changchun Institute of Optics Mechanics and Physics, CAS, China	wangjianli@ciomp.ac.cn
Jingxu	Zhang	CIOMP, Chinese Academy of Sciences, Changchun, China	wangjianli@ciomp.ac.cn
Johnston	Gary	Geoscience Australia, Canberra, Australia	gary.johnston@ga.gov.au
Juping	Chen	Shanghai Astronomical Observatory, China	zzp@shao.ac.cn

Kim	Kyunhee	KAIST / STRC, Korea	
Kirchner	Georg	Austrian Academy of Sciences, Graz, Austria	kirchner@flubpc04.tu-graz.ac.at
Klosko	Steven	SGT Inc., USA	sklosko@sgt-inc.com
Koidl	Franz	Austrian Academy of Sciences, Graz, Austria	koidl@flubpc04.tu-graz.ac.at
Kolbl	Josef	Deggendorf University of Applied Sciences, Germany	josef.koelbl@fh-deggendorf.de
Kucharski	Daniel	Space Research Centre, Polish Academy of Sciences, Poznan, Poland	Kucharski@cbk.poznan.pl
Kudo	Nobuo	Japan Aerospace Exploration Agency, Tsukuba-City, Japan	kudoh@nobuo@jaxa.jp
Kulagin	Oleg	Institute of Applied Physics, RAS, Nizhny Novgorod, Russia	ok@appl.sci-nnov.ru
Kunimori	Hiroo	NICT, Koganei, Japan	kuni@nict.go.jp
Lee	Sang Hyun	KAIST / STRC, Korea	
Lemoine	Frank	NASA Goddard Space Flight Centre, USA	flemoine@puuoo.gsfc.nasa.gov
Lewova	Dana	Czech Technical University, Prague, Czech Republic	Lew.Dana@gmail.com
Li	Xin	Institute of Seismology, China Earthquake Administration, China	lxcomcn@yahoo.com.cn.
Lim	Hyung-Chul	Korea Astronomy & Space Science Institute, Daejeon, Korea	
Lu	Ma	UAO	
Luceri	Vincenza	e-GEOS, CGS, Matera, Italy	cinzia.luceri@telespazio.com
Luck	John	Stromlo SLR, EOS, Canberra, Australia	John-luck@bigpond.com
Luton	Geoff	Geoscience Australia, Canberra, Australia	Geoff.luton@ga.gov.au
McClure	David	Honeywell Technology Solutions Inc., USA	david.mcclure@honeywell-tsi.com
McGarry	Jan	NASA/GSFC, Greenbelt, USA	Jan.McGarry@nasa.gov
Michaelis	Harald	DLR, Institute of Planetary Research, Berlin, Germany	harald.michaelis@dlr.de
Moore	Chris	Stromlo SLR, EOS, Canberra, Australia	cmoore@eos-aus.com
Moshkov	Vladislav	IPIE, Moscow, Russia	Natalia.n@g23.relcom.ru
Mueller	Horst	DGFI, Muenchen, Germany	mueller@dgfi.badw.de
Mullaney	Jennifer	Registration Coordinator, EOS, Australia	
Murphy	Tom	University of California at San Diego, La Jolla, USA	tmurphy@physics.ucsd.edu
Nemec	Martin	Czech Technical University, Prague, Czech Republic	nemecM1@troja.fjfi.cvut.cz
Noomen	Ron	Delft University of Technology, The Netherlands	r.noomen@tudelft.nl
Noyes	Vince	MOBLAS 5 Yarragadee, EOS, Australia	moblas@midwest.com.au
Ogaja	Clement	Geoscience Australia, Canberra, Australia	clement.ogaja@ga.gov.au
O'Gara	Daniel	University of Hawaii Institute for Astronomy, Maui, USA	ogara@ifa.hawaii.edu
Osipova	Liene	Institute of Astronomy, University of Latvia, Riga, Latvia	lieneosipova@inbox.lv
Otsubo	Toshimichi	NICT, Japan	t.otsubo@srv.cc.hit-u.ac.jp
Parkhomenko	Natalia	Institute for Precision Instrument Engineering, Moscow, Russia	Natalia.n@g23.relcom.ru
Pavlis	Erricos	JCET/UMBC Nasa Goddard SFC, USA	epavlis@umbc.edu
Pearlman	Michael	Harvard-Smithsonian Centre for Astrophysics, Cambridge MA, USA	mpearlman@cfa.harvard.edu
Pearson	Matthew	EOS, Canberra, Australia	mpearson@eos-aus.com
Peltier	Richard	University of Toronto, Canada	peltier@atmosp.physics.utoronto.ca

Pierron	Monique	Observatoire de la Cote d'Azur, Grasse, France	monique.pierron@obs-azur.fr
Pierron	Francis	Observatoire de la Cote d'Azur, Grasse, France	francis.pierron@obs-azur.fr
Qian	Li	Beijing SLR Station of Chinese Academy of Surveying and Mapping, China	bjslr@casm.ac.cn
Ricklefs	Randall	University of Texas, Center for Space Research, Austin, USA	ricklefs@csr.utexas.edu
Salminsh	Kalvis	Institute of Astronomy, University of Latvia, Riga, Latvia	kalvis@lanet.lv
Sang	Jizhang	EOS, Canberra, Australia	jsang@eos-aus.com
Schreiber	Ulrich	Fundamental Station Wettzell, Germany	schreiber@fs.wettzell.de
Seemueller	Wolfgang	DGFI, Munich, Germany	seemueller@dgfi.badw.de
Shargorodsky	Victor	Institute for Precision Instrument Engineering, Moscow, Russia	Natalia.n@g23.relcom.ru
Shelus	Peter	Center for Space Research, University of Texas, Austin, USA	pjs@astro.as.utexas.edu
Sierk	Bernd	TIGO Observatory (BKG), Concepcion, Chile	sierk@tigo.cl
Smith	Craig	EOS, Canberra, Australia	csmith@eos-aus.com
Sperber	Peter	University of Applied Sciences, Deggendorf, Germany	peter.sperber@fh-deggendorf.de
Tangyong	Guo	Institute of Seismology, China Earthquake Administration, Wuhan, China	guoty@21cn.com
Tanqiang	Wang	Beijing SLR Station of Chinese Academy of Surveying and Mapping, China	bjslr@casm.ac.cn
Thompson	Ron	EOS, Canberra, Australia	ronthompson@eos-aus.com
Titov	Oleg	Geoscience Australia, Canberra, Australia	Oleg.titov@ga.gov.au
Torre	Jean-Marie	Observatoire de la Cote d'Azur, Grasse, France	torre@obs-azur.fr
Torrence	Mark	SGT Inc/NASA-GSFC, Greenbelt, USA	mark.h.torrence1@gsfc.nasa.gov
Tregoning	Paul	School of Earth Sciences, Australian National University, Canberra, Australia	Paul.tregoning@anu.edu.au
Urschl	Claudia	Astonomical Institute, Uni of Bern, Switzerland	claudia.flohrer@aiub.unibe.ch
Varghese	Thomas	Cybioms Corporation, Rockville MD, USA	tvarghes@cybioms.com
Wang	Peiyuan	Institute of Seismology, China Earthquake Administration, Wuhan, China	yangroot@yahoo.com.au
Wanzhen	Chen	Shanghai Astronomical Observatory, China	cwz@shao.ac.cn
Wasiczko	Linda	US Naval Research Laboratory, USA	linda.wasiczko@nrl.navy.mil
Wetzel	Scott	NASA SLR / Honeywell TSI, USA	scott.wetzel@honeywell-tsi.com
White	Nathan	EOS, Canberra, Australia	nwhite@eos-aus.com
Wiant	Jerry	McDonald Observatory, University of Texas, USA	jrw@astro.as.utexas.edu
Wilson	Peter	Stromlo SLR, EOS, Canberra, Australia	pwilson@eos-aus.com
Xiangming	Zheng	Yunnan Observatory, National Astronomical Observatories China (NAOC), Kunming, China	KMzxm@hotmail.com
Yechun	Tan	Institute of Seismology, China Earthquake Administration, Wuhan, China	tanyechun@21cn.com
Zhao	You	Changchun Observatory of NAOC, China	youzhao@cho.ac.cn
Zhongping	Zhang	Shanghai Astronomical Observatory, China	zzp@shao.ac.cn
Zhulian	Li	Yunnan Observatory, NAOC, Kunming, China	KMzxm@hotmail.com

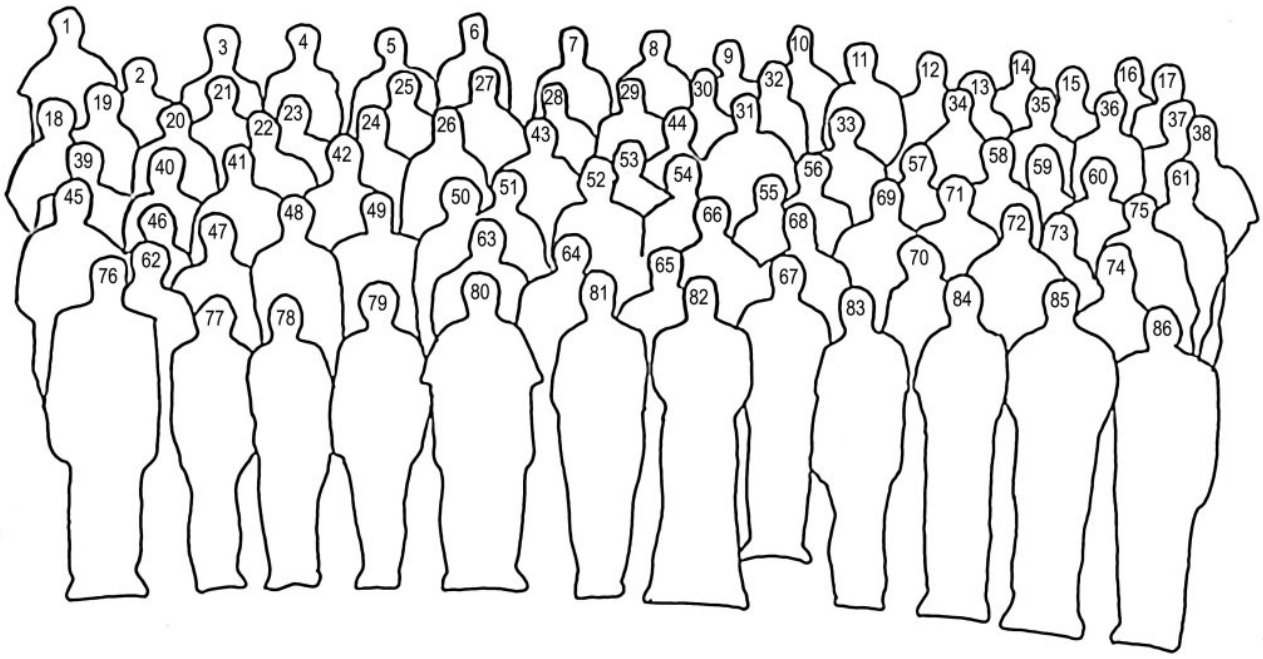

1 Paul Tregoning
2 Hyung-Chul Lim
3 David McClure
4 Howard Donovan
5 Christopher Clarke
6 Ron Noomen
7 Randy Ricklefs
8 Tom Murphy
9 Jerry Wiant
10 Nathan White
11 Mike Pearlman
12 Georg Kirchner
13 Steve Klosko
14 Daniel Kucharski
15 Vlasislav Moshkov
16 John Luck
17 Zuheir Altamimi
18 Wang Peiyuan
19 Kyung-Hee Kim
20 Zhang Zhongping
21 Sang-Hyun Lee
22 Dan O'Gara
23 Franz Koidl
24 Jean-Marie Torre
25 Vince Noyes
26 Ulrich Schreiber
27 Mark Davis
28 Jorge Garate
29 Pippo Bianco
30 Giovanni Delle Monache
31 David Coulot
32 Cinzia Luceri
33 Li Xin
34 Toshi Otsubo
35 Mark Elphick
36 Nobuo Kudo
37 Zhao You
38 Bernd Sierk
39 Craig Smith
40 Chris Moore
41 Scott Wetzel
42 Kalvis Salminsh
43 Pete Shelus
44 Florent Deleflie
45 Vladimir Burmistrov
46 Galina Glotova
47 Nina Platova
48 Ma Lu
49 Guo Tangyong
50 Philip Gibbs
51 Jan McGarry
52 Peter Dunn
53 Graham Appleby
54 Horst Mueller
55 Frank Lemoine
56 Hiroo Kunimori
57 Dave Arnold
58 Yang Fumin
59 Li Zhulian
60 Zheng Xiangming
61 Martin Nemec
62 Natalia Parkhomenko
63 Peter Sperber
64 Wolfgang Seemueller
65 Erricos Pavlis
66 Werner Gurtner
67 Ramesh Govind
68 Harald Michaelis
69 Dave Carter
70 Monique Pierron
71 Francis Pierron
72 Clement Ogaja
73 Dana Lewova
74 Andriy Dmytrotsa
75 Karel Hamal
76 Vladimir Glotov
77 Julie Horvath
78 Tan Yechun
79 Chen Wanzhen
80 Mark Torrence
81 Jennifer Mullaney
82 Ron Thompson
83 Claudia Urschl
84 Randall Carman
85 Peter Wilson
86 Viktor Shargorodsky